PIERS 2002

Progress In Electromagnetics Research Symposium

Proceedings

July 1–5, 2002

Cambridge, Massachusetts, USA

www.piers.org

PIERS 2002 Proceedings

Published by The Electromagnetics Academy.
P.O. Box 425518, Kendall Square, Cambridge, MA 02142, USA.
www.emacademy.org

Printed by Courier, Stoughton, MA, U.S.A.
ISBN: 0-9679674-2-2

Progress in Electromagnetics Research Symposium

July 1-5, 2002
Cambridge, Massachusetts, USA

PIERS 2002 ORGANIZATION

PIERS Chair

J.A. Kong, MIT, USA

PIERS 2002 General Chair

M.B. Silevitch, Northeastern University, USA

PIERS 2002 Executive Committee

E. Miller (Co-Chair)	C. Rappaport (Chair)	R. T. Shin	Y. E. Yang
Y. Zhang			

PIERS 2002 Technical Program Committee

J. J. Akerson	F. Ares	C. Berginc	W. Boerner
J. Bolomey	G. Brown	H. Braunisch	M. Chatterjee
K.S. Chen	M. Cheney	W. Chew	I. Chuang
G. F. Crosta	J. Dowling	M.A. Fiddy	T. M. Grzegorczyk
H. Han	J. Harvey	W. Hong	H. Ikuno
J. Johnson	D. Kasilingam	K. Kobayashi	N. Khazenie
Y. Kotsuka	Y. Lai	D. Lesselier	J. S. Lee
L.-W. Li	K.M. Luk	S. Maci	A. Massa
D. Mirshekar-Syahkal	M. Miyakawa	N.V. Nghiem	D.P. Nyquist
E. Pottier	T. K. Sarkar	C. Seoa	T. Sengor
A. Sivhola	W. Stachnik	L. Tsang	H.A. Zebker
L. Zurk			

PIERS 2002 International Advisor Committee

S. Anderson	Y. Antar	A. Blanchard	N. Gershenfeld
T. M. Habashy	T. Hagfors	A. Ishimaru	E. Jakeman
J. Kim	R. Lang	T. Le Toan	K. F. Lee
M. S. Leong	S. Mano	R. McCoy	R.C. McPhedran
H. Ogura	P. Pampaloni	E. Pike	M. Pollock
A. Priou	Y. Rahmat-Samii	M. Raugi	H. Rott
J. Saillard	G. L. Tyler	G. Whitman	W. Wiesbeck
W. X. Zhang			

PIERS 2002 Administrative Committee

C. O. Ao	T. M. Grzegorczyk	Y. Hara	M. Lai
J. Pacheco	F. L. Teixeira	B.-I. Wu	Y. Zhang (chair)

PIERS 2002 SESSION ORGANIZERS

Alvarez-Melcon, A.	Ammari, H.	Anderson, S. J.	Ao, F.
Ares-Pena, F.	Awadallah, R. S.	Barmada, S.	Berginc, G.
Bergman, D. J.	Bertero, M.	Blaikie, R.	Blaunstein, N.
Bolomey, J. Ch.	Braunisch, H.	Caorsi, S.	Castañer, M. S.
Castañon, D. A.	Chiba, J.	Chien, C.-P.	Crosta, G. F.
de Jager, L.	DiDomenico, L.	Dowling, J.	Dutta, G.
Encinar, J. A.	Eremin, Y.	Erni, D.	Felsen, L. B.
Freilikher, V.	Galdi, V.	Habashy, T.	Hadley, G. R.
Hafner,Ch.	Hanson, G.	Hernandez-Figueroa, H.	Hocking, W.
Huang, H.C.	Karam, M. A.	Kikuchi, H.	Kobayashi, K.
Kotiuga, P. R.	Kotsuka, Y.	Las Heras Andres, F.	Lee, J.-S.
Lesselier, D.	Li, L.-W.	Liou, K.-N.	Mainguy, S.
Maradudin, A. A.	Martin, O. J. F.	Massa, A.	Maystre, D. R. C.
Mazar, R.	Meaney, P. M.	Meecham, W. C.	Méndez, E.
Mishchenko, M. I.	Miyakawa, M.	Musolino, A.	Nepa, P.
Novotny, L.	O'Neill, K.	Ogura, H.	Overfelt, P. L.
Pampaloni, P.	Pande, K.	Pichot, Ch.	Pribetich, J.
Rachidi, F.	Radhakrishnan, K.	Ramer, R.	Rawat, B.
Rott, H.	Sánchez-Gil, J. A.	Sengor, T.	Shahriar, S. M.
Saghafi, S.	Shestopalov, Y. V.	Sihvola, A.	Smith, D. R.
Stolen, R.	Stover, J. C.	Tayeb, G.	Teixeira, F. L.
Terzuoli, A. J.	Vassal'lo, J.	Wang, J. R.	Yakovlev, A.
Yamada, Y.	Zaki, K. A.	Zurk, L.	

PIERS 2002 SPONSORSHIP

- ☐ The Electromagnetics Academy
- ☐ MIT Lincoln Laboratory
- ☐ Mitsubishi Electric Corporation
- ☐ Cold Regions Research and Engineering Laboratory
- ☐ MIT Department of Electrical Engineering and Computer Science
- ☐ MIT Center for Electromagnetic Theory and Applications, Research Laboratory of Electronics

PIERS 2002 SESSIONS

Session 1Aa1

SAR and Polarimetric SAR

Polarization Orientation Estimation from Polarimetric SAR Data

J.-S. Lee, D. L. Schuler, and T. L. Ainsworth
Remote Sensing Division, Code 7263, Naval Research Laboratory
Washington, DC 20375-5351, U.S.A.

D. Kasilingam
University of Massachusetts, Dartmouth
Dartmouth, MA, U.S.A.

Interferometric synthetic aperture radar (SAR) has been successfully applied to measure topography. Radar interferometry requires the use of dual antennas separated by a baseline in a single pass system, or by a repeated pass configuration. In recent studies, Schuler et al. applied polarimetric imaging radar derived orientation angles to measure topography, and Lee et al. used orientation angles for polarimetric SAR data compensation. The results from this technique generally agree well with the DEM map. However, the accuracy is not as good as that from SAR interferometry. Accurate estimation of geophysical parameters, such as soil moisture, surface roughness, snow depth, etc requires such compensation for terrain variations. Many different techniques [1–5] for the estimation of orientation angles have been proposed. However, in these studies, inconsistency in the estimation of orientation angles was encountered in several areas, introducing noisy and erroneous results. To support these applications, it is important to accurately estimate shifts in orientation angles induced by the azimuth slope variations. However, in many cases, inconsistency in the estimation of orientation angle shifts was encountered in several areas, introducing noisy and erroneous results.

In this paper, we develop a unified analysis of estimation algorithms based on the circular polarization covariance matrix. The concept of reflection symmetry is used to explain the soundness of the circular polarization method, and to show problems associated with other algorithms. The relationship between several algorithms will also be explored from different viewpoints, and a theoretical model will be used to explain the results. The effect of radar frequency, scattering media, and polarimetric calibration will also be discussed. L-band polarimetric synthetic aperture radar images of Camp Roberts, CA are used to substantiate this theory.

REFERENCES

1. Lee, J. S., D. L. Schuler, and T. L. Ainsworth, "Polarimetric SAR data compensation for terrain azimuth slope variation," *IEEE Transactions on Geoscience and Remote Sensing*, Vol. 38, No. 5, 2153–2163, September 2000.
2. Roweis, S. T. and L. K. Saul, "Non-linear dimensionality reduction by locally linear embedding," *Science*, Vol. 290, 2323–2326, 2000.
3. Schuler, D. L., J. S. Lee, T. L. Ainsworth, and M. R. Grunes, "Terrain topography measurement using multipass polarimetric synthetic aperture radar data," *Radio Science*, Vol. 35, No. 3, 813–832, May–June 2000.
4. Pottier, E., D. L. Schuler, J. S. Lee, and T. L. Ainsworth, "Estimation of the terrain surface azimuthal/range slopes using polarimetric decomposition of POLSAR data," *Proceedings of IGARSS'99*, 2212–2214, July 1999.
5. Kasilingam, D., H. Chen, D. Schuler, and J. S. Lee, "Ocean surface slope spectra from polarimetric SAR images of the ocean surface," *Proceedings of International Geoscience and Remote Sensing Symposium 2000*, 1110–1112, Honolulu, Hawaii, July 2000.

Studies of Ocean Current Fronts and Internal Waves using Polarimetric SAR Coherences

D. L. Schuler and J.-S. Lee
Naval Research Laboratory
Washington, DC 20375-5351, U.S.A.

D. Kasilingam
University of Massachusetts, Dartmouth
Dartmouth, MA, U.S.A.

F. De Grandi
European Union Commission, Joint Research Centre
Ispra, Italy

Land-based studies [1] have shown that polarimetric SAR coherence values may be used as estimators of surface roughness. In particular, the circular-pol, complex coherence, ρ_{RRLL}, has been used for roughness studies involving both synthetic dielectric surfaces (in an anechoic chamber) and for slightly-rough terrain (Mojave Desert).

The measurement concepts developed in [1] have been applied to a new study of ocean current fronts and the surface manifestations of internal waves. This study uses the fact that the roughness sensitivity of ρ_{RRLL} is largely due to distributions of surface slopes present in the ocean features. Functionally, ρ_{RRLL} responds to SAR azimuthal direction slopes and to the look angle, but there is no dependence on the dielectric constant. The image data used is NASA JPL/AIRSAR P-, L-, and C-band quad-pol data. Data for the current front was obtained during the 1990 NRL Gulf Stream Experiment. Preliminary studies [2] of current fronts located within the Gulf Stream indicate the presence of sharp changes in the polarimetric orientation angle at the frontal boundary. An image of the coherence magnitude $|\rho_{\mathrm{RRLL}}|$ reveals a (related) sharp drop in the value of $|\rho_{\mathrm{RRLL}}|$ at the front. A theoretical composite-surface Bragg scatter model has been used to predict the relation between $|\rho_{\mathrm{RRLL}}|$ and the slope induced variance of the orientation angles. Another estimator, the linear-pol coherence, ρ_{HHVV}, is used to measure slopes in the orthogonal SAR range direction.

The coherences, ρ_{RRLL} and ρ_{HHVV}, are then used in a second study of polarimetric SAR imaging of the surface effects of internal waves. AIRSAR data on internal waves was used from 1) the 1992 Joint US/Russia Internal Wave Remote Sensing Experiment in the New York Bight, and 2) the 1991 Straits of Messina Experiment. Significant sea-truth is available for both experiments. Surface wave cross-section spectral perturbations, for the type of internal waves encountered in the New York Bight, have been calculated by Thompson. Related perturbations also occur in the ocean wave height and slope spectra. These perturbations are near zero for ocean wavelengths shorter than 0.1 m and longer than about 10 m. A spectral peak of about three times ambient relative modulation is reached for wavelengths of 0.5–1.0 m and this peak can be detected by $|\rho_{\mathrm{RRLL}}|$. For aircraft flight-lines which place the internal wave propagation direction (and the slope perturbations) in the azimuthal direction, the estimator $|\rho_{\mathrm{RRLL}}|$ can measure the variance of these sub-pixel slope distributions. SAR measurements from both data sets will be compared with sea-truth.

REFERENCES

1. Schuler, D. L., J. S. Lee, D. Kasilingam, and G. Nesti, "Surface roughness and slope measurements using polarimetric SAR data," *IEEE Trans. Geosci. Remote Sensing*, (In press).
2. Lee, J. S., R. W. Jansen, D. L. Schuler, T. L. Ainsworth, G. O. Marmarino, and S. R. Chubb, "Polarimetric analysis and modeling of multifrequency SAR signatures from gulf stream fronts," *IEEE J. Oceanic Eng.*, Vol. 23, No. 4, 322–333, 1998.

Modulation of Polarimetric Radar Coherence by Ocean Features

D. Kasilingam
University of Massachusetts, Dartmouth
North Dartmouth, MA 02747, U.S.A.

D. L. Schuler and J.-S. Lee
Naval Research Laboratory
Washington, DC 20375, U.S.A.

S. Malhotra
University of Massachusetts, Dartmouth
North Dartmouth, MA 02747, U.S.A.

Polarimetric SAR images have been used to retrieve useful geophysical information over terrain and the oceans. Information such as digital elevation maps (DEM), surface roughness and wave slope spectra have been successfully estimated using polarimetric SAR images. In this study, the use of polarimetric coherence as a measure of surface properties over the ocean is investigated. The study focuses on two L-band, SAR images off the west coast of North America, which were obtained by the JPL AIRSAR polarimetric SAR and the SIR-C shuttle imaging radar sensor, respectively. The focus of the study is to understand the relationship between the modulation of the co-polarized coherence, ρ_{HHVV}, circularly-polarized coherence, ρ_{RRLL}, and the geophysical properties of the oceanic features. The effects on both the magnitude and the phase of the coherence are investigated.

The features investigated in these images are a fresh water plume generated by a river outflow, a weather front, long surface waves and a ship wake. Complex images of the scene are calculated from the satellite data in the different polarizations (HH, VV, HV, RR and LL) and the corresponding image intensity maps and the coherence maps (ρ_{HHVV} and ρ_{RRLL}) are generated. The study shows that a plume off the coast of northern California, is not visible in the intensity images, because the plume does not modulate the small scale roughness significantly. In this same region, the magnitude of the co-polarized coherence, $|\rho_{HHVV}|$, is shown to decrease and thus render the plume visible. The estimator, $|\rho_{RRLL}|$, does not show any significant change within the plume, because it is insensitive to changes in the dielectric constant. It will be shown that the modulation of $|\rho_{HHVV}|$ is mainly due to the change in dielectric constant caused by the mixing of fresh water and seawater.The surface waves are visible in the $|\rho_{HHVV}|$ image, but not visible in the $|\rho_{RRLL}|$ image. It is argued that the modulation of $|\rho_{HHVV}|$ is caused by the change in local incidence angle due to long wave tilts. The incidence angle dependence of $|\rho_{HHVV}|$ is supported by the range dependence of $|\rho_{HHVV}|$, in the AIRSAR image.

The study also found that changes in short-scale roughness do not significantly change $|\rho_{HHVV}|$. In the SIR-C image off the coast of Chiapas, Mexico, the weather front is shown to be a region of increased short-scale, surface roughness. The increased roughness within the weather front, can be deduced from the almost ten-fold increase in backscatter. However, $|\rho_{HHVV}|$ did not change significantly in this region. This suggests that $|\rho_{HHVV}|$ is insensitive to changes in small-scale roughness. In the Chiapas image, $|\rho_{RRLL}|$ shows a corresponding increase around the border of the weather front. It is concluded that small changes in $|\rho_{HHVV}|$ will be manifested as larger increases in $|\rho_{RRLL}|$, if the cross-polarized component, HV, is not small compared to the co-polarized component. Further studies are planned with images of other ocean features such as internal waves and current boundaries.

Helicity, Orientation, Depolarization and Scattering Mechanism Derived from Polarimetric SAR Data

T. L. Ainsworth, S. R. Cloude, and J.-S. Lee
Remote Sensing Division, Code 7263, Naval Research Laboratory
Washington, DC 20375, U.S.A.

Fully polarimetric SAR data analysis has found wide application for terrain classification, land-use, soil moisture and ground cover classification. New methods and algorithms for extracting geophysical parameters from polarimetric data continue to be developed. One method of analyzing polarimetric SAR data that has gained great popularity is the Cloude-Pottier eigenvalue/eigenvector decomposition of coherency matrices [1]. The eigenvalue spectrum uniquely describes the scattering entropy, anisotropy and span (total power). The eigenvalues are also employed in the calculation of averaged quantities, e.g., average scattering mechanism, $\overline{\alpha}$. Here the eigenvectors are analyzed in greater detail.

A general 3×3 Hermitian coherency matrix is described by nine real parameters. Three of these are the eigenvalues. Therefore the three complex eigenvectors (18 real variables) contain at most six independent real variables. Four are required to parameterize the first eigenvector. Orthonormality conditions (10 additional real constraints) severely limit the remaining two eigenvectors. In earlier work [2] we noted that once two eigenvectors are specified the third is fixed and that no new information is provided by the third eigenvector. Here we present a new method for analyzing the eigenvectors that explicitly incorporates the orthonormal properties of the eigenvectors [3]. The circular basis is convenient for describing the scattering mechanism, orientation angle, helicity and depolarization parameters. By construction these variables are independent and describe distinct polarimetric information. This new parameterization of the eigenvectors provides a consistent framework within which to compare and discuss the information content of polarimetric SAR data.

We employ SIR-C, ESAR and EMISAR polarimetric data at both L- and C-band to illustrate the eigenvector analysis and to compare current results with previous work. The diversity of SAR systems and varied scene characteristics may allow general conclusions to be drawn from the data.

REFERENCES

1. Cloude, S. R. and E. Pottier, “A review of target decomposition theorems in radar polarimetry,” *IEEE Trans. Geosci. and Remote Sensing*, Vol. 34, 498–518, 1996.
2. Ainsworth, T. L., J. S. Lee, and D. L. Schuler, “Multi-frequency polarimetric SAR data analysis of ocean surface features,” *IEEE Proceedings of the Int. Geosci. and Remote Sensing Symposium*, 2000.
3. Cloude, S. R., “A new method for characterizing depolarization effects in radar and optical remote sensing,” *IEEE Proceedings of the Int. Geosci. and Remote Sensing Symposium*, 2001.

Modelling of the Mueller Matrix for Rough Surface Scattering with a Modified Version of the IEM

J. L. Alvarez-Perez, I. Hajnsek, and K. P. Papathanassiou
Deutsches Zentrum für Luft- und Raumfahrt e.V.
Institut für Hochfrequenztechnik und Radarsysteme
Weßling, D-82234, Germany

A corrected version of the Integral Equation Model (IEM) by A.K.Fung for rough surface scattering has been previously developed by one of the authors to bridge the gap between the small perturbation method (SPM) and the Kirchhoff approximation (KA). This new Integral Equation Model unifies analytically SPM and KA beyond ad-hoc implementations such as two-scale models and shares its vocation with the small slope approximation (SSA) developed by Voronovich or the phase-perturbation model by Ishimaru. Whereas SPM, SSA and KA are based on the assumption of small values for height, slope and curvature of the surface profile respectively, the corrected version of IEM proposed here relies on the validity of assuming Fresnel coefficients which can be evaluated for the global incident angle instead of the local incident angles. Therefore, some compromise for height, slope and curvature values is required.

In the work presented here this new model is used to calculate all the elements of the Mueller matrix. To date the backscattering coefficients corresponding to the upper-left four elements of this matrix have been extensively studied in the literature and most of the physical models have focused on them. However, a fully polarimetric description of the scattering phenomenon requires the knowledge of the entire Mueller matrix. Analyzing the polarization properties of a scattered wave contributes to a finer interpretation of the properties of the target and facilitates a physical interpretation of measured data acquired by multipolarization synthetic aperture radar (SAR). We investigate the predictions of the model for various surface rms heights and correlation lengths and test its performance against numerical simulations based on the method of moments.

Multi-Frequency SAR Analysis of Vegetation Type and Biomass for Annual and Perennial Pastures in Western Australia

M. J. Hill
Bureau of Rural Sciences and CRC for Greenhouse Accounting
Kingston, ACT, 260, Australia

J.-S. Lee
Remote Sensing Division, Code 7263, Naval Research Laboratory
Washington, DC 20375-5351, U.S.A.

G. E. Donald and D. Henry
CSIRO Livestock Industries
Floreat Park, WA 6014, Australia

Synthetic aperture radar (SAR) has significant advantages for agricultural monitoring in highly seasonal environments where the growing season is defined by rainfall and hence cloudiness limits the use of optical imagery. The advent of satellite systems with multi-frequency polarised SAR has the potential to greatly increase the utility of SAR data for biomass and land cover monitoring compared with current single frequency systems. Grasslands and pastures constitute a difficult target for SAR analysis since they often lack the regular row arrangement of scattering targets and uniformity of scattering types seen with crops and single-species tree plantations. However, recent backscatter modelling with various crop types suggests that quantitative measurement of biomass and detailed discrimination of vegetation type with fully polarimetric multifrequency SAR data are close at hand. In this study, we use JPL POLSAR data to characterise pasture and crop types, and estimate pasture biomass.

The Cervantes area of Western Australia is located near the coast north of Perth. The landscape is predominantly agricultural interspersed with areas of remnant native vegetation. Agricultural land cover consists of cropping, primarily with wheat, lupins and canola, and pasture, primarily made up of annual grasses and legumes, but including some perennial grasses and the tree legume, tagasaste. NASA JPL polarimetric SAR data were collected on the PACRIM2 mission on September 7, 2000 over Cervantes. At or around the time of collection, botanical composition, wet and dry pasture biomass, pasture height along 25 m transects, and soil moisture were collected at 37 sites throughout the area. POLSAR data were subjected to two types of analysis:

1) A coherence version of the POLSAR data (a 9 channel image consisting of the sum, and difference between hh and vv for each frequency, and the cross pole channel for each frequency) was processed with a segmentation scheme based on polarimetric scattering decomposition and the complex Wishart classifier. The resulting classification was compared with field records of crop and pasture types. The classification was used to define land cover types across the POLSAR scene.

2) Regressions were constructed between single POLSAR channels and field measurements of dry and wet vegetation biomass, and calculated volumetric water content of soil and vegetation. The best channel combination was then used to estimate pasture biomass for classified land cover types across the scene. The potential for routine biomass estimation from satellite-based multifrequency SAR is discussed.

Segmenting SAR Images with Robust Competitive Clustering

P. R. Kersten and T. L. Ainsworth
Remote Sensing Division, Code 7263, Naval Research Laboratory
Washington, DC 20375, U.S.A.

R-Y. Lee
RF Sensors Division, Code 455, Naval Air Warfare Center - Aircraft Division
Patuxent River, MD 20670, U.S.A.

Polarimetric Synthetic Aperture Radar (POLSAR) Images have many practical applications. The value of these images is increased provided they can be efficiently segmented prior to image classification. This presentation describes a competitive robust clustering algorithm to segment the POLSAR images.

POLSAR images are constructed from the four possible polar combinations of transmit-receive pairs of the radar: HH, HV, VH, and VV. These coherent returns are complex and symmetry assumptions allow a real 9-D vector representation of the Coherence Matrix. This feature vector, which is associated with each pixel of the image lattice, is used for both clustering and classification. Considerable preprocessing is required to form, register, and calibrate the image [1].

The statistics associated with POLSAR images are far from benign and contain outliers along with the small clusters of high-energy returns. Moreover, the number of clusters required to efficiently segment an image is unknown. The basic clustering algorithm studied is the fuzzy c-means (FCM) clustering algorithm, which demands the number of clusters be specified before the algorithm can be applied [2]. One technique around this problem is to over-estimate the number of clusters and then use a competitive robust FCM (CRFCM) clustering technique to remove those clusters whose cardinality drops below a threshold [3]. CRFCM is applied to simultaneously cluster and reduce the number of clusters to a parsimonious set. We present the current state of this algorithm along with illustrations applied to SAR images.

REFERENCES

1. Lee, J.-S, M. Grunes, and G. de Grandi, "Polarimetric SAR speckle filtering and its implication for classification," *IEEE Transactions on Geoscience and Remote Sensing,* Vol. 37, 2363–2373, Sept. 1999.
2. Bezdek, J., *Pattern Recognition with Fuzzy Objective Function Algorithms,* Plenum Press, New York, 1981.
3. Frigui, H. and R. Krishnapuram, "A robust competitive clustering algorithm with applications in computer vision," *IEEE Transactions on Pattern Analyis & Machine Intelligence,* Vol. 10, No. 5, May 1999.

Optimal Polarimetric Decomposition Variables — A Non-linear Dimensionality Reduction

T. L. Ainsworth and J.-S. Lee
Remote Sensing Division, Code 7263
Naval Research Laboratory
Washington, DC 20375-5351, U.S.A.

Analysis of polarimetric SAR data typically involves identifying important degrees of freedom in the data. Derived parameters (e.g., entropy, polarization fraction) and/or models of polarimetric response are used to reduce the dimensionality of the data and, hopefully, preserve the most relevant polarimetric information. Procedures for choosing the appropriate variables are often based upon empirical or model-based observations, thus the resulting variables are *ad hoc*, one-size-fits-all choices. The powerful eigenvector/eigenvalue techniques for polarimetric decomposition are arguably one of the best methods for reducing the dimensionality of polarimetric SAR data whilst retaining polarimetric information. However, even these techniques tend to exclude the possibility that the polarimetric data may lie on a low-dimensional manifold within the high-dimensional polarimetric data.

The aim of this work is to determine, from the data, a reduced set of variables that "optimally" represents the polarimetric information. We test two related methods of non-linear dimensionality reduction to identify low-dimensional structures (manifolds) that provide meaningful representations of the imagery. Once the manifolds are determined segmentation and classification of the data, now embedded in the manifold, can proceed. In both methods the important ("optimally chosen") variables describe the relative location of the data on the manifold rather than how the manifold is embedded in the higher-dimensional observation space.

The only free parameter in these techniques is the size of the local neighborhoods. A small-size neighborhood tends to segment the data onto disjoint manifolds. Large neighborhoods tend to collect more data onto one large manifold. Employing smaller neighborhoods allows these methods to follow tighter folds, twists and turns in the non-linear manifolds than would larger neighborhoods. Both methods are neighborhood preserving.

We apply the proposed methods of non-linear dimensionality reduction to simulated data and to polarimetric SAR imagery data. Analysis of the derived optimal variables and comparison with standard polarimetric decomposition methods are made.

REFERENCES

1. Tenenbaum, J. B., V. de Silva, and J. C. Langford, "A global geometric framework for non-linear dimensionality reduction," *Science*, Vol. 290, 2319–2323, 2000.
2. Roweis, S. T. and L. K. Saul, "Non-linear dimensionality reduction by locally linear embedding," *Science*, Vol. 290, 2323–2326, 2000.

Segmentation of Polarimetric SAR Images Based on Three-Component Scattering Model

J.-S. Lee, M. R. Grunes, T. L. Ainsworth, and D. L. Schuler
Remote Sensing Division, Naval Research Laboratory
Washington, DC 20375-5351, U.S.A.

Terrain and land-use classification is arguably the most important application in polarimetric SAR. Many supervised and unsupervised classification methods have been proposed. Unsupervised classification automatically segments polarimetric SAR data into several classes. Recently, Lee et al. [1] and Pottier and Lee [2] have applied polarimetric target decomposition to initially segment the data, followed by iterated refined classification based on the Complex Wishart classifier. The final classification can be drastically different from the initial segmented results, and pixels of different scattering mechanisms can be mixed together. In this paper, we propose a new segmentation algorithm that has better stability in convergence and preserves the homogeneous scattering mechanism of each class. In addition, in order to produce an informative classification map, class color selection is important, so we have developed a procedure that automatically colors the map using its scattering characteristics categorized as surface scattering, double bounce scattering, volume scattering and mixed.

The proposed algorithm initially segments the polarimetric SAR images by applying the scattering decomposition of Freeman and Durden [3]. Each pixel is decomposed into four scattering categories: volume, surface, double bounce, and mixed. Pixels in each category are divided into 30 or more initial clusters based on the power of the scattering categories. Within each category, the initial clusters are merged based on the between-class Wishart distance into a desirable number of classes. The complex Wishart classifier is then applied within each category iteratively for the final classification. This ensures the class homogeneous in scattering characteristics. For example, a double bounce dominated pixel will not be assigned to a specular scattering class even if the Wishart distance is the shortest. After the final classification, the color selection for each class is automatically assigned: blue colors for the surface scattering classes, green colors for volume scattering classes, red colors for double bounce classes, and gray shades for mixed classes.

In summary, this paper presents a new polarimetric SAR image classification algorithm that preserves scattering mechanism for each pixel. It applies the complex Wishart classifier in each scattering category, producing classes that contains pixels with the same type of scattering mechanism. Consequently, better classification results are obtained, and the final classified images show improved convergence stability. JPL AIRSAR and ESAR L-Band and P-Band data are used for illustration.

REFERENCES

1. Lee, J. S. et al., “Unsupervised classification using polarimetric decomposition and the complex Wishart classifier,” *IEEE TGRS,* Vol. 37, No. 5, September 1999.
2. Pottier, E. and J. S. Lee, “Unsupervised classification scheme of PolSAR images based on the complex Wishart distribution and the H/A/Alpha — Polarimetric decomposition theorem,” *Proceedings of EUSAR 2000,* May 2000.
3. Freeman, A. and S. L. Durden, “A three-component scattering model for polarimetric SAR data,” *IEEE TGRS,* Vol. 36, No. 3, 963–973, May 1998.

Session 1Ac2

Numerical Methods in Electromagnetics

Determination of Multiple Angle Arrival in Linear Antenna Array Using Genetic Algorithms

B. Galindo de Góes, A. Duarte Dória Neto, and W. da Mata
UFRN
Natal, Brazil

The adaptive antennae have been widely applied in radar, sonar and mobile communications, where the objective is to magnify the directivity in the direction of the interest signal, canceling the action of interference signals. In this case, it is necessary to know the Angle Of Arrival (AOA) of the incident signals in the antenna array. This is possible through methods of spectrum estimation as the method of Bartlett, Pisarenko, MUSIC, ESPRIT, MVDR and others. This work deals with the study to Genetic Algorithms as an auxiliary tool in the determination of the arrival angle in linear antennae arrays. The Genetic Algorithms are random and evolutionary methods generally used in the solution of search and optimization problems. Its functioning is based on the genetic and in the Darwin's theory of the species evolution. The method presented in this work consists on the development of a Genetic Algorithm to determine the points of global maximum generated by the MVDR spectrum. Such points correspond to the angle of arrivals of the incident signals in the array. With intention to verify the efficiency of the developed method, many simulations had been done. One of them consisted of two incident angle signals ($-45°$ and $20°$) in an array of 5 elements and a relation sign/noise equal to 10, resulting in found angles of $-44.97°$ and $19.98°$, after 13 generations. The algorithm revealed fully capable to determine the angle of arrivals with low computational time and presenting a small index of error, never bigger than 0.05, between the exact value and the solution presented by the algorithm. By this way, the Genetic Algorithms are presented as a tool of great interest in the branch of the Adaptive Antennas.

A Matrix Robust Algorithm Applied to an Adaptive Antenna

F. A. L. Gomes
UNICAMP – Faculdade de Engenharia Elétrica
São Paulo, Brazil

A. D. D. Neto
UFRN – Departamento de Engenharia de Computação e Automação
Natal, Brazil

A. D. de Araújo and W. da Mata
UFRN – Departamento de Engenharia Elétrica
Natal, Brazil

The adaptive antenna theory has been studied in several application fields such as radar, sonar, mobile communications, geophysics exploitation, etc. In all these cases, the different methods used to solve problems in the adaptive antenna approach generally use the same procedure, which is related to the increasing of the directivity of the antenna array and to the interfering signals adaptive cancellation. The research to obtain more efficient methods has motivated the adaptive antennas approach to use traditional Least Mean Square (LMS) method or state space variables methods such as Kalman Filter and State Observers. This work presents an algorithm to obtain the optimum gains of the Generalized Side Lobe Canceller Filter (GSC Filter) using a pseudo inverse matrix. Additionally, the importance of the regularization factor to the robustness of the method is verified. The method is recursive, with low computational complexity and fast calculation of the optimum gains. The method is applied to the cancellation of interfering signals in a non-stationary condition of an adaptive antenna array. A matrix regularization process is developed to get a robust method and a better matrix conditioning. The simulation results show the efficiency of the proposed method to cancel interfering signals in planar antennas. The simulation results were done with a 3×3 half wavelength elements in planar array for both signals (desired and interfering). A 40 dB was considered for the relationship between the desired signal and the interfering signal. The irradiation diagrams were obtained in two dimensions for a fixed angular coordinate. The method seems to be efficient to generate null signals in the interfering signal direction. The LMS method was used to compare the performance with the proposed method.

Spectral Methods for Radiative Transfer

A. D. Kim
Department of Mathematics, Stanford University
Stanford, CA 94305-2125, U.S.A.

M. Moscoso
Departamento de Matemáticas, Escuela Politécnica Superior, Universidad Carlos III de Madrid
Leganés, 28911, Spain

We present some computational methods for solving the radiative transfer equation which models wave propagation in a medium that scatters, absorbs, depolarizes and emits radiation. In this method, we use spectral approximations for the spatial variables of the intensity. After substituting these approximations into the radiative transfer equation, one obtains a coupled system of integral equations for the angle dependent expansion coefficients. Using Gaussian quadrature rules to solve these integral equations, we then obtain a linear system whose sparsity can be exploited to yield an efficient method for computing solutions. These methods exhibit super-algebraic convergence rates typical of spectral methods.

This basic idea easily extends to a broad variety of problems that includes pulses, polarization and inhomogeneous media. Hence, we begin by developing this method for the continuous plane wave problem involving only one spatial dimension. From that derivation, we show that modifications needed to consider more general problems such as inhomogeneous media, polarization, and higher dimensions are straightforward. Finally, we present some recent results for polarized waves and narrow optical beams in plane-parallel media.

The Role of Time-Varying Thevenin Equivalent in Electromagnetic Theory

B. Z. Kaplan
Department of Electrical and Computer Engineering,
Ben-Gurion University of the Negev
Beer-Sheva, 84105, Israel

U. Suissa
Department of Electrical and Electronic Engineering,
Negev Academic College of Engineering
Beer-Sheva, 84100, Israel

L. Frumkis
Department of Electrical and Computer Engineering,
Ben-Gurion University of the Negev
Beer-Sheva, 84105, Israel

We have recently found that the Thevenin equivalent, which is known in its applicability for receiving antennas, is of great value in treating DC field sensors. Other authors treat sensors by different methods. The association of field sensors with antennas, and hence their possible representation by the Thevenin equivalent appear at a first glance obvious. Sensors gather signals originated in the measured field sources, and are, therefore, related to receiving antennas. Further contemplation, however, suggests that ELF, ULF, and especially DC field sensors consist a separate entity. The latter sensors operate at wavelengths of some 10^6 and more times longer than the sensor dimensions. Hence, we deal with a near field, and the sensed signal is obtained through reactances. The situation is different from that of antennas, where the coupling to the Thevenin representation of the field sources is by radiation resistance, and real power is transferred (transmitted) to the sensing element (receiving antenna). Furthermore, the lower the frequency, the larger the radiation reactance in comparison to the radiation resistance. The practical cancellation of the radiation reactance by matching for maximum power transfer is useful in the highest portion of the VLF, and in higher frequency bands. The receiving antennas there are 'power receptors'. The situation, however, at the lower frequencies is that the antennas are in fact 'field sensors', power transfer is negligible, and due to the enormous ratio of radiation reactance to radiation resistance matching is impossible. The radiation resistance there is even smaller than the sensor structure resistance. Hence, the related devices are coupled to the sources by relatively large reactances. Their Thevenin equivalent is a voltage source connected to the measuring device through a relatively small capacitance. The voltage of the source in the Thevenin equivalent is the surrounding field intensity multiplied by the sensor effective antenna length.

DC field sensors deserve a separate treatment since the series capacitive reactance tends to infinity at DC, and the voltage source in the Thevenin equivalent is cut off from the measuring device. Coupling to the sources is restored in many of the DC sensors by making them time varying. Some sensors like the Covering Fieldmill possess in their equivalent a time varying series capacitance, which enables the signal current to reach the measuring device even at DC. Other DC field sensors (like Eforks and a sensor developed by us) possess Thevenin equivalents, where both the series capacitance and also the voltage source are time varying. A second capacitance, which is also time varying and should be taken into account, is in parallel to the measuring device terminals. It is due in the Covering Fieldmill, for example, to the capacitance between the rotating and the stationary groups of wings inside the sensor, while the series capacitance is due to the capacitance between the latter groups outside the sensor.

The paper explains our unique method for the systematically simple evaluation of electric DC field sensors. Furthermore, the rules of EM Duality permit the method to treat also magnetic DC field sensors (like fluxgates) by employing the Norton equivalent instead of Thevenin's.

Benchmarks Solutions for Two Body Resonators

S. M. Booker and S. S. Vinogradov
Department of Mathematics, University of Dundee
Dundee, DD1 4HN, Scotland

There are few problems in electromagnetics for which an analytic solution can be obtained, as a result considerable reliance must be placed on numerical solutions of Maxwell's equations. In order to ensure the accuracy, efficiency and robustness of any numerical solution scheme there is a need for benchmark problems, the solution of which can be accurately and reliably determined.

In this paper we discuss a benchmark problem for scattering by an important class of two body resonators. These resonators are defined by two open, concentric spherical shells with a common axis of rotational symmetry; this axis defines the direction of propagation of an incident time-harmonic field. Two cases may be considered, one with the apertures of the two shells oriented in the same direction and one with the apertures of the two shells oriented in opposite directions (see figure below). A solution may be obtained for this time-harmonic scattering problem via the Method of Regularisation. This involves a transformation from a first kind to a second kind system of equations and yields a stable numerical solution to within any pre-determined accuracy. Since the regularised numerical solution takes the form of a rapidly converging series, a benchmark solution can be obtained either for a wideband scattering problem or for a transient scattering problem (via Fourier transformation).

This benchmark problem has a number of important properties. Firstly, since the scattering target possesses edges, cavities and inclusions within cavities, it possesses a range of scattering mechanisms similar to those encountered in many practical situations. Secondly, the parameters of the model may be varied to emphasise different scattering mechanisms. Thirdly, a number of canonical results may be recovered by a suitable choice of the model parameters. Fourthly, the resonators defined by this problem are of potential practical interest.

We illustrate how this scattering problem can be used to benchmark a numerical solution scheme. We consider both far-field properties, such as scattering cross sections, and near-field properties, including the energy stored within each of the resonator's spherical cavities.

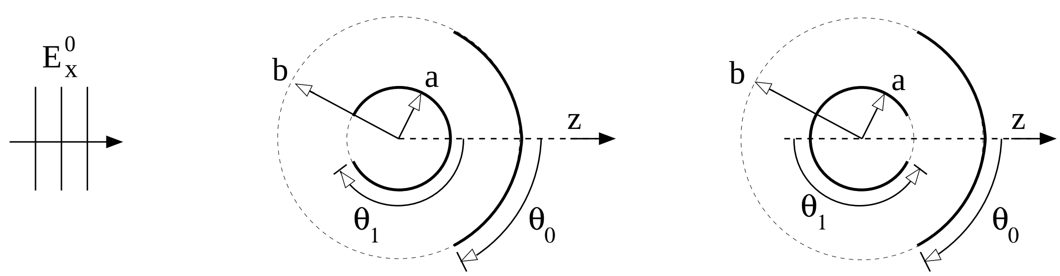

Equivalent Electric Networks for the Evaluations of Radiated Electromagnetic Fields

S. Barmada and R. Rizzo
Dip. di Sistemi Elettrici ed Automazione, Università di Pisa
Pisa, 56100, Italy

The study of the emissions of electromagnetic fields during the operation of electrical devices is of growing interest because of the presence of international rules about the limitation of such emissions when they are not intentional.

An integral method with equivalent electric networks for the analysis of the electromagnetics fields in presence of conductive materials and linear dielectrics is presented.

This methodology is based on the subdivision of the examined system in volume elements in which a uniform current density (for the conductive regions) and polarization (for dielectrics) is assumed. If we respectively indicate with N_d and N_s the number of the volume elements in which we decompose the dielectric bodies and conductive regions, and with N_r the number of branches constructed with the centres of several elementary volumes, the following expressions for the potential functions can be written:

$$\begin{aligned}
\varphi(P,t) &= \frac{1}{4\pi\varepsilon_0}\sum_{i=1}^{N_s}\int\limits_{S_i}\frac{\sigma_i(Q,t-\Delta t_{P,Q})}{r_{P,Q}}dQ + \frac{1}{4\pi\varepsilon_0}\sum_{i=1}^{N_d}\int\limits_{S_i}\frac{\vec{P}_i(Q,t-\Delta t_{P,Q})\cdot\vec{n}}{r_{P,Q}}dQ;\\
\vec{A}(P,t) &= \frac{\mu_0}{4\pi}\sum_{i=1}^{N_r}\int\limits_{V_i}\frac{\vec{J}_i(Q,t-\Delta t_{P,Q})}{r_{P,Q}}dQ.
\end{aligned}$$

By discretizing the volume such as the maximum dimension of each elementary volume is much smaller of the smallest wavelength of the source, in the previous equations we can replace the term $\Delta t_{P,Q}$ (time delay), variable in the integration domain, with a constant delay respect to the centre of the domain.

Integrating, inside the conductive regions, the Ohm's law and the law expressing the continuity of the current, and writing the constitutive equation for the dielectrics in the form of $\vec{P}(P,t) = \varepsilon_0(\varepsilon - 1)\vec{E}(P,t)$, we can obtain a set of equations that can be seen as the equilibrium equation set of an equivalent electric network. In such network we can see resistive and inductive terms coming from the integration of Ohm's law and capacitive terms taking in account the law of the conservation of charges.

The knowledge of the currents and the charge density allows the evaluation of the electromagnetic field in the whole space.

An application of the methodology for the study of antennas is presented.

REFERENCES

1. Harrington, R. F., *Field Computation by Moment Methods*, McMillan, 1968.
2. Gimignani, M., Musolino, A., and Raugi, M., "An integral formulation for nonlinear magnetostatic and eddy currents analysis," *IEEE Trans. On Mag.*, Vol. 30 No. 5, 3024–3027, September 1994.
3. Albanese, R. and Rubinacci, G., "Numerical procedures for the solution of nonlinear electromagnetic problems," *IEEE Trans. On Mag.*, Vol. 28, No. 2, 1228–1231, March 1992.

On the Setting of Multipoles for MMP and GMT

C. Hafner
Swiss Federal Institute of Technology
Zurich, CH-8092, Switzerland

The Multiple Multipole Program (MMP) is the most prominent and most advanced version of the Generalized Multipole Techniques (GMT). Its latest version is contained in the MaX-1 code. Since GMT is a boundary method that is very close to analytic solutions, it allows one to obtain very reliable and accurate results with relatively small matrices. It is well known that these matrices tend to high condition numbers depending on the placement of the multipoles that are used for expanding the field in all domains of a given model. In order to overcome the problems caused by the high condition numbers, two subproblems must be solved: 1) An appropriate method for computing the parameters of the MMP expansions must be used. 2) The multipoles must be placed in a reasonable way. Up to now, the best solution of the first subproblem is the Generalized Point Matching (GPM) technique that works with overdetermined systems of equations. This technique is so successful that it can handle almost all practical problems – provided that the multipoles are correctly set.

It is known that one can reduce the condition number by placing the multipoles close to the boundaries, but this usually leads to relatively inaccurate results. For simple 2D cases, the optimal placement of multipoles can be obtained from conformal mapping techniques. Unfortunately, this cannot be easily generalized for arbitrary boundaries and structures consisting of several materials. Moreover, the optimally placed multipoles can cause very ill-conditioned matrices. Earlier attempts of using numerical optimizers for finding the optimal multipole locations for arbitrarily shaped domains turned out to be extremely time-consuming and not sufficiently robust – even in the simple 2D electrostatic case. Therefore, several simple geometric rules for the multipole setting were proposed and semi-automatic routines based on these rules were implemented. With a sufficient overdiscretization, these routines allow one to easily construct sets of multipoles that are useful for obtaining reasonable results.

However, as soon as the MMP code shall be embedded in an optimizer (for designing optimal antenna, waveguides, filters, etc. with desired characteristics), such semi-automatic routines are not sufficient and fully automatic procedures are required that generate MMP models with 1) appropriate locations and orders of the multipoles and 2) appropriate locations of the matching points along the boundaries. Both tasks depend on each other. First of all, the matching point density depends on the variation of the field along the boundaries. Thus, an optimal placement of the matching points can be obtained when the solution is already known – which is usually not the case. Here, the situation is similar to the mesh generation in Finite Elements (FE). Adaptive mesh generators start with a suboptimal mesh and improve the mesh iteratively from the solutions obtained. Similarly, one can also design adaptive matching point generators and adaptive multipole setting routines.

Session 1Ac3

Recent Advances on Microwave Inverse Scattering Techniques

Diminished 3D Wave Propagation Artifacts with Reduced Background Contrast

P. M. Meaney, N. Yagnamurthy, M. Fanning, S. Pendergrass, and K. D. Paulsen
Thayer School of Engineering, Dartmouth College
Hanover, NH 03755, U.S.A.

We have previously demonstrated in both simulation and phantom experiments that our 2D imaging system is capable of imaging 3D objects with some limitations. In particular the relative permittivity images were quite good in cases where high contrast spheres were illuminated at multiple planes with our monopole array, demonstrating an effective imaging system slice thickness of 4.2 cm at 500 MHz [Meaney et al. 2001]. The corresponding images for conductivity counterpart were disappointing with the conductivity distribution for the recovered object sometimes exhibiting an increase in conductivity rather than a decrease. These 3D effects are important considerations with respect to our liquid coupled microwave breast imaging system where a typical breast presents itself as nearly conical when pendant in the liquid-filled illumination tank.

We have recently performed a number of simulations and phantom experiments with lower contrast ratios between the coupling medium and imaging objects that clearly demonstrate reductions in 3D wave propagation effects as a function of contrast. Figure 1 shows a sequence of three images of a 4.6 cm sphere at multiple planes in 1.3 cm intervals for a background contrast of 2:1 within a 13 cm diameter imaging area. With respect to the relative permittivity images, using the image slice thickness metric developed in the previous analysis, the slice thickness is significantly reduced when the contrast is reduced (Figure 2). For the conductivity counterparts, the slice thickness is considerably larger; however, the presentation of images as a function of imaging slice position is well behaved with no evidence of unexpected object disappearance or inversion observed. These findings are significant with respect to our breast imaging system. In addition, our new clinical interface prototype has been redesigned to require considerably less liquid during exams since any alternative to water will inevitably be more costly. A patient- and environment-friendly coupling medium has been identified which is readily available at modest costs and can be diluted with water to provide a desired lower contrast background medium for breast imaging.

This work was supported by NIH/NCI grant # R01 CA55034–09.

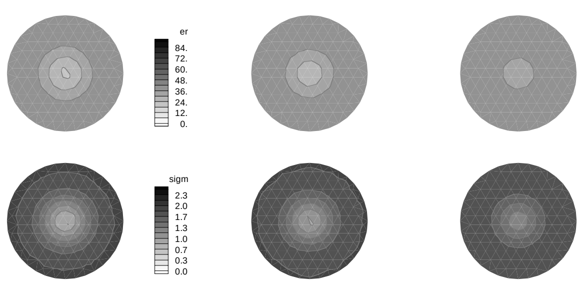

Figure 1. 900 MHz simulation images of a 4.6 cm diamater sphere (2:1 contrast with background) at three planes beginning with the centered position.

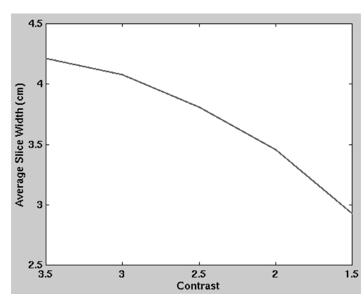

Figure 2. Plot of the effective imaging slice width as a function of contrast with the ackground medium.

REFERENCES

1. Meaney, P. M., K. D. Paulsen, S. Geimer, S. Haider, and M. W. Fanning, "Quantification of 3D field effects during 2D microwave imaging," *IEEE Transactions on Biomedical Engineering,* 2001 (submitted).

Microwave Imaging of a Homogeneous Dielectric Cylinder

A. Qing
Temasek Laboratories, National University of Singapore
Kent Ridge Crescent, 119260, Singapore

Locating, identifying and recognizing dielectric objects is a standard electromagnetic inverse problem with many practical applications. The higher nonlinearity and the presence of nonradiating source make it more difficult to deal with than that of perfectly conducting objects.

Microwave imaging of a homogeneous dielectric cylinder under TM-z plane wave illumination is considered in this paper. The cylinder contour is denoted by a shape function $\rho = F(\theta)$ in the local polar coordinate.

Existing algorithms for the problem can be classified into either the contrast-source type volume integral equation method or the surface equivalent integral equation method. The number of unknowns for the first approach is very large while the second approach is mathematically tedious.

In this paper, the surface equivalence principle is used to derive the governing electromagnetic field integral equation for the scattering problem while the inverse problem is solved using the real-coded genetic algorithm. The local shape function is approximated as closed cubic B-splines of N control points instead of trigonometric series of $N/2$ order. The control points together with the location parameters are the optimization parameters for the inverse problem which is recast into an optimization problem.

Reconstructions with both synthetic and real scattering data are carried out. Good agreement between true profiles and reconstruction results are observed, even when the real measuring data is very noisy.

Identification of Pipes Buried in the Ground from the Measured Data by the Iterative Inversion with Levenberg-Marquardt and Genetic Algorithm

D.-H. Je, K.-S. Oh, and J.-W. Ra
Department of Electrical Engineering and Computer Science, Korea Advanced Institute of Science and Technology
Yuseong-gu, Daejeon 305–701, Republic of Korea

The iterative inversion method in the spectral domain by using the Levenburg-Marquardt and Genetic algorithm may be used to reconstruct the shape and the distribution of permittivities and conductivities of large and high contrast dielectric and conducting two-dimensional objects [1]. The same algorithm is also used for finding the multiple parameters of the air tunnel and the surrounding medium such as the location, size, permittivities and conductivities of the target and the background from the in-situ measured data obtained by the cross-borehole measurement [2]. This multi-parameter inversion techniques give the reconstruction of multiple cylinders of either conducting or dielectric medium buried in the ground from the calculated scattered fields above the ground interface [3].

A newly developed multi-frequency continuous-wave ground-penetration-radar with a highly isolated transmitting and receiving antennas measure the fields coupled between antennas though the surface region and scattered by the underground multiple targets of either conducting and dielectric material above the ground interface. One may reduce the direct coupling through the ground interface region further by taking the Fourier transform of the measured total fields along the measurement direction above the ground interface and eliminating the spectral components near the zero spatial frequency. We like to show that the realistic reconstruction of the buried targets from these measured fields are possible by using this iterative inversion method with the Levenberg-Marquardt and Genetic algorithm and discuss the pitfalls, such as the illposedness, the local minima, the resolution, and the sufficient number of independent data, etc. of the inversion method.

REFERENCES

1. Park, C. S., S. K. Park, and J. W. Ra, "Moment method and iterative reconstruction of two-dimensional complex permittivity by using effective modes with multiple sources in the presence of noise," *Radio Sci.*, Vol. 31, 249–253, 1996.
2. Choi, H. K. and J. W. Ra, "Detection and identification of a tunnel by iterative inversion from cross-borehole CW measurement," *MOTL*, Vol. 21, 458–465, 1999.
3. Kim, J. S. and J. W. Ra, "Location and imaging of two-dimensional pipes buried in a lossy half earth," *MOTL*, Vol. 31, 140–143, 2001.

Microwave Imaging in the Time Domain Using the FDTD Method

I. T. Rekanos
Radio Laboratory, Helsinki University of Technology
Espoo, FIN-02015, Finland

Microwave imaging utilizing wideband incident fields has attracted considerable interest during the last years. Actually, the idea of applying wideband incidences and inverting time-domain field measurements can be realized as the extension of using multiple but distinct excitation frequencies. The use of multiple distinct frequencies — implemented as a frequency-hopping scheme — has been proven advantageous compared to the use of monochromatic illuminations of the scatterer domain. This can be attributed to the fact that the lower frequencies insure the convergence of iterative inverse scattering techniques, while the higher frequencies improve the resolution of the reconstructed scatterer profiles.

In our study, we have developed a time-domain inverse scattering method, which combines the FDTD method and the Polak-Ribière conjugate gradient optimization algorithm. This method is based on the minimization of a cost functional representing the discrepancy between the measured and the estimated values of the total (incident plus scattered) field. Actually, the Fréchet derivatives of the cost functional with respect to the functions that describe the unknown electromagnetic properties of the scatterer are derived analytically by setting an augmented functional stationary. This augmented functional combines the aforementioned cost functional with the Maxwell's curl equations, which are set as constraints. The constraint of fulfillment of the Maxwell's curl equation by the field is introduced by using Lagrange multipliers. An analysis based on the calculus of variations has proven that, similarly to the electromagnetic field, the Lagrange multipliers satisfy the Maxwell's curl equations and the radiation condition. Hence, both the electromagnetic field and the Lagrange multipliers can be calculated by means of the FDTD method.

The presented method has been successfully applied to the reconstruction of two-dimensional scatterers, which can be dielectric, lossy, and magnetic. We mention that the spatial distributions of the dielectric permittivity, conductivity, and permeability of the scatterer are reconstructed simultaneously. In numerical results, we have examined both the TM- and TE-polarization cases. Furthermore, the robustness of the method to the presence of noise in the set of measurements has been investigated.

Recovering a Lossy Dielectric Cylinder in a Lossy Dielectric Box

Yu. V. Shestopalov
Karlstad University
Karlstad, Sweden

We reconstruct the shape S or complex permittivity ε_o of a lossy dielectric cylinder placed in a lossy thin-wall dielectric box. The covered cylinder is situated inside a perfectly conducting rectangular cavity. The structure is irradiated through thin slots cut in the walls. The direct scattering problem is reduced to nonselfadjoint boundary value problems for the Helmholtz equation, the unknown function coincides with the longitudinal component of the electric or magnetic fields.

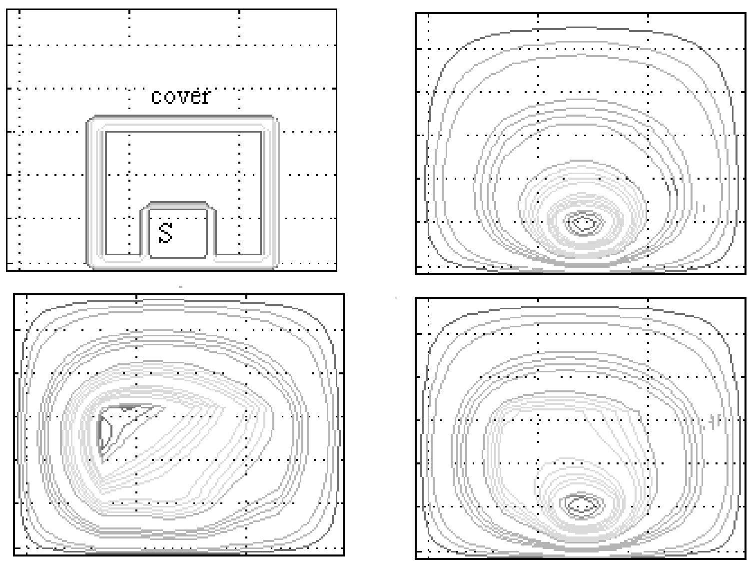

The direct problem is solved numerically using finite differences. The inverse problems of recovering (a) S (ε_o is given) or (b) ε_o (S is given) from the boundary field is considered within the frames of the following setting: to model the most rarefied mesh that still allows one to reconstruct (to 'see') the inclusions and requires minimum CPU resources. A combination of rectangular domains facilitates the solution and substantially reduces the CPU time, which enables one to obtain results using a PC in the resonance frequency range.

The figures shows the typical reconstructed shapes. The number of mesh nodes was as low as 400–2500, the cavity diameter $D = 3 - 10\lambda$, the permittivities $\mathrm{Re}\,\varepsilon_c = 10 - 50,\ \mathrm{Im}\,\varepsilon_c = 0.001 - 30$ (cover) and $\mathrm{Re}\,\varepsilon_o = 30 - 80,\ \mathrm{Im}\,\varepsilon_o = 0.01 - 50$; the cover wall thickness was $0.001 - 0.05D$, and the size of amounted S to $0.5D$

The results enable us to conclude that (i) the imaginary part of the field components carries the essential information about the reconstructed object; (ii) the reconstruction procedure weakly depends on the source location; and (iii) when the difference $|\mathrm{Im}\,\varepsilon_c - \mathrm{Im}\,\varepsilon_o|$ lies within a certain interval, the reconstruction is possible (the cover is virtually transparent to the field), and outside this interval, the effect of the lossy cover becomes pronounced and may violate the reconstruction (see figures).

Inversion of Borehole Radar Data for Electrical Properties

T. Tanaka
Division of System Science, Graduate School of Science & Technology, Nagasaki University
Nagasaki, 852-8521, Japan

T. Takenaka
Department of Electrical & Electronic Engineering, Nagasaki University
Nagasaki, 852-8521, Japan

In our previous work, the forward-backward time-stepping (FBTS) algorithm [1] was proposed to reconstruct the electrical parameter profiles of unknown objects from time domain field data and the effectiveness of the algorithm was demonstrated for a full-view measurement case where transmitter and receiver positions surround the objects on all sides. In borehole radar imaging, it is not possible to transmit or receive waves from all positions around a reconstruction region containing targets. This restriction on the data collection decreases the amount of information about the unknown objects as compared with a full-view measurement case. Moreover, the search region is generally large with respect to the illumination wavelength. The reconstruction in a large search region with limited-view measurements often fails trapped in a local minimum when we use a gradient-based optimization method to solve the inverse scattering problem.

In this paper, we propose a two-step iterative approach to the cross-borehole radar imaging. In the first step, in order to perform coarse reconstruction, we regard all the targets as homogeneous objects with circular cross-sections, although they may not be so. The general geometrical structure (location and size) of the unknown targets is determined in a large search region by using FBTS algorithm under the assumption. Using this geometrical information, the original search region can be reduced to several smaller regions each of which contains only one target. In the second step, detailed reconstruction is performed in the several small search regions by using FBTS algorithm to determine more accurately the shapes, locations and electrical parameter profiles of the targets. Reduction of a search region saves the memory storage and computation time, and speeds up the convergence rate. Numerical examples show the efficiency of the combination of the coarse and detailed reconstruction. Good reconstruction is obtained even when reconstruction with the detailed reconstruction algorithm alone fails.

REFERENCES

1. T. Takenaka, H. Jia, and T. Tanaka, ”Microwave imaging of electrical property distributions by a forward-backward time-stepping method,” J. Electromagn. Waves Applic., vol.14, pp. 1609-1626, Dec. 2000.

Furtivity and Masking Problems in Time Dependent Acoustic and Electromagnetic Obstacle Scattering

F. Zirilli
Dipartimento di Matematica "G. Castelnuovo", Università di Roma "La Sapienza"
Roma, 00185, Italy

We consider "furtivity" and "masking" problems in time dependent acoustic and electromagnetic obstacle scattering. Roughly speaking a "furtivity" ("masking") problem consists in making "undetectable" ("unrecognizable") and object immersed in a medium where an acoustic or electromagnetic wave that scatters on the object is propagating. The detection (recognition) of the obstacle must be made through the knowledge of the field scattered by the object when hit by the propagating wave. These problems are interesting in several application fields. We formulate a mathematical model for the "furtivity" and "masking" problems considered consisting in optimal control problems for the wave equation or for the Maxwell equations. Using the Pontryagin maximum principle we show that the solution of these control problems can be characterized as the solution of suitable exterior problems for systems of coupled wave equations. The numerical solution of these systems involving partial differential equations in four (space, time) independent variables is a critical issue when reliable and efficient procedures to solve the furtivity or masking problem are required. High performance parallel algorithms are desiderable to solve these systems. We suggest a computational method well suited for parallel computing and based on an adapted version of the operator expansion method. Some numerical results for the acoustic case in the form of computer animations can be found in the website hhtp://www.econ.unian.it/recchioni/w8.

3-D Blind Deconvolution of Point-Spread Functions from Microwave Scatterers

A. E. Yagle
University of Michigan
Ann Arbor, MI, U.S.A.

In microwave inverse scattering of an isolated target having finite spatial support inside a dielectric medium, a major difficulty is accounting for the propagation effects of the dielectric medium containing the target. This is difficult enough even when the effects of the medium on microwave propagation are known. In practice, the effects are often unknown, which makes the inverse scattering problem even harder.

We apply the Born approximation to the Lippman-Schwinger integral equation of inverse scattering, resulting in a linearized integral equation relating the target reflectivity to external measurements. The kernel of the equation is the Green's function (in optics, the point-spread function) of the medium. However, the Green's function is often unknown, or known only approximately. Our experience has been that uncertainties in the Green's function itself are more significant than the multiple scattering that is neglected in the linearization of the integral equation, for imaging an isolated target.

This leads to a 3-D blind deconvolution problem, in which the goal is to reconstruct both the target reflectivity and the Green's function from noisy measurements of their convolution. Although this seems to be one equation in two unknowns, it is actually a heavily overdetermined problem, so that a reasonably-conditioned (not extremely sensitive to variations in the data) solution can be obtained from noisy data. The problem is how to do this without having to numerically process 3-D data sets.

We present a new algorithm for solving the 3-D blind deconvolution problem, and apply it to a microwave scattering problem. The algorithm computes the maximum-likelihood estimate of the target reflectivity. We assume that:
(1) The target has unknown reflectivity but has known finite spatial extent;
(2) The point-spread function is even (symmetric); this is a common state of affairs in optics and electromagnetic field propagation in general;
(3) The additive noise is a zero-mean 3-D white Gaussian noise random field.

The algorithm has the following features:
(1) We use the 2-D Fourier transform to decouple the 3-D problem into a set of 1-D blind deconvolution problems. Not only are the 1-D data sets much smaller, but the 1-D problems can be solved separately and in parallel;
(2) We assemble a resultant matrix from the Fourier-transformed data whose nullspace is the Fourier transform of the target reflectivity. Due to the small size of the 1-D problem matrix, this nullspace is well-defined and it can be computed relatively quickly;
(3) The minimum least-squares perturbation of the data so that the matrix is singular is computed using an iterative and absolutely convergent algorithm.

The algorithm proceeds as follows, in parallel for each 1-D subproblem:
(1) Compute the minimum singular value and vectors of the resultant matrix;
(2) Subtract off the outer product associated with the minimum singular value;
(3) "Toeplitzify" the resulting matrix by averaging along diagonals to produce a matrix having the form of the resultant matrix;
(4) Continue until convergence, which is guaranteed.

A New Approach to Microwave Imaging Based on a Memetic Algorithm

S. Caorsi
Department of Electronics, University of Pavia
Pavia, 27100, Italy

A. Massa
Department of Information and Communication Technology, University of Trento
Trento, I-38050, Italy

M. Pastorino, M. Raffetto, and A. Randazzo
Department of Biophysical and Electronic Engineering, University of Genoa
Genova, 16145, Italy

In recent years, electromagnetic imaging is became a more and more important topic. The number of its applications grows day by day. Let us consider medical applications, non-destructive test and evaluation, mine localization, archaeology tasks, etc. Consequently, suitable methods, accurate and faster, are required. However, inverse scattering problems (resulting from the mathematical description of typical microwave imaging procedures) are generally ill-posed and nonlinear. This implies the use of nonlinear methodologies able to overcome ill-posedeness and to avoid the solution be trapped in local minima of the arising cost function. To this end, many iterative techniques have been successfully used [1]. However, as far as optimization methods are concerned, a large amount of computational resources is generally required. For example, let us consider the class of stochastic algorithms and in particular the genetic algorithms (Gas). In the recent years, a lot of approaches based on GAs has been developed and many efforts have been done to produce hybrid code [2] in order to increase the convergence rate. Memetic Algorithms (MAs) [3] are hybrid optimization algorithms where the population is composed by local minima of the cost function. This results in an increase of the convergence rate of the minimization procedure. The trial solution moves in the search space by ”jumping” from a minimum to another one, exploring only the optimum values of the cost function. The population is generated by means of a local minimization procedure (e.g., conjugate gradient method) and the evolution is performed by using standard genetic operators, like crossover and mutation.

In this paper, the effectiveness of the MAs in the framework of microwave imaging is assessed. The reconstruction of dielectric and geometric characteristics of a multi-layer elliptic cylinder (in this case the scattered field can be analytically computed [4]) is performed. Selected results of numerical simulations are presented in order to point out capabilities but also current limitations of the proposed approach.

REFERENCES

1. Pastorino M., “Short-range microwave inverse scattering techniques for image reconstruction and applications,” *IEEE Trans. Instrum. Meas.*, Vol. 47, 1419–1427, 1998.
2. Caorsi S., A. Massa, and M. Pastorino, “Recent advances on optimization techniques based on genetic algorithms (GAs) for electromagnetic inverse scattering problems,” *PIERS2001*, Osaka, Japan, p. 223, July 18–22, 2001.
3. Merz P. and B. Freisleben, “Fitness landscape analysis for QAP,” *IEEE Trans. Evolutionary Comp.*, Vol. 4, 337–352, 2000.
4. Caorsi S., M. Pastorimo and M. Raffetto, “Electromagnetic scattering by a multilayer elliptic cylinder under transverse-magnetic illumination: series solution in terms of Mathieu functions,” *IEEE Trans. Antennas Propagat.*, Vol. 45, 575–560, 1997.

Inverse Treatment in Microwave or Millimeter Wave Radiometry

G. Tittelein, R. Ringot, J. C. Van de Velde, and B. Bocquet
Institut d'Electronique et de Microélectronique du Nord U.M.R. CNRS 8520
Département Hyperfréquences et Semiconducteurs
Université des Sciences et Technologies de Lille
Lille, France

Principle: Microwave radiometry measures the power of an electromagnetic noise signal emitted by each dissipative material. The classical Planck's law describes the specific intensity of this random signal. Our principal interest is the development of microwave or millimeter radiometry for industrial or medical applications, quite different of remote sensing and radioastronomy applications.

Investigation: Our investigations concern the near field or far field radiometers. These radiometers are designed for a power or correlation measurement. Technologies of such radiometers are different. In near field radiometry, generally, it is necessary to take into account the emissivity factor for a quantitative retrieval of the temperature. Then, we have developed radiometers, which are capable to measure emissivity and temperature.

Two another important factors are the measurement time and the image synthesis. Recently, we have developed a real time calibration method based on a digital signal processing which are realized a real-time and multi-sensors calibration.

Inverse Treatment: The quantitative retrieval of the temperature is not easy in radiometry. Microwave or millimeter wave radiometry is described by a Freedholm equation, which represents a class of ill-posed problem. We have developed a method based on deconvolution and regularization of the solutions. Also, it is necessary to describe the response of the radiometer in its environment. We will see how we can apply this treatment on the different kind of radiometer (near field, far field, correlation) and the possibility to use this principle without a-priori information on the depth if we work with a multi-frequency radiometer.

Applications: I give several applications to illustrate this point of view. A first example concerns the medical field with a Microwave Radiometric Mammography (near field imagery) for the early characterization of beast cancers [1, 2]. Other example is dedicated to the observation of scene in bad weather conditions (fog, clouds, rain, . . .) for automotive or aircraft transportation (far field millimeter imagery) [3, 4]. The last example concerns the development of a microthermal sensor for the temperature measurement of dissipative transmission lines in electronic circuits. We use here a near-field and multifrequency correlation radiometer [5].

REFERENCES

1. Leroy, Y., B. Bocquet, and A. Mamouni, "Non-invasive microwave radiometry themmometry," *Physiological Measurement*, Vol. 19, 127–148, 1998.
2. Bocquet. B., G. Tittelein, and R. Ringot, "Clinical results in microwave radiometric mammography (MRM)," *PIERS'2001*, Osaka, Japan, 18–22, July, 2001,
3. Chamseddine, A., B. Bocquet, P. A. Rolland, A. Cappy, M. Klingler, and M. Heddebaut, "Real-time Low cost passive imaging system for automotive applications," *IEEE VTC Symposium 2000*, Boston, 24–28, September, 2000.
4. Chamseddine, A., M. Klingler, M. Heddebaut, B. Bocquet, A. Cappy, and P. A. Rolland, "Millimeter-wave passive imaging system for survey and obstacle detection in ITS," $8^{\rm th}$ *Conf. on Intelligent Transportation Syst.*, Sydney, September $30^{\rm th}$– October $4^{\rm th}$, 2001.
5. Allal, D., B. Bocquet, and Y. Leroy, "Synthetic bandwidth correlation radiometer for the resolution improvement of a thermal mlcrosensor," *Microwave and Optical Technology Letters*, Vol. 19, No. 2, 94–100, 1998.

Session 1Ac4

Composite Materials and EMC Applications

Complex Permeability of Spinel Ferrite Composite Materials and Microwave Absorbing Characteristics of Single-Layer Absorbers

T. Tsutaoka
Graduate School of Education, Hiroshima University
Kagamiyama, Higashi-Hiroshima 739–8524, Japan

T. Kasagi
Beppu Women's Junior College
Beppu, Ohita 874–8567, Japan

K. Hatakeyama and T. Nakamura
Faculty of Engineering, Himeji Institute of Technology
Syosha, Himeji 671–2201, Japan

High frequency complex permeability $\mu_r{}^*$ and permittivity $\epsilon_r{}^*$ of spinel ferrite (Ni-Zn ferrite and Mn-Zn ferrite) composite materials have been studied in the microwave frequency range. Fig. 1 and 2 show the $\mu_r{}^*$ and $\epsilon_r{}^*$ spectra of these two types of composite materials. In both ferrite composites, frequency dispersion of $\mu_r{}^*$ locates above 100 MHz. This is originated by the domain wall and spin rotational resonance. Though there is no frequency dispersion of $\epsilon_r{}^*$ in Ni-Zn ferrite composites up to 6 GHz, it is found that Mn-Zn ferrite composites show frequency dispersion of $\epsilon_r{}^*$ in several GHz.

Figure 3 shows the return loss of single-layer microwave absorber using these ferrite composites as a function of frequency.
The matching frequencies locate below 1 GHz for Mn-Zn ferrite composite absorbers, and above 1 GHz for Ni-Zn ferrite composite ones. This frequency increases with decreasing ferrite content in both composite absorbers. Thus we can control the matching frequency by changing the ferrite content. Further we can construct the several types of absorbers using these composite materials.

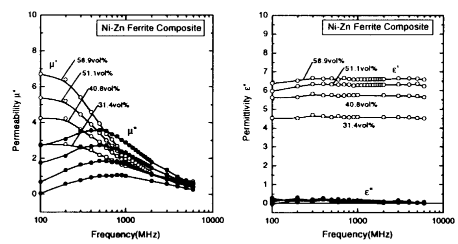

Figure 1: Complex permeability and permittivity spectra for Ni-Zn ferrite composite materials.

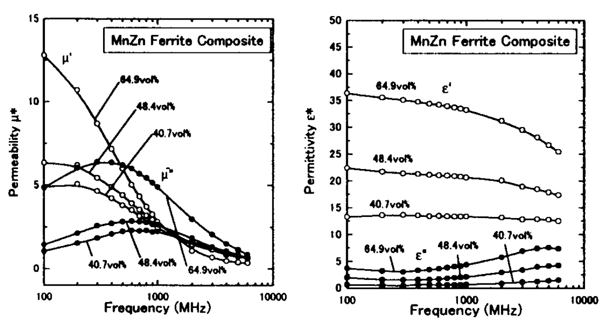

Figure 2: Complex permeability and permittivity spectra for Mn-Zn ferrite composite materials.

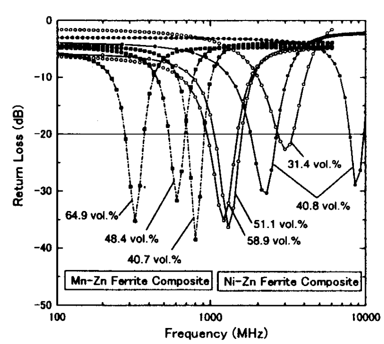

Figure 3: Microwave absorbing characteristics of single-layer absorbers using spinel ferrite composite materials.

Permeability Spectra of Some Ferrites and Their Application to EM-Wave Absorber

T. Nakamura, K. Hatakeyama, and Y. Yamada
Faculty of Engineering, Himeji Institute of Technology
Himeji, Hyogo 671-2201, Japan

In spinel ferrites, the permeability values in the radio frequency region are limited with the natural resonance phenomena. It is called the Snoek's limit, and provides some limitations to radio frequency device applications. In this study, we study the permeability spectra in polycrystalline spinel and hexagonal ferrites. Thin electromagnetic wave absorbers using hexagonal ferrites are proposed.

The complex permeability is numerically evaluated by the combination of spin rotation component and domain wall motion contribution [1, 2]. The spin rotational component plays a major role in the frequency region above hundreds MHz. The product of static spin susceptibility and spin resonance frequency corresponds to the Snoek's product [3]. The Snoek's product of spinel ferrite is proportional to the magnetization. The Snoek's product values of hexagonal ferrite exceed the dashed line. It indicates that the high-frequency permeability of hexagonal ferrite is not limited by the Snoek's law.

The utilization of hexagonal ferrite enables us to obtain thin quasi-microwave absorber, since the permeability values of hexagonal ferrite are far beyond the Snoek's limit. By changing the chemical composition of the hexagonal ferrite, the center frequency is tunable in the range from 700 MHz to 4 GHz. The matching thickness decreases from 3.5 to 1.5 mm, as the center frequency shifts higher.

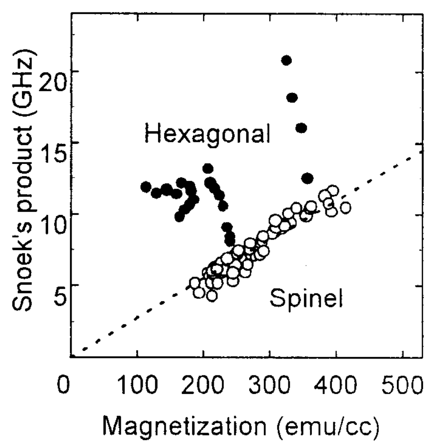

Figure 1: Snoek's product vs. magnetization for spinel and hexagonal ferrites.

REFERENCES

1. Nakamura, T., T. Tsutaoka, and K. Hatakeyama, *J. Magn. Mater,* Vol. 138, No. 139, 1994.
2. Nakamura, T., *J. Magn. Mater,* Vol. 168, No. 285, 1996.
3. Nakamura, T., *J. Appl. Phys.* Vol. 88, No. 348, 2000.

Study on Measuring Method of Shield Effectiveness and Numerical Analysis of the Conductive O-ring

T. Yamada and H. Hyakutake
NOK Corporation
Fujisawa-shi, Kanagawa-ken 251-0042, Japan

K. Hatakeyama
Faculty of Engineering, Himeji Inst. of Tech.
Shosha, Himeji 671-2201, Japan

Rubber packing and O-rings are used for automobiles and other outdoor equipments to seal water, oil ,and dust. NOK is the largest supplier of O-rings in Japan. We have succeeded in developing high conductive rubber without compounding any forms of metals and apply this material to O-rings for EMI shielding. Since there is no defined evaluation method of shield effectiveness available, we have also developed a new evaluation device.

There are two ways in fixing O-rings, cylinder fixing type and plane fixing type as shown in Fig. 1. Accordingly, our evaluation device corresponds to both forms as shown in Fig. 2. A sample is inserted into P1 section if it is a cylinder fixing type and into P2 section if it is a plane fixing type, and is connected with the input/output ports of 50 ohm line on both sides. Our conductive rubbers are EPDM, CR, and NBR based and are compounded with carbon and other materials, which raise electric conductivity up to about 2000 S/m.

We calculated the characteristic impedance of the device and transmission characteristic by the transmission line model. The electromagnetic field of the P section spreads in radiation state between the two pole plates. We solved the Maxwell equation under the condition that electromagnetic field does not change in Z direction for the reason that the gap between the two pole plates is narrow. Then it can be expressed by the Hankel function. As a result, we found it possible to measure up to 1 GHz because reflection is very low during that range, and also found that the correction compensation is necessary for transmission characteristic when putting in samples. The measured value of the conductive O-ring (cross section axial 2.4 mm, inter diameter 20 mm) by this device is shown in Fig. 3. In the figure, the solid line represents the plane fixing type and the broken line represents the cylinder fixing type. Though materials are the same, the characters are different because the correction compensation is different. And, it corresponded well to the result of the same thickness plate sample measured in the uniformity line of characteristic impedance. Consequently, this result confirms that this device enables us to make quantitative evaluation of the transmission characteristic of O-rings. Also, the high shield effectiveness of our EMI O-ring, added conduction to the conventional material, was confirmed quantitatively.

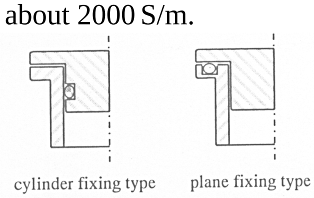

Fig.1 Two ways in fixing O-rings

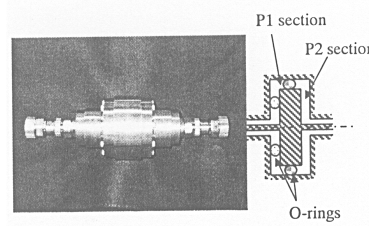

Fig.2 Photograph of outside and cross section view of the evaluation device

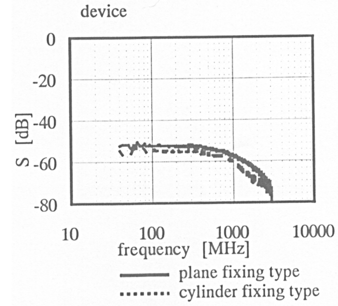

Fig.3 Transmission characteristic of O-rings

The Matching Characteristics of EM Wave Absorbers with a Surface of Printed Conductive Line Patterns

M. Amano and Y. Kotsuka
Department of Communications Engineering, Tokai University
Hiratsuka, Kanagawa-ken 269-1292, Japan

EM wave absorber with a surface-printed conductive line patterns is newly proposed. The advantage of this absorber is to be able to control the matching frequency both toward a higher frequency or a lower frequency region and to offer twin-peaks characteristic using a single absorbing material.

The authors have proposed simple methods of changing the matching characteristics of microwave absorber only using a single material from the viewpoints of effective use of materials and the necessity of quickly responding to recent demands for various kinds of EM wave absorber [1, 2]. The magnetized ferrite absorber is one of the examples for this purpose [1]. Its matching frequency characteristics are changed toward higher frequency regions by controlling both the strength of a static magnetic field that is applied perpendicularly to the surface of a ferrite absorber and the ferrite thickness simultaneously. As a more simple method, a rubber ferrite absorber with multi-holes can provide the method of broadly changing the matching frequency region toward a higher frequency region by adjusting the hole size and the adjacent hole space [2]. However these EM wave absorbers have the matching characteristic of only changing the matching frequency toward higher frequency regions.

This paper proposes a new method of changing a matching frequency both toward higher frequency or lower frequency regions and realizing twin-peaks characteristic using a single absorbing material. Square conductive patches with a checkered pattern attached to a dielectric absorbing material have been proposed [3].

Present EM wave absorber is constructed with conductive thin line patterns printed periodically on the surface of magnetic absorbing material such as a ferrite.

The conductive line patterns printed on the surface of absorbing material can give the nature of capacitance or inductance for the absorbing material depending on wavelength. In this paper, first, a few models of absorber are introduced. Then, the detailed matching characteristics of microwave absorber printed with periodical square frames is investigated for the case of normal incidence, particularly focusing on the method of realizing a thin EM wave absorber. To investigate present fundamental matching characteristics, FDTD analysis is introduced. It is clarified that matching frequency characteristic is shifted toward a lower frequency region as the square size of loop or frame width of the loop is increased and as the adjacent space between squares is decreased when the other parameters are kept as constants. A thin absorber with a thickness of 2.0 mm is obtained at the frequency of 2.45 GHz, using a carbonyl iron absorber.

REFERENCES

1. Kotsuka, Y. and H. Yamazaki, "Fundamental investigation on a weakly magnetized ferrite absorber," *Trans. on IEEE*, Vol. 42, No. 2, May 2000.
2. Kotsuka, Y. and M. Amano, "A method of effective use of ferrite for microwave absorber," *2001 IEEE MTT-S Int. Microwave Symp. Dig.*, 1187–1190, Phoenix, USA, May 2001.
3. Ojima, T., "Reflectivity calculation of a periodical-patch-loaded absorber by the FD-TD method," *1999 IEEE Int'l Symp. on EMC*, 340–344, Seattle, WA, August 1999.

EM Wave Absorber with a Surface of Periodical Conductive Materials

M. Amano and Y. Kotsuka
Department of Communications Engineering, Tokai University
Hiratsuka, Kanagawa-ken 269-1292, Japan

The EM wave absorber with thin conductive lattices attached to the surface of a magnetic absorber has been proposed [1]. In the same construction as ours, square conductive patches with a checkered pattern have been proposed. This paper treats the case of using a dielectric material as an absorber [3].

In the case of our EM wave absorber however, a magnetic absorber has been introduced from the investigation based on the transmission line theory. That is, the magnetic absorber like a ferrite can be expressed using an equivalent circuit with series connections of resistance and inductance at the end of the transmission line. Therefore, a capacitance is added to this equivalent circuit if conductive materials are attached to the surface of ferrite material. As the result, the equivalent circuit becomes to have a nature of resonant circuit. This is a reason why our present EM absorber adopted magnetic materials. This absorber has a special feature that the matching characteristics is changed toward low frequency regions using a single material and it has also the possibility of making a thinned absorber. However, there are many parameters such as a lattice size, adjacent space between conductive lattice, and material constant to determine characteristics.

In this paper, the detailed matching frequency characteristics are investigated by taking these many kinds of parameters to establish a method of computer-aided design.

For the analysis of matching characteristics, FDTD method has been introduced. A slab waveguide is introduced as an analytical model for calculating reflection coefficients [2]. Since the present absorber has a periodical structure, periodical boundaries are introduced and at the opposite side of ferrite absorber, a 16 layer PML absorbing boundary is set up. We introduced changeable cell size in order to model an absorber in details. General charts for the design of present absorber are provided particularly from the view points of how to select a width of size of lattice and an adjacent space between lattices for several frequencies.

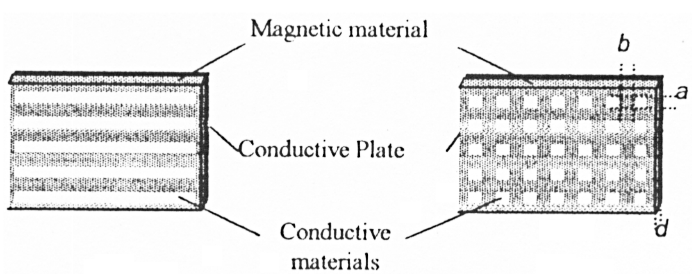

(a) (b)

Figure 1: EM wave absorbers with the surface of periodical conductive materials.

REFERENCES

1. Kotsuka, Y. and H. Yamazaki, “Fundamental investigation on a weakly magnetized ferrite absorber,” *Trans. on IEEE,* Vol. 2, No. 2, May 2000.
2. Kotsuka, Y. and M. Amano, “A method of effective use of ferrite for microwave absorber,” *IEEE MTT-S Int. Microwave Symp. Dig.,* 1187–1190, Phoenix, USA, May 2001.
3. Ojima, T., “Reflectivity calculation of a periodical-patch-loaded absorber by the FD-TD method,” *IEEE Int’l Symp. on EMC,* 340–344, Seattle, WA, August 1999.

Site Attenuation on an Absorber-Lined Ground Plane

K. Fujii, A. Sugiura, and Y. Matsumoto
Tohoku University, 2-1-1, Katahira
Aoba-ku, Sendai 980–8577, Japan

A. Nishikata
Tokyo Institute of Technology, 2-12-1 Ookayama
Meguro-ku, Tokyo 152–8552, Japan

Recently, EMI measurements performed in a free-space environment have been discussed in various international standard organizations. In this respect, placing ferrite tiles over a ground plane is considered to be a promising way for realizing the free-space condition at an open area test site. However, the performance below 100 MHz has not been sufficiently analyzed because the tiles are placed very close to an equipment under test (EUT) and a measuring antenna. The present paper therefore employs the Sommerfeld integral representation for the reflected waves from a ground plane lined with ferrite tiles in order to analyze the site attenuation (SA) rigorously.

The SA is defined in terms of the following two measurement results [1]: (1) When a pair of antennas are arranged on a test site as shown in Fig. 1(a), the maximum voltage V_S is measured during the receiving antenna scanned. (2) When the cables are connected directly to each other as in Fig. 1(b), the voltage V_D is measured. Then, the SA is calculated from $SA = V_D - V_S$ [dB]. The numerical evaluation of the SA was performed using the moment method with the Sommerfeld expression for the reflected waves from ferrite tiles placed on a ground plane.

The results are shown in Fig. 2(a) for the 3-m SA and Fig. 2(b) for the 10-meter SA. The either case was calculated for horizontal polarization and half-wave tuned dipole antennas used. From these figures it is concluded that ferrite tiles are very effective for reducing the ground reflection for the 3-m SA measurement. However, in the case of the 10-m SA measurements, ferrite tiles are less effective because of an oblique incidence of the waves.

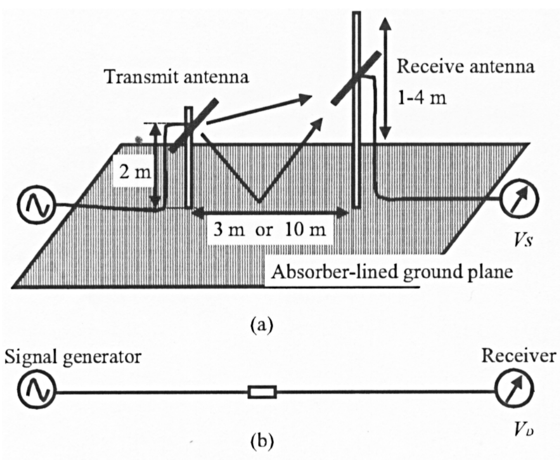

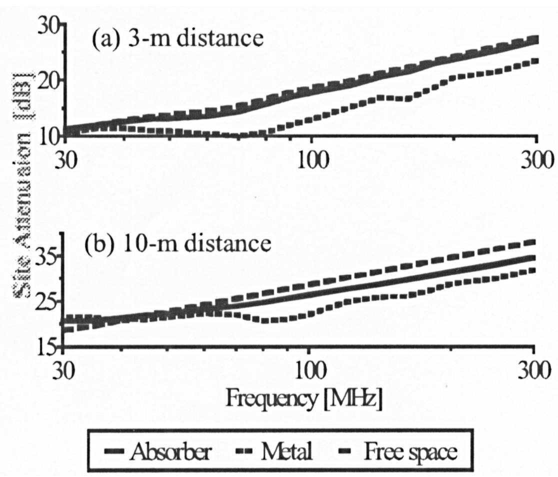

Figure 1: Site attenuation measurements. Figure 2: Site attenuation (Ferrite tiles: TOKIN TFA-10057)

REFERENCES

1. CISPR 16–1.
2. Stratton, J. A., "Electromagnetic theory," McGrawHill Book Co., 1941.

Development of Pyramidal Ferrite Absorber for Anechoic Chambers

K. Shimada, T. Hayashi, and M. Kaneko
Riken Eletech Corporation
Suehiro, Kumagaya-shi, Saitama-Ken 360-8522, Japan

M. Tokuda
Musashi Institute of Technology
Tamazutsumi, Setagaya-Ku, Tokyo 158-8557, Japan

Pyramidal ferrite absorber has been developed to reduce reflection of conventional ferrite absorbers in the frequency range above 1 GHz [1]. The pyramidal ferrite is compounded of ferrite powder and polypropylene? and it is molded into a pyramidal shape, and its height is slightly 8 cm. It is used as a hybrid absorber for anechoic chamber as shown in Fig. 1, and it is consist of pyramidal ferrite, ferrite tiles and metal reflector. This paper describes the characteristics of pyramidal ferrite and measurement NSA results for a semi anechoic chamber.

Fig. 2 shows the reflection coefficient of ferrite, pyramidal ferrite and hybrid absorber. The reflection of ferrite tends to increase as the frequency goes up from 200 MHz. The pyramidal ferrite absorbs electromagnetic wave well from 2 GHz. The hybrid absorber presents low reflection coefficient less than -20 dB from 70 MHz to 10 GHz. Further more, the reflection of pyramidal ferrite in high frequency range is reduced by containing carbon powder as shown in Fig. 3. These pyramidal absorbers are suitable in order to design superior anechoic chambers for EMC testing or antenna testing of microwave band. Because these absorbers are very tough, they are also the most suitable for walkway absorber.

The hybrid absorbers were installed on walls and ceiling of a compact semi anechoic chamber with 4.7 m width $\times$ 7.0 m Length $\times$ 3.1 m Height. Measured NSA deviation was within + 4 dB deviation from 30 MHz to 18 GHz as shown in Fig. 4 and Fig. 5.

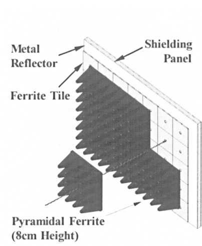

Fig. 1 Construction of Hybrid absorber for wide-band from VHF to microwave band

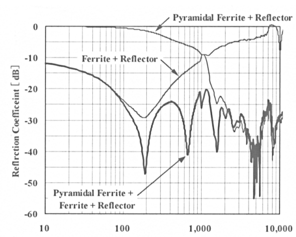

Fig. 2 Reflection Coefficient of Hybrid absorber for wide-band from VHF to microwave band

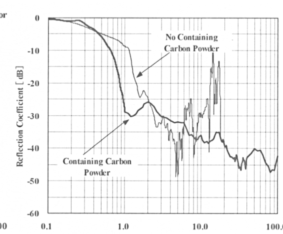

Fig. 3 Reflection Coefficient of Pyramidal Ferrite for microwave band and millimeter wave band

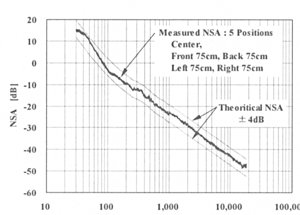

Fig. 4 Measurement NSA Results at Horizontal Polarization

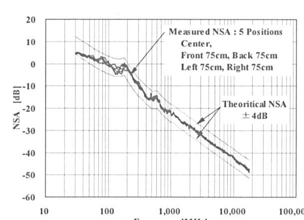

Fig. 5 Measurement NSA Results at Vertical Polarization

REFERENCES

1. Shimada, K., et al., "Fully compact anechoic chamber using pyramidal ferrite absorber for immunity testing," *IEEE EMC Symposium*, 2000.

Structural and Magnetic Properties of Zr^{4+} Substituted $\mathrm{Mg\_Zn}$ Ferrites

R. B. Pujar and B. K. Chougule
Department of Physics, Shivaji University.
Kolhapur, 461004, India

Polycrystalline ferrites with the general formula $\mathrm{Zn}_x\ \mathrm{Mg}_{1-x+y}\ \mathrm{Zr}_y\ \mathrm{Fe}_{2-2\mathrm{y}}\mathrm{O}_4$ with $x = 0.1,\ 0.2,\ 0.3,$ 0.4, 0.5, and $y = 0.01,\ 0.03,\ 0.05,\ 0.07$ were prepared by double sintering ceramic method and characterised by x-ray diffraction. The spinel ferrites are most widely used at low frequency. The lattice parameter is found to increase monotonically with Zn and Zr contents which is attributed to ionic volume differences of the cations involved. The increase in bond lengths with Zr concentration suggests the decrease in ionocovalent character of the ferrites.

IR absorption bands ν_1 and ν_2 are assigned to the fundamental vibrations of tetrahedral and octahedral and octahedral complexes respectively. The splitting of ν_2 band indicates the presence of Zr^{4+} ions on B site. The addition of Zn and Zr reduces the strong bonding between oxygen ions and metal ions leading to the decrease of force constants Ko and Kt respectively.

The increase in magnetisation with Zn up to $x = 0.3$ obeys Neel's two sub lattice model while the decrease in magnetisation for $x > 0.3$ obeys Y.K. Model. The increase in magnetisation at lower concentration of Zr is due to the increase in A_B interactions by the transfer of Mg ions from A to B site. For $Y > 0.05$, Fe^{3+} ions behave like super paramagnetics. Hence the decrease in magnetisation is observed at higher concentration of Zr. The variation of a.c. susceptibility with temperature and the small values of $\frac{Mr}{Ms}$ suggest the MD particles in the samples.

The dependence of initial permeability on Zr content obeys Globus model. The change in initial permeability is caused by the positive contribution of anisotropy constant to the total anisotropy during the conversion of Fe^{3+} ions into Fe^{2+} ions.

Investigation of the Wire Termination Metrology for Automotive EMC Simulation

B. Mazari and F. Duval
Institut de Recherche en Systèmes Electroniques Embarqués
Mont Saint Aignan, 76131, France

J.-M. Poinsignon and P. Matossian
Research Department, RENAULT Automobile
Guyancourt, 78310, France

This paper presents a new metrology, based on simulation, allowing to predict the conduced disturbance caused by the wire termination in an electrical network. These measurements are carried out in a specific frequency bandwidth. This is of particular interest for the automotive industry and its suppliers, which are forced to decrease their costs, as it reduces the number of EMC compliance tests.

In order to obtain a reliable simulation, we need an accurate measurement of the strands final load and its behavior. In an automotive electrical network, the main loads are the rotating machines, and especially the direct current electric motors. It has to be noticed that the model of this type of motor can not be applied from 10 MHz.

These equipments consist in several functions (electronic systems, coils, *etc.*), therefore, the measurement has to be adapted. We can consider two different levels of complexity in the measurements.

When the equipment represents a single terminal load, the measurement has to be carried out with a network analyzer, calibrated in the connector plane. The measurement is done directly by considering the device's stress (place of the ground plane, switching, connectors, angular position of the rotor, *etc*).

When the equipment consists in several terminal loads, a matrix solving is necessary after the measurement, in order to restitute the physical impedances of the system. These impedances are representative of the equipment's internal cross-talks and of the loads in relation to the reference plan.

As rotating machines are concerned, measurements of the impedances and of the established source generators are necessary. In main way, the mathematical equations of rotating machines can provide a first suitable approach of the source generator.

To conclude, the measurements of equipments are a main step to obtain simulation models of conducted perturbations.

Effect of Temperature and Frequency on Initial Permeability of Some Substituted $\mathrm{Mg\_Zn}$ Ferrites

R. B. Pujar and B. K. Chougule
Department of Physics, Shivaji University.
Kolhapur, 461004, India

Ferrites are iron oxide based ceramic magnetic materials which behave as ferrimagnets. High initial permeability (Mi) at low frequency is the technological requirement of ferrites. These ferrites are invariably used for low frequency inductors, transformer cores, wavefilters, oscillators, logic functions and memory devices, ultrasonics and radiofrequency electronics. Polycrystalline spinel ferrites with the chemical formula $\mathrm{Zn}_x\,\mathrm{Mg}_{1-x+y}\,\mathrm{Zr}_y\,\mathrm{Fe}_{2-2y}\mathrm{O}_4$ with $x = 0.1$ to 0.5 and $y = 0.01$ to 0.07 were prepared by a standard ceramic method. They were characterised by x-ray diffraction to confirm the formation of single phase.

The variation of Mi with temperature shows sudden drop at curie point because anisotropy decreases more rapidly than the saturation magnetisation. The presence of single peak is the evidence for the single phase formation of compound. The tailing effect is attributed to the minor phases or weak magnetic interactions. The maximum value of Mi corresponds to a point of Zero anisotropy field. The positive values of temperature coefficients indicate the increase in Mi and vice versa. The presence of pores hinders the domain wall motion and causes for the local demagnetising field which modifies the domain pattern near the grain boundaries and results in the low value of Mi.

The value of Mi varies sharply at low frequencies and attains maximum value at certain frequency. The dispersion of Mi at low frequency is caused by domain wall displacement. The absence of resonance at these frequencies is due to the absence of domain wall rotation. The absorption at highest frequency is attributed to the rotational resonance of domains under the combined effect of anisotropy and demagnetising field. The negative values of Mi beyond resonance indicate that the relaxation effect is not pronounced above such frequencies.

Session 1Aa5

Magnetic Diffusion Modeling, Surface Impedance, and Scatterer Characterization

Analysis of UXO Classification Capability With the Low Frequency EMI Sensor Responses

F. Shubitidze
Thayer School of Engineering, Dartmouth College
Hanover, NH 03755, U.S.A.

K. O'Neill
ERDC Cold Regions Research and Engineering Laboratory
Hanover, NH 03755, U.S.A.

K. Sun and K. D. Paulsen
Thayer School of Engineering, Dartmouth College
Hanover, NH 03755, U.S.A.

Clearing of buried unexploded ordinance (UXO) poses an enormous, persistent and expensive problem thought the world. Most UXO are either wholly or at least partly metallic and therefore may readily be detected. However, with current technology it is extremely difficult to distinguish UXO reliably from typically widespread pieces of metal clutter. The false alarm rate induced by clutter is extremely high and can result in the majority of remediation costs being spent on excavating innocuous items. Thus a current research goal is to isolate ways to discriminate objects of concern from surrounding metallic clutter, once an item has been detected. For this purpose we must be as interested in the scattering characteristics of diverse, arbitrary clutter shapes as in the morphological effects of the dangerous targets we are ultimately concerned about. The key to this is an understanding of the effects of various basic object features on the scattered signals our instruments record. Many clutter items have sharp edges or points, or consist of isolated sections of thin shells. By contrast, UXO typically comprise bodies of revolution, or smooth and closed shapes, which are hollow. Many if not most UXO are composite objects with distinct, relatively homogeneous sections, each consisting of different metal, e.g., head, body, tail and fins, copper banding, etc. Further, in many highly contaminated sites, multiple UXO together with widespread clutter appear simultaneously within the field of view of the sensor.

One potential methodology for target identification exploits broadband scattered electromagnetic induction (EMI) responses. EMI sensing has some distinct advantages relative to ground penetrating radar (GPR): while still range limited, the practical depth of penetration of EMI signals is typically not limited by the lossiness of conductive soils, and signal clutter due to dielectric heterogeneity is negligible. At the same time, resolution and processing approaches that are well established for GPR do not carry over to EMI surveying. In the frequency domain, EMI responses are typically characterized by two components, one in-phase with the transmitted field and another in phase quadrature with it. Different induced phenomena are associated with each of these components; in particular the quadrature component is associated with volume currents in the scatterer. These are negligible at both the lowest (near static) frequencies and at the highest EMI frequencies, where currents are concentrated essentially only on the surface. The quadrature response reaches a peak between those frequency extremes.

The main goal of this paper is to investigate the frequency dependence of the broadband EMI response by different classes of scatterer's. We will analyze sensitivities to sharpness (points, edges) and to wall thickness. Viewed conversely, will be demonstrated key scattering sensitivities, which may either be useful in or may limit object classification capability and will show what features of frequency response might effectively group different objects into separate classes.

Applicability of the TSA Approximation in Magneto-Quasistatic Scattering over the Entire Induction Frequency Band, for High Permeability Objects

K. Sun[1], K. O'Neill[2], F. Shubitidze[1], and K. D. Paulsen[1]
[1] Thayer School of Engineering, Dartmouth College, *Hanover NH 03755, U.S.A*
[2] ERDC Cold Regions Research and Engineering Laboratory, *Hanover NH, 03755, U.S.A.*

Electromagnetic induction (EMI) sensing of buried metallic objects has recently emerged as one of the most promising avenues for discriminating objects of urgent interest (e.g., unexploded ordnance) from innocuous clutter. The analysis and simulation required to understand scattering between a few Hz and 100's of kHz is complicated by the fact that "primary" or transmitted fields from outside the object typically penetrate the object, but only slightly. This penetration cannot be ignored, but also cannot easily be resolved. In approaching this numerically, we have devised the Thin Skin Approximation (TSA), initially designed to treat the higher frequency portion of EMI spectrum [K. Sun et al, IEEE TGARS, in press]. The governing equation outside the scatterer is based on the recognition that the irrotational magnetic fields in that realm may be expressed entirely via a scalar potential, ψ, such that $\mathbf{H} = -\nabla\psi$. The governing integral equation applied at points on the object surface is

$$\alpha(\mathbf{r})\psi(\mathbf{r}) + \int ds' \left[\psi(\mathbf{r}')\frac{\partial g(\mathbf{r},\mathbf{r}')}{\partial n'} - g(\mathbf{r},\mathbf{r}')\frac{\partial \psi(\mathbf{r}')}{\partial n'}\right] = \psi^{pr}(\mathbf{r}) \tag{1}$$

where the integration is over the object surface, $\partial\psi/\partial n = -H_n$, g is the static Green function, ψ^{pr} is the primary field, and $\alpha = 1/2$ on smooth portions of the surface. A similar equation with $\alpha = 1$ is applied at points outside the object to obtain the scattered field. Inside the object only the divergence relation is applied, $\nabla\cdot\mathbf{H} = 0$. On the inside of the surface, the tangential H fields and their tangential derivatives in the divergence equation may be expressed in terms of exterior tangential fields, and hence in terms of ψ. Interior H_n and its normal derivative are re-expressed via the TSA: $H_n \approx H_n(n=0)e^{i\alpha_n kn}$, where the default value of α_n is unity, and lower values of α_n are required to make the relation precise when the default relation degenerates. Given standard compatibility condi- tions at the boundary, this closes the system, so that the exterior integral equation and interior divergence relation are both expressed entirely in terms of ψ and H_n.

The startling result in numerical application of this system is that it appears to apply well to calculation of solutions not just at high frequency, but also over the entire EMI band, including steady state (magnetostatics), for high permeability materials. Analysis explains this result, and shows that it is not an artifact of the numerical tests. Using analytical magneto-quasistatic scattering solutions for the sphere and the infinite cylinder subjected to transverse excitation, we can express all terms in the system of two equations exactly, applying the TSA however where $\partial H_n/\partial n$ is required. The resulting scattered far field is proportional to $1-3/[1+(2+ika\alpha_n)/\mu_r]$ and $1-2/[1+(+ika\alpha_n)/\mu_r]$ for the sphere and cylinder, respectively, where μ_r, is relative magnetic permeability. These expressions may be examined for sensitivity to accuracy of the TSA, i.e. to the parameter α_n. At the lowest frequencies the ka term vanishes and sensitivity is negligible, as the system collapses to the static formulation. At highest frequencies sensitivity is likewise negligible as both expressions tend to unity in the PEC limit. In between sensitivity reaches a maximum. Higher values of μ_r, shift the region of maximum sensitivity virtually entirely up into the region where the TSA is accurate. For details, see "Numerical Modeling of Electromagnetic Induction ..." in http://www-nml.dartmouth.edu/geophysprg/subsurface_uxos.html

Evaluation of Approximate Analytical Solutions for Magneto-Quasistatic Scattering From both High and Low Permeability Objects

I. Shamatava[(1)]**, K. O'Neill**[(2)]**, F. Shubitidze**[(1)]**, and K. Sun**[(1)]
[(1)]Thayer School of Engineering, Dartmouth College, *Hanover NH 03755, U.S.A*
[(2)]ERDC Cold Regions Research and Engineering Laboratory, *Hanover NH, 03755, U.S.A.*

Progress in the emerging field of electromagnetic induction (EMI) remote sensing of metallic objects has been impeded by the lack of tractable analytical solutions for scattering from non-spherical objects. In recent progress, formulations are presented and evaluation problems attacked for scattering from prolate spheroidal shapes under axially oriented magnetic field excitation [Braunisch, H. et al., *IEEE TGARS*, Vol. 39, 2689–2701, 2001]. Special high frequency approximations are employed to extend the range over which solutions may be evaluated. Building on this, C. A. Ao et al. formulate solutions for scattering from both axial and transverse excitation of prolate spheroids; and for both prolate and oblate spheroids they propose approximations assuming small penetration of the object (SPA) [Ao, et al., *IEEE TGARS*, in press, and *Proc. SPIE*, Vol. 4394, 1304–1315, 2001]. The devices applied in SPA are reminiscent of impedance boundary condition formulations, assuming simplified complex exponential forms for the dependency of tangential fields on distance normally inwards from the surface. In a parallel development, recent numerical work has applied a Thin Skin Approximation (TSA) [Sun, et al., *IEEE TGARS*, in press]. The TSA assumes exponential dependency of the interior normal magnetic field components and beyond that only applies the divergence equation for magnetic field inside the scatterer. Surprisingly, analysis and numerical experience both show that, for high permeability scattering material (e.g. $\mu_r = \mu/\mu_0 \sim 100$ for steel), the TSA system produces accurate results over the entire EMI band, from a few Hz to a few 100 kHz. Using detailed numerical solutions from the Method of Auxiliary Sources (MAS) [Shubitidze, et al., *IEEE TGARS*, in press] we test here the accuracy of the SPA, as a function of frequency and μ, under variation of aspect ratio, for both prolate and oblate spheroids. While the system based on the SPA indeed performs best in the higher frequencies, it is remarkably accurate, for even slightly magnetic materials, over all but the lowest frequency portion of the EMI spectrum. Like the TSA, for $\mu_r \sim 100$ and higher it is very accurate overall.

For additional approximate solutions we also test here some new, simple formulations for finite cylinders and plates under axial excitation, i.e. transmitted magnetic field parallel to the long axes. The solutions are based on general expressions for the magnetic moment produced by the electromagnetic responses induced in the scatterer [Braunisch, H., et al., op cit.]. Here those responses are considered to be approximately the same, per unit length or area, as would appear in an infinite body of the same diameter or thickness. For cylinders with length to diameter ratios greater than unity and plates with diameter to thickness ratios greater than about 5 or 10, the approximate results compare favorably with MAS solutions for $\mu_r = 1$ (non-magnetic). More extreme aspect ratios produce better agreement. For $\mu_r > 1$ the solutions degenerate. Analysis shows that this is associated with error in the assumption that internal magnetic fields normal to the surface continue unaltered right up to the surface, in magnitudes based on the infinite case. For highly magnetic materials this would imply a jump from object interior to exterior such that secondary magnetic fields at the ends of the induced dipole would be orders of magnitude greater than the original primary field. However analysis reveals that total fields never become greater than about twice the primary field as μ increases and the fields at the objects ends "saturates".

We note that, in remote sensing practice applied to common metallic objects, the two cases of importance are: non-permeable scattering materials (aluminum, copper, brass, stainless steel), and magnetic steel with $\mu_r \sim 100$ or perhaps greater. Thus this second class of solutions for low μ cases combines with those described above for high μ scatterers, to form a broadly applicable compendium of approximate analytical solutions.

Shielding of Time-Harmonic Magnetic Fields by Permeable and Conducting Plane Screens

G. Mrozynski
Institute of Electromagnetic Theory, University of Paderborn
Paderborn, D-33098 , Germany

E. Baum
Fundamentals of Electrical Engineering, University of Applied Sciences Fulda
Fulda, D-36012 , Germany

H. Pankratz
Institute of Electromagnetic Theory, University of Paderborn
Paderborn, D-33098 , Germany

This paper deals with the shielding of the quasi-stationary magnetic field excited by a current carrying loop of arbitrary contour, position and orientation placed above a permeable and conducting plane screen. The frequency range is restricted to low frequencies so that all current elements in the loop have the same amplitude and phase.

In a first step of the analysis a magnetic dipole is considered lying in a plane parallel to the plane of the screen. The field excited by this dipole is computed from a vector potential ; to ensure zero divergence of the vector potential it is derived from a second order vector potential by applying the curl-operator. The electric field is shown to be transverse with respect to the unit normal of the plane screen.

In a second step the field of a current carrying loop is computed by integrating the contributions of all elementary dipoles lying in a special area enclosed by the contour of the loop and stretching out to infinity in one direction. For the special area chosen it is possible to carry out one integration by analytical means so that only a line integral over the contour of the loop remains.

The analysis offers the possibility to study the impact of the form of the current carrying loop on the shielding performance. Moreover the closed form solution derived in this paper can serve as a reference for comparing results obtained by numerical methods.

To verify the results the shielding efficiency for a screen shielding the low impedance field of a magnetic dipole is computed and compared with results from the well known Schelkunoff-formulas.

A Magnetic Diffusion Model for Magnetic Nondestructive Evaluation of Aircraft Skins and Naval Vessel Hulls

B. F. Phelps and W. Czura
Department of Physics, Royal Military College
Kingston, ON, Canada

W. Zhu
Tektrend International
Kingston, ON, Canada

S. Dubois
Department of Physics, Royal Military College
Kingston, ON, Canada

The magnetic vector potential equation is the standard equation describing time varying electromagnetic phenomena. At low frequencies, wave effects may be neglected, resulting in a diffusion equation. If strictly harmonic source terms are implemented, then a complex formulation becomes possible, in which the first order time derivative may be replaced with its explicit representation, reducing the problem to that of an elliptic equation in each instantaneous time frame.

A very large 3D grid is required to describe the problem geometry. The grid must be solved for each time frame. The finite difference method is easier to code and to implement than the more difficult finite element method, and the rectangular finite difference grid is also easier to generate than a triangular prism finite element mesh.

The goal is to model the output signal received in a magnetic sensor coil, when a square pulse is sent through a magnetic exciter coil, with both coils located in close proximity to the sample being studied. The square pulse is expressed in its Fourier expansion. The modeling is done for a collection of known defect configurations, such as linear cracks, and corrosion pits in aircraft aluminum materials and naval ferromagnetic materials. Comparison to finite element solutions is given. Comparison to analytical solutions is also given for simple problem geometries.

Detection of Mine-Like Objects by using Surface Impedance Concept

I. Akduman and A. Yapar
Istanbul Technical University
Istanbul, Turkey

E. Gago-Ribas
University of Valladolid
Valladolid, Spain

Impedance Boundary Conditions (IBC), which gives a relation between the electric and magnetic field vectors on a given surface in terms of a coefficient called surface impedance is one of the main tools which is used in the solution of electromagnetic scattering problems. The surface impedance is commonly used to model imperfectly conducting scatterers, perfectly conducting objects coated with a penetrable or absorbing layer or scatterers with corrugated or rough surfaces and it contains all the information about the scattering body. If the scattering object is highly conductive, the main contribution to the scattering field comes from a very thin layer just below the surface. Then, the surface impedance will characterize this layer. If this layer contains inhomogeneities, this will effect the impedance function and it will be inhomogeneous. When the surface impedance is determined, some information about the above mentioned inhomogeneities can be recovered. This property can be used to detect the inhomogeneities embedded in the earth surface. Especially, when we consider the dielectric mines, they are buried structures very close to the earth surface. In such a case, if one illuminates the region of the earth surface where the mines are buried, and collects the scattering data through the measurements performed by an equipment flying in the air, a small aircraft for example, the surface impedance of the region of interest can be obtained. Then by observing the anomalies in the impedance function one can detect and locate the mines. To the best our knowledge there is no available publication in the open literature using surface impedance concept described above.

The main objective of this paper is to give a new method for the detection of mine-like objects, which is based on the determination of the surface impedance of the area where the objects are located. The boundary condition considered here is the Standard Impedance Boundary Condition (SIBC). For the sake of simplicity, we will consider only cylindrical bodies buried in a half-space which are located as parallel to each other. Similar analysis can be carried out easily for the three-dimensional bodies. The surface impedance of the half-space where the bodies are located is obtained directly from the SIBC, which requires to know the field and its derivative at the interface. To obtain these values, the half space containing the bodies is illuminated by a time harmonic plane wave from the other half-space, and the scattered field is measured on a certain line in the same region. Then the analytical continuation of the measured data to the interface yields to get the required field expressions. The method is tested by considering illustrative examples. It has been observed that it yields very accurate results.

Session 1Ab5

Sub-Surface Remote Sensing

Statistical Signal Processing for Subsurface Object Detection and Identification Using the NIITEK Ground Penetrating Radar

L. Collins and Q. Zhu
Department of Electrical and Computer Engineering, Duke University
Durham, NC 27708-0291, U.S.A.

S. Frasier and F. Clodfelter
NIITEK, Inc.
Fairfax, VA 22031, U.S.A.

Ground penetrating radar has been proposed as an alternative sensor to classical electromagnetic induction techniques for the problem of subsurface object detection. Like metal detectors, however, a persistent problem associated with traditional ground penetrating radar sensors involves not just detection of dielectric discontinuities, but the discrimination of objects of interest from clutter. In most fielded sensors, the processing that is performed essentially consists of anomaly detection, and this often leads to excessively large false alarm rates. When each subsurface anomaly must be excavated in order to determine whether it is a target of interest, significant costs are incurred both due to lost time, and costs associated with digging. The false alarm problem is particularly pernicious in real world landmine detection scenarios.

Bayesian signal detection theory prescribes a method for optimally processing signals for detection and identification in an uncertain or random environment. When applied correctly, this approach guarantees optimal performance in the sense of minimum probability of error, or a maximum detection/identification rate for a given false-alarm rate. Uncertainties in the response of a target, or uncertainties in the response that result from a non-deterministic environment, can be incorporated into the processing strategy in the form of *a priori* density functions. Signal detection theory also affords quantitative performance-evaluation measures in the form of a functional relationship between probability of detection (P_d) and probability of false alarm (P_{fa}) termed the receiver operating characteristic (ROC). In the case where probability density functions are not known a priori, or phenomenological models cannot be employed to determine target signatures, other statistically-based techniques have been employed to effect discrimination using ground penetrating radar data. Fuzzy logic, hidden markov models, and principal components analysis have all proven useful. However, these techniques have relied upon human expertise to determine appropriate features. We propose to implement an alternative algorithm that automatically extracts pertinent features and then utilizes these features within a Bayesian construct.

Independent Components Analysis (ICA) has been proposed as a viable solution for the problem of blind source separation. The blind source separation problem consists of recovering unobservable signals, or sources, from several observed mixtures. The adjective “blind” is used to emphasize the fact both the source signals and the mixing properties are unobservable. This approach has achieved success in several application areas, and as an alternative to principal components analysis and other linear methods such as factor analysis and projection pursuit. It is applicable to data from high fidelity ground penetrating radars since the measured signal at a particular object/sensor orientation consists of a mixture of reflections from various surfaces of the subsurface object, and the relative weights of these reflections changes as a function of target/sensor orientation, or equivalently sensor position. Multi-position data can be processed by ICA to extract the functional forms of the individual reflections. In the context of this research, we utilize ICA to extract the features associated with a particular object, and then utilize a Bayesian approach to discriminate targets of interest from clutter using the extracted features.

Electromagnetic Response of a Buried Conducting Mine to a Generalised Gaussian Pulse

S. F. Mahmoud and M. G. Hussain
Electrical Engineering Department, Kuwait University
Safat, Kuwait

Recently, the Ground Penetrating Radar (GPR) technique using wideband frequency spectrum received attention as means of detecting buried targets such as mines. A relevant problem in this respect is the scattering of electromagnetic waves from a finitely conducting circular disc buried in a homogeneous earth. We present a full wave analytical solution to this problem in both frequency and tim domains. The main feature of the solution is the expansion of the induced currents on the disc in terms of a complete set of orthogonal vector functions over the area of the disc. The frequency response of the scattered fields associated with a given current eigenfunction is obtained as a single integration over the radial spectral wavenumber. For a given exciting field, application of the boundary condition at the discs surface leads to a set of linear equations for the unknown coefficients of the current expansion. The eigencurrents is chosen to have the form:

$$\vec{j}^{a}_{np}(r,\phi) = \frac{n}{k_p r} J_n(k_p r) \sin n\phi \, \hat{r} + J'_n(k_p r) \cos n\phi \, \hat{\phi} \tag{1}$$

$$\vec{j}^{b}_{np}(r,\phi) = J'_n(k_p r) \sin n\phi \, \hat{r} + \frac{n}{k_p r} J_n(k_p r) \cos n\phi \, \hat{\phi} \tag{2}$$

where $J_n()$ is the Bessel function of order n and the prime denotes differentiation with respect to the argument, k_ρ, and $p = 1, 2, \ldots$ identifies the radial behavior of the vector function and is chosen such that $J_n(k_p a) = 0$ for type (a) functions and $J'_n(k_p a) = 0$ for type (b) functions. Note that this ensures the vanishing of the radial current component at the disc's edge $r = a$ for every eigenfunction of type *(a) or (b)*. The total induced current on the disc is then expressed as a linear sum over the modal currents in (1)–(2) with coefficients to be determined from the boundary condition at the discs surface. The radiated fields in the air region are then determined in simple forms in the frequency domain. The advantage of the adopted current distribution over the disc is that only few terms of the current series are needed to accurately represent the current as the numerical examples indicate [1].

In the time domain, the generalized Gaussian pulse, introduced in [2], is taken as a source of excitation to the disc. The advantage of the generalized Gaussian pulse is that its frequency spectral width can be controlled through a single parameter, that it is free of a D.C. component, and is mathematically easy to manipulate. Two approaches are used to derive the time domain response to the generalized Gaussian pulse. The first is the convential inverse FFT of the frequency response. The second is the estimation of the amplitude and phase of the frequency response as a truncated power series of frequency. This leads to the derivation of the time response as a sum of closed form terms.

REFERENCES

1. Samir F. Mahmoud "Full wave analysis of electromagnetic wave scattering from an imperfectly conducting disc", *Journal of Electromagnetic Wave applications*, Vol 15, July 2001.
2. Malek G. Hussain, "Principles of space-time array processing for Ultra-Wideband impulse radar and radio communications", *IEEE Trans. On Vehicular Technology*, May 2002.

Inversion of Stratified Inhomogeneous Layers

E. A. Hashish
Electronics and Communications Department, Faculty of Engineering, Cairo University
Giza, Egypt

M. A. Karam
Northrop Grumman Corporation, Electronic Systems
Azusa, CA 91702, U.S.A.

The problem of subsurface probing of homogeneous stratified dielectric media has been widely considered by many authors. Such a subsurface probing is usually performed through the inversion of scattered wave data due to the incidence of either a plane wave or a spherical wave excited by a point source on the top of the media.

The scattered wave data may be measured with the variation of frequency, time, distance or angles of incidence. The Fast Fourier Transform FFT inversion algorithms are among different algorithms that have been employed for the data inversion.

Recently, a FFT inversion algorithm for discrete layered models has been introduced using either the impedance or reflection data due to the incidence of a plane wave on homogenuous stratified media [1]. This algorithm has proved to be quite accurate even in the case of band limited data.

In this study, the above FFT inversion algorithm is extrended to an inhomogeneous multilayered model satisfying the WKB condition for each layer. A uniform plane wave is obliquely incident on the top surface of the model and the reflection coefficient is sampled over a finite frequency band. The spectrum of these data is then obtained using the FFT inversion algorithm. Furthermore, with the aid of the algorithm, the height and the permittivity profile of each layer are obtained. The results of an example for inverting a three layer model are presented.

REFERENCES

1. E. A. Hashish, "Improved FFT Inversion Method for Discrete Multi-layer Dielectric models", Electromagnetic Waves and Applications, vol. 11, 1997, pp 161-173.

The Steepest Descent Fast Multipole Method for Clutter Statistics in Minefields Using Monte Carlo Simulations

M. El-Shenawee
Department of Electrical Engineering, University of Arkansas
Fayetteville, Arkansas 72701, U.S.A.

C. Rappaport
Department of Electrical and Computer Engineering, Northeastern University
Boston, Massachusetts 02115, U.S.A.

A rigorous electromagnetic model has been developed to analyze the scattering mechanism of a target buried near a clutter-object under the two-dimensional random rough ground (3-D scattering problem). In realistic landmine fields, the anti-personnel (AP) nonmetallic mine is often buried nearby a rock, tree root, etc. The presence of a second object buried near the nonmetallic mine can easily obscure the target and/or cause a false alarm during the detection process.

The rigorous model is based on the classical electromagnetic equivalence theorem leading to producing six new integral equations. Using the Method of Moment (MoM), the new integral equations are transformed into a linear system of equations to be solved for the unknown electric and magnetic currents on the surface of three scatterers; rough ground, target and clutter-object. The MoM impedance matrix completely represents every interaction between these three scatterers. The Steepest Descent Fast Multipole Method (SDFMM) is used to tremendously accelerate the computations of the unknown MoM surface currents.

In previous work, we thoroughly investigated the effect of ground roughness on the signature of the target when it is buried alone under the ground. In this work, we will present numerical results for parametric investigations of the objects proximity, orientations, materials, and shapes. The results show that in certain situations, the target can be completely obscured due to the presence of the nearby clutter-object (e.g., tree root). In other cases a false indication of presence of a third buried object is observed. When the sources of clutter (e.g. the rough ground and the clutter object) are removed, by subtracting the return from both the rough ground and the clutter-object, the signature of the target can be clearly observed and analyzed. The numerical results show that the ground roughness along with the separation distance, between the target and the clutter-object, play a significant role on the probability of true or false alarm in the detection process.

The Potential of Passive Sensors in Monitoring Buried Temperature Anomalies

M. A. Karam and A. Shrekenhamer
Northrop Grumman Corporation Electronic Systems
Azusa, CA 91702, U.S.A.

Buried temperature anomalies are present in different forms in nature. They may be tumors in human bodies or permafrost or geothermal source beneath soil, or electric utilities within a wall or within a road, etc. In this study a mathematical evaluation of the potential of passive sensors (microwave, millimeter wave, and thermal infrared) for monitoring buried temperature anomalies is presented. The anomalies are considered as a buried layer within a stratified medium. For thermal infrared sensors the solution of the classical heat conduction equation in stratified media is used. For microwave and millimeter wave sensors the solution of heat conduction equation is combined with a coherent brightness temperature formulation based on the fluctuation dissipation theorem. The solution of the classical heat conduction equation is based on the thermal wave characteristics of heat conduction. Those characteristics are considered in two transform domains: Laplace transform domain to account for initial temperature conditions, and Fourier transform domain to facilitate numerical calculations in the quasi-steady solution of heat conduction equation. Numerical simulations are performed to investigate characteristics of anomalies monitored by each sensor, i.e. location of the anomalies, and their properties in contrast with the properties of the surrounding media.

Session 1Aa6

Antenna Arrays

Analysis of Microstrip Antenna Arrays Using Floquet's Harmonics

M. Wnuk, W. Kołosowski, M. Amanowicz and R. Dufrène
Military University of Technology, Electronics Faculty
Warsaw, Poland

Microstrip antennas have been one of the most innovative areas of antenna technology for a dozen of years now. It is an area combining field and circuit problems, requiring the application of highly complex analytical methods. But individual radiating elements made with the use of this technology have a rather narrow frequency band (in the range of a few percent) as well as large transverse radiation patterns. These disadvantages can be eliminated through the use of periodic systems – antenna arrays and multilayer structures. Such a construction makes it possible to achieve required parameters and antenna array patterns.

A spectral response of a periodic antenna array on a homogenous dielectric medium depends on the geometry of a single radiating element, the medium parameters, polarization and geometry of the exiting field. By changing the size and shape of the individual elements of the antenna we can effectively modify its spectral characteristics. During analyses we have to take into account that each antenna array has limited dimensions. But if we focus on analysing centrally situated cells of the periodic antenna structure, we can shown such values $2M + 1$ and $2N + 1$, above which the field generated by these centrally situated elements will cease to change. So can assume that in areas from the distance the array edge the antenna array has unlimited dimensions and that the number of single elements of the array i.e. cells of the periodic antenna structure is unlimited. In this case the two-dimensional antenna array can be treated as a periodic structure, which makes the application of many well-known analytical methods possible. Another condition, along with that of an unlimited number of antenna elements, which is indispensable to obtain results suitable for a direct analytical interpretation, is to assume a homogenous (linear) phase correlation of individual antenna elements excitations. When the condition of antenna periodicity and its excitation with a linear, homogenous phase modulation is satisfied, the problem of EM field scattering on such a structure can be reduced to analysing a single, basic antenna cell, usually in a spectral space containing a whole system of corresponding Floquet's harmonics. In case of structures with smaller dimensions and a smaller number of elements, effects connected with these limitations, especially edge effects occurring on external cells, can influence the radiation patterns of antennas and should be taken into account. Therefore, the authors have proposed to consider limited dimensions of the antenna array through the application of "windows function" imposed on the sought currents distribution. In this case we can use the results obtained from analisys of infinite periodic structure. The problem was analysed with the use of the spectral modification of the Galerkin method, with an eye to EM field distribution on harmonic Floquet's using vectors distribution on basis functions. We educed generalised dispersion and transmission matrixes for individual planar elements of the antenna, and eventually obtained a generalised dispersion matrix for the entire antenna structure by combining the particular transmission matrixes. Through solving a system of algebraic equations, this function makes it possible to analyse antenna arrays with any shift of phase between the particular antenna elements as well as with any amplitude of the field exiting the elements. The method that is proposed here also makes it possible to analyse antenna arrays with variable dimensions of the elementary cell. According to the authors knowledge, the procedure of EM field scattering on the antenna arrays presented here is an original solution. Calculations were made and compared with the results of measurements of an antenna array model. A high conformity of results was achieved.

A Simple Technique for the Analysis of Large Finite Aperture-Coupled Printed Arrays

J. A. Zornoza and J. A. Encinar
Polytechnic University of Madrid
Madrid, Spain

The analysis of finite arrays can be accomplished from two completely different approaches, either by computing element-by-element couplings, or by applying convolution techniques to the results of the infinite array. Meanwhile the first one gives an exact solution, the second only finds an approximation. However, the last one is very suitable for arrays with a large number of elements, since the element-by-element approach needs a huge amount of computation not available by actual computers.

In this work, an efficient and simple technique based on that proposed in [1] is applied to the analysis of finite aperture-coupled printed arrays. The proposed technique, which can be applied to multi-layer arrays with arbitrarily shaped patches, allows the computation of the active input impedance for all the array elements at once.

The active input impedance of a single element in the infinite array environment must be computed in the whole u-v domain, i.e. for all possible scanning angles and beyond, but the domain is reduced to a small region due to symmetry and periodicity properties exhibited by the infinite array impedance. In this first step, the infinite array analysis is carried out by a modular technique based on the Spectral Domain Method of Moments [2]. Next, a proper convolution technique [1] over the infinite array impedance computed before, gives the active input impedances of the elements belonging to the finite array. Through the Fourier Transform and an appropriate truncation, the computation of the final integral expression is simplified and all the element impedances are obtained at the same time for a beam radiated in a given direction, in a smart and fast way. Thus, the method presented allows a rapid approximated evaluation of the active input impedance for large phased arrays, including stacked configurations.

A one-layer 16x16 array of squared patches uniformly fed has been analyzed. The results show ripple behavior on the active impedance, which increases with the element proximity to the edge of the array, as it could be expected. Some examples will be discussed at the oral presentation.

REFERENCES

1. A. Ishimaru, R. J. Coe, G. E. Miller and W. P. Geren, "Finite Periodic Structure Approach to Large Scanning Problems," *IEEE Trans. on Anten. and Propag.*, AP-33, No. 11, pp. 1213–20, Nov. 1985.
2. P. Gay-Balmaz, J. A. Encinar and J. R. Mosig, "Analysis of Multilayer Printed Arrays by a Modular Approach Based on the Generalized Scattering Matrix," *IEEE Trans. on Antennas and Propag.*, Vol. 48, pp. 26–34, Jan. 2000.

Scattering Properties of Fractal Reflectarray

S. Erdem and B. Saka
Hacettepe University
Ankara, Turkey

The multiband system antennas are very important for communication systems such as frequency hoping schemes in radar and spread spectrum techniques in some communication systems. Fractal reflectarray is multiband array antenna, which combines the some of the best features of the array, reflector and fractal antennas.

A reflectarray consists of a flat array of microstrip patches or dipoles printed on a thin dielectric substrate. A feed antenna illuminates the array whose individual elements are designed to scatter the incident field with the proper phase required to form a planar phase surface in front of the aperture. This operation is similar in concept to a parabolic reflector that naturally forms a planar phase front when a feed is placed at its focus, thus, the form flat reflector is sometimes used to describe the reflectarray.

Fractals are usually self-similar structures, which means that several copies of the main shape are found at several scales within the fractal body. This property can be used to design multifrequency antennas and arrays as it was first suggested by Puente et al. Research in this area has recently yielded a rich class of new designs for antenna elements as well as arrays.

In this study, we introduce the fractal reflectarray antenna based on Sierpinski Carpet in order to combine the best features of the reflector, array and fractal antennas. The geometry under study consists of a Sierpinski carpet fractal array of microstrip patches on a thin dielectric substrate.

The overall design procedure for fractal reflectarray procedures are as follows:

1) The back scattering properties of the squared shaped patches are calculated for a given incident angle using MOM-Galerkin's techniques with subdomain rooftop basis functions. The resonant frequencies of the patches are determined with aid of the back-scattered fields.

2) The back-scattered field pattern of the fractal reflectarray is calculated using array theory.

The back scattering field patterns of the fractal reflectarray are calculated in the range of 5 GHz to 50 GHz. We determined 15 resonant frequencies and calculated the scattering patterns at the resonant frequencies in the specified frequency range.

Estimation of Signal Correlation in Antenna Arrays

I. Salonen and P. Vainikainen
Smart Antenna Development for Mobile Communications
Helsinki University of Technology
Espoo, Finland

The correlation between received signals is a basic parameter for the use of an antenna array or an antenna pair in diversity systems. In many systems the signal can arrive from different directions. It is shown in this paper that in the case of uniform distribution of the angle of arrival the correlation matrix between element ports responses can be simply calculated from the scattering matrix measured by e.g. a vector network analyzer. The result is equal to that obtained from array element pattern measurements, which is shown by a formula based on the law of the conservation of energy. The correlation calculated in this manner defines the minimum correlation level that can be reached with an antenna pair or with a dual-polarized antenna. Naturally this level decreases with increasing element spacing.

We have shown with microstrip array prototypes that the correlation matrices calculated using scattering matrices or element patterns agree well, which indicates that the idea of using scattering matrices for the correlation calculations in the case of many sources in a horizontal plane is useful. Further we demonstrate, how the equality of the correlations calculated using scattering matrix or element patterns allows to estimate the signal envelope correlation dependency on the absolute value $|S_{ij}|$ of the scattering parameter between an antenna pair. The mutual coupling coefficient $|S_{ij}|$ is very easy to measure and gives thus a simple method to estimate the correlation between in an antenna pair.

The envelope correlation level of about 0.7 is usually defined as a practical limit to obtain significant diversity gain with signal combining. For this limit we have estimated the dependency of the allowed levels for the scattering parameter $|S_{ij}|$ from the angular spread of incoming signals.

The uncorrelated noise in array ports is usually an assumption for signal processing algorithms. The noise correlation decreases the system performance. In future systems the role of different interferers and other noise sources is increasing and the model of signal arriving from all directions with different delays can be used as well for the estimation of antenna noise correlation.

Model-Based Beam Pattern Analysis of a Particular Structure Circular Array

H. H. Chang
Chinese Military Academy
Kaohsiung, Taiwan

S. S. Bor, C. L. Wang, Y. X. Zeng, and K. P. Chen
Feng-Chia University
Taichung, Taiwan

L. P. Chi
Chung-Shan Institute of Science and Technology
Tao-Yuang, Taiwan

We joined a project to design proto-type smart antenna system which the antenna array developed by this joint project is an 18-element circular array. All array elements of this circular array are folded-dipole antenna attached on the surface of a centered conducting cylinder. The analysis of beam pattern of this particular structure circular array is difficult theoretically because the existence of this centered conducting cylinder may cause image effect as well as the array element pattern is not isotropic and there can also be mutual coupling among array elements etc. In this paper we use a model-based approach to deal with this problem, which we may encounter known and unknown two types of parameters on modeling this array. The known parameters can be derived based on known array geometry which we assume all array element patterns are isotropic, and the unknown parameters will be used to take into account the overall effects caused from the existence of conducting cylinder, the element pattern and mutual coupling, etc. In this paper the unknown parameters are estimated and evaluated from measurement data collected from indoor chamber.

The contents of this paper have three major parts described in the following:

(1). The modeling and derivation of the steering vector associated this circular array.
The steering vector $\mathbf{a}(\theta)$ associated with $\mathrm{AOA} = \theta$ is modeled and defined as follows:

$$\mathbf{a}(\theta) = [a_1\gamma_1 e^{j\psi_1}\ a_2\gamma_2 e^{j\psi_2}\ \cdots a_{18}\gamma_{18} e^{j\psi_{18}}]^T = \mathbf{A}(\theta)\mathbf{a}_o(\theta)$$

In this equation we define a steering vector, $\mathbf{a}_o(\theta) = [a_1\ a_2 \cdots a_{18}]^T$, based on the ideal conditions when all array element patterns are isotropic, where $a_i = e^{j2\pi(R/\lambda)\cos(\theta-\alpha_i)}$ and R is radius, λ the wavelength and the angel between element i and the reference direction. $\mathbf{A}(\theta)$ is a diagonal matrix containing the unknown parameter $\gamma_i e^{j\psi_i}$ which is the narrowband channel response of element i caused by a combination of all factors such as pattern of array element, mutual coupling effect, the existence of cylindrical metal shell, etc.

(2). The analysis of LCMV-based adaptive beam pattern of this array.
The LCMV (linear constraint minimum variance) algorithm is widely used for both narrowband and wideband beamforming and thus is applied upon this circular array for adaptive beam pattern analysis and comparison.

(3). The comparison of computer simulation results.
Array pattern examples are presented to evaluate and compare the proposed model-based approach of beam pattern analysis. Both the LCMV-based and quiescent beam examples show that the beam pattern will be greatly distorted if these unknown antenna parameters are ignored. We have reasons to believe that there could be errors on the estimation of these unknown parameters, thus we demonstrate also many examples how will array patterns be effected under different degrees of errors.

Scattering of a Large Planar Dipole Array Paralleled to a Finite Imperfectly Conducting Plane

Z. Li
Chongqing Three Gorge College
Chongqing, 404000, P. R. China

Scattering of an electromagnetic plane wave by a finite circular or square disk or a circular hole in a conducting plate is a classical problem and has been studied using various methods for many years. But the analysis of scattering of an incident electromagnetic waves induced by a large planar dipole array over or closed to a finite imperfectly conducting plate seems not available so far due to the complicated diffraction and scattering mechanism. In this paper, a hybrid technique is applied to solve this kind of problem.

The analysis of scattering of a large planar array parallel to a finite imperfectly conducting plate is presented by a hybrid technique combing the moment method and uniform physical theory of diffraction, the former is used to obtain the current distributions of the array while the latter to get the field scattered by a finite imperfectly conducting plate.

This study can be extended to handle the scattering of any array near a finite opaque scatterer by introducing the modification to the induced source and the field equivalence theorem.

Session 1Ab6

Antenna Technology

Dielectric Resonator Antennas Mounted on a Slotted Ground Plane for Circular Polarization

C.-Y. Huang
Department of Physics, National Kaohsiung Normal University
Kaohsung, Taiwan 802, Republic of China

Circularly polarized dielectric resonator antennas with a slotted ground plane are proposed. By embedding suitable slots in the finite ground plane of a feed substrate, the excited surface currents on the ground plane and radiating patch can be strongly meandered. The proposed antennas with two pairs of narrow slots in the ground plane for achieving compact or circularly polarized radiation have also been successfully implemented. Detail of the proposed designs and experimental results of the constructed prototypes are presented.

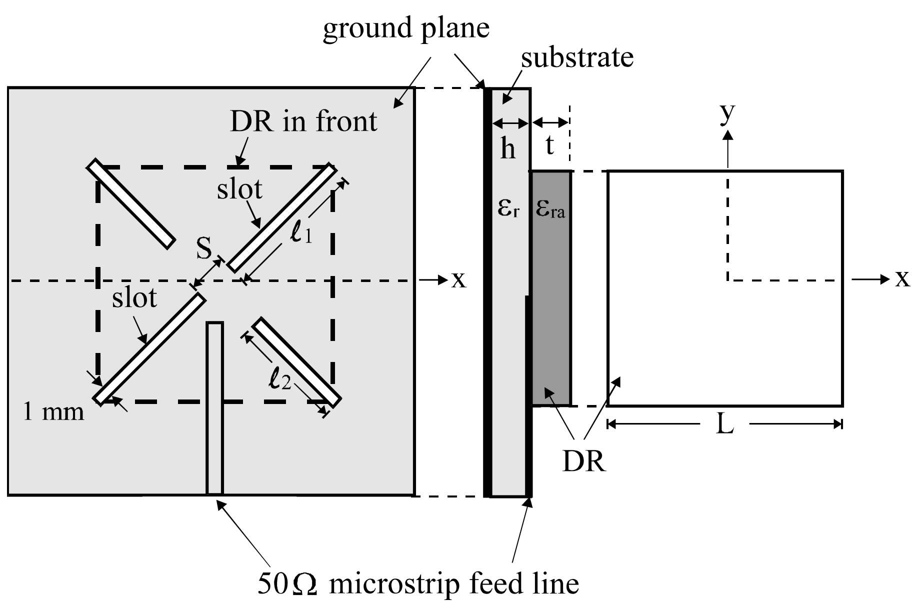

Rigorous Analysis of Dielectric Horns With A Mixed Integral Equation-Mode Matching Method

N. Fognani
University of Florence, Electrical Eng. Dept.
Florence, Italy

G. G. Gentili
IET (CNR), Politecnico di Milano, Dip. Elettronica e Inf.
Milano, Italy

R. Nesti
CAISMI (CNR)
Florence, Italy

G. Pelosi
University of Florence, Electrical Eng. Dept.
Florence, Italy

Horns partially loaded with dielectrics are a practical solution to feed antenna realization, since their radiation characteristics are similar to those of corrugated horns and their fabrication is considerably simpler, especially at millimeter wavelength. Circular dielectric loaded horns support "local" hybrid modes, the dominant being HE_{11}. The varying cross section excite the full set of HE_{1n} and EH_{1n} modes, all having the same azimuthal variation. The concept of "local modes" has been exploited to analyze the structure by a mixed mode-matching, integral equation approach. In particular mode-matching has been used to model the internal horn geometry and up to the terminal section. With respect to previous works on the mode-matching analysis of dielectric loaded horn, the improvement implemented in this work is an automatic algorithm for the computation of the local mode spectrum including complex modes. The algorithm is based on a 1D FEM analysis along the radial variable and its main advantage is a quick computation of the mode spectrum without the need of iterative searches in the complex plane. Since the appearance of complex modes is rather difficult to predict, the advantage of the method described is the possibility to optimize the structure without worrying about the existence of complex modes. The external part of the horn is modelled by an integral equation approach (IE) based on a combined electric field equation and magnetic field equation. By the IE we can model the external shape of the boundary and the terminal section and couple it to the model of the internal part to obtain a rigorous full wave simulation of the horn including the exact external horn geometry. This is also an improvement with respect to several methods available in the literature.

The availability of a rigorous full-wave simulation open the way to an optimization of the whole structure, including dielectric filling shape, metalization geometry and external profile.

Low Profile, Low-Cost, High Efficiency Microstrip Planar Antenna for Single and Dual Polarized Operations

S. Raut, A. Petosa, and M. Cuhaci
Communications Research Centre Canada
Ottawa, ON P. O. Box 11490, Canada

The design of a low profile microstrip planar array antenna is considered. The main goal of the design is to obtain a high efficiency antenna that can be achieved with minimum manufacturing costs. The chosen operating band is 5.7 GHz - 5.85 GHz, which is the unlicensed band for terrestrial wireless application.

To achieve a high efficiency antenna, it is necessary to minimize the losses associated with the radiating structure. In most printed antenna arrays the feed lines are the primary source of losses. As the array size becomes larger, the line losses increase accordingly and provide a low overall antenna efficiency. A method to lower the line lengths, which is related to total line losses, is presented in this paper. This design incorporates a phase rotation technique within the corporate feed method to reduce line lengths. Less expensive substrate materials were considered to keep the manufacturing cost to a minimum. Furthermore, the design of the antenna emphasizes structure simplicity to limit manufacturing steps. However, a compromise between the substrate cost and loss performance of the substrate material is needed to properly balance the economical and practical aspects of the design.

The present design for the single polarization case implements a single substrate that can accommodate the desired frequency band. A 8x8 size array is considered and designed on an Arlon 25 FR and Rogers R4003 60 mils material. The aperture size for the array is about 29.3 cm $\times$ 29.3 cm for both substrate cases. For the centre frequency of 5.775 GHz, the array provides a gain 23.8 dBi (Efficiency : 60%) on Rogers 4003 and about 23.0 dBi (Efficiency: 51%) on Arlon 25 FR. Dual polarized array is being designed by implementing a two-layer structure.

Analysis on Excitation of Magnetostatic Surface Waves In an In-plane Magnetized YIG by The Integral Kernel Expansion Method

Y. Ando and M. Hayakawa
The University of Electro-Communications, Department of Electronic Engineering
Tokyo, Japan

Magnetostatic waves (MSWs) have possibilities of the application to signal processing in microwave bands. From practical point of view, we need to establish the analysis to characterize excitation of magnetostatic surface waves (MSSWs) in an in-plane magnetized ytttium-iron-gannet (YIG) for efficient design of MSSW devices. The purpose of this paper is to analyze the excitation within reasonable accuracy. In the present problem, the current density distribution over a metal strip which determines the excitation of the mode, can be used to formulate an integral equation, and then, we solve the equation by using the integral kernel expansion method.

Consider a microstrip line with an YIG substrate, as shown in Fig. 1, where a bias magnetic field is applied in the direction making an angle θ with the z-axis. Under the quasi-static approximation, the current density flowing in the metal strip, $J_z(y)$, can be formulated as an integral equation as follows: $\int_{-\infty}^{\infty} G(k)\tilde{J}_z(k)e^{-jky}dk = 0$ with $-w \leq y \leq w$ where $G(k)$ can be written in terms of the saturation magnetization of YIG, the applied magnetic field, and the gyromagnetic ratio. We can solve this equation by using the integral kernel expansion method. The integral kernel, e^{-jky} and the unknown current density, $\tilde{J}_z(k)$ are expanded as follows: $e^{-jky} = \sum_{m=0}^{\infty}(-j)^m(2m+1)j_m(kw)P_m\left(\frac{y}{w}\right)$; $\tilde{J}_z(k) = \frac{w}{2}\sum_{n=0}^{\infty} a_n j^n J_n(kw)$ where $P_m(z), j_m(z)$ and $J_n(z)$ are the Legendre polynomial, the spherical Bessel function, and the cylindrical Bessel function. The a_n's are unknown coefficients to be determined. After substituting the basis function expansion into the integral equation, we can truncate the infinite expansion by a finite number of terms to calculate the unknown coefficients, a_n, so that we obtain an approximate solution for $\tilde{J}_z(k)$.

Figures 2 and 3 show the numerical results of the insertion loss of the microstrip transducer and the corresponding experimental results for the case of $\theta = 0°$ and $30°$, respectively. The solid lines indicate the numerical results by the present method. The numerical results by the conventional method which assumes that the current density is of constant magnitude over the metal strip, are given by the dotted line for comparison. In order to verify the validity of the present method, we plotted the experimental results. As you can see, the present method shows excellent agreement with the experiment, on the other hand the conventional method has significant discrepancy for both cases.

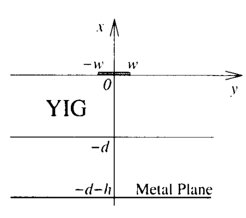

Fig. 1 Configuration for analysis.

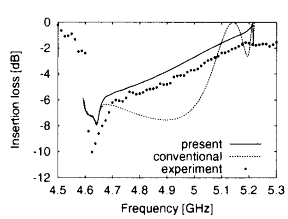

Fig. 2 Comparison of the numerical results by the present and the conventional methods with the experiment in the case of $\theta = 0°$.

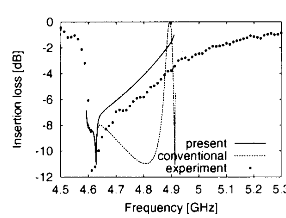

Fig. 3 Same as Fig. 2, but in the case of $\theta = 30°$.

Session 1Ac8

Wavelets/Multiwavelets with Applications

Solving Nonlinear Semiconductor Equations by Using Multiwavelet

G. Pan and K. Wang
Dept of electrical engineering, Arizona State University
Tempe, AZ 85287, U.S.A.

B. Gilbert
Mayo Foundation
Rochester, MN 55905, U.S.A.

The computer simulation of semiconductor devices invloves highly nonlinear equations such as Boltzmann transport equation, hydrodynamic equation, and drift-diffusion equation. Due to the mixed elliptic/parabolic/hyperbolic nature of those partial-differential equstions, conventional FEM and FD schemes always result in oscillatory and thus fail when the cell Reynolds number of the system is large. Based on the drift- diffusion model, several schemes have been proposed, namely, the Gummel scheme, Petrov-Galerkin method and upwind scheme. The Gummel scheme is the most successful one yet suffers the so-called crosswinding effect and lacks the ability of extension to higher order. Futhermore, it is imposible to be incorporated into the Boltzmann transport equation. Petrov-Galerkin method, on the other hand, is more like an empirical scheme without the mathematic background; the relative weight of its symmetric and antisymmetric bases is not easy to be determind. Upwind scheme is probably the most adaptive one among those three. However, its numerical error is also the largest.

A new approach of multiwavelet based finite element method(MWFEM) to solve the semicondutor drift-diffusion system is presented here, which has already been shown efficient to solve electromagnetic problems. In this approach, the multiscalets (multiscaling functions) are employed as the basis functions. Because of the interpolator property of the multiscalets in terms of the basis function and its derivatives, fast convergence in approximating a function is achieved. The new basis functions are $\in C^1$, i.e., the first derviatives are continuous on the connecting nodes. The multiscalets, along with their derivatives, are orthonormal in the discrete sampling nodes. Therefore no coupled system of equations in terms of the function and its derivative is involved, resulting in a simple and efficient algorithm. Due to its ability of tracking the tendency, namely, the first derivative of the unknown function, MWFEM shares the versatile of the conventional FEM while keeps stable in a highly nolinear system. Comparison among Gummel scheme, upwind FEM, conventional FEM and MWFEM shows the MWFEM performs excellently under both small and large cell Reynolds number conditions. A complete 1D drift-diffusion solver base on WMFEM was implemented. Numerical results demonstrated high efficiency and accuracy of the new method.

On Sampling-Biorthogonal Time-Domain Scheme Based on Daubechies Wavelets

S. Ogurtsov
Dept. of Electrical Engineering, Arizona State University
Tempe, AZ 85287, U.S.A.

Y. V. Tretiakov
IBM Microelectronics
Burlington, VT 05452, U.S.A.

G. Pan
Dept. of Electrical Engineering, Arizona State University
Tempe, AZ 85287, U.S.A.

The positive sampling function and its biorthogonal dual were proposed by G. Walter, a pioneering mathematician. In this presentation, we provide a rigorous analysis of the multiresolution time domain (MRTD) technique, employing the positive sampling functions and their biorthogonal dual. We call our approach the sampling biorthogonal time-domain (SBTD) technique. The introduced sampling and dual functions are both originated from Daubechies scaling functions of order 2 (referred to as D_2), and form a biorthonormal system. This biorthonormal system has exact interpolation properties that simplify the treatment of excitation sources, boundary conditions and circuit parameter extraction of the scattering matrix, currents, etc.

In the talk, we present the SBTD treatment of the dielectric interface and absorbing boundary conditions. We estimate the finite-difference space approximation and numerical dispersion for the SBTD in comparison with Yee's FDTD and the S-MRTD. The SBTD approximates the curl operator by spatial finite-difference with higher precision and smaller numerical dispersion, while using less terms than the Battle-Lemarie based S-MRTD. Numerical examples demonstrate the superiority of the SBTD over the standard FDTD in terms of memory and speed in a wide range of applications, including resonators, microstrip antennas and package and device interactions.

Modeling of On-Chip Interconnects on Lossy Silicon Substrate Using Wavelets

M. Toupikov
Analog Devices
Wilmington, MA 01887, U.S.A.

Y. V. Tretiakov
IBM Microelectronics
Burlington, VT 05452, U.S.A.

G. Pan
Dept of electrical engineering, Arizona State University
Tempe, AZ 85287, U.S.A.

The lossy nature of the highly dopped silicon substrate have a significant impact on the performance of on-chip interconnects in CMOS integrated circuits, such as increased loss and dispersion.

At the frequencies of interest the most important losses occur in the metal layers that form a device as well as in the bulk Si substrate that appears below the device. Interconnect models in available design tools are based on lossless or low loss substrates and therefore can not accurately model interconnects on substrates with significant losses. Measurement results for on-chip interconnects on lossy silicon substrate with low bulk resistivity clearly show that induced frequency dependent substrate currents (eddy currents) are a dominant source of loss in these substrates.

In this paper we express the resistance and inductance of each conductor in terms of the surface currents and it's normal derivatives. A system of coupled integral equations is then derived to relate these quantities through the diffusion equation inside the conductors and Laplace's equations outside. The lossy substrate is treated as an additional lossy conductor with current described by diffusion equation.

In this presentation, we propose the use of the Coifman wavelets (Coiflets) as basis functions for the solution of the surface integral equations.The Dirac-delta-like property of the Coifman scaling functions and vanishing moments property of the Coifman wavelets make the calculation of the moment matrix elements much easier. In fact, the majority of the matrix entries can be evaluated without performing the time consuming numerical integration using Gaussian or other quadrature formulas and no thresholding procedure is required.

On Analysis of Finline Transformer via Multiwavelets

V. Sokolev
Mayo Foundation
Rochester, MN 55905, U.S.A.

X. Xie and G. Pan
Dept of Electrical Engineering, Arizona State University
Tempe, AZ 85287, U.S.A.

A nonuniform finline is designed to bridge the W-band waveguide with a spripline/micrsrip environment. The design and analysis of the finline structure are aimed to minimize, in a large frequency bandwidth, the impedance mismatch between a waveguide of several hundred ohms and the uniform parallel plate finline of 35 ohms.

In this talk, we applied a new set of shape functions of multiwavelets in the edge based finite element method (EEM). Because of the smoothness, completeness, compact support, and interpolation property of the multiscalets in terms of the basis function and its derivatives, fast convergence in approximating a function is achieved. The new basis functions are $\in C^1$, i.e., the first derivatives of the bases are continuous on the connecting nodes. Thus the divergence-free condition is satisfied at the end points. The multiscalets, along with their derivatives, are orthonormal in the discrete sampling nodes. Therefore no coupled system of equations in terms of the function and its derivative is involved, resulting in a simple and efficient algorithm. Numerical results demonstrate high efficiency and accuracy of the new approach.

Malvar Wavelet Based Fast Algorithms for Thin-Wire Antennas and Scatterers

Y. V. Tretiakov
IBM Microelectronics
Burlington, VT 05452, U.S.A.

M. Toupikov
Analog Devices
Wilmington, MA 01887, U.S.A.

Recently, wavelets found their application in solving integral equations, resulting in sparse impedance matrices. Smooth local trigonometric systems (SLT) were proposed by Malvar. The SLT are trigonometric functions multiplied by a smooth bell shaped window and form an orthogonal basis in the L^2. Similar to wavelets, the SLT system constructs its basis functions utilizing both translation and dilation of a single function. However, the construction is in a more flexible manner, thereby overcoming the inconvenience of conventional wavelets in handling the end points of non-periodic functions.

In this presentation we apply the smooth local cosine (SLC) functions to the generalized Pocklington integral equations for thin-wire scattering and radiation problems. Despite the strong singularity of the the Green's function, the SLC performs very stable. Numerical examples of thin-wire scatterer and antenna are presented. The results are compared with those obtained by using the standard pulse-based MoM. It has been noticed, that the use of the fast discrete cosine transform DCT-IV can drastically reduce computational time and increase accuracy of numerical calculations.

Application of Physical Spline FEM to Waveguide Problems

X. Zhou
Agere Systems, Inc.
Allentown, PA 18109, U.S.A.

G. Pan
Dept of electrical engineering, Arizona State University
Tempe, AZ 85287, U.S.A.

In this presentation, physical spline is applied to the finite element method (FEM) for the first time. Traditionally, linear or higher order Lagrange interpolations are employed in the FEM. Although one can achieve higher order differentiable interpolations by increasing the order of Lagrange polynomials, the discontinuities at joint ends still exist which is physically unacceptable. Furthermore, if higher order Lagrange interpolation is used, sometimes the continuity within an element may be overabundant. We employ the physical spline FEM to overcome the above difficulties. It is well known that cubic splines are twice continuously differentiable. However, since the first and second order differentials are not available in most cases, it is very difficult to apply the cubic spline directly to the FEM. This problem is resolved by introducing a new concept of the physical spline. The wave equation is discretized by the cubic spline interpolations. For waveguide problems, the resulting nonlinear eigenvalue problem is solved by the initial estimate based on the Lagrange interpolation, and then the solutions are improved by a few iterations.

The bandwidth of the resultant matrix from the physical spline is the same as that of linear Lagrange interpolation and is also sparse. As a result, sparse matrix solver can be used. Three classical examples are demonstrated and compared with the analytical solutions and with the Lagrange interpolation results. It is observed that the present method converges faster than the Lagrange interpolation method.

On the Use of Orthogonal Functions in Computational Electromagnetics

Y. V. Tretiakov
IBM Microelectronics
Burlington, VT 05452, U.S.A.

M. Toupikov
Analog Devices
Wilmington, MA 01887, U.S.A.

In this presentation, different orthogonal systems are applied to modern computational electromagnetics, including compactly supported orthogonal wavelets of Coifman (Coiflets) and Daubechies, smooth local trigonometric, and sampling based biorthogonal functions.

Owing to the vanishing moments of both the scaling function and mother wavelet of the Coiflets, the one-point quadrature integration rule in the method of moments (MoM) is implemented. The Coiflet-Galerkin MoM demonstrated superiority over the traditional MoM with pulse expansion and point matching.

The smooth local trigonometric (SLT) functions are employed in the Galerkin's MoM. The SLT is more suitable in handling electrically large scattering problems where the integral kernel behaves in a highly oscillatory manner. Numerical examples show the effectiveness of the SLT for two dimensional scatterers with sharp edges as well as with smooth contours.

Daubechies' wavelet based positive sampling functions are used in the wavelet-Galerkin time-domain (WGTD) technique to solve the Maxwell's equations. This biorthogonal sampling system has an exact interpolation property and demonstrates its superiority over the standard finite-difference time-domain (FDTD) and multi-resolution time-domain (MRTD) techniques in terms of computation time, use of computer memory and accuracy.

Session 1Pa1

Microwave Remote Sensing of Vegetated Terrains: Basic Studies and Applications

Retrieval of Bare Soil Parameters from SAR Data by Inversion of Surface Scattering Model

N. Pierdicca and P. Castracane
Department of Electronic Engineering, University of Rome "La Sapienza"
Roma, 00184, Italy

P. Ciotti
Department of Electrical Engineering, University of L'Aquila
L'Aquila, 67040, Italy

The objective of the work is the estimation of bare soil geophysical parameters (i.e., roughness and soil moisture) using polarimetric SAR data. IEMM model and a Semi-Empirical Model (SEM) have been implemented to simulate the measurements of a multifrequency radar polarimeter. Both models were introduced in an inversion scheme aiming to estimate roughness and dielectric properties of bare soil. The model output have been compared against polarimetric data acquired by the AIRSAR sensor (by JPL/NASA) during the MAC Europe campaign over an Italian test site (Montespertoli, close to Florence) and SIR-C data acquired from Space Shuttle over the same site. Three frequency bands (P, L, C) were available from AIRSAR and two frequency bands (L, C) from SIR-C, plus an X band at single polarization. Some fields of bare soil have been selected in the images whose roughness was determined by different rural tillage (ploughed, arrowed and rolled fields). The noise has been considered in the multidimensional space of the elements of the polarimetric Covariance Matrix and an additive calibration error has been introduced on the simulated measurement in order to evaluate its effect on the system parameters optimization, the occurrence of the calibration error has been demonstrated to affect the optimized incidence angle for parameter retrieval. Different inversion algorithms have been compared: a multivariate polynomial regression, a maximum likelihood algorithm, a minimum variance algorithm and a neural network. A correlation between the roughness parameter has been imposed in the simulation for the different inversion algorithms in order to evaluate its effect on the estimation accuracy. The methods have been tested on simulated data to compare their performance as function of number of looks, incidence angles and frequency bands. Using different frequency bands and polarizations strongly contribute to improve the inversion results with respect to single frequency or single polarization data.

Synergy of Active and Passive Low Frequency Microwave Sensing to Estimate Surface Soil Moisture and Canopy/Roughness Factor: Constraints Imposed by Spatial Patterns

E. G. Njoku
Jet Propulsion Laboratory
Pasadena, CA 91109, U.S.A.

D. Entekhabi
Massachusetts Institute of Technology
Cambridge, MA 02139, U.S.A.

Low frequency microwave brightness temperature and radar backscatter may be used to sense surface soil moisture because of the large contrast between the dielectric constant properties of water and soil. Surface roughness and attenuation by vegetation cover adversely affect the estimates. Development and validation of algorithms that can retrieve soil moisture in the presence of unknown vegetation and roughness factors is an area of intense study. The effects of these factors can be estimated by the use of either auxiliary information (e.g. optical vegetation indices) or by the use of multi-channel/multi-polarization measurements. The objective of this study is to use active and passive polarized L- and S-band measurements to simultaneously retrieve surface soil moisture, effective L- and S-band emitting temperatures, and two polarization-independent but frequency-dependent canopy extinction variables (five unknowns). The measurements are taken from the Passive/Active L/S-band sensor (PALS) that was flown over the Little Washita watershed during the 1999 Southern Great Plains field experiment. Although the measurements are made at an off-nadir constant incidence angle, the passive L-, S-band H, V measurements are not independent and hence do not generally provide enough constraints to solve for even four unknowns. In this study we condition the problem by taking advantage of the active measurements, and information in spatial patterns of the measurements, to reduce the numbers of degrees of freedom in the inversions. The problem is solved variationaly and the spatial patterns constraint is added with a lagrange multiplier. The key result of the study is demonstration of the feasibility of using the synergy of active and passive measurements to retrieve surface soil moisture in the presence of vegetation canopies.

Sensitivity of Vegetation Biomass Estimation Accuracy to SAR Parameter-Diversity using an Analytically Based Algorithm

M. Moghaddam
Jet Propulsion Laboratory
Pasadena, CA 91109, U.S.A.

Estimating vegetation biomass has long been regarded as a potential contribution of the synthetic aperture radar (SAR) to Earth science research. Many researchers have established the correlation of airborne and spaceborne SAR measurement at various frequencies and polarizations to the amount of biomass on the Earth surface. Many have also estimated biomass based on empirical or regression models applied to SAR data, which have often been quite limited in polarization and/or frequency diversity, especially on large scales. Dictated by the present lack of parameter-diverse SAR data and the need for large-scale knowledge of vegetation biomass, this paper studies how the accuracy of biomass estimation is affected as the number and independence of SAR data channels is reduced. As opposed to the previous empirical and regression-based analyses, the biomass estimation algorithm used here is based on analytical scattering models which take advantage of species knowledge and their allometric relations. The algorithm first estimates the canopy geometric variables (vegetation "biovolume") and their moisture content. It then deduces vegetation biomass based on these two pieces of information. The sensitivity analysis is carried out for an area in the Canadian boreal forest for which various SAR data sets exist. This area was part of the BOREAS project, and has been covered with the 3-frequency polarimetric AIRSAR, L-band HH-polarized JERS-1, and C-band VV-polarized ERS-1/2. The AIRSAR data present the most diverse data set available, but have a very small coverage area. Conversely, the two satellite systems each have only one data channel, but have covered the boreal zone on a large scale. The accuracy of biomass estimates using the AIRSAR will be compared to that possible using JERS-1 and the combination of JERS-1 and ERS-1/2. The modification of the estimation algorithm in the latter two cases to reduce the number of unknowns will be discussed, and its impact on estimation accuracy presented. This information is critical in deriving the large-scale biomass map of the north-American boreal zone from the JERS-1 and ERS-1/2 data sets.

Interferometric Coherence of Vegetated Areas in Mountain Regions

H. Rott, T. Nagler, and A. Kamelger
Institute of Meteorology and Geophysics, University of Innsbruck
Innsbruck, A-6020, Austria

Interferometric SAR data of mountainous regions in the Eastern Alps and in Patagonia (Southern Argentina) were analyzed in order to study effects of coherence on InSAR applications for topographic mapping and monitoring of mass movements at mountain slopes. Below the tree line the land cover of the Alpine test area is dominated by coniferous forests and cultivated meadows, and at higher elevations by dwarf-shrubs, sedges, grasses and bare rock. Interferograms were generated from C-band SAR data of ERS-1 and ERS-2 over time spans ranging from one day to a few years. The coherence images show dominating influence of vegetation type and density, and also pronounced seasonal effects. Over dense vegetation, such as forests and agricultural areas, the signal decorrelates almost completely during one-day periods, with the exception of cold periods in winter when the surfaces are covered by dry snow. Surfaces in alpine areas, covered by dwarf shrubs, low sedges and grass, show sufficient coherence for interferometric analysis even over annual intervals if acquired during the snow-free period. However, the phase decorrelates over time spans of a few weeks in winter because of changing phase delays in the snowpack due to accumulation, mematorphosis etc.

The investigations in Patagonia were based on ERS-1 and ERS-2 data from different years, as well as on one-day and three-day repeat pass data from SIR-C/X-SAR acquired at L-, C-, and X-band during the SRL-2 Mission in October 1994. The test area in the region of Lago Argentino extends from the ice-covered Cordillera to the dry steppe of eastern Patagonia. In the wet western part the elevation zones below 1000 m are covered by dense deciduous forests. The forest density decreases towards the east, and the vegetation cover changes to dry grassland. The coherence in the three frequencies clearly reflects the density of vegetation and the availability of water, enabling the identification of characteristic vegetation types. The investigations in both regions demonstrate the information content of interferometric coherence for discriminating main vegetation classes. For characterizing dense vegetation short interferometric time spans are necessary, and multiple-wavelength data are particularly valuable. A critical factor, reducing interferometric coherence even over short time spans, are precipitation events shortly before or during the SAR data acquisition.

Scattering and Interferometric Phase Center of Randomly Distributed Dielectric Cylinders Upon a Reflecting Surface

G. Macelloni
CNR-IROE
Florence, Italy

F. Marliani
ESA/ESTEC, TOS-EEE
Noordwijk, The Netherlands

G. Nesti
European Commission, JRC
Ispra, Italy

S. Paloscia, P. Pampaloni, and R. Ruisi
CNR-IROE
Florence, Italy

P. Poggi and P. Bruscaglioni
Department of Physics, University of Florence
Florence, Italy

Backscattering from vegetation covered soils is often dominated by the cylindrical structures such as stems in crops and trunks and branches in forests. In order to investigate the scattering properties of these important elements, a study has been performed based on an experimental model realized with dielectric circular cylinders distributed with different densities and inclinations, upon a reflecting surface.

Multi-frequency polarimetric and interferometric scattering measurements were carried out by using the European Microwave Signature Laboratory (EMSL) of the Joint Research Centre of Ispra, Italy. The experimental model consisted of an ensemble of glass pipes (inner diameter = 6.3 mm, length = 700 mm) filled with water. The pipes were mounted on a perfectly conductive plate, all parallel but with a random spatial distribution (two different densities and two inclinations). After the standard polarimetric monostatic calibration, backscattering measurements at different azimuth position for vertical and inclined pipes were carried out for the following configurations:

- A single pipe
- Couples of pipes at four different distances
- Dense distribution (two scenarios)
- Sparse distribution (two scenarios)

The measured frequency band was 1.0-9.0 GHz. The incidence angle was constant $(45°)$, while the azimuth aspect angle was changed in steps. Further measurements were performed on the same targets aiming at measuring the effective phase centre of the scattering sources. In this case, the incidence angle was changed in small steps around the nominal value of $45°$, while the azimuth aspect angle was changed in larger steps to obtain fully decorrelated data samples.

Experimental results were compared with model simulations obtained by using both incoherent and coherent approaches. In the incoherent model the intensity was obtained by calculating the scattered intensity by each element and then summing all intensities. In the coherent models, the electric fields scattered by each element were added coherently and the attenuation in the target was computed by means of Foldy's approximation. In both cases scattering from a cylinder was computed by using the infinite cylinder approximation.

From this research it has been possible to evaluate the mechanisms that influence the single scattering. In particular, the results of this investigation confirmed the importance of double scattering for vertical cylinders and of direct scattering for cylinders inclined perpendicularly to incidence direction. In addition, this study pointed out when the single scattering is no more sufficient to characterize the backscattering and when the effects of multiple scattering become important. The comparison of model results with experimental data, as well as the evaluation of the main scattering mechanisms that influence total backscattering, are discussed in the paper.

Session 1Pb1

Microwave Remote Sensing of Snow and Ice

Scattering by Dense Media of Small Particles Based on Monte Carlo Simulations and Applications to Microwave Remote Sensing of Snow

J. Guo, C.-T. Chen, and Q. Li
Dept. of Electrical Engineering
University of Washington, Box 352500
Seattle, WA 98195-2500, U.S.A.

K. H. Ding
Air Force Research Laboratory, Sensors Directorate/SNHE
Hanscom AFB, MA 01731-2909, U.S.A.

L. Tsang
Dept. of Electrical Engineering
University of Washington, Box 352500
Seattle, WA 98195-2500, U.S.A.

The frequency dependence of scattering by geophysical medium at microwave frequencies is an important scattering topic because multi-frequency measurements are useful in remote sensing applications. Classically, the independent scattering states that if the particles are small, scattering is proportional to the fourth power in 3-D scattering and frequency to the third power in 2-D scattering. If particle sizes are comparable to the wavelength, then the frequency dependence is weaker and scattering becomes independent of frequency at the geometric optics limit. In the case of sparse concentration of random distribution of particles, independent scattering is valid, and the frequency dependence follows that of single particle. However, does the frequency dependence of scattering change with the concentration of particles? We will show that the frequency dependence of scattering of dense media is different from that of sparse concentration of particles. When the particles are densely packed together, they can adhere to form aggregates. The correlation of scattering and the near field interaction between particles have to be taken into account.

In this paper, we will present Monte Carlo simulation results of dense media scattering using typical parameters found in microwave remote sensing of snow. The dense media consists of densely packed small particles. Solutions are based on Maxwell's equations and rigorous methods of generating dense media. The extinction rates of three-dimensional Monte Carlo simulations are compared with the QCA results at 18, 35, 60 and 90 GHz. For typical snow grains, the diameters are in millimeter ranges (e.g., 1 mm). For such cases, ka values are ranging from 0.2 to 1 depending on the frequencies. Particles with and without interparticle forces are both used in simulations to study the frequency-dependence of the extinction rate rigorously. It is shown that for densely packed sticky particles exhibit a weaker frequency dependence of scattering rate than that of independent scattering. The numerical parameters are chosen such that the results converge. The number of multipoles chosen for simulations depends on ka values. When frequency increases (large ka), higher order multipoles are included. The number of particles used in the simulations is chosen such that sufficient incoherent waves are introduced in the system. This will assure the calculated scattering rate is reliable. Many realizations are used to ensure the convergence of results. Up to 50 realizations are used in this paper. For most of the cases, the results converge within 20 to 30 realizations. The number of particles used in this study is between 100 and 2000 depending on the fractional volume and frequency. Numerical results indicate that the frequency dependence of densely packed small sticky particles is weaker than the frequency to the fourth power of independent scattering

Application of Huygens' Wavefront Principle in Analysis of Interferometric Signatures of Snow Events and Evolution

S.-S. Li
Geophysical Institute, University of Alaska
Fairbanks, AK, U.S.A.

M. Sturm
U.S. Army Cold Regions Research & Engineering Laboratory
Fairbanks, AK, U.S.A.

When a radar beam enters a snow layer from the air, the radar wavelength changes because of the refraction of the beam at the air and snow interface. A pair of synthetic aperture radar (SAR) images acquired before and after a snow event will have different wavelengths in the space that is occupied by the new snow accumulation. A question has been asked: will these two radar beams produce coherent interferometric patterns for the new snow accumulation? The traditional answer will be no, because two beams of different wavelengths will not coherently interfere with each other. People do see noisy interferometric patterns that are related to new snow accumulations. However, there are also examples of coherent interferometric patterns for some new snow event. A theoretical analysis is needed to explain these two seeming contradictory phenomena. We applied Huygen's wavefront principle to depict the interferometric patterns in the space of new snow accumulation. The resulting constant interferometric phase surfaces in the space of new snow accumulation are almost parallel to the surface of the new snow layer and are highly compact within the layer. This means that any irregularities in the thickness of the new snow layer will cause great variations of the interferometric phase values in the vicinity of a SAR pixel due to randomly distributed scatterers with significantly different individual interferometric phase value in the pixel neighborhood. This analysis explains why new snow, which is rarely of uniform thickness, tends to reduce interferometric phase coherence. When the new snow accumulation is uniform or the variation of new snow layer is less than 1.5 cm in terms of snow water equivalence, high interferometric coherence can be maintained. This result explains why different degrees of coherence can be related to new snow accumulation. The new method is able to explain interferograms that are related to various snow events. Especially, the new method verifies possible maintenance of coherent interferometric pattern during a new snow event. The results of this new method also warrant a radar-path-length-based method, which has been applied for interpretation of SAR interferograms in snow applications.

Mapping Global Snow Water Equivalent Using Passive Microwave Imagery: Problems and Progress

R. E. J. Kelly and A. T. C. Chang
NASA/Goddard Space Flight Center Hydrological Sciences Branch/Code 974
Greenbelt, MD 20771, U.S.A.

We present an approach to global mapping snow water equivalent (SWE) using the Special Sensor Microwave Imager (SSM/I) in preparation for the Advanced Microwave Scanning Radiometer – EOS (AMSR-E) aboard Aqua. The methodology first detects dry and wet snow using a well established brightness temperature difference scattering signal and polarization signal at 37 GHz. We also screen for non-snow scattering and snow free surfaces. Generally, cloud-free snow cover area mapping agrees well with Terra MODIS snow maps albeit with an underestimation of snow area by the SSM/I at the start of the season caused by shallow snow packs. Estimation of SWE is calculated using the brightness temperature difference at 19 and 37 GHz channels plus a dense media radiative transfer model (DMRT) that is parameterized by a single layer snow pack hydrology model. The DMRT is used to characterize critical snow pack properties (especially snow grain size) that are needed for the SWE estimation. The algorithm is tested on the Red River and Colorado River catchments in the USA and the Ob River in Siberia. In all cases, results show reasonable agreement with ground observations of snow water equivalent.

Determination of Errors in Visible/Near-Infrared and Passive-Microwave-Derived Snow Maps in Different Land-Cover Types

D. K. Hall, R. E. J. Kelly, A. T. C. Chang, and J. L. Foster
Code 974, NASA/Goddard Space Flight Center
Greenbelt, MD 20771, U.S.A.

Accurate snow maps are required for hydrological and climatological applications and by operational agencies to monitor snow conditions, and to predict spring water supply. Visible/near-infrared-based snow maps have the advantage that the spatial and temporal resolution is very good, and albedo can be measured, while passive-microwave snow maps have good temporal resolution, but poor spatial resolution. A tremendous advantage of passive-microwave sensors is that the potential exists to map snow depth and snow-water equivalent (SWE) as well as snow extent. Interpretation of many operational snow maps is hampered by cloud obscuration and therefore the combined use of visible/near-infrared and passive-microwave data is under study by many investigators. NASAs Moderate Resolution Imaging Spectroradiometer (MODIS) from the Terra and Aqua satellites, and the Advanced Microwave Scanning Radiometer (AMSR) currently produce or will produce snow maps. The Terra satellite, launched in December of 1999, has the MODIS as part of its payload of five instruments, while the Aqua satellite, to be launched in 2002, contains a second MODIS instrument, the AMSR-E and four other instruments. Snow maps have been produced since February 2000 from the MODIS sensor, and snow maps from the Defense Meteorological Satellite Program/Special Sensor Microwave/Imager (DMSP/SSM/I) have been produced since July 1987. AMSR-derived snow maps will be available beginning in about the summer of 2002. From October 2001 to March 2002, MODIS snow maps at ~ 5.6-km resolution are compared with ~ 25-km resolution SSM/I-derived snow maps. Results confirm previous results by several authors that correspondence between the MODIS- and SSM/I-derived snow maps improves as the winter progresses. Early in the season, the SSM/I snow mapping algorithms are unable to identify shallow and wet snow as snow cover, while the MODIS snow maps perform well under those circumstances, but cannot map snow through clouds and cannot provide estimates of SWE. By January when the snow temperatures are colder, and liquid water in the snowpack is minimal, the agreement between MODIS- and SSM/I-derived snow maps improves. In the present paper, we also define snow-mapping errors for the MODIS and SSM/I snow maps in each of seven land covers in North America. Land-cover type is determined from a MODIS-derived land-cover map developed by Boston University. NOAA operational Interactive Multisensory Snow and Ice Mapping System (IMS) snow maps and Landsat Enhanced Thematic Mapper Plus (ETM+) images are used as "ground truth".

Relationship Between Passive Microwave Measurements and Snow Parameters

N. C. Grody
NOAA/NESDIS/Office of Research and Applications
Camp Springs, MD 20746, U.S.A.

Measurements from the Advanced Microwave Sounding Unit (AMSU) will be used to demonstrate the variations in emissivity due various snow parameters (e.g., snow depth, grain size, fractional volume and stratification). AMSU was first launched in 1998 aboard the NOAA – K operation satellite, and contains window channels at 23, 31, 89, 150 GHz. The AMSU measurements will be used to identify metamorphic changes in the spectral characteristics as the snow ages in addition to the effects of melting and re-freezing of the snow surface. Ice crusts on the surface and within the snow pack are also shown to affect the satellite measurements. The paper will also provide models to account for the satellite observations and develop relationships between the AMSU channel microwave measurements and snow parameters.

Satellite Wind Scatterometer Estimates of Greenland Snow Accumulation

M. R. Drinkwater
European Space Agency-ESTEC
Noordwijk, Netherlands

D. G. Long
Microwave Earth Remote Sensing Lab, Brigham Young University
Provo, UT, U.S.A.

Data collected by the C-band ERS-2 wind scatterometer (EScat), the Ku-band ADEOS-1 NASA Scatterometer (NSCAT), and the Ku-band SeaWinds on QuikScat (QSCAT) satellite instruments are used to illustrate spatio-temporal variability in snow accumulation on the Greenland ice sheet. Microwave radar backscatter images of Greenland are derived using the scatterometer image reconstruction (SIR) method at 3-day intervals over the period 1991–98, and 1996–97 for EScat and NSCAT, respectively. The backscatter coefficient σ° normalized to 40° incidence, A and gradient in backscatter, B in the range $20-60^\circ$ are compared with historical snow accumulation data and recent measurements made in PARCA shallow snow pits. Empirical relationships derived from these comparisons reveal different exponential relationships between C- and Ku-band A values and dry-snow zone mean annual accumulation (Q). Frequency difference images between overlapping scatterometer images suggest that C-band data are more sensitive to snow layering and buried inhomogeneities, whereas Ku-band data are more sensitive to volume scattering from recently accumulated snow. Direct comparisons between NSCAT B values and in situ Q measurements show a linear relationship between ln(Q) and B, with a negative rank correlation of $R=-0.8$. The root mean square residual in fitting regression line equation ln$(Q)=3.08-17.83B$ to the data is 5 cm snow water equivalent. This value is of comparative order of magnitude to errors inherent in making in-situ estimates from snow pits. This simple Ku-band empirical relationship is exploited to investigate decadal changes in dry-snow zone accumulation between Seasat (1978) and NSCAT (1996). Additional comparisons between NSCAT and recent QSCAT (1999) data reveal significant upslope shifts in the dry snow line along the southwestern flank of the ice sheet. Recent acceleration in the increase in intensity of scattering is observed in the percolation zone, suggesting increased melting between 2000 and 3000 m elevation in the southern half of the ice sheet.

Retrieval of Glacier Properties from Single-Channel and Multi-Parameter SAR Data

H. Rott, D. Floricioiu, and T. Nagler
Institute of Meteorology and Geophysics
University of Innsbruck, Austria
Innsbruck, 6020, Austria

Spacebome SAR images are an excellent basis for studies of the dynamic behavior and mass balance of glaciers which is of significant importance for the hydrology of mountain regions and for global climate research. In order to learn about possibilities and limits of SAR for monitoring the mass balance and flow behavior of mountain glaciers, we studied backscattering signatures and interferometric data sets acquired by the European Remote Sensing Satellites ERS-1 and ERS-2 SAR (operating at C-band VV) in the years 1992 to 2000 and by the Shuttle Imaging Radar SIR-C/X-SAR (C- and L-Band polarimetric, X-Band VV) in 1994. Comprehensive field measurements of snow and ice properties and motion were carried out for comparison with the SAR data. The test sites are located in the Austrian Alps, with typical glacier size of several km^2, and in the Southern Patagonian Icefield (Argentina), where the large outlet glaciers cover areas up to several hundred km^2.

Among the main glacier characteristics, derived from SAR data, were ice motion and the areal extent and physical properties of the diagenetic glacier facies (glacier ice, wet snow zone, percolation zone and dry snow zone). The extent and temporal dynamics of these zones is related to the mass balance of a glacier which is a key parameter for climate studies. Because the data base covers different seasons and years, it was possible to study short term and seasonal changes of signatures. Backscatter model calculations were carried out in order to assist in the interpretation of the signatures and to study the sensitivity of the backscattering parameters in dependence of snow and ice properties. The IEM approach was used for surface scattering, and conventional and dense medium radiative transfer theory for volume scattering. Though good agreement of modeled and SAR derived signatures can be obtained for single frequencies, the models are not able to reproduce the frequency dependence of backscattering adequately. Main reasons for this are the complexity of the ice surfaces, covering different scales of roughness, and the wide range of scatterers found in refrozen multiyear firn. Nevertheless, the characteristic surface and volume scattering contributions of glacier ice and firn enable good classification of ablation and accumulation areas, key parameters for estimating the mass balance. For this classification it is important to take into account the melting or freezing state of the top ice and snow layers which may be subject to fast temporal changes, in particular during the transition periods between summer and winter.

Ice motion was analysed by means of one-day repeat pass interferometric SAR data of ERS on glaciers in the Alps and in Patagonia, and with one-day repeat pass L-, C-, and X-band SIR-C/X-SAR data in Patagonia. Whereas the investigated Alpine glaciers show maximum velocities of 10 cm/day, the Patagonian glaciers move up to 4 m/day. Due to the strong shear along the glacier boundaries, L-band data are most suitable for motion analysis of fast flowing glaciers, whereas the C-band data are better suited for motion mapping on the Alpine glaciers. The one-day interferometric motion was compared with GPS measurements of motion over annual intervals at selected points. The GPS and interferometric motions agree within a few per cent, which confirms that the annual variability of ice velocity is small in both test sites

Session 1Pc2

Fundamental Questions: Teaching, Learning, Concepts

Primary Forms of Maxwell's Equations in Free Space

A. D. Yaghjian
A.J. Devaney Associates
Boston, MA, U.S.A.

The traditional form of Maxwell's equations that include electric and magnetic polarization densities ($\mathbf{P}$ and $\mathbf{M}$) and magnetic charge-current, as well as electric charge-current, is given by

$$\nabla \times \mathbf{E} + \frac{\partial \mathbf{B}}{\partial t} = -\mathbf{J}_m \quad (1), \qquad \nabla \cdot \mathbf{B} = \rho_m \quad (2)$$

$$\nabla \times \mathbf{H} - \frac{\partial \mathbf{D}}{\partial t} = \mathbf{J}_e \quad (3), \qquad \nabla \cdot \mathbf{D} = \rho_e \quad (4)$$

with the constitutive relations $\mathbf{D} = \epsilon_0 \mathbf{E} + \mathbf{P}$ and $\mathbf{B} = \mu_0(\mathbf{H} + \mathbf{M})$. The constitutive relations can be used to eliminate $\mathbf{D}$ or $\mathbf{E}$ and $\mathbf{B}$ or $\mathbf{H}$ from Maxwell's equations in favor of $\mathbf{P}$ and $\mathbf{M}$. Maxwell's equations (1)–(4), which hold in polarized material with the given constitutive relations, can be derived from the free-space Maxwell equations beginning with either bound electric charge-current or bound magnetic charge-current. However, in order to arrive at the same general Maxwell equations (1)–(4) beginning with either bound electric or magnetic charge-current, one must begin with different forms of Maxwell's equations in free space, namely

$$\nabla \times \mathbf{E} + \frac{\partial \mathbf{B}}{\partial t} = 0 \quad (5), \qquad \nabla \cdot \mathbf{B} = 0 \quad (6)$$

$$\nabla \times \mathbf{B} - \epsilon_0 \mu_0 \frac{\partial \mathbf{E}}{\partial t} = \mu_0 \mathbf{J}_e \quad (7), \qquad \nabla \cdot \mathbf{E} = \rho_e / \epsilon_0 \quad (8)$$

for electric charge-current, and

$$\nabla \times \mathbf{D} + \epsilon_0 \mu_0 \frac{\partial \mathbf{H}}{\partial t} = -\epsilon_0 \mathbf{J}_m \quad (9), \qquad \nabla \cdot \mathbf{H} = \rho_m / \mu_0 \quad (10)$$

$$\nabla \times \mathbf{H} - \frac{\partial \mathbf{D}}{\partial t} = 0 \quad (11), \qquad \nabla \cdot \mathbf{D} = 0 \quad (12)$$

for magnetic charge-current, provided we retain the usual definitions of $\mathbf{P}$ and $\mathbf{M}$ in terms of bound charge and current

$$\mathbf{P}(\mathbf{r}, t) = \lim_{D \to 0} \frac{1}{\Delta V} \int_{V_D} \rho_{eb}(\mathbf{r}', t) \mathbf{r}' dV' = -\lim_{D \to 0} \frac{\epsilon_0}{2\Delta V} \int_{V_D} \mathbf{r}' \times \mathbf{J}_{mb}(\mathbf{r}', t) dV' \quad (13)$$

$$\mathbf{M}(\mathbf{r}, t) = \lim_{D \to 0} \frac{1}{2\Delta V} \int_{V_D} \mathbf{r}' \times \mathbf{J}_{eb}(\mathbf{r}', t) dV' = \lim_{D \to 0} \frac{1}{\mu_0 \Delta V} \int_{V_D} \rho_{mb}(\mathbf{r}', t) \mathbf{r}' dV'. \quad (14)$$

Therefore, the vectors $\mathbf{E}$ and $\mathbf{B}$ are the primary fields in free space produced by electric-charge current, and the vectors $\mathbf{D}$ and $\mathbf{H}$ are the primary fields in free space produced by magnetic charge-current. This result and some of its consequences, as well as the primary equations given in Maxwell's Treatise, are discussed in the talk.

In Search of a Geometrical Basis for the Ubiquitous Electromagnetic Energy

J. F. Nystrom
Computing & Mathematical Sciences, Texas A&M University – Corpus Christi
Corpus Christi, TX 78412, U.S.A.

Are photons a tetrahedral package of energy? Is current flow a geometrical dance of interconnected tetrahedral and octahedral forms? In the past, scientific investigations aimed at uncovering a geometrical basis of electromagnetic (EM) energy would not have been practical. Only over the past few decades have computational tools evolved to a level where it is possible to peruse the structure underlying the time-domain behavior of EM energy in detail. That is, our scientific capabilities are now at alevel wherein we can ask deeper questions about the underlying nature of the EM energy. Consequently, I query: Wherein the electromagnetic form?

In this presentation I first describe the recently developed *isotropic vector field decomposition methodology* [1], and then report on an exciting application thereof. The isotropic vector field decomposition methodology purports to provide a heretofore unavailable perspective for computations involving vector fields, and also an opportunity to search for underlying geometrical forms of the EM energy [2, p.221]. The isotropic vector field decomposition methodology utilizes a computational grid (the isotropic vector matrix – IVM) wherein all vertices are equally spaced from their twelve nearest neighbors; discretizes a vector field upon the IVM in such a way as to preserve the isotropic nature of space; and contains an algorithm whereby the vector curl operator can be calculated. Figure 1 shows a vector equilibrium (VE) cell from which an IVM is built. (Also shown in Figure 1 are the six IVM basis vectors at the center of the VE cell, and the four hexagonal planes which compose the outer layer of the VE cell.) The vector curl algorithm utilizes field values on two of the four exterior hexagonal planes for each of the resulting six IVM basis vectors at the center of the VE cell. (That is, each unique pair of exterior planes of a VE cell begets one of the six IVM basis vectors at the center of that VE cell.)

The first application of the isotropic vector field decomposition methodology will be the construction of computational electromagnetic solvers. Investigations – utilizing visualization and data mining techniques on resulting time-domain data – will also be undertaken to uncover an underlying geometrical basis for EM energy. The hope is that eventually, when our grandchildren ask – "Wherein the electromagnetic form?" – we may have ananswer.

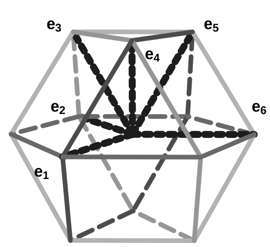

Fig 1: The IVM basis vectors e_1–e_6.

REFERENCES

1. Nystrom, J. F., "The isotropic vector field decomposition methodology," submitted to *ACES 2002: The 18th Annual Review of Progress in Applied Computational Electromagnetics*, Monterey, CA, March 18–22, 2002.
2. Nystrom, J.F., "Tensional computation: further musings on the computational cosmography," Applied *Mathematics and Computation*, 120, 211–225, 2001.

The Effect of Electromagnetic and Mechanical Forces on Single Items Used in Electrical Machines

C. Grabner, J. Bacher
Institute of Electrical Machines and Drives
Graz, Austria

E. Schmidt
Institute of Electrical Drives and Machines
Vienna, Austria

It has been reported in literature that the mechanical behaviour of Roebel bars utilised in stator slots of large synchronous machines mainly depends on forces of electromagnetic origin. The problem of mechanical forces occurring through necessary assembling is omitted there. Hence, this paper investigates the common interaction of appearing mechanical and electromagnetic forces.

Based on a linear mechanical deformation process we are able to obtain the common deformation through superposition of the mechanical and electromagnetical deformation. In a first step, the indispensable mechanical pre-load is applied to the slot wedge.

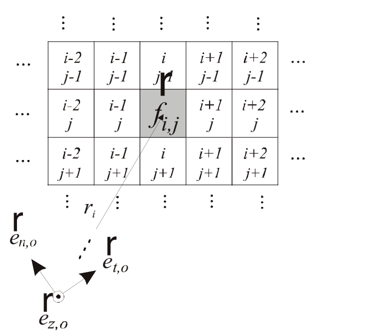

$$\vec{f}_{i,j}^{FE}(V)=(J_{z,i,j}\,B_{n,i,j})\,\vec{e}_{t,0}-(J_{z,i,j}\,B_{t,i,j})\,\vec{e}_{n,0}$$

Figure 1: Volume force densities are caused by current carrying conductors.

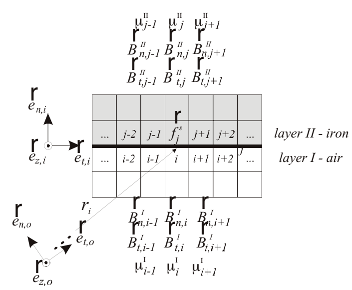

$$\vec{f}_i^{s,FE}(V)=\frac{1}{2\mu_0}\left(\frac{\mu_{r,i}^{I}-\mu_{r,i}^{II}}{\mu_{r,i}^{I}\,\mu_{r,i}^{II}}\right)(B_{n,i}^2+B_{t,i}^2)\,\vec{e}_{n,i}$$

Figure 2: Surface forces densities acting at material boundaries.

Roebel bars have the qualification to carry electrical currents in large quantities, so we have to consider secondly the mechanical deformation of inlaid parts caused by electromagnetic forces. Volume force densities inside copper regions are numerically received from nonlinear electromagnetic quantities according Fig.1. Local field values of layer I and II, as well as nonlinear iron permeability values of layer II must be used for the correct evaluation of mechanical surface force densities at material boundaries, as it is depicted in Fig.2. Thus, a unique correspondence of finite elements situated in both layers along the contour under investigation is generated.

The interrelationship of varying electrical current and varying mechanical pre-load, as connected by the requirement that no free space inside the slot arises during electrical failure conditions, is of important interest. Thus, the paper will explain the applied algorithm for often repeated numerical solving of the coupled electromagnetic-mechanical field problem until the secondary condition is fulfilled. The implementation finally results in the searched characteristic. We obtain, for a chosen operating point of the characteristic line, for several investigated composite materials significant differences in the distribution of compressive stress.

Consequently, our investigation shows obvious that the mechanical behaviour of both Roebel bars is mainly determined by the mechanical pre-load of the slot wedge, forces of electromagnetic origin are of secondary interest in normal operation state. This result is contrary to conventionally assumptions and therefore of usefulness for an enhanced construction process.

The Internal Losses of Magnets by Electromagnetic Waves are Determined with Finite Element Methods

J. Bacher and C. Grabner
Institute of Electrical Machines and Drives, Technical University Graz
Graz, Austria

Permanent magnets are normally characterised by the product of the magnetic flux density and the magnetic field strength. This magnetic field energy per unit depends essentially on the temperature. At higher temperature, this characteristic parameter reduces considerably. This fact will be illustrated by Nd-Fe-B. The reasonable working for this high-quality magnetic material is in the region from 20 to 120° C. This illustrates the small temperature range of such high-quality magnetic materials. In view of this fact the temperature in magnetic material and its connection with electromagnetic waves is treated in more detail in this paper.

The temperature of the magnetic material increases under the action of electromagnetic waves. If the electric conductivity of the magnet is finite, currents are induced to flow in the magnetic material. The amplitude and frequency of the magnetic wave are criterions for the heat development in the material. Practical electromagnetic waves have a defined frequency spectrum which can be found by a Fourier analysis. Here the higher harmonics must be divided into two classes. First, there are higher harmonics which have been produced by a magnetic non-linear steel parts. These higher harmonics have the same speed as the first harmonic. The second class consists of the higher harmonics from the power supply. In this case its speed can be calculated by its harmonic order and the speed of the first harmonic. The super position of the effects of the higher harmonics is not allowed. The relationship between the wave parameters and the internal losses in the material is determined by finite element methods. The magnet is divided into thin layers of the penetration depth of the individual higher harmonics. The eddy currents flow in these layers. All regions of the magnet are carrying different currents. The variation of the current density in the layers because of changing temperature can not be neglected. The current density in the layers will depend very much on the frequency spectrums of the electromagnetic waves. The choice between various types of frequency spectrums will result in an optimal temperature rise of the magnetic material. In contrast to the general assumption that the temperature in the magnet rises uniformly, this analysis considers the temperature distribution in the magnetic material. A further complication in this connection is the design of the magnet. Neither the current densities in the layers nor the temperature distribution in the magnet are independent of the magnet design. On the one hand the design affects the eddy currents in the magnetic material and on the other hand the surface of the magnet plays a very important role in connection with the final temperature.

In this paper electromagnetic effects are coupled with thermal effects. Such coupled problems can be solved by finite element methods. In view of the various application field of magnets, the knowledge of the temperature distribution which is caused by electromagnetic waves is absolutely necessary to design and to calculate magnets correctly.

Electromagnetics Teaching: How Much Bandwidth Is Needed to Transmit Real Understanding?

A. Sihvola
Electromagnetics Laboratory, Helsinki University of Technology
Espoo, 02015, Finland

It is difficult to teach electromagnetics. Many university professors and other teachers would agree with this. Someone may even say that it is impossible. How, then, about learning electromagnetics? Certainly it is safe to assume that most PIERS participants hold the opinion that it is difficult to learn electromagnetics. But only the most cynical of us would say that it would be impossible. Much of our electromagnetics understanding comes slowly, through our research work when we solve electromagnetics problems. Is there any role for a teacher to assist us in becoming an expert in electromagnetics?

My presentation tries to argue for a positive answer to this question. Teachers are needed. But the role is challenging. Difficulties in the teaching of electromagnetics courses are very much caused by the facts that fields are functions of space and time and also often vectors. To get a useful and true picture of their behavior requires considerable mental efforts. The visualization of electromagnetic fields can be made very much easier with today's computers, interactive software, and web-based applets.

Help that user-friendly computers can offer is extremely valuable. Visually effective teaching materials can certainly be distributed through computer networks and can be accessed using basic browsers. But even if we had gigacycles of bandwidth, the channel is nevertheless too narrow to be able to transmit the interaction which is so essential in the teaching and learning process, and to compete with the human teacher–learner connection that should always be required in electromagnetics education. It is important to remember, as Parker J. Palmer has expressed [1], that good teaching cannot be reduced to technique, good teaching comes form the identity and integrity of the teacher.

REFERENCES

1. Parker J. Palmer: *The courage to teach.* Jossey-Bass, San Francisco, 1998.

Inverse Obstacle Problem in Ellipsometric Scatterometry

M. Yeung
Department of Manufacturing Engineering, Boston University
Boston, MA 02215, U.S.A.

Scatterometry is the measurement of the shapes of sub-wavelength diffractive structures by characterizing the scattered light produced under different incidence conditions. Because the phase of the scattered light is difficult to measure, the inverse obstacle problem in scatterometry is usually formulated in terms of the measured intensity, rather than the complex electric field. Recent advance in scatterometry, however, has allowed the phase of the scattered electric field in one incident polarization relative to that in the other, orthogonal polarization to be measured accurately by ellipsometric technique. Using such information, it becomes possible to formulate the inverse obstacle problem in terms of the complex ratio between the scattered electric fields in two orthogonal incident polarizations.

In this paper, the inverse obstacle problem in ellipsometric scatterometry is formulated for dielectric diffraction grating structures. An extension of a well-known theorem on domain derivatives for perfectly conducting objects to the case of dielectric objects is presented. It is then used in an efficient numerical solution of the inverse obstacle problem by a Newton like iteration method. Numerical results demonstrate the usefulness of the present approach for the non-destructive metrology of sub-micron integrated circuit structures in microelectronics manufacturing, as shown in Fig. 1.

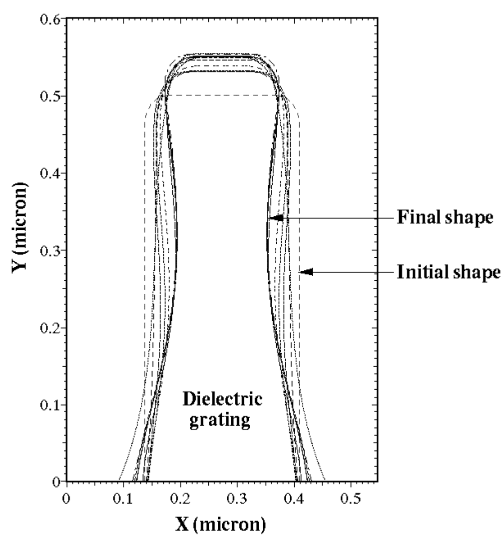

Figure 1: Shape reconstruction of a dielectric diffraction grating with a period of 0.5464 micron.

Although in this paper the inverse obstacle problem is discussed within the context of diffraction gratings in optics, the present formulation based on the measured complex ratio of scattered electric fields can be easily generalized for inverse obstacle problems in other areas of electromagnetics such as radar shape reconstruction. The data requirements for application of the ellipsometric inverse obstacle method to such areas are discussed.

Phenomenology-Based Inverse Scattering

L. Perlovsky, D. Choi, K. Ding, K. Kim, M. Rangaswamy, E. Tichovolsky, and B. Weijers
AFRL/SNHE
Hanscom AFB, MA 01731, U.S.A.

Whereas solving complex inverse problems remains a challenge, biological systems solve these problems with ease: e.g., an eye-brain system constantly reconstructs properties of surrounding objects from scattered fields. One of the main principles utilized by biological systems is relying on practically available knowledge concerning phenomenology of objects and their scattering properties. The classical Tikhonov's regularization and inversion method cannot take into account available knowledge of object phenomenology. Morozov's modification permits using an estimate of the expected error. Recent developments using this approach result in accurate inversions of three-dimensional objects, this however, works for regularly shaped objects, in absence of clutter that might contain a number of irregularly shaped objects, which properties are not of interest in a particular application. This presentation will discuss an inversion method that can take into account available information on object properties and propagation environment, that might be practically available (even if imprecise or approximate). This additional information leads to a better performance for complex problems, such as when noise is strong, even when object signals are below noise or clutter (or when a large number of objects of no interest are present). This method can be described as defining the Tikhonov's regularization parameter in a way to account for the available information. Whereas the original Tikhonov's regularization parameter is a scalar, in our approach it is an operator. The discussed method can incorporate uncertain information including unknown parameters. In this case, the regularization parameter becomes a nonlinear operator, which depends on the unknown parameters characterizing available knowledge, and on the uncertainty of these parameters. The method is iterative and convergence theorems will be presented. We will also present some initial examples of applications of this method.

REFERENCES

1. Tikhonov, A.N., "Regularization of Incorrectly Posed Problems", *Soviet Math.* Doklady 4, pp.1624-1627, 1963.
2. Morozov,V.A., "On the Solution of Functional Equations by the Method of Regularization", *Soviet Math.* Doklady 7, pp.414-417, 1966.
3. D. Colton, K. Giebermann, and P. Monk., "A regularized sampling method for solving three dimensional inverse scattering problems", *SIAM J. Scientific Computation*, 21, pp.2316-2330, 2000.

Nonlinear Electrodynamics May Be the Unified Field Theory

A. A. Chernitskii
Department of Physical Electronics, St.-Petersburg Electrotechnical University
Alexander Friedmann Laboratory for Theoretical Physics
St.-Petersburg, 197376, Russia

The idea to consider some nonlinear electrodynamics model as the general theory of matter goes back to the articles by G. Mie, also by M. Born and L. Infeld. In such approach the electron and the other elementary particles must be represented by some electromagnetic solitons. In general, this representation is characteristic for the unified field theory approach, instead of the description of each kind of particles by individual fields which are interacting with each other. This last approach is characteristic for quantum field theory but, as we think, it can be considered as some approximation to more general theory based on the unified field. The question pertinent to nonlocal behavior of the quantum objects is discussed in the article by A.A. Chernitskii [8], where it is shown that the nonlocal correlations must exist in the framework of local field theory. Electromagnetic field satisfying nonlinear system of equations can be considered as the real candidate for the unified field [2,4]. In particular, this opinion is based also on the results indicative for the possibility of description of gravitation in the framework of nonlinear electrodynamics [1,3,4]. In this approach there is the model for particle with spin which include two dyon with equal electric and opposite magnetic charges [4,5,6]. Also there is the spinor representation for nonlinear electrodynamics equations [7].

The unified field theory approach promises considerable advantages for the nanotechnology because it must be giving more deterministic predictions about the behavior of the micro objects. This approach must help to construct the Avogadro-scale or quantum real computer.

REFERENCES

1. A.A. Chernitskii, *Theoret. and Math. Phys.* **90**(3) (1992) 260.
2. A.A. Chernitskii, *Helv. Phys. Acta* **71**, 274 (1998); http://arXiv.org/abs/hep-th/9705075.
3. A.A. Chernitskii, *J. High Energy Phys.* 11 (1998) 015; http://arXiv.org/abs/hep-th/9809175.
4. A.A. Chernitskii, *J. High Energy Phys.* 12 (1999) 010; http://arXiv.org/abs/hep-th/9911093.
5. A.A. Chernitskii, http://arXiv.org/abs/hep-th/0002083.
6. A.A. Chernitskii, “Bidyon”, in “Concise encyclopedia on supersymmetry and noncommutative structures in mathematics and physics”, Eds. P. Fayet, J. Gates, S. Duplij, to be published by Kluwer Academic Publishers, Dordrecht, 2001.
7. A.A. Chernitskii, http://arXiv.org/abs/hep-th/0009121.
8. A.A. Chernitskii, http://arXiv.org/abs/quant-ph/0102101.

Spectral Problems in Small Ferrite Resonators – Structural Elements for Microwave Composites

E. O. Kamenetskii, R. Shavit, and M. Sigalov
Department of Electrical and Computer Engineering,
Ben-Gurion University of the Negev
Beer-Sheva, 84105, Israel

Rich multi-resonance spectrums of the so-called magnetostatic (MS) oscillations in small ferrite disk resonators excited by the microwave magnetic field, were experimentally observed more than 40 years ago. Since then, the effect of conversion of electromagnetic power into spin-wave power spectrums (with two-four order differences in wavelength) was a topic of serious experimental and theoretical investigations.

Recently, we have shown that MS oscillations in a small ferrite disk resonator can be characterized by *a discrete spectrum of energy levels* [1]. Concerning the problem, one should keep in his mind the fact that when in classical electrodynamics structures the spectral problems are characterized by *wavenumbers* and/or *squared frequencies* as spectral parameters, in quantum mechanical structures there are *energy eigenstates* as spectral parameters. This fact allows analyzing the MS oscillations similarly to quantum mechanical problems and gives a basis for a clearer understanding the nature of the observed multi-resonance spectrum. This fact also displays a very important aspect of the artificial-electromagnetic-material principles that, as we discussed in [2], the "microscopic" (on the scales of the structural-element sizes) properties of artificial electromagnetic materials should be based on the non-electromagnetic (quantum mechanical like) laws.

In a ferrite disk resonator, the MS potential function can be considered as a probability distribution function. We obtained the scalar-function wave equation that contains a first derivative with respect to time and a second derivative with respect to space coordinates. The form of this equation is similar to the Schrodinger equation, but there is no certain analogy between the quantum mechanical constants and parameters, on the one hand, and our coefficients, on the other hand. In this paper we give the results of energy spectrum calculations for MS oscillations in a ferrite disk resonator. We show the energy level diagram and the MS potential and magnetization distribution functions for energy eigenstates. Transitions between the energy levels correspond to portions of the magnetic energy. Our calculations are made based on the so-called model of an "open ferrite disk resonator" (the OFDR model). This model gives a good correlation between the pictures of the calculated and experimental resonance spectrums. The role of the non-uniform DC magnetic field is considered as an additional factor that, certainly, can lead to distortion of an initial discrete spectrum in a ferrite disk but does not imply a fundamental character.

An analysis of MS oscillation spectra shows that small ferromagnetic resonators can be considered in microwaves as "artificial atomic structures".

REFERENCE

1. Kamenetskii, E. O., "Energy eigenstates of magnetostatic waves and oscillations," *Phys. Rev. E,* 63, 066612, 2001.
2. Kamenetskii, E. O., "Quasistatic principles in macroscopic electrodynamics of bianisotropic media," *Phys. Rev. E,* 58, 7965, 1998.

Session 1Pc3

All SOP Fiber Optics: Circuitry and Applications

Polymer Optical Fibre and Gratings

P. L. Chu
Optoelectronics Research Center, City University of Hong Kong
Kowloon, Hong Kong

Polymer optical fibre is receiving intense attention recently because of its potential applications to short distance communication systems. It has many advantages over glass fibres: (1) Large core diameter ($\sim$ 1 mm) facilitating ease of connection, (2) Large numerical aperture enabling it to carry much more optical power than the glass fibre, (3) Large flexibility allowing it to negotiate sharp bends with ease, (4) Small Young's Modulus making it to have large strain at small stress, and (5) Light weight.

In this paper, we firstly survey the latest development of low loss polymer fibre and then report on our study of its photosensitivity and writing of Bragg gratings in single mode polymer fibre and finally the applications of these gratings.

The standard material for polymer optical fibre is Polymethacrylate (PMMA) which in commercial term, is Perspex. This material is easy to handle and its refractive index can be varied readily by adding appropriate dopants into its monomer phase. However, the resultant fibre loss is rather high, about 150 dB/km. A new fibre has recently been developed which replaces the hydrocarbon in PMMA with fluorine and the resultant fibre is called perfluorinated fibre. It has an experimental loss figure of 13 dB/km. This fibre will find applications in local area networks with bandwidth in Gigahertz.

We have shown that Bragg gratings can be written in both PMMA fibres and Perfluorinated fibres. The passband wavelength of these gratings can tuned both mechanically and thermally. In the case, of PMMA fibre, the tuning range is 73 nm by mechanical stretching and 18 nm by thermal tuning. For perfluorinated fibre, the thermal tuning range is 10 nm. These figures are much larger than those afforded by glass fibre Bragg gratings. Hence polymer fibre gratings open up a new area of application where wavelength tenability is an advantage. Examples are tunable Add-Drop multiplexer-demultiplexer, simple optical spectrum analyzeer, and tunable dispersion compensator etc.

Specialty Fibers as Optical Components

R. Stolen
Dept. of Electrical & Computer Engineering, Virginia Tech
Blacksburg, VA, U.S.A.

Fiber Optics was once viewed simply as a light pipe between a transmitter and a receiver. This was in contrast to microwave technology where systems could be constructed from off-the -shelf components. The scope of Fiber Optics technology has grown with time and lightwave transmission systems have become quite complex. Fiber compatible components and devices such as directional couplers, filters, isolators, and optical amplifiers are now readily available. Improvements in connectors and splicing permit the connection of these individual components into systems that go well beyond simple optical transmission. These fiber compatible components are fabricated using microoptic, integrated optic, exposed core, or all-fiber technologies.

The goal of a complete set of fiber components and devices has largely been realized- the exception is a truly effective all-fiber modulator. However, the potential of the all-fiber components has barely been tapped. While these components share functions with bulk optics components and microwave components they have features that are unique. Examples are the modal coupling features seen in fused taper all-fiber components such as the directional coupler; coupling between core light and cladding modes; and the recently invented fiber waveplates.[1]

To take full advantage of these properties will require improvements in fiber design and fabrication. The state of the art has seen dramatic improvement over the years but it is clear that there is much more that can be done. The interplay of applications, theory, and fabrication technologies will stimulate progress. The ultimate goal is totally all-fiber integrated systems for communications, sensors and fiber lasers.

REFERENCES

1. Huang, H. C., "Fiber-optic analogs of bulk-optic wave plates," *Appl. Opt.*, Vol. 36, 6968, 1997.

Fabrication and Simulation of Photonic Crystal Fiber

Z. D. Shi and Q. Guo
Shanghai University
Jia-Ding, Shanghai 201800, P.R.China

Y. J. Zhu and X. P. Dong
University of Xiamen
Xiamen, 361005, P.R.China

The Photonic Crystal Fiber (PCF) is a novel kind of optical fiber featured by a periodic modulation of refractive index of its clad. This modulation can be realized by holes or by other material rods embedded in the clad. The mechanism of lightwave guidance in a PCF is essentially based on the photonic bandgap effect and total internal reflection. The PCFs display unusual wave-guiding properties potentially applicable to fiber-optic communication and sensors. The size of the mode spot depends strongly on the ratio of wavelength λ to lattice pitch Λ, allowing either very strong or very weak nonlinear coefficients, with the result that the zero dispersion point may be shifted into the visible part of the spectrum. For small hole diameters ($d/\Lambda < 0.4$), the fibers are found to be "endlessly single-mode". Analysis and simulations on this novel fiber can be found in the literature, including a scalar description for a PCF with small air fill-fractions, and a vector method for the field structures of a PCF with large air fill-fractions. It has been found that asymmetries, elliptical holes and deformations of the inner ring can cause significant birefringence in a PCF.

In manufacturing a porous clad PCF, assembling rods and tubes is usual procedure to form fiber preform. The size, shape and distribution of holes in clad must be controlled and maintained during drawing of preform down to fiber dimension. The balance of pressure within the hole against viscous forces of the surrounding material must be precisely kept at very high temperature. In order to effectively overcome these difficulties and reduce contamination, holes may be filled with some material with suitable different refractive index. The "sol-gel" is a promising alternative method for PCF fabrication, in which different size, shape and distribution of holes in clad can be controlled under varying consolidation conditions.

The Finite Difference Time Domain (FDTD) method was employed for the analysis of the transmission characteristics of PCF. A two-dimensional FDTD algorithm has been set up for the calculation. The results of the calculation of the PCF propagation characteristics, including the mode field distribution and chromatic dispersion, etc., agree with the published theoretical and experimental data, which are useful in an optimal design of the PCF. Based on the data of calculation, our efforts are now directed to the technique of producing low-loss, hi-bi (highly birefringence) PCF with particular emphasis on obtaining an essentially circular-shaped mode field. Our research project is conducted under the support of the National Natural Science Foundation of China. (Grant No. 60177026)

Study of Polarization Mode Dispersion (PMD) in a High Bit Rate Optical Link Using a System Simulator

J.-L. Verneuil, C. Aupetit-Berthelemot, and J.-M. Dumas
ENSIL, University of Limoges
Limoges, 87068, France

Fiber and optoelectronic component improvements together with the insertion of Erbium doped fiber amplifiers (EDFA) lead to increases in the bit rates and span lengths of long haul optical transmission systems. However, the Polarization Mode Dispersion (PMD) is still a fiber detrimental effect that has to be overcome. In this communication, we report results on the impact of the PMD on the performance of a high bit rate optical link, using a system simulator.

The major cause of PMD is the asymmetry of the fiber-optic strand. It is due to various process dependent and/or fiber deployment stresses. The residual anisotropy produced by core ellipticity or non-circular stresses induces two modes of polarization. The difference in the propagation constants gives rise to a differential transit time for the propagated data stream. So, PMD results in a pulse dispersion responsible for high bit error rates.

We investigated the impact of PMD on a 40 GBits/s link by means of the simulator COMSIS (IPSIS, F-Rennes). Figure 1 illustrates the simulated link. The basic building block parameters are extracted from our participation in a French national telecommunication project named ERMIONE, involving operators, equipment manufacturers and universities. These parameters can be found elsewhere [1].

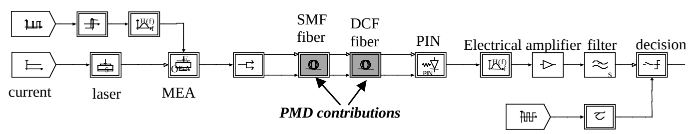

Figure 1: Blocks diagram of the simulated fiber optic system.

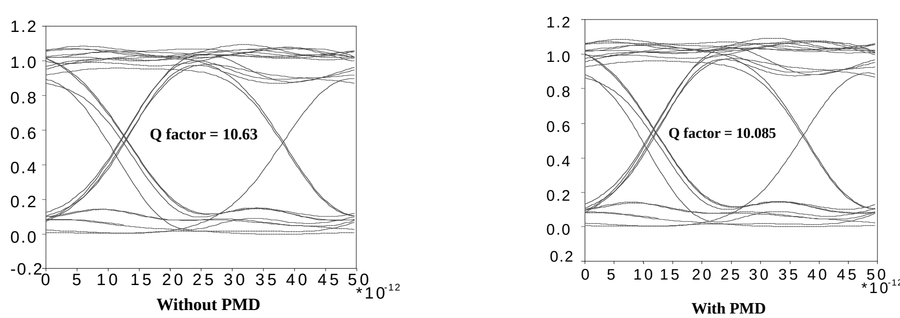

Figure 2: Simulated eye diagrams and Q factors for the system illustrated in figure 1. SMF and DCF fiber lengths are respectively 53 and 11.25 km (optimized terrestrial span length).

By carefully choosing the DCF and SMF fiber lengths for a given span length, one can note that PMD is negligible. However, PMD becomes a penalizing effect for longer span lengths. Other results will be presented.

REFERENCES

1. ERMIONE project reports, 2001.

Fiber-Optic Quarter Waveplate and Its Application in All-fiber Electric Current Sensor

H.-C. Huang
Shanghai University
Shanghai, Jia Ding 201800, P. R. China

This paper describes a fiber-optic quarter waveplate of the author's invention in connection with its one exceedingly useful application example in structuring an all-fiber current sensor. The underlying principle of this particular application is *not* based on the best-known function of a quarter waveplate which transforms linear light into circular light or vice versa, but is based on the less-known function of this element by which a disordered linear light orientation is made ordered, and hence easily detectable. This technological approach to Faraday-rotation sensing is entirely new.

Analytically, the transform between linear light and circular light involves a single supermode only, while the transform of a disordered orientation to an ordered orientation involves two supermodes. Drastic difference exists between these two transforms in their power transfer pattern: the power transfer through single supermode process is gradual, but the power transfer through dual supermode process exhibits a beating-like pattern with violent power conversions–reconversions in the neighborhood of one or the other terminal of the fiber-optic quarter waveplate. In a comparative study, these two kinds of polarization transforms are treated exactly by an asymptotic mathematical approach in the text.

On the basis of the theory, a prototype all-fiber current sensor is constructed in the author's laboratory, in which a single piece of fiber-optic quarter waveplate spliced (in-line) in the fiber circuitry replaces the entirety of the traditional bulk-optic elements and sophisticated signal processors that are otherwise indispensable in a current-sensing scheme. Experimental results have confirmed the theoretical prediction in all aspects. The utmostly simple current sensor thus constructed has been continuously observed to work stably without the need of re-tuning in a long-run operation.

Full-Vectorial Finite-Difference Mode Solver for Optical Waveguides with Corners

Y.-C. Chiang and H.-C. Chang
Department of Electrical Engineering, National Taiwan University
Taipei, Taiwan 106-17, Republic of China

The computation of modal fields in dielectric waveguides is fundamental to the analysis of integrated optical devices. Such structure often contains corners, and it is well known that singularities of the fields at corners are manifestations of the vector nature of electromagnetic waves. Accurate modeling of these field singularities with full-vectorial modal analysis is very difficult. Because of the simplicity to implement and sparsity of the resultant matrix, the finite-difference method (FDM) is an attractive numerical method for analyzing the fields in optical waveguides. But corners of optical waveguides are abstruse to model because field singularities occasionally occurring there may cause the finite-difference method not applicable. Some improved formulas have been proposed for this problem, including the introduction of a suitable singularity function in the formulation. In this paper we propose a rigorous full-vectorial finite-difference formulation for treating optical waveguides with oblique or curved step-index interface. We use the new formulations and model the corner as a tiny section of arc to investigate the singular behavior at the corner.

The structure under consideration is a piecewise homogeneous medium with an oblique or curved step-index interface. We assume that there is a curved interface between the mesh point (m, n) and another mesh point nearby, $(m+1, n+1)$ for example. The fields at point $(m+1, n+1)$ can be expressed as the linear combinations (but not the simple Taylor series expansion) of the fields and their derivatives at point (m, n) via the process of two-dimensional Taylor series expansion, local coordinate transformation, and interface conditions matching. The fields at other nearby points can similarly be expressed referring to point (m, n). Finally, these similar relations derived between a mesh point and its eight nearby mesh points are combined and expressed in an algebraic form as $\overline{F} = \overline{\overline{M}} \cdot \overline{D}|_{(m,n)}+$ higher order terms, where $\overline{F}$ is a vector composed of the fields at nine mesh points, $\overline{\overline{M}}$ is the matrix representing the coefficients of the linear combinations mentioned above, and $\overline{D}|_{(m,n)}$ is a vector composed of the fields and their derivatives at mesh point (m, n). The final finite-difference formulas can be obtained after taking the inverse of $\overline{\overline{M}}$.

The proposed formulas have been applied to calculate the E_x^{11} and E_y^{11} modes of a buried square channel waveguide. We model the corner as a tiny section of arc and adopt nonuniform division in the computation domain. The singular behaviors near the corner are investigated. We have also applied the method to a rib waveguide and a passive polarization rotator structure. The results show that the singular behavior appears when the effective radius of the arc that replaces the corner gets small enough, and no additional singular functions need to be introduced in the formulation.

Optical Fiber Designs: Trends, Tradeoffs, and Techniques

A. Safaai-Jazi
Bradley Department of Electrical and Computer Engineering
Virginia Polytechnic Institute and State University
Blacksburg, VA 24061-0111, U.S.A.

The design of optical fibers has evolved from simple step-index fibers to sophisticated structures such as photonic crystal fibers over the past three decades. In the 70s', the main design issues were dispersion and attenuation. The first generation of single-mode fibers were designed to provide negligible chromatic dispersion in the $1.3\,\mu$m window and take advantage of a local attenuation minimum in this wavelength range. However, the lowest attenuation of silica glass occurs at the $1.55\,\mu$m wavelength. This motivated fiber designers to propose a new design, to become known as 'dispersion-shifted fiber', which would provide negligible dispersion in the $1.55\,\mu$m window. This fiber could not have a simple step-index profile, because it required high index differences between the core and cladding and thus high attenuation. This difficulty was remedied by using a triangular index profile or designs with multiple cladding layers.

The continuously rising demand for more information capacity and longer repeater spacing for optical fiber links during the 80s' and 90s' resulted in revolutionary advances in fiber optic technology. The advent of erbium-doped fiber amplifiers satisfactorily solved the attenuation problem, and made all-optical transmission over very long distances a practical reality. The issue of increasing the information capacity, on the other hand, was resolved by implementing wavelength division multiplexing techniques. In fact, several orders of magnitude increase in information capacity has been recently achieved using dense wavelength division multiplexing (DWDM). However, with DWDM the light intensity in the fiber is far stronger than that in a fiber carrying only one optical channel. This made fiber nonlinearity a serious new source of signal distortion. Ordinary dispersion-shifted fibers were found not to perform satisfactorily for DWDM applications. New fiber designs were required to mitigate the nonlinearity. This gave rise to another generation of optical fibers known as 'large effective-area fibers'. It was further realized that with DWDM very small chromatic dispersion allows the four-wave mixing phenomenon to occur which in turn causes more signal distortion. Thus, large effective-area fibers with a limited amount of dispersion were deemed more desirable. With this development, yet another design referred to as 'nonzero dispersion-shifted large effective-area fiber' was introduced.

In addition to attenuation, chromatic dispersion, and nonlinearity, there exists the phenomenon of polarization-mode dispersion that is recognized as another factor limiting the fiber capacity. Can optical fibers be designed to provide low nonlinearity and be free of polarization-mode dispersion? We report recent progress made toward achieving this goal. In designing optical fibers, many requirements need to be taken into consideration, including large effective-area, small bending loss, small absorption and scattering losses, negligible polarization-mode dispersion, small dispersion slope, and a wide wavelength range for single-mode operation. The conflicting nature of some of these requirements necessitates tradeoffs. How can optimum designs be achieved? This presentation also addresses design tradeoffs and optimization techniques such as genetic algorithms. Results for nonzero dispersion-shifted, large effective-area, low loss fibers with zero polarization-mode dispersion due to core ellipticity are presented.

High Power Diode Pumped Lasers

T. F. Morse
Laboratory for Lightwave Technology, The Photonics Center,
Boston University
Boston, MA, U.S.A.

Double clad optical fiber lasers circumvent the restrictions of the brightness theorem by having a single mode core with a larger multimode structure. The multimode structure guides the radiation from the diode. As this radiation interacts with a rare earth doped core, it is absorbed and a population inversion is created in the single mode core. This artifice allows for an increase in brightness (over the original diode source) of at least several orders of magnitude. Powers in excess of 100 W out of a 9 micron core have been reported, and the material limitations of the silica fiber are far from being reached.

We have developed a process for the fabrication of optical fiber lasers that uses an aerosol of organic liquids into which are dissolved the solid organic precursors of the rare earth dopants needed for lasing. With piezoelectric generation of the aerosol at 1.6 MHz, droplet size of the precursor liquid is of the order of 5 microns. This provides the possibility of convective transport of solid materials (dissolved in the liquid aerosol droplets). When these particles encounter a large temperature increase, decomposition results in molecular fragments from which a homogeneous glass is produced. The process is analogous to a sol-gel process, and it is a new way of making glass. We believe this to be the best technique for the fabrication of rare earth doped fiber lasers.

With an ability to fabricate rare earth doped fiber lasers, we have investigated several techniques for laser combining to achieve ultra-high power radiation. Work is in progress in this area. We have previously demonstrated that by combining rare earth doped fibers in a more complex gain structure, that many of the difficulties of phase combination of lasers is avoided. If the laser cavity consists, for example, of 1/2 of a 2×2 fused taper coupler fabricated of erbium doped fiber in a "wishbone" configuration, then with Bragg gratings on each leg of the "wishbone", this complex cavity produces coherently combined radiation, since there is only a single more complex cavity. This process can be extended to higher powers. We believe that it is possible using a combination of a polarizing high power beam splitter and a series of 1/4 wave plates, that a linear cavity can be made that possesses an arbitrary number of ports for end pumping. This is a possible way of combining many individual gain fibers into a single cavity.

Session 1Pb4

Optical Computed Tomography and Optical Imaging

Optical Tomographic Imaging with the Equation of Radiative Transfer

A. H. Hielscher, G. Abdoulaev, A. K. Klose, A. Bluestone, and J. Lasker
Depts. of Biomedical Engineering and Radiology, Columbia University
New York, NY, U.S.A.

Optical Tomography (OT) is a fast developing new medical imaging modality that use near-infrared light to probe various sections of the human body. The light from laser diodes is delivered through optical fibers to several locations on the surface of the body part under investigation. Measurements of backreflected and transmitted light intensities at other positions on the surface are recorded and analyzed. The technology for making these measurements is nowadays readily available and has mainly been applied to breast and brain imaging. However, a major challenge that still remains is the development of efficient numerical schemes that transform these data into useful cross-sectional images of the interior. Unlike x-rays, near-infrared photons do not cross the medium on a straight line from the source to the detector. Besides being absorbed, light is strongly scattered throughout the body. Therefore, backprojection algorithms that are commonly used in computerized tomography (CT) have limited applicability for the tomographic image reconstruction in OT. Furthermore, the reconstruction problem is highly ill posed. Currently, the most promising type of algorithms for OT are so-called model-based iterative image reconstruction (MOBIIR) schemes. These schemes are computationally much more demanding than backprojection methods, but they more rigorously account for the underlying physics of light propagation in tissue. Furthermore, model-based algorithms allow incorporating prior knowledge about the region of interest into the reconstruction process, which makes the problem less ill posed. During this talk I will give a review of state-of-the-art reconstruction techniques for OT and show numerical and experimental results from studies on tissue-phantoms, limbs, finger joints, and brains. An example, for a 3-dimensional reconstruction of changes in oxy- and deoxy-hemoglobin in the human forehead during a Valsalva maneuver ($\sim$ breath hold) is shown in Fig, 1. Challenges and possibilities that this novel imaging modality provides will be discussed, and possible extensions of MOBIIR techniques to other imaging problems in non-medical areas, such as geophysics, nuclear science, and astrophysics are pointed out.

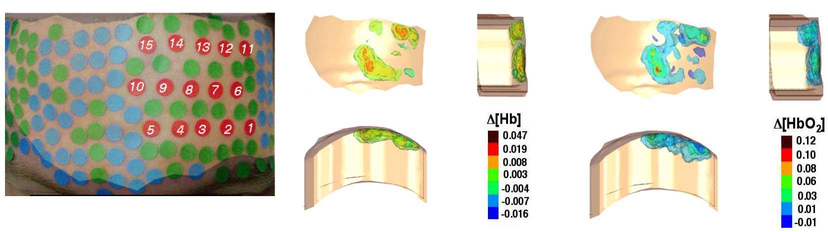

Figure 1: (left) Placement of sources and detectors on forehead. The 15 source/detector position are indicated by the encircled numbers. The lighter shaded area depicts the outer surface of the finite-element mesh, which was used for the volumetric image reconstruction. Reconstructed changes in deoxyhemoglobin (middle) and oxyhemoglobin (right) at maximal signal change during a Valsalva maneuver (breath hold). The changes are given in units of [mM]. Shown are a frontal view (upper left), a side view (upper right), and an aerial view (lower left) of the human forehead.

Multispectral Near-Infrared Tomography For Hemoglobin-Based Imaging of Cancer *in Vivo*

B. Pogue
Thayer School of Engineering, Dartmouth College
Hanover, NH 03755, U.S.A.

S. Poplack
Dept. of Diagnostic Radiology, Dartmouth-Hitchcock Medical Center
Lebanon, NH 03756, U.S.A.

S. Jiang and H. Dehghani
Thayer School of Engineering, Dartmouth College
Hanover, NH 03755, U.S.A.

W. Wells
Dept. of Pathology, Dartmouth-Hitchcock Medical Center
Lebanon, NH 03756, U.S.A.

K. D. Paulsen
Thayer School of Engineering, Dartmouth College
Hanover, NH 03755, U.S.A.

Hemoglobin imaging in tissue is now possible with the use of both multispectral tomographic measurements and model-based reconstruction algorithms. Measurements of diffuse near-infrared light transmission through tissue in multiple overlapping projections, are used to reconstruct the absorption coefficient images at multiple wavelengths. These images are then used to reconstruct concentrations of the chromophores, hemoglobin, oxyhemoglobin, water and lipids which are present in the tissue. The clinical utility of these images is being assessed in a patient trial to assess their predictive value in imaging breast cancer. The results to date include 8 patients with tumors and over 35 normal control patients. Images of both the symptomatic and contralateral breasts will be shown for comparison, suggesting that there is a significant rise in hemoglobin concentration, and hence blood volume within tumor tissue, related to the increase in angiogenesis at the site of the tumor. In this small sample of patients there is a good correlation between the hemoglobin concentration and the pathology assay of epithelial to stromal ratio.

Development of this type of imaging system poses significant challenges both in numerical image reconstruction methodology as well as in multispectral data collection. Recent specific advances our work include 3-dimensional image reconstruction and multi-diode laser imaging capabilities to allow a patient imaging session to be done in less than 5 minutes, and image reconstruction within a few minutes. A summary of clinical data will be presented, along a discussion of where future additions and applications of this technology are going.

Optical Imaging Using Picosecond Time-Resolved Measurements

Y. Yamada
Dept. of Mechanical Engineering and Intelligent Systems, University of Electro-Communications
Chofu, Tokyo 182-8585, Japan

F. Gao, H. Zhao, Y. Tanikawa, Y. Onodera, and A. Sassaroli
Institute for Human Science and Biological Engineering, National Institute of Advanced Industrial Science and Technology (AIST)
Tsukuba, Ibaraki 305-8564, Japan

Light propagation in biological tissues is essentially diffuse, and it is impossible to know the propagation path and pathlength by continuous wave measurements. The measurement using a picosecond time-resolved (TR) technique makes it possible to estimate the optical pathlength in biological tissues. We have used a multichannel TR measuring system consisting of picosecond pulse diode lasers in the near infrared wavelength range, optical switches, multichannel devices combining optical attenuators, fast photomultipliers, miniaturized CFD/TAC modules, A/D converters, and signal acquisition units. With this system we measured the temporal profiles of the diffusely propagated light pulses, and these data were used to reconstruct optical tomographic images and to measure the average optical pathlengths in human heads.

TR transmittances and reflectances of the picosecond light pulses can be measured and incorporated into reconstruction algorithms of optical tomography. The total numbers of the TR measured data are huge and the previous algorithms had difficulty to tackle with such large number of data. We propose two algorithms which can use the TR data. First algorithm uses a modified generalized pulse spectrum (GPST) technique which converts the time-domain data to the complex-frequency-domain data by Laplace transform and inverts the latter data. This algorithm successfully reconstructed the images of both the absorption and reduced scattering coefficients simultaneously from simulated data and from measured TR data for a cylindrical phantom. The second algorithm incorporates the full TR curves and its performances to improve the image qualities have been shown by the reconstructed images from simulated data for a 2D phantom.

Another application of the multichannel TR system is the measurement of the optical pathlength in human heads. The optical pathlengths are much longer than the distance between the source and detector positions, and the ratios of the optical pathlength to the S-D distance (DPF) were measured at various surface areas in human heads. These data are useful for both optical mapping and spectroscopy of brain functions towards the quantitative imaging.

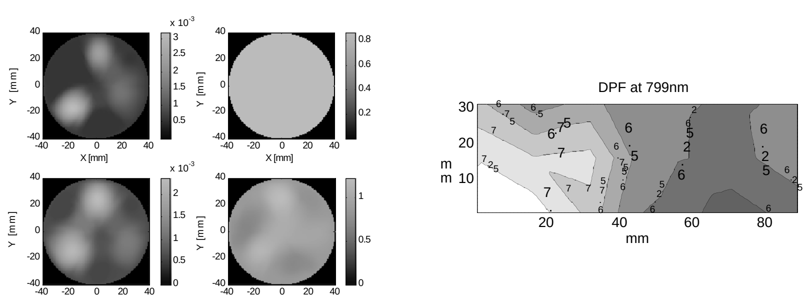

Figure 1: [Left images] Reconstructed images of the absorption (left column) and reduced scattering (right column) coefficients by a conventional (upper row) and modified (lower row) GPST. [Right image] Measured DPF profiles at the right foreheads of eleven human subjects at the wavelength of 799 nm.

Frequency-Domain Optical Mammography: A Novel Imaging Technique to Detect Breast Cancer

S. Fantini, V. Pera, and E. L. Heffer
Bioengineering Center
Department of Electrical Engineering and Computer Science
Tufts University
Medford, MA 02155, U.S.A.

L. Götz, A. Heinig, and S. Heywang-Köbrunner
Martin Luther Universitaet Halle/Wittenberg
Institut für Diagnostische Radiologie und CT
Halle, D-06097, Germany

O. Schütz and H. Siebold
Siemens AG, Medical Technology
Erlangen, 91050, Germany

Optical mammography has a relatively long history as it was first proposed in 1929 and led to diaphanograpy in the 1970's. The potential of optical mammography lies in the sensitivity of near-infrared light to the concentration and oxygen saturation of hemoglobin inside breast tissue. However, the empirical approach of diaphanography resulted to be strongly operator-dependent and yielded a large number of false positive cases. Recent developments in the field of light propagation in tissues have led to the introduction of time resolved methods, where the light emission is not constant with time (as in diaphanography) but is either pulsed (time-domain) or harmonically modulated (frequency-domain). This advance, in conjunction with the use of a physical model to describe light propagation in breast tissue, allows for a more quantitative and rigorous approach to optical mammography.

We present clinical results obtained with a prototype for frequency-domain optical mammography developed by Siemens Medical Engineering. This instrument operates at a modulation frequency of 70 MHz and uses laser diodes at four different wavelengths (690, 750, 788, and 856 nm) as light sources. The breast is slightly compressed between two glass plates. The optical mammogram is obtained by performing a planar tandem scan of the source and detector optical fibers that are located on opposite sides of the breast (transmission geometry). The raw frequency-domain optical data (amplitude and phase) are processed using an algorithm that minimizes edge effects resulting from the breast geometry. The edge-corrected image (that we call N-image) is further processed to enhance the contrast of the optical mammograms. Finally, the spectral information (from images at four wavelengths) is used to obtain an estimate of the oxygenation of the detected breast lesions.

We studied the optical mammograms collected on a clinical population of patients having breast abnormalities. In each case, we know the size, location, and type of tumor from x-ray mammography, fine needle biopsy, or histology. We have performed analyses aimed at obtaining ROC (receiver operating characteristic) curves [i.e., sensitivity vs. (1-specificity)] for the N-images, the contrast-enhanced images, and the spectral images.

The contrast-enhanced N-images confirm the capability of frequency-domain optical mammography to detect breast tumors with high contrast. The results of our spectral analysis (limited to the four wavelengths at which data were collected) indicate that spectral information may provide useful indications about the benign or malignant nature of breast lesions.

Optical Topography – Visualization of Brain Activation by Near-Infrared Spectroscopy

T. Yamamoto and A. Maki
Advanced Research Laboratory, Hitachi, Ltd.
Hatoyama, Saitama 350-0321, Japan

Y. Tanikawa
National Institute of Advanced Industrial Science and Technology
Namiki, Tsukuba 305-8564, Japan

M. Kiguchi
Advanced Research Laboratory, Hitachi, Ltd.
Hatoyama, Saitama 350-0321, Japan

E. Okada
Department of Electronics and Electrical Engineering, Keio University
Hiyoshi, Yokohama 223-8522, Japan

Y. Yamada
Department of Mechanical Engineering and Intelligent Systems, University of Electro-Communications
Chofu, Tokyo 182-8585, Japan

H. Koizumi
Advanced Research Laboratory, Hitachi, Ltd.
Hatoyama, Saitama 350-0321, Japan

Methodology of optical topography (OT) was proposed to visualize the brain activation in the cortex[1]. The method is based on near-infrared spectroscopy (NIRS) to estimate blood volume change in the cortex associated with the brain activation. Array of optodes is arranged on the scalp in the 30 mm-interval like the grid, the reflected intensity change is detected. Then, the topographic image of the brain activation is obtained. Subjects just wear the helmet with optodes; the method is applicable for the subjects with moving. Topographic images of the language function activation and paroxysm of epilepsy were obtained.

The effective optodes arrangement was examined to improve the spatial resolution of the topographic image. Light is strongly scattered by the living tissue (skull, for example), the pair of optodes detects the blood volume change in the wide area. Though the optodes are arranged in high density, there is a limit to improve the resolution. The measuring method with two faces of optodes array was proposed. Additional optodes are arranged in the midpoint of optodes pair. An adult head phantom was prepared; the phantom also simulates the brain activation. The activation was reconstructed to the topographic image; resolution of the image was investigated and the efficacy became clear.

REFERENCES

1. Koizumi, H., et al, "Higher-order brain function analysis by trans-cranial dynamic near-infrared spectroscopy imaging," *J. of Biomed. Opt.*, Vol. 4, 403–413, 1999.

Near Infrared Spectroscopy Used *In Vivo* for Tumor Oximetry and Assisting Neurosurgery

H. Liu
The University of Texas at Arlington
Arlington, Texas, U.S.A.

C. A. Giller, R. P. Mason
The University of Texas Southwestern Medical Center
Dallas, Texas, U.S.A.

This presentation demonstrates the development of Near Infrared (NIR) spectroscopy for two particular clinical applications. The first one is to show the feasibility of a novel application of NIR spectroscopy for tumor oximetry. The second one is for precise mapping of neural structures during neurosurgery performed to alleviate symptoms of Parkinson's disease.

It is known that hypoxic tumor cells are relatively more resistant to radiotherapy, chemotherapy, and photodynamic therapy. Measurement of oxygen tension (pO_2) of tumor tissue or saturation of oxygen (SO_2) in blood of the tumor vascular bed could be valuable for optimizing treatment plans. We have used our recently developed, frequency-domain system to measure changes in hemoglobin oxygen saturation and total concentration in the vascular bed of rat prostate and breast tumors *in vivo* non-invasively and in real-time. For comparison, tissue pO_2 values of the tumors were also measured using ^{19}F NMR EPI of hexafluorobenzene, which provides regional tumor oxygenation tension at millimeters resolution. These measurements were taken while the inhaled gas was alternated between air and carbogen (95% O_2, 5% CO_2). Both techniques showed significant changes in tumor oxygenation accompanying respiratory challenge, with changes in vascular SO_2 preceding tissue pO_2 change. These changes in SO_2 could be modeled with two exponential components yielding two time constants. Using the Fick Principle, we further derived a simplified model to relate the time constants to tumor blood perfusion rates. This study demonstrates that the NIRS technology can provide an efficient, real-time, non-invasive means for monitoring vascular oxygenation dynamics of tumors and facilitate investigations of tumor vascular perfusion.

For the seond application, we have designed and implemented a portable optical system, which includes a miniature spectrometer, a 30-cm-long fiber optic reflectance probe, and a lap-top computer for data acquisition and real-time display. Our 1.3-mm-diameter probe contains seven 100-μm fibers, one delivering light and six collecting the reflected light from the human brain to the spectrometer. During surgery, the probe was placed against the surface of the brain, and the spectrum between 450-850 nm was recorded. Measurements were repeated at 1-mm increments from the surface of the brain to 70-mm deep near the targeted lesion. The measured reflectance from the brain can be used to identify gray or white matter by calculating the spectral slope between 700-850 nm. The capability of differentiating gray and white matter allows us to localize the lesion accurately. The neural structure maps obtained from the optical method are in good agreement with the corresponding MRI images. Furthermore, we have further developed analytical expressions to quantify the optical properties of the brain tissue, and thus to determine regional hemoglobin oxygen saturation in the brain. Both Monte Carlo simulations and *in vitro* experimental results support our close-form expression.

Measurement of Skin Colors of World Population and its Applications of Cosmetics Products

S. Takata
Product Deveropment Center, Shiseido Research Center
Yokohama, 224-8558, Japan

M. Akimoto
Institute of Science and Technology, Kanto Gakuin University
Yokohama, 236-0032, Japan

M. Miyakawa
Department of Biocybernetics, Faculty of Engineering, Niigata University
Yokohama, 950-2181, Japan

The expression of skin color is an extremely important element in the evaluation of cosmetics. Skin color differs largely depending on sex, age, or race, and it has been pointed out that the data reported so for has not necessarily been adequately quantitated. There are also large discrepancies due to a difference in measuring instruments, while reliable measurement values have been sought. In this study, we attempted to analyze the skin color of women from the world using identical conditions. The skin colors of women over the world were measured to clarify the characteristics of skin color. The data were used to design new cosmetics in consideration of the optical properties of skin.

A total of 1703 women at 20-40 years of age including Caucasian, Mongoloid, and Negroid were used for color evaluation at an identical skin site. The skin colors at right and the left sites on the check and the forehead were determined under the same conditions for a period as long as seven years from 1992. Skin color measurement was performed by using a spectrometric colorimeter. Spectra reflectance was measured for each interval of 10 nm in a range of 400 700 nm. The light reflected from an area of approximately 12mm in diameter is received. The contact pressure was kept constant to minimize the measurement error due to the head contact with the skin.

The mean value of Munsell scale was 3.1YR6.4/3.7 for the Caucasian women, 4.9YR6.2/3.8 for the Mongoloid, and 4.8YR4.1/3.4 for the Negroid. The Caucasian women's skin was more reddish than the other. The mean lightness of Negroid women's skin was lower by about two than either lightness of Caucasian and Mongoloid women, showing that the former skin was different from the latter two in respect of skin lightness. The skin color differences among races were well reflected in these values. These facts suggest that melanin pigment and blood hemoglobin in the skin might be the important determinants of skin color. Quantitative evaluation was made to clarify the effects of melanin pigment and hemoglobin on skin color. Conventionally, erythema and melanin indices have been well known as such determinants. These determinants were defined on the basis of pigment absorption, which varies with wavelength, but no data of all visible light range were taken into consideration. Therefore, we modified those conventional indices and defined new respective indices which reflect various spectral information of whole visible region. There was very close correlation between the factors related to melanin and hemoglobin, indication that skin color differences between Caucasian and Negroid women could be expressed with two factors as to hemoglobin and melanin. The present results were applied to formulate new cosmetics in consideration of the optical properties of skin.

It was demonstrated that the skin color can be expressed with two factors; hemoglobin factor and melanin factor. The present results were applied to formulate new cosmetics in consideration of the optical properties of skin. We succeeded to produce highly effective make-up foundations applicable to the skin of any colored women in the world. Thus, it became possible to correct the skin problem and produce translucent and beautiful skin of high lightness by using make-up cosmetics formulating the two novel powders.

Session 1Pc5

Subsurface Imaging and Reconstruction

Assessing the Degree of Non-Linearity and Retrievable Information in Location and Imaging of Buried Objects

O. M. Bucci
Dipartimento di Ingegneria Elettronica e delle Telecomunicazioni and Istituto per il Rilevamento Elettromagnetico dell'Ambiente IREA-CNR
Napoli, Italy

L. Crocco
Istituto per il Rilevamento Elettromagnetico dell'Ambiente IREA-CNR
Napoli, Italy

T. Isernia
Dipartimento di Ingegneria Elettronica e delle Telecomunicazioni
Napoli, Italy

Microwave techniques have gained a great deal of attention in subsurface sensing applications owing to their non invasive capabilities. Whenever there is the need of an accurate quantitative reconstruction of the region under test, such as for example in demining applications, the problem can be formulated as an inverse scattering one. As it is well known, this kind of problems are already ill-posed in case the unknown scatterers are located in free space. The situation is still worse in the subsurface sensing case, in which available data are unavoidably aspect limited. This lack of information, together with the non-linear nature of the problem, implies that a particular care has to be taken in the development of solution procedures.

In order to assess the kind of non-linearity of the problem (which affects possible approximations and overall difficulty) and to get an understanding of the kind of information which can be effectively retrieved we preliminary addressed the canonical problem of accurately locating and imaging dielectric objects buried in a (possibly lossy) half space.

As a first step, we deeply investigated the sources of non-linearity of the problem, and new tools were developed for quantifying the 'degree on non-linearity' of the problems at hand as a function of the properties of the permittivity distribution and of characteristics of the background.

On the other side, we focused our attention to quantifying the maximum amount of information one can get by single frequency scattering experiments, as well as to qualifying the kind of information one can get about the unknown permittivity distribution. To this end, it proves fruitful to refer to the Singular Value Decomposition (SVD) of the operator A_e relating the primary sources to the incident fields, and of the operator A_a relating the induced currents to the anomalous fields. By definition, the singular values σ_n and the singular functions u_n, v_n, of A_e obey the relationships: $A_e u_n = \sigma_n v_n$, and $A_e^+ u_n = \sigma_n v_n$ wherein A_e^+ is the adjoint of A_e. As a consequence, the left singular functions u_n are a convenient basis for the primary sources, and the right singular functions v_n a convenient basis for the incident fields. Moreover, it is simple to prove that A_a admits the same decomposition of A_e, but with reversed roles of u_n and v_n. As a consequence, u_n are also a convenient basis for the scattered fields, and v_n a useful basis for the induced currents. By using the u_n as primary sources, and projecting the corresponding scattered fields onto the u_n as well, it turns out that the overall inverse scattering problem can be conveniently formulated in term of a 'scattering matrix' which encodes all possible information arising from scattering experiments.

Due to the behavior of the singular values σ_n, the scattering matrix has an essentially finite number of terms. This number allows to quantify the maximum amount of independent information one can collect. Then, analysis of the expression of the elements of the scattering matrix, and behavior of the singular functions v_n, also allows to understand the kind of permittivity distributions which can be actually retrieved when solving the inverse problem. It comes out that the class of permittivity functions which can be accurately retrieved exhibit intrinsic multiresolution properties, which suggest suitable modifications to classical solution schemes exploiting Fourier analysis.

Subsurface Imaging and Time Domain Numerical Simulation Techniques

F. Akleman and M. O. Ozyalcin
ITU Department of Electronics & Communication Engineering
Istanbul Technical University
Maslak/Istanbul, 80626, Turkey

L. Sevgi
Electronics & Communication Engineering Department
Engineering Faculty, DOĞUŞ University
Acıbadem, 81010 Kadıkoy, Istanbul, Turkey

Landmines and unexploded ordnance are among the top world wide public concern. They are significant barrier to economic and social development in many parts of the world, seriously affecting countries such as Vietnam, Cambodia, Laos, Afghanistan, Middle East, Armenia, Iraq, Bosnia, etc. The UN lists nearly 70 countries affected by mines, where more than 100,000,000 mines are estimated to be buried in the ground.

Detection and clearance of buried mines and unexploded ordnance is a crucial and urgent humanitarian as well as a military problem. The problem is aggravated by the wide usage of cheaper plastic mines and explosives with little metal content. While mine fielding is a quick, safe and cheap process, humanitarian demining is slow, dangerous and expensive. Dense vegetation and erosion are the most common obstacles to demining, which make systematic clearance almost impossible. Experts say that demining and clearance may take approximately 500 years with today's technologies. Because of all these, world wide efforts have been put on developing better devices and/or techniques for demiming and clearance.

Humanitarian demining efforts still rely almost exclusively on metal detectors, dogs and manual probing. The main problem in practical realization of mass scale of demining and clearance are; (i) unacceptable rate of false alarms of almost all available sensors, (ii) unacceptable lower speed. Detection of land mines with variety of shapes, materials, weight, etc. necessiates (i) to picture subsurface as clear as possible (ii) to distinguish targets from noise, clutter and interfering objects. To achieve these, understanding subsurface EM characteristics is a must.

Ultra wide band (UWB) ground penetrating radar (GPR) is one of the most promising technologies for detection and identification of buried landmines. The operational parameters of the GPR depends on particular application, mostly the kind of mine one is looking for, its size, shape and depth, electrical properties of both mine and soil. One should compromise between resolution and detection depth, since they require higher and lower operating frequencies, respectively.

In this invited presentation, theoretical and practical studies in Turkey will be discussed. First, two time domain numerical simulation techniques will be outlined in relation to subsurface imaging. Two GPR algorithms, which are based on the Finite-Difference time-Domain (FDTD) and Transmission Line Matrix (TLM) techniques were prepared to simulate UWB subsurface imaging. The effects of absorbing boundary simulations, plane as well as cylindrical wave excitations on subsurface imaging have been investigated. Extensive amount of different scenarios have been tested. These numerical simulation issues will be discussed in detail. Then, the problems and the results of, and experience gained from a three-year Turkish project in designing and realising a portable multi-sensor detector will be outlined (the project was given to TUBITAK-MRC, Marmara Research Center by the Ministry of Defense, R&D Department, started in 1997 and its first phase ended in 2000).

Time Domain Forward Computational Models of Complex Dispersive Media for Subsurface Sensing Applications

C. Rappaport
Northeastern University
Boston, MA 02115, U.S.A.

In time domain modeling of lossy, dispersive background media (such as biological tissue or soil) for subsurface imaging and detection applications, the electric flux and the current are convolutions $\epsilon(t)$ and $\sigma(t)$ with $E(t)$ respectively. To avoid these memory-intensive computations, the convolutions can often be accuracy and simply modeled as second order difference equations. In particular, by matching the corresponding Z-transform of the E-field/current (or E-field/flux) relation to an approximation of frequency-dependent conductivity (or dielectric constant) results in a ratio of polynomials (a rational function) in Z^{-1} (where $Z = \exp[j\omega\Delta t]$). Using a 1-pole/2-zero model, it is possible to find a good fit to measured tissue data over almost two decades in frequency. Since the Z-transform variable corresponds to a unit time delay in the time domain, using this type of dispersion model fits the FDTD algorithm well. The only modeling error occurs in fitting the measured dielectric parameters values to the rational function; not in the time discretization.

It has been found that choosing a constant average value of real permittivity $\epsilon(t) = \epsilon_{\mathrm{Av}}$, and fitting conductivity to the rational function $\sigma(Z) = (b_0 + b_1 Z^{-1} + b_2 Z^{-2})/(1 + a_1 Z^{-1})$, leads to wave propagation characteristics (velocity and attenuation) that match those of the measured values to within 15%. The standard FDTD Courant stability test is modified for this choice of dispersion model. The stability test involves finding the roots of a third degree polynomial for all frequencies of interest, and ensuring that these roots remain within the unit circle. With judicious parameter selection it is possible to maintain stability for most of the media investigated for various time steps.

As an example, for high water content biological tissue in the frequency range 200 MHz–10 GHz, the choice of b_0=77.3845, b_1=-129.99, b_2=52.743, a_1= -0.8785, and ϵ_{Av}= 8.437 gives errors of 4% in velocity and 10% in decay rate. This compares with 12% and 70% modeling error respectively for the simple minded nondispersive model.

A low-order model of this type is needed for fast and efficient modeling of short pulse excitations for wave-based medical imaging, and ground penetrating radar underground sensing applications. Ignoring dispersive media effects in a computational model can lead to errors that are greater than the perturbative scattering of a small or low-contrast target.

Location and Imaging of Homogeneous Objects Buried in a Realistic Soil

O. M. Bucci
Dipartimento di Ingegneria Elettronica e delle Telecomunicazioni,
Università di Napoli Federico II
Napoli, Italy

L. Crocco
Istituto per il Rilevamento Elettromagnetico dell'Ambiente IREA-CNR
Napoli, Italy

T. Isernia
Dipartimento di Ingegneria Elettronica e delle Telecomunicazioni,
Università di Napoli Federico II
Napoli, Italy

When tackling the canonical problem of reconstructing an unknown permittivity profile embedded in an homogeneous half space, several circumstances have to be taken into account. First, the fact we deal with an essentially finite amount of independent information implies that only a finite dimensional representation of the unknown permittivity can be hopefully retrieved. Second, the class of permittivity distributions which can be effectively retrieved exhibit intrinsic multiresolution properties. Finally, the possible occurrence of false solutions is greatly reduced by using, in the representation of the unknown, a number of parameters as low as possible.

Taking into account the above results, we developed a solution scheme which makes use of a wavelet representation of the unknown permittivity distribution. This choice allows to take into account in a natural and effective fashion the expected multiresolution properties of the class of retrievable functions, with beneficial effects on both ill conditioning and false solutions problems. Moreover, the use of wavelets also can allow 'synthetic zooming' operations, which also implies an optimal use of the finite amount of independent data one deals with. These choices already allow considerable ameliorations with respect to more classical processing schemes. On the other side, the approach as developed up to now did not exploit the fact that in many cases the sought target is characterized by a constant (possibly unknown) permittivity. Moreover, the developed tools did not take into account the fact that the interface is not actually planar.

In order to deal more effectively with the case of homogeneous scatterers we added to this approach a regularization scheme which exploits the homogeneous nature of the target. The approach allows to achieve a clear, well defined and quantitatively accurate image whereas the usual approach only furnishes a 'smoothed' image of the inclusions under test.

Starting from this basis, in this communication we deal with the case of targets buried in a more realistic environment. Accordingly, we introduce several complications to our model such as for instance a rough air-soil interface and the presence of targets which are not the object of the survey.

To cope with this problem we modify the regularization approach of in such a way that different homogeneous permittivities are looked for in different parts of the region under test. In the (preliminary) 2-D case we deal with, we are able to achieve a quantitative reconstruction of the target and, at the same time, a "coarse" reconstruction of the non planar interface profile, which allows a better estimation of the target with respect to the canonical half space scheme.

The developed approach brings to satisfying quantitative reconstruction and appears to be robust in rejecting clutter and false targets also in cases wherein objects having the same dimensions and permittivity of plastic landmines are considered.

Adaptive Approaches to Rough Surface Underground Imaging - I: Interface Profile Reconstruction

V. Galdi†, J. Pavlovich, W. C. Karl, D. A. Castañon, and L. B. Felsen
Boston University
Boston, MA 02215, U.S.A.

In ground penetrating radar (GPR) applications, a major source of variability in the observed signals is due to the distortion introduced by the twice-traversed rough air-ground interface, which the interrogating signal encounters on its way to and from the targets of interest.

In this two-part sequence, with particular reference to anti-personnel plastic land mine detection/classification, we present an adaptive framework for subsurface sensing in the presence of a moderately rough air-soil interface. The proposed approach is based on the use of physical and statistical modeling techniques to estimate, and compensate for, the related clutter, it works with sparse data, and it is built on recently developed Gabor-based narrow-waisted Gaussian beam (GB) fast forward scattering models [1].

Here, in the first part, we deal with the prior (coarse-scale) interface estimation problem, which, by exploiting the GB fast forward models, is posed as a nonlinear optimization problem [2, 3]. Algorithmic aspects, accuracy and computational issues are discussed, with presentation of examples for both frequency-stepped and pulsed GPR configurations.

These results set the stage for the adaptive underground imaging techniques discussed in Part II [4].

REFERENCES

1. V. Galdi, L.B. Felsen, and D.A. Castañon, *IEEE Trans. Antennas Propagat.*, vol. 49, No. 9, pp. 1305-1314, Sept. 2001; ibid, “Quasi-ray Gaussian beam algorithm for short-pulse two-dimensional scattering by moderately rough dielectric interfaces,” submitted to *IEEE Trans. Antennas Propagat.*,Apr. 2001. See also our paper in Session “Gaussian beams for efficient computation of propagation and scattering in complex environments,” organizers: L. B. Felsen and V. Galdi.
2. V. Galdi, D.A. Castañon, and L.B. Felsen, “Multifrequency reconstruction of moderately rough interfaces via quasi-ray Gaussian beams,” to be published in *IEEE Trans. Geosci. and Remote Sensing*, 2002.
3. V. Galdi et al., “Moderately rough dielectric interface reconstruction via short-pulse quasi-ray Gaussian beams,” submitted to *IEEE Trans. Antennas and Propagat*, Oct. 2001.
4. V. Galdi et al., “Adaptive approaches to rough surface underground imaging – II: Target reconstruction,” this Conference.

† also with University of Sannio, Benevento, Italy

Adaptive Approaches to Rough Surface Underground Imaging – II: Target Reconstruction

V. Galdi†, H. Feng, D. A. Castañon, W. C. Karl, and L. B. Felsen
Boston University
Boston, MA 02215, U.S.A.

Having established in the first part of the presentation [1] the possibility of reconstructing the coarse scale profile of the air-soil rough interface from sparse backscattered field observations, this second part is concerned with the *target imaging* in the presence of a known roughness profile. In particular, we focus on the important and challenging case of shallowly-buried low-contrast mine-like targets.

The proposed approach is based on an approximate Born-linearized forward model for the target scattering, wherein the distortion introduced by the twice-traversed roughness profile is accounted for by using previously developed Gabor-based quasi-ray fast forward solvers [2]. The resulting reconstructed interface profile is used to correct the raw backscattered field data observed at the receivers so as to compensate for the corresponding clutter; at this stage, statistical models can be used to account, in addition, for noise, estimation error and residual unmodeled effects.

The forward scattering model is finally inverted to retrieve the unknown dielectric permittivity contrast in a suitable test domain. In this connection, use is made of pixel-based and object-based regularization and reconstruction techniques [3].

Numerical implementations of the algorithms are discussed and interpreted, with performance examples presented for both frequency-stepped and pulsed excitations.

REFERENCES

1. V. Galdi et al., "Adaptive approaches to rough surface underground imaging – I: Interface profile reconstruction," this Conference.
2. V. Galdi, L.B. Felsen, and D.A. Castañon, *IEEE Trans. Antennas Propagat.*, vol. 49, No. 9, pp. 1305-1314, Sept. 2001; ibid, "Quasi-ray Gaussian beam algorithm for short-pulse two-dimensional scattering by moderately rough dielectric interfaces," submitted to *IEEE Trans. Antennas and Propagat.*, Apr. 2001.
3. V. Galdi, et al., "Moderately rough surface underground imaging via short-pulse quasi-ray Gaussian beams," submitted to *IEEE Trans. Antennas and Propagat.*, Oct. 2001; ibid, "Multifrequency subsurface sensing in the presence of a moderately rough air-soil interface via quasi-ray Gaussian beams," submitted to *Radio Science*, Oct. 2001.

† also with University of Sannio, Benevento, Italy

3-D Physics-Based Underground Imaging via Edge-Preserving Regularization

J. Pavlovich, W. C. Karl, V. Galdi†, D. A. Castañon, L. B. Felsen
Boston University
Boston, MA, U.S.A.

Detection, localization and classification of shallowly-buried plastic objects via ground penetrating radar (GPR) is a challenging problem, with many potential applications. Prominent among them are humanitarian applications, such as anti-personnel landmine remediation.

In this paper, we address the problem of subsurface imaging of shallowly-buried plastic mine-like objects via ultra-wideband (UWB) GPR. The proposed approach relies on an approximate, Born-linearized, three-dimensional forward scattering model. In this preliminary investigation, the air-soil interface roughness is neglected, and the needed half-space dyadic Green's function is efficiently approximated via ray optics.

The data is preprocessed with a robust adaptive filter to suppress the ground reflection and other spurious contributions in the received backscattered waveforms, thereby isolating the subsurface target scattering. Next, the linearized forward scattering model is used to invert this preprocessed data and obtain the three-dimensional distribution of the unknown dielectric permittivity contrast. The inversion process suppresses noise and spurious structure through the incorporation of prior information on the field in the form of edge and negativity preserving penalties. The resulting reconstructions have good energy localization and are computationally efficient.

The proposed approach has been validated and calibrated against real GPR data, collected at Northeastern University test-bed facility in Dedham, MA, using a recently developed forward-looking UWB GPR system [1].

REFERENCES

1. C.M. Rappaport et al., ”Hand-held forward-looking focused array mine detection with plane wave excitation”, in *Detection and Remediation Technologies for Mines and Minelike Targets V, Proc. SPIE*, vol. 4038, pp.1118-1126, Aug. 2000.

† also with University of Sannio, Benevento, Italy

Adjoint-Field Methods for Shape-Based and Image-Based Diffuse Wave Inverse Problems

G. Boverman and E. L. Miller
Northeastern University
Boston, MA 02115, U.S.A.

Research interest in Diffuse Optical Tomography (DOT) has been increasing steadily in recent years. This imaging modality offers the prospect of a new method for the detection and classification of tumors in the breast, as well as a means of functional brain imaging with very high temporal resolution and potentially strong spatial resolution as well. However, there are significant research challenges in terms of signal processing, modeling, and inversion that must be overcome before this clinical potential is realized. Specifically, accurate and fast physical models for the transport of light within tissue must be developed, and regularization methods are needed for the ill-posed inverse problem.

Over the last year and a half, we have addressed both of these issues. First, we have developed a highly efficient, preconditioned Krylov subspace algorithm for solving the forward DOT problem, a 3D frequency domain diffusion equation. Using this code as a base, we have developed two regularized, fully three dimensional inversion methods. The first, is an imaging approach based on the nonlinear conjugate gradient method, and produces a fully voxelated reconstruction of the region under investigation. Exploiting the fact that in many DOT applications one is primarily interested in localizing and characterizing small anomalous regions, we have also synthesized a "shape" based inversion routine designed to determine the position, size, and contrast of that homogeneous sphere which best localizes an underlying anomaly. Both of these methods make great use of adjoint field calculations for gradient computations. In the poster accompanying this abstract, we shall elaborate on the details of our algorithms and provide results using simulated data.

Finally, an area of some interest in the application of DOT for brain imaging is the accuracy of the diffusion model. For the brain application, the presence of non-scattering regions implies that this model, which is a simplification of the true transport-based physics is not strictly correct. Work to date has not resolved whether such modeling errors have a significant impact specifically on shape-estimation types of inversion routines. Results from a study in which we use transport generated synthetic data in our diffusion-based inverse shape routine will also be presented.

Session 1Pa6

Flat Reflector Antennas for Space Applications

Multi-Beam Reflectarrays

J. A. Encinar and J. A. Zornoza
Polytechnic University of Madrid
Madrid, Spain

Microstrip reflectarrays are a type of antennas that combine the advantages of reflectors and phased arrays. Comparing to phased arrays, the reflectarray eliminates the complexity and losses of the feeding network and exhibits a higher efficiency. Reflectarrays are easier to manufacture than reflector antennas and present less cross-polarization at the cost of a narrower bandwidth. Multilayer printed reflectarrays made of stacked rectangular patch arrays have been proposed to overcome the narrow band limitation [1]. In that configuration, the phase of the reflected field is controlled by adjusting the dimensions of the patches. In addition, reflectarrays can perform several functions that reflectors cannot, such as multi-beam patterns with a single feed or change from linear to circular polarization, based on a local full phase control for each polarization.

Multi-beam reflectarray applications are investigated in this work. First, multi-beam reflectarrays are designed assuming a unique feed. The phase corresponding to the superposition of several beams was obtained on the surface of a reflectarray illuminated by one feed, and a multi-beam radiation pattern was achieved. Due to the constraint on the amplitude distribution, the side lobe levels were high (-10dB), but they can be reduced by phase-only optimizations. When the several beams are close one to each other, a contoured beam is obtained. This technique has been used to get a starting phase distribution for contoured beam applications.

As a particular case, a reflectarray with two beams separated 55^o at 11.95 GHz has been designed, built and measured with satisfactory results. Both, frequency and angle between beams correspond to the TV channels of ASTRA and HISPASAT satellites seen from Madrid.

For multiple beam applications with different channels, such as those used in communications with frequency reuse, a cluster of feeds can be used, in a similar way than in multi-fed reflectors. Then, the reflectarray is designed to generate a beam associated to each feed. For this problem, the feed positions have been optimized in order to minimize aberrations due to the feed defocusing. For further improvements, not only the feed positions but also the patch dimensions on the reflectarray can be optimized.

REFERENCES

1. J. A. Encinar, "Design of two-layer printed reflectarrays using patches of variable size," *IEEE Trans. Antennas and Propagat.*, Vol. 49, No. 6, pp. 1403-1410, Oct. 2001.

Reflectarrays Technologies for Space Applications

J. M. Andrés Matey
EADS CASA Space Division
Madrid, Spain

J. Vassal'lo
CSIC, Institute of Applied Physics
Madrid, Spain

Reflectarrays are becoming a mature technology for earth based antenna applications. They can substitute parabolic reflectors and they are mainly presented in a flat design.

Electrical design studies show that flat reflectarrays can constitute a design alternative to parabolic reflectors for space applications. Now is the time that structural, mechanical and thermal studies show if this technology can be implemented on space systems and be competitive.

Flat reflectarrays implementations could provide several advantages with respect to conventional space parabolic reflectors:

- They do not require specific moulding tools as parabolic reflectors. They are reusable and consequently the cost can be low.
- The structure implementation on space applications of planar surfaces have lower thermoelastic distortions with a better control than in the case of curved surfaces.
- A reflector surface in the range from 5 to 20 m in diameter, is demanded at this moment for space environment. Large flat reflectors can be designed in a number of tiles that can be stored in compact size when folded away for launching, and they can be deployed to final size and shape once in space.
- Reflectarrays technologies for space applications would require space qualified materials and structural schemes able to withstand launching and in-orbit thermo-mechanical environments. The technologies developed for planar array antennae can be use for the purpose as they have already been implemented in space systems and they provide a number of technological solutions for large flat reflectarrays: space qualified materials and components, multilayer circuits, support structure designs and deployable panels. An example of this technology is the ASAR antenna of the ENVISAT platform, having a radiating surface of 1.5×10 m.

The aim of this contribution is to present a review of the structural problems of flat reflectors technology, showing drawbacks and advantages versus different electrical solutions and applications.

The work described in this contribution is sponsored by the Spanish Ministry of Science and Technology (TIC2000-0401-P4-09).

Performance Review of Fresnel Zone Flat Reflectors

A. Pedreira
Polytechnic University of Madrid
Madrid, Spain

J. Vassal'lo
Institute of Applied Physics, CSIC, Madrid
Madrid, Spain

The basic technology of flat reflectors with reflectors Fresnel zones is known many years ago, but its application presents a serious drawback of loss of gain and bandwidth, to be compared with parabolic reflectors. It makes difficult its selection as an antenna candidate of any development.

On the contrary, parabolic reflector technology had many years of experience and it is successfully verified. So, designers, manufacturing companies and costumers reject not experimented alternative concepts, because they do not like to assume risks on this antenna market.

In the case of space applications, the cost could not be a great problem. Any technological concept could be considered as an alternative if it will be possible to reduce the time of the manufacturing process. But it is not an easy task, because the manufacturing process of parabolic reflectors are very well optimised.

The solution to the use of Fresnel Zone Flat Reflectors on space applications, could be to provide a kind of performance that was not possible to supply by parabolic reflectors. One of them could be to generate simultaneous beams, or to provide a separation of feeders versus frequency sub-bands.

The aim of this paper is to present a review of the state of the art of this kind of reflector, making a comparison with parabolic reflectors and reflectarrays performance, in order to know the possibilities of this technology.

Element Design Methodology for Printed Reflectarray Antennas

J. Huang
Jet Propulsion Laboratory, California Institute of Technology
Pasadena, CA 91109, U.S.A.

The printed reflectarray antenna has recently been paid attention by many researchers. Its flat or slightly curved reflecting surface can be conformally mounted onto existing supporting structure with relatively small incremental mass and volume. With a proper phase design or phase changing device incorporated into each element of the reflectarray, the main beam can be tilted or scanned to large angles from the aperture broadside direction. Another significant advantage of the reflectarray is that it can perform as a high-gain phased array with thousands of elements but without any complicated beamforming network and expensive transmit/receive amplifier modules. Many researchers have developed reflectarrays with good pattern performance, such as side-lobe level and cross-pol level. However, to achieve reasonable aperture radiation efficiency (above 40%) remains to be a challenge for reflectarray designers.

The efficiency of a reflectarray is primarily governed by its element design. There are several element types for printed reflectarrays such as the ones that use variable element size to achieve the desired phase change, the ones that use identical element size but with different-length phase-delay lines attached, and those that use identical elements but variable rotational angles (circular polarization only). No matter what element type is used, in order to achieve good radiation efficiency, one must pay attention to the following three factors when designing reflectarray elements. First, one must characterize the phase change versus the element change (size change, phase delay line length change, or rotation angle change). In other words, a curve for the amount of phase change versus the amount of element change should be generated. Second, as element phase changes, its radiation amplitude should not be sacrificed. For an example, the input impedance of a patch element should be matched to its attached phase delay line. Third, as element phase changes, the change in element's resonant frequency should be minimized. Several mathematical methods can be used to predict theses three factors. These are element radar cross-section calculation, infinite array computation, or waveguide simulator calculation. A more detailed discussion on these element design methodologies will be given during the presentation.

Analysis of Periodic Structures with Cross Dipole Metallizations and Its Application to Multi-Frequency Reflectarrays

A. Pedreira and J. A. Encinar
Polytechnic University of Madrid
Madrid, Spain

A printed reflectarray is an array of microstrip patches on a grounded substrate with a certain tuning to locally control the phase of the reflected field when illuminated by a feed. Rectangular and cross dipole patches have been used, and the phase control has been achieved by adjusting the patch dimensions [1]. For dual-frequency applications, a two stacked array configuration was proposed [2]. Another alternative for multiple-frequency applications is to use several printed elements in the same periodic cell, each of them resonating at an individual frequency. For that purpose, cross dipoles are preferred because of their small surface.

In this work, a Spectral Domain Method of Moments has been implemented to analyze a periodic array composed of several crosses and/or dipoles of different sizes in the periodic cell. The metallizations are defined in a general way, which allows combinations of both dipoles and crosses with the only limitation of being parallel to the lattice axes. The method accounts for any mutual coupling between printed elements. Entire domain basis functions have been used, because they present two advantages compared with sub-domain basis functions: First, a reduction in CPU time is achieved, and second, they are more appropriated to be used in optimization routines for the adjustment of the dimensions. For dipoles, the sine and cosine customary functions are used. Additional cross-current functions have been considered for the crosses in order to improve the numerical convergence.

The program implemented computes the Generalized Scattering Matrix (GSM) of the periodic surface, which relates incident and scattered Floquet harmonics. A cascade connection involving GSM matrices is performed to analyze multi-layer configurations. In particular, multi-resonant arrays with crosses and dipoles printed on the upper side of a grounded substrate have been analyzed due to their applications to multi-frequency reflectarrays. The phase of the reflected wave versus the arm length is analyzed for the different bands of interest.

REFERENCES

1. D. M. Pozar, S. D. Targonski, and H. D. Syrigos, "Design of millimeter wave microstrip reflectarrays," *IEEE Trans. Antennas Propagat.*, vol. 45, pp. 287–295, Feb. 1997.
2. J. A. Encinar, "Design of a dual frequency reflectarray using microstrip stacked patches of variable size," *Electr. Lett.*, vol. 32, pp. 1049–1050, June 1996.

A Simulated Image Array Model for Vertical Antennas above a Dielectric Half-Space

R. M. Shubair
Department of Communication Engineering, Etisalat College of Engineering
Sharjah, U.A.E.

Using the induced EMF method, the input impedance of a vertical antenna in *homogeneous free-space* can be obtained in closed-form in terms of Sine and Cosine integrals. In doing this, the induced EMF method assumes a sinusoidal current distribution along the vertical dipole and uses the free-space potential Green's function expressed as a spherical wave.

This paper extends the use of the induced EMF method for vertical antennas *above a dielectric half-space.* To do this, we must first obtain a spherical-wave representation of the half-space potential Green's function. This is done using the simulated complex image technique which was introduced to model microstrip [1] and multilayered structures [2]. Using this technique here allows us to model the effect of the lower dielectric half-space by introducing a finite set of simulated image antennas. The complex amplitudes and physical locations of the simulated images can be obtained in a way similar to [2]. The result is an equivalent problem in which the lower dielectric half-space has been replaced with free-space so that the simulated image antennas form a *simulated image array* located in homogeneous free-space. The derivation of this simulated image array allows for the use of induced EMF method to calculate the input impedance of the original vertical antenna. This results in a closed-form expression which represents the superposition of the antenna's self-impedance, and the mutual impedances due to the presence of image antennas within the derived simulated image array. It should pointed out that as one simulated image array is found for a given height above the dielectric half-space, then for a different antenna height, say upwards, the image array remains unchanged except that it is bodily translated downwards by the same distance. This means that as the induced EMF method is applied once, then at other heights the convergence is even faster since the simulated image antennas need not to be recalculated.

To verify the accuracy and convergence of method, numerical results are obtained showing the complex coefficients of the simulated image antennas, as well as, the input impedance as a function of height above the dielectric half-space, with or without loss.

REFERENCES

1. Y. L. Chow et. al., *IEEE Trans. Microwave Theory* & *Tech.,* Vol. 47, No. 9, 1777–1781, Sept. 1999.
2. R. M. Shubair, *IEEE Antennas* & *Prop. Symposium Digest*, 838–841, July 2001.

Session 1Pb6

Antenna Measurement Techniques

Radiation Pattern Determination using Infrared Thermograms

J. M. González-Arbesú, S. Blanch, A. Aguasca, and J. Romeu
Universitat Politècnica de Catalunya, Signal Theory and Communications Department
Barcelona, 08034, Spain

Infrared thermograms of electromagnetic fields have demonstrated their usefulness in the measurement of fields radiated by microwave antennas when close to radiant structures [1]. A portion of the electromagnetic energy radiated by the antenna is transformed into heat when a lossy detection screen is placed near by the radiator. The temperature gradient of the lossy material is instantly detected by an infrared camera and transferred to a computer, where the equivalence between measured temperatures and field intensities are solved for the whole detection screen.

If a planar screen of a lossy material is placed in front of a directive antenna, each pixel of the thermal image (thermogram) acquired with the infrared camera becomes a sample of the electromagnetic field intensity radiated by the antenna. Processing these field intensities, using a conventional phase retrieval technique and a classical near to far field transformation, the result is the radiation pattern of the antenna.

Fundamentals of the method (microwave/infrared correlation), detection screen design, infrared camera specifications and details of the measurement set-up for radiation pattern determination are going to be shown in the paper. Measurement results of an slotted waveguide and a pyramidal horn using this technique will be shown too in the presentation.

The conclusions arrived at this paper are that electromagnetic near-field sensing and radiation pattern determination using an infrared camera is a quick, conceptually simple, and economic technique useful for the measurement of electromagnetic fields in a noninvasive way.

REFERENCES

1. Norgard, J. D., "Infrared/microwave correlation measurements," *Optical Engineering*, Vol. 33, No. 1, Jan. 1994.

Near to Far Field Transformation for a Cylindrical Measurement System: Tests and System Error

A. Castello, J. J. Serrano, L. de Haro, and J. L. Besada
Grupo de Radiación, Dept. de Señales, Sistemas y Radiocomunicaciones
E.T.S. de Ingenieros de Telecomunicación, Universidad Politécnica de Madrid
Madrid, 28040, Spain

Radiation Group of the Polytechnic University of Madrid is mounting a new planar and cylindrical system, which it will be fully available in a few months. The software, that this measurement system will need, in order to transform near to far field is being developed and tested.

This transformation is based on Friis equation and reprocity equations written in terms of scattering matrices in order to obtain the expansion in cylindrical modes. The algorithm has been implemented by using two cascaded Fast Fourier transformations. Measurement sampling spacing in z and ϕ is selected according sampling theorem. Transmission spectrum is considered band limited both in γ $(|\gamma| \geq k)$ and m $(|m| \geq ka)$ where γ and m are expansion variables related with z and ϕ, respectively, k is the wave number and a is the measurement radius cylinder.

Pattern probe correction coefficients has to be computed previously using and equivalent algorithm as the applied to antenna under test measurement. Polarization probe correction for dual polarization probes has been implemented pre-correcting measurements with matrix relationships between each input polarization fields and the voltage at probe output gates.

This software is being tested using theoretical patterns from currents distributions computed in near field. The current line is described as a set of short dipoles, that can be expressed in near field. Moreover, some polarization errors in current line can be included to test cross-polar algorithm performances. After that, mechanical tolerances of the cylindrical will be tested using developed software. Presented paper will emphasize last mentioned topics.

Measurement of Electrically Small Antennas

A. K. Skrivervik, J.-F. Zürcher, and J. R. Mosig
Laboratoire d'Electromagnétisme et d'Acoustique
Ecole Polytechnique Fédérale de Lausanne
Lausanne, 1015, Switzerland

Electrically small antennas are difficult to measure properly because they are often neither purely symmetrical nor antisymetrical due to the limited size of ground planes or feeding baluns. Therefore, when such an antenna is connected to a measuring device, a current will flow on the outer conductor of the cable connecting the antenna, creating spurious radiations. When no special care is taken, this spurious radiation can be so important that it will frequently mask completely the characteristics of the antenna under test and will cause overestimation of the gain up to 10 dB or more [1]. Impedance measurements are also affected, as the measurement will yield the impedance of the antenna formed by the small antenna plus the connecting cable. Furthermore, when a small antenna is mounted on a casing, the latter will participate to the radiation, and its effect should be taken into account when characterizing a mobile communication device. To complicate the problem, the polarization is seldom well defined. Thus, the only way to obtain useful information about the antenna behavior of an electrically small mobile communication device is to test it under operating condition, and the relevant features will be its gain and efficiency.

An original solution to obtain the maximum gain [2] and since recently also the efficiency of electrically small antennas matching the above conditions has been developed in our laboratory, and will be presented here. It is based on the following considerations :

- The electrically small antenna under test should be mounted in its definitive environment (casing) for the measurements.
- The antenna should be fed using a stable VCO of known (measured) output power, enclosed with the batteries in the shielded case, in order to avoid all connecting cables.

Several results will be presented for both gain and efficiency of electrically small antennas.

REFERENCES

1. Staub, O., J-F. Zürcher, and A. Skrivervik, "Some considerations on the correct measurement of the gain and bandwidth of electrically small antennas," *Microwave and Optical Technology Letters*, Vol. 17, No. 3, 156–160, February 1998.
2. Zürcher, J-F., O. Staub, A. K. Skrivervik, and M. Hermanjat, "Accurate measurement of the maximum gain of electrically small antennas," *Microwave and Optical Technology Letters*, Vol. 23, No. 6, 328–331, December 20, 1999.

Design and Construction of a Planar and Cylindrical Antenna Measurement System at Polytechnique University of Madrid

J. L. Besada-Sanmartín, M. Sierra-Castañer, P. C. Almena, and J. M. S. Puente
Grupo de Radiación, Dpto. Señales, Sistemas y Radiocomunicaciones
Universidad Politécnica de Madrid., E.T.S.I. Teleocomunicación. Ciudad Universitaria
Madrid, 28040, Spain

Radiation Group of the Polytechnic University of Madrid is mounting a new planar and cylindrical system, which it will be fully available in a few months. The design, construction and evaluation of the planar scanner and the cylindrical system for antenna measurement is presented.

This new system shares the anechoic chamber with a compact range system that has been working for the last seven years. The RF equipment: network analyzer, rotary joints, cables . . . has been acquired from different commercial providers. But, the mechanical structure, the position controller and the acquisition and near field — far field transformation field has been implemented at the facilities of the University, so the price of the system has been really low.

The free dimensions for the planar scanner are 4.5 meters by 4.5 meters. The cylindrical system is placed at the middle of the planar scanner. The system will work from 900 MHz until 40 GHz. The maximum diameter of the Antenna Under Test will be 2.5 meters. Everything is fabricated with Aluminium.

The rotors are controlled with commercial encoders. These equipment are controlled by a six axes equipment designed and constructed at the facilities of the University. The equipment is based on a PC (Pentium 200) completed with different commercial cards to control the encoders and to communicate with GP-IB bus.

The software required to control both the positioning system and the RF equipment is designed under Windows environment. This software is completed with the planar near field and cylindrical near field to far field conversions.

The evaluation tests for the whole system has been implemented and the results of this evaluation will be available in March.

Accurate Diagnosis of Large Arrays from Near-Field Measurements

O. M. Bucci
Dipartimento di Ingegneria Elettronica e delle Telecomunicazioni
Università di Napoli "Federico II"
Napoli, 21 80125, Italy

M. D. Migliore and G. Panariello
Dipartimento di Automazione, Elettromagnetismo, Informazione, Matematica Applicata Università di Cassino
Cassino, Italy

P. Sgambato
Dipartimento di Ingegneria Elettronica e delle Telecomunicazioni
Università di Napoli "Federico II"
Napoli, 21 80125, Italy

Near-field measurements are an effective tool for arrays diagnosis. The most used algorithm evaluates the excitation coefficient of the array by a Discrete Inverse Fourier Transform of the array factor, which is obtained by Fourier transforming the near-field data collected on a plane into far-field and dividing by the element factor. However, this methods suffers of a number of drawbacks. In fact, notwithstanding of its numerical efficiency, due to the use of FFT, it can not be used in case of more complex arrays, like conformal arrays or planar arrays with not periodic geometry. Furthermore, in case of patch or slot antennas the use of the array factor concept causes a significative error due to the different behaviour of the elements in the center and on the border of the array. Finally, the method is sensitive respect to the truncation of data, and large scanning areas are required in order to reduce the truncation of near-field data at negligible level.

The above drawbacks can be avoided using a matrix method. If $\underline{\underline{A}}$ is the matrix relating the excitation vector $\underline{e}$ and the measurement vector $\underline{\underline{E}}$, then the inversion of the linear system $\underline{\underline{Ae}} = \underline{\underline{E}}$ gives the required excitation coefficients of the array. The formulation is completely general, and includes conformal arrays and any scanning geometry. Furthermore, it can include the measurement probe effect.

However, the solution of the system is not trivial at all. A first problem is that in case of large arrays the standard $\lambda/2$ sampling strategy would lead to a strongly rectangular matrix that requires large computer memory, and long measurement time. However, the standard $\lambda/2$ sampling step is highly redundant. The redundancy of data can be reduced by taking into account some "a priori" information of the source, like its maximum dimension, its shape, and its position in the space. In particular, it is possible to represent the field on a surface surrounding the antenna within a given representation error with a number of measured data almost equal to $4\Sigma/\lambda^2$ wherein Σ is the area of the minimum convex surface including the antenna under test. The second problem is that the matrix is very ill conditioned in case of large arrays, so that a regularization procedure is required. A linear inversion algorithm particularly suitable in terms of speed, numerical stability and reasonable computational effort is the generalized Landweber iterative algorithm.

A large numerical investigation on arrays of more than 2000 elements has been carried out. Each simulation required a global computation time of less than 3.5 hours on a Pentium III 450 MHz personal computer using a not optimized program written in Matlab. The results will be shown in the conference and confirm the effectiveness of the technique.

Advances and Review of Applications of Equivalent Principle-Source Reconstruction Method

F. Las-Heras
Dept. Ingenieria Eléctrica, Universidad de Oviedo
Gijon, Asturias 33204, Spain

T. K. Sarkar
Dept. EECS, Syracuse University
Syracuse, NY 13244, U.S.A.

The source reconstruction technique, based on the equivalent principle and the minimization of cost functions involving integral equations that relates electric field components and equivalent magnetic current components, is presented as a general method for different electromagnetic applications.

In particular, the near-field to far-field (NF-FF) transformation for antennas measurement is addressed in combination with some approximations and recursive algorithms to reduce the number of equations to solve and the unknowns involved in these equations. It results in efficient NF-FF transformation methods for the typical canonical acquisition configurations (planar, cylindrical, spherical).

Also the source reconstruction is directly used for diagnosis purposes over aperture and arrays antennas.

Another addressed application is the NF-FF transformation from amplitude only electric field data. The general method allows the transformation from the knowledge of the amplitude near field data over one or more arbitrary surfaces. Also the particular acquisition cases of spherical scanning and planar scanning over two planes are considered.

Finally, the pattern synthesis as a source reconstruction application from the knowledge of a given far field pattern is considered. Adequate cost functions are addressed both for the case of direct pattern specification as well as when the pattern specification is given by a template.

Some advances regarding optimization algorithms and multilevel techniques are discussed when applied to the source reconstruction method.

In all NF-FF cases, numerical examples and measurements performed at near field measurement ranges in anechoic chambers are presented to verify the performances of the equivalent principle-source reconstruction method.

Evaluation of Array Pattern Synthesis Methods Based on Artificial Neural Networks

R. G. Ayestarán and F. Las-Heras
Dept. Ingenieria Eléctrica, Universidad de Oviedo
Gijon, Asturias 33204, Spain

The evaluation of antenna array pattern synthesis methods based on artificial neural networks is presented.

Classical and more recently developed methods use analytical and numerical procedures in order to establish a connection between the excitation of the elements of the array antenna and the radiated far field at different aspect angles. Methods based on artificial neural networks do not implement any mathematical relation directly, but they adapt themselves through a learning process. The network gets information using different sets of field data and their correspondent excitation coefficients. If the learning process is performed with an enough representative and independent number of sets, the neural network is able to adapt itself automatically to output the excitation coefficients corresponding to any set of field data.

Artificial neural networks can interpolate and extrapolate values, so a good training process may adjust the neural network in such way that no additional modification is needed any more and its operation becomes definitive.

The neural network is based on a combination of a defined number of layers, and layers on a combination of processing elements (neurons) implementing a simple mathematical operation. The adaptation process selects automatically the weights that are used for any element, while the number of neurons and layers are design parameters. The designer also selects the learning procedure.

The training procedure is performed via electromagnetic simulation of aperture distributions that radiate an electric field at different aspect angles or using the array factor of one-dimensional and two-dimensional arrays. Once trained, the network outputs the excitation coefficients that must be used to implement the antenna array with the target radiaton pattern.

A detailed evaluation of the implementation and its performances is presented. Some examples regarding BTS antennas and radar antennas are considered. Also, a comparison between this synthesis method and classical or optimization-based methods is addressed.

Session 1Pc7

WindSat Mission: Sensor Design and Expected Performance

WindSat — Space Borne Remote Sensing of Ocean Surface Winds

P. W. Gaiser and D. Spencer
U.S. Naval Research Laboratory, Code 7223
Washington, DC 20375, U.S.A.

The high demand for operational ocean surface wind vector data and the success of recent aircraft campaigns gave impetus to developing a space borne polarimetric microwave radiometer. WindSat is a satellite-based multi-frequency polarimetric microwave radiometer being developed by the Naval Research Laboratory for the U.S. Navy and the National Polar-orbiting Operational Environmental Satellite System (NPOESS) Integrated Program Office (IPO). WindSat is designed to demonstrate the viability of using polarimetric microwave radiometry to measure the ocean surface wind vector from space. The sensor provides risk reduction data that the IPO will use in the development of the Conical Microwave Imager Sounder (CMIS). WindSat is the primary payload on the Air Force Coriolis satellite, which is scheduled to launch in November 2002. The WindSat design allows both forward and aft views of the Earth, thus allowing comparison of wind vector retrievals using one- or two-looks. This is a critical part of the experiment because the added costs and complexity of achieving two looks, if necessary, will be significant for operational sensors such as CMIS. WindSat must perform its wind mission without impairing the capability to measure other environmental parameters currently provided by SSM/I.

The WindSat radiometer operates in discrete bands at 6.8, 10.7, 18.7, 23.8, and 37.0 GHz. The 10.7, 18.7 and 37.0 GHz channels are fully polarimetric, while the 6.8 and 23.8 GHz channels are dual polarized only (vertical and horizontal). It uses a 1.8 m offset reflector antenna and will be launched into an 830-km sun-synchronous orbit. The WindSat design and ground processing algorithms focus on the primary mission of measuring the sea surface wind vector. However, it will produce a unique data set with numerous environmental remote sensing applications.

This talk will address the WindSat mission motivation, objectives, and timeline. Furthermore, the WindSat sensor design will be presented. Lastly, this talk will provide an overview of the WindSat ground segment.

WindSat — Sensor Design and Expected Performance

P. W. Gaiser and E. M. Twarog
U.S. Naval Research Laboratory, Code 7223
Washington, DC 20375, U.S.A.

The WindSat radiometer operates in discrete bands at 6.8, 10.7, 18.7, 23.8, and 37.0 GHz. The 10.7, 18.7 and 37.0 GHz channels are fully polarimetric, while the 6.8 and 23.8 GHz channels are dual polarized only (vertical and horizontal). It uses a 1.8 m offset reflector antenna and will be launched into an 830-km sun-synchronous orbit. The primary objective of the WindSat mission is to demonstrate the capability of polarimetric radiometry to measure the ocean surface wind vector. Several aircraft radiometer systems have demonstrated that there is a measurable wind direction signal. WindSat is the first space borne polarimetric radiometer to be developed.

The fundamental limit to the utility of polarimetric data is the capability to measure the Stokes vector, which translates into isolating the orthogonal polarizations. Because the wind direction driven ocean surface brightness temperature variations are so small, approximately 1% of the vertical or horizontal polarization signals, successful measurement requires low noise and very stable calibration. More importantly, a polarimetric radiometer measures cross-polarization of the microwave radiation emitted from the Earth's surface. Therefore, the limiting factor in measuring the Stokes vector is the cross-polarization performance and characterization of the antenna.

The WindSat development program included several stages of testing and system characterization. An outdoor antenna range was built to meet the rigorous antenna measurement requirements. The WindSat antenna range is capable of measuring the cross-polarization with accuracy of less than -30 dB. The radiometer sensitivity, or NEDT, was characterized using highly stable, high accuracy calibration targets in a thermal/vacuum chamber. This talk will address the antenna polarization testing and resulting performance. The radiometer sensitivity and stability will also be discussed.

Fourth Order Small Slope Theory of Thermal Emission from the Sea Surface

M. A. Demir and J. T. Johnson
Department of Electrical Engineering and ElectroScience Laboratory
The Ohio State University
Columbus, OH 43212, U.S.A.

In recent years, models based on a small slope approximation (SSA) for emission from a rough surface have been applied to study sea surface brightness temperatures. The formulation of these models is based on a small perturbation method (SPM) solution for scattering from a rough surface, which has been shown to yield a small slope theory when applied to the computation of surface emission. The majority of previous studies have employed the second order SSA theory, either alone or in combination with a geometrical optics approach to obtain a "two-scale" model. These second order SSA-based theories predict that the influence of surface roughness on brightness temperatures can be expressed as an integration over the surface directional spectrum multiplied with an emission "weighting function." A third order SSA theory has also been derived recently, and obtains a correction to second order results in terms of a quadruple integration over the surface bi-spectrum. Because the bispectrum vanishes identically for a surface described as a Gaussian random process, third order SSA results only provide limited information on the accuracy of second order predictions for the near-Gaussian process sea.

In this paper, a fourth order SSA model for emission from the sea surface is considered to assist in estimating the accuracy of second order SSA predictions. The derivation of the emission model requires determination of the fourth order SPM coherent reflection coefficient correction, made possible by a recently developed systematic SPM solution. Expressions for the fourth order emission correction will be presented first in terms of the surface spectrum and tri-spectrum, but reduced to a quadruple integration over a product of two spectra for a Gaussian random process sea. Results from the theory will be presented for some example cases, and approximate forms derived to simplify the computations. A discussion of the expected accuracy of the second order theory based on the results obtained will then be provided.

Effects of Foam on the Four Stokes Parameters of Passive Microwave Remote Sensing of Ocean

L. Zhou, L. Tsang*, and Q. Li
Department of Electrical Engineering, University of Washington
Seattle, WA 98195-2500, U.S.A.

The effects of ocean wind on the four Stokes parameters have been studied extensively both in theory and experiments. However, when the ocean is covered with foam, there is little known concerning how the foam affect the four Stokes parameters. Recently, we have developed a dense medium radiative transfer theory for foam. In this paper, we study the microwave emission of wind roughened ocean covered by a layer of foam. We combine the dense media radiative transfer theory with roughness boundary conditions created by the ocean wind. The iterative method is employed to solve DMRT equations. Firstly, the differential radiative transfer equations are converted into integral equations, and then the boundary conditions are incorporated into the integral equations from which the first- and second-order solutions are derived. The boundary conditions of the radiative transfer theory are derived by using the small perturbation method (SPM) An empirical wind-generated ocean surface spectrum is used to generate small-scale ocean surfaces that depend on various wind speeds. The frequency, polarimetric, azimuthal, and wind dependence of four Stokes parameters are studied in this work. Results are illustrated for 19 GHz and 37 GHz and for all four Stokes parameters. The simulated results show that the brightness temperature is more dependent on polarization at 19 GHz than at 37 GHz. Results also show that the brightness temperatures are less sensitive to the surface roughness at 19 GHz than at 37 GHz. When a layer of foam is present, it is found that the vertical and horizontal brightness temperatures increase and the U and V components decrease. The results are also illustrated as a function of foam layer thickness. As the foam layer thickness further increases, the four Stokes parameters level off to constant values.

* Also with City University of Hong Kong

The WindSat Ocean/Atmosphere Retrieval Algorithm: Methodology and Results

C. K. Smith
Computational Physics, Inc.
Washington, DC, U.S.A.

R. M. Bevilacqua, P. W. Gaiser, K. M. St. Germain
Remote Sensing Division, Naval Research Laboratory
Washington, DC, U.S.A.

N.-Y. Wang
NOAA/NESDIS/ORA
Camp Springs, MD, U.S.A.

We describe the WindSat retrieval algorithm for sea surface temperature and wind vectors, columnar water vapor and cloud liquid water. This physically based algorithm uses the optimal estimation approach, developed originally for retrieval of atmospheric temperature and composition profiles by C.D. Rodgers (1976, 1990).

The optimal estimation approach, which uses a-priori information about the retrieval parameters, has been applied successfully to numerous atmospheric and geophysical retrieval problems where the solution is under-determined, i.e., not unique. Here, the problem is over-determined, but the solution for the wind vector is not unique; several solutions ("ambiguities") exist, corresponding to local minima of the chi-square function (weighted sum square difference between the model function and measurements). As in atmospheric profile retrievals, the global minimum chi-square solution is not necessarily the best solution, due to measurement noise. This is especially true at low wind speeds, where the directional signal is 1K or less. The optimal estimation technique is designed to yield a single, best solution.

Our implementation of the optimal estimation technique is general; the retrieval driver is independent of the physics of the problem. All physics of the ocean/atmosphere radiative transfer is specified in the retrieval forward model module. The modularity and generality of the implementation allows straightforward addition of other retrieval parameters.

The a-priori data can be used as a first guess and also to constrain the retrieval. The algorithm requires specification of two covariance matrices, one for the a-priori data and one for the measurements, and the weighting of the a-priori data and measurements in the solution is governed by their relative values. Thus, the a-priori covariance terms are considered tunable parameters, to be adjusted to minimize the retrieval errors.

We will describe the algorithm and parameterizations of the physics in the retrieval forward model in some detail. Retrieval results using simulated brightness temperatures for a variety of realistic conditions will be shown.

The Effect of Surface Roughness and Whitecaps on Sea Surface Microwave Emissivity

W. E. Asher
University of Washington
Seattle, WA, U.S.A.

S. C. Reising
University of Massachusetts
Amherst, MA, U.S.A.

L. A. Rose
Naval Research Laboratory
Washington, DC, U.S.A.

With its upcoming launch in late 2002, WindSat will be the first spaceborne polarimetric radiometer, specifically designed to measure the ocean surface wind vector. This instrument motivates a renewed interest in understanding the relationship between wind speed and microwave emission from the ocean surface. Although the microwave emissivity of the sea surface is known to depend upon surface roughness and foam coverage, the exact form of this dependence has not been determined, primarily because of the difficulty of acquiring time series of radiometric data with concurrent measurements of the relevant air-sea interaction parameters. For example, aircraft-mounted radiometers are capable of providing high-quality radiometric data, but the high costs associated with aircraft operations make it difficult to obtain sufficiently long time series of radiometric data. Conversely, a ship can maintain station for several weeks to study the temporal changes in brightness temperature, but changes in incidence angle caused by ship motion due to waves and swell make it difficult to acquire high-quality radiometric data. In September 2000, the Fluxes, Air-Sea Interaction and Remote Sensing (FAIRS) experiment was conducted in the northeastern Pacific Ocean aboard the R/P FLIP. Because FLIP functions as a 120 m long spar buoy with minimal platform motion, it was possible to acquire a long-term radiometric time series for use in studying the response in ocean surface microwave emission to changes in the environmental forcing functions.

Sea surface microwave brightness temperatures were measured at X-band (10.8 GHz) and Ka-band (36.5 GHz) at incidence angles of 45, 53 and 65 degrees for wind speeds ranging from 2 m/s to 15 m/s. Fractional area whitecap and foam coverage in the field of view of both radiometers was measured using a boresighted video camera. In addition to the microwave and video data, air-sea interaction parameters such as sea-surface skin temperature and friction velocity were also measured. When combined, these data sets are well-suited for testing parameterizations of the sea surface microwave emissivity that include the effects of fractional-area foam coverage and surface roughness.

We show that for the low to intermediate wind speeds, fractional-area whitecap coverage can be parameterized in terms of a cubic dependence on wind speed. Using the relationship for whitecap coverage and the foam emissivities measured by *Rose et al.*, we then compare predicted versus measured increases in sea surface brightness temperature as a function of wind speed at both X-band and Ka-band. For these comparisons, we initially parameterize increases in brightness temperature due to roughness using previously published relationships based on wind speed, but also investigate whether scaling roughness in terms of friction velocity instead of wind speed results in a more accurate relationship.

WindSat Atmospheric Forward Model Comparisons

N.-Y. Wang and P. S. Chang
NOAA/NESDIS/ORA
Camp Springs, MD, U.S.A.

R. M. Bevilacqua, C. K. Smith and P. W. Gaiser
Naval Research Laboratory
Washington, DC, U.S.A.

WindSat is a satellite-based multi-frequency polarimetric microwave radiometer designed and built by the Naval Research Laboratory (NRL) for the U.S. Navy and NPOESS Integrated Program Office. The radiometer will measure fully polarimetric radiometric brightness temperatures (TB) at 10.7, 18.7 and 37.0 GHz, and linearly polarized brightness temperatures at 6.8 and 23.8 GHz. The primary goal of Windsat is to demonstrate the capability of polarimetric microwave radiometry in remote sensing of the ocean surface wind vector. Sea surface temperature, atmospheric water vapor, and cloud liquid water, are among some of the other geophysical parameters that can also be measured. To retrieve these environmental parameters from the multi-frequency polarimetric radiometer measurements, a forward model that characterizes the measured brightness temperature components due to emission from the surface and the intervening atmosphere, and its transmission through the atmosphere is essential.

The atmospheric component of the forward model includes the calculation of three principal parameters used to evaluate the atmospheric contribution to the brightness temperature measurements. These are up-welling radiation, down-welling radiation, and attenuation (loss) due to the atmosphere. This study looks at the attenuation due to clear air and non-precipitating clouds in the frequency range of SSM/I, TRMM/TMI, Windsat and CMIS spaceborne passive microwave instruments. For clear air, the atmospheric optical depth is the sum of contributions from dry air and water vapor. Several atmospheric absorption models have been developed in the literature. Uncertainties in current models for water vapor absorption in the 20–40 GHz frequency range is estimated to be up to a few percents, which may translate into significant biases in up-welling and down-welling brightness temperatures. A performance assessment of the current radiative transfer models and atmospheric absorption models is performed using comparisons with existing measurements from spaceborne passive radiometers such as SSM/I and TMI with near-coincident radiosonde profiles of the atmosphere and buoy observations of the surface wind fields. The intercomparions focus on the modeling at Windsat channels of 10.7, 18.7, 23.8 and 37 GHz. Results of this effort will be reported.

WindSat On-Orbit Radiometric Calibration

W. L. Jones
Microwave Remote Sensing Consultants
Cocoa Beach, FL, U.S.A.

K. M. St. Germain and P. W. Gaiser
Remote Sensing Division, Naval Research Laboratory
Washington, DC, U.S.A.

The WindSat Program is a proof of concept satellite experiment that uses passive microwave polarimetry to measure the ocean surface wind vector. This satellite remote sensor will demonstrate several technology advances in multi-frequency microwave radiometry; but the most important of which is the unique measurements of the 3^{rd} and 4^{th} Stokes parameters. The geophysical retrieval of ocean surface wind direction will be based upon the anisotropy of the Stokes parameters with wind direction. By measuring the full Stokes matrix (four parameters), the wind direction may be derived from a "single forward or aft look" fully polarimetric measurement.

The dynamic range of the 3^{rd} and 4^{th} Stokes parameters are about two orders of magnitude smaller than that of the vertical and horizontal brightness temperatures; therefore instrument calibration is much more stringent than usual (e.g., SSMI or SSMIS). This is especially important for polarization-purity of the antenna that measures vertical, horizontal, $\pm 45°$, and left-hand & right-hand circular polarizations. The WindSat antenna is probably the best-characterized reflector antenna to fly in space.

Thus, the on-orbit radiometric calibration is critical to the success of the WindSat program. The radiometer error budget will be presented and the calibration issues will be addressed. Further, the on-orbit calibration plan will be described that includes a special satellite pitch maneuver that allows the WindSat instrument to view space, simultaneous aircraft under-flights and the possible use of ground-based calibration aids.

Rainfall and WindSat

T. Wilheit
Department of Amospheric Sciences (3150), Texas A&M University
College Station, TX 77843–3150, U.S.A.

Wind retrievals can be degraded by rainfall. If the rainfall is heavy enough, it simply obscures the surface and even at modest rates it will reduce the signal-to-noise through partial obscuration of the surface. It also has more subtle impacts. The primary wind speed signal and essentially all of the wind direction signal is in the polarization of the radiances. Normally the reduction of polarization by atmospheric absorption is accompanied by an increase in the individual brightness temperatures so that corrections can be made to a very high accuracy. However, the scattering associated with rainfall reduces the brightness temperature so that the polarizations would be undercorrected in rain. Rainfall is also highly structured spatially. In considering a single pixel, this would not normally be a problem since the rainfall would be the same for all polarizations. However, not all frequencies and polarizations are coincident in the WindSat radiometer. They are rectified to a common field of view by resampling with observations spaced somewhat wider than the Nyquist intervals. This high spatial frequency noise will corrupt the resampled brightness temperatures, thus degrading the wind retrievals. In heavy rain, the impact of the drops on the surface will change the emissivity.

On the other hand, WindSat has many of the same frequencies as other radiometers used for rainfall retrieval, (e.g. SSM/I, TMI, AMSR). A rainfall product can be derived from WindSat that will complement those of other satellites permitting a more complete picture of the earth's rainfall to be assembled. The future GPM mission will consist of many satellites of varying designs in a variety of orbits. The combination of WindSat, two SSM/Is, two AMSRs and TRMM which should be available for a few years after the launch of WindSat will provide an early development test bed for the data combination issues of GPM.

Effects of Large Scale Ocean Waves on Polarimetric Sea Foam Emission

T. M. Grzegorczyk, C. O. Ao, Y. Zhang, and J. A. Kong
Research Laboratory of Electronics
Massachusetts Institute of Technology
Cambridge, MA 02139, U.S.A.

It has long been recognized that sea foam has a disproportionately strong effect on thermal emission from a wind-driven ocean surface. An empirical formula due to Stogryn for sea foam emission which was based on early experiments is still widely used today. Recently, attempts have been made to derive a physical model of foam emission where the foam is idealized as a collection of air bubbles with sea water shell.

The foam layer is typically assumed to overlay a flat ocean surface. Therefore, the effects of the rough ocean surface are not taken into account in such models. In this work, we want to introduce the roughness of the ocean surface by incorporating the large scale variations included in the commonly used two-scale model. Hence, a realistic Cox-Munk slope distribution is used to characterize the slope distribution of the random sea-foam surface.

The solution to this problem is obtained in two steps. First, the dense medium radiative transfer theory is used to compute the thermal emission from a foam layer on a flat interface. Second, the emission from a tilted foam layer is calculated using coordinate and polarization transformations. In doing so, it is assumed that dominant effects of the rough ocean surface on foam emission is the geometric tilting of emission vectors.

Using this approach, we examine polarimetric foam emission for different sea surface foam parameters as well as wind speed and direction. We will present results of brightness temperatures as a function of looking angles and frequencies. When combined with the commonly used two-scale theory of thermal emission from plain ocean surface, one can arrive at a simple but physics-based description of *foam-covered* ocean emission that can be used as a basis of parameterized inversion from real data.

Session 1Pa8

Bistatic and Multistatic Radar at HF and VHF: Active and Passive – Part I: Target Focus

Passive Airborne Bistatic Detection: Principles and Challenges

M. Lesturgie
Office National d'Études et de Recherches Aérospatiales (ONERA)
Palaiseau, F-91761, France

During the last ten years, passive detection has been the object of many theoretical and experimental investigations, in Europe, USA and other countries. The techniques usually addressed the re-use of non cooperative ground-based transmitters like broadcasting TV or radio emitters radiating in low frequency bands (HF, VHF, UHF).

Passive detection concepts are well known to present several advantages in terms of low detectability, reduction of vulnerability compared to classical active radar operating. This paper deals with the airborne concept of passive detection. More than for ground surveillance systems, stealth and discretion are determinant for the survivability of a military aircraft. Then, combined with stealth, passive airborne modes can help to approach the "full discretion" concept.

Another interest of passive radar results from the access to non-radar frequency bands, (specially in VHF/UHF) without any request for frequency allocation.

However, airborne bistatic configuration induces many differences both in radar operating and signal processing techniques. Selection of suitable emitters is described : ground broadcast emitters (radio or TV in VHF-UHF bands), airborne or space borne emitters. More generally, the paper describes different class of emitters usable for passive airborne detection. Each class of emitter is represented by a set of generic parameters which is used to compute a first estimation of coverage radar performances. The paper gives a quick look of experimental results obtained from low frequency emitters in a motionless passive configuration, to reinforce the interest of using these emitters either in ground or airborne configuration.

The second part of the paper raises probably one of the main challenges in airborne bistatic detection, consisting of signal processing. More than a classical matched filter based on a correlation, signal processing needs to solve the problem of clutter and direct path rejections. Basic components of signal processing are described for a motionless configuration; then airborne motion configuration is considered, with 2 cases:

- if the emitter is not moving, clutter ground echoes are spread in Doppler, but conventional STAP (Space Time Adaptive Processing) algorithms seem to be efficient to reduce the clutter and direct path effect, with similar techniques as used for monostatic active airborne radar. Doppler value is related to the azimuth direction of ground echoes, so that STAP weighting vectors can be easily estimated from the covariance matrix with a negligible dependence on the range.

- if both emitter and receiver are moving (2 aircraft or 1 aircraft / 1 satellite) the range-dependence of the Doppler echoes, for each direction implies to design a larger weighting vector, whose components are more complex to estimate. Larger the dimension of the STAP weighting vector, more restricting and difficult is the covariance matrix estimation.

Then, extrapolation from ground motionless concept to airborne motion passive concepts required to assess the technical feasibility of clutter and direct path with specific STAP techniques. As a conclusion, the paper summarizes the bistatic configurations of greatest interest for airborne passive detection, and gives a first estimation of signal processing feasibility, addressing the corresponding technical challenges to be overcome in the next few years.

Low Frequency Bistatic Radar Network for Precision Positing of Air Targets

H. Hellsten
Ericsson Microwave Systems AB
Mölndal, SE 431 84, Sweden

As is well known, stealth and electronic countermeasures challenge the usefulness of the traditional microwave monostatic surveillance radar. As for stealth, an often-claimed remedy is to decrease frequency to become more or less resonant with target dimensions, thus making many of the stealth techniques ineffective. It is obvious that keeping to the monostatic concept, a VHF radar will either possess a very low angular resolution or the antenna dimensions will be unpractically large. Also lack of directional resolution will make it sensitive to jamming. However as frequency decreases, coherent integration time increases, so there may not necessarily be a power budget problem even though antenna gain is low.

The last observation opens for an alternative system concept, viable at low frequency. The idea is to combine low frequency (VHF or UHF) with bistatic imaging geometries. Target detection is achieved with a uniformly laid out ground grid of small and compact low frequency radars. On the basis of prolonged integration times, but without the usual directional antenna, air targets become detected and represented as a function of range and time (Doppler and possibly higher order motion parameters) with respect to several of these radars. The positioning of the targets is achieved by triangulation in a post detection stage.

The big challenge is to device robust methods of dealing with the triangulation assignment problem. Clearly given radar range measurements from three different sites, any three detections at these sites, would lead to a unique target track, independently if the detections applied to the same target or not. If there is more than a three-fold overlap between independent measurements, ghost tracks only appear with a certain probability. The probability of ghost tracks must however be very small, since a radar network must be able to deal with - maybe - thousands of targets. The required large degree of overlap can be realized by exploiting the overlapping radars in combined monostatic and bistatic modes. In a radar grid in which each bistatic pair covers one grid distance around, there are of the order 30 independent configurations covering each point in space.

An important feature of this type of system is that, since targets are detected only in the state subspace of no angular resolution, a very high resolution would not lead to undue data rates. However by means of this high resolution, targets can be positioned with accuracy better than the typical target extension. Fast methods of solving the assignment problem, for the very large state space, is required but can be found. Position accuracy becomes so good that a radar network of the indicated type can be used as a collision avoidance system or — oppositely — for precision steering of anti-aircraft missiles.

The combined use of low frequency and bistatic radar geometries is of particular significance for stealth targets. Large bistatic angle radar measurements will in fact detect the diffraction fringes of the forward scattering beam. The fringes are highly apparent for radar wavelengths down to one magnitude or so below the size of the target. Hence, stealth targets will be detected and accurately positioned by this type of radar system.

The bistatic radar network can be devised to be quite robust with respect to jamming, by providing each radar site with a rudimentary antenna directivity, which can be achieved without compromising the smallness of the individual antenna installations.

Methods for Processing Data from a Low Frequency Bistatic Radar Network

M. Herberthson
Swedish Defence Research Agency
Linköping, Sweden

In this talk we address the specific problem of correctly associating data in a radar network as described in the talk 'Low Frequency Bistatic Radar Network for Precision Positioning of Air Targets'. We will assume that talk and therefore consider the following principle problem. Consider a set of radar stations monitoring the air territory. The stations perform individual monostatic measurements and, for nearby stations, also bistatic measurements. The association problem is then to correctly match data from different radar facilities, so as to produce the correct and precise location of the air targets.

The problem can be most easily seen in the simplest case with three monostatic stations overlooking the same region. Suppose each station sees N targets. By assumption, only distance and radial speed is known for each target, i.e., we have no angular information. The three stations can, in principle, associate the given data in N^3 ways. The association problem is then to from these N^3 candidates eliminate all false associations (ghosts) and keep the true ones (targets). A solution, in theory, uses redundant measurements, which overdetermine the equations. For the case with several radar stations, allowing also bistatic measurements, the problem is then how to effectively use the redundancy and associate the targets.

As the number of stations and targets grow, there arises a need for effective processing of radar data. We will discuss two different processing methods, shortly described below. The targets are to be located in a six-dimensional state-space S^6 (position and velocity). In the first method we discuss, the idea is to divide S^6 into cells (regions of suitable size). One then deletes all cells which cannot contain any targets, and then refine the division on the surviving cells. After the division, further (smaller) cells can be deleted, and the surviving cells are again divided. This procedure, which contains non-trivial steps, is iterated until some criterion is met. The second method uses the fact that a pair of stations which produce two monostatic and one bistatic measurements, can process these three data sets in a two-dimensional subspace S^2 of S^6. This is possible because of a rotation symmetry around the axis going through the two stations. In S^2, data can be effectively pre-processed, and the remaining processing burden is then seen to be reduced.

Phased Antenna Arrays in Bistatic Forward Scattering Radar System

A. B. Blyakhman
Nizhny Novgorod Research Radiotechnical Institute
Nizhny Novgorod, 603950, Russia

A. V. Myakinkov and A. G. Ryndyk
Nizhny Novgorod Technical University
Nizhny Novgorod, 603155, Russia

In bistatic forward scattering radar systems with continuous quasi-harmonic sensing signal, detection and measurement of echo-signal parameters are provided by way of evolving of envelope of interference signal, which is made owing to summing of the direct transmitter signal and echo-signal from the moving target in the receive antenna. Measuring parameters allowing defining the path of target moving are the following: Doppler frequency and direction of signal arrival.

The signal of Doppler frequency can be easily made owing to amplitude detector at the output of the partial receiver channel.

The drawback of systems using multibeam antenna systems is because of the influence of the direct signal level in receiver channels on the gain relationship. This influence is stipulated by the fact that the amplitude detector gain depends on the direct signal level. In partial channels (except the central channel) the direct signal level is defined by the side lobes level. That's why it's fortuitous in fact.

The more prospective can be the realisation of space signal processing in bistatic forward scattering radar systems with the use of the phase antenna array with coherent signal postprocessing from the outputs of its elements. However, it is rather difficult to carry out coherent signal processing in bistatic forward scattering radar systems because of high separation of the transmitter and receiver in space. To provide the coherent mode it is necessary to transmit the signal over the dedicated communication channel or to release the reference voltage from the direct signal. The both approaches have serious technical problems.

So, in this paper it is considered the possibility of the use PAA by way of receiver arrays in bistatic forward scattering radar systems.

It is shown that while forward scattering the presence of powerful forward transmitting signal provides measurement of direction of signal arrival by signal processing from amplitude detector outputs. Thereby, as in radar with previously formed partial channels for space-time receiving signal processing, it is not required the reference signal synchronized by transmitter deviations, which is the essential factor for processing in monostatic radar with PAA. It is also shown that for postdetection integration of antenna directivity characteristics, ambiguity of angle coordinate measurement is created. We offer the method, which allows eliminating this defect. Estimated accuracy measurement characteristics such as Doppler frequency and signal direction of arrival when space-time processing in shape of twofold Fourier transform.

Presented simulation results of measurement of parameters of air target trajectory in bistatic forward scattering radar system with PAA.

So, it is shown the possibility of the effective tracking in bistatic forward scattering radar system with postdetection signal processing in PAA.

HF/VHF Bistatic SAR for Buried Target Detection Experiment Results

H. Bascom and J. Clancy
Emergent
Rome, NY 13440, U.S.A.

R. Ogrodnik
USAF Research Laboratory (AFRL/SNRD)
Rome, NY 13441-4514, U.S.A.

Foliage and ground penetrating radar imaging systems have considerable military and commercial utility. Lower frequency radar systems are needed to penetrate foliage or propagate deep into the ground. Systems operating at frequencies from VHF down into the HF portion of the spectrum are emerging to meet the penetration requirement. These systems encounter the inevitable tradeoff between the choice of operating frequency and resolution or bandwidth requirements. Use of low operating frequencies implies high percent bandwidths or ultra wideband systems. Signal bandwidths are inherently limited at low frequencies and thus limit the down range resolution achievable. Cross range resolution at low frequencies is reduced since wavelengths are longer. Conventional synthetic aperture techniques at low frequencies yield inadequate resolution for target detection and characterization. These considerations spurred interest in radar imaging based on narrowband, wide angle tomographic imaging principles.

This paper reviews results from ongoing experiments conducted at the Air Force Research Laboratory, Rome Research Site, Verona NY test facility. These experiments are investigating bistatic and multistatic radar imaging concepts, using the HF/VHF band, applied to buried target detection. In support of these experiments, a multistatic testbed was developed allowing for ground based data collection. The system hardware is composed of a wide band HF/VHF illuminator, developed under this program, and deramping receiver, provided GFE. A controlled scene was developed containing both surface and buried targets. A variety of targets filled the scene, including log periodic antennas, corner reflectors, oil drums and vehicles.

The basic design problems for radar detection of underground targets for the various purposes outlined above are: 1) to provide adequate signal to noise of the scattered return from the buried target at depths of 10 to 30 meters in dry and wet ground, 2) a means of detecting the target return from clutter signals scattered from the earth's surface, and 3) a means of characterizing the type of targets or features detected. Satisfying the last two requirements sets the resolution requirements for the radar, which are on the order of 10 to 20 meters for the larger targets, and 1 to 5 meters for the detection of 55 gallon drums.

Capabilities and Limitations of FW-CW Systems to Measure Impulse Response of Aircraft RCS in the HF-VHF Frequency Band

C. Barès, C. Brousseau, A. Bourdillon
Laboratoire ART, Equipe Radar-Polarimétrie, FRE CNRS $N°$ 2272
Rennes, 35072, France

Two methods can be used to measure impulse response of aircraft Radar Cross Section (RCS): the first one consists in sending a very short and powerful pulse and the second one consists in generating a FM-CW (Frequency Modulation - Continuous Wave) signal with a time duration larger than the equivalent pulse which has the same frequency band. Then, the impulse response of target RCS can be obtained by calculating the inverse Fourier transform of its frequency response.

In the last few years, the technical advances in Direct Digital Frequency Synthetizer (DDFS) allow the use of low cost electronic circuits to generate a FM-CW signal. Due to the current limitations of Digital to Analog Converter (DAC), the maximum usable frequency is about 500 MHz without frequency translation.

In this study, the capabilities and the limitations of DDFS to measure impulse response of aircraft RCS is evaluated. In a first part, the influence of the DDFS parameters that decrease the accuracy of the measurements is considered. Thse parameters are the following :

- Frequency bandwidth,
- Amplitude flatness of the signal as a function of frequency,
- Phase noise,
- Number of steps used to generate the frequency band,
- Limitations due to the FM-CW pattern.

In a second part, the influence of the FM-CW radar system on the measurement of impulse response of aircraft RCS is studied. Two parameters can decrease the quality of the measurements. The first one is the frequency bandwidths and the cut-off frequencies of the filters used in the receiver, and the second one is the displacement of the antenna phase center as a function of frequency. This displacement is determined on a log-periodic antenna and then, its effect on the measurements is evaluated.

Finally, many measurements realised on a FM-CW synthetizer using DDFS technology are shown in the 1 - 300 MHz frequency band. These measurements show the effects of the parts of the synthetizer which are the most critical.

Session 1Pb8

Bistatic and Multistatic Radar at HF and VHF: Active and Passive – Part II: Environment Focus

Non-Cooperative Bistatic (Multistatic) Radar Technology and Applications Using Beyond the Horizon HF Transmitters of Opportunity

J. G. McGraw
Photon Research Associates, Inc.
Arlington, VA 22209, U.S.A.

D. Lodwig
Lockheed Martin Mission Systems
Gaithersburg, MD 20879, U.S.A.

F. J. Ryan
Maritime Surveillance Division, Space and Naval Warfare Systems Center
San Diego, CA 92152-5001, U.S.A.

J. D. Sahr
Department of Electrical Engineering, University of Washington
Seattle, WA 98195-2500, U.S.A.

The development of advanced integrated circuits has made the digital implementation of radio communications receivers compact, relatively cheap and reliable, while having the capability to simultaneously cover the entire HF through UHF bands. Recently, non-cooperative bistatic (multistatic) radar based on Line of Sight (LOS) — limited television [TV] or frequency modulated [FM] VHF/UHF broadcasts and available commercial receiver technology has been demonstrated to have potential utility for all-weather air surveillance. This paper describes bistatic (multistatic) radar systems via Beyond The Horizon Radar HF signals as a practical extension to the FM/TV broadcast-based system. System configuration, performance measures and signal processing techniques applicable to air and missile defense missions will be discussed.

VHF Passive Bistatic Radar Observations of Ionospheric Targets with Distributed Digital Receivers

J. D. Sahr, C. Zhou, D. M. Gidner, and M. G. Meyer
Department of Electrical Engineering, University of Washington
Seattle, WA 98195-2500, U.S.A.

F. D. Lind
MIT Haystack Observatory
Westford, MA 01886, U.S.A.

We have designed and built a completely passive radar, observing the scatter of commercial FM broadcasts at 100 MHz. By computing the cross-ambiguity function of two widely separated receivers, we are able to generate full, unambiguous, range-Doppler profiles of radio scatter from ionospheric turbulence, meteor trails, and aircraft.

We'll briefly describe the principles of our radar's operation, and then proceed to demonstrate our recent experience with modern digital receivers. These receivers directly sample the RF (after amplification), and then digitally down convert and synthesize nearly arbitrary bandpass functions through digital downsampling. The resulting data is nearly perfect, eliminating IQ channel mismatch and DC offsets which plagued our earlier analog implementation.

Although digital receivers offer superb performance, care is required to achieve their promise. In particular one must limit the spectral content which is passed to the high speed (but nevertheless aliased) analog-to-digital conversion. For example, with our sample rate of 56 MHz, we would suffer from aliasing of VHF LO television broadcasts from 54 to 84 MHz. Woe awaits those who assume that the enormous potential dynamic range of these receivers is easily achieved.

Each digital receivers have two antenna inputs; we'll show early results from beam forming excercises to strip multipath from the reference signals, as well as estimation of azimuth information in the scattered signals.

We have expended considerable effort to address the large computational burden. Our standard process requires about 10 GFlops to keep up with raw data for ionospheric range-Doppler profiles. We'll describe some compromises that reduce this to about 1 GFlop with little performance sacrifice.

We'll present recent data outputs, and encourage interested observers to examine fresh data at

http://www-rcs.ee.washington.edu/∼radar/

3D Inverse Problem of HF Radar Sounding of TIDs

V. G. Galushko, Y. M. Yampolski, and V. S. Beley
Institute of Radio Astronomy, National Academy of Sciences of Ukraine
Kharkov, Ukraine

B. W. Reinisch and V. V. Paznukhov
Center for Atmospheric Research, University of Massachusetts
Lowell, MA, U.S.A.

The study of traveling ionospheric disturbances (TIDs) is of considerable importance for increasing our knowledge of the physical processes in the upper atmosphere, as well as for the practice of environmental protection and monitoring and "space weather" forecasts. Indeed, the TIDs represent signatures of atmospheric gravity waves (AGW) propagating through the ionosphere and playing an outstanding role in the energy exchange and coupling between various regions of the geospace. In addition, the AGW/TIDs, being an important agent transferring energy from the Earth surface and lower atmosphere to ionospheric and higher altitudes and back, are kind of an indicator of their primary sources.

Among the experimental methods of TID diagnostics the radar sounding techniques stand out. This is particularly true for the passive radar techniques that use the radiation from commercial radios in the capacity of probe signals. Such radars are relatively inexpensive to construct and operate and, with account of the great number of simultaneously operating broadcasting stations, could be used for organizing a global network of routine ionospheric monitoring at a comparatively low cost.

The Institute of Radio Astronomy, National Academy of Sciences of Ukraine (Kharkov, Ukraine) and the Center for Atmospheric Research, UMass Lowell (MA, USA) combined their efforts in developing a passive HF radar techniques for TID diagnostics [1] and implementing these with the DPS (Digisonde Portable Sounder) system of the UMass [2]. The methods were based on measurements of HF signal trajectory parameters (for the most part, from HF broadcasting radios) and allowed recovering basic parameters of TIDs in the model of a perfectly reflecting surface that moved at ionospheric heights. However, the model evidently was an oversimplification and did not allow fully comprehending TID dynamics.

In this paper we extend the TID restoration technique to the model of electron density waves propagating through a realistic ionospheric layer. Within the perturbation method for the ray optical eikonal relations are derived to connect trajectory parameter variations with TID characteristics. The inverse problem is solved in the spectral domain. Examples of computer simulation and results of real data processing are presented.

REFERENCE

1. Beley, V. S., V. G. Galushko, and Y. M. Yampolski, "Traveling ionospheric disturbance diagnostic using HF signal trajectory parameter variations," *Radio Sci.,* Vol. 30, 1739–1752,1995.

2. Beley, V. S., V. G. Galushko, D. Paznukhov, B. W. Reinisch, and Y. M. Yampolski, "HF radar sounding of TIDs with the use of the DPS system and signals from broadcasting stations," *PIERS-2000, Cambridge, Mass., Book of Abstracts,* p. 602, 2000.

HF/VHF Multisite Radar Diagnostics of Ionospheric Disturbances

V. G. Galushko, Y. M. Yampolski, and V. S. Beley
Institute of Radio Astronomy, National Academy of Sciences of Ukraine
Kharkov, 61002, Ukraine

J. C. Foster, P. J. Erickson
Atmospheric Sciences Group, MIT Haystack Observatory
Westford, MA 01886-1299, U.S.A.

B. W. Reinisch, V. V. Paznukhov
Center for Atmospheric Research, University of Massachusetts
Lowell, MA 01854, U.S.A.

Results of simultaneous ionospheric sounding with the use of coherent HF (oblique and vertical) and incoherent VHF scatter radars are reported. The measurement campaign, aimed at recovering large-scale wavelike processes in the upper atmosphere, was carried out during 10 days (13 to 22 March, 2001) at the site of MIT Haystack Observatory (Millstone Hill, MA, USA). A Digisonde Portable Sounder (DPS) of the University of Massachusetts (Lowell, MA) was used in the vertical sounding mode to provide electron density profiles every 5 min. Another DPS was operated in the oblique sounding mode. The instrument was upgraded to implement the passive technique of TID diagnostics developed at the Institute of Radio Astronomy, National Academy of Sciences of Ukraine (Kharkov, Ukraine). The radio signals used for the diagnosis were emissions from Radio CHU of the Canadian Time Service (Ottawa, Ont.) at 3.33 MHz and 7.335 MHz. Time-varying angles of arrival (azimuth and elevation angle) and Doppler frequency shifts of the probe signals were recorded every 4 minutes and were used for recovering basic parameters of wavelike disturbances (amplitude, propagation direction and velocity of motion) in the model of a perfectly reflecting surface.

During 3 days (14 to 16 March) the DPS-based measurements were accompanied by parallel round-the-clock operation of the incoherent scatter radar of the Massachusetts Institute of Technology that followed a special program. The vertically oriented and the steerable antennas of the radar were used to measure the electron density and the electron and ion temperatures of the ionospheric plasma through the height range 130 to 800 km. The fully steerable antenna was oriented in three consecutive directions, in order that the expected reflection point of the broadcast sounding signal should occur at the center of the corresponding angular sector. Such angular spacing of the antenna patterns corresponded to a nearly 70 km linear separation at the reflection height of the Radio CHU diagnostic signal. The data taking cycle (interrogating all the antennas and orientations) lasted for 5 minutes. This methodology allowed using the triangulation method to identify the direction of motion and speed of the wavelike ionospheric disturbances, similar like in paper.

Comparison of the measured data showed consistency of the results obtained by the three diagnostic methods. The difference between the motion directions of wavelike disturbances determined by the different methods was within 10 or 15 degrees, while that of the velocity and wavelength measurements was 10 to 12%. The conclusion of paper was validated that the moving solar terminator is a regular source of wavelike disturbances. The correlation length of the disturbances over the ionopheric layer thickness was determined.

Radar Applications of the Low Frequency Array (LOFAR)

F. D. Lind
MIT Haystack Observatory
Westford, MA 01886, U.S.A.

The Low Frequency Array is a new radio telescope being developed for operation in the 15 to 240 MHz frequency range by a collaboration between ASTRON (Netherlands), NRL, and MIT. This system will consist of approximately 13,000 dipoles in the frequency range from 15 to 90 MHz and 213,000 dipoles in the 110 to 240 MHz band. The instrument will possess one square kilometer of collecting area at 15 MHz in its current design. The antennas will be organized in a spiral configuration of roughly 100 stations with inter-station baselines of up to 400 km. These stations will be linked with optical fibers and digital receivers will be used at the antenna element level. Between 2 and 4 MHz of spectral bandwidth will be transmitted for processing at any instant in time out of a digitized bandwidth of 32 MHz. High performance digital systems and signal processing will be used to allow real time beamforming of multiple independent beams, transient detection and capture, and flexible remote operation of the instrument. I will describe the current state of the array's design, mention the scientific applications, and discuss plans for using this instrument in multistatic active and passive radar applications. In particular I will also discuss the potential applications of the array for the imaging of ionospheric irregularities using FM radio transmitters as radar signals of opportunity.

Differential Propagation Effects in Passive Radar Systems at HF

S. J. Anderson
Defence Science and Technology Organization
Edinburgh, SA 5111, Australia

The exploitation of transmitters of opportunity as illuminators for passive radar systems is based on the assumption that the receiving station can intercept faithfully both the original transmitted signal (the reference) and the echoes of that signal after scattering from targets in the joint field of view. In the case where the physical mechanism of propagation is line-of-sight space wave, this assumption is generally well-founded, and the process of information extraction via space-time-Doppler registration can be carried out on the basis that the received reference signal is essentially identical to the signal which was incident on the scatterer of interest.

At HF, and to a significantly lesser extent at VHF, it is possible, in principle, to exploit signals which have propagated via ground wave or skywave, thereby achieving an 'over-the-horizon' passive radar capability. These introduce an additional complication in the form of the signal transformations which arise in the course of propagation across a rough sea surface or via reflection from the ionosphere. The critical issue which must be addressed in such cases is the extent to which differential propagation effects compromise system performance.

We have conducted a number of experiments, incorporating both ground wave and skywave propagation paths, to establish the characteristics of differential propagation at HF. In the case of ground wave propagation, the modulation signature of a representative sea path was measured using a transmitter mounted in a small boat together with a high resolution multi-beam shore-based receiver. This signature was then compared with predictions based on a Green's function representation of the multiple scattering series. Using the validated multiple scattering model, the differential signatures and cross-ambiguity functions of triangular ground wave configurations were calculated for a range of sea conditions, yielding predictions of the fidelity of target parameter estimates.

For skywave propagation, we compared two-way signatures of echoes from differentially displaced scattering patches on the distant earth's surface. Measurements were carried out over a range of ionospheric propagation conditions. The resulting signal modulations were assessed in terms of their intrinsic impact on cross-ambiguity functions and on their identifiability and compensation. A similar procedure was applied to hybrid propagation paths.

The results of these investigations confirm our suspicion that significant degradation of passive radar modes can be introduced by differential propagation effects, but suggest that there is some prospect for reducing the deleterious effects by physics-based signal processing.

Session 2Ac1

Rough Surface Scattering

Backscattering from a Rough Surface when Strong Shadowing is Present

I. M. Fuks
Zel Technologies, LLC and NOAA Environmental Technology Laboratory
Boulder, CO 80305-3328, U.S.A.

In all existing models of wave scattering by a rough surface $z = \zeta(\boldsymbol{r})$, the probability distribution function (PDF) $W(\boldsymbol{\gamma})$ of surface slopes $\tilde{\boldsymbol{\alpha}} = \nabla\zeta(\boldsymbol{r})$ is one of the more informative statistical function describing the surface roughness. For low grazing angles, the surface shadowing can play a significant role in forming the micro radio wave backscattering cross sections. In particular, the PDF $W_{IL}(\boldsymbol{\gamma})$ of illuminated surface slopes can differs substantially from $W(\boldsymbol{\gamma})$. For rough surfaces, modeled as a stationary (spatial uniform) random function, the relation between these two functions was established in the following general form (see, for details, *F. G. Bass and I. M. Fuks* "*Wave Scattering from Statistically Rough Surfaces*", Oxford: Pergamon, 1978):

$$W_{IL}(\gamma) = \theta(\tan\psi - \gamma)W(\gamma)Q(\psi), \tag{1}$$

where ψ is an angle of grazing (complementary to the incidence angle), γ is the surface slope in the plane of incidence, and the factor $Q(\psi)$ does not depend on the slope γ, and is fully determined by a function $\Lambda(\psi) = \int_{\tan\psi}^{\infty}(\gamma\cot\psi - 1)W(\gamma)d\gamma$. It is seen from (1) that the slopes γ of the illuminated part of the surface have the same probability distribution as the whole surface: only "selfshadowed" slopes are excluded by the factor $\theta(\tan\psi - \gamma)$, and the normalization factor $Q(\psi)$ appears, which takes into account the total decrease of illuminated surface area. This is a direct result of supposed statistical independence of height ζ and slope γ at every given point of the surface.

Real rough surfaces do not satisfy this condition in general. For example, at rough sea surface, we can see that the characteristic slope at the upwind sea wave face grows with the elevation increase, and vise versa for slopes at downwind face. We obtained the explicit equations for $W_{IL}(\gamma)$ in the opposite limiting case, when height ζ and slope γ are fully correlated. As a result, factor $Q(\psi)$ converts to the function not only on ψ but also on γ, and PDF $W_{IL}(\gamma)$ of illuminated surface slopes can differ substantially from the $W(\gamma)$. It was shown that at low grazing angles ψ, the functional dependence between ζ and γ can lead to the essential increase of the slope PDF $W_{IL}(\boldsymbol{\gamma})$ for steep enough slopes (several r.m.s. of γ), and, correspondingly, to the grows of the backscattering cross section in the upwind direction. For downwind backscattering cross section the opposite effect takes place.

Rigorous Multi-Scale Solver for Rough-Surface Scattering Problems: High-Order-High-Frequency and Variation of Boundaries

O. P. Bruno
Department of Applied and Computational Mathematics
California Institute of Technology
Pasadena, CA 91125, U.S.A.

A. Sei and M. Caponi
Ocean Technology Department, TRW
Redondo Beach, CA 90278, U.S.A.

The electromagnetic scattering from rough surfaces plays an important role in a wide range of applications, including SAR imaging, remote sensing, detection, etc. The analysis of the scattering processes involved in these applications poses a rather challenging scientific problem as it requires description and understanding of diffraction by complicated surfaces. Computationally, the main difficulty arises from the multiple-scale nature of rough surfaces (such as the ocean surface), whose spectrum may span a wide range of lengthscales. A number of techniques have been developed to treat associated limiting cases. For example, the high frequency case, in which the wavelength λ of the incident radiation is much smaller than the surface lengthscales, can be handled by asymptotic methods such as geometrical optics or physical optics approximations. On the other hand, resonant problems where the incident radiation is of the order of the surface scale are treated by perturbation methods, typically first or second order expansions in the height h of the surface.

However, when a multitude of scales is present on the surface none of the techniques above is adequate, and attempts to combine them in a so-called two-scale approaches have been given by various authors. The two-scale models imply a splitting of the surface into a large and small scale, where typically a first order approximation in wavelength (Kirchhoff approximation) is used to treat smooth components of a surface and a first order in surface height (Rayleigh-Rice method) is used to deal with the rough components of the surface. The results provided by these methods are not always satisfactory — precisely as a result of the limitations imposed by the low orders of approximation used in both, the high-frequency approximation and the small perturbation methods.

To alleviate these drawbacks, our approach to multi-scale scattering is based on use of expansions of *very high order* in both parameters λ and h — which leads to algorithms based on complex variable theory and analytic continuation. The resulting approach expands substantially on the range of applicability over low order methods, and can be used in some of the most challenging cases arising in practice. Furthermore, this new method does not require separation of the length-scales in the surface into large and small, but instead it is able to deal with a continuum of scales on the surface. Indeed the high order expansions we utilize have a common “overlap” region in the (λ, h) plane where both components are highly accurate. More precisely, there is a range of surface heights and incident wavelengths for which both methods produce results with machine accuracy. Therefore by dividing the scales of a surface at a point in the overlap region we obtain a general method which is applicable to surfaces containing a continuum of length-scales — which is ideal for evaluation of scattering from rough surfaces with wide spectral distributions.

Optimizing Rough Surface Vibration Detection by Means of Adaptive Photo-EMF Detectors

S. Stepanov, P. Rodriguez Montero and J. Castillo Mixcoatl
INAOE
Puebla, 72000, Mexico

Operation of adaptive photo-EMF detectors [1] is based on generation of transient electrical current through a photo-conductor illuminated by vibrating light pattern, e.g. by regular interference or irregular speckle-like pattern. Between the most important areas of applications of these novel detectors, which were demonstrated recently, are laser vibrometry and profilometry of optically rough surfaces, but OCT oriented application is another highly promising area. These detectors allow us to detect fast general displacement of complicated light patterns in presence of relatively slow changes of position and shape of these patterns. They can utilize a big number of mutually uncorrelated speckle spots at the same time, which keeps average detected signal power and, finally, the output signal more or less constant, in contrast to tremendous fluctuations in output signal, which are inevitable for conventional (i.e. vibrometric or OCT) systems working with one fluctuating speckle spot.

Very much was done on understanding of detection of regular sinusoidal light patterns by photo-EMF detectors (i.e. when phase modulation in plane or in Gaussian waves is detected) recently [1]. The main problem, which is addressed in this work is - how the speckle structure of the detected signal beam influences the efficiency of the detection process, and which are the optimal conditions of photo-EMF detectors operation in this case. More precisely, large speckle spot number reduces output signal fluctuations and increases focal depth of the optical system. At the same time this needs utilization of photo-EMF detectors with bigger inter-electrode spacing, which makes their matching with preamplifiers more difficult and speed of the device suffers strongly.

Original experimental data obtained with GaAs photo-EMF detectors show that utilizing a moderate speckle number around 10x10 in the detected signal wave seems to be optimal. On one hand this enables reasonable focal depth of the detection optical system (about 1 cm for numerical aperture of the collecting lens ~ 0.1), and on the other hand - this keeps fluctuations in the detected output signal at a relatively low level $\leq 10\%$. Experimental demonstrations of measurements of vibrations, laser-induced ultrasonic displacements, and profiles of optically rough surfaces by GaAs photo-EMF detectors are presented.

REFERENCES

1. S. Stepanov, “Photo-electromotive-force effect in semiconductors”, in ‘Handbook of Advanced Electronic and Photonic Materials and Device’ ed. By H.S. Nalwa (Academic, San Diego, 2000), pp.205-272.

Investigation of the Near Fields Scattered by Small and Large Scale Rough Surfaces and Lateral Fluctuations in the Permittivity and Permeability of Nanostructures for the Syntheses and Modification of the Electrical Characteristics

E. Bahar
Electrical Engineering and Center for Electro-Optics
University of Nebraska
Lincoln, NE 68588-0511, U.S.A.

The electromagnetic near fields scattered by nanostructures due to fluctuations in the surface height and/or lateral variations in the electromagnetic medium parameters such as the complex electric permittivity, conductivity, and magnetic permeability are investigated. Since the scales of the medium fluctuations of the nanostructures considered could be significantly smaller or larger than the electromagnetic wavelengths, the familiar perturbation and physical/geometrical optics solutions based on the Kirckhoff approximations of the fields on the boundaries cannot be used nor is it possible to investigate sub-wavelength structures based on the far-field measurements. A full wave approach which employs complete field expansions that include propagating and evanescent waves as well as lateral waves and surface waves are used in the analysis of the total scattered near fields.

The surface is regarded as a ensemble of facets of arbitrary orientations and the cross sections are shown to be stationary over a broad range of facet sizes. The full wave approach can be used to determine the scattered near fields as well as far fields. Both large scale and small scale (including subwavelength) fluctuations of the rough surface are accounted for in the analysis.

The full wave solutions are not restricted in electromagnetic scattering by layered media with irregular interfaces. Scattering due to lateral variations in the complex electrical permittivities and magnetic permeabilities in each layer are also accounted for in the analysis. The full wave approach can also be used to determine the coupling between the propagating and evanescent waves, the lateral waves and the guided (surface) waves of the layered structures. Thus realistic, physically realizable models of nanostructures can be analyzed. The lateral waves and surface waves as well as evanescent waves are not accounted for in the familiar perturbation and physical optics analysis.

It is shown using the full wave approach, that in the physical optics large (compared to electromagnetic wavelength) scale limit, the near fields are expressed as integrals over the (spatial) propagating and evenscent wave vector spectrum of quantities related to the stationary phase, specular point surface element scattering coefficients and the surface slope probability density functions. In the very small (nanoscale, sub-wavelength) perturbation limit, the near fields are expressed as integrals over the (spatial) propagation and evenscent wave vector spectrum of quantities related to the small slope surface element scattering coefficients and the surface height spectral density functions. Since the surface height spectral density function is the Fourier transform of the surface height auto-correlation function, the full wave analysis can be applied to the synthesis and modification of nanostructure surfaces. It contributes to the fundamental understanding of the physical, analytical and optical characteristics of artificially engineered surfaces due to nanoscale roughness. Since the full wave analysis accounts for scattering due to lateral fluctuations in the electrical and magnetic properties of stratified structures, synthesis and modification of nanostrutures such as quatum dots can also be considered.

Fast and Exact Method for Calculating Bistatic Scattering from Periodic Rough Surfaces

D. Kasilingam
University of Massachusetts, Dartmouth
North Dartmouth, MA, U.S.A.

Even though in the past, scattering calculations have focussed on the backscatter component, in recent years there has been an increased interest in calculating bistatic scattering from targets and natural surfaces. Methods for bistatic calculations have followed the techniques used for backscatter calculations, where a single incidence and scattering direction are identified and the scattering components are calculated in these directions. However, ideally bistatic scattering calculations should calculate the bistatic scattering components in all possible scattering directions.

For periodic surfaces, the scattering components can be calculated exactly since the solution involves a discrete set of scattering modes known as Floquet modes. However, this set includes an infinite set of evanescent modes, which do not carry any power but are necessary to match the boundary conditions at the periodic surface. In practice, the series of evanescent fields is truncated at a point beyond, which the contributions from these modes are negligibly small. The number of evanescent modes varies according to the roughness of the surface. For calculations of scattering from slightly rough to moderately rough surfaces, the number of evanescent modes may be small. However, for more complicated surfaces, a large number of such modes may have to be included. Furthermore, due to their exponential dependence, the computation of evanescent modes and their projections are generally tedious and may result in significant computational errors due to the large fluctuation in their values.

In this paper, a technique, which eliminates the need to compute the evanescent modes, is presented. The evanescent modes are not simply substituted out, but instead they are factored out of the calculations by projecting the boundary conditions onto a subspace, which is orthogonal to all the evanescent modes. The method is exact and generates results which are consistent with the computationally more demanding methods. The method is compared with other analytical and numerical techniques and found to produce results with greater consistency. Since the number of propagating modes is finite, the computation speed is significantly faster. In addition, the elimination of the fast-changing, evanescent modes also improves the accuracy of this method. For lossless media, it is shown that the scattering components can be related to the incident components through a unitary linear transformation. This unitary transformation defines a model that provides the bistatic scattering components in terms of all possible incident scattering components. Several examples of bistatic scattering from ocean and terrain like surfaces are presented.

Mean Dyadic Green's Functions of a Random Medium Layer with Rough Boundaries

S. Mudaliar
ARCON Corporation
Waltham, MA 01731, U.S.A.

For studying scattering in statistical environments the concept of the mean Green's function is useful. It plays a role similar to the ordinary Green's function in deterministic problems. Furthermore, it is important in the analysis of the second moment of the fields which is essential for the computation of the scattering cross sections. This paper is on the derivation of the mean dyadic Green's functions for electromagnetic waves in a random medium layer with rough boundaries. The geometry of the problem consists of a random medium layer bounded by rough surfaces which are parallel planes on the average. The permittivity of the random medium layer has a deterministic part and a randomly fluctuating part. All the fluctuations of the problem are small and smooth and independent of each other. The bottom surface is a perfect conductor.

The Green's functions are defined as a system of differential equations with appropriate boundary conditions. Based on the fact that the fluctuations in boundaries are small and smooth, the boundary conditions are translated onto average planar surfaces. This enables us to use the unperturbed Green's functions and reduce the problem to a single integral equation, where all the fluctuations of the problem are represented by a zero mean random operator. Smoothing leads to an integral equation for the mean Green's functions. On applying the wave operator to this equation we obtain an integro-differential equation for the mean electric fields within the layer. We employ a multi-scale analysis to obtain the first order solutions to the mean propagation constants. We next use boundary operators on the smoothed integral equation. This leads to integral equations for the various coefficients of the mean Green's functions. It turns out that these equations can be solved by transform methods. Further details of the analysis and some properties of the mean dyadic Green's functions are given in the paper.

Bi-Spectrum Scattering Model for Dielectric Randomly Rough Surface

N. Liu and Z. Li
Tsing Hua University
Beijing, 100086, China

Because Kirchhoff model (KM) and small perturbation model (SPM) is valid to predict the scattering coefficient of dielectric randomly rough surface only in high and low frequency band, it is necessary to develop the theoretical model with wider valid range. The integral equation method is more complex to be applied for the dielectric surface for the complexity of the integral equations leads to the complex deducing process and result. To obtain an analytical expression, two physical simplification are taken to be "Discard terms in the tangential field expression involving the sum of $R_\perp$ and $R_{||}$" and "Approximate the local incident angle in $R_\perp$ and $R_{||}$ by the incident angle for surfaces with small scale roughness and by the specular angle for surfaces with large scale roughness".

Though numerical simulations and experiments have proved that IEM shows wider application range, these approximations cause to two problems to be improved: the bistatic scattering coefficient does not satisfy the reciprocal theorem and the angle of Fresnel reflection coefficient is ambiguous.

The traditional two-scale model (TSM) for dielectric model considers the scattering characteristics at different incident angle and use Kirchhoff and small perturbation method to analyze the field at near-normal and non near-normal angle. Because the model needs the probability distribution of the large-scale surface's slope, the common surface must be separated into large scale and small perturbation parts and assumed its slope's distribution. This assumption brings further parameters that are not necessary in IEM and not facile to be achieved. So the valid range of TSM is narrower than IEM.

Brown's two-scale model presented a method that split the surface in spectral domain. This idea avoids the separation according to the incident angle and shows a reasonable splitting way for the common surface. Yet because of the rectangle-windowed splitting filter, the approximations and deducing method, only backscattering coefficient for conducting surface is achieved and its final expression is not convenient to be calculated. There is no further study to extend this model to dielectric surface in bistatic case.

Basing on the aim to simplify the analyzing and the results, a bi-spectrum model (BSM) is built by splitting the surface in the spectral domain. Because the component in the lower frequency band approach Kirchhoff conditions nearly, the scattering field is approximated by Kirchhoff method. The surplus surface is forced to satisfy the small perturbation condition, so its scattering field is derived by perturbation method in which the affection of Kirchhoff surface is considered either. The analyses are concluded into four steps: splitting the surface in the spectral domain, analyzing the surface field of the split surface, solve the Kirchhoff field and the small perturbation field, achieving the final expression of scattering coefficient.

BSM use a scale-compression filter and the perturbation theory which are different to Brown's model, so it has a simple bistatic expression that is easy to be calculated. The analytical expression of BSM can degenerate to KM and SPM when the surface satisfies KM and SPM conditions. Its reciprocity can be proved theoretically from the bistatic scattering coefficient expression. Comparisons with IEM and experimental results show that BSM is suitable for common randomly rough surface. If the surface is near the Kirchhoff conditions, BSM can predict the scattering coefficient with high accuracy. To the surface doesn't satisfy Kirchhoff conditions extraordinarily, it is still possible to calculate the scattering coefficient with acceptable accuracy. Namely, the validity range of BSM is wider than KM and SPM.

Polarization Dependent Scatter Cross Sections of Random Rough Surfaces-Stationary Two-Scale Full Wave Approach

E. Bahar and P. Crittenden
Electrical Engineering Department and Center for Electro-Optics
University of Nebraska
Lincoln, NE 68588-0511, U.S.A.

A full wave approach that also accounts for the excitation of surface waves and lateral waves by plane waves incident upon rough surfaces is used to determine the radar cross sections of composite rough surfaces at near grazing incidences.

Using the small height/slope perturbation solution, it is shown that the vertically and horizontally polarized backscatter cross sections of random rough surfaces have a significantly different dependence upon the incident angle. Thus, for highly conducting surfaces, the ratio of the two cross sections σ^{PP} (P=Vertical, Horizontal) is $\frac{\sigma^{W}}{\sigma^{HH}} = \left|\frac{1+sin^2\theta}{cos^2\theta}\right|$. As the incident angle θ approaches 90^o, this ratio becomes very large. The corresponding expressions for the physical optics solutions are polarization independent. The physical optics and perturbation solution for the backscatter cross sections are in agreement only for normal incidence (specular scatter).

Ample experimental data, however, indicate that the backscatter cross sections σ^{PP} (P = V or H) can be of the same order of magnitude and also significantly larger than the values predicted by both physical optics and perturbation theory.

A unified full wave approach is used to express the backscatter cross sections as weighted sums of two cross sections. One is associated with the larger scale rough surface cross section, multiplied by the magnitude squared of the smaller scale rough surface height characteristic function. The second is the cross section associated with the smaller scale surface height, modulated by the slopes of the larger scale surface. When the composite rough surface is characterized by a continuous surface height spectral density function, it becomes necessary to judiciously separate the smaller scale surface from the larger scale surface. It is shown that this can be done reliably using the full wave approach by seeking stationary solutions to the cross sections over a wide range of mean square values for the small (or large) scale surface heights. These stationary values for the polarization dependent backscatter cross sections can be practically equal and also significantly larger than the corresponding physical optics and perturbation results.

At a free space-dielectric (nonmagnetic) interface only vertically polarized surface waves can be excited. Since these surface waves have complex propagation coefficients, they attenuate along the interface and contribute to a reduction in the vertically polarized backscatter cross sections (compared to the backscatter cross sections for perfectly conducting interfaces that do not support surface waves).

Bistatic Scattering from Inhomogeneous Soil Profile

C.-Y. Hsieh
E.C.E., National Kaohsiung Institute of Marine Technology
Kaohsiung, Taiwan

In the remote sensing area theoretical models of microwave scattering properties from bare soil field are needed to interpret the measured data, and to generate simulated data for developing retrieval algorithms when the measured data is scarce or does not exist at all. The remote sensing of soil moisture using microwave sensors require accurate and realistic scattering models for the wave scattering from random rough soil profile. In this paper we show the model developed for electromagnetic wave bistatic scattering from bare soil field. The model is based on a pair of integral equations. For evaluating the measurement the comparisons of model prediction with the measured data are made. The unknown quantity in the model is the surface correlation length. The surface correlation length is chosen to fit the measured data. The parameters of soil moisture content, surface rms height, surface correlation length will affect the scattering strength from bare soil. Further the soil composition of sand, loam and clay will also influence the scattering coefficient from bare soil surface. It is seen that satisfactory agreement is obtained between the model prediction and measured data.

Interpretations for a part of the soil data have already been published in the literature. Between 1984 and 1992 many campaigns were carried out systematically by using the mobile measurement system to the signature studies on agricultural fields. Between 1989 and 1993 Wegmuller et al. Selected sets of data where only one soil parameter changed to study the dependence of the bistatic scattering coefficient and of the emissivity on the surface roughness and the soil moisture.

In this paper we developed a model for bistatic scattering coefficients from bare soil surfaces at microwave band. To account for bistatic scattering properties in the plane of incidence we develop a formulation for estimating the tangential surface fields on the randomly rough dielectric surfaces and show the method to characterize the surface roughness parameters of bare soils and fields. The parameters of bare soil surface includes the surface standard deviation, surface correlation length, soil moisture content, the ration of surface component-clay, sand and loam. The model prediction of bistatic scattering behaviors from bare soil surfaces with different surface parameters are also studied. Finally the comparisons of model predictions with the measured data are made.

From the model prediction, integral equation model is compact and has relatively simple algebraic form. For bistatic scattering from soil surfaces the only unknown parameter is the surface correlation length. The surface correlation length is chosen for data fitting. The difference between integral equation model and the measured data by truck-based radar is less than a dB. No modification to ground truth were made.

REFERENCES

1. Wegmuller, U. and C. Matzler, “Active and passive microwave signature catalogue on bare soil (2–12 GHz),” *Report of the Institute of Applied Physics*, University of Bern, Sidlerstrasse 5, CH3012 Bern, Switzerland, 1993.
2. Saatchi, S. and U. Wegmuller, “Modeling and measurement of microwave emission and backscattering from bare soils surfaces,” *Proceedings of IGARSS’92,* Houston, Texas, IEEE No. 92CH3041-1, Vol._, 1190–1192, 1992.

Session 2Aa2

Computational Wave Electromagnetics I – Photonics

A Full-Vector Finite Solution of Photonic Crystal Fibers

M. Koshiba
Division of Electronics and Information Engineering
Hokkaido University
Sopporo, 060-8628, Japan

In recent years, there has been a significant interest in a photonic crystal fiber (PCF) consisting of a central defect region surrounded by multiple air holes running along its length. Light confinement is explained by two different mechanisms: the index-guiding effect [1, 2] and the photonic band-gap effect [3, 4]. Band-gap guidance has no analogue in conventional fibers and allows for novel features such as light confinement to a low-index core. Especially, index-guiding PCFs, also called holey fibers (HFs) possess numerous unusual properties such as wide single-mode wavelength range, bend-loss edge at short wavelength, extremely large or small effective-core-area at single-mode region, anomalous group-velocity dispersion at visible and near-infrared wavelengths, and strong wavelength-dependent beam divergence. To accurately model PCFs with large refractive-index difference between the pure silica and air region, it is crucial to use a full-vector model. In particular, a complete vector model is required to predict sensitive quantities such as dispersion and birefringence.

An early full-vector model for HFs has been based on a modal decomposition technique using sinusoidal functions (plane-wave expansion method: PWE) [5, 6], Hermite-Gaussian functions (localized function method: LFM) [7, 8], or cylindrical functions (multipole method: MM) [9]. Recently, published models utilize other direct, numerical analysis techniques such as finite element method (FEM) [10] and finite-difference time-domain (FDTD) [11]. FEM can treat not only HFs but photonic band-gap fibers (PBGFs) with arbitrary shaped, sized, and arranged air holes, and a recently developed full0vector FEM with curvilinear hybrid edge/nodal elements [12] is very useful for avoiding spurious solutions and for accurately modeling curved boundaries of air holes in PCFs.

In this paper, using the full-vector FEM, the single-mode nature of HFs is accurately analyzed as a function of wavelength. The cladding effective index which is a very important design parameter for realizing a single-mode HF and is defined as the effective index of the fundamental space-filling mode (FSM) of the infinite photonic crystal cladding if the core is absent, is also determined using the FEM. In traditional fiber theory, a normalized frequency, V, is often used to determine the number of guided modes in step-index fibers. In order to adapt the concept of V-parameter to HFs, the effective core radius, a_{eff}, should be determined for each given ratio of hole size to hole pitch. The value of a_{eff} is calculated using the actual numerical aperture, NA, given by the FEM. In addition, using the effective index of the fundamental HE_{11} mode of HFs, computed, n_{eff}, computed as a function of wavelength, the group velocity dispersion is accurately calculated. Finally, modal birefringences in HFs and PBGFs are numerically investigated.

REFERENCES

1. Knight, J. C., *et al.*, *Opt. Lett.*, Vol. 21, 1547–1549, Oct. 1996.
2. Birks, T. A., *et al.*, *Opt. Lett.*, Vol. 22, 961–963, July 1997.
3. Knight, J. C., *et al.*, *Science*, Vol. 282, 1476–1478, Nov. 1998.
4. Cregan, R. F., *et al.*, *Science*, Vol. 285, 1537–1539, Sept. 1999.
5. Fernando, A., *et al.*, *Opt. Lett.*, Vol. 24, 276–278, Mar. 1999.
6. Fernando, A., *et al.*, *J. Opt, Soc. Am. A*, Vol. 17, 1333–1340, July 2000.
7. Mogilevtsev, D., *et al.*, *J. Lightwave. Technol.*, Vol. 27, 2078–2081, Nov. 1999.
8. Monro, T. M., *et al.*, *J. Lightwave. Technol.*, Vol. 18, 50–56, Jan. 2000.
9. Steel, M. J., *et al.*, *Opt. Lett.*, Vol. 26, 488–490, Apr. 2001.
10. Breched, F., *et al.*, *Opt. Fibers Technol.*, Vol. 6, 181–191, Apr. 2000.
11. Lizier, J. T., *et al.*, *IEEE Photon. Technol. Lett.*, Vol. 13, 794–796, Aug. 2001.
12. Koshiba, M., *et al.*, *J. Lightwave Technol.*, Vol. 18, 737–743, May 2000.

Negative Index Behavior in Hexagonal-Symmetry Photonic Crystals

G. R. Hadley
Sandia National Laboratories
Albuquerque, NM 87185-5800, U.S.A.

Previous work [1] has shown that photonic crystals fabricated by etching a hexagonal array of holes into a slab waveguide structure can exhibit unusual properties in certain wavelength regimes. In particular, they may diffract light in a manner that is describable in terms of a negative index of refraction. Such behavior has a number of important practical applications such as focusing of a diverging beam, allowing the formation of a guiding lens train, or the construction of a ring laser cavity using the juxtaposition of positive and negative refractive index materials [1]. We have investigated this phenomenon theoretically by modelling the photonic crystal waveguide in two dimensions using triangular mesh finite difference methods. The purpose of this investigation is to both increase our understanding of the basic phenomenon as well as design more useful devices.

The present understanding of the cause of negative index behavior in photonic crystals relies on the existence of star-shaped equifrequency surfaces near the lowest band-edge [1]. However, simulations performed for frequencies in this regime showed no negative index behavior, whereas such behavior was seen at much higher frequencies in the vicinity of bands 5 and 6 where the surfaces are essentially circular. It thus appears that a detailed understanding of the origin of this behavior is still lacking, and we have constructed several numerical tools to examine this phenomenon, including (1) a 2D Helmholtz solver that simulates propagation through a large domain (20×20 unit cells) of the photonic crystal, (2) a 2D periodic eigenmode solver that allows the construction of band diagrams, and (3) a 3D periodic eigenmode solver to investigate propagation through a realizable slab structure, including out-of-plane loss.

REFERENCES

1. Notomi, M., *Phys. Rev. B*, Vol. 62, No. 16, 10696, 2000.

Full-Vectorial Integral Equation Analysis of Arbitrary-Shaped Waveguides Including Leakage, Losses and Gain

S. V. Boriskina, T. M. Benson, and P. Sewell
School of Electrical and Electronic Engineering, University of Nottingham
Nottingham, NG7 2RD, UK

A. I. Nosich
Institute of Radio Physics and Electronics, National Academy of Sciences of Ukraine
Kharkov, 61085, Ukraine

A fast and accurate algorithm based on a full-vectorial contour integral equation (IE) analysis of the natural modes of microwave and optical dielectric waveguides of arbitrary cross-section is presented. Galerkin's method, together with the Analytical Regularization procedure, is applied to discretize the IEs and solve the eigenvalue problem. The contour of a waveguide cross-section is characterized by a parametrical curve with a finite curvature at each point, which avoids the singularity points at corner regions. However, the analysis provides numerically convergent and accurate results even for waveguides with sharp corners (e.g., rib and rectangular dielectric waveguides and fibers with a triangular-shaped core region) where this curvature approaches infinity. One of the attractive features of the approach proposed is that it is formulated in the complex domain and so immediately allows calculation of leaky and complex modes as well as the treatment of lossy and amplifying media.

Both the fundamental and higher-order mode propagation characteristics and the field distributions of several common and novel waveguide geometries have been studied in bound and leaky regimes. Numerical results consistent with other theories and experimental data will be presented for a wide range of practical waveguides to demonstrate the efficiency, accuracy and versatility of the method developed. These include waveguides of arbitrary geometrical shapes, such as rib waveguides of various profiles, double-core or multi-cladding fibers, dielectric image guides and buried optical waveguides. Finally, the study of the polarization-dependent properties of waveguide structures with either deliberate or accidental shape imperfections (e.g., cuts or air bubbles) will be discussed.

Wide-Angle FD-BPM Analysis of TM Modes in Nonlinear and Nonreciprocal Integrated Optical Waveguides

L. D. S. Alcantara
Escola de Engenharia Elétrica da USP, São Carlos, SP, Depto. de Engenharia Elétrica
São Carlos, 13560-250 SP, Brazil

F. L. Teixeira
Department of Electrical Engineering and ElectroScience Laboratory, The Ohio State University
Columbus, OH 43212, U.S.A.

A. C. Cesar and B.-H. V. Borges
Escola de Engenharia Elétrica da USP, São Carlos, SP, Depto. de Engenharia Elétrica
São Carlos, 13560-250 SP, Brazil

New all-optical network concepts are placing increasing demands on both active and passive optical component technologies. Particularly important for passive components is the ability to perform different tasks simultaneously. Nonlinear devices are commonly employed as logical gates and switches, whereas nonreciprocal devices are used as isolators and circulators. The use of optical devices employing nonlinear and nonreciprocal materials simultaneously paves the way for obtaining such functions in a single device.

Due to their inherent complexity, a detailed analysis of any such device is possible only through numerical methods. In this work, we introduce a novel finite-difference beam-propagation (FD-BPM) formalism for the simulation of integrated optical waveguides composed of both Kerr-type nonlinear and magnetooptic nonreciprocal materials. The formalism can handle various Kerr-type nonlinearity mechanisms (e.g., heating, electronic distortion, molecular orientation). The formalism can also simulate structures with longitudinal variation more adequately since longitudinal derivatives of the permittivities are explicitly taken into account.

When magnetooptic materials are involved, it is often convenient to separate the solutions into TE and TM modes. When a static magnetic field is properly applied across the structure, the nonreciprocal behavior is observed only for TM modes. Because of this and due to their added complexity (the entries on the electric permittivity tensor depends on two electric components simultaneously), we focus here on the TM propagation analysis.

Interesting features unveiled by the FD-BPM simulations include (1) the effect of the power density on the modal effective index, (2) the nonreciprocal phase shift, and (3) high-index channels induced in the non-linear medium for high input power densities.

A special iterative algorithm is introduced to accelerate the convergence in the nonlinear medium, and both a transparent boundary condition (TBC) and a generalized perfectly matched layer (PML) are used to truncate the computational domain. FD-BPM results are compared against finite-difference time-domain (FDTD) simulations, showing good agreement.

Simulation of Transverse Anisotropic Waveguides by an Efficient H-Field Finite-Element BPM

J. P. Silva, H. E. Hernández-Figueroa and A. M. F. Frasson
School of Electrical and Computer Engineering (FEEC), University of Campinas
São Paulo, 13083-970 , Brazil

In the last ten years or so, a considerable effort has been done to simulate in an efficient and accurate manner the electromagnetic propagation along optical waveguides. One of the most powerful numerical tool used in these simulations is the beam propagation method (BPM). Among the numerical methods available to discretize the waveguides' cross section, it is quite well established by now, the superior performance achieved when the finite-element method is adopted. So far, a number of scalar, semivectorial and vectorial finite-element (FE) BPM schemes have been reported in the literature.

For dielectric media, it is quite clear that high accuracy and flexibility is attained by choosing the magnetic field as the wave equation's unknown, due to its continuity over the dielectric interfaces. This permits the use of nodal elements, which are simpler than the edge ones, specially for high order. For this situation, spurious solutions can be efficiently suppressed by forcing the divergence condition into the formulation, which permits, as additional advantage, to eliminate the axial field component. As a consequence, a highly efficient scheme which solves the magnetic field's transverse components, is obtained.

All this has been widely and thoroughly reported in the literature, specially in connection with the so called modal (eigenvalue) analysis, see [1] and references therein. For the BPM situation, such approach has been exploited by Obayya $et al.$ [2] and Pinheiro $et al.$ [3]. In the former isotropic media was considered, including PML and the wide-angle Padé approach; while in the latter, transverse anisotropy was treated, however, hard boundary conditions (perfect electric or magnetic walls) and paraxial propagation were adopted. The limitations exhibited in [3] are mainly due to the simplifications introduced in that formulation, making unclear and cumbersome the introduction of proper radiation boundary conditions and wide angle features. Here, the corresponding vector operators are manipulated and presented in such a way that only one minor and well acceptable simplification is needed, facilitating the straightforward introduction of both PML and Padé approximants.

The careful analysis of key examples such as, anisotropic channels with angular displacement from the optical axis, and nonreciprocal magnetooptic Y-junctions demonstrate the usefulness and effectiveness of the present scheme.

Acknowledgment – The authors heartily thank the Brazilian Agencies CAPES and CNPq (Proc. No. 301 209/94-4), and CAPES PICDT-Federal University of Espirito Santo, for their financial support.

REFERENCES

1. Hernández-Figueroa, H. E., F. A. Fernndez, and J. B. Davies, "A Vectorial Finite Element Formulation for Analysing 2D Leaky Waveguides," *IEEE Transactions on Magnetics*, Vol. 31, No. 3, 1710–1713, May 1995.
2. Montanari, E., S. Selleri, L. Vincetti and M. Zoboli, "Finite element full-vectorial propagation analysis for three-dimensional z-varying optical waveguide", *IEEE/OSA J. Lightwave Tech.*, Vol. 16, No. 4, 703–114, Apr 1998.
3. Obayya, S. S. A., B. M. A. Rahman, and H. A. El-Mikati, "New full-vectorial numerically efficient propagation algorithm based on the finite element method," *IEEE Journal Lightwave Technology*, Vol. 18, No. 3, 409–415, Mar 2000.
4. Pinheiro, H. F., and H. E. Hernández-Figueroa, "Novel finite-element formulation for vectorial beam propagation analysis in anisotropic medium", *IEEE Photonics Technology Letters*, Vol. 12, No. 2, 155–157, Feb 2000.

Polarized Spatial Solitons in Cubic Chiral Materials

H. Torres-Silva and M. Zamorano
Department of Electronics, Faculty of Engineering, University of Tarapacá
Arica, Chile

Recent results [1] showed that in the presence of linear and nonlinear competing mechanism of polarization rotation in an isotropic medium, novel elliptically polarized temporal soliton exist which can propagate without rotation of the axes of polarization. These new soliton states influence the whole dynamics of soliton-like pulse propagation in nonlinear media with chiral optical activity. The aim of the present work is give a contribution to the study of spatial soliton propagation in anisotropic chiral media. We found that two new stationary vector solitons appear as a result of the joint action of nonlinearity and chirality in the fundamental generalized nonlinear Schrödinger equation. We start from the double curl wave equation,

$$\nabla \times \nabla \times \vec{E} - 2\omega t_c\sqrt{\mu_0\varepsilon_0} = \left(\frac{\omega}{c}\right)^2 (\varepsilon_c/\varepsilon_0 - t_c^2)\cdot\vec{E} - \left(\frac{\omega}{c}\right)^2 P^{NL} \tag{1}$$

where $E = \sum_{j=x,y}\Psi_j(z,t)E_j(x,y)\exp(i(kz-\omega t)+cc)$ is the electric field, ω is the angular frequency, c is the light velocity in vacuum, ε_c is the permittivity tensor, t_c is the chirality parameter and P^{NL} is the spectral amplitude of the nonlinear induced polarization which can lead to rotation of the polarization ellipse of the plane electromagnetic wave.

To investigate the stability of stationary solutions we can use a combined analysis of the system of the two coupled nonlinear Schrödinger equations in the weak guidance approximation, which is obtained from equation (1), and the evolution of the Stokes vector $S = (S_1, S_2, S_3)$ on the Poincare Sphere.

In one of the standard conventions the Stokes parameters are defined as $S_i = \Psi_j^*(\sigma_i)_{jk}\Psi_k$, where σ_i are the Pauli spin matrices and with small anisotropy along the direction of propagation the evolution equations of S_i take the form:

$$\frac{dS_1}{dz} = -2kt_cS_2 + k(1-B)S_2S_3, \quad \frac{dS_2}{dz} = 2kt_cS_2 - k(1-B)S_1S_3, \quad \frac{dS_3}{dz} = kBS_1S_2 \tag{2}$$

where B is a coefficient which take into account the energy interchange between the circular components. Without solving equation (1) exactly, and for different values of t_c and B we can study the polarization dynamics of solitons in the case that the solution of (1) is nearly circular. Some results are obtained for the output polarization state of an optical beam propagating along a birefringent single mode fiber when the input polarization is given. The output Stokes polarization parameters are either periodic or aperiodic depending of t_c and B. When new elliptically polarized solitons appear beyond the bifurcation points the circulary polarized solutions loses its stability.

Numerical results of elliptical solitons which appear as a result of bifurcation from the circulary polarized solutions will be discussed and presented at the Conference.

ACKNOWLEDGEMENTS

The authors thank the Chilean Agency CONICYT for their financial support. FONDECYT No. 1010300, PM.UTA No. 8723–0. and Proyecto de Internacionalización, Universidad de Tarapacá.

REFERENCES

1. Torres-Silva, H. and M. Zamorano, "Chiral effects on optical solitons," submitted to *Journal Mathematics and Computers in Simulation on "Nonlinear Waves: Computation and Theory II"*, 2001.

Session 2Ab2

Computational Wave Electromagnetics II – Electronics

Three-Dimensional Dynamic Modelling of Liquid Crystal Display Cells Using a Vector Approach and Finite Elements

F. A. Fernandez, S. E. Day, P. Trwoga, H. Deng, and R. James
Department of Electronic and Electrical Engineering, University College London
London, WC1E 7JE, England

A new approach for the dynamic, three-dimensional modelling of liquid crystal cells is presented. The method is based on a variational approach to the Oseen-Frank free energy formulation that establishes a balance between electric and elastic energies in the liquid crystal. The method considers three elastic constants and uses a vectorial rather tensorial representation of the director field. A simpler form that uses only two constants and is faster to operate is obtained as a by-product of the full three-constants model. Finite elements over a mesh of tetrahedral elements are used in the solution of both the electric potential and director distributions and these are combined within a finite difference time stepping procedure.

The nonlinear interdependence of the electric potential and directors is resolved by iterations within the time steps until consistence is achieved. Finite differences in the time domain are used as a base for the time stepping process, which due to computing time restrictions has been based on a simple forward iteration scheme. A variational approach of the energy formulation leads to the dynamic representation of the behaviour of the liquid crystal cell and the finite element representation of the director field leads to an expression containing third order powers of nodal values of director components. This causes difficulties for the numerical solution of the problem. However, after some manipulation, the higher order terms can be modified into a form that becomes linear if the elastic coefficients K_{22} and K_{33} are considered equal. Thus, a simpler, less accurate but faster form of the method can be constructed using this approximation. Furthermore, this modification leads to a simpler implementation of the remaining terms. The full three constants implementation for an accurate calculation, requires the inclusion of the nonlinear term, which is cubic in terms of director values. Linearization of this term for the numerical solution of the problem is performed by iterations using the values of directors at the previous time step.

Dirichlet boundary conditions are imposed directly on the resultant matrix equation, thus reducing the order of the system. Neumann boundary conditions, required at the lateral edges of the cell, are implemented by defining auxiliary prismatic elements at the edges, and forcing the normal derivatives of potentials and/or directors to be zero there. Periodic boundary conditions are also implemented by forcing the same surface mesh on corresponding sides. Results of the analysis of practical liquid crystal cells show agreement with experimental results and with results from other numerical approaches.

Electromagnetic Response of Fractal Media in Geophysical Environment

V. J. da C. Farias
Mathematics Department, Federal University of Pará
Abaetetuba, Pará, 66000-000, Brazil

B. R. P. da Rocha
Electrical Engineering Department, Federal University of Pará
Belém, Pará, 66075-000, Brazil

A quantitative interpretation of Induced Polarization data in geophysical prospecting is an hard task due to the fractal nature of geologic environment. To carry out this interpretation, it's necessary a physical model to explain the behavior of the polarizable medium within a large frequency range.

The "Fractal Model to Complex Resistivity" used here considers the fractal effects of the porous surface and includes the bulk response of rocks. The parameters of this model include the DC resistivity (ρ_0), the chargeability (m), two relaxation times (τ_1 and τ_2), a diffusion constant (K) and a fractal parameter (η). The later two parameters are related to the fractal rough pore interfaces between the conductive grains (metallic or clay minerals) which are blocking the pore path and the electrolyte. The introduction of the fractal roughness factors permits the investigation of the texture of rocks which is very important factor in explaining their electrical property.

In this paper, the induced polarization response over an horizontally and cylindrically stratified media was obtained. We considered the fractal model to complex resistivity to a intrinsic electrical properties of the polarizable layer. It was used four electrode array in order to measure the ground resistivity. The results showed that: 1) the fractal parameter (η) dominates the phase response of the apparent resistivity in low frequency. This result is very important for petrophysics interpretation of field data; 2) the measurements, in both the situation considered here, permit the determination of the medium properties, been the electromagnetic coupling negligible to frequencies lower than 10^4 Hz.

Computation of the Dynamic of a Gas Spark Discharger

D. S. das Virgens Alves
Computation Department, Centro de Estudos Superiores do Pará
Belém, Pará, Brazil

B. R. P. da Rocha
Electrical Engineering Department, Federal University of Pará
Belém, Pará 66075-900, Brazil

An hybrid code for modeling a discharge in a gas protection device is presented. It is composed by a radiation code, a plasma code and a wavefront code used for the numerical simulation of the dynamic of a gas spark discharger.

This work presents a model based in physical links to describe the arcs formation in the gas spark discharger terminals due to surge input, the arcs attachment and the arcs collapse due to surge end.

The radiation code is based on the finite differences in time domain method applied to the Maxwell curl equations for the electromagnetic fields computation.

The plasma code is based on the FDTD method applied to the Aflvén equations. The electric and magnetic force equation acting on the anions SF_6^- and on the cations SF_6^+ and on the electrons, and the continuum equation of heat, electric charge, mass, momentum, energy and magnetic flux for the electromagnetohydrodynamic coupling computation, considering thermal, electric and magnetic arc constrictions.

The wavefront code is based on the FDTD method applied to the Huygens operator on the Poynting vector for the energy transfer computation, considering the electric properties evolution due to the forerunners propagation.

Session 2Ac3

Optics and Photonics, Lasers, Gyrotrons

Analysis of High Reflectivity in Brillouin-Enhanced Four Wave Mixing

F. Ao, H. Hang, S. Li, D. Zhang
Guilin Institute of Electronic Technology
Guilin, Guangxi 541004, P. R. China

In this paper we analyze the conditions for high reflectivity of transient interaction in Stimulated Brillouin-enhanced Four Wave Mixing system under pump depletion. By choosing system's input parameters properly, we can achieve a high reflectivity almost 10^7 through stimulation.

Stimulated Brillouin-Enhanced Four Wave Mixing (SBEFWM or BEFWM) has been received considerable attention recently [1, 4, 5], because it has many advantages to overcome the main shortages of four wave mixing and stimulated Brillouin scattering. SBEFWM has the form of nearly-degenerate four-wave mixing in which four beams are coupled by the Brillouin nonlinearity, and can obtain the high phase conjugate reflectivities (more than 10^6) [1] which is very useful for some cases, for example, using this technique, one can get a low threshold phase conjugate reflectivity, amplify the very weak optical signal, and control the high power laser optical systems.

The reference [2] studied the stationary saturate characteristic of the system, and got the reflectivity and the convert efficiency of the system for stationary conditions, but did not solve the transient response. Reference [3] had analyzed the transient behavior, but did not get the theoretical results that it would be possible to realize the high reflectivity. This paper is mainly analyze the transient behavior, and uses the model of reference [3] to get the conditions in which the high reflectivity can be obtained.

We will change the input parameters, such as the input weak optical signal, the pump ratio and the gain parameter, and then analyze these factors which influence the high reflectivity. In the process not only the intensity of input signal, but also the response time will influence the high reflectivity. We hope to establish the relationship between the reflectivity and the input optical signal to obtain high reflectivity and high response speed.

References

1. Scott, A. M. and K. D. Ridley, "A review of Brillouin-enhanced four wave mixing," *IEEE J. Quantum Electron.,* Vol. 25, No. 3, 438–459, 1989.

2. Shuh, C.-C., "Analytical theory of four-wave stimulated Brillouin scattering in the saturation regime," *IEEE J. Quantum Electron.,* Vol. 23, No. 9, 1452–1457, 1987.

3. Schroeder, W. A, et al., "Single-frequency phase conjugate laser resonator using stimulated Brillouin scattering," *IEEE J. Quantum Electron,* Vol. 25, No. 3, pp. 460-469, 1989.

4. Dansereau J. P., et al., "Analysis of Brillouin-Enhanced four wave mixing phase conjugation systems," *SPIE. Nonlinear Optics*, Vol. 1409, pp. 67-82, 1991.

5. Ackerman J. R., et al., "Optimization of the field of view of a Brillouin-Enhanced four-wave mixing phase conjugator," *Optics Letters,* Vol. 19, No. 23, pp. 2015-2017, 1994.

A Lattice Gas Model for Optics Wave Propagation in Complex Environments

S. Li and W. Lin
Guilin University of Electronic Technology
Guilin, Guangxi 541004, P.R. China

The lattice gas model has been an effective numerical tool to model the complex situations for which traditional numerical techniques are hardly applicable.

Several researchers have succeeded in simulating the problem of wave propagation in urban environments based on the lattice Boltzman method [1, 2]. Optic wireless communication of indoor, or outside of door has been recently found many applications in the field of mobiling computer system. When this system is designed for satisfying with the communication between multiple users, the characteristics of optic wave propagation, which are the characteristic delay of multiple channel and path loss due to complex environments and weather conditions, are key designed parameters of the communication system. Because both the scales of environment space comparing with the wave length are very large and the lattice gas model naturally takes into account complicated boundary condition, the same as the reference [1], a lattice Boltzman model is presented to simulated and predict optics wave propagation in the complex environment of indoor and outside of door in this paper, but the pulse source model is provided in our simulation, and the absorbed effect in the fog is also considered in this paper.

REFERENCES

1. Chopard, B., P. O. Luthi, and J.-F. Wagen, "A lattice Boltzmann method for wave propagation in urban microcells," http://cui.unige.ch/l̃uthi/tlm.
2. Bertoni, H. L., W. Honcharenko, L. R. Maciel, and H. Xia. "UHF propagation prediction for wireless personal communications" *IEEE Proceedings*, Vol. 82, No. 9, 1333–1359, 1994.

The Research on the Utilization of Optical Fiber Grating for the Under Water Communications

D. Zhang, S. Li, and F. Ao
Guilin University of Electronic Technology
Guilin, Guangxi, P.R. China

The optical filter is very important in the case of free space optical communications where the son radiation is existing. The bandwidth, the transparent ratio etc. of the optical filter will play an important role for the sensibility of optical receiver and for reducing the transmitting power of the optical transmitter.

Theoretically, using the atomic resonant optical filter (AROF) is a good method for underwater optical communications, as the bandwidth of the AROF is smaller than 0.1 Å, which is very good for improving the sensitivity. But practically, we can use AROF only at some specific wavelength, and it need some critical conditions, such as the mode of the optical source, the environment conditions. So in practically, we can not use AROF as well as we hope, there are many problems need us to solve. The bandwidth of the traditional optical birefringent filter is as wide as several nm. the optical filter characteristic is poor, we do not use it for the underwater communications.

At present time, for the bandwidth is as small as several tenth of a nm, the insert loss is also very small (the transparent is as big as 80%), the optical fiber grating filter (OFGF) is used in practical optical fiber communication systems. If use the OFGF for the free space optical communications, it will be a good ideal. As we can design the central wavelength as we need, so the match between OFGF and the optical source is easy.

For free space communication, the match between optics come from free space and the OFGF is the key problem. Some examples had shown that, by lens system, the match ratio may be 50%, and the transparent ratio may be as small as that of AROF. So the usability of OFGF for underwater communication will be increased greatly.

All of these are planned to be realized.

REFERENCES

1. Bilodean, F., et al., “High-return-lose narrowband all-fiber band pass bragg transmission filter,” *IEEE Photo. Technol. Lett.*, Vol. 6, No. 1, 80–82, 1994.
2. Kashyap, R., et al., “All-fiber narrowband reflection gratings at 1500 nm,” *Electron Lett.*, Vol. 26, 730, 1990.

Synchronization for PPM with Any Pulse-Shape

C. Zou, N. He, and F. Ao
Department of Telecommunication Engineering
Guilin Institute of Electronic Technology
Guilin, Guangxi, P.R. China

Pulse-position modulation (PPM) is a power-efficient communication, and finds its way to optical communication and impulse radio (IR). PPM encodes K bits of binary information into one of $Q = 2^K$ positions, or time slots, in a frame of duration T as shown in Fig. 1. The PPM frame consists of Q time slots in modulation time T_S preceded by a dead time T_D. A single pulse transmitted at the ith slot $(i = 0, 1, 2 \ldots Q$-1) of modulation time per frame conveys the K bits of information.

In this article, the maximum-likelihood (ML) rules of frame and block synchronization are derived for the PPM pulse sequences with any shape and multi-samples per chip. However, the ML rules are computationally complicated process, so it is presented three of suboptimal approximation rules: high signal-noise ratio (HS) rules, correlation (CR) rules and simplified correlation (SCR) rules, which are easier to implement. Further, the rules of designing sequences of synchronization marker that have a maximum peak-to-sidelobe distance of the autocorrelation are proposed and the designing method for single sample per chip orthogonal PPM sequences is extended to the PPM pulse sequences with any shape and multi-samples per chip. The new methods of keeping synchronization are also proposed. Finally, the optimal ML rules as well as three of the suboptimal approximations are identified and performances are studied through computer simulations.

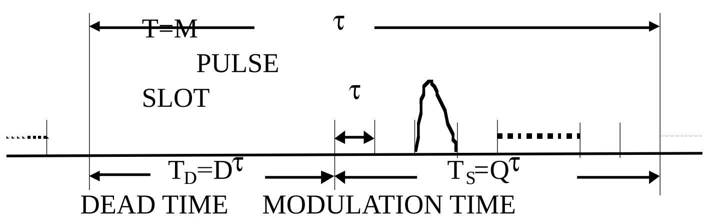

Figure 1: The digital PPM frame structure.

REFERENCES

1. P.T. Nielsen, "Some optimum and suboptimum frame synchronizers for binary data in Gaussian noise," *IEEE Tran. Commun.*, Vol. COM-21, 770–772, June 1973.
2. C.N. Georghiades, "Modulation and coding for throughput-efficient optical systems," *IEEE Transactions on Information Theory,* Vol. 40, No. 5, 1313–1326, September 1994.
3. T.W. Barrett, "History of UltraWideBand (UWB) Radar & Communications: Pioneers and Innovators," *Proceedings of Progress in Electromagnetics Symposium 2000 (PIERS2000)*, Cambridge, MA, July 2000.

Laser Beam Acquire Technology and Analysis on Accuracy of Pointing and Tracking in Optical Inter-Satellite Links

Y. Hu and T. Luo
Institute of Applied Physics, UEST of China
Chengdu, 610054, China

Optical Inter-Satellite Links (OISL) is established by acquisition, pointing and tracking (APT) system. Laser beam's divergence angle is so narrow and communication distance is far away that give APT system more stringent than other Inter-Satellite Links. So it is important to study for laser beam acquisition, pointing and tracking.
This paper firstly presents the acquisition technologies of OISLs, including acquire method, acquisition probability, uncertain area and acquisition time and so on.
Secondly, this paper analyzes the accuracy of tracking and pointing system, inlcuding analyzing tracking error sources, point-ahead error and budget of error tracking and pointing system. It is shown that accuracy of tracking and pointing is affected by systematic error and random error. The systematic error easily cancelled. Random error caused by such a detector noise, satellite platform jitter, so must ensure accuracy and disturbance compensation in tracking and pointing.
Finally, the designed ground demonstration laser communication system is representative of OISLs, explains its acquisition, pointing and tracking performance and accuracy of tracking.

Vibration Suppression in Optical Inter-Satellite Communications

T. Luo and Y. Hu
Institute of Applied Physics, UEST of China
Chengdu, 610054, P. R. China

Optical inter-satellite communications is a promising technology in space-based communications. The advantages for optical ISL include higher bandwidth, lower power requirement, and small antenna size. However, because of the small beam divergence and the low available signal power, the spatial tracking requirement for an optical ISL is more stringent than that of a conventional microwave link. The establishment of an optical ISL requires that both cooperating terminals achieve mutual spatial alignment of their optical system boresights. So laser communications between satellites imply stringent demands concerning the accuracy of the acquisition, pointing and tracking subsystem. In addition, optical communication transceiver is impacted by vibration of platform and space environment as satellite's payload. Pointing error analysis has shown that S/C vibration is the dominant contributor to mis-pointing. Therefore, the ATP functions have the be demonstrated to clearly and effectively compensate for spacecraft vibration environment.

This paper summarily explains the design requirement of acquisition, pointing and tracking system firstly, then presents the vibration of satellite and typical vibration's power spectral density. It also provides the feasible method of vibration suppression and design methods of APT system. A tracking subsystem with composite axis control is designed. Finally, uses some simulations to verify tracking and vibration suppression performance of the designed system and gives the simulation results.

The Improvement of Multiapertures Transmitting to the Scintillation Effect in Atmospheric Wireless Optical Communications

Y. Hu and Y. Tan
Institute of Applied Physics, UESTC of China
Chengdu, 610054, China

Scintillation effect is one of the problems those perplex the atmospheric wireless optical communications. We propose the multiapertures transmitting to improve the performance and also get the probability of error. When laser travels through the atmospheric turbulence, scintillation effect occurs. It causes fades in the received optical power. We will see the fluctuation of the power as noise at the receiver.

$$p(I, \sigma_x^2) = \frac{1}{2I\sqrt{2\pi\sigma_x^2}} \exp[-\frac{(\ln(I) + 2\sigma_x^2)^2}{8\sigma_x^2}] \tag{1}$$

The above expression performs a theoretical analysis for a two transmitting apertures system.

$$p(I, n) = \frac{I^{n-1}\, e^{-nl} n^n}{\Gamma(n)} \tag{2}$$

The above expression performs a n theoretical analysis for a transmitting apertures system. $\Gamma(n)$ is the Euler gamma function. We can calculate the mean and the standard deviation of the $p(I, n)$.

When the number of the transmitting apertures increases, the fluctuation decreases, and on the other hand the noise decreases. We use MATLAB to simulate a multiapertures transmitting system's probability of error under. From these figures, we compare the number of apertures, and can see that when the number increases, the probability of error decreases largely. From the figures, we also can see that the number increases, the curves of probability of error approximate to the curve of that of no turbulence. In conclusion, the multiapertures transmitting can improves the performance of wireless optical atmospheric communication.

The Optical CDMA Receiver in Poisson Channel

Y. Hu and S. Wan
Institute of applied physics, UEST of China
Chengdu, 610054, China

OCDMA attract many people's attention. The application of CDMA for optical communication not only preserve it's anti-jamming, security, soft capacity, asynchronous access, simple network protocol and etc., but also talk full advantage of the large bandwidth of optic, at the same time, the large number of address codes make it a fit technology for LAN application. Same as the RF(radio frequency) CDMA system, the performance of the conventional OCDMA correlation receiver degrade rapidly when the number of users increased. Some multiuser detection proposed, but the multiuser receiver demodulate all users symbol and require information of other active users, which increase the system's complexity.

In this paper, we estimate the MAI according to the maximum a posteriori probability(MAP), the estimated MAI is then used to demodulate the desired user's signal. If the system is chip synchronous, the interference can be seen as binomial distribution, if the number of active users are large, it can be seen as Gaussian distribution. In this paper, we give the system's performance by approximate the MAI by these two distribution respectively.

Presume the MAI is I, then the signal can written as

$$n(t, I) = Wn_s + In_s + Wn_b \tag{1}$$

the priori probability is $p(I)$,then the MAP of I can be written as

$$P(I|k) = \frac{P(k|I)P(I)}{\Sigma P(k|I)P(I)} \tag{2}$$

if all symbol's probability are equal, then, maximizing the MAP equals to maximizing the $P(k|I)P(I)$, it can be written as

$$\max_{\hat{\mathrm{I}}} \quad \{logP(k|I) + logP(I)\} \tag{3}$$

According to estimator, we can get the decision rule. The Fig.1 are the structure of receiver.

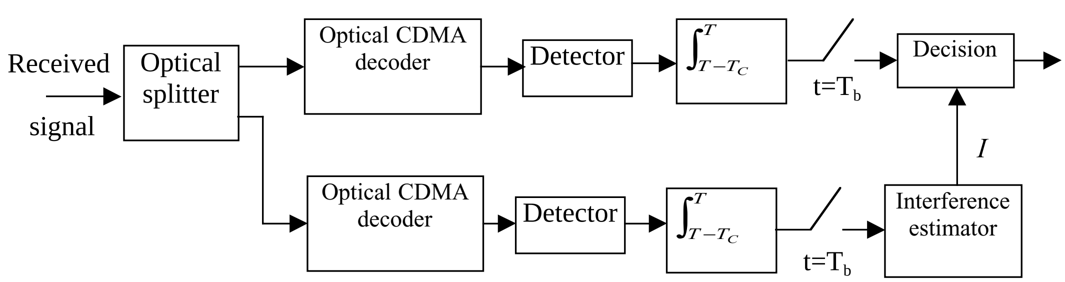

Session 2Ac4

RF, Microwave and Millimeter Wave Devices

Present Status of Compound Semiconductor Nanoelectronics for Applications to Sub-Millimeter Wave and Terahertz Regions

H. Hasegawa
Research Center for Interface Quantum Electronics
Graduate School of Electronics and Information Engineering, Hokkaido University
Sapporo, 060-8628, Japan

In view of applications to various areas including ultra wide-band/ultra high speed (Tera-bit) telecommunications, imaging and near object analysis, remote sensing, etc., considerable interests exist currently to develop science and technology for semiconductor devices that are useful for generation, amplification and detection of submillimeter-wave to terahertz regions of the electromagnetic spectrum. Since the spectral range falls in between the microwave/millimeter wave region and the optical region, the approach to fill up the so-called THz gap is two-fold. Namely, one is to push up the electron device approach to higher frequencies and the other is to push down the photonic device approach to longer wavelengths. The common feature of these two approaches is "nanoelectronics" where the nano-scale feature sizes are required for metallization dimensions and/or basic semiconductor structures.

The purpose of the present paper is to review the present status and future prospects of compound semiconductor nanoelectronics for generation, amplification and detection of sub-millimeter wave/terahertz portion of electromagnetic spectrum.

The paper will begin with the approach of pushing up of the electron devices to higher frequencies by reducing the feature sizes into nanometer region. Present status of devices such as FETs, HBTs, Schottky diodes, heterostructure barrier diodes etc are reviewed. Then, the second approach based on artificial semiconductor nanostructures will be discussed. Here, one notes that the inter-subband/ inter-sublevel energy separation of quantum states in artificial quantum nanostructures such as quantum wells, wires, dots and superlattices can be matched very well with those of THz photons (4 meV for 1 THz) by proper material and structural design. Various devices based on inter-subband transitions, photon assisted tunneling, single electron transport etc will be covered.

AlInGaN-based Microwave Field Effect Transistors

R. Gaska
Sensor Electronic Technology, Inc.
Latham, NY 12110, U.S.A.

Simin and A. Khan
Department of EE, University of South Carolina
Columbia, SC 29208, U.S.A.

M. S. Shur
Department of ECSE and CIEEM, Rensselaer Polytechnic Institute
Troy, NY 12180, U.S.A.

The use of Strain and Energy Band Engineering (SEBE) approach in quaternary AlInGaN material system allowed us to nearly independently control built-in strain and energy band discontinuity. The combination of SEBE with Pulsed MOCVD (Pulsed Atomic Layer Epitaxy – PALE) technique opened up the way for deposition of high aluminum content AlInGaN heterostructures at reduced growth temperatures suitable for the incorporation of significant amounts of In.

We have demonstrated Metal-Oxide-Semiconductor Heterostructure Field Effect Transistors (MOSHFETs) and AlInGaN/InGaN/GaN Double Heterostructure FETs (DHFETs). The incorporation of a SiO_2 insulating layer with a high quality SiO_2/AlInGaN heterointerface reduced the gate leakage by more that than 6 orders of magnitude, which is particularly especially important for large periphery devices. Strain control in the DHFETs resulted in the current collapse-free rf performance. We expect that the combination of the insulated gate and InGaN channel designs will yield stable high microwave power device performance of the devices.

We will also review our studies on the fabrication and microwave performance of novel GaN-based Highly Doped channel Metal Semiconductor Field Effect Transistors (HDMESFETs). The estimated electron sheet density, n_s, in our devices varied from 5×10^{12} cm^{-2} to 1.5×10^{13} cm^{-2}, which is in the same range as the typical values of ns for AlGaN/GaN-based Heterostructure Field Effect Transistors. The electron Hall mobility in the structures grown over SiC substrates was up to 330 cm^{-2}/Vs. Our simulation results show that these improved values of mobility should lead to the performance approaching that of AlGaN/GaN HFETs for short channel devices (with one micron and shorter gate lengths).

We measured the unity current gain cut-off frequencies, f_t, up to 13 GHz and the maximum frequencies of oscillation up to 28 GHz for HDMEFET devices with the source-drain spacing of 3 μm and the gate length of 1 μm. The pulsed microwave power at 2 GHz was up to 2.7 W/mm with the maximum power added efficiency of 25%. This is the highest microwave power of GaN-based MESFETs reported to date.

Our experimental data and modeling results show that, with further design improvements, GaN HDMESFETs should be able to compete with AlInGaN-based HFETs in terms of microwave performance offering, at the same time, advantages of fewer fabrication steps, better yield, and less pronounced non-ideal effects. This makes these devices to be potential candidates for the first commercial GaN-based high power transistors.

Broadband Attenuator Circuit Using PIN Diodes

A. A. Shirakawa, C. P. Moreira, and H. Tertuliano
Electrical Engineering Department, UFPR
Curitiba, Parana, Brazil

In the past few years the broadband CATV networks starts to provide not only pay TV but also Internet access, telephony, videoconference and other services. So, the management of this network has become more critical. To make possible that from a center point of the network (headend) make re-alignments and interact with the equipments in the distribution system we propose a circuit attenuator using PIN diodes controlled by a voltage level. So, an intelligent system can interact with the headend operator and, then, control the voltage level of this circuit.

We propose in this paper a circuit (Pi) attenuator using PIN diodes. The PIN diode is a current controlled resistor at radio and microwave frequencies. It is a silicon semiconductor diode in which a high resistivity intrinsic I-region is sandwiched between the P-type and N-type regions. When the diode is forward biased, the charges are injected in the I-region. So, controlling the bias current it is possible to control the resistance of the element.

Using this mechanism we propose a bias circuit that minimize the noise insertion. We had chosen the Pi architecture for this circuit because it can reduce the distortion inserted by the PIN diodes in the CATV signal.

In our laboratories, we had done tests to evaluate the insertion loss, return loss and the distortions of the circuit. The circuit presented an insertion loss that can vary from 0,5 dB to 10,5 dB, a return loss 16 dB and the distortion less than -80 dBc.

Two-Dimensional Space Charge Waves in Semiconductor Films and Microwave Frequency Conversion Under Negative Differential Conductivity

V. Grimalsky
Electronics Department, National Institute for Astrophysics, Optics, and Electronics
Puebla,, Z.P. 72000, Mexico

S. Koshevaya, M. Tecpoyotl-Torres, and J. Escobedo-Alatorre
Center for Investigations on Engineering and Applied Science, Autonomous State Univ. of Morelos
Morelos, Z.P. 62210, Mexico

In the report, the nonlinear interaction of two-dimensional space charge waves including the amplification, parametric interaction and a multiplication in GaAs semiconductor films is analyzed. In order to obtain a negative differential mobility, the electric bias field must be $E_0 > E_{crit} \approx 4\,\mathrm{KV/cm}$.

The coordinate system is chosen as follows: X-axis is directed perpendicularly to the film, the drift field E_0 is applied along Z one, exciting and receiving antennas are parallel to Y-axis. 2D model of electron gas in the thin n-GaAs epitaxial film and i-GaAs substrate is used. Thus, 2D electron concentration is present only in the plane $x = 0$. The space charge waves possessing phase velocity equal to drift velocity of electrons $V_0 = V(E_0)$, $E_0 = U_0/L_z$, are considered, where U_0 is bias voltage, L_z is the length of the film. Generally, a non-local dependence of the drift velocity v of electrons on the electric field takes place [1, 2]. The following system for description of nonlinear space charge waves is used:

$$\begin{gathered}\frac{\partial\tilde{n}}{\partial t} + div(n\vec{v} - D(w)\nabla\tilde{n}) = 0; \qquad \frac{d(m(w)\vec{v})}{dt} = e\vec{E} - \frac{m(w)\vec{v}}{\tau_p(w)};\\ \frac{dw}{dt} = e\vec{E}\vec{v} - \frac{w-w_0}{\tau_w(w)}; \quad D(w) = \frac{2}{3}\frac{\tau_p(w)}{m(w)}\left(w - \frac{1}{2}m(w)v^2\right); \quad \vec{E} = E_0\vec{e}_z + \tilde{\vec{E}} + \tilde{E}_{ext}\vec{e}_z;\\ \tilde{\vec{E}} = -\nabla\varphi; \quad \Delta\varphi = -\frac{e}{\varepsilon_0\varepsilon}\tilde{n}\delta(x); \quad \tilde{E}_{ext} = \sum_{j=1}^{2} E_{0j}\sin(\omega_j t)\exp\left(-\left(\frac{z-z_1}{z_0}\right)^2 - \left(\frac{y-y_1}{y_0}\right)^2\right).\end{gathered} \tag{1}$$

The Eqs. (1) are added by boundary conditions (the sizes of the film are L_z, L_y):

$$\begin{gathered}\varphi(x, y; z=0) = \varphi(z=L_z) = 0; \quad n(y; z=0) = n(z=L_z) = n_0;\\ E_y(x, y=0, z) = E_y(y=L_y) = 0; \quad \frac{\partial n}{\partial y}(y=0, z) = \frac{\partial n}{\partial y}(y=L_y) = 0.\end{gathered} \tag{2}$$

Here φ is the varying part of potential, $n = n_0 + \tilde{n}$ where n_0 is constant electron concentration, $\tilde{n}$ is its varying part. The mean energy and mean effective mass of electron are denoted by w and $m(w)$, the equilibrium value of w is w_0; $\tau_{p,w}$ are relaxation times. D is the diffusion coefficient, and e is the lattice dielectric permittivity of GaAs.

Numerical simulations of Eqs. (1) have demonstrated a high efficiency of parametric up-conversion with an amplification of space charge waves. It has been shown that the local field approximation for the dependence of the drift velocity on the electric field is valid if carrier frequencies are $f < 50\,\mathrm{GHz}$. Non-locality leads to an increase of noises under frequency conversion. Some reduction of noises can be achieved when the optimal width of the film L_y and the optimal sizes of input antenna are chosen.

Recent Advances in Space Photonics Research

A. K. Ghosh
Canadian Space Agency
Quebec, Canada

Rapid growth of photonics networks for terrestial fiber optic communication and demand to develop improved space payloads for satellite communications, remote sensing and space science have encouraged significant research in the area of the application of photonics for space.

In this paper, some of the recent advances in space photonics with regard to microwave photonics (signal generation, distribution and processing), high speed optical databus, and optical inter-satellite link will be reviewed. A new emerging technology of photonic bandgap materials for improved phased-array antennas, integrated optical and electromagnetic devices for space applications will be discussed.

In one of the areas of microwave photonics, the synthesis of microwave signal by optical techniques is of practical interest for space application due to possibilities of achieving reduced size, less power consumption and wide bandwidth. In addition to reviewing various approaches, a novel patented technique based on optical serodyning will be reported which has high spectral purity with fast hopping capabilities.

Photonics also has the promise to develop novel architecture for phased array systems for space based radar (e.g. synthetic aperture radar) as well as advanced satellite communication antennas. Various techniques of optical beam forming and beam steering will be reviewed. Recent investigations of the use of fiber optic devices such as fiber optic gratings, wavelength division multiplexers to achieve true time delay phase control for active phased array systems will be presented. Another important requirement for optical phased array systems is the development of low loss RF fiber optic links. The results of investigations of signal distribution at L-band, C-band and X-band will be discussed.

In the area of signal processing, photonic technique based on optical correlation for on board processing is of interests for space applications. A novel technique based on optical ring resonator using two optical correlation fillers for pattern recognition will be discussed.

The demands for high speed (e.g. 10 gb/sec) intersatellite optical links as well as high speed optical databus are increasing constantly for future space missions. Although there are compelling reasons to adapt terrestial fiber optic communication components namely, semiconductor diode laser along with EDFA (Erbium Doped Fiber Amplifier) for optical intersatellite link due to ease of component availability, we report an OISL system based on Ytterbium Doped Fiber Amplifiers because of its overwhelming power advantage over EDFA.

Next, the discovery of realizing photonic (electromagnetic) bandgap in artificially constructed periodic structure has opened up exciting activities in developing improved microwave/millimeterwave antennas, in particular phased array antennas, microwave devices, as well as integrated optical devices. The potential application of this new technology for space will be discussed. Lastly, the issues of space radiation effects on photonic components based on recent investigations will be reported.

Modeling of Open-Ended Coaxial Probe for Near Field Scanning Microwave Microscopy

M. A. El Sabbagh and K. A. Zaki
Electrical and Computer Engineering Department, University of Maryland
College Park, U.S.A.

A. Schwartz and V. Talanov
Neocera, Inc.
Beltsville, U.S.A.

There is a need to develop non-destructive microscopy techniques to quantitavely measure the microwave properties of semiconductors and dielectric samples (thin or bulk) on a length scale much smaller than the free space wavelength. Open-ended coaxial lines are often used for non-destructive measurements of the complex permittivity of materials. For non-destructive measurements of permittivity, the open end of the coaxial line is terminated by the sample material and the input reflection coefficient of the system is measured at a dexired frequency. The data obtained are then related to the complex permittivity of the material. The spatial resolution is determined by the volume over which the fields extend beyond the end of the line, and this volume is determined by the dimensions of the coaxial line.

In this paper, the open end of the coaxial probe is modeled as a one port structure using the finite element method (FEM). The modeled probe is a 50Ω coaxial transmision line with an inner cylindrical conductor of diameter $125\mu\mathrm{m}$ and an outer cylindrical conductor of inner and outer diameters $420\mu\mathrm{m}$ and $670\mu\mathrm{m}$ respectively. These dimensions were chosen to match a UT-20 coaxial probe used experimentally. With these dimensions, the probe has a measurement spot size area of approximately 0.5 mm^2. The region between the inner and outer cylinders is filled with PTFE that has a relative dielectric constant of 2.1. The probe is assumed to be at a constant height above the sample, typically between $1\mu\mathrm{m}$ and $10\mu\mathrm{m}$. To account for radiation losses from the sample area, the probe is considered to be surrounded by a radiation boundary condition. It was proven through simulations that if the probe is surrounded by a perfect metallic boundary, identical results are obtained as long as the boundaries are far away (at least twice the inner probe diameter) from the coaxial probe. For the different structures studied, the reflection coefficient (magnitude and phase) is obtained as a function of the sample parameters such as the loss tangent and the dielectric constant. In this paper, we report some new results, using FEM commercial software HFSS from Agilent technologies, for bulk dielectrics, thin films on top of bulk dielectrics, and semiconductors. The bulk dielectrics considered have a thickness variation between $50\mu\mathrm{m}$ and $1000\mu\mathrm{m}$ while the thin films have a thickness variation between $0.1\mu\mathrm{m}$ and $10\mu\mathrm{m}$. Experimental results obtained with a UT-20 coaxial probe were compared to the simulation results and they are in good agreement, which shows the validity of the model used.

Computer-aided Diagnosis of Symmetric Coupled Resonators Filters

H.-T. Hsu, Z. Zhang, and K. A. Zaki
Department of Electrical and Computer Engineering, University of Maryland at College Park
College Park, MD 20742, U.S.A.

A. E. Atia
Orbital Sciences Corporation
Dulles, VA 20116, U.S.A.

The increasing need for high-performance microwave filters which possess optimum responses consistent with minimum weight and compact size is apparent. Coupled-resonator filters in a symmetric folded configuration (the canonical form) is a preferable candidate. Accurate knowledge of the parameters (resonant frequencies of individual resonators and couplings between resonators) is essential for the design and tuning of such high performance filters for modern communication systems applications.

This paper presents a diagnosis method with its applications in the design and measurement for canonical filters. The parameters of the filter can be accurately diagnosed by the zeros and poles locations of the input impedance functions of the even- and odd-mode bisected networks. The corresponding zeros and poles locations can be determined either by EM simulation or measurement. In the case of EM simulation, half of the structure is simulated twice by putting PEC and PMC at the plane of symmetry. The zeros and poles are then determined from the phase response of the input reflection coefficients of the corresponding bisected networks (S_{11even} and S_{11odd}). As for applications in real measurements, however, it is impossible to physically impose PEC and PMC at the symmetric plane. An approach to obtain S_{11even} and S_{11odd} from measurement of the whole filter network is proposed. In this approach, S_{11even} and S_{11odd} can be efficiently derived through the magnitude and phase of S_{11} and S_{21} of the original filter. Special attention on the reference planes for measurement must be paid to accurately determine the zeros and poles of the bisected networks.

Design example together with application in filter measurement will be presented to show the powerfulness of the proposed diagnosis method.

Experimental Studies of Local ME Coupling in Small Ferrite Resonators

A. K. Saha
Department of Electrical and Electronic Engineering, Yamaguchi University,
Tokiwadai, Ube shi 755-8611, Japan

E. O. Kamenetskii
Department of Electrical and Computer Engineering, Ben-Gurion University of the Negev
Beer-Sheva, 84105, Israel

I. Awai
Department of Electrical and Electronic Engineering, Yamaguchi University,
Tokiwadai, Ube shi 755-8611, Japan

An idea that small ferromagnetic resonators with special-form surface electrodes can be considered in microwaves as "bianisotropic molecules" — the particles with properties of *local internal magnetoelectric (ME) coupling* modeled as glued pairs of small electric and magnetic dipoles, has been put forth recently by one of the authors. Our recent experimental investigations showed that quasi-static microwave ME effect really exists in such particles. The effect is characterized by rich spectrums of ME oscillations that can be excited by the external RF electric or magnetic fields or their combinations [1]. Experimental results of the ME coupling in *different types of ferrite resonators and different types of surface electrodes* were reported and some important conclusions were drawn observing the oscillation spectra of those particles [2].

A physical ground for point ME particles was found in small ferromagnetic resonant specimens where the so-called magnetostatic (MS) multi-resonance oscillations occur. The MS oscillations take place in ferromagnetic bodies with sizes much less than the electromagnetic wavelength in a microwave region but much more than the characteristic length of the exchange interaction. In our experiments we have a certain evidence that a ferrite ME particle, being responded to the external quasistatic electric field, shows a property of the electric polarization. This can be considered as a quite surprising fact since the nature of the MS oscillations does not exhibit any properties of the electric potential fields and, therefore, any properties of the electric polarization. Moreover, in the quasistatic free-space region (the region much less than the free-space electromagnetic wavelength) one has an effective transformation of energy of electric polarization to energy of magnetization or, in other words, the effective transformation of the quasielectrostatic energy to the quasimagnetostatic energy.

In new experimental results shown in this paper, an essential attention is paid for uncovering the main physics of such effective quasielectrostatic to quasimagnetostatic energy transformation. The nature of the observed effects arises from the eigen-electric-moment properties of MS oscillations found recently in small ferrite disks [3]. The unified ME (produced by two locally coupled electric and magnetic dipoles) field can exhibit the symmetry properties different from the symmetry properties of the electromagnetic field. Our experimental results verify this fact.

REFERENCES

1. Kamenetskii, E. O., I. Awai, and A. K. Saha "Experimental evidence for magnetoelectric coupling in a ferromagnetic resonator with a surface metallization," *Microw. Opt. Technol. Lett.*, Vol. 24, No. 1, 56, 2000.

2. Saha, A. K., E. O. Kamenetskii, and I. Awai, "Microwave magnetoelectric particles: An experimental study of oscillating spectrums," *Phys. Rev. E*, Vol. 64, 056611, 2001.

3. Kamenetskii, E. O., A. K. Saha, and I. Awai, *Phys. Rev. Lett.* (submitted).

Coupling Characteristics of Square Shaped Ceramic Resonator at 60 GHz

F. Kuroki, M. Yamaguchi, and S. Sonoo
Kure National College of Technology
Aga-Minami, Kure 737-8506, Japan

T. Yoneyama
Tohoku Institute of Technology
Kasumi-Chou Yagiyama, Taihaku-Ku Sendai 982-8577, Japan

The cylindrical ceramic resonators with TE_{0nd} resonant modes are usually used at centimeter frequencies due to their low loss natures. However they have a difficulty in making wide-band band-pass filters in the millimeter-wave region because of their poor coupling factors between the resonators and input/output waveguides. Having this fact in mind, we propose the use of the square shaped ceramic resonators as shown in Fig. 1, where the thin square ceramic piece is located at the horizontal mid-plane in a below cutoff parallel metal plate waveguide. In order to keep the symmetrical shape, the ceramic piece is supported by square shaped teflon pieces from the upper and lower sides, where they have the same cross sectional dimensions as the ceramic reso-nators. Since the resonator is fed by NRD guide, we assumed the electric wall on the y-z plane and mag-netic wall on the x-y plane, respectively. Figure 2 shows the calculated resonant frequencies for each resonant mode versus the side lengths of the square ceramic piece, where the relative permittivity and thickness of the ceramic piece was set to be 24 and 0.4 mm, respectively, and the separation of the below cutoff parallel metal plate waveguide is selected to be 2.25 mm so as to be less than half a free space wave-length. It is obvious that 5 types of resonant modes appear in the 60 GHz frequency band. The electric field distributions for the lower modes are shown in Fig. 3. From among these modes, the EH_{12d} mode is chosen as the dominant mode because the resonant frequencies of the neighboring HE_{10d} and HE_{11d} modes are away from that of the EH_{12d} mode. The coupling coefficients between two resonators have been calculated as shown in Fig. 4. For the compari-son, the calculated coupling coefficients of the EH_{11d} mode in cylindrical ceramic resonator with the rela-tive permittivity of 24 are shown in this figure. The ceramic resonator supported by the upper and lower teflon discs is designed to be 2.0 mm in diameter and 0.45 mm in thickness so as to resonate at 60 GHz and is inserted in the same parallel plate waveguide. From this result, it is confirmed that the coupling factor of the square shaped ceramic resonator is larger than that of the cylindrical one as predicted. Next step of this research is to apply the square shaped ceramic resonator in the millimeter-wave integrated circuits.

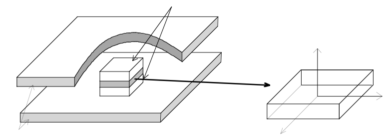

Fig.1 Plane view of square shaped ceramic resonator and its coordinates

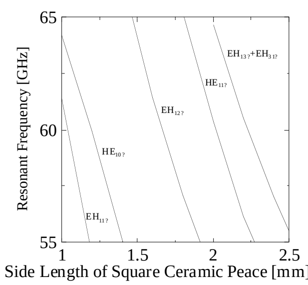

Fig.2 Calculated mode chart of square shaped ceramic resonator

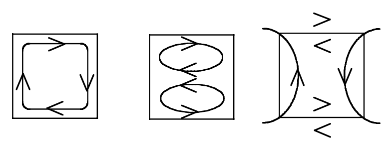

Fig.3 Electric field distributions of resonant modes

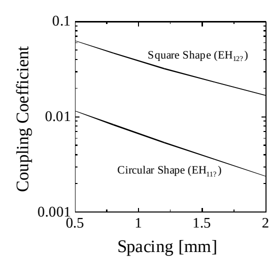

Fig.4 Calculated coupling coefficients between two resonators

Feasibility of Near-Field Measurement on Devices

B. Mazari and C. Anne
Institut de Recherche en Systèmes Electroniques Embarqués
Mont Saint Aignan, 76131, France

C. Arcambal, F. Dhondt, and P. Eudeline
Thales Air Defence
Ymare, 76620, France

D. Gasquet, L. Nativel, and M. Castagné
Centre d'électronique et de microoptoélectronique de Montpellier
Montpellier, 34095, France

In the radar Transmit/Receive (T/R) module from Thales Air Defence, MMICs are often used. The current simulation tools does not allow to compute the electric field close to complex active devices. Thus, the EMC characterization of MMICs needs near field measurement. In this purpose, a simple near field mapping system based on micro monopole antenna has been developed by CEM2. Passive circuits like 50Ω lines, filters and an area of a MMIC have been measured. The measurements on passive circuits have been compared to 3D electromagnetic simulations realized by IRSEEM. The goal of this paper is to prove the feasibility of this low cost and rather reliable method. This measurement technique can be of a great help to optimize the circuit reliability, topology and packaging.

The system of near field measurement has been used in C and X band and is built with a micro monopole antenna. This antenna (length 300 μm, diameter $150\,\mu$m) is moved vertically above a microwave circuit by a motorized X-Y table driven by a PC. The maximal associated mechanical resolution is about 1 μm. The antenna is cascaded with a 60 dB low noise, wide band, amplifier. It is also possible to insert a double slug adapter between the antenna and the first stage of amplification. The amplified signal is detected and is then transmitted to the PC. The PC software controls the displacement, the measurement, and processes the electromagnetic field datas.

In order to prove the feasibility of near field measurement on MMICs and to understand the measured phenomena, we have chosen to investigate the near field above very basic samples. A bend 50Ω line loaded either by a short circuit or an open one and a line-coupled filter loaded with 50 ohms have been characterized at 11 GHz. These same structures have been simulated with HFSS and Ensemble. Therefore, we can conclude that the vertical component of the electric field is measured. These first results show the interest of such a measurement. Indeed, this set up allows us to know the near field with a sufficient dynamic and accuracy.

After having characterized passive structures with our probe, we have chosen to measure an active device provided by Thales Air Defence and working in C-band. Due to amplifiers and attenuators, the power, within the chip, spreads over a large range; that allows us to obtain exploitable measurements. By simulation with MDS, only the electrical power distribution is available and not the radiated power. In practice, the probe was placed as close as possible to the circuit's surface (about 300 μm).

The first results about the chip are very interesting as they permitted to identify clearly the high field areas. These data are complementary of the electrical simulations. We can now identify the part of the chip in which the field is the higher.

In this paper we want to show that by means of a relatively simple experiment it is possible to investigate the electromagnetic behavior of a complex MMIC under working conditions. However, this very innovative work is only a first step. Numerous points must be cleared. As an example we must clearly understand the phenomenon that is measured. Then the influence of the probe must be evaluated.

Session 2Ac5

Sub-Surface Imaging and GPR

Low-Frequency Radar for Planetary Subsurface Resource Investigation: A Feasibility Study

G. Tacconi, R. Filippini, R. Marcialis, and S. Pagnan
Institute for Naval Automation of National Research Council (IAN-CNR)
Genova, 16149, Italy

Among the low frequency radar techniques TDEM (Time Domain Electromagnetic Method) technique is one of the most employed for the Earth subsurface prospecting. It allows to obtain a detailed map of the subsoil by means of a EM field opportunely generated by a source (transmitter-TX) coil where the source input is a step-like function. The time rate of change of the source field, caused by the ideal instantaneous turnoff, determines a secondary field in the subsoil according to the physical law of induction. The secondary field is therefore recorded by a receiver (RX, coil or magnetometer) and the shape of the recorded response carries all the information about the subsoil (conductivity profile), the response consisting of a sum of infinite contributions translated in time and space of more or less conductive strata, which interpretation is quite complex with the exception of few cases. The TDEM has been successfully employed for the Earth resources exploration (mine industries, petroleum, groundwater, geothermal energy and more) thanks to its higher sounding capability (resolution and depth of investigation) with respect to other techniques.

The aim of this paper is to investigate on the feasibility of the TDEM technique in a planetary exploration context. The challenge of such a proposal relies upon the strong limitations imposed by the mission constraints, namely the reduced power and mass budget. Although these limitations are not a problem in the Earth exploration, they could represent a bottleneck for the system performance in the planetary context. The paper wants to face all those problems from a mathematical point of view evaluating the performance of a TDEM system in function of the mass and power limitations and for different targets of investigation. As performance measure we take the sounding capability expressed as maximum depth of penetration of the field in the subsoil. As targets, different exploration scenarios will be addressed, according to the main strategic issues of the planetary exploration programs: water deposits (ice or liquid), permafrost, sedimentary deposits (correlated to the existence of past forms of life).

Into approaching the problem we'll model the system and the subsoil as follows: TX and RX antennas are modeled with the respective transfer function, EM noise at the receiver is statistically characterized and a laterally uniform subsoil model, where the target is just one of the layers, represents the medium.

The study aims to put the basis for the project of technologically advanced system for the in-situ planetary exploration, that could perform and/or support: 1) the subsoil resources mapping for mining (human consumption, storage and energy production) 2) the exobiology programs (search of present and past traces of life).

The work is conducted in the framework of the ESA (European Space Agency) Topical Team ”Electromagnetic and other geophysical techniques for in-situ and orbital planetary exploration”.

The Contrast Increasing of the Tomography Images of the Subsurface Objects by Means of Filtering of the Space Spectrum of Scattered Field

A. A. Vertiy*, S. P. Gavrilov, I. V. Voynovskyy, V. N. Stepanyuk, and S. Aksoy**
TUBITAK-M.R.C., Turkish-Ukrainian Joint Research Laboratory
Gebze-Kocaeli, 41470, Turkey

The results of consideration about the contrast-improving problem in the case of reconstruction of the subsurface objects images by using of the tomography algorithm are given in this paper. In modeling the back-scattered field data were used at 17 frequencies in frequency range from 3.5 to 4.0 GHz with the constant frequency step. Dielectric objects with sizes of $d \cong 1 \div 5\lambda_0$ ($\lambda_0 = 0.075m$) and heights of $h \cong 0.5 \div 2\lambda_0$ were studied. Relative dielectric permittivity was taken 5.0 for medium surrounding an object, 4.0 for the studied object and 1.0 for medium containing incident plane wave. The tomography setup used in experiment was described in [1]. In analyses and experiments the normal incidence of the probing wave is used. Data about scattered field are determined at a fixed probing line above the medium surface investigated. In the inverse a complex function of the space coordinates representing the normalized polarization currents in the region of the object cross-section under investigation is reconstructed. The image of the investigated object cross-section is modulus of this function. Formulae based on inverse Fourier transform and plane wave spectrum of scattered field [1] are used in the reconstruction algorithm. This spectrum can be calculated from the measuring of amplitude and phase of the back-scattered field in the case when electromagnetic wave, with the varied frequency, probes the studied half-space containing the embedded object. As the plane wave spectrum of electromagnetic field scattered by the medium surface is centralized near to zero spatial frequency, this part of the spectrum can be removed by means of narrowband filter tuned on zero spatial frequency. Some part of spectrum appertaining to the quest will be also deleted in this case, but this part has small size.

It is shown by calculations and experiments that filtering a little compresses the object image in the direction of scanning. This compressing can be compensated in the image processing. It is ascertained that plane wave spectrum of the back-scattered field contains constituents given by the finite length of the scanning line. These constituents of spectrum can not be removed by the filtering and brings to the image false details. Constituents given by finite length of the scanning line can be removed at the image reconstruction by a special algorithm.

The results obtained may be applied in practical tomography setups for detection and observation of different subsurface objects.

REFERENCES

1. Vertiy A.A., Gavrilov S. P., Voynovskyy I.V., Aksoy S., Kudelya A. M., Salman A.O. "Diffraction tomography method application in wide frequency range", *International Journal of Infrared and Millimeter Waves*, Vol. 21, No: 2, 321-339, February 2000.

* Also with IRE, National Academy of Science of Ukraine, 12 Acad. Proskura St., Kharkov, Ukraine
** Also with GIT, Gebze Institute of Technology, 41470, Gebze, Kocaeli, Turky

Experimental Application of Brewster Geometry for Subsurface Tomography Imaging

S. Aksoy, A. A. Vertiy, S. P. Gavrilov
TUBITAK-MRC, Turkish-Ukrainian Joint Research Laboratory
Gebze, Kocaeli 41470, Turkey

One of the most important problems for imaging of subsurface objects based on plastic materials by microwave tomography method is undesired reflection effects from surface. Microwave tomography experiments are performed at and show that the level of surface reflection is extremely effective to damage for the image of subsurface objects. If investigated subsurface object is buried especially close to surface or extremely deeply from surface, due to the undesired reflection effects from surface, it is very difficult or sometimes impossible to obtain subsurface object images from weakly subsurface scattered objects like mine etc. materials. This paper points out experimental investigation that if transmitter antenna is arranged at Brewster angle geometry or using of dielectric waveguide as a transmitter and receiver antenna [1], undesired effects from surface reflection is minimized and obtained images of subsurface weakly scattered objects by microwave tomography method is more clear and better than previous case. Two experimental results are investigated by using dielectric waveguide and Brewster angle geometry for imaging of subsurface objects which are buried close to surface or more deeply from surface.

It is shown that using of dielectric waveguide as a receiver and transmitter antenna or geometry of Brewster angle for transmitter antenna, reflection from surface will be minimized and the image of subsurface objects based on plastic materials will be more qualified and satisfied. If one compares using of Brewster angle geometry versus dielectric waveguide structure for subsurface objects which are buried close to surface, the performance of two system and the images of investigated subsurface objects are approximately same but for investigated subsurface objects which are buried more deeply from surface, using of Brewster angle geometry for transmitter antenna provides better images according to the using of dielectric waveguide as a transmitter and receiver antenna. The obtaining of subsurface images in the case of more deeply ($\geq 4\lambda$) placement from surface is generally impossible by using dielectric waveguide svstem for experimental microwave tomography setup.

The obtained results may be used in practical application of tomography setup for obtaining of more qualified images of investigated subsurface objects.

REFERENCES

1. S. Aksoy, A.A. Vertiy, S. Gavrilov, "The Investigation of Buried Object Imaging by using Leaky Waves from a Dielectric Waveguide", p.276, July 18-22 *PIERS* 2001, Osaka, Japan

Electrical and GPR Tomographies for Archaeological Investigations at Mit-Raheina Village, Giza, Egypt

A. G. Hassaneen, S. S. Osman, M. A. Abd Allah, and F. A. Shaaban
National Research Institute of Astronomy and Geophysics
Cairo, Egypt

The studied area lies on the the western side of the River Nile, SW of Giza City. This area is characterized by a number of archaeological tells occupying topographically high sites, such as Tell El-Rabi'a, Tell El-Qalaa, Tell El-Fakhri and Tell El-Nawa. This work aims to investigate the near-surface sedimentary cover of the area for tracing the archaeological relics, that are probably buried.

Resistance scanning survey have been conducted, using the RM15 Resistance Meter, at Tell El-Rabi'a (behind Hathour Temple). A total number of 12 square grids, with grid length of 20 m, are conducted. The field data are processed and illustrated using the GEOPLOT software.

Sixty-five detailed, GPR profiles were measured at Tell El-Rabi'a using the Surface Interface Radar, SIR-2000 instrument, and utilizing a 400 MHz antenna with a time window 100 ns. 38 profiles east to Hathour temple, with profile length of 60 m and with profiles apart of 1 m and 27 profiles north to the temple with profile length of 40 m and profiles apart of 1 m are carried out.

The RADAN program, designed by the Geophysical Survey System Inc. (GSSI), was used to treat the GPR surveying data. The field data of the detailed GPR profiles, that were conducted in the Tell El-Rabi'a area for archaeoprospection, are presented vertically in sections and laterally in time slices. The analysis of the radar sections and the time slices representations with the available excavation data allowed for identification and constructions of the shape and extension of the expected archaeological targets beneath the earth surface.

The coordination of the geophysical surveys and the available excavation information as well as the borehole data in the investigated sites proved to be valuable in detecting buried archaeological relics at different depths beneath the ground surface.

Integrated Geophysical Interpretation for Groundwater Exploration at Nukhl Area, Central Sinai, Egypt

A. G. Hasaneen and S. A. Sultan
National Research Institute of Astronomy and Geophysics.
Helwan, Cairo, P. O. 11722, Egypt

B. S. Mohamed
Geological Survey of Egypt and Mining Authority
3 Salah Salem Road, Abbassiya, Cairo, Egypt

Different geophysical tools were carried out on the studied area to define the stratigraphic units, structural elements and the depth to the basement surface. These geophysical tools are geoelectric, magnetic and gravity methods.

Three deep vertical electric soundings were measured with current electrode spacing ranged from AB = 3 m. to AB = 8000 m. to detect the deep aquifer at the studied area to define the main aquifers in the studied area. One VES station was measured beside a borehole, which was drilled in the area, for correlation, calibration and interpretation purposes.

Quantitative interpretation of the vertical electrical sounding curves was done by using the two layer standard curves and generalized Cagniard graphs (Koefoed, 1960) and (Orellana and Money, 1966) to determine the thickness and true resistivities for each geoelectrical unit in order to obtain a preliminary models. All VES stations are re-interpreted as a final models using IPI-1D program to compute these final models by using the results of the manual interpretation as an initial ones. The actual thicknesses and resistivities were used to construct geoelectrical cross-sections to define subsurface stratigraphic units and water bearing aquifer.

One hundred twenty land magnetic stations were measured to cover the studied area. The interpretation of the magnetic data started with reduction to the magnetic pole, then depth to the upper surface of the basement was determined applying Eulier deconvolution technique.

Gravity measurements were done using Autograv gravimeter of sensitivity 0.01 mGal at the same stations of magnetic measurements. The gravity measurements were corrected to give the Bouguer gravity anomaly map. The quantitative interpretation of Bouguer gravity anomaly map started with separation of residual and regional gravity anomalies applying high and low pass filter technique using Geosoft program, (1994). However, the residual gravity anomalies reflect the anomalies, that have been resulted from shallow sources, while the regional gravity anomalies reveal the effects, which have been produced from deeper sources. The structural elements can be determined from the residual gravity anomalies. Also, gravity modeling was carried out along three profiles to define the depth of water bearing Nubian sandstone aquifer and the upper surface of the basement using GM SYS program.

A Feasibility Study on the Detection of Anomaly Inside Wood by Using Ground-Penetrating Radar Probing

S.-Y. Hyun and S.-Y. Kim
Korea Institute of Science and Technology
Seoul, Korea

A number of extremely beautiful but very old temples and palaces are preserved as the national treasures in Korea. But our National Treasure Agency worries about sudden collapse of the old architectures due to the weakness of those wooden columns. Hence we suggest GPR(ground-penetrating radar) as an effective tool for identifying any anomalies inside wooden column, because GPR has been widely used for subsurface probing on buried targets and geological structures and testing of concrete status on building, road, dam, bridge, etc.
A feasibility study is performed on the detection of anomaly inside wood by using GPR. At first, an actual GPR system including the self-fabricated antenna is installed in our laboratory. An empty cavity is made artificially inside a long rectangular wooden column. The scanning of the GPR system along the wooden column is performed in various directions. The measurement data illustrated that the location of each anomaly inside the wooden column corresponds to its actual position one-to-one.
To verify the accuracy of the GPR experiment, an efficient GPR simulator is also developed by combining the CP-FDTD (contour path finite difference time domain) method and the extended PML (perfectly matched layer) condition. And an improved model on the antenna feed was also added. The complex permittivity of wooden column is measured by employing an open-ended coaxial probe designed in our laboratory. In case of the same situation of our actual GPR experiment, the simulated numerical results approach to the measured data very closely. And a number of numerical simulations are performed to find the possibility of a GPR on identifying some abnormal wooden columns among the total columns of an old architecture.

Scattering from Non-Shallow Targets Buried Beneath Two-Dimensional Random Rough Surfaces Using the Multiple Interaction Model

M. El-Shenawee
Department of Electrical Engineering, University of Arkansas
Fayetteville, Arkansas 72701, U.S.A.

The multiple interaction approach is used with the robust Steepest Descent Fast Multipole Method (SDFMM) to compute the signature of non-shallow penetrable scatterers buried beneath 2-D random rough surfaces. The most attractive feature of the proposed model is removing the quasi-planar structure constraint of the Steepest Descent Fast Multipole Method (SDFMM) when used in analyzing non-quasi-planar scatterers. The basic idea of the multiple interaction model is to decompose certain non-quasi-planar structures into two quasi-planar scatterers where the conventional SDFMM can be applied separately to each one. The interactions between the sub-quasi-planar scatterers are calculated directly using the electromagnetic vector potentials near-field expressions. Significant reductions in the CPU time and computer memory are achieved by using the SDFMM in the model. A variety of geometries are used to test the model and their numerical results are validated with the conventional MoM.

The results show that the buried object's signature is largely due to the first interaction mechanism (i.e. ground-object-ground). However, the contribution of each additional interaction is explicitly calculated using the model. Interestingly, the contributions from repeating this mechanism become insignificant especially for lossy background soil. This conclusion depends on the physical properties of the scatterer.

The multiple interaction model successfully demonstrates the exploitation of the SDFMM robustness when applied to the multilayered rough ground where the burial depth of the underground rough layer is on the order of a wavelength.

Electromagnetic Induction (EMI) Response from Conducting and Permeable Spheroidal Shells

B. E. Barrowes, C. O. Ao, and J. A. Kong
Research Laboratory of Electronics, Massachusetts Institute of Technology
77 Massachusetts Ave, Room 26-305
Cambridge, MA 02139-4307, U.S.A.

K. O'Neill
US Army Cold Regions Research and Engineering Laboratory
Hanover, NH 03755, U.S.A.

Broadband electromagnetic induction (EMI) methods are promising in the detection and discrimination of subsurface metallic objects such as unexploded ordnance (UXO) [1]. In previous works [2, 3, 4], we have presented the EMI solution for prolate and oblate solid spheroids under arbitrary excitation. This paper extends these anlayses to include spheroidal shells with a hollow cavity enabling the computation of the EMI response from hollow metallic objects such as needles, spheres and disks. It is expected that these hollow geometries will more closely resemble actual UXOs therefore leading to more accurate detection and discrimination.

We give an exact analytic formulation for the EMI response of a conducting and permeable prolate and oblate spheroidal shells. This formulation is based on the separation of variables in spheroidal coordinates. We assume that the medium surrounding the spheroidal shell is poorly conducting and only weakly magnetic. Thus, in the frequency range of interest, $\sim$20Hz–30kHz, volume and surface effects from the surrounding medium may be conveniently ignored by approximating the background wavenumber $k_2 \approx 0$. This is in contrast to higher frequency subsurface detection techniques such as ground penetrating radar (GPR) in which case scattering must be accounted for due to the nonzero wavenumber of the background medium.

Numerical results for the far-field response from both prolate and oblate spheroidal shells for varying elongations and relative permeabilities are presented as a function of size parameter. These results are compared and contrasted to results for solid spheroids in limiting cases to validate the method. Results are presented as real (in-phase) and imaginary (quadrature) relaxation curves normalized to the high frequency limit. Results indicate that EMI responses from spheroidal shells differ in resonance frequency, crossover point, and DC dipole magnitude when compared to solid spheroids.

REFERENCES

1. Won I. J., D. A. Keiswetter, and T. H. Bell, "Electromagnetic induction spectroscopy for clearing landmines" *IEEE Trans. Geosci. Remote Sensing*, vol. 39, num. 4, pp 703–709, April, 2001.
2. Braunisch H., C. O. Ao, K. O'Neill, and J. A. Kong, "Magnetoquasistatic response of conducting and permeable spheroid under axial excitation" *IEEE Trans. Geosci. and Remote Sensing*, vol. 39, no. 12, pp 2689–2701, Dec. 2001.
3. C. O. Ao, H. Braunisch, K. O'Neill, and J. A. Kong, "Quasi-magnetostatic solution for a conducting and permeable spheroid with arbitrary excitation" *IEEE Trans. Geosci. and Remote Sensing*, accepted for publication.
4. C. O. Ao, H. Braunisch, K. O'Neill, J. A. Kong, L. Tsang, and J. T. Johnson, "Broadband electromagnetic induction response from conducting and permeable spheroids," in Detection and Remediation Technologies for Mines and Minelike Targets VI, Orlando, Apr. 16-20, 2001, vol. 4394 of Proc. SPIE, pp 1304–1315.

A Minimum Entropy Image Restoration Approach to Enhance GPR Images Produced by Frequency-Wavenumber Migration

X. Xu and E. L. Miller
Department of Electrical and Computer Engineering, Northeastern University
Boston, MA 02115, U.S.A.

In this paper we present an optimized frequency-wavenumber (F-K) migration method to image subsurface reflectivity using ground penetrating radar (GPR) sensing. F-K migration has been used to provide high quality images in many GPR applications. For example, in landmine detection, the hyperbolic curves usually seen in the GPR data can be collapsed to a point representing the position of the landmine. Essentially F-K migration is designed to back-propagate waves so that the position of a point source, i.e., the landmine, can be identified. Underlying this approach is the so called "exploding reflector" model in which the scattered fields from the landmine are assumed to arise from a point source located in a homogeneous medium emitting spherical waves. The power of this model is its simplicity. Specifically, it leads to a migration approach which has an efficient, Fourier-based implementation. However, by ignoring effects arising from the presence of an air-earth interface as well as the roughness of the surface, the resulting images tend to be corrupted by artifacts making their interpretation difficult.

In this paper, we discuss an optimized approach to F-K migration using a constrained minimum entropy method which is designed to remove artifacts arising from the imperfect model. Under ideal conditions where the exploding reflector model holds, the F-K images should contain point-like features indicating the position of the mines. Such images are known to have small entropy especially compared to the cluttered results one obtains in practice. To remove this clutter and essentially auto-focus the image, we have developed a means of locally varying the velocity of propagation in the medium within the context of the efficient, nominal F-K algorithm. Thus, by employing a rigorous optimization approach, we look for that set of velocities which yields a reconstructed image of the lowest entropy. Before applying the optimized F-K migration to a GPR image, we use histogram equalization to pre-process the raw image in order to better enhance the hyperbolic curves. Histogram equalization modifies an image so that its histogram has a desired shape, which in turn, transforms the image for the ease of detection and localization. Using histogram equalization, landmine reflected signals that are difficult to detect can be enhanced thereby making the subsequent optimized F-K migration more effective.

Using field data from a number of time-domain GPR systems, we show that optimized F-K migration can produce images of a highly focused mainlobe and suppressed sidelobes.

A Thin Layer Modelling and Radiometric Evaluation of a Dielectric Slab

S. Aktas
Turkish Airforce Academy, Electronic Engineering
Yesilyurt, Turkey

O. Yildirim
Turkish Airforce Academy, Research & Development Center
Yesilyurt, Turkey

S. Yalcin
Bahcesehir University
Bahcesehir, Turkey

As is well-known, dielectric properties of soils have been extensively studied using laboratory techniques. To reveal the interactions of soil properties and microwave emission better, a series of field and laboratory experiments have been conducted for many years.

Microwave radiometers are being used to estimate surface soil moisture, soil texture, bulk density. It measures the spectral radiance of the thermal emission as the brightness temperature which depends on the thermal temperature and reflectivity or emissivity of the surface. The thermal emission varies according to both the dielectric and temperature profiles of the soil. The assumption of uniform vertical properties requires that the depth of the soil that affects the microwave emission is known. This problem has been studied theoretically and experimentally.

The brightness temperature can be observed by a airborne radiometer looking down at the slab surface through an absorbing and radiating features. The surface emission model determines both the slab reflection and the slab emission characteristics. The soil moisture sampling depth of the microwave sensors is only a few tenths of a wavelength. The longer wavelengths showed a greater ability to penetrate a loss dielectric media and a deeper soil moisture sampling depth.

In this study, a slab of soil is modelled as a thin layer with different temperatures, humidities. We determine the relationship between the reflection coefficient and the soil moisture content. The reflectivity of the soil surface is determined via dielectric properties of the soil. The radiometric temperature of the slab is added by evaluating the thermodynamic temperatures of the soil slab lying the sensor field of view.

Accordinative Study Between The Vertical Electrical Sounding and TEM Methods for Exploring Groundwater Along Cairo-Alexandria Road (Egypt)

E. A. Al-Sayed, S. S. Osman, and A. G. Hassaneen
National Research Institute of Astronomy and Geophysics (NRIAG)
Cairo, Egypt

Shallow geophysical methods in the form of VES and TEM survey are carried out along Cairo - Alexandria Road. This survey achieved for exploring the groundwater potentialities and prospecting the geologic capabilities of water bearing sequence and to determine the more suitable technique for exploring groundwater, which is considered as the main aim of this work. However the vertical distribution of the produced resistive, as have been concluded from the interpretation of fifty two TEM soundings and thirteen VESes carried out in the studied area, investigated shallow sections into nearly four layers.
These layers are classified electrically and hydrologically into four main zones. The upper high resistivity zone is devoid from water. The second low resistivity zone shows the aquiclude of the aquifer. The third zone exhibits the main aquifer, and the fourth zone represents the barren section. From the interpretation of the VESes and TEM data and comparing the results with the wells, which are present in the area of study we can deduce that, the TEM technique is considered the more suitable one for the exploring of groundwater at least in the conditions of the area of study.

Session 2Ac6

Recent Mathematical Advances in Solving Inverse Problems in Electromagnetics

On the Local Dirichlet-to-Neumann Map

G. Uhlmann
University of Washington
Seattle, WA, U.S.A.

We will consider in this talk the problem arising in Electrical Impedance Tomography (EIT) of determining the conductivity of a body by making voltage and current measurements at the boundary of the body. The information is encoded in the so-called Dirichlet-to-Neumann (DN) map. Significant progress has been made in the last twenty years or so in both the theoretical and applied aspects of EIT. In particular the construction of complex geometrical optics solutions has led to many results. These results have for the most part assumed that we can make the measurements on the whole boundary.

In this talk we will survey recent progress on the determination of a conductivity by making electrical measurements on part of the boundary. The speaker and A. Bukhgeim have shown that one can prove unique identifiability of the conductivity by measuring the DN on particular open subsets of the boundary. The method of proof uses Carleman estimates to construct appropriate complex geometrical optics solutions. We will also discuss recent joint work with H. Ammari. We prove that we can determine the conductivity in the interior by measuring the DN map on arbitrary open subsets of the boundary by applying voltage potentials in the same open subset, if one knows a-priori the conductivity in a neighborhood of the boundary.

Identification of Conductivity Imperfections of Small Diameter

S. Moskow
University of Florida
Gainesville, FL, U.S.A.

We show asymptotic formulae for a voltage potential in the presence of small inhomogeneities. We then discuss several possible techniques using these formulae to determine the location, size, and/or conductivities of these imperfections. This is a joint work with Habib Ammari and Michael Vogelius.

Inversion of 2-D Buried Scatterers by Controlled Evolution of Level Sets: State-of-Art and Perspectives

C. Ramananjaona, M. Lambert, and D. Lesselier
Département de Recherche en Électromagnétisme
Laboratoire des Signaux et Systèmes (CNRS-SUPÉLEC-UPS)
Gif-sur-Yvette, France

J.-P. Zolésio
INRIA
Sophia-Antipolis, 06902, France

So-called controlled evolutions of level sets are increasingly considered as fast yet powerful solution tools of time-harmonic, non-linearized wavefield inverse scattering problems. Such tools apply when one wishes to retrieve the unknown shapes of scatterers, those having known electromagnetic contrasts with respect to those of their known embedding (or known Boundary Condition holding on them, e.g., perfectly conducting objects), from some knowledge of the field scattered off when a probing wave is impinging upon them. (One may speak of topological identification.) No information about the number, connectivity and/or location of interior points of such objects is usually given, and the main topological prior is that they remain contained in some prescribed box, and the main restriction to practical use, in addition to the knowledge of contrasts (unless those are retrieved simultaneously) or BC, is that the boundary contours are and remain smooth enough.

Most analyses so far —not every one, e.g., Dorn, "A level set approach to low-frequency electromagnetic imaging in 3D," SIAM annual meeting, July 2001, San Diego— appear to have been led in 2-D scalar cases, i.e., for objects elongated enough in one direction with respect to the characteristic length of the probing signal to be considered as pure cylinders, as investigated here.

The authors, and colleagues before, have devoted much effort to free space cases (the objects are sought in a homogeneous space) as well as buried cases (the objects are sought within a half space and illuminated and the data collected from an other half space). For detail, one should refer to Litman *et al.*, *Inverse Probl.* 14 (1998) 685-706, and to Ramananjaona *et al.*, *Inverse Probl.* 17 (2001) 1087-111, respectively, and references therein. The (simpler) TM and (more involved) TE polarization cases have been considered. Like methods (so-called fixed point ones) have been studied also with no much exposition yet, whilst most recent works are carried upon the strongly ill-posed simultaneous retrieval of the topology (the cross-sections of the cylinders) and of the material contrasts. Key questions, like the strategy of evolution from one level set iterate to the next, the penalization of the cost functionals, and stopping criteria are also of interest.

Here the authors will attempt to exhibit, without dwelling on the sophisticated mathematics beneath the level-set approaches and like ones, the main results obtained in practice, and to outline questions ahead. This will be done with the help of a small number of results reached by numerical simulations (free of *inverse crime*) and laboratory-controlled experimentations in illustrative cases.

Inverse Scattering Transform Technique for Soliton Propagation in Random Media

J. Garnier
Laboratoire de Statistique et Probabilités, Université Paul Sabatier
Toulouse, France

The investigation of the competition between randomness and nonlinearity for wave propagation phenomena in the one-dimensional case is of great interest for applications such as nonlinear optics and optical transmission systems. As it is well known, in one-dimensional linear media with random inhomogeneities strong localization occurs, which means in particular that the transmitted intensity decays exponentially as a function of the size of the medium. On the other hand, in some homogeneous nonlinear media wavepackets called solitons can propagate without change of form or diminution of speed.

We study the transmission of a soliton through a slab of nonlinear and random medium. We first consider the one dimensional nonlinear Schrödinger (NLS) equation, and we assume that inhomogeneities affect the potential, the nonlinear coefficient, and the dispersion. We study the influence of the random perturbations on the propagation properties of the integrable NLS equation. Several asymptotic behaviors can exhibited when the amplitudes of the random fluctuations go to zero and the size of the slab goes to infinity. The mass of the transmitted soliton may tend to zero exponentially (as a function of the size of the slab) or following a power law; or else the soliton may keep its mass, while its velocity slowly decays to zero.

Second the Korteweg-de Vries equation is considered with the initial condition given by a soliton. A random perturbation is added to this integrable system. It is shown that this problem is very different from the NLS case in that many small-amplitude solitons are generated. We give the precise description of the scattered wave in terms of a main soliton, a soliton gas, and radiation.

Fourier Integral Operators in Synthetic Aperture Radar

M. Cheney
Rensselaer Polytechnic Institute
Troy, NY, U.S.A.

C. J. Nolan
University of Limerick
Limerick, Ireland

This talk considers Synthetic Aperture Radar and other synthetic aperture imaging systems in which a backscattered wave is measured from a variety of locations.

For the received signal, we give a mathematical model that includes the effects of limited bandwidth and the antenna beam pattern. The model includes antennas with poor directionality, such as are needed in the problem of foliage-penetrating radar, and can also accommodate other effects such as antenna motion and steering.

We show that this model for the received signal can be naturally formulated so as to involve a Fourier Integral Operator (FIO), for which an extensive mathematical theory has been developed [1, 2, 3]. This theory is built to deal with singularities, such as wavefronts and the jumps in wave speed that occur at the boundaries between materials.

FIO techniques have been developed for linearized inverse problems [4], and these can be applied to the SAR problem to give an approximate inversion formula for SAR. This inversion formula can accomodate non-ideal aspects, such as a changing antenna beam pattern and limited bandwidth. Under certain conditions, the inversion process accurately reconstructs features of the scene that correspond to singularities, such as walls and edges. The FIO formulation can be analyzed to determine exactly what is reconstructed and to determine the resolution of the image.

REFERENCES

1. J. J. Duistermaat, *Fourier Integral Operators*, Birkhauser, Boston, 1996.
2. A. Grigis and J. Sjöstrand, Microlocal Analysis for Differential Operators: “An Introduction, London Mathematical Society Lecture Note Series,” Vol. 196, *Cambridge University Press*, 1994.
3. F. Treves, “Introduction to Pseudodifferential and Fourier Integral Operators,” Vol. I and Vol. II, *Plenum Press*, New York, 1980.
4. G. Beylkin, “Imaging of discontinuities in the inverse scattering problem by inversion of a causal generalized Radon transform,” *J. Math Phys.*, Vol. 26, 99–108, 1985.

High Order Methods in Direct and Inverse CEM

O. P. Bruno, J. Chaubell, and E. M. Hyde
Department of Applied and Computational Mathematics
California Institute of Technology
Pasadena, CA 91125, U.S.A.

We are concerned with direct and inverse problems of scattering by penetrable bodies.

With regards to direct solvers, we present a new high order integral algorithm for the solution of scattering problems by heterogeneous bodies in two and three dimensions. Here a scatterer is described by a (continuously or discontinuously) varying refractive index $n(x)$ within a bounded region; solutions of the associated Helmholtz equation under given incident fields are then obtained by high-order inversion of the Lippmann-Schwinger integral equation. The algorithm runs in $\mathcal{O}(Nlog(N))$ operations where N is the number of discretization points. A wide variety of numerical examples provided include applications to highly singular geometries, high-contrast configurations, as well as electrically large problems for which supercomputing resources have been used recently. Our method provides highly accurate solutions for such problems on small desktop computers in CPU times of the order of seconds. In particular, applications of this method to the *inverse problem* of low-coherence interferometry, described below, are given.

Low-coherence interferometry is a non-invasive imaging technique based on the use of light sources exhibiting a low degree of coherence. Low coherence interferometric microscopes have been successful ([Tearney, Brezinski and Southern, *Opt. Lett.*, Vol. 20, No. 21, 1995]; [Hettinger, Mattozzi and Myers, *Plant Physiology*, May 2000, Vol. 123]) in producing internal images of thin pieces of biological tissue; typically samples of the order of 1mm in depth have been imaged, with a resolution of the order of 10 to 20μm in some portions of the sample. Such images have been produced through renderings of the intensities of certain interference fringes as functions of the position of the light-focus within the sample; quite generally, limited post-processing of this data has been used. Our discussion addresses, in a mathematically rigorous manner, the inverse (Maxwell) problem of producing the actual values of the refractive index within the sample from given low-coherence interferometric data. We show that use of the low coherence properties of light lead to well conditioned inverse problems. Once obtained, the refractive index maps are useful in a variety of ways; in particular, a straightforward display of this map yields an image of the internal structure of the sample. As opposed to the direct renderings used earlier, the present rigorous mathematical treatment allow to account for various loss mechanisms such as scattering and absorption in a rigorous manner, and, thus, to produce images that remain faithful throughout the body of the sample.

Boundary Perturbations and Analytic Continuation in Electromagnetic Scattering

O. P. Bruno
Applied Mathematics, Caltech
Pasadena, CA, U.S.A.

F. Reitich
School of Mathematics, University of Minnesota
Minneapolis, MN, U.S.A.

The advantages of the use of boundary perturbation methods for electromagnetic scattering calculations have been recognized now for several decades. Besides the simplicity of their implementations, perturbation approaches generally lead, quite efficiently, to very accurate results within their domain of applicability. Indeed, it was these characteristics that prompted a number of investigations in the last thirty years, mainly in the area of scattering by corrugated surfaces, and which resulted in a variety of low-order theories. These, of course, are limited to fairly small departures from an exactly solvable geometry and, in fact, attempts at extending their domain of applicability by simply raising their order encountered very limited success, and they led to substantial confusion over the validity of perturbation expansions.

In an effort to overcome these limitations we have developed over the last few years a general *high-order* method based on variation of boundaries. In this presentation we shall first review the main ideas that led us to devise these numerical algorithms. In particular we will present a new mathematical demonstration of our main observation, namely that electromagnetic fields depend *analytically* upon (smooth) boundary deformations. We will next explain how this result, which settled a long-standing controversy in the electromagnetic community, guarantees that the applicability of perturbative schemes can be significantly enhanced through the use of appropriate mechanisms of *analytic continuation*. In fact, we will show that, with this addition, the resulting numerical codes effectively provide direct scattering predictions that, in some cases, may be substantially more accurate than those that can be garnered with classical methods. Further, we shall also show that these mechanisms can be used to advantage in solution of inverse scattering problems when these are cast in terms of the minimization of a (least squares) functional. Indeed, we will show that the aforementioned ideas of analytic continuation can be advanced to enable a *global* line search at each step of a minimization algorithm; through a number of numerical examples we will further demonstrate that such globalization may be necessary to overcome nonconvexity. Finally, we will show that our new proof of analyticity of electromagnetic fields provides insight into the validity and applicability of all classical perturbative treatments of scattering problems. In particular, we shall explain how our analysis predicts that the numerical conditioning of the problem deteriorates with increasing boundary roughness. We will illustrate this effect on the classical "Operator Expansion" method which we will show to be unsuitable for high-order calculations due to a pronounced numerical ill-conditioning; possible ways to stabilize these and other perturbative algorithms will also be discussed.

The Linear Sampling Method in Inverse Electromagnetic Scattering

P. Monk
University of Delaware
Newark, DE 19711, U.S.A.

I shall discuss computational and theoretical advances in the use of the linear sampling method for solving certain inverse scattering problems for the time harmonic Maxwell equations for frequencies in the resonance region. The Linear Sampling Method, due to Colton and Kirsch, can reconstruct the boundary of a scatterer using single frequency bistatic data. The advantages of the method are that information is not needed concerning the nature of the scatterer (for example the boundary condition on the scatterer need not be known), and the method easily reconstructs multiple scatters (disconnected). In addition the method only involves solving multiple linear ill-posed problems. The main disadvantages are the need for a substantial amount of bistatic data, and that only data for a single wavenumber can be used. In addition non information can be obtained about other properties of the scatterer such as the boundary conditions or composition of the scatterer.

Recently, substantial progress has been made in the theoretical understanding of the Linear Sampling Method. For example it has recently been justified for “mixed” scatterers involving both perfect conducting and imperfect conducting boundary conditions on a single surface. In addition the method is justified (under rather restrictive assumptions that do not seem necessary in practice) for penetrable media. Besides these theoretical advances, three dimensional numerical tests of the method have also been completed for some simple scattering geometries.

In the talk I shall outline the Linear Sampling Method and give an overview of it’s analysis. I shall mainly concentrate on the numerical implementation of the Linear Sampling Method, various numerical results and their implications.

A New Algorithm for the Reconstruction of Conductivity Inhomogeneities

H. Ammari
Ecole Polytechnique
Palaiseau, France

In this talk we will discuss a recent joint work with J. Seo on the reconstruction of conductivity inhomogeneities. We will derive accurate asymptotic expansions of the steady-state voltage potentials in the presence of a finite number of diametrically small inhomogeneities with conductivities different from the background conductivity. We will then apply these asymptotic formulae for the purpose of identifying the location and certain properties of the shapes of the conductivity inhomogeneities. Our designed algorithm is based on the observation of the pattern of simple weighted combinations of the input currents and the output voltages. Our mathematical analysis indicates that our algorithm is with a high resolution and accuracy.

Identifying Imperfections of Small Diameter

H. Ammari
Center for Applied Mathematics, Ecole Polytechnique & CNRS UMR 7641
Palaiseau, France

M. S. Vogelius
Department of Mathematics, Rutgers, The State University of New Jersey
Piscataway, NJ 08854-8019, U.S.A.

D. Volkov
Dept. of Mathematical Sciences, New Jersey Institute of Technology
Newark, NJ 07102, U.S.A.

The objective of our work is the detection of small dielectric imperfections in an otherwise homogeneous electromagnetic medium. In the presence of such imperfections, we try to identify their location, and possibly to evaluate their electromagnetic properties such as their conductivity and derive information about their geometry. The only data that we use is the electric and magnetic fields measured on the boundary of the medium.

The time harmonic Maxwell equations form an elliptic system of PDE's. If both tangential electric and magnetic fields are known, the corresponding elliptic boundary problem is overdetermined. This lead us to believe that the overdetermined boundary data conveys information on the presence and characteristics of imperfections.

Denoting H_ρ, where the subscript ρ is a dilation coeffcient for fixed imperfections, the magnetic field in presence of imperfections and H_0 the magnetic field in absence of imperfections, we derived an expansion in the parameter ρ for the difference $H_\rho - H_0$ assuming that the same tangential electric field is prescribed. We obtained in this expansion terms that are relevant for characterizing the location, polarization, conductivity, permittivity and permeability of the imperfections.

The rigorous derivation of these formulas was an interesting and challenging mathematical problem in the three dimensional case. We also found and rigorously derived an expansion for the eigenvalues of the Maxwell equations in that case. The two dimensional case is related to cylindrical geometries, T.E. and T.M. waves. We conducted many numerical simulations in this case. Some of them were based on minimization algorithms. In another approach, special boundary currents were applied in order to measure the Fourier transform of Dirac functions centered at the imperfections. The location of the imperfections were then recovered by using a FFT algorithm.

We are currently researching related problems. We want to implement a method for finding the locations of imperfections in a situation where measurements are available on only one part of the boundary. In another frame of work, instead of relying on boundary measurements, we analyze the scattered field of imperfections in free space illuminated by an incident wave.

Session 2Ac7

Left-Handed Medium and Other Electromagnetic Metamaterials I

Macroscopic Electromagnetic Field Modeling in Metamaterials

S. A. Cummer
Electrical and Computer Engineering Department, Duke University
Durham, NC 27708, U.S.A.

Recent papers have explored the fascinating theoretical properties of electromagnetic materials with simultaneously negative permittivity and permeability. More importantly, materials with a negative refraction index in a limited frequency range have actually been manufactured using metallic inclusions, and some properties of these materials have been verified experimentally. These structures have been based on carefully designed metallic inclusions, and detailed numerical simulations of a unit cell of these inclusions have also demonstrated some of their unusual properties. However, these microscale simulations are to detailed to easily simulate the fields in a larger region of space like one might encounter in an actual application of these materials. The bulk dielectric properties of these materials have been experimentally verified and are well-understood, making analytical simulation an option. But in strongly dispersive materials like these, non-sinusoidal solutions are not easy to derive, and they are typically only analytically tractable for very simple material geometries and inhomogeneities. A numerical method for simulating the macroscopic fields in a relatively large region of LH materials would be valuable for simulating applications and including effects like losses that are not easy to treat analytically.

Thus far physically realized materials with these properties are simply a combination of dispersive electric and magnetic field material responses. The combination of these material effects leaves a linear, isotropic,and temporally dispersive medium that can be simulated with finite difference techniques. We demonstrate the accuracy and stability of such a technique and investigate some of the important properties of these materials, including the exponential growth of waves with imaginary wave number and associated subwavelength focusing. Energy limitations and the achievability of sinusoidal steady state solutions will be discussed. Absorbing boundary conditions for this material present an interesting problem. Ordinarily, the perfectly matched layer (PML) is straightfowardly adaptable to dispersive materials, but we show analytically and numerically that the opposite directions of phase and energy velocity cause the fields in the negative index band to grow exponentially in the PML.

Scattering of Light from, and its Transmission through, a Slab of a Left-Handed Medium with a Random Illuminated Surface

T. A. Leskova
Institute of Spectroscopy, Russian Academy of Sciences
Troitsk, Moscow obl. 042090, Russia

A. A. Maradudin
Department of Physics and Astronomy and Institute for Surface and Interface Science
University of California, Irvine
Irvine, CA 92697, U.S.A.

I. Simonsen
Nordic Institute for Theoretical Physics – Nordita
Copenhagen, DK-2100, Denmark

Recently a physical medium was fabricated [1] in which both the effective permittivity $\epsilon(\omega)$ and the effective permeability $\mu(\omega)$ are simultaneously negative over a restricted frequency range. Thus, in this frequency range, such a medium is "left-handed", and is characterized by a negative refractive index. It was shown recently that in contrast to nonmagnetic media with a negative dielectric function, the planar surface of a left-handed medium can support both p- and s-polarized surface electromagnetic waves [2, 3]. The reflectivity of such a surface as a function of the angle of incidence displays structure associated with the existence of a Brewster angle in both polarizations and the existence of a critical angle for total internal reflection in both polarizations [3]. A study of the scattering of p- and s-polarized electromagnetic waves from a weakly rough one-dimensional random surface of a left-handed medium has shown that the angular distribution of the intensity of the light that has been scattered incoherently displays an enhanced backscattering peak, and Yoneda bands, for both polarizations of the incident light [3]. In this paper we study the scattering of p- and s-polarized light from, and its transmission through, a slab of a left-handed medium bounded by a rough one-dimensional random surface. We assume that the surface profile function is a single-valued function of the coordinate in the mean plane of the surface that is normal to its grooves and ridges, and constitutes a zero-mean, stationary, Gaussian random process. Since both the effective permittivity $\epsilon(\omega)$ and the effective permeability $\mu(\omega)$ are simultaneously negative in the frequency range we are interested in, the electric and magnetic excitations give rise to both p- and s-polarized surface polaritons in the slab. When light is scattered from or transmitted through the slab bounded by a random rough surface not only the enhanced backscattering and enhanced transmission peaks but also satellite peaks appear in the angular distributions of the intensity of light. We show that as in the case of a semi-infinite left-handed medium, the angular distributions of the intensity of the light that has been scattered from or transmitted through the slab display unusual features associated with the left-handedness of the material of the slab.

REFERENCES

1. Smith, D. R., W. J. Padilla, D. C. Vier, S. C. Nemat-Nasser, and S. Schultz, "Composite media with simultaneously negative permeability and permittivity," *Phys. Rev. Lett.*, Vol. 84, 4184–4187, 2000.

2. Ruppin, R., "Surface polaritons of a left-handed medium," *Phys. Lett. A*, Vol. 277, 61–64, 2000.

3. Leskova, T. A., A. A. Maradudin, and I. Simonsen, "Scattering of electromagnetic waves from the random surface of a left-handed medium," *SPIE*, Vol. 4447, 6–16, 2001.

Electromagnetic Modeling of Negative Permeability and Left-Handed Metamaterials Including Bianisotropy

R. Marqués, F. Medina, F. Mesa and R. Rafii-El-Idrissi
Departamento de Electrónica y Electromagnetismo, Facultad de Física and E.T.S. de Ingeniería Informática, Universidad de Sevilla
Sevilla, 41012, Spain

Left-handed media were first theoretically proposed by Veselago [1] and, recently, a left-handed artificial medium (metamaterial) has been realized by D.R.Smith and his co-workers [2]. The metamaterial proposed in [2] is a composite of two artificial media with negative electric permittivity (NEPM) [3] and negative magnetic permeability (NMPM) [4] in the microwave range, respectively.

Bi-isotropic artificial media were first proposed and realized by Lindmann [5] and, henceforth, the analysis, modeling and realization of such media became an active field of research in the microwave community. Artificial bianisotropic media are a straightforward generalization of the bi-isotropic media proposed in [5]. These media are characterized by the most general linear and local constitutive relationships:

$$D_i = \varepsilon^{i,j} E_j - j(\mu_0 \varepsilon_0) k^{i,j} H_j \;\; ; \;\; B_i = j(\mu_0 \varepsilon_0) k^{j,i} E_j + \mu^{i,j} H_j \; ,$$

where the constraints imposed by the Onsager symmetry relationships for reciprocal media have been included.

There are some physical analogies between the behavior of these artificial bianisotropic media and the aforementioned NMPM, which suggests the presence of bianisotropy in both NMPM and left-handed metamaterials.

In this contribution we present an electromagnetic model for the analyzed left-handed metamaterial [2]. Our work is based on previous models for the NEPM and on a quasi-static analysis of the constitutive particles of the NMPM (which is justified by the small electrical size of these particles) together with the well-known Lorentz local field theory. This analysis accounts for a possible bianisotropy of the aforementioned constitutive particles.

In particular, two cases are considered: the edge coupled split rings resonator (ECSRR) proposed in [3] and a novel broadside coupled split rings resonator (BCSRR). It is shown that the ECSRR is also a bianisotropic particle, whereas the BCSRR does not show bianisotropy. A comparative analysis of these two particles is carried out. It is shown that, for a given working frequency, a smaller electrical size is expected for the BCSRR.

REFERENCES

1. Veselago, V. G., *Sov. Phys. USPEKHI*, Vol. 10, 509, 1968.
2. Smith, D. R., W. J. Padilla, D. C. Vier, S. C. Nemat-Nasser, and S. Schultz, *Phys. Rev. Lett.*, Vol. 84, 4184, 2000.
3. Pendry, J., A. Holden, W. Stewart, and I. Youngs, *Phys. Rev. B*, Vol. 57, 15261, 1998.
4. Pendry, J., A. Holden, D. Robbins, and W. Stewart, *IEEE-MTT*, Vol. 47, 2075, 1999.
5. Lindmann, K., *Annalen der Physik*, Vol. 63, 621, 1920.

Pulse Propagation in Left-Handed Metamaterials

A. Kaso and S. Sridhar
Physics Department, Northeastern University
Boston, MA, U.S.A.

As has been already shown, a material with both ϵ and μ negative can sustain propagating waves. The permittivity ϵ and permeability μ cannot be negative constants as this would violate the causality principle. Therefore a dispersive expression is needed for each of them. We consider the expressions obtained by theoretical considerations of the metamaterial used in the Smith and al. experiment and disregard their dissipative part. Then the material presents two stop bands, one LH band and one RH band. We consider several useful cases of pulse propagation:

1. A gaussian enveloped pulse with a carrier frequency is considered and the properties of its propagation (group velocity v_g, the spreading of the wave packet in time in the dispersive medium) are obtained.
2. A slab of material is considered for which transmission and reflectivity are computed for a normal incidence of the pulse on the slab. This treatment can be easily extended for incidence other than normal.
3. An antenna is treated of as included in a slab of material and its radiation in free space is considered.

All the above situations can prove useful in the applications of this new metamaterial, such as in delay lines where high values of the index of refraction are needed. Particular attention is given to the frequency region where the material displays $n = -1$. The transmission of the near field of a electric dipole in front of the slab will be considered, as it pertains to the construction of a perfect lens. Furthermore Ohmic losses will be included in the calculation.

Waves Propagation in a Rectangular Waveguide Simultaneously Filled with Left-Handed and Right-Handed Media

T. M. Grzegorczyk, Y. Zhang, and J. A. Kong
Research Laboratory of Electronics, Massachusetts Institute of Technology
Cambridge, MA 02137, U.S.A.

Propagation of electromagnetic waves is at the basis of many communication systems, ranging from microwave to optical frequencies. In order to increase the overall transmission characteristics of such channels, engineers are constantly looking for versatility in design, materials or geometries. The recent appearance of left-handed media, where the permittivity and the permeability are simultaneously negative over a frequency band, thus allows for new investigations in the domain of guiding wave devices.

In this work, we first review the simple parallel-plate waveguide geometry, and compute the Green's function for arbitrary excitation. This is done by solving the traditional Helmholtz wave equation with Dirichlet boundary conditions, first in its homogeneous version and then including the source. In a second step, the method of scattering superposition is applied to obtain the Green's function of a rectangular waveguide filled with two dielectrics, one of which has both the permittivity and the permeability negative, whereas the other has them both positive.

As for the parallel-plate waveguide case, the Green's function is obtained in an integral form, which kernel is composed of sine and cosine vector wave functions. This form is particularly well-adapted for further implementation in MoM-type methods, since the surface integrals may still be computed analytically.

With this basis, we conduct a detailed investigation on the fields inside the two dielectrics. Since the negative permittivity is a frequency dispersive phenomenon, it can be used to tune the left-handed dielectric properties and thus, to tune the field distribution inside the waveguide.

From a transmission point of view, this configuration can sustain two waves propagating in two opposite directions, or two waves propagating in the same direction, with a specific control on the velocity of the waves. Further work will investigate the applicability of such properties to waveguide devices.

Flux Distributions in a Non-Resonant Magnetic Metamaterial

E. Shamonina and L. Solymar
Department of Engineering Science, University of Oxford
Oxford, OX1 3PJ, UK

V. A. Kalinin
Transense Technologies Ltd.
Oxon, OX25 5HD, UK

M. Lapine and K. H. Ringhofer
Department of Physics, University of Osnabrück
Osnabrück, D-49069, Germany

The response of a 3D lattice of lossy metallic loops inserted into a homogeneous time-varying magnetic field is investigated theoretically. The current distribution is found by taking into account the magnetic coupling between any pair of loops in the approximation of no retardation. Knowing the current distribution and using the principle of superposition the electric and magnetic fields are then determined analytically in terms of elliptic functions. This makes the analysis very efficient in calculation time and data storage and permits obtaining a solution with an ordinary PC for a lattice comprising of a couple of thousands elements.

The main aim of the study is to find out how the magnetic flux varies inside and outside the loops, how the volume average of the magnetic field within a unit cell depends on the relative position of the unit cell within the structure and to show how the exclusion of the magnetic flux from the lattice occurs for different shapes (cubic, tall and flat structures) and for different packing densities. Conditions for approaching an ideal diamagnet are discussed and comparison with the current and magnetic field distribution in Type I superconductors are made.

Meta-Materials for Wireless Communications

E. D. Isaacs
Bell Laboratories, Lucent Technologies
Murray Hill, NJ, U.S.A.

D. R. Smith
University of California, San Diego
San Diego, CA, U.S.A.

S. H. Simon
Bell Laboratories, Lucent Technologies
Murray Hill, NJ, U.S.A.

Since Maxwell first wrote down the fundamental theory of electromagnetic radiation in the late nineteenth century and these concepts were broadly applied during World War II to radar, conventional wisdom has been that antennas must have linear dimensions of order the wavelength of the radiation. However, for many modern radar and communications applications such as integrated radios for hand held devices and multiple transmit and receive designs it is essential to have compact, efficient and lightweight antennas. Meta-materials offer a new approach to engineering material composites that open up the possibility of high-gain antennas even for substantially sub-wavelength dimensions. Utilizing the plasma resonance of the medium, which can be tuned from below 1 GHz to 20 GHz, meta-materials have been demonstrated to have very large linear responses in the microwave region.[1]

Consisting of arrays of very small conducting wires and dielectric elements, meta-materials are a natural for combining compact antenna designs with a range of new approaches to enhanced channel capacity for wireless. These approaches include multiple transmit and receive elements for Bell Labs LAyered Space-Time (BLAST) processing and/or highly directional beams. Another path to increased channel capacity is through the electric and magnetic polarization degrees of freedom[2] of the radiation field. Meta-materials have been demonstrated to be sensitive not only to the electric polarization, but also to the magnetic polarization of microwaves,[1] a property which at chosen wavelengths results in a Left Handed Medium with a **negative** refractive index.[1]

REFERENCES

1. Composite Medium with Simultaneously Negative Permeability and Permitivity, D.R. Smith, *Phys. Rev. Lett.* 84, 4184 (2000).
2. Tripling the Capacity of Wireless Communications Using Electromagnetic Polarization, M. Andrews, et al., *Nature* 409, 316 (2001).

Experimental Investigation of Negative Index Meta Materials

A. F. Starr, D. R. Smith, R. A. Shelby, and S. Schultz
Department of Physics, University of California
San Diego, CA 92093, U.S.A.

Meta-materials, or artificially structured materials designed for particular electromagnetic properties, have drawn much interest recently with the introduction of materials with simultaneously negative permittivity and permeability. This results in a negative index of refraction. These materials present challenges in characterization. As traditional methods of electromagnetic characterization are being modified to accommodate this new class of materials, we find that indirect methods are of great utility.

One particular experimental method investigates negative refraction as given by Snell's law as one implication of a negative index. Here we present details of an Angle Resolved Microwave Spectrometer (ARMS) used to study the angular refraction characteristics of electromagnetic meta-materials. This apparatus uses parallel conducting plates to confine EM propagating modes to two dimensions. A microwave source is coupled into the region between the plates, launches a propagating mode (single mode for certain plate separations) which is subsequently collimated. The collimated beam encounters a sample in the form of a prism. The beam is refracted upon exiting the sample into a direction characterized by an angle theta with respect to the sample normal. The beam width is also limited by an aperture at the sample. A detector located some distance, and at a variable angle from the sample detects the microwave power. Thus the apparatus allows for frequency and angle swept data.

More details of the experimental setup will be presented. Experimental results for positive index and negative index meta-materials are then presented, demonstrating negative refraction. The impact of dispersion, losses, and diffraction on the observed radiation patterns is discussed. Theoretical modeling of the structure also accompanies the discussion.

Numerical Studies of the Transmission Properties of Left-Handed Materials

P. Markoš and C. M. Soukoulis
Ames Laboratory and Department of Physics and Astronomy, Iowa State University
Ames, IA 50011, U.S.A.

Transmission of the electromagnetic (EM) waves through arrays of split-ring resonators (SRR) and through left-handed materials (LHM) is studied numerically using an improved version of the transfer-matrix method. The transmission and reflection amplitudes as well as the absorption are calculated [1,2].

For an array of SRRs, the resonance frequency band is found, in which transmission decreases by many orders of magnitude. We assume, in accordance with theoretical prediction of Pendry *et al.* [3], that the *effective* permeability of the entire structure is *negative* in this frequency region.

We study the dependence of the resonance frequency on the structural parameters of the split rings - the ring thickness, inner diameter, radial and azimuthal gap - as well as on the orientation of the SRR and on the electrical permittivity of the board and the embedding medium, where SRR resides. Qualitatively good agreement with previously published analytical results is obtained.

By combining an array of SRRs with an array of thin metallic wires, the left-handed meta-material is constructed. The LHM has both the *effective* permittivity and the *effective* permeability *negative* within the resonance band [4]. We indeed found a sharp transmission peak in the frequency dependence of the transmission. We present how the transmission properties of the LHM depend on the real and imaginary part of the electric permittivity of the metal, the length of the system, and the size of the unit cell.

The obtained numerical data for the transmission, reflection and the absorption are in very good agreement with the predictions of the simple homogeneous model with negative permittivity and permeability. Data for the reflection, absorption and for their phases have also been used for the direct calculation of the *effective* refraction index and impedance of the analyzed meta-materials. In the resonance frequency gap, *negative* real part of the refraction index was found [5].

REFERENCES

1. P. Markoš and Soukoulis. C. M, "Transmission studies of left-handed materials",*Phys. Rev.* B 64 (2001), cond-mat/0105618
2. P. Markoš and Soukoulis. C. M, " Numerical studies of left-handed materials and arrays of split-ring resonators", *physics/0111135*
3. J. B. Pendry *et al.*, *IEEE Trans. Microwave Theory Tech.* 47, 2075 (1999)
4. D.R. Smith *et al.*, *Phys. Rev. Lett.* 84, 4184 (2000)
5. D.R. Smith, Schultz. S, Markoš. P. , and Soukoulis. C. M," Determination of permittivity and permeability of metamaterials from scattering data", (unpublished).

Multiple Antennae, Multipole Radiation, and Beam Formation: Counting Electromagnetic Degrees of Freedom

A. S. Polyakov
New York University & Bell Labs, Lucent Technologies
New York, NY 10003, U.S.A.

P. P. Mitra and M. R. Andrews
Bell Labs, Lucent Technologies
Murray Hill, NJ 07974, U.S.A.

We propose an algorithm to design localized multi-antennae capable of directed beams with multiple degrees of freedom, by studying an appropriate concentration problem. We describe electromagnetic waves emerging from a localized region of space in terms of the electric and magnetic multipole moments of the source. Maximizing the concentration, defined as the normalized radiated energy within a solid angle, leads to an eigenvalue equation analogous to that studied earlier by Slepian, Landau, and Pollak in the context of the spectral concentration problem. This approach allows us to define a principled measure of the number of electromagnetic degree of freedom in a given solid angle. Since the channel capacity at high signal-to-noise ratio scales linearly with the number of degrees of freedom, this method should help us to design useful directed multi-antennae. In particular, by combining electric and magnetic multipole elements we find we can double the number of radiated degrees of freedom compared to electric-only or magnetic-only designs.

This talk will build on and generalize our previous work towards increasing the capacity of wireless communication through novel use of polarization [1]: Classically, radio communications have relied on a single channel per frequency, although it is well understood that the two polarization states of planar waves allow two distinct information channels; techniques such as "polarization diversity" already take advantage of this. We showed that in environments with scattering, an extra factor of three in channel capacity can be obtained relative to the conventional limit using dual-polarized radio signals. The extra capacity arises because there are six distinguishable electric and magnetic states of polarization at a given point, rather than only two as have been usually assumed.[1]

REFERENCES

1. Andrews, M. R., P. P. Mitra, and R. Decarvalho, "Tripling the capacity of wireless communications using electromagnetic polarization," *Nature*, January 18, 2001.

[1] A similar summary and talk were given at URSI-02 in January, but at PIERS 2002 we intend to present further results

Electromagnetic Energy Transfer through Nano Particle Arrays

Q. Wei, K. Su, N. Fang and X. Zhang
Department of Mechanical and Aerospace Engineering,
University of California at Los Angeles
Los Angeles, CA 90095, U.S.A.

The strong interactions of conductive electrons in an individual metal particle with high frequency electromagnetic waves, such as visible light, lead to an excitation of collective motion of electrons at the surface plasmon frequencies, with the metal particle behaving dominantly as an oscillating dipole. The surface plasmon frequency is defined by the particle material, the particle shape, and refractive index of surrounding medium. When another metal particle is present in close proximity, the dipole of this metal particle excited by the light wave will induce a plasmon oscillation of electrons in the second metal particle as a result of the near field electro-dynamic interactions. Recently, it has been proposed and shown theoretically that the strong interaction of the metal particles with light and strong near-field coupling between particles can be employed to fabricate wave guides by simply forming linear arrays of closely spaced nano metal particles [1, 2]. This kind of waveguides will have a feature size much smaller than the light wavelength. Analogous experiments with microwaves have demonstrated similar effects which are in accordance with the theory. In this paper, we will present our recent experimental investigations on nano metal particle arrays as waveguides. The results on the effects of the particle shapes, particle spacing, and light frequency on the waveguide properties will be discussed.

REFERENCES

1. M. Quinten, A. Leitner, J. R. Krenn, and F. R. Aussenegg, *Opt. Lett.* 23, 1331-1333 (1998)
2. M. L. Brongersma, J. W. Hartman, H. A. Atwater, *Phys. Rev.* B. 62, R16356 (2000)

Session 2Ac8

Electromagnetic Interaction on Rough Surfaces and by Particles: Phenomena and Applications

Ultrarefraction Properties of Photonic Crystals

D. Maystre, S. Enoch, and G. Tayeb
Institut Fresnel, Faculté des Sciences et Techniques de S^t Jérôme (case 262)
Marseille, 13397, France

Photonic crystals have been the subject of considerable interest since the end of the 80's. They have many potential applications, for example the development of efficient semiconductor light emitters, filters, substrates for microwave antennas, lossless mirrors.

More recently, some authors have predicted a phenomenon of ultrarefraction generated by such structures at the edge of the transmission gaps. In these conditions, a photonic crystal can simulate a homogeneous material having a real optical index less than unity [1–4]. Comparable considerations can be found in Ref [5] in the context of modulated planar waveguide. The first explanations of this phenomenon were based on heuristic considerations lying on dispersion properties. Then, numerical results based on rigorous electromagnetic theories [6, 7] have confirmed the validity of these predictions [8].

The first aim of this communication will be to propose intuitive and rigorous interpretations of this strange phenomenon. Rigorous numerical results will illustrate these explanations. It will be shown that the physical meaning of the phenomenon is close to that given to the Goos-Hanschen phenomenon. In contrast with the classical Goos-Hanschen phenomenon the photonic crystal allows to get this translation phenomenon for the transmitted beam, and close to the normal incidence.

A special attention will be paid to the notion of effective index: is it possible to associate to an inhomogeneous material such as a photonic crystal a homogeneous medium having the same refractive properties? It will be shown that in general, the answer is negative since the effective index depends on the angle of incidence on the crystal. However, considerations based on three-dimensional dispersion diagrams will demonstrate that in some conditions, this effective index becomes independent of the angle of incidence [9]. As a consequence, an object made of the photonic crystal may behave like a homogeneous object with a real optical index close to zero. A spectacular numerical example of a convergent concave microlens made of photonic crystal will be given.

Finally, numerical results will illustrate the phenomenon of negative refraction, where a photonic crystal seems to simulate a homogeneous medium with negative refractive index.

REFERENCES

1. Dowling, J. P. and C. M. Bowden, *J. Mod. Optics*, 41, 345–351, 1994.
2. Wisser, P. M. and G. Nienhuis, *Optics Comm.*, 136, 470–479, 1997.
3. *Photonic Band Gap Materials*, 71–91, C. M. Soukoulis Ed., Kluwer, 1996.
4. *Confined Electrons and Photons: New Physics and Applications*, 585–633, E. Burstein and C. Weisbuch Ed., Plenum Press, 1995.
5. Zengerle, R., J. Mod, *Optics*, 34, 1589–1617, 1987.
6. Felbacq, D., G. Tayeb, and D. Maystre, *J. Opt. Soc. Am. A*, 11 2526–2538, 1994.
7. Maystre, D., *Pure Appl. Opt.*, 3, 975–993, 1994.
8. Enoch, S., G. Tayeb, and D. Maystre, *Optics Communications*, 161, 171–176, 1999.
9. Gralak, B., S. Enoch, and G. Tayeb, *J. Opt. Soc. Am. A* 17, 1012–1020, 2000.

Coherent and Incoherent Scattering of Light from a Dielectric Film with a Two-Scale Random Surface on a Reflecting Substrate

M. Kretschmann, T. A. Leskova, and A. A. Maradudin
Department of Physics and Astronomy and Institute for Surface and Interface Science,
University of California, Irvine
Irvine, CA 92697, U.S.A.

In this work we study the coherent and incoherent scattering of s-polarized light from a dielectric film deposited on the planar surface of a semi-infinite perfect conductor. The vacuum-dielectric interface is a weakly rough one-dimensional random surface whose surface profile function $\zeta(x_1)$ is the sum of two components, $\zeta(x_1) = \zeta_1(x_1) + \zeta_2(x_1)$. Each of the two functions $\zeta_{1,2}(x_1)$ is a zero-mean, stationary, Gaussian random process defined by the two-point correlation function $\langle\zeta_j(x_1)\zeta_j(x_1')\rangle = \delta_j^2 W_j(|x_1 - x_1'|)(j = 1,2)$, where $\delta_j = \langle\zeta_j^2(x_1)\rangle^{\frac{1}{2}}$ is the rms height of the surface, and the angle brackets denote an average over the ensemble of realizations of the corresponding surface profile function. It is assumed that the surface height autocorrelation function $W_j(|x_1|)$ has the Gaussian form $W_j(|x_1|) = \exp(-x_1^2/a_j^2)(j = 1,2)$. The function $\zeta_1(x_1)$ defines a long-scale (smooth) component of the surface profile function, while the function $\zeta_2(x_1)$ defines a small-scale roughness component of the surface profile. Thus we assume that $\delta_1 < \delta_2$, while $a_1 \gg a_2$. We also assume that the functions $\zeta_1(x_1)$ and $\zeta_2(x_1)$ are completely uncorrelated. The contribution to the mean differential reflection coefficient from the coherent component of the scattered light is expressed in terms of the averaged single-particle Green's function for the guided waves in the system, and the contribution to the mean differential reflection coefficient from the incoherent component of the scattered light is expressed in terms of the averaged two-particle Green's function for these guided waves. To obtain the single-particle Green's function we use the two potential formalism, in which the equation for the Green's function is written in the form $G = G_0 + G_0(V_1 + V_2)G$, where G_0 is the Green's function in the absence of any roughness, the scattering potential V_1 is proportional to the Fourier transform of $\zeta_1(x_1)$, while the scattering potential V_2 is proportional to the Fourier transform of $\zeta_2(x_1)$ on the background of the long-scale component $\zeta_1(x_1)$. A Green's function G_1, associated with the long-scale roughness, is defined as the solution of $G_1 = G_0 + G_0V_1G_1$. The Green's function G is then the solution of the equation $G = G_1 + G_1V_2G$, which is solved in the approximation of small-amplitude perturbation theory in powers of V_2. The results are then used to obtain the contributions to the mean differential reflection coefficient from the coherent and incoherent components of the scattered light. The angular positions of the peaks in the latter function now depend on the angle of incidence. We show also that the straightforward application of small-amplitude perturbation theory can produce the analogous dependence even in the case of a single-scale surface roughness.

Scattering of a Plane Wave by Rough Surfaces: A New Curvilinear Coordinate System Based Approach

G. Granet and K. Edee
Université Blaise Pascal
Les Cézeaux Aubiére, France

Scattering of waves by rough surfaces has aroused the interest of physicists and engineers for many years because of its large domain of application in optics, radio wave propagation and radar techniques. When the geometrical parameters are close to the incident light wavelength, rigorous vectorial methods are to be used. For periodic surfaces, i.e. gratings, the curvilinear coordinate method (C.C.M) is now well established and is known to provide both simplicity and versatility. We believe that it should also be very powerful in the field of rough surfaces. Indeed it has already been extended to the case of non periodic surfaces that are invariant along one direction [1], [2]. In our opinion, from the numerical point of view; the two above approaches cannot be extended to the general case of 2D rough surfaces with geometrical parameters in the resonant domain because they would be too much time and memory consuming even for modern computers. In this communication, we investigate a new approach in order to reduce the size of the matrices involved in the computation: first we calculate the magnetic and electric currents on the profile by using the C.C.M. and then we make them radiate.

The essence of the C.C.M method is to choose a coordinate system in such a way that the boundaries of the physical problem coincide with coordinate surfaces. The simplest one is the so called translation coordinate system given by: $x = u$, $y = v + p(x) = v + p(u)$, $z = w$. Then, the surface $v = 0$ is the profile itself. The TE and TM fields are derived from the same scalar eigenequation in which the geometry appears in terms of the derivative of the profile function. This system is solved by using the method of moments in discrete Fourier space. The second and very new step consists in calculating the induced currents on the profile. It is then elementary to obtain the radiated field. This method keeps on all the advantages of the classical C.C.M; at the same time it proves to be numerically more efficient. At present it is implemented for one dimensional surfaces and conical incidence.

REFERENCES

1. A. Benali, J. Chandezon, and J. Fontaine, “A new theory for scattering of electromagnetic waves from conducting or dielectric rough surfaces,” *IEEE Trans. Antennas Propagat.*, vol. 40, no. 2, Feb. 1992.
2. R. Dusséaux and R. de Oliveira, “Scattering of a plane wave by a 1-dimensional rough surface - Study in a non orthogonal coordinate system,” *J. of Electromagnetic Waves and Appl.*, vol. 15, no. 10, pp. 1365–1366, 2001.

Emissivity of Structured Surfaces: from Homogeneization to Geometrical Optics

T. Ghabara and F. Ghmari
Université de Tunis II
Tunis, Tunisia

J.-J. Greffet
University of Rochester
Rochester, NY 14627, U.S.A.

It is known that the emissivity of a surface can be changed dramatically by modifying its surface profile. The purpose of this paper is to investigate the different mechanisms that enhance the absorption of an interface when ruling a grating. It will be seen that the mechanisms that are responsible for the enhancement of the absorption depend very much on the period of the grating. For gratings with a period much smaller than the wavelength, the roughness essentially behaves as a transition layer with a gradient of the optical index. Such a layer reduces the reflection thereby increasing the absorption. For periods much larger than the wavelength, the mechanism is analog to what happen in a cavity where a ray is trapped and undergoes a large number of reflections.

In order to explore very different period/wavelength ratios ranging from the homogeneization regime to the geometrical optics limit, we have used a differential method. The code has been implemented for both s and p-polarizations. We have explored the limits of the geometrical optics approximation systematically. New theoretical results [1] support the assumption that the phenomenological theory of emission should be accurate for subwavelength structures provided that no multiple scattering appears. A numerical evaluation of these predictions will be presented.

REFERENCES

1. Carminati R., Greffet J.J., Near-field effects in spatial coherence of thermal sources. *Phys. Rev. Lett.* 82, (1999) 1660-1663.

Polarised Reflectance from Composite Scattering Media

P. N. Raven, D. L. Jordan, and R. M. J. Watson
QinetiQ ltd
Worcestershire, United Kingdom

Bidirectional reflectance has become increasingly developed to characterise the properties of smooth surfaces based on small angle scatter, as in this regime the power spectral density of a rough surface can be linked to the bidirectional reflectance distribution function (BRDF). In the large angle scatter regime the measured BRDF cannot be unambiguously linked to a surface structure. However measurement of the polarised BRDF and polarised spectral directional hemispherical reflectance (DHR) can provide a characterisation of the composition and morphology of a coating.

Many materials do not comprise a single compound, but are a composition of multiple constituents, each with characteristic absorption spectra. Scattering, diffraction and interference can also take place creating characteristic spectral features. The reflectance spectrum of the whole material is a combination of the constituent spectra. However, the morphology of the material affects the impact of the optical properties of the individual constituents on the change of the polarised reflectance spectrum with incident and reflectance angle. Scattering by particular constituents and surface structure of the host matrix affect the degree of polarisation of the reflected radiation.

This paper discusses materials consisting of scattering pigment in a polymer binder. Such pigmented media are representative of paints and moulded plastics. The test samples include examples of scattering pigments and flake pigments, and different surface finishes. The results of DHR and BRDF measurements are reported. The spectral DHR measurements have been taken with incident radiation in parallel (P) and perpendicular (S) polarisation states at a range of incident angles across the visible and IR. The BRDF measurements have been taken in the polarisation states SS, PP, SP and PS, where the first letter retfers to the incident state and the second letter the reflected state.

The separation of the reflectance into different polarisation states can be used to partially separate the reflectance spectra arising from the pigment and the binder. A powder pigment tends to reflect radiation through volume scattering, with depolarisation of reflected radiation. The outer surface of the host binder reflects radiation through a single surface interaction, often with partial polarisation of the reflected radiation.

Although a modelling of the polarised reflectance is desirable, models of the unpolarised reflectance arising from differellt scattering sources can be helpful in data analysis. A calculation of the coating reflectance can be made from knowledge of the optical properties of the individual constituents, which can be done for the unpolarised reflectance from scattering pigments using the Mie theory based code SCATCAD. Alternatively the measured data can be approximated by standard simple lineshape models, and these can be used to suggest the degree of importance of different reflectance mechanisms.

The combination of the DHR and BRDF sources of data allows a characterisation to be made of the constituents and morphology of the material, and their impact on the observed directional reflectance spectrum.

Coupling between Surface and Volume Scattering by a Radiative Approach

S. Durant and J.-J. Greffet
Laboratoire EM2C, Ecole Centrale Paris
Chatenay-Malabry, France

O. Calvo-Perez and N. Vukadinovic
Dassault Aviation
St. Cloud, 92552, France

The purpose of our study is to compute the Bidirectional Reflection Distribution Function (BRDF) of a rough slab that contains dielectric scatterers with a fast approximate model. This study is motivated by the evaluation of the optical properties of rough paints with dielectric inclusions.

It has been shown [1] that for a large volume fraction of small particles, the coupling is mainly due to the modification of the effective index. By taking this into account, the scattering can be obtained by merely adding the contributions of the surface and the volume. In this work, the scattering medium is a collection of spherical particles with a size parameter near Mie resonances. The volume fraction is such that the correlation between particles can be neglected. In addition, we assume that there are no correlations between the roughness and the distribution of the particles. This is a reasonable approximation for low concentrations. The BRDF is calculated by solving the phenomenological scalar Radiative Transfer Equation (RTE) in the slab by means of the discrete ordinate method. The roughness effects are taken into account when writing the boundary conditions for the specific intensity at the rough interfaces [2]. We have used either the Kirchhoff approximation [3] or the Mean Field Theory [4] to describe the scattering by the rough surfaces.

Our goal is to study the effects of the coupling between volume and surface scattering for the regime of Mie particles. To investigate the different contributions, we first consider a slab with scattering particles and without roughness. A second computation case is based on a rough slab with a homogeneous volume. We find that the addition of both results is very close to the result obtained for the full system when the rms of surface height distribution is less than 0.4 wavelength. Results of different cases will be presented and we will discuss the origin of this behaviour.

REFERENCES

1. Sentenac A., Giovannini H. and Sailard M., “Scattering from rough inhomogeneous media- splitting of surface and volume scattering ” Accepted to be published in *J.O.S.A. A*, 2001.
2. Fung A. K. and Chen M. F., “Scattering from a Rayleigh Layer with an irregular interface,” *Radio Science*, Vol. 16, pp. 1337–1347, 1981.
3. Ulaby F. T., Moore R. K. and Fung A. K., “Microwave Remote Sensing Volume 2, Radar Remote sensing and Surface Scattering and Emission Theory,” Addison-Wesley Publishing Company, 1982.
4. Calvo-Perez O., Sentenac A. and Greffet J. J., “Light Scattering by a two-dimensional, rough penetrable medium: A mean-field theory,” *Radio Scientce*, Vol. 34, pp. 311–335, 1999.

Characterization of Thermo-Optical Properties of Infrared Structures

T. Lanternier and S. Mainguy
Commissariat à l'Énergie Atomique, Centre d'Études Scientifiques et Techniques d'Aquitaine
Le Barp, BP2 33114, France

Over the last ten years, a set of optical devices was developed at CEA/CESTA to characterize properties of infrared structures.

Such set-up allow us to measure surfacic and/or volumic optical scattering of various structures placed into controlled environmental conditions. Two types of experimental set-up were defined: one for directional emissivity measurement and one for Bidirectional Scatter Distribution Function (BSDF) measurement.

For directional emissivity measurement, we have acquired capabilities for measuring samples placed in atmospheric conditions or under vacuum and within temperature domains of respectively $80 \leftrightarrow 600$°C and $-20 \leftrightarrow 80$°C. Directional emissivity figures can be determined at any observation angle, over 3–12 μm wavelength range and with spectral resolution of 0.2 μm. Directional emissivity measurement of articles placed under vacuum and at low temperature was carried out using a liquid nitrogen cooled cryostat. Samples were measured over the same spectral range with identical spectral resolution. To get directional emissivity characteristics, we have also considered use of hemispherical directional reflectivity (HDR) technique, which is related to directional emissivity. In that case, the sample placed in atmospheric conditions and at room temperature and measurements are performed over 3–12 μm wavelength range with spectral resolution of 1 μm.

For BSDF measurements, samples are placed in atmospheric conditions and room temperature. Devices with heated ceramic rod or monochromatic laser sources (0.632, 5.4 and 10.6 μm) have been developed and qualified. BSDF figures can be determined within incidence plane, at wavelength values ranging 3–12 μm and with spectral resolution of 1μm. To improve spectral resolution up to 0.1 μm, a FTIR spectrometer was installed on a similar BSDF metrology system. BSDF benches calling for laser sources are more specifically utilized for low level BSDF or backscattering measurements. Moreover, a "special" device has been designed to measure BSDF figures outside the incidence plane and over a wide angular distribution [1].

All apparatus are calibrated and fully operated respecting standards or absolute calibration methods. Comparison of our metrology devices with similar systems used by other laboratories were conducted. This affords to assert validity of our measurement means and procedures. Results of BSDF and HDR measurement intercomparison campains [2] will be presented.

REFERENCES

1. Mainguy, S., M. Olivier, M. Josse, and M. Guidon, "Description and calibration of a fully automated infrared scatterometer," *SPIE Proceedings*, 1530, J. C. Stover (Ed.), 1991.
2. Boucher, Y., C. Deumié, C. Amra, L. Pinard, J.-M. Mackowski, S. Mainguy, L. Hespel, and J.-F. Perelgritz, "Round Robin of painted targets BRDF measurements," *SPIE Proceedings*, 4029, 2000.

Conception and Validation of Infrared Structures with Controlled Thermo-Optical Properties

S. Mainguy
Commissariat à l'Énergie Atomique
Centre d'Études Scientifiques et Techniques d' Aquitaine
Le Barp, France

Recent history has shown the relevance of infrared and laser techniques. In the study of articles with controlled thermo-optical behavior and monitored infrared signature, infrared properties of the object are mainly conditioned by the nature and the geometry of the materials that constitute its external envelope, their surface state and surface temperature. The main properties that describe the infrared behavior of this envelope are emissivity and reflectivity of the coating materials. The calculation of these properties is achieved in the framework of three different approaches: geometrical optics, electromagnetic optics and radiative transfer. Possibilities of coupling between approaches also exist.

The aim of this talk is to emphasize on infrared structures with controlled thermo-optical behavior currently studied in our laboratory. We will more particularly focus on radiative properties. Figures of interest were calculated using one of the previously described theoretical approaches. Experimental validations were achieved throughout emissivity or scattering measurements using a variety of optical devices developed in our laboratory. The spectral range of interest includes visible spectrum and near to medium infrared covering [2–12] μm wavelength. Structures such as "optical" gratings with wide period compared to wavelength and diffraction gratings (Fig. 1) with infrared resonant absorption will be examined. Then this work will deal with dielectric and metallic 1D and 2D random rough surfaces (Fig. 2). At last smooth or rough films filled with dielectric inclusions, corresponding to paint coatings or plasma-sprayed ceramics, will be exposed.

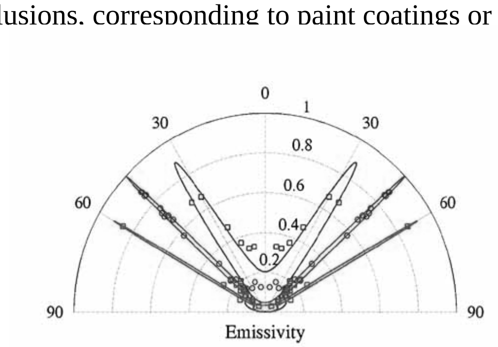

Fig.1 —Comparison between calculated and measured emissivity of a SiC grating at room temperature. The measured emissivity (markers) is deduced from specular reflectivity measurements from $\varepsilon_\lambda = 1 - R_\lambda$. The emission spectra are given for wavelengths 11.04 m, 11.36 m and 11.86 m with increasing emission angle from the normal, respectively.

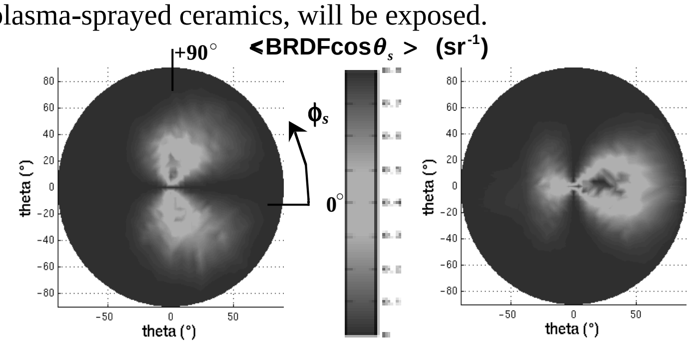

Fig.2 —Co-polarized and cross-polarized scattering by a 2D randomly rough Gaussian perfectly conducting surface with rms height $\sigma = 0.5\ \lambda$ and correlation length $T = 3\lambda$. The incident field is a s-polarized plane wave with incidence angle of 20° from the normal. The results are calculated for ss (left figure) and for sp (right figure) polarizations, using an electromagnetic method based on Rayleigh hypothesis and coupled to a Monte-Carlo technique.

Scattering of Electromagnetic Waves from Two Dimensional Rough Dielectric Surfaces: Theoretical and Experimental Comparison

J.-P. Segaud
Office National d'Etudes et de Recherches Aérospatiales
Toulouse, Cedex 4 31055, France

Scattering of electromagnetic waves from two-dimensional rough surfaces of **dielectric** materials has been theoretically studied. A sparse matrix flat surface iterative approach [1, 2] has been used to obtain the rigorous solution of the diffraction problem. Randomly rough surfaces with **gaussian** height distribution and autocorrelation function have been considered. A beam decomposition technique has been used to enlarge the surface dimensions under illumination [3]. Monte Carlo simulations has been performed to found an ensemble averaged scattering coefficient. Horizontal polarized incident waves (electric field perpendicular to the plane of incidence) have been considered. The convergence processes has been particularly investigated to know the number of iterations required for a given significant accuracy. The computation needs and the calculation times are specified for two different supercomputers used.

Numerical results are compared with experimental investigations of the angular distributions distribution of the light scattered from rough interface separating air from dielectric media [4]. Bi-directional reflectance distribution function are shown for a large angular domain. The polarimetric effects has been particularly investigated. Co-polarized and cross-polarized contribution to the mean differential reflection coefficient are shown.

Numerical simulations for the same surfaces in the case of perfectly conducting materials have also been performed. The material and geometrical effects are separated in that manner. It appears that the influence of the material nature can be taken into account in first approximation by the use of its Fresnel reflectivity coefficient for the co-polarized component.

REFERENCES

1. Pak, K., L. Tsang, and J. Johnson, *JOSA A*, Vol. 14, No. 7, 1515–1529, July 1995.
2. Soriano, G. and M. Saillard, *JOSA A*, Vol. 18, No. 1, 124–133, January 2001.
3. Saillard, M. and D. Maystre, *J. Opt*, Vol. 19, No. 4, 173–176, 1988.
4. Chaikina, E. I., R. Hernadez-Walls, and E. R. Mendez, *J. of Mod. Opt.*, Vol. 47, No. 6, 1013–1024, 2000.

Session 2Ac9

Poster Session - I

Fluctuations of Transient Reflections in Chaotic Medium with Strong Inhomogeneities

A. U. Bubnovsky, I. L. Kiriluk, and B. M. Shevtsov
Pacific Oceanological Institute
Vladivostok, Russia

With the help of an invariant imbedding method, the characteristics of a corn of back scattering operator are investigated numerically for the normal incidence of a plane wave on one-dimensional chaotic medium. The strong fluctuations of a local reflection coefficient of the medium are simulated by solution of Lorenz's equations at parameters according to a strange attractor. Instead this solution any other chaotic process may be took, but they are known not so good as Lorenz's process, which likes the random non-gauss process. Therefore the research approach advanced earlier for the investigation of the scattering in random media can be applied with completing by the special methods for the analysis of the chaotic processes. The numerical approach and algorithm for this problem were developed in (A. U. Bubnovsky, B. M. Shevtsov, Izv. Vuzov, Radiofizika, 2001, No. 11). The time dependence of the first eight single-point cumulants and correlation functions of delta-impulse reflections in the chaotic medium is considered here. The chaotic dynamics of non-stationary reflections at the multiple back scattering is investigated. The characteristics of reflections in the chaotic medium are compared with the results obtained earlier for a medium with a Gauss noise. In was shown, that the average intensity of reflections decreases in the time faster, and the fluctuations of reflections have more strong oscillations for a chaotic medium on the comparison with a random one. In the both cases, the correlation radius of the reflection decreases in the time when the multiple back scattering occurs, it means, that the chaos and randomness in the reflections grow in time. For chaos reflections, this conclusion is confirmed by the behaviour of reflected signals in reconstructed phase spaces and by the growth of the reflected signal fractional dimension. The temporary oscillations of reflection cumulants in the chaotic and random media are very different. It may be find the application in the remote sounding.

Open Loop Resonator Filter Using Aperture

S. Im, C. Seo, and J. Kim
School of Electronic Engineering, Soongsil Univ.
Dongjak-ku, Seoul, 156-743 , South Korea

Y. Kim, and N. Kim
Electronics and Telecommunications Research Institute.
Daejeon, 305-350, Korea

In modern satellite communication system, RF filter is required to be small, be easy to be fabricated, give flat group delay and especially, wider bandwidth for data increasing more and more. Although the saw filter has been widely used in mobile communication owing to high selectivity, it is not applicable to broadband system because of bad group delay ripple property and narrow bandwidth. Microstrip open loop resonator filter has advantage of the smaller size than other microstriop half wave length type filter. But they are mainly focused on the narrow band with high selectivity for mobile communication not on broadband application, for example IF filter for satellite communication.

The aperture can expand the bandwidth of microstrip open loop resonator filter with little degrading pass-band ripple. Conventionally, the bandwidth of microstrip filter can become wider with narrower strip line and slot width between loops. However, as the slot width has to be extremely narrow for wide bandwidth, circuit can be very sensitive with slot width and it will be a serious problem for fabrication. So employing aperture is alternative solution for wide bandwidth. Reduced coupling between loop and ground plane, and increased coupling between two loops can be achieved by aperture on the ground plane

We applied the aperture to six pole open loop resonator filter on the ground. Bandwidth is increased by 25%, from 148 MHz to 185 MHz at center frequency of 1.25 GHz. All geometric parameters of two filters are exactly same except whether aperture is used or not.

An Improved Model for Urban Non Line of Sight Propagation Using Penetrable Structures

G. A. Ellis
Department of Electrical and Computer Engineering
National University of Singapore
10 Kent Ridge Crescent,, 119260, Singapore

The interiors of buildings located in urban areas are usually composed mostly of air. Several studies have shown that radiowave propagation into buildings at 900 and 1800 MHz varies with between 5 - 12 dB of attenuation. Building penetration can become a major factor in modern cellular systems resulting in interference between adjacent cellular base station sites or cells. Cellular providers often plan base station location such that the presence of large buildings can be used for isolation. Frequency reuse is also used whereby the same frequencies are utilized in geographically distinct areas or cells such that signal path loss over distance can be exploited. One of the drawbacks with frequency reuse however, is the potential for interference due to multipath reflections between buildings in nearby cells.

In this paper, an improved three-dimensional electromagnetic propagation model for field strength prediction in non line of sight (NLOS) urban areas using penetrable building walls is described. The model, which is based on ray theory and uniform theory of diffraction (UTD) takes into account first-order effects such as singly reflected and diffracted rays, second order effects such as doubly reflected and diffracted rays, and third order effects such as triple reflections and diffractions. The simplified model of Raffles Place, the central business district of Singapore, was modeled using more than 360 plates and compared with data measured at 937.6 MHz along drive routes at the site.

It is found that inclusion of second or third order interactions alone may not result in accurate predictions for NLOS situations. Building structures that are modeled using penetrable walls having between 10-15 dB of thru attenuation results in less variation in the predicted fields, which is more consistent with the measured data than using walls that are non-penetrable. It is also found that in NLOS situations, radio wave propagation may be dominated by third order interactions. This may result in propagation paths, which may not be intuitively obvious.

Magnetic Levitation of Saturn's (Planetary) Rings

A. Yu. Pospelov and V. V. Tchernyi
General Physics Institute, Russian Academy of Sciences
Moscow, Russia

S. Girich
Volgograd State University
Volgograd, Russia

Many problems of Saturn's (planetary) rings, including data gathered by US Voyager missions, are resolved by the physical effects and phenomena characteristic of superconductors in a magnetic field. A superdiamagnetic liquid film demonstrates behavior comparable to planetary rings, supposing a huge number of superconducting particles in a planet's magnetic field.
Problem of Planetary Rings. Superconductive Effect (Distinctive Parameter):

1.The origin, dynamics and evolution of planetary rings. The Meissner-Ochsenfeld Effect: the display of perfect diamagnetism by superconducting particles.

2. The existence of a temperature border in the distribution of planetary systems with rings within the Solar system (the asteroid belt). The existence of the superconducting transition at certain temperature (Tc).

3. The extraordinary flatness of ring systems $(h/R = 10-6)$. Sharp edges of rings, incomplete rings and arcs. The phenomenon of the pushing out of diamagnetic matter out of areas with a greater density of magnetic flux.

4. The thin structure of Saturn's rings. The phenomenon of the formation of periodic structures in diamagnetic liquid film under the influence of a normal magnetic field.

5. The existence of planetcentrical dust flows of sub-micron particles in rings systems. The disappearance of diamagnetic properties by superconductive particles with dimensions similar to London's depth of magnetic field penetration $(\sim 10-510-6\,\text{cm})$.

6. The azimuthal brightness variations of Saturn's ring A. The orientation of elongated diamagnetic particles normally to the force lines of a magnetic field.

7. The formation and development of spokes in Saturn's B ring relative to special magnetic longitudes. The repulsion of superconductive particles out of the rings plane or their reorientation by magnetic anomaly.

8. The high reflection and low brightness of ring particles in the radio frequency range. The existence of a critical frequency $(\sim 1011\,\text{Hz})$ below which electromagnetic waves are fully reflected, and above which they are absorbed by the superconductor.

9. Saturn's rings own wide band pulse radiation in the frequency range $20\,$kHz–$40.2\,$MHz, correlated to particle collisions. The non-stationary Josephson Effect (the generation of electromagnetic radiation from points of contact between superconductors with frequency $4.83594 \times 1014\,$Hz/V).

10. Frequency anomalies in the thermal radiation of Saturn's rings in the spectrum range 100mm – 1cm. The existence of energetic slit $(\sim 3.5\,\text{kTc})$ in energetic spectrum of electrons in superconductors.

11. Color differentiation of Saturn's rings in a small scale. The greatness of pushing out forces acting upon an adulterated superconductor in magnetic field is dependent on the volume of superconducting phase.

12. The phenomenon of the anomalous inversion of the reflection of radio waves $(>\ 1\,\text{cm})$ with circular polarization from Saturn's rings. The Andreev's reflection mechanism at the normal-to superconducting interface, in which electron and hole quasiparticles are interconverted and the excitation trajectory undergoes retro-reflection.

Session 2Pc1

Remote Sensing of Earth, Ocean and Atmosphere

Ground Based Remote Sensing of Small Scale Phenomena in the Earth's Atmosphere

W. K. Hocking
Department of Physics & Astronomy, University of Western Ontario
London, Ontario, Canada

Radars have been used for many years to investigate dynamical motions in the atmosphere, both in regard to the neutral air and the ionized. Small refractive index perturbations due to turbulence and stratification effects, as well as wave phenomena, produce sufficient radar backscatter for successful signal detection and interrogation. Assuming that the perturbations drift with the wind, radars have utilized this backscatter to measure wind speeds. However, the details about the dynamical phenomena causing these refractive index perturbations are still not well understood. Certainly turbulence contributes to some of the inhomogeneity, but other phenomena such as viscosity waves and other small scale organized motions seem to also play a role. Similar processes seem to be active in height regions ranging from the ground up to 100 km in altitude, but the relative importance of these different phenomena seems to change with height. In this talk, we will consider the mechanisms responsible for these inhomogeneities, and review our current understanding about them. We will also demonstrate that by better comprehending their generation, we will also be able to make better use of them in interpreting the physics of the atmosphere in their immediate vicinity.

Microwave Rain Attenuation over Global Oceans from TOPEX-Poseidon

A. K. Varma and S. M. Bhandari
Ocean Science Division, Space Applications Centre
Ahmedabad, 380015, India

The knowledge of space-time variability of attenuation in the earth-space path is essential for all space-based microwave remote sensing and microwave communications experiments. For reliable uninterrupted earth-space-earth communications, information about cumulative probabilities of attenuation due to rain at different time scales ranging from a minute to hours and days provides an essential input in deciding the link margins and in exploitation of space diversity. The rain attenuation increases with signal frequency and is of great consequence as satellite communications move to Ku band and above. A number of satellite-based sensors (radar altimeters, scatterometers and SARs) for monitoring the ocean surface roughness leading to information about ocean surface winds, waves and images of manifestations of a variety of ocean surface and subsurface processes, operate in the Ku-band. These measurements get adversely affected due to presence of rain in the intervening atmosphere. Precise values of path attenuation allow a correction of the rain-affected measurements towards a valid retrieval of the surface parameters.

In this paper, we use the ocean surface backscatter information collected by simultaneous dual frequency radar pulse transmission and reception by the TOPEX-Poseidon satellite in orbit around the earth since 1992. Rain events are identified using both the TOPEX passive microwave radiometer (operating at 18, 21 and 37 GHz) as well as the TOPEX-Poseidon dual frequency [C (5.3 GHz) and Ku (13.6 GHz) band] radar altimeter observations using the method developed earlier by the authors [1]. This study was restricted for the SW monsoon season for a particular year over the Indian region. Presently, we extend the analysis of improved TOPEX-Poseidon data sets extending over several years and covering the global oceans within the TOPEX coverage zone (± 66 deg. Lat.). Results are presented in the form of maps of monthly average rain attenuation over global oceanic areas. Rain attenuation exceedence probabilities are calculated for various CCIR climatological regions and compared with different models available in the literature.

Continued availability of dual frequency radar altimetric measurements from space from TOPEX-Poisedon since 1992 and the recent launch of TFO and Jason-1 satellites provide an excellent opportunity for operational realization of highly reliable database of rain attenuation statistics over the global oceans.

REFERENCES

1. Bhandari S.M. et al., URSI Commission F Symp. on "Wave propagation and Remote Sensing", Ahmedabad, India, 1995 (Derivation of Rain-rate Statistics over Indian Tropical Oceanic Regions from Dual-Frequency TOPEX Radar Altimetric Measurements).

Ocean Parameter Retrieval Algorithms from Polarized Microwave Simulations and TRMM Data Using Neural Network Approach

R. M. Gairola, A. K. Varma, and V. K. Agarwal
CETP/CNRS
Velizy, France

The variations in global distribution of rain amounts, total water columns, wind speed and sea surface temperature are key parameters in climate dynamics. The latent heat release during condensation in tropical cloud clusters contribute significantly to the atmospheric energy balance. Water vapor determines the development of clouds and rain. The temporal variation of water vapor amounts might indicate global climate changes caused by rising surface temperatures. Thus the retrieval techniques using measurements from passive microwave sensing as derived from space borne microwave radiometers are highly useful for determination of these geophysical fields.

Recently, artificial neural networks have been recognized as being useful for retrieval operations in remote sensing of the atmosphere and oceans. The use of neural network in statistical estimation is often effective because they can simultaneously address nonlinear dependencies and complex statistical behavior. We have used neural network approach for the retrieval of geophysical parameters like wind speed, sea surface temperature, columnar water vapor and liquid water simultaneously from TRMM Microwave Imager (TMI). Using advanced radiative transfer model and ECMWF analyzed fields of geophysical input parameters, a large database of simulated of brightness temperatures at TMI frequencies has been created. The different neural network architectures for all the parameters have been optimized to ascertain best achievable accuracies. The interest of present approach is that the future retrieval and applications of the geophysical parameters to be obtained from various microwave radiometric observations from different satellites planned in future, like MADRAS (Measurement and Detection of Rain and Atmospheric Systems) sensor of MEGHA-TROPIQUES and AMSR of the ADEOS-II and TMI like radiometers in Global Precipitation Mission (GPM).

In Evaluation of Soil Resources by Remote Sensing Techniques: A Case Study Ranga Raddy District of Andhra Pradesh, India

V. Sudarshan, P. R. Saxena
Department of Applied Geochemistry, Osmania University
Hyderabad, 500 007, India

M. R. Saxena
National Remote Sensing Agency, Balanagar
Hyderabad, 500 037, India

Systematic evaluation of soils is very important for the efficient utilization of land resources which lead to the economic and agricultural development of the region. Mapping of soils by Remote Sensing techniques is well established by virtue of its accuracy in boundary delineation, cost effectiveness besides time factor.

The soil and land capability map of the Kandukur area (Lat. 16° 57’ 54” N to 17° 07’ 16” N and Long. 78° 27’ 16” E to 78° 37’ 24” E) has been prepared on 1:20,000 scale using IRS - IB LISS II A2 (Path 25, Row 56) satellite images and other collateral data with limited field surveys. Land resources were evaluated for agricultural and non-agricultural purposes.

The study area consists of Archaean granites / gneisses traversed by dolerites. The valley fills and flood plains of the streams comprise alluvium of recent origin.

Preliminary visual interpretation of satellite data has been carried out initially and representative sample strips covering various physiographic and image element variations were selected for intensive examination of soil profiles and for establishing relationship between physiography and soils.

After preliminary visual interpretation, a general field traverse was conducted to obtain the overall idea about the relationship between geology, physiography and soils. Based on this concept, final sample strips were selected. Intensive profile examination and auger bore studies were carried out in the sample strips and random observations were made in other areas, wherever necessary.

The soil profiles were studied for the morphological characteristics and representative soil samples were analyzed for chemical characters.

The soils in the study area have been finally classified as per Soil Taxonomy up to family level and soil map on 1:50,000 scale has been prepared based on morphological, physical and chemical characteristics, soil moisture and temperature regimes. Subsequently this map has been suitably enlarged to 1:20,000 scale.

Land capability classification is the key factor for land evaluation and useful in understanding the potential and limitations of individual land class. The study area has been evaluated into several land capability classes based on soils, slope, erosion, salinity/alkalinity hazard, water logging and other characters and six land capability classes have been identified.

Remote Sensing Techniques for Environmental Impact Assessment (EIA) Analysis of 'Bhavaninagar Site and Environs, U.P. India

P. R. Saxena and V. Sudarshan
Department of Applied Geochemistry, Osmania University
Hyderabad, 500 007, India

M. R. Saxena
National Remote Sensing Agency, Balanagar
Hyderabad, 500 037, India

The relation of man with environment can be considered both in terms of unity and conflict in the sense that survival depends on exploiting natural wealth and changing the environment in many unavoidable ways. In order to maintain some kind of balance between the natural environment and human activities, it is necessary pre-requisite for carrying out an environmental impact assessment (EIA) before executing any project.

Remote sensing techniques have added a new dimension in carrying resources evaluation and environmental management plan, with their ability to generate a wealth of information continuously and objectively. Earth observation satellites help in mapping and monitoring changes resulting due to urbanization/industrialization, mining, and deforestation and to assess and prepare a comprehensive plan for management and sustainable development of resources.

The present work highlights the use of satellite imagery of IRS LISS-II (B2) for generating the land-use/land-cover information and area information for Bhavaninagar site and 5 kms radius around the site. The study area falls in the district of Rae Bareli in Uttar Pradesh State, India. The area is well bounded within latitude 26° 21'16" N to 26° 27' 39" N and longitude 81° 23' 09" E to 81° 29' 12" E covering an area of 7857.00 ha. The area has semi-arid climate. The maximum rainfall occurs in the month of June to September. The maximum temperature is about 39°C while the minimum temperature reaches up-to 8.5°C.

Based on the study the area is confined to alluvial plain and the area has predominantly levelled landscape. The existing land-use/land-cover comprising built-up land (3.58%) in specified site and 4.64% of impact zone (0-5 Kms radius excluding Agricultural land accounting to 38.44% of specified site and 72.49% of total study area. Salt affected land accounting for 30.05% of specified site and 9.90% of total study area, water logged (27.65% of specified site and 11.99% of total study area), water bodies 0.2 8% of specified site area 0.82% of total study area. Further based on satellite data of different seasons, it is observed that the area is inundated due to water logging and affected by salinity.

Application of Remote Sensing Techniques for Integrated Planning for Micro Watershed Development – a Case Study in Andhra Pradesh, India

V. Sudarshan, P. R. Saxena
Department of Applied Geochemistry, Osmania University
Hyderabad, 500 007, India

M. R. Saxena
National Remote Sensing Agency, Balanagar
Hyderabad, 500 037, India

The socio-economic development of our country is interlaced with our natural resources and the manner in which they are managed and exploited. Reliable and timely information on the available natural resources is very much essential o formulate a comprehensive landuse plan for sustainable development. The land, water, minerals and biomass resources are currently under tremendous pressure. Consequently over exploitation and mismanagement of resources are exerting detrimental impact on the natural Eco-system. The striking manifestations of this phenomenon are various kinds of land degradation, water and air pollution and biomass deterioration. To reverse the process of degradation, the need of the hour demands to conserve and enhance the resource base of our country keeping pace with the accelerating technology.

Watershed management has been accepted as an approach to the integrated area development program, which signifies development of all sorts of resources for planning and implementation in a unit area. Conservation/harvesting of water resources on watershed basis should receive top priority in the strategy for development of dry lands.

The present work envisages to assess natural resources of the Kandukur area of Ranga Reddy district, Andhra Pradesh and to identify the problems and potential of the area and to generate a resource based landuse plan for the overall development on a sustainable basis.

Different thematic maps viz. Landuse/landcover map, hydrogeomorphological map, soil map, slope map, drainage and surface water body map and integrated action plan map of the study area has been prepared on 1:20,000 scale using IRS 1B LISS II A2 satellite imagery with necessary field checks.

The study has helped in identifying the degraded areas, assessing the problems and potentiality of the area, availability of water resources for agriculture and other sectors and this helped in generating a resource based action plan for sustainable development.

Evaluation of Forest Cover (under Bench Mark Study) and Preparation of Forest Cover Maps using IRS-1B LISS II Data in Andhra Pradesh State, India

P. R. Saxena
Department of Applied Geochemistry, Osmania University
Hyderabad, 500 007, India

M. R. Saxena
National Remote Sensing Agency, Balanagar
Hyderabad, 500 037, India

V. Sudarshan
Department of Applied Geochemistry, Osmania University
Hyderabad, India

Forest as a major biological investment of earth system and its contribution exerts an influence on other subsystems; the demand for preservation of former cannot be simply overlooked. Forest plays a significant role in economic development of any country. They protect watersheds and natural environment. Forest provides a large variety of products vital to human being, which range from cosmetic to medicine. They have an immensely positive role in food production that goes all but unnoticed except to the discerning eye.

A comprehensive information on forest cover (land-use/land-cover) is a basic pre-requisite for land resource evaluation, environmental assessment, utilization and management. Today, with increasing population pressure on land and the resulting change in the land use pattern and processes, a considerable degree of land transformation and environmental deterioration is being witnessed. Therefore, it is important to understand the 'cause and effect' of the change through scientific studies.

The synoptic coverage of satellite based remote sensing provide capabilities for integration of real time information on regional and global scales for forest management. Realizing the potential of satellite remote sensing techniques, forest cover assessment study is being taken up in parts of nine districts of Andhra Pradesh, India. The interpretation essentially consists of a set of image elements or characteristics like tone/color, texture, pattern, size, shape and so on which help in the recognition or identification of various forest cover classes systematically on the satellite imagery during visual interpretation. A preliminary interpretation key was prepared for IRS data, which was used for visual interpretation. Here, the reference details including the reserved forest boundaries are transferred from SOI topographical maps in scale of 1:50,000 and enlarged to 1:25,000 scale. Micro-watershed boundaries have also been delineated on the basis of slope and stream flow direction, which was incorporated in the final maps for better planning. This was then finalized after the ground truth, wherever it was found necessary.

A Study of Infrasonic Waves in the Atmosphere

M. Lal
Indian Institute of Geomagnetism
Tirunelveli, 627011, India

Continuous observation of the infrasonic wave has been recently studied at low latitude northern hemisphere, Tirunelveli (8.70N, 77.80E), India. Major interest is in the infrasounds frequently radiated into the atmosphere by the geomagnetic storm and substorms. In detection of the infrasonic signal in the turbulent boundary layer, it is often indispensable to reduce the irregular noise caused by the turbulent fluctuation of the wind. In the present study, a new type of circular noise reducer has been designed. The circular noise reducer is noise-reducing lines of pipe typically consisting of about 300 meter of pipe of various diameters, tapering from 3 inch (inside diameter) pipe at the center in steps to 0.5 inch (inside diameter) pipe at the ends. The pipe line is equipped with capillary ports to the atmosphere usually set at 10 ft intervals, and the input to the microphone is connected to the venter of this spatial filter. From several field tests, it has been shown that the wind noise is remarkably attenuated by the use of multi-pipe line microphone. The infrasonic waves observed due to microbaroms, earthquake and magnetic storm will be presented in details.

Application of Model-Based Spectral Analysis to Wind-Profiler Radar Observations

E. Boyer
LESiR/ENS Cachan, UPRESA 8029
Cachan, 94235, France

M. Petitdidier and W. Corneil
CETP
Velizy, 78140, France

C. Adnet
THALES Air Defense
Bagneux, France

P. Larzabal
IUT de Cachan, CRIIP, Universite Paris Sud, also LESiR/ENS Cachan
Cachan, 94234, France

A classical way to reduce a radar's data is to compute the spectrum using FFT and then to identify the different peak contributions. But in case of overlapping between the different echoes (atmospheric echo, clutter, hydrometeor echo...) exists, Fourier-like techniques provide poor frequency resolution, and sophisticated peak-identification may not be able to detect the different echoes. In order to improve the number of reduced data and their quality relative to Fourier spectrum analysis, three different methods are presented in this paper and applied to actual data. Their approach consists of predicting the main frequency-components, which avoid the development of very sophisticated peak-identification algorithms. The first method is based on spectrum properties generally used to determine the shift between two close identical echoes. We will see in this paper that this method cannot provide a better estimate than Fourier-like techniques in an operational use. The second method consists of an autoregressive estimation of the spectrum. Since the tests were promising, this method was applied to reduce the radar data obtained during two thunderstorms. The autoregressive method, which is very simple to implement, improved the Doppler-frequency data reduction relative to the FFT spectrum analysis. The third method exploits a MUSIC algorithm, one of the numerous subspace-based methods, which is well adapted to estimate spectra composed of pure lines. A statistical study of performance of this method is presented, and points out the very good resolution of this estimator in comparison with Fourier-like techniques. Application to actual data confirms the good qualities of this estimator for reducing radar's data.

Seasonal Variation of Solar Tides in the Troposphere and Lower Stratosphere over Gadanki: Comparisons with the GSWM

H. A. Basha, B. Bapiraju, P. Balasubrahmanyam, M. A. A. Siddiqui, and G. Dutta
Anwarul-Uloom College, Osmania University
Hyderabad, India

Atmospheric tides are one of the important means of transferring energy and momentum between different regions of the atmosphere. Tidal perturbations, generated in the lower and middle atmosphere, grow in amplitude as they propagate upwards, and help in determining the heat and momentum budgets of the upper atmosphere. Diurnal cycle hourly wind measurements by VHF radar have been used to investigate the characteristics of diurnal, semidiurnal and terdiurnal tides as functions of height and their seasonal variations in the troposphere and lower stratosphere over a tropical Indian station, Gadanki (13.5° N, 79.2° E). The observations have been compared with the recent updated Global Scale Wave Model (GSWM-00).

Observed diurnal (24h) amplitudes are found to be much higher (0.5 - 3 m/s) for zonal wind and (0.3 - 2 m/s) for meridional wind compared to the model values. Departures of the observed values from the model ones are more prominent in zonal wind case, especially for summer and equinox with strong maxima between 10 and 16 km. Observed amplitudes are found to be larger than GSWM by factors of 6.5 and 3 in summer, equinox and winter respectively. Meridional amplitudes show closer agreement with model values. The phase structures indicate interfering modes with short vertical wavelengths.

Maximum amplitudes of the 12h semi-diurnal oscillation are found to be $\sim$2 m/s for both zonal and meridional winds during summer which are an order larger than the theoretical values of GSWM. Observed phases lag behind the model values by 3-4 h for EW component whereas NS phases show excellent agreement with calculated ones. Both model and observed phases are found to be almost constant with height suggesting evanescent structure of tidal modes.

Amplitudes of the components of terdiurnal (8 h) are found to be quite significant with maximum values $\sim$1.5 m/s in summer for zonal wind and 1 m/s for meridional wind. Phase structures show short vertical wavelength and remain almost constant with height. Energy densities of tidal components become maximum in the upper troposphere and get reduced in the lower stratosphere.

VHF Doppler Radar Measurements during Thunderstorms

P. Balasubrahmanyam, H. Aleem Basha, B. Bapiraju, T. S. P. L. N. Prasad, and G. Dutta
Anwarul-Uloom College, Osmania University
Hyderabad, 500 001, India

Convection occurs when a fluid in the presence of gravity is heated from below or cooled from the top at such a rate that molecular diffusion can not redistribute the modified density field fast enough to maintain equilibrium. The fluid layer then becomes buoyantly unstable and overturns macroscopically to stabilize the stratification of density. The buoyant parcel of air pushes ambient air out of its path and the surrounding atmosphere adjusts by sending out a spectrum of gravity waves. The forcing mechanisms responsible for generating convection waves are not yet well understood. Different mechanisms like mechanical oscillator effect (Fovell et al., 1992), obstacle effect (Pfister et al., 1993) and forcing by transient or steady heat source (Pandya et al., 1993) have been suggested.

Various workers have observed gravity waves generated by convective storms using different techniques like VHF doppler radar (VanZandt et al., 1979; Röttger, 1980; Lu et al., 1984; Gage et al., 1989), aircraft observations (Kuettner et al., 1987; Frittz & Nastrom, 1992; Pfister et al., 1986, 1993), satellite cloud images (Bergman and Salby, 1994) and so on. But our knowledge of convection waves is still inadequate due to the sporadic nature of convective events both in space and time.

The MST radar at Gadanki (13.5° N, 79.2° E) was operated during thunderstorm activity in June, 2000. Two convective events of 355 minutes and 265 minutes could be captured on 21 and 22 June, 2000 respectively. Control observations were taken on a regular basis for 9 days (between 19 June and 29 June, 2000). Vertical velocities are found to be 2-9 m/s during convective events which are 5-10 times larger compared to a normal day. The events are found to be associated with strong wind shear and higher radar reflectivity. SNR profiles during convection show erosion of sharp tropopause structure indicating troposphere - stratospher exchange during convection. Waves of vertical wavelength between 4 - 10 km and periods between 10-60 minutes could be identified. The amplitudes of the waves in all the period bands were found to be enhanced by almost an order of magnitude compared to control day values. Maximum amplitudes $\sim$ 1.0 - 1.3 m/s were observed in mid-troposphere between 8 and 14 km whereas the control day values range between 0.01 - 0.08 m/s. The data sets have been further analyzed by PSD method and the PSD components have been integrated to obtain variance values during convective events and on control days. The ratio of active variance to quiet variance is found to increase by $\sim$ 20 times in mid-troposphere around 8 km. A quantitative assessment of the vertical wind spectra shows an enhancement of the slope of frequency spectra from 1.0 - 1.5 in the troposphere.

Evidence of Kilometer-Scale Waves in the Lower E Region from High Resolution VHF Radar Observations over Gadanki

A. K. Patra
Space Physics Laboratory, Vikram Sarabhai Space Centre
Thiruvananthapuram, 695022, India

S. Sripathi, V. Siva Kumar, and P. B. Rao
National MST Radar Facility
Tirupati, India

High resolution VHF radar observations made at Gadanki revealed the kilometer-scale waves in the low altitude lower E region. These waves are found to occur in a narrow altitude range of 92 - 97 km and have vertical wavelengths of $\sim$ 0.5 km and wave periods of $\sim$ 40 seconds. They resemble quite closely to that reported recently for midlatitude using the MU radar. The signal intensities associated with these waves, shown in SNR, are found to be as high as 25 dB, quite comparable to that observed at higher altitudes. It is in contrast to the much weaker mid-latitude lower E region echoes reported by the MU radar. The wave structures show both positive and negative altitude rates with values in the range of 15 - 20 ms-1, which are in good agreement with the observed Doppler velocities. The spectral widths are found to be relatively lower, implying the lower E region wave structures to be less turbulent compared to their counterpart at higher altitudes. The observed wave structures bear remarkable resemblance to that simulated for the equatorial E region through nonlocal nonlinear gradient drift instability. In this paper we present these new structures and discuss the results in the light of current understanding of the kilometer scale wave structures.

Rayleigh LIDAR Observations in Troposphere, Stratosphere and Mesosphere: A New Interpretation

M. V. Ratnam, W.-N. Chen, and J.-B. Nee
Department of Physics, National Central University Chung-Li
Tirupati, 32054, Taiwan

S. V. B. Rao and D. N. Rao
Department of Physics, Sri Venkateswara University
Tirupati , 517 502, India

In general, temperature of the atmosphere is sensed (remote or in situ) by satellite, rocket, balloon, or lidar. The ability of high spatial and temporal resolution measurements makes lidar to be extensively applied to study high altitude (above stratosphere) atmospheric dynamics such as gravity wave, planetary waves and mesospheric temperature inversions. The upper tropospheric and low stratospheric temperature plays an important parameter on the research of the stratosphere-troposphere exchange of mass and global change. The routinely monitored radiosonde flights could not provide the better understanding of these processes due to poor spatial and temporal resolutions. Moreover Raleigh Lidar couldn't provide high-resolution measurements at these lower heights. Hence, how to make lidar temperature measurement at these lower altitudes with more accuracy is of present interest.

Rayleigh lidar system installed at Gadanki ($13.50°$N, $79.20°$E) has been used to obtain nighttime high-resolution temperature profiles in the altitude range 5–85 km since March 1998. In this present study, the lidar temperature algorithm and a new atmospheric transmission correction method are introduced. The uncertainties in estimating the temperature using this new method are discussed in detail. The temperature profiles obtained using this new method by lidar are compared with routinely monitored radiosonde data, CIRA-86 model and also with HALOE data. The results show excellent agreement between these instruments showing the accuracy of this new method. This new technique will lead to understand middle atmosphere dynamics fluently especially stratospheric-tropospheric mass exchange and interaction between various atmospherics layers.

Characteristics of MF Radar Echoes from the Mesosphere and Lower Thermosphere Region over the Magnetic Equator

T. K. Ramkumar and S. Gurubaran
Equatorial Geophysical Research Laboratory, Indian Institute of Geomagnetism, Krishnapuram
Tirunelveli, 627 011, India

The medium frequency (MF) radar at Tirunelveli (8.7°N, 77.8°E, geographic; 0.2°N, dip latitude), India, operated in a spaced antenna mode, has proved to be a potential tool for the dynamics studies of the middle atmosphere, in particular, the altitude region of 80-98 km. The focus in recent times has been on understanding the nature of the echoes received by the radar located close to the magnetic equator. With a wide transmitting beam, the radar probes sheets of electron density irregularities whose horizontal scale size covers one Fresnel zone. The echoes from higher altitudes (above 90 km) have the signatures of equatorial electrojet, an enhanced east-west current system flowing at $\sim$105 km in a narrow latitudinal belt centered about the magnetic equator. These echoes have a characteristic distinct from those received from the lower altitudes (70-90 km).

Two potential problems have received our attention: (1) the possibility of total reflection of the 1.98 MHz signal at heights above 90 km that causes a saturation of the receivers and (2) the electrojet influence of the measured drifts. Both these factors contribute to the uncertainties in the estimates of neutral winds. The full correlation analysis of *Briggs* [1984] is adopted in the present work in an attempt to understand these influences and the processes that contribute to the differing characteristics of the echoes at various heights. Some of the results from this study will be presented.

Session 2Pc2

Advances in Computational Electromagnetics

A Fast High-Order Algorithm for Predictions of the Electromagnetic Scatter Produced by Thin Penetrable Bodies

O. P. Bruno
Applied Mathematics, Caltech
Pasadena, CA, U.S.A.

F. Reitich
School of Mathematics, University of Minnesota
Minneapolis, MN, U.S.A.

We present a new approach to the numerical simulation of electromagnetic scattering processes that is ideally suited for the treatment of "thin" penetrable bodies, that is, of bodies that present a characteristic length of no more than a few wavelengths in a particular direction. As we explain, the interest of such a specialized algorithm is twofold: on the one hand it allows for an efficient and high-order treatment of specific geometries that arise naturally in applications (e.g. coatings): and, on the other hand, it also provides the appropriate means for the treatment of thin regions near material discontinuities when integrated with a (fast) solver for general penetrable scatterers, which typically can only attain high-order convergence away from jumps in the optical properties of a given configuration. Our new algorithm is based on the (iterative) solution of Lippman-Schwinger type equations. It is based on the introduction of a partition of unity—to localize the integration, parametric volume representations—to distinguish the "thin" direction—, changes of independent variables in the "tangential" (i.e. not thin) directions—first to mollify the singularity of the Green's function and then to effect a systematic refinement near singular points—and, finally, on a suitable splitting of the integral in the "transverse" (thin) direction—to avoid integration through a singular point—. As we shall show this framework then allows for the use of quadratures with superalgebraic convergence properties. Finally, we show that an acceleration algorithm based on planar arrays of equivalent sources can be incorporated to yield a high-order method with a significantly reduced operation count.

On Fast, High-Order Solution of Surface Scattering Problems

O. P. Bruno
Department of Applied and Computational Mathematics
California Institute of Technology
Pasadena, CA 91125, U.S.A.

L. Kunyansky
Department of Mathematics, University of Arizona
Tucson, AZ 85721, U.S.A.

The calculation of electromagnetic and acoustic scattering by large objects remains one of the most important and challenging problems in computational science. Roughly, these problems present difficulties as they require accurate descriptions and manipulation of highly oscillatory functions; we approach these problems through consideration of the associated systems of integral equations. Scattering problems involving one dimensional integrals have been efficiently treated by means of high order integrators (including the exponentially accurate trapezoidal rule and other high-order schemes), which reduce dramatically the complexity necessary to meet a given accuracy requirement. Problems of scattering by surfaces in three dimensional space require much more delicate treatments, however.

In this context, use of high-order integrators is necessary to guarantee accurate results but generally not sufficient: in large scattering problems direct evaluation of a simple-minded discretization scheme would usually lead to inordinately long computing times. We thus present a fast, high-order algorithm for the solution of problems of scattering from smooth and non-smooth surfaces in three dimensions. Based on analytic resolution of singularities and FFT acceleration, the present algorithm computes scattered fields in $\mathcal{O}(N^{6/5}\log N)$ to $\mathcal{O}(N^{4/3}\log N)$ operations (depending on the geometric complexity of the scatterer), where N is the number of variables in the discretized problem.

Our basic high-order integrator involves use of partitions of unity — to deal with topological characteristics of closed surfaces — and analytical resolution of singularities — to avoid costly refinement strategies. Use of this algorithm without acceleration would lead to the customary $O(N^2)$ operation count. The constant of proportionality in this complexity estimate is rather small, however, so that, even without acceleration, our high-order integrator is an efficient solver for small to medium-sized problems. For large problems, however, use of acceleration is imperative.

The use of (three-dimensional) FFT acceleration, in turn, is made possible through introduction of certain "equivalent sources" which, lying on a three-dimensional cartesian grid, reduce the integration problem to a discrete three-dimensional convolution. Our acceleration scheme differs significantly from the one used in other Adaptive Integral Methods, by the number of sources used, their location and the technique exploited to calculate intensities of the sources. These differences lead to a considerably faster, higher-order acceleration scheme with reduced memory requirements.

The combination of the above-mentioned high-order local integrator and acceleration scheme gives rise to an efficient algorithm, which outperforms some of the most competitive methods available. In fact, the present approach allows one to calculate accurately on PC type computers scattering from the bodies of electrical sizes of several hundreds — a goal, otherwise achievable only by supercomputing.

A Finite-Difference Frequency Domain Method with a Localised Integral Equation Regularisation for Scattering in Cavities

C. Fiachetti
IRCOM (seconded to ONERA)
Toulouse, 31055, France

B. Michielsen
Electromagnetics and Radar Department, ONERA
Toulouse, 31055, France

We are working on the numerical modelling of a so-called Mode-Stirred Chamber (MSC), which consists of a large reverberating chamber with a so-called mode-stirrer, a highly asymmetric metallic object, which scatters the cavity field in order to create different field configurations for every mode-stirrer orientation. The heart of this modelisation problem then is to compute the scattering of an electromagnetic wave by the mode stirrer paddles in the presence of the quite large reverberation room.

In order to account for the presence of the reflecting walls of the reverberation chamber, we might think of using implicit methods such as integral equations with periodical Green's functions or of the Ewald transform. However, this would lead to long computation times and full systems, which are difficult to handle at the frequencies of interest in MSC work.

In this contribution, we investigate another possibility. Starting from the efficiency of Finite Difference discretisations in parallellepiped cavities, we would like to be able to account for the oblique surfaces of the mode stirrer paddles without the usual staircase approximations. The basic idea then is to introduce a local regularisation, accounting for the presence of magnetic field discontinuities. If we subtract a field, $\{E^d, H^d\}$ (called the regularising field), which shows the correct discontinuities, from the exact field, $\{E, H\}$, then the remainder field, $\{E^s, H^s\}$, should be smooth and convenient for conventional finite difference discretisations. Such a regularising field can be obtained locally by truncated integral representations parameterised by a boundary element discretised surface current distribution J:

$$E^d(x) = [-j\omega\mu_0 - \frac{1}{j\omega\epsilon_0}\nabla\nabla\cdot]\int_S G_x J \quad H^d(x) = \nabla \times \int_S G_x J$$

where $G_x(y) = \chi(\|x-y\|)e^{-jk_0\|x-y\|}/4\pi\|x-y\|$ is the truncated Green's function for the Helmholtz equation with some smooth truncation function $\chi : \mathbb{R}_+ \to [0,1]$, which vanishes identically outside a sphere with a radius of the order of, for example, $2h$ where h is the cell size of the surface triangulation. The J in this integral representation represents the discontinuity in the tangential magnetic field. The discretisation of this surface current introduces a supplementary set of unknowns in addition to the unknowns of the finite difference discretised field $\{E^s, H^s\}$

The method can also be considered from the point of view of integral equations. Thinking in this way, we have decomposed the Green's function into a truncated free-space Green's function and a residual which is a finite difference solution of a Helmholtz problem with a source term derived from the parameterised truncated field representation.

As a result, we get a system matrix with a large but very sparse FDFD block, another near diagonal block representing the surface integral equation, based on the truncated Green function, plus two relatively small interaction blocks coupling the FDFD field to the surface currents on the paddles. This kind of linear systems is very suitable for iterative solution methods. We shall present the results of numerical experiments on the convergence and efficiency of this method.

Dispersion in Non-Orthogonal FDTD Meshes

I. J. Craddock and R. Nilavalan
Department of Electrical and Electronic Engineering, University of Bristol
Bristol, BS8 1UB, UK

The standard FDTD model is well-known and widely-used for full-wave electromagnetic analysis. Numerical dispersion is one of the main sources of error that degrade the accuracy of the analysis - for each structure of interest, the users of the model must attempt to generate a mesh that will avoid introducing high levels of dispersion.

One of the main limitations of the traditional FDTD method is that it is restricted to structures described in orthogonal (usually Cartesian) co-ordinates. In order to model curved and angled structures, the Non-Orthogonal FDTD method may be used, however the Non-Orthogonal mesh cells introduce further dispersion into the analysis. Little information is however available on how the dispersion properties of the Non-Orthogonal FDTD algorithm vary with mesh size, mesh angle and direction of propagation - and hence it is difficult for users to make appropriate choices in their mesh generation.

The aim of this contribution is to quantify the dispersion in realistic Non-Orthogonal FDTD models of microstrip structures directly through numerical simulations. A test structure is considered, discretised using a number of Non-Orthogonal mesh configurations, including single and multiple skew angles. Based on these results, recommendations are made concerning the range of cell angles for which dispersion stays within acceptable bounds.

Results are compared to previously unpublished predictions from the Numerical Dispersion Relation (NDR) for the algorithm. It is shown that, although the NDR gives a guide to the algorithm dispersion under some circumstances, the Non-Orthogonal FDTD method suffers from additional dispersion effects that are not adequately described by the NDR - the origin of these effects is discussed.

A Symbolic Procedure for the Generation of Universal Functions in Accelerated EM Computing: A Fast-MoM Approach

A. R. Baghai-Wadji
Vienna University of Technology
Vienna, A-1040, Austria

The numerical accuracy of diagonal- and near-diagonal elements of impedance matrices in the MoM decisively determines the overall quality of our simulations. Most difficulties in calculating near-field interaction terms stem from inadequate regularization of kernel singularities in integral equations. Standard methods suffer from various deficiencies: (1) A case-by-case problem diagnosis is required. (2) Schemes valid in a certain frequency region fail to produce satisfactory results in other bands. (3) Approximate-, numerical-, and asymptotic solutions are required for the near-, intermediate-, and the far field, respectively: A coherent methodology has been lacking. (4) Modifying the material or the geometry, accuracy and robustness criteria have to be re-examined, and extensive tests conducted.

In this presentation simple recipes will be presented for a unified and automatic regulariza- tion of singularities of all types. Since the manipulatory steps are all physics-based, details can be communicated fairly easily and intuitively. We will address the following important topics: (i) Notions of weak-, strong-, and hyper-singular kernels will be explained. (ii) The concept of Hadamard's Finite Part will be discussed, and existing regularization techniques surveyed. (iii) A novel regularization will be introduced for converting slowly decaying, or even diverging integrands to virtually band-limited and bounded signals. (iv) Ill-conditioned rapidly oscillating integrals will be transformed into equivalent fast-decaying counterparts. (v) Robust techniques for numerical Fourier transform in d-dimensions will be detailed, along with the Fourier analysis on finite groups. (vi) A library of eigenpairs (primitive building blocks for the construction of dydic Green's functions) will be presented. Adopting a meta language, recipes for the construction and regularization of Green's functions will presented. (vii) Moments of Green's functions will be formulated in a sophisticated manner. (viii) Material parameters, the frequency, and geometric features will be scaled out, and a large number of universal functions derived. universal functions are astonishingly smooth, and can be tabulated inexpensively, and processed easily (Fast-MoM). (ix) By sampling precalculated universal functions at few (typically 4, 8, 16) points we can calculate the near-, intermediate-, and far-field interaction terms consistently and uniformly. (x) Numerical examples will include: Printed and space Antennas, MEMS, RF-MEMS, interconnects, packaging, ceramic filters (dielectrics with voids and holes), photonic crystals, SAW- and BAW devices. EM scattering problems in two- and three dimensions will serve to explain field singularities at sharp geometrical edges and corners.

We will conclude by reviewing the family of multipole-, multiresolution-, and multigrid techniques, and discuss their relevance to the Fast-MoM.

Mathematical Modelling of Optical PCM System by Wavelet Technique and Optimisation by Simplex Matlab Tool

C. D. Gupta, M. K. Panda, R. S. Bagul
Department of Electrical Engineering, Indian Institute of Technology
Kanpur, India

D. Bhowmik
Department of Electronics and Computer Science, Visvesvaraya Regional College of Eng.
Nagpur, India

In the proposed paper mathematical modeling of Pulse Code Modulation system of audio signal both by means of Free Space Optics and Optical Fiber (Relatively of longer distance compare to that in FSO) have been studied. For the purpose of laboratory study we have used a cheaper version of Chinese semiconductor Laser pointer typically used for the purpose of lecture demonstration with 5 mill watt of power. We have used the PIN diode photo detector developed by our sister unit in the department which operates very satisfactory over a wide band down to infra red region starting from visible spectrum of less than 800 mm . The typical rise time of the detector diode is less than 10ns. What is quite satisfactory for the purpose of studying the PCM system for audio range. As expected noise level for intensity modulator is inferior to that of PCM system. In order to optimize of implementing the hardware of PCM system we have isolated the A/D and D/A part of the commercially available sound card which is widely used in multimedia system.

In order to optimize the SNR mathematical modeling of the system is being done by “Wavelet technique “[Forming the product of oscillatory and decay function yield the wavelet] and optimization of the different operating parameter by simplex MATLAB tool. The system are being studied for both FSO and optical fiber which will be operated in much longer distance.

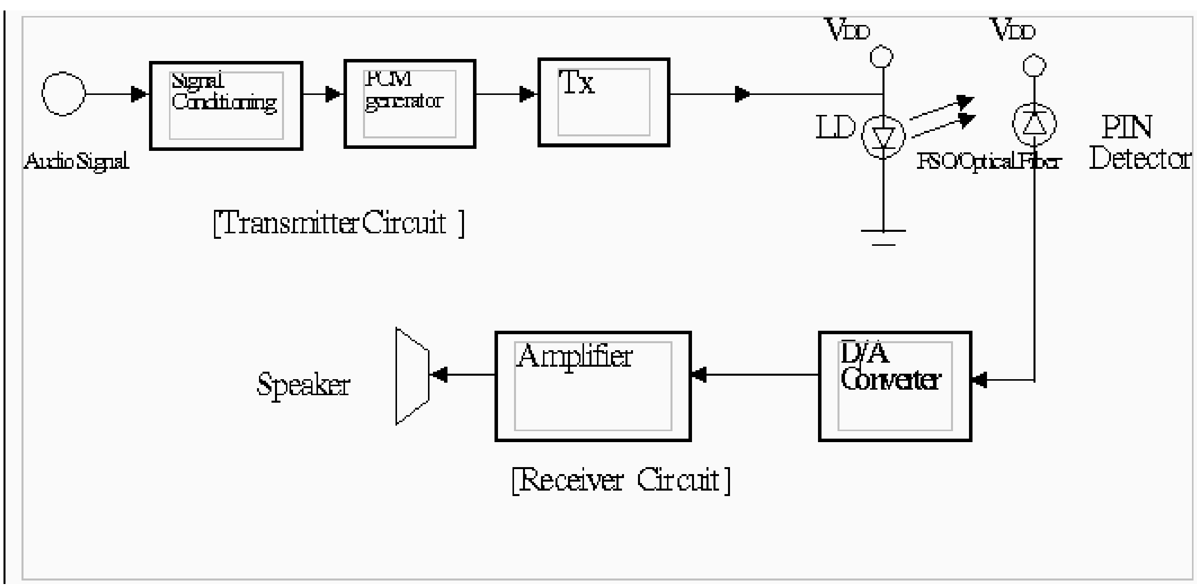

Enhancing a Geometrical Optics Aperture Integration Scheme for Arbitrarily Shaped Cavities Using Fuzzy Logic

S. M. Khan
Department of Engineering Technology, Kansas State University
Salina, KS 67401, U.S.A.

The computation of electromagnetic backscattering from arbitrarily shaped cavities has generated quite a lot of interest over the past few years; many pure and hybrid techniques have been proposed to deal with this problem. One approach used to study backscattered fields from large cavities utilizes a geometrical optics aperture integration (GO-AI) scheme. In this approach, the incident field is collimated into tubes of equal cross section and traced back to the aperture through shooting and bouncing (SBR). The exiting tubes have angles and cross sections that depend on the construction and configuration of the cavity. The magnitude of the fields within the exiting tubes is obtained by assuming power conservation inside the ray tube, which originates and terminates at the aperture. The field distribution within the exiting tube is assumed to be uniform inside the sub-aperture. The total backscattered far field is found by integrating and summing the contributions of the sub-apertures of each of the exiting ray tubes. While the above technique seems to work well for large cavities (say a 50 λ aperture) and compares favorably to modal schemes, inaccuracies develop at relatively smaller ones (say a 5 λ aperture). An explanation of this discrepancy can be made if the arbitrarily shaped cavity can be seen as being composed of different piecewise uniform sections. Problems occur when the ray angles in any uniform section (of some length) exceed the modal angle for the highest order mode in that section. This occurs because the modes struck up at such angles are non-propagating modes which would attenuate and as such the conservation within the tubes would not hold.

This paper will demonstrate a scheme to overcome the aforementioned problems with the conventional GO-AI scheme using some fundamental ideas of fuzzy logic. Fuzzy considerations are used to tap out power from the exiting ray tubes at the aperture. The field inside the exiting ray tubes are reshaped to resemble a trapezoidal distribution (fuzzy distribution) and its cross section adjusted by taking into consideration the frequency of the wave, length of travel, angles of travel, and the number of reflections that each tube undergoes. Results obtained from studying backscattering from an offset bend and an S-shaped cavity will be presented and compared with conventional ray trace schemes, modal schemes and a hybrid integral equation approximate modal technique.

Analysis of Dielectric Slab Layers in Stratified Media Using a 1-D Pseudo-Spectral Time Domain (PSTD) Method

M.-S. Tong and V. Krozer
Institute of High Frequency Engineering, Faculty of Electrical and Information Engineering
Technical University of Chemnitz
Chemnitz, D-09126, Germany

Throughout the last few decades, the Finite Difference Time Domain (FDTD) has been popularly applied for solving complicated electromagnetic (EM) problems. This numerical method is easy to be implemented, since its basic idea is to directly discretize the time dependent Maxwell's curl equations using the central finite differences. Additionally, the method possesses a number of advantages, namely, geometrical flexibility, no matrix inversions, and broadband computations.

However, one of its major disadvantages is that it requires a huge amount of computational memory space for storage of the discretized EM field information. This is due to the fact that the FDTD requires usually at least a one-tenth of the minimum discretized guided wavelength in order to maintain the accuracy up to the corresponding maximum frequency bandwidth. There is also a limitation on the maximum allowed spatial grid size with respect to the temporal step due to the fact that their ratio must be bounded by the speed of light traveling in free space.

Recently, an alternative algorithm, called the Pseudo-Spectral Time Domain (PSTD), was proposed. The idea is to apply a hybrid approach, in which the temporal derivatives from the Maxwell's equations are still expanded using the second order central finite differences, while the spatial derivatives are expanded using the properties of the Fourier Transform (FT). Since it is known that the FT has in general an infinite accuracy, the accuracy due to the spatial discretization can be well maintained. Indeed, it can be deduced that the spatial discretization can be taken as coarse as two times of the minimum discretized guided wavelength according to the Nyquist sampling theorem. In addition, due to the nature of periodicity of the FT, the PSTD method is especially suitable for the EM problems which involve periodical structures.

In this presentation, it is going to be shown how a one-dimensional (1-D) PSTD method is applied for analysis of the dielectric slab layers in stratified media. Time domain data and frequency properties in terms of propagation characteristics are to be analyzed. It is found that the PSTD method satisfies the Nyquist sampling theorem in the cases of both single and periodical dielectric slab layer structures. Comparisons will also be made with the results obtfained from the conventional FDTD algorithm. An unsplit anisotropic perfectly matched layer (APML) is adopted as the absorbing boundary conditions (ABCs).

Convergence of Beam Mode Expansion Coefficients for Corrugated and Conical Feed Horns

E. García, F. Martín, and L. de Haro
Politécnica de Madrid
Madrid, Spain

J. A. López Fernández, and F. Tercero
Centro Astronómico de Yebes (CAY-OAN). Ministerio de Fomento.
Yebes, Guadalajara, Spain

B. Galocha
Politécnica de Madrid
Madrid, Spain

A. Barcia
Centro Astronómico de Yebes (CAY-OAN). Ministerio de Fomento.
Yebes, Guadalajara, Spain

J. L. Besada
Politécnica de Madrid
Madrid, Spain

This paper presents a convergence study of the Beam Mode Expansion (BME) coefficients for corrugated and conical feed horns used in radiotelescopes. Gaussian Beam analysis has been employed to study the behavior of these radioastronomy feeds.

Beam Mode Expansion consists of expanding the electric field in the aperture in terms of a set of Gaussian-Laguerre modes. Near and far field patterns are easy calculated in a same manner with these modes by summing their contributions. The modes are solutions of the wave equation within the paraxial approximation, and their propagation can be calculated in a simple and well defined way.

A quasioptical analysis software for corrugated and conical feed horns has been developed. Using the number of modes desired, the field pattern of the feed horns can be represented. According to the number and type of modes selected, it is possible to compare several fields patterns. So we can analyze the convergence of the field by increasing the number of the studied modes. We have 34 symmetric modes for the corrugated feed horn, while for the conical feed horn, we have 33 symmetric modes and 30 asymmetric modes. As we present in this paper, in both cases the number of modes is sufficient for an accurate field level calculation.

To contrast the accuracy of the Beam Mode Expansion a 22 GHz conical feed horn for the Yebes Astronomical Observatory (CAY-OAN) has been measured. We present the convergence results of the Beam Mode Expansion establishing an evaluation of the weight and influence of the symmetric and asymmetric modes in the field pattern.

Fundamental mode is suitable to analyze the principal lobe of the field, i.e., high values of the field. If we want to study lower levels of field (i.e. secondary lobes), it is necessary to increase the number of modes. In this paper we present that the adequate amount of symmetric modes used in the calculation of field levels from -30 dB and upper in the case of corrugated feed horn is 10 modes. For the conical feed horn, using 10 symmetric and 10 asymmetric modes we guarantee an accurate calculation of field values from -30 dB and upper, which agrees with the measurements done to the 22 GHz feed horn.

A Far to Near Interpolation

N. Bartoli and F. Collino
CERFACS
Toulouse, France

We discuss the interaction between an antenna and some surrounding elements. To study radiant structures like antennas, we measure generally the phase and the amplitude of scattered fields in the far zone, as a function of spherical angles. In many cases, industrials are interested in deducing the interaction of this antenna with other elements, using only the knowledge of the far field measurements.

Our purpose is to approximate the near field issued from the antenna on the different elements. This far to near transformation can be performed in many ways. A first and obvious approximation consists in using an interpolation of the far field at each point weighted by two terms: a term in $1/r$ and a phase term e^{ikr}, where r characterizes the distance antenna-point. This approximation is easy to implement but remains valid only if the distance is large enough.

A more accurate approximation is based on a multipol expansion. The field on each element is directly given by the antenna's far field via an adaptation of the Fast Multipol Method, in the close vicinity of the antenna (more than a quarter of wavelength). The main advantage is also to use all the new techniques developed in the context of FMM, to reduce the CPU cost. This process is particularly appropriate for large obstacles.

Both of these transformations need to interpolate the far field measurements, in which case the simulation requires more data. For this purpose, we develop an interpolation process using a spherical harmonic expansion of the field. Some numerical results will be presented to illustrate these far to near transformations.

Computer-Aided Calibration of Direct Far-Field from UHF To mm Wave Region and of the Optical System Both in Two-Dimensional and Three-Dimensional Forms

C. D. Gupta, M. K. Panda
Department of Electrical Engineering, Indian Institute of Technology
Kanpur, Uttar Pradesh, India

R. S. Kumar
Department of Electronics Engineering, Regional Engineering College
Tiruchirapalli, Tamilnadu, India

The original papers [1,2,3], presented by the author have been combined in modified form focusing mainly on the computer aided calibration of direct far-field from UHF to mm region and of the optical radiation plot as envisaged earlier in the two dimensional form has been extended here for three dimensional too. The relevance of the three dimensional radiation plot will have due importance for experimental evaluation of inverse scattering problems.

Besides the direct measurement of the far-field, of optical radiation both in two and three dimensional forms it is planned to have microprocessor detection of the radiating source. The later part of the work will be quite useful in terms of installing the units in FSO systems, the emerging field of immense commercial interest, particularly in the western countries.

It had been found by the author during his visit to Boston [1] that this system only in terms of direct measurement of far-field that too in two dimensional form only over a band of microwave frequency was being quoted for price of US $40,000. Thus, it can be concluded that when this work will be further regularized will have tremendous commercial importance.

Before measuring the radiation plot of any unit to be developed it is necessary to know its input impedance matching characteristics preferably within a wideband. Our sister unit have developed the computer aided measurement system as a substitute of wideband network analyzer system for which HP quotes the price of more than US $50K. They have done by suitable implementation of the software along with 1-20 GHz frequency synthesizer.

We have developed the program by MATLAB of Smith Chart to be implemented with computer aided measurement by network analyzer.

REFERENCES

1. C. Das Gupta: Experimental study of fan beam Cassegarian antenna with planar metal dielectric feeder. *Proceedings 2001 IEEE APS/URSI International Symposium*, Boston, USA. Orally Presented.
2. C. Das Gupta: Computer aided measurements of antenna parameters from UHF to far microwave region. Presented at *2nd International Conference on Cybernatics and Technologies of 21st century*, October 2001, Voronetz, Russia.
3. C. Das Gupta: Computer aided calibration of far field of the off set optical Cassegarian antenna, *URSI National Radio Science Meeting*, University of Colorado at Boulder, January 2002. (Accepted for presentation).

A Parallel Genetic Algorithm for Profiled Corrugated Circular Horn Optimization

L. Lucci
Department of Electronics and Telecommunications
University of Florence
Florence, 50134, Italy

R. Nesti
Arcetri Astrophysical Observatory, National Astrophysic Institute
Florence, 50125, Italy

G. Pelosi and S. Selleri
Department of Electronics and Telecommunications
University of Florence
Florence, 50134, Italy

Profiled Corrugated Circular Horns (PCCH) are the preferred feed for high performance reflector and lens antennas. This is due to the fact that PCCH exhibit very high polarisation purity and very small size as compared to classical horns. No direct analytic or computer based techniques are available for the design of PCCH and hence design is carried out either by a trial-and-error or via some sort of numerical optimization procedure be it deterministic or stochastic. Both these methods require an accurate full wave code for the analysis. A very accurate method of analysis is a hybrid technique relying on a Mode Matching solution for the interior of the horn and the solution of a Combined Field Integral Equation (CFIE) on the outer boundary to correctly keep into account of the exterior horn structure. This latter solution can be accomplished, for example, in the framework of a weighted residual method. The two solutions are matched at the horn aperture via an appropriate application of the equivalence theorem.

In any case, even exploiting any — eventual — rotation symmetry to speed up the CFIE solution computing costs are extremely high, in the order of some minutes per frequency points on a 750 MHz Pentium III. If any kind of optimization procedure is to be applied many simulations on many frequency points would be necessary, leading to computing times in the order of days or even weeks. This is particularly true if a stochastic optimization procedure like Genetic Algorithms (GA) are used. GA are an extremely powerful and versatile procedure, but they require a relatively large amount of analyses hence, even if they are free from the convergence and local minimum issues of deterministic techniques, they are generally slower.

On the other hand GA work on a population of possible solutions to the problem which are updated altogether at each iteration on the basis of their performance against a given — analysis based — cost function. Many analyses must then be computed for each step, one — over many frequency points — for each member of the population. These analysis need not to be performed sequentially but can rather be performed in parallel, hence greatly speeding up the process.

This intrinsic parallelism can be very efficiently exploited by creating a parallel GA code and by keeping the original non-parallel analysis code. It is the task of the GA to spawn single-CPU analysis all over a parallel machine. Hence a Beowulf cluster with four dual-CPU nodes has been set up and an appropriate GA devised to take full advantage of the cluster without having to rewrite the non-parallel analysis code. Thanks to the presence of a virtual 8CPU machine the CPPH design process is nearly 8 times faster than on an equivalent single CPU machine.

Profile and corrugations parameters are considered as variables in the optimization process, seeking for compact horns which, nevertheless, present a phase center as stable as possible. Cross-polarization level and return loss are also considered in the cost function.

Detection and Classification of Defects in Metallic Plates Using Fuzzy Entropy Algorithms

M. Versaci, S. Calcagno, and F. C. Morabito
Dipartimento DIMET – Facoltà di Ingegneria, Università “Mediterranea” Reggio Calabria
Reggio Calabria, Italy

In several industrial applications, Non Destructive Testing (NDT) in the field of defects identification on metallic elements plays a remarkable role with special regard to those sectors where the integrity of the material is strictly required (i.e. structural elements in aircrafts, parts of nuclear reactors, etc). Being moreover NDT non invasive techniques, they allow the designer as well as the manufacturer on one side don't to damage the specimen before the installation and on the other hand to investigate, if necessary, on the specimen itself during the in-service test. As a consequence, detection of defects in metallic plates together with the consequent defect shape classification provides the operator useful information on the actual mechanical integrity of the specimen. Defects on metallic plates nevertheless rarely look as well-known geometrical shapes (square, triangle, circle, . . .) but take a shape which roughly approaches regular geometry. This paper aims to suggest a methodology to detect and classify the shape of a defect by applying the fuzzy logic. Having the position of a defect been located by using fuzzy inference automatic extraction algorithms, next step is to classify the defect by introducing the fuzzy entropy concept. Fuzzy entropy is mainly employed to measure how far is a defect from a well-known geometry.

Experimental measurements have been carried out in Reggio Calabria NDT lab on thin metallic plates. The applied sensor was the FLUXSET® type, moved along the surface under investigation by a step-by-step motorized scanning system. An external exciting field at a proper frequency is generated close to the specimen, thus inducing eddy currents on the surface as well as on subsurface layers. The measured pick-up voltage is proportional to the magnetic field component parallel to the longitudinal axis of the sensor itself. To develop the training phase, a number of plates were employed equal to the defects with well-known geometry. Only one defect could be found on each of these plates. In the following training phase, holes with non regular geometry have been analyzed. The plates have been step-by-step scanned along x and y axis in order to obtain a whole 2D measurements map.

In the near past neural networks have been successfully employed to locate defects on metallic plates. In this paper the use of fuzzy inference techniques allowed to obtain banks of *IF ... THEN* fuzzy rules, in virtue of which the system under investigation behaves as a linguistic structure thus helping to take decisions. The use of fuzzy inferences automatic extraction algorithms, provided with training routines, leads to the writing of rules everyone including all the useful variables, thus reducing the computational complexity.

The fuzzy logic can represent a solution to define how much a defect is far (approaches) from well-known shapes. In particular, the fuzzy entropy approach translates into a value in the range [0,1] the belonging of the shape of a defect to one of the well-known classes. From a geometric point of view, the translation takes place by means of the unitary ipercube, each vertex of which represents a geometrically well-known class of defects (each vertex represents a crisp point of behaviour, the shape of the defect being perfectly known, without any uncertainty). The degree of belonging of the shape of a defect to the well-known classes located at the single vertexes is given by the measurement of the fuzzy entropy. The applied algorithms to calculate the entropy have been got from Kosko Theory.

Encouraging results comes out from the investigation of metallic plates based on Eddy Currents methodology aimed to locate and classify defects. The produced fuzzy inferences give the expert verifiable rules about the behaviour of the system. The fuzzy entropy looks as a powerful instrument to classify defects on the plates. The geometric representation by means of ipercubes moreover provides a graphical reading of the classification.

Session 2Pa3

Laser Beam Characterization

The Characterization of Hard-Edged Diffracted Flattened Gaussian Beams

B. Lü, X. Ji, and S.-R. Luo
Institute of Laser Physics & Chemistry, Sichuan University
Chengdu, 610064, China

In recent years much attention has been paid to the parametric characterization of laser beams including their propagation properties and beam quality. In a document from the International Organization for Standardization the second-order-irradiance moments-based M^2 factor (beam propagation factor) is recommended as a criterion for characterizing different laser beams. In addition, the shape features of laser beams, such as the symmetry and degree of flatness, can be described by the skewness and kurtosis parameter K, respectively. On the other hand, beams with a flat-topped transverse profile are of particular interest owing to the practical application purpose. It has been shown that the flattened Gaussian beam (FGB) introduced by Gori is a useful model for simulating such a type of beam. As yet the propagation properties, beam quality of FGBs and correspondence between FGBs and super-Gaussian beams have been studied extensively. However, most publications are limited to the unapertured case, whereas in practice beams are apertured more or less.

This talk presents some recent results of our group in studying hard-edged diffracted FBGs. First, by using the technique of expanding the rect function into a finite sum of complex Gaussian functions, an approximate closed-form propagation equation of FGBs passing through paraxial ABCD systems with hard-edge aperture is derived, which allows us to study propagation properties of hard-edged diffracted FGBs both analytically and numerically. Then, the generalized M^2 factor and K parameter of hard-edged diffracted FGBs are derived. As a special case, the M^2 factor of truncated plane waves is shown to be $4\sqrt{3}/3$. Furthermore, from a practical point of view, a key parameter, i.e., the power in the bucket (PIB) (alternatively, the β-parameter), is chosen as the beam characteristic parameter, and the beam quality of hard-edged diffracted FGBs are illustrated with numerical examples. It is also pointed out that some additional parameters, such as the pointing stability, uniformity (or fill factor) and sustainability, have to be used to characterize the beam quality of real laser beams in accordance with the application aim. Finally, a brief summary of the main results and future studies are concluded in the talk.

Spatial Frequency Content of Ultrashort Pulsed Beams

C. J. R. Sheppard and M. D. Sharma
Physical Optics Department, School of Physics A28, University of Sydney
Sydney, NSW 2006 , Australia

The propagation behaviour of ultrashort pulsed beams depends on the relationship between the characteristics of the different spectral components. For a particular relationship called isodiffracting beams, or Type 3 pulsed beams, space-time couplings are reduced. This is also an important practical case as this is the type of pulse formed in a mode-locked laser cavity. The propagation behaviour of different types of pulsed beam can be investigated using the concept of the generalized three-dimensional pupil function. This approach specifies the three-dimensional spatial frequency content of the beam, and has been found to be particularly useful for the study of highly-convergent focused beams. The amplitude in the focal region as a function of time is then given simply as a three-dimensional Fourier transform of the generalized pupil function. The properties of two special cases, of Bessel beams and Gaussian beams, are investigated. The connection of the former with focused wave modes (FWM) and X-waves is also discussed. The FWM is a special case of the Type 3 pulsed Bessel beam. The treatment for the Gaussian beam is based on the concept of the complex source/sink point model.

Characterising Flat-Top Beams Produced in Lasers Employing Unstable Resonator

S. Saghafi, M. Withford, and J. A. Piper
Physics Department, Macquarie University
Sydney, NSW 2109, Australia

For many laser applications, a beam with a flat-top intensity profile (i.e. uniform irradiance over a defined cross section) is highly desired. As a result, many lasers are designed to produce flat-top beams and various beam processing techniques have been developed to obtain uniform (flat-top) beams from Gaussian and other non uniform laser beams. There are three main models, all based on the paraxial approximation, which can predict the beam diameter, intensity profile and phase at any point along the propagation axis for beams with uniform irradiance distribution. Each models have their strengths and may be preferred in particular situations. The beam parameters M^2 and k are used to describe propagating laser beam. To use any of these models, their individual model parameter describing the beam characteristics must be defined.

In this paper, we establish:

1) a general relationship between M^2 and k,
2) the relationship between these beam parameters and the model parameter describing the beam characteristic in each of three analytical models (that enable us to switch from one model to the other depending on the application),
3) testing the validity of these results against beam profile measurements of a high power Copper Vapour Laser with unstable resonator (Figs. 1 and 2), and
4) presenting the possible application in optical data storage system.

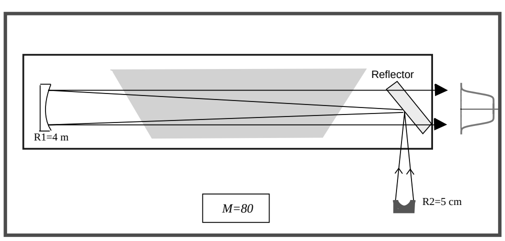

Figure 1

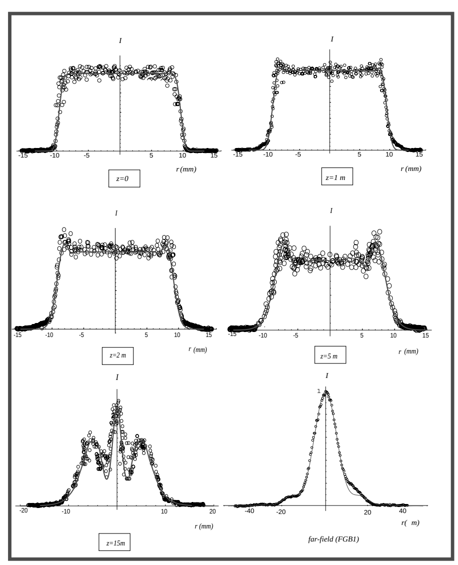

Figure 2

Characterization of the Coherent Features of Partially Coherent Source Through Intensity Measurements

R. Borghi and G. Guattari
Dipartimento di Ingegneria Elettronica, Università Roma Tre and Istituto Nazionale per la Fisica della Materia
Roma, Italy

F. Gori and M. Santarsiero
Dipartimento di Fisica, Università Roma Tre and Istituto Nazoinale per la Fisica della Materia
Roma, Italy

It is well known that many real lasers oscillate on a superposition of transverse modes of the cavity.[1] Such modes oscillate inside the cavity at slightly different frequencies, when no degeneration occurs, and often they can be supposed to be totally uncorrelated. The determination of the transverse modal content of a real laser beam represents a key problem in order to characterize the beam itself as well as the source and keeps on attracting the interest of opticists.

A recurrent question is whether the measurements of the intensity distribution across a single transverse section of the beam is sufficient to recover the modal weights. Generally speaking, since the information content carried by a partially coherent beam is extremely greater than that pertinent to a coherent beam, the knowledge of the sole spatial intensity distribution is generally not sufficient to warrant a unique reconstruction of the coherence properties, i.e., of the cross-spectral density of the beam.[2] However, when an *a priori* knowledge on the physical properties of the partially coherent beam is available, then the number of degrees of freedom necessary for the characterization of the beam reduces, and one can expect that the solution of the corresponding inverse problem becomes possible. This happens, for instance, inside a multimode stable-cavity laser, where the modes can be approximately assumed to be mutually uncorrelated Hermite-Gaussian (HG) beams.[1] In such a case, due to the uncorrelation hypothesis and to the shame invariance property of the HG modes,[1] the recovery of the modal weights pertinent to each HG mode can be done by means of a very simple technique, as recently shown.[3,4] However, for a general partially coherent source neither the uncorrelation nor the HG-shaped mode statements are fulfilled. This, in particular, happens when lasers having unstable resonator geometries are considered.

Here we propose a novel general method that allows the complete modal distribution of a typical partially coherent source to be achieved starting from sole-intensity measurements on the radiated beam. The method makes use of a generalization of the Fourier transform-based technique employed in Ref. 3, and has been implemented in a fair and efficient way by means of standard FFT techniques. The method is then applied to the case of the of the incoherent superposition of two (equally intense) fundamental Gaussian beams with the same spot-size and whose centers, across their common waist plane, are displaced from one another. In this circumstance the proposed method is able recover all correlation coefficients in closed-form terms. Further examples are also given in order to numerically verify the feasibility of the method.

We believe that the proposed technique could be of interest for studying the coherence features of beams emitted by multimode unstable-cavity lasers and for their characterization.

REFERENCES

1. A. E. Siegman, *Lasers*, (University Science Books, Mill Valley, California, 1986).
2. F. Gori, M. Santarsiero, and G. Guattari, "Coherence and space distribution of intensity," *J. Opt. Soc. Am. A* **10**, 673-679, (1993).
3. F. Gori, M. Santarsiero, R. Borghi, and G. Guattari, "Intensity-based modal analysis for partially coherent beams with Hermite-Gaussian modes," *Opt. Lett.* **23**, 989-991 (1998).
4. M. Santarsiero, F. Gori, R. Borghi, and G. Guattari, "Evaluation of the modal structure for light beams with Hermite-Gaussian modes," *Appl. Opt.* **38**, 5272-5281 (1999).

Optimization of Chirped Pulse Amplification Systems Using Martinez Stretcher

Y. Song, Z. Zhang, and Q. Wang
School of Precision Instrument and Optoelectronics Engineering, University of Tianjin
Tianjin, 300072, P. R. China

Martinez stretcher [1] is most commonly used in the chirped pulse amplifications, however, it has not been thoroughly examined because of the lack of the calculation formula. Numerical ray-tracing method was claimed in many papers during the last 10 years. Unfortunately, in most theoretical papers, Treacy formula [2] with an opposite sign was still the unique tool used to predict the performance of Martinez stretcher and Offner stretcher as well. The fatal problem of using Treacy formula to imitate Martinez stretcher (and Offner stretcher) is that a real stretcher has significant mirror aberration, which will transfer to phase dispersion.

We derived a formula for calculating the phase of Martinez stretcher, based on 2-dimensional ray-tracing. With this formula, we analyzed the phase dispersion of a CPA system including a multipass amplifier or a regenerative amplifier. The simulation revealed some new characteristics. First, the grating position in the stretcher is a sensitive parameter to affect the system phase and can be used to compensate the high order term; a compromise between the high order dispersion and the stretching ratio has to be reached. Second, for a regenerative amplifier, adjusting any of available parameters including mixed gratings will not result in a broader bandwidth greater than 100 nm. Third, in a multipass amplifier, combining gratings of 1200 l/mm and 1100 l/mm in the stretcher and the compressor respectively, a very broad phase window ($\sim$ 200-nm bandwidth) can be achieved for supporting further short pulse amplifications. Experimental confirmation is being conducted.

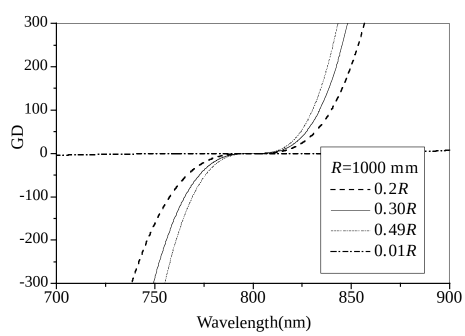

Fig. 1 Group delay of a stretcher and compressor system as a function of wavelength when tuning the grating position with no material dispersion.

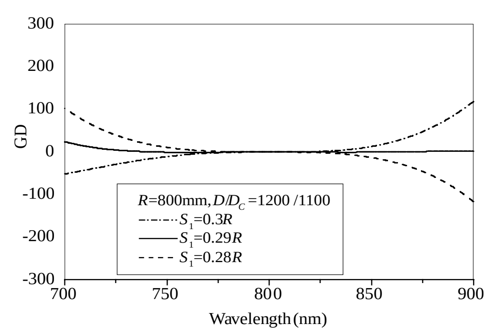

Fig.2 The optimized group delay of a multipass amplifier combining the four parameters: R=800mm, γ_a =10°, D=1200/mm, D_C=1100/mm, S_1=0.30R, 0.29R, 0.28R, respectively.

(R: curvature radius of the spherical mirror, D, DC: the grating groove densities in stretcher and compressor respectively, γ_a: incident angle equals Littrow angle plus γ_a, S_1: grating position.)

REFERENCES

1. Martinez, O. E., *IEEE Journal of Quantum Electronics*, Vol. QE-23, 59–64, 1987.
2. Zhang, Z., T. Yagi, and T. Arisawa, *Appl. Opt.*, Vol. 36, 3393–3399, 1997.

Session 2Pb3

Optical Devices and Communication Systems

Electromagnetic Simulations of MEM Optically-Controlled GaAs Microstrip Switches: ON/OFF Ratio Enhancement

C. Canseliet, C. Algani, F. Deshours, and G. Alquié
Instruments and Systems Department, Pierre and Marie Curie University
Paris, France

S. Formont and J. Chazelas
Thalès Airborne Systems, Microwaves Photonics R&D Department
Elancourt, France

Optical and optoelectronic systems are required in telecom networks to achieve high speed data transmissions. Performance of such optical/electrical and electrical/optical interfaces become an industrial stake. In case of optical to electrical conversion, photoconductive effect is mainly used with semiconductor substrates.

Through photoconductive effect, inducing local photoconductance Gg (2), a discontinuity (gap) of a microstrip conductor, subject to optical beam satisfying the material absorption condition (1), provides efficient switching and sampling of a microwave signal that feeds the line. Some photoswitches lightened by continuous optical source have already been designed on GaAs, GaAs:Cr^+ and Si and InP with different gap structures reaching a maximum isolation between ON and OFF optical source states of 8 dB for a microwave signal frequency of 20 GHz.

$$\lambda_{\text{opt}}(\mu\text{m}) \leq \frac{1.24}{E_g(\text{eV})} \tag{1}$$

$$G_g = \frac{e}{hv}(\mu_n + \mu_p)\eta\alpha\tau(1-R)\frac{P_{opt}}{A}\frac{w_{\text{eff}}}{L_g}\frac{1}{(1-\alpha^2L^2)}\left[\frac{1}{\alpha} - L\frac{\alpha L^2 + v_s\tau}{L + v_s\tau}\right] \tag{2}$$

Optimizations on switching performances occur at two levels, by modifying surface and volume structure. Gap capacitance is reduced to a few femtofarads by changing, in the first case, discontinuity geometry, and in the second case, material relative permittivity under the gap.

Volume optimisations have been realized with moment's method simulations, assuming multilayered structure under the microstrip gap.

Volume optimizations associated to MEMs technology have been realized with 2.5 D commerical software using moment's method simulations, assuming multilayered structure under the microstrip gap, with a 10 μm-height polymide $(\varepsilon_r = 3.4)$ and 4 μm-height nitride $(\varepsilon_r = 7.2)$ layers usually necessary in fabrication process. Substrate is hollowed in a depth of 10 μm under the discontinuity corresponding to a local air layer, and a 10 μm-height layer of silica $(\varepsilon_r = 2.25)$ is added on the microstrip line, to design a lateral optics-integrated photoswitch. Lightening is synthesized by a $100\,\Omega$ resistance placed in parallel with OFF state S-parameters data box obtained from 2.5 D simulations. An isolation of 45 dB between OFF and ON states is achieved at microwave frequency of 20 GHz, assuming a gap length of 160 μm and a 200 μm GaAs height. For the same structure without local air layer, an ON/OFF ratio of maximum 30 dB is obtained at the same frequency. 3 D simulations are in progress in order to complete simulations results from those obtained from 2.5 D.

Scattering of Light in Photonic Crystals

B. J. Hoenders, M. Doosje, and J. Knoester
Institute for Theoretical Physics, University of Groningen
Groningen, AG 9747, The Netherlands

Photonic crystals are regular structures with periodically varying optical properties, such as the dielectric function. These crystals are characterised by their photonic band structure and Bloch wave eigenfunctions, the knowledge of which is not sufficient to determine the scattering process by a photonic crystal.

We report on the results of a new and exact scattering theory, which describes reflection and transmission of light at the surface of an arbitrarily shaped photonic crystal in terms of "equivalent surface current distributions", (strata). Such a theory is needed because the underlying assumptions for the dynamical theory of X-ray diffraction are not satisfied for photonic crystals. A current stratum is a 'surface current distribution' generating the pertinent electromagnetic field. Each surface current element acts as a point source which generates an elementary electromagnetic field, described by a Green dyadic response function. The pertinent electromagnetic fields inside- and outside the crystal are obtained by the superposition of all the elementary electromagnetic fields (Huygens's principle).

The continuity conditions for the electromagnetic field at the boundaries lead to a set of coupled linear integral equations for the two surface current distributions generating resp. the electromagnetic fields inside and outside the crystal, which are then solved numerically. The knowledge of these quantities enables us to determine the physical quantities of interest, like the surface field distribution and the amount of energy scattered in all directions.

We consider in particular the scattering of an incoming plane wave by a photonic crystal occupying an infinite half space or slab. We will present results of such calculations for two-dimensional photonic crystals and present a generic model which allows us a qualitative interpretation of the calculated transmitted intensity.

Second-Order Statistics of Multi-Layer Optical Coatings

H. E. Rowe
Department of Electrical and Computer Engineering, Stevens Institute of Technology
Hoboken, New Jersey 07030, U.S.A.

Optical mirrors, windows, beam-splitters, and filters are made from multiple dielectric layers. Random errors, in thickness or index of refraction of the different layers, limit the performance of these devices. Given the desired performance, we wish to determine the required tolerances. Alternatively, given the tolerances, we require the performance that is attained.

The response of a specific device is given as a matrix product; each matrix is determined by the thickness and index of the corresponding layer. With random errors, the matrices are random. Kronecker product methods yield exact values for the statistics of such random matrix products. However these methods yield statistics for only the reciprocals of the transfer function or transmittance, rather than the desired statistics of these quantities themselves. Similarly, they do not yield the desired reflection statistics directly.

Consequently, it is necessary to combine perturbation theory with Kronecker product methods to determine the desired transmission and reflection statistics in terms of the thickness and index statistics. The resulting transfer function statistics are only approximate, valid for small departures from the design. We validate these approximate results by comparison with exact results for special cases in which the imperfections, in layer thickness or index, have a discrete probability distribution.

Prior work has compared perturbation theory, for the average transmittance vs. frequency, with exact results for a 13-layer filter with independent binary thickness errors. Beyond the perturbation region, the transmittance exhibits varied frequency dependence for different filters, representing unacceptable performance.

We study the second-order transmission transfer function statistics for this 13-layer filter, and compare the approximate and exact results for this case, as a function of the magnitude of the thickness errors. For sufficiently small errors, the transfer functions depart only slightly from their ensemble average. The average time response, determined from the approximate second-order transfer function statistics, is a useful measure of performance in this case.

A Compact Phase Tracking Interferometer Based on a Quarter Waveplate-Polarizing Cube Beamsplitter Combination and Which Uses Polarized Beams

G. P. Riblet
Microwave Development Laboratories, Inc.
Needham Heights, MA 02491-1483, U.S.A.

In the case of the Michelson interferometer with conventional beamsplitter only the transmitted power P_t is detected. This power P_t has a $\cos\theta$ dependence on the phase difference θ of the paths in the two arms of the interferometer. The power P_r reflected back toward the source remains undetected. Of course if it were measured by a second detector, it would also have a $\cos\theta$ dependence but of opposite sign. This is necessitated by the requirement for energy conservation. The ambiguity in the determination of θ itself would remain even if P_r were measured. Suppose instead that a polarization sensitive beamsplitter is used. Furthermore, suppose the power in each transmitted polarization state and in each reflected polarization state were detected. The power in one of the two transmitted polarization states might have a $\cos\theta$ dependence and the power in one of the two reflected polarization states might have a $\sin\theta$ dependence without violating energy conservation. In this case θ could be determined to within $\pm 180°$.

A quasioptical version of such a phase tracking interferometer can be based on a quasioptical 8-port circuit which I described at PIERS 2000 [1]. It consists of a quarter waveplate wire grid combination. Furthermore, linearly polarized beams making a $45°$ angle with the grid wires are assumed. In this presentation it was shown that the resulting quasioptical circuit functions as an 8-port correlator network. Such an 8-port network is well known in the microwave industry. It is equivalent to a 4^{th} order Buttler network. A Martin-Puplett interferometer (MPI) may be modified to form a new interferometer which includes the above quasioptical 8-port correlator circuit. If the roof lines of the reflecting roof mirrors of the MPI are set at $22.5°$ rather than $45°$, then half of the reflected power will pass back through the wire grid toward the source. If an oriented quarter waveplate is now placed in this reflected beam, the 4 normalized powers in the above linearly polarized modes are $(1+\cos\theta)/4,\ (1-\cos\theta)/4,\ (1+\sin\theta)/4,$ and $(1-\sin\theta)/4$. This result follows from the known S-matrix of the correlator network. The sum of these 4 normalized powers is 1 independent of θ as it must be if energy is to be conserved.

Experimental verification of the phase tracking properties of such a modified Martin-Puplett interferometer would be expensive. A stable polarized source in the far infra-red would be needed. On the other hand a laser diode provides an inexpensive and stable linearly polarized optical source. In this regard, it has been found that the quarter waveplate wire grid combination of the modified MPI can be replaced by a quarter waveplate-polarizing cube beamsplitter combination at a known optical frequency. As a result experimental verification of phase tracking has been possible using inexpensive optical components. It can be shown that with a suitable choice of orientation of the orthogonal electric field vectors in the input and output paths, a quarter waveplate-polarizing cube beamsplitter combination can also be made to function as a compact 8-port optical correlator network at a given frequency. In the case of the experimental interferometer, the roof mirrors of the MPI have been replaced by hollow retro reflectors. This facilitates beam alignment. Since the source and reflected beams are now displaced, the reflected beam can pass by a mirror, through a quarter waveplate and then a polarizer to the second detector. The orientation of the polarizers in both the transmitted and reflected beams are adjusted experimentally for optimal phase sensitivity.

REFERENCES

1. Riblet, G. P., "A broadband quasioptical 6-port network using a single wire grid and a quarter waveplate," *Progress Electromag. Res. Symp. Dig.*, p.876, 2000.

Polarization-Resolved Chaos in an Optically Injected Vertical Cavity Surface Emitting Laser

Y. Hong, P. S. Spencer, P. Rees, S. Bandyopadhyay, and K. A. Shore
University of Wales, Bangor School of Informatics, Bangor LL57 lUT,
Wales, UK

Recently vertical cavity surface emitting lasers (VCSELs) have been given considerable attention owing to their impressive characteristics, such as a low threshold current, single longitudinal mode operation, circular output-beam profile and wafer scale integrability. In addition to the properties of stand-alone VCSELs, effort has also been given to understanding the response of VCSELs subject to optical feedback and optical injection. Specific interest arises in regard to the effects of optical injection on the polarization of VCSEL emission. For example, in recent work we have demonstrated experimentally how the properties of VCSELs can be influenced by detuned optical injection [1–3].

In this paper, we will report our investigations of a VCSEL biased just above threshold so that it supported only the fundamental transverse mode of one polarization and subject to external optical injection over a large frequency detuning range and optical injection power. We make what we believe to be the first report of the observation of two chaotic regimes in a VCSEL subject to optical injection. These two chaotic regimes are located on the negative and positive detuning sides of the injection locking region. This contrasts to the case of edge-emitting lasers where two chaos regimes are located on the same detuning side of the injection locking regime [4]. From the time trace of the light emission, we have also confirmed that the observed chaos in the VCSEL is polarization chaos: the total output power is almost stable, but the polarized resolved output power exhibits chaotic dynamics. We also observed other dynamical behaviours in the VCSEL; namely, nearly degenerate four-wave mixing (NDFWM), injection locking, limit cycle and period doubling.

When the injection power is at a low level, we observed nearly degenerate four wave mixing, limit cycles and injection locking, but no chaotic dynamics. With higher injection power the chaos in the negative detuning region from the stable injection locking regime was eliminated. For further increases of injection power the chaos was fully suppressed.

REFERENCES

1. Hong, Y., K. A. Shore, A. Larsson, M. Ghisoni and J. Halonen, "Pure frequency-polarisation bistability in vertical cavity surface-emitting semiconductor laser subject to optical injection," *Electron. Lett.,* Vol. 36, pp. 2019–2020, 2000.

2. Hong, Y., K. A. Shore, A. Larsson, M. Ghisoni and J. Halonen, "Polarisation switching in a vertical cavity surface emitting semiconductor laser by frequency detuning," *IEE Proc-Optoelectron.,* Vol. 148, pp. 31–34, 2001.

3. Hong, Y., P. S. Spencer, and K. A. Shore, "Power and frequency dependence of hysteresis in optically bistable injection-locked VCSELs," *Electron. Lett.,* Vol. 33, pp. 569–570, 2001.

4. Kovanis, V., A. Gavrielides, T. B. Simpson, and J. M. Liu, "Instabilities and chaos in optically injected semiconductor lasers," *Appl. Phys. Lett.,* Vol. 67, pp. 2780–2782, 1995.

Numerical Calculation of Leakage-Loss in W-Tunneling Optical Fiber

M. N. Ji
Optical Fiber Research Center, Physics Department
Kun Ming University of Science and Technology
Kun Ming, 650093, P. R. China

A W-Tunneling optical fiber is single polarization single mode (SPSM) when one of the fundamental modes is cutoff and the other is guided. The fiber can be used as a polarizer and is useful in gyroscope, coherent telecommunication and interferometric sensors. To determine the extinction ratio and single polarization bandwidth, it is necessary to know the leakage loss of the fundamental mode below cutoff. Though the leakage loss of a W-profile fiber with circular core and circular inner cladding can be calculated easily, the problem will become much complicated when a W-Tunneling optical fiber with an elliptical inner cladding is considered. Until now only an approximate method given by Marcuse is used in this calculation. But his results are only order-of-magnitude estimates. In this paper, a new numerical method based on point-matching is presented to calculate the leakage loss of the fundamental mode in W-Tunneling optical fibers. The main idea of this method is to put the boundary conditions of Maxwell's equation in matrix form. From this matrix form, the leakage loss of the fundamental mode can be obtained simply by solving a set of algebraic equations.

The effectiveness of the method is confirmed by stability calculation and by comparing with the experiment data. It is found in calculation that the loss coefficient α is insensitive to the semimajor axis a when the inner cladding is highly elliptical $(a/b \geq 5)$, but is sensitive to the semiminor axis b and the index depth d. It decreases quickly with the increase of b and d. These numerical results are important in designing a W-Tunneling optical fiber.

Simultaneous Effect of Optical Radiation, Temperature and Hydrostatic Pressure on GaAs Based Device Parameters

S. Bose
Institute of Electro-Optical Engineering, National Chiao Tung University
Hsinchu, 30010, Taiwan, R.O.C.

M. Gupta and R. S. Gupta
Semiconductor Devices Research Laboratory, Department of Electronic, Science University of Delhi South Campus
New Delhi , -110 021, India

C.-L. Pan
Institute of Electro-Optical Engineering, National Chiao Tung University
Hsinchu, 30010, Taiwan, R.O.C.

There is no doubt that the semiconductor, GaAs has now become widely acclaimed in semiconductor industry in comparison to other compound semiconductors. This is because of its some highly useful properties like high carrier mobility, direct and wide bandgap etc. for high-speed digital, optoelectronics and high temperature applications. Also, the technology of GaAs based devices such as GaAs MESFET is more mature than those of other compound semiconductors. For the past few years, GaAs has also become the study of intense research for the generation of THz (Tera-hertz) radiation.

Therefore, it is very much essential to study the effect of temperature and optical radiation on the important parameters of GaAs, which are responsible for its widespread use. It is also true that the hydrostatic pressure plays a significant role on energy gap and thus other parameters.

In the present work, a theoretical study has been carried out to notice the simultaneous effect of optical radiation, temperature, and hydrostatic pressure on important parameters like bandgap energy, carrier mobility etc. and hence the generalized expressions for these parameters have been obtained which are useful for simulation purpose.

It is observed that the effect of optical radiation (having energy greater than or equal to bandgap) is negligible on the parameters whereas temperature and hydrostatic pressure have noteworthy effect. The bandgap energy is found to increase with temperature and decrease with pressure. The electron mobility increases with temperature initially due to weak scattering rate and at elevated temperatures, it decreases because of increased scattering. With the pressure, the mobility decreases. Using this study, an analytical model for GaAs MESFET has been carried out.

Session 2Pc4

Electromagnetic Scattering by Nonspherical Particles

Optimum Configuration for Polarisation Photon Correlation Spectroscopy

P. C. Y. Chang
School of Electrical and Electronic Engineering, University of Nottingham
Nottingham, UK

K. I. Hopcraft and E. Jakeman
Theoretical Mechanics Division, School of Mathematical Sciences, University of Nottingham
Nottingham, UK

J. G. Walker
School of Electrical and Electronic Engineering, University of Nottingham
Nottingham, UK

Polarization Photon Correlation Spectroscopy (PPCS) uses correlations between the fluctuations in different polarization components of scattered light to deduce information about the shape of the scattering particles in addition to the size information available from conventional Photon Correlation Spectroscopy (PCS). The technique exploits a generalisation of the well-known Siegert relation or factorisation theorem of Gaussian light to include polarization, namely

$$\varepsilon_{ab}(\tau) = \frac{\langle I_a(t) I_b(t+\tau)\rangle}{\langle I_a\rangle\langle I_b\rangle} = 1 + \frac{|\langle E_a(t) E_b^*(t+\tau)\rangle|^2}{\langle I_a\rangle\langle I_b\rangle} \tag{1}$$

Here the subscripts on the intensity, I, and fields, E, refer to different polarisation states, denoted by a and b, of the scattered radiation for a given input state. The deviation of this intensity cross-correlation function at zero delay time from the value of two, expected for spherical particles, provides a measure of particle shape. The experimental arrangement used in such measurements is similar to that used in PCS and requires that the particles are sufficiently numerous for the scattered coherent light to be in the Gaussian scattering regime, but sufficiently sparse for multiple-scattering effects to be neglected. The cross-correlation function of intensities scattered into separate polarization states depends on the input polarization state, the scattering angle, relative refractive index of the particles and their shape, and this information can be used to recover the aspect ratio of the particles.

In this paper, combinations of input and output polarization states are analysed for their sensitivity to photon noise and other experimental uncertainties and optimal configurations for the instrument are identified. The optimum configurations are to illuminate with light whose polarization is

1. in the plane 45° to the horizontal and by detecting and correlating the scattered horizontal and vertical components

2. left-circularly polarized and detecting and correlating the scattered left and right circularly polarized states.

The robustness of the technique in these configurations is demonstrated by reconstructing from experimental data the aspect ratios of particles having a variety of sizes and shapes.

Statistics of the Scattered Intensity by Two-Particle Systems

S. Cotera, F. Moreno, J. M. Saiz, and F. González
Departamento de Física Aplicada, Grupo de Óptica, Universidad de Cantabria
Santander, 39005, Spain

G. Vidden
Army Research Laboratory, AMSRL-CI-EM
Adelphi, MD 20783, U.S.A.

Many years ago, it was shown [1] that the statistical analysis of the scattered radiation (in particular, that of the factorial moments of its statistical fluctuations) in the non-Gaussian regime (a few effective scatters in the scattering region) is a powerful tool to obtain information of particle scattering system when the particles scatter as independent. Much more recently, a lot of research has been done about wave propagation through random media where multiple scattering is an important effect. The statistical analysis of the speckle fluctuations produced when light propagates through disordered media has constituted an important part of that research.

The purpose of this contribution is to go deeper in understanding of the scattered light statistics of particle scattering systems when multiple scattering has a non-negligible contribution. In particular, we focus on the analysis of the second order factorial moment of the intensity fluctuations and its relation to particle interaction. Both, particles in a volume (scattering volume case) or particles on a substrate (scattering surface case) are considered. A two dipole-like particle model is adopted because its simplicity allows to extract the physical information in an easier way. Previously, the two-particle model has been successfully used by other authors for studying the enhanced backscattering effect [2] and the frequency shift of localized plasmons in small particles [3].

Numerical calculations of the scattered intensity have been performed using the coupled dipole method for the scattering volume case and the coupled dipole method plus the image theory [4] for the scattering surface case. The polarizability, α, has been chosen to evaluate the strength of particle interaction.

REFERENCES

1. Pusey P. N., "Statistical properties of the scattered radiation", *Photon Correlation Velocimetry*, H.Z. Cummins and E.R. Pike (Eds.), NATO ASI Series: Series B, Physics, Vol. 23, pp. 45-141, Plenum Press, New York 1977.
2. Ismagilov F.M., Kratsov Y.A., "Backscattering enhancement polarization effects on a system of two small randomly oriented scaters", *Waves in Random Media*, Vol. 3, pp. 17-24, 1993.
3. Markel V.A., "Scattering of light from two interacting spherical particles", *Journal of Modern Optics*, Vol. 39, no. 4, pp. 853-861, 1992.
4. Moreno F., González F. Eds, *Light Scattering from Microstructures*, Springer-Verlag, Berlin, 2000.

Two-dimensional Angular Optical Scattering (TAOS): Analysis of Aggregate Scattering

S. Holler
Sandia National Laboratory
Albuquerque, NM 87185-1423, U.S.A.

G. F. Crosta and S. Zomer
Department of Environmental Sciences, University of Milan, Bicocca
Milan, I 20126, Italy

Y.-L. Pan
Department of Applied Physics, Yale University
New Haven, CT 06520-8284, U.S.A.

J. R. Bottiger
U.S. Army Edgewood Chemical Biological Center
Aberdeen Proving Ground, MD 21010-2742, U.S.A.

R. K. Chang
Department of Applied Physics, Yale University
New Haven, Connecticut 06520-8284, U.S.A.

Real-world aerosols are often non-spherical conglomerates of smaller primary particles. The myriad of intricate non-spherical particles that exist precludes the use of Mie theory for studying their scattering properties. The increased complexity associated with the aggregation of smaller particulates leads to a corresponding complexity in the intensity distribution of the angularly scattered light; gone is the familiar ring structure associated with Mie scattering from spherical obstacles. A complicated speckle pattern emerges due to the interference of light scattered from different primary particles that are in close proximity to each other.

In this paper we present the two-dimensional angular optical scattering (TAOS) from aggregates containing several different micron-sized spherical primary particles. Clusters of primary particles are generated by an ink-jet aerosol generator (IJAG) and are illuminated by a pulse from the second harmonic (532 nm) of a Q-switched Nd:YAG laser. The scattered light is collected with a camera lens used in the Abbé sine condition. The light then emerges parallel and is record with an intensified-CCD (ICCD) array. The data is then stored on a computer for future analysis.

The features of these TAOS patterns are studied using a principal components analysis (PCA) technique. Here the Euclidean distance (on the ICCD array) between the peaks and valleys in the TAOS patterns is used to define the variables for the PCA. Using PCA allows us to seek out patterns in the TAOS data, and based on the principal components of known samples, we may construct basis TAOS images that may be used to characterize unknown aerosols.

Implementation of the PCA technique will allow for a greater understanding of the relevant parameters in TAOS data from aggregates while also leading to enhanced characterization and improved methods for the inverse scattering problem.

Finite Groups in the Surface Green's Function and T-Matrix Formulations of Electromagnetic Scattering

F. M. Kahnert
Department of Physics, University of Bergen
Bergen, 5007, Norway

Electromagnetic scattering computations based on rigorous theory can place considerable demands on computer time and memory resources, especially when considering ensembles of particles consisting of many different sizes and geometries. This paper discusses how the electromagnetic scattering solution simplifies for particles with discrete symmetries. Two different formulations of the electromagnetic scattering problem are considered— the surface Green's function (SGF) formulation and the T matrix formulation.

Particles with discrete symmetries can be classified by finite groups (so-called point-groups) that contain all the symmetry elements of a given particle. For each point group one can identify a minimum set of symmetry elements that give rise to independent symmetry relations of the electromagnetic scattering solution. This is demonstrated by using the T matrix formulation of the scattering problem. For each of these symmetry elements it is straightforward to derive symmetry relations of the T matrix.

Symmetry relations are also derived for the SGF of star-shaped padrticles with discrete symmetries. The symmetry relations of the SGF are shown to be equivalent to those of the T matrix. It turns out that the symmetry relations of the SGF are simpler to derive and more appealing to intuition than those of the T matrix. In addition, the SGF concept prrovides a link between surface integral methods and finite-difference methods. This amy open up the possibility to exploit finite groups in finite-difference methods in teh future. On the other hand the symmetry relations of the T matrix can be readily used in practical implementations.

Exploiting finite groups in the null-field method leads to a substantial reduction in computer resource requirements. For a point-group of order M the CPU time for the T matrix computation is reduced by a factor of M^2. Depending on the point-group this can amount to several orders of magnitude. For ensembles of randomlu oriented particles the CPU time for the analytic procedure for orientational averaging is reduced by a factor of M. It is shown that the necessary matrix inversion in the null-field method can be performed with LU-decomposition without destroying the symmetry-related sparsity of the matrix.

Application of Electromagnetic Scattering by Nonspherical Particles to Remote Sensing of Clouds and Aerosols

K. N. Liou, Y. Takano, and S. C. Ou
Department of Atmospheric Sciences, University of California, Los Angeles
Los Angeles, CA 90095-1565, U.S.A.

P. Yang
Department of Meteorology, Texas A&M University
College Station, TX 77843, U.S.A.

We discuss the application of the results of electromagnetic scattering by nonspherical particles to the remote sensing of clouds and aerosols using bidirectional reflectance and polarization. The theories for light scattering by ice crystals and nonspherical aerosols developed by the authors are first reviewed, followed by a presentation of the transfer of solar radiation in randomly and horizontally oriented particles. We then describe the principle of the remote sensing of cirrus cloud optical depth and ice crystal size based on the correlation technique and present pertinent results using two solar channels on AVHRR/NOAA and MODIS/TERRA satellites. Finally, the feasibility of determining the cloud thermodynamic phase, and ice crystal shape and orientation using the reflected polarization of sunlight is further presented.

Effective Medium Approach to Aggregate Scattering

D. W. Mackowski
Department of Mechanical Engineering
201 Ross Hall Auburn University
Alabama, AL, U.S.A.

Formulations and algorithms are discussed to approximate the scattering by aggregated particles. The approach is to use an effective medium model to obtain a moment solution to the multiple sphere interaction equations. The T matrix for the aggregated particle obtained in this way will maintain the energy conservation, convergence, and origin invariance properties required of the T matrix. Comparisons are made between effective medium and exact results for various configurations of aggregated spheres, and results are very promising. In addition, the application of the method to the discrete dipole approximation is discussed. It is shown that the resulting discrete dipole moment method (DDMM) provides a relatively simple and efficient means to calculating the T matrix for an arbitrarily nonspherical particle. Comparisons are presented between DDMM, EBCM, and standard DDA approaches for calculating the T matrix.

Geometrical Renormalization Approach to Optical Properties of Fractal Nanoaggregates

V. A. Markel
Department of Radiology, Washington University
St. Louis, MO 63110, U.S.A.

Optical properties of fractal aggregates of small nanometer-sized particles have been intensively studied during the past two decades. There are two important classes of such systems: aggregates of noble metal particles (typically, silver or gold) in colloidal solutions and different soots that form at high temperatures during combustion. The former are interesting because they exhibit a number of fascinating nonlinear optical effects which are, generally, explained by strong fluctuations and enhancement of local fields on subwavelengths scales. The optical properties of soot attracted attention because of its importance for atmospheric physics, climate research, remote sensing of fires, etc.

The usual physical model for fractal aggregates described above is agglomerates of identical spheres which are small compared to the incident wavelength. Although rigorous numerical methods for solving the electromagnetic scattering problem for such systems has been developed, they are not always practically applicable. In metal aggregates, the electromagnetic interaction is very strong in both visible and IR spectral ranges which makes application of the usual numerical or theoretical approaches not feasible. The same is true for carbonaceous soots in the far IR spectral region.

To overcome these difficulties, we have proposed a method which is based on a geometrical renormalization of fractal clusters. The method is statistical in nature. It replaces a random ensemble of aggregates by another ensemble with geometrically intersecting primary spheres whose number and size are renormalized, but keeps unchanged the total volume of material, average gyration radius of the clusters and the density-density correlation function. The method allows to enormously simplify the problem while keeping the important characteristics of the physical system under investigation unchanged. In my talk I'll review the formulation and justification of this method, its application to several problems of practical interest, and comparison of the obtained results with experimental data.

Scattering Matrix of Quartz Aerosols: Comparison of Laboratory and Lorenz-Mie Results

M. I. Mishchenko and L. Liu
NASA Goddard Institute for Space Studies
New York, NY 10025, U.S.A.

This paper compares the results of laboratory measurements of the Stokes scattering matrix for nonspherical quartz aerosols at a visible wavelength in the scattering angle range $5°$-$173°$ and the results of Lorenz-Mie computations for projected-area-equivalent spheres with refractive index of quartz. A synthetic normalized phase function is constructed based on the laboratory data and the assumption that the diffraction forward-scattering peak is the same for spherical and nonspherical projected-area-equivalent particles. We demonstrate that the scattering matrix for the nonspherical quartz particles is poorly represented by the Lorenz-Mie results, whereas the asymmetry parameters for the synthetic phase function and for the equivalent spherical particles are similar. Implications of these results for atmospheric remote sensing are discussed.

Solving Nonspherical Boundary Value Problems by Use of the Method of Lines - The Surface Green's Function

T. Rother
German Aerospace Center
Wessling, Germany

Conventional Finite-Difference techniques have been widely applied to solve nonspherical boundary value problems like light scattering on nonspherical particles, for instance. Although being simple in concept and execution these methods are accompanied with two essential disadvantages if compared to surface integral equation approaches.

The first drawback is concerned with the fulfilment of the radiation condition at infinity. Due to the necessary finite discretization volume this nonlocal condition must be replaced by a local approximation, the so-called Absorbing Boundary Condition. Different types of Absorbing Boundaries are known but it is often a difficult task to choose that one which is matched best to a certain problem. Surface integral equation techniques are not suffering from this disadvantage since employing the free-space Green's function. This function incorporates the radiation condition analytically.

The second drawback is related to the process of orientation averaging – a necessity in remote sensing applications, for instance. Within the conventional Finite-Difference methods each new orientation of the same scatterer requires a new solution of the whole problem. With surface integral equation approaches a decoupling of the physical constitution and geometry of the scatterer from its orientation in the incident field can be achieved. This results in much less computational effort to perform orientation averaging.

These two disadvantages of the conventional Finite-Difference techniques are overcome with the Method of Lines, a special Finite-Difference approach which applies the discretization scheme to the angular coordinates only. The radial coordinate remains unaffected. The Method of Lines is the mathematical background of the Discretized Mie formalism we have developed recently to treat light scattering problems on nonspherical particles. In this paper we will demonstrate how we can derive the corresponding surface Green's function belonging to the Helmholtz equation in spherical coordinates. The boundary values are assumed to be given on a nonspherical but sufficiently smooth boundary surface. This reveals new and interesting conceptional aspects not only of the Method of Lines but also of the conventional Finite-Difference techniques. We will demonstrate the strong relation to the Separation of Variables method and resulting consequences.

Light Scattering on Finite Hexagonal Ice Crystals

K. Schmidt and J. Wauer
German Aerospace Center, Remote Sensing Technology Institute
Neustrelitz, D-17235, Germany

T. Rother
German Aerospace Center, Remote Sensing Technology Institute
Wessling, D-82234, Germany

Cirrus clouds play an important role in the Earth radiation budget and climate system. Depending on their optical thickness and microphysical properties cirrus clouds may either heat or cool the earth surface. Natural ice crystals in cirrus clouds tend to be highly irregular. However, hexagonal shapes are also of some importance especially in producing well-known halo phenomena or as basic constituents of more complex ice particles. Since the scattering characteristics of ice crystals differ significantly from that of spherical droplets it is important to have a more realistic phase function for these non-spherical particles in remote sensing applications and climate modeling. The computation of such phase functions in moderate size parameter regions still represents a problem. This is due to fact that, on one hand, ray-tracing techniques valid for sufficiently large particles can not be applied for smaller scatterers and, on the other hand, approaches like the Discrete Dipole Approximation can be employed only with extravagant expenses or even fail for larger objects. Therefore, the scattering behaviour of ice particles with moderate size parameters has been often modeled by prolate/oblate spheroids or finitely extended circular cylinders in using the Anomalous Diffraction Theory and Watermans T-matrix approach, respectively. In recent years, Finite Difference Time Domain techniques have been successfully applied to infinite and finite hexagonal cylinders. But these methods have an essential disadvantage if the scattering problem in open spaces is considered. It is related to the requirement of a finite discretization volume. Absorbing boundary conditions must be introduced which allow only an approximate fulfillment of the non-local radiation condition.

Alternatively, we developed a generalization of the Separation of Variables Method for infinitely extended but non-circular cylinders and, based on this rigorous approach, an approximation to finite non-circular cylinders by applying Huygens principle. Both approaches allow an exact incorporation of the radiation condition.

In our talk we want to present numerical results for finite hexagonal ice crystals. These results are again obtained within a generalization of the Separation of Variables Method. For checking their accuracy comparisons with recently published numerical values, gained within the same method, are given. The results are also compared with the former mentioned approaches for infinitely and finitely approximated hexagonal cylinders, and the relevance of the latter approaches is discussed.

Radiative Properties of Ice Crystals within Cirrus Clouds: Effect of Particle Morphology and Size

P. Yang
Department of Atmospheric Sciences, Texas A&M University, TAMU 3150.
College Station, Texas, U.S.A.

K. N. Liou
Department of Atmospheric Sciences, University of California.
Los Angeles, CA 90095, U.S.A.

Ubiquitous ice clouds or cirrus located in the upper portion of the troposphere or the lower part of the stratosphere constitute a unique and important component of the terrestrial atmosphere. The effect of these clouds has been identified as being largely uncertain in atmospheric research. In recent years, the atmospheric radiative transfer and remote sensing community has made a concerted effort to improve the characterization of cirrus clouds. A number of airborne and balloon-borne observations have demonstrated that cirrus clouds are essentially composed of nonspherical ice crystals with various habits (or shapes) and sizes. In our previous effort, we have developed several numerical models to calculate the single-scattering properties of nonspherical ice crystals with small and large size parameters. In this paper, we report some recent progresses concerning single and multiple scattering by nonspherical ice crystals.

Atmospheric radiation in the terrestrial window region (8-12μm) contains a wealth of information that is useful for the retrieval of ice cloud properties. We have successfully applied the finite-difference time domain method to small compact (i.e., particles with aspect ratio of unity) nonspherical ice crystals with sizes up to 40 μm. For particles larger than 40 μm, the stretched scattering potential method, a modified version of the eikonal approximation, has been developed to calculate the extinction and absorption efficiencies. To calculate the phase function of large ice crystals at the strong absorbing spectral region, an asymptotic method based on the principles of geometric optics can be employed, which fully accounts for the inhomogeneity of refracted wave.

It is a common practice in cirrus study to assume that the habits and sizes of ice crystals are vertical uniform though it is not the case in reality. Using in situ microphysical data, we have investigated the effect of the vertical variation of particle sizes and shapes on the bulk radiative properties of cirrus. It is shown that the effect is small at visible wavelength. On the contrary, this effect can be potentially large at near-infrared wavelength. In addition, it has been noticed that the small particles at the top portion of cirrus clouds are important to cirrus bi-directional reflectance. The "quasi-spherical" concept applied to these small particles is quite misleading. We have defined a droxtal geometry on the basis of observation for light scattering calculation concerning natural small ice crystals. In addition to particle geometry, we also show that the ice crystal size is critical to the optical properties. As a result, the bin resolution used to discretize size distribution can substantially affect the simulated bulk optical properties of cirrus clouds.

Optical Scattering at Resonance and Pattern Measurement in Large Angles

Y.-L. Pan, K. Aptowicz, and R. K. Chang
Department of Applied Physics, Yale University
New Haven, CT 06520-8284, U.S.A.

Real-time characterization of airborne particles by optical scattering continues to be a challenge in fundamental research and applications. The angular distribution of elastic optical scattering is mainly dependent on the particle's shape, size, and refractive index. This distribution becomes more complicated when the particle acts as a microcavity and the whispering gallery modes (WGMs) are on or off resonance. Theory has successfully predicted the internal field distribution and scattering properties of various shapes of particles and even clusters. However, novel experiments are needed for various shapes of particles and clusters in order to test and challenge the theory.

In this paper, we first present the optical scattering results from a square-shaped μ-cavity (with 200μm edge fused silica, n=1.456) on or off resonance. We achieved greater than 75% energy transfer to the WGMs at resonance by evanescent-wave coupling via using a prism with frustrated total internal reflection. The coupling efficiency and the WGM linewidth of the resonances were found to be dependent on the prism-cavity coupling gap as well as the angle and position of the incident light on the prism surface. Such multimode elastic scattering also can be obtained by focusing the incident beam along one square edge. The scattering properties were greatly changed when the square-shaped dielectric fiber is illuminated uniformly by a plane wave in steady of focused along the cavity face.

Second, we present the two-dimensional angular optical scattering (TAOS) patterns that span huge range of angles. In the experiment, an ellipsoidal reflective mirror and an ICCD detector were used for collecting and detecting scattering light. Assume θ is the angle from the illuminating light propagating (Z or -Z) direction, and ϕ is the angle on the X-Y plane from X-axis and rotated about the Z-axis, TAOS patterns over large angle (θ ranges from 20° to 120° or 60° to 160°, and ϕ ranges from 0° to 180°) were recorded. If the illuminating light was aligned to propagate perpendicular to the mirrors optical axis, the near forward and near backward TAOS in large angle (θ ranges from 10° to 50° and from 130° to 170°, and ϕ ranges from 0° to 180°) can be recorded simultaneously. This novel design greatly increases the TAOS information for single-shot illumination of single particle.

Session 2Pc5

Earth's Subsurface Electromagnetic Imaging and Inversion

A New Inversion Algorithm Based on Fast and Accurate Approximations of Electromagnetic Scattering

C. Torres-Verdín and G. Gao
The University of Texas at Austin
Austin, TX, U.S.A.

T. M. Habashy
Schlumberger-Doll Research
Ridgefield, CT, U.S.A.

We have developed a nested loop optimization algorithm to approach the solution of large-scale inverse electromagnetic (EM) scattering problems. The algorithm is based on the iterative minimization of a quadratic cost function that includes both data and model penalty functions. There are two nested loops used in the construction of the algorithm. First, an inner minimization loop is constructed with the use of approximate solutions to the electromagnetic scattering problem. Specifically, we have made use of Born, Extended Born, and Modified Extended Born EM scattering approximations to construct the inner-loop minimization algorithm. This inner loop is a stand-alone minimization entirely based on an approximation to the forward problem and hence can be solved in a very efficient and expeditious manner. Once the inner-loop minimization is completed, a model solution is obtained and entered into an accurate numerical EM solver to quantify the corresponding fit to the measurements. If the discrepancy between the simulated data and the measurements is large, we use that discrepancy to start a new inner-loop minimization algorithm. The process repeats itself to provide a monotonic decrease of data misfit, and is halted when the fit to the measurements falls within the expected tolerance. An intrinsic advantage of the nested-loop inversion procedure is that at no point in the algorithm does one need to explicitly compute an accurate solution for the Jacobian matrix of the cost function. The algorithm only requires a small number of accurate simulations of the measurements and this represents a considerable improvement in computer performance. We describe and quantify the conditions whereby the nested-loop minimization algorithm will produce model solutions consistent with those obtained using a rigorous Gauss-Newton minimization strategy.

Examples drawn from EM well logging applications are used to illustrate the relative benefits of the algorithm with respect to standard inversion procedures. We also present an analysis of the efficiency of the algorithm based on the type of approximate EM scattering solution used to construct the inner-loop minimization. In addition to Born, Extended Born, and Modified Extended Born scattering approximations, we have implemented a variety of approximate scattering solutions stemming directly from natural preconditioners of the Method-of-Moments stiffness matrix. The latter strategy provides us with practically unlimited possibilities to improve the accuracy and computer efficiency required for the solution of the inner loop minimizations.

A Fast Preconditioner for the 3D Electromagnetic Inverse Problems

G. A. Newman
Sandia National Laboratories
Albuquerque, NM 87185-0750, U.S.A.

M. J. Tompkins
University of Wisconsin-Madison
Madison, WI 53706, U.S.A.

Storage and computational issues can make Newton and Gauss-Newton solution approaches to the 3D electromagnetic (EM) inverse problems prohibitive, especially when realistic problem geometries are considered. Given these considerations, a common approach to the problem is to employ gradient type methods in the solution process, including conjugate gradient and steepest-descent techniques. A drawback of gradient type methods is their slow convergence rates. To overcome this limitation we have developed a preconditioning scheme, that when combined with a gradient-type search for the solution, accelerates the convergence rate by a three to four fold factor with a similar reduction in computational run time. The effect of the preconditioner is to change the search direction produced by the gradient-type method to a direction that economically approximates the Newton direction. Application of the preconditioner results in significant savings in computational time and storage compared with solution treatment based on a Newton or Gauss-Newton approach. Key to the method is the use of approximate model sensitivities in the preconditioning step. The method has been applied to both synthetic and field 3D crosswell data sets with encouraging results.

Three-Dimensional Cross-Well Electromagnetic Imaging Based on the Localized Quasi-Linear Approximations

M. S. Zhdanov, K. Yoshioka and E. Tartaras
University of Utah, Department of Geology and Geophysics
Salt Lake City, UT 84112, U.S.A.

In this paper we develop a new technique for 3-D cross-well electromagnetic imaging using the localized quasi-linear (LQL) approximation for forward modeling and focusing inversion. The quasi-linear approximation has proven to be a powerful tool in electromagnetic forward modeling. It is based on an assumption that the anomalous electrical field within an inhomogeneous domain is linearly proportional to the background (normal) field through an electrical reflectivity tensor λ. In the original formulation of the quasi-linear approximation (Zhdanov and Fang, 1996), this tensor was determined by solving a minimization problem based on integral equation for the scattering currents. However the electrical reflectivity tensor depends on the illuminating (background) field. In other words, for any new position of the transmitter we have to recalculate the tensor coefficient λ. This slows down the calculations for multi-array sources, which are typical for many geophysical applications, for example for a cross-well tomography, or for well logging modeling and inversion. In this paper we use a new approach to quasi-linear approximation based on so-called localized electrical reflectivity tensor that is independent on the source position. It is based on ideas similar to those developed by Habashy et al. (1993) for localized nonlinear approximation.

We develop a new fast 3-D EM inversion method using the LQL approximation. The modern inversion methods are usually based on Tikhonov regularization that provides a stable solution of the inverse problem. This goal is reached, as a rule, by introducing maximum smoothness stabilizing functional. It is important to emphasize, however, that regularization doesn't necessarily mean the "smoothing" of the solution. The main basis for regularization is an implementation of a priori information about the geological structure in the inversion procedure. The traditional inversion algorithms providing smooth solutions for geological structures have difficulties in describing the sharp boundaries between different geological formations, while in real geological situations the sharp boundaries may constitute an important goal of interpretation. In these situations, it can be useful to search for the stable solution within the class of inverse models with the blocky geological structures.

The mathematical technique for solving this problem is based on the minimum support or minimum gradient support stabilizing functionals. We call this technique a focusing regularized inversion to distinguish from the traditional smooth regularized inversion. We develop a method of cross-well electromagnetic imaging based on the combination of the LQL approximation for the forward modeling and the focusing inversion. The numerical examples demonstrate effectiveness of this technique in 3-D cross-well electromagnetic imaging.

3-D Fast Forward and Inverse Methods for Subsurface Electromagnetic Induction Sensing

Z. Q. Zhang and Q. H. Liu
Duke University
Department of Electrical and Computer Engineering
Box 90291
Durham, NC 27708, U.S.A.

Electromagnetic induction (EMI) is an important technique for geophysical subsurface sensing. Applications of EMI subsurface sensing include resources exploration, environmental site characterization, detection and characterization of landmines and unexploded ordnance (UXO). In oil exploration, induction tools are also used inside a borehole to measure the conductivity distribution in rock formation.

Three-dimensional forward and inverse problems are essential for interpretation of EMI measurements. However, conventional methods such as finite-element, finite-difference, and method of moment methods can only solve small scale 3-D problems. We have developed an efficient stabilized biconjugate-gradient fast Fourier transform (BCGS-FFT) method for the 3-D forward EMI method. It solves the volume electric field integral equation through the weak-form discretization. The convolution of induced sources with the Green's function is accelerated by the FFT algorithm, and the discretized system of equations is solved by a stabilized biconjugate-gradient method. This BCGS-FFT method has been applied to solve unprecedented 3-D electromagnetic wave scattering problems of up to 21 million unknowns. For large scale EMI problems, the BCGS-FFT method is even more efficient as the number of iterations is small for induction problems. The total computational complexity of this method is $O(N \log_2 N)$.

Our 3-D inverse solver for EMI problems is based on the extended Born approximation (EBA) preconditioned contrast source inversion method. This method combines the advantages of the EBA and CSI methods, reducing the number of iterations. We have applied this preconditioned contrast source inversion (PCSI) method for large scale 3-D inverse problems. Numerical results will be presented to demonstrate the applications of these fast forward and inverse EMI solvers.

Level Set Methods for Cross-Borehole ERT

M. Khames Ben Hadj Miled and E. L. Miller
Center for Subsurface Sensing and Imaging Systems, Northeastern University
Boston, MA, U.S.A.

Electrical resistance tomography (ERT) is a widely used method for earth subsurface imaging with applications in fields such as geophysical prospecting and environmental monitoring and remediation. Typical inversion methods are based on the solution to a non-linear optimization problem and address the ill-posed nature of this inverse problem through the use of a Tikhunov-type of functional to enforce a degree of smoothness in the recovered profile. The profile itself is based on a fine scale voxelation of the region of interest. In this paper we explore an alternate inversion strategy based on the realization that for many problems one does not necessarily require information about a large number of voxels, but rather the goal is to localize particular structures of interest: mineral deposits, pollution plumes, etc.

For problem with these characteristics there has been significant interest in the use of "shape-based" methods for explicitly recovering the geometry of the object. Techniques employing parametric representations of contours in two dimensions (such as B-splines, Fourier descriptors and the like) have been proposed for a variety of inverse scattering problems. More recently, curve evolution methods based on level set evolution have received considerable attention. Compared to other alternatives, level sets are distinguished by their natural ability to describe and track moving boundaries for multiple, disconnected regions without a need for a prior knowledge on their number and localizations or any constraints on their shapes. By definition, a level set function is an infinite number of contours that propagate according to a space varying velocity function. In our approach, we explore the flexibility in defining such a function as a remedy for the inherently low sensitivity (which leads to the ill-posedness) found in the ERT problem. Extending the current state of the art in the use of level sets for known binary media, we describe both 2-D and 3-D implementations for the N-ary problem both when the contrasts of the object as well as the background are and are not known. Results using synthetic as well as experimental data from lab-level ERT testbeds will be provided to validate the practical utility of the method.

A Level Set Method for Shape Reconstruction in 3D Electromagnetic Induction Tomography

O. Dorn
Department of Computer Science, University of British Columbia
Vancouver, B.C. V6T 1Z4, Canada

We present a novel two-step nonlinear shape reconstruction algorithm which combines the advantages of the so-called *adjoint-field inversion technique*, the *level set technique* for modelling propagating interfaces, and the *fast forward modelling code EH3D*, for achieving fast, fully 3D inversions from relatively few electromagnetic surface-to-borehole data.

A key point of the scheme is the use of the *level set technique* for modelling and propagating the shapes during the reconstruction process. Since the number of obstacles which we are looking for is not known a priori, topological changes of these shapes typically occur in the iterative reconstruction process and a flexible tool for tracking the boundaries of the shapes is therefore of great importance for the success of the reconstruction method.

We have chosen to use the level set technique for describing the moving shapes, since this method is able to easily model topological changes of the boundaries. In this technique, the shapes are given as the zero level set of a higher dimensional level set function f, which in our case is a function from $\mathbb{R}^3$ to $\mathbb{R}$. Those points $x \in \mathbb{R}^3$ where $f(x) = 0$ define the boundaries of the shapes. If we change the function $f(x)$, for example by adding an update $\delta f(x)$, we move the shapes accordingly. This relation is used in the level set technique when constructing updates $\delta f(x)$ to a given level set function $f(x)$ such that the shapes are deformed in a way which decreases a given cost functional. This iterative reconstruction scheme starts with the result of a preprocessing step which is based on the adjoint field inversion technique.

In our numerical experiments, the propagation of the electromagnetic fields is described by the full 3D system of Maxwell's equations in the frequency domain. As sources we use large horizontal electric current loops at the surface, and the receivers are small horizontal electric wire loops which are distributed in several boreholes surrounding the domain of interest. The electric conductivity has to be recovered from the data gathered at a frequency of 1 KHz.

We show that the presented shape reconstruction algorithm is able to provide stable reconstructions of one or more objects in the earth with good accuracy from relatively few data if approximate values of the parameters inside these objects are given and the (typically inhomogeneous) background is known. We also discuss possibilities to extend the presented method to the simultaneous reconstruction of the shapes and the contrast of the sought object.

This is joint work with E. Haber, D. Oldenburg and U. Ascher (University of British Columbia, Vancouver).

Minimization Methods Applied to Resistivity Logging

A. Litman and L. Jammes
Schlumberger Riboud Product Center
Clamart, France

T. M. Habashy
Schlumberger Doll Research Center
Ridgefield, CT, U.S.A.

In oil exploration, the estimation of oil in place is accomplished by an integrated interpretation of all available logging data. In particular, deep-resistivity measurements are commonly used to provide an estimation of the virgin zone resistivity, which is strongly dependent on the hydrocarbon content of the rock.

However these electromagnetic tools are sensitive to important parasitic effects, such as borehole, invasion or shoulder-bed effects. Traditionally, sequential chart-book type corrections are applied on the logging measurements to estimate a usable value of the virgin zone resistivity. This may lead to inaccurate representation of the rock physical properties and therefore of the estimation of hydrocarbon volumes.

These drawbacks can be overcome by simultaneously taking into account borehole, shoulder and invasion effects through a Forward-Model based inversion technique. Furthermore, with the development of robust minimization algorithms and the availability of fast forward-modeling codes, inversion techniques are becoming a usable tool for the interpreter.

The application that will be presented is based on the following methodology:

1. A zone of interest is selected and represented as a sequence of parallel beds, which are the most appropriate to the downhole conditions from where the logs were obtained. A set of physical / petrophysical properties is assigned to each bed.

2. The minimization algorithm (either a Gauss-Newton, a BFGS or a Levenberg-Marquardt method) is then applied to estimate user-selected parameters (any sub-set of the formation properties can be fixed).

After explaining the methodology and the major difficulties encountered, the influence of the several minimization algorithms will be analyzed via synthetic and real data cases. Results obtained on selected benchmarks extracted from real data will also be presented and compared with those obtained through more traditional approaches. Estimation of associated a-posteriori uncertainties will also be discussed. Finally the influence of a-priori information and the way this information can be introduced in the algorithm will be discussed.

Low Frequency Models and Characterization of an Ellipsoidal Body in the Context of Earth's Exploration

G. Perrusson and D. Lesselier
Département de Recherche en Électromagnétisme
Laboratoire des Signaux et Systèmes (CNRS-SUPÉLEC-UPS)
Gif-sur-Yvette, France

P. Vafeas and G. Dassios
Division of Applied Mathematics, Department of Chemical Engineering,University of Patras,
and ICEHT-FORTH
Patras, Greece

Inductive electromagnetic means that are currently employed in the exploration of the Earth's subsurface and embedded voluminous bodies often call for an intensive use – both at the modeling stage and at the inversion stage – of computationally demanding tools of field calculation, which are usually based on the use of finite differences, finite elements, or method of moments to deal with appropriate partial differential, variational or Green-integral formulations of the (diffusive) wave fields. Even if much studied approximations like those of the extended Born kind might yield considerably faster calculations, they are at risk to fail whenever high contrasts of electric parameters (conductivities) between the bodies (mostly conductive) and the surrounding Earth (mostly resistive) are faced with. On the other hand, simple models that involve equivalent sources representations as those discussed in Bourgeois *et al.*, *Inverse Probl.* 16 (2000) 1225-1262, certainly require a robust expertise of geophysical exploration to be handled properly.

In this contribution, the authors will attempt to confirm that the rather traditional low frequency scattering theory – fields are expanded in positive integral powers of (jk), k complex wavenumber of the exterior medium, the coefficients of the expansions being found by solving a succession of coupled magnetic and electric boundary value problems– can be employed to model the response of an impenetrable (perfectly conducting) ellipsoidal anomaly (possibly reduced to a sphere) to a time-harmonic magnetic dipole placed nearby; then, they will attempt to use that model in order to invert for an equivalent ellipsoidal body in an effective manner synthetic or experimental vector magnetic field data in a borehole nearby.

Today's work is in continuation of Perrusson *et al.*, "Low-Frequency electromagnetic modeling and retrieval of simple orebodies in a conductive Earth," Proc. 3rd ISAAC Congress, Berlin (2001) *submitted*. Static fields have been modeled and confronted to simulated and real data therein, which means that the generally but not necessarily much weaker quadrature component of the anomalous magnetic fields is left aside. Most of the attention is now focused on the mathematical calculation in a proper ellipsoidal system of coordinates and numerical manipulation of the second-order terms (those appearing at power 2 in jk) which enable, in principle, to fit both in phase and quadrature field components.

Image Reconstruction of Buried Cylindrical Objects Using Synthetic Aperture Processing and Inverse Scattering Method

T. Tanaka
Division of System Science, Graduate School of Science & Technology, Nagasaki University
Nagasaki, 852-8521, Japan

T. Takenaka
Department of Electrical & Electronic Engineering, Nagasaki University
Nagasaki, 852-8521, Japan

Ground penetrating radar has been attracting interest in recent years for purposes of detecting pipes, tunnels and other subsurface structures in situations calling for nondestructive exploration and evaluation. Not only the locations and sizes but also the electrical property distributions of buried objects are of interest.

The inverse scattering problem of imaging buried objects can be cast as an optimization problem where a cost functional defined as the difference of the measured field data and calculated field data for an estimate of electrical properties needs to be minimized. A gradient search method is used to minimize the cost functional. In our previous work, the forward-backward time-stepping (FBTS) algorithm was proposed for reconstructing electrical property distributions from the knowledge of measured time-domain field data. This algorithm was shown to be effective for reconstruction of high-contrast objects. However, very long calculation time is required with widening a search region.

Synthetic aperture processing can quickly estimate the location of underground objects. Therefore we combine the synthetic aperture processing with FBTS algorithm. The basic procedure of the combined algorithm is as follows:

1. The location of the buried object is estimated by the synthetic aperture processing, and a vicinity of the estimated location of the object is chosen as a reconstruction region.

2. The inverse scattering method (FBTS algorithm) is applied to the reconstruction region.

3. If the result of reconstruction is not satisfactory, the reconstruction region is expanded, and reconstruction is carried out again using the FBTS algorithm.

The numerical calculations for noise-contaminated data are carried out in order to show the effectiveness of the proposed algorithm.

Constrained Maximum Likelihood Reconstruction with Side Information of Layered Media from Noisy Impulse Reflection Response Measurements

A. E. Yagle
University of Michigan
Ann Arbor, MI, U.S.A.

The one-dimensional inverse scattering problem for a discrete layered medium probed with an impulsive plane wave at normal incidence arises in many areas. For example, the radar reflection from a stratified lossless dielectric medium (such as an airplane skin) can be used to reconstruct the permittivity of the medium in each layer if the magnetic permeability is assumed to be constant. The geophysical subsurface imaging problem for a layered medium in 2-D or 3-D can also be formulated in this way.

The goal of this paper is to present a simple algorithm that computes the constrained maximum-likelihood estimates of the reflection coefficients of a discrete layered medium, from measurements of the impulse reflection response to which a Gaussian noise process with known mean and covariance is added. All multiple reflections are included; no approximations are used anywhere.

The side information is that some of the reflection coefficients are known. Such information could come either from previous knowledge of a homogeneous slab inside the layered medium, or from thresholding small noisy estimates of the reflection coefficients. Such thresholding strategies are common in signal processing applications, so this is useful in this regard.

It is important to note that due to the nonlinearity of the exact (meaning all multiple reflections included) inverse scattering problem, we cannot solve this problem by simply setting the noisy reconstructed reflection coefficients to their known values. Note that we could do this in the Born approximation (linearization of the inverse scattering problem), but the nonlinearity implies that alteration of (interface) reflection coefficients will produce a complex alteration of the impulse reflection response. Two almost-identical impulse reflection responses can arise from two very-different sequences of (interface) reflection coefficients.

Our procedure is simple, noniterative, and requires only solutions of systems of linear equations. Examples show that it is necessary to alter some of the non-constrained reflection coefficients, as well as the constrained ones, to obtain the maximum-likelihood estimate. We also show that the side information improves reconstruction of UNCONSTRAINED reflection coefficients, as well as constrained ones, due to the nonlinearity of the inverse scattering problem. Examples include discrete layered media and a continuous 1-D inverse scattering problem with reflectivity function a realization of a $1/f$ fractal process, except in a known band.

Session 2Pb6

Pattern Synthesis for Antenna Arrays

Pencil Beam Pattern Synthesis with a Uniformly Excited Multi-Ring Planar Antenna

M. Vicente-Lozano, F. Ares, and E. Moreno
Grupo de Sistemas Radiantes, Dept. de Física Aplicada
Facultad de Física, Universidad de Santiago de Compostela
Santiago de Compostela, 15706, Spain

Phased array antennas are often used in radar systems for seeking and tracking multiple targets, and in commercial satellite communications systems. Their main drawback in comparison with reflector antennas is their high cost: the number of elements needed is usually large, and the beam-forming network complex and expensive. When power is strictly limited, as in the case of satellite-borne antennas, a further problem is the need to balance effective isotropic radiated power (EIRP) against sidelobe level (SLL): the former can be maximized by exciting all the elements equally at the highest possible power level, but for arrays with conventional geometry this produces power patterns with higher sidelobes than are tolerable in satellite communications.

We show a method that improves some previous solutions to this problem. The simulated annealing technique is used to determine ring radii that afford optimal performance in multiring antennas with circular patches excited with circularly polarized signals. Pencil beam patterns with low sidelobes and good directivity can be synthesized for those multi-ring antennas with small numbers of uniformly excited elements. In this case there is no accompanying power loss, and the pencil beam can be easily scanned in the usual way by introducing a phase factor.

In this work we obtain examples with 10 rings with $4n$ and $8n$ elements per ring ($n =$ number of ring) that show the effectiveness of the method.

Arbitrary Footprint Patterns from Planar Arrays with Complex Excitations

A. Trastoy, F. Ares, and E. Moreno
Universidad de Santiago de Compostela, Spain
Santiago de Compostela, Spain

A procedure for synthesizing arbitrarily shaped footprint patterns with controlled side lobe level and ripple using planar arrays with complex excitations is presented. This method extends a method due to Ares et al. [1] for synthesizing shaped patterns using a real modified Taylor distribution to apertures and arrays with complex excitations. Since the use of complex excitations allows a given footprint to be synthesized using a smaller array than with real excitations, this procedure provides the best performance for arbitrary footprint patterns from planar arrays. As a example, for a square footprint pattern generated by an equispaced squared rectangular grid of no more than 24 elements long, compared with the performance achieved for the same array size when real excitations are used, footprint size and ripple are approximately halved, and the dynamic range ratio is reduced by about two orders of magnitude.

The method involves two steps; firstly, a transformation P is accomplished that shrinks or stretches a virtual circular aperture in each direction φ so that its radius in that direction is inversely proportional to the desired beamwidth in that direction [1]; the array grid is then trimmed to the resulting shape, and each remaining element E, with coordinates (α_E, β_E), is assigned the excitation corresponding to the point $P^{-1}(\alpha_E, \beta_E)$ of a modified complex circular Taylor distribution [2]. Secondly, an optimization procedure (the Simulated Annealing) that provides the best modified complex circular Taylor aperture for the desired pattern is undertaken. A cost function containing both terms measuring the difference between the synthesized pattern and the desired pattern and terms favouring the efficiency of the excitation distribution is minimized using the complex positions of the roots as variables of the algorithm.

REFERENCES

1. Ares F., R. S. Elliott, and E. Moreno, "Design of planar arrays to obtain efficient footprint patterns with an arbitrary footprint boundary", *IEEE Trans. Antennas Propagat.*, vol. 42, no. 10, pp. 1509–1514, 1994.
2. Elliott R. S., G. J. Stern, "Shaped patterns for a continuous planar aperture distribution", *IEE Proceedings*, vol. 135, Pt. H, no. 6, pp. 366–370, 1988.

Power Pattern Synthesis of Shaped Beam Reflectarrays

J. A. Zornoza and J. A. Encinar
Polytechnic University of Madrid
Madrid, Spain

Because of its easy development, its low cost and its deployable facility, flat printed reflectarrays are becoming an emerging alternative to the bulky, costly and complex onboard reflectors used in DBS applications. In this way, a contoured beam reflectarray based on the previous design of a conformal surface reflector has already been manufactured [1]. Nevertheless, a reliable and efficient method which permits synthesize any required power pattern, with no dependence on reflectors, would be desired. The present paper deals with the study of these possible synthesis methods.

A reflectarray antenna consists on a passive microstrip array illuminated by a feed (a horn in our case of study). Then, it can be established that the reflected field amplitude on each element at the reflective surface, is fixed and imposed by the position and the pattern of the horn (pedestal cosine), meanwhile the phase can be adjusted changing the reflection coefficient of the patches [2]. Taking into account that the far field radiated is closely related to the field at the reflective surface by the Fourier Transform, it can be said that the power pattern synthesis of conformal beam reflectarray is constrained to cases where is only possible to modify the phase distribution of the reflected field at the array. In phased array literature, this kind of synthesis is known as phase-only synthesis.

Iterative numerical methods are required because: a) phase-only power pattern synthesis has a high non-linear nature, and b) a general method capable of reaching any desired pattern is searched.

Two different iterative methods have been implemented. The first one minimizes a multivariable error function, defined as the least-squared error between the desired (called mask) and the computed radiation patterns. The optimization algorithm computes the gradients of the function [3]. The second approach, minimizes the distance between two sets: the objective and the calculated array factors. This method has been used satisfyingly in the synthesis of phased array with amplitude constraints [4]. Both approaches require a good initial point for the optimizations, which is obtained by the superposition of the phase distributions corresponding to individual beams. Some synthesized patterns will be shown at the oral presentation.

REFERENCES

1. D.M. Pozar, S.D. Targonski, and R. Pokuls, "A shaped-beam microstrip patch reflectarray", *IEEE Trans. Antennas Propagt.*, vol. 47, no.7, pp. 1167–1173, Jul. 1999.
2. J. A. Encinar, "Design of two-layer printed reflectarrays using patches of variable sizes", *IEEE Trans. Antennas Propagt.*, vol, 49, no. 10, pp. 1403–1410, Oct. 2001.
3. J. A. Zornoza and J. A. Encinar, "Multi-layer printed reflectarrays as an alternative to shaped reflectors", *24th ESTEC Antenna Workshop on Innovative Periodic Antennas*: Photonic Bandgap, Fractal and Frequency Selective Structures, Noordwijk, Holland, 2001.
4. O. M. Bucci, G. Franceschetti, G. Mazzarella, and G. Panariello, "Intersection approach to array pattern synthesis", *IEE Proceedings*, vol. 137, Pt. H, no. 6, pp. 349–357, Dec. 1990.

Near-Field Beamforming for Hyperthermia Applications Using Waveguide Aperture Arrays

B. P. Kumar and N. Karnik
Department of Electrical and Electronic Engineering
California State University, Sacramento
Sacramento, CA 95819, U.S.A.

G. R. Branner
Department of Electrical and Computer Engineering
University of California, Davis
Davis, CA 95616, U.S.A.

This paper describes the design, fabrication and testing of a multi-element conformal waveguide aperture array. Techniques are described to focus the array in the near-field of array, and to control the focus point of the array. The array contains a central element that serves as the focusing element, and other elements serve as directing elements. The frequency range of the array is the K band range of 18–26 GHz, which enables to get a millimeter range focus resolution. The array is designed with application for microwave hyperthermia applications for the therapeutic treatment of surface and sub-surface tumors in the human body. Preliminary simulation and measured results show good agreement, and confirm the predicted high resolution of the array.

Synthesis of Shaped Beams in Conformal Semi-Active Antennas

L. Vaskelainen
VTT Information Technology
Otakaari, Finland

Semi-active feed system [1] consists of Butler-matrix type circuits, where every output of the circuit is connected to an element in different sector of a circular array antenna. The number of input and output ports in these feed circuits is the number of sectors in a circular array. The power distribution in outputs of the feed circuits can be controlled by phases of the input signals. In this kind of antenna it is thereby possible to direct beams in all azimuth angles around the antenna by phase control of inputs of the feed circuits.

This kind of semi-active feed system can be used also in spherical (or in other conformal) arrays. Elements in the array must be divided for example in four sectors on the sphere. All outputs of the four-port Butler-matrices are connected to elements in different sectors. The distances of elements connected in outputs of the same Butler-matrices should be as equal as possible. Genetic algorithm can be used to find the most optimal connection combination between the elements and the Butler-matrices.

When the geometry is found, a phase synthesis problem of finding the input phases of the feed circuits for a given beam shape must be solved. It will be shown, that any phase synthesis method of conformal array antennas can be used by writing the matrix, which transforms element currents to feed circuit excitations, and by multiplying the original matrix, which gives the field intensity in different directions from element currents, by this transform matrix. One feasible phase synthesis method is published by the author [2].

In synthesis examples it will be shown that this kind of spherical antenna can direct a pencil-beam or different kind of shaped beams to any direction, where a suitable amount of elements on the sphere are directed. With circularly polarized elements the cross-polarization problems are avoided. When very wide beams are synthesized, some compromise between side-lobe level and beam shape must be done.

REFERENCES

1. Shelley M., D. Price, and A. Roederer, “Application of semi-active antennas to terrestrial systems”, *COST245 ESA Workshop on Active Antennas*, 27-28 June 1996, Estec, Noordwijk, the Netherlands, pp. 295–301.
2. Vaskelainen L. I., “Phase Synthesis of Conformal Array Antennas”, *IEEE Trans. Antennas Propagat.*, vol. 48, pp. 987–991, June 2000.

Array Synthesis: Extention of a Classical Technique, and the Wideband Application of Numerical Approaches

D. A. McNamara
School of Information Technology & Engineering
University of Ottawa
Ottawa, Ontario K1N 6N5, Canada

The original formulation for the synthesis of Chebyshev arrays is applicable to the case of an even $(2N)$ or an odd $(2N+1)$ number of elements for inter-element spacing $d \geq \lambda/2$. The restrictrion on d is to ensure that the transformation needed for the $polynomial \Leftrightarrow array\ factor$ correspondence provides a radiation pattern that is indeed optimal in the sense of supplying the minimum first-null-beamwidth for the given number of elements and specified sidelobe level. This same transformation does not guarantee optimality if $d < \lambda/2$. Subsequent formulations showed how the transformation must be altered to reclaim optimality if $d < \lambda/2$, but only for arrays of an odd number of elements. In this paper we broaden the formulation to provide a means of synthesising such optimal arrays for an even number of elements when $d < \lambda/2$. This is done in an exact manner using existing polynomials.

The anticipated increased data rates in future wireless communication systems will require wider, or several, operating frequency bands. Antennas are key components in such systems. There is thus some renewed interest in antenna array configurations that are able to provide a performance that is relatively invariant over wider frequency bands. Modern array synthesis techniques based on numerical algorithms are attractive because of their flexibility (e.g., relative ease with which both pattern and excitation constraints can be reliably implemented; ability to deal with arbitrary inter-element spacings). This paper will present and compare the results of the application of such synthesis approaches to the wideband and multiband array synthesis problem.

On the Existence of Radiation Patterns Satisfying Constraints Imposed on Nulls and on Dynamic Range Ratio in Antenna Arrays

R. Vescovo
Dipartimento di Elettrotecnica Elettronica ed Informatica, Università di Trieste
Trieste, 34127, Italy

The synthesis problems for antenna arrays usually involve constraints of various kind. In this paper we consider the case where a synthesis problem involves constraints on nulls and on the dynamic range ratio of the excitations. An example of such a problem is the following: given an array of arbitrary geometry consisting of N elements, let $F(\mathbf{a}_0, \hat{\mathbf{r}})$ be the radiation pattern, where $\hat{\mathbf{r}}$ specifies the generic space direction and $\mathbf{a}_0$ denotes the excitation vector. Determine an array pattern $F(\mathbf{a}, \hat{\mathbf{r}})$ minimizing the mean-square distance from $F(\mathbf{a}_0, \hat{\mathbf{r}})$ while satisfying the following conditions:

(a) $F(\mathbf{a}, \hat{\mathbf{r}})$ vanishes in $M(\leq N-2)$ prescribed space directions $\hat{\mathbf{r}}_1, \cdots, \hat{\mathbf{r}}_M$, that is:

$$F(\mathbf{a}, \hat{\mathbf{r}}_m) = 0 \quad \text{for } m = 1, \cdots, M \tag{1}$$

(b) The dynamic range ratio dyn(**a**) of the excitations does not overcome a given threshold u_0, that is:

$$dyn(\mathbf{a}) \leq u_0 \tag{2}$$

where $\mathbf{a} = [a_1, \cdot, a_N]$ is the excitation vector and $dyn(\mathbf{a}) = max_n\{|a_n|\}/min_n\{|a_n|\}$.

Before solving this problem, we put ourselves the following question: has the system of equations (1) and (2) solutions for any $u_0(\geq 1)$? The answer is no, in general, and we intended to determine the set of all values of u_0 for which the system has solutions. Some results of our investigation are summarized below.

Theorem 1

Let D be the space of the excitation vectors whose radiation patterns satisfy equation (1). If $M \leq N-2$, the set T of the dynamic range ratios of all vectors of D is a closed unbounded interval: $T = [c_0, +\infty]$.

The minimum c_0 plays an important role, as is stated by the following theorem.

Theorem 2

If $M \leq N-2$, a necessary and sufficient condition for the existence of excitation vectors satisfying the system of equations (1) and (2) is that $u_0 \geq c_0$. If $u_0 > c_0$ the set of such solutions has the cardinality of the continuum.

We first devised an iterative technique to determine the minimum c_0. Then we applied this technique to several arrays, such as equispaced linear arrays, equispaced circular arrays and arc arrays, and verified that if M is small compared to N it results $c_0 = 1$, so that the system of equations (1) and (2) has solutions for any $u_0 \geq 1$, by Theorem 2. Furthermore we solved the above synthesis problem, which consists in determining a pattern $F(\mathbf{a}, \hat{\mathbf{r}})$ approximating a given pattern $F(\mathbf{a}_0, \hat{\mathbf{r}})$ while satisfying equations (1) and (2), in many cases where $c_0 = 1$: we observed that, although the value of u_0 may strongly affect the shape of the synthesized pattern, the required nulls were achieved for any $u_0 \geq 1$. Both the technique used to evaluate c_0 and that used to solve the synthesis problem are iterative, and are based on the method of alternate projections. The method can be applied in such a way as to take the mutual coupling into account.

Session 2Pc7

Left-Handed Medium and Other Electromagnetic Metamaterials II

A 'Fibre Optic Bundle' for the Near Field-Perfect Fibre Optics

J. B. Pendry and S. A. Ramakrishna
Imperial College
London, UK

M. C. K. Wiltshire
Marconi Optical Components
Caswell, UK

W. J. Stewart
Marconi Optical Components
London, UK

A bundle of optical fibres will transfer an object placed in front of one end of the fibre to the other end. Each pixel of the image is picked up by a fibre and transferred to the other end with the same phase change for each pixel. Thus a coherent image is produced. However the resolution of the image is limited by the diameter of the fibres which in turn is limited by the wavelength of light in the fibre medium.

Recent work has shown that the wavelength of light need not be a limit to the resolution of an image formed by a lens. Here we show that we can specify a medium which has the same effect as a bundle of fibres, except that the resolution is in principle unlimited.

If we analyse the fibre bundle in k- space, the field as defined by,

$$\mathbf{E}(\mathbf{r},t) = \sum_{\sigma,k_x,k_y} \mathbf{E}_\sigma(k_x,k_y)\exp(ik_z z + ik_x x + ik_y y - i\omega t)$$

Let us take the source to be at $z = 0$. In free space,

$$k_z = \sqrt{\omega^2 c_0^{-2} - k_x^2 - k_y^2}$$

and the fields are gradually defocused as we move away from the source because the Fourier components lose their phase relationship. In a fibre bundle we have a different situation: k_z is independent of (k_x, k_y) at least for a limited range of values,

$$k_z = k_c,\ k_x >> d^{-1},\ k_y >> d^{-1}$$

where d is the diameter of the fibre. Hence in this instance the Fourier components satisfying the above inequalities retain the correct relative phase and remain in focus throughout the length of the fibre. The secret is to find a medium in which k_z remains independent of (k_x, k_y) for all values of (k_x, k_y). This is possible if we can produce an anisotropic medium such that,

$$\varepsilon_x = \varepsilon_y = 0,\ \varepsilon_z = \infty.$$

Inside the medium the wave vectors obey the following relationship,

$$\frac{k_x^2}{\varepsilon_z} + \frac{k_y^2}{\varepsilon_z} + \frac{k_z^2}{\varepsilon_x} = k_0^2$$

where k_0 is the wave vector in free space. This ensures that whatever the value of k_x, it is always true that $k_z = 0$.

In other words all Fourier components of the image are translated to the other side of the anisotropic slab with zero phase change and zero amplitude change where a perfect image is reproduced. We give a simple practical recipe for manufacturing a suitable meta material which approximates these dielectric properties and show how the performance of the "perfect fibre bundle" degrades as we depart from the ideal values of the dielectric response.

Left-Handed Materials with High Transmittance and a New Way to Realize Photonic Band Gaps

J. Li, Z. Lei, P. Sheng, and C. T. Chan
Physics Department, Hong Kong University of Science and Technology
Clear Water Bay, Hong Kong

Material that has simultaneously negative permeability and permittivity is called left handed (LH) material. It has recently been demonstrated that such LH material can be realized in the microwave regime and the effective negative refraction index properties are clearly demonstrated. However, the transmission coefficients of previously fabricated samples are typically low, partly due to absorption and partly because of the impedance mismatch. With the help of accurate computer simulations, we found that it is possible to realize resonance structures which not only have an effective negative refraction index, but also an overall effective impedance that matches well with that of vacuum, leading to a LH material with fairly high transmittance.

In addition, we will show that negative refractive index materials can be combined with ordinary materials to create a composite that exhibits stop bands, which has different characteristics when compared with conventional stop band that originates from Bragg scattering. Conventional photonic band gaps are created through Bragg scatterings so that periodicity and symmetry are essential. Through a general physical argument and a rigorous proof for one-dimensional systems, we find stop bands can be created which is independent of the periodicity but just the proper volume average of refraction index. Such stop bands can only be realized in composites consisting of both positive and negative refractive index of materials, but not in heterogeneous systems containing one type alone (either positive or negative n). Distinct from the Bragg scattering mechanism, the new mechanism shows many unusual properties. First, the gap remains at the same frequency if the unit cell is rescaled by a factor. Second, the gap is insensitive to weak disorder. We will also go beyond simple mathematical models, and show numerically that such unconventional stop bands do exist when the full dispersion of a realistic resonance structure is taken into account.

Negative Refraction Phenomena with a Positive Effective Index

C. Luo, S. G. Johnson, and J. D. Joannopoulos
Department of Physics and Center for Materials Science and Engineering
Massachusetts Institute of Technology
Cambridge, MA 02139, U.S.A.

J. B. Pendry
Condensed Matter Theory Group, The Balckett Laboratory, Imperial College
London, SW7 2BZ, United Kingdom

Negative refraction of electromagnetic waves has become of great interest recently because it is the foundation for a variety of novel phenomena, including a super-lensing effect that can potentially overcome the diffraction limit inherent in conventional lenses. These phenomena have been described in the context of an effective medium theory with negative permittivity and negative permeability. The current class of periodic metallic structures that realize such materials is known as “Left-Handed Materials”, which use an assembly of resonances due to internal inductance and capacitance and exhibit negative behavior at the high frequency side of the resonance. However, they appear to be limited to the microwave or millimeter regime only.

To explore the possibility of negative refraction at optical frequencies, we have turned to photonic crystal structures as interesting alternatives. Recent work indicates that negative refraction phenomena in photonic crystals are possible for a limited range of incident angles in the regimes of negative group velocity and negative effect index. To our knowledge, however, both the “Left-Handed Materials” and the recent photonic crystal work involve either the long wavelength limit or regions near the Brillouin zone center (Γ).

In this work, we show that *single-beam* negative refraction in photonic crystals is possible for *all* incoming angles in a regime of positive effective index of refraction. In particular, we focus on the lowest photonic band near a Brillouin zone corner furthest from Γ. Interestingly, this band has a positive group velocity but a negative photonic “effective mass”. The frequency range is chosen so that for all incident angles, one obtains a single negative-refracted beam. We call this effect All-Angle Negative Refraction (AANR) and present the set of sufficient criteria for its observation. To illustrate this phenomenon, we design and numerically simulate a photonic crystal micro-superlens. We believe that this work could help pave the way towards realization of all-angle negative refraction at optical frequencies.

Anomalous and Nonlocal Effective Behavior of Wire Mesh Photonic Crystals

D. Felbacq
LASMEA UMR-CNRS
Clermond-Ferrand, France

F. Zolla
Institut Fresnel UMR-CNRS
Marseille, France

G. Bouchitté
University of Toulon
Toulon, France

Metallic photonic crystals have recently attracted the attention for their ability of exhibiting a very low plasma frequency and a somewhat exotic homogeneous behavior (for instance a negative relative permittivity or permeability) [1-6]. It was also pointed out that 3D wire mesh photonic crystals could lead to new devices [7]. In this work, we consider a simple geometry where the crystals is made of parallel highly conducting rods of finite length and we aim at describing the effective electromagnetic properties of the structures when the period η of the crystal tends to zero (and accordingly the number of rods tends to infinity). That way, we obtain as a limit problem a scattering problem, and not an electrostatic one.

For infinitely long fibers there are two critical sizes. For E// incident waves, the homogenized crystal is an infinitely conducting material when the radius of the rods is of the order of the period ($r_\eta \propto \eta$), whereas for very small rods with respect to the period ($\eta^2 \log |\mathrm{r}_\eta/\eta| \propto cste = \gamma$) the equivalent medium is dielectric with a negative permittivity [3,5]. The H// case is less known: there is only one critical size ($r_\eta \propto \eta$) and the effective medium is **anomalous**: it is a **dielectric with a surface current**.

For the finite-size rods, and hence for any incident wave, we still distinguish between the two critical sizes. When the rods are very small in radius, we assume, that the mean conductivity σ of the set of rods does not depend on the small parameter η. In that case, there appears vertical microscopic currents on the rods ($\mathbf{e}_3$ direction), and these currents give rise to a macroscopic current J$\mathbf{e}_3$ at the limit when η tends to 0. We have performed a rigorous limit analysis of Maxwell equations when the period tends to 0. Our conclusion is that the Maxwell system writes at the limit: $\bigtriangledown \times \mathbf{E}$ = i$\omega\mu_0\mathbf{H}$, $\bigtriangledown \times \mathbf{H}$ = -i$\omega\varepsilon_0\mathbf{E}$ + $\sigma J\mathbf{e}_3$. The crucial point here is that current J is linked **nonlocally** to the electric field through the propagation equation: ∂_3J+(k^2+2i$\pi\gamma/\sigma$)J=2i$\pi\gamma/\sigma E_3$ so that the effective medium exhibits **spatial dispersion**. This situation is reminiscent of that of quantum wires where such a spatial dispersion is also encountered.

REFERENCES

1. D. R. Smith and al., *Appl. Phys. Lett.*, no. 75, pp. 1425, 1999.
2. R. A. Shelby, D. R.Smith, and S.Schultz, *Science*, pp. 292, 2001.
3. J.B. Pendry and al., *Phys. Rev. Lett.*, no. 76, pp. 4773, 1996.
4. C.A. Moses and N. Engheta, *Wave Motion*, no. 34, pp. 301, 2001.
5. D. Felbacq and G. Bouchitté, *Waves in Random Media*, no. 7, pp. 245, 1997.
6. D. Felbacq, *J. Phys. A: Math. Gen.*, no. 32, pp. 1, 1999.
7. D. F. Sievenpiper and al., *Phys. Rev. Lett.*, no. 76, pp. 2480, 1996.

Negative Refractive Index Metamaterials Based on L-C Loaded Transmission Lines

G. V. Eleftheriades, A. K. Iyer, A. Grbic, and O. Siddiqui
The Edward S. Rogers Sr. Department of Electrical and Computer Engineering
University of Toronto
Toronto, ON M5S 3G4, Canada

Starting from the transmission line representation of free-space we show how to synthesize negative refractive index metamaterials (left handed media) by appropriately loading a host transmission line medium with inductors and capacitors. This simple approach provides valuable intuition into the operation and synthesis of negative refractive index metamaterials [1]. This fresh approach led to the design of new classes of negative refractive index metamaterials that go beyond the standard medium of split-ring-resonators/wires [2]. The so far synthesized media exhibit a number of interesting and desirable properties. These include the ability to guide on-board 2-D transverse-magnetic (TM) waves which is key for practical microwave-circuit applications, small unit cells due to the use of lumped elements which is essential for low-frequency RF applications, and the ability to easily form isotropic or anisotropic versions of the metamaterials. In addition and unlike [1], the new media do not rely on distributed (ring) resonators to synthesize the negative permeability which thus can lead to wider operating bandwidths and lower absorption losses. Furthermore, the new metamaterials can be easily controlled by incorporating variable inductors and capacitors for wireless beamforming applications.

These new kinds of negative refractive index metamaterials have been utilized to demonstrate reversed refraction, focusing as well as backward-wave beam formation analogous to reversed Cherenkov radiation first predicted by Veselago [3, 4], and interesting "superluminal" pulse propagation effects when operating within negative group velocity regions near (synthesized) absorption lines. Validating results will be presented based on a combination of circuit and full-wave electromagnetic simulations as well as experiments at microwave frequencies.

REFERENCES

1. Iyer, A. K. and G. V. Eleftheriades, "Negative refractive index metamaterials supporting 2-D waves," To be presented at *IEEE MTT-S International Microwave Symposium in Seattle*, Washington, June 2–7, 2002.
2. Shelby, R. A., D. R. Smith, and S. Schultz, "Experimental verification of a negative index of refraction," *Science*, Vol. 292, 77–79, April 2001.
3. Pendry, J. B., "Negative refraction makes a perfect lens," *Phys. Rev. Lett.*, Vol. 85, No. 18, 3966–3969, Oct. 2000.
4. Veselago, V. G., "The electrodynamics of substances with simultaneously negative values of e and m," *Sov. Phys. Usp.*, Vol. 10, No. 4, 509–514, Jan.–Feb. 1968.

Equivalent Circuit of Split Ring Resonators

L. Solymar
Department of Engineering Science, University of Oxford
Oxford, OX1 3PJ, UK

V. A. Kalinin
Transense Technologies Ltd.
Oxon, OX25 5HD, UK

M. Shamonin
H. Rosen Engineering
Lingen (Ems), D-49811, Germany

E. Shamonina
Department of Engineering Science, University of Oxford
Oxford, OX1 3PJ, UK

3D arrays of split ring resonators have been investigated in the last few years with a view to produce a metamaterial with negative effective permeability [1, 2]. Although an analysis yielding a resonant frequency is already available [1] we are looking here at an alternative approach in terms of an equivalent circuit. It is derived by the following considerations: Firstly there must be currents in each of the two rings caused by the induced emf. The relevant impedance consists of the resistance and self-inductance of the ring plus the capacitance due to the gap between the ends of each of the rings. The coupling between the two ring currents is caused by the mutual inductance between the rings and by the scattered capacitance which is due to the electric field in the gap of one ring spilling over to the surface of the other ring. A full equivalent circuit is then derived from which the resonant frequency can be determined. In contrast to previous work [1] we conclude that the capacitance between the two rings is not among the parameters. Comparison with numerical and experimental results show good agreement for the resonant frequency.

REFERENCES

1. Pendry, J. B., A. J. Holden, D. J. Robbins, and W. J. Stewart, “Magnetism from conductors and enhanced nonlinear phenomena,” *IEEE Trans. MTT,* Vol. 47, 2075–2084, 1999.
2. Smith, D. R., W. J. Padilla, D. C. Vier, S. C. Nemat-Nasser, and S. Schultz, “Composite medium with simultaneously negative permeability and permittivity,” *Phys. Rev. Lett.,* Vol. 84, 4184–4187, 2000.

Waves in a Resonant Metamaterial

E. Shamonina and L. Solymar
Department of Engineering Science, University of Oxford
Oxford, OX1 3PJ, UK

V. A. Kalinin
Transense Technologies Ltd.
Oxon, OX25 5HD, UK

K. H. Ringhofer
Department of Physics, University of Osnabrück
Osnabrück, D-49069, Germany

One of the potential applications of metamaterials is in Magnetic Resonance Imaging when a densely packed structure made up of so-called Swiss rolls, have already been successfully used [1]. We have investigated an alternative structure composed of capacitively loaded coupled metallic loops in one, two and three-dimensional configurations.

It is shown that the magnetic guiding takes place via slow waves whose velocities are independent of the velocity of light. In the simplest case the dispersion relationships (which may exhibit both forward and backward waves within a pass band) may be obtained from a circuit model which can also provide the value of the terminal impedance leading to a pure travelling wave. The conclusions remain more or less unchanged when we rely on a field model instead which takes into account interactions between any two loops within the structure but then it is necessary to resort to a numerical solution. The waves are shown to be able to follow a moderate radius of curvature but losses become excessive as the radius of curvature declines.

REFERENCES

1. Wiltshire, M. C. K., J. B. Pendry, I. R. Young, D. J. Larkman, D. J. Gilderdale, and J. V. Hajnal, "Microstructured magnetic materials for RF flux guides in magnetic resonance imaging," *Science*, Vol. 291, 849–851, 2001.

Effective Electromagnetic Properties of Periodic Media

S. Nemat-Nasser and A. V. Amirkhizi
Center of Excellence for Advanced Materials, University of California San Diego
La Jolla, CA 92093-0416, U.S.A.

For an infinite medium with periodically distributed heterogeneities, we have developed a homogenization method to extract the long-wave-length effective electromagnetic parameters. The homogenization is achieved by the introduction of periodically distributed magnetic and electric polarization vector fields. These fields are then calculated by requiring that the resulting electromagnetic field variables for the homogenized medium in the presence of polarization vector fields be the same as those of the original heterogeneous medium. The resulting equations are called the consistency conditions. Since only the effective electromagnetic parameters are to be calculated, the consistency equations are averaged over a unit cell, and are solved approximately for the effective parameters which are functions of both the wave vector and frequency. Introducing these into the basic equation for the homogenized medium yields the desired dispersion relations. The method is illustrated through a number of examples.

Experimental Investigation of Left-Handed Materials

A. Houck, D. Kong and J. Brock
Center for Bits and Atoms, MIT Media Laboratory
Cambridge, MA 02139, U.S.A.

B.-I. Wu, J. Pacheco, T. M. Grzegorczyk and J. A. Kong
Research Laboratory of Electronics
Cambridge, MA 02139, U.S.A.

I. Chuang
Research Laboratory for Electronics, MIT Media Lab
Cambridge, MA 02139, U.S.A.

We present experimental investigations of materials which theoretically have simultaneously negative permittivity and permeability, resutling in a negative index of refraction. Following Pendry et. al, a periodic lattice of wires and split- ring resonators is used to independently engineer the permittivity and permeability. Transmission measurements on lattices with wires only and resonators only are found to be consistent with a narrow band of negative permeability which overlaps with a broad band of negative permittivity.

Three different experimental configurations, all using a two dimensional waveguide, are used to test the composite material for left handed behavior in this overlap frequency regime:

1. We replicate the setup of R.A.Shelby et al (footnote science paper) and measure the angular power distribution of microwaves normally incident on a prism with a single angled surface.
2. We measure the linear displacement of collimated microwaves obliquely incident on a flat slab of the material.
3. We place a point source in front of a large flat slab of the material, and use a moveable antenna to measure a two-dimensional map of both the transmitted and reflected electric field.

Results from these three geometries all indicate that the material studied was extremely lossy. Possible signatures of negative index behavior are discussed and compared with theoretical simulation results.

Theoretical and Numerical Simulations of Propagation through Left-Handed Materials

J. Pacheco, C. D. Moss, B.-I. Wu, T. M. Grzegorczyk, Y. Zhang, and J. A. Kong
Research Laboratory of Electronics
Massachusetts Institute of Technology
Cambridge, MA 02139, U.S.A.

A. Houck, I. Chuang
Center for Bits and Atoms, MIT Media Laboratory
Cambridge, MA 02139, U.S.A.

Left-handed materials, so called due to the anti-parallel nature of the wave vector and the Poynting vector arising from simultaneous negative permittivity and permeability were first given theoretical consideration by Veselago in 1968. Theory predicts a number of interesting properties including a negative index of refraction and backward waves. Recently, a meta-material structure composed of a periodic arrangment of rods and split ring resonantors was demonstrated to have a negative index of refraction. To better understand this initial experimental result, and other experiments done by the MIT Media lab, we have studied the propagation through left-handed materials (LHMs) using both analytical and numerical techniques.

To study the propagation through LHMs, we take two approaches. The first one is a macroscopic approach where the assumption of isotropic homogenous media is made, while the second is a microscopic approach where the actual structure of the meta-materials is modeled using the FDTD technique. Results of both approaches will be presented, although the emphasis will be on the macroscopic techniques. A more complete study of the microscopic simulations will be presented in a separate paper.

For the macroscopic approach, the analytic technique used is based on the Green's function methodology. In particular, we determine the electromagnetic field expressions due to a linear antenna, i.e. infinite line source, located outside a slab of LHM. The case of a dipole antenna can be treated in an analogous manner. As an example, the integral expressions for the fields arising under the conditions necessary for producing a perfect image are studied. We find that for certain regions of space, the integral expressions diverge exponentially and can not be evaluated in the usual sense. Yet, using an analytic continuation argument, a closed form expression for the fields at all spatial points can be found. Remarkably, we find that inside the slab there is a convergence of power, formed at the first image point while in the transmitted region an equivalent source forms at the second image point. While this source-sink-source solution satisfies Maxwell's equations, the boundary conditions, and the radiation conditions, it may not be unique in this case since the slab is lossless.

Additionally, experimental proof of the perfect lens effect has not been demonstrated. In order to understand current experimental results, frequency dispersive models for permittivity and permeability, which include losses, are introduced into the simulations. The effects of loss are discussed and comparisons with experimental results will be presented.

Pulse Propagation and Negative Group Delay in Metamaterials

M. Mojahedi, O. Siddiqui, J. Woodley, and G. V. Eleftheriades
Department of Electrical and Computer Engineering
University of Toronto
Toronto, Ontario, M5S 3G4, Canada

Metamaterials in which both permittivity and permeability are negative quantities have received much attention in recent times. These materials are expected to exhibit many unusual behaviors such as inverted refraction, Doppler shift, and Cherenkov radiation. Perhaps, a less investigated, and yet equally exciting aspect of metamaterials is the dynamics of the pulse propagation when an electromagnetic wave packet (EMWP) is propagated through such media.

Previous work has shown that under appropriately design circumstances an EMWP can travel with group velocities exceeding the speed of light in vacuum (superluminal) or with negative group velocities without violating the requirements of special relativity [1–3]. While for these abnormal velocities to occur the former case requires a passive optical barrier such as photonic crystals [1], the later has been demonstrated in an active medium such as an inverted Cesium vapor [3]. The metamaterials provide a possibility to obtain a negative group velocity and a negative group delay (a group advance) without the need for an active medium.

In this work the possibility of negative group delay for metamaterials is investigated. First, the transmission phase, and hence the group delay, for a slab having the permittivity and permeability of the split-ring-resonator/wire is calculated. Second, the pulse propagation through a suitably designed passive RLC loaded transmission line which emulates the aforementioned dispersion relation [4] is considered. It is observed that metamaterials in addition to supporting the backward waves also support a negative group delay. This means that the peak of the transmitted pulse would leave the medium prior to the peak of the incident EMWP entering it. Despite this counter intuitive behavior, there is no violation of the principle of causality, since there is no causal connection between the incoming and outgoing peaks, and the pulse front remains luminal under all circumstances. This phenomenon can be understood in terms of pulse reshaping by means of constructive and destructive interferences and can be used in designing faster interconnects and transmission lines.

REFERENCES

1. Mojahedi, M., E. Schamiloglu, F. Hegeler, and K. J. Malloy, "Time-domain detection of superluminal group velocity for single microwave pulses," *Phys. Rev. E*, Vol. 62, 5758–5766, 2000.
2. Bolda, E. L., J. C. Garrison, and R. Y. Chiao, "Optical pulse-propagation at negative group velocities due to a nearby gain line," *Phys. Rev. A*, Vol. 49, 2938–2947, 1994.
3. Wang, L. J., A. Kuzmich, and A. Dogariu, "Gain-assisted superluminal light propagation," *Nature*, Vol. 406, 277–279, 2000
4. Iyer, A. K. and G. V. Eleftheriades, "Negative refractive index metamaterials supporting 2-D waves," To be presented at *IEEE MTT-S International Microwave Symposium*, Seattle, Washington, June 2–7, 2002.

Electromagnetic Properties of Left-Handed Metamaterials and Their Constituents

O. J. F. Martin, P. Gay-Balmaz, and M. Paulus
Electromagnetic Fields and Microwave Electronics Laboratory
Zurich, ETH-Zentrum 8092, Switzerland

The exciting properties of left-handed (LH) metamaterials are currently attracting a lot of interest. In this contribution we present some of our recent work on that topic. We both investigate the electromagnetic response of LH materials per se - assuming a negative permittivity and a negative permeability - as well as the properties of specific electromagnetic elements that have been used to create a LH metamaterial thus far.

For the general properties of LH materials, we study the response of a LH slab with negative permittivity and permeability. Our approach is based on the Green's tensor associated with a stratified medium [1]. The computation of this dyadic has been extended to account for negative permittivity and permeability. In particular, the location of the poles that occur in the Fourier representation of the Green's tensor (Sommerfeld integrals) must be carefully located in that case. The intrinsic properties of the Green's tensor allow us to obtain the response of a dipolar source in the vicinity of such a system. Radiation patterns and lifetime for a dipolar source are computed as a function of the material properties.

Considering the constituents of LH metamaterials, we concentrate on the physics of split-ring resonators. We show the magnetic character of the coupling between such elements placed at a short distance from each other. At the resonance, a magnetic flow can be induced from one resonator to the other, leading to a strong coupling. The dependence of this coupling on the different geometrical parameters is investigated in detail both numerically, with the mixed potential method of moments, and experimentally, using simple split ring resonators placed in a rectangular waveguide.

REFERENCES

1. M. Paulus, P. Gay-Balmaz and O.J.F. Martin, "Accurate and efficient computation of the Green's tensor for stratified media," Phys. Rev. E 62, 5797-5807 (2000).

Session 2Pa8

Novel Mathematical Methods in Electromagnetics - I

Unified Analysis of Near Field Property for Changing Charges including Discharge Process by the Spatial Networks for Vector and Scalar Potentials

N. Yoshida
Division of Electronics and Information Engineering, Hokkaido University
Sapporo, Japan

Recently, the EMC problems such as “Electromagnetic Interference(EMI)” have become serious ones in the development of the digital technology including downsizing in devices and performing high-speed operation. Since these problems are so complicated that analyses by the numerical method on the three-dimensional space and the time domain become very effective. But, the conventional time-dependent methods such as the FD-TD and the TLM essentially simulate only the propagation of the solenoidal wave because of assumption in the formulation that the divergence for both electric and magnetic fields does not been taken into consideration. Therefore, some radiation mechanisms in the EMI problems, especially such as the “Electro-Static Discharge (ESD)”, in that not only the solenoidal radiation field from the current sources but also the laminar field from the space charges are included, cannot be analyzed by using only above methods. The scalar field must be analyzed independently by using the Poisson’s equation or the scalar Helmholtz wave equation. To perform the overall analysis of the EMI problems, introducing of the scalar field, that is, the laminar field to the time-dependent method for the conventional solenoidal field should be essential.

I have already proposed the condensed node “Spatial Network” for the vector potential and the equivalent network for the scalar potential field as the three-dimensional and time-dependent numerical method. In the networks, the connection between the vector potential and the scalar potential, which is theoretically related by the Lorentz gauge condition, is expressed by the equivalent current source. By using this method, it has been already presented that the static field caused by the changing charges including DC component, which includes both the Poissons field and the retarded potential field, can be simulated in the network for the vector potential [1]-[2].

In this paper, the near field property for the set of changing positive and negative charges are observed by presenting the variation of the divergent and rotational components through the total conditions from charging process to discharging one. Especially, in the discharge process, not only both the discharge current but also the decreasing charges cause the complicated fields near the sources. This treatment will be useful in the analysis of the radiated and static fields caused by current and charge sources to be appear often in the actual EMC problems.

REFERENCES

1. N.Yoshida: “Connection of Scalar Field to Condensed Node Spatial Network for Vector Potential and Hertz Vector,” *Proc. of PIERS 2000*, 1022 (July 2000).
2. N.Yoshida: “Treatment of the Gauge Conditions in the Condensed Node Spatial Network for the Vector Potential and Hertz Vector,” *Proc. of PIERS 2001*, 667 (July 2001).

Coupling Mechanism of Highly Decoupled Antennas in Layered Medium for Ground Penetration Radar

D.-H. Je and J.-W. Ra
Dept. of Electrical Engineering and Computer Science,
Korea Advanced Institute of Science and Technology
Daejeon, 305-701, Republic of Korea

In the subsurface explorations and identifications of the objects such as pipes, cables, voids, and plastic mines, the continuous multi-frequency radar is advantageous over that of impulse in coping with the dispersion of the ground medium, the accuracies of the measurement, and the minimum detectable signal strength. It requires, however, a good isolation between the transmitting and the receiving antennas, since the time gating of the transmitting signal is impossible for the continuous wave radar. In addition to the large isolation, wide bandwidth of operation is required for the high enough resolution of the fine targets.

Wideband decoupled planar dipoles inside the air waveguide backed by the perfect magnetic conductor plate is suggested as a subsurface transmitting and receiving antenna. Its coupling mechanism is shown to be the contributions of the branch point, i.e. the evanescent lateral waves, and the poles, i.e. the leaky waves, while the guided modes inside the dielectric slab are cut-off for the relative dielectric constant of the waveguide is smaller than that of the ground. It is shown that the contributions of the evanescent lateral waves and the leaky waves, respectively, decrease and increase as the operating frequency increases, which makes it possible to design the optimum center frequency that gives the maximum decoupling and the widest bandwidth of operation for given dimensions of the antenna. This antenna gives a good radiation efficiency and the isolation more than 60 dB between the transmitting and receiving dipoles over 55 percent bandwidth of its center frequency 320 MHz for the planar dipoles of 0.4 m by 0.05 m located 0.03 m from the perfect magnetic conducting plane and separated by 1.0 m inside the air-waveguide. Asymptotic contributions of the lateral waves and the leaky waves will be shown and discussed.

Interaction of Oscillations in Slotted Resonators Close to the Degeneration Points

Yu. V. Shestopalov and O. V. Kotik
Karlstad University
Karlstad, Sweden

We consider intertype interaction of oscillations in cylindrical resonators whose cross sections are formed by two slotted rectangular domains Ω^1 and Ω^2. We calculate the electromagnetic field distribution by reducing the initial boundary eigenvalue problem to an integral equation with a logarithmic singularity of the kernel and then to infinite systems with respect to the unknown Fourier coefficients of the solution. The system operator is represented finally as a Fredholm operator-function $I - A(z)$ of the spectral (frequency) parameter z , where I is the identity operator and $A(z)$ is a compact analytical operator-function of z. The dispersion equation (DE) has the form $F(z, w) = det(I - A(z, w)) = 0$, where F is the infinite determinant. We study interaction by analyzing the variation of the spectrum $\sigma = \sigma(w)$ of eigenfrequencies when the chosen parameter w is varied. The analytical surface $\sigma_0 = \{(z, w) : F(z, w) = 0\}$ is associated with the DE. If (z_0, w_0) is an isolated critical point (ICP) of $F(z, w)$ situated close to σ_0, then the local structure of σ_0 is specified by its position and type. We focus on intertype interaction of oscillations when a geometric parameter (e.g., the width $w = a_1$ of the upper partial rectangular domain Ω^1) is varied in the vicinity of an ICP, where the double frequency degeneration takes place. ICPs of other types lie in the vicinity of the points where eigenvalues of the Laplacian of the partial rectangular domains coincide (as in Fig. 1a). The interaction manifests itself, in particular, as the development of hybrid field configurations accompanied by a sharp increase in the field amplitude; σ_0 acquires locally a saddle-shaped structure (Fig. 1b). Eigenfrequencies are obtained explicitly in the form of segments of asymptotic series in powers of the characteristic small parameter (logarithm of the relative slotwidth of one of the slots).

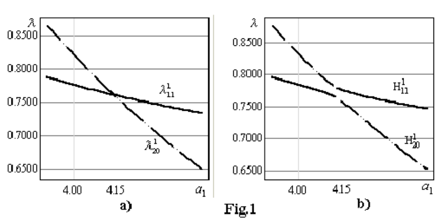

Figure 1: shows H-type eigenfrequencies $\lambda^{(1)}_{11}$, $\lambda^{(1)}_{20}$ vs. a_1. The curves intersect (in the absence of the slot) when $a_1 = a^* \approx 4.156$. At this point $\lambda^{(1)}_{11}(a^*) = 0.7616$, $\lambda^{(1)}_{20}(a^*) = 0.7618$.

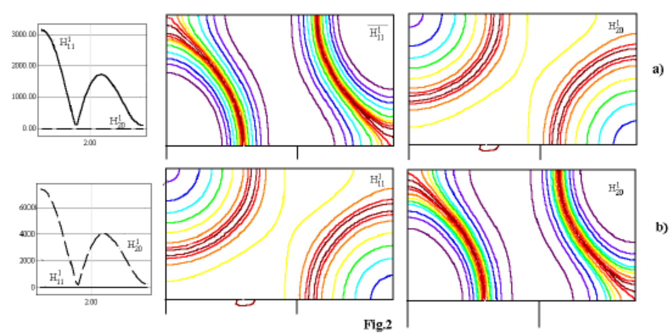

Figure 2: displays the field behaviour in the vicinity of the ICP when the width $a_1 = 4.156$ (Fig. 2a) and $a_1 = 4.157$ (Fig. 2b). One can see that the oscillations 'exchange' their types.

Mathematical Analysis of Electromagnetic Radiation and Leaky Fields from Tapered Optical Waveguides Using Conformal Mapping Method

Y. Miyazaki
Department of Information and Computer Sciences,
Toyohashi University of Technology
Toyohashi, 441-8580, Japan

Very small output of tapered optical waveguides and fiber probes are very useful for sensing the optical characteristics of material objects in nano-meter spaces. These characteristics are related with fundamental properties of scanning atomic microscopes.

Near field characteristics of optical tapered waveguides and probes have been studied by approximate mode methods with integral equations and numerical methods of FDTD, FEM and beam propagation method. Integral equation method with Green's function using conformal mapping method is very useful for electromagnetic field analysis of complicated boundary problems. Tilted and curved waveguides, and optical fibers have been investigated by this integral equation method using conformal mapping.

The tapered couplers of optical fibers have similar characteristics as electromagnetic properties of tapered optical near field probes. Electromagnetic fields in tapered couplers have been studied by this method of integral equation with conformal mapping and optimum index distribution for field matching is shown.

Two dimensional tapered probes are transformed to semi-infinite straight slab guide in new mapped space by analytic function $\dot{Z} = \dot{z} + a\tan^{-1} c\dot{z}$. For mapped straight guide with inhomogeneities, optical wave field equations with inhomogeneous coefficients given by metric coefficients in new mapped space can be analyzed by integral equation using Green's function of straight slab guide. Near field and reflected modes are shown by Born iteration method for integral equation when incident wave is dominant mode.

Three dimensional tapered probes with circular cross section can be transformed to semi-infinite straight optical fiber with inhomogeneities in new mapped space by similar analytic function. Electromagnetic near field and reflected mode are shown for incident fundamental HE_{11} mode.

Virtual Sources for the Paraxial Wave Equation

S. R. Seshadri
Madison, WI 53705-2718, U.S.A.

For the physical space $z > 0$, a beam propagating along the z-axis and generated by sources outside $z > 0$ is considered. External to the physical space and at its boundary is the input plane $z = 0$. The wave function $F_{m,n}(x, y, z)$ which specifies the scalar beam and which is governed by the Helmholtz equation is separated out as $F_{m,n}(x, y, z) = f_{m,n}(x, y, z) \exp(ikz)$ where m and n are integer indices indicative of the nature of variations in the x and y directions, $f_{m,n}(x, y, z)$ is a slowly varying function of its arguments and k is the wave number. Assuming that the input beam width w_0 is large compared to the wavelength $2\pi/k$, $f_{m,n}$ is expanded into a series:

$$f_{m,n} = f^{(0)}_{m,n} + \delta^2 f^{(2)}_{m,n} + \delta^4 f^{(4)}_{m,n} + \dots$$

where $\delta = 2/kw_0$ [1]. A secondary source for generating $f^{(0)}_{m,n}(x, y, z)$ which satisfies the paraxial wave equation is assumed as

$$f^{(0)}_{m,n}(x, y, 0) = \frac{(-1)^{m+n}}{\pi w_0^2} H_m\left(\frac{x}{w_0}\right) H_n\left(\frac{y}{w_0}\right) \exp\left(-\frac{x^2 + y^2}{w_0^2}\right)$$

where $H_m()$ and $H_n()$ are Hermite polynomials. The solution $f^{(0)}_{m,n}(x, y, z)$ of the paraxial wave equation is shown to be the field generated by a higher-order point source situated at $x = y = 0$ and $z = ib = i0.5kw_0^2$ [2, 3]. The first nonparaxial field $f^{(2)}_{m,n}$ generated by the paraxial field $f^{(0)}_{m,n}$ is determined from the inhomogeneous differential equation via the wave number domain linked to the complex source point associated with the paraxial field. The behavior of $f^{(2)}_{m,n}$ is found to be inconsistent with the predictions of Fresnel diffraction theory. It is concluded that the regular series solution is inadequate for the treatment of nonparaxial fields. The correct behavior of the first-order nonparaxial field can be recovered by using additional first-order nonparaxial sources at the same complex source point. The first-order nonparaxial field can be made to vanish along the beam axis by introducing additional first-order nonparaxial sources at the same complex source point. However, the requirement that the nonparaxial fields vanish on the beam axis is shown to be not acceptable in general [4]. The complex source point technique carried out directly in conjunction with the wave equation is presented as a rigorously valid procedure for the determination of the nonparaxial fields [2].

REFERENCES

1. M. Lax, W. H. Louisell, and W. B. McKnight, "From Maxwell to paraxial wave optics," *Phys. Rev. A* 11, 1365–1370, 1975.
2. L. B. Felsen, "Evanescent waves," *J. Opt. Soc. Am.*, 66, 751–760, 1976.
3. S. Y. Shin and L. B. Felsen, "Gaussian beam modes by multipoles with complex source points," J. Opt. Soc. Am., 67, 699–700, 1977.
4. M. Couture and P. A. Belanger, "From Gaussian beam to complex-source-point spherical wave," *Phys. Rev. A*, 24, 355–359, 1981.

Parameterizing Guided-Mode Dispersion Dynamics Directly in the Time Domain

L. B. Felsen
Boston University
Boston, MA, U.S.A.

Temporally dispersive (i.e., frequency dependent) wave propagation characteristics can be grouped into two major categories: a) *intrinsic* dispersion which can occur in "complex" bulk materials; b) *structural* dispersion which can occur in layered or completely bounded regions filled with nondispersive material. When a dispersive environment is subject to transient excitation, the resulting space-time-dependent field response is conventionally synthesized by first Fourier or Laplace-transforming to the frequency domain (FD), obtaining the space-dependent response in the FD by wavenumber spectral decomposition, and *thereafter* frequency-inverting back to the time domain (TD). This conventional approach is ill-suited to physics-based modeling of the temporally well-resolved space-time observables due to wideband/short pulse (SP) excitation. Under these conditions, it is preferable to perform the frequency inversion *before* the wavenumber inversion, thereby representing the response in terms of time-dependent wavenumber spectra *directly* in the TD.

In this paper, attention is focused on a review of the TD dynamics of two types of SP-excited *structurally* dispersive wavefields: a) leaky waves (LW) excited by a single pulsed dipole in a grounded nondispersive dielectric slab [1-3]; b) Floquet waves excited by a periodic line array of sequentially-pulsed dipoles in free-space [4]. While these canonical studies have been carried out during the past decade, they have not yet been applied systematically to SP-excited practical guided wave and phased array configurations. After a summary of the *direct-TD* spectral analysis and synthesis procedure, high frequency asymptotic methods are applied to extract phenomenology-matched wave physics from the formal spectral integrals. The outcome is an algorithm which parameterizes TD-LW and FW dispersion in terms of time-dependent wavenumbers and frequencies that are tuned dynamically so as to satisfy the FD dispersion relation at each instantaneous frequency. For the TD-LW, this leads to polarization-sensitive self-consistent hybrid ray-mode trajectories that connect the SP dipole source with an exterior observer. For the TD-FW, analogous considerations lead to instantaneous arrival directions to the observer. Numerical examples demonstrate the accuracy and utility of the algorithms in various parameter regimes.

REFERENCES

1. L.B. Felsen and F. Niu, "Spectral analysis and synthesis options of short pulse radiation from a point dipole in a grounded dielectric layer," *IEEE Trans. Antennas Propagat.*, vol. 41, pp. 747-754, 1993.
2. F. Niu and L.B. Felsen, "Time domain leaky modes on layred media: dispersion characteristics and synthesis of pulsed radiation," *IEEE Trans. Antennas Propagat.*, vol. 41, pp. 755-761, 1993.
3. F. Niu and L.B. Felsen, "Asymptotic analysis and numerical evaluation of short pulse radiation from a point dipole in a grounded dielectric layer," *IEEE Trans. Antennas Propagat.*, vol. 41, pp. 762-769, 1993.
4. L.B. Felsen and F. Capolino, "Time domain Green's function for an infinite sequentially excited periodic line array of dipoles," *IEEE Trans. Antennas Propagat.*, vol. 48, pp. 75-85, 2000.

Session 2Pb8

Novel Mathematical Methods in Electromagnetics - II

Source and Image Coefficients for Wedge Diffraction

K. Uchida
Fukuoka Institute of Technology
Higashi-ku, Fukuoka 811-0295, Japan

This paper is concerned with a theoretical discussion on simplifying analytical treatments for electromagnetic diffraction by an edge or a wedge. Starting from the rigorous solution to the plane-wave diffraction by a conducting half-plane, we derive an approximate solution to wedge diffraction of an incident spherical-wave.

Based on the rigorous solution to the half-plane diffraction problem, we propose the source-coefficient and image-coefficient to analyze complicated diffraction problems in a simplified way. The rigorous analysis is applicable only to the two-dimensional structure in the case of a plane-wave incidence. As a result, we cannot apply the rigorous treatment straightforwardly to a complicated diffraction problem. Overcoming this difficulty is a main motivation of the present paper.

First, we extend the rigorous solution to an approximation that can be applied to a line-source case. Next, we deal with the edge diffraction of a plane-wave in case of oblique incidence, and we introduce an approximate solution for a spherical-wave with arbitrary polarization. Finally, we derive an approximate solution applicable to the wedge diffraction.

Numerical examples will be shown to demonstrate the effect of incident angle and polarization of the incident wave on field distributions.

Generalized Eigenfunction Expansions in the Presence of Modal Degeneracies

G. W. Hanson
University of Wisconsin-Milwaukee
Milwaukee, Wisconsin 53211, U.S.A.

A. I. Nosich
National Academy of Sciences
Kharkov, Ukraine

Eigenfunction expansions associated with differential operators are used extensively in theoretical electromagnetics, and in performing computations in electromagnetics applications. Eigenfunctions are often preferred over other expansion functions because they have physical (modal) significance, and offer convergence improvements compared to other series expansions. It is often implicitly assumed that there are "enough" eigenfunctions, i.e., that they span the solution space in question. Fortunately, for the differential operators that commonly occur in electromagnetics, it is usually true that the eigenfunctions form a complete set in the function space of interest. One exception is when modal (eigenvalue) degeneracies occur, at which points the ordinary eigenfunctions may not be "enough," and the series expansion must be augmented with associated eigenfunctions, as in a Jordan chain.

While there has been considerable work in this area from the differential operator view, the theory is somewhat complicated and difficult to apply in practice. An alternative is found through the use of Green's functions, which are well known to electromagnetics researchers. Pole singularities and residues of the Green's function are associated with eigenvalues and eigenfunctions, respectively, of the corresponding differential operator. Therefore, the residue series form of a Green's function can be associated with an eigenfunction expansion, and the question of completeness becomes moot if the Green's function can represent any solution of the original (Maxwell's equations) problem. Poles of multiple order associated with a nontrivial modal degeneracy correspond to the presence of associated or generalized eigenfunctions, and are easily obtained using residue theory.

In this paper previous work on expansions in associated eigenfunctions will be surveyed, the general approach based on Green's functions will be presented, and some applications to inhomogeneously-layered planar waveguides will be discussed.

Polygonal Trefftz Finite Elements for Electromagnetics

Y. O. Shlepnev
Innoveda, Inc.
Camarillo, CA 93010, U.S.A.

Trefftz Finite Element method (TFEM) has been recently introduced into computational electromagnetics [1,2]. As the conventional finite element method, the TFEM is based on a division of a boundary value problem for Maxwell's equations into small elements. Though, instead of polynomial functions, plane-wave solutions of the Maxwell's equations are used as the intra-element basis functions to expand electric and magnetic fields inside the element. To impose inter-element boundary conditions, an additional set of basis functions for the electric and magnetic fields is defined on the surface of the element. Admittance matrix formulation is used to relate the surface field expansion coefficients. The element admittance matrix construction procedure involves integration over the element boundaries only and is independent of the surrounding elements. The method can be considered as a generalization of the method of minimum autonomous blocks, introduced by V.V. Nikol'skii and T.I. Lavrova in the late 70th.

Though, the basic concepts of the method are quite general and straightforward, it is rather cumbersome for a manual implementation and only brick-shaped elements of the first order have been built so far [1,2]. This presentation introduces and explores a formalized computer-automated procedure to build elements of polygonal shapes. A planar TM problem in frequency domain is studied as an example. N plane waves are used to expand fields inside a convex polygonal element with N sides. Constant vector functions tangential to the sides of the polygon are used to expand electric and magnetic fields on the surface of the polygon. It gives $2N$ unknown surface expansion coefficients in addition to the N interior field expansion coefficients. Projections of the interior fields on the sides of the polygon reduce total number of unknown coefficients to 2N. An N by N admittance matrix relates the surface expansion coefficients. The admittance matrix can be expressed as a product of two N by N matrices $Y = M_h \times M_e^{-1}$. Matrix M_e contains projections of the electric field components of the interior field expansion plane waves on the surface electric field basis functions. Matrix M_h contains projections of the magnetic field components of the interior field expansion plane waves on the surface magnetic field basis functions. The elements of the matrices can be expressed directly if a point-matching projector is used to project the interior fields on the surface of the element. Numerical integration over the polygon sides is required in a general case to compute the elements of the matrices if a Galerkin-type projector is used. The algorithm is implemented in a computer program for building polygonal elements with arbitrary number of sides and for re-composition of the elements. A set of benchmark problems is solved to investigate numerical properties of the element building procedure and features of the TFEM in general.

REFERENCES

1. Y.O. Shlepnev, "Trefftz-type brick finite elements for electromagnetics," *Proceedings of the 17th Annual Review of Progress in Applied Computational Electromagnetics*, Monterey, CA, March 19–23, 2001, pp. 345–352.
2. Y.O. Shlepnev, "Trefftz finite elements for electromagnetics", Accepted for publication in *IEEE Trans. on Microwave Theory and Techniques*.

High-Frequency Diffraction by a Finite Parallel-Plate Waveguide with Three-Layer Material Loading

S. Okada
Department of Electrical, Electronic, and Communication Engineering, Chuo University
Bunkyo-ku, Tokyo 112-8551, Japan
S. Koshikawa
Laboratory, Antenna Giken Co., Ltd.,
Miyagayato, Saitama 330-0011, Japan
K. Kobayashi
Department of Electrical, Electronic, and Communication Engineering, Chuo University
Bunkyo-ku, Tokyo 112-8551, Japan

Analysis of the scattering from open-ended waveguide cavities is an important subject in target identification problems since these obstacles contribute significantly to the radar cross section (RCS) due to the interior irradiation. Cavity structures are encountered in many radar targets such as aircrafts and ships; therefore it is often required to reduce the RCS either by loading the interior of cavities with absorbing materials or by shaping cavities. A number of diffraction problems involving two-dimensional (2-D) and three-dimensional (3-D) cavities have been solved thus far by using various analytical and numerical methods. However, the solutions deduced via these methods are not uniformly valid for arbitrary cavity dimensions. In this paper, we shall consider a finite parallel-plate waveguide with three-layer material loading as a 2-D geometry that can form a cavity, and analyze the plane wave diffraction rigorously by means of the Wiener-Hopf technique.

The geometry of the waveguide is shown in Fig. 1, where $-L < D_1 < D_2 < D_3 < D_4 < L$, and ϕ^i is the incident field of E or H polarization. The waveguide plates are perfectly conducting and of zero thickness, and the material layers I $(D_1 < z < D_2)$, II $(D_2 < z < D_3)$, and III $(D_3 < z < D_4)$, are characterized by the relative permittivity/permeability ($\varepsilon_{rm}/\mu_{rm}$) for $m = 1, 2$ and 3 respectively. Introducing the Fourier transform for the scattered field and applying boundary conditions in the Fourier transform domain appropriately, this problem is formulated in terms of the simultaneous Wiener-Hopf equations satisfied by unknown spectral functions, which are solved exactly in a formal sense via the factorization and decomposition procedure. It should be noted, however, that the formal solution involves branch-cut integrals with unknown integrands as well as infinite series with unknown coefficients. Applying a rigorous asymptotics with the aid of the edge condition, we shall derive approximate expressions of the branch-cut integrals and the infinite series, which are then led to efficient approximate solutions. The approximate solution involves numerical inversion of matrix equations. Numerical computation is carried out for the case where region II $(D_2 < z < D_3)$ is composed of perfect conductors so that two cavities are formed at the right $(D_3 < z < L)$ and the left $(-L < z < D_2)$ sides of the waveguide. Illustrative numerical examples of the RCS are presented for various physical parameters and the far field scattering characteristics of the waveguide are discussed in detail.

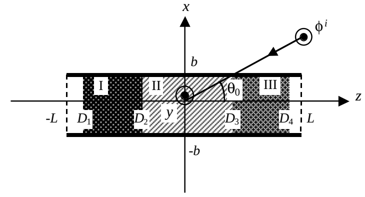

Figure 1: Geometry of the waveguide.

An Incremental Theory of Diffraction Formulation for Wedges with Impedance Boundary Conditions

R. Tiberio, A. Toccafondi, and A. Polemi
Department of Information Engineering, University of Siena
Siena, 53100, Italy

The developments of high-frequency techniques have mainly been based on an appropriate use of solutions of local canonical problems, that in most instances have an infinite, uniform cylindrical configuration. In order to overcome those difficulties that occur in applying ray methods close and at caustics, it is useful to define local, incremental field contributions to be distributed and then integrated along specific lines on the actual object. problems. To this end, a field based quite general systematic procedure was developed for defining such incremental field contributions, which may provide effective tools for describing a wide class of scattering and diffraction phenomena at any aspect, within a unitary, self-consistent framework. In particular, typical spectral integral solutions for infinite uniform local canonical configurations are transformed into a spatial integral representation along the axis of the cylinder. This is achieved by establishing a Fourier transform pair between a spectral integral representation and a spatial integral convolution. This process, which is referred to as Incremental Theory of Diffraction (ITD), provides a systematic procedure for representing the field of the cylindrical canonical structure as a superposition of incremental field contributions that are distributed along a generatrix of the cylinder. As a consequence, the integrand of the spatial integral representation is directly used to define the desired incremental field contribution. The purpose of this paper is to develop a ITD formulation for non p.c. local canonical problems. Among them, a wedge with impedance b.c. is a significant and not straightforward starting problem.

Typically, the 3D solution for the electric and magnetic fields, that exhibit uncoupled boundary conditions (b.c.) at a uniform cylindrical canonical problem such as a perfectly conducting wedge, may be obtained by spectral synthesis of the 2D solution of the same canonical problem. This spectral representation is naturally well suited to apply the ITD procedure. Unfortunately, this not the case for a wedge with impedance b.c. on its faces. However, it has been shown (Bucci and Franceschetti,1976; Senior and Volakis, 1995) that, at least for an edge impedance discontinuity on a plane, an impedance half-plane and an impedance right angled wedge, convenient combinations of the spectrum functions of the longitudinal (z) components of the fields can be found that exhibit uncoupled b.c.; for the sake of convenience, they are now referred to as potential functions, that allow to directly derive the expressions of the various field components. Due to their specific property, the 3D solution for such potential functions may be obtained by spectral synthesis of the 2D solution of the same canonical problem. Consequently, this Fourier spectral synthesis representation of the exact solution quite naturally leads to the desired spatial integral convolution representation of the same exact solution. So far, it is worth pointing out that the uncoupled b.c. property, which allows the applicability of the ITD procedure, is the same as that used to find a Maliuzhinets method solution of the actual canonical problem.

The above Fourier transform convolution procedure yields expressions for the incremental fields that are in spectral integral form. In order to provide practical tools, the above spectral integrals need to be asymptotically evaluated. To this end, a somewhat involved asymptotic analysis is required to define the most appropriate critical point which provides the dominant contribution of the four fold spectral integrals. This analysis yields closed form high-frequency expressions that are applicable at any incidence and observation aspects.

Scattering from TVFD/TDFV Dielectric to PEC Half-Plane Junctions

T. Sengor
Yildiz Tech. University
Istanbul, 80750, Turkey

Abstract. The wave diffraction in materials having time dependent and frequency varying (TDFV) and/or time varying and frequency dependent (TVFD) characteristics are considered. The perspective of the paper includes convenient transformation [1]-[2]. The junctions of dielectric-to-perfectly electric conducting boundaries are studied in TDFV/TVFD cases.

Introduction. Let us consider a homogeneous region in a TDFV/TVFD medium. The following presentation will be adequate to use in the TDFV/TVFD characterization of the medium [2]: $\vec{E} \equiv \vec{E}(\vec{r};t\,|\,\tilde{\omega}:\omega)$, $\vec{H} \equiv \vec{H}(\vec{r};t\,|\,\tilde{\omega}:\omega)$. Here $;t\,|$ is time domain in physical sense and $|\,\tilde{\omega}:\omega$ is the actual frequency domain. The $\tilde{\omega}$ illustrates the continuously varying frequency distributed around a specific location of ω. The Maxwell's equations are written as (see [1-2].)

$$\mathrm{rot}\,\underline{\vec{\mathrm{E}}} + \mathrm{i}\tilde{\omega}\left[\tilde{\mu}(\vec{\mathrm{r}}\,|\,\tilde{\omega}:\omega) * \tilde{\vec{\mathrm{H}}}(\vec{\mathrm{r}}\,|\,\tilde{\omega}:\omega)\right] \equiv -\underline{\vec{\mathrm{J}}}^{\mathrm{m}}(\vec{\mathrm{r}}\,|\,\tilde{\omega}:\omega)$$

$$\mathrm{rot}\,\underline{\vec{\mathrm{H}}} - \mathrm{i}\tilde{\omega}\left[\tilde{\varepsilon}(\vec{\mathrm{r}}\,|\,\tilde{\omega}:\omega) * \tilde{\vec{\mathrm{E}}}\right] \equiv \tilde{\sigma}(\vec{\mathrm{r}}\,|\,\tilde{\omega}:\omega) * \tilde{\vec{\mathrm{E}}}(\vec{\mathrm{r}}\,|\,\tilde{\omega}:\omega) + \underline{\vec{\mathrm{J}}}^{\mathrm{e}}(\vec{\mathrm{r}}\,|\,\tilde{\omega}:\omega)$$

$$\mathrm{div}\,\left[\tilde{\varepsilon}(\vec{\mathrm{r}}\,|\,\tilde{\omega}:\omega) * \tilde{\vec{\mathrm{E}}}(\vec{\mathrm{r}}\,|\,\tilde{\omega}:\omega)\right] \equiv \underline{\rho}^{\mathrm{e}}(\vec{\mathrm{r}}\,|\,\tilde{\omega}:\omega),\ \mathrm{div}\,\left[\mu(\vec{\mathrm{r}}\,|\,\tilde{\omega}:\omega) * \tilde{\vec{\mathrm{H}}}(\vec{\mathrm{r}}\,|\,\tilde{\omega}:\omega)\right] \equiv \underline{\rho}^{\mathrm{m}}(\vec{\mathrm{r}}\,|\,\tilde{\omega}:\omega)$$

when $\tilde{\omega} = -\omega$ for solving the effects of non-time variations in the region, where frequency varies continuously. Here the convolution $(*)$ is defined with respect to $\tilde{\omega}$ [1]. The dependence of constitutive parameters on time generates some specific currents in the material, which we call dispersion currents. The dispersion currents induce some specific charges on the material, which we call dispersion charges.

Dispersion Currents. Let us consider the junction of an isotropic and non-conducting TVFD/TDFV medium and a PEC material on a regular surface S. The interface can hold the surface charges and currents; therefore, surface electric charge ρ_S^{e}, surface electric current J_S^{e}, dispersion currents J_S^{ed} and J_S^{md}, and dispersion charges ρ_S^{ed} and ρ_S^{md} are induced on interface. So, we write followers, $\tilde{\omega} = -\omega$ by modified separation method [1-2]:

$$f_{\varepsilon^+}(:\omega)U_n^{e+}(\vec{r_S}\,|\,\tilde{\omega}:\omega)\tilde{T}_{\varepsilon^+}(\tilde{\omega}:\omega) * \tilde{T}_n^{e+}(\tilde{\omega}:\omega) = U_S^{\rho^{e}}(\vec{r_S}\,|\,\tilde{\omega}:\omega)\underline{T}_S^{\rho^{e}}(:\omega) + U_S^{\rho^{\mathrm{ed}}}(\vec{r_S}\,|\,\tilde{\omega}:\omega)\underline{T}_S^{\rho^{\mathrm{ed}}}(:\omega)$$

$$f_{\mu^+}(:\omega)U_n^{h+}(\vec{r_S}\,|\,\tilde{\omega}:\omega)\tilde{T}_{\mu^+}(\tilde{\omega}:\omega) * \tilde{T}_n^{h+}(\tilde{\omega}:\omega) = U_S^{\rho^{\mathrm{md}}}(\vec{r_S}\,|\,\tilde{\omega}:\omega)\underline{T}_S^{\rho^{\mathrm{md}}}(\omega)$$

Here, the U and T illustrate spatial and time parts of corresponding quantities, respectively.

Conclusions. The junctions of dielectric-to-perfectly electric conducting boundaries are studied in TDFV/TVFD cases. The boundary conditions are obtained.

REFERENCES

1. T. Sengör, "Analytic classification of time and frequency dependence basics in dielectric materials," *Helsinki Univ. Tech. Electromagnetics Lab. Rept.* 344, Nov. 2000.
2. T. Sengör, "Wave equation and solution in time varying and frequency dependent medium: plane case," *Helsinki Univ. Tech. Electromagnetics Lab. Rept.* 347, Dec. 2000.

A Closed-Form Formula for the Array Factor of Arrays with a Polygonal Contour

A. Cucini and S. Maci
Department of Information Engineering, University of Siena
Siena, 53100, Italy

In this paper, a closed-form formula for evaluating the array factor (AF) of planar phased arrays with a polygonal contour is presented. The derivation is based on the Floquet wave (FW) diffraction theory [F. Capolino et al., *IEEE Trans. Antennas Propagat.*, Vol. 47, No. 1, pp. 67–85, Jan. 2000]. In this theory the conventional element-by-element representation of the array Green's function (AGF), is replaced by an efficient 'global' asymptotic representation given in terms of a few ray-type contributions associated to *i*) FWs relevant to the infinite periodic structure, which are truncated at the array border, *ii*) FW-induced edge diffracted waves and *iii*) FW-induced vertex diffracted waves. The asymptotic result is cast in the format of a generalized periodicity-induced uniform geometrical theory of diffraction.

At the present state, the above theory is restricted to the treatment of rectangular periodic arrays with a rectangular grid. Here, in the same framework, a solution is presented for the AF of periodic arrays with a polygonal grid and a skewed grid. The solution is obtained starting from the solution relevant to the canonical problem of a planar sectoral array of elementary point sources. To this end, the formulation proposed in [F. Capolino et al., *Radio Science*, Vol. 35, No. 2, pp. 579–593, Mar.–Apr. 2000] is here extended to arbitrary sector angles and skewed grids, with limitation to observation in the far zone, maintaining the linear phase shift and constant amplitude distribution.

The solution is cast in a compact form of vertex diffraction coefficients, which exhibit singularities on the diffraction cones associated to the two confluent edges of the array sector. From this solution the AF is obtained by just superimposing the diffraction coefficients from each vertex of the polygonal rim. Thus, the final output is an elegant and simple way to exactly represent the AF in terms of a few contributions, which is independent of the number of sources. The singularities associated to the various diffraction coefficients compensate one to the other, thus giving a well-behaved field everywhere. The numerical impairment associated to the cancellation of singularities can be overcome by an *a priori* summation of contributions in the critical directions. Numerical examples will be presented tor illustrating possible applications and benefits.

This formulation constitutes the basis for a general extension of a uniform asymptotic field solution at finite distance from the array.

Session 3Ac1

Coherent Effects in Random Media

Fresnel Approximation for Wave Scattering in Random Medium

V. I. Tatarskii
Zel Technologies and NOAA/ETL
Boulder, CO 80303, U.S.A.

In the conventional theory of scattering by random medium the transverse scale L of the scattering volume is defined as $L = (\lambda/a)R$, where λ is the wave-length, a is the antenna diameter, and R is the distance from antenna to the scattering slab. In the far zone of antenna where $\sqrt{\lambda R}/a \gg 1$, we have $L = (\sqrt{\lambda R}/a)\sqrt{\lambda R} \gg \sqrt{\lambda R}$. On the other hand, the opposite assumption $L \ll \sqrt{\lambda R}$ is used in the Fraunhofer diffraction (scattering) theory. These two conflicting assumptions are simultaneously used in the conventional Fraunhofer scattering theory from extended scatterers.

We consider the single scattering of waves in a medium containing weak inhomogeneities of refractive index using Fresnel diffraction approximation. In this case, the assumption $L \ll \sqrt{\lambda R}$ is not necessary. We do not introduce the scattering volume but consider the transmitting antenna with the Gaussian distribution of current and receiving antenna with Gaussian distribution of attenuation across the aperture. The results obtained are valid both in the near and far zones of antenna.

Similarly to the Fraunhofer diffraction approach, the scattering intensity obtained is proportional to the Bragg component of the inhomogeneities that are averaged in Fourier space with some specific weighting function (spectral window) depending on antenna size and pulse duration. The width of spectral window in the transverse direction, $\Delta k = \gamma K_{\mathrm{Bragg}}$, where $\gamma = \lambda/a$ is the angular size of the antenna diagram, and K_{Bragg} is the Bragg wave number.

In the case considered in this paper, we deal with the scattering of Gaussian beam. The incident wave has different energy flux in different parts of the scattering volume, and receiving antenna summarizes scattered fields from different parts of scattering volume coherently. In such conditions we are unable to determine the scattering cross-section using common definition. To describe the relative scattering intensity, we use the ratio of the mean squares of the electric field at the antenna horn in the cases of scattering from random inhomogeneities and reflection from ideal mirror.

Statistical Analysis of Target Detection for Subsurface Radar Sensing of Buried Objects in Random Media

Y. Miyazaki and K. Takahashi
Department of Information and Computer Sciences,
Toyohashi University of Technology
Toyohashi-shi, 441-8580, Japan

Subsurface radar is one of useful target methods of buried objects, such as gas and water pipes, archaeological remains and mines. The soil is an inhomogeneous medium consisting of several kinds of compositions. Received signals have random fluctuations due to many undesirable scattered waves. In this paper, characteristics of unwanted scattered wave are studied for reduction of unwanted signals and improvement of SN ratio of received signals is shown. In a simulation model, the target is buried in random media. Incident electromagnetic pulse is scattered by the target and many obstacles buried in the random media. Transient response of EM pulse by buried objects is numerically simulated using FDTD method.

In this model, random media consist of many scatterers, which are statistically distributed with small and large sizes comparing with the wavelength of pulse spectrum. Impulse width around 1 nsec is considered. The permittivity and conductivity of dry soil with water content of 5% are assumed to be 4.0 and 0.007 S/m respectively at main pulse spectrum. Each scatterer has several shapes with random size, center coordinate and relative permittivity. The bow-tie antennas are used for transmitting and receiving pulses. The transmitting antenna is fixed to be y-directed, and the direction of receiving antenna is for co-polarized response and cross-polarized response y and x directions. Statistical properties of received signals and random media are analyzed using statistical correlation functions. The received signals are evaluated by correlation coefficient and variance, considering received signals in homogeneous media and in inhomogeneous media. Correlation coefficient between the signals of two cases decreases with variance of permittivity and variance increases.

For the image of the buried object, received signals at several different positions on the ground surface are synthesized as signal processing. SAR is a conventional tool for detection of buried target and resolution can be improved. In this paper, the characteristics of detection of buried target are discussed for various random media, using synthetic aperture processing.

As a result of image processing, distributed received signals from the target yield the actual scattering images.

To obtain more rigorous characteristics, further simulations at various situations and the comparison with the theory of wave scattering from random media, are discussed. Based on these computer simulations, the optimum detection systems of subsurface radar in random media can be constructed.

Resonances in 1D Anderson Localization of EM Waves: Local and Average Field Intensities

J. A. Sánchez-Gil
Instituto de Estructura de la Materia, C.S.I.C
Madrid, 28006, Spain

V. Freilikher
The Jack and Pearl Resnick Institute of Advanced Technology, Department of Physics, Bar-Ilan University
Ramat-Gan, 52900, Israel

I. V. Yurkevich
School of Physics and Space Research, University of Birmingham
Birmingham, B29 4LU, UK

We investigate the one-dimensional propagation of EM waves in the strong localization regime. In particular, the occurrence of anomalously large transmission coefficients for given realizations and/or frequencies (resonant or quasi-transparent realizations) is studied, with emphasis on the field intensity distributions along the direction of propagation. For that purpose, we make use of both an analytical formulation and rigorous numerical simulation calculations. As an example of a one-dimensional disordered system we consider a waveguide formed by two parallel, perfectly conducting planes, one of which presents random height deviations with Gaussian statistics and correlation function. The frequency ω and waveguide thickness are chosen in such a manner that only one p-polarized guided mode is supported. In addition, the surface roughness parameters and waveguide length guarantee that the Anderson localization regime is reached ($L \gg \xi_{loc}$, where L is the length of the rough segment and ξ_{loc} is the localization length). The analytical consideration is based upon the invariant embedding method and averaging over rapid phase; the numerical calculations exploit the invariant embedding equation formulation for a surface disordered waveguide.

We examine the frequency dependence (in a narrow frequency range) of the transmission coefficient $T(\omega)$ for a given realization. Whereas the spectral response yields typically very low values of T, as expected from the average $\langle LnT\rangle \sim -L/\xi_{loc}$ over an ensemble of realizations, there exist very narrow resonances at which the transmission coefficient can be even close to 1. The EM field for a resonant frequency/realization exhibits high intensity concentration in a narrow region around the center of the system, in contrast with typical, low transmission frequency/realization for which the intensity decays monotonically.

Numerical simulation calculations are also carried out for the mean EM field intensity $\langle I\rangle$ inside the waveguide for fixed $\omega,\ L$, and statistical parameters of the roughness. Averages are done separating typical and resonant realizations according to a threshold value of T_r (typically, $T_r \gg \langle T\rangle$). We find that the average over resonant realizations $\langle I\rangle_{res}$ is a broad distribution with a maximum (larger than the incoming wave intensity) at some point near the center of the waveguide. The distribution depends on both L and ξ_{loc}. On the contrary, the averaging over typical realizations yields the coordinate dependence, $\langle I\rangle_{typ}$, that is a rapidly decaying monotonic function practically independent on L. As a result from both contributions, the total average $\langle I\rangle$ exhibits a nearly at (L-dependent) plateau at the entrance of the waveguide, its shape resembling the analytical prediction.

Spectral Representation of Wave Field Scattered from a Periodic Random Surface

J. Nakayama[1] **and V. Freilikher**[2]

[1] Kyoto Institute of Technology, *Kyoto 606-8585, Japan*
[2] Bar-Ilan University, *Ramat-Gan 52900, Israel*

This paper deals with a spectral representation of wave field scattered from a periodic random surface, of which average and two-point correlation function are periodic. Let us consider a two-dimensional case, where the periodic random surface is mathematically given by a periodic stationary process $f(x,\omega)$ with the period L,

$$z = f(x,\omega), \quad (-\infty < x < \infty) \tag{1}$$

Here, ω is a probability parameter denoting a sample point in the sample space Ω. We note that $f(x,\omega)$ satisfies the shift invariance: $f(x+mL,\omega) = f(x,T^m\omega)$, where m is any integer and T is a measure-preserving transformation in Ω. If we define a displacement operator D^m that carries (x,ω) into $(x+mL,T^{-m}\omega)$ as $D^m f(x,\omega) = f(x+mL,T^{-m}\omega)$ the periodic random surface becomes invariant under the operator D^m for any integer m.

A periodic stationary process $f(x,\omega)$ is periodic on average and is known to have a harmonics series representation,

$$f(x,\omega) = \sum_{m=-\infty}^{\infty} [f_m^{(a)} + f_m(x,\omega)] e^{imk_L x}, \tag{2}$$

where $k_L = 2\pi/L$, $f_m^{(a)}$ is the Fourier coefficient of the average $\langle f(x,\omega)\rangle$ and $f_m(x,\omega)$ is a band-limited stationary process with zero mean and correlation function $R_{mn}(x_1 - x_2)$=$\langle f_m(x,\omega) f_n^*(x,\omega)\rangle$, the angle brackets and the asterisk denoting ensemble average and complex conjugate, respectively.

We denote the wave field by $\psi(x,z,\omega)$, which satisfies the wave equation and a boundary condition on (1). Regarding $\psi(x,z,\omega)$ as a functional of the periodic random surface (1), we define a linear transformation as

$$\Psi(x,z,\omega|p) = \sum_{m=-\infty}^{\infty} D^m[\psi(x,z,\omega)e^{-ipx}] = \sum_{m=-\infty}^{\infty} \psi(x+mL,z,T^{-m}\omega)e^{-ip(x+mL)} \tag{3}$$

Then, the spectrum $\Psi(x,z,\omega|p)$ becomes invariant under D^m, i.e. $D^m\Psi(x,z,\omega|p) = \Psi(x,z,\omega|p)$. This means that $\Psi(x,z,\omega|p)$ is a periodic stationary process of x. Thus, we write its harmonics series representation as

$$\Psi(x,z,\omega|p) = \sum_{m=-\infty}^{\infty} e^{imk_L x} \times [\Psi_m^{(a)}(z|p) + \Psi_m(x,z,\omega|p)] \tag{4}$$

where $\Psi_m^{(a)}(z|p)$ is the Fourier coefficient of the average spectrum $\langle\Psi(x,z,\omega|p)\rangle$ and $\Psi_m(x,z,\omega|p)$ is a band-limited stationary process with zero mean.

From (3), we find the inverse transformation $\psi(x,z,\omega) = \frac{1}{k_L}\int_{-k_L/2}^{k_L/2}\Psi(x,z,\omega|p)e^{ipx}dp$ which is a spectral representation of wave field scattered from a periodic random surface. Using (4), we find a representation of the coherent wave,

$$\langle\psi(x,z,\omega)\rangle = \frac{1}{k_L}\sum_{m=-\infty}^{\infty} e^{ik_L mx} \times \int_{-k_L/2}^{k_L/2} \Psi_m^{(a)}(z|p)e^{ipx}dp. \tag{5}$$

The spectral representation may be applicable to inhomogeneous problems such as the scattered wave from a periodic random surface with finite extent and Green's function over a periodic random surface. Some of these applications will be discussed.

Ultrasonic Multiple Scattering

J. Scales
Colorado School of Mines
Golden, CO 80401, U.S.A.

In many fields involving wave propagation in heterogeneous media, multiply scattered waves are often regarded as a source of “noise”, best removed from the data. Partly this is because data processing algorithms are usually based on single-scattering theory, such as the Born approximation; but also, there is a sense that multiply scattered waves are “chaotic” or unstable. Recent work has shown that this need not be the case and that multiply scattered waves can be exploited to make inferences about the scattering medium. Despite the complexity of multiply scattered wave-fields, there are many potential advantages to exploiting these waves. In particular, multiply scattered waves are sensitive to small changes in the medium, since those small changes are amplified upon repeated scattering. Further, these waves tend to sample the medium more uniformly, providing increased aperture of illumination of the target.

In order to study the propagation of multiply scattered waves, it is useful to have a medium in which the scattering properties can be easily controlled. Here we describe such a system; it involves the propagation of ultrasonic surface waves in a medium with an aligned, disordered, pattern of grooves. Waves propagating parallel to the grooves see a homogeneous medium; waves propagating perpendicular to the grooves are strongly scattered. By varying the source-receiver orientation with respect to the grooves and the distance between source and receiver, we are able to map out the transition from ballistic to diffusive propagation. In addition, by using an optical detection system we are able to measure the wave motion *inside* the scattering medium. We measure the angle-dependent macroscopic properties of the medium, such as the phase and group velocity; but also the mean free path and the diffusion constant in the strong-scattering regime. We will also show examples of the measurement and analysis of multiply scattered waves in rocks, which are randomly heterogeneous.

Numerical Analysis of Bistatic Cross-Sections of Concave-Convex Conducting Cylinders in Continuous Random Media

M. Tateiba and M. Nakashima
Dept. of Computer Science and Communication Engineering, Kyushu University
Higashi-ku, Fukuoka 812–8581, Japan

Z. Q. Meng
Dept. of Electrical Engineering, Fukuoka University
Jonan-ku, Fukuoka 814–0180, Japan

As well known, the backscattering enhancement was found out in theory and experiments as a fundamental phenomenon in a random medium, which is produced by statistical coupling of incident and backscattered waves due to the coherent effect of double passage. When the average scattered intensity is enhanced in the backward direction, it is predicted to decrease in some other directions from the law of energy conservation. To make clear numerically the prediction as well as the scattering characteristics, we need to analyze the bistatic cross-section(BCS).

We have analyzed numerically the BCS of a conducting circular cylinder in a continuous random media for E- and H-wave incidence. The numerical results of BCS agree well with the law of energy conservation. Both the BCS enhancement and diminution phenomena, which have been predicted for a point scattering, are made sure numerically for the cylinders of resonance region size. We have found out that second peaks of BCS appear outside the valleys where the diminution occurs. This appearance is caused by the interference of incident and scattered waves in a small cone of which center is the cylinder and central axis is in the back-ward direction.

Here we extend the cylinder cross-section from a circle to an arbitrary shape and analyze numerically the BCS of the cylinder in a continuous random medium for E- and H-wave incidence. The results agree well with the law of energy conservation. we also find the second peaks outside the valleys. The medium effect on the BCS is almost the same for the change in cross-section shape of the cylinder under the condition that the spatial coherent length of incident waves around the cylinder is much larger than the cross-section size of the cylinder.

Effective Propagation Constant Model of a Disordered Waveguide System

A. Komiyama
Osaka Electro-Communication University
Hatsu-cho Neyagawa-shi, 572-8530, Japan

In an ordered system composed of identical cores of equal spacing mode waves are extended over the entire system. On the other hand, in a disordered waveguide system composed of randomly different cores in size mode waves are localized into a narrow region of several cores[1]. In this paper a simple model of a disordered waveguide system is presented on a basis of the concept of an effective propagation constant which simulates the localization properties of mode waves in a disordered waveguide system. For an electronic system the model was introduced by Soven[2] under the name of the coherent-potential model.

At every core in the waveguide system we place an effective propagation constant β_c and denote the Green's function for the ordered system by $\overline{\mathbf{G}}_\mathbf{0}$. The Green's function $\mathbf{G}$ for a d-dimensional disordered waveguide system is represented in the form of an infinite perturbation series,

$$\mathbf{G} = \overline{\mathbf{G}}_\mathbf{0} - \sum_{\ell} \overline{\mathbf{G}}_\mathbf{0} \bar{\mathbf{t}}_\ell \overline{\mathbf{G}}_\mathbf{0} + a^d \sum_{\ell} \sum_{p \neq \ell} \overline{\mathbf{G}}_\mathbf{0} \bar{\mathbf{t}}_\ell \overline{\mathbf{G}}_\mathbf{0} \bar{\mathbf{t}}_\mathbf{p} \overline{\mathbf{G}}_\mathbf{0} - \cdots \tag{1}$$

where a is a spacing between cores and $\bar{\mathbf{t}}_l$, is a scattering matrix describing the scattering of a wave from the perturbing propagation constant $\beta_l - \beta_c$ of the ℓth core. The unknown effective propagation constant β_c is determined by the requirement that there is no further scattering from the perturbing propagation constants on average,

$$< \bar{\mathbf{t}}_\ell >= 0 \tag{2}$$

We approximate the average Green's function as follows:

$$< \mathbf{G} >= \overline{\mathbf{G}}_\mathbf{0} \tag{3}$$

In order to verify the validity of the model we calculate the modal density of states of one- and two-dimensional waveguide systems. The theoretical results are in good agreement with the results obtained by numerically solving the coupled mode equation. It is found that the effective propagation constant model is adequate for describing the localization properties of the mode waves.

REFERENCES

1. A. Komiyama, *Opt. Comm.*, 151, pp. 25–30, 1998.
2. P. Soven, *Phys. Rev.*, 156, pp. 809–813, 1967.

Asymptotic Form for Random Cylindrical Waves and Localization in 2-Dimensional Random Medium

H. Ogura
Kinki University
Uchita, Wakayama 649-6493, Japan

Random wave field in a 2D homogenous and isotropic random field is shown to have the angular mode with quantum number M defined by the rotation operator arising from the stochastic rotational symmetry of random medium, which we call the random cylindrical wave in analogy to the one in the free space [1]. Such an angular mode is studied in the polar coordaintes using the polar spectral representations for a homogeneous and isotropic random field [2]. The isotropic mode ($M = 0$) is calculated for a narrowband medium which describes a random grating having an isotropic narrow band spectrum with central spatial frequency $2k$ twice as much as the wave number k. The asymptotic form in the radial direction is obtained by solving a set of coupled equations for the inward and outgoing cylindrical waves, and the exponential factor $e^{\gamma kr}/\sqrt{kr}$, $\gamma = \alpha + i\beta$, is obtained in terms of the spectrum. The same exponential factor can be obtained for the 2D random plane wave by the analysis based on the translation operator associated with the homogeneity of the random medium.

The exponential index γ is concretely calculated assuming a Gaussian spectrum; $\alpha = \pm 0.0538\sigma^2/\sqrt{\Delta}$, $\beta = 0.0602\sigma^2/\sqrt{\Delta}$, where σ^2 denotes the variance and Δ/k the spectral width. It can be compared with 1D random plane wave [3] where the exponential factor $e^{\gamma kx}$, $\alpha = \pm 0.1556\sigma^2/\Delta$, $\beta = 0$ for a similar Gaussian spectrum. Since σ^2/Δ equals the spectral height the extra factor $\sqrt{\Delta}$ in 2D case comes from the interactions in 2D spectral space. The exponential factor, representing the stochastic decay or growth of the amplitude in the radial direction, describes the localized nature of an isotropic random wave field generated by a symmetric source or by a source-free resonance wherever the resonant condition is satisfied.

REFERENCES

1. H. Ogura: Stochastic theory of wave localization in 2-dimensional random media, *Proceedings, URSI Int. Symp. on EMT*, Victoria, pp. 573-576 (2001).
2. H. Ogura: Polar spectral representation for a homogeneous and isotropic random medium, *J. Phys. Soc. Japan*, Vol. 21, pp. 1370-1380 (1968).
3. H. Ogura: Theory of waves in a homogeneous random medium, *Physical Review A*, Vol. 11, No. 3, pp. 942-956 (1975).

Is a Linear Dependence of Physical Quantities on the Surface Roughness Possible in Rough Surface Scattering?

V. Freilikher
The Jack and Pearl Resnick Institute of Advanced Technology, Bar Ilan University
Ramat Gan, Wakayama 52900, Israel

T. A. Leskova
Institute of Spectroscopy, Russian Academy of Sciences
Troitsk, Wakayama 142090, Russia

A. A. Maradudin
Department of Physics and Astronomy and Institute for Surface and Interface Science, University of California, Irvine
Irvine, California 92697, U.S.A.

N. M. Makarov
Instituto de Ciencias, Universidad Autónoma de Puebla
Puebla, Pue. 72050, México

Literally thousands of theoretical studies have treated the problem of the scattering of electromagnetic waves from weakly rough random surfaces. The weakness of the surface roughness assumed allows this problem to be treated perturbatively, and a number of different versions of perturbation theory were developed to attack different aspects of the scattering problem. The roughness-induced effects were shown to be of $\mathcal{O}(\delta^2)$, where δ is the rms height of the surface roughness. Recently, Makarov and Moroz [1] developed a new approach that they call the "exact–scattering operator" approach, for studying the spectrum of waveguide modes in a planar TH waveguide bounded by weakly rough, random, perfectly conducting surfaces. The result of their study was quite unexpected and unconventional. They showed that in the limit of small roughness the real parts of the wavenumbers of the waveguide modes exhibit a linear dependence on δ. For a semi-infinite medium their result implies that the imaginary part of the roughness-induced corrections to the average reflection coefficient should also exhibit a linear dependence on δ. To check the results of [1], in this paper we calculate the average reflection coefficient of light scattered from the weakly rough random surface of a semi–infinite perfect conductor. We do this with the use of the different approaches developed up to now: self–energy perturbation theory, phase perturbation theory, the small–slope approximation, small–contrast perturbation theory, modified to apply to the perfect conductor (infinite–contrast) case, and the exact scattering operator approach developed in [1]. In no case is a linear dependence on δ found.

REFERENCES

1. N. M. Makarov and A. V. Moroz, "Spectral theory of a surface-corrugated electron waveguide: The exact scattering-operator approach", Phys. Rev. B**60**,258-269 (1999).

Anomalous Transmission in Waveguides with Correlated Surface Disorder

F. M. Izrailev and N. M. Makarov
Instituto de Física, Universidad Autónoma de Puebla
Puebla, Pue., 72570, México

Wave transmission through a single-mode waveguide of average width d and randomly corrugated surface characterized by the variance σ^2, is described by using the theory of one-dimensional localization. The corresponding localization length is [1]

$$L_{loc}^{-1} = (\sigma/\pi)^2(\pi/d)^6 W(2k_1)/(2k_1)^2. \tag{1}$$

Therefore all transport properties of such a waveguide are determined by the Fourier transform $W(k_x)$ of surface-roughness binary correlator (x runs along the waveguide). In particular, if $W(2k_1)$ vanishes within some interval of the wave number $k_1 = \sqrt{(\omega/c)^2 - (\pi/d)^2}$, the waveguide is entirely transparent. We can construct a disordered surface profile $\xi(x)$ that results in perfect transparency in a given range of k_1, by representing $\xi(x)$ in the following form:

$$\xi(x) = \sigma \int_{-\infty}^{\infty} dx'\, Z(x-x')\, \beta(x'), \tag{2}$$

with some function $\beta(x)$ determined by the Fourier transform $W(k_x)$,

$$\beta(x) = \int_{-\infty}^{\infty} (dk_x/2\pi) \exp(ik_x x)\, W^{1/2}(k_x). \tag{3}$$

Here $Z(x)$ is a delta-correlated random process ("white noise") with $\langle Z(x)\rangle = 0$ and $\langle Z(x)Z(x')\rangle = \delta(x-x')$. Equations (2) and (3) allow practical solution of an inverse scattering problem of constructing a corrugated surface from its binary correlator.

Based on the method suggested, we demonstrate a possibility of fabricating rough surfaces that possess any desired combination of transparent and non-transparent windows depending on the frequency ω of an incoming wave. This can be done by proper choice of specific long-range correlations along the waveguide. Direct numerical solution of the corresponding wave equation proves effectiveness of the theoretical predictions. The results presented here can be used for experimental realization of waveguides with preselected transmission selectivity. Note that random surfaces with discontinuous dependence $W(k_x)$ were recently fabricated in an experimental study of backscattering enhancement [2].

The research was supported by Consejo Nacional de Ciencia y Tecnología (CONACYT, México) grants 34668-E, 38072-E and by Universidad Autónoma de Puebla (BUAP, México) grant II-63G01.

REFERENCES

1. Freilikher, V., N. M. Makarov, and I. V. Yurkevich, *Phys. Rev. B,* Vol. 41, 8033, 1990.
2. West, C. S. and K. A. O'Donnell, *J. Opt. Soc. Am. A,* Vol. 12, 390, 1995.

Session 3Ac2

Microelectronic Packaging I

The Development of a 2D Unconditionally Stable Transmission-Line-Modeling Method

Y.-M. Lee and C. C.-P. Chen
Department of Electrical and Computer Engineering
University of Wisconsin at Madison
Madison, WI 53706 , U.S.A.

The TLM (Transmission-Line-Modeling) method has been successfully applied to simulate VLSI packaging and PCB applications especially for the grid or plan structure. Due to the miniature features, the time-steps are limited by the CFL stability condition. As a result, it is often that millions of time-step is required to complete a reasonable simulation especially for Deep-Sub-Micron on-chip VLSI applications. So far, most of the researchers are working on developing the unconditionally stable FDTD (Finite Difference Time Domain) method [2–4]. Since TLM explains everything in terms of circuit concept, we think it is of great interests to develop an unconditionally stable TLM method for VLSI applications [1].

In this paper, we will present our recent progress on the development of a 2D TLM method based on the ADI (Alternating-Direction-Implicit) algorithm. The proposed algorithm, with linear runtime and memory requirement, is also unconditionally stable which ensures that the time-step is not limited by any stability requirement. Theoretical analysis and extensive experimental results show that the proposed algorithm is not only orders of magnitude faster than fully implicit method but also extremely memory saving and accurate for deep-sub-micron VLSI applications.

REFERENCES

1. Christos Christopoulos, *The Transmission-Line Modeling Method TLM*, Oxford University Press, 1995.
2. Allen Taflove, and Susan C Hagness, *Computational Electrodynamics - the Finite-Difference Time-Domain Method*, Artech House Publishers, 2000.
3. Takefumi Narniki, "A new FDTD algorithm based on alternating-direction implicit method," *IEEE Trans. on Microwave Theory and Techniques,* Vol. 47, No. 10, 1999.
4. Fenghua Zheng, Zhizhang Chen, and Jiazong Zhang, "Towards the development of a three-dimensional unconditionally stable Finite- Difference Time-Domain method," *IEEE Trans. on Microwave Theory and Techniques,* Vol. 48, No. 9, pp. 1500–1558, 2000.

Simulations of Large Number of Vias in Electronic Packaging Structure

L. Tsang*, **H. Chen, Q. Li, C.-C. Huang, and V. Jandhyala**
Department of Electrical Engineering, University of Washington
Seattle, WA 98195, U.S.A.

Via structure is extensively used in electronic package to connect signal traces residing on different layers of the circuits because of ever-increasing density and routing complexity in IC design. The via problem represents major coupling because waves decay as the square root of distance due to the parallel plate waveguide effects. The signals (current or voltage) on the active via cylinders excite waveguide modes along the plane and affect other active or passive vias. The affected vias can in turn influence the original signal. This poses considerable design and simulation problems for reliability. Such coupling can cause unreliable circuit behavior or complete signal failure, such as signal integrity loss, higher delays, and inappropriate switching of devices.

In this paper, we developed a semi-analytical technique by using Foldy-Lax equations to compute the full wave solution of multiple interactions among cylindrical vias in a planar waveguide with either infinite or finite ground plane. Using the equivalence principle, the structure is decomposed into interior and exterior problem. The interior problem consists of large number of vertical cylinders placed in parallel plate waveguide. The exterior problem consists of coupled transmission lines bent into the vertical via sections outside the parallel plate waveguide. For the interior problem, Foldy-Lax equations in vector cylinderical waves, waveguide modes and resonator modes are derived to describe the multiple scattering among the cylinders excited by the magnetic current sources. The exterior problem is analyzed using the MOM method. The exterior and interior problems are combined into a matrix equation by relating the port voltages and currents. It is solved by iterative method of which the solution gives the propagation characteristics of the entire structure.

The procedure can give the solution of several thousand vias with moderate CPU and memory requirement. Based on the developed algorithm, simulations are done to model multiple scattering among large number of vias with numerical results shown for several thousand vias. Because of the importance of differential signaling, also illustrated are the results for common mode and differential mode in differential signaling, including the effects of several thousand idle vias and shorting vias. For the multi-layered via structure, it is decomposed into several single-layered via structure and their transfer matrices are cascaded together to give the final transfer matrix of multi-layered via structure. The simulation results are given for cases with different vias radius, anti-pad radius, layer thickness, number of layers, and for infinite and finite power/ground planes.

---

* Also with City University of Hong Kong

Evaluating the Effectiveness of SMT Decoupling Capacitors Placed in Proximity to IC Power/Ground Pin Connections for Mitigating High-Frequency Power Bus Noise

S. Luan[1], J. Fan[2], W. Cui[3], J. Drewniak[1], J. Knighten[2], T. VanDoren[1]
[1]UMR EMC Laboratory, ECE Department, University of Missouri-Rolla, *Rolla, MO, USA*
[2]NCR Corporation, Teradata Division, *San Diego, CA, USA*
[3]Intel Corporation, *Chandler, AZ, USA*

Switching IC devices that are powered through a DC distribution topology which uses entire layers for power and ground in a multi-layer printed circuit board (PCB) produce high-frequency noise that is easily propagated throughout the system on the parallel-plane transmission line formed by the power and ground planes. This high-frequency noise, with a spectrum into gigahertz frequencies for current high-speed devices can lead to SI and EMI problems. Surface mount technology (SMT) decoupling capacitors are typically used in high-speed digital design to mitigate high-frequency noise on the DC power bus that results from the active device. For multi-layer PCBs that employ entire layers for power and ground, some design maxims specify placing SMT capacitors in proximity to an IC device to mitigate the simultaneous switching noise. The reasoning is to decouple the high-frequency noise that results from a particular device. In this sense, the SMT capacitor is designated as a local capacitor. Other design maxims purport that SMT decoupling capacitors should be distributed in an approximate uniform distribution over the PCB, and that the noise mitigation benefits are global, i.e., these capacitors are shared by all devices. These differing design maxims are often advanced as absolute, and, hence, one must be in error. However, recent work has shown that for certain layer stackups noise mitigation benefits can be achieved through placing a capacitor in proximity to an IC device. The specific physics is a consequence of the mutual inductance between the vias of the IC and the decoupling capacitor. The magnetic flux linkage giving rise to this mutual inductance is between the power and ground planes. This effect is frequency independent (for electrically short vias), and consequently, capacitors placed in proximity to an IC device can have an effect to very high frequencies, even beyond the normal series resonance of the capacitance and interconnect inductance. From these physics, an equivalent circuit, and figure of merit quantifying the noise mitigation benefits of an SMT decoupling capacitor in proximity to an IC has been developed. The benefit of an SMT capacitor placed in proximity to an IC is essentially quantified through the coupling coefficient for the mutual inductance, and the ratio of the portion of the interconnect inductance above the planes, to that between the planes.

A means for quantifying the portion of the interconnect inductance between the planes, and the portion above the planes in order to evaluate the ratio has been developed. The PCB geometry that includes the multi-layer stackup, vias, and power and ground planes is modeled using a mixed-potential integral equation formulation. A quasi-static approximation to the Greens function for a multi-layer medium is made, and a SPICE model extracted from the formulation, as opposed to solving the MOM problem. In this sense, the method is a variation of the partial element equivalent circuit (PEEC) method. Using this formulation, the inductance for the portion of the via between the planes has been extracted, as a function of the via location, and an empirical equation developed. Similarly, the coupling coefficient between two coupled vias between the planes has been extracted from the PEEC formulation. Then, knowing the total inductance of the SMT interconnect, the part of the inductance due to the portion of the interconnect above the planes can be determined. Finally, the ratio of the portion of the inductance above the planes, to that between the planes can be evaluated, and the noise mitigation benefits of the local SMT assessed.

The results show that only for certain types of layer stickups can appreciable power bus noise mitigation be achieved by placing a decoupling capacitor in proximity to an IC device. However, with the proposed approach, this can be easily quantified, and design formulas for engineering application have been developed.

Fast Lumped-Element Models for 3D Vertical Interconnects in Multilayer PCBs

G. V. Eleftheriades and R. Abhari
The Edward S. Rogers Sr. Department of Electrical and Computer Engineering
University of Toronto
Toronto, ON M5S 3G4, Canada

Presently, the telecommunications and personal computer industries have to cope with electrical data signals with multigigabit/sec bit rates. It is well established that the bottleneck for increased data rates will arise from interconnect and heat dissipation restrictions rather than from intrinsic semiconductor device limitations. Metallic interconnects can no longer be regarded as traces that can instantaneously propagate digital signals (1's and 0's) from one point to another. Such interconnects have to be carefully accounted for and their effect on signal integrity has to be predicted and minimized to the best possible extend. Interconnect effects such as propagation delay, ground-noise and associated cross-talk, reflections and package resonances, dispersion and intersymbol interference have to be included in the overall digital design, both at the printed circuit board (PCB) as well as the chip levels.

In order to become able to predict and minimize the undesired effects of interconnects to the signal integrity of next generation high-speed, high-density PCBs, fast but accurate models for the interconnects are urgently required. To this end, in this overview talk we will be presenting lumped element models for 3D vertical interconnects (i.e., vias) in multilayer printed-circuit-boards that are based on radial transmission line theory. Although these CAD via models are circuit based and thus fast, nevertheless they *can accurately* predict the induced ground noise, a purely distributed effect. The models have been applied to a great variety of situations, including multilayer PCBs, coupled traces, as well as the prediction of reflections and package resonances. In all cases the accuracy of the models will be assessed against full-wave finite difference time domain (FDTD) simulations as well as time-domain-reflectometry (TDR) measurements.

The developed models have been utilized for investigating ground noise reduction techniques. Such techniques include the use of decoupling capacitors and the employment of differential traces and vias. In addition, a novel technique for ground noise suppression/isolation is proposed and investigated based on electromagnetic band-gap (EBG) ground-planes with compact texture.

Accurate and Efficient Simulation of Crosstalks

J.-S. Zhao and W. C. Chew
University of Illinois at Urbana-Champaign
Urbana, IL 61801, U.S.A.

In high-speed digital and analog circuits, accurate and efficient prediction of rise time, time-delay, ground bounce, crosstalk, and reflection is very important. Because digital system clock speeds have become increasingly faster, original circuit model cannot capture all the electromagnetic information. Traditional full wave electromagnetic simulation is inapplicable due to the limitation of computer resources. Hence, fast full wave solver is needed. In addition, since the packaging and signal lines have become progressively smaller, the skin depth is comparable to the radius of the signal line. Here, the skin effect (finiteness of skin depth) cannot be ignored as opposed to high frequencies analysis.

We developed a code to accurately and efficiently simulate crosstalks between lossy conducting structures. Many new techniques are applied in the code. First, an accurate impedance boundary condition for very thin lossy wires at very low frequencies is presented. Numerical results show that this boundary condition is accurate for low-frequency problems. Then the Y matrix in the frequency domain of a lossy structure is calculated by using the surface integral equation with loop-tree basis and applying the low-frequency multilevel fast multipole algorithm (LF-MLFMA) to decrease the computation complexity. The application of loop-tree basis allows the surface integral equation be accurately solved down to very low frequencies. The application of LF-MLFMA decreases the memory requirements and work load from $O(N^2)$ to $O(N)$, where N is the number of unknowns. Therefore, large linear systems can be solved efficiently. A generalized formula to calculate the current and voltage at each port from the Y matrix and arbitrary sources and loads is also given. After the voltages and currents at each ports in the frequency domain are calculated, crosstalks are then obtained by using the fast Fourier transform (FFT) to transform the response from the frequency domain to the time domain. In this approach, all frequency spectra are included and calculated accurately and efficiently. The simulation is powerful, efficient, and accurate.

A Surface Integral Equation Based Technique for General Coupled Circuit-Electromagnetic Simulation

V. Jandhyala, Y. Wang, D. Gope, S. Chakaraborty, and R. Shi
Department of Electrical Engineering, University of Washington
Seattle, WA 98195, U.S.A.

Incorporating electromagnetic (EM) effects into circuit-level simulation is critical for a variety of high-speed and high-frequency circuit applications, including systems-on-chip, as well as electronic packaging, interfacing, and interconnects. Several mature approaches rely on equivalent circuit models, or state-space models, that describe EM interactions. Such models are then incorporated, in conjunction with model-order reduction, into circuit-based simulation tools such as SPICE and its myriad variants.

The partial equivalent electric circuit (PEEC) method is a successful approach, especially for digital interconnects, that is used to develop equivalent circuits that describe EM interactions through inductive, capacitive, and inductive coupling between basis functions described using brick-shaped filaments. However, there are some existing limitations of the PEEC approach, including the inability to model arbitrarily-shaped three-dimensional structures, problems with the fast solution of SPICE-level matrices with large dense sub-matrices, and ad-hoc nature of reduced-order models.

In this work, a surface-only approach to coupled circuit and electromagnetic simulation is presented. This method can be interpreted as both a generalization of PEEC as well as a means to use the surface-based method of moments (MoM) approach in a circuit scenario. Rao Wilton Glisson (RWG) basis functions are used to represent equivalent surface currents, and the exterior and interior of conductors are modeled using relevant Green's functions. In particular, interactions in the interior of non-perfect conductors are modeled using a lossy medium Green's function, for which special quadrature techniques are developed. These techniques enable the complete method to be used at both high frequencies, where surface impedance approximations are valid, and at very low frequencies, where skin depth is larger than the cross section of the conductors.

A coupled EM-circuit system is constructed wherein the EM interactions are described through a multi-region MoM formulation, the circuit interactions are described through modified nodal analysis (MNA), and the EM-circuit interactions are described through relevant boundary conditions. These boundary conditions include simple current continuity for flat structures, and a more involved implementation of the continuity equation for 3D structures with specified input and output terminal faces. Laterally infinite dielectric layers are incorporated through multilayered Green's functions, and both quasi-static and full-wave analyses are included.

Fast $\mathcal{O}(N \log N)$ solution methods are presented for the coupled system solution. The MoM matrix is compressed using low-rank decompositions of inductance and potential matrices, and this QR decomposition is used for both fast iterative and direct solution. The fast direct solver is particularly important for multiple right-hand-side problems such as substrate coupling. Several numerical examples are provided to demonstrate accuracy, efficiency, and generality of the complete approach.

Hybrid EM Solutions for SI and PI Simulation of Electronic Packaging System

R. Y. Chen
Sigrity, Inc.
4675 Stevens Creek Blvd., Suite 130
Santa Clara, CA 95051, U.S.A.

In electronic packaging systems, Signal Integrity (SI) and Power Integrity (PI) issues such as reflection noise, crosstalk, and ground bounce are all related to wave propagation, EM coupling, resonance and other EM phenomena. A 3D full-wave field solution, based on FEM, FDTD or MoM, will provide accurate simulation results. The vast computation resource requirement renders such methods inadequate for system level simulation. In the generalized field solver approach, all conductors need to be discretized, resulting a huge number of unknowns for all geometry details in a package or PCB.

We found that the geometry features for interconnects are not arbitrary 3D in shape. A typical package or PCB contains only traces, planes, and vias. In addition, the 3D EM fields generated inside this multi-layer structure are not arbitrary 3D either. Therefore the fields can be solved using special algorithms with necessary accuracy and much improved efficiency. We propose a hybrid approach to handle different types of interconnect geometry using different EM solutions. This hybrid method resolves:

1. Transmission line effects for sections which exhibit such behavior;
2. Full-wave effects for sections of the structure comparable to a wavelength;
3. Lumped circuit perturbations for parasitics that do not require a full-wave description and do not behave like a transmission line.

The special geometry handling, requires multiple solvers working together, such as transmission line solvers, full-wave field solvers, and circuit solvers. And all the different solvers need to be connected to each other using appropriate algorithms to account for the interactions between different geometry features in situations such as a via passing through planes then branching into a trace, or a trace over a plane gap, *etc*.

This hybrid method can deliver either frequency domain or time domain solutions. If all the solvers are in frequency domain, then the direct results can be S, Y, Z parameters at any locations of a complex packaging system; if all the solvers are in time domain, then the direct results can be voltage and current waveforms anywhere in the system, including the effects of non-linear IC component switching activities.

Since the full-wave solver is no longer responsible for solving all the geometry details, its algorithm can be greatly improved to handle specialized cases. The computation mesh setting can be much relaxed. Some of the field components can be eliminated during computation. Different EM solving techniques may be combined to achieve more accurate and more efficient solutions. For example, FD can be used to model the planes; meanwhile, BEM may be used to model the reflection and radiation at the packaging edges.

In essence, this hybrid approach provides necessary field-solution-based accuracy for SI and PI simulation of electronic packaging systems with much improved simulation speed.

The Development of an Efficient Time Domain PEEC Solver and Inductance Sparsification

T.-H. Chen and C. C.-P. Chen
Department of Electrical and Computer Engineering, University of Wisconsin at Madison
Madison, WI 53706, U.S.A.

Parasitic on-chip inductance is growing into another design concerns as the VLSI technologies march toward ultra deep sub-micron and approach frequency in the gigahertz range. Inductive coupling effect becomes more important as the higher frequency signal contents, denser geometries, reduction of both resistance and capacitance by copper and low-K devices. Inductance effects presents not only in IC packages, but also in on-chip interconnects such as power grids, clock nets and bus structures. It causes overshoot, undershoot and oscillation of signal, aggravates crosstalk and power grid noise, which seriously impact signal integrity on-chip.

One of the main problem with inductance modeling is the long range coupling effects and return paths uncertainty since inductance is a function of a closed loop, which is hard to predict in advance before simulations. In fact, return paths are also frequency dependent and may change in a cycle-by-cycle basis due to different logic switch patterns and gate resistance. For this reason, A. Ruehli developed the famous Partial Element Equivalent Circuit method (PEEC) [3] models for parasitics modeling. PEEC method defines the partial self and mutual inductance for each wire segment with the assumption that each wire has return loop in infinity. Basically, PEEC models can be used to solve the inductance issues in either frequency and time domain. In the frequency domain, FastHenry [4] utilizes a multi-pole acceleration technique to speed up the extraction process. As in the time domain, [5] proposes to directly simulate the PEEC model in the time domain to determine the return paths. This method has been shown to be accurate in a wide range of frequencies.

The PEEC models, however, lead to a large scale dense inductance matrix since the long range effects of inductive coupling and the uncertainty of current return paths require the consideration of millions of mutual inductance terms to capture inductance effects. The traditional circuit simulation engines may require hours or even days for such a large scale dense matrix simulation. To effectively reduce the mutual inductance terms, sparsification is crucial.

In this paper, we propose to develop and integrate novel inductance sparsfication methods, advanced circuit formula-tion techniques, and excel matrix solving algorithms to develop an efficient, accurate, and inductance-wise interconnect simulation engine under time-domain PEEC model, INDUCTWISE. Extensive simulations show that the combination of inductance reduction method (8X) and advanced matrix solving techniques (50X) achieve a total over 400X speed up over SPICE3.

REFERENCES

1. Beattie, M. W. and L. T. Pileggi, “Inductance 101: Modeling and extraction,” In *DAC*, June 2001.
2. Gala, K., D. Blaauw, J. Wang, V. Zolotov, and M. Zhao, “Inductance 101: Analysis and design issues,” In *DAC*, June 2001.
3. Ruehli, A. E., “Inductance calculatioin in a complex integrated curcuit environment,” *IBM Journal of Research and Development,* 470–481, September 1972.
4. Kamon, M., M. J. Tsuk, and J. K. White, “Fasthenry: A multipole-accelerated 3-d inductance extraction program,” In *DAC*, June 1993.
5. Lillis, J., C. K. Cheng, Norman Chang, and Shen Lin, “Inteconnect analysis and synthesis.

Modeling of Plane Discontinuities for Power-Distribution Networks

J. Miller and I. Novak
Sun Microsystems
Burlington, MA 01803, U.S.A.

Accurate printed circuit board (PCB) modeling is critically important for the design of robust power-distribution networks. Models are required for the power and ground planes (including irregularities, such as cutouts) and discontinuities, such as vias. Several approaches have been proposed for accurate modeling of the power and ground planes including the transmission-line grid method and the analytic plane-impedance method. This report examines approaches to modeling discontinuities, such as vias and anti-pads, in terms of model accuracy and efficiency. Accurate plane models are needed to ensure that impedance targets are met for the power-distribution network and to satisfy DC power requirements. Accurate modeling of discontinuities is important for several reasons: 1) The inductance of these discontinuities can exceed the horizontal component of the plane, 2) discontinuities can significantly alter the impedance profile and resonance locations and 3) accurate current return paths depend heavily on the handling of discontinuities within the overall power-distribution network.

In this report, modeling of vias and anti-pads within the context of the overall power-distribution system is studied. A simple model for handling vias which minimizes the number of circuit elements is shown to be accurate. A methodology is presented for assessing the accuracy of the simplified via model for a particular PCB technology application. This assessment is made by comparing the contribution of the partial mutual inductance to the loop inductance. By using this approach, a trade-off can be made between simulation efficiency and simulation accuracy. For example, for via lengths less than 30 mils and via diameters less than 20 mils, the simplified model introduces less than 30% error for a via pair separation greater than 40 mils center-to-center. This analysis is performed on via pairs and extended to the case of multiple surrounding vias. Formulas are presented for calculating the model parameters. These closed form expressions are compared to 3D field solutions and to frequency domain PCB measurement data. Good agreement is obtained.

Session 3Ac3

Novel Radar Methods for Studying the Structure and Dynamics of the Atmosphere and Ionosphere

Measurement Physics of Standard and Interferometric Radar Wind Profilers

A. Muschinski
CIRES, University of Colorado, and NOAA Environmental Technology Laboratory
Boulder, CO 80305-3328, U.S.A.

The forward problem for the first three auto- and cross-spectral moments (orders $m = 0, 1, 2$) of radar wind profiler signals is solved in a very general fashion. It is shown that the *instantaneous m*th cross-spectral moment,

$$M_{12}^{(m)} = \int S_{12}(\omega)\omega^m d\omega, \tag{1}$$

can be written in terms of the spatial statistical structure of the refractive-index field and the spatial deterministic structure of the wind velocity vector field:

$$M_{12}^{(m)} = (-1)^m \iiint \iiint H_{12}(\mathbf{r},\mathbf{k})\Phi_{nn}(\mathbf{r},\mathbf{k})[\mathbf{u}(\mathbf{r})\cdot\mathbf{k}]^m d^3r d^3k. \tag{2}$$

Here, $H_{12}(\mathbf{r},\mathbf{k})$ is an instrument function, $\Phi_{nn}(\mathbf{r},\mathbf{k})$ is the local and instantaneous wavenumber spectrum of the refractive-index perturbations, $\mathbf{u}(\mathbf{r})$ is the instantaneous velocity field, and $\mathbf{k}$ is the wave vector. This general solution is valid for a very wide class of applications, including frequency–domain interferometry, range imaging, and multi-receiver interferometry. For didactic purposes, the general solution is discussed in detail for the specific case of the standard monostatic radar wind profiler in the far field. The Gaussian model by Doviak and Zrnic (1984) is used as the basis for the instrument function. Closed–form solutions for the backscattered power, the Doppler shift, and the spectral width are derived for two scenarios: first, refractive–index turbulence that is isotropic at the Bragg wave number; second, refractive-index turbulence that is strongly anisotropic at the Bragg wave number. In both cases, the refractive-index perturbations are assumed to be statistically stationary during the observation period and statistically homogeneous within the scattering volume; the velocity field is assumed to be deterministically stationary during the observation period and deterministically homogeneous within the scattering volume.

The concept of *instantaneous statistical stationarity* for wind profiler signal time series is introduced as a temporal equivalent of *local statistical homogeneity* of random spatial fields, a concept that is familiar in turbulence physics. The integral time scales of profiler signals are usually on the order of a tenth of a second and therefore about three or four orders of magnitude shorter than typical integral time scales of meteorological variables in the middle of the atmospheric boundary layer. It is shown that the integral time scale of the profiler signal is a function of the refractive-index and velocity fields' *instantaneous* spatial characteristics and not of their temporal characteristics. It is explained why in many cases, statistically stable spectral moments can be obtained for dwell times as short as one second. These so-called *instantaneous* spectral moments may be considered random variables with respect to the longer time scales associated with boundary-layer dynamics and weather. It is shown how the temporal characteristics of the instantaneous spectral moments are related to the temporal characteristics of the refractive-index and velocity fields.

Cross-Correlation Ratio Method to Estimate Both Transverse and Radial Wind

R. J. Doviak
NSSL
Norman, OK 73069, U.S.A.

G. Zhang
NCAR/RAP
Boulder, CO 80307, U.S.A.

Wind velocity can be measured by either Doppler or interferometric methods. The Doppler method is routinely used to measure radial velocity, whereas interferometric techniques, with closely spaced receiving antennas, are used to measure winds transverse to the beam. The Doppler method uses the phase of auto-correlation function while the interferometric technique uses the magnitude of cross-correlation function of the signals from spaced receiving antennas. A problem of using phase information is aliasing at the Nyquist velocity ($\lambda/4T_s$). Interferometric techniques do not have that problem but they have not been used to determine the radial wind. Furthermore, transverse wind estimation typically uses the Full Correlation Analysis (FCA) method that might not be optimal.

In this paper, we propose a cross-correlation ratio (CCR) method and use it to determine both transverse and radial wind using the interferometric technique. The CCR method estimates wind velocity from the ratio of cross-correlation functions at positive and negative lags. First, we apply CCR to estimate transverse wind from SA measurements. The standard error of the velocity estimated with the CCR method is analyzed and compared with that from FCA. It is shown that the CCR method gives less estimation error than the FCA method for antenna separations less than half the transmitting antenna size. Second, the CCR method is used to determine radial wind by correlating signals from two range gates in a single receiver; this is called range interferometry (RI). The cross-correlation function of signals from different range gates is derived. The standard errors of the estimated range cross-correlation magnitude and that of derived radial velocities are presented. The dependence of errors on radar parameters, and medium properties (i.e., mean wind and turbulence) are studied. To determine the velocity aliasing index, the number of required independent samples M_I must satisfy the condition

$$M_I > \left(\frac{4\pi\sigma_r\sigma_t}{\lambda v_r}\right)^2, \tag{1}$$

in which λ is the wavelength, v_r the mean radial velocity, σ_t the velocity spectrum width due to turbulence, and σ_r the range resolution. Having practical numbers for M_I requires fine range resolution and/or low levels of turbulence.

High-Resolution Radar Observations Using Multiple-Frequency and Multiple-Receiver Techniques

T.-Y. Yu
National Center for Atmospheric Research
Boulder, CO 80301-2260, U.S.A.

Range imaging (RIM) was developed recently to improve the range resolution of conventional pulsed radars using multiple transmit frequencies. RIM has shown promise in revealing the fine-scale structure of the atmosphere within the radar volume in range. In this work, the idea of RIM is further exploited to generate synthesized time series data at subgates within the radar volume. At each subgate, synthesized data are obtained by combining signals from shifted frequencies such that these signals are added coherently. As a result, total power, radial velocity, and spectral width can be obtained at each subgate using synthesized data. Moreover, if multiple frequencies and multiple receivers are used simultaneously, the same process can be implemented independently on signals from each individual receiver and shifted frequencies. A horizontal wind can be estimated at each subgate by applying full correlation analysis (FCA) on synthesized data from spaced receivers. The combination of RIM and FCA is shown to reveal the vertical wind shear within the radar volume using simulated data. This technique is further verified using the multiple antenna profiler radar (MAPR) of the National Center for Atmospheric Research (NCAR), which has been modified to transmit multiple frequencies. These high-resolution products obtained by RIM and FCA are extremely helpful to the investigation of small-scale dynamics such as turbulent processes and atmospheric instabilities.

A Review of Generalized Radar Imaging of the Atmosphere and Recent Experimental Results

R. D. Palmer
Department of Electrical Engineering
University of Nebraska-Lincoln
Lincoln, NE 68588-0511, U.S.A.

Generalized radar imaging of micro-scale, reflectivity structures within the resolution volume of atmospheric Doppler radar systems has the potential to unlock many new discoveries. The general mathematical formulation will be reviewed illustrating the relationship between the visibility function and the brightness distribution. This formulation will show how the three-dimensional reflectivity structure, on scales smaller than the resolution volume, can be imaged by exploiting both spatially separated receivers and signals with distinct transmitter frequencies. Two special cases are presented which separately take advantage of these two experimental configurations. Coherent Radar Imaging (CRI) can be achieved through the examination of differences in backscattered signals received at spatially diverse locations. It will be shown that Fourier CRI, or traditional beamforming, is a special case of the general three-dimensional formulation and that more sophisticated algorithms can be exploited for increased resolution without loss in robustness. Range IMaging (RIM) is a recently developed method used to investigate horizontally stratified scattering structures with vertical scales much smaller than the resolution dictated by the radar bandwidth. This increased altitude resolution is achieved by using the subtle differences in backscattered signals which have slightly different wavelengths. RIM will be shown to have distinct similarities to CRI resulting in a fundamental understanding of the generalized radar imaging problem. Experimental CRI results will be presented from the Turbulent Eddy Profiler (TEP), which is a unique 915 MHz boundary layer radar consisting of 90 independent receivers. The TEP configuration allows sophisticated CRI algorithms to be implemented providing significant improvement in angular resolution. Observations of polar mesosphere summer echoes using the RIM technique will also be presented. The results were obtained using the EISCAT VHF radar system in Tromsϕ, Norway, and are possible because of the frequency agility of the radar.

Radar Range Imaging Studies of the Lower Troposphere

P. Chilson
NOAA Environmental Technology Laboratory
University of Colorado - CIRES
Boulder, CO 80305-3328, U.S.A.

The available range resolution of pulsed radar wind profilers is usually limited by bandwidth restrictions. Range imaging (RIM) has recently been developed as a means of mitigating these limitations by operating wind profilers over a small set of distinct transmitter frequencies. In conventional pulsed radar processing, the angular resolution and the range resolution are given by the beamwidth and the pulse width, respectively. In RIM, the conventional radar sampling volume is partitioned in range into individual slices or subgates," which define a RIM sampling subvolume. It will be shown that images of the reflectivity field and Doppler velocities can then be obtained for each of these subvolumes. A brief overview of how RIM works and how it can be implemented on wind profilers will be presented. Data collected with two 915-MHz profilers in Colorado will be shown and discussed. These profilers were operated using four separate carrier frequencies. Both RIM and conventional processing was performed. Results from the experiments include high-resolution images in time and height of thin, persistent scattering layers, Kelvin-Helmholtz billows, thermal plumes, and even bird echoes. Furthermore, it will be shown how Doppler time-series data for each of the RIM subvolumes can be synthesized from the returned signals at the four frequencies. The synthesized data can then be further processed to obtain Doppler spectral moments for each of the subvolumes. It will be demonstrated that RIM has great promise as a tool for studying and monitoring the atmospheric boundary layer and lower free troposphere.

Dual-Frequency Radar Applications in the Atmospheric Boundary Layer and Troposphere

W. L. Clark, T. E. VanZandt, and K. S. Gage
NOAA Aeronomy Laboratory
Boulder, CO 80303, U.S.A.

This talk focuses on atmospheric probing with UHF radar dual-frequency wind profiler systems. Such systems are significantly better than mono-frequency systems at discriminating turbulent and particulate (e.g., rain, bugs, birds, bats, and dust) scatter. This discrimination then allows more accurate and reliable retrieval of many atmospheric parameters, including wind speed, rain-rate, and drop size distribution. Further use of the dual echoes may allow determination of ε, the turbulent eddy kinetic-energy dissipation rate per unit mass. This latter measurement technique, still under development, is the major focus of this talk.

Briefly, for a given kinematic viscosity ν, the magnitude of ε in a cascade of turbulent kinetic energy specifies the length scale at which viscous effects will become important. In the boundary layer and lower troposphere, this scale tends to be around 5 cm, coinciding with the Bragg wavelength of S-band radars. Since the reflectivity damping in the inertial- to viscous-dissipation transition region has been quantitatively modeled as a function of ε and ν, and since the amount of damping for a given echo may be determined by comparing S-band reflectivities to simultaneous returns from a longer-wavelength 'reference' radar (whose wavelength lies in or near the inertial subrange) it is possible to deduce the value of ε for any altitude, with the relatively constant ν value determined from a standard atmosphere.

This technique has been used successfully over the Tiwi Islands, located just north of Darwin, Australia, during the November-December 1995 Maritime Continent Thunderstorm Experiment (MCTEX). The analysis yielded observation of the daytime vertical and diurnal structure of ε for much of the campaign. In contrast, attempts to apply this technique to 9 months of data taken during 1994–1995 at the Flatland Atmospheric Observatory near Urbana, Illinois, have proved more problematical, due to the frequent presence of small particulate echoes that mix with the turbulent echoes in the profiler Doppler spectra.

The technique has some limitations: 1) For any given wavelength, the observable range over ε is confined to approximately two orders of magnitude (e.g., if $\lambda = 10\,\mathrm{cm}$, then $\sim 10^{-5} < \varepsilon_{observable} <\sim 10^{-3}\,\mathrm{m^2s^{-3}}$ in the lower atmosphere). This range may be slightly extendable on the low ε side by increasing the profiler sensitivities and dynamic ranges, but the high limit is due to flattening of the viscous damping curve as it approaches the inertial range. 2) The technique can work in rain or bugs only if it is possible to separate the particulate echo from the turbulent echo. 3) The ideal radar wavelength increases slowly, but significantly, with altitude due to the dependence of kinematic viscosity on the ambient atmospheric density.

A Study of Snow Development Using Two UHF Profiler Radars

W. O. J. Brown and S. A. Cohn
National Center for Atmospheric Research
Boulder, CO 80307, U.S.A.

The National Center for Atmospheric Research deploys Integrated Sounding Systems (ISS) consisting of wind profilers, radiosondes, and various other instruments at NSF sponsored projects for universities and other institutions. A recent project was the Inhibition of Snowfall by Pollution Aerosol project carried with the Desert Research Institute (DRI). The project aims to examine the effect of pollution on snow formation and also to improve forecasting of snow events in the Rockies. The DRI operates the Storm Peak Laboratory on top of Mt Werner at Steamboat Springs, Colorado, at which in-situ measurements of snow and cloud physical and chemical properties at the 3300 meter level can be made. An ISS was positioned near the base of the mountain, 1100 meters lower. Although absolute microphysical properties cannot be measured by the ISS directly, the profiler can provide information on the variation of snow properties with altitude, and the radiosondes indicate cloud levels. For example, if snowflakes are growing (and becoming heavier) by riming in a super-saturated cloud, the profiler can report the altitude profile of fall speeds and identify riming heights. Knowledge of snow crystal types as measured at the Storm Peak Lab is critical to interpreting the profiler observations.

One difficulty is separating air motion from snow fall speeds; snow generally falls at 0.5–1 m/s, and vertical air motion is often of a similar magnitude. Two profilers were deployed at the Steamboat project, one operating at 915 MHz and the other at 1299 MHz. This difference in wavelength is such that if the reflectivity of the snow echoes is matched on the two profilers, then there is a 6 dB difference in the clear-air echo signal. The clear-air component of the Doppler spectra can be removed, and snow fall speed distributions as a function of height can be produced. Preliminary results from the experiment, carried out in January and February 2002, will be presented.

Performance Enhancements to the VHF Boundary Layer Technique

B. G. W. Vandepeer, B. M. Fuller, A. J. Murphy, D. J. O'Connor, E. Alexe, R. A. Orr, D. M. Cox, P. Aryal, and S. M. Ludborzs
Genesis Software Pty Ltd
Adelaide, South Australia 5006, Australia

Recent years have seen an increased interest in the scientific and operational applications of VHF boundary layer radar systems. Such systems are now emerging as viable alternatives to the more expensive traditional UHF profilers and provide significant performance improvements in some areas. In particular, the higher altitude performance of the VHF systems is of note, with higher-powered systems potentially reaching the tropopause and beyond.

Traditionally, the focus of most VHF boundary layer radar designs has been the extension of the height coverage to the lowest possible altitudes, usually to the detriment of the higher ranges. It is possible, however, through the use of novel multiplexing techniques to maximise boundary layer performance at the lowest heights without sacrificing the upper-tropospheric returns. In this presentation we describe some of these techniques and demonstrate their efficacy using the example of an operational system. We present results showing the altitude performance of the boundary layer troposphere radar system, and demonstrate that the temporal resolution of the results are not degraded as a consequence of the multiplexing techniques utilised.

A Hybrid Yagi/Loop Antenna System for VHF Boundary Layer Studies

W. K. Hocking
Department of Physics and Astronomy, University of Western Ontario
London, Ont. N6A 3K7, Canada

Traditionally, boundary layer radar studies have been dominated by radars which operate at frequencies above 400 MHz. At higher altitudes, VHF radars are used alongside UHF and higher frequency radars, and indeed upper atmospheric windprofiling began with VHF radars. VHF radars have many advantages, including reduced sensitivity to particulates, hydrometeors and insects. However, at low heights in the atmosphere (below 2 km altitude) VHF radars have several disadvantages. Firstly, it is not possible to use them in Doppler mode, since if the radar array is chosen to be of a suitable size for Doppler studies, then altitudes of 1 km and less are often in the near field. Furthermore, pulse lengths of 150 meters require bandwidths which cover a significant spectral range, and after-pulsing effects can also delay the lowest height of useful detection with the radar.

VHF boundary layers do exist, however. Some of these problems discussed above have been solved in the past by using the spaced antenna method, which uses antenna arrays with physically small areas, thereby avoiding the near-field problems. Many such radars can record data as low as 700 meters above ground level, but measurements down to 400 meters and less are rarer. This is especially due to the effects of after-pulse phenomena, and production of results at these low altitudes often requires very carefully designed transmit-receive switches. It is therefore useful to examine alternative options for the construction of VHF boundary layers, which might help improve the response at lower altitudes.

In this talk, we describe an interesting alternative VHF boundary layer radar, which has no need for transmit-receive switches. We employ separate antennas for transmission and reception. Transmission is accomplished with Yagi antennas, and reception is performed using loop antennas. By using these two different types of antennas, and by careful selection of locations of the antenna elements, we have been able to substantially diminish the antenna-antenna coupling between transmitters and receivers, enabling us to achieve measurements to low altitude. The system is restricted in achieving its ultimate capability by limitations in the transmitter pulse, but nevertheless we have been able to achieve useful results to altitudes as low as 600 meters. Comparisons with radiosondes over the summer of 2001 are shown, and the potential for this type of VHF hybrid will be discussed.

A Comparison of Mesospheric OH Temperatures and IDI Winds with Coincident Meteor Radar Measurements

M. J. Taylor
Center for Atmospheric and Space Sciences and Physics Department, Utah State University
Logan, UT, U.S.A.

F. T. Berkey and C. S. Fish
Space Dynamics Laboratory, Utah State University
Logan, UT, U.S.A.

W. K. Hocking
Department of Physics and Astronomy, University of Western Ontario
London, ON, Canada

G. O. L. Jones
British Antarctic Survey
Cambridge, UK

In October 2000, an all-sky SKiYMET meteor radar system on loan from the University of Western Ontario, was installed at Bear Lake Observatory, Utah (41.9°N, 111.4°W) for comparative measurements alongside two site instruments: a Mesospheric OH Temperature (MTM) and a NOAA dynasonde operating as an Imaging Doppler Interferometer (IDI). The MTM was developed under support from the NSF CEDAR Program and utilizes narrow band (∼1.2 nm) image measurements of selected emission lines in the near infrared OH nightglow emission to determine mesospheric temperature at the ∼87 km level with a high precision (1–2 K in 3 min). Imaging Doppler Interferometry is a MF-HF partial reflection remote sensing radar technique developed in the 1980s and more recently implemented on the dynasonde by colleagues at the British Antarctic Survey. The weak partial reflections are utilized as tracers of the mesospheric neutral wind.

Joint measurements were obtained over a 5-month period, between November 1999 and March 2000. Analyses of the radar wind data indicate remarkable agreement between the datasets, with exceptions during the months of November and March. Imaging Doppler Interferometry is a relatively new remote sensing radar application that has been accompanied by substantial controversy. The high level of correlation between the IDI and SkiYMET data further establishes the validity of the recently implemented IDI wind measurements capability at Bear Lake Observatory. Similarly, comparison of the OH temperature measurements with the newly developed meteor radar temperature algorithm provides an excellent test of this technique for mid-latitude, nighttime conditions. This paper will present the main results of these two studies, focusing on short and long-term variability in each parameter.

Meteor Radar Temperatures at Mid-Latitudes Compared with OH* Rotational Temperatures and Lidar Observations

W. Singer
Leibniz-Institute of Atmospheric Physics
Rostock University
Kuehlungsborn, 18225, Germany

Meteor radars can be used to estimate temperatures in the mesopause region after different techniques as shown in recent papers by Hocking. The most promising method provides absolute measurements of a height-averaged temperature at about 90 km based on the height dependence of the meteor decay times but requires an approximation of the mean temperature gradient at the peak altitude of the meteor layer. Usually, the gradient is given by a global empirical model. At least, several hundred meteor detections are necessary and several thousand meteors are desirable to obtain a representative height distribution of meteor decay times for a reliable temperature determination.

An improved model of the seasonal course of the mean temperature gradient for mid-latitudes has been derived from potassium lidar observations at Kuehlungsborn ($54.1°$ N) in combination with meteor radar temperatures obtained over the time period from 1999 to 2001 at Juliusruh ($54.6°$ N) and OH* rotational temperatures measured at Wuppertal ($51.3°$ N) at the same time. The initial gradient model has been modified that an optimum agreement exists between meteor temperatures, OH* rotational temperatures and lidar results. The Juliusruh meteor radar at 32.5 MHz generally provides temperatures at about 90 km which are daily averages based on about 1500 to 3500 meteor detections.

We describe the seasonal variability of the meteor radar temperature over the time period from November 1999 to August 2001, its response to stratospheric warmings in winter and the relation of the low temperatures in summer (~ 150 K) with the appearance of strong mesopheric radar echoes in the VHF range and of noctilucent clouds. In addition, meteor radar temperatures deduced at arctic latitudes ($69°$ N) during fall, winter, and spring are compared with lidar observations and rocket measurements.

Session 3Ac4

Transmission Line and Waveguiding Structures: Novel Structures and New Effects

Properties of Waveguides with Periodic Side Walls of Finite Width

R. B. Hwang and S. T. Peng
Microelectronics and Information System Research Center, National Chiao Tung University
Hsinchu, Taiwan

The development of artificial materials by constructing lattice structures has gained considerable attention in recent years; in particular, the stop-band phenomenon associated with a lattice structure has found many applications. For example, a 1D periodic array of dielectric uniform layers has been shown to exhibit many interesting phenomena, such as spontaneous emission and localization of electromagnetic energy. Such periodic arrays of dielectric materials were employed as a novel waveguide to mold the flow of electromagnetic energy. The basic concept of this class of applications can be traced back to the early work of Larsen and Oliner who had used one-dimensionally (1D) periodic dielectric slabs to form waveguide walls that are operated in their stop-band or below-cutoff condition due to the Bragg phenomenon.

In this work, a rigorous formulation is presented for the dispersion characteristics of localized modes in a uniform layered region bound on both sides, each by a periodic structure with a finite number of unit cells. The dispersion characteristics of this class of waveguides are analyzed in terms of the multiple reflections between two waveguide walls. In particular the leakage phenomenon critically evaluated in the presence of only a finite number of unit cells. Since the reflection of plane wave by periodic layers depend on the incident angle as well as the frequency, contours of constant reflection coefficient are plotted with the incident angle and the frequency as variables. Though not shown, these contours provide a simple and useful procedure for the design of a waveguide for a desired number of modes, as we shall follow throughout this work.

Fig. 1 shows the phase constant versus the frequency for the lowest mode of a waveguide with its configuration inserted as an inset. In this case, we have designed the cutoff frequency (d/λ) at around 0.3 to ensure the single-mode operation. We have observed that the increase of the number of unit cells has a negligible effect on the phase constant, but it reduces appreciably the attenuation due to the leakage of energy through the finite periodic structures, as depicted in Fig. 2. Extensive, interesting results have been obtained and will be presented together with their physical implications in talk at the conference.

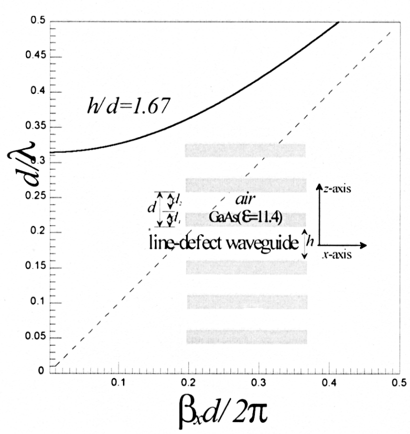

Figure 1: Variation of the phase constant versus normalized frequency.

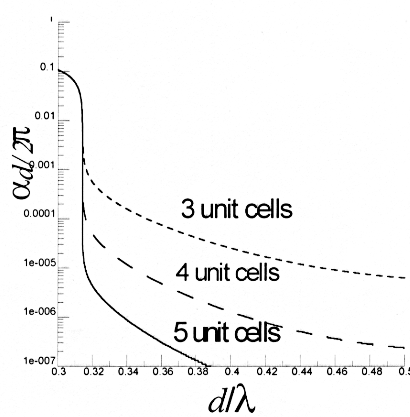

Figure 2: Variation of the attenuation constant versus normalized frequency.

Scattering by 3D Periodic Structures Containing Metallic Components

C.-H. Lin, K. M. Leung and T. Tamir
Department of Electrical and Computer Engineering, Polytechnic University
Brooklyn, NY 11201, U.S.A.

Owing to their strong scattering of electromagnetic waves, metals can often be found in electromagnetic devices. This is especially true at lower frequencies where the waves penetrate little into the metal and consequently they are not absorbed appreciably. At these frequencies, the real part of the dielectric constant of the metal is very large and negative. This often causes inaccuracies, convergence problems and even instabilities in numerical computation of the various electromagnetic properties. Fortunately it is in this regime that the metals behave more like a perfect electric conductor (PEC), and these devices can therefore be modelled accurately by treating the metals as PECs.

This present work deals with three-dimensional periodic strictures containing arbitrary combinations of layers involving uniaxial dielectric materials and metallic cavities. The approach is based on the use of modal fields inside the dielectric and metallic cavities. The pertinent boundary conditions are treated using a general transmission-line formalism. Highly accurate results can be obtained with relatively modest computational resources for the scattering and absorption properties, and for the field distributions, even in the presence of rather large dielectric contrasts.

Application of the present theory to model and improve the performance of a new class of quantum-well infrared photodetectors is discussed. These devices typically involve many homogeneous and periodic layers containing high and low dielectric materials and metallic components. In addition the dielectric materials may be uniaxial and absorbing.

Leakage Behavior When a Wave is Guided at an Angle on a Periodically Grooved Dielectric Layer

A. A. Oliner
Polytechnic Univ.
Brooklyn, NY, U.S.A.

S. T. Peng
National Chiao Tung Univ.
Hsinchu, Taiwan

Wave guidance at an **angle** on a periodically grooved dielectric layer produces a variety of new physical effects, none of which are present when the wave propagates normal to the periodic structure. We have recently presented the results of such a study for the frequency range in which one finds non-radiating stop bands. The present talk examines the **radiation** behavior that occurs when the frequency is raised so that the bound mode guided by the periodically grooved layer turns into a **leaky** mode. A set of new physical effects are found, some of them quite unexpected.

When the mode travels perpendicularly to the periodic grooves, the angle of leakage begins at backward endfire. When the mode travels at an angle to the periodic grooves, however, the leakage does not occur first in the principal plane but instead at some **skew** angle, and the beam then rises from the ground as the frequency is increased further. Alternatively, the frequency may be kept constant, but the angle ϕ of excitation or guidance increases away from the normal. If the guided mode is already leaky at normal incidence, then, as ϕ increases, the beam swings out from the principal plane, and moves down toward the ground and away from the principal plane, until the beam hits the ground.

In the first of the above considerations, we are asking what effects are produced when the angle of the excitation is kept the same but the frequency is varied. For this purpose, the most convenient plane to use is the band-structure plot (or Brillouin diagram), although when the angle ϕ of the excitation is not zero, the details of the band-structure plot are different. Each time the angle ϕ is changed, however, a whole new plot must be obtained. Alternatively, when the frequency is kept constant and the excitation angle ϕ is varied, the appropriate plane is the wavenumber diagram, which plots the transverse wavenumber against the propagation wavenumber. If the frequency is then changed, a new plot is needed. Both types of planes will be discussed in the talk, and it will be shown how each is used.

Numerical results will be presented to illustrate the leakage-angle performance mentioned above. Rigorous calculations were also made of the leakage rate α, where it was found that the value of α remains approximately constant as angle ϕ is varied until the beam approaches the ground, at which point α rapidly drops to zero. It is also interesting, and unexpected, that the leakage rate for TE excitation is almost an order of magnitude larger than that for TM excitation.

As the frequency is increased further, the second stop-band region is approached. For excitation at normal incidence (ϕ = 0), an open stop band is known to occur as the beam reaches broadside. When $\phi > 0$, we again find **four** stop bands, similar to what we found earlier for the first Bragg region except that now everything is complex. Detailed plots of the behavior will be presented.

The final aspect to be discussed is that of **mode conversion**. It was clear that mode conversion would occur, but the amount of it was quite unexpected. For example, for TE excitation there is no radiated power in TM form when ϕ = 0, but, as ϕ increases, the proportion of radiated power in TM form increases gradually to a peak of almost 80%. The case for TM excitation is even more dramatic. Numerical plots will be presented for these unusual results.

Radiation from a Source on a Covered Microstrip Line

W. L. Langston, J. T. Williams, and D. R. Jackson
Department of Electrical and Computer Engineering, University of Houston
Houston, TX 77204-4005, U.S.A.

F. Mesa
Department of Applied Physics 1, University of Seville
Seville, 41012, Spain

Radiation from sources and discontinuities on integrated circuit structures becomes important at high frequencies, where it results in crosstalk, power loss, and spurious package effects. Understanding the nature of the radiation from a source or discontinuity is important for understanding the spurious effects that may occur at high frequencies. In this presentation, the radiation from a voltage gap source on a covered microstrip line is examined. The covered microstrip line is a practical structure, which is representative of a general class of structures that are open transversely and closed vertically by perfectly conducting planes. It consists of a conventional microstrip line with a conducting top plane above the substrate. The microstrip line is infinite in the z direction, and is excited by a gap voltage source at $z = 0$.

The gap voltage source excites a current on the microstrip line, which consists of the desired bound mode of propagation, together with a continuous-spectrum current. Mathematically, this decomposition is performed by using a semi-analytical spectral-domain method to solve for the Fourier transform of the current, and then expressing the current in terms of an inverse Fourier transform integral in the k_z wavenumber plane. The residue contribution from the bound-mode pole defines the amplitude of the bound-mode current, while a branch-cut integration defines the continuous-spectrum current. The branch-cut integral may be deformed to a steepest-descent path, capturing residues from physical leaky-wave poles in the process. This allows the continuous-spectrum current to be resolved into a set of one or more physical leaky-mode currents, together with a "residual-wave" current. Asymptotically, for large distances from the source, the residual-wave current decays as $z^{-3/2}$.

After the current on the line is determined, the radiation from the current is calculated. Because of the closed nature of the covered microstrip, the field radiated by the line current takes the form of a parallel-plate mode field. The vertical dimensions are chosen so that only the fundamental TM_0 parallel-plate mode is a propagating mode, and hence only this mode is important at distances more than a fraction of a wavelength from the line. The radiation fields from the bound-mode, leaky-mode, and residual-wave currents are calculated and studied separately, in order to examine the nature of the radiation field from each type of current. It is interesting to note that the bound-mode current does produce a radiation field, even though the bound mode is a slow-wave with respect to the TM_0 parallel-plate mode, since the bound-mode current has a slope discontinuity at $z = 0$. The "far-field" radiation from each current is also calculated, as the radial distance from the source becomes large, and the shapes of these patterns are studied. Results are studied for various frequencies, to examine the role of each radiation field in producing crosstalk at high frequency.

Proper Continuous-Spectrum Current and Near Field of Microstrip

J. Lee, D. P. Nyquist, and M. J. Havrilla
Department of Electrical and Computer Engineering, Michigan State University
East Lansing, MI 48824, U.S.A.

The continuous spectrum currents/fields of integrated open waveguide structures have been, until recently, neither conceptualized nor quantified adequately. That spectrum can be identified as a branch-cut contribution due to the singularity expansion of those currents/fields in the complex axial-transform plane. Singularities in that plane include poles associated with the guiding structure and branch points contributed by the layered background environment. The manner in which singularities of the background environment manifest themselves as branch points in the complex axial-transform plane is reviewed.

Based on a transform-domain integral-equation formulation, approximate and analytical expressions for the spectral-domain microstrip current are obtained. The delta-gap feed model is exploited. That approximation is based on the Maxwell distribution for the transverse current profile. The spectral-domain current is inverted into the space domain by integration-contour deformation on the top sheet of the axial-transform plane. This result is the representation of currents in terms of the proper propagation-mode spectrum. That spectrum consists of bound propagation modes associated with pole singularities and a continuous spectrum associated with integration around branch cuts contributed by the background environment. During integration around the branch cuts, singularities in the transverse-transform plane migrate in a complicated manner. The trajectories of this migration are identified and suitably accommodated during the real-axis integration in that plane. This overall procedure leads to a decomposition of the total currents into bound modes and continuous-spectrum contributions. This representation is validated by real-axis integration in the axial-transform plane. A similar analysis leads to the near-zone electric field of the guiding structure. The quasi-TEM characteristic impedance of the principal bound mode is calculated.

Numerical results are obtained, which compare the bound mode and continuous-spectrum contributions of the microstrip currents. It is found that current is dominated by that of the bound mode. The characteristic impedance of the bound mode is validated by comparison with well-known empirical formulae. The continuous-spectrum current is maximal near the feed point and decays rapidly with axial distant from the feed. The near field is dominated by the continuous-spectrum contribution. Extensive numerical results for near-zone fields are obtained.

Unexpected Influence of Nonphysical Solutions on Physical Behavior in Printed-Circuit Transmission Lines

M. Tsuji and H. Shigesawa
Department of Electronics, Doshisha University
Kyotanabe, Kyoto 610-0321, Japan

It is well known that a leaky-wave solution in printed-circuit transmission lines is improper but physical and measurable within a sector of space near the guiding structure. On the other hand, the eigenvalue solutions that do not satisfy physical conditions based on a finite-source excitation are called nonphysical solution. Therefore such solutions have been ignored with respect to their influence on the physical field excited by a source, although the evolution in their properties serves to explain certain changes in the character of the physical modes. While it is true that they do not contribute directly to the excited fields, we have found out that under the right conditions, two types of nonphysical solutions, that is, real and leaky ones can indirectly influence the physical field in significant but different ways. Actually, we have observed at a finite distance from a source that nonphysical real solution behaves like a bound mode, whereas nonphysical leaky one behaves like a leaky mode.

In the talk, we will show the quantitative verification of the contribution of nonphysical solutions to the physical fields, by comparing the calculated results by the finite-difference time domain method with those by the spectral-domain method, and also present the experimental verification by measuring the field variation along the guide axis. Furthermore we will investigate such indirect effects of nonphysical solutions for various printed-circuit transmission lines and prove that they occurs on most, if not all, printed-circuit lines, so that they are rather general.

Graphical Approach for Localizing Modal Poles in Guided- and Leaky-Wave Structures

A. S. Omar and A. H. Kamel
University of Magdeburg
Magdeburg, D-39016, Germany

Modal poles of most guiding and radiating structures are usually determined numerically by looking for the zeros of a certain characteristic function. This task is computationally inefficient as these zeros are generally complex and the searching algorithm is consequently two dimensional. Characteristic functions with closely located zeros and poles complicate the task further and lead sometimes to overlooking some of the searched zeros. Another serious problem arises when the characteristic function becomes flat in the vicinity of one of its zeros. Successfully catching the zero in this case necessitates that the zero-searching routine should be initiated with a guess value very close to the searched zero.

In this contribution we present a graphical approach for providing sufficiently small subregions on the complex plane, where one and only one zero of the characteristic function exists. These sub-regions can be inputted to any iterative zero-searching routine to end up with the accurate value of the modal pole. The proposed approach is based on firstly cleaning up the characteristic function from all finite poles (by crating an auxiliary function with the same zeros but with all poles at infinity). Through successive variable transformations, modal poles are obtained as the intersections between two families of two-dimensional contours.

The proposed approach has been applied to a number of both lossless and lossy open structures. An excellent agreement with other independent approaches has been achieved.

Wave Phenomena on Ferrite Planar Slab Waveguides Using Singularity Theory

G. W. Hanson
Department of Electrical Engineering, University of Wisconsin-Milwaukee
Milwaukee, Wisconsin 53211, U.S.A.

A. B. Yakovlev
Department of Electrical Engineering, The University of Mississippi
University, Mississippi 38677, U.S.A.

The dynamic and magnetostatic modes of planar ferrite slab waveguides are of considerable interest in electromagnetic applications. Although the properties of some of the fundamental modes are relatively well understood, the mode spectrum is very complicated and difficult to characterize in a general fashion. In particular, leaky modes have not been studied extensively, nor has possible modal interactions and mode coupling.

In this paper we present some general results based on singularity theory which helps to characterize properties of ferrite slab modes, including leakage and modal interactions. The analysis is based on the fundamental understanding of singularities associated with modal effects on isotropic slab waveguides, which serve as the background for the investigation of wave phenomena on biased ferrite slabs. By introducing a biasing magnetic field and varying the direction of the applied field, these singularities migrate in the complex frequency plane. In particular, it has been observed that singularities associated with isotropic dielectric slabs and corresponding to leaky-wave cutoff split into two similar-type branch-point singularities associated with forward and backward leaky waves when the slab becomes a ferrite. Furthermore, as the orientation of the applied bias field varies, certain frequency-plane branch points approach the real frequency axis, resulting in the interaction of leaky-waves. Numerical results are presented for a variety of ferrite slab structures, and the role of complex-frequency and complex-wavenumber singularities associated with the dispersion function is described.

Conditions for the Appearance of Complex Modes in Strictly Bidirectional Waveguides

M. Mrozowski
Department of Electronics, Technical University of Gdansk
Gdansk, 80-952, Poland

Complex modes are the least known type of waves which may exist in lossless waveguiding structures. A single complex wave can not exist because it always gives rise to a second complex wave having a complex conjugate propagation constant. Such a pair stores reactive energy. These basic facts about complex modes have been established by many researchers. It has also been shown that complex waves above cutoff are a result of the degeneracy between forward and backward waves. However, the circumstances accompanying the appearance of complex waves below cutoff have not been explained. In this contribution this problem will be addressed and explained. The analysis is based on the generalized telegraphist equations, the theory of symmetric matrix pencil and the general orthogonality and energy relations for modes in inhomogeneous anisotropic waveguides. The theory, valid for arbitrary strong inhomogeneities, predicts that the complex waves below cutoff result from the coupling of nearly degenerate pair of waves, each having different energy properties. The energy stored in electric field of one wave taking part in the interaction has to exceed the energy stored in the magnetic field and the opposite must be true for the second wave. A new fact which was established for a complex wave is that while it cannot transport energy the average value of electromagnetic momentum is nonzero. The theory explains which guide geometries are prone to complex waves and allows one to predict the approximate frequency range of the complex wave pair. These theoretical findings will be illustrated at the conference by the numerical investigation of energy relations in several waveguiding structures.

Session 3Ac5

Recent Advances on Microwave Inverse Scattering Techniques for Buried Object Detection, Reconstruction and Imaging

Design of UWB Antennas for Step-Frequency or Impulse Radars Applied to the Detection of Thin Layers and Buried Objects

E. Le Brusq, J. Y. Dauvignac, and C. Pichot
Université de Nice-Sophia Antipolis
Valbonne, France

C. Fauchard, X. Dérobert, and P. Côte
Laboratoire Central des Ponts et Chaussées
Bouguenais, France

The detection and identification of buried inhomogeneities using electromagnetic waves are of crucial importance for nondestructive testing civil engineering and geophysics applications. For example, identifying the thickness of roadway pavement layers is one of the major interest topics in civil engineering. Other major interest topic concerns the detection of buried pipes and inhomogeneities in the geophysics domain. For road construction and maintenance, the need for information on the thickness of asphalt layers, e.g. thin asphalt layers TAS (average layer-thickness ≤ 4 cm), very thin asphalt layers VTAS (average layer-thickness between 2 and 3 cm) and ultra thin layers UTAS (average layer-thickness < 2 cm), is not satisfied by means of commercial impulse GPR, due to the inability of such devices to operate over ranges of several GHz (central frequency and band width limited to 2 GHz). As a result, research has been focused on the design of ultra-wide band antennas (UBW) either with a step-frequency radar technique able to work with very high-frequency synthetic pulses or with impulse radar.

Ultra-wide band (UWB) Vivaldi antennas having a bandwidth (SWR ≤ 2) greater than a decade (458 MHz-10 GHz) for road applications and (150 MHz – 3.5 GHz) for geophysics applications have been developed. The directivity of such antennas enables a bistatic configuration with low offset. First, the antennas were tested on various bituminous concrete samples with a network analyzer operating over the frequency range 500 MHz-6 GHz. Different parameters were studied, including bandwidth, offset between antennas, and height and shape of the frequency-dependent pulse, as well as depth, object shape and type were studied. A comparison has been made with a commercial impulse radar (GSSI radar with 1.5 GHz central frequency antenna). Second, GPR dynamic measurements were carried out on selected road construction and maintenance test sites (e.g. on a circular pavement fatigue test track composed of a number of known structures). Third, measurements have been made on a special test site for geophysics applications for different buried objects (e.g. pipes filled with different materials buried at various depths) with H-H, V-V and H-V polarization configurations.

Synthetic Focusing into the Ground and into Buildings, Using Real Aperture Radar

R. Benjamin, I. J. Craddock, E. McCutcheon, and R. Nilavalan
University of Bristol
Bristol, UK

The performance of Surface-Penetrating Radars (SPRs) is normally severely limited by clutter and attenuation. In applications such as landmine detection, or in-building imaging (as could be used for search and rescue activities, for example), it is quite possible to make use of a real (rather than synthetic) radar aperture - exploiting this extra degree of freedom yields far greater immunity to clutter.

The Real Aperture, Synthetically Organised Radar (RASOR) technique described herein, like Synthetic Aperture Radar (SAR), transmits from all antenna elements in turn. However, where normal SAR employs N antennas in one dimension, yielding N monostatic signal paths, in RASOR the echoes from each of the N transmitting antennas are received by the other N-1 antennas. The combination of these N(N-1) bistatic signal paths yields a significant processing gain, against clutter, compared to conventional SAR.

The operational RASOR system described herein switches a single transmitter consecutively to all antennas, and at each antenna operates it repeatedly, so that a single receiver and digitiser can be switched to all relevant receiving antennas in turn. The bistatic use of all antennas within view of a target ensures that all potentially relevant signals are collected. The recorded data from the separate bistatic paths may then be coherently focused onto all potentially relevant resolution cells in the medium.

In this contribution the authors demonstrate successful use of the RASOR system for the detection of buried landmines and also describe its use for imaging of human subjects through both partition and concrete walls. The latter demonstration opens up interesting new possibilities in areas such as in-building search-and-rescue.

A New Kernel-Based Learning Algorithm for Buried Object Detection

E. Bermani and A. Boni
University of Trento
Trento, Italy

S. Caorsi
University of Pavia
Pavia, 27100, Italy

A. Massa
University of Trento
Trento, Italy

By a numerical point of view, the main drawbacks of nonlinear inverse scattering methodologies are the computational efforts and memory resources required for the reconstruction process, generally resulting from an iterative minimization procedure. In order to effectively deal with this problem, different strategies have been proposed. A first class of methodologies resorts to very fast direct electromagnetic solvers [1]. Other approaches consider a numerical implementation of optimization techniques on parallel computers in order to reduce computational time by sampling the search space in an efficient way [2]. Neural network-based learning algorithms have been also applied to obtain real-time results for a class (e.g., object detection and localization) of inverse scattering problems [3][4]. These approaches, though have been shown remarkable performances in solving such a kind of problems, do not fully exploit the a-priori information about the inverse scattering data (scattered field collected in the so-called observation domain external to the investigation domain) and the scatterers under test. In the last few years, a new framework for machine learning based on the theory of Reproducing Kernel Hilbert Space (RKHS), has been developed. Such a theory permits one to change the domain of work of a given algorithm from its input space to a higher, possibly infinite, feature space where one can usually manipulate simpler linear functions. This task is accomplished by means of special kernel operators, which, in practice, play the role of hiding such a mapping. Support Vector Machines (SVMs), designed by Vapnik [5], represent the first framework based on a kernel method, and have been successfully applied for classification and function approximation tasks. The main advantage with respect to traditional learning algorithms consists in structure of the optimization problem. Furthermore, the kernel operator can be specifically designed in order to embed the prior knowledge of the problem [6]. In this work, we propose a new and innovative kernel-based approach for buried object detection and describe how to build specifically-oriented kernel functions. Numerical results show the effectiveness of our method with respect to previous neural network and standard kernel-based algorithms.

REFERENCES

1. W. C. Chew and Y. M. Wang, "Reconstruction of two-dimensional permittivity distribution using the distorted Born iterative method," *IEEE Trans. Medical Imag.*, vol. 9, pp. 218–225, 1990.
2. J. J. Mallorqui et al., "Parallelization of a Newton-Kantorovich reconstruction algorithm for microwave tomography," *PIERS 1998*, Nantes, France, p. 1017, July 13–17, 1998.
3. S. Caorsi and P. Gamba, "Electromagnetic detection of dielectric cylinders by a neural network approach," *IEEE Trans. Geosci. Remote Sensing*, vol. 37, pp. 820–827, 1999.
4. I. T. Rekanos, "Radial basis function neural networks for on-line inverse scattering applications," *PIERS 2001*, Osaka, Japan, p. 139, July 18–22, 2001.
5. V.N. Vapnik, *The Nature of Statistical Learning Theory*, John Wiley & Sons, NY, USA, 2nd edition, 1999.
6. B. Schölkopf, P. Y. Simard, A. J. Smola, and V. N. Vapnik, "Prior knowledge in support vector kernels," in *Advances in Neural Information Processings Systems*, M. I. Jordan, M. J. Kearns, and S. A. Solla, Eds., vol. 10, pp. 640–646, Cambridge, MA, 1998. MIT Press.

On the Effectiveness of a Class of Genetic Algorithm-Based Techniques for Buried Object Detection, Reconstruction and Imaging

S. Caorsi and G. Cevini
Department of Electronics, University of Pavia
Pavia, Italy

A. Massa
Department of Information and Communication Technology, University of Trento
Trento, Italy

M. Pastorino and M. Raffetto
Department of Biophysical and Electronic Engineering, University of Genoa
Genova, Italy

In the inverse scattering framework, the sensing of buried targets is a very difficult and complex topic. This is due, for instance, to aspect-limited data, noisy environments, wave-ground interactions, etc. In the past, many inversion methods have been proposed aiming at reconstructing objects buried in a half space or multi-layered media (see [1] and the references therein). Among these methods, the modified gradient-based approaches [2] and the algorithms using the distorted Born iterative method [3] demonstrated their effectiveness. Recently, a growing effort has been devoted to develop inversion procedure based on genetic algorithms [4]. On the other hand, GA-based procedures have shown their capabilities when microwave imaging problems, where dielectric structures belong to a free-space background [5], have been addressed. This work is aimed at further developing those methodological approaches by considering the framework of buried object detection. To this end, some inverse scattering methods are presented to detect 2D buried objects by using GA-based schemes. In these approaches, the air-earth interface is taken into account and the earth can be either lossy or lossless. The inverse problem is cast as an optimization problem where a cost function, proportional to the difference between measured field data and the fields calculated from estimated parameter configurations, has to be minimized. In order to reduce the ill-posedness (caused by errors or noise in the measured scattered fields) of the inversion procedure a suitable filtering strategy is developed and discussed. Both the permittivity and conductivity profiles of buried objects are reconstructed. Moreover, the influence of a gaussian noise on the object localization and on the dielectric profile reconstruction is evaluated. Finally, a general overview on GA-based strategies and a discussion about capabilities and current limitations for buried object detection are also presented.

REFERENCES

1. Lesselier, D. and B. Duchêne, "Wavefield inversion of objects in stratified environments: from back propagation scheme to full solutions," in *Review of Radio Science*, 1993–1996, W. R. Stone Ed., Oxford University Press, pp. 235–268, 1996.
2. Soriau, L., B. Duchêne, D. Lesselier, and R. Kleinman, "Modified gradient approach to inverse scattering for binary objects in stratified media," *Inverse Problem*, vol. 12, pp. 463–481, 1996.
3. Cui, T. J., W. C. Chew, A. A. Ayudiner, and S. Y. Chen, "Inverse scattering of 2D dielectric objects buried in a lossy earth using the distorted Born iterative method," *IEEE Trans. Geosci. Remote Sensing*, vol. 39, pp. 339–346, 2001.
4. Kim, J. -S. and J.-W. Ra, "Location and imaging of two-dimensional pipes buried in a lossy half heart," *Microwave Optical Technology Letters*, vol. 31, pp. 140–143, 2001.
5. Caorsi, S., A. Massa, and M. Pastorino, "A computational technique based on a real-coded genetic algorithm for microwave imaging purposes," *IEEE Trans. Geosci. Remote Sensing*, vol. 38, no. 4, pp. 1697–1708, July 2000.

Buried Mines Classification from Three-Dimensional Radar Data

L. Capineri, P. Falorni, and L. Masotti
University of Florence
Florence, Italy

C. Windsor
Didcot, UK

The identification and classification of buried mines is performed in 3-D from raster scans using ground-penetrating radar. A method for extracting relevant features from scattered waves in 3-D has been developed and presented in a previous work. This method is based on the estimation of 3-D hyperbolic patterns deriving from the range variation between the buried object and the scanning probe that can be measured by the time-of flight. These patterns can be detected by using the gradient information of the 3-D data set and for each pattern can be determined the apex position in real space and a score that explain the correlation with the hyperbolic template. A classification of the objects has been achieved by an analysis of the arcs into “pendants” corresponding to each buried object. Each pendant consists of a series of points defining the lateral position, depth and intensity of each arc “apex” from the given object. For objects of size comparable with the wavelength (typically 0.1 m @ 1 GHz), several such points are found. Apex points within a pendant are located by choosing a strong apex point and searching for both more shallow and deeper apex points which

(i) lie within a specified vertical area,

(ii) have a depth change within a specified margin from a quarter wavelength,

(iii) have the correct alternating phase.

The relative intensities within a pendant provide the necessary features for classification by, for example, a K-nearest-neighbour or neural net classifier. The method is demonstrated using radar images from buried isolated mines and also in proximity with other objects. The aim of this classification scheme is the identification of one object (mine) type against more “point-like” signals from “clutter” objects small compared to the wavelength.

A New Method for Solving an Inverse Scattering Problem Using Topological Sensitivity in the Context of Detection of Buried Objects with a Ground-Penetrating Radar

P. Millot and X. Ferrieres
ONERA, DEMR Department
Toulouse, 31055, France

J. Pommier
UMR MIP, INSA
Toulouse, 31077, France

M. Masmoudi
UMR MIP, Université Paul Sabatier Toulouse 3
Toulouse, 31062, France

This paper presents a new method to detect buried objects. We apply a strategy based on the topological sensitivity to solve an inverse diffraction problem. Topological sensitivity has already been used with success in electromagnetics for optimization problems [1]. The method is a shape optimization method, which does not require any assumption on the final solution. Therefore it could be very useful in the context of object detection where the number and the shape of the objects to find are unknown. The topological sensitivity can be seen as a space function, giving for each point of the space the variation of the cost function when we put or remove at this point a small metal cell.

The topological sensitivity function can be also accurately approximated by the product between the scattered fields and the adjoint scattered fields, taken at the positions where one wants to evaluate this function. In frequency domain, by solving Maxwell's equation for a source S, the electromagnetic fields u are given by a linear system $A(\Omega)u = S$, where $A(\Omega)$ is a matrix which depends on the distribution Ω of the objects in the soil. Let $J(u)$ be the function cost to minimize, then the adjoint fields w are given by $\overline{A}(\Omega)w = -\partial J(u)/\partial u$, where $\overline{A}(\Omega)$ is the adjoint operator of $A(\Omega)$. In time domain, the adjoint operator of the Maxwell's equations consists in solving them with a time reversal process.

To apply this method to detect buried objects in soils; we first take an initial Ω_0 empty distribution of objects. As we don't know exactly the soil composition, we assume it as an homogeneous soil with an average dielectric constant value. With these hypothesis, it is very fast to compute the fields and the adjoint fields of the problem. This evaluation can be analytical. After computing the topological sensitivity, we define a new distribution Ω_1 and a new cost function that can be used for computing a new iteration step of the optimization process. In general, the first iteration step is sufficient.

We have compared this method with other methods that are more classical in radar imaging. In particular, we have compared the topological sensitivity of synthetic data given by FDTD with conventional B-SCAN GPR imaging, SAR-like monostatic GPR tomography [2]. The proposed method seems to lead to more resolved radar images and also, to provide an answer to the question of multiple interactions between scatterers occuring with methods based on the linearization of the Greens function.

REFERENCES

1. J.Pommier, M. Masmoudi, and X. Ferrieres, "The topological asymptotic method," *APS*, 9–14, April 2000, Davos (Switzerland).
2. P.Millot, E. Le Brusq, E. Guillanton, C. Pichot, and J.Y. Dauvignac, "Radar Imaging of shallow buried objects with an ultra-wide band technique with specific antennas and synthetic antenna processing," *PIERS 2000*, Cambridge, MA, 7–10 July 2000.

Three-Dimensional Imaging of Multi-Component Ground-Penetrating Radar Data

J. van der Kruk
Institute of Geophysics, Swiss Federal Institute of Technology
Zurich, Switzerland

C. P. A. Wapenaar, J. T. Fokkema, and P. M. van den Berg
Delft University of Technology
Delft, 2628 RX, The Netherlands

Scalar imaging algorithms originally developed for the processing of remote sensing measurements (e.g., synthetic-aperture radar (SAR) method) or seismic reflection data (e.g., Gazdag phase-shift method) are commonly used for the processing of ground-penetrating radar (GPR) data. Unfortunately, these algorithms do not account for the radiation characteristics of GPR source and receiver antennas and the vectorial nature of radar waves. We present a new vector (multi-component) imaging algorithm designed specifically for electromagnetic wave propagation.

The multi-component three-dimensional imaging procedure is based on the expression for the scattered field using the Born approximation. Taking into account that the orientation of the source and receiver is parallel to the interface, four different source-receiver combinations are possible, which is written as a two-by-two tensor formulation for the scattered field due to a contrasting domain. The vectorial Green's functions, which describe the propagation of the electric field from the source to the contrasting domain and the propagation from the contrasting domain to the receiver, for the four different source-receiver combinations are combined in the tensorial wavefield extrapolator. A bounded inverse wavefield extrapolator is obtained by inverting the forward wavefield extrapolator in the spatial Fourier domain (Van der Kruk et al. [1]). When this approach would be carried out for a single-component measurement, a non-stable inverse would be obtained. To assess the performance of the multi-component, SAR and Gazdag algorithms, we compute their spatial resolution function, which is defined as the image of a point scatterer at a fixed depth using a single frequency. Application of the new multi-component imaging algorithm results in a circularly symmetric resolution function, demonstrating that the radiation characteristics of the source and receiver antennas do not influence the derived image. In contrast, the two tested scalar imaging algorithms return distinctly asymmetric resolution functions, which could result in erroneous images of the subsurface when these algorithms are applied to GPR data.

The multi-component and the two scalar imaging algorithms are tested on data acquired across numerous buried objects with various dielectric properties and different strike directions. Images of oblique and spherical objects produced by the multi-component algorithm have noticeably higher amplitudes than those produced by the two scalar algorithms. Phase differences between the different images are similar to those observed in the synthetic examples. Of the tested algorithms, we conclude that the multi-component approach produces the most reliable results.

REFERENCES

1. van der Kruk, J., C. P. A. Wapenaar, and J. T. Fokkema, "Multi-component 3-D imaging of ground penetrating radar data using matrix inversion in the spatial fourier domain," In *Proceedings Eight International Conference on Ground-Penetrating Radar, Queensland, Australia*, 508–513, 2000.

Binary Contrast Source Inversion of Immersed Objects from Laboratory-Controlled Data

B. Duchêne and J.-M. Geffrin
Département de Recherche en Electromagnétisme (DRÉ)
Laboratoire des Signaux et Systèmes (L2S / CNRS-Supélec-UPS)
Gif-sur-Yvette, F-91192, France

We investigate, herein, the characterization of objects immersed in water from laboratory-controlled data obtained in the microwave frequency range.

The objects are immersed in a water tank and are illuminated by a time-harmonic incident wave radiated by a biconical antenna operating in the frequency band 150–850 MHz. The scattered electric field, which results from wave – object interaction, is measured at several discrete frequencies by means of an antenna which is similar to the source and displaced step-by-step on a line.

The situation is such that a 2D-TM configuration is considered, and the modeling of the wave – object interaction is led through two coupled domain integral representations of the fields. The first equation, the so-called observation equation, relates the scattered field data to the Huygens type sources (or contrast sources) induced inside the object which are proportional to a contrast function representative of its constitutive physical parameters and to the total field within the object; the second equation, the so-called coupling equation, links these sources to themselves.

The inverse scattering problem then consists in retrieving, in a prescribed test domain assumed to contain an object, the unknown contrast function from measurements of the scattered field, through the inversion of the aforementioned two coupled integral equations. As is well-known, this problem is non-linear and ill-posed. It is dealt with by means of the so-called "binary contrast source inversion", which is a specialization to the case of homogeneous objects of the contrast source inversion method (van den Berg P. M. and Kleinman R. E., *Inverse Problems*, Vol. 13, pp. 1607–1620). The binary specialization has been developed for highly ill-posed problems which require a strong regularization, such as those encountered in the aspect-limited data configuration considered here, where the introduction, in the inversion algorithm, of a priori information on the object to be retrieved is a prerequisite to their resolution. This binary constraint is introduced, herein, in a way similar to that of "L. Souriau *et al.*, *Inverse Problems*, Vol. 12, pp. 463–481", where it was applied to the modified gradient method. As the latter, the contrast source inversion method is an iterative gradient-type method where the solution is obtained by minimizing a cost functional which accounts for both the observation and the coupling equation, however, contrarily to it, where the unknown contrast and the unknown field within the object are simultaneously looked for, here the contrast sources and the contrast are alternately updated at each iteration step, and this leads to a much faster and efficient algorithm.

Emphasis will be put on the way used to deal with the difficulties linked to both the high attenuation of the fields in water and the aspect-limited data configuration considered here, and the results obtained for objects of various natures (dielectric and metallic) and cross-sections will be presented.

Microwave Radiometry Techniques for Buried Landmine Detection

S. Dill, M. Peichl, S. Schulteis, and H. Süß
Institute of Radio Frequency Technology and Radar Systems
Oberpfaffenhofen, Germany

At present many million anti-personnel (AP) mines are polluting our environment in many countries. They cause a considerable limitation of the living space and make the land unuseable for agricultural purposes. Because the mine clearance procedures are much slower than the mine laying operations the number of polluting mines and the related contanimated areas are nowadays still increasing. Many mine polluted regions are former combat areas or belong to formerly highly frequented places. Thus the ground is contaminated additionally by many artificial impurities. For the current mine detection technologies and for the most modern mines, which become continuously smaller and have less metal content, a high false alarm rate of up to 1.000 to 1 is therefore very likely.

Classical mine detection procedures like using metal detectors or dogs, or brute-force methods like mechanical plowing through the soil by tank-like vehicles are not able to solve satisfactorily the mine contamination problem. They suffer mainly from many drawbacks like a high false-alarme rate, sensitivity to extraneous causes, high costs, and a destroying mode of operation, which cannot be tolerated in each situation. Thus an advanced mine detection system consists of multiple sensors based on different physical phenomena and principles and benefits from fusing their data. By doing this the different advantages of each sensor can be isolated from its shortcomings and merged to match as comprehensive as possible the specific mine detection requirements.

In this paper we illustrate the phenomenological background, the design, and some experimental results of a multi-spectral low-frequency microwave radiometer as a part of a multi-sensor mine detection system. The overall system is intended to work in a hand-held operation allowing the use in areas of difficult access without excluding missions in more friendly environments. Thus the radiometer antenna is operated in an extreme near-field mode to achieve a corresponding ground resolution in the order of the active antenna aperture size. In particular, the radiometer receiver is swept in low-bandwidth steps through a broad frequency range to vary the penetration depth and the reflectivity properties of the actually observed ground part. This provides significantly increased information about the location and shape of buried objects for discrimination purposes. The relevant theoretical aspects of this interference based effects are illustrated and attempts to interprete the frequency spectrum for specific layered arrangements as in the case of buried objects are presented.

Session 3Ac6

Computational Optics for Ultra-Dense Treatment of Light Fields

Simulating Nanoscale Near-Field Optical Microscopy

G. W. Bryant
National Institute of Standards and Technology
Gaithersburg, MD 20899-8423, U.S.A.

Nanooptics is a rapidly emerging branch of optics driven by the goal to control and manipulate light on the nanoscale. Key applications include photonic devices and circuits, microscopy with nanometer resolution, atom trapping and guiding, and quantum computing. Simulations of light fields in nanooptics are challenged by the need for a nanoscale description of light fields that are calculated from the near field out to the far field. In this presentation, we discuss new insights gained from addressing this challenge for nanoscale optical microscopy.

Near-field scanning optical microscopy (NSOM) has been used intensively to obtain nanoscale resolution in optical microscopy. The key to NSOM is to place a nanoscale optical probe in the near-field of the sample. The drawback is that the near-field optics is significantly perturbed by the nanoscale environment and a strong coupling between probe and sample. A critical problem for NSOM metrology is to identify and quantify the mechanisms that provide contrast in NSOM images. Even the simplest samples can provide counterintuitive images that are difficult to interpret.

We address this problem by considering simple, well-characterized imaging experiments. We have performed detailed simulations of these experiments by use of a variety of approaches including finite-difference and finite-element time domain methods, and the coupled dipole method. Two examples are considered here.

Holes in a dielectric film appear dark in illumination-mode NSOM images collected in transmission, counter to the expectation that probe light should pass more easily through the holes than through the film. Our finite-element simulations show that this contrast reversal is not determined by how the probe light scatters from the holes, as one might expect. Rather, the image contrast is determined by how light is extracted from the NSOM probe. Our simulations show that more light is extracted from the probe when the probe is over a thin dielectric film than when the probe is just in air. The holes in a film are dark in NSOM images because less light is extracted from the probe when the probe is above a hole.

NSOM images of small particles and metal templates can show detailed structure. Normally, it is assumed that the probe interrogates the sample, producing structure in the images that arises from light scattering by the sample. Our coupled-dipole simulations show that the roles of sample and probe can be switched with the structure in the images revealing information about light diffraction around the probe rather than about light scattering by the sample.

These simple but surprising explanations provide a step toward making NSOM a qualitatively and quantitatively accurate nanoscale metrology. This understanding is only possible with nanoscale simulations of the light scattering by the sample, the light emission by probe and the probe/sample coupling.

Optical Fields with Sub-Wavelength Structures: Experimental and Theoretical Studies

R. Dändliker, A. Nesci, L. Vaccaro, M. Salt, and H. P. Herzig
Institute of Microtechnology, University of Neuchatel
Neuchatel, Switzerland

In this paper we will present experimental and theoretical studies of optical fields with sub-wavelength structures, in particular phase singularities and coherent detection methods with nano-metric resolution. We intend to gain a better understanding of the interaction of light with microstructures in order to determine their optical properties. We have employed different numerical methods to get rigorous solutions for the electromagnetical field produced by microstructures, such as Fourier modal methods (FMM) for periodic structures and finite integration time domain methods (FITD) for fully three-dimensional simulations of scanning (near-field) probes. An electromagnetic field is characterized by an amplitude, a phase and a polarization state. Therefore, experimental studies require coherent detection methods, which allow to measure amplitude and phase of the optical field with sub-wavelength resolution. We will present two instruments, a heterodyne scanning probe microscope (heterodyne SNOM) and a high resolution interference microscope (HRIM).

We discuss some basic properties of phase distributions. Light waves diffracted by microstructures can give birth to phase dislocations, also called phase singularities. Phase singularities are isolated points where the amplitude of the field is zero. The time-averaged Poynting vector is zero and the energy flows around the phase singularity. Phase dislocations can be observed in the near- and far-field of optical microstructures, such as gratings. The position of phase dislocations depends essentially on the period, the height, the shape and the fill-factor of the grating. Therefore, according to the position of the phase singularity, the structure of the grating can be recovered by comparing the measured positions with rigorous calculations of the diffraction. However, the relationship between the position of the phase dislocation and the structure is not straightforward.

We will present theoretical and experimental results for a holographically recorded 1 mm pitch surface relief grating for TE- and TM-mode excitation. The behavior of phase singularities have been studied with a spatial resolution of 10 nm. Comparison of the calculated and measured amplitude and phase for the TE- and TM-mode with the heterodyne SNOM gives interesting information about the field conversion by the fiber tip probe. Our conclusion is that the longitudinal component of the electrical field contributes nearly as much as the transverse component to the light detected by the fiber probe. These findings have to be compared with the results from the theoretical modeling of fiber tips. Phase measurements obtained with a high resolution interference microscope show similar spatial resolution for the phase singularities. However, in this case only the transverse components of the electric field vector contribute to the measured amplitude and phase.

In conclusion, comparison of theoretical field calculations and experimental measurements of amplitude, phase and polarization, using coherent detection methods with nano-metric resolution, is the key for the understanding of the interaction of light with sub-wavelength structures.

Numerical Study of the Lifetime of a Molecule Close to a Lossy Nanostructure

M. Thomas and R. Carminati
Laboratoire EM2C, Ecole Centrale Paris, CNRS
Chatenay-Malabry, France

J.-J. Greffet
University of Rochester, The Institute of Optics
Rochester, NY 14627, U.S.A.

One of the most promising techniques in near-field optics uses a tip to enhance locally the electromagnetic tip [1]. A major goal for this technique is to achieve spectroscopy of a single molecule. While the tip produces a strong enhancement of the field, it also introduces new channels for the desexcitation of the molecule. Using an ellipsoid particle as a model for the tip, it has been shown qualitatively that there is a competition between the enhancement factor and the induced losses in the tip [2]. A quantitative model of these competing processes is still an open question. The purpose of this work is to present a first step towards a quantitative model based on a numerical solution of the problem.

The relevant quantity to study in this context is the Greens tensor of the system. On one hand, it yields the lifetime of the molecule. On the other hand, its trace yields the local density of states. From a simple point of view, this amounts to compute the electric field scattered at the location of a dipolar source.

In order to be able to deal with any possible shape of the scatterer and to take losses into account, we have used surface integral equations. The numerical scheme that we use to solve these equations is the standard moment method. We will discuss the effect of the shape and the dielectric properties of the particle on the lifetime of the molecule.

REFERENCES

1. E.J. Sanchez, L. Novotny, and X.S. Xie, “Near-field fluorescence microscopy based on two-photon excitation with metal tips,” *Phys. Rev. Lett.*, vol.82, pp.4014-4017, 1999.
2. J. Azoulay, A. Debarre, A. Richard and P. Tchenio, “Quenching and enhancement of single-molecule fluorescence under metallic and dielectric tips, *Europhys. Lett.*, vol.51, pp.374-380, 2000.

SNOM Simulation Using the MaX-1 Software

C. Hafner
Swiss Federal Institute of Technology
Zurich, CH 8092, Switzerland

The main problem of Scanning Nearfield Optical Microscopy consists in finding structures that cause small spots of high field intensity. At low frequencies, such spots can easily be created in the vicinity of conductors with small radii of curvature. At optical frequencies, no sufficiently good conductors are available. Therefore, it is very difficult to design bright spots that are much smaller than the wavelength. Since the fabrication and measurement of promising SNOM structures is difficult, numerical simulations of such structures are highly desirable.

Traditional SNOM structures - such as optical fiber tips with metallic cladding - cause huge problems for all kind of numerical methods for several reasons. First of all, a very high accuracy is required because the field near the tip can be several orders of magnitudes smaller than the incident field. Second, the entire SNOM structure may be big compared with the wavelength, i.e., the structure may have a huge number of resonances and requires a fine discretization at the same time. Furthermore, for detailed studies, many different models must be generated and computed, which is a very time-consuming process. In order to keep the expenditure for the simulations reasonably small, it is important to focus on simplified models and to take advantage of user-friendly software with advanced modeling tools. Since full 3D simulations are very demanding, one often starts with 2D models that are not very realistic. A much better insight is obtained from axisymmetric models. In many cases, the expenditure for axisymmetric models is not much higher than for 2D cylindrical models. This even holds when the field is not axisymmetric.

MaX-1 is a general purpose code for computational electromagnetics that also contains the most advanced version of the Multiple Multipole Program (MMP). Previous MMP versions had already successfully been applied for SNOM simulations years ago. MaX-1 considerably simplifies the modeling and provides several tools that are useful for axisymmetric cases. Therefore, various traditional structures as well as new promising structures can be studied with a reasonable effort.

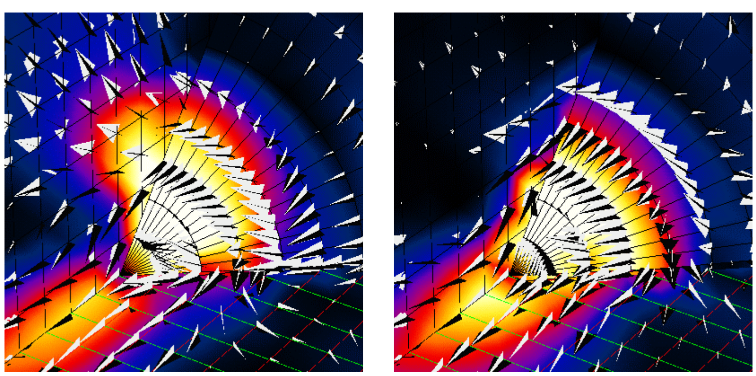

Figure 1: Poynting vector field of a conical SNOM tip (triangular cross section) illuminated by a laser beam from the back hand side. Relative permittivity of the tip 2.2 (left) and 4.0 (right).

Field Enhancement Near Laser-Illuminated Metal Tips

L. Novotny
The Institute of Optics, University of Rochester
Rochester, NY 14627, U.S.A.

Recently, anovel method has been proposed and implemented for near-field optical microscopy [1, 2] and near-field optical trapping [3]. The method makes use of the strongly enhanced electric field close to a sharply pointed metal tip under laser illumination. The energy density close to the metal tip is shown to be orders of magnitude stronger than the energy density of the illuminating laser light. The tip is held a few nanometers above the sample surface so that a highly localized interaction between the enhanced field and the sample is achieved. In order to obtain a high image contrast, the method takes advantages of nonlinear optical interactions based on multi-photon processes. Resolutions on the order of 20nm have been demonstrated by making use of the field enhancement effect combined with two-photon excitation of the sample.

To analyze the tip-enhancement effect we performed simulations based on the multiple-multipole (MMP) method. The rotational symmetry of the metal tip allows us to reduce the problem to two dimensions by applying ring-multipoles as expansion functions. Solutions along the semi-infinite cylindrical tip-shaft are expanded in cylindrical waveguide modes. We calculate the induced surface-charge density and show that the field enhancement depends strongly on the polarization properties of the irradiating laser light. To calculate the temperature distribution due to laser irradiation we use the results of the MMP calculations as source terms for a heat-diffusion equation which is solved by the finite-difference time-domain (FDTD) method.

The strong field gradients near the irradiated metal tip exert electromagnetic forces on polarizable particles. We analyze the trapping potential near the tip by rigorously evaluating Maxwell's stress tensor. We find that the trapping forces can overcome uctuations due to Brownian motion and that a stable near-field trap is feasible for particles with sizes on the order of the tip radius.

REFERENCES

1. L. Novotny, E. J. Sanchez, and X. S. Xie, "Near-field optical imaging using metal tips illuminated by higher-order Hermite-Gaussian beams," *Ultramicroscopy,* Vol. 71, pp. 21-29, 1998.
2. E. J. Sanchez, L. Novotny, and X. S. Xie, "Near-field uorescence microscopy based on two-photon excitation with metal tips," *Phys. Rev. Lett.,* Vol. 82, pp. 4014-4017, 1999.
3. L. Novotny, Bian. R. X, and Xie. X. S, "Theory of nanometric optical tweezers," *Phys. Rev. Lett.,* Vol. 79, pp. 645-648, 1997.

MMP Computations of Photonic Crystals: Band Structure of Perfect Crystals and Waveguides

E. Moreno, D. Erni, and C. Hafner
Laboratory for Electromagnetic Fields and Microwave Electronics, Swiss Federal Institute of Technology
Zurich, Switzerland

Understanding the behavior of defect-free photonic crystals and designing devices based upon them require a knowledge of the wave propagation properties in the crystal [1,2]. This information is contained in the band structure and eigenmodes of the periodic system. In the most basic level, it is important to find perfect crystal structures with improved features. In this context, new geometries have been investigated, e.g. the Kagomé structure [3], and symmetry techniques to enhance the gaps have been applied [4]. The next level comprises the characterization of crystals with impurities, such as cavities and channel waveguides, which are likely needed for the design of devices with useful functionalities. The band structure and modal fields are essential tools here as well.

In this paper, a method for the computation of the band structure of two-dimensional photonic crystals will be presented. It is well suited for crystals including materials with arbitrary frequency-dependent dielectric constants. The technique can be applied to study photonic crystals with irregularly shaped (non circular) elements. This method is based on the multiple multipole method (MMP) [5]. In order to find the solutions of the non-linear eigenvalue problem, a multipolar source is introduced which acts as an excitation. By varying the frequency of the source, the various eigenmodes are excited and can be localized as resonances in an appropriately chosen function. The approach will be demonstrated for several systems including perfect photonic crytals and photonic crystals with defects. Various materials are investigated, such as non-dispersive dielectrics and highly dispersive metallic media.

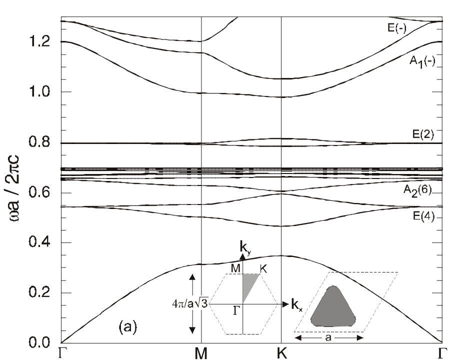

Band structure of two-dimensional photonic metallic crystal

REFERENCES

1. J. D. Joannopoulos, R. D. Meade, and J. Winn. “Photonic crystals. Molding the flow of light”, *Princeton University Press, New Jersey*, 1995.
2. K. Sakoda, “Optical properties of photonic crystals”, *Springer, Berlin*, 2001.
3. J. B. Nielsen, T. Sondergaard, S. E. Barkou, A. Bjarklev, J. Broeng, and M. B. Nielsen, *Electron. Lett.* 35(20), 1736 (1999).
4. C. M. Anderson and K. P. Giapis, *Phys. Rev.* B 56(12), 7313 (1997).
5. Ch. Hafner, *Post-modern Electromagnetics.* “Using Intelligent MaXwell Solvers”, John Wiley and Sons, Chichester, 1999.

Analysis of Resonant Coupling between Dielectric Waveguides via Rectangular Microcavities

M. Hammer and E. van Groesen
MESA^{+} Research Institute, University of Twente
Enschede, 7522 DA, The Netherlands

While traditionally most concepts for applications of integrated optical microresonators in optical wavelength division multiplexing deal with smooth cylindrical, elliptical, or spherical geometries, recently configurations with square cavity shapes have been proposed [1] and considered experimentally [2]. A typical resonator element consists of a compact rectangular cavity, that couples evanescently two adjacent parallel dielectric waveguides. We consider these devices in a two-dimensional setting by means of two different techniques.

Upon viewing the structure as a sequence of three longitudinally homogeneous waveguide segments, on a wide lateral computational window the electromagnetic field is expanded into the local modes of these segments, including propagating and evanescent, forward and backward traveling terms. Matching adjacent fields at the segment boundaries yields the transmission characteristics of the resonator [3]. These mode expansion simulations allow an efficient and quite rigorous numerical assessment.

Alternatively, we propose to apply a coupled mode theory based on the guided fixed-frequency modes of the two port waveguides and the cavity, regarding the latter as a short segment of a thick multimode slab waveguide. Forward and backward traveling versions of the basic modes are coupled over the extension of the cavity. Combined with the numerically computed guided wave reflectivity of the cavity end facets, the coupled mode equations for both propagation directions allow to evaluate the power transmission of the resonant coupler. Being of a more approximate nature, where the high refractive index contrast and the long light path in a resonant configuration constitute somewhat extreme conditions, the coupled mode approach is nevertheless an ab-initio model without free parameters, that gives some insight in the functional behaviour and proper design of the rectangular resonators.

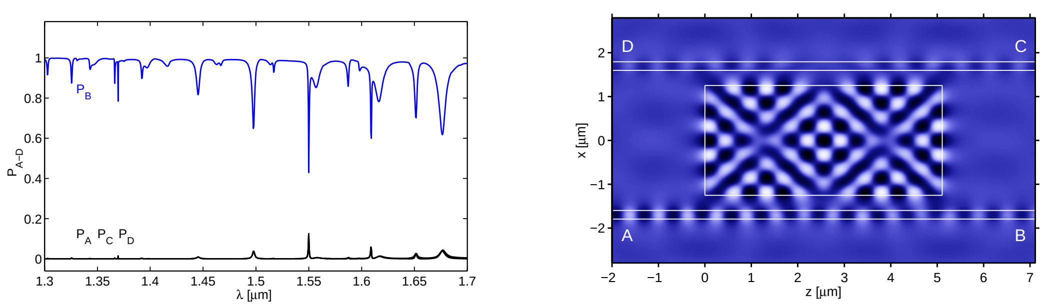

Figure 1: Spectral response (left) and resonant field pattern (right, $\lambda = 1.55\mu$m) for TE light propagation through a rectangular microresonator. $P_A - P_D$ are the relative powers transmitted or reflected into ports A to D, versus the vacuum wavelength λ of the incoming light, that enters the structure in port A. Cavity dimensions: $2.5\mu m \times 5.108\mu m$, waveguide core width: $0.194\mu m$, gap width: $0.35\ \mu m$, refractive indices: 3.2 (guiding regions) and 1.4 (cladding).

REFERENCES

1. C. Manolatou, M. J. Khan, S. Fan, P. R. Villeneuve, H. A. Haus, and J. D. Joannopoulos. “Coupling of modes analysis of resonant channel add-drop filters,” *IEEE Journal of Quantum Electronics,* 35(9):13221331, 1999.
2. A. W. Poon, F. Courvoisier, and R. K. Chang, “Envanescent and refractive side-coupled high-Q resonances of non- circular 2-D micropillars,” In A. V. Kudryashov and A. H. Paxton, editors, Laser Resonators IV, Vol. 4270 of SPIE Proceedings, 131-138, 2001.
3. M. Lohmeyer. “Mode expansion modeling of rectangular integrated optical microresonators,” *Submitted to Optical and Quantum Electronics,* 2001 (accepted).

Fourier Methods for Modelling Photonic Crystal Devices

P. Lalanne, J.-P. Hugonin, and E. Silberstein
Laboratoire Charles Fabry de l'Institut d'Optique, Centre National de la Recherche Scientifique
Orsay, F-91403, France

Numerical characterization and modeling of guided-wave passive components have been an important research topic in the past four decades. This is due to increased research and development in millimeter-wave and photonic integrated circuits. In the early 60's, efforts were devoted to establish the foundations of the theory. In the late 1980's, more than a dozen of numerical methods were invented and the somewhat more classical methods have been refined. Most of the presently existing methods have been known from that time. The development of waveguide theory continues today responding to the demands of the increasingly widespread applications of integrated optics. It features improvements of the existing methods regarding numerical stability, convergence speed and versatility... Most of this can be said for grating theories as well. Clearly, because they rely both on the same foundation, the theory of electromagnetism, waveguide and grating methods share many common features. However, probably because they are directed to the modeling of different structures and because the applications are rather different, it appears that these theories were mainly developed independently and that clear bridges between these theories were rarely made in the literature.

In this work, we use the Rigorous Coupled Wave Analysis [1] (RCWA) to solve many non-periodic diffraction problems in integrated optics. The RCWA is a frequency-domain method widely used in grating theory. It has been developed over many years. The RCWA is based on the computations of the grating modes as eigenvectors and on Fourier expansions for the permittivity and for the electromagnetic fields inside the grating region.

The extension of the RCWA to model waveguide diffraction problems relies on the introduction of absorbers to satisfy the outgoing wave condition [2]. Perfectly-matched layer [3] are used in our numerical implementation. Up-to-date problems like the diffraction of guided waves by 2D gratings [4], the losses of photonic crystal waveguides above the light line and waveguide airbridge microcavities [5] will be considered in the oral presentation. The theory is also tested against experimental data for photonic crystal waveguides.

REFERENCES

1. M.G. Moharam et al., "Formulation for stable and efficient implementation of the rigorous coupled-wave analysis of binary gratings", *J. Opt. Soc. Am.* A 12, 1068 (1995). Ph. Lalanne and Morris. G. M, "Highly improved convergence of the coupled-wave method for TM polarization", *J. Opt. Soc. Am.* A 13, 779 (1996). L. Li, "New formulation of the Fourier modal method for crossed surface-relief gratings", *J.Opt. Soc. Am.* A 14, 2758 (1997).
2. Ph. Lalanne and Silberstein. E, "Fourier-modal method applied to waveguide computational problems", *Opt. Lett.* 25, 1092 (2000).
3. J.P Bérenger, "A perfectly matched layer for the absorption of electromagnetic waves", J. Computational. Physics, 114, 185-200 (1994).
4. Ph. Lalanne and H. Benisty, "Out-of-plane losses of two-dimensional photonic crystal waveguides: electromagnetic analysis", *J. Appl. Phys.* 89, 1512 (2001).
5. Eric Silberstein et al., "On the use of grating theories in integrated optics", *J. Opt. Soc. Am. A,* to be published in the special issue on Diffractive Optics, November 2001.

Generating and Analysing Short Optical Pulses in Dielectric Waveguide Structures for Obtaining Spectral Data Using the FDTD

R. M. de Ridder
University of Twente
Enschede, The Netherlands

R. Stoffer
Alcatel Optronics Netherlands
Enschede, The Netherlands

The spectral analysis of photonic crystal structures containing waveguides and resonators is often difficult due to the lack of efficient direct spectral methods. Such structures can be well analysed using a general-purpose time-domain method like the Finite-Difference Time-Domain (FDTD) method. A very inefficient way of calculating the spectral response using such a method would be to perform many separate calculations of the response to a CW stimulus at several frequencies of interest. A better method, applicable if no optical nonlinearities are involved, is to perform a single time-domain calculation of the response to a short pulse, providing all the necessary data, which can be transformed afterwards to the frequency or wavelength domain.

An additional problem arises when the light is coupled into or out of the structure using conventional dielectric slab or channel waveguides, since the modal field distributions in these waveguides may be strongly frequency-dependent. If the spatial distribution of the input pulse is matched to the modal field at a particular frequency, then there will be a mismatch for other frequency components contained in the pulse, leading to a large amount of radiated energy. So the problem is how to launch an extremely short pulse (a few fs is needed for covering a sufficiently broad wavelength range of about $1.0 - 2.0\mu$m) efficiently into a single-mode dielectric waveguide.

A similar problem occurs in gathering the response data from the structure. The simplest approach would be to just take the time series of field values at a single position in a waveguide. However, the results turn out to be very sensitive to the exact position of the ‘collection point’ since beat patterns will occur due to interference of several modes with slightly different frequencies. Also, contributions will be found of light that is not guided in a mode (and that would be seen to radiate away if the calculation window would be sufficiently long). This problem is the inverse of the former one: how to decompose the time-domain output field into the modal fields for each frequency involved.

We will demonstrate an approach for solving both these problems. A Gaussian pulse in a discrete time domain will have a discrete Gaussian frequency spectrum $S_0(\omega)$. For each frequency component ω_i a (transversal) fundamental modal field $M_1(\omega_i, x, y)$ is calculated. This leads to different frequency spectra $S_1(\omega, x, y) = S_0(\omega)M_1(\omega, x, y)$ at different points (x, y) in a transversal plane. The spectrum in each of these points is then back-transformed into the time domain, leading to a complicated space-time pattern $E_1(t, x, y)$ that will efficiently excite the fundamental mode of the waveguide over the entire spectrum. In the analysis, the emerging time-space dependent field pattern $E_2(t, x, y)$ – possibly in a different waveguide – will be Fourier transformed into spectra $S_2(\omega, x, y)$ at each point in the transversal plane. For each frequency ω_i in this space-frequency pattern, the overlap integral $m(\omega_i)$ of $S_2(\omega_i, x, y)$ with the fundamental waveguide mode $M_2(\omega_i, x, y)$ is calculated. The transmission spectrum for the light entering the structure in the fundamental mode of waveguide 1 and leaving in the fundamental mode of waveguide 2 is then given by $T_{12}(\omega) = m(\omega)/S_0(\omega)$.

PBG Device Simulation

R. Zaridze, D. Karkashadze, K. Tavzarashvili, F. Bogdanov, A. Bijamov and V. Tabatadze
Tbilisi State University
Tbilisi, 380028, Georgia

C. Hafner, D. Erni and E. Moreno
Swiss Federal Institute of Technology
Zurich, CH-8092, Switzerland

Finite Photonic Cristals (PC) allow one to easily obtain integrated optical circuits consisting of various devices, including optical waveguides, splitters, filters, resonators, etc. Although it is easy to obtain such devices, it is hard to find an appropriate solution when the desired characteristics of the device are given. For an efficient design, a smart optimizer combined with a reliable and accurate simulation tool are required. In this paper we present such a simulation tool based on the Multiple Multipole Program (MMP) and on the Method of Auxiliary Sources (MAS) combined with the well-known Mie-Vekua-Yasuura approach.

First, we focus on the relatively simple problem illustrated in Fig. 1: In an arbitrary dielectric (complex, biisotropic, chiral properties can also be handled) with surface S one has some circular dielectric rods of radius R on a regular grid with defects. This crystal is excited by a harmonic wave incident from the exterior region.

The field inside the area bounded by S and the surfaces of the rods is composed of both the scattered field of the rods (approximated by high multipoles) and the field of Auxiliary Sources (AS) located outside S on the auxiliary surface S_1. Inside the rods the field is described by Bessel functions. Finally, the exterior field (outside S) is modelled by a superposition of AS on S_2 and the incident field.

Unknown amplitudes of the AS are determined from the boundary conditions on S and on the surfaces of the rods.

For non-circular rods, the Mie-Vekua-Yasuura approach turns out to be inefficient and can be replaced either by a MMP or a pure MAS approach. Software packages with user-friendly GUIs were developed based on both approaches. Figure 2 shows a simple example.

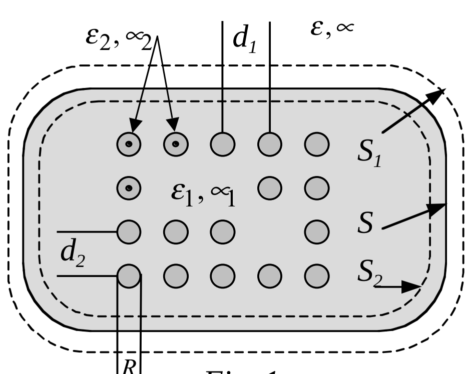

Fig. 1

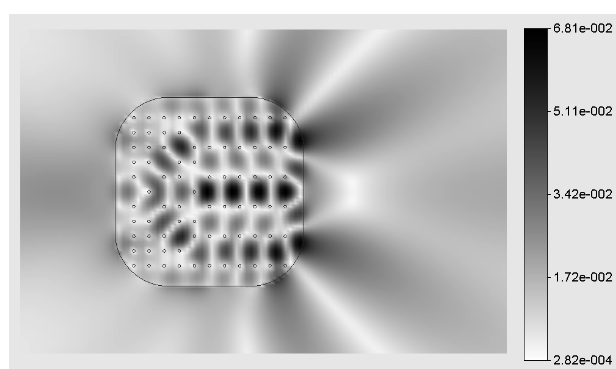

Fig. 2

Session 3Ac7

Electromagnetics for Novel Meta Materials and Structures

DARPA's Interests in Meta Materials

V. M. Browning
Defense Advanced Research Project Agency(DARPA)
Defense Science Office(DSO)
Arlington, VA 22203-1714, U.S.A.

An overview of the motivation, goals, and current focus of the Defense Advanced Research Project Agency (DARPA) Meta-Materials Program will be presented. Metamaterials are engineered composites that exhibit superior properties that are not observed in the constituent materials or nature. DARPA's interests in metamaterials was motivated, in part, by recent developments in the processing and synthesis of nanoscale composite materials as well as new understandings of how the physics of materials changes at low dimensions and/or small scale. Recent advances in material processing and synthesis capabilities now allow 3D, composite materials to be engineered and assembled with great precision. In addition, new theoretical understandings and predictive models suggest that superior properties may be observed in materials that contain inhomogeneities that have features that are small compared to the coherence length of the physical property of interest (ferromagnetic exchange length, electron mean free path, electromagnetic wavelength, etc.). The primary goal of the DARPA program is to explore and exploit these new developments by developing and demonstrating a broad range of metamaterials with superior properties that will fill the void in the design space for a number of important DoD and commercial applications. Among the metamaterial efforts that will be discussed are:

1. "left-handed" or negative index of refraction composites for antenna, communication, and frequency selective surface applications;
2. superparaelectric/nanocomposite ferroelectrics for microwave radar components;
3. super radiant (IR) emitting structures for thermal management applications;
4. composite dielectrics/magneto-dielectrics for antenna applications;
5. low loss, high permeability magnetic composites for power electronics.

Experiments and Simulations on Left-Handed Metamaterials

D. R. Smith and S. Schultz
University of California, San Diego
La Jolla, CA 92093-0319, U.S.A.

In the sixties, V. G. Veselago [1] suggested that a *left-handed* medium, in which the electric permittivity, ε, and the magnetic permeability, μ, were simultaneously negative, would have remarkable electromagnetic properties. These properties included negative refraction, reversal of the electromagnetic Doppler shift, and the reversal of Cerenkov radiation.

To date, a naturally occurring material having both ε and μ simultaneously negative has not been reported. Recently, however, our group performed experiments [2] on a fabricated structure that could be characterized by an $effective\ \varepsilon$ and an $effective\ \mu$, both of which could be simultaneously negative over a band of frequencies. The structure made use of an array of wires to produce an electric response [3], in which was interleaved an array of split ring resonators (SRRs) to produce a magnetic response [4]. In particular, the property of negative refraction was demonstrated [5], confirming one of Veselago's initial conjectures.

In this talk, we will describe the sequence of design that led to the structures used in the experiments, as well as the results of those experiments. We will show that the totality of experimental and simulation data indicates that, over at least some range of frequencies, metamaterials can be well described by bulk frequency-dependent electromagnetic material parameters, which can assume values not readily observed in naturally occurring materials. This result is central to the metamaterials concept.

1. V. G. Veselago, *Sov. Phys. Usp.* , Vol. 10, 509 (1968).
2. D. R. Smith, W. J. Padilla, D. C. Vier, S. C. Nemat-Nasser, S. Schultz, *Phys. Rev. Lett.*,, Vol. 84, 4184 (2000).
3. J. B. Pendry, A. J. Holden, W. J. Stewart, I. Youngs, *Phys. Rev. Lett.*, Vol. 76, 4773 (1996).
4. J. B. Pendry, A. J. Holden, D. J. Robbins, W. J. Stewart, *IEEE Trans. Microwave Theory Tech.*, Vol. 47, 2075 (1999).
5. R. A. Shelby, D. .R. Smith, S. Schultz, $Science$ 292, 77 (2001).

Progress in Left Handed Material Research

C. G. Parazzoli, R. B. Greegor, K. Li, A. Vetter
Physics Technology, The Boeing Company
Seattle, WA 98124, U.S.A.

D. R. Smith
Department of Physics, UCSD
La Jolla, CA 92093, U.S.A.

R. Schuhmann
Darmstad University of Technology, Comp. Electromagn. Laboratory
Darmstad, 64289, Germany

Modeling and experiments to better understand the behavior of Left Handed Materials (LHM) are currently in progress in a DARPA funded project. The modeling of the elementary cells structures occurring in LHM is in progress using a variety of numerical algorithms. Significant understanding of the behavior of the elementary cells has been achieved in our simulations. The collective performance of the materials has also been gained. In parallel with the simulation effort an experimental effort is in progress. We have designed a test anechoic cell where a collimated RF beam between 5 and 20 GHz is generated. The RF fields in the cell have been computed by numerical simulation and verified by direct measurements. The performance of the elementary LHM cells have been measured and compared to the simulation results. A full LHM sample is placed in the test apparatus and its scattering parameters obtained. From the measured scattering parameters the effective ε and μ are retrieved.

Electrodynamics of Metallic Photonic Crystals and Problem of Left-Handed Light

A. L. Efros and A. L. Pokrovsky
Department of Physics, University of Utah
Salt Lake City, UT, U.S.A.

An analytical theory of electromagnetic waves in a metallic photonic crystal is presented. We consider the cases $\omega\tau << 1$ and $\omega\tau >> 1$, where τ is the relaxation time in a metal. In the low frequency case the modes, obtained before experimentally and by computations, are studied. The dispersion equation and the expression for the electric permittivity are obtained. It is shown that the modes have a cutoff frequency, which is the root of the permittivity. The results for the cutoff frequency are in a good agreement with the experimental and computational data but they are far from proposed earlier analytical expressions. It is shown that if the system is embedded into a medium with a negative magnetic permeability, it has no propagating modes at any frequency. Thus, such a system cannot support the left-handed light (LHL). We think that the recently observed LHL is due to the anomalous dispersion rather than to the negative permeability. It is shown that in the high frequency case ($\omega\tau >> 1$) there is a spatial dispersion of the dielectric constant. In general there are five different branches of the EMW that cover almost all frequency range under consideration. The theory of refraction is proposed which is unusual because of the spatial dispersion.
The work has been funded by NSF grant DMR-0102964.

A Superlens for Nanoscale Imaging in Far-Field?

N. Fang and X. Zhang
Dept. of Mechanical and Aerospace Engineering, University of California at Los Angeles
Los Angeles, CA 90095, U.S.A.

In a paper published in 1968 [1], Veselago predicted from Maxwell equations that electromagnetic waves in a medium having simultaneously negative permittivity and permeability ("left-handed medium", or LHM) would propagate with wavevector k in a direction opposite to the energy flow. Therefore, a slab of LHM will function as a 1:1 imaging lens at designed wavelength and working distance. Recently, this left-handed medium is realized in microwave range by Schultz's group in UCSD [2,3]. From a quasi-static theory, Pendry [4] presents a radical prediction in contrast to the diffraction limit of conventional optical imaging: with a loss-free thin slab of LHM, one can observe a real image of the object of interest at near-field, without losing the subwavelength details.

However, Pendry's quasi-static theory did not specify the following questions: how can we achieve reduction/magnification with LHM? how does the loss affect the imaging quality? and finally, how can we realize imaging in far-field? In this paper, we present the numerical experiment results to address these important issues. We examined the quality of imaging subwavelength features using a LHM superlens. Examples of image reduction and magnification with LHM are demonstrated and resolution limits are discussed. For the first time, we demonstrated the possibility of far-field imaging with perfect tuning of permittivity and permeability.

Tunable Split-Ring Resonator Arrays for Left-Handed Electromagnetic Meta-Materials

E. Niver and K. Um
ECE Department, NJIT
Newark, NJ 07102, U.S.A.

A. A. Zakhidov
Physics Department, Moscow State University
Moscow, Russia

R. Baughman and A. A. Zakhidov
UTD-NanoTech Institute, University of Texas at Dallas
Dallas, TX 75070, U.S.A.

Tunability of split ring resonator (SRR) arrays and back plane strip elements (plasmon meshs), known to achieve left handed metamaterial was investigated using varactor diodes connected between the split rings. Finite element based numerical simulations and experimental measurements were carried out when these elements were placed in a slotted microwave waveguide. The slotted waveguide medium was preferred to simplify the connectivity of the bias voltage power supply to change the junction capacitance of varactor diodes. The resonance frequency of the split ring resonator and back plane strip configuration was determined using single element loaded waveguide measurements. The effect of the arrays of such elements, assembled into 2-d and 3-d structures were measured and additional resonances were observed below the expected resonance frequency of the split ring resonator configuration due to internal interaction of the structure with the surrounding waveguide. Reverse bias voltage was applied to varactor diodes and tunability in terms of shift of the resonance frequency of SRR, broadening of the stop band region and further increase in the transmission loss due to loading with varactor diodes were observed. Preliminary numerical simulations are in agreement with the measurements. Further optimization for higher tunability is in progress for achieving tunable left handed metamaterials.

Experimentally the tunability of split ring resonators has been investigated in the waveguide environment as will be shown. Rectangular waveguides have been thoroughly analyzed and provide advantages over the open region structures due to well defined wave interactions such as propagating modes. The waveguide used in this study was WR-187 waveguide with physical dimensions (1.872×0.872 inches) and a cut-off frequency of 3.152 GHz. For the accurate verifications of the resonance frequency, measurements were also carried out in a WR-284 waveguide of dimensions (2.840×1.340 inches) and a cut-off frequency of 2.078 GHz. The dominant TE10 mode was excited during these simulations and measurements.

The split ring resonator dimensions are similar to one used by Smith *et al.* (*Phys. Rev. Lett*., 84, pp. 4184-4187, 2000). The substrate material used was GETEK with thickness of 10 mils and relative dielectric constant $\varepsilon_r = 4.2$. The tuning element consists of an array of three split ring resonators coupled to a strip on its back plane. In left-hand configuration, the back plane strip of the three-element array is grounded. Each such cell in an array has the inter cell spacing of 17.5 mm. The split ring resonator and the back plane strip are initially placed into a WR-187 waveguide. The purpose in the choice of this type of the waveguide is to keep the resonance frequency away from the cut-off frequency. Numerical simulations of the above described geometry was carried out on a finite element based HFSS (High Frequency Structure Simulator).

SRR tunability have been observed up to 5 GHz which is primarily limited by the varactor diode limitations. Additional resonances appeared due to interaction between the waveguide and the tuning array elements. There is pass band region which is a precursor to the left hand media observed between 3.6 and 3.8 GHz. However, only three arrays did not induce high losses as reported for the left handed media. As observed before shifting the bias to 10 V introduced only slight loss.

Diffraction in Left-Handed Materials and Theory of Veselago Lens

A. L. Efros and A. L. Pokrovsky
Department of Physics, University of Utah
Salt Lake City, UT 84112, U.S.A.

The theory of diffraction in the system consisting of the left-handed and the right-handed materials is constructed. The theory is based upon the Huygens principle and the Kirchhoff integral and it is valid if the wavelength is smaller than any relevant length of the system. The theory is applied to the calculation of the smearing of the foci of the Veselago lens due to the finite wavelength. We show that the Veselago lens is a unique optical instrument for the 3D imaging, but it is not a "superlens" as it has been claimed recently.

Electromagnetic Scattering by Canonical Objects Composed of Left-Handed Materials

J. Pacheco, B. E. Barrowes, and J. A. Kong
Research Laboratory of Electronics
Massachusetts Institute of Technology
Cambridge, MA 02139, U.S.A.

Left-handed materials, so called due to the anti-parallel nature of the wave vector and the Poynting vector arising from simultaneous negative permittivity and permeability, were first given theoretical consideration by Veselago in 1968. A number of remarkable and potentially useful electromagnetic properties exist for left-handed materials (LHMs) including backward waves, reverse Doppler shift, reverse Čerenkov radiation, near field focusing phenomena, and a negative index of refraction. Recently, a two dimensional meta-material consisting of rods and split ring resonators printed on dielectric sheets was shown to exhibit LHM properties in the microwave regime. Motivated by this demonstration and in anticipation of possible applications of LHMs, we analyze the scattering from various canonical objects such as layered planar, cylindrical, and spherical media that are composed of LHMs.

In order to examine the electromagnetic properties of an object composed of left-handed material (LHM), we begin by studying a sphere composed of a homogeneous LHM. Although the Mie scattering theory has been extensively studied in the past, the details of the theory have been reviewed for the purposes of handling LHMs. In particular, in a LHM, there is an ambiguity in the choice of sign for the wavenumber, which if not properly accounted for, can lead to incorrect scattering results. It turns out that the Mie scattering coefficients in their most general form are independent of this sign choice, however, the form of the coefficients presented in many textbooks often contain certain simplifications of these coefficients that implicitly assume a certain sign for the wavenumber of the LHM. Accordingly, care must be taken to choose the correct sign for this wavenumber when these references are used directly.

After deriving the Mie scattering coefficients, the scattering properties of the LHM sphere can be studied. The characteristics of the scattered fields produced by plane wave incidence will be presented. For instance, inside LHM spheres a focusing point exists, which is not present in RHM spheres. For a more quantitative comparison, the near-field and far-field patterns for a LHM sphere are also compared.

We next examine the scattering from layered planar, spherical, and cylindrical media. The formulation presented is general, and each layer can be composed of either LHMs or RHMs. In view of RCS reduction applications, the backscattering from conducting objects coated with LHMs is calculated. To characterize the scattering properties over a wide bandwidth, various frequency dispersive models for LHMs, such as the Lorentz and Drude model, are used. The RCS reductions obtained by using LHMs and by using standard radar absorbing materials are compared.

Finite-Difference Time-Domain Simulation of Propagation Through Left-Handed Metamaterials

C. D. Moss, Y. Zhang, T. M. Grzegorczyk, and J. A. Kong
Massachusetts Institute of Technology
Cambridge, MA 02139, U.S.A.

Materials with both negative permittivity and negative permeability are known as 'left-handed' (LH), because the power propagates in the opposite direction of the wave vector. These materials are a popular topic of current research due to their recent physical realization [1]. Predicted properties of these materials include a reversed Doppler effect, reversed Cerenkov radiation, and a negative index of refraction [2]. As such, the range of imaginable applications extends to the field of antenna design, vehicle coatings for altering radar cross section properties, and perhaps even the realization of a perfect lens [3].

Currently, the LH materials are metamaterial structures, composed of periodic arrays of metal microstrip lines (for negative permittivity) and split-ring resonators (SRRs, for negative permeability) [1]. The first demonstration of the LH nature of these structures was inferred by observing the transmission and reflection coefficients of a slab over frequency. For regions where either the permittivity or the permeability is negative, there is no transmission (because of an imaginary wave number). However, in the band where the two parameters are simultaneously negative, transmission occurs. This pass-band phenomenon was indeed observed in LH metamaterials, but it is not specific to them: many different types of metamaterial geometries can result in pass-band or stop-band transmission characteristics, and hence measurements of this type are not sufficient to demonstrate that a given material is LH. A more rigorous test to demonstrate the LH nature of a material is to measure the index of refraction of a prism constructed with LH metamaterials. Snell's law dictates that the angle of transmission into or out of any positive ('right-handed') material must be on the opposite side of the surface normal with respect to the incident angle. For LH materials, however, the angle of transmission is on the same side of the normal, and has been theoretically demonstrated and experimentally verified [2, 4].

The purpose of this work is to develop a numerical model to study LH metamaterials, and use the model to further understand the characteristics and behaviour of these structures. A greater understanding of these materials will allow for design criteria to be acheived and will allow for the optimal design of LH structures (i.e. increased frequency band, controled index of refraction, smaller material cost, etc). In particular, we will focus on a three dimensional Finite-Difference Time-Domain (FDTD) approach to model a prism of LH metamaterial structure in a parallel plate waveguide, similar to the setup presented in [4]. Using the numerical model, we show two measurement techniques that demonstrate the LH nature of the metamaterial, and we describe in detail the electromagnetic fields generated in the structure.

REFERENCES

1. Smith, D. R. et al., "Composite medium with simultaneously negative permeability and permittivity," *Physcial Review Letters*, Vol. 84, No. 18, May 1, 2000.
2. Veselago, V. G., "The electrodynamics of substances with simultaneously negative values of ϵ and μ," *Soviet Physics*, Vol. 10, No. 4, January 1968.
3. Pendry, J. B., "Negative refraction makes a perfect lens," *Physical Review Letters*, Vol. 85, No. 18, October 30, 2000.
4. Shelby, R. A., D. R. Smith, and S. Schultz, "Experimental verification of a negative index of refraction," *Science*, Vol. 292, April 6, 2001.

Lateral Displacement of a Gaussian Beam in the Presence of a Slab with Negative Permittivity and Permeability

B.-I. Wu, J. A. Kong, and Y. Zhang
Research Laboratory of Electronics, Massachusetts Institute of Technology
Cambridge, MA 02139-4307, U.S.A.

A medium with negative permittivity and permeability was introduced by Vesalago in 1968, and was called a left-handed medium because the wavevector, the electric field vector, and the magnetic field vector form a left-handed system. Theoretically, it has been shown that such medium possesses negative refraction index and has negative ϵ and μ macroscopically. Experimentally, the left-handed medium has recently been realized by using wires and split ring resonators. A prism of such design exhibits a reversed light bending effect at microwave frequencies. Another effect of the perfect lens realization has also been suggested.

In this paper, we demonstrate an effect which can serve as a means to identify an isotropic material that possesses simultaneously negative values of ϵ and μ. We construct a Gaussian beam incident upon a homogeneous, lossless, isotropic dielectric slab and provide the analytic solutions to the electric and magnetic fields both inside and outside the slab. It is shown that the field values in all regions can be unambiguously determined. By examining the distribution of the time-averaged power density on the interface where the transmitted/reflected Gaussian beam emerges, we can describe quantitatively the amount of lateral displacement of the beam position, from which we can determine if the dielectric slab is a left-handed medium.

Numerical simulations are carried out and the field values as well as the power densities are computed for all regions and a dramatic negative lateral shift is observed when both ϵ and μ are negative.

Session 3Aa8

Electromagnetic Waves in Complex Media

Symmetry Conditions for Linear Constitutive Relations

R. E. Raab and O. L. de Lange
University of Natal
Scottsville, Pietermaritzburg 3209, South Africa

Constitutive relations for the response fields $\mathbf{D}$ and $\mathbf{H}$ are used in macroscopic theories of transmission and reflection effects. Usually, empirical forms are adopted for these relations. However, Post [1] showed in a covariant theory that constitutive relations that are linear in arbitrary fields $\mathbf{E}$ and $\mathbf{B}$, namely

$$D_i = A_{ij}E_j + T_{ij}B_j, \tag{1}$$
$$H_i = U_{ij}E_j + X_{ij}B_j, \tag{2}$$

are subject, for real fields in the absence of dissipation, to the symmetries

$$A_{ij} = A_{ji}, \qquad U_{ij} = -T_{ji}, \qquad X_{ij} = X_{ji}, \tag{3}$$

where A_{ij}, T_{ij}, U_{ij}, and X_{ij} are macroscopic material properties.

Various effects are known to be induced in matter by space and time derivatives of the fields $\mathbf{E}$ and $\mathbf{B}$ [2, 3]. As it is not possible to express such field derivatives in covariant form (i.e. as components of a 4-tensor), Post's theory is inapplicable. The question then arises whether any symmetries exist, equivalent to those in (3), which must be imposed in such instances on the material properties of the medium.

To seek an answer, we restrict consideration to the fields of a harmonic plane wave

$$\mathbf{F} = \mathbf{F}_0 e^{i(\mathbf{k}\cdot\mathbf{r}-\omega t)}, \quad \mathbf{F} = \mathbf{E} \quad \text{or} \quad \mathbf{B}, \tag{4}$$

where the wave vector $\mathbf{k}$ and angular frequency ω are real for a lossless medium.

Then all space- and time-derivative fields in $\mathbf{D}$ and $\mathbf{H}$ can be related to $\mathbf{E}$ and $\mathbf{B}$ to obtain, for a linear response by the medium, constitutive relations of the forms of (1) and (2). However, now the fields and the material constants are complex.

From the differential of the Lagrangian density for complex fields and using the property that it is real and a perfect differential, one derives the symmetry relations for complex material properties in (1) and (2), namely [4]

$$A_{ij} = A^*_{ji}, \qquad U_{ij} = -T^*_{ji}, \qquad X_{ij} = X^*_{ji}. \tag{5}$$

Because a Lagrangian density is invariant under a shift of the coordinate origin, the coefficients in (5) are also. The results in (5) have also been derived from Poynting's theorem [5].

Some examples are discussed of how the symmetries in (5) and also origin independence are achieved in a multipole theory of constitutive relations. These examples show that these constraints are insufficient to specify completely the material constants in such a theory. A further symmetry condition is suggested, namely that the Fresnel reflection matrix must satisfy reciprocity, a form of time-reversal symmetry.

REFERENCES

1. E. J. Post, *Formal structure of electromagnetics*, 1962 (Amsterdam: North-Holland).
2. R. E. Raab and J. H. Cloete, *J. Electromagn. Waves Applic.*, 1994, **8**, 1073.
3. R. W. Ziolkowski, J. M. Arnold, and D. M. Gogny, *Phys. Rev.* A, 1995, **52**, 3082.
4. R. E. Raab and O. L. de Lange, *J. Opt. A: Pure Appl. Opt.*, 2001, **3**, 446.
5. J. A. Kong, *Electromagnetic wave theory*, 1986 (New York: Wiley).

Singular Integral Equations Method for Analysis of the Microstrip Lines on Narrow Anisotropic Substrate

L. Knisevskaja
Microwave Laboratory, Semiconductor Physics Institute
Vilnius, 2600, Lithuania

K.-F. Berggren
Department of Physics and Measurement Technology, Linköping University
Linköping, S-58183, Sweden

M. Tamov
Microwave Laboratory, Semiconductor Physics Institute
Vilnius, 2600, Lithuania

Modern progress of the microwave integrated-circuits design and production technologies has realized higher performances microstrip structures. The electrooptic techniques based on the Pockels effect has been frequently applied to optoelectronics.

In this paper we study the microstrip lines (MSL) with a substrate having an anisotropic semiconductor $LiTaO_3$ that are used for optoelectronics modulaters acting on the Pockels effect. For studying these MSL we used the methods of singular integral equations in the quasi-TEM approximation. The computation algorithm allows us to take into account the conductor thickness and the substrate width. The method of singular integral equations is almost universal: the line cross-section shape can be arbitrary, the line can be either open or screened, it may contain dielectric, anisotropic materials, and metal. The complex dielectric permittivity of the anisotropic substrate may changes in very wide range.

The dependence of the MSL wave impedance, attenuation coefficient, wavelength, effective permittivity and capacity per unit length on the strip conductor width, its distance from the substrate edges has been studied. By varying the MSL substrate width, it is also possible to select the required microstrip line characteristics. This may be useful for adjusting the MSL to other waveguide lines.

The dependences of the MSL characteristics on the strip conductor width are presented. Curves in figures show that the real part of the line wave impedance depends on the line substrate width, but the influence of the latter parameter is less than the effect of the strip conductor width w. The obtained dependences may be applied for determining the geometric parameters of the line in order to create a microstrip device with the required wave impedance and other line characteristics.

Radiation Characteristics of HTS Microstrip Antenna Arrays on Anisotropic Substrates

A. G. d'Assunção
Federal University of Rio Grande do Norte
Natal, RN 59072-970, Brazil

S. G. Silva
Federal University of Paraíba
Natal, RN 59072-970, Brazil

J. R. S. Oliveira
Federal University of Maranhão
São Luís, Brazil

Recently, a growing interest has been observed in the development and use of new materials in microwave technology. Particularly, a special interest has been observed in the use of superconducting materials in microwave and millimeter wave integrated circuits, which is due to their main characteristics, such as small losses (with reduction of the attenuation and noise level) and very small dispersion, even for higher frequencies (dozens of GHz).

The microstrip antenna structure considered in this work was obtained from the deposition of a very thin patch of superconducting material on a dielectric substrate, which is mounted on a ground plane. This patch, actually, is constituted of a High Temperature Superconductor (HTS), with high critical temperature, T_c, greater than 77 K. Planar and circular antenna arrays were also analyzed.

A fullwave analysis is presented, which combines the Galerkin method, Hertz vector potentials and the two fluid model of Gorter and Casimir, in the Fourier domain, as well as antenna array theory.

Curves for the resonant frequency, f_r, and for the quality factor, Q, are shown as function of the geometry dimensions and of the dielectric substrate and superconducting patch characteristics. Radiation pattern results are also presented.

The method presented here gives better results than those obtained by using approximate methods, such as the cavity and the modified cavity models. As a matter of fact, an excellent agreement was observed between our results and the measured ones reported in the literature for the resonant frequency of HTS microstrip patch antennas.

Furthermore, the analysis presented here is quite general and can be extended to study the characteristics of other types of microstrip patch antenna arrays on multilayered substrates.

Frequency Dependence of Initial Permeability of (Co Ti) Substituted Barium, Strontium and Calcium Hexaferrites

S. B. Narang, I. S. Hudiara, and A. Kumar
Department of Electronics Technology, Guru Nanak Dev University
Amritsar, India

Hexagonal ferrites are characterized by a hexagonal crystal structure and are made up of oxides of alkaline earths and Fe_2O_3 in different ratios. M type hexagonal ferrites (they are iso-structural with the naturally occurring mineral magnetoplumbite, which has the composition $PbFe_{7.5}Mn_{3.5}Al_{0.5}Ti_{0.5}O_{19}$) have attracted much attention due to the wide range of applications in industry, particularly as permanent magnets, recording media and microwave devices. An electromagnetic wave propagating through the ferrite encounters strong interaction with spinning electrons and gives rise to desirable properties in ferrites. The properties of ferrites depend on the chemical composition, microstructure, method of preparation, etc. The effect of substitution of cations having different magnetic moments for Fe^{3+} ions have been reported in literature. Initial permeability is an important parameter of a magnetic material which describes the effect of the magnetic properties of a medium on the propagation of electromagnetic waves and thus represents the state of magnetization of the material. In the present work, variation in permeability with different amount of substitution of $Co^{2+}Ti^{4+}$ ions in $BaFe_{12}O_{19}$, $SrFe_{12}O_{19}$ and $CaFe_{12}O_{19}$ hexaferrites at different frequencies has been studied.

Three ferrite series of the composition $Ba(CoTi)_yFe_{(12-2y)}O_{19}$, $Sr(CoTi)_yFe_{(12-2y)}O_{19}$ and $[Ca(CoTi)_yFe_{(12-2y)}O_{19}]96.0[La_2O_3]4.0$ where y varies from 0 to 1.0 in steps of 0.2 have been synthesized. Addition of 4.0wt.% of La_2O_3 to calcium hexaferrite has been reported to produce magnetoplumbite structure with optimum ferromagnetic properties. The ferrites were synthesized from stoichiometric mixtures of $BaCO_3$, $SrCO_3$, $CaCO_3$, $CoCO_3$, TiO2, Fe_2O_3 and La_2O_3 of 99.9% purity using normal ceramic method. The reagents were crushed and mixed thoroughly for 6h in acetone in a ball mill. The material was dried and calcined at 10000C for 12h in air in case of barium, 4h in case of strontium and for 3h in case of calcium hexaferrite. During calcination, the evolution of gases takes place and ferrite is partially formed. This is an important homogenization operation that produces ferrites with reasonably high densities, uniform crystal structure, chemical composition and particle size. The calcined material was again crushed for 8h and then pressed to form samples, which were finally sintered for 12h at 13000C in case of barium hexaferrites, for 12h at 12500C case of in case of strontium hexaferrites and for 3h at 11800C in case of calcium hexaferrites. X-ray diffraction analyses of a few typical samples confirmed magnetoplumbite structure for these ferrites. It indicates that for the substitution performed, the ions of Co and Ti occupy such lattice positions as to maintain M-type hexagonal structure.

Initial permeability of toroidal samples having outer diameter 16mm, inner diameter of 10mm and thickness of 3mm approximately, was determined as a function of frequency of the applied field in the frequency range from 10 KHz to 10 MHz following the method described by Heck using a Hewlett Packard LCR meter Bridge model 4275A.

The variation of initial permeability as a function of concentration of $Co^{2+}Ti^{4+}$ ions in initial permeability. $Ba(CoTi)_yFe_{(12-2y)}O_{19}$, $Sr(CoTi)_yFe_{(12-2y)}O_{19}$ and $[Ca(CoTi)_yFe_{(12-2y)}O_{19}]96.0[La_2O_3]4.0$ hexaferrite series has also been found at various frequencies. This can be explained on the basis of site preferences of Co^{2+} and Ti^{4+} ions in these ferrites. The smaller substitutions prefer 12k sites but with increased substitution these ions show a marked preference for 4fv1 and 2b sites. So substitution of a part of Fe^{3+} ions in these HexaFerrites with (CoTi) can be used to control the properties of ferrites at various frequencies.

On Contradictions in Macroscopic Electrodynamics of Bianisotropic Media

E. O. Kamenetskii
Department of Electrical and Computer Engineering,
Ben-Gurion University of the Negev
Beer-Sheva, 84105, Israel

The question about local coupling of electric and magnetic polarizations [magnetoelectric (ME) coupling] arises in a subject of so-called chiral and bianisotropic media. In classical electromagnetic theory of such complex media one becomes faced with *serious problems*. One cannot consider (classical electrodynamically) two coupled electric and magnetic dipoles – the ME particles – *as point sources* of the electromagnetic field. One cannot construct a classical model of duality symmetry in points with local sources. In nature, such duality symmetry appears to be spoiled by the fact that one can observe point electric charges, but not magnetic ones. One should come to the conclusion that the unified ME fields originated by ME particles may exist with the symmetry properties distinguished from that of the electromagnetic (EM) fields.

Because of these problems the notion "condensed bianisotropic media" bears a formal character. In the attempts to create a macroscopic electrodynamics of bianisotropic materials – artificially constructed media having electromagnetic properties not generally found in nature – one becomes faced with certain *contradictions*. These contradictions become evident even on the *macroscopic level of consideration*.

Contradiction 1: The balance of electromagnetic energy in bianisotropic media is determined not only by the material constitutive parameters, but also by the *structure of the electromagnetic field*. To vary the energy in bianisotropic media, a certain *time-domain correlation* between amplitudes of the fields is essential. Necessary *constraints* to the structure of the quasimonochromatic field should be imposed.

Contradiction 2: In characterization of different physical processes in bianisotropic media one should use different-form constitutive relations. In a general case, one form of the constitutive relations cannot be reduced to another. This fact is illustrated by an analysis of the Lorentz reciprocity theorem and the Onsager-Casimir principle for bianisotropic media.

Contradiction 3: In attempts to create the so-called *homogenization theory for dense bianisotropic composites*, the question about the near-zone fields of every bianisotropic particle arises. Because of the *internal coupling* between electric and magnetic dipoles in every particle, these fields should be described by two *coupled Laplace equations* (for the quasielectrostatic and quasimagnetostatic fields). In the classical description, such equations are unknown at present time.

It becomes evident that instead of the macroscopic electrodynamics of bianisotropic media it is more correct to talk about the *generalized field-medium continuum*. Such a continuum is conceived as a physical object described by the combined (different-scaled quasistatic ME and vortex EM) fields.

Plasma and Complex Waves in Semiconducting Superlattice

A. A. Bulgakov and O. V. Shramkova
Institute of Radiophysics and Electronics of the NAS of Ukraine,
12 Ac. Proskura St
Kharkov, 61085, Ukraine

The present work studies the instability of plasma polaritons and inhomogeneous (complex) waves in infinite structure derived by the periodic recurrence of two alternation semiconductor layers. The application of an electric field in one of the layers produces a drift of particles in this layer. We have considered structures without losses.

We have derived analytically and numerically the dispersion relation for plasma and complex waves in semiconducting superlattice. The special property of complex waves in semiconducting structure is the complex transversal wave vector component. The imaginary part of wave vector is much greater than the real one. A quantization of the imaginary part of wave vector takes place. This means that the appearance of the complex plasma waves is possible only in the case when the width of each slab equals an integer number of $\lambda_z/2$ quantities (λ_z is the spatial period of an inhomogeneous plane wave in the direction perpendicular to the slab interfaces). The appearance of large amount of inhomogeneous modes is one of the most important properties of complex waves.

We have discussed the field distributions and energy flows of complex waves. Second important characteristic of complex polaritons is the dependence of the energy flow (Poynting's vector) on coordinates. Complex eigenmodes are not orthogonal and the modes can exchange their energy. The energy of highest complex modes localizes in certain points of lattice. The energy is carried on closed circuits.

We have considered the excitation of the inhomogeneous waves by the drift of carriers.

Session 3Ab8

Air Force Institute of Technology Research

Emergency Communications with Near Vertical Incident Skywave (NVIS) Antennas

R. Allnutt, A. Terzuoli, and M. Temple
Air Force Institute of Technology
Dayton, OH, U.S.A.

J. T. Johnson
The Ohio State University
Columbus, OH, U.S.A.

Near Vertical Incident Skywave (NVIS) techniques involve a physical propagation using the electromagnetically reflective canopy of ionosphere overhead. All High Frequency (HF) communications between roughly 2 and 30 MHz can be reflected from the ionosphere as well as the earth's surface. HF radio transmission is normally optimized for distances beyond 1000 miles. However, NVIS techniques optimize communication between 20 and 100 miles.

A void exists in communication distances beyond line of sight and closer than several hundred miles. Line of sight communications can easily be accomplished with transmitters above 90 MHz. This includes everything from commercial FM radio to VHF and UHF radios developed during WWII for the military, but now ubiquitous in amateur, business, and personal communications. Long distance communication around the globe can be accomplished with HF radio. Amateur radio operators and over water air traffic controllers have long exploited this propagation technique for intercontinental communication. Unfortunately, HF communication is frequently disrupted by the peculiar nature of "skip". "Skip" is the tendency for HF waves to be heard in the immediate vicinity of the transmitter and also heard several hundred miles away, but to be missing (skipping) the interval between.

A system is tested which expands on the common use of HF radio waves. To a large extent, "skip" exists because the antenna designer builds it into the system. The system utilized in this work is designed to eliminate skip. The NVIS technique involves use of transmission and receiving antennas optimized for nearly vertical propagation. Instead of aiming for long distance, contiguous short distance is the goal. The techniques of NVIS communications purposely attempt to circumvent the generation of "skip", making medium distance communication possible

Man portable, very low power transceivers (5 watts maximum) and low dipole antennas are used in an NVIS communication system for this work. Digital and analog techniques are compared for effectiveness at the lower edge of unable signal to noise ratio. Digital techniques include PSK and MFSK coding.

This exploration of an unusual and little researched communication technique poses immediate usefulness to a society dependent on technologically advanced techniques prone to sabotage and disruption. It is also vitally important to understand these techniques from a counter terrorism perspective, as they are inexpensive and difficult to disrupt.

Target-In-Motion SAR Signature XPatch$^{\mathrm{TM}}$ Predictions for Algorithm Development

M. Fernandez-Covas
Department of Electrical Engineering, Air Force Institute of Technology
Dayton, Ohio 45433, U.S.A.

A. Terzuoli
Air Force Institute of Technology
Dayton, Ohio 45401, U.S.A.

W. Wood
Department of Electrical Engineering, Air Force Institute of Technology
Dayton, Ohio 45433, U.S.A.

J. Westerkamp
Department of Electrical Engineering, University of Dayton
Dayton, Ohio, U.S.A.

The research presented in this paper is a methodology for predicting synthetic aperture radar (SAR) signatures of targets in motion within a scene. The research is in support of Synthetic Aperture Radar data processing algorithm development efforts. The algorithm uses inherent data within the signature's video-phase history to determine the target's characteristic invariant scattering centers, which can then be analyzed by automatic target recognition algorithms. Until now, the predicted-data target pool and motion have been limited to simple shapes and noisy simplistic trajectories. The development effort has out-grown rudimentary tools, and seeks to increase the target pool and complexity. The research establishes a *cookbook* approach to generating the necessary signal histories for algorithm testing using existing tools: specifically, MatLab$^{\mathrm{TM}}$ and XPatch$^{\mathrm{TM}}$.

This first step effort limits the target dynamics to whole-unit, generalized movement and translation. Effects of independent element's motion such as that from wheels and turrets have been deferred. Mass effects in acceleration and turning have also been disregarded from the trajectory at this time.

The basic process uses MatLab to generate the initial trajectory position parameters (i.e., roll, pitch, yaw, target center and target x, y coordinates). These parameters go to XPatch$^{\mathrm{TM}}$ as an ASCII file. Once the signal history is generated, a subsequent MatLab routine formats the signal history parameters as needed for submission to the algorithm under test. The resulting processed data can then be compared against the *truth* data of the target model to refine the algorithm.

Minimum Antenna Coupling Solutions for Air Force One Using Genetic Algorithms and Hybrid Optimization Techniques

E. M. Koper and W. D. Wood
Department of Electrical Engineering, Air Force Institute of Technology
Dayton, Ohio 45433, U.S.A.

S. W. Schneider
Air Force Research Laboratory
WP AFB, Ohio, U.S.A.

This research combines existing global optimization techniques with local search algorithms to determine the best placement of a new navigation and communication system for Air Force One. The Air Force One aircraft are uniquely modified Boeing 747–200's with a dense array of command-and-control and communications systems. The coupling problems are compounded by limited real-estate on the surface of the fuselage making the addition of this or any other new system difficult.

On the verge of a major electronic system upgrade for Air Force One, this research will construct an efficient approach to solve this and more complicated intra-system interference problems using optimization algorithms that automatically interface with computational electromagnetic software. Genetic and local search algorithms will be combined to achieve the most efficient use of time and computer resources from a fixed performance aspect. Fitness evaluations will be made considering feasibility of antenna patterns and aircraft logistics constraints. Simple Genetic Algorithms, micro-Genetic Algorithms, and Response Surface Methodology techniques will be used individually and in a combinational fashion to minimize coupling problems of 2 variables (single movable antenna) and 16 variables (all in-band antennas movable). During the optimization process, all variable combinations and solutions evaluated will be retained and global response models built giving the design engineer additional domain knowledge not inherent in these GA and local search techniques alone. The techniques will be compared and evaluated based on fitness of solution and computational efficiency. The optimization algorithms will interface with and direct a uniform theory of diffraction computational engine operating on a complex spline-lofted geometric model of Air Force One.

For validation of the uniform theory of diffraction code and techniques, first principle moment method techniques will be used on a wire-grid 747-200 model and compact antenna range measurements using a 1/100 scale model will be taken.

The techniques used here can be applied to any antenna placement optimization problem and interface with any suitable computer code for the problem at hand. In addition, variable types can be expanded to include different types of antennas or directional antenna radiation patterns.

Target Recognition Using Late Time Scattering

K. J. Pascoe, W. D. Wood, P. S. Maybeck, and A. W. Wood
Air Force Institute of Technology
Wright-Patterson AFB, OH, U.S.A.

Late-time electromagnetic scattering from objects illuminated by ultra-wideband, short pulse radars has predictable properties that may be used to identify the objects. This work attempts to exploit these properties in a practical target recognition algorithm.

Late-time scattering occurs after the incident radar pulse has transited an object, so shorter pulses provide better results and ultra-wideband near-impulses are preferred. Singularity Expansion Method theory states that the late-time return from perfectly conducting objects is composed of a sum of damped sinusoids whose frequencies of oscillation and damping are independent of target aspect angles. The coefficients of these terms are dependent on aspect, however.

These frequencies can be found via the Matrix Pencil Method, ESPRIT, genetic (evolutionary) algorithms, or other techniques. Identifying signal parameters is challenging, given the low signal power of late time resonance. Ideally, several measurements of the object from different azimuths would be analyzed together for a best-fit from all azimuths. The most significant frequencies form a description of the target, which can be used to identify it.

A recognition algorithm based on Kalman filters can easily exploit the known signal parameters. The target description is used to build a linear, time invariant state-space model that forms the basis of the filter. For this type of model the Kalman filter is the optimal state estimator. We can arrange a bank of filters in a parallel algorithm. Each filter assumes a different set of frequencies specific to a given target. The algorithm is similar to the Multiple Model Adaptive Estimation — Maximum a Posteriori technique used in automatic control systems. Each filter models the expected signal given the assumed frequencies and estimated coefficients. The difference between the model and measurements is used to form a scaled residual. The filter with the smallest scaled residuals represents the most likely match to the object.

The views expressed in this article are those of the author and do not reflect the official policy or position of the United States Air Force, Department of Defense, or United States Government.

Electromagnetic Scattering from a Gap in a Magneto-Dielectric Coating on an Infinite Ground Plane

G. R. Simpson, P. J. Collins, and W. D. Wood
Air Force Institute of Technology
Dayton, OH, U.S.A.

A hybrid Green's function/Method of Moments (MoM) based numerical method is developed for the problem of determining the electromagnetic scattering from a gap in a magneto-dielectric coated infinite ground plane. In this context, the gap forms a break in the magneto-dielectric slab coating while the ground plane is continuous. The magneto-dielectric slab material is a general material medium that can possess relative permittivity and permeability greater than one and each may be lossy. The model can represent a gap that is of a general two-dimensional trapezoidal shape and may be filled with a material possessing isotropic permittivity and permeability differing from that of the slab material. The scattering from the gap is then evaluated for illumination that is either transverse magnetic (TM) or transverse electric (TE) with respect to the gap.

The volume equivalence theorem is used to convert the gap region to a trapezoidal cylinder region containing unknown volumetric magnetic and electric equivalent currents. The hybrid Green's function weighting these equivalent currents contains a direct coupling term and a term that adds a correction to account for the grounded-slab geometry. This bounce correction term is formulated via periodic surface theory and the terms for each individual equivalent current element is found using the Array Scanning Method (ASM). A set of coupled integral equations based on these equivalent currents is then solved via the MoM.

In this work, the ASM is an alternative approach to computing the spectral domain modal Green's function integral where the continuous spectral domain variable of integration is split into continuous and discrete components. Due to the functional form of the resulting integrands, the ASM approach produces a set of rapidly converging integral expressions that enable efficient numerical evaluation of the slab geometry bounce correction terms. The ASM technique was originally developed at the Ohio State University by Prof. B.A. Munk and his colleagues.

The hybrid Green's function/MoM is validated using both existing MoM reference codes and measured data. The results show that the hybrid method is accurate and more time efficient than methods relying on the existing reference codes. The end result is a computational tool with which various gap filler treatment materials can be evaluated in a rapid and efficient manner.

Session 3Ac9

Poster Session - II

Evaluation of a New Spectral Analysis Multilook Strategy for Synthetic Aperture Radar Processing

A. Vidal, C. Bachiller, A. A. San Blas, and M. Ferrando
Universidad Politécnica de Valencia
Valencia, Spain

Synthetic Aperture Radar (SAR) sensors are becoming a very important source of information for modern Earth Observation Remote Sensing programs. Furthermore, most recent satellites like ENVISAT or RADARSAT carry on-board Scanning SAR (ScanSAR) instruments because they can explore a wider swath. One of the most interesting SAR processor for ScanSAR systems is provided by the Spectral Analysis (SPECAN) technique. This method exploits time-frequency latching of linear frequency modulated signals by deramping, carried out via complex multiplication and spectral estimation. SPECAN has been identified as a good candidate to process ScanSAR raw data thanks to its high efficiency concerning computation time. Meanwhile, the data size that have to be processed simultaneously is reduced when compared with traditional high-resolution processors.

On the other hand, Multilooking is an important step that is performed in order to improve image radiometric resolution at the cost of geometric resolution. It is carried out in ScanSAR systems for an adjustment on range spatial resolution and for azimuth system look exploitation. The process is not straightforward because deramping exploits the time-frequency relation, and it is usually defined in the spatial or alternatively in the frequency domain. For that reason, traditional SPECAN Multilook can be applied using different approaches specially adapted to that situation, which are based on continuous deramping. In this work we propose a new technique that does not use that principle. The deramping template is precisely computed according to the properties of each data burst and the system return time. Furthermore, the corresponding burst spectrum is computed around its Doppler Centroid frequency. Samples around that frequency present the highest Signal to Noise Ratio (SNR) of all Doppler Spectrum and can be specially positioned to avoid interpolation before look summation.

The new idea has been tested in one-dimensional simulated data and in a ScanSAR simulated environment using ERS raw data. The conclusion obtained from this study is that the new Multilook strategy presents practical advantages in the context of SPECAN processing. It eases Multilook summation and preserves the most important part of the Doppler spectrum when compared to the traditional Multilook formation with SPECAN techniques.

Nonlinear Diffraction, Focusing of Secondary Waves

G. Koshevarov, L. Melnikov, V. Matus, V. Gandurin, and S. Stepanenko
Moscow Scientific Research Institute of Instrument Engineering
Moscow, 121170, Russia

An excitation of combination frequency waves in nonlinear medium was investigated in [1–3]. It has been theoretically found that neither availability of dispersion nor availability of anisotropy is a necessary condition for effective nonlinear diffraction. But there are restrictions on a size and a form of the homogeneous medium or on the spatial distribution of the nonlinearity of inhomogeneous medium.

It was established, that regardless of the shapes of phase surfaces of primary wave, there are so-called focusing surfaces. If the medium is nonlinear only on one of focusing surface the secondary waves are in-phase at a certain point (focus). Theory and application of focusing effect are the objectives of this paper.

Each focusing surface corresponds to the certain phase of secondary waves in focus point. If the nonlinear medium is localized in volume V, situated between focusing surface, corresponding to the phase ψ_1, and focusing surface, corresponding to ψ_2, all elementary secondary waves in focus point have phases in the range from ψ_1 to ψ_2. If ψ_1 and ψ_2 differ reasonably little, all elementary secondary waves are nearly in-phase in focus point. In this sense the volume V is a focusing volume. The position of the focus is invariant with respect to a medium evolution within a focusing volume.

If one of the primary waves changes the direction of propagation, the position of the focus will also change. In this sense the focusing surface for any of the primary waves serves as a lens. The position of focus and the shape of focusing surface depend on the parameters of the primary waves.

Conditions of secondary wave focusing on an infinity are determined, i.e. conditions under which a combination frequency secondary wave has minimum divergence.

The focusing effect can be used for phasing of arbitrary located wave exciters or receivers. A case in point is the nonlinear-diffraction phasing of non-rigid or conformal antenna arrays [4–6].

References:

1. Bakhrakh L., S. Stepanenko, A. Neudakin and V. Horoshulin, “Excitation of Combination Frequency Waves When Monochromatic Waves Are Superimposed of an Irregular Non-linear Medium,” *Proc. URSI Int. Symp. on EM Theory,* St. Petersburg, Russia, p. 534, 1995.

2. Stepanenko S., V. Horoshulin, A. Fleck and I. Savinkow, “Nonlinear Diffraction in Inhomogeneous or Limited Nonlinear Medium,” *Abstracts. XXVth General Assembly of the International Union of Radio Science*, Lille, France, p. 91, 1996

3. Stepanenko S., N. Povarenkin, L. Bakhrakh, V. Andrianov and V. Loss, “Nonlinear diffraction. Theory and application,” *Proc. URSI Int. Symp. on EM Theory*, Thessaloniky, Greece.

4. Bakhrakh L., S. Stepanenko, A. Neudakin and V. Horoshulin, “New Approach to Phasing of Non-rigid Antenna Arrays and Non-stationary Interferometers,” *Proc. URSI Int. Symp. on EM Theory*, St. Petersburg, Russia, p. 200, 1995.

5. Stepanenko S., G. Koshevarov, L. Melnikov, V. Matus, N. Grigoruk and O. Iatsenko, “Phasing of the Non-rigid Active Receiving Antenna Arrays,” *Proc. Progress in Electromagnetics Research Symposium*, Seattle, USA, p. 639, 1995.

6. Bakhrakh L., S. Stepanenko, V. Horoshulin and A. Fleck, “Non-rigid Active Receiving Antenna Arrays with the Nonlinear-diffraction Phasing Means,” *Abstracts. XXVth General Assembly of the International Union of Radio Science*, Lille, France, p. 774.

The Enhancement Factor for Absorption of Light by Carbon Particles in Micro-Droplets of Water: Averaging over Size Parameters

V. A. Markel
Department of Radiology, Washington University
St. Louis, Missouri 63110, U.S.A.

The absorption of electromagnetic radiation by carbonaceous soot aerosol is of considerable interest for climate and radiation energy transfer modeling. The optical properties of free soot have been extensively studied. In the visible and near IR, the first Born approximation or the mean-field theory provide accurate results for the absorptive properties of atmospheric soot. However, it is known that the soot often forms agglomerates with water microdroplets, especially in the clouds. When soot particles are placed inside a water droplet, they are no longer excited by plane waves, but rather by internal modes of a high-quality optical resonator. To complicate things further, the resonator modes can effectively couple to the modes of clusters themselves. As a result, the absorption spectra of soot particles inside the microdroplets are very different from those of free soot.

The above fact stimulated a lot of interest in scattering and absorption by inhomogeneous spheres. The previous work focused mostly on a given incident light wavelength λ and the sphere radius R and, therefore, on a fixed size parameter $x = kR = 2\pi R/\lambda$. However, in most practical cases the microdroplets are polydisperse and excited by a broad-band radiation. This leads to a broad distribution of size parameters. We have performed an averaging over the size parameter of microdroplets and studied the effects of narrow morphology-dependent resonances on the absorption enhancement factor, $G(x)$. In particular, we have shown that the integral effect of these resonances is not small, and they should be accounted for in order to calculate the averaged enhancement factor, $\langle G \rangle$, accurately. We have also shown that $\langle G \rangle$ averaged over a wide range of the droplet size parameters is a few times larger than that for off-resonant values of x. This increase is attributed to the integral effect of the morphology-dependent resonances.

A systematic study of the dependence of $\langle G \rangle$ on the resolution in x with which the averaging is done is presented in this poster. This question is important since the averaging over size parameters is expected to yield the "true" result only for a sufficiently small step in x, Δx. We show that, first, a well-defined limit for $\langle G \rangle$ exists when $\Delta x \to 0$ and, second, in this limit $\langle G \rangle$ is close to 25, a number significantly larger than previously reported.

Chaos Synchronization with Coupling-Delay Lag Time in Diodes Subject to Optical Feedback

E. M. Shahverdiev, S. Sivaprakasam, and K. A. Shore
School of Informatics, University of Wales
Wales, UK

Recently chaos synchronization in coupled systems have been extensively studied in the context of laser dynamics, electronic circuits, chemical and biological systems. Chaos synchronization can be applied in secure communications, optimization of nonlinear system performance, modeling brain activity and pattern recognition phenomena.

Due to finite signal transmission times, switching speeds and memory effects time delay systems are ubiquitous in nature, technology and society. Therefore the study of synchronization phenomena in systems with time delay is of high practical importance. Time delay systems are also interesting because the dimension of their chaotic dynamics can be made arbitrarily large by increasing the delay time. From this point of view these systems are especially appealing for secure communication schemes.

In lag synchronization the driver (transmitter) output is synchronized with the retarded output of the response (receiver) system. Numerical simulations and experimental investigations of this phenomenon in unidirectionally coupled semiconductor lasers with optical feedback have established different results for the lag or retardation time. Most experimental investigations of chaos synchronization in unidirectionally coupled external cavity semiconductor lasers have found that the lag time between the master and slave lasers is equal to the coupling delay time. However, numerical results show that the lag time should be equal to the difference between the delay time in the coupling and round-trip time of the light in the transmitter's external cavity for the coupled identical systems. Knowledge of the exact lag time is of considerable practical importance as experiments on message transmission using fibre lasers and diode lasers have shown that the recovery of message at the receiver critically depends on the correction made for the lag time.

In this paper we report an analytical approach to lag or retarded synchronization in unidirectionally coupled external cavity semiconductor lasers governed by two characteristic delay times, where the delay time in the coupling is different from the feedback delay time in the coupled systems. We derive existence conditions for lag synchronization manifolds for both identical and non-identical transmitter and receiver systems.

We find that for identical systems (no parameter mismatches) the lag time is equal to the difference between the coupling delay time and the feedback delay time in the coupled systems. Also for the first time we demonstrate that differences between the lasers' cavity losses can explain why the experimentally measured lag time between the transmitter and the receiver waveforms is equal to the coupling delay, and is independent of the round-trip time of the light in the external cavity of the transmitter.

Analysis of the Flange Effects for an Open-Ended Dielectric Probe

R. Olmi
IROE - Italian National Research Council
Firenze, 50127, Italy

R. Nesti
Arcetry Astrophysical Observatory
Firenze, 50125, Italy

G. Pelosi and C. Riminesi
Department of Electronics and Telecommunications, University of Florence
Firenze, 50134, Italy

An open-ended coaxial line has been studied by many researchers in order to use it as an electromagnetic sensor for the dielectric characterization of materials. These studies include formulations of the electromagnetic problem under various simplifying assumptions as quasi-static formulation [1] and coax opening on an infinite conducting plane [2]. In this paper, we evaluate the aperture field distribution for both a coaxial opening on a conducting infinite plane and a coaxial opening with a conducting flange with finite extension, in the case of TEM exicitation. In the former case a full-wave formulation of the problem is used and solved in terms of the free-space dyadic Green's function, while in the latter case the method of moments (MOM) is adopted. Thanks to the numerical code [3] the contribution of the flange and the external surface current of the coaxial probe can be accurately taken in to account in the computation of the aperture field distribution. The field on the coaxial aperture ($z = 0$) is expressed as a superposition of the dominant TEM mode and the TM_{0n} modes which are the subset excited by symmetry. The continuity of the magnetic field is imposed in $z = 0$ at the aperture. A comparison between results related to the different methods are presented showing the difference on the reflection coefficient as a function of the flange geometry and frequency. The results also show how the error on the reflection coefficient propagate on the material permittivity through the inversion numerical procedure. Simulation results obtained are compared with measurements for a probe with a conducting flange which extends up to 8 mm in the 2–3 GHz frequency range.

REFERENCES

1. Misra, D., "A quasi-static analysis of open-ended coaxial lines," *IEEE Trans. Microwave Theory Tech.*, Vol. MTT-35, 925–928, Oct. 1987.
2. Olmi, R., M. Bini, A. Ignesti, and C. Riminesi, "Non-destructive permittivity measurement of solid materials," *IOP-Measurement Science and Technologies*, Vol. 11, 1623–1629, 2000.
3. Contu, S., G. G. Gentili, R. Nesti, and G. Pelosi, "Electromagnetic analysis of coaxial horns," *10th Microcoll*, Budapest, Hungary, March 21–25, 1999.

Electromagnetic Resonances of Lossy Dielectric Spheres Immersed in a Lossy Dielectric Medium

S. Dewald
Department of Electronic Engineering and Information Technology
Universität Karlsruhe (TH)
Karlsruhe, 76227, Germany

R. Bansal
Department of Electrical & Computer Engineering, University of Connecticut
Storrs, CT 06269, U.S.A.

This paper investigates the complex resonance frequencies of a lossy dielectric sphere immersed in a lossy dielectric medium. It extends the work of C. Chen (1998) and M. Gastine et al (1967) on lossless dielectric spheres surrounded by a lossless medium to lossy targets and lossy ambient media. This problem has potential applications in the area of target classification using the complex natural resonances (CNR) of the target. An example from the biomedical field is the classification of suspicious growths in breast cancer diagnosis. Since the differences between a tumor and the healthy tissue as well as those between different types of tumors occur most significantly in the conductivity of the tissues, the breast and the tumor tissue cannot be assumed to be lossless. Spherical targets were chosen for this study because the associated electromagnetic problem can be solved analytically and the results can be analyzed to gain insight into the relationship between the properties of the target and its CNR.

In this investigation both the spherical target and the surrounding medium are assumed to be homogeneous, isotropic, nonmagnetic ($\mu_r = 1$) and dispersive. The frequency dependence of the dielectric properties is taken into account by using the Debye model. Maxwell equations are solved by matching the fields at the boundary of the sphere. An eigenvalue equation is obtained that is both complex and transcendent. A numerical method is employed to compute the complex natural frequencies.

The computed complex frequencies are characterized into internal and external resonances. Both transverse electric (TE) and transverse magnetic (TM) modes are investigated. The differences between lossy and lossless media can be seen both in the damping factor and in the real part of the resonance frequencies.

Application of Aerodynamic Method In the Development of Relativity

X. Yang
Airfoil Center, Northwest Polytechnic University
Xi'an, 710072, China

Equivalent of Maxwell equation and Euler equation

Momentum equation is $\partial \mathbf{V}/\partial \mathbf{t} = -\omega \times \mathbf{V} - (P/\rho + \mathbf{V}^2/2)$ (1). Where $\mathbf{V}(x,t)$ is the velocity field, ω is the vortices field, $P(x,t)$ is the pressure and ρ is the density. Define Lamb Vector $\mathbf{F}_1$ as a cross vector product of ω and $\mathbf{V}$. $\mathbf{F}_1 = \omega \times \mathbf{V}$, put $\phi = P/\rho + \mathbf{V}^2/2$, and from Eq. (1).
$\partial \mathbf{V}/\partial \mathbf{t} = -\mathbf{F}_1 - \nabla\phi$ (2). Take curl of Eq. (2) $\partial\omega/\partial t = \nabla \times \mathbf{F}_1$ (3). From continuity Eq. $\nabla \cdot \mathbf{V} = 0$ (4). Take Curl of Eq. (4) give $\nabla \times \omega = 0$ (5). Write Eq. (2) into
$\mathbf{F}_1 = -\partial \mathbf{V}/\partial \mathbf{t} - \nabla\phi$ (6). Takes diverge of Eq. (6) .$\nabla \cdot \mathbf{F}_1 = -\nabla \cdot \partial \mathbf{V}/\partial \mathbf{t} - \nabla^2\phi$. Consider
$\nabla \cdot \mathbf{V} = 0;$ $\nabla \cdot \mathbf{F}_1 = -\nabla^2\phi$ (7), can write derivative of Lamb vector $\mathbf{F}_1$ to time t as

$$\partial \mathbf{F}_1/\partial t = \partial(\omega \times \mathbf{V})/\partial t = \partial\omega/\partial t \times \mathbf{V} + \omega \times \partial \mathbf{V}/\partial \mathbf{t} \quad (9)$$

And $\partial \mathbf{F}_1/\partial t = -\partial(\omega \times \mathbf{V})/\partial t = -(\nabla \times \mathbf{F}_1) \times \mathbf{V} + \omega \times (-\mathbf{F}_1 - \nabla\phi)$ (10). Through further deduction Eq. (10) charge to:

$$\partial \mathbf{F}_1/\partial t = \mathbf{V}^2 \nabla \times \omega - \nabla \times (\mathbf{V} \cdot \omega)\mathbf{V} + \mathbf{V}(\nabla^2\phi) - 2(\mathbf{F}_1 \cdot \nabla)\mathbf{V} - \omega \times \nabla(\phi + \mathbf{V}^2) \quad (11)$$

Let us define a "current", as follows $\mathbf{j} = \nabla \times (\mathbf{V} \cdot \omega)\mathbf{V} - \mathbf{V}(\nabla^2\phi) + 2(\mathbf{F}_1 \cdot \nabla)\mathbf{V} + \omega \times \nabla(\phi + \mathbf{V}^2)$ (12) Thus Eq. (12) write to $\partial \mathbf{F}_1/\partial t = \mathbf{V}^2 \nabla \times \omega - \mathbf{j}$ (13).
So the proof of the equivalent of this two-equation system is complete. We have the Eq. from Continuity medium mechanic, which equivalent Eq. of electromagnetic: $\nabla \cdot \mathbf{F}_1 = -\nabla^2(\phi)$; $\partial \mathbf{F}_1/\partial t = \mathbf{V}^2 \nabla \times \omega - \mathbf{j}$; $\partial\omega/\partial t = -\nabla \times \mathbf{F}_1$; $\nabla \cdot \omega = 0$. Though we can deduce the father expressions from N. S. equation, but we are interest at expressions from non-Newtonian fluid.

Relation of force and vortex as using principle of Boltzman and visco-elastic model

Relation of stress and strain of Newtonian fluid can express to $\tau = \mu r/t$ where τ is stress, μ is constant, γ is rate of strain. Let us use Boltzman's principal, of superimposition to construct the relation between stress and strain. $\tau(t) = \int_{\gamma(-\infty)}^{\gamma(t)} G(t-\tilde{t})d\gamma(\tilde{t}) = \int_{-\infty}^{t} G(t-\tilde{t})\frac{\partial r}{\partial t}(\tilde{t})d\tilde{t}$ and make it a partial integral $\tau(t) = G_0\gamma(t) - \int_{-\infty}^{t} \frac{\partial\gamma}{\partial t}(\tilde{t})\frac{dG(t-\tilde{t})}{d\tilde{t}}d\tilde{t} = G_0\gamma(t) - \int_{-\infty}^{t} M(t-\tilde{t})\gamma(\tilde{t})d\tilde{t}$. In the expression $(t-\tilde{t})$ is modulus of relaxation, $M(t-\tilde{t})$ is function of memory. In simple shear flow, its different equation is $\tau + \lambda\partial\tau/\partial t = \mu\partial\mathbf{r}/\partial t$, where λ is the proportion of viscous coefficient and modulus of elasticwith the initial condition $t = -\infty,$ $\tau = 0$, gives $\tau = \int_{-\infty}^{t} \frac{\mu}{\lambda} e^{-\frac{(t-\tilde{t})}{\lambda}} \frac{\partial r(\tilde{t})}{\partial \tilde{t}} d\tilde{t}$ (14). Originally the momentum is deferent with Euler equation only in the added viscous term.
$\partial \mathbf{V}/\partial \mathbf{t} + \nabla(\mathbf{V}^2/2) + \mathbf{F}_1 = -1/\rho\nabla P + 1/\rho\nabla \cdot \{\tau\}$ (15). Take curl of it: $\partial\omega/\partial t = \nabla \times \mathbf{F}_1$ (16) Eq. (15) can be also written to $\nabla \cdot \mathbf{F}_1 = -\nabla^2\phi + \nabla \cdot [\nabla \cdot \{\tau\}/\rho]$. Put $\mathbf{F}_4 = \lambda_2/\rho\partial\tau/\partial t$. So $\nabla \cdot (\mathbf{F}_1 + \mathbf{F}_4) = -\nabla^2(\phi)$ (17). $\mathbf{F}_4$ express the force on account of stress acceleration.

$$\partial \mathbf{F}_1/\partial t = \partial^2 \mathbf{V}/\partial t^2 - \nabla(\partial\phi/\partial t) + 1/\rho\nabla(\partial\boldsymbol{\tau}/\partial t) \quad (18)$$

The third term of r.h.s of Eq. (18) can only be present in $\partial\tau/\partial t = \mu/\lambda_2[\varepsilon] - 1/\lambda_2\tau = \zeta\rho[\varepsilon] - \lambda_3\rho\tau$. Where $\zeta = \mu\rho/\lambda_2$, and $\lambda_3 = 1/\rho/\lambda_2$, and $[\varepsilon]$ can be expanded to $\partial\tau/\partial t = \zeta\rho\{\partial v_i/\partial x_j + \partial v_j/\partial x_I\} - \lambda_3\rho\tau$. So the last term of r.h.s. of Eq. (18) become $1/\rho\nabla \cdot \{\partial\tau/\partial t\} = \zeta\nabla \times (\omega) - \lambda_3\nabla \cdot (\tau)$. Institute the contribution of viscosity to $\mathbf{F}_1/t$ ins the last term of r.h.s. of Eq. (18) and consider the rest of contribution construct inviscid part as Eq. (11) become $\partial \mathbf{F}_1/\partial t = \mathbf{V}^2 \nabla \times (\omega) - \mathbf{j} + \zeta\nabla \times (\omega) - \lambda_3\nabla \cdot (\tau)$. After arrangement

$$\partial \mathbf{F}_1/\partial t = (\mathbf{V}^2 + \zeta)\nabla \times (\omega) - \mathbf{j}' \quad (19)$$

And $\mathbf{j}' = \mathbf{j} + \lambda_3\nabla \cdot [\tau] = -\mathbf{V}\nabla^2\phi + \nabla \times (\mathbf{V} \cdot \omega)\mathbf{V} - \mathbf{V}(\nabla^2\phi) + 2(\mathbf{F}_1 \cdot \nabla)\mathbf{V} + \omega \times \nabla(\phi + \mathbf{V}^2) + \lambda_3\nabla \cdot (\tau)$ (20) So Eq. (5), Eq. (16), Eq. (17), Eq. (19) give the same equivalence of Maxwell equations system, and brought the concept of metafluid in EM field.

Session 3Pc1

Radio Waves in the Atmosphere

Estimation of the Ionospheric Irregularities by Site Dependent Total Electron Content (TEC) Amplitude Fluctuation Index

C. B. Erol
Department of Biomedical Engineering, Baskent University
Ankara, 06530, Turkey

S. G. Tanyer
TUBITAK
Ankara, Turkey

The scintillation effects are known to degrade the tracking performance of a GPS receiver. Possible Doppler shift observed on the GPS signal due to rapid phase variations could extend the bandwidth exceedingly, forcing the phase locked loop to its tracking limits, and the lost of signal can be observed especially at the frequency L2. For this, accurate estimation of the ionospheric irregularities is often not possible since ionosphere is usually assumed to be locally isotropic. In this study, short time (15 min.) amplitude fluctuation index (f_a) that is function of time, orbit number and satellite number, and hourly amplitude fluctuation index (F_a) that function of hour and orbit number only, are defined. f_a can be calculated at any point on the surface of the earth for each 15 minute long time section using only one satellite, and F_a can be calculated hourly and using satellites in the vicinity of the receiver. It is shown that utilizing the amplitude fluctuation indices f_a and F_a, oblique examination of the index is possible, without assuming a perfect vertical path. Finally, the variations on the total electron content corresponding to different cases are discussed on numerical results.

Modeling of the Monthly Median foF2 Value by Utilizing Radial Basis Function Neural Networks

M. A. Kanaki
PATHE, Special Service of Public Works
Thermi, GR-57001, Greece

I. T. Rekanos
Radio Laboratory, Helsinki University of Technology
Espoo, FIN-02015, Finland

The estimation and forecasting of the electromagnetic properties of the upper layer of the ionosphere (F2-layer) are very interesting issues, since the characteristics of the F2-layer play crucial role in long distance, high frequency (HF, 3-30 MHz) radio links. For instance, the presence of the ionosphere has a direct impact on the time-delay and the variance of the amplitude of signals in earth-satellite HF links. One of the properties of the F2-layer, which is frequently mentioned and has been studied extensively, is the critical frequency foF2. Unfortunately, modeling of foF2 is a very difficult problem because foF2 depends nonlinearly on many parameters such as time, location, and solar activity. A promising approach to model the variation of foF2 is the use of neural networks, which can approximate any nonlinear mapping.

In this work, we propose the application of radial basis function neural networks (RBFNNs) in the estimation of the monthly median foF2 value. Actually, the RBFNNs are constructed and trained by utilizing the orthogonal least squares algorithm. By applying this algorithm we can obtain the network size while the free parameters of the networks are computed in a straight-forward manner. Consequently, the computational burden of selecting an optimum network-structure by trial and error $-$ a common strategy for multilayer perceptron neural networks $-$ is significantly reduced.

We have applied the RBFNNs to the data obtained from the ground stations of Slough (51.5° N, 0.6° W) and Rome (41.9° N, 12.5° E). In particular, the RBFNNs we developed map the calculated values of the critical frequency (foE) of the ionospheric layer E and the cosine of the elevation angle of the sun (cosx) to the frequency foF2. The modeling of foF2 is carried out within the time intervals [09:00, 15:00] and [08:00, 16:00] for Slough and Rome, respectively. We have trained one network for each month i.e., 12 neural networks for Slough and for Rome, respectively. The training set of each network has been composed of the calculated values of foE, the cosx, and the observed values of foF2 in the years between 1967 and 1988. After the completion of the training procedure, we examined the generalization ability of the trained RBFNNs, by testing their response to the data we had obtained from the two ground stations in the years between 1989 and 1994. In results, we observed that most of the estimated values of foF2 diverged less than 5% from the corresponding observed values. Actually, we noticed that during the summer period (when the solar activity is higher and the daily variation of the observed foF2 values is smoother) the estimation of foF2 is more accurate compared to the rest of the year.

Daily Mean Ionospheric Total Electron Content (TEC) Estimation Using Global Ionospheric Maps

C. B. Erol
Department of Biomedical Engineering, Baskent University
Ankara, 06530, Turkey

S. G. Tanyer
TUBITAK
Ankara, Turkey

The seasonal, diurnal, latitudinal and longitudinal variations of ionospheric total electron content (TEC) is investigated using Global Ionospheric Maps (GIM) corresponding to a twenty-four month period (1999–2000) at Ankara (39.88°N, 32.35°E), Turkey. The dependence of those TEC values on solar zenith angle and season is also examined. It is observed that the daily mean TEC values for one month is sufficient to extrapolate the corresponding values both for the previous and the following months. This is illustrated on interpolation for a whole twenty-four month period using only the daily mean values corresponding to February, May, August and November. It is interesting to note that the variations of solar and geomagnetic indices are reflected on the daily mean TEC values with a delay about 1 to 3 days and 1 to 2 days, respectively. It is also interesting to note that for the year 2000, winter anomaly was not concentrated in high mid-latitudes as usually expected.

Fuzzy Model of Corona Currents due to EHV Lines

P. Kumar and R. Garg
Delhi College of Engineering, Department of Electrical Engineering,
Delhi University
Delhi, 110042, India

The ionization of air surrounding the EHV conductor due to electrostatic field of EHV lines generates corona currents in the form of pulses. It depends on various factors such atmospheric conditions, size of conductors, conductor configuration and voltage gradient, etc. The corona generated currents change with the atmospheric conditions and also with the terrain which cannot be defined accurately and are uncertain in nature. To deal with such currents it is appropriate to represent them with fuzzy logic model as it takes into account the uncertainties and vagueness of the parameters. Fuzzy logic identifies the truthness or belongingness to a certain function. It can be described in three basic process-i) fuzzification ii) processing, and iii) defuzzification. Fuzzification is the process of getting a set of membership values from the crisp values by using trigonometric and geometric relations. These set of values are then, processed according to the framed rules and the output is in form of set of processed values. In order to find out a single value corresponding to crisp values of various parameters at particular condition, centroid method has been employed in the present work.

The authors, in this paper, have presented the fuzzy-corona signal model for EHV lines assuming triangular fuzzy functions. First the excitation function has been computed [1]. This has been then fuzzified and processed based on the rules emerged from the simulation studies carried out.

The corona generated currents, i per unit length are then computed using the equation (1)

$$i = \frac{\omega C}{2\pi\varepsilon} \cdot \frac{q}{\rho} \cdot \frac{d\rho}{dt} \tag{1}$$

Here, q is the charge, C is the capacitance per unit length of line and depends as the geometry of conductors, ω is the angular frequency of injected corona currents. The factor $(\underline{q}/\rho) \cdot d\rho/dt$ depends upon the characteristics of space charge, its quality and law of its movements. It is generally called corona excitation function, Γ. Thus equation (1) can be re-written as:

$$i = \frac{\omega C \cdot \Gamma}{2\pi\varepsilon}$$

The results obtained using fuzzy model, conventional model and field model are compared and presented in this paper.

REFERENCES

1. Kumar, P., M. S. Thomas, and R. Garg, "Sensitivity analysis of corona noise interference due to EHV lines," *Journal of the Institute of Engineers (India)*, Vol. 79, 182–185, Feb. 1999.

Information of Polarizing Parameters of a Radar Signal

A. B. Shupiatsky
Central Aerological Observatory Dolgoprundy
Moscow, 141700, Russia

The review of theoretical and experimental studies of meteorological events by dual-polarization radars are presented. Theoretical and experimental foundations of the polarization methods of detecting dangerous weather phenomena are made. Theoretical models of polarization characteristics (linear and elliptical) of radar signals from different kinds of clouds and precipitation are worked out and described. From common case of elliptically polarization is shows sensibility echo signal from microstructure of reflected particles. A choice of optimal polarization may by make.

Algorithms of the detection of a variety of hydrometeors and optimal polarization are discussed. Creation of algorithms of connection of microstructure and dangerous weather phenomena with polarization characteristics of radar signals are presented.

Requirements to the equipment and up-dating of existing radars are formulated. These algorithms and requirements were realized on basis of polarization airborn and ground dual-polarization weather radars. These diversity-polarization radar are described.

The airborn polarization meteoradar to study clouds and precipitation and solve problems of polarization identification was elaborated and manufactured at the Central Aerological Observatory (CAO). This radar with a digital-processing system is able to measure backscatter during aircraft flying time, using measurement results.

Methods and means for remote detection of pre-storm state, increased electrical activity, zones of icing, hail and shower clouds, heavy precipitation, turbulence and other weather phenomena and conditions which are dangerous for flights of air vessel and human activities.

In results our work done: Theoretical and experimental foundation of the polarization methods of detection dangerous weather phenomena. Solution of direct and inverse problem of electromagnetic waves with different atmospheric objects. Change of polarization of radio waves due to reflection and propagation through them. Creation of algoritms (know-how) of connection of micro-structure and dangerous weather phenomena with polarization characteristics of radar signals. Requirements to the equipment and up-dating of existing radars. Preparation of the programs of recording and real time processing of variable polarizations components of the signal.

It is necessary to note one more important developed direction in polarizing radiometeorology. It is a bistatic mode of reception of signals.

With this mode considerably extends information of the polarizing characteristics of a signal. Theoretically and experimentally is shown, that with reception of signals not only with a return corner of dispersion of 180 degrees, but also in a general case with other corners of dispersion, volume of the information about reflecting object considerably extends. So from the point of view of meteorological tasks the detection of large particles in a cloud, spectrum of their distribution, phase structure is possible.

The theoretical substantiation developed a technique and the equipment for realization of this mode of operations is resulted.

Ultra-Low Frequency Electromagnetic Vortical Structures in E-Region of the Ionosphere

G. D. Aburjania
Vekua institute of applied mathematics, Tbilisi state university.
Tbilisi, 380043, Georgia

G. V. Jandieri
Physics department, Georgian technical university
Tbilisi, 380075, Georgia

O. A. Kharshiladze
Physics department, Tbilisi state university
Tbilisi, 380026, Georgia

Physical mechanism of generation of slow and fast ULF waves of electromagnetic type caused by regular action factor—latitude variation of geomagnetic field in dissipative E-region of the ionosphere is suggested. It is shown that slow waves are generated due to dynamo field in the ionosphere, fast waves by vortical electric field. Slow electromagnetic wave is analog of the Rossby planetary wave; fast one is a new mode of proper oscillation of E-layer. Linear waves propagate both to the east and west directions along parallel against a background of the mean zonal flow in dynamo region of the ionosphere. Phase velocity of fast waves if a few km$\cdot s^{-1}$, frequencies are in the range $10^{-2} \div 10^{-4} s^{-1}$ and the wavelength is of the order of 10^3 km and more. Phase velocities of slow waves and local winds are the same by an order of magnitude, frequencies $10^{-4} \div 10^{-5} s^{-1}$ and the wavelength is in the order of 10^3 km or more. Fast waves generate intensive magnetic fields in the order of few hundred nanotesla (nT); slow one in the order of few ten nT.

Nonlinear theory of fast and slow planetary electromagnetic waves in E-region of the ionosphere is considered for the first time in this paper. It was established that these perturbations are self-localized in the form of nonlinear solitary vortical structures in dynamo-region of the ionosphere and move to the west (fast) to the east (slow) directions against a background of the mean zonal flow. Nonlinear structure consists of couple of reverse-rotatory vortices cyclone-anticyclone type and transfer trapped medium particles. Energy and entropy of large-scale vortices weakly attenuate and are long-lived. Vortical structures generate magnetic fields by an order of magnitude greater than corresponding linear waves. Theoretical investigations of the features and parameters of electromagnetic wavy structures are in a good agreement with experimental observations of large-scale ULF wavy perturbations in the ionosphere.

Resolving Diffractive Structures in Planetary Radio Occultation

C. S. Han
Stanford University
Stanford, CA 94305, U.S.A.

G. L. Tyler
Stanford University
Stanford, CA 94305, U.S.A.

In planetary radio occultation, the Abel transform is often used to generate profiles of atmospheric refractivity, temperature, and pressure. But being based in geometrical optics, this inversion technique cannot typically resolve structure with scales smaller than the diameter of the first Fresnel zone, $\sim 2\sqrt{\lambda D}$ where D is the distance from the spacecraft to the observed ray periapse. Planetary atmospheres have such sub-Fresnel-scale structures (e.g., waves, temperature inversions) that cause diffraction, and even planetary limbs diffract. These "sharp-boundary" structures often overwhelm the inversion process with diffractive noise and limit the efficacy of Abel inversion in yielding well-resolved profiles.

By manipulating the angular spectrum of the data to reverse propagate the observed fields, a new effective observation distance much less than D can be attained, reducing the Fresnel scale and resulting in vertical resolutions finer than that achievable by applying Abel inversion alone. In simulation, this technique resolves a smooth, 40 m refractivity perturbation of magnitude 10^{-7} superposed over the refractivity profile for a Mars-like atmosphere. The simulated atmosphere has a refractivity of $\sim 4\times10^{-6}$ and a scale height of approximately 9 km. The diameter of the first Fresnel zone in this simulation is approximately 500 m.

Diffraction from planetary limbs, an effect clearly seen in real occultation data (i.e., Mars Global Surveyor), has also been verified in multiple phase screen simulations of Mars and Pluto occultation. In these simulations, the diffraction resembles a knife-edge effect, even with very smooth limbs, and has been shown to obscure, if not complelely conceal, more subtle atmospheric radio wave interaction that must be discerned for accurate profile reconstruction. This is of special concern when attempting to image near-surface atmospheric structure. The back-propagation method applied here also simultaneously resolves the planetary limb and sub-Fresnel-scale atmospheric artifacts.

Inversion Methods for GPS Occultations

C. O. Ao, G. A. Hajj, and A. J. Mannucci
Jet Propulsion Laboratory, California Institute of Technology
Pasadena, CA 91109, U.S.A.

Radio occultations have long been used in the remote sensing of planetary atmospheres. Recently, thanks to the GPS satellite constellation, similar techniques have been applied to provide vertical profiling of the Earth's atmosphere and ionosphere as well. The GPS Meteorology (GPS/MET) proof-of-concept experiment, which operated from April 1995 to February 1997, has already provided a wealth of interesting data for scientific analysis. The currently operating CHAMP and SAC-C spacecrafts, carrying the more advanced BlackJack GPS receiver, are capable of tracking deep into the lower troposphere and yield approximately 300 occultations per day.

The standard retrieval method converts the excess phase measurements due to atmospheric refraction into the raypath's bending angle α as a function of impact parameter a. The relation $\alpha(a)$ is then integrated — via Abel inversion — to yield the vertical profile of the refractive index. This method assumes that the atmosphere is locally spherically symmetric and that geometric optics is valid. However, sharp refractivity gradients could cause multiple signals to arrive at the receiver simultaneously. In this case, which is quite common in the lower troposphere, the retrieval system infers multiple values of bending for the same impact parameter. An *ad hoc* procedure must then be applied to the data to compute the Abel inversion integral, which results in retrieval biases.

Radioholographic methods such as backpropagation, radio optics (or sliding spectral method), and canonical transform, have been proposed to circumvent difficulties encountered by the standard retrieval method and to improve the vertical resolution of the retrievals. These methods use both the amplitude and phase of the received signal in reconstructing the ray structure of the refracted field. We shall present assessments in the performance of radioholographic methods versus the standard retrieval method.

It is important to recognize that the final step of these radioholographic methods, where the refractivity profile is computed, is still carried out through Abel inversion. Thus the basic assumption of a locally spherically symmetric atmosphere remains. This constraint is especially problematic in the ionosphere or when weather fronts are present in the troposphere. To bypass such limitation, we investigate the inversion of radio occultation data based on a least-squares minimization technique. A fast forward model is implemented through the use of dynamic ray tracing. The unknown coefficients of the properly parameterized refractivity profile can then be obtained by minimizing the cost function that characterizes the differences between the computed signal and the measured signal. The parameterization can accommodate horizontal as well as vertical refractivity variations; therefore, the least-squares method has the potential of unraveling 3-D refractivity structures from occultation measurements.

An Alternate Method for Local Vertical TEC Estimation

C. B. Erol
Baskent University
Baglica Kampusu, Ankara 06534, Turkey

F. Arikan
Hacettepe University
Beytepe, Ankara 06532, Turkey

O. Arikan
Bilkent University
Bilkent, Ankara 06533, Turkey

Total Electron Content (TEC), which is defined as the number of free electrons along the ray path above one square meter, is a direct way to investigate the structure of ionosphere and upper atmosphere. Both short term and long term variations, including irregularities and disturbances in the ionospheric structure can be observed utilizing TEC values. In recent years, Global Positioning System (GPS) dual frequency signals are widely used to estimate both regional and global TEC values. The advantages of GPS signals include the large number of satellites at an altitude of 20,000 km, global coverage and commercially available receivers. Theoretically, TEC values are estimated from GPS signals using the P1 and P2 pseudoranges provided by the GPS receivers. The TEC values are proportional to the difference of P1 and P2, which is then modified by a constant related to the frequencies of the satellite. Various factors complicate this virtually simple computation procedure when the TEC values are estimated using active GPS satellite signals. The GPS receivers can receive signals from as many as 12 different satellites at a given instant. All of these satellites have different orbits and thus traverse the GPS receiver range with different paths in elevation and azimuth. Most of the estimation procedures provided in the literature assume both the spatial homogeneity of ionosphere for a wide range of elevation and azimuth angles and a temporal stationarity period of at least 15 minutes. This way some of the important spatial and temporal variations over the receiving station may not be observed. In order to compensate such difficulties some of the TEC computations are based on observations from only one satellite and for very limited time periods.

In this paper, we devised a novel technique which can combine signals from all the satellites for a given instant and given station and estimate the vertical TEC (VTEC) values for any desired period without missing any important feature in temporal or spatial domain. The raw GPS signals are downloaded from the Internet site of International GPS Geodynamics Service (IGS), (www.igs.egn.fr) and preprocessed to reduce the anomalies due to satellite, receiver or multipath from the signals. The preprocessed signals from all the satellites that are received for a certain time period are weighted according to their positions with respect to the local zenith. A two-step regularization algorithm combines these signals and provides smooth VTEC estimates for the desired time period. The first step of the regularization includes the minimization of error utilizing a high pass penalty function. This step requires the determination of two regularization parameters, which are to be chosen from the error function formed by the L2 norm of the difference between the estimated and actual VTEC values. An optional weighting function is an added feature to the regularization algorithm, which helps to reduce the error in calculation of VTEC due to inhomogeneous structure of ionosphere in elevation. The second step of regularization includes a sliding window median filter, which further reduces the undesired features in the estimated VTEC values. The window length of the sliding median filter is another parameter to be determined.

The estimation algorithm is tried on VTEC values obtained from four stations Kiruna (67.32° N, 20.09° E), Kiev (50.22° N, 30.30° E), Ankara (39.53° N, 32.45° E) and M. Dragot (31.35° N, 35.23° E) for the solar maximum period of April 23 to April 28, 2001. Within this period we observed both the typical quite day structure of VTEC and also the VTEC values of most positively and most negatively disturbed days of the month. The estimation procedure is highly accurate in detecting disturbances and irregularities for various time scales without changing the parameters chosen for quiet day conditions.

Doppler Radar Complex for Measurement of the Characteristics of Atmosphere

V. N. Efremov
Central Asian Hydrometeorological Research Institute
Tashkent, Republic of Uzbekistan

Up to the present it has been considered to be impossible to measure the wind field using single Doppler radar. In the paper a methodical approach is considered for evaluation of the wind field by data obtained with the use of single Doppler radar and automatic complex assigned for that. This technique provides the opportunity to measure dynamic characteristics of atmosphere in the radius of 60 kilometres. Thus, information about reflectivity from meteorological objects, wind radial component over the radar and wind field with the step of network equal to 2.5 and 5.0 kilometres may be reproduced on the screen of monitor and printed. Due to this complex full survey and analysis of data obtained by single Doppler radar are carried out for 5-10 minutes.

The estimation of the vector wind field measuring accuracy using single Doppler radar on the data of field experiments has been carried out. The analysis of the obtained data has shown the satisfactory accuracy of the experiments (1m/s by module, 15 degrees by direction).

In the paper a methodical approach is considered for evaluation of the wind field, its characteristics in clouds and precipitations by data obtained with the use of single Doppler radar.

Session 3Pa2

Microelectronic Packaging II

Correlating Measured Dielectric Properties with Kramers-Kronig Relations

A. Enver
Compaq Computer Corporation
Shrewsbury, MA 01545-4112, U.S.A.

M. Tsuk
Compaq Computer Corporation
Marlborough, MA 01752-3085, U.S.A.

F. Azam
Department of Physics, Government Womens College
Islamabad, Pakistan

Printed wiring boards (PWB) are commonly manufactured from the FR-4 type composite, consisting of an epoxy matrix reinforced by a woven glass cloth. These boards, operating at high frequencies — in the microwave range — exhibit frequency-dependent dielectric characteristics. Experimental data indicate significant differences between low frequency and microwave-frequency values of permittivities. Some PWB heating has been observed in these systems indicating energy losses at high frequencies. These losses could be attributed to the chemical composition of the PWB materials as well as their laminar nature. The permittivity for such a material would vary as a function of frequency, temperature, water content (dependent upon the environmental conditioning of the material), and relative proportions of its components. The commonly used measure of dielectric loss, the loss tangent, is defined as the ratio of the imaginary part of the permittivity to the real part. The Kramers-Kronig relations determine the relationship between the real and imaginary parts of the permittivity as a function of frequency and therefore put significant constraints on the physically allowable behavior of the loss tangent.

In order to verify the experimental data in the literature, we have used the Kramers-Kronig relations to obtain the imaginary part of the permittivity from the experimental values of the real part and vice versa. Since the experimental results span a finite frequency range, appropriate high-frequency approximations and physically reasonable bounds on the permittivity were employed to evaluate the integrals over a significantly wide frequency range. The calculations show that there is a significant change in the permittivity at gigahertz frequencies — in the range of operation of the Compaq high performance Alpha microprocessor — as shown in the experimental results. This would have an impact on the performance of the Alpha-based systems that operate in this range of frequencies.

The present analysis extended to the study of PWBs from several manufacturers would help identify those with the optimum performance characteristics for Compaqs future high-performance servers. The analysis has been carried on data from the work of several investigators and reasonably good correlation has been obtained with the experimental results. In conclusion, the PWB materials that are currently used in high-end servers do show dielectric losses that could impact their performance.

Coupling between Microstrip Lines and Finite Ground Coplanar Lines Embedded in Polyimide Layers for 3D-MMICs on Silicon

G. E. Ponchak
NASA Glenn Research Center
Cleveland, OH 44135, U.S.A.

N. Bushyager, J. Papapolymerou, E. M. Tentzeris, and J. Laskar
School of Electrical and Computer Engineering
Georgia Institute of Technology
Atlanta, GA 30332-0250, U.S.A.

Three-dimensional circuits built upon multiple layers of polyimide are required for constructing Si/SiGe monolithic microwave/mm-wave integrated circuits on CMOS (low resistivity) Si wafers. It is expected that these circuits will replace the ones fabricated on GaAs and reduce the overall system cost. However, the closely spaced transmission lines that are required for a high-density circuit environment are susceptible to high levels of cross-coupling, which degrades the overall circuit performance. In this paper, theoretical and experimental results on coupling and ways to reduce it are presented for two types of transmission lines: a) the microstrip line and b) the Finite Ground Coplanar (FGC) line. For microstrip lines it is shown that a fence of metalized via-holes can significantly reduce coupling, especially in the case when both lines are on the same polyimide layer or when the shielding structure extends through several polyimide layers. For closely spaced microstrip lines, coupling is lower for a metal filled trench shield than a via-hole fence. Coupling amongst microstrip lines is dependent on the ratio of line separation to polyimide thickness and is primarily due to magnetic fields. For FGC lines it is shown that they have in general low coupling that can be reduced significantly when there is even a small gap between the ground planes of each line. FGC lines have approximately 8 dB lower coupling than coupled coplanar waveguides (CPW). In addition, forward and backward characteristics of the FGC lines do not resemble those of other transmission lines such as microstrip. Therefore, the coupling mechanism of the FGC lines is different compared to thin film microstrip lines.

System-on-a-package (SoP) Solution for High Performance RF/Microwave Systems

L. M. Franca-Neto
Wireless Technology Lab (WTL), Intel Corporation
Hillsboro, OR 97124, U.S.A.

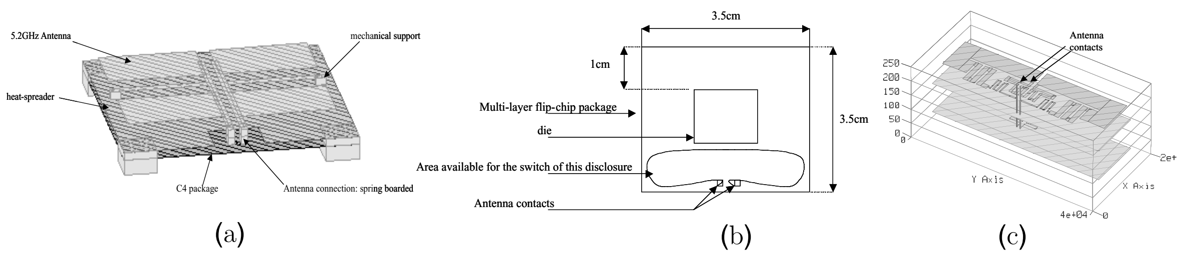

Figure 1: System-on-a-Package (SoP): antenna on the heat-spreader and critical high Q tuned passive components on the multi-layer flip-chip package. (Note: dimensions in micrometers unless explicitly stated).

RF/Microwave front-end integration in mixed signal ICs approximates active device performance limits when critical tuned passive components are realized with high quality factor (Q) components. Assuming metal thickness of at least two skin depths, the Q of microwave microstrips and striplines follow closely equation 1, where h is the height from signal trace to ground plane(s), σ is the metal conductivity, and f is the frequency of operation. Thus, geometric considerations alone makes realization of these critical components 10x higher Q than equivalent realizations on the IC for typical cases: $\mathcal{Q} \infty h\sqrt{\sigma f}$. Figure 1 shows System-on-a-Package (SoP) developed from the above observations. Antenna structure for 5.2 GHz frequency of operation case mounted over the heat-spreader of a C4 package is shown. Heat-spreaders can extend over more than one C4 chip, thus higher foot-print antenna structures (for lower frequencies or smart antennas) and omnidirectional operation can also be accommodated. A switch to make receiver and transmitter share the same antenna, the Power Amplifier's (PA's) impedance transformer networks plus RF chokes, and the Input Match Networks (IMN) for the receiver's Low Noise Amplifiers (LNA) are all realized on the top four metal layer of the package (Figure 1 (b) and (c)).

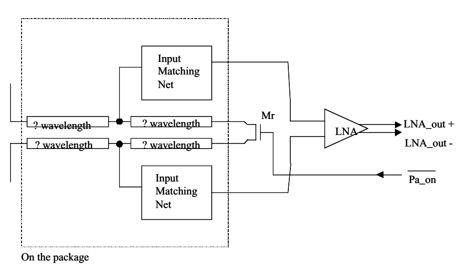

Figure 2: Receiver front-end.

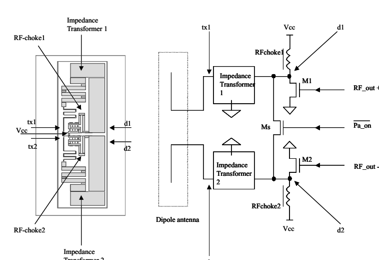

Figure 3: Transmitter front-end.

Figure 2 shows the receiver circuitry on the package and Figure 3 shows the electric equivalent of the microstrips on the package for the transmitter-end (PA).

LNA reaches noise figures of 1.3 dB and 2.3 dB at 2.4 GHz and 5.2 GHz respectively, only 0.1 dB above the values with ideal lossless input matching networks. PA's impedance transformers transfer more than 80% of the power from the PA to the antenna.

Development of Highly Integrated 3D Microwave-Millimeter Wave Radio Front-End System-on-Package (SOP)

M. Davis, K. Lim, S. Pinel, E. M. Tentzeris, and J. Laskar
Packaging Research Center, School of ECE
Georgia Institute of Technology, Yamacraw Design Center
Atlanta, GA 30332, U.S.A.

Multi-layer integrated components, and optimized PGA technology for microwave packaging are critical to meet the cost and performance requirement of highly integrated wireless systems. Embedded components technology allows a higher level of integration in the development of a wireless transceiver system. They offer the potential for saving the assembly time and cost by considerably reducing the MMIC real estate and the amount of discrete elements used in the module. The current drawbacks of most commercially available microwave and millimeter wave front-ends, such as the Ku-band satellite transceivers for outdoor units, are their relatively large size, heavy weight primarily caused by discrete components such as the filters, and separately located modules. Multi-layer SOP-based implementation is capable of overcoming this limitation by integrating components as part of the module package that would have otherwise been acquired in discrete form. In this paper, we present the development, implementation and measurement of a 3D-deployed RF front-end System-on-Package (SOP) topology in a standard low-loss multi-layer ceramic (LTCC) technology. A compact 14 GHz GaAs MESFET-based satellite transmitter integrated with a low-loss embedded filter for outdoor units were built on a $400 \times 310 \times 35.2\,\mathrm{mil}^3 .943$AT tapes. The LTCC filter exhibits a measured maximum insertion loss of 1.8 dB while the entire transmitter chain yields a $32 - 34$ dB of gain in the 13.5 to 14.5 GHz range. These results suggest the potential feasibility of building highly SOP integrated microwave and millimeter wave radio front ends. In addition, a highly integrated transceiver module for OFDM Communication System using Multilayer Packaging technology as well as Multilayer Integrated Passives using Fully Organic System on Package (SOP) technology demonstrate the capabilities of SOP for applications in the area of 5.8 GHz. The three-dimensional transmitter architecture that has been incorporated yields more than 40% savings of real estate. This development suggests the potential feasibility of building highly SOP integrated microwave and millimeter-wave radio front ends.

Loop Inductance and Planar Circuits

H. Braunisch and K. Radhakrishnan
Intel Corporation
Chandler, Arizona 85226-3699, U.S.A.

Loop inductance is an important concept in electronic packaging. As an example take the power delivery loop between a group of switching devices, such as a microprocessor core cell, and the interface between two stages of the decoupling hierarchy. The effectiveness of a decoupling capacitor at the aforementioned interface in suppressing simultaneous switching noise is related to the loop inductance that serves as a figure of merit quantifying electrical package performance.

For an arbitrary two-port characterized in the frequency domain by Z parameters, the loop inductance seen at port 1 with respect to port 2 can formally be defined as

$$L_{\text{loop}} = \lim_{\omega\to 0} \operatorname{Im}\left\{\frac{Z_{\text{in}}}{\omega}\right\} = \lim_{\omega\to 0} \operatorname{Im}\left\{\frac{Z_{11}\,Z_{22} - Z_{12}^2}{\omega\,Z_{22}}\right\} \tag{1}$$

where Z_{in} is the input impedance at port 1 with port 2 shorted and ω the angular frequency.

In the case of a general transmission line of length ℓ and with transmission line parameters per unit length R, L, G, and C, the definition (1) can be shown to lead to

$$L_{\text{loop}} = \frac{1}{4\,G^2}\sqrt{\frac{G}{R}}\left[2\ell\sqrt{RG}\,(RC+GL) - (RC-GL)\,\sinh 2\ell\sqrt{RG}\right]\operatorname{sech}^2\ell\sqrt{RG} \tag{2}$$

In the limit as $G\to\infty$ or $\ell\to 0$, the transmission line is shorted at port 1 and L_{loop} vanishes exponentially and linearly, respectively. As G approaches zero, $L_{\text{loop}} \to L\,\ell$ as expected, supporting the notion that decoupling capacitors should be placed as close as possible to the switching devices in order to minimize L_{loop}.

An electromagnetic cavity formed by two parallel rectangular plates with widths a, b and filled with a dielectric medium of thickness d and permeability μ constitutes a simplified model of a pair of power and ground planes in an electronic package, multi-chip module, or printed circuit board. Utilizing the Z parameters given by Lei *et al.* (1995/99) for rectangular ports of widths w_{xi}, w_{yi}, $i = 1,2$, centered about $\overline{\rho}_i = (x_i, y_i)$ where $0 < x_i < a$ and $0 < y_i < b$, we derive

$$L_{\text{loop}}(\overline{\rho}_1, \overline{\rho}_2) = \frac{\mu d}{ab}\sum_{m,n=0}^{\infty}\frac{\varepsilon_m\,\varepsilon_n}{k_{\rho mn}^2 + \delta_m\,\delta_n}\left[f_1(\overline{k}_{\rho mn}) - f_2(\overline{k}_{\rho mn})\right]^2 \tag{3}$$

where $f_i(\overline{k}_{\rho mn}) = \cos(k_{xm}\,x_i)\,\cos(k_{yn}\,y_i)\,\operatorname{sinc}(k_{xm}\,w_{xi}/2)\,\operatorname{sinc}(k_{yn}\,w_{yi}/2)$. Here $\operatorname{sinc} x$ is the analytical continuation of $\sin(x)/x$, the $\overline{k}_{\rho mn}$ are given by $(k_{xm}, k_{yn}) = (m\pi/a, n\pi/b)$ and we set $\varepsilon_m = 2 - \delta_m$ with the discrete Dirac delta δ_m. Result (3) is interesting from both analytical and numerical points of view. The loop inductance of the planar circuit depends not only on the distance from one port to the other but on port location with respect to the boundaries of the system; it is also seen to be *laterally scale invariant*. Convergence of the doubly infinite series depends on port size and there is a relation with the classical two-wire transmission line in the limiting case $a, b \to \infty$.

Session 3Pb2

Electromagnetics in Biology and Medicine

Risk Evaluation of Potential Environmental Hazards From Low Energy Electromagnetic Field Exposure using Sensitive *In Vitro* Methods (REFLEX)

F. Adlkofer
VERUM Foundation
München, Germany

Introduction: Although the biological effects of EMF exposure have been under study for the past 30–40 years, no consensus has been achieved with respect to either findings or their interpretation. The reasons for this are numerous: difficulties in measuring EMF exposure at the putative sites of action, vast differences in exposure and experimental conditions and the complete lack of agreement on biological endpoints appropriate for study. In the REFLEX project essential central elements in the function of various cell systems and in the development of disease are investigated using the most powerful molecular biological tools currently available. This will ensure a better understanding of the biological effects of EMFs, the prerequisite for an objective assessment of potential health hazards as well as of potential therapeutic effects.

Project objectives: Eleven research groups from all over Europe cooperate within the REFLEX project. The following five priority areas are investigated under strictly controlled conditions: 1. Direct and indirect genotoxic effects of EMFs. 2. Effects of EMFs on differentiation and function of embryonic stem cells. 3. Effects of EMFs on gene expression and protein targeting. 4. Effects of EMFs on the immune system. 5. Effects of EMFs on cell transformation and apoptosis.

Preliminary results and discussion: ELF-EMF $(50\,\text{Hz})$ exposure at flux densities $>\ 20\,\mu T$ increased the number of DNA strand breaks in cultured human diploid fibroblasts, but not in human lymphocytes. Induced damage reverted within 24h to baseline values. Reactive oxygen species may not be generated by ELF–EMF, since the 8–OHdG level in cellular DNA remained unchanged after exposure. A low but statistically significant up-regulation of c–jun, p21 and egr–1 mRNA levels was found in p53-deficient but not in wildtype mouse embryonic stem cells after exposure to powerline ELF–EMF $(50\,\text{Hz}$, $2.3\,\text{mT}$, on/off – $5/30\,\text{min})$ for 6 hours during the initial stage of their differentiation. The growth of human neuroblastoma cells increased significantly at a flux density of $100\,\mu T$, while DNA synthesis, cell cycle and membrane activation markers of human peripheral blood mononuclear cells were not affected through ELF-EMF exposure $(50\,\text{Hz}$, $50\,\mu T)$.

RF-EMF exposure $(1800\,\text{MHz}$, 1.5-$2.0\,\text{W/kg}$, on/off – $5/30\,\text{min}$, $217\,\text{Hz}$ pulse modulation) did not influence cell cycle length, differentiation and gene expression in wildtype mouse embryonic stem cells during the first 3 days of differentiation, but resulted in a low but statistically significant up–regulation of mRNA of c–jun, p21 and c–myc in p53-deficient embryonic stem cells. Furthermore, short–term exposure $(900\,\text{MHz}$, 2 W/kg, 1h) of human endothelial cells induced significant changes in gene expression as well as in protein expression and protein phosphorylation suggesting activation of a variety of yet unidentified cellular signalling pathways. No effect of RF–EMF on the apoptosis of endothelial cells and of U937 human monocytes was observed.

Conclusion: The results reported in the literature and obtained so far in the REFLEX laboratories suggest EMF effects on living cells at the DNA level. Whether these effects will have any significance in cell physiology or pathology remains to be established. In the ongoing studies the new techniques of genomics and proteomics which allow the simultaneous screening of large numbers of genes and proteins will be used. This technology appears to be the method of choice for providing a much deeper insight into cellular processes than previously considered possible.

1800 MHz Radiofrequency Exposition of Human HL60 Cells is Correlated with DNA Strand-Breaks as Measured by the Alkaline Comet Assay

K. Schlatterer, R. Tauber, and R. Fitzner
Department of Clinical Chemistry
University Hospital Benjamin Franklin, Free University of Berlin
Berlin, D-12200, Germany

Goal of these studies was to determine if radiofrequency electromagnetic fields induce structural alterations on the genetic level with proven relevance for cellular growth behaviour and cancerogenesis. Analysis was focussed the detection of DNA strand-breaks. The human promyelocytic leukaemia cell line HL60 was continuous wave-exposed to 1800 MHz at SAR 1.3 and 1.0 W/kg over 24 hours. DNA strand-breaks were examined by means of the single cell gel electrophoresis (SCGE), i.e., Comet assay. The Comet assay is used as a very suitable test system to study genotoxic effects on the single cell level with high sensitivity. Applying the alkaline Comet assay, single as well as double strand-breaks can be detected.

HL60 cells were cultured in RPMI 1640 medium with 10% FCS under temperature- and pH-control conditions at 37° C. For radiofrequency exposure experiments the initial seeding density per 35 mm petri dish was 7.5×10^5 cells. Exposure and sham-exposure were performed double-blinded. Subsequently, cells were monitored for DNA breakage by use of the alkaline Comet assay. 1000 cells per slide were scored manually by fluorescence microscopy for Comet formation according to Diem et al. [1], generating a tail factor by a simple mathematical approach. This tail factor allows to quantitatively compare the induction capacity of different environmental noxes concerning DNA-stand-breakage.

The tail factor determined in these experiments is increased for HL60 cells exposed at 1.3 W/kg as compared to sham-exposed controls. For 1.0 W/kg no such effect can be found. As positive control for DNA strand-breakage the tumour initiator 7,12-dimethylbenz[a]anthracene (DMBA) was used at a concentration of 25 μg/ml culture medium (0.01 mM). The effect of 1800 MHz radiofrequency exposure exerts that of DMBA clearly. As DMBA was solubilized in dimethylsulfoxide (DMSO), an additional group of cells, treated solely with DMSO, was included into the experimental set-up as a solvent control to ensure that this solvent, which itself is cytotoxic, exerts no genotoxic effects at the concentration used. Evaluation of the tail length showed that treatment of cells with DMBA causes a higher tail factor as compared to the DMSO solvent control, which is in accordance to previous studies performed for Hep G2 cells [2].

Our findings for the HL60 cell system reflect a correlation between radiofrequency exposure and DNA effects examined in the HL60 cell system. The increased rate of DNA strand breaks and its meaning for the cell system has to be further elucidated. After all, the findings of Lai and Singh in 1995 should be noted, who had shown increased single strand-breakage in rat brain cells after exposure to 2450 MHz radiofrequency fields.

REFERENCES

1. Diem, E. and H. W. Rüdiger, "Mikrokerntest und Comet Assay: Ein Ergebnisvergleich bei Normalprobanden," *Arbeitsmedizin Sozialmedizin Umweltmedizin*, 34, 437–441, 1999.
2. Yusuf, A. T., L. Vian, R. Sabatier, and J. P. Cano, "In vitro detection of indirect-acting genotoxins in the comet assay using Hep G2 cells," *Mutat. Res.*, 468, 227–234, 2000.
3. Lai, H. and N. P. Singh, "Acute low-intensity microwave exposure increases DNA single-strand-breaks in rat brain cells," *Bioelectromagnetics*, 16, 207–210, 1995.

Mobile Phone Radiation Effects on Cancer Induction and Blood-Brain Barrier Permeability: Hypothesis of the Possible Molecular Mechanism

D. Leszczynski
Radiobiology Laboratory, Department of Research and Environmental Surveillance
STUK - Radiation and Nuclear Safety Authority
Helsinki, FIN-00880, Finland

The question of whether mobile phone radiation is hazardous to health remains unanswered. In the earlier study (Leszczynski & Joenväärä, Differentiation, 2002, in press) it has been demonstrated that the 1-hour non-thermal exposure of human endothelial cell line EA.hy926 to SAR of 2W/kg (900 MHz GSM signal) leads, among others, to:

- transient increase in phosphorylation of hsp27 stress response protein, which was prevented by SB203580, a specific inhibitor of p38 mitogen-activated protein kinase (p38MAPK),
- transient changes in protein expression levels of hsp27 and p38MAPK.

Activated (phosphorylated) and/or over-expressed hsp27 has been shown to inhibit apoptosis and to affect the permeability of blood-brain barrier. It is hereby proposed that the activation of hsp27 by mobile phone radiation might be the molecular mechanism underlying some of the in vivo observed biological and potentially health-related effects.

In normal circumstances the apoptosis-preventing activity of hsp27 protects cells from "undesired" and "accidental" apoptotic death. However, activation of this preventive measure in damaged or transformed cells could help these cells to escape programmed death and to give rise to abnormal cell clone(s) that could, in favorable circumstances, develop into tumor. The molecular mechanism for hsp27-induced inhibition of apoptosis has been recently determined. It has been shown that phosphorylated form of hsp27 forms complex with the apoptosome (complex of Apaf-1 protein, pro-caspase-9 and cytochrome c) or some of its components and prevents proteolytic activation of pro-caspase-9 into the active form of caspase-9. This, in turn prevents proteolytic cleavage of down-stream pro-caspase-3 into active caspase-3. Thus, induction of the increased expression and phosphorylation of hsp27 by the mobile phone radiation might lead to inhibition of the apoptotic pathway that involves apoptosome and caspase-3. This event, when occurring in brain cells, which have earlier underwent either spontaneous or external-factor-induced transformation/damage, could support survival of the transformed/damaged cells what, in favorable circumstances, could help clonal expansion of the transformed/damaged cells — a known prerequisite for the tumor development.

Phosphorylated hsp27 has been also shown to regulate several endothelial cell functions that, when occurring in endothelial cells lining brain's capillary blood vessels, might be of critical importance for the stability and proper functioning of blood-brain barrier. The increased expression and/or phosphorylation of hsp27 has been shown to stabilize endothelial cell stress fibers due to increased actin polymerization. The stabilization of stress fibers was shown to cause: (i) cell shrinkage, (ii) increase in permeability and pinocytosis of endothelial monolayer, (iii) stronger responsiveness to estrogen causing secretion of bFGF, and (iv) formation of apoptosis-unrelated blebs obstructing blood flow, and inhibition of formation of apoptosis-related blebs.

Thus, the effects of hsp27/p38MAPK stress signaling pathway on apoptosis and endothelial permeability might be a molecular mechanism, which could facilitate the development of brain cancer and cause increase in blood-brain barrier permeability. These events, when occurring repeatedly over a long period of time might become a health hazard because of the possible accumulation of brain tissue damage. Furthermore, this hypothesis suggests that mobile phone radiation unrelated cell-damaging factors (mutagens) may have a co-participating role in the tumor development caused by mobile phone radiation.

The Effect of a 50 Hz Magnetic Field on the Immune Status of the Mouse, *Mus musculus*

L. de Jager
School for Health Technology, Technikon Free State
Bloemfontein, South Africa

G. J. Van Zyl, and H. J. Geyer
Dept. of Anatomy and Cell Morphology, University of the Free State
Bloemfontein, South Africa

L. De Bruyn
Clinical Skills Lab., University of the Free State
Bloemfontein, South Africa

Recent studies on the influence of low frequency electro- magnetic fields on biological systems suggest that there may be an interaction between magnetic fields (MF) and biological systems. It has been suggested that magnetic fields may act as a promoter or co- promoter in carcinogenesis or play a role in carcinogenesis through effects on the immune system. The immune system, with natural defense mechanisms, protects the body against infections and, in addition, the immune system plays an important role in the immune surveillance mechanisms of the body against tumor cells It has been suggested that MF exposure affect the immune system; Mevissen observed *in vivo* immunosuppressive effects of magnetic fields in rats. In a previous study we demonstrated a shortened life-expectancy in mice exposed to a time-varying power line magnetic field. The mice died at an earlier age because of non-specific illnesses. These findings prompted us to evaluate the *in vivo* effect of long- term exposure to a time varying 50 Hz magnetic field on the immune status of a mammal, namely the mouse.

An exposed and sham- exposed group of mice, *Mus Musculus* of the BALB/c strain were used in the study. The mice were housed in two laboratories under controlled conditions. The mice in the exposed group were exposed for 24 hours per day, to a rms 50 Hz magnetic field randomly varying between 0.5 and 77μT with an average of 2.75μT. Groups of mice were exposed or sham- exposed 14 weeks and 12 months. After the exposure period the quantitative status, as well as the qualitative status, of the immune system of the mice were determined. The B- lymphocytes ($CD19^+$), T- helper cells ($CD8^+$), T- suppressor ($CD4^+$) and natural killer ($CD56^+$) were determined quantitatively by means of immuno- phenotyping in conjunction with whole blood cell counts. The capacity of T- helper and B- lymphocytes cells to be activated was determined by means of the blast cell transformation test. Results were statistically analyzed by means of the Student's *t* or Mann- Whitney tests.

Statistically significantly differences between the number of cells in the subpopulations of lymphocyte in the exposed and sham-exposed groups were found. After 14 weeks of exposure the MF exposed group of mice showed a significantly decrease in the total number of lymphocytes, as well as in the T- helper cells and T suppressor cells, as well as a statistically significantly difference in the relation of $CD4^+$ to $CD3^+$. A suppression of T, as well as B- cell proliferative capacity was found in the exposed group after 14 weeks of exposure. The same tendency, thus a statistically significantly decrease in the total number of lymphocyte cells and T suppressor cells, was found in the MF exposed group after one year of exposure. The relation of $CD4^+$ to $CD3^+$ also showed a statistically significantly change after one year of exposure.

The immune surveillance system has repeatedly been proposed as a potential link in MF effects on carcinogenesis. In evaluating the potential role of MF effects on the immune system, long term *in vivo* studies are essential to accommodate a possible humoral effect that would be missed *in vivo* and/or short term studies. In this study we found that a decrease in the number of cells in sub populations of lymphocytes as well as in the proliferative capacity of the T and B lymphocyte cells. Our results thus indicate that long term exposure to a time varying magnetic field has an effect on the immune system if mice that could lead to a decrease in the capacity of the immune surveillance system, these observations are in line with those of Mevissen who reported on immunosuppressive effects of MF exposure in rats.

Influence of Measured Dielectric Properties to SAR Values

D. Simunic, J. Bartolic, and S. Skokic
Faculty of Electrical Engineering and Computing, University of Zagreb, Croatia
Zagreb, HR-10000, Croatia

Electromagnetic dosimetry measurements of mobile phones, as recommended by European Commission, are performed by three-axes isotropic electric field probe and a three axes positioner. Such a system performs a real-time high-frequency electric field sampling in a homogeneous liquid dielectric with losses, that simulates human tissue. Also, it processes the measured data, so that a deposited electromagnetic energy in human body, i.e., its standardized measure Specific Absorption Rate (SAR) can be calculated. Presently, there is no consensus on measured data of "in vivo" dielectric properties of tissue. Furthermore, clear dependence of measured SAR on dielectric properties of liquids has not been investigated thoroughly. We considered it as a very important issue, because the dielectric data are the starting point in the process of measuring the deposited energy, which could significantly influence measured SAR.

Therefore, we mixed liquids with different percentage of NaCl, sugar and water and measured their complex dielectric properties at different frequencies in the frequency range from 400 to 2900 MHz. The measurements have been performed with an open coaxial probe, based on the method of Stuchly [1] and Mosig [2]. During the process, it has been realized that the contact between dielectric and the probe has to be as homogeneous as possible, because it significantly influences acquired values of reflection coefficient and thus complex permittivity. After acquiring values of permittivity and conductivity, as recommended in a recently issued CENELEC norm 50361 related to mobile communications dosimetry, we performed measurements of SARs in a homogeneous liquid and found interrelationship between variations of SARs and permittivity.

REFERENCES

1. Mosig, J. R., J. E. Besson, M. G. Fabry, and F. E. Gardiol, "Reflection of an open-ended coaxial line and application to nondestructive measurement of materials," *IEEE Trans. Instrum. Meas.*, Vol. IM-30, 46–51, March 1981.
2. Athey, T. W., M. A. Stuchly, and S. S. Stuchly, "Measurement of radio frequency permittivity of biological tissues with an open-ended coaxial line: part I," *IEEE Trans. Microwave Theory Tech*, Vol. MTT-30, January 1982.

MISYA: A Microwave Stirred Room for Woodworm Disinfestation of Artistic Painted Boards

R. De Leo
Universita' di Ancona
Ancona, Italy

Many artistic objects, like wooden paintings or old furniture or carpets are infested by parasites. Actually they are cured essentially by use of toxic gases that creates serious ambient problems or by low efficiency surface treatments.

Based on an idea developed in the past at the IROE (the well-known Italian CNR Institute) a large system called MYSIA has been developed for threading large artistic objects.

In particular a 50 cubic meter($6050 \times 2440 \times 2200$ mm) screened room equipped by three rotating stirrers has been realized. This system is fed by three 20 kW magnetrons and the temperature at the surface of the artistic objects is controlled in real time by use of an infrared thermography system while a mathematical thermo model is used in order to estimate the temperature inside the object. In this way we ensure to reach in the objects a temperature higher than the parasitic lethal one (typically from $52°C$ to $60°C$) and low enough to avoid any damage to the disinfested artistic object.

The treatment takes only few minutes and the object is ready to be used while the traditional systems need up to 28 days. The system is self-powered and can be easily sent to any museum by using a truck.

At the Conference the main characteristics will be presented along with the specific experimented results. In particular:

- the electric field inside the stirred ambient that denotes a fairly constant average value in the central zone of the room
- The temperature profiles that are obtained in a wooden object
- The effects of metallic parts (like for example golden plates or nails)
- Results upon the mortality of infestants as a function of the temperature reached inside the object.
- The control of electromagnetic field outside the room..

Session 3Pc3

Optical Components and Systems

Dynamic Characteristics of Integrated Optical Amplifiers Using Er-Yb Codoped Garnet Crystal Waveguide

Y. Miyazaki and K. Takei
Department of Information and Computer Sciences, Toyohashi University of Technology
Toyohashi-shi, 441-8580, Japan

Optical integrated-type amplifiers are very important components of communication and signal processing as amplification and signal repeaters. For the integrated optical circuits, they have additional advantages such as compactness and high-efficiency. Er doped amplifiers have good efficiency for signal amplification in the communication wavelength band of 1.55 μm. Sensitization with Yb allows high gain and broader pumping wavelength range. Garnet material is useful for the fabrication of active integrated optical devices. The authors have earlier reported Nd doped garnet waveguide amplifier with a high gain of 15 dB/cm at 1.064 μm wavelength. Fundamental characteristics of Yb-Er codoped waveguide amplifiers have so far not been reported.

Steady state and transient amplification characteristics of waveguide amplifier based on Yb-sensitized Er-doped Garnet crystals are studied using time-dependent rate equations and propagation equations. Steady state response of these waveguide amplifiers is analyzed to get optimum condition of the signal gain. It is shown that a high gain of around 10 dB/cm is possible for a coupled pump power of 30 mW with 980 nm pump wavelength. The concentration effects of Yb ions have also been considered. RF-sputtered Er-Yb doped Garnet thin films are fabricated, and experimentally determined parameters such as loss, absorption and emission cross-sections have been used for the theoretical simulations. Optical characteristics of Er-Yb codoped waveguide amplifiers are compared with Er doped waveguide amplifiers.

Dynamic characteristics of these waveguide amplifiers are discussed for the input modulated signal. Pulse propagation characteristics are studied for applications in high-speed communication systems. The amplifier medium, particularly the population dynamics plays an important role in the pulse amplifications. Dynamic amplification characteristics of our proposed amplifier using time-dependent rate equations are shown. Because of the slower gain dynamics of the Yb-sensitized Er-doped Garnet amplifier medium, the longer signal input pulses with the duration of the order of excited state lifetimes are observed to be distorted upon amplification. Short pulses are amplified without change in the pulse shape. Er fluorescence bandwidth of 10 nm corresponds to a frequency bandwidth of 1.3 THz, and a pulse width limitation of 0.7 psec, and this model has the limitation of analysis of pulses shorter than 0.7 psec. Sub-psec pulse amplification has also been investigated considering the gain bandwidth. From dynamical studies with respect to various parameters, we obtain optimum performance of the amplifier to be able to use in the integrated optical circuits and systems for THz and super high femto second bit rate communications.

New Frontiers of Non-Invasive Sensing Applications Using Infrared Optical Fibers

R. Bruch
Department of Physics, University of Nevada, Reno
Reno, NV 89557, U.S.A.

B. S. Rawat
Department of Electrical Engineering, University of Nevada, Reno
Reno, NV 89557, U.S.A.

J. Gietl
Nevada Business and Science Foundation
Reno, NV 89509, U.S.A.

Optical fibers, in the near-infrared (NIR) and middle-infrared (MIR) wavelength regions, have found new opportunities in biomedical, environmental, and industrial applications. There is a race to find the fiber that works best for MIR non-invasive optical sensing techniques. In this study, we will report about the use of polycrystalline infrared (PIR) fibers. These fibers are very flexible, transparent in the wide spectral region of 4-18 μm, and very durable in the temperature range from $-200°$C up to +$250°$C. They are produced by Advanced Research and Technology (ART) Photonics using an innovative extrusion method from pure $AgCl : AgBr$ solid solution crystals in a core/clad structure, providing improved quality fiber products. The superior optical properties of these PIR fibers play an important role in modern Fourier Transform Infrared (FTIR) spectroscopy, in particular for the Fiberoptical Evanescent Wave (FEW) sensing technique. Such FTIR interferometers generally use infrared black body sources and more recently, tunable NIR and MIR laser systems.

In this study, we present our current results associated with numerous applications of FTIR-FEW spectroscopy for surface and subsurface structural analysis at the molecular level. The FTIR-FEW method utilized in this work can be applied to many fields including: (i) noninvasive biomedical diagnostics of human tissue and body fluids, (ii) skin tissue cancer diagnostics and other diseases in *vivo*, (iii) remote monitoring of chemical processes and the environment, (iv) surface analysis of polymers and other materials, (v) characterization of the quality of food, as well as (vi) agricultural, forensic, geological, mining, and archaeological field measurements. In particular, we present FTIR-FEW spectra of living skin tissue surfaces, polymers, and food products. In addition, fiberoptical results concerning the vibrational spectral analysis of normal and pathological skin tissue in the wave-number region 850 to 4000 cm^{-1} are discussed. Furthermore, we will provide a comparison of different NIR and MIR fiber characteristics, as well as multichannel MCT/PIR-fiber detectors for fast pyrometry and multispectral sensing applications.

Connector Offset Effects on Bandwidth-Distance Product of Multimode Fiber

A. S. Andrawis
South Dakota State University
Brookings, SD 57007, U.S.A.

P. T. Huang
Kennedy Space Center
Kennedy Space Center, FL 32899, U.S.A.

The local area network (LAN) market has undergone significant changes over the last few years. The major motivation of the market transformation is the exponential growth of the data moving across the network. Recently, the IEEE Gigabit Ethernet Committee completed the Gigabit Ethernet (GbE) standard to meet the explosive demand. The dominant fiber base used in LANs is multimode fiber (MMF) however, its modal bandwidth imposes an upper limit on the achievable bit rate and link distance.

Two types of optical modes, meridional ray modes and skewed ray modes, propagate in an overfilled (OFL) MMF. Mainly, meridional ray modes, as well as low order skewed ray modes limit the modal bandwidth in a MMF. If these modes are eliminated, MMF bandwidth-distance product improves significantly.

There have been several successful attempts to overcome the OFL bandwidth-distance product limit by selective excitation of only higher order skewed ray modes.

This paper is to explore the possibility of selective excitation of modes using a technique simpler than the ones reported in literature. This technique is expected to be easier to implement than reported attempts. It consists of SMF-to-MMF lateral offset ferrule connector. Offset launch condition is controlled such that only higher order modes are selectively excited. Selective mode excitement results in extending the bandwidth-distance product as well as reducing the modal noise.

A short description of offset ferrule connector will be initially introduced in this paper. Then, performance test results for eye pattern, Jitter, power loss, bit error rate (BER) and optical power distribution for several connector-offset values will also be presented.

Various Achievable Applications Using Versatile SOAs

J. Le Bihan and A. Sharaiha
Ecole Nationale d'Ingénieurs de Brest
Brest, France

Research studies on semiconductor optical amplifiers (SOAs) began earnestly twenty years ago. By now, we know for sure that SOAs will be key components in the architecture of optical transmission and optical switching systems. SOAs can be achieved at both 1.3μm and 1.5μm telecom windows. Their technology is the same as that of a Fabry-Perot laser diode, except that here cavity reflections are blocked using an antireflection coating. Today, SOAs can provide 25 dB of signal gain with low power consumption (~ 200 mW), saturation output powers up to 13 dBm and a noise factor of $6-7$ dB over a bandwidth of about 50 nm. SOAs have a polarization sensitivity of less than 1 dB and exhibit non-linear distortions. Moreover, SOA simplicity and compactness make them suitable for integration with semiconductor optical circuits and devices.

SOAs are used in both linear and non-linear modes of operation and they present a large number of applications for future optical systems. They have demonstrated their multifunctional capability by combining optical amplification with either modulation or in-line photodetection. By using modulation and photodetection abilities, we had proved the feasibility of a bi-directional optical bus with SOAs used as emitter-receiver at 1.5Gb/s.

In non-linear mode, SOAs are efficient for gating, wavelength conversion and optical signal processing. Several all optical switches have been achieved by utilizing SOAs in interoferometric configurations or by using the self-induced gain modulation in cascaded SOA configuration by counterpropagating the data and control signals.

Wavelength conversions allow to fully benefit of wavelength division multiplexing (WDM) to increase the capacity and the flexibility of optical telecommunications networks. The used all-optical wavelength conversions are based on non-linearities in SOAs, in particular cross-gain modulation (XGM) and cross-phase modulation (XPM). The simplest all-optical scheme is XGM in a single SOA. Wavelength conversion using XGM has been demonstrated for signals at bit rates up to 100Gb/s by using a SOA of 2mm length.

The limitation of SOAs with WDM channels is overcome thanks to clamped – gain SOAs (CG-SOA) where the signal induced gain fluctuations are suppressed by clamping the gain by a lasing oscillation outside the optical bandwidth. High performance 4-SOA arrays have been realized at low operating current (25 mA) for parallel optical loss compensation or for fast path selection. CG-SOAs have also been integrated in arrays of 4.

In this paper, we review the role of SOAs in future optical fiber systems. We give some of the more important equations governing the SOAs performances. Then a number of applications are discussed considering both the current state of laboratory experiments and the future performance expectations. Multifunctionality and potential of integration are essential advantages of SOAs, allowing to design future complex optical functions for telecom systems.

Erbium-Doped Dual-Core Fibre as C-Band and L-Band Amplifier

P. L. Chu
City University of Hong Kong
Kowloon, Hong Kong

Erbium-doped fibre amplifier (EDFA) forms the backbone of modern optical communication. For WDM systems in which many wavelengths of light are transmitted through one fibre, the spectral gain flatness of EDFA becomes an important issue. The standard EDFA has a gain peak at 1530nm followed a gain trough around 1550nm. The gain variation between the peak and the trough can be as high as 10dB. Many approaches have been suggested to flatten the gain spectrum and the incorporation of fibre Bragg gratings is one of the popular methods.

In this paper, we report a new method for gain flattening relying on the use of dual core fibre in which one core is doped with Erbium while the other is undoped. The two cores are closely spaced so that evanescent field coupling is possible between them. Since the two cores are unsymmetrical (the doped core is active while the undoped core is passive), the coupling is also unsymmetrical. The parameters of the fibre such as core diameters, core refractive indices and core to core spacing etc, can be adjusted so that part of the excessively amplified signal at 1530nm is coupled from the doped core to the undoped core and is wasted without coupling back to the doped core. In this manner, the gain of the amplifier can be flattened over a wide wavelength range. Our experimental results show that with the fibre 11 metres long, the gain can be flattened to within a ripple of 0.7dB over the wavelengths 1525nm to 1560nm. Furthermore, the noise figure over this range is less than 4dB. It is also important to note that although the amplifier is made up simply by a dual core fibre, only the doped core is needed for access at both ends. The undoped core is simply parasitic. Thus it does not pose any connection problem. This is a C-band optical fibre amplifier.

Furthermore, the dual-core approach can be further used to design an L-band amplifier for wavelengths from 1565nm to 1625nm. Over this range, the emission cross-section of Erbium decreases with the increase of wavelength making the gain to decrease accordingly. In order to flatten the gain, the dual core fibre can be designed to have a coupling coefficient to increase with wavelength so as to compensate for the reduction of the Erbium emission cross-section. We show experimentally that this can be achieved with a gain variation of 0.6dB over the range.

Dynamics and Spectra of Vertical Cavity Surface Emitting Lasers Subject to Optical Injection

Y. Hong, S. Bandyopadhyay, P. Rees, P. S. Spencer, and K. A. Shore
University of Wales
Wales, UK

External optical injection in semiconductor lasers have been widely investigated because of promising results in areas such as single mode operation under high-speed modulation, reduction of spectral linewidth and frequency chirping. Many phenomena, such as injection locking, four-wave mixing, mode-hopping, chaos and optical bistability, have been reported in edge-emitting diode lasers subject to optical injection. Such studies have been extended to vertical cavity surface emitting semiconductor lasers (VCSELs) which have many impressive characteristics, including a low threshold current, single-longitudinal mode operation, circular output-beam profile and wafer-scale integrability. Nearly degenerate four-wave mixing and injection locking in VCSELs show similar behaviour to those of edge-emitting laser diodes. Unlike edge emitting laser diodes the polarization of a transverse mode in VCSELs is randomly oriented in the plane of the active layer. Work has demonstrated that the linear polarization state of single-mode VCSELs can be switched by optical injection. However, VCSELs often operate in several transverse modes at high injection current, and so investigation of the optical injection dynamics of VCSELs with multimode operation is expected to be of some interest.

In this paper, we will report experimental investigations of VCSELs subject to external optical injection. Particular interest will be given to VCSELs supporting to two-transversemodes. The spectra of VCSELs with two parallel-polarized modes demonstrate significantly different behaviours, compared to the VCSEL with two orthogonally-polarized transverse modes. In a VCSEL with two orthogonally-polarized transverse modes, the experimental results confirm theoretical predictions that external optical injection can be used to achieve single-mode operation. However, in the case of a two parallel-polarized transverse modes VCSEL, single-mode operation cannot be obtained via optical injection. When the injection frequency is close to one of the modes, the coexistence of the injected beam and the mode give rise to very rich dynamical behaviours, however, the other mode is unperturbed by the optical injection. We will also report experimental and numerical studies of a form of antiphase dynamics which has been identified in VCSELs subject to optical injection.

Analysis of Cross-Talk and Cell Phase Shift of AOCA System for DWDM Application

B. S. Rawat and Y. Weng
Department of Electrical Engineering, University of Nevada
Reno, NV 89557, U.S.A.

The rapid growth in demand for high-capacity and high-speed telecommunication networks especially due to internet applications has resulted in very high increase in the use of dense wavelength division multiplexing (DWDM) for optical communications. With the advent of tunable lasers with extremely narrow line widths, it has become possible to have very closely spaced signal channels in DWDM. At present 0.8 nm channel spacing has been accepted as the industry standard for a highly cost effective long-haul optical communication link. The MUX/DEMUX is an important optical component used in a DWDM system. A new type of MUX/DEMUX using acousto-optic cell array (AOCA) system was first proposed by Rawat et. al. in 1998. This new type of tunable MUX/DEMUX consists of a phased array of AO Bragg cells with very large deflection capability compared to recently developed AOTF. This large flexibility is achieved by controlling the RF signal that is used to produce an acoustic signal with appropriate transducers. Besides tuning the RF signal, proper selection of number of cells, N and phase shift between consecutive AO cells directly related to cell spacing S, is used to optimize the system performance on demand. The phase-shift between two consecutive cells varies at a faster pace as the number of channels increases and can be controlled by adjusting separation between consecutive cells or by acoustic signal frequency.

The narrow channel spacing in DWDM links gives rise to crosstalk, which is the unwanted signals arriving in a given channel from other channels. It is an important issue in DWDM systems with large number of channels. The crosstalk can be introduced by almost any component in a DWDM system like fiber nonlinearities, optical switches, passive routers, optical add-drops, wavelength MUX/DEMUX etc. The crosstalk can severely limit the number of nodes allowed in the network and degrade the system performance of individual components. In this paper the effects of crosstalk and phase shift between consecutive cells of an AOCA system have been thoroughly investigated and simulated results for 4-channel and 8-channel DEMUX have been presented.

Optical Devices for Terhertz Bandwidth Optical Communication

J. Nishizawa and K. Suto
Semiconductor Research Institute, Aoba-ku
Sendai, 980-0862, Japan

As the bases of optical communication, semiconductor injection laser, optical fiber communication and graded index optical fiber, as well as pin photodiode and avalanche photodiode were proposed world first by the author in early 1950s to 1960s. Following the invention of the semiconductor injection laser, a proposal was made to utilize molecular lattice vibration effect to optical communication, such as generation of terahertz wave as well as optical frequency conversion in 1963. Since then, semiconductor Raman lasers and amplifiers have been extensively studied.

Semiconductor Raman lasers and amplifiers are promising devices for use in future terahertz bandwidth optical communication as well as high density wavelength division multiplexing (WDM) systems with total band width extending over 1 THz to 10 THz. In particular, semiconductor Raman amplifiers have a function of light frequency discrimination. Waveguide structure Raman amplifiers with a GaP core layer and $Al_xGa_{1-x}P$ cladding layers have a large gain coefficient with a frequency band width of 25 GHz, and the center frequency of light can be tuned by varying the pump light frequency.

We have also shown that the semiconductor Raman amplifiers have a function of high speed time gate amplification. Using a mode-locked pump source, pulse width of 80 ps, repetition frequency of 80 MHz and the amplification of 20 dB have been demonstrated. This function is quite suitable for pulse channel selection, within a selected single wavelength channel, at each subscriber connected by an optical fiber broadband network. We will discuss a possibility to further increase the optical gain by using the tapered waveguide structure. In the present, the Raman amplification is caused only by the backward interaction. We will discuss a possibility of obtaining fast traveling type forward interaction of the pump light and the signal light.

Ideal (ballistic) static induction transistors (ISIT) can be used as a multiplexing and demultiplexing circuits of the terabit light signals. ISITs make up a traveling wave type delayed circuits. Terabit light signals are directly detected by photosensitive ISITs which are gated with electric pulses transmitting a delayed circuits on which ISITs are placed.

In 1990, Photodynamic Research Center also started by following the author's guidance as the branch of the Institute of Physical and Chemical Research, and one department was settled to realize THz devices utilizing lattice vibrations and Dr. Kawase and Prof. Ito succeeded.

Session 3Pc4

Electromagnetic Scattering by Small or Resonant Obstacles

Microparticle Photophysics: Photonic Atom Microsensors

S. Holler
Sandia National Laboratory
Albuquerque, NM 87185-1423, U.S.A.

S. Arnold
Microparticle Photophysics Laboratory (MP^{3}L), Polytechnic University
Brooklyn, NY, U.S.A.

F. Vollmer
The Rockefeller University
New York, NY, U.S.A.

An isolated micro-sphere stimulated into a high angular momentum state has become known as a photonic atom because of the geometric similarity with orbital motion, and the ability of the problem to be cast in a form analogous to the Schrödinger equation in quantum mechanics.

The orbital analog derives from the fact that photons confined in high-Q whispering gallery modes circulate the micro-sphere's center similar to how an electron orbits a nucleus. The spectral characteristics of the photonic atom modes is highly dependent on the size, temperature, and refractive index of the micro-sphere resonator. As a result of the sensitivity to these parameters, the micro-sphere may be incorporated into a variety of sensor devices.

Access to the photonic atom modes is accomplished through "photon tunneling" from a fiber waveguide in close proximity to the micro-sphere. For the work presented here, we used either a fiber optic that has been etched to narrow ($\sim 4\mu\mathrm{m}$) waist, or evanescent access block in which a fiber optic embedded in a glass block is polished to be within $\sim 1\mu\mathrm{m}$ of the core. The spherical micro-cavities we used are either commercially available ball lenses, or fabricated by melting a ball at the end of a fused silica fiber.

We have observed shifts in the resonant frequency of the micro-sphere resulting from changes to the environment external to the micro-cavity. Principally, we are interested in the adsorption of chemical or biological species to the micro-sphere surface. The associated shift in the resonant frequency may be used to infer the thickness of the adsorbed layer. Furthermore, coating micro-spheres with analyte specific receptors will allow sensitive detection of chemical and biological agents through observed resonant frequency shifts due to molecular binding.

Shape Reconstruction from Scattering Amplitude Data at the Nyquist Limit

G. F. Crosta
Department of Environmental Sciences, University of Milan Bicocca
Milano, Italy

The experimental data processed herewith belong to the IPSWICH set. A perfectly electrically conducting right cylinder of axis **z** and unknown cross section, Ω, was illuminated by vertically **(z)** polarized plane waves at $10\,$GHz. For incidence directions spaced by 10 degrees in the $(\mathbf{x}, \mathbf{y})$ plane, (RADAR cross section, relative phase) pairs were measured in the same plane every 10 degrees within a sector of 170 deg. The latter sector depended on the incidence direction.

The scattering problem is scalar. The inversion algorithm used to reconstruct $\partial\Omega$, the boundary of Ω was based on approximate forward propagation, developed by the author [1]. In brief, the unknowns are the $\{\psi_i \,|\, 1 \le i \le I\}$ shape parameters; an approximation order, L, is chosen; the scattered wave on the obstacle surface is represented by a linear combination, of order L, of outgoing cylindrical waves, $\{w_\lambda | \lambda \in \Lambda(L)\}$; the coefficients $\{c_\lambda^{(L)} | \lambda \in \Lambda(L)\}$ in the combination are such that the DIRICHLET boundary condition is fulfilled in the least squares sense; the far zone scattered wave is represented by a linear combination of the asymptotics of w_λ by coefficients $\{f_\lambda^{(L)} | \lambda \in \Lambda(L)\}$. The latter coefficients are related to $\{c_\lambda^{(L)}\}$ by an affine map, the approximate forward propagator, which depends on $\{\psi_i\}$. Given I and L, the reconstruction of $\partial\Omega$ is carried out by minimizing the far zone defect, F, with respect to $\{\psi_i\}$, where the computed scattering amplitude is compared to the measured one.

The new feature of the algorithm described herewith consists of a method for determining the best value of L. Namely, a simple initial shape, usually an ellipse, and an initial value, say $L = 4$, are chosen, the corresponding minimizer $\{\psi_i\}$ is computed. Then L is increased by one and the previous minimizer used as initial shape guess. The procedure continues until the far zone defect keeps decreasing. Eventually the optimal L and $\{\psi_i\}$ are simultaneously determined.

Sampling of the far zone has occurred every 10 degrees: if 36 samples were indeed available, then the maximum value of L i.e., the NYQUIST limit, would be 18. In fact experimental data come from a limited aperture and are noisy. Computation typically returns optimal L's of 16 when data from 18 separate incident directions are assimilated.

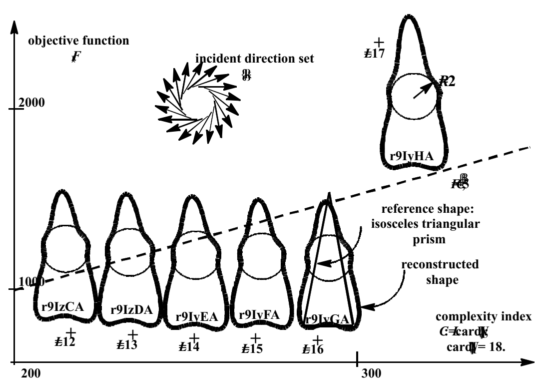

REFERENCES

1. Crosta, G. F., "The Forward propagation method applied to the inverse obstacle problem," *FIELDS Institute Communications*, 25, 225–238, 2000.

Numerical Performance of Forward Propagation Algorithms in the Inversion of Intensity Only Data

G. F. Crosta and S. Zomer
Department of Environmental Sciences, University of Milan Bicocca
Milano, Italy

Let electromagnetic scattering occur in the resonance (RAYLEIGH – KLEINMAN) region. If the shape to be reconstructed is the cross sectional boundary, $\partial\Omega$, of a perfectly electrically conducting, right cylinder illuminated by a plane wave such that the $\boldsymbol{E}$ vector is parallel to the axis of the cylinder, then the scattering problem is scalar.

Let $\partial\Omega$ be described by the set of shape parameters $\boldsymbol{\psi} := \{\psi_n | 1 \leq n \leq N\}$. Reconstruction of $\partial\Omega$ by the approximate forward propagation (AFP) algorithm consists of minimizing the far zone intensity defect

$$G := \int_{\phi} (I_C - I_M)^2 d\varphi, \tag{1}$$

where $\boldsymbol{\phi}$ is the aperture, $\varphi \in \boldsymbol{\phi}$ is azimuth, I_M is the scattered intensity measured in $\boldsymbol{\phi}$ and I_C is the computed intensity i.e.,

$$I_C = |\Sigma_\lambda f_\lambda[\{\psi_n\}] w_\lambda|^2. \tag{2}$$

Let L denote the approximation order, then λ is an index pair in the finite set $\Lambda(L)$, $\{w_\lambda\}$ are the asymptotics to the outgoing cylindrical wave functions and $\{f_\lambda\}$ are the far zone scattering coefficients, which depend on $\{\psi_n\}$ as described in a previous paper.

The numerical performance of the AFP with measured scattering amplitude data at 10 GHz has been known for some time and recently improved by means of the automatic determination of the best L according to the available data sets.

The numerical results yielded by applying AFP to intensity only data will be described. Simple shapes e.g., ellipses and other star shaped and smooth obstacles will be dealt with.

Scattered intensities will come both from numerical simulations (used for consistency verification) and measurements (IPSWITCH data).

Analytical Inversion Methods for Diffuse Light with Sampling and Truncation of Data

V. A. Markel and J. C. Schotland
Department of Radiology, Washington University
St. Louis, MO 63110, U.S.A.

The propagation of near-IR light in biological tissues is characterized by strong multiple scattering and relatively weak absorption. Under these conditions, the spatial distribution of the energy density of electromagnetic radiation $u(\mathbf{r})$ can be described by the diffusion equation $\partial_t u = \nabla \cdot D\nabla u - \alpha u + S$ with position-dependent absorption and diffusion coefficients, $\alpha(\mathbf{r})$ and $D(\mathbf{r})$, where $S = S(\mathbf{r}, t)$ is the source function. There has been a considerable interest in the possibility of recovering the functions $\alpha(\mathbf{r})$ and $D(\mathbf{r})$ using multiple source-detector pair intensity measurements with the application to biomedical imaging.

In a typical experimental set up, the imaged medium is located between two measurement planes $z = 0$ and $z = L$ and is characterized by deviations of the absorption and diffusion coefficients, $\delta\alpha(\mathbf{r})$ and $\delta\alpha(\mathbf{r})$ from the constant (known) background values. We have recently proposed [PRE 64(3), R035601 (2001)] an explicit inversion formulas for the linearized (in $\delta\alpha(\mathbf{r})$ and $\delta\alpha(\mathbf{r})$) inverse scattering problem for the diffusion equation with general boundary conditions imposed on the measurement planes. These inversion formulas are computationally efficient and can be regularized to make reconstructions stable in the presence of noise. However, these inversion formulas require knowledge of *complete data*, i.e., continuously measured over the infinite planes. In practice, the data are samples on a square grid with step h and dimension $W = Nh$, where N is an integer. The influence of the parameters h and N on the resolution of diffusion tomography is an important practical question. We have generalized our approach for the case of finitely sampled data and studied systematically resolution limits.

In this talk we will review the reconstruction algorithm and its generalization for the case of discrete data, and discuss the results of numerical simulations. We show that the fundamental limit (in the absence of noise) of transverse resolution scales as the the transverse separation between nearest sources (detectors) and can be as small as $\lambda_{\text{diff}}/40$, where λ_{diff} is the diffuse wavelength. The depth resolution is strongly influenced by noise and in the absence of noise - by the numerical precision of the computer.

A Generalized Numerical Scheme for Light Scattering and Absorption by Particles in a Dielectric Medium: Finite-Difference Time Domain Technique with a Uniaxial Perfectly Matched Layer Absorbing Boundary Condition

W. Sun and N. G. Loeb
Center for Atmospheric Sciences, Hampton University
Hampton, VA 23681 2199, U.S.A.

Q. Fu
Department of Atmospheric Sciences, University of Washington
Seattle, WA 98195 1640, U.S.A.

The three-dimensional (3D) finite-difference time domain (FDTD) technique has been extended to simulate the light scattering and absorption by nonspherical particles embedded in a dielectric medium. A uniaxial perfectly matched layer (UPML) absorbing boundary condition (ABC) in Sacks et al. (1995) is used to truncate the computational domain. We have formulated a numerical scheme to represent the propagation of an incident plane-wave pulse in a homogeneous dielectric medium. We have also used an equalization factor in the FDTD scheme to reduce errors related to the numerical dispersion.

A Mie solution for light scattering and absorption by spherical particles in an absorbing medium developed by Fu and Sun (2001) is used to examine the accuracy of the UPML FDTD program. We have examined the particle internal fields and absorption efficiencies. It is found that the global errors in the internal fields and the errors in the absorption efficiency from the UPML FDTD are typically smaller than 1%. For light scattering by particles in free space, the UPML FDTD scheme shows the similar accuracy as our previous PML FDTD model (Sun et al. 1999), though the formulations of PML and UPML have different Gauss' Laws.

With the use of UPML ABC, the memory requirement for the absorbing boundary layer has been further reduced and the simulation can be done on a personal computer for a size parameter as large as 20. This generalized FDTD scheme might have potential applications to remote sensing of ocean color. The dynamic memory allocation feature of C++ makes this numerical model user-friendly and it is easy to be integrated into optical software for biological study and fiber optics applications.

Shape Reconstruction in Scattering Media with Voids Using a Transport Model and Level Sets

O. Dorn
Department of Computer Science, University of British Columbia
Vancouver, B.C. V6T 1Z4, Canada

A two-step shape reconstruction method for diffuse optical tomography (DOT) is presented which uses adjoint fields and level sets. The propagation of near-infrared photons in tissue is modeled by the time-dependent linear transport equation in 2D, of which the absorption parameter has to be reconstructed from boundary measurements of the outgoing flux. In the shape reconstruction approach, it is assumed that the inhomogeneous background absorption parameter and the values inside the obstacles (which typically have a high contrast to the background) are known, but that the number, sizes, shapes, and locations of these obstacles have to be reconstructed from the data. An additional difficulty arises due to the presence of so-called clear regions in the medium.

The first step of the reconstruction scheme is a transport-backtransport (TBT) method which provides us with a low-contrast approximation to the sought objects during the early iterations. The second step uses this approximate result of the TBT method as the starting guess for an iterative shape reconstruction routine. Since the number of obstacles which we are looking for is not known a priori, topological changes of these shapes typically occur during the iterations and a flexible tool for tracking the boundaries of the shapes is therefore of great importance for the success of the reconstruction method.

We have chosen to use the *level set technique* for describing the moving shapes, since this method is able to easily model topological changes of the boundaries. In this technique, the shapes are given as the zero level set of a higher dimensional level set function f, which in our case is a function from $\mathbf{R}^2$ to $\mathbf{R}$. Those points $x \in \mathbf{R}^2$ where $f(x) = 0$ define the boundaries of the shapes. If we change the function $f(x)$, for example by adding an update $\delta f(x)$, we move the shapes accordingly. This relation is used in the level set technique when constructing updates $\delta f(x)$ to a given level set function $f(x)$ such that the shapes are deformed in a way which decreases a given cost functional.

Numerical experiments in 2D are presented which show that this novel method is able to recover one or more objects very fast and with good accuracy from time-dependent boundary data in situations where clear layers are present. In the talk we will also present a detailed sensitivity analysis of the TBT method which gives us valuable information about how to design the imaging experiment in an efficient way.

Scattering from Deformed Cylinders and Cylindrical Shells

A. Z. Elsherbeni
Electrical Engineering Department, The University of Mississippi
University, MS 38677, U.S.A.

True smooth surfaces can only exist in theory; thus every surface in nature has some kind of roughness that may affect its response to electromagnetic waves. Random roughness is very difficult to analyze; however, a specified class of roughness can be incorporated in many solution techniques to predict the corresponding electromagnetic response. In most of these attempts, it is cumbersome to compute the required data in a convenient time using moderate resources. In addition to the natural roughness, man made roughness involving specific patterns, usually called deformations or corrugations, are important to consider.

In this paper the scattering characteristics of periodically deformed cylinders and circular shells are presented. The scattering problem is two dimensional (2D) and the analysis is therefore suited to be investigated using scatterers that are generally constructed from a set of parallel circular cylinders. The problem of the scattering by parallel cylinders has been under continuous investigation for decades using different techniques. Among these, is the boundary value point matching technique which will be used for this investigation. Deformed scatterers of conducting, dielectric, or combinations of conducting and dielectric materials are examined. The excitation is represented by a plane wave, or a line source field for both TM and TE types of polarizations. For practical applications and experimental conditions, a bounded incident beam rather than the infinitely extended or omni-directional cylindrical wave should be considered. Therefore, this investigation is further extended to analyze the scattering from deformed scatterers excited by a 2D Gaussian beam. This type of excitation represents a more practical excitation than the plane wave or the line source field.

Sample of the numerical results obtained using this simulation procedure is shown in the Figure. The scatterer consists of a circular dielectric cylinder of radius equal to $0.45\,\lambda$ and $\varepsilon_r = 4$. The dielectric cylinder is partially coated by a corrugated metal sheet which is simulated by a circular arc deformed by a sinusoidal function and consisting of 63 perfectly conducting cylinders. The depth of deformation is $0.05\,\lambda$ and the thickness of the sheet is $0.015\,\lambda$. This composite geometry is excited by an incident plane wave propagating along the x axis. The polar plot shows the scattered field pattern for the dielectric cylinder alone along with the pattern of the partially loaded cylinder. The effect of the loading is clearly shown, specially in the backward direction.

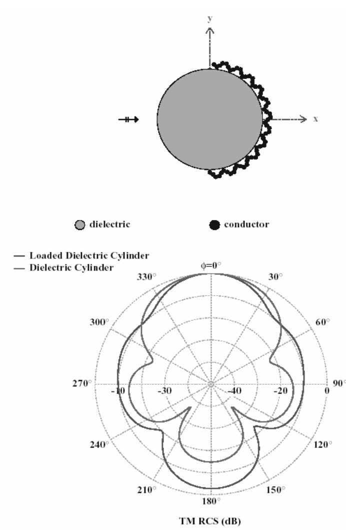

Imaging with Evanescent Waves

P. S. Carney
University of Illinois at Urbana-Champaign
Urbana, IL 61821, U.S.A.

D. G. Fischer
NASA Glenn Research Center
Cleveland, OH 44135, U.S.A.

J. C. Schotland
Washington University in Saint Louis
St. Louis, MO 63130, U.S.A.

Inverse scattering, three-dimensional imaging, and tomography, have repeatedly added greatly enhanced capability to existing imaging and spectroscopic modalities. Examples abound: the paradigm shift from X-ray shadow-grams to computed tomography; from magnetic resonance spectroscopy to magnetic resonance imaging; from X-ray diffraction to crystallography; from optical microscopy to optical coherence tomography; and many more. In microscopy, the classical Abbe-Rayleigh resolution limit of order λ may be overcome in the modalities which fall under the broad umbrella known as near-field optics (NFO) [1]. These modalities include near-field scanning optical microscopy (NSOM), photon scanning tunneling microscopy (PSTM), and an array of variations on the techniques. The ability to form images on subwavelength scales is important in number of applications where conditions dictate the use of a probe field whose free-space wavenumber is much smaller than the spatial frequencies attributable to the features of interest in the sample.

There has been recent progress made in bringing tomographic capabilities to the NFO modalities. In recent investigations of the information content of the optical near-field, it was demonstrated that the high spatial-frequency Fourier components of the scattering object are encoded in the scattered field components [2]. An explicit solution to the three-dimensional inverse problem has been presented for several modalities within the context of a scalar model for the field [3]. It is the presence of evanescent waves in the NSOM and PSTM modalities which makes possible the formation of subwavelength resolved images. Such waves are also generated and used to probe samples in the dark field technique known as total internal reflection microscopy (TIRM). Since TIRM makes use of evanescent waves to probe the sample, it offers a means to control the depth of penetration of the illuminating field into the sample. The super resolved imaging capability of the instrument however remains largely untapped.

We present an analysis of the inverse scattering problem for the TIRM experiment. The results enable a technique we call total internal reflection tomography (TIRT). We take into account the polarization effects as well as the effects of the presence of the boundary at the surface of the prism. We will also report on the progress being made in the experimental efforts in TIRT.

REFERENCES

1. M. A. Paesler and P. J. Moyer, *Near Field Optics*. Wiley, New York, 1996; J.-J. Greffet and R. Carminati, Prog. Surf. Sci. **56**, 133 (1997).
2. D.G. Fischer, J. Mod. Opt. **47**, 1359 (2000); D.G. Fischer, Opt. Lett. **25**, 1529 (2000).
3. P. S. Carney and J. C. Schotland, Opt. Lett. **26**, 1072, (2001); P. S. Carney and J. C. Schotland, Appl. Phys. Lett. **77**, 2798, (2000); P. S. Carney, V. A. Markel and J. C. Schotland, Phys. Rev. Lett., **86**, 5874 (2001).

Electromagnetic Scattering by Two External Spheres, One with Small Radius

J. A. Roumeliotis and V. Douvalis
Department of Electrical and Computer Engineering
National Technical University of Athens
Athens, 15773, Greece

The scattering of a plane electromagnetic wave by a dielectric or metallic sphere external to another one, also dielectric or metallic, of electrically small radius, is examined. The method of separation of variables is used, in conjunction with translational addition theorems for spherical vector wave functions. The sphere radii are R_1 and R_2, respectively, while d is the distance between their centers O_1 and O_2 origins of two cartesian coordinate systems with parallel axes. The origin O_2 lies at the general position (d, θ_0, φ_0) of the system $O_1x_1y_1z_1$. We examine first the scattering from the sphere with radius R_1, being alone in the space, i.e. in the absence of the second sphere with small radius R_2 (unperturbed problem) and next the scattering in the presence of the second small sphere (perturbed problem). In the latter case the initial unperturbed fields $\vec{V}(0)$ are slightly perturbed and expressed in the form $\vec{V} = \vec{V}(0) + \delta\vec{V}$, where $\delta\vec{V}$ is the first order perturbation of $\vec{V}(0)$, due to the presence of the second small sphere, which is expressed analytically. Analogous forms are obtained for the various scattering cross sections, with analytical expressions too. Their first order perturbations are proportional to R_2^3. By the formulas derived in this work we can easily calculate the scattering cross sections for each small value of the ratio R_2/R_1, if the other parameters of the problem remain constant. The correctness of our results is checked by the use of the forward scattering theorem, for various values of the parameters.

Inverse Electromagnetic Source Problem Using the Delayed Time-Domain Boundary Integral Method

S. Alestra, E. Duceau, G. P. Piau, and I. Terrasse
Numerical Modeling Group and Hyperfrequency Group, EADS CRC
Suresnes, 92150, France

We consider the numerical resolution of electromagnetic scattering problem by a perfect conductive obstacle Ω, illuminated by a set of ponctual electric sources $\vec{E}_{inc}$. By using a boundary integral equations (BIE), the unknowns are the scattered field $\vec{E}^+$ and $\vec{H}^+$ in the exterior of Ω, satisfying Maxwell Time Domain equations with the null initial conditions and the perfect boundary conditions. By an appropriated extension of the fields inside Ω, the classical BIE electromagnetic unknown on the interface is $\vec{j} = [\vec{H} \wedge \vec{\nu}]$.

This integral equation (1st constrained equation) is solved in space by a surfacic finite element method. The boundary Γ of the object is meshed with N_h triangular elements. A P(div) discretization in space and a P1 discretization in time are used.

After discretization, we obtain a forward time marching matricial system. The corresponding numerical scheme is unconditionnaly stable and convergent. Moreover, all the electromagnetic matrices are real, sparse and symmetric.

Once the electric currents are known, the electric field outside the object can be computed, using the post treatment equation (2nd constrained equation). We suppose that the incident electric field E_{inc} is (I, the number of emitters):

$$E_{inc}^n = \vec{E}_{inc}(x, t_n) = \sum_{p=1}^{I} \frac{f_p(t_n - |x - x_p|)}{4\pi|x - x_p|} \qquad x_p \text{ is the emitter for the source } f_p$$

We denote by $E_{tot} = E_{diff} + E_{inc}$ the total computed electric field data for the source f_p and E_{obs} the total observed electric field data. The inverse problem is the identification of the emitter functions (f_p, for each time sampling $i : (f(i\Delta t))_p = f_p$) given the measured electric field E_{obs} for some points in near field.

Let K and $capt_k$, the sensors number and position, and (t_m) the time sampling data. The cost function is given by:

$$j(f_p) = J(E_{tot}(f_p)) = \frac{1}{2} \sum_{m=1}^{n} \sum_{k=1}^{K} (E_{tot} - E_{obs})^2 (capt_k, t_m)$$

The optimal source function $(f_p)_{opt}$ is given by $Minj(f_p) \forall f_p \in R^n$ under the two discretized direct constrained equations. We have been developing a robust time domain integral equation for wave propagation. The time scheme is unconditionnaly stable (no CFL restriction). That allows the use of a classical optimal approach for inverse and optimization procedure. Direct and adjoint codes have exactly the same properties. We show some examples of the validity and stability of the method. These first encouraging results can be applied to an Hyperfrequency dipole identification problem, an EMC identification or optimization problems for the protection of electronic devices from the effects of lightning, or the parasite source emitters identification problem.

Electromagnetic Scattering from Traveling Wave Along Aircraft Fuselage

H. Zhang
Beijing Electromechanical Institute
Beijing, China

B. F. Wang and D. H. Qin
Beijing University of Aeronautics & Astronautics
Beijing, 100083, China

In general, the surface of an aircraft is often coated with a thin lacquer layer for the protection of the fuselage from adverse environmental condition. It will lead traveling wave to happen along the surface of the aircraft. The propagation of a TM surface wave along a conducting plane with a thin layer of dielectric has been investigated by Attwood [1].The results of this analysis have shown that a thin film of dielectric (such as varnished aircraft) leads to a large increase in the concentration of the field near the surface. So far nearly all the computer-aided design (CAD)–based 3–D computer codes contains first-order & multiple bounces scattering effects. What is missing and urgently needed is a description of the scattering arising from traveling wave. Hence, in the computation of the Radar Cross Section (RCS) the effect of traveling wave has to be taken into account.

Based on the analysis of surface wave in case that the radar target is much large with respect to the observing wavelength, a method of computing scattering effect caused by traveling wave is provided. The method is summarized bellow.

1. A target is first constructed by using a solid geometry modeling package developed at Beijing University of Aeronautics & Astronautics called BUAA–RCSAS–CAD.

2. By neglecting the losses, the traveling wave currents is calculated as a sum of the individual contribution due to each classified plane surface having surface wave.

3. The back scattering fields of traveling current distributions can be calculated by Stratton-Chu equation in source-from region.

4. Contributions from all traveling currents are summed up at far-field observation point to give rise to the final scattered fields [3].

The above method is both general and flexible. The calculating results are in close agreement with the measured data for some typical rectangular sheet coated with a thin varnished layer. The validity of this method is verified by a simple example. Finally the numerical results for a given aircraft are given.

REFERENCE

1. Attwood, S. S., “Surface wave propagation over a coated plane conductor,” *J. Appl.*, Vol. 22, 504–509, April, 1954.

2. Collin, R. E., *Field Theory of Guided Waves*, McGRAW–HILL BOOK COMPANY, INC. 1960.

3. Matsuzuka, I. and K. Nagasawa, “Unidirectional patterns of traveling wave rectangular antenna.” *IEEE Trans. On AP*, Vol. AP-30, No. 4, July 1982.

Session 3Pc5

Scattering and Propagation in Periodic or Quasi-Periodic Structures

Conical Propagation of a Surface Plasmon Polariton Across a Classical Metallic Grating

M. Kretschmann, T. A. Leskova, and A. A. Maradudin
Department of Physics and Astronomy and Institute for Surface and Interface Science
University of California, Irvine
Irvine, CA 92697, U.S.A.

By the use of the homogeneous form of the reduced Rayleigh equation for the electric field above and on a two-dimensional rough metal surface in contact with vacuum, we obtain the dispersion relation for a surface plasmonpolariton propagating across a classical metallic diffraction grating when the sagittal plane is not perpendicular to the generators of the surface. This dispersion relation is given by the vanishing of the determinant of a pair of infinite order coupled matrix equations for the p- and s-polarized components of the electric field in the vacuum. It is exact within the domain of validity of the Rayleigh hypothesis on which its derivation is based. It is solved numerically for three different forms of the surface profile function: (i) a sinusoidal profile function; (ii) a symmetric sawtooth profile function; and (iii) a periodic array of parallel Gaussian ridges. The parameters characterizing the roughness of the grating profiles are such that small-amplitude perturbation is invalid for obtaining these dispersion curves. Particular attention is paid to the dependence of the position and width of the gap between the two lowest frequency branches of the dispersion curve that occurs at the boundary of the one-dimensional first Brillouin zone defined by the periodicity of the grating on the angle between the sagittal plane and the generators of the surface. It is found to decrease to zero as this angle increases from zero to $90°$, at which point the surface plasmon polariton is propagating parallel to the generators of the surface. The ability to vary the gap by changing this angle may be useful for the design of filters for surface plasmon polaritons.

Electromagnetic Scattering from Two-Dimensional Photonic Crystals Embedded in a Dielectric Slab

K. Yasumoto, H. Toyama
Department of Computer Science and Communication Engineering, Kyushu University
Fukuoka, 812-8581, Japan

Periodic dielectric or metallic structures are widely used in the design of frequency selective or polarization selective components in microwave and optical wave regions. Recently photonic crystals in discrete periodic system have received a growing attention because of their potential applications to narrow-band filters, high-quality resonant cavities, and substrates for antennas. A periodic array of cylindrical scatterers is a typical example of discrete periodic system. When the array is multilayered, it constitutes two-dimensional photonic crystals. We shall discuss here a very accurate and efficient method for analyzing the electromagnetic scattering from two-dimensional photonic crystals consisting of multilayered periodic arrays of circular cylinders embedded in a dielectric slab.

In the method, the reflection and transmission matrices for a set of space harmonics are first calculated for each periodic arrays in isolation. The matrices are expressed in terms of the lattice sums and the aggregate T-matrix of cylinders located within a unit cell. The lattice sums characterize uniquely a periodic arrangement of scatterers, and are independent of the polarization of the incident field and the individual configuration of scatterers. The details of scattering from each array element are included in the aggregate T-matrix, which is obtained in closed form for circular cylinders. The array elements per unit cell can contain two or more cylinders, which may be dielectric, conductor, gyrotropic medium, or their mixtures with different dimensions.

When the arrays are multilayered, the reflection and transmission matrices are concatenated to obtain the generalized reflection and transmission matrices for the entire layered system. This yields a recurrence formula for the generalized reflection and transmission matrices. The dimensions and configurations of cylindrical elements in different layers may be different so long as the array periods are identical over all layers. For an N-layered arrays, the recursion process requires $N-1$ times computations of inversion of matrices. When the layered system consists of identical arrays separated with equal distance, a concept of Floquet modes propagating in the layered direction is incorporated into the concatenation to calculate the generalized reflection and transmission matrices without using the recursion process. Most of the photonic crystals consisting of layered periodic arrays of circular cylinders can be efficiently analyzed by combining the recursion process with the concept of Floquet modes.

Propagation and Radiation Properties of 2D Photonic Band Gap Structures

P. Viktorovitch, C. Grillet, J. Mouette, X. Letartre, P. Rojo-Romeo, and C. Seassal
Ecole Centrale de Lyon Laboratoire d'Electronique (LEOM)
Ecully, Cedex 69131, France

M. Le Vassor d'Yerville, D. Cassagne, and J. P. Albert
Groupe d'Etude des Semiconducteurs, Universite Montpellier II
Montpellier, Cedex 05 34095, France

Photonic crystals (PC) are recognized as candidates to provide an effective control of light at micrometer size [1]. In particular, for applications in the fields of optical telecommunications and interconnects, they can be used to elaborate Photonic Integrated Circuits comprising sources, detectors, modulators, wavelength filters, and wave-guides.

As they can be fabricated on semiconductor layers using mature microelectronic and optoelectronic technologies, two-dimensional PC (2D PC) have recently been the subject of intensive theoretical and experimental investigations. In this case the vertical confinement is insured by index contrast with substrate and cladding layers. For example, an efficient confinement is achieved with semiconductor membranes suspended in air or bonded to a low index material such as silica [2-4].

Unfortunately, due to their finite height, 2D PC wave-guides can suffer losses if mode frequencies are above the so called "light line" of these confining materials, i.e. if guided modes can interact with radiated modes through the corrugation of the PC.

In this work, we emphasize the study of light propagation along single line defect PC wave-guide fabricated on an InP suspended membrane. Our approach consists in the study of both open and closed wave-guides. Closed wave-guides can be considered as a long linear cavity where Fabry-Perot oscillations of guided modes occur. We show that the resulting spectral response allows for the determination of the optical mode group velocity and propagation losses. Identification of the guided modes is obtained by comparison of experimental data with 3D plane-wave expansion (PWE) calculations. In particular, clear distinction can be made between lossy wave-guided modes, which can couple to radiative modes and loss-less modes which are allowed to propagate "below" the light-line.

Although considered as detrimental in the context of the development of Photonic Integrated Circuits based on 2D PC, it turns that the coupling of wave-guided modes to radiative modes can be usefully exploited for the manipulation of photons in free space. It is shown in this presentation that interaction of radiative and guided modes through a 2D PC, especially under conditions where the later correspond to extrema of the dispersion characteristics of the 2D PC, results in resonance phenomena which can be used practically for the development of passive (for example wavelength selective reflector) as well as active (for example cavity-less wavelength selective surface emitting optical sources).

REFERENCES

1. E. Yablonovitch, Phys. Rev. Lett. 58, 2059 (1987).
2. P. Pottier, C. Seassal, X. Letartre, J.-L. Leclercq, P. Viktorovitch, D. Cassagne, and C. Jouanin, J. Lightwave Technol. 17, 2058 (1999)
3. C. Monat, C. Seassal, X. Letartre, P. Viktorovitch, P. Regreny, M. Gendry, P. Rojo-Romeo, G. Hollinger, E. Jalaguier, S. Pocas, B. Aspar, Electron. Lett 37, 764 (2001)
4. X. Letartre, C. Seassal, C. Grillet, P. Rojo-Romeo, P. Viktorovitch, M. Le Vassor D'Yerville, D. Cassagne, C. Jouanin, Appl. Phys. Lett. 79, 2312 (2001).

Propagation in Photonic Crystal Waveguides

L. C. Botten, A. A. Asatryan[†], T. N. Langtry
Department of Mathematical Sciences, University of Technology
[†] also School of Physics, University of Sydney
Sydney, NSW 2007, Australia

R. C. McPhedran and C. M. de Sterke
School of Physics, University of Sydney
Sydney, NSW 2006, Australia

Waveguides may be introduced into two-dimensional photonic crystals (PC) by a channel defect, the most common example of which is removal of a line of scatterers that leaves a line shaped void. In this paper we present two theoretical models and the results of computational studies of propagation in photonic crystal waveguides.

In the first of these, an infinite waveguide is modelled as a structure characterised by plane wave reflection and transmission matrices $\mathbf{R}$ and $\mathbf{T}$ sandwiched between two semi-infinite PCs, each characterised by a reflection matrix $\mathbf{R}_\infty$ to form a resonant cavity. The calculations for Fig. 1, which shows dispersion curves for a family of waveguides, were generated from the solution of the eigenvalue equation $\det(\mathbf{I} - \mathbf{R}^2) = 0$ where $\mathbf{R}$, a function of wavenumber k and propagation constant β, is given by $\mathbf{R} = (\mathbf{I} - \mathbf{R}_\infty \mathbf{R})^{-1} \mathbf{R}_\infty \mathbf{T}$. The data in Fig. 1 corresponds to the ΓX direction for TM polarisation in a square lattice of period d, with a single cylinder of refractive index $\nu = 3$ and radius $a = 0.3d$ in each unit cell. The shaded regions correspond to modes of the perfect crystal where a line defect cannot have modes. Fig. 1 shows that multi-mode propagation arises in guides of sufficient width and that single mode propagation can be sustained even for very thin guides, with the dispersion curve approaching the upper band edge.

While this method is very useful in computing the dispersion properties of guides and in predicting the location of Fabry-Perot interference phenomena (e.g., nodal and antinodal separation in finite guides, and wavelengths of transmission maxima etc.), it is not a tool with which we may readily calculate energy properties.

Accordingly, we introduce an alternative technique in which we model a waveguide by a stack of cylinder gratings, each with multiple cylinders per cell and with the channel modelled by the absence of a cylinder. In this method, the cut-off frequency of the guide appears as a band gap of the photonic crystal constructed from the multi-cylinder grating layers. For long guides (i.e., stacks of sufficient length), the energy properties are governed by the propagating Bloch modes, facilitating a simple and elegant asymptotic analysis of the wave propagation within the guide and the calculation of reflection and transmission coefficients associated with impedance mismatches at their ends.

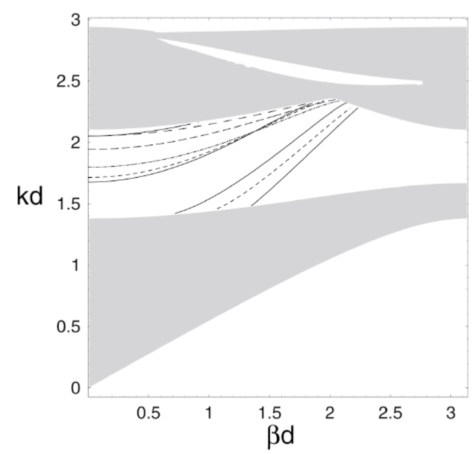

Figure 1: Waveguide dispersion diagrams showing normalised free space wavenumber kd vs normalised propagation βd constant for different thickness: Solid curve $h/d = 5$; short dashed $h/d = 3$; dash-dotted $h/d = 1$; long-dashed $h/d = 0.7$; medium dashed $h/d = 0.4$.

Sharp Filtering of Unpolarized Light by Gratings

D. Maystre, A. L. Fehrembach, and A. Sentenac
Institut Fresnel, Unité Mixte de Recherche, Faculté des Sciences et Techniques de St Jérôme
Marseille, Cedex 20 13397, France

The communication is devoted to a presentation of a phenomenological theory of sharp filtering by one-dimensional and two-dimensional diffraction gratings made by perturbing a planar dielectric waveguide. Sharp peaks in the reflectivity and transmittivity of such structures occur when the spatial and temporal frequencies imposed by the incident beam are close to that of an eigenmode of the structure. These anomalies have been widely studied in the case of classical one-dimensional gratings illuminated with in-plane mountings in particular when only one order is reflected or transmitted by the grating. It has been shown that the reflectivity of these gratings is in general close to that of the planar structure except for a sharp peak culminating at 100% corresponding to the excitation of a guided mode, at least for 1D shallow surfaces. This remarkable property may be valuable for light filtering, but unfortunately, it is limited to polarized light. In order to use this property for many technological applications of filtering, it has been suggested to use off-plane (conical) mounting or two-dimensional gratings in order to design filters for unpolarized light [3]. However, the main difficulty is to handle the large number of parameters describing these gratings, since the behavior of the reflectivity versus the wavelength, angle of incidence and incident polarization in the general vectorial case is still little understood. The aim of our work is to overcome this difficulty.

As in [1, 2], we study the behavior of the scattering matrix, that relates the incident beam to the reflected and transmitted beams, by using the notion of analytic continuation of complex functions of a real variable in the complex plane. To account for the polarization states of the beams,the scattering matrix is of size 4×4. The definition of poles and roots of the eigenvalues of hermitian matrices derived from this scattering matrix allows us to predict the performances of the structures for filtering of unpolarized light.

Our first result is that high efficiency filtering properties for unpolarized light is impossible to obtain if the incident light excites only one mode of the structure. Thus, it is necessary to design a grating that supports two independant modes for the same spatial and temporal frequency. This goal is reached with structures with symmetry properties illuminated under a direction of symmetry, when the two guided modes propagate in almost orthogonal directions. It is worth noticing that the filtering property reported in [3] is obtained in these conditions. This interesting property is interpreted in terms of Brewster effect and perturbation approach. Rigorous numerical results will confirm these theoretical predictions for some kinds of gratings.

REFERENCES

1. Maystre, D., “General study of grating anomalies,” *Electromagnetic Surface Modes,* A. D. Boardman (ed.), 661–724, John Wiley & Sons, Chichester, 1982.
2. Popov, E., L. Mashev, and D. Maystre, “Theoretical study of anomalies of coated dielectric gratings,” *Opt. Acta,* Vol. 33, 607–619, 1986.
3. Mizutani, A., H. Kikuta, K. Nakajima, and K. Iwata, “Nonpolarizing guided mode resonant grating filter for oblique incidence,” *J. Opt. Soc. Am.,* Vol. 18, 1261–1266, 2001.

Losses and Dispersion of Microstructured Optical Fibres

B. Kuhlmey, G. Renversez, and D. Maystre
Institut Fresnel, U.M.R. CNRS 6133
Marseille, Cedex 20 13397 cedex 20, France

The aim of the communication is to describe the results given by a rigorous electromagnetic theory of microstructured optical fibres (MOF). Our method based on multipole formulation was developed in the past few years and was recently generalized to MOF structures [1]. It can predict nearly all the properties of these structures, specially losses and dispersion properties. Our theory fully takes into account the finite size of the holes region in the fibre cross-section. Moreover, it can deal with MOF fibres surrounded by a cladding. For MOFs with regularly arranged holes, our formalism obeys the symmetry properties [2], so that no symmetry-breaking is induced. Furthermore, it has been adapted to take into account those symmetry properties to increase computational efficiency. Finally, our method uses the frequency as an input parameter, the output being the propagation constant. It is thus well-suited for calculations involving material dispersion.

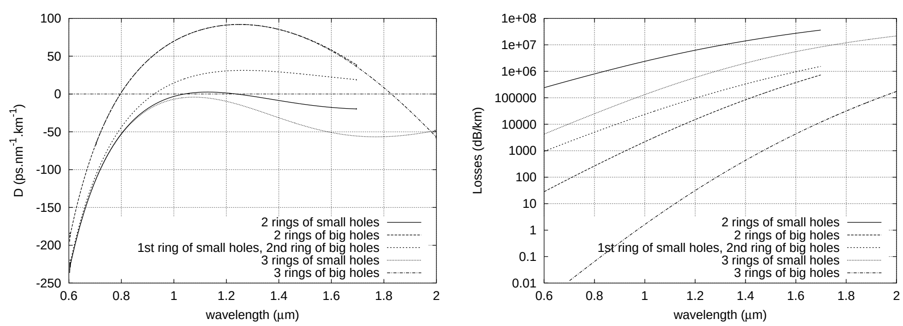

Figure 1: Dispersion and losses for different MOFs. The centers of the holes are regularly spaced on a triangular lattice. The core of the fiber consists of a missing hole in the middle of the MOF. The pitch is always $1.55\,\mu m$. Small holes diameter is $0.6\,\mu m$, big holes diameter is $1.0\,\mu m$.

The results we obtained for the dispersion are in very good agreement with published experimental measurements [3]. The great number of structural parameters defining a MOF (hole number, positions and diameters) enables a much more versatile control on dispersion properties than that obtained from conventional optical fibers. However in order to use these MOF in practical applications, both the dispersion and the losses should be studied. In figure (1), we show both the group velocity dispersion (GVD) and the losses for different MOF. As it can be seen multiple zero GVD wavelengths are found for a simple MOF but the corresponding losses are not acceptable. Nevertheless, the great set of dispersion curves we have computed allows us to believe that MOF structural parameters should provide a structure either with multiple zero GVD wavelengths either with a flatten nearly zero GVD but in all cases with low losses.

REFERENCES

1. B. Kuhlmey, T. P. White, *et al.* Multipole method for microstructured optical fibers I: formulation and II: implementation and results. *J. Opt. Soc. Am. B*, submitted.
2. P. R. Mc Isaac. Symmetry-induced modal characteristics of uniform waveguides-I: Summary of results. *IEEE Transactions on Microwave Theory and Techniques*, 23(5):421–433, 1975.
3. M. J. Gander, R. McBride, *et al.* Experimental measurement of group velocity dispersion in photonic crystal fibre. *Electronics Letters*, 35(1):63–64, 1999.

Coupled Cavity Systems Applied to PBG Waveguides

A. L. Reynolds
Nortel Networks UK Limited Harlow Laboratories, London Road,
Harlow, Essex CM17 9NA, UK

Considerable effort has and continues to be focused on exploring the properties of perfect photonic crystals with continuous waveguides placed within the crystal. By placing several defects within the crystals each of which can couple to at least its nearest neighbour a system of coupled cavities can be created. In this manner a small band of allowed transmission results creating a waveguiding mechanism in the photonic band gap region of the perfect crystal. These systems are attracting considerable interest due to their wavelength selectivity and the potential for device miniaturisation. By extending coupled cavity systems into 2- and 3-dimensional periodic systems many more degrees of control are afforded.

The spectral properties of such waveguides and devices are characterized by the nature of the defects and their spacing within the crystal, both broadband and narrow band devices can be created. However, while such systems are designed inherently for their transmission properties they have an associated inherent reflectivity. We present analysis of coupled cavity systems that form both straight and bent waveguides, a Y-shaped symmetric power splitter and for a waveguide incorporating two bends. We show that next nearest defect interaction is critical in governing the consequential reflection from a waveguide bend and that the criterion for a zero reflection system is stringent. For the simple Y-shaped power splitter we also find that the coupled cavity transmission system narrows the spectral range of the device. Furthermore the overall reflectivity of the crystal depends on the shape and type of interface of the crystal.

Bragg Fibers and Microstrutured Air-Silica Fibers for the Management of the Chromatic Dispersion : Modelling and Experimentation

J. Marcou, A. Peyrilloux, F. Bréchet, D. Pagnoux, P. Roy, and S. Février
IRCOM/CNRS, University of Limoges
123 Avenue Albert Thomas
Limoges Cedex, 87060, France

G. Melin
Alcatel Research and Innovation, Route de Nozay
Marcoussis, 91460, France

T. Chartier
CORIA/CNRS, University of Rouen
Rouen, France

The cancellation of the chromatic dispersion at short wavelengths into optical fibers is of great interest for telecommunications and non-linear optics applications. It can be achieved into two kinds of non-conventionnal fibers, with a quasi-periodic cladding structure theoretically and experimentally studied in this paper.

First, Bragg fibers with a cladding made of a quasi-periodic succession of concentric high and low index layers (transverse Bragg grating) and a low-index core are modelled by means of a cylindrical 2D Finite Difference BPM method, using the Wijnand's technique. We show that such fibers, in which the core index is lower than the mean index of the cladding, exhibit even no guiding or, at a proper wavelength, a single-mode propagation. With realistic values of the thickness of the layers and of the index difference between the layers, the index profile can be designed so to cancel the chromatic dispersion at wavelengths as short as $0.85\,\mu$m. A fiber with zero dispersion @$1.06\,\mu$m has been designed and manufactured. It has been experimentally demonstrated to propagate well-confined light into its low-index core. Its propagation characteristics (dispersion, attenuation, $\cdots$) will be presented at the conference.

The second kind of attractive fibers allowing a large management of the chromatic dispersion are the Microstructured Air-Silica (MAS) fibers. They consist in a regular quasi-periodic arrangement of some layers of thin holes (the "cladding") surrounding a pure silica core. These fibers are accurately and reliably modelled by means of a vectorial Finite Element Method. The field distribution and the effective index of the guided mode (and thus its effective area and its chromatic dispersion) are computed, taking into account the polarisation effects. It is demonstrated that the chromatic dispersion and its slope can be changed by adjusting the dimension of the air holes and the pitch between these holes. The experimental characterisations of different MAS fibers manufactured at the laboratory will be detailed at the conference.

Emission of Partially Coherent Light by Thermal Sources with Periodic Microstructures

J.-J. Greffet , R. Carminati, K. Joulain, F. Marquier, and J.-P. Mulet
Laboratoire EM2C, CNRS
Châtenay-Malabry, 92295 Cedex, France

S. Mainguy
Commissariat à l'Energie Atomique, Groupe Optique
Le Barp, 33114, France

Y. Chen
Laboratoire de photonique et de nanostructures, CNRS
Bagneux, 92220, France

It is usually taken for granted that light spontaneously emitted by different points of a thermal source cannot interfere. By contrast, different points of an antenna emit waves that interfere constructively in particular directions producing well-defined angular lobes. The intensity emitted by a thermal source is the sum of the intensities emitted by different points so that it cannot be directional. However, it has been shown recently by Carminati et al. (1999) and Shchegrov et al. (2000) that some thermal sources may have a large coherence length and can be quasi monochromatic in the near-field. This paves the way for the construction of a thermal source that could radiate light within narrow angular lobes as an antenna instead of having the usual quasi lambertian angular behaviour.

In this paper, we report experimental measurements demonstrating that it is indeed possible to build an infrared antenna by ruling a grating on a polar material such as a semiconductor. Such an antenna radiates infrared light in a narrow solid angle when it is heated. A remarkable property of this source is that the emissivity is enhanced by a factor of 20 compared to the emissivity of a flat surface.

Another remarkable property is that its emission spectrum depends on the observation direction. This behaviour was first predicted by E. Wolf (1986) as a consequence of spatial correlations of random sources. This effect has been demonstrated experimentally for artificial secondary sources but has never been observed for primary thermal sources.

REFERENCES

1. Carminati R. and Greffet J.J., "Near-field effects in spatial coherence of thermal sources," *Phys. Rev. Lett.*, Vol. 82, pp. 1660-1663, 1999.
2. Shchegrov A., Joulain K., Carminati R. and Greffet J.J., "Near-field spectral effects due to electromagnetic surface excitations" *Phys.Rev.Lett.*, Vol. 85, pp. 1548-15451, 2000.
3. Wolf E., "Invariance of the spectrum of light on propagation," *Phys.Rev.Lett.*, Vol. 56, pp. 1370, 1986.

Session 3Pc6

Microwave Application of Photonic Bandgap Materials

The Excitation of Remarkably Non-Dispersive Surface Plasmons on a Non-Diffracting, Dual-Pitch Metal Grating

A. P. Hibbins and J. R. Sambles
University of Exeter
Exeter, EX4 4QL, England

C. R. Lawrence
QinetiQ, Structures and Materials Centre
Farnborough, GU14 0LX, England

A non-diffracting and dielectric filled metallic lamellar grating formed from three equally spaced grooves per repeat period is examined at microwave frequencies ($11.3 < \lambda_0 < 16.7$ mm). One of the grooves is slightly shallower than the other two and while it is the deep, short pitch component of this profile creates a flat-banded surface plasmon polariton (SPP) mode outside the light line, it is the shallow long pitch component that provides the necessary extra in-plane momentum to allow incident photons to couple to this high-momentum region of the dispersion curve. The net result is a structure that, when correctly orientated with respect to the incident beam, demonstrates remarkable angle-independent excitation of the SPP mode and selective absorption of the incident power, powerfully illustrating the potential of "designer" surfaces of very short pitch. Experimental observations, which have been recorded as a function of wavelength at seven different angles of incidence, show excellent agreement with the predictions from a rigorous coupled wave theory.

Microwave Reflectivity of a Dual-Pitch Non-Diffracting Metal Bi-Grating

M. J. Lockyear, A. P. Hibbins, and J. R. Sambles
University of Exeter
Exeter, EX4 4QL, United Kingdom

C. R. Lawrence
QinetiQ
Farnborough, GU14 0LX, United Kingdom

The excitation of self-coupled surface plasmons on zero-order gratings with large depth-to-pitch ratios has been shown to lead angle-dependent absorption of radiation [1]. In this present experimental study the surface plasmon modes supported by a much shallower, non-diffracting 90° bi-grating formed in an aluminium alloy substrate is explored. The grating profile consists of one shallow and two deep grooves per repeat period running in two orthogonal directions of a two-dimensional surface plane. The surface modes that propagate across the sample are characterised by studying the reflectivity from the structure as a function of the angle of incidence and the incident wavelength ($7.5 < \lambda_0 < 16.7$ mm). Compared to a dual-pitch mono-grating study [2], the bi-grating supports two remarkably angle-independent modes. In addition, a further, lower-energy mode is observed which is more dispersive, and exhibits band splitting. By comparing the experimentally recorded reflectivity measurements with those calculated using a finite element model and studying the electromagnetic fields at the resonant frequencies, the origins of each of the modes are explored.

REFERENCES

1. "Flat surface-plasmon-polariton bands and resonant optical absorption on short-pitch metal gratings", W.-C. Tan, T. W. Preist, J. R. Sambles, and N. P. Wanstall, *Phys. Rev. B 59*, 12661 (1999).
2. "The excitation of remarkably non-dispersive surface plasmons on a non-diffracting, dual-pitch metal grating", Alastair P. Hibbins, J. Roy Sambles and Chris R Lawrence, submitted for publication to *Applied Physics Letters* (November 2001).

Microwave-Tunable Photonic Bandgap Devices using Arrays of Ferromagnetic Nanowires

A. Saib and I. Huynen
Microwaves, Université Catholique de Louvain, Bâtiment Maxwell
Louvain-la-Neuve, B-1348, Belgium

Periodic inclusions having adequate dimensions in a planar substrate yield Photonic Bandgap effects at microwaves. We show that it is possible to tune the bandgap of microwave stopband filters by using a substrate containing a periodic array of ferromagnetic nanowires.

Topology under scope - It consists of a periodic arrangement of "nanowired zones" in a porous polymer substrate (Fig. 1). Pores are vertical and distributed randomly, and have a nanosized diameter (Fig. 1b). A microstrip line is deposited on the top side of the substrate, while the back side is metallized to form a ground plane (Fig. 1a). Nanowired zones are distributed periodically along the length of the microstrip: each zone is formed by deposition of magnetic metallic nanowires inside the pores under the microstrip, over a length d. Ferromagnetic nanowires can be of different type: Ni(ckel), Co(balt), iron(Fe), NiFe alloy.

Simulations show that this topology has interesting stopband properties at microwaves. First, it has been shown that a microstrip line lying on a porous polymer substrate containing ferromagnetic nanowires has stopband properties. The stopband center frequency is a function of the kind of material filling the pores, and is tuned by applying a DC magnetic field. Next, the ferromagnetic material has an equivalent permeability which is higher than unity in the vicinity of the ferromagnetic resonance frequency. Hence a periodic arrangment of nanowired zones of length d can yield a bandgap absorption. Its design is based on the equivalence between PBG and FBG. Figure 2 illustrates this new feature for Ni nanowires. The solid curve shows the transmission factor of the RF signal on a micro-strip line lying on a fully nanowired substrate (d equal to length of microstrip): it shows a bandgap due to ferromagnetic absorption at 17 GHz. The dashed curves are simulated for a periodic arrangment of porous nanowired zones in the substrate. A second stopband occurs at 27 GHz: its center frequency does not shift when applied DC magnetic field varies from 5 kOe to 7 kOe. The first stopband is shifted, due to ferromagnetic resonance. Fig. 3 confirms the PBG nature of this second stopband: its position depends on the periodicity of the nanowired zones (number of sections over microstrip length).

From these results, a set of potential applications is currently investigated: the position of zeros in multiple stopband filter responses can be tuned by combining PBG effects and ferromagnetic resonance. Also, simulations show that such a combination may also occur above 40 GHz. Finally, the random pore distribution in Fig. 1 corresponds to the technology now available at UCL, for future experimental validation. A better control of the patterning will allow a periodic disposition of nanowires, and should yield similar effects at optical wavelengths, based on magnetooptic interactions in nanowires.

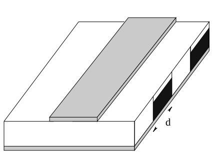

Fig. 1a

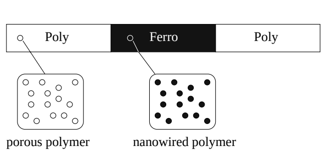

Fig. 1b

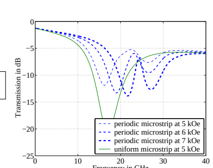

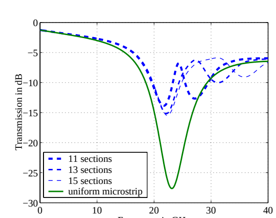

Applications of 1D Photonic Bandgap (PBG) Structures with Defects to Microstrip Circuits

A. Griol, D. Mira, A. Martinez, and J. Marti
Universitat Politècnica de València
València, Spain

Microstrip PBG structures have attracted great interest mainly due to its good performance and potential applications. A readily way to implement PBG microstrip structures consist on drilling a periodic pattern through the substrate or etching a one or two dimensional periodic pattern of circles in the ground plane of a microstrip line. PBG topologies show certain bands of frequencies where field propagation is not allowed (bandgap).

In this paper, novel nonperiodic patterns of etched circles in the ground plane of a 50 Ohm microstrip line are studied. The topologies are based on breaking the etched circles periodicity introducing some additional space between periodic circle patterns. This topology may be considered as the insertion of defects (small phase shifts) in the periodic circles pattern as depicted in figure 1.

The results show that a resonance appears in the bandgap when microstrip PBG structures depicted in figure 1 are used. The resonance depends on the defect's size (*ad; see figure 1*). The resonant mode is the only one that may exist in the defect and its propagation may be explained as the coupling of the microstrip line mode energy to the resonant mode in the defect by the evanescent field across the array of holes. As this basic structure (defect) is repeated along the microstrip ground plane, it is observed the splitting of the single defect resonance into n resonances, where n is the number of introduced defects. It is noticed that a complete passband inside the bandgap is formed due to the coupling of individual resonance modes when the defects number is high enough. This splitting effect may be explained by using the Tight-Binding formalist, which are applied to study the overlap of atomic wave functions in condensed-matter physics. This paper reports the verification of TB theory in microstrip technology. All the studied effects may be used in order to design different microwave and millimeter waves circuits such as diplexers, passband filters or channelisers.

In conclusion, different PBG microstrip structures have been studied and a good agreement between FDTD simulated and experimental results was obtained. These topologies are based on breaking periodicity of the circles pattern etched in the ground plane of a microstrip line. It has been demontrated that resonances in the bandgap appear obtaining a verification of TB theory for microstrip technology. This effect is proposed to design different microwave circuits. It is demonstrated that PBG microstrip circuits based on a periodic pattern of etched holes where some defects are introduced in the ground plane of a microstrip line may be designed.

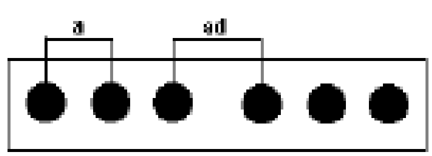

Figure 1: Ground plane for proposed PBG microstrip structure

Microstrip Multistage Coupled Ring Bandpass Filters using Photonic Bandgap (PBG) Structures for Harmonic Suppression

A. Griol, J. Marti, and J. L. Corral
Universitat Politècnica de València
València, Spain

There has been a growing interest in harmonic suppressed microstrip bandpass filters and resonators at microwave and millimetre wave frequencies. Several techniques for harmonic suppression in microstrip bandpass filters have been proposed, e. g. stepped impedance low-pass filters, notch filters located in the feeding lines or into the rings and also active components have been used to reduce harmonic levels. All these harmonic suppression techniques implies a modification in the microstip ring topology which introduces size penalties and manufacturing limitations.

In this letter, a smart technique for harmonic suppression based on using microstrip PBG structures is proposed and demostrated. PBG topologies show certain frequency bands where propagation of electromagnetic fields is not allowed (bandgap). This bandgap may be tuned in order to attenuate the harmonics characteristic of coupled ring bandpass filters. This PBG harmonic suppression technique does not imply a modification of the microstrip coupled ring structure avoiding size penalties or manufacturing limitations, because the PBG structure is achieved by etching a one dimensional periodic pattern of circles in the ground plane of the microstrip multistage ring bandpass filters.

Two topologies based on placing the PBG structures either into or out of the ground plane of the coupled rings have been considered and a performance comparison between both structures has been carried out. The embedded PBG structures were designed in order to set a notch filter at the second bandpass filter harmonic frequency. Both topology were FDTD simulated and implemented on a Rogers 6010 substrate with relative permitivity of 10.5. The results show that a very good bandpass filter response (insertion loss < 1.5 dB, return loss of ~ 15 dB) and harmonic suppression ratios over 35 dB may be achieved for both filter topologies.

In conclusion, a high increase in the rejection band of microstrip multistage coupled ring bandpass filters was obtained by using a technique based on using PBG structures for harmonic suppression.

Microstrip Circuit Applications Based on 1D Photonic Bandgap (PBG) Structures with Defects

A. Griol, D. Mira, A. Martinez, and J. Marti
Universitat Politècnica de València
València, Spain

Microstrip PBG structures have attracted great interest mainly due to their good performance and potential applications. A readily way to implement PBG microstrip structures consist of drilling a periodic pattern through the substrate or etching a one or two dimensional periodic pattern of circles in the ground plane of a microstrip line. PBG topologies show certain bands of frequencies where field propagation is not allowed (bandgap).

In this paper, novel nonperiodic patterns of etched circles in the ground plane of a 50 Ohm microstrip line are studied. The topologies are based on breaking the etched circles periodicity introducing some additional space between periodic circle patterns. This topology may be considered as the insertion of defects (small phase shifts) in the periodic circles pattern.

The results show that a resonance appears in the bandgap when microstrip PBG structure with one defect is used. The resonance depends on the defect's size. The resonant mode is the only one that may exist in the defect and its propagation may be explained as the coupling of the microstrip line mode energy to the resonant mode in the defect by the evanescent field across the array of holes. As this basic structure (defect) is repeated along the microstrip ground plane, it is observed the splitting of the single defect resonance into n resonances, where n is the number of introduced defects. It is noticed that a complete passband inside the bandgap is formed due to the coupling of individual resonance modes when the defects number is high enough. This splitting effect may be explained by using the Tight-Binding formalist, which are applied to study the overlap of atomic wave functions in condensed-matter physics. This paper reports the verification of TB theory in microstrip technology. All the studied effects may be used in order to design different microwave and millimeter waves circuits such as diplexers, passband filters or channelisers.

In conclusion, different PBG microstrip structures have been studied and a good agreement between FDTD simulated and experimental results was obtained. These topologies are based on breaking periodicity of the circles pattern etched in the ground plane of a microstrip line. It has been demontrated that resonances in the bandgap appear obtaining a verification of TB theory for microstrip technology . This effect is proposed to design different microwave circuits. It is demonstrated that PBG microstrip circuits based on a periodic pattern of etched holes where some defects are introduced in the ground plane of a microstrip line may be designed.

Photonic Crystal Components for Microwave Applications

I. Ederra, R. Gonzalo, J. J. Fernández, and B. Martínez
Electrical and Electronic Engineering Department, Universidad Pública de Navarra
Pamplona, Navarra E-31006, Spain

P. de Maagt
Electromagnetics Division, European Space Research and Technology Centre, ESTEC
Noordwijk, AG 2201, The Netherlands

This paper deals with the design of different passive Photonic Crystal (PC) components in planar parallel-plate technology at microwave frequencies. Photonic Crystals are periodic materials that show the interesting property of not allowing the propagation of electromagnetic waves in certain frequency ranges. During the last years they have been used in a wide range of applications. In the microwave range they have already been successfully used in filter and antenna applications. They have shown very promising features, which can overcome the limitations of current planar technology with respect to waveguiding losses, surface wave excitation and efficiency.

In order to get the most of this technology, a fully integrated receiver or emitter system should be developed in which all the components were designed using PC technology. The first step in order to achieve this goal is the design of the individual components.

The components, which will be presented in this paper, were based on a 2D rectangular lattice of air holes drilled in a dielectric which is sandwiched between a parallel plate waveguide. By using conventional microwave printed circuit technology the Photonic Crystal waveguide can be directly accessed by microstrip lines. Due to the natural transition from microstrip technology to the PC-waveguide the matching losses are very low in a wide frequency range, and the PC components can be easily integrated in microstrip circuits.

The different components are obtained by introducing defects in the 2D Photonic Crystal structure. Two different waveguiding mechanisms have been considered: producing a row of defects or coupling between local defects (Coupled Cavity Waveguide). Bends, couplers, resonators and filters have been designed using ANSOFT-HFSS software and several prototypes fabricated on a ROGERS 6010 substrate (dielectric constant of 10.2). Good agreement between simulation and measurements has been obtained and will be presented in this paper.

Application of Microstrip Ring for Tunable Photonic Bandgap Structures

M.-Y. Jang, L.-H. Fang, C.-S. Kee, I. Park, and H. Lim
Department of Molecular Science & Technology, and Division of Electronic Engineering, Ajou University
Suwon, 442-749, Korea

Microwave photonic band-gap (PBG) structures, which are usually implemented on the microstrip PBG plates, can be employed for various purposes such as to improve the performance of microwave antennas, increase the output power of microwave amplifiers, suppress higher order harmonics coming from resonators, and to design new type of duplexers. However, microwave PBG structures usually have a serious drawback coming from its quite large physical dimensions. Thus, some compact microstrip PBG structures have been proposed for the miniaturization. In this talk, we propose a new compact microwave PBG structure based on the microstrip ring with a narrow gap. The proposed structure does not require a periodic structure to obtain the PBG. Thus it is compact and needs only few design parameters. Moreover, the tunability of the PBG using externally mounted varactors can open new application of microwave PBG structure as microwave switches.

We show that the microstrip ring directly connected to the feed lines exhibits the PBG characteristics that is generally believed to be created by a periodic array, when a narrow gap is introduced in the ring. The multiple reflections with fixed phase correlations that is necessary to make the PBG come from the large impedance mismatch at the two sides of the narrow gap in the microstrip ring, and the stop band is formed around the center frequency whose quarter wavelength in the medium and its odd multiples are equal to the distance between the gap and the input feed point. Thus the center frequency of the first PBG generally decreases with the increase of the ring radius.

It is observed that the relative bandwidth of the first PBG, i.e., the bandwidth of the stop band divided by the center frequency, is observed to increase with the decrease of the ring radius for a given ring line width. To clarify the physical origin of this observation, the dependence of the center frequency and the line shape of the first PBG on the ring line width is extensively studied. From this study, it is found that the PBG center frequency at a given mean radius of the ring is determined mainly by the whispering gallery mode when the ring line width is rather narrow and then the influence of LC parameter of the ring increases with the increase of the ring line width. From the above observations, we have developed the way to increase the bandwidth of the stop band at a given center frequency by modifying the shape of the outer circumference of the ring. The center frequency and the line shape of the stop band can also be tuned by varying the capacitance or inductance value after a variable capacitor or inductor is mounted between the gap. The stop band increases (decreases) with the increase of the mounted inductance (capacitance).

Sub-Wavelength Planar Structures With Photonic Band Gap Effects

L. Zhou, W. J. Wen, J. Li, C. T. Chan and P. Sheng
Hong Kong Univ. of Science and Technology
Clear Water Bay, Hong Kong

Photonic band gap structures can reflect electromagnetic (EM) waves incident from all directions. Conventionally, such materials are constructed employing the ideas of Bragg scattering, which dictates that the periodicity is comparable to the wavelength. This means that the thickness and the lateral dimension of a functional photonic crystal slab must be a few times that of the wavelength. This restriction, which is a natural consequence of Bragg scattering, makes photonic crystal too bulky for many applications in the microwave and radio wave regime.

We show that a specific class of planar structures exhibits a series of intrinsic self-similar resonances, which give arise to series of alternating stop bands and total transmission bands for incident electromagnetic waves. We demonstrate both by theory and experiment that the planar structure behaves like a "sub-wavelength" photonic band gap material. It has frequency selective properties and can reflect certain ranges of frequencies while allowing near complete transmission for other frequencies. The frequency and the size of the stop bands are independent of the incident angle of the incoming EM wave. The size of the stop band can be increased substantially by stacking two of such planar structures together. This class of planar structure has an important sub-wavelength property, in the sense that it can reflect an electromagnetic wave with wavelength much larger than its all three dimensions. We will show both theoretical and experimental results which demonstrate that a small plate containing the planar structure, measuring 28x29x2mm, can shield microwave of 3.85 GHz in the forward direction generated by a whip antenna placed at 9mm from the plate. For comparison, a metal plate of exactly the same dimension failed to reflect the microwave when placed at the same configuration. It takes a substantially larger piece of metal to have the same reflection effect.

It is always desirable to have the ability to tune the optical property of a photonic band gap material by an external "nob". In principle, that can be achieved via non-linear effects, but the effect is typically too small in practice. We will show both numerical simulations and experimentally measured results that the transmission/reflection properties of the planar structure can be modulated by an external source.

Plasmonic Band-Gap Materials

A. K. Sarychev and V. M. Shalaev
Purdue University
West Lafayette, IN, U.S.A.

We show that metal nanostructures, such as a metal wire mesh [1] and metal spheres embedded in a dielectric host, can be employed as robust photonic band-gap materials, with large and scaleable gaps, for various applications in photonics [2-4]. A band gap in this case does not show much sensitivity to the periodicity because it occurs primarily because of the large and *negative* permittivity of metals. Thus, metals are intrinsically band-gap materials because of their negative permittivity and they can have a band gap even in random composites. We also show that because of a large skin effect in metals, which expels light from the metal structures, losses can be relatively small. This opens new avenues for fabricating low-loss robust band-gap metal structures with large gaps in various parts of the spectrum, including the visible and infrared.

We developed a first-principle theory for the effective dielectric permittivity in metal meso- and nanostructures. Our approach is based on the direct solution of the Maxwell equations (with the use of expansion in multipole series). We also found the band structure, transmittance, and losses in these plasmonic materials.

REFERENCES

1. J.B. Pendry, A.J. Holden, W.J. Stewart, I. Youngs, *Phys. Rev. Lett.*, 76, 4773 (1996)
2. A.K. Sarychev and V.M. Shalaev, *Phys. Reports*, 335, 275 (2000)
3. A.K. Sarychev, R.C. McPhedran, and V.M. Shalaev, *Phys. Rev.* B 62, 8531 (2000)
4. Andrey K. Sarychev and Vladimir M. Shalaev, arXiv: cond-mat/0103145 (2001).

Session 3Pc7

Rough Surface Scattering and Related Phenomena

Angular Spectrum Redistribution from Rough Surface Scattering

Z.-H. Gu
Surface Optics Corporation
San Diego, CA 92127-1441, U.S.A.

T. A. Leskova and A. A. Maradudin
Department of Physics and Astronomy and Institute for Surface and Interface Science University of California, Irvine
Irvine, CA 92697-4575, U.S.A.

In a series of papers [1] Wolf considered radiation from a three-dimensional quasihomogeneous source and showed that if the degree of spectral coherence of the source is suitably chosen, the spectrum of the emitted radiation can be redshifted or blueshifted with respect to that of the source, even if the radiation propagates in free space. Subsequently, Lagendijk [2] pointed out that the enhanced backscattering of light from a strongly scattering disordered medium, which is due to the coherent interference between multiply scattered optical paths and their time-reversed partners, can be regarded as due to the reemission of light from an extended source in the random medium that possess just the type of source correlation required to produce a Wolf redshift. In a theoretical study of changes in the spectrum of light multiply scattered from a system with a random surface [3], it was shown that these spectral changes can exhibit features that are absent in scattering from disordered volume systems, and can be much larger than the effect predicted for disordered volume systems. In this work we present experimental results for the angular spectrum redistribution resulting from the scattering of s-polarized light from a 5 mw AlGaInP diode laser source from one-dimensional random gold surfaces. The measured spectrum of the incident light is fitted by a Gaussian profile. The experimental results are compared with results obtained by means of rigorous computer simulations. The experimental and theoretical results agree in showing a red shift of the spectrum of the scattered light compared to that of the incident light. The shift is small, but measurable.

REFERENCES

1. Wolf, E., *Nature*, Vol. 326, 363, 1987; *Phys. Rev. Lett.*, Vol. 58, 2646, 1987; *Opt. Commun.*, Vol. 62, 12, 1987.
2. Lagendijk, A., *Phys. Lett. A*, Vol. 147, 389, 1990; *Phys. Rev. Lett.*, Vol. 65, 2082, 1990.
3. Leskova, T. A., A. A. Maradudin, A. V. Shchegrov, and E. R. Méndez, *Phys. Rev. Lett.*, Vol. 79, 1010, 1997.

Alternative Representations for Scattering from Periodic Surfaces

J. A. DeSanto
Department of Mathematical and Computer Sciences, Colorado School of Mines
Golden, CO 80401, U.S.A.

One method to describe the scattering from rough surfaces is to use integral equations. A version of these can be derived using Green's Theorem in a domain between the rough surface and a line (or plane) above the highest surface excursion. We illustrate the result for a periodicity of the fields. The result is a representation for the field in the domain in terms of integrals on the rough surface (involving the usual boundary unknowns of field and normal derivative for a scalar problem or currents for an electromagnetic derivative or currents). The usual integral equation formulation results from the domain field being set on the rough surface. There are several approaches of this type and they are well known.

Here we set the domain field on the line. The result is a representation of the scattered field on the line purely in terms of integrals over the rough surface involving the boundary unknowns. Using the periodic Green's function we can write this as a phased Fourier modal sum whose amplitudes are boundary integrals involving topological basis modes. In addition, the Green's theorem result can be evaluated outside the domain. If the evaluation is on a line below the lowest surface excursion the result is also a related to the incident field on this lower line. The set of equations can also be expressed in spectral space in several ways. Examples of Dirichlet, Neumann and transmission problems will be discussed.

Is Surface Scattering Caused by Fluctuations in Roughness Height or Slope?

N. M. Makarov
Instituto de Ciencias, Universidad Autónoma de Puebla
Puebla, Pue., 72050, México

Yu. Tarasov
Institute for Radiophysics and Electronics, NASU
Kharkov, 61085, Ukraine

In this contribution we discuss two essentially different mechanisms of surface scattering for quantum or classical waves. The first one is caused by fluctuations in local height of the roughness, while the other is due to fluctuations in roughness slope. According to this, we identify the *by-height* (BH) and *by-slope* (BS) scattering mechanisms that may well compete and lead to unconventional dependence of the wave scattering length on the r.m.s. height σ and correlation length R_c of the roughness as well as on other parameters of the problem.

We calculate and analyze the average transmittance for a plane waveguide with zero (Dirichlet) boundary conditions on both randomly rough edges of the waveguide. In order to separate properly the BH and BS mechanisms, it is convenient to solve the problem within a discrete representation of normal waveguide modes, which obey the exact boundary conditions and exist for any realization of the rough edges. In this representation the Hamiltonian for an n-th mode contains perturbation operators of two types. The first one is determined by local displacement of the edges from straight lines and is therefore responsible for the BH scattering. The other random operator depends on gradients of the roughness and describes the BS scattering. In accordance with the localization theory for one-dimensional disordered systems, the average transmittance of a single-mode waveguide exhibits ballistic behavior for small waveguide length L and shows exponential decrease as L exceeds the localization length L_{loc}. The BH and BS scattering operators contribute additively to the inverse localization length, $1/L_{loc} = 1/L_{loc}^{(BH)} + 1/L_{loc}^{(BS)}$. The BH length $L_{loc}^{(BH)}$ has the conventional dependence on σ and R_c as well as on average waveguide width d and longitudinal wave number $k_1 = \sqrt{k^2 - (\pi/d)^2}$. For Gaussian correlations we get

$$R_c/L_{loc}^{(BH)} \sim (\sigma/d)^2 (R_c/d)^4 \exp(-k_1^2 R_c^2)/(k_1 R_c)^2. \tag{1}$$

In particular, the inverse BH length is quadratic in the roughness r.m.s. height σ. At the same time, the inverse BS length shows an unexpected dependence on the parameters of the problem,

$$R_c/L_{loc}^{(BS)} \sim \begin{cases} (\sigma/R_c)^4 (R_c/d)^2 & \text{for} \quad R_c \ll d, \\ (k_1\sigma)^4 (R_c/d)^2 \exp(-k_1^2 R_c^2/2) & \text{for} \quad R_c \gg d. \end{cases} \tag{2}$$

Obviously, the value $L_{loc}^{(BH)}/L_{loc}^{(BS)}$ is highly sensitive to the statistical properties of the rough edges and can be in arbitrary proportion to the unity. The BS mechanism can be dominating (i.e., $L_{loc}^{(BS)} \ll L_{loc}^{(BH)}$) even for weak wave-surface scattering when the edge roughness is both low ($\sigma \ll d$) and mildly sloping ($\sigma \ll R_c$). If the BS scattering prevails, then the inverse localization length is proportional to the fourth power of the roughness r.m.s. height, $1/L_{loc} \propto \sigma^4$.

This research was supported by Consejo Nacional de Ciencia y Tecnología (CONACYT, México) grant 38072-E and by Universidad Autónoma de Puebla (BUAP, México) under grant II-63G01.

Localized Optical Excitations in Disordered Metal Surface

J. A. Sánchez-Gil
Instituto de Estructura de la Materia
Madrid, 28006, Spain

We study the physical mechanism underlying the appearance of localized optical modes upon illuminating a rough metal surface supporting surface-plasmon polaritons (SPP) with a laser beam. Localized optical modes give rise to strong and narrow (both in real and frequency space) concentrations of EM field intensity bound to the metal surface, and are thus believed to underlie surface nonlinear optical processes and surface-enhanced Raman scattering (particularly, *hot spots* which are candidates for single molecule detection sites).

First, we investigate whether such modes are connected with the phenomenon of Anderson localization of SPP, namely, whether there exist resonances linked to the Anderson localization of SPP that can be excited by both plane wave or SPP illumination. To this end, we perform numerical calculations on the p-polarized scattering from 1D randomly rough metal surfaces, on the basis of the k-space, integral equation formulation for the scattering amplitude obtained by the use of the impedance boundary condition. Both (physical) self-affine fractals and Gaussian-correlated profiles are considered with nanoscale (sub-100 nm) features. We observe intense optical modes when illuminating with a plane wave. However, no evidence of Anderson localization of SPP is found for the same finite surface profiles, with a SPP incident on one of its edges; or, at least, the localization length is larger than the profile length. The transmission coefficient decays very rapidly with increasing surface length due to radiation damping (rather than to Anderson localization). In addition, the frequency dependence of the SPP transmission coefficient shows no evidence of low-probability resonances.

Second, we analyze in detail the connection of localized optical excitations with surface features with the help of numerical calculations based on the Green's theorem integral equation formulation, in the case of a p-polarized Gaussian beam incident on 1D randomly rough surfaces as mentioned above. The scattered near EM field indicate that localized optical modes appear predominantly in two locations of the rough surface: crevices and ridges. Interestingly, the strongest modes on the randomly rough surfaces being studied are found at ridges for a wide frequency range (visible and near IR).

Emissivities and Back-Scattering Coefficients of Soil and Ocean at Microwave Frequencies Based on 3-Dimensional Numerical Simulations

L. Zhou, Q. Li, and L. Tsang†
University of Washington
†also City University of Hong Kong
Seattle, WA, U.S.A.

C. H. Chan
City University of Hong Kong
Hong Kong, P. R. China

K. S. Chen
National Central University
Chung-Li, Taiwan

The surfaces of ocean and soil are random rough in two-dimensional. The measurements of ocean and soil surface scattering and thermal emission at microwave frequency can provide the means to predict soil moisture and ocean wind velocity. However, the interactions of rough surfaces with microwave are still not understood because of lack of accurate theoretical results. Classical analytical theories of rough surface scattering are limited by inherent approximations and do not give the correct frequency and polarimetric dependence of electromagnetic wave scattering and emission. Neither can they be used to make quantitative comparisons with real-life experiments. On the other hand, numerical simulations can provide the accurate results by solving Maxwell's equations exactly. In this paper, numerical simulations are used to study the emissivities and backscattering coefficients of soil and ocean surfaces at microwave frequencies. The computational method used in the simulations is the sparse matrix canonical grid method (SMCG) combined with the physics-based two-grid method (PBTG), which is developed for the fast simulations of wave scattering and emission from lossy dielectric rough surfaces with large number of surface unknowns. The computer code has been implemented for parallel computation on low cost Beowulf PC clusters. The use of PBTG with RWG basis functions is to ensure that the emissivity can be calculated accurately For soil surfaces, the goal is to determine the frequency dependence and polarimetric dependence of scattering and emission of soil using the same physical roughness parameters for a variety of soil moisture and roughness conditions. Based on the simulation results, it is found that the brightness temperatures are higher at C band than at L band in horizontal polarization and lower at C band than at L band in vertical polarization with the same physical surface roughness parameters. Since the permittivities of wet soil with the same soil moisture are comparable at L and C bands, the surface roughness have a large effect on C band than at L band. The simulated backscattering coefficients are compared with the experimental measurements from real life soil surfaces. The power law spectrum is used to generate real life soil surfaces in the simulations. The reasonable agreements are obtained at multi-frequency bands and multi incidence angles. For ocean surface, the four Stokes parameters of emission and their azimuthal variations are simulated at 19 GHz. The frequency, polarimetric, and azimuthal dependence of ocean emission is studied in this paper.

Diffuse Scattering of Light from Characterized Surfaces

E. I. Chaikina, G. A. Navarrete, T. A. Leskova, and E. R. Méndez
División de Física Aplicada,
Centro de Investigación Científica y de Educación Superior de Ensenada, Apdo. Postal 2732
Ensenada, B.C. 22800, México

Wave scattering by randomly rough characterized metallic, dielectric and semiconductor surfaces is becoming increasingly important in various areas of research and applications. There is a considerable interest in experimental investigations of scattering properties of random surfaces with different statistical properties as a tool to test the validity of theoretical approaches to the scattering problem.

In this work we present experimental and theoretical studies of the scattering of light from randomly rough gold surfaces. We consider both one-dimensional and two-dimensional surfaces. The samples were fabricated in a photoresist, and their metallized surfaces constitute a good approximation to Gaussian-correlated, Gaussian random processes. The correlation lengths of both the one- and two-dimensional surfaces vary in the range 3–19 μm, and the standard deviations of the surface heights vary between 0.3 and $1.6\,\mu$m. The measurements were carried out for incident light of $10.6\,\mu$m wavelength and several angles of incidence. The angular distribution of the intensity of the light scattered diffusely from the two-dimensional surfaces is presented for various polarization combinations of the incident and detected light. Because the surfaces are only weakly rough, the experimental results are compared with the results of perturbation theories and the Kirchhoff approximation. The measured angular dependence of the intensity of the light scattered from the one-dimensional random rough surfaces is also compared with results of numerical simulations of the problem.

Scattering of Electromagnetic Waves from a Semi-Infinite, Inhomogeneous Dielectric Medium

R. M. Fitzgerald
Department of Physics, University of Texas at El Paso
El Paso, TX 79968, U.S.A.

G. Sewell
Department of Mathematics, University of Texas at El Paso
El Paso, TX 79968, U.S.A.

We consider an s-polarized plane wave of frequency ω, with plane of incidence the x_1x_3-plane, incident from the vacuum onto a dielectric medium characterized by a dielectric constant ϵ, that has a planar surface and a number of two-dimensional scatterers with dielectric constant ϵ_d distributed in its volume. The electric field satisfies:

$$\left(\frac{\partial^2}{\partial x_1^2}+\frac{\partial^2}{\partial x_3^2}+\frac{\omega^2}{c^2}\epsilon\left(x_3\right)\right)E_2\left(x_1,x_3|\omega\right) = \frac{-\omega^2}{c^2}\Theta\left(-x_3\right)\left(\epsilon_d-\epsilon\right)\sum_{i=1}^{N_{obj}}S\left(\mathbf{x}-\mathbf{x}_i\right)E_2\left(x_1,x_3|\omega\right),$$

where $\epsilon\left(x_3\right)=\Theta\left(x_3\right)+\epsilon\Theta\left(-x_3\right)$, $\mathbf{x}=\left(x_1,x_3\right)$, $\mathbf{x_i}=\left(x_{i1},x_{i3}\right)$ is the position of the ith defect, $\mathbf{S}(\mathbf{x})$ is the characteristic function of the defect, which equals unity if $\mathbf{x}$ is inside the cross section of the defect and zero otherwise, and $\Theta\left(x\right)$ is the Heaviside unit step function. The solution for the scattered electric field is

$$\begin{aligned} E_{2scatt}\left(x_1,x_3|\omega\right) &= \frac{\left(\epsilon_d-\epsilon\right)}{4\pi}\frac{\omega^2}{c^2}\int dx_1^{'}\int dx_3^{'}G\left(x_1,x_3|x_1^{'},x_3^{'}\right) \\ &\times\sum_{i=1}^{N_{obj}}S\left(\mathbf{x}'-\mathbf{x}_i\right)E_2\left(x_1^{'},x_3^{\prime}|\omega\right), \end{aligned}$$

where $G\left(x_1,x_3|x_1^{'},x_3^{'}\right)$ is the corresponding Green function.

Numerical calculations for the electric field and the cross section were performed for wavelengths larger than the size of the scatterers for the specific case of an ice medium containing volume inhomogeneities, and the results compared with those obtained from calculations using the Finite Element Method. The impact on the cross section of increasing the density of volume inhomogeneities is presented.

Subsurface Sensing of Targets Buried Beneath 2-D Multilayered Random Rough Surfaces: Use of the Steepest Descent Fast Multipole Method

M. El-Shenawee
Department of Electrical Engineering, University of Arkansas
Fayetteville, Arkansas 72701, U.S.A.

The scattering of electromagnetic waves from a penetrable shallow target buried beneath 2-D multilayered random rough surfaces will be presented. There are several applications for this work, e.g. detection of anti-personnel mines, anti-tank mines, water and/or gas pipes, location of underground water, etc. In reality, these targets are buried under the Earth's surface, which is a randomly rough interface and also is not simply composed of a single layer, but is a multilayered media. The closer the real environment is incorporated into the electromagnetic model, the more accurate and practical inferences can be gained from the numerical results. Without modeling the multiple ground layers, many targets *cannot be detected*. One unobtrusive way these buried targets can be detected is by bombarding the Earth's surface with electromagnetic waves, and comparing the scattered signature of the ground alone with that of the ground with the buried target.

A rigorous electromagnetic model based on the equivalence theorem and the method of moments (MoM) is developed to analyze this 3-D scattering problem. Three layers are considered in this work; air, dry-soil and wet-soil. The penetrable target is buried between the air/dry-soil interface and the dry/wet-soil interface. The Steepest Descent Fast Multipole Method (SDFMM) is implemented to significantly accelerate the computations of the unknown electric and magnetic surface currents. The effect of the lossy underground rough layer (wet soil) on the target signature will be investigated. Moreover, images based on the scattered electric fields for the buried target will be presented.

Propagation of Pulses in Waveguides With Rough Walls

V. Freilikher
The Jack and Pearl Resnik Institute of Advanced Technology
Department of Physics, Bar-Ilan University
Ramat-Gan, 52900, Israel

Yu. Tarasov
Institute for Radiophysics and Electronics, National Academy of Sciences of Ukraine
Kharkov, 61085, Ukraine

The propagation of quantum wave packets and pulses of electromagnetic radiation in disordered media is a classic problem with a long-standing history. The continued interest of physicists in this problem is stimulated both by the quest to better understand such fundamental problems of disorder as correlations in momentum-energy space, localization of time-dependent fields, Wigner time delay, etc., and also by the growing number of applications that pulsed signals find in modern electronics, communications, optics, and geophysics. Considerable theoretical and experimental investigations have been expended to study the propagation of pulses in randomly inhomogeneous media in diffusive regime. Much less studied is the space-time evolution of wave packets in disordered one-dimensional and layered systems where the interference of multiple scattered fields is of crucial importance. The typical example of one-dimensional random systems is a one-mode waveguide with rough boundaries. To explore the multiple scattering and localization effects in such a waveguide we have reduced the problem to studying the wave propagation in an infinite dielectric medium with the permittivity depending on one coordinate only. A narrow-band signal radiated by a point source in a randomly layered absorbing medium is studied asymptotically in the weak-scattering limit by means of the resonant expansion method. It is shown that in a disordered stratified medium that is homogeneous on average, as well as in a waveguide with cylindrical roughness, the pulse is channelled along the layers in a narrow strip in the vicinity of the source. The space-time distribution of the pulse energy is calculated. Far from the source, the shape of wave packets is universal and independent of the frequency spectrum of the radiated signal. Strong localization effects manifest themselves also as a low-decaying tail of the pulse and a strong time delay in the direction of stratification. The frequency-momentum correlation function in a one-dimensional random medium is calculated.

Quantum Chaos and Chaotic Scattering in Waveguides with Corrugated Surface

F. M. Izrailev
Instituto de Física, Universidad Autónoma de Puebla
Puebla, Pue, México

In this talk we discuss chaotic properties of waveguides with corrugated surface, by making use of methods developed in the theory of quantum chaos and in solid state physics. A particular interest is in waveguides with flat low boundary $z = 0$ and upper profile $z(x) = d + af(x)$ where $f(x)$ is assumed to be "random" enough and $< f(x) >= 0$, $< f^2(x) >= 1$, $a \ll d$.

In the case of one transverse mode, $N = 1$, this model is equivalent to a 1D solid state model with the potential $\phi(x)$ determined by the profile $f(x)$ [1]. The approach developed recently [2] for 1D tight-binding models allows the construction of such random potentials that result in perfect transparancy in a given range of wave vector k_x. The predictions have been confirmed experimentally on measurements of a transmission through single-mode microwave waveguides with inserted correlated delta-like scatters [3]. The application of this approach to waveguides with corrugated surfaces [1] reveals a non-trivial role of long-range correlations in $f(x)$, and shows how specific profiles that result in a selective transport, can be practically constructed.

For many channels, $N \gg 1$, the "rippled billiard" model with simple periodic profile $f(x) = \cos(2\pi x/L)$ has been studied in great detail in connection with classical and quantum chaos (see [4] and references therein). It was found that even in a deep semiclassical region corresponding to strong classical chaos, quantum eigenstates have remarkable regular properties. This phenomenon is due to an interplay between classical unstable periodic orbits and quantum coherent effects.

The analysis of this model is based on the canonical transformation to new coordinates, $u = x$, and $v = y/[d + af(x)]$. This allows the represention of the Hamiltonian in the form of two interacting "particles" moving in the billiard with flat boundaries. In this way, the effect of the corrugated boudary $f(x)$ is embedded in the interaction term. The important point is that this interaction depends both on $f(x)$ and on its derivative $f'(x)$.

We have studied how the structure of eigenstates of the periodic waveguide depends on the complexity of the profile defined as a sum of a number M harmonics with random amplitudes, $f(x) = \sum_l^M A_l \cos(2\pi lx/L)$ (with fixed variance of $f(x)$). One of the most interesting effects is that with an increase of M, the influence of the derivative $f'(x)$ increases, and for a very large $M = 100$, (analog of a "random" profile), even low-energy eigenstates are strongly modified. Another interesting effect is that there are huge fluctuations in the value of localization length of eigenstates, that do not disappear with an increase of energy.

REFERENCES

1. F.M. Izrailev and N.M. Makarov, *Optics Lett.*, Vol. 26, 1604, 2001.
2. F.M. Izrailev and A.A. Krokhin, *Phys. Rev. Lett.*, Vol. 82, 4062, 1999.
3. F.M. Izrailev, A.A. Krokhin, and S.E. Ulloa, *Phys. Rev. E.*, Vol. 63, 041102(R), 2001.
4. U.Kuhl, F.M. Izrailev, A.A. Krokhin, and H.J. Stoeckmann, *Appl. Phys. Lett.*, Vol. 77, 633, 2000.
5. G.A. Luna-Acosta, J.A. Méndez-Bermúdez, and F.M. Izrailev, *Phys. Rev. E.*, Vol. 64, 036206, 2001.
6. G.A. Luna-Acosta, J.A. Méndez-Bermúdez, and F.M. Izrailev, in preparation.

Inverse Problem for Rough Surface Scattering

A. G. Voronovich
Environmental Technology Laboratory/NOAA
Boulder, CO, U.S.A.

Retrieving parameters of rough surfaces based on information regarding the field scattered from the roughness represents an interesting and important practical problem. It can be considered both in deterministic and statistical formulations. The situation seems to be relatively simple (at least in principle) in the case of Bragg scattering, when there is a linear relation between scattered field and elevations or the roughness spectrum. However, in many cases, related, in particular, to geophysical remote sensing applications, Rayleigh parameter is large and Bragg scattering description is not valid. In these cases the relation between roughness and scattering amplitude (or scattering cross-section) is strongly non-linear, and analytical solution of the problem does not exist.

Still there is a possibility to get an analytic answer in the cases when the scattering can be adequately described in the Kirchhoff or the first order of the small-slope approximation. This can be done, for the expense of selection of a special set of scattering data. The solution makes use of a particular form of the expression for the scattering amplitude (or scattering cross-section) where elevations (or correlation function) enter into the exponent with a proportionality factor equal to the sum of vertical components of the incident and scattered waves. Then, if information regarding scattering amplitude is available for sufficiently broad set of incident and scattering angles, then the data should be selected that correspond to a fixed value of this parameter. Then application of the Fourier transform with respect to the other parameter, which is a difference between horizontal projection of the incident and scattering wave-vector will provide necessary inversion.

When only back-scattering measurements are possible, then the scattering data should be known within a sufficiently wide frequency band. When the frequency is fixed, then bi-static measurements are necessary. Possible practical approach to collecting a necessary set of scattering data for the case of scattering from the rough sea- or terrain surface will be presented.

Inverse Scattering of Layered Structures with Far-Field Amplitude Data

E. R. Méndez and D. Macías
División de Física Aplicada, CICESE
Ensenada, B.C. 22800, Mexico

The interaction of optical waves with rough surfaces and films has been a well-studied subject for many years. Much attention has been given to the direct problem of determining the angular distribution of the scattered light under given conditions of illumination. For this problem, rigorous numerical techniques that can model situations in which multiple scattering is important have been developed and are now routinely used for one-dimensional surfaces and films. On the other hand, the inverse problem is more complex and has received less attention. Previously [1], we have studied an algorithm to retrieve the profiles of dielectric and metallic one-dimensional rough surfaces. We have also developed a sampling strategy and studied the effects of noise on the reconstructions.

In this work, we explore the possibility of reconstructing the interior interfaces of multilayer objects. We show that to profile interior surfaces the algorithm must be modified. Moreover, the modifications must be adapted to the local depth of the interior layer. The proposed procedure is tested using scattering data corresponding to multilayer objects with one-dimensional roughness. The data was obtained numerically by solving the direct scattering problem using with an integral equation technique The approach is rigorous, and takes into account multiple scattering and the possible excitation of waveguide modes and surface plasmon-polaritons. We find that the algorithm is fairly robust but encounters difficulties when the interfaces have large slopes.

REFERENCES

1. Mací as, D., E. R. Méndez, and V. Ruiz-Cortés, *Scattering and Surfaces Roughness*, A. A. Maradudin and Z. H. Gu (eds.), Proc. SPIE 4100, 57–64, 2000.

Two-Dimensional Random Surfaces that Act as Circular Diffusers

T. A. Leskova and A. A. Maradudin
Department of Physics and Astronomy and Institute for Surface and Interface Science
University of California
Irvine, California 92697, U.S.A.

E. R. Méndez
División de Física Aplicada, Centro de Investigación Científica
y de Educación Superior de Ensenada
Ensenada, B.C. 22800, México

We propose a method for designing a two-dimensional random Dirichlet surface which, when illuminated normally by a scalar plane wave offrequency ω, scatters light with a circularly symmetric distrib ution of intensity. It is based on the geometrical optics limit of the Kirchhoff approximation, which yields the mean differential reflection coefficient in the form

$$\left\langle \frac{\partial R}{\partial \Omega_s} \right\rangle = \frac{1}{S}\left(\frac{\omega}{2\pi c}\right)^2 \int d^2u_\parallel \exp(-i\mathbf{q}_\parallel \cdot \mathbf{u}_\parallel) \times \int d^2x_\parallel \langle \exp[-ia\mathbf{u}_\parallel \cdot \nabla\zeta(\mathbf{x}_\parallel)]\rangle. \tag{1}$$

In this expression the angle brackets denote an average over the ensemble of realizations of the surface profile function $\zeta(\mathbf{x}_\parallel)$, S is the area of the plane $x_3 = 0$ covered by the random surface, $\mathbf{q}_\parallel$ is given in terms of the polar and azimuthal scattering angles by $\mathbf{q}_\parallel = (\omega/c)\sin\theta_s(\cos\phi_s, \sin\phi_s, 0)$, and $a = (\omega/c)(1+\cos\theta_s)$. The surface profile function $\zeta(\mathbf{x}_\parallel)$ is assumed to be a function of the radial coordinate $r = |\mathbf{x}_\parallel|$ alone, $\zeta(\mathbf{x}_\parallel) = H(r)$, and $H(r)$ chosen to have the form

$$H(r) = a_n r + b_n \quad nb \le r \le (n+1)b, \quad n = 0, 1, 2, \dots, \tag{2}$$

where the $\{a_n\}$ are independent random deviates, b is a characteristic length, and the $\{b_n\}$ are determined in such a way as to make $H(r)$ a continuous function of r

$$b_n = b_0 + (a_0 + a_1 + \cdots + a_{n-1} - na_n)b \quad n \ge 1. \tag{3}$$

We seek the probability density function (pdf) of a_n, $f(\gamma) = \langle\delta(\gamma - a_n)\rangle$ such that the resulting profile function yields a mean differential reflection coefficient of a prescribed form. The result is

$$f(\gamma) = 8\pi \frac{\gamma}{(1+\gamma^2)^2} \left\langle \frac{\partial R}{\partial \Omega_s} \right\rangle (\gamma), \tag{4}$$

where $\gamma = \tan(\theta_s/2)$. A long sequence of $\{a_n\}$ is determined from this pdf by the rejection method, and a realization of the random surface is then calculated from Eqs. (2) and (3). The method is applied to the design of a surface that scatters light uniformly within a circular region and produces no scattering outside this region, and a surface that acts as a Lambertian diffuser. It is tested by computer simulations, and a procedure for fabricating such surfaces on photoresist is described.

High Order Correlation from Rough Surface Scattering

Z.-H. Gu
Surface Optics Corporation
San Diego, CA 92127-1441, U.S.A.

There are similarities between *Universal Conductance Fluctuations* in mesoscopic conductors and rough surface scattering. There are three types of correlations which play different roles in multiple scattering regime. The short-range correlation $C^{(1)}$, also known as *Memory Effect*, is the dominant part in the system where the dimension size of the sample d is much larger than the thickness l, while the long-range $C^{(2)}$ and the infinite-range $C^{(3)}$ correlations take the dominant part when $l \geq d$.

We will report the measurement of high order correlations for a 1-D rough dielectric film on a glass substrate, the thickness of photo-resist is about 5 μm, while the thickness of glass is about 6 mm. When the laser beam size is reduced to 2-3 mm, which is comparable to the thickness of glass, $C^{(2)}$ and $C^{(3)}$ are measured. The measurements are comparable with theoretical prediction.

Session 3Pa8

Novel Mathematical Methods in Electromagnetics - III

3-D FDTD Analysis of Periodic Waveguide for Asymmetric Corrugation

T. Shibazaki and I. Matsuda
Tokyo Metropolitan College of Technology
Tokyo, Japan

T. Kinoshita
Tokyo Institute of Polytechnics
Kanagawa, Japan

For the composition of the delay circuit and filter, the periodic structure of the waveguide is well used. The authors have shown the efficient FDTD analysis method for the lossless waveguide with periodic structure [1]. This method has been expanded from the 2-D FDTD method [2], and is based on Floquet's theorem. First, the propagation constant of the waveguide β is given. Next, the periodic condition is adopted, and field equations are discretized. At this time, the analysis region of the periodic waveguide covers only 1 period. Therefore, the calculation capacity and calculation time can be drastically reduced. The $k-\beta$ diagram is obtained in the same way of 2-D FDTD method. In Ref. [1], we have analyzed the corrugated waveguide where the width of the rectangular waveguide changed. Comparisons have been made with the modal expansion method, and it is shown that both values agreed well. In this report, we analyze the propagation characteristics for asymmetric corrugation, and will show the effectiveness of our method at the frequency at which the higher modes can propagate.

The geometry for the corrugated waveguide is shown in Fig. 1. In the figure, the periodic structure is a tooth form that changes in the electric field direction of the TE10 mode. Each component of the electromagnetic field changes with $\sin(\pi y/a)$ or $\cos(\pi y/a)$ in the y axial direction. Each of them is assumed to be expressed as $E_x(x,y,z;t) = \sin(\pi y/a)E_x(x,z;t)$, $E_y(x,y,z;t) = 0$, $E_z(x,y,z;t) = \sin(\pi y/a)E_z(x,z;t)$, $H_x(x,y,z;t) = \cos(\pi y/a)H_x(x,z;t)$, $H_y(x,y,z;t) = \sin(\pi y/a)H_y(x,z;t)$, and $H_z(x,y,z;t) = \cos(\pi y/a)$ $H_z(x,z;t)$. Then, we obtain the field distribution by the equations (1) and (2) where the electric field $E(x,y,z;t)$ and the magnetic field $H(x,y,z;t)$ are described in propagation constant β for the direction of propagation. Here, Maxwells equations for the component that is not the zero of the electromagnetic field can be transformed by the equations (3)-(8). By approximating these equations in finite difference, equations of the successive approximation for the FDTD scheme are obtained.

$$E(x,y,z;t) = \mathrm{Re}[\mathbf{e}(x,y,z;t)e^{-j\beta z}] \quad (1)$$

$$H(x,y,z;t) = \mathrm{Re}[\mathbf{h}(x,y,z;t)e^{-j\beta z}] \quad (2)$$

$$-\frac{\pi}{a}h_z - \frac{\partial h_y}{\partial z} + j\beta h_y = -\varepsilon\frac{\partial e_x}{\partial t} \quad (3)$$

$$\frac{\partial h_y}{\partial x} - \frac{\pi}{a}h_x = \varepsilon\frac{\partial e_z}{\partial t} \quad (4)$$

$$\frac{\pi}{a}e_z = -\mu\frac{\partial h_x}{\partial t} \quad (5)$$

$$\frac{\partial e_x}{\partial z} - j\beta e_x - \frac{\partial e_z}{\partial x} = -\mu\frac{\partial h_y}{\partial t} \quad (6)$$

$$-\frac{\partial e_z}{\partial x} = -\mu\frac{\partial h_y}{\partial t} \quad (7)$$

$$-\frac{\pi}{a}e_x = -\mu\frac{\partial h_z}{\partial t} \quad (8)$$

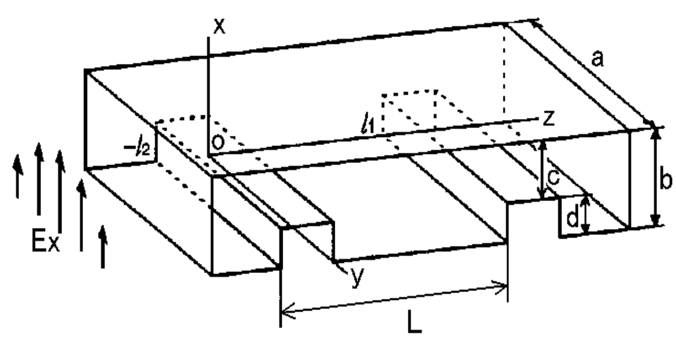

Figure 1: The geometry for the corrugated waveguide.

REFERENCES

1. T. Shibazaki, I. Matsuda, and T. Kinoshita, *FESS-MMNA'01*, August 2001, Nakhodka, Russia.
2. S. Xiao, R. Vahldieck, and H. Jin, *IEEE Microwave Guided Wave Letters*, vol. 2, pp. 165–167, May 1992.

Scattering by Truncated Periodic Arrays via the Discrete Wiener-Hopf Method

F. Capolino
University of Houston
Houston, TX, U.S.A.

M. Albani
University of Messina
Messina, Italy

Modeling large truncated periodic arrays requires intense numerical effort due to the large number of array elements and because the convenient assumption of pure periodicity that permits the analysis of a single-periodicity cell is not valid. Several approximate techniques that use the periodicity information have been proposed in the past. Among those, in [L.Carin and L.B.Felsen, *IEEE Trans. AP*, **4**, 1993] a hybrid (ray)-(Floquet)-(MoM) efficient formulation have been used for an array of strips (2D case), however truncation effects were accounted for using a Kirchhoff approximation. Succesively, a 3D case (semi-infinite array of dipoles) have been studied in [F.Capolino et. al., *IEEE Trans. AP*, **1**, 2000] observing that truncation effects can be effectively modeled as Floquet wave-modulated-diffracted fields. These new localization properties have been used by A. Neto et al. [*IEEE Trans. AP*, **3**, 2000] and by O.A. Civi et al. [*Radio Sci.*, **2**, 2000], in numerical techniques based on a method of moments that uses basis functions shaped as FW-modulated-diffracted fields.

Here, the scattering fundamentals pertaining to semi-infinite arrays are analyzed analytically by a discrete Wiener-Hopf technique. 2D problems such as semi-infinite arrays of strips or slots, and 3D problems such as a semi-infinite linear array of dipoles are analyzed first. Then, formulation and results are generalized to the 3D case of a semi-infinite array of small radiators (e.g. dipoles), or more in general to a semi-infinite array of ”single-mode” elements. The discrete Wiener-Hopf technique has already been applied in [N.L. Hills and S.N. Karp, *Comm. Pure Appl. Math.*, **18**, 1965] to treat a semi-infinite grating of small cylinders under the hypothesis of electrically-large interelement spacing (this restriction is removed in our approach, and it represents only a limit case), and in [W. Wasylkiwskyj, *IEEE Trans. AP*, **3**, 1973] where the coupling between elements in a semi-infinite array is analyzed, without introducing the concept of diffracted terms and asymptotic trends.

The discrete Wiener-Hopf is implemented using a Z-transform of the sampled current distribution. The topology (singular points) of the z-spectral plane is shown explicitly by using the infinite Poisson summation formula. A complete correspondence between the discrete z-spectral representation and the standard continuous plane wave k_x-spectral representation is established in relation with the Wiener-Hopf solving procedure. Solutions for the two limit cases of large and small interelement spacings are automatically obtained from our formulation and will be addressed in details. Efficient analytic-numerical algorithms are analyzed for the factorization in the z-spectral plane. Asymptotics is performed via path deformation and SDP (steepest descent path) evaluation directly in the z-plane (showing the correspondence to the k_x plane). Asymptotic results are performed in a uniform fashion for both radiated fields and currents on the array elements, thus treating also the important transitional case, where a Floquet wave is close to cutoff (i.e. close to grazing propagation). The radiated field is then found asymptotically as a sum of Floquet waves with domain of existence bounded by shadow boundary planes plus diffracted fields arising from the truncation of the array.

Numerical Analysis of a Variable Slab Using Body Fitted Grid Generation Method with Moving Boundaries

M. Kuroda, N. Miura and R. Takahashi
School of Engineering
Tokyo University ofTechnology
Tokyo, Japan

A new numerical technique is proposed for the analysis of the electromagnetic waves transmitted through a tunable slab. The study of the electromagnetic field for a moving or a rotating body is an important problem for a realization of new optical devices or microwave devices as well as the electromagnetic probing of moving bodies. To model these devices, it is necessary to simulate the electromagnetic field distribution in dielectric materials with moving boundaries. Due to limitations of the conventional numerical technique, it was difficult to simulate these time dependent moving boundary problems. The proposed technique is based on the finite-difference time-domain method and a kind of grid generation. Employing the transformation with time factor it would be able to apply the grid generation technique to analyze the moving object. With such grid, the FD-TD method can be solved very easily on a square grid in a rectangular computational region regardless of the shape and the motion of the physical region. We have already applied this technique to the Poisson's equation, the Laplace's equation and the Navier-Stokes equation for the flow and the heat transfer problems and the electromagnetic problems This paper presents the general theory of body-fitted grid generation method with moving boundaries, where the relativistic motion is also taken into account. The numerical results of the phase shift of the electromagnetic wave transmitted through a tunable slab are demonstrated. This technique will be an important tool to simulate new optical devices or microwave devices.

Extended Physical Optics for Wedge Diffraction

S.-Y. Kim
Korea Institute of Science and Technology
Seoul, Korea

The geometrical theory of diffraction (GTD) has played the key role in analyzing high-frequency diffraction by perfectly conducting objects. In spite of some improved GTD versions, the applicability to the diffraction by penetrable objects has been hindered by the lack of rigorous diffraction coefficients of some canonical structures such as a penetrable wedge and a cone. In contrast, the physical optics (PO) consists of the geometrical optics (GO) terms and the edge-diffracted field, but its diffraction coefficients cannot satisfy not only the boundary condition but also the edge condition. Its improved version is called the physical theory of diffraction (PTD). However there is no systematic way to obtain the non-uniform currents of penetrable wedge and cone. In this paper, we suggest an extended PO including virtual rays in order to provide more accurate diffraction coefficients of composite wedge.

The diffraction by a composite wedge consisting of perfect conductor and lossless dielectric is formulated into the dual integral equations. At first, the uniform currents induced along the lit region of the wedge are expressed by the GO terms. Then one may easily obtain the conventional PO solution. In particular, the PO diffraction coefficients are expressed by finite series of cotangent functions, of which amplitudes and poles are equal to the amplitudes and propagation angles of the GO rays, respectively. This means that each ray corresponds one of the PO cotangent function completely. In case of diffraction by a perfectly conducting wedge, however, the PO and the exact diffraction coefficients are represented by two and four cotangent functions, respectively. To reconstruct the exact diffraction coefficients of a perfectly conducting wedge by employing the PO approximation, one may find two additional rays.

In this paper, an extended GO is implemented by sum of the ordinary rays in the physical region and the virtual rays in its complementary region. To construct a complete one-to-one correspondence of the extended GO and its PO diffraction coefficients directly, a new ray-tracing law applicable to the complementary region is developed in case of diffraction of a perfectly conducting wedge. Applying this new ray-tracing law to the diffraction by the composite wedge, we obtain an extended PO solution. To satisfy the null-field condition in the complementary region, the angular period of the extended PO diffraction coefficients is changed from 2π to $2\pi\nu$, where ν is the minimum positive value satisfying the edge condition at the tip of the composite wedge. Then the extended PO diffraction coefficients can be expressed into the closed form as finite series of cotangent functions. The validities of the extended PO are assured here.

An Exact Line Integral Representation for the PO Field from a Flat Perfectly Conducting Surface Illuminated by Elementary Dipoles

M. Albani
Universita' degli Studi di Messina
Messina, Italy

S. Maci
University of Siena
Siena, Italy

In this paper, a line integral representation for the PO radiation integral from a flat perfectly conducting surface, illuminated by an arbitrary oriented elementary electric dipole, is pre-sented. No restriction is imposed on the position of the source and of the observation point. The main application of this result is concerned with the acceleration of the numerical PO integration for electrically large surfaces. In spite of the fact that other solutions have been sug-gested in the literature by several authors, starting from the original, scalar work of Rubino-vitch [*J. Opt. Soc. Am.*, vol. 52, no. 6, pp. 717–718, June 1962], our final outcome appears quite simple, clearly interpretable, and easily applicable. A systematic attempt to express PO in terms of line integration, was due to Asvestas [*IEEE Trans. Antennas Propagat.*, vol. 34, no. 9, pp. 1155–1159, Sep. 1986]; his technique, based on a mathematical theorem, was applied by Johansen and Breinbjerg [*IEEE Trans. Antennas Propagat.*, vol. 43, no. 7, pp. 689–696, July 1995], which geometrically interpreted the Asvestas formulation, and expressed in explicit form the PO line integrand. However, the final result is constituted by a large number of in-volved contributions, that render their applicability quite cumbersome. For this reason there is still a motivation for investigating on simpler and easily applicable expressions. To this purpose, we remark that the exact incremental diffraction PO contribution (i.e., the integrand of the final exact line integral representation) is not unique; indeed, an arbitrary irrotational field can be added to the integrand without affecting the final closed contour integration. The exact formulation used here for spherical source dipoles, takes inspiration from both the procedure presented in [*J. Opt. Soc. Am.*, vol. 52, no. 6, pp. 717–718, June 1962] and in Breinbjerg [*IEEE Trans. Antennas Propagat.*, vol. 43, no. 7, pp. 689-696, July 1995] but is essentially different from both. From Johansen and Breinbjerg our procedure maintains the clever idea of the projection surface from the observation point on which the geometrical construct is based; from the original Rubinowicz scalar work [*J. Opt. Soc. Am.*, vol. 52, no. 6, pp. 717-718, June 1962] (re-addressed for the electromagnetic case by Sakina and Ando in [*IEICE Transaction on Communications*, September 2001] without including reactive incident field components) the present formulation preserves the elegant and physical appealing application of the equivalence theorem. The final outcome is a simpler, but nevertheless "exact", alternative to [*IEEE Trans. Antennas Propagat.*, vol. 43, no. 7, pp. 689-696, July 1995] of the incremental PO coefficients.

Application of Path Integral Methods in Seismo-Acoustic Wave Propagation and Inversion

L. Fishman
MDF International
Slidell, LA 70461, U.S.A.

Recently, de Hoop and co-workers developed a microlocal (asymptotic) seismic inversion algorithm for application in complex environments supporting multi-pathed and multi-mode wave propagation. This inversion is based on the Born/Kirchhoff approximation, and employs the global, uniform asymptotic extension, associated with Maslov, of the geometrical method of "tracing rays" to account for caustic phenomena. While this microlocal (asymptotic) seismic inversion approach has successfully inverted the multicomponent, ocean-bottom data from the Valhall field off the coast of Norway, accounting for severe focusing effects, it is still an inherently "high-frequency" approximation, which neglects wave effects, in addition to being incapable of treating the more rapidly-varying medium properties (as measured on the scale of a typical wavelength). This algorithm can be extended to incorporate wave phenomena in, ultimately, a nonlinear inversion scheme through the application of two constructions which are well-known (at least physically and from a formal mathematical viewpoint) in the wave propagation communities: (1) directional wavefield decomposition and (2) the generalized Bremmer coupling series.

While seismic wave propagation modeling is often most appropriately formulated in the time domain, numerical calculations are most often carried out, by computational necessity, in the frequency domain. In the frequency-domain formulation, the square-root Helmholtz operator is the focus of both the directional wavefield decomposition and generalized Bremmer coupling series constructions. This operator provides for the construction of the right- and left-traveling wavefield components, and, in exponentiated form, represents the formal, fundamental, one-way wavefield solutions (propagators) in the tracking of the multiple scattering in the generalized Bremmer coupling series. The application of phase space and path (functional) integral methods then provides for explicit, exact and uniform asymptotic constructions of the square-root Helmholtz operator symbol, and, subsequently, phase space path integral representations of the fundamental wavefield solutions. Taken together, these methods and constructions suggest a seismic inversion algorithm, which can be interpreted as a method of "tracing waves". The phase space path integral plays the primary role in what is essentially a multiple-sweep algorithm that "traces the wave constituents" in the environment.

As an alternative to the generalized Bremmer coupling series, the exact, well-posed, one-way reformulation of the elliptic Helmholtz equation, in terms of appropriate Dirichlet-to-Neumann (DtN) operators, provides for a complementary approach to seismo-acoustic wave propagation and inversion. The DtN operator, which generalizes the square-root Helmholtz operator, accounts for the fully coupled, two-way nature of the problem. The corresponding phase space path integral represents the multiple-scattering process in a single-sweep algorithm, unlike the case of the generalized Bremmer coupling series, and provides the basis for layer-stripping-type inversion algorithms. A final alternative formulation would be provided by the construction of an exact configuration space path integral representation for the Helmholtz Green's function.

This talk is intended to provide an overview of these methods, stressing the role of the path integral constructions, and intertwining some of the most recent results with the basic outline of the theory.

Session 3Pb8

Novel Mathematical Methods in Electromagnetics - IV

Scattering of Electromagnetic Waves by Inhomogeneous Dielectric Gratings with Perfectly Conducting Strip

T. Yamasaki, T. Hinata, and T. Hosono
Dept. Electrical Eng., College of Science and Tech., Nihon University
Chiyoda-ku, Tokyo 101-8308, Japan

Recently, the refractive index can easily be controlled to make the periodic structures such as optoelectronic devices, photonic bandgap crystals , frequency selective devices, and other applications by the development of manufacturing technology of optical devices. Thus, the scattering and guiding problems of the inhomogeneous gratings have been considerable interest, and many analytical and numerical methods which are applicable to the dielectric gratings having an arbitrarily periodic structures have been proposed. However, most the theoretical and numerical studies have considered the dielectric gratings. In this paper, the scattering of electromagnetic waves by inhomogeneous dielectric gratings with perfectly conducting strip are analyzed using the combination of improved Fourier series expansion method and point matching method.

In the grating region S_2 $(-d < x < 0)$, the permittivity profile $\varepsilon_2(x, z)$ is generally not separable with respect to the *x* and *z* variables. Main process of our method to treat these problems is as follows (1) The grating layer is approximated by an assembly of *M* stratified layers of modulated index profile with step size $d_\Delta(d/M)$. (2)Taking each layer as a modulated dielectric grating, electromagnetic fields are expanded appropriately by a finite Fourier series. (3) In the dielectric grating with the perfectly conducting strip region $(j < l < j + 1)$, see Fig.1(b), the electromagnetic fields are matched using point matching method for the boundary conditions between inhomogeneous dielectric region and metallic region. (4) Finally, all stratified layers include the metallic materials are matched using appropriate boundary conditions to get the inhomogeneous dielectric gratings with perfectly conducting strip.

Numerical results are given for the transmitted scattered characteristics for the case of incident angle and frequency by inhomogeneous dielectric gratings with perfectly conducting strip both TM and TE waves.

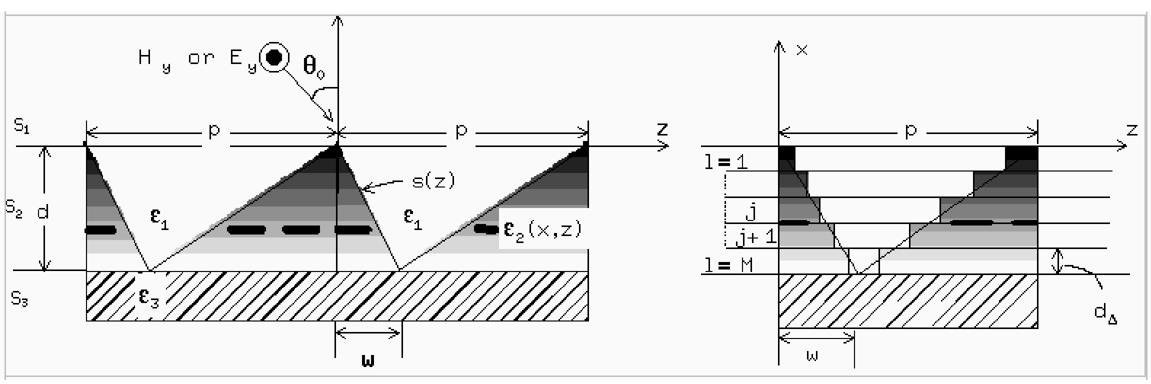

(a) (b)

Fig.1 Structure of columnar dielectric gratings consisting of inhomogeneous layer. (a) Coordinate system, (b) Approximated inhomogeneous layers.

Transmission Matrix Analysis of PBG Substrate Microstrip and Coplanar Circuits

A. S. Andrenko
Fujitsu Laboratories LTD.
Yokosuka, Japan

Over the last decade, photonic band-gap (PBG) structures have attracted a considerable interest in microwave and mm wave circuits and antenna applications. Among them are planar patch antennas on periodic substrates to increase radiation efficiency and eliminate surface wave excitation, design of broadband power amplifiers, and waveguide band pass filters. The PBG structures are usually being analyzed by using direct numerical methods and, taking into account the complexity of PBG configurations used, the EM simulations can be time consuming. On the other hand, the transmission matrix method is long known as a straightforward yet efficient tool for analyzing two-port microwave filters and circuits. This paper presents an analytical analysis of a PBG air-block periodic substrate microstrip and coplanar line circuits by the transmission matrix method and discusses the advantages of the structure considered for the design of active integrated antenna amplifiers and mobile communications transmitter front-ends.

In applying the transmission matrix approach to the analysis of a PBG rectangular air-block substrate configuration, the circuit is treated as a finite periodic structure and the F-matrix (transmission matrix) relating currents and voltages at the input and output ports is being derived. First, the F-matrix of one period element as a two-element microstrip over air block (or material implant) and conventional dielectric substrate is defined in terms of the characteristic line impedance and phase length. The total transmission matrix is then calculated as a matrix series product of all elements forming the periodic circuit. Next, S-parameters of the PBG periodic substrate microstrip/coplanar circuit can be obtained through A,B,C,D parameters of the total transmission matrix for deriving the analytical condition of passband $|S_{11}| = 0$ and that of stopband $|S_{11}| = 1$. These formulas can be further simplified by employing the condition of symmetry of a transmission circuit for the case of lossless structure and the reciprocity relation for a circuit with equal impedance input and output ports. If a PBG circuit consists of a few elements the conditions of passband and stopband are derived analytically whereas for a large number of elements the passband/stopband frequencies should be calculated by a numerical matrix multiplication. As a particularly important result, it was found that the number of passbands on the frequency axis from 0 Hz to the lower limit of stopband is always equal to the number of periodic elements forming the circuit while the stopband width depend on the period and length of substrate implants along the transmission line.

The formulas obtained here serve as a basis for analyzing stopband/passband properties of periodic PBG structures and contribute to efficient optimization of the PBG circuit design parameters. EM simulation results obtained offer a variety of applications of the periodic substrate PBG microstrip and coplanar circuits such as novel stopband filters and tuning elements in active integrated antenna amplifiers for transmitter front ends.

Scattering by a Dielectric Wedge for Oblique Incidence

E. Marx
National Institute of Standards and Technology
Gaithersburg, MD 20899-8212, U.S.A.

Electromagnetic scattering of an incident plane monochromatic wave by dielectric or finitely conducting infinite cylinders of arbitrary cross section can be reduced to the solution of scalar Helmholtz equations in two dimensions for the components of the electric and magnetic fields parallel to the generator of the cylinder as functions of the coordinates in the plane perpendicular to the generator. In the single-source integral equation method, two unknown boundary functions are required for oblique incidence and arbitrary polarization [1].

Sharp edges on the scatterer lead to divergent boundary functions for singular integral equations, a problem that is related to divergent fields components at the edge of a wedge [2]. A rigorous solution of the scattering by an infinite dielectric wedge might yield the asymptotic behavior of the unknown function at the edge of the wedge, which could then be used near the edge in computations. Nonrigorous solutions [3] provide an asymptotic behavior for the fields equal to that of static fields, which is not necessarily supported by numerical experiments. The field behavior cannot be immediately applied to the boundary functions. Alternatively, hypersingular equations, [4], [5], can be derived for boundary functions that tend to a constant at the edge, but the difficulties with the divergent unknown function are shifted to integration difficulties due to the higher singularity of the kernel. The behavior of the unknown boundary functions near edges affects mainly the fields near the boundary, while the far fields are less sensitive to the details of the approximation, although computed images of a broad dielectric strip on a substrate can present anomalies due to these divergences. The behavior of arbitrary static fields near the edge of a wedge has also been determined as functions of the angle of incidence of the corresponding scattering problem [6].

Numerical experiments for TE and TM modes generate fields near the edge of a finite wedge that agree only at times with the expected behavior [2], [5]. These numerical experiments are now extended to oblique incidence. Scattered fields near the edge are compared to static fields in a transition between the TE and TM modes for arbitrary direction of incidence and polarization, for both singular and hypersingular integral equations. The behavior of the unknown boundary functions near the edge for singular integral equations is also shown.

REFERENCES

1. E. Marx, "Scattering by an Arbitrary Cylinder at a Plane Interface," in *Radar Cross Sections of Complex Objects*, W. R. Stone, Ed., IEEE Press, pp. 356-370, 1990.
2. E. Marx, "Computed Fields Near the Edge of a Dielectric Wedge," *IEEE Trans. Antennas Propagat.*, vol. 38, pp. 1438–1442, 1990.
3. J. Meixner, "The Behavior of Electromagnetic Fields at Edges," *IEEE Trans. Antennas Propagat.*, vol. 20, pp. 442–446, 1972; G. I. Makarov and A. V. Osipov, "Structure of Meixner's Series," *Radio Phys. Quantum Electron.*, vol. 29, pp. 544-549, 1986.
4. R. E. Kleinman and P. A. Martin, "On Single Integral Equations for the Transmission Problem in Acoustics," *SIAM J. Appl. Math.*, vol. 48, pp. 307–325, 1988.
5. E. Marx, "Electromagnetic Scattering from a Dielectric Wedge and the Single Hy-persingular Integral Equation," *IEEE Trans. Antennas Propagat.*, vol. 41, pp. 1001–1008, 1993.
6. E. Marx, "Scattering by a Dielectric Wedge: Oblique Incidence" *1995 Digest of the IEEE Antennas and Propagation Society International Symposium*, pp. 1072–1075, 1995.

Application of Adaptive Multigrid Method to Eigenvalue Problem of Inhomogeneous Waveguide

M. Yokota
Department of Electrical and Electronic Engineering, Miyazaki University
Miyazaki, 889-2192, Japan

Numerical techniques such as FD-TD method, BPM, FEM and BEM are very important and useful for solving the propagation and the scattering problems for the complicated shapes. It is desirable to develop the rapid method to obtain the accurate solutions since the systems of equations are becoming large recently. The multigrid method [1], [2], which has been applied to the scattering problem [3] and the analysis of a microstrip line [4], is one of the fast solvers for the large system. The usefulness and the efficiency have been shown.

When we discretize the differential equation, the equally spaced grids are usually used for the simple structure. But when the geometry of the problem and/or the profile of the refractive index becomes complex, it is efficient that the size of the grid changes adaptively [5].

In this paper, the adaptive multigrid method is applied to the eigenvalue problem for the two-dimensional inhomogeneous waveguide. Both of TE and TM cases are formulated. The eigenvalue for the inhomogeneous waveguide is obtained as follows. At first, the initial electric field and the initial propagation constant are given, and then the propagated electric fields are obtained by the finite difference beam propagation method to which the multigrid method is applied adaptively. The size of the grid is selected in accordance with the profile of the refractive index. In this research, the fine grid is used when the index profile changes rapidly, and on the other hand, the grid size is coarse for the small refractive index difference. The propagation constant is updated by using the consecutive electric fields. This procedure is repeated until the propagation constant changes less than the criterion. The Hidgon absorbing boundary condition is used.

As the numerical examples, the effect of the distributions of the grids, the iteration numbers and the levels of the multigrid method on the eigenvalues is examined.

REFERENCES

1. W. H. Press, S. A. Teukolsky, W. T. Vetterling and B. P. Flannery, *Numerical Recipes in FORTRAN(2nd Edition)*, ch. 19, Cambridge University Press, 1992.
2. R. Hiptmair, "Multigrid method for Maxwell's equations", *SIAM J. Numer. Anal.*, vol. 36, pp.204-225, 1998.
3. D. J. Donohue, H.-C. Ku and D. R. Thompson, "Application of iterative moment-method solutions to ocean surface radar scattering", *IEEE Trans. Antennas Propagat.*, vol. 46, pp.121-132, 1998.
4. C. L. Tsai and W. S. Wang, "An improved multigrid technique for quasi-TEM analysis of a microstrip embedded in an inhomogeneous anisotropic medium", *IEEE Trans. Microwave Theory Tech.*, vol. 45, pp.678-686, 1997.
5. U. Rude, "Fully adaptive multigrid methods", *SIAM J. Numer. Anal.*, vol. 30, pp.230-248, 1993.

Solving the Electric Field Integral Equation Using the Method of Moments with Pulse-Basis Functions and Point Matching

R. A. Shore and A. D. Yaghjian
Air Force Research Laboratory/SNHA
Hanscom AFB, MA 01731, U.S.A.

Unlike the magnetic-field integral equation (MFIE), the conventional form of the electric-field integral equation (EFIE) cannot be solved accurately with the method of moments (MoM) using pulse-basis functions and point matching. It has been demonstrated that it is the highly singular kernel of the EFIE, rather than the derivatives of the current, that precludes the use of the pulse-basis function point-matching MoM. A new form of the EFIE has been derived whose kernel has no greater singularity than the free-space Green's function. This new form of the EFIE has been solved for a perfectly electrically conducting body of revolution (BOR) using the pulse-basis function point-matching MoM, and a computer program has been written to implement the solution. Derivatives of the current are approximated with finite differences using a quadratic Lagrangian interpolation polynomial. Bistatic radar cross section calculations performed for a perfectly conducting sphere and prolate spheroid demonstrate that reasonably accurate results can be obtained with the new lower-order singularity EFIE using the pulse-basis function point-matching MoM. However, like the original EFIE, the new lower-order singularity EFIE requires considerably more unknowns than are needed by the MFIE to yield the same accuracy. This increased point density is the result of using finite differences to approximate the first and second order derivatives of the current that appear in the lower-order singularity EFIE, whereas current derivatives do not appear in the MFIE.

Analysis of a Passive Circular Loop Antenna Radiating in the Presence of a Layered Chiral Sphere Using Method of Moments

L.-W. Li and M.-S. Leong
Dept. of Electrical & Computer Engineering, National University of Singapore
Singapore

W. X. Zhang
State Key Laboratory of Millimeter Waves, Southeast University
Nanjing, P. R. China

P.-N. Jiao
China Research Institute of Radiowave Propagation
Xinxiang, China

Characterization of electromagnetic waves in artificial and natural chiral media and fabrication of artificial chiral media have been two subjects that attract a lot of research interests of many scientists and engineers in over the past two decades. The considerable attention it receives is due to its versatility in microwave and millimeter wave applications such as waveguides, antennas, radomes, shielding, scatterers. From the previous studies, it has been found that the chiral media have a distinct feature of changing the polarization state of a radio wave. Due to this characteristic, the layered chiral media have been considered to be a good polarization transformer. Also, due to the electromagnetic coupling in the constitutive relations, not only the polarization state but also field strength and patterns are varied when a radio wave passes through, or is scattered by, a chiral medium.

On the other hand, the analysis of a thin circular loop antenna radiation has been another area of interests to many antenna engineers and academia. However, the performance of a loop antenna is seriously affected when its surrounding environment is changed, for instance, in the presence of a layered chiral sphere to be considered in this work. This thus motivates the present work. To formulate the current distribution along the loop wire and to obtain its field pattern, the method of moments is usually utilized regardless of presence or absence of an environment. However in the formulation of current distributions, some existing works made a wrong assumption which certainly leads to incorrect results. This work will clarify why the assumption is wrong in a comparative way.

In this paper, radiation patterns of a thin circular passive antenna, illuminated by a plane wave in the presence of a layered chiral medium, are obtained. The method of moments is employed in this work to formulate the current distribution along the circular loop out of a spherically layered chiral medium. The dyadic Green's functions defining electromagnetic fields are applied. In the Galerkin's procedure for the method of moments, basis functions used in the work are sine and cosine functions which form a Fourier series. The formulation itself here is quite compact, straightforward, and easy-to-use. Effects of various geometrical and dielectric parameters of the chiral medium are discussed. For different chiral medium parameters, waves and fields in such an electromagnetic system are characterized. Comparison of results obtained using the correct formulation and wrong assumption is made for correct and efficient analysis.

New Hybrid Method for the Electromagnetic Diffraction Problems

Yu. G. Smirnov
Penza State University
Penza, 440600, Russia

An exterior problem of electromagnetic wave diffraction by an arbitrary system of dielectric and perfectly conducting bodies is considered. A hybrid method is used that reduces the problem to a system of volume and surface equations in a finite space region. For the system of Maxwell's equations, the problem is not elliptic. An equivalent formulation of the original boundary problem is presented in the form of a system of Helmholtz equations. The system is proved to be elliptic.

In recent years, hybrid method have found increasing use in solving exterior problems of electromagnetic diffraction by a system of dielectric and perfectly conducting bodies. The idea of the hybrid method for solving the diffraction problem is as follows. An auxiliary closed surface is chosen that encompasses the system of dielectric and perfectly conducting bodies. Outside this surface, the solution to the problem is written in an explicit form in terms of surface potentials. Inside the surface, the problem is solved by a well-known method and then the exterior and interior solutions are joined with the help of coupling conditions. As a result, the equations inside the auxiliary surface (in volume) are supplemented by additional surface equations on the auxiliary surface, which is the reason why the method is named hybrid.

This method allows one to go from the exterior diffraction problem to an interior problem with additional surface equations. The main advantage of the method is that it is universal for diffraction by a system of bounded bodies. One of its major disadvantages is that the operator of the electromagnetic diffraction problem is not elliptic.

The goal of this paper is to provide a new formulation of the hybrid method so that the operator of the problem is elliptic. The theoretical foundations of such approach were developed also.

It is well known [4] that Galerkin method is convenient to obtain an approximate solution to an equation with an elliptic operator. In this case the necessary and sufficient condition for Galerkin method to be convergent is that it must possess the approximation property.

Numerical results for solutions of some diffraction problems are also presented.

Session 4Ac1

Measurements in Atmospheric Water Vapor

Radiosonde Humidity Soundings and Microwave Radiometers during Nauru99

E. R. Westwater[1,2], B. B. Stankov[2], D. Cimini[3], Y. Han[1]
J. A. Shaw[2], B. M. Lesht[4], and C. N. Long[5]

[1] University of Colorado, *Boulder, CO, U.S.A.*
[2] NOAA/Environmental Technology Laboratory, *Boulder, CO, U.S.A.*
[3] Università di L'Aquila, *L'Aquila, Italy*
[4] Argonne National Laboratory, *Argonne, IL, U.S.A.*
[5] Pacific Northwest National Laboratory, *Richland, WA, U.S.A.*

During June–July 1999, the NOAA R/V *Ron H. Brown (RHB*) sailed from Australia to the Republic of Nauru. On Nauru, the Department of Energy's Atmospheric Radiation Measurement (ARM) Program has set up a long-term climate observing station. The purpose of the *RHB* cruise was to determine how well island measurements represent the surrounding ocean environment. During July, when the *RHB* was in close proximity to the island of Nauru, detailed comparisons of ship- and island-based instruments were possible. These data provided a rare opportunity to compare basic observations necessary for developing radiative transfer models. Essentially identical instruments were operated from the ship and the island's Atmospheric Radiation and Cloud Station (ARCS-2). These instruments included simultaneously launched Vaisala radiosondes, the Environmental Technology Laboratory's (ETL) Fourier Transform Infrared Radiometer (FTIR), and the ARM Program's Atmospheric Emitted Radiance Interferometer (AERI), as well as cloud radars and ceilometers to identify clear conditions.

The ARM Microwave radiometer (MWR) operating on Nauru provided another excellent data set for the entire Nauru99 experiment. The calibration accuracy was verified by a liquid nitrogen blackbody target experiment and by consistent high-quality tipping calibrations throughout the experiment. The data thus provide an excellent baseline for evaluation of the quality and consistency of Vaisala radiosondes that were launched from the Nauru ARCS-2 and from the *RHB*. Comparisons were made for calculated clear sky brightness temperature (T_b) and for precipitable water vapor (PWV). Our results indicate that substantial errors, sometimes of the order of 20% in PWV, occurred with the original radiosondes. When a proprietary Vaisala correction algorithm, based on the age of the radiosondes, was applied, better agreement with the MWR was obtained. However, the improvement was noticeably different for different radiosonde lots and was not a monotonic function of radiosonde age. When the Rosenkranz (1998) absorption model was applied to newer radiosondes, both from the *RHB* and the R/V *Mirai*, agreement with the ARM MWR was substantially better.

Brightness temperature calculations based on three absorption algorithms, those of Liebe and Layton (1987), Liebe et al. (1993), and Rosenkranz (1998), were also compared. The Liebe 87 model was in reasonable agreement with Rosenkranz 98, but neither was in agreement with Liebe 93. For the 23.8 GHz vapor-sensitive channel, the Liebe 87 model and the Rosenkranz 98 model differed by only 0.1 K in T_b comparisons. At 31.4 GHz, the difference was about 0.5 K between the two. It was also possible to scale radiosonde soundings using data derived from the MWR. Infrared spectral radiance calculated from scaled radiosonde data, using all of the microwave radiative transfer models, was compared with AERI observations from the ARCS-2 site; the best agreement was obtained with the Rosenkranz 98 model. In addition, the radiosonde observations scaled by the MWR PWV agreed better with the AERI measurements than did the radiosondes corrected by the Vaisala proprietary algorithm.

Early on Orbit Performance of the Jason-1 Microwave Radiometer

C. S. Ruf
Department of Atmospheric, Oceanic & Space Sciences, University of Michigan
Ann Arbor, MI, U.S.A.

S. J. Keihm
NASA Jet Propulsion Laboratory, California Institute of Technology
Pasadena, CA, U.S.A.

S. T. Brown
Department of Atmospheric, Oceanic & Space Sciences, University of Michigan
Ann Arbor, MI, U.S.A.

The Jason-1 satellite is scheduled for launch on 7 December 2002. The Jason Microwave Radiometer (JMR) on board will measure radiometric brightness temperature (TB) at 18.7, 23.8, and 34.0 GHz in the nadir direction, from which will be estimated the excess path delay (PD) through the atmosphere experienced by the radar altimeter signal due to water vapor and suspended cloud liquid water. JMR is a follow on and improvement to the earlier TOPEX Microwave Radiometer (TMR). There is one significant change in the instrument design from TMR to JMR. In the case of TMR, absolute calibration was referenced to a warm black body load and a cold sky view of space. These calibration reference points bracket the range of Earth TBs measured over the life of the mission. In the case of JMR, the cold sky horn has been replaced by a trio of internal noise diodes that provide a hot reference point above that of JMR's warm black body load. This new approach to radiometer calibration represents a significant relaxing of the demands on sensor complexity and spacecraft accommodation to support the cold sky view. This change also presents two new issues that will be examined during on-orbit validation. Firstly, the calibration points will no longer bracket the Earth TBs. Absolute calibration will involve an extrapolation from, rather than an interpolation between, reference points. The second issue involves the stability of the noise diode's Excess Noise Ratio and possible aging effects in the space environment. Three noise diodes were used to improve reliability and also in order to correct for independent short term variations in their noise power. Correlated drifts due, for example, to radiation exposure, cannot be internally detected and corrected. An external absolute reference is required to monitor such drifts. On-orbit assessment of JMR performance will include comparisons with TMR cross-overs and with near-coincident radiosonde profiles of the atmosphere and ground-based upward looking water vapor radiometer measurements of PD and TB, and examination of stationary statistical properties of the Earth's TB probability distribution. Early results of the on-orbit calibration and validation effort will be presented.

Retrieval of Low Column Water Vapor from Radiometric Measurements of MIR and SSM/T-2

J. R. Wang
Microwave Sensors Branch, Laboratory for Hydrospheric Processes
NASA Goddard Space Flight Center
Greenbelt, MD, U.S.A.

W. Manning
Joint Center for Earth Systems Technology, University of Maryland at Baltimore County
Baltimore, MD, U.S.A.

Radiometric measurements near the strong water vapor line of $183.3\,\mathrm{GHz}$ from both MIR (Millimeter-wave Imaging Radiometer) and SSM/T-2 (Special Sensor Microwave/Temperature 2) are used to retrieve column water vapor $W \leq 0.8\,\mathrm{g/cm^2}$ over Arctic and Midwest regions. For the SSM/T-2, three channels at 150, 183.3 ± 3, and $183.3 \pm 7\,\mathrm{GHz}$ were used so it is necessary to assume a frequency-independent surface emissivity over the 150-$183\,\mathrm{GHz}$ range. For the MIR, an additional frequency at $220\,\mathrm{GHz}$ is available; thus, both 3-channel and 4-channel retrieval methods could are possible. The 4-channel retrieval method allows implementation of a linear frequency dependence of surface emissivity. Results derived from the MIR data using both retrieval methods are used to examine the effect of surface emissivity on the estimation of W. Several nearly concurrent measurements of SSM/T-2 and MIR acquired during February 1997 and May 1998 are examined in this study.

The retrieval results from the MIR compared well with those derived from the nearly concurrent rawinsonde data. The spatial variations of W displayed features that are consistent with topographical variations. The 3-channel retrieval, which assumes a frequency-independent surface emissivity, can have errors of $\pm 0.1\,\mathrm{g/cm^2}$ due to the assumption; the retrieval tends to over-estimate W if surface emissivity increases with frequency, and vice versa. Excellent agreement was found between the W values retrieved from both MIR and SSM/T-2, which suggests that the radiometric measurements are consistent for both sensors. An earlier study examined how surface temperature variability effected the retrieval performance using modeled numerical simulations. This effect is explored more fully and discussed more explicitly in this paper, using data from both aircraft and satellite platforms.

Retrieval of Column Precipitable Water Using Millimeter-wave Radiometric Measurements: Applying Knowledge Gained from Regional Field Experiments to the Global Special Sensor Microwave/Temperature-2 (SSM/T-2) Radiometer Data Set

W. Manning
JCET/UMBC
Baltimore, MD, U.S.A.

J. R. Wang
NASA GSFC
Greenbelt, MD, U.S.A.

E. R. Westwater
CIRES/NOAA/ETL
Boulder, CO, U.S.A.

P. E. Racette
NASA GSFC
Greenbelt, MD, U.S.A.

Y. Han
CIRES/NOAA/ETL
Boulder, CO, U.S.A.

Water vapor plays a primary role in the energetics of the atmosphere both through the release of latent heat and through radiative interactions. When estimating polar surface radiation budgets, uncertainties in quantifying atmospheric precipitable water can create errors in satellite-derived estimates of surface albedo and temperature. Additionally, atmospheric water vapor is the sole source of ice contained in the continental ice sheets; therefore, the transfer of water vapor into and within the atmosphere above these ice sheets is of increasing concern when considering their mass and energy balance.

Several recent studies strongly suggest that robust precipitable water vapor retrievals can be achieved for dry atmospheric conditions using a combination of passive microwave radiometer channels located on the wings of the strong water vapor absorption line at 183.31 GHz along with a window channel at 150 GHz. In this study, a similar retrieval procedure using recent SSM/T-2 data is tested for all global areas where the atmospheric conditions are sufficiently dry.

The objective of this study is to thoroughly assess the performance of the SSM/T-2 precipitable water vapor retrieval procedure. A two year global set of radiosonde calculated column precipitable water vapor point values, with integrated column amounts less than 0.6 cm, are merged with matching SSM/T-2 overpasses that occur in close proximity in both time and space. Additionally, radiosonde and the Atmospheric Radiation Measurement (ARM) Program's microwave radiometer (MWR) precipitable water data gathered during two separate field experiments in the Arctic region are compared with the SSM/T-2 retrieved results. Combined, these comparison data sets provide a meaningful and descriptive basis for discussions related to the strengths and weakness inherent to the proposed retrieval method. Finally, a time series of retrieved values over the Greenland ice sheet for the 2000-2001 time period is presented and discussed.

Boundary Layer Activities Observed by a Multi-Channel Radiometer and an Integrated Sounding System During GIMEX

Y. Liou
Center for Space and Remote Sensing Research, National Central University
Chungli, 32054, Taiwan

Y. Liou and C. Wang
Institute of Space Sciences, National Central University
Chungli, 32054, Taiwan

H. Lai and P. Lin
Department of Atmospheric Sciences, National Central University
Chungli, 32054, Taiwan

B. J. Jou
Department of Atmospheric Sciences, National Taiwan University
Chungli, 32054, Taiwan

Heavy precipitation and strong winds associated with severe weather systems, such as typhoons and Mei-Yu fronts, threat Taiwan and other places around the world every year. They cause severe damage to agriculture and industry, and serious loss of human life. It is hence an obvious demand to improve quantitative precipitation forecasting. Partially under the demand, Taiwan Weather Research Program (TWRP) is formed and co-sponsored by National Science Council and Central Weather Bureau of Taiwan. As an initial effort of the TWRP, Green Island Mesoscale Experiment (GIMEX) was conducted in May to June 2001. Scientific objectives of the GIMEX include a better understanding of the mesoscale circulation associate with the Mei-Yu front, the evolution and structure of mesoscale circulation induced by the complex Taiwan topography, the structure and development of the land/sea breeze and mountain/valley wind, and the interaction among mesoscale circulation systems, lee vortices, and local circulations.

In this paper, we will present the use of a ground-based multi-channel radiometer and an Integrated Sounding System (ISS) to interpret the observed boundary layer activities, including land-sea breeze and turbulence. The radiometer is manufactured by the Radiometrics Corporation, USA (http://www.radiometrics.com). Its operating frequencies include five channels in the range of 20-30 GHz to primarily provide water vapor distribution, and seven channels in the range of 51-59 GHz to determine temperature profile. The combined 20-30 and 51-59 GHz bands together with IR radiometer-derived cloud base temperature allow us to derive cloud liquid profile associated with the weather systems of interest. The ISS includes a 915 MHz wind profiler to offer the vertical structure of wind fields and to infer the occurrence of the associated turbulence.

Implicit Precipitable Water Retrievals within Oceanic Rainfall Algorithms

T. Wilheit, R. Chen, K. Feng, S.-W. Hong, J. Huang, K.-W. Jin, and R. Weitz
Department of Atmospheric Sciences, Texas A&M University
College Station, TX, U.S.A.

J. Thomas-Stahle
Department of Atmospheric Sciences, Colorado State University
Fort Collins, CO, U.S.A.

C. Bellows
Flight Design and Dynamics-Navigation, United Space Alliance
Houston, TX, U.S.A.

Rainfall provides the dominant, but not the only, contribution to microwave brightness temperatures observed over oceanic rain. For the SSM/I frequencies (and TMI above 19 GHz) the water vapor contribution is quite significant. A very robust Precipitable Water algorithm can be made using only the 19.35 and 21.4 (or 22.235 for SSM/I) GHz channels. This algorithm is tolerant of significant contamination by land or rain. This rainfall tolerance is exploited to retrieve precipitable water in the presence of rain.

In retrieving rainfall intensity, knowledge of the freezing level is needed as it determines thickness of the liquid precipitation layer. The radiative transfer model used specifies the atmospheric temperature lapse rate and the relative humidity profile. These assumptions couple the freezing level and the precipitable water. While these assumptions may not be reasonable under all circumstances, they are quite reasonable in the presence of rain.

The Texas A&M oceanic rainfall retrieval algorithm uses the 19/21 GHz combination to retrieve the precipitable water but expresses this retrieval in terms of the freezing level via the translation implicit in the thermodynamic assumptions of the radiative transfer model.

The freezing level so retrieved has been compared with an independent determination of the freezing level derived from the bright-band observations in the TRMM Precipitation Radar data. The accuracy of the retrieval is better than 200 m.

These comparisons, combined with radiosonde observations, have been used to refine the absorption coefficient for water vapor near the 22 GHz line. Small adjustments are needed that can be expressed in terms of either the strength parameter or the pressure broadening parameter. Expressing the change in terms of the pressure broadening parameter is physically more realistic and produces an answer consistent with published values.

Surface Emissivity of Sea Ice at 89, 157 and 183 GHz during the SEPOR-POLEX Campaign

N. Selbach
Institute of Environmental Physics, University of Bremen
Bremen, 28334, Germany

T. J. Hewison, and J. P. Taylor
Met Office
Farnborough, GU14 0LX, UK

G. Heygster
Institute of Environmental Physics, University of Bremen
Bremen, 28334, Germany

A. J. McGrath
Met Office
Farnborough, GU14 0LX, UK

Recent studies in atmospheric and oceanic circulation have shown that polar regions play an important role in the global climate variability and change. Due to the remoteness of these areas and their demanding climate, direct measurements of many useful geophysical parameters in polar regions are very sparse. Satellite microwave radiometry, due to its good spatial and temporal coverage, potentially provides a valuable tool for global observations of atmospheric parameters. Difficulties to separate the atmospheric and the surface part of the signal arise from the large and highly changeable surface emissivity at microwave bands from the ice and snow covered surface together with the very low water vapor burden in polar regions. Measurements of the surface emissivity at millimeter wavelengths over snow and ice in these regions are rare. Data from the airborne SEPOR–POLEX (Surface Emissivities in Polar Regions–Polar Experiment) campaign in the Arctic in March 2001 are used to derive surface emissivities at 89, 157 and 183 GHz. The key instrument operated on the Met Office C-130 aircraft was the microwave radiometer MARSS (Microwave Airborne Radiometer Scanning System) with frequencies close to those of the SSM/T2 and AMSU-B. Five flights were performed over various ice types in the Arctic including new, glacier, first year and multi-year ice. Each flight consisted of a long low level run over the ice, a profile ascent and a run back to the base (Tromsø, Norway) at high level along the same track. During the high level run dropsondes were released to gain information about atmospheric profiles of pressure, temperature and humidity. Data of high and low level flights are used to calculate the surface emissivity using coincident surface temperature measurements from an IR-radiometer onboard the aircraft. Surface temperature and emissivity are retrieved from the thermal infrared measurements of an interferometer onboard the aircraft, as well. To derive the surface emissivity from data collected at high flight level the atmospheric contribution needs to be known. This is derived from radiative transfer calculations using measurements from the dropsondes as input. To retrieve the emissivity from low level flights both, downwelling and upwelling radiation, have to be considered as well as the surface temperature. Problems arise in defining and measuring an effective surface temperature for a non-isothermal volume-scattering medium due to the different penetration depths in the infrared and microwave frequency ranges. First results of this study will be presented.

Session 4Ac2

Bioelectromagnetic Imaging and Visualization

Evaluation of the Jacobian Matrix for Two Different Gauss-Newton Image Reconstruction Formulations

P. M. Meaney, D. Li, Q. Fang, N. Yagnamurthy, and K. D. Paulsen
Thayer School of Engineering, Dartmouth College
Hanover, NH 03755, U.S.A.

The Jacobian matrix is the essential component in determining the electrical property updates at each iteration during the Gauss-Newton image reconstruction scheme. The updates are solved using $[J]\{\Delta k^2\} = \{E^m - E^c\}$ where $[J]$ is the Jacobian matrix, $\{\Delta k^2\}$ is the property update and $\{E^m - E^c\}$ is the difference between the measured and computed electric fields. In our original algorithm, it is comprised of derivatives of the electric fields measured at receiver (r), due to source (s), and with respect to the electric property at the reconstruction parameter node (n), and can be represented as $\partial E_{rs}/\partial k_n^2$, for all possible combinations of $r,\ s,$ and n. Perhaps the most informative way to study the behavior is to plot 2D contours of the Jacobian over the reconstruction parameter mesh for fixed transmitter and receiver pairs. Figures 1a and b show such a distribution (magnitude and phase) for the first iteration at an operating frequency of 900 MHz of a reconstruction where the object being recovered is a simulated 10 cm diameter breast ($\varepsilon_r = 20,\ \sigma = 0.2$ S/m) with a 2.5 cm diameter tumor inclusion ($\varepsilon_r = 57,\ \sigma = 1.2$ S/m). The background medium is saline ($\varepsilon_r = 77,\ \sigma = 1.7$ S/m) for an array of monopole antennas on a 15 cm diameter circle surrounding the 13 cm diameter reconstruction parameter mesh. Two important observations can be made from this. First, both exhibit curved patterns roughly connecting the transmitter and receiver, with the phase displaying waves of wrapping extending out in parallel with this curved line. We have previously described limitations in image reconstruction due to phase wrapping and this probably contributes to that problem. Second, the magnitude exhibits a "banana"-like distribution between the transmitter and receiver with it being essentially zero outside of this band. In addition, there is a pronounced trough in the center of the band and two peaks closer to the transmitter and receiver. This implies that this algorithm has a distinctly lower sensitivity in the parameter mesh center than nearer its perimeter.

The log-magnitude and phase reconstruction algorithm introduced by Meaney et al. [2001] produces distinctly different distributions than observed with the previous implementation. There is no perceptible phase wrapping and the "banana" shape in the log-magnitude component has no perceptible null near the center of the mesh. Visual comparison of the rows (r and s held constant) of these Jacobians clearly demonstrate the potential improvement from utilizing the new log-magnitude/phase algorithm.

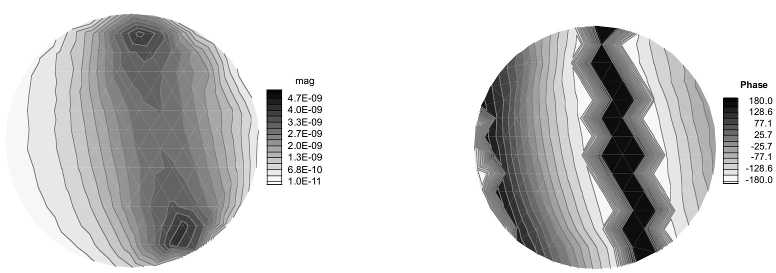

(a) (b)

Figure 1: (a) Magnitude and (b) phase of a single row of a jacobian matrix at 900 MHz as plotted on the reconstruction parameter mesh.

A Linear Model for CP-MCT

M. Bertero, P. Boccacci, F. Conte
DISI – DIFI, Università di Genova
Genova, 16146, Italy

M. Miyakawa
Department of Biocybernetics, University of Niigata
Niigata, 950-2181, Japan

M. Piana
DIMA, Università di Genova
Genova, 16146, Italy

Chirp-Pulse Microwave Computerized Tomography (CP-MCT) is an imaging technique developed at the Department of Biocybernetics, University of Niigata, and based on the following procedure: i) the source antenna S and receiving antenna R move in the direction θ along two parallel straight lines delimiting the scanning region; ii) the input is a chirp signal with frequencies between 1 and 2 GHz; iii) part of the input signal is multiplied in a mixer by the signal registered on the receiving antenna. The high-frequency components of the mixed signal are filtered out.

Here we propose a linear model for data acquisition in CP-MCT based on scattering theory. We assume that the positions of the source S and the receiver R on the θ,$\theta^{\perp}$ coordinate system are given by $x_S = (s, d/2)$ and $x_R = (s, -d/2)$ respectively, where d is the distance between the two antennas. Then, according to our model the CP-MCT projection $g_\theta(s)$ in the direction θ is given by

$$g_\theta(s) = \int\int R(s-s', |y'|)c(s',y')ds'dy' \tag{1}$$

where (s', y') are the θ,$\theta^{\perp}$ coordinates of a point x' in the plane, $c(x')$ is proportional to the attenuation constant in x' and the function $R(s-s', |y'|)$ is the normalized response of the device to a point source placed in x'. We compute this function by conveniently solving the Lippmann-Schwinger equation. In Figure 1 the impulse response is plotted for different distances of the pixel from the center. In particular Figure 1(a) shows that in a region close to the center the model can be considered space invariant and the projection equation (1) can be approximated by the convolution equation

$$g_\theta(s) = \int R(s-s')(\int c(s',y')dy')ds' \quad . \tag{2}$$

In these conditions a simple two-step algorithm for image restoration from CP-MCT projections can be naturally derived: a) perform a regularized deconvolution of $g_\theta(s)$ by means of an effective regularization method reducing the numerical instabilities due to the presence of noise on the data; b) apply the Filtered Back Projection algorithm to the result of the regularized deconvolution. A generalization of this algorithm to a space-variant situation is in due course. In this case the difficulties implied by the notable computational complexity can be addressed by means of techniques suitably mutuated from SPECT imaging modality.

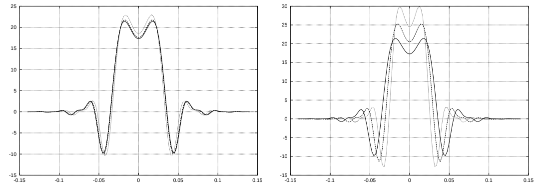

Figure 1: Plot of the response functions corresponding to different distances r from the center. *Left:* $r = 0$m (full), $r = 0.025$m (dashed), $r = 0.050$m (dotted). *Right:* $r = 0$m (full), $r = 0.075$m (dashed), $r = 0.1$m (dotted)

FDTD-Based Computation to Find an Optimal Configuration of the Printed Array Antenna Used for a Fan Beam Scanner of Chirp Pulse Microwave Computed Tomography (CP-MCT)

M. Miyakawa, W. Jing, and K. Sugawara
Niigata University, Faculty of Engineering, Department of Biocybernetics
Niigata, 950-2181, Japan

M. Bertero
INFM & DIFI, University of Genova
Genova, I-16146, Italy

Feasibility of a fan beam scanner of CP-MCT and its optimal antenna-configuration have been investigated. There is no doubt that the rotational scan will contribute to reduce the data acquisition time. The most effective way of arrangement of the transmitting- and receiving antennas has been explored from the viewpoints of data acquisition time and quality in the tomographic image. The receiving antenna consists of approximately fifty dipole-antenna elements. The appropriate configuration is practically determined by the distance between the transmitting- and receiving-antennas, microwave attenuation between them and distance among adjacent receiving antenna elements.

For the configurations shown in Fig. 1, Fig. 2 and Fig. 3, the quality of the reconstructed images is firstly compared. The estimated spatial resolution is almost the same value (10 to 12 mm) in all scanners, regardless of the antenna configuration. In other words, those element antennas are so arranged to satisfy the requirement of equal spatial resolution.

Configuration as shown in Fig. 1 is the most effective in respect of the target size as compared to the (short) antenna distance between the transmitting and receiving antennas, although the distance depends on the location of the receiving antenna element. In contrast, the antenna distance is kept at constant regardless of the position in Fig. 2. Instead, the distance is longer than that of the configuration in Fig. 1. Configuration as shown in Fig. 3 can reduce the antenna distance as compared to Fig. 2. The signal to noise ratio is improved, although number of the elements of the receiving antenna is decreased.

In CP-MCT, the configuration of the scanner such as one as shown in Fig. 3 is the best in respect of the SN ratio, spatial resolution.

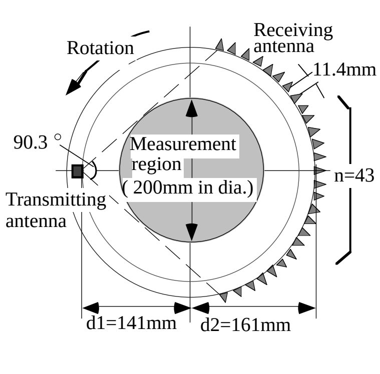

Figure 1: Configuration-1

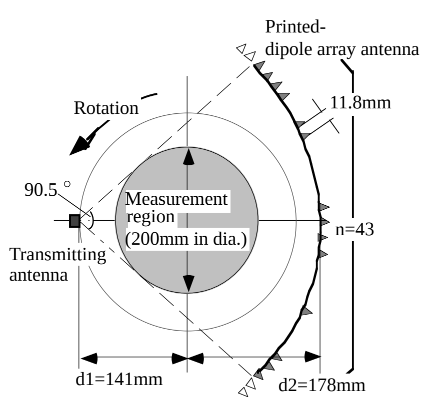

Figure 2: Configuration-2

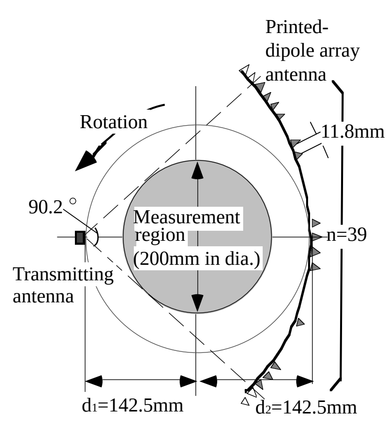

Figure 3: Configuration-3

Computational Imaging of the Breast- and Head-Models in CP-MCT

M. Miyakawa and K. Sugawara
Niigata University, Faculty of Engineering, Department of Biocybernetics
Niigata, 950-2181, Japan

M. Bertero and M. Piana
INFM & DIFI, University of Genova
Genova, I-16146, Italy

The FDTD-based after-effect function method (AEFM) has been developed to obtain numerically the tomographic images of a biological object by chirp pulse microwave computed tomograhy (CP-MCT). In this study, high resolution-type CP-MCT using a chirp pulse microwave from 2 to 3 GHz has been considered instead of the prototype system working at 1–2 GHz. The evaluated spatial resolution of the high resolution-type CP-MCT is approximately 6 to 7 mm, while resolution of the prototype system has been estimated at 10 to 12 mm.

Two dimensional imaging of a head has been attempted numerically by using a head model developed by ourselves from X-ray CT images. Figure 1(a) is the attenuation image of the head model while Fig. 1(b) is the image of the same head with a temperature variation of 4°C at the right upper region of the model. The CP-MCT prototype is assumed in this computation. Due to the long wavelength of the prototype system, the anatomical structure is not clearly observed. However, information on the temperature variation is derived successfully from the subtracted image of those tomograms, regardless of the complexity of electric structure of the head.

Three dimensional imaging of the head has also been attempted by employing a model developed for dosimetric studies by the Radio Frequency Radiation Branch, United States Air Force Research Laboratory.

Figure 2 is a model of a breast suffering from an early stage cancer. The 10 mm spherical tumor is not realistic as an early stage cancer but it is consistent with the spatial resolution of the high resolution-type CP-MCT. Figure 3(a) and (b) are tomographic images of two sections of the breast: the first is that containing the tumor while the second is 5 mm apart. Direct localization is not feasible but the effects are surely observable.

By making use of TAEFM, we have investigated the applicability of CP-MCT to specific purposes. The results demonstrated that the cooperative use with traditional imaging modalities, CP-MCT would provide useful information for clinical diagnosis.

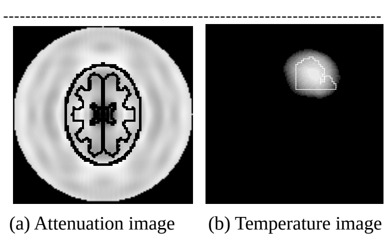

Figure 1: Computational imaging of a head model with prototype CP-MCT (1–2 GHz).

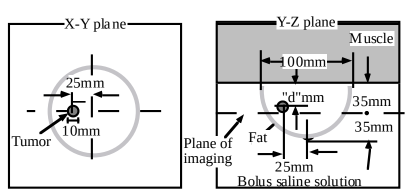

Figure 2: A model of the breast with a tumor.

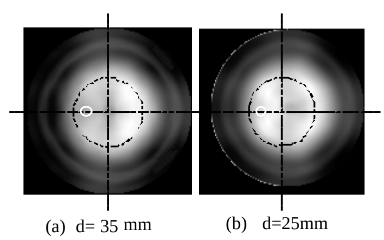

Figure 3: Three dimensional imaging of the breast tumor with high resolution-type CP-MCT.

Efficient Image Reconstruction of Breast Tumors

T. Tanaka
Division of System Science, Graduate School of Science & Technology, Nagasaki University
Nagasaki, 852-8521, Japan

T. Takenaka
Department of Electrical & Electronic Engineering, Nagasaki University
Nagasaki, 852-8521, Japan

Microwave imaging has considerable potential for detection of breast cancer because of high contrast in dielectric properties of normal breast tissue and breast tumors at microwave frequencies. Several methods of imaging biological objects by microwave have been proposed during the last two decades. They are roughly categorized into two groups. One is based on beamforming techniques. The methods determine the location and shape of strong scatterers in a biological object. The other is related to inverse scattering problems. The inverse scattering techniques reconstruct the electrical parameter profile of a biological object, so that not only the location and shape but also the electrical property of malignant breast tissue can be determined. For a large and high-contrast object, however, the inversion methods need much longer processing time than the methods based on beamforming techniques.

In this paper we propose a combination of beamforming and inverse scattering techniques. High-contrast tissues and a large cross section of a breast compared to the wavelength in the normal tissue make the inverse scattering problem of breast tumor detection highly nonlinear. To avoid being trapped in local minima when we use a gradient-based inversion method, an initial guess should be chosen properly. First, we use a 'time-shift-and-add' algorithm of beamforming technique [1, 2] to roughly estimate the location and size of malignant breast tissue in the large cross section of a breast. Then, a small square area including the roughly detected malignant breast tissue is selected as a reconstruction domain for inverse scattering. The reduction of reconstruction domain decreases the nonlinearity of the problem. The forward-backward time-stepping method [3] is applied to the small reconstruction domain. Numerical examples show the reliability and effectiveness of the proposed two-step procedure.

REFERENCES

1. S. C. Hagness, A. Taflove, and J. E. Bridges, "Two-dimensional FDTD analysis of a pulsed microwave confocal system for breast cancer detection: Fixed-forcus and antenna-array sensors," *IEEE Trans. Biomed. Eng.,* Vol. 45, 1470–1479, Dec. 1998.
2. E. C. Fear, and M. A. Stuchly, "Microwave detection of breast cancer," *IEEE Trans. Microwave Theory Tech.,* Vol. 48, 1854–1863, Nov. 2000.
3. T. Takenaka, H. Jia, and T. Tanaka, "Microwave imaging of electrical property distributions by a forward-backward time-stepping method," *J. Electromagn. Waves Applic.,* Vol. 14, 1609–1626, Dec. 2000.

Brain Electrical Imaging by Means of Parametric Projection Filters

J. Hori
Department of Biocybernetics, Niigata University
Niigata, 950-2181, Japan

B. He
Department of Bioengineering, University of Illinois at Chicago
Chicago, IL 60607, U.S.A.

In the present paper, spatial filters for inverse estimation of an equivalent dipole layer from the scalp-recorded potentials have been explored for their suitability in achieving high-resolution electroencephalogram (EEG) imaging.

It is of importance and interesting to image brain electrical activity from noninvasive electrical measurements on the scalp. However, the spatial resolution of conventional EEG is limited due to the smearing effect caused by the head volume conductor. Moreover, as the measurement electrode number is always much smaller than the dimension of the unknown dipole layer vector, this problem is an underdetermined non-unique inverse problem.

Spatial enhancement, which attempts to deconvolve the low-pass spatial filtering effect of volume conduction in the head, is one of the approaches to overcome such difficulty. In particular, cortical dipole imaging technique, which attempts to estimate the cortical potentials from scalp potentials through an intermediate source layer, have an advantage that no *ad hoc* information about the nature of sources is required.

In the present study, we consider the influence of non-uniform additive noise, which is characterized by noise covariance. We have applied the parametric projection filter (PPF), which uses the information of noise covariance, to perform the inverse regularization in cortical dipole imaging, and examined the feasibility of these spatial filters in a volume-conductor head model.

In a clinical situation, the noise information may be estimated from data that is known to be source free, such as pre-stimulus data in evoked potentials. We applied above restoration methods to the inverse problem in the conditions of various noises, such as Gaussian white noise (GWN) and non-uniform noise to simulate noise-contaminated scalp potential measurements.

The present results suggest that the PPF are effective for the condition of low correlation between signal and noise and that have similar restorative ability to the general inverse with truncated singular value decomposition and the Tikhonov regularization method for the GWN and the condition of high correlation between signal and noise. Further investigation using experimental data is necessary to fully validate the performance of PPF for cortical dipole imaging.

A Study of Electrical Properties of the Epidermal Stratum Corneum

M. Egawa and L. Yang
Graduate School of Natural Science and Technology, Niigata University
Niigata, 950-2181, Japan

M. Akimoto
Institute of Science and Technology, Kanto Gakuin University
Kanazawa-ku, Yokohama 236-0032, Japan

M. Miyakawa
Department of Biocybernetics, Faculty of Engineering, Niigata University
Niigata, 950-2181, Japan

Human skin is composed of an array of layers varying in their thickness. The most superficial layer is the stratum corneum. Stratum corneum not only retards water loss from the inner hydrated layers but also prevents the invasion of toxic agents and microorganisms. This character of stratum corneum is called barrier function. Dielectric analysis in the wade range of frequency region is attracting considerable interest as a noninvasive technique to measure of skin. The relationships obtained between the impedance and the stratum corneum at a few frequencies have been reported; however, to date, the study in this field has not yet been complete. The present paper reports on the electrical properties of the stratum corneum, and it has as its goal a contribution to skin impedance analyses. This paper embodies three main parts. First, the impedances of layers removed by stripping are determined and the electrical properties of these layers are elaborated. Secondly, the average resistivities and dielectric constants at two parts of the skin are determined and the dispersion characteristics as a function of frequency are shown. Thirdly, the mathematical expression for the direct current resistivity of the stratum corneum is determined.

The dielectric measurements were performed using automatic swept-frequency network and impedance analyzers. The frequency range 5 Hz to 10 MHz was covered by an HP4192A impedance analyzer, an HP8753C was used in the frequency range 300 KHz to 1 GHz. Open- ended co-axial probes were used to interface the measuring equipment with the samples in all cases. A impedance-matched conical co-axial probe was adapted to interface the sample to the HP4192A impedance analyzer. The probe is characterized by a fringing capacitance and conductance which are functions of its physical dimension and can be measured with the impedance analyzer.

An experimental investigation of dielectric properties of skin was undertaken using two experimental techniques with overlapping frequency coverage extending from 5 Hz to 1 GHz. It was shown that, for measurement on the low-frequency experimental set-up, electrode polarization errors affect the results below 1 KHz and become significant below 100 Hz in the case of tissue samples. Appropriate corrections were made for electrode polarization and for the lead inductance effect. The corrected data fall well within the values in the literature. The impedance of the skin and the impedance of the stratum corneum were investigated by using tape to remove the stratum corneum. The epidermal stratum corneum behaves as a very important element for the skin impedance. Therefore, there is a need for an adequate study of the electrical properties of the stratum corneum. The essential results of this study are as follows. The impedance of the removed layers of stratum corneum does not show the Cole- Cole circular arc, but the skin impedance remaining after some stripping shows the Cole-Cole circular arc. There are a few frequency dispersions in the skin impedance based on different origins. That is, the dispersion based on the stratum corneum formed from the laminated configuration of extinct cells and the three dispersion based on living deeper tissues containing granular layer can be separated and evaluated distinctly. The skin stratum corneum forms a high electric-resistance layer. The resistance of this layer, however, does not become homogeneous, but becomes low toward the part. We believe that the dielectric analysis based on the stratum corneum model presented in this study is useful to the integrity of stratum corneum.

Temperature Retrievals by Microwave Radiometry in Canonical Models of Tissues

F. Bardati and G. Marrocco
Dipartimento di Informatica, Sistemi e Produzione,Universita' di Roma "Tor Vergata"
Rome, 00133, Italy

P. Tognolatti
Dipartimento di Ingegneria elettrica, Facoltà di Ingegneria, Università dell'Aquila
L'Aquila, 67100, Italy

Microwave Radiometry is based on receiving, measuring, and processing spontaneous thermal radiation from lossy bodies. It has been considered for non-invasive measurement of temperature in connection with biomedical applications such as diagnosis of pathological conditions, monitoring of temperature and temperature dosimetry. Recently it has been considered for the measurement of deep brain temperature in newborn infants subjected to hypothermia treatments [1], [2].

Modern radiometric systems provide multifrequency radiometric data, g_n, that are equal to the body temperature, T, if T is uniform over Ω. Ω is the body which provides the thermal radiation received by the radiometric antenna. In the general case

$$\int_{\Omega} W_n(\underline{r})\, T(\underline{r})\, d\underline{r} = g_n \tag{1}$$

where W_n is the weighting function at frequency f_n with unitary integral over Ω. Its computation, for given antenna and frequency, requires the solution of Maxwell's equations for the radiation problem into tissues. Tissues are characterised by the permittivity $\in$, which depends on tissue type and frequency, while variations with temperature are negligible for thermal changes of a few degrees as is expected in living bodies. In most studies the permittivity is kept constant within each type of tissue. Both realistic and idealised models of head have been solved especially in connection with recent studies on a possible damage by cellular phones. The layered sphere is a widely adopted canonical model for the head.

Equation (1) is a Fredholm integral equation of the first kind. The retrieval of T is an ill-conditioned problem, hence additional "a priori" information on temperature is required for inversion. A layered sphere is a useful model for the computation of main heat exchanges in the head and to the environment [3].

The interest in canonical models such as layered spheres for both the electromagnetic and thermal modelling is in the evidence which is given to the dependence of temperature retrievals on the various physical parameters affecting a radiometric temperature retrieval. In this paper some application-oriented inversion techniques are discussed with reference to simulated radiometric measurements on a newborn head.

1. K. Maruyma, Mizushina S. , Sugiura T., Van Leeuwen G.M.J., Hand J.W., Marrocco G., Bardati F., Edwards A.D., Azzopardi D., Land D. (2000), "Feasibility of non-invasive measurement of deep brain temperature in new-born infants by multi-frequency microwave radiometry", *IEEE Trans. Microwave Theory Techn.* , Vol. 48, pp. 2141-2147, Nov. 2000.

2. F. Bardati, Hand. J.W., Marrocco G., Mizushina S., Tognolatti P., van Leeuwen G.M.J., "Brain temperature measurement by microwave radiometry in new born infants", *Atti Fond. G. Ronchi*, LVI (4-5), p. 647, 2001

3. X. Xu, Tikuisis P., Giesbrecht G., "A mathematical model for human brain cooling during cold-water near drowning", *J. Appl. Physiol.*, Vol. 86, pp. 265-272, 1999.

Reconstruction of the Refractive Index in Electromagnetic Scattering by Using a Propagation-Backpropagation Method

M. Vögeler and F. Natterer
University of Muenster
Muenster, Germany

This talk deals with an inverse problem in electromagnetic scattering.

Assume an inhomogeneous object, which is embedded in a homogeneous medium, is irradiated by an incident time-harmonic planar wave. We consider the inverse problem of determining the 3D complex-valued refractive index inside the object. We use a PBP-Method that has been shown to work in ultrasound tomography.

In order to determine the refractive index of the scatterer, the knowledge of the complex-valued scattered electromagnetic wave is assumed to be known at some distance from the object for a finite number of directions of the incident waves.

The scattering process for the electric field is described by a second order elliptic partial differential equation, which is shown to be equivalent to the Maxwell-equations for a smooth refractive index. Solving the Cauchy problem for this equation leads to a nonlinear operator from the set of refractive indices to the measurement space. The Fréchet differentiability of this operator is shown and a stability result for solving the Cauchy problem is given. The nonlinear problem is solved iteratively in a Kaczmarz-Newton-like fashion.

Finally numerical reconstructions of the refractive index of 3D-objects are shown.

Session 4Ac3

Numerical Modeling of Photonic Crystal Structures

Efficient Modelling of Photonic Crystal Structures Based on Vectorial Eigenmode Expansion

P. Bienstman
Massachusetts Institute of Technology
Cambridge, MA 02139, U.S.A.

We will present an efficient and flexible method for the calculation of photonic crystal structures. The method is based on the principle of vectorial eigenmode expansion. Rather than spatially discretising the structure under study, the electromagnetic field is expanded into the eigenmodes of each longitudinally invariant layer. Subsequently, scattering matrices are computed to describe the behaviour of the entire component. The method can be used equally well to model infinite and finite structures.

For infinite structures and band structure calculations, the model has the advantage that it can easily be applied to dispersive media, which will be illustrated with examples. Also, because it uses eigenmodes rather than plane waves as basis functions, it converges faster than more conventional approaches. Special care will be given to numerical stability.

For the modelling of finite structures containing periodic sections, the method has the advantage that computation times are logarithmic in the number of periods, rather than linear. Also, the use of advanced absorbing boundary conditions like PML (perfectly matched layer) means that the method is able to model radiation loss accurately, which is important for practical applications.

The model will be illustrated with numerous design examples of photonic crystal components, like structures to butt-couple light into single mode fiber, tapers to couple dielectric waveguides to photonic crystal waveguides, out-of-plane scattering losses in photonic crystal slabs and coupled-resonator optical waveguides. The extension to three-dimensional problems will be discussed as well.

The modeling code (called CAMFR or Cavity Modelling FRamework) is freely available from
http://camfr.sourcefore.net

Electromagnetic Properties of 3D Photonic Bandgap Structures Embedded in Waveguides

O. J. F. Martin and M. Paulus
Electromagnetic Fields and Microwave Electronics Laboratory
Zurich, ETH-Zentrum 8092, Switzerland

The experimental realization of Photonic bandgap (PBG) structures for optical transmission at the usual wavelengths is quite difficult. It requires the realization of periodic structures with an extremely high accuracy, both for the periodicity and for the dimensions of the individual scatterers.

From a modeling point of view, the simulation of realistic PBG structures is also quite challenging. Whereas the band diagram is reasonably simple to compute for an infinite lattice of infinitely long scatterers, the electromagnetic properties of a finite structure, composed of scatterers with a finite length, are much more difficult to characterize. However, any practical realization of a PBG structure relies only on a finite number of scatterers. Further, in a realistic device, the PBG structure must be embedded into a stratified background with a guiding layer, which provides the vertical light confinement.

We recently developed a new computational approach that can handle scatterers placed in a stratified background [1-3]. This technique relies on the Green's tensor associated with the stratified background and is very well suited for simulating planar waveguides with embedded scatterers. One of the attractive features of this approach is that only the scatterers must be discretized, the stratified background forming the guiding layers being accounted for in the Green's tensor. For the simulation of PBG structures embedded in waveguiding structures, this means that the discretization is limited to the scatterers forming the PBG, irrespective of the number of layers composing the stratified background.

Using this fully vectorial three-dimensional approach, we investigate specific properties of realistic PBG structures embedded in optical waveguide structures. In particular, we study the radiation losses from the PBG structure into the substrate or into the air; the coupling between the unperturbed waveguide into the PBG structure and the corresponding insertion losses. We also discuss the correlation between the band diagram for an infinite lattice and the transmission properties of a finite PBG structure embedded in a waveguide. Finally, we study the guiding properties of a channel waveguide defined through the PBG structure within the background waveguide. Practical implications such as the fabrication tolerances for the realization of a PBG structure embedded in a stratified waveguide are also discussed.

REFERENCES

1. M. Paulus and O.J.F. Martin, "Light propagation and scattering in stratified media: A Green's tensor approach," J. Opt. Soc. Am. A 18, 854-861 (2001).
2. M. Paulus and O.J.F. Martin, "A Fully vectorial technique for scattering and propagation in three-dimensional stratified photonic structures," Opt. and Quantum Electronics. 33 315-325 (2001).
3. M. Paulus and O.J.F. Martin, "Green's tensor technique for scattering in two-dimensional stratified media," Phys. Rev. E 63, 066615.1-066615.8 (2001).

Coupling to and Transmission Through Photonic Crystal Waveguides

T. J. Karle, D. H. Brown and R. Wilson
Ultrafast Photonics Collaboration, School of Physics & Astronomy, University of St Andrews
St. Andrews, KY16 9SS, Scotland

M. Steer
EPSRC Central Facility for III-V Semiconductors, Department of Electronic and Electrical Engineering,
University of Sheffield
Sheffield, S1 3JD, U.K.

T. F. Krauss
Ultrafast Photonics Collaboration, School of Physics & Astronomy, University of St Andrews
St. Andrews, KY16 9SS, Scotland

We explore the characteristics of two dimensional Photonic Crystal (PhC) based waveguide structures. Transmission measurements are presented for Coupled Cavity Waveguide (CCW) samples, with high throughput observed for closely coupled defects. A slab waveguide GaAs/GaAlAs heterostructure is preferred, providing confinement in the vertical direction. A triangular lattice of air holes etched through this dielectric waveguide provides a platform for our investigations.

The CCWs consist of a chain of missing hole defects orientated along the Γ-K crystal axis. Both single (H1) and seven (H2) missing hole cavities are examined. The coupling mechanism along the chain is examined using FDTD simulation to study the modal properties of the cavities. The 'air holes in dielectric' system is distinct from its converse lattice structure of 'dielectric rods in air', in that the defect modes have a higher symmetry. We also address the input/output coupling from access waveguides. As with 1D PhCs, (eg. Fibre Bragg Gratings) there exists a group velocity mismatch, in coupling between a fast and a slow wave structure, and this requires an "impedance match" to transform the modes. Here we can take advantage of the 2D nature of the crystals. We examine various methods to achieve this within the restrictions of our fabrication methods.

Laser transmission measurements are obtained using a lithographic tuning technique. Spectral bandwidths of the order of tens of nanometres can be realised with high transmission. We observe good comparison between simulation and physical experiment. Enhanced transmission performance is demonstrated, for various crystal and access waveguide configurations.

Photonic Crystal Technologies for Chip-Scale Photonic Circuits

D. W. Prather
University of Delaware
Newark, DE 19716, U.S.A.

Next generation integrated circuit (IC) processors will continue to benefit from two progressing trends in microelectronics technology: decreasing device sizes and increasingly more parallel architectures. As the first trend results in both higher device density and faster operational speeds, the second trend results in ICs with increased throughput, due to the ability to perform multiple instructions simultaneously. However, while both of these trends enable the realization of significantly more sophisticated processors they tend to exacerbate an already serious problem: the communication infrastructure between the devices, components, and circuits within the processor.

As a result of this challenge we are currently developing photonic crystal technologies for the monolithic integration of on-chip interconnect infrastructures. This technology is based on the relatively new field of photonic crystal devices, which we use to create a three dimensional mesh of guided wave channels that have dimensions on the nanometer scale, are monolithic, and can be wavelength selective. As a result, this approach allows for the incorporation of fiber optic communication principles, such as high bandwidth, multi-channel, add/drop, and WDM, into the design of interconnect infrastructures on a chip.

In the course of this talk we will discuss the design, fabrication, characterization, and integration of photonic crystal devices for the above integrated circuit applications. More specifically we will present our design tools that are based on computational electromagnetic methods, such as the plane wave method and the finite-difference time-domain method. For fabrication we will present our newly developed methods for multi-layer photonic crystals in silicon, patterned with electron beam lithography. For characterization we will present our work on using a broad-band source to illuminate the photonic crystal structures and an optical spectrum analyzer to characterize their response. Lastly, we will also discuss proposed methods for their integration into actual chip-scale photonic circuits.

Out-of-Plane Losses of Single-Row Defect Photonic Crystal Waveguides

G. R. Hadley
Sandia National Laboratories
Albuquerque, NM 87185-5800, U.S.A.

Previous work has solidly established photonic crystals as a promising technology for future photonics circuitry. These structures possess some very unusual properties in being able to guide light around corners with small radii of curvature. However, the first issue that must be resolved before these devices are taken seriously concerns the propagation loss of simple straight waveguides. These waveguides are commonly fabricated by etching a lattice of holes into a slab waveguide structure with the modification of a single (or multiple) row of holes to form a so-called single-row defect waveguide. So far, these waveguides have indeed been shown to guide light. However, detailed measurements of their propagation losses have been rare, and when they have been reported indicate losses in the $50 - 100$ cm^{-1} range[1]. These values are unacceptably high for many applications, and in any event are at odds with the prevalent view that such devices should exhibit regimes of zero loss. The purpose of this work is to address the question of the fundamental causes of loss in these devices theoretically and to thereby suggest some strategies for designing lower loss waveguides. For concreteness we will restrict our investigation to the case of waveguides formed by the omission of a single row of holes.

We calculate the out-of-plane losses on single row defect waveguides using a 3D finite difference eigenmode solver that includes the exact slab structure with absorbers as top and bottom layers together with radiation boundary conditions[2]. The loss is determined from the imaginary part of the complex propagation constant eigenvalue. This loss has been calculated over a wide frequency range for two common slab structures in use, and shows significant wavelength dependence and significant variation between structures, ranging from values around 10 cm^{-1} for high-contrast AlOX structures to around 50 cm^{-1} for lower-contrast AlGaAs structures. The resulting calculations lead to a simple coupled-mode-theory picture in which propagation losses result from coupling of energy out of the fundamental waveguide mode into lossy radiation modes by the effective corrugation of the hole pattern. The conclusions of this work are therefore that (1) lower-loss waveguides are possible, perhaps with losses below 5 cm^{-1}, and (2) design of such devices involves engineering the slab structures so that their radiation modes are either weak or optimally positioned so that the minimum of energy from the fundamental mode is coupled into them.

REFERENCES

1. C. J. M. Smith, H. Bensity, S. Oliver, M. Rattier, C. Weisbuch, T. F. Krauss, R. M. DeLaRue, R. Houdre, and U. Oesterle, *App. Phys. Lett.* 77, No. 18, 2813(2000).
2. G. Ronald Hadley, To Be Published in *Photonics Technology Letters*.

Iterative Eigensolver Techniques and Maxwell's Equations in Periodic Systems

S. G. Johnson and J. D. Joannopoulos
Massachusetts Institute of Technology
Cambridge, MA 02139, U.S.A.

Optical systems have been the subject of enormous practical and theoretical interest in recent years, with a corresponding need for mathematical and computational tools. One fundamental approach in their analysis is eigenmode decomposition: the possible forms of electromagnetic propagation are expressed as a set of definite-frequency (time-harmonic) modes. In the absence of nonlinear effects, all optical phenomena can then be understood in terms of a superposition of these modes, and many forms of analytical study are possible once the modes are known. Of special interest are periodic (or translationally-symmetric) systems, such as photonic crystals (or waveguides), which give rise to many novel and interesting optical effects. The solutions of such periodic systems are governed by Bloch's theorem, a critical tool for both theoretical understanding and computational analysis of these structures. Another important basic system is that of resonant cavities, which confine light to a point-like region. There, the boundary conditions are, in principle, irrelevant if the mode is sufficiently confined – so they can be treated under the rubric of periodic structures as well via the supercell technique. In this talk, we describe a fully-vectorial, three-dimensional method for computing general eigenmodes of arbitrary periodic dielectric systems, including anisotropy, based on the preconditioned block-iterative solution of Maxwell's equations in a planewave basis. A new effective dielectric tensor for anisotropic systems is presented as an important technique for accelerating convergence and tolerating coarse grid resolutions, and we suggest that a similar effective tensor could be employed in other electromagnetic calculations, from finite-difference time-domain (FDTD) to beam-propagation methods (BPM). We also describe a technique for computing eigenvalues in the interior of the spectrum (e.g. defect modes) without computing the underlying bands, which is exceedingly useful for resonant-cavity calculations. We present comparisons of different iterative solution schemes, preconditioners, and other aspects of frequency-domain calculations. This work is also available as a free and flexible computer program downloadable from the Web (http://ab-initio.mit.edu/mpb/).

Modelling of Waveguide Photonic Crystal and Photonic Wire Device Structures

R. M. De La Rue, I. Ntakis, A. S. Jugessur, H. Chong, and P. Pottier
Optoelectronics Research Group, Department of Electronics and Electrical Engineering
University of Glasgow
Glasgow, G12 8QQ, Scotland, U.K.

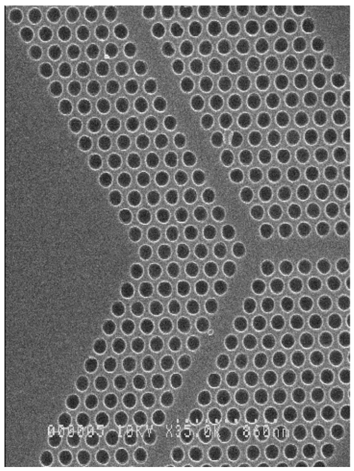

Fig. 1(a): Photonic crystal channel junction

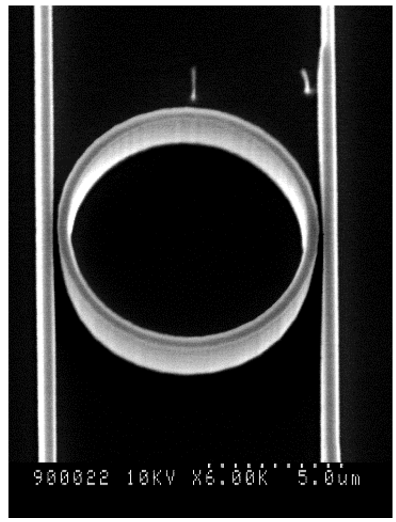

Fig. 1(b): Photonic wire structure.

In this presentation we shall describe new results for planar-waveguide based photonic crystal and photonic wire device structures. Examples of device structures investigated include large angle junctions [Fig. 1(a)], bends, tapers, waveguide microcavities and planar resonators. A photonic wire example is shown in Fig. 1(b). Computational modelling has been used extensively but with the central aim of designing useful devices – and predicting their characteristics and performance. Heavy reliance has been placed on commercial software, e.g. Fullwave from RSoft and FIMMPROP from Photon Design. Some commercial software is explicitly restricted to modelling two-dimensional situations and is therefore intrinsically limited in its ability to describe the frequency-dependent propagation of light through realistic waveguide-based device structures.

Because of the approach that we have taken, subjective factors such as ease-of-use and visualisation have inevitably played a major role. But it has been equally important to recognise that serious questions of accuracy can appear, with the possibility of substantial errors occurring. It is clear that prediction of the experimentally observed Q-factor and resonant frequency of, e.g., photonic crystal waveguide microcavities may be difficult, even where state-of-the-art fabrication technology is used and accurate post-fabrication measurements are made. The problems of obtaining good agreement between experiment and theory have been recognised for some time [1] and have not gone away [2]. We shall, where possible, address these problems in the presentation.

REFERENCES

1. T.F. Krauss et al, Nature, **383**, pp. 699-702, 24th Oct (1996).
2. T.P. Pearsall et al, LEOS Annual Meeting, San Diego, 11-15 Nov. 2001 , paper TuB3.

Vector Finite Element Method for Anisotropic 2D Dielectric Photonic Crystals

V. F. Rodríguez-Esquerre and H. E. Hernández-Figueroa
Department of Microwaves and Optics, School of Electrical and Computer Engineering, University of Campinas, UNICAMP
São Paulo, Campinas 13083-970, Brazil

A Vector Finite Element Method (VFEM) is used for computing the band structure in 2D photonic crystal structures made of full anisotropic dielectric material ($\bar{\bar{\epsilon}}_r$). Recent results showed the advantage of using anisotropic materials to optimize the band gap in photonic crystals. In those works diagonal anisotropy is analyzed. Here we introduce total permittivity anisotropy. We start from the double curl wave equation,

$$\nabla \times \bar{\bar{\phi}}_r \; \nabla \times \vec{H} = \left(\frac{\omega}{c}\right)^2 \vec{H} \tag{1}$$

where H is the magnetic field, ω is the angular frequency, c is the light velocity in vaccum, and the tensor $\bar{\bar{\phi}}_r$, which is the inverse of the relative anisotropic permittivity tensor, is given by,

$$\bar{\bar{\phi}}_r = \frac{1}{\bar{\bar{\epsilon}}_r} = \begin{bmatrix} \phi_{xx} & \phi_{xy} & \phi_{xz} \\ \phi_{yx} & \phi_{yy} & \phi_{yz} \\ \phi_{zx} & \phi_{zy} & \phi_{zz} \end{bmatrix} = \bar{\bar{\phi}}_T + \vec{\phi}_{yx}\hat{z} + \hat{z}\vec{\phi}_{xy} + \phi_{zz}\hat{z}\hat{z}; \qquad \bar{\bar{\phi}}_T = \begin{bmatrix} \phi_{xx} & \phi_{xy} \\ \phi_{yx} & \phi_{yy} \end{bmatrix}$$

$$\vec{\phi}_{xy} = (\phi_{zy}\hat{y} + \phi_{zx}\hat{x})\,; \qquad \vec{\phi}_{yx} = (\phi_{yz}\hat{y} + \phi_{xz}\hat{x})$$

The computational domain is the plane xy and the propagation is parallel to this plane with no variation in the axial direction $\partial/\partial z = 0$, then we can write $\nabla = \nabla_T$, where $\nabla_T = \partial/\partial x\,\hat{x} + \partial\partial y\,\hat{y}$, and $\vec{H} = \vec{H}_T + \vec{H}_z$. Plugging into (1), we obtain the following transverse and axial equations, respectively,

$$\nabla_T \times \phi_{zz} \; \nabla_T \times \vec{H}_T + \nabla_T \times \vec{\phi}'_{xy} \times \nabla_T \times \vec{H}_z = \left(\frac{\omega}{c}\right)^2 \vec{H}_T \tag{2a}$$

$$\nabla_T \times \bar{\bar{\phi}}_T \; \nabla_T \times \vec{H}_z + \nabla_T \times \vec{\phi}'_{yx} \times \nabla_T \times \vec{H}_T = \left(\frac{\omega}{c}\right)^2 \vec{H}_z \tag{2b}$$

where $\vec{\phi}'_{xy} = \phi_{zy}\hat{x} - \phi_{zx}\hat{y}$, and $\vec{\phi}'_{yx} = -\phi_{yz}\hat{x} + \phi_{xz}\hat{y}$.

Since spurious solutions may occur in solving (2), a careful numerical approach is required. To avoid such undesired solutions and observing that $\nabla_T \cdot \vec{H}_T = 0$, (2) can be solved in an efficient manner using solenoidal edge elements for $\vec{H}_T = 0$ and nodal elements for $\vec{H}_z = 0$. Proper boundary conditions can be applied taking into account that $\vec{H} = \vec{h}e^{-j\vec{k}_T\cdot\vec{r}}$, where $j = \sqrt{-1}$, $\vec{k}_T = k_x\hat{x} + k_y\hat{y}$ is the wave vector, $\vec{r} = x\hat{x} + y\hat{y}$ and $\vec{h}$ is the envelope. The latter is periodic over the unitary cell's boundary. Full anisotropy provides more freedom degrees than the isotropic case, this permits the design of waveguide structures with novel polarization characteristics. To show the validity and usefulness of the proposed algorithm, numerical results for a variety of anisotropic photonic crystal structures will be discussed and presented at the Conference.

The authors thank the Brazilian Agencies FAPESP and CNPq for their financial support. FAPESP Process No. 98/16202-0. CNPq Process No. 301209/94-4.

Use of Negative Refraction Characteristics of Photonic Crystals for Coupling into Single-Row Defect Photonic Crystal Waveguides

D. W. Peters
Sandia National Laboratories
Albuquerque, NM 87185-0603, U.S.A.

The usefulness of single-row defect photonic crystal waveguides has been limited to date by the mismatch and subsequent high losses incurred when coupling light from a conventional waveguiding structure. Recent work describing photonic crystals with negative refractive index characteristics offer a potentially attractive solution to this problem. In particular, the negative index photonic crystal may be used to focus a diverging Gaussian beam to a small spot where it may then couple efficiently into a row-defect waveguide.

In this paper we investigate this coupling mechanism by numerically simulating two identical photonic crystals comprising air holes etched into a slab waveguide but rotated at 90 degrees with respect to each other. Light is injected into the first crystal along the $\Gamma - K$ direction at a frequency corresponding to the 5^{th}-6^{th} band where negative index behavior is known to occur. Near the focal point the second photonic crystal, oriented in the $\Gamma - M$ direction, is positioned so that focused light enters the single-row defect waveguide. Coupling efficiency depends both on the alignment of the two crystals as well as the divergence of the incident beam.

The performance of this coupling device is investigated using a 2D triangular mesh finite difference model. The effective index approximation has been employed to reduce the 3D problem to two dimensions. One novel aspect of this device is that the row-defect waveguide as shown below must be operated at a much higher frequency than its usual value in the lowest band gap. Waveguide performance at these frequencies still remains to be explored. An alternative solution is to use photonic crystals with widely different lattice constants and hole diameters. Relative performance of these geometries will be discussed.

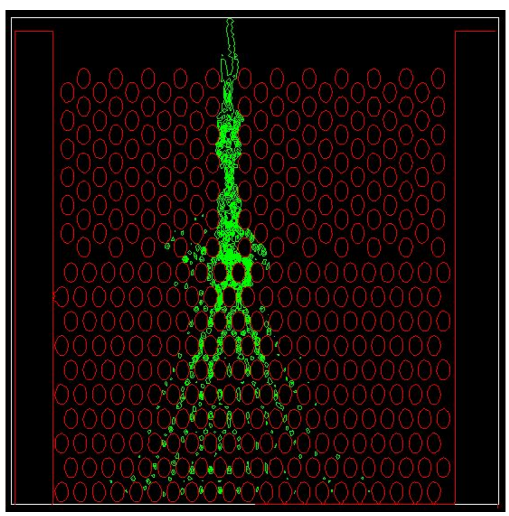

Figure 1. Photonic crystal focusing light into row-defect photonic crystal waveguide.

Negative Refraction at Optical Frequencies in Photonic Crystals near the Photonic Band Edge

M. Notomi
NTT Basic Research Laboratories
Atsugi, 243-0198, Japan

We demonstrate that light propagation in strongly-modulated multi-dimensional dielectric photonic crystals becomes *refraction-like* in the vicinity of the photonic band gap. Such a crystal behaves like an isotropic material having an effective refractive index whose sign and absolute value can be controlled by the photonic band structure. When this index is negative, various interesting light-propagation phenomena (mirror-like imaging effect, image-transfer effect, etc.) relating to *negative refraction* occur. This negative refraction is similar to that recently discussed and observed in left-handed meta-materials consisting of split-ring resonators and grid arrays of UCSD group, but the basic physics is totally different and it can be realized in *optical frequencies*.

We first study the light propagation phenomena in weakly-modulated photonic crystals, and show that appropriate effective refractive index cannot be defined in them. Nevertheless, the effective-index approximation becomes meaningful for the propagation states of strongly-modulated photonic crystals near the photonic band edge. In other words, we can use Snell's law to describe the light propagation in such strongly-modulated photonic crystals with a constant effective index (that can be negative) for all incident angles. The situation is analogous to the effective-mass approximation in electron-band theory.

We analyze propagation states near the photonic band edge by using photonic band calculations for 2D square and hexagonal photonic crystals, and directly show that negative refraction really occurs for such photonic crystals by numerical simulation using finite-difference time-domain (FDTD) method. The result shows the predicted negative refraction and imaging effect take place in such strongly-modulated photonic crystals in optical frequencies.

REFERENCES

1. M. Notomi, Phys. Rev. B 62, 10696 (2000).

Session 4Ac4

Novel Microwave Circuits and Antennas: Numerical Methods and Practical Applications

Power Synthesis for Conformal Arrays, Using Radiation Pattern Phase Distribution

G. Castaldi and G. Gerini
Physics and Electronics Laboratory TNO
The Hague, Netherlands

Since a few years, conformal array antennas have attracted a growing interest of both antenna and platform designers. These arrays, in fact, can offer some advantages compared to planar array antennas. They can fulfil the structural and/or aerodynamic requirements without appreciable degradation of the antenna performance, can have wider scan angles without rotating/moving antennas, can reduce radar cross section of the platform and the interaction between radome and antenna.

Unfortunately, the analysis and synthesis of such arrays are more complicated, since it is impossible to factorize the expression of the radiation pattern into an element pattern and an array factor. Furthermore, the polarization properties of the array depend, not only on the elements, but also on the geometry of the array itself. As a result, the analytical methods developed for planar arrays are not suitable for conformal antennas.

Nowadays, because of the stringent constrains on the required radiation pattern amplitude, the synthesis problems need to exploit the radiation phase distribution, as a further degree of freedom. As a result, the synthesis problem is not linear and therefore, this has motivated, in the last years, the development of algorithms like iterative least square synthesis, and generalized projection method.

In this communication, we propose a robust and reliable approach for synthesis of conformal arrays, using the radiation pattern phase distribution. This method, by using the least square technique, reduces the power synthesis problem to the minimization of a functional, representing the squared distance between the actual and required radiation pattern. The unknowns are the feeding currents and the radiation pattern phase distribution. Gram-Schmidt method allows expressing the feeding currents in terms of the phase distribution, which, therefore, becomes the only unknown of the problem.

For the minimization of the objective functional, we propose an iterative technique, based on the optimization theory for constrained functions. In order to improve the reliability and robustness of the algorithm, we use a continuation method, introducing a suitable parametric transformation of the functional. By slowly increasing the continuation parameter, this functional is minimized, starting from the previous local solution.

This technique has been applied to the pattern synthesis of some significant conformal array structures. Numerical simulations have shown that the algorithm is more reliable and robust to spurious solutions and obtains a mean square error lower than the iterative least square synthesis, at the cost of a slightly higher computation time.

A Simple Waveguide Diplexer for Satellite Communications

A. Alvarez-Melcon
Information and Communications Department, Technical University of Cartagena
Cartagena, Murcia 30202, Spain

M. Mattes and J. R. Mosig
Ecole Polytechnique Fédéderal de Lausanne (EPFL)
Laboratoire d'Electromagnétisme et d'Acoustique (LEMA)
Lausanne, 1015, Switzerland

This paper presents the design of a very simple diplexer in waveguide technology, which uses only inductive discontinuities. Due to the simplicity of the structure proposed, it can be very easily designed using efficient software full wave simulators, therefore reducing the experimental work to the final manufactured hardware. The structure is composed of two four-pole inductive filters, one with centre frequency of 9.5 GHz and the other of 10.65 GHz, which are then connected to a single input entry with the aid of a simple H-plane T-junction. For the analysis of this structure, first the inductive filters are optimised separately with a full-wave software simulator based on [1]. The T-junction is then analyzed using an improved theory of cavities as described in [2], which is then coupled to the inductive filters analysis. For the optimization of the whole structure the procedure described in [3] has been used. Following this technique only the first cavity of the filters need to be re-designed to compensate for the reactive behaviour of the opposite branch, and for the re-adjustment of the input coupling of each filter in the presence of the T-junction walls. For the final optimization, the response of the first cavity of each filter is obtained alone. Then the first cavity of each filter is connected to the T-junction, and the couplings and lengths of the structure are modified until the behaviour of the cavities alone are recovered. Once the first cavity is re-designed in this way, the rest of the filters can be added to complete the diplexer. The result is a complete design of the whole structure in a few minutes. Furthermore, due to the accuracy of the software employed the experimental iterations in the laboratory are reduced to one. The diplexer has been manufactured and tested. The final design is shown in Fig.(a), while Fig.(b) presents comparison between predicted and measured response. Results show that the software derived is indeed accurate, and the procedure efficient for the design of this type of hardware. During the conference full details on the software developed and the design procedure will be given.

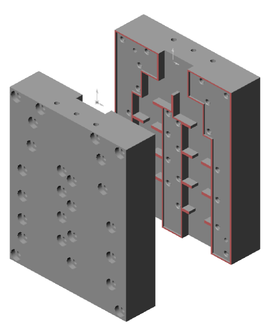

(a)

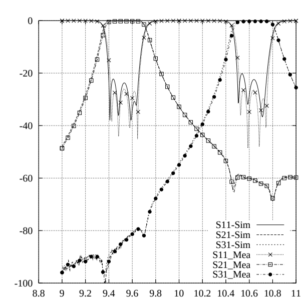

(b)

REFERENCES

1. Conciauro et. al. *Advanced Modal Analysis, CAD Techniques for Waveguide Components and Filters*, Wiley, 2000, pp. 213.
2. Michael Mattes et. al. *European Microwave Conference*, 3-5 October 2000, Paris, France, pp. 274-277.
3. Guglielmi. *IEEE Trans. Microw. Theory and Tech.*, Vol. 42,. No. 7, 1994, pp. 1347-1352.

Efficient Analysis and Design of Dichroic Plates for Large Reflector Antennas

M. Bozzi and L. Perregrini
Dept. Electronics, University of Pavia
Pavia, 27100, Italy

Large reflector antennas for radio-astronomy applications usually operate in more than one frequency bands. The feeding system of such antennas frequently consists of a beam waveguide, where the combination of the signals at different frequencies can be performed by dichroic plates.

In the basic configuration, dichroic plates consist of a thick metal screen perforated periodically with apertures: the geometry of the apertures and the thickness of the metal screen determine the frequency bands where the dichroic plate is transparent and the ones where it is a perfect mirror. More complicated configurations are sometimes used, in order to achieve better performance: multigrid structures and metal plates perforated periodically with stepped-waveguides have been proposed.

Recently, we have developed an efficient method for the analysis of dichroic plates [1]. This method, named the MoM/BI-RME method, is based on the infinite array approximation and permits the analysis of dichroic plate with arbitrarily shaped apertures. The peculiarity of the method consists in the use of the Boundary Integral-Resonant Mode Expansion (BI-RME) method for the numerical calculation of entire-domain basis functions, needed in the analysis by the Method of Moments (MoM).

The MoM/BI-RME method was implemented in fast and flexible computed codes. One of them applies to the analysis of single-grid dichroic plates, perforated with arbitrary apertures and illuminated by a uniform plane wave incident at an arbitrary angle. This code permits the wideband analysis of dichroic plates in few seconds on a standard PC. This code was used for the design of a S-/X-band dichroic mirror to be operated in the deep space antenna of the European Space Agency (ESA) in Perth, Australia [2]. This antenna is required for future deep space missions by ESA, such as Rosetta and Mars Express. Another code was implemented for the analysis of multigrid dichroic plates. By using the segmentation technique and the infinite array approximation, the structure reduces to a number of step discontinuities between a metallic waveguide and a waveguide with periodic boundary conditions, where the field is expressed as a combination of Floquet modes.

Finally, a code was implemented for the analysis of metal plates perforated with stepped waveguides. In this case, the structure reduces to the cascade of two types of discontinuities: the discontinuity between two metallic waveguides with different cross sections and the one between a metallic waveguide and a waveguide with periodic boundary conditions.

REFERENCES

1. M. Bozzi, L. Perregrini, J. Weinzierl, and C. Winnewisser, “Efficient Analysis of Quasi-Optical Filters by a Hybrid MoM/BI-RME Method,” *IEEE Transactions on Antennas and Propagation,* Vol. AP-49, No. 7, pp. 1054-1064, July 2001.
2. P. Besso, M. Bozzi, L. Perregrini, L. Salghetti Drioli, and W. Nickerson, “Deep Space Antenna for Rosetta Mission: Design and Testing of the S/X-Band Dichroic Mirror,” accepted for publication in the *IEEE Transactions on Antennas and Propagation*.

Efficient Techniques for the Accurate Analysis and Design of Passive Waveguide Components with Arbitrary Geometry

V. E. Boria, S. Cogollos, H. Esteban, and A. A. San Blas
Universidad Politécnica de Valencia
Valencia, Spain

B. Gimeno
Universidad de Valencia
Valencia, Spain

Present manufacturing techniques, e.g. computer-controlled milling, spark eroding or electro-forming, usually introduce internal rounded corners during the low-cost manufacture of passive rectangular waveguide components. If the CAD tools employed to design these devices had accurate and efficient analysis engines for considering the cited mechanization effects (rounded corners), the industrial production of such waveguide components would be highly improved in terms of accuracy, costs and development times. For these reasons, the presence of rounded corners in passive waveguide devices has recently become a topic of great interest in the technical literature [1, 2].

In this paper, we present two novel hybrid techniques for the accurate and efficient analysis of passive waveguide components with arbitrary geometry in the H-plane and in the cross-section of the waveguides. Results for inductively coupled rectangular waveguide filters including rounded corners in the H-plane of coupling windows and cavities, as well as in the cross-section of waveguides, have been successfully validated through numerical and experimental data (see Fig. 1).

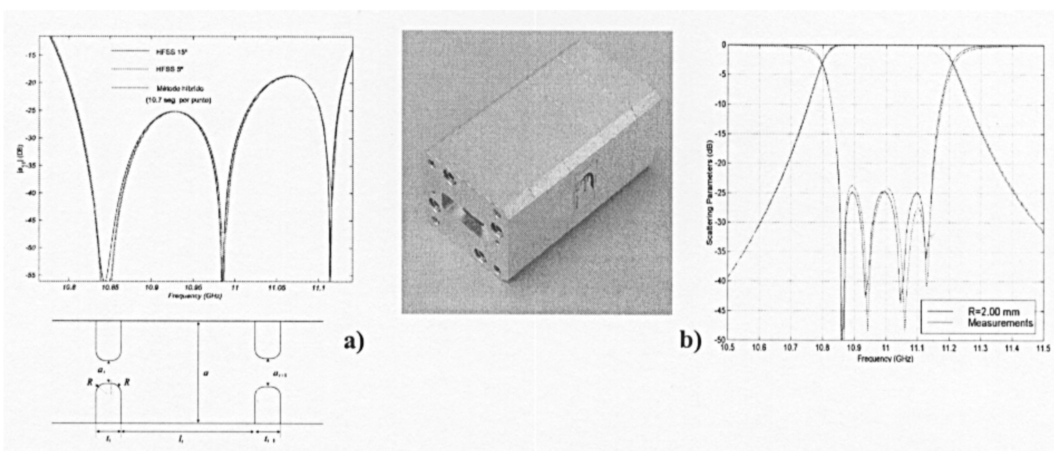

Figure 1: Effect of rounded corners in the H-plane in a), and in the cross-section of the waveguides in b).

REFERENCES

1. Reiter, J. M. and F. Arndt, "Rigorous analysis of arbitrarily shaped H- and E-plane discontinuities in rectangular waveguides by a full-wave boundary contour mode-matching method," *IEEE Trans. Microwave Theory and Tech.*, Vol. 43, 796–801, April 1995.
2. Bressan, M., L. Perregrini, and E. Regini, "BI-RME modeling of 3D waveguide components enhanced by the Ewald technique," *IEEE MTT-S Int. Symp. Dig.*, 1097–1100, Boston, June 2000.

Integral Equation Analysis of Multilayered Shielded Transmission Lines

J. L. G. Tornero and A. Alvarez-Melcon
Information and Communications Department, Technical University of Cartagena
Cartagena, Murcia 30202, Spain

T. M. Grzegorczyk
Massachusetts Institute of Technology
Cambridge, MA 02139, U.S.A.

This paper presents the analysis of multilayered and multiconductor shielded transmission lines using the Integral Equation Technique (IE). The formulation uses the 2D multilayered media shielded Green's functions for the electric field expressed in terms of infinite series of modal expansion functions (infinite wire in a box). The basic modal expansions used are those of a parallel plate waveguide (normal incidence), modified to allow for a propagating factor in the longitudinal direction of the structure. The coefficients of the expansion are traditional voltage terms calculated in equivalent transverse transmission lines along the stratification axis [1]. The integral equation is formulated and solved with the Method of Moments (MoM), which leads to an homogeneous system of linear equations that can be solved for the unknown propagating factor. In order to assure good convergence rate in the infinite series used to express the kernel of the integral equation, the modal expansion under normal incidence in a parallel plate waveguide of equivalent magnetic walls is used as basis and test functions in the MoM, following similar ideas as those presented in [2]. Fig. (a) shows the convergence behavior of the kernel as a function of the ratio strip width/box width, while Fig. (b) shows a comparison of the dispersion relation for the dominant TEM mode between the technique derived in this paper, results obtained with a spectral domain approach, and results obtained with the technique [3]. Results show that the technique is accurate and convergence is attained fast, so efficient computer codes can be developed.

The technique derived has also been adapted to account for any arbitrary periodic structure printed along the longitudinal axis. In this case a two dimensional integral equation is applied to a unit cell by using a Fourier series expansion of Floquet modes [4]. Finally, a modified structure consisting in opening the top cover of the box has been implemented. This has been accomplished by defining proper magnetic currents at the top cover through the use of the surface equivalence principle, combined with the 2D infinite current filament free space Green's functions for the external region. The technique leads to a coupled system of integral equations which is solved for the complex propagating factor. The resulting software has allowed to explore the leaky and surface wave propagation properties in these novel transmission line structures. A thorough discussion will be presented at the conference, including side coupled and broadside coupled lines printed on a slab.

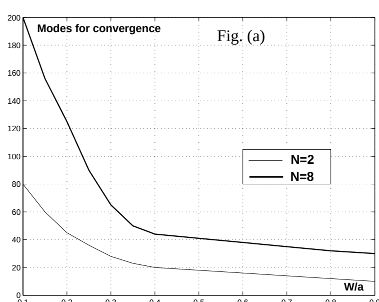

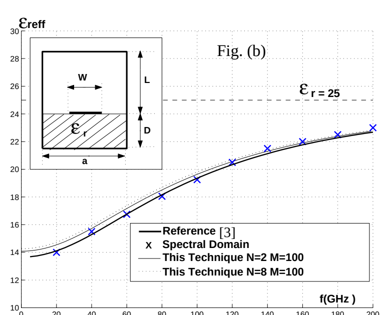

$\epsilon_r = 25,\ L = 10\text{mm}$,
$\mathrm{D} = 0.254\text{mm}$,
$\mathrm{a} = 0.726\text{mm}$,
$\mathrm{w} = 0.0807\text{mm}$

Acknowledgment: This work has been developed under contract CICYT No. TIC2000/0591/C03/03, and PROFIT No. PNE028 /2001-C-01.

REFERENCES

1. Michalski et. al. *IEEE Trans. Antennas and Propagation*, Vol. 45, No. 3, 1997, pp. 508-519.
2. Melcon et. al. *IEEE Trans. Microw. Theory and Tech.*, Vol. 47, No. 7, 1999, pp. 1045-1058.
3. Guglielmi et. al. *IEEE Trans. Microw. Theory and Tech.*, Vol. 43,. No. 11, 1995, pp. 2621-2626.
4. Pozar et. al. *IEEE Trans. Antennas and Propagation*, Vol. 32, No. 6, 1984, pp. 602-610.

Efficient Technique for the Analysis of Cylindrical Dielectric Resonators in Rectangular Waveguide Cavities

D. Camilleri, B. Gimeno, A. Coves, and M. V. Andrés
Dpto. de Física Aplicada - I.C.M.U.V., Universidad de Valencia
Valencia, Spain

A. A. San Blas, H. Esteban, and V. E. Boria
Dpto. de Comunicaciones, Universidad Politécnica de Valencia
Valencia, Spain

Cylindrical dielectric resonators are usually axially loaded in rectangular enclosures for mechanical reasons. In fact, dielectric-loaded cavities find increasing applications as microwave filters in satellite and mobile communications because of their small size, low loss and temperature stability [1]. In this paper we present a novel technique for the efficient analysis of inhomogeneous cylindrical resonators, located in an arbitrary position of a rectangular waveguide cavities bounded by perfect electric conductors [2]. This new procedure takes advantage of some mathematical properties which leads to a computationally efficient and versatile method. This approach also provide high numerical precision, which is a requirement to model high Q resonators.

In Figure 1 we show the results (S_{21} parameter) provided by our novel technique for the case of a dielectric resonator arbitrarily placed within a metallic cavity. We have compared our results with the numerical data provided by the technical literature [3]. As we can in figure 1, an excellent agreement between our results and the numerical data has been obtained, thus fully confirming that the novel method proposed in this paper is very accurate.

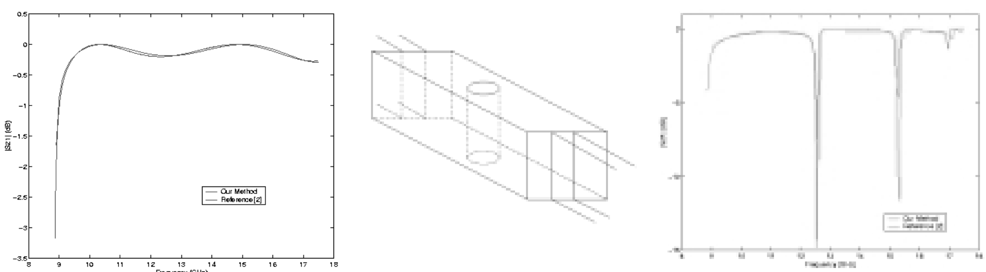

a) **b)**

Figure 1: Scattering parameter (S_{21}) of a dielectric resonator ($\varepsilon_r = 2.17$) placed in the center of the cavity in (a), and shifted respect to the center of the cavity in (b).

REFERENCES

1. Liang, X.-P. and K. A. Zaki, “Modeling of cylindrical dielectric resonators in rectangular waveguides and cavities,” *IEEE Trans. Microwave Theory and Tech.*, Vol. 41, No. 12, 2174–2181, Dec. 1993.
2. Monsoriu, J. A., M. V. Andrés, E. Silvestre, A. Ferrando, and B. Gimeno, “Analysis of dielectric-loaded cavities using an othonormal-basis method,” Accepted to be published in *IEEE-MTT*.
3. Esteban, H., S. Cogollos, V. E. Boria, A. San Blas, and M. Ferrando, “A new hybrid mode-matching/numerical method for the analysis of arbitrarily shaped inductive obstacles and discontinuities in rectangular waveguides,” Accepted to be published in *IEEE-MTT*.

Acknowledgments: This work was supported by the European Commission under the Research and Training Networks Programme, Contract No. HPRN-CT-2000-00043, and by the Ministerio de Ciencia y Tecnologa (Spain) under the Project No. TIC2000-0591-C03-03

Use of Broadside Conductor-Backed CPW-Fed Twin Linear-Slot Antennas for Increased Radiation Efficiency on Two-Layer Dielectric Substrates

J. P. Jacobs, J. Joubert, and J. W. Odendaal
Centre for Electromagnetism
Department of Electrical, Electronic and Computer Engineering
University of Pretoria
Pretoria, 0002, South Africa

Slot antennas fed by coplanar waveguide (CPW) without conductor backing have been found in recent years to exhibit several benefits, including wider impedance bandwidth than microstrip patch antennas. For many applications, however, it is necessary that a conducting back plane forms part of the antenna structure. An important drawback of conductor-backed coplanar waveguide (CBCPW)-fed slot antennas is the excitation of parasitic parallel-plate modes at the discontinuity posed by the radiating slot. Even for antennas on a two-layer dielectric substrate that precludes propagation of the parallel-plate TEM mode, power leakage into the TM0 mode may degrade radiation efficiency to the extent that the antenna becomes unsuited for practical usage. This may occur even though the CBCPW feeding line itself is not leaky.

In earlier reports, a technique has been described for increasing the radiation efficiency of single linear-slot antennas on thick dielectric substrates. This involves placing appropriately spaced, in-phase driven twin elements broadside to each other, which results in partial phase cancellation of the dominant surface-wave mode. More recently, a similar effect has been demonstrated for twin linear slots on either thick or thin substrates with a ground reflector positioned a quarter free-space wavelength away from the conductor side of the antenna. It has furthermore been shown that guided leaky-wave cancellation can be enhanced even further for a similarly layered structure with a substrate height not exceeding a quarter dielectric wavelength by using twin arc-slot radiators of appropriate radius of curvature and length.

In this paper, we focus on twin linear slots on a conductor-backed two-layer substrate with a high-low combination of dielectric permittivities (the high permittivity layer being adjacent to the slots). The twin slots' CBCPW feeding lines are taken into account explicitly. We show that radiation efficiency can be significantly improved compared to the radiation efficiency of a single slot when the slots are appropriately spaced. A systematic investigation is furthermore presented of how radiation efficiency is affected by parameters such as substrate layer heights and dielectric constants, radiating slot length, and feeding line dimensions. Radiation pattern characteristics are also addressed. Theoretical findings will be discussed in conjunction with measured data.

Characteristics of Microstrip Antennas on Ferrimagnetic Substrates

J. R. S. Oliveira and R. N. L. Martins
Centro Federal de Educação Tecnológica do Maranhão (CEFET-MA)
Department of Eletronics, CEFET-MA
São Luís, Brazil

A. G. d'Assunção and S. G. da Silva
Universidade Federal do Rio Grande do Norte (UFRN)
Centro de Tecnologia, Departamento de Engenharia Elétrica
Natal, RN, Brazil

The interest on microwave devices using microstrip antenna on ferrimagnetic layers has increased. Mainly, this is due to the possibility of altering the performance of these devices by changing the properties of the ferrimagnetic substrates according, to the magnitude and direction of the external applied magnetic field.

In this work, the characteristics of a microstrip antenna on ferrimagnetic and dielectric layers are investigated. The analysis is developed using the the Hertz vector potentials and Galerkin methods. In this analysis, it is assumed that a uniform external magnetic field $\mathbf{H}_0$ is applied perpendicularly to the microstrip ground plane. Then the permeability tensor $\vec{\mu}$ of the ferrimagnetic substrate is given by:

$$\vec{\mu} = \begin{bmatrix} \mu & 0 & ik \\ 0 & \mu_0 & 0 \\ -ik & 0 & \mu \end{bmatrix}$$

where μ and k are $\frac{\mu}{\mu_0} = 1 - \frac{\gamma^2 H_0 4\pi M_s}{\omega^2 - (\gamma H_0)^2}$, $\frac{k}{\mu_0} = \frac{\gamma 4\pi M_s}{\omega^2 - (\gamma H_0)^2}$ and $4\pi M_s$ is the saturation magnetization, γ is the gyromagnetic ratio and ω is the operating frequency. The permeability of free-space is μ_0.

Numerical results for microstrip antenna on dielectric substrates are presented as a particular case. That is obtained by imposing $k = 0$ and $\mu = \mu_0$ in the derived equations.

Fig. 1 shows the variation of the resonant frequency $H_0/(4\pi M_s)$. When the value of $H_0/(4\pi M_s)$ increase, the value of the resonate frequence also increase, suggesting the possibility of a external tuning with the variation of the external static magnetic field.

As can be seen from the results, there is an influence of the use of a magnetized magnetic material as substrate of a microstrip antenna. The use of the Hertz vector potential associated with the Galerkin methods is efficient for this analysis and the results have an excellent agreement with other results of the literature.

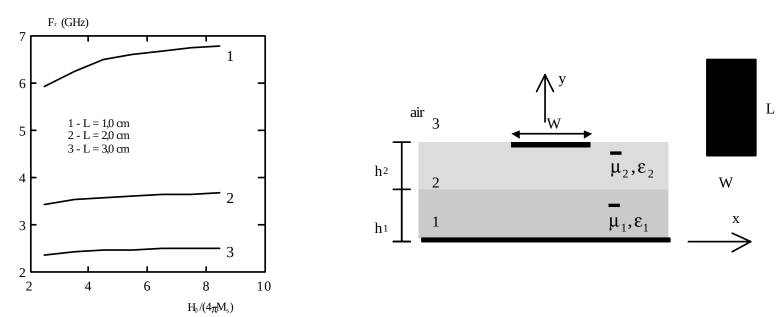

Figure 1: Freqüência de ressonância versus $H_0/(4\pi M_s) w = 0,4\,\mathrm{cm}$, $h_1 = 0,127\,\mathrm{cm}$, $h_2 = 0,0635\,\mathrm{cm}$, $\varepsilon_{r1} = 15,2$, $\varepsilon_{r2} = 2,35$, $4\pi M_s = 1200,0\,\mathrm{G}$.

Accurate and Efficient Numerical Integration of Weakly Singular Integrals in Galerkin EFIE Solutions

D. Taylor
Naval Research Laboratory
Washington, DC 20375, U.S.A.

The electric field integral equation (EFIE) solution for scattering from an arbitrary three-dimensional geometry was published by Rao, Wilton and Glisson (RWG) in 1982. Since that time this formulation has been utilized to solve a large variety of scattering and radiation problems. Experience has taught us that the accuracy of quantities derived from the original RWG solution are a function of the electrical size of the problem, which is reflected in the order of the system of equations that must be solved, and the electrical dimensions of the triangular patches.

The ill-conditioned matrices that result from electrically small patches have been addressed with the 'loop-star' approach. For electrically large problems, with large order systems of equations, the confidence one has in the solution depends on the numerical accuracy of the Galerkin inner products, which populate the method of moments (MoM) impedance matrix. A new treatment of these inner products is presented here which improves the accuracy and efficiency of the numerical integration of the singular surface integrals that result from the Galerkin formulation.

A Galerkin discretization of the electric field integral equation (EFIE) for PEC surfaces using Rao-Wilton-Glisson (RWG) basis functions requires the numerical evaluation of integrals with singular kernels over triangular regions. These singularities have been traditionally handled by utilizing a 'singularity extraction' procedure to produce a regular integral and an analytic function to replace the original singular integral. A new approach is presented here, in which the 4-dimensional weakly singular integrals unique to the Galerkin RWG EFIE solution for PEC surfaces are transformed into integrals with regular integrands. The transformations allow some of the integrations to be performed analytically, in some cases reducing the original 4-D integral into a 1-D numerical integration. The accuracy and convergence properties of the new method are demonstrated by evaluating the scalar potential function over a unit triangle.

Application of the Solar Antenna "SOLANT" Concept to a LEO Satellite Spacecraft

S. Vaccaro and J. R. Mosig
Ecole Polytechnique Fédérale de Lausanne
Lausanne, CH 1015, Switzerland

P. de Maagt
ESA - ESTEC
Noordwijk, NL 2201, The Netherlands

T. M. Grzegorczyk
Massachusetts Institute of Technology
Cambridge, MA 02139, U.S.A.

The possibility to combine solar cells and antennas has been largely demonstrated in series of previous publications including several by the authors. The application of SOLANT to a "real life" space mission, presented here, will provide a step forward in the demonstration of the applicability of this concept. The selected space mission is the MITA platform, an Italian satellite developped to accept different scientific payloads. Actually, the spacecraft uses separate solar cells and antennas that are in competition for the limited space available. The utilization of a SOLANT antenna will, on one hand improve the antenna capabilities and on the other hand increases the surface available for the solar cells. All this can be done without increasing neither the volume nor the mass of the spacecraft. MITA satellite has two solar panels mounted on both sides of the satellite.

On top of the satellite, between the two panels, it has not been possible to place more solar cells because of the presence of the antenna. Thanks to the use of the SOLANT antenna, it would be possible to cover with solar cells the entire topside of the satellite keeping the antenna in place.
For this particular application, two antennas have been used to replace the helix antenna embarked on MITA, one is a small array of four slots in sequential rotation requirements and the second is a 4x4 elements array with conical beam. Figure 1 shows the radiation patterns of the two antennas. Thanks to the two antennas used, the requirements of MITA are fully covered.

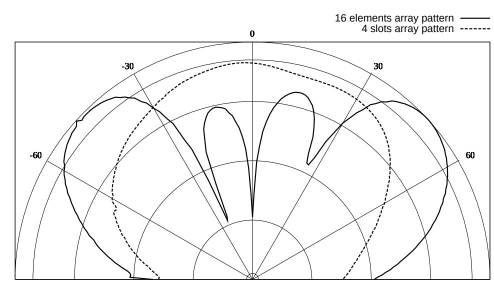

Figure 1: Radiation pattern of the 16 elements array and of the 4 slots array.

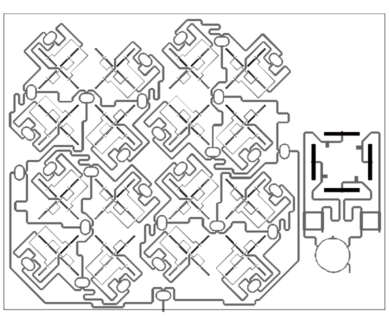

Figure 2: SOLANT array. On the left the 4x4 elements array, on the right the single slot CP slot antenna.

The 4x4 elements array has been designed to be circularly polarized and to have a conical beam. Each array element is a circularly polarized slot shaped with a sophisticated geometry where the cross is composed by four folded slots, one per crosss arm. This produces a very small element while retaining most of the characteristics of a simpler cross-slot. The array, depicted in figure 2, is composed by four subarrays turned of 90 degrees respect to each other. In order to obtain the conical beam, all the elements are fed in phase. However, since the elements are turned of 90 degrees between them, the sought-conical pattern is obtained. Each array element integrates a solar cells module composed by four solar cells.

Analysis of a Compact Microstrip Patch Antenna with Tuning Stubs for Dual Frequency Trimming and Dual Polarization

G. S. Binoy, C. K. Aanandan, P. Mohanan, and K. Vasudevan
Centre for Research in Electromagnetics and Antennas
Department of Electronics, Cochin University of Science & Technology
Cochin, Kerala, India

A novel printed antenna element embedded with tuning stubs capable of providing dual polarized operation over two widely separated frequency bands is described.

Dual Frequency dual-polarized antennas are generating great interest due to the development of wireless communication over recent years. They find applications in satellite communication systems to realize frequency reuse for doubling the system capability. They can also be used in mobile communication systems to obtain polarization diversity for enhanced reception and transmission functions into one antenna for reducing the antenna size.

The antenna geometry consists of a square patch loaded in the centre with a square slot having four extended arms (Placed at right angles to each other). It is fabricated on a substrate of thickness h and relative permittivity ε_r. The square slot is centered in the square microstrip patch antenna. It is observed that two distinct operating frequencies are excited. Here, the slot geometry creates another resonance near the fundamental resonance of the antenna, which will result in dual frequency operation. By changing the length of the tuning slot arms, the frequency ratio of the proposed antenna can be varied effectively. The optimum feed position remains practically the same even when the arm slot length is changed.

With a square slot alone, it is observed that the antenna is resonating at 1.611 GHz, whereas the introduction of the first base arm as well as the other three stubs initiates an additional resonance frequency at 1.155 GHz. It is also observed that the second resonance frequency falls to 1.341 GHz from 1.61 GHz. It can be concluded that the slot is effectively increasing the patch dimensions and hence lowering the resonant frequencies. Both the two resonant frequencies are well below the resonant frequency of the standard square patch. By changing the length of the slot arm, the frequency ratio of the proposed antenna can be tuned effectively. By varying the number of stubs from one to four we can also trim the frequency of operation over a wide band. The transmission characteristic studies reveals the orthogonal polarization studies of the antenna.

The analyses of the antenna by simulating the antenna geometry using the Zeland IE3D also were carried out. IE3D is an integrated full wave electromagnetic simulation and optimization package for the analysis and design of three dimensional microstrip patch antennas. The experimental observations are found to be in very close agreement with the IE3D results.

The area requirements of ordinary square patches operating at f_1 and f_2 frequencies of the new design are found to be more; typically when $f_1 = 1.155$ GHz and $f_2 = 1.341$ GHz, the reduction in patch areas are $\sim 69\%$ and 54% respectively. By changing the slot arm dimensions we can merge or shift apart the resonating frequencies. It is observed that the percentage bandwidth remains almost invariant even when the slot arm dimensions are changed to reduce the operating frequencies. The reduction in relative gain of the newly designed antenna is found to be 1.8 dB less compared to standard rectangular patch.

Session 4Ac5

Electromagnetic Theory

Coherent-Difference Detection of Electromagnetic Waves and Propagation Medium Parameters

A. V. Siniavski
Low Temperature Laboratory, Yerevan Physics Institute
Yerevan, 375036, Armenia

In the classical spectroscopy techniques based on the dispersion resolving of analyzed Electromagnetic Waves (**EMW**), today it is achieved high precision of spectral lines positions and width determination. The sources investigated in optical and radio astronomy and space communication systems, in majority present themselves as high coherence sources owing to large distance between objects. Spectrally resolved waves propagated in disperse medium, have high sensitivity to phase shift of neighbor spectral components, and produce the perceptible shift of spectral lines – e.g., phase shift of one wavelength demonstrates a shift proportional to same value of magnitude. Registration of this type of shift requests a specific configuration of coherent measuring system.

The conducted calculation shows that gravitation fields, scattering medium, exotic particles are able to produce on the astronomical or information systems distances relative phase shifts of observed **EMW** sources in some wavelengths. Results of traditional astronomical and information system's parameter measurements allow the various interpretation of spectral shifts observed, and method described can be applied to precision measurements in the optical, **IR**, and microwave spectroscopy, space communication channels, as well as in the long length optical fiber communication system.

We revue several developments that are being carried on, focusing mainly on the application to radiation negligible wave changes in the number of precision measurements of the **EMW** parameters. The physical model of the method is described and experimental investigations of spectral, phase, temporal parameters of radiation flows are included.

It has be pointed out that coherent mixing of spectrally resolved **EMW**'s in broad range of energies – **X**-rays, optical, **IR**, microwave, etc. – has high sensitivity to wave parameters due to propagation medium influence and radiation source characteristics.

References

1. Siniavski, A., "Coherent-Difference Detection of Optical Radiation Pulses," *Quantum Electronics, (Kvantovaya Elektronika* & *Turpion Ltd., UK),* vol. 25, p. 605, 1995.

2. Siniavski, A., "Superconductor Bolometer in the WIMP Coherent Registration Systems," Abstract of LTD-6, 6th Low Temperature Detectors Workshop, BO-19, Beatenberg, Switzerland, 1995.

Spectral Domain Analysis of Coupled Microstrip Using Spheroidal Wave Functions

C. A. Carter
Department of Electrical and Computer Engineering
Stevens Institute of Technology
Hoboken, NJ 07030, U.S.A.

This paper presents a study of coupled microstrip transmission lines using spheroidal wave functions and the spectral domain method. The electromagnetic field equations and boundary conditions are formulated in the spectral, or Fourier transform, domain. This formulation is used to derive an equation that expresses the Fourier transform of the electric field in terms of the current distribution on the microstrip. Galerkin's moment method is then applied. This yields a system of equations that can be used to solve for the unknown propagation characteristics.

Microstrip is an important element in microwave integrated circuits (MICs), millimeter-wave circuits, and microwave networks. While single microstrip lines have found numerous uses in MICs, their usefulness can be extended when two lines are coupled. Coupled microstrip can be used to produce a variety of devices including directional couplers, filters and delay lines. Two microstrip lines placed in parallel form a simple directional coupler.

The current distribution on the microstrip lines is modeled as an expansion of known basis functions with unknown coefficients. Walsh functions, sinusoidal functions, sinusoidal functions with edge conditions and Chebyshev polynomials have been utilized as basis functions. Spheroidal wave functions have been successfully used to model the current distribution in the analysis of single microstrip transmission lines. These functions modeled the current over a broad frequency range and required fewer expansion terms than other previously used basis functions. Basis functions used in the analysis of single microstrip transmission lines have also been used in the analysis of coupled lines.

This paper examines the use of spheroidal wave functions for the analysis of coupled microstrip in the spectral domain and the determination of characteristic quantities associated with such structures. A brief overview of the theory of spheroidal wave functions will be included but the primary focus will be on practical issues of computation. A set of steps, allowing these functions to be computed, will be outlined. Results obtained will be compared to those obtained with other standard basis functions.

Spin-up Instability of a Levitated Molten Drop in MHD-flow Transition to Turbulence

B. Abedian
Mechanical Engineering Department, Tufts University
Medford, MA 02155, U.S.A.

R. W. Hyers
NASA Marshall Space Flight Center
Huntsville, AL 35812, U.S.A.

When an alternating magnetic field interacts with induced eddy currents in a conducting body, there will be a repulsive force between the body and the driving coil system generating the field. The eddy currents in the conducting body may also generate Joule heating and a mechanism for containlessness processing of different materials. Axial rotation of electromagnetically levitated objects is a common observation in levitation systems and often an undesirable side effect of such experiments on 1-g and μ-g. There have been recent efforts to use magnetic damping and suppress this tendency of body rotation.

The first report of rotation in EML drops was attributed to a slight asymmetry of the shape and location of the levitation coils could change the axis and speed of rotation. Other theories of sample rotation include a frequency difference in the traveling electromagnetic waves and a phase difference in two different applied fields of the same frequency. All of these different mechanisms share the following characteristics: the torque is small, constant for constant field strength, and very weakly dependent on the samples temperature and phase (solid or liquid).

During experiments on the MSL-1 (First Microgravity Science Laboratory) mission of the Space Shuttle (STS-83 and STS-94, April and July 1997), a droplet of palladium-silicon alloy was electromagnetically levitated for viscosity measurements. For the non-deforming droplet, the resultant MHD flow inside the drop is inferred from motion of impurities on the surface. These observations indicate formation of a pair of co-rotating toroidal flow structures inside the spheroidal levitated drop that undergo secondary flow instabilities. As rise in the fluid temperature rises, the amplitude of the secondary flow increases; and beyond a point in the experiments, the surface impurities exhibit non-coherent chaotic motion signifying emergence of turbulence inside the drop.

In this work, a background of these set of observations will be given followed by a presentation of our results on the digital particle tracking analysis that has been performed on a number of available videos. The analysis indicates that the levitated drop attains a constant rotational speed during the melting phase and formation of the co-rotating axi-symmetric laminar toroidal structures. However, the rate of axial rotation increases dramatically during the deformation of the toroidal structures and their breakup into chaotic entities. This new data suggests an interaction between the flow inside the levitated molten drop and the driving coils in the experiments. Possible mechanisms for this interaction will be reviewed. The data will also be used to make an assessment of existing theories on droplet rotation.

The Extinction Theorem for a Periodic Structure – a Suggestion

C. G. Ribbing
Ångström Laboratory, Uppsala University and Swedish Defence Research Agency
Linköping, Sweden

In the classical Extinction Theorem attributed to P. P. Ewald and C. W. Oseen it is proved that the interactions between an impinging electromagnetic wave and a bulk medium can be completely described within a scattering formalism. The reflected and transmitted electromagnetic waves are obtained as the result of interfering waves that are scattered from the atoms of the media. The authors showed that the Fresnel equations in optics can be obtained without the assumption of a smooth, abrupt interface. In a sense one can say that the relationship between the Extinction Theorem and the Fresnel equations is analogous to that between the Laue Equations and the Bragg equation.

It is suggested that the Extinction Theorem should be rederived for a solid body with the more complex geometry of a photonic crystal. A photonic crystal is a periodic structure for which the length scale of the periodicity is comparable to the wavelength of the electromagnetic wave one wishes to manipulate. Thus for optical or IR wavelengths, the lattice constant in a photonic crystal is 10^2 to10^5 times that of an ordinary atomic crystal. A photonic crystal consists of at least two media whose dielectric functions are different at the wavelengths in question. The derivation under these new circumstances should take advantage of the periodicity to sum up all waves scattered from the two constituents. It seems probable that Fourier-transformation to momentum space is one of the steps that should be undertaken.

If this new formulation of the Extinction Theorem can be obtained, it should corrrespond to results that have already been obtained by a combination of Maxwell's equations and quantum mechanics, i.e. the appearance of photonic band structure of large current interest. The bands would be obtained as branches of dispersion relations: hv=f($\mathbf{k}$), where the definition of the momentum vector $\mathbf{k}$ is given by the Fourier transformation, just as in the derivation of the Laue Equations. The appearence of photonic gaps, i.e. energy intervals within which the wave is extinguished will be dependent upon sufficient contrast between the dielectric functions of the two constituents and the choice of symmetry for photonic crystal.

Roads to Maxwell's Equations

D. Sterc
University of Osijek
Osijek, 31000, Croatia

D. Butkovic and V. Mikulicic
University of Zagreb
Zagreb, 10000, Croatia

This paper introduces several new derivations of Maxwell's equations which vary considerably in content and perspective. They are designed to span as much ground as possible and explore the roads less traveled.

The **first** one is a Dirac-like inference it is based on enforcing the generalized Huygens principle by pulling a sort of a square root out of the free wave equation for a vector field. This field, which is later identified as the Faraday field, must be transversal for the procedure to work this is justified both by experiments and symmetry arguments.

The **second** derivation appears as a variation of the first one. The arguments are applied in a reverse order transversality is the starting point and the wave equation is deployed in the end to fix the linear operator that governs the time evolution as demanded by the Huygens principle.

The **third** one is a potential-based reasoning it shifts the perspective since in classical electrodynamics introduction of the potentials seems to serve merely as a calculational convenience. Here, the D'Alembertian is not split right away instead, the implications of applying a source (current) are considered. Demanding the transversality at this point kills the longitudinal component of the current and spoils the locality which is the reason for having a field theoretic description in the first place. The rescue comes from the conservation of charge which permits us to trade a manifestly nonlocal term for an additional field component. Consequently, the D'Alembertian is split more naturally and a radiation gauge emerges.

The **fourth** road is yet another potential-based approach, this time with emphasize on gauge invariance. Careful examination shows that the previous inference might have applied the transversality condition overzealously even where experiments did not indicate it was necessary at the location of the source. Hence, locality need not be spoiled entirely only locality in time, but not in space, is to be sacrificed and no new degrees of freedom (fields) are required so a temporal gauge comes out. In effect, this means removing the longitudinal part of the Laplacian (instead of the current).

The **fifth** derivation has a more traditional taste it focuses on mending Ampere's law through a series of approximations. They come from projecting out the longitudinal part of the current and repairing the damage it does to locality by adding further nonlocal terms containing time-derivatives. The result is recognized as a Born series expansion for the Green function of the D'Alembertian temporal derivatives are treated pertubatively, which is the essence of quasistatic approximations.

It proves beneficial to compare these approaches with the derivations of Maxwell, Feynman, Schwinger and Weinberg. Gilbert Strang wrote that "a revolution [in a textbook presentation] is very likely to end at 2π", and this appears to apply very well here the derivations we have presented start from dynamic considerations close to the modern elementary particle physics and gradually arrive very close to Maxwell's original *ansatz*. We are inclined to perceive this more as a blessing than a curse displaying the curvature of our minds.

On Equiconvergence with the Fourier Integral of Spectral Expansion Related to the Non-Hermitean Sturm-Liouville Operator

E. G. Saltykov
Department of Computational Mathematics and Cybernetics
M. V. Lomonosov Moscow State University
Moscow, 119899, Russia

The spectral expansion of a function f equiconverging with the Fourier integral is associated with the operator

$$1\varphi = -d^2\varphi/dz^2 - k^2(z)\varphi,$$

where $k(z)$ is a complex-valued piecewise continuous function defined over the whole line R. $k(z) = k_1 = \text{const}$ if $z < 0,\ k(z) = k_2 =$ const if $z > H$. It is represented by the formula

$$\sigma_\wedge(z, f) = \int_R \theta(\wedge, z, z')f(z')dz'$$

provided that $f^{(k)} \in L_1(R),\ k = 0, 1.$

The spectral function θ has the form

$$\theta(\wedge, z, z') = \sum_{i=1}^{2} \int_0^{M_i(\wedge)} u_i(z, \mu)u_i(z', \mu)dp_i(\mu), \tag{1}$$

where u_i are eigenfunctions satisfying equations

$$lu_i = \left(\mu^2 - k_i^2\right) u_i, \quad i = 1, 2.\ \mu \in R,\ M_i(\wedge) \sim \wedge,\ \wedge \to \infty$$

The formula (1) is obtained from the representation

$$\theta(\wedge, z, z') = \frac{1}{2\pi i} \int_{C_\wedge} \alpha g(z, z'; \alpha)d\alpha,$$

as the integral around the circle $C_\wedge$ of the radius $\wedge$ in the complex plane α can be reduced to branch-cut integrals connected with branches in Green's function $g(z, z'; \alpha)$ which satisfies the equation

$$(1 + \alpha^2)g = \delta(z - z')$$

and has no poles in the complex plane α.

This result can be considered as the mathematical justification of the approach connected with the alternative representations of Green's function for conductive medium [1].

REFERENCES

1. Felsen, L. B. and N. Marcuvitz, *Radiation and Scattering of Waves,* Vol. 1, Prentice-Hall, Inc., Englewood Cliffs, New Jersey, 1973.

Spectral Domain Analysis of the Tuning Properties of Microstrip Circuits on Magnetized Ferrites

G. León, R. R. Boix and F. Medina
Microwaves Group, Department of Electronics and Electromagnetism
University of Seville
Seville, 41012, Spain

The propagation constant and characteristic impedance of microstrip transmission lines on magnetized ferrite substrates can be adjusted over a wide range by varying the magnitude and/or the orientation of the bias magnetic field (G. León et al., *JEWA*, vol. 15, pp. 223-252), which can be used for the design of tunable phase shifters (C. S. Teoh et al., *IEEE-Magnetics*, vol. 31, pp. 3464-3466). Also, the resonant frequencies of microstrip resonators printed on magnetized ferrites can also be tuned by means of the bias magnetic field (H. How et al., *IEEE-MTT*, vol. 42, pp. 988-994; V. Losada et al., *IEEE-MTT*, vol. 48, pp. 1057-1064). This latter fact has been used for the fabrication of tunable antennas (D. M. Pozar et al. *Electron. Lett.*, vol. 24, pp. 729-731) and tunable bandpass filters (M. Tsutsumi, *Electron. Lett.*, vol. 33, pp. 687-688). Thus, magnetized ferrites show a potential application as substrates of tunable microstrip circuits.

In this paper the authors carry out a full-wave three-dimensional analysis of one-port and two-port microstrip circuits fabricated on magnetized ferrites. In particular, the tuning properties of the circuits with respect to variations in the magnitude and/or the orientation of the bias magnetic field are studied in detail. In order to obtain the scattering parameters of the circuits, these are fed by finite length microstrip lines excited by impressed voltage sources. The current density on the feeding microstrip lines and the metallizations of the circuits are obtained by means of Galerkin's method in the spectral domain. Rooftop basis functions are used in the approximation of the current density. The process of de-embedding the scattering parameters of the circuits is carried out via two different approaches. In the first approach the scattering parameters are directly extracted from the standing wave current pattern by means of the matrix pencil technique (E. Drake et al. *IEEE-MTT*, vol. 48, pp. 1394-1403). In the second approach, a short-open calibration technique similar to that reported in (L. Zhu et al. *IEEE-MTT*, vol. 48, pp. 347-356) is used to characterize the voltage sources parasitic effects, which leads to the accurate determination of the scattering parameters. Both approaches give similar results, but the approach based on the matrix of pencil technique seems to be more stable than that based on the short-open calibration. The results obtained for the reflection coefficient of an open-ended microstrip line printed on ferrite substrate have been compared with those obtained in (H. Y. Yang, *IEEE-MTT*, vol. 12, pp. 2423-2428), and good agreement has been found. Also, new results have been obtained for filters fabricated on ferrite substrates which can be tuned by means of variations in the magnitude and/or the orientation of the bias magnetic field. However, the results have shown that these filters cannot operate in the frequency bands in which magnetostatic mode propagation (E. B. El-Sharawy et al. *IEEE-MTT*, vol 38, pp. 730-737) is allowed along the ferrite substrates.

Modified Saddle Point Method

X. Chen, B.-I. Wu and J. A. Kong
Research Laboratory of Electronics
Massachusetts Institute of Technology
Cambridge, MA 02139, U.S.A.

The saddle point method is a useful tool in evaluating the asymptotic value for an integral containing a very large parameter, and has a wide application in solving electromagnetic problems. It is well known that the leading terms for the integration

$$I(\xi) = \int_{\Gamma} d\alpha F(\alpha) e^{\xi f(\alpha)} \qquad (\xi \to \infty) \tag{1}$$

is $F(\alpha_0)e^{\xi f(\alpha_0)}\sqrt{\frac{2\pi}{-\xi f''(\alpha_0)}}$, where α_0 is the saddle point. But when $f''(\alpha_0)$ approaches to zero, the above leading term obviously is not good.

This paper presents a modified saddle point method for the case $f''(\alpha_0) \approx 0$. First, change the intergral expression so that $f''(\alpha_0) = 0$. Then let

$$-s^3 = f(\alpha) - f(\alpha_0) \tag{2}$$

$$\alpha(s) = \alpha_0 + \sum_{n=1}^{\infty} a_n s^n \tag{3}$$

So, the integral becomes

$$I(\xi) = e^{\xi f(\alpha_0)} \Big\{ \int_{\Gamma_1 \infty}^{\Gamma_1 0} ds \frac{d\alpha}{ds} F[\alpha(s)] e^{-\xi s^3} + \int_{\Gamma_2 0}^{\Gamma_2 \infty} ds \frac{d\alpha}{ds} F[\alpha(s)] e^{-\xi s^3} \Big\} \tag{4}$$

Please note that $a_1 = (\frac{-6}{f'''(\alpha_0)})^{\frac{1}{3}}$ takes different values on Γ_1 and Γ_2. On the steep descent path near the saddle point, $\alpha(s) - \alpha_0 \approx a_1 s$. Since s is positive real, the angle of a_1 is same as that of $\alpha(s) - \alpha_0$.

In (4),

$$I_{\Gamma_2}(\xi) = F(\alpha_0) e^{\xi f(\alpha_0)} \Big\{ \frac{\Gamma(\frac{1}{3})}{3\xi^{\frac{1}{3}}} a_1 + \frac{\Gamma(\frac{2}{3})}{3\xi^{\frac{2}{3}}} [2 \frac{-a_1^2}{12} \frac{f^{iv}(\alpha_0)}{f'''(\alpha_0)} + \frac{F'(\alpha_0)}{F(\alpha_0)} a_1^2] + \dots \Big\} \tag{5}$$

and $-I_{\Gamma_1}(\xi)$ takes the same form as $I_{\Gamma_2}(\xi)$ in (5) except a_1 differs. Therefore, $I(\xi)$ is got by adding the above two parts.

An example of the applicaton of the above method is to calculate the asymmptotic expression for $H_\nu^{(1)}(\xi) = \frac{1}{\pi}\int_\Gamma d\alpha e^{i(\xi \cos\alpha + \nu\alpha - \nu\frac{\pi}{2})}$ when ν and ξ are both large but $|\nu - \xi|$ is not.

Rewrite it as $H_\nu^{(1)}(\xi) = \frac{1}{\pi}\int_\Gamma d\alpha e^{i(-\nu\frac{\pi}{2} + \alpha\nu - \alpha\xi)} e^{\xi(i\cos\alpha + i\alpha)}$. Note that a_1 takes the value of $6^{\frac{1}{3}} e^{i\frac{5\pi}{6}}$ on $\Gamma_1$and $6^{\frac{1}{3}} e^{i\frac{3\pi}{2}}$ on Γ_2, respectively. The leading term is

$$H_\nu^1(\xi) \approx \frac{1}{\pi} \frac{\Gamma(\frac{1}{3})}{\sqrt{3}\xi^{\frac{1}{3}}} 6^{\frac{1}{3}} e^{i\frac{5\pi}{3}} + \frac{1}{\pi} \frac{\Gamma(\frac{2}{3})}{\sqrt{3}\xi^{\frac{2}{3}}} 6^{\frac{2}{3}} e^{i\frac{4\pi}{3}} (\nu - \xi) \tag{6}$$

The above result is correct according to [1]. The advantage of the method in this paper is that we can expand $I(\xi)$ in higher powers of $\xi^{-\frac{1}{3}}$.

REFERENCES

1. Wang, Z. X. Guo, D. R., *Special Functions*, pp.394, World Scientific, 1989.

Constructing the Solutions of the EM Field in Cylindrically Stratified Media by the Counter-Propagation Deduction (CPD) Method

Q. Zhang
China University of Mining and Chinese Academy of Science
Beijing, China

J. Zhu
China University of Mining and Technology
Beijing, China

Due to many natural and artificial media can be modeled as a stratified medium, the analysis of EM fields in stratified medium occupies an important position in EM theory. As early as in the fifties in the last century, Russian scientist Π. M. Brecobckhc systematically studied the various kinds of waves in stratified media, including Electromagnetic, sound, and elastic waves, etc. As far as the analytical methods for the EM waves in a multi-layer medium are concerned, the contributions made by J. R. Wait, J. A. Kong, W. C. Chew should be mentioned due to their popularity and familiarity among the researchers in this area. J. R. Wait has given a close explanation of a theoretical method which involves in the calculation of the wave impedance of total field and reflection coefficient at each layer, and is similar to the one for analyzing the voltage and current in a multiple tandem transmission line. By means of reflection coefficient and taking the form of the propagation matrix, J. A. Kong has presented a general method for analyzing the EM field excited by four types of dipoles. Still by means of the reflection coefficient and the propagation matrix, W. C. Chew has analyzed the fields in horizontally, spherically and cylindrically stratified media in a united way.

Though the methods mentioned above are quite classical, however, because of their involving in the iterative calculations of the reflection coefficients, with the increasing of the number of the layers, the analysis becomes impractical.

Different from the traditional idea — to search for the solution according to the boundary conditions, the Counter — Propagation Deduction (CPD) Method, which is put forward by the authors for the first time, is characterized by constructing the solution directly. Just like bricks making a building, by introducing a new conception named Boundary Originated Set (BOS) of waves, the direct solution of the EM field in an arbitrary layer can be expressed as a superposition of the component waves of the BOSs. Due to the regularity in the constructing procedure as well as in the expression structure, the rigorous numerical solution can be easily obtained by programming. As far as the horizontally stratified medium is concerned, beside the case that the field source is a uniform wave, the CPD method can also be applied to the analysis of the fields excited by a vertical and horizontal electrical dipole. The efficiency of the method has been proved by the numerical analysis of the field excited by an arbitrary shape of a loop antenna.

This paper investigates its application to the case that the medium is cylindrically stratified.

As the study made by W. C. Chew shows, because the r-component and f-component of $\mathbf{E}$ and $\mathbf{H}$ can be deduced from E_z and H_z according to the two curl-equations in Maxwell's equations, the key step for analysis of the fields in cylindrically stratified media is to deduce E_z and H_z in each layer. Here, instead of searching for them by the transportation matrix, this paper will apply the CPD method to construct their analytical expressions directly.

The paper is organized as follows. In Part one, the background for presenting the CPD method is introduced. In Part two, the mechanism of the CPD method is illustrated. The BOS corresponding to E_z and H_z in the case of cylindrically stratified media is found in Part three. Part four presents an illustrative example to show how the solutions of the field are constructed.

Clausius-Mossotti Approximation for Nonlinear Composites with Coated Ellipsoidal Particles

A. Pinchuk
Radiophysical Faculty
Kyiv T. Shevchenko University
Kyiv, Ukraine

Last time considerable attention has been devoted to nonlinear composite structures due to their potential applications for integrated optical devices (such as optical switching and signal processing devices, ect.) In particular, an intrinsic optical bistability (IOB) phenomenon has been extensively studied theoretically as well as experimentally. We consider a heterogeneous system of oriented but randomly distributed coated ellipsoidal particles with a nonlinear core and a linear metallic confocal shell embedded in a linear lossless host medium. An external electric field with a wavelength much larger than the characteristic dimension of the coated ellipsoidal particles is applied parallel to one of the principal axes of the oriented ellipsoid, i.e., we are working in the framework of the quasi-static approximation. We study an effective nonlinear dielectric permittivity of such a heterogeneous composite structure. We derive an expression for the effective dielectric permittivity tensor of such a system following the Clausius-Mossotti approximation. We obtain the conditions for the existence of optical bistability phenomenon in a single coated ellipsoidal particle with a nonlinear core and a metallic shell. The Clausius-Mossotti approximation for a suspension of coated spheres with the same heterogeneous structure was also generalised. We present numerical results for the effective dielectric permittivity of the composite nonlinear structure which consists of GaAs oriented spheroids coated with a silver shell and embedded in a silica glass matrix. We have calculated the change of the real and imaginary parts of the effective dielectric permittivity of such a structure depending on the applied intensity. We observe a broader hysteresis loop for higher concentrations of the coated spheroids. Thus we predict more prominent bistability phenomena for denser nonlinear composite structures with heterogeneous nonlinear spheroids

Transverse Resonance Method of Solution of Unilateral Fin-Line by Means of Rayleigh-Ritz Technique and Optimization by Simplex MATLAB Tool

C. D. Gupta, M. K. Panda, and R. S. Bagul
Indian Institute of Technology
Kanpur, Indian

D. Bhowmik
Visvesvaraya Regional College of Enginerring
Nagpur, India

In the present paper an approximate method of solution for designing unilateral fin-line by transverse resonance method [1] by simple equation has been developed. The experimental unit is composed at Ku -band with center frequency 16 GHz and RT Duroid substrate of permittivity κ = 10.2 and thickness t = 1.5 mm, for the sake of economical experimental set up. On the basis of these experimental results oversized fin-line models at mm and upper mm (i.e. 100GHz) are proposed by Raleigh Reitz Technique. Optimization of parameters is to be done by standard SIMPLEX MATLAB TOOL [3].

To find the eigen equations for the unilateral fin line by transverse resonance method we can treat the metallic fins to effectively act like series LC circuit [2] in the equivalent transmission line representation and finally find the eigen equations [2] as:

$$lh\ \cot(hd_1) + \cot(hd_2)) + h^2 \cot(hd_1)\cot(hd_2)\tan(lt) - l^2 \tan(lt) + (1/(X_L - X_C))\,(h\cot(hd_1)\tan(lt) + 1) = 0 \tag{1}$$

$$\beta^2 = l^2 + (m\pi/b)^2 - \kappa k_0^2 = l^2 + (m\pi/b)^2 - k_0^2 \tag{2}$$

where, the symbols have following meaning:

β	=	propagation constant in the fin line $= 2\pi/\lambda$
h, l	=	wave numbers in the air and the dielectric, respectively
b	=	b-dimension
κ	=	permittivity of the dielectric
k_0	=	$2\pi/l_0 = 2\pi f_0/c$

The capacitive reactance are given by [2]

XC	=	$1/wC$, where $C = \kappa \in_0 L/[0.885 + d/t]$
d	=	separation between the conducting stripes
t	=	thickness of the dielectric substrate

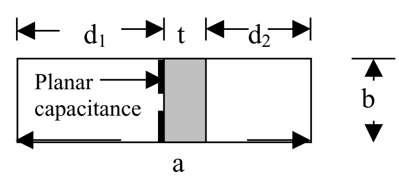

schematic diagram of experimental unit (cross sectional)

REFERENCES

1. R. E. Collin, *Field Theory of Guided Waves*.
2. C. D. Gupta, "A new microwave method of measuring complex dielectric constant of high permittivity thin films," *IEEE Transactions on Instrumentation and Measurement*, March 1975.
3. C. D. Gupta, "UHF Ferroelectric Antenna Parameter Optimization by Genetic Algorithm," A Broad Based Tutorial Paper. *Proceedings 2001, IEEE APS / URSI International Symposium*.

Session 4Ac6

Light Scattering by Layered Substrate Features

The Effect of Surface Oxide Layers on Particle Scattering

J. C. Stover
ADE Corporation
Westwood, MA 02090-1806, U.S.A.

Yu. A. Eremin and N. V. Grishina
Moscow State University
Moscow, 119899, Russia

During the last several years a lot of effort has been spent developing rigorous models to predict polarized light scattering from pits and particles of different materials on bare and filmed substrates. Confirmation of the models has been accomplished by measurement of scattering from polystyrene latex spheres of known sizes on bare silicon wafers. By combining several measurements with the model information, the type of defect can be identified (pit, particle, particle material, etc.), and then the models can be used again to obtain an estimate of true defect size. If the surface is covered with a film, the scattering results change. This paper illustrates the use of these models to explore the effect of surface film thickness on the scattering from particles of different materials. This is an issue as there is a thin native oxide layer present on most surfaces, and it is important to know under what conditions it may affect scanner calibration, defect identification, and sizing estimates.

The models used here are based on the Discrete Sources Method (DSM). This technique constructs the scattered field everywhere outside an axial-symmetric particle as a finite linear combination of the fields resulting from multipoles distributed over the axis of symmetry inside the particle. The solution satisfies Maxwell's equations and required conditions at infinity. The Green Tensor of a layered substrate is employed to account for the complete interaction of the particle with the stratified interface. Then the unknown discrete source's amplitudes are determined from transmission conditions enforced at the surface of the particle. The DSM model controls convergence and stability of the result by a posterior evaluation of the surface residual.

The figure shows modelled scatter from a silicon wafer into a circular aperture centred 53° from normal and 135° azimuthally from 100 nm particles of different materials illuminated by a P polarized source of wavelength 532 nm incident at 65° from normal. There is no significant change in the detected scatter signal for film thicknesses less than 10 nm. So for this situation there is no effect expected from native oxide layers, which are typically 4 nm thick on silicon. Several detector configurations were modelled with similar results.

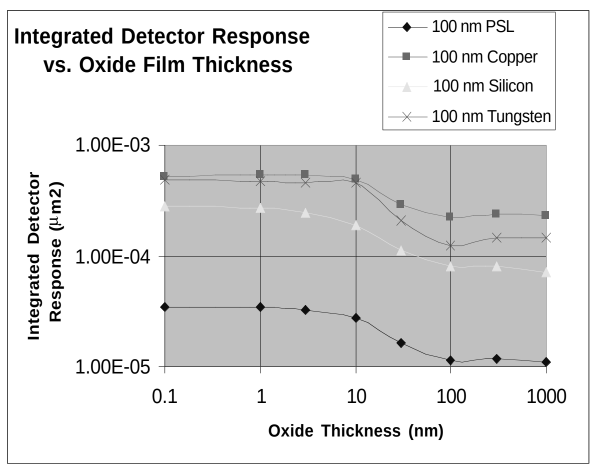

Evanescent Waves Scattering by Large Particle on a Substrate Surface

Yu. A. Eremin
Moscow State University
Moscow, Russia

T. Wriedt
Institut fuer Werkstofftechnik
Bremen, Germany

The wide potential of application of scattering microscopy especially in biology, materials science and information technology gives rise to a renewed interest in the computer simulation of evanescent waves scattering by a penetrable obstacle deposited near a dielectric prism surface [1]. In the past mainly scattering by spherical particles has been analysed using approximate models, which do not account for particle-prism interacting. In recent papers [2-3] a computer model for evanescent wave scattering analysis has been developed based on the Discrete Sources Method (DSM). The model takes into consideration complete scatterer-prism interaction and provides an opportunity to investigate evanescent wave scattering by any axial symmetric obstacle. It has been demonstrated that only a rigorous model can adequately describe scattering of evanescent waves by a particle near a plane interface [2]. In the present paper we represent an improved scheme of DSM enabling to analyse larger penetrable particle near the plane surface.

The new version of DSM gives an extension of its range of validity from particle diameter 1μm up to 5μm for corresponding exciting wavelength λ_0=632.8nm. The real need to investigate scattering by larger particles consists in the necessity to calibrate a modern particle scanner design to be able to demonstrate its ability of measuring several orders of magnitude of angle resolved Differential Scattering Cross-Section.

The main novelties of the extended DSM scheme consist in the following:

1. Different numbers of discrete sources are used for the representation fields inside and outside penetrable particle. The number of discrete sources is proportional to the relation between refractive indexes of the corresponding media.
2. The number of discrete sources now depends on the number of Fourier harmonic involved. For higher harmonic we use the lower number of discrete sources.
3. For large particles higher Fourier harmonics are computed using advanced Fresnel approximation for Weyl integrals.

All the innovations mentioned above have allowed to decrease the error of the numerical results, increase considerable the results accuracy and, as a consequence, extend the range of validity of the DSM scheme from particle diameter of 1μm up to 5μm.

REFERENCES

1. Ch. Girard, A. Dereux Near-field optics theories: *Rep. Prog. Phys*. 1996, **59**, 657-699.
2. A. Doicu, Yu.A. Eremin and T. Wriedt. Scattering of evanescent waves by a particle on or near a plane surface: *Opt. Commun*. 2001, **190**, 5-12.
3. A. Doicu, Yu.A. Eremin and T. Wriedt. Scattering of evanescent waves by a sensor tip near a plane surface: *Comput. Phys. Commun*. 2001, **134**, 1-10.

Modeled Results for Particle Identification and Sizing of Features on Filmed Wafers

V. I. Ivakhnenko and J. C. Stover
ADE Corporation
Westwood, MA, U.S.A.

Yu. A. Eremin
Moscow State University
Moscow, Russia

An important problem in semiconductor manufacturing is the detection and characterisation of micro-defects on silicon wafers. Defects are found using instruments that sense flashes of scattered light created when a scanning laser beam illuminates surface features. The scanners are calibrated with polystyrene latex (PSL) spheres. These particles make an ideal reference standard because they are commercially available in (nominally) single diameter batches, very spherical, and have a well-known refractive index. Calibration is accomplished by depositing PSL spheres on a wafer and then relating the scanner signal to the sphere size. In this way different model scanners can report defects in PSL light scattering equivalent (LSE) signals. The object is to learn as much as possible about the surface features from these scatter signals. Unfortunately, LSE gives true particle size for spherical PSL particle only. Because particle scatter is a strong function of material, scanners do not actually size the particles they detect. In the case of metal and semiconductor particles the sizing error can approach 300%.

Sophisticated models to predict light scatter signals using computer simulations based on rigorous mathematical models of polarized light scattering [1-2] were developed recently. Based on these models the numerical approaches for particle identification and sizing for features on bare Si wafer were suggested in [3-4]. The results are that actual particle size can be closely estimated and a material type (metal, dielectric or semiconductor) can be identified for most cases. This is a significant development for the semiconductor industry because it increases the speed with which contamination sources can be found, and it allows far more accurate sizing of the contaminating particles. In fact, it opens the way for true defect sizing rather than the use of LSEs.

This paper explores the numerical approach for particle identification and sizing for features on filmed wafer. For this study models were used to generate scatter patterns from particles with oblate and prolate shapes of various sizes, aspect ratios and materials. Then the numerical approach discussed in [4] was used to attempt identification of the particle material and average diameter. We investigate the influence of different collected data set (p- polarized source only; both p- and s- polarized sources) and the error in film thickness measurement on the accuracy of results.

REFERENCES

1. A. Doicu, Yu Eremin, and T. Wriedt, *Acoustic and Electromagnetic Scattering Analysis Using Discrete Sources*, Academic Press, 2000.
2. N. V. Grishina and Yu. A. Eremin, "Analysis of the Scattering Properties of Defects of Multilayered Substrates," *Opt. Spectroscopy*, 88, no.2, 2000.
3. J. C. Stover, V. I. Ivakhnenko, C. A. Scheer, and Yu. A. Eremin, "Use of light scatter measurements to identify particle material," *Proc. of SPIE*, vol. 4449-17, San Diego, CA, Jul. 29–Aug.3, 2001.
4. V. I. Ivakhnenko, J. C. Stover, C. A. Scheer, and Yu. A. Eremin, "Effect of particle shape on particle identification and scatter measurements," *Proc. of SPIE*, vol. 4449-18, San Diego, CA, Jul. 29–Aug.3, 2001.

Green's Tensor of Stratified Media in Surface and Volume Based Methods

A. A. Dmitrienko
Tomsk State University
Tomsk, Russia

Yu. A. Eremin
Moscow State University
Moscow, Russia

O. J. F. Martin
IFH, ETH-Zentrum
Zurich, Switzerland

Many important areas of today science and technology rely on scattering of electromagnetic waves by features embedded in or deposited on multilayered backgrounds. These areas include in particular the discrimination of defects on silicon wafers using laser beam scattering analysis, high resolution imaging of nanostructures employing the field scattered from a local probe microscope or remote detection and identification of buried objects via electromagnetic sensing. In each case the feature under investigation is embedded in a complex background involving several material layers with different electromagnetic properties, which strongly affects the response of the feature.

The Green's tensor of multilayered structures plays a key role in scattering calculations, as it enables to take into account all the reflections and refractions occurring at the different interfaces. For light scattering by a local feature on or inside a stratified medium, the Green's tensor allows to take into account analytically all possible interactions between the feature and the interfaces. This approach is widely used in surface and volume based methods. In that context, the efficient and accurate computation of the different components of the Green's tensor is strongly required.

During the last few years a lot of efforts have been spent developing rigorous models to predict polarized light scattering from a feature of a substrate. To examine such a class of scattering problems the Discrete Sources Method (DSM) has been developed. DSM technique enables to construct a representation of the scattered field everywhere outside a local feature, as a finite linear combination of the fields resulting from multipoles distributed inside. Vector potentials of the multipoles are constructed from the Green's tensor of a half-space. Therefore, the solution satisfies the boundary conditions imposed by Maxwells equations at an infinite interface. The unknown discrete sources amplitudes are then determined from transmission conditions enforced at the local feature surface.

One of the most known volume based approach is the Volume Integral Equation (VIE), where the unknowns in the problem are expressed in terms of volume currents induced inside the scattering feature. Using the Green's Tensor VIE can be formulated for the unknown total electric field inside the feature only. Using the method of moments (MOM) the VIE can be converted into a matrix equation. Modern VIE approach has some peculiarities:

1. It allows solving scattering problems for inhomogeneous obstacles.
2. The radiation conditions at infinity and transmission conditions at the interface surface are automatically satisfied.
3. Using a uniform mesh for discretization in the spatial domain allows one to get well-structured matrices and to apply 3D Fast Fourier Transformation with an iterative solver.

Continuous progress in semiconductor manufacturing requires the analysis of light scattering by defects of Silicon Oxide Interface (SOI) wafers, which necessitates the computation of the stratified Green's tensor for more than one interface, possibly for many different layers. This can be achieved using Sommerfeld integrals, which must be evaluated numerically.

Scattering Characteristics of Inhomogeneous Surface Bound Particles

V. I. Ivakhnenko
ADE Corporation
Westwood, MA, U.S.A.

Yu. A. Eremin
Moscow State University
Moscow, Russia

Control of silicon wafer surface contamination is of prime significance in semiconductor manufacturing. As the minimum line width of wafer structures continues to decrease, the importance of proper detection and characterization of scattering features grows and the new generation of advanced wafer inspection systems that can classify features of various shapes and materials on the wafer surface is strongly desirable. Only very recently numerical methods able to distinguish features of different shapes and materials have been developed [1,2]. These methods are based on known scatter signals in scanner collectors from particles with oblate and prolate shapes of various sizes, aspect ratios and materials. The discrete sources method (DSM) [3] is used to model light scattering by particles on a silicon wafer and to simulate responses of scanner collectors.

DSM seems to be one of the most efficient and flexible tools for modeling of a light scattering by the axial symmetric structures with homogeneous or piece – wise homogeneous permittivity. The DSM outlines consists of representing an approximate solution for scattered field as a finite linear combination of the fields multipoles, deposited at inside a particle volume. Therefore, the solution satisfies the system of Maxwell's equations everywhere outside medium discontinuity and infinity conditions. Multipoles fields are constructed based on Green Tensor of the layered substrate. Hence, the solution fits the transmission conditions at an interface surface. The amplitudes of the Discrete Sources (DS) are to be determined from boundary conditions enforced at the discontinuity surfaces of the local obstacle. A completeness of a DS fields system provides a convergence of the approximate solution to the exact one.

Unfortunately, real world particles could have arbitrary shape and profile of permittivity distribution. In this case the scattering models could be based on volume integral equation (VIE) [4]. In VIE the unknowns in the problem are expressed in terms of volume currents flowing in the scattering feature. The following features of the VIE approach make this method attractive for application: 1. The VIE allows to solve scattering problem for arbitrary shaped inhomogeneous defect. 2. The radiation condition at infinity is automatically satisfied by their solutions. 3. Using a uniform mesh for discretization in the spatial domain allows one to get well structured matrices and to apply 3D fast Fourier transform (FFT) with an iterative solver, to find the resultant matrix equation rapidly.

In this paper using VIE and DSM we estimate the effect of different permittivity distribution profiles on scattering characteristics. The knowledge of this effect allows us to formulate the area of application of axial symmetric problems for obstacles with homogeneous or piece – wise homogeneous permittivity.

REFERENCES

1. J. C. Stover, V. I. Ivakhnenko, C. A. Scheer, and Yu. A. Eremin, "Use of light scatter measurements to identify particle material," *Proc. of SPIE*, vol. 4449-17, San Diego, CA, Jul. 29–Aug. 3, 2001.
2. V. I. Ivakhnenko, J. C. Stover, C. A. Scheer, and Yu. A. Eremin, "Effect of particle shape on particle identification and scatter measurements,"*Proc. of SPIE*, vol. 4449-18, San Diego, CA, Jul. 29–Aug. 3, 2001.
3. A. Doicu, Yu Eremin, and T. Wriedt, *Acoustic and Electromagnetic Scattering Analysis Using Discrete Sources*, Academic Press, 2000.
4. Yu. A. Eremin and V.I. Ivakhnenko, "Analysis of inhomogenities on substrates based on integral transformation method," *Differential Equations*, vol. 36. No. 9, pp. 1238–1247, 2000.

Plane Wave Scattering by Stochastically Rough Spheroid

Yu. A. Eremin and V. Lopushenko
Moscow State University
Moscow, Russia

In many fields of science, such as astronomy, biology, medicine, meteorology, there is an urgent need to learn more about the scattering characteristics of realistic particles having stochastically rough surfaces [1]. The particles with surfaces slightly fluctuating near some average shape may be a subject of special interest, because in this case semi-analytical methods can considerably improve the performance of the computational algorithm. This is a point where the well-known techniques, developed to predict the scattering from particles in free space, can be combined with the approaches describing the scattering from rough surfaces.

In the present paper we will use the integral equation (IE) method, because it offers a simple perturbation theory scheme to calculate the scattering from the rough spheroid if roughness height is small in comparison with wavelength. The reference problem, formulated for the smooth spheroid, is solved with the Discrete Sources Method (DSM). It has been demonstrated [2] that DSM is a rigorous approach and describes the scattering of electromagnetic waves by particles of different shapes. DSM is based on the representation of the scattered field everywhere outside a local feature via a finite linear combination of the fields produced by multipoles distributed inside. Maxwells equations and required conditions at infinity are satisfied automatically. The unknown discrete sources amplitudes can be found from transmission conditions enforced at the particle surface.

Assuming that the surface of the spheroid is Gaussian, the statistical properties of refractive index can be derived and the approach like [3] can be implemented to calculate the first order perturbation theory approximation for the scattered field produced by the surface roughness. Formally, the rough surface is considered as medium with randomly fluctuating refractive index, making it possible to apply a volume technique to surface scattering. It can be shown that the averaging over the ensemble of realizations of the random surface can be performed analytically and the calculation of the total scattered intensity requires only integration over the angular variables.

The presented approach was applied to the rough spheroids with different aspect ratios and size parameters. To estimate the contribution of the surface roughness, we calculated also the scattered intensity for smooth spheroids.

REFERENCES

1. K. Lumme, J. Rahola. Comparison of light scattering by stochastically rough spheres, best-fit spheroids and spheres: J. Quant. Spectrosc. Radiat. Transfer 1998, 60, 439-450.
2. Yu.A. Eremin, N.V. Orlov, and A.G. Sveshnikov. Models of Electromagnetic Scattering Problems Based on Discrete Sources Methods, Generalizes Multipole Techniques for Electromagnetic and Light Scattering. Ed. T. Wriedt. Elsevier Science, Amsterdam, 39-79.
3. V. Lopushenko. Applying mean-field theory in scattering from microroughness of filmed wafers: Proc. of Fifth International Conference on Light Scattering by Nonspherical Particles. Halifax, Canada, August 28-September 1, 2000, 196-199.

Sizing Distribution Accuracy in Particle Deposition Systems

J. C. Stover and C. A. Scheer
The Scatter Works, Inc.
North Attleboro, MA 02760, U.S.A.

Defects are found on silicon wafers using instruments that detect the flash of scattered light created when a scanning laser illuminates the surface feature. Scanners are calibrated with polystyrene latex (PSL) spheres. Depositing PSL spheres on wafers and relating the resulting scanner signal to the sphere size has been the technique used for scanner calibration. Difficulties arise because the mean size of commercially available spheres is not always well established and because in many cases the distribution of sphere diameters present in a given bottle may be as large as +/-20% of the nominal mean diameter. Because it is important to know the PSL sphere diameter to within a few percent, this imposes accuracy requirements on the particle deposition systems used to create the calibration wafers. This paper reviews these issues and the differential mobility analyzer (DMA) "filter technique" used to reduce deposition inaccuracies.

The DMA works by subjecting charged particles to an applied electric field that is transverse to flow direction. Particle of only one size pass through a slit and progress towards the deposition surface. The modeled transfer function of a DMA is found from the applied voltage and the related airflows through the system [1]. It has a triangular shape whose peak (center) value can be swept through a range of diameters by changing the applied voltage, while the base width remains a constant percentage of the mean diameter. In the figure the central distribution is a Gaussian with a 0.7 nm standard deviation representing the NIST 100.7 nm PSL Standard Reference Material. The outer Gaussian curve is the modeled convolution of the DMA transfer function with the diameter distribution. The discrete points are measurements of the same convolution. They fall very close to the modeled results. The implication is that the deposition system method used to calculate the mean value of the NIST PSL spheres is accurate and that the transfer function of the deposition system is well characterized. Actual depositions, with the DMA fixed at a constant voltage (and diameter), can be no broader than the transfer function of the DMA. Thus knowing the maximum width of the transfer function allows an upper percentage limit to be placed on diameter distributions of depositions made with the system with these settings.

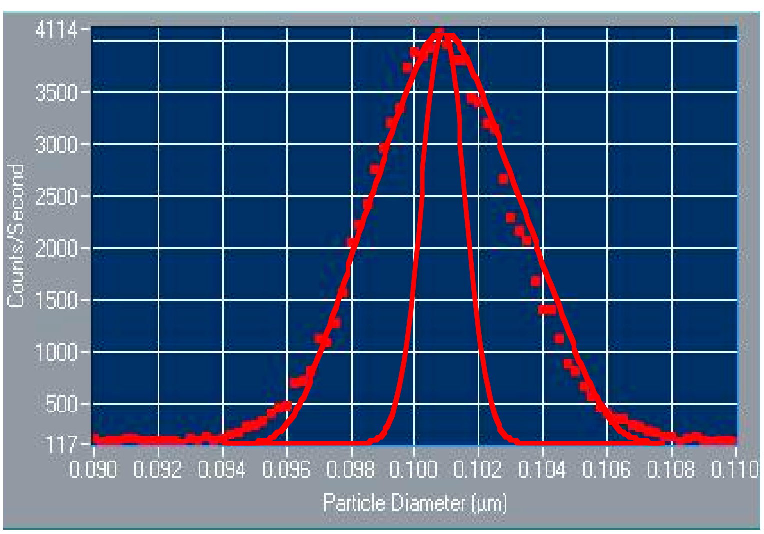

REFERENCES

1. P.D. Kinney, D.Y.H. Pui, G.W. Mulholland, and N.P. Bryer, "Use of the Electrostatic Classification Method to Size 0.1 mm SRM Particles – A Feasibility Study," *J. Res. Natl. Inst Stand. Technol.*, 96, 147, 1991.

Calculation of Particle Diameter Distributions from Electrostatic Classifier Data

J. C. Stover
The Scatter Works, Inc.
North Attleboro, MA 02760, U.S.A.

V. I. Ivakhnenko
ADE Corporation
Westwood, MA 02090, U.S.A.

C. A. Scheer
The Scatter Works, Inc.
North Attleboro, MA 02760, U.S.A.

An important problem in semiconductor manufacturing is the detection and characterisation of micro-defects on silicon wafers. Defects are found using instruments that sense flashes of scattered light created when a scanning laser beam illuminates surface features. The scanners are calibrated by measuring the scattering signal from known diameter of polystyrene latex (PSL) spheres, which are deposited on wafers. Ideally PSL spheres of known diameter would be available with very narrow diameter distributions. Unfortunately, narrow distributions are available in only a few sizes, and the problem is much worse for the smaller spheres where the distribution widths can approach +/-20% of the mean diameter. This paper reviews an inverse convolution technique developed to calculate the diameter distribution from measurements made with a differential mobility analyser (DMA).

The DMA works by subjecting charged particles to an applied electric field that is transverse to particle flow direction. Particles of only one size pass through a slit and progress towards the deposition surface. The modeled transfer function of a DMA can be found from the applied voltage and the related airflows through the system [1]. It has a triangular shape whose peak (center) value can be swept through a range of diameters by changing the applied voltage. Its base width changes, but remains a constant percentage of the mean diameter. If the DMA is swept through a distribution of particles then the particle count rate, as a function of diameter, becomes a measure of the convolution of the DMA transfer function with the available particle diameter distribution. By knowing the transfer function of the DMA and the general shape of the distribution, it is possible extract the distribution shape from the convolution data.

The figure shows one example. The outer solid plot is a model of an unusually complicated particle distribution. The inner plot is the convolution of a narrow triangular DMA transfer function with the distribution. Using this data the particle distribution was reconstructed as the dotted plot, which overlays the input distribution almost exactly. The slight shift of the peaks between the convolution and the particle distribution is caused by the increase in the transfer function width as it sweeps towards larger diameters. The diameter distribution in an actual deposition can be found by multiplying the transfer function, centered at the diameter of interest, times the distribution. This provides data needed for accurate scanner calibration.

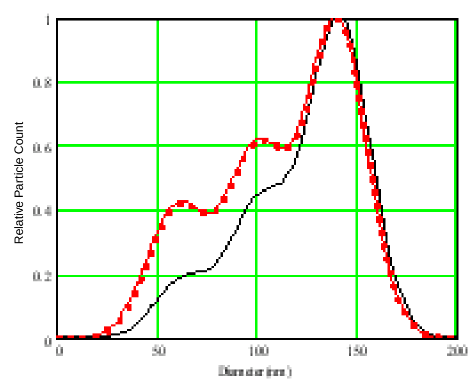

REFERENCES

1. P. D. Kinney, D. Y. H. Pui, G. W. Mulholland, and N. P. Bryer, "Use of the Electrostatic Classification Method to Size 0.1 mm SRM Particles – A Feasibility Study," *J. Res. Natl. Inst Stand. Technol.*, 96, 147, 1991.

Modeling of Light Scattering by Non-spherical Particle Inside a Film via Discrete Sources Method

E. Eremina
Moscow State University, Physics Faculty
Moscow, 119899, Russia

The progress in chips production requires more rigid cleanness standards. Modern chips are made on the base of silicone wafers, so the problem of maintenance of cleanness of a wafer surface becomes more and more important. Especially difficult is the problem of detection microcontaminating particles inside a film deposited on a substrate, or the film defects. It is connected with a fact that the scattered signal from the particles inside a film is essential lower, than for the particles on a substrate.

The problem of wafers defects and contaminations detection can be considerably facilitated by using a mathematical simulation. In this paper electromagnetic waves scattering by particles situated in a film on a substrate is considered. For modeling of diffraction process the discrete sources method (DSM) [1] is used. In difference from earlier paper [2], where the axisymmetrical defects were considered, the generalization of DSM on case of nonaxisymmetrical particles of any shapes is conducted.

In the frame of DSM the approximate solution of the difraction problem is constructed on the base of linear combinations of multipoles fields and satisfy all conditions of a problem except of conditions on particle surface. To account a layered structure it is necessary to use the Green tensor of a stratified medium. The amplitudes of discrete sources are found from satisfaction of interface conditions for electromagnetic fields on a particle surface by a generalized method of collocations. That approach allows to solve a problem simultaneously for a set of polarizations P/S and for all incident angles.

Using the program realization of developed method the analysis of scattering properties of equvolume particles with various geometries was conducted. Was shown, what even for small particles, their shape and arrangement in relation to an incident plane render essential influence for the characteristics of scattering. It was revealed, that in difference from particles on a substrate, S polarized radiation gives a more precise picture of scattering, than P polarized.

REFERENCES

1. Yu.A. Eremin, J.C. Stover, N.V. Grishina, “Discrete Sources Method for light scattering analysis from 3D asymmetrical features on a substrate”, Journal of Quantitative Spectroscopy & Radiative Transfer. 70 (2001). p. 421-431.
2. H.Yu.Eremina, A.G. Sveshnicov, “Analysis of Light Scattering by Particle Inside a Layer via Discrete Sources Method”, Moscow University Physics Bulletin. Allerton Press, Inc. N1. 1999. p. 8-16.

Session 4Ac7

Surface Plasmon Photonics

Polarization Singularities in Random Media and Rough Surface Scattering

I. Freund
Department of Physics, Bar-Ilan University
Ramat-Gan, 52900, Israel

The scattered, free space electromagnetic field can exhibit a variety of singularities. These include singularities of phase (optical vortices and edge dislocations), of amplitude (divergent caustics), and of polarization (vector, elliptic, and Stokes singularities). In general, in passing from a disordered medium or rough surface into the far field, one can expect all possible singularities to make an appearance. Phase singularities and caustics have been widely studied, but in the area of random media and rough surface scattering, polarization singularities are for the most part terra incognita. Vector singularities are points (V-points) or lines (V-lines) at which the direction of the electric (and magnetic) vector of linearly polarized fields becomes undefined. Conventionally, V-points are characterized by a conserved topological quantum number, the Poincaré-Hopf index η, which measures the rotation of the vectors in the surrounding vector field. Generically $\eta = \pm 1$, although we have recently shown how to generate optical V-points with any positive or negative value for η, including true singularities with $\eta = 0$. Optical V-lines are nongeneric, but also these can be generated. Elliptic singularities are points or lines at which the parameters of the ellipses in elliptically polarized fields become undefined. At C-points and on C-lines the field is circularly polarized, and the orientation of the major (and minor) axis of the ellipse becomes undefined. Conventionally, C-points are characterized by the conserved topological singularity index I_C, which measures the rotation of the ellipses in the surrounding ellipse field. Generically, $I_C = \pm 1/2$, although we have recently shown how to generate optical C-points with any positive/negative half-integer or integer value for I_C, including zero. C-lines are nongeneric, but also these can be generated. Under propagation, V-points typically convert to C-points. Such conversions are best discussed using a new conserved index, the Stokes index σ_{12}, which is defined in terms of the directly measurable Stokes parameters S_1 and S_2. Conservation of this index requires, for example, a single $\eta = +2V$-point to decay into four $I_C = +1/2$ C-points. At L-points and on L-lines the polarization ellipse collapses to a line, and the handedness, right or left, becomes undefined. Only zero index L-points are possible, and although these can be generated, they are nongeneric. In a random field the generic L-singularity is an L-line, and these lines always separate regions of left handed and right handed polarization. At a Stokes singularity all three normalized Stokes parameters become undefined, and the *state* of polarization becomes indeterminate. Unlike the other polarization singularities, Stokes singularities ($\sum$-points or $\sum$-lines) cannot be represented as points or lines on the Poincaré sphere. There are only a few specific examples of $\sum$-points currently available (and none of $\sum$-lines), and at present little is known about the properties of these singularities. Examples of the various singularities in random fields will be presented, their dynamic and topological interactions will be examined, and their evolution and interconversions under propagation will be discussed.

Channel Polaritons

A. A. Maradudin and I. V. Novikov*
Department of Physics and Astronomy and Institute for Surface and Interface Science
University of California, Irvine
Irvine, CA 92697, U.S.A.

We determine the dispersion relation for surface electromagnetic waves guided by a straight channel cut into the otherwise planar surface of a solid in contact with vacuum. The solid can be either a metal or a dielectric medium, and is characterized by a real, frequency-dependent dielectric function $\epsilon(\omega)$ that is negative in some range of frequencies. It is assumed that the generators of the channel are parallel to the x_2-axis, and the region $x_3 > \zeta(x_1)$ is vacuum while the region $x_3 < \zeta(x_1)$ is the solid. The surface profile function $\zeta(x_1)$ can be either a single-valued function of x_1, or a multi-valued function of x_1. The application of Green's second integral identity in the plane to the regions $x_3 > \zeta(x_1)$ and $x_3 < \zeta(x_1)$, and the boundary conditions at the interface $x_3 = \zeta(x_1)$, lead to a system of four coupled homogeneous integral equations for the values of the components of the electric and magnetic vectors parallel to the generators of the surface, evaluated on the surface, and for the values of their normal derivatives evaluated on the surface. To deal with the possible multi-valued nature of the surface profile function $\zeta(x_1)$ a parameterization of it due to Mendoza-Suárez and Méndez [1] is used in deriving these integral equations The integral equations are converted into a system of four matrix equations by the use of a numerical quadrature scheme. The dispersion relation is then obtained by equating to zero the determinant of the matrix of coefficients in this system, and searching for the roots. Three forms of the shape of the channel were used in these calculations: (i) a Gaussian groove; (ii) a nearly rectangular groove; and (iii) a truncated circular groove. The latter is described by a double-valued profile function. Each channel supports an infinite number of modes propagating in the x_2-direction that are spatially localized in the vicinity of the channel. The dispersion curves for the three lowest frequency modes and the three highest frequency modes have been obtained in the case that the solid is a simple free electron metal. These propagating bound electromagnetic modes are called *channel polaritons*.

REFERENCES

1. Mendoza-Suárez, A. and E. R. Méndez, *Appl. Opt.*, Vol. 36, 214, 1997.

* Present address: Stanford Research Systems, 1290 Ream Wood Avenue, Sunnyvale, CA 94089

Giant Light Transmission through Subwavelength Apertures in Metal Films

T. Thio
NEC Research Institute
Princeton, NJ 08540, U.S.A.

The transmission of light through a single aperture in an otherwise smooth and opaque metal film is expected to be extremely small when the hole diameter is smaller than the optical wavelength, scaling as $(d/\lambda)^4$. However, when a metal film is perforated with a periodic *array* of such sub-wavelength holes, the transmission is enhanced by up to several orders of magnitude, and can be larger than the fraction of the area occupied by the holes. The transmission enhancement is the result of a resonant interaction of the incident light with surface plasmon polaritons, collective electronic excitations at the metal surface; the interaction is made possible by a periodic corrugation of the surface. The transmission spectra therefore provide a probe for the surface plasmon dispersion relation, with high transmission occurring when the energy and momentum of the incident light matches that of the surface plasmons. Deep and sharp minima in the transmission spectra are due to Wood's anomaly, a diffraction effect.

The surface plasmon enhancement of the transmission also occurs for the case of a single subwavelength aperture surrounded by an array of indentations in the metal surface. Spatially resolved transmission data suggest that the enhancement is a highly local phenomenon, with the transmission spectrum of each aperture depending only on the surface structure in the immediate vicinity of the aperture. Although surface plasmons clearly play an important role in the transmission enhancement, the details of the enhancement mechanism are not yet understood.

The wavelength at which the enhancement occurs may be tuned by controlling the geometry of the hole/indentation array, the refractive index of the adjacent dielectric, and the incident angle. Such tunability, together with the high transmission, make these structures attractive for use in a variety of novel devices such as high-transmission NSOM, flat-panel displays and subwavelength photolithography.

Overcoming Optical Diffraction from a Sub-Wavelength Aperture

H. J. Lezec, T. W. Ebbesen, E. Devaux, and A. Degiron
ISIS, Université Louis Pasteur
Strasbourg, NJ 67000, France

F. J. Garcia-Vidal
Departamento de Fisica Teórica de la Materia Condensada, Universidad Autónoma de Madrid
Madrid, NJ 28049, Spain

L. Martin-Moreno
CSIC, Instituto de Ciencia de Materiales de Madrid
Madrid, NJ 28049, Spain

R. A. Linke
NEC Research Institute
Princeton, NJ 08540, U.S.A.

The transmission of light through a sub-wavelength aperture in a smooth, opaque metal film can be boosted up to several orders of magnitude by patterning the surface of incidence around the hole with periodic indentations. This enhancement can be explained by coupling of light to surface-plasmon (SP) modes at specific frequencies, which results in a substantial increase in optical intensity at the hole entrance.

Here we specifically explore the additional effect of adding a periodic corrugation to the exit side of the film. By using focused-ion-beam fabrication and a free-standing Ag membrane as our substrate of choice, we are able to pattern bulls-eye or rectangular groove arrays on both sides of the film, centered about circular or slit-shaped apertures, respectively. At wavelengths leading to SP resonance on both sides of the film, a further order-of-magnitude transmission enhancement is typically observed for both hole- or slit-device configurations.

Contrary to what is expected for a plain sub-wavelength aperture, which typically diffracts light uniformly in all directions, the light transmitted through the present structures is observed to have a very small angular divergence ($\sim \pm 5°$). This is especially surprising given our additional observation that surface emission is mainly confined to an area with lateral dimensions comparable to the wavelength. Another interesting phenomenon is specifically revealed in the case of the patterned-exit-surface slits: directional control of the low-divergence transmitted beam as a function of wavelength.

A simple model, validated by numerical simulations, has been derived which predicts the observed effects. In this model, the collimation and directionality of the transmitted beam can be explained by the interference of fully-diffracted light emitted from the point-source aperture with light emitted weakly from the centers of the nearest-neighbor grooves. This weak emission corresponds to reradiation by surface-plasmons launched at the hole and Bragg-scattered to form a standing wave on the periodic exit surface.

The unique combination of strong localization, high efficiency, narrow divergence, and directionality displayed in their transmission characteristics suggests that these novel SP-activated sub-wavelength apertures are potentially useful in a wide range of photonic applications.

Light-Controlled Extraordinary Optical Transmittance and Photonic Circuits in Plasmonic Nanomaterials

Andrey K. Sarychev[†]**, V. A. Podolskiy**[‡]**, and Vladimir M. Shalaev**[†]

[†]Purdue University
West Lafayette, Indiana, U.S.A.

[‡]New Mexico State University
Las Cruces, New Mexico, U.S.A.

Recently it has been shown that light can experience extraordinary optical transmittance (EOT) through subwavelength hole arrays in optically thick metal films [1-5]. The plasmon-enhanced EOT exceeds the ordinary (with no plasmon excitation) transmittance for a film with such small holes by 10^5. This effect is of great importance because it opens up new ways to control light. Shalaev and Sarychev predicted theoretically that the EOT could occur even without holes, if there is a periodic modulation in the refractive index n at the metal-dielectric interface. Such n-modulation makes possible the excitation of surface plasmon polaritons (SPPs), resulting in the EOT [5]. The light itself can induce the n-modulation, in particular, by using the optical nonlinearity. Photorefractive quantum wells are known to produce a large n-modulation, even at very low light intensities, $\sim 10\mu$W. Thus, by covering a metal film with a photorefractive quantum well and irradiating the sample with two interfering beams incident on the surface from the opposite sides (see the *left* figure), one can create the n-grating and thus control the EOT for the fundamental beam, propagating normal to the surface. Note that the light-gated EOT represents an example of manipulating photons with photons, similar to the manipulation of current in conventional electronics. Note that by arranging nano-holes in special patterns one can perform light circuiting along a metal film, similarly to electron circuits (see figure in the *right*). Another related effect we plan to discuss is optical bistability. If there is a small correction to the refractive index that depends on the light intensity, then the SPPs induced by the light on the n-modulated surface would result in larger local fields and increased n-modulation, which in turn would lead to enhanced amplitudes of the SPPs. This positive feedback can give rise to bistability in the optical transmission [5] (as verified by our simulations), which can be used for developing novel nanostructured optical switches, operating with femtosecond-scale switching times – by far faster than switches in electronics. The extraordinary optical transmittance through nanostructured metal-photorefractive composite films and arrays of nanoholes are expected to result in novel applications in the emerging area of nanophotonics.

REFERENCES

1. T.W. Ebbesen, H.J. Lezec, H.F. Ghaemi, T. Thio and P.A. Wolff, *Nature*, 391, 667 (1998).
2. L. Martin-Moreno, F.J. Garcia-Vidal, H.J. Lezec, K.M. Pellerin, T. Thio, J.B. Pendry, and T.W. Ebbesen, *Phys. Rev. Lett.*, 86, 1114 (2001).
3. V.A. Shubin, A.K. Sarychev, J.P. Clerc, and V.M. Shalaev, Phys. Rev. B 62, 11230 (2000); A.K. Sarychev, R.C. McPhedran, and V.M. Shalaev, *Phys. Rev.* B 62, 8531 (2000).
4. A.K. Sarychev and V.M. Shalaev, *Phys. Reports* 335, 275 (2000).
5. A. K. Sarychev, V. M. Shalaev, *Proceedings of SPIE*, v. 4467 (2001), p. 207

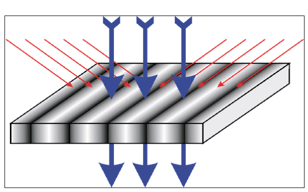

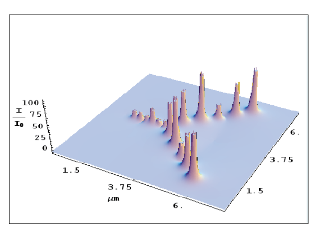

Extraordinary Optical Transmission Through Nanostructured Metals

L. Martin-Moreno
Department of Condensed Matter Physics, Universidad de Zaragoza
Zaragoza, 50009, Spain

F. J. Garcia-Vidal
Department of Theory of Condensed Matter Physics, Universidad Autonoma de Madrid
Madrid, 28049, Spain

We show how surface plasmons can help to enhance optical transmission through transmission gratings [1] and 2D hole arrays [2]. We will analyze the similarities and differences between both cases.

First we analyze the case of transmission gratings with very narrow and deep slits. In this case we show that there are two possible ways of transferring light from the upper surface to the lower one: either by the resonant excitation of surface plasmons on both surfaces of the metallic grating or by the coupling of the incident light with cavity plasmon modes located in the slits.

Next, we present a fully 3D theoretical study of the extraordinary transmission of light through subwavelength hole arrays in optically thick metal films [3]. Good agreement is obtained with experimental data. An analytical minimal model is also developed, which conclusively shows that the enhancement of transmission is due to tunneling through surface plasmons formed on each metal-dielectric interfaces. Different regimes of tunneling (resonant through a ”surface plasmon molecule”, or sequential through two isolated surface plasmons) are found depending on the geometrical parameters defining the system.

Finally, and in order to visualize the dynamics of the transmission process, we will show some real-time evolutions of the electromagnetic fields impinging on the structured metal.

REFERENCES

1. J.A. Porto, F.J. Garcia-Vidal and J.B. Pendry, Phys. Rev. Lett. 83, 2845 (1999).
2. L. Martin-Moreno, F.J. Garcia-Vidal, H.J. Lezec, K.M. Pellerin, T. Thio, J.B. Pendry and T.W. Ebbesen, Phys. Rev. Lett. 86, 1114 (2001).
3. T.W. Ebbesen et al., Nature (London) 391, 667 (1998).

Surface-Plasmon Polariton Excitation in Nanostructured Metal Surfaces: EM Mechanism in SERS

J. V. García-Ramos and J. A. Sánchez-Gil
Instituto de Estructura de la Materia, CSIC
Madrid, Spain

E. R. Méndez
Departamento de Óptica, CICESE
Ensenada, México

By means of numerical simulation calculations based on the Green's theorem integral equation formulation, we study the p-polarized near electromagnetic (EM) field scattered in the vicinity of one-dimensional, randomly rough metal surfaces. Two rough surface models are considered with different statistical properties: self-affine (physical) fractals and Gaussian-correlated profiles. In both cases, the statistical parameters of the surface roughness (lower scale cutoff and correlation length, respectively) are chosen in such a manner that sub-100 nm features are present. Thus surface-plasmon polaritons are more efficiently excited by the incoming beam. For sufficiently rough surfaces (small enough nanostructures with large enough height deviations), strong surface EM field excitations (*hot spots*) are found. Typically, they yield local enhancement factors of the EM field intensity (normal component) of up to $\sim 10^4$ for a wide range of incoming wavelengths covering the visible and near infrared up to $\lambda \approx 2\mu$m. These hot spots could very likely play the role of active sites in connection with SERS (surface-enhanced Raman scattering) detection of single molecules.

We also analyze the EM contribution to the average SERS enhancement factor from the numerical calculations of the average and fluctuations of the surface EM field intensity for ensembles of random realizations. As a consequence of the large values acquired by the average and fluctuations, the average SERS response can be enhanced by a factor exceeding 10^4 for a wide spectral range, provided that the statistical parameters of the surface roughness are such that large nanoscale features are present. Our results might shed light onto the EM mechanism in SERS, including SERS single molecule detection, on well known metal substrates exhibiting self-affinity. Furthermore, it is predicted that non-fractal, randomly rough metal surfaces of controlled statistics (Gaussian-correlated in this case), which can be fabricated, might well be used as SERS substrates.

Surface-Enhanced Raman Spectroscopy on Rough Metal Surfaces of Controlled Statistics

J. V. García-Ramos and J. A. Sánchez-Gil
Instituto de Estructura de la Materia, Consejo Superior de Investigaciones Científicas
Madrid, 28006, Spain

E. R. Méndez
Departamento de Óptica, División de F'ısica Aplicada
Centro de Investigación Científica y de Enseñanza Superior de Ensenada
Ensenada, Baja California 22860, México

Surface-Enhanced Raman Scattering (SERS) has been reported from a great variety of substrates: electrodes, colloids, silver islands, etc. All of these substrates have different properties that make them SERS active, but present nontrivial drawbacks. Rigorous numerical simulation calculations for the contribution from the electromagnetic (EM) mechanism to the enhancement factor in SERS provide conclusive results in favor of the use of rough metal surfaces with controlled statistics (Gaussian statistics and Gaussian correlation function) as substrates for SERS spectroscopy; typical average SERS enhancement factors of four orders of magnitude and even larger have been predicted.

One-dimensional and two-dimensional randomly rough metal surfaces with Gaussian statistics and Gaussian correlation functions have been fabricated by exposing photoresist-coated plates to laser speckle patterns. The resulting sample with the desired statistics and correlation function is then covered with a metal layer by evaporation techniques. This kind of metal surfaces has been commonly used in elastic rough surface scattering. Typically, such randomly rough metal surfaces have correlation lengths above 1 μm. On the other hand, if sub-100 nm surface features are needed, ground glass or polished metal surfaces can be employed. Alternatively, UV-lithography could potentially extend the above mentioned laser speckle technique to fabricate Gaussian-correlated samples with correlation lengths in the range of or smaller than a hundred nanometers.

The randomly rough metal surfaces thus fabricated have been employed as SERS substrates. By depositing heterocyclic compounds in a controlled manner, SERS spectra have been obtained. The experimentally inferred SERS enhancement factors, and other relevant information extracted from the SERS spectra, are compared with the rigorous numerical simulation calculations for similar surface models. Roughness-induced excitation of surface-plasmon polaritons lies on the basis of the SERS enhancement factor for the substrates with ~ 100 nm features; in contrast, multiple scattering of light might be the underlying intensification mechanism for the substrates with micron-sized correlation lengths. The potential use of such substrates for SERS single molecule detection is analyzed.

Study of Enhanced Specular Peaks in Diffuse Light Scattering from Weakly Rough Metal Surfaces

K. A. O'Donnell and E. R. Méndez
Centro de Investigación Científica y de Educación Superior deEnsenada
Ensenada, Baja California, México

The diffuse scatter from a weakly rough surface may contain interesting effects due to the excitation of surface plasmon polaritons. In particular, the roughness can permit the incident wave to launch plasmon polaritons and, conversely, surface waves can be roughness-coupled to contribute to the diffuse scatter escaping from the surface. Such processes are well-known to produce effects such as backscattering enhancement. On the other hand, if the surface roughness is also appropriate to couple counter-propagating plasmon polaritons to one another, we demonstrate that such processes should produce a distinct peak at the specular angle in the diffuse scatter. This peak arises from a four-fold scattering process and thus appears in a contribution to the mean diffuse intensity that is of eighth order in the standard deviation of surface height. In their lowest perturbation orders, the specular peak presents an angular width twice that of the backscattering peak.

The specular peak is investigated using perturbation theory based on the reduced Rayleigh equations, and with Monte Carlo computational techniques. The peak is either absent or quite indistinct for a number of common surface roughness power spectra. By employing a spectrum composed of two rectangular forms centered near the plasmon polariton wavenumber, and at twice this wavenumber, it is found that the specular peak may be made to appear at high levels in the scattering distribution. Surface parameters intended to optimize the peak visibility are discussed and, finally, we discuss the plausibility of the experminental observation of the peak.

Surface Profile Reconstruction Using Far-Field Intensity Data

D. Macías, G. Olague, and E. R. Méndez
División de Fí sica Aplicada, CICESE
Ensenada, B. C. 22800, Mexico

We study inverse scattering problems using an evolutionary approach. The input data consists of far-field angle-resolved scattered intensity data, and the objective is to retrieve the surface profile function that produced the scattering data. To simplify the problem, the surface is assumed to be one-dimensional, random, and perfectly conducting.
The fitness function is defined as

$$f(\zeta(x_1), k_j) = \sum_{j=1}^{N_{ang}} \int \left| I^{(m)}(q|k_j) - I^{(c)}(q|k_j) \right| dq,$$

where $I^{(m)}(q|k_j)$ represents the measured intensity data, $I^{(c)}(q|k_j)$ is the intensity data calculated with a proposed surface profile function, N_{ang} is the number of angles of incidence considered, $k_j = (\omega/c)\sin\theta_j$, and $q = (\omega/c)\sin\theta_s$. The minimum of the fitness function is searched using the evolutionary strategies (μ, λ) and $(\mu + \lambda)$.
On the assumption that some knowledge about the statistical properties of the unknown surface profile is given or can be obtained, the search space is restricted to surfaces that belong to that particular class. In our case, as the original surface, the trial surfaces constitute realizations of a stationary zero-mean Gaussian random process with a Gaussian correlation function. The numerical results are encouraging. We have found that for the conditions and parameters employed the surface profile can be retrieved with high degree of confidence. Some aspects of the convergence and the lack of uniqueness of the solution will be also discussed.

Session 4Ac8

Wavelets in Electromagnetics

On the Application of Electromagnetic Boundary Conditions in Wavelet-Based Time Domain Numerical Techniques

C. D. Sarris and L. P. B. Katehi
Radiation Laboratory, Department of Electrical Engineering and Computer Science
University of Michigan
Ann Arbor, MI 48109-2122, U.S.A.

The use of wavelet bases for the discretization of Maxwell's equations through the Method of Moments has led to the development of Multiresolution Time Domain (MRTD) technique Research into several aspects of this technique, as formulated in wavelet bases ranging from Haar to biorthogonal wavelets, is motivated by the fact that it provides a most natural framework for the implementation of dynamically adaptive grids, following the spatio-temporal evolution of field quantities under determination.

However, the multilevel field expansions that the application of wavelet methods are based on, also imply that local field values are represented as a weighted sum of basis functions, not necessarily collocated and corresponding to multiple levels of resolution (introduced by the wavelets). In consequence, the enforcement of localized boundary conditions at points, lines or planes of the computational domain typically presents a complexity that can potentially compromise the advantages that the use of wavelets can produce at electromagnetically homogeneous parts of the domain.

For the Haar wavelet-based MRTD scheme, the authors have formulated and applied a numerical interface with the Finite Difference Time Domain (FDTD) technique, that was shown to facilitate the modeling of perfect electric conductors (PECs) within the computational domain and perfectly matched layer (PML) absorbers for mesh termination. Employing this technique, modeling of perfect electric conductors of width that is less than the cell size can be accomplished at a minimum complexity and without the need to invoke image theory and split the domain below and above the conductor.

This paper revisits the problem of modeling localized boundary conditions that are applied at points, lines or planes contained within MRTD cells, from a broader, basis-independent point of view. Three classes of boundary conditions are considered: Sources, hard boundaries (PECs) and absorbing boundary conditions, including PMLs. As a general strategy, boundary conditions are realized in the domain of scaling functions at the maximum resolution of the wavelet-based scheme and then transformed to the wavelet domain. Thus, locally modified expressions that implement certain types of electromagnetic boundary conditions are explicitly deduced for Haar wavelet and spline based MRTD schemes.

The proposed formulations of the boundary conditions are validated in practical microwave circuit structures. In particular, the performance of absorbing boundary conditions and PML absorber formulations is tested in open problems of printed antennas and open waveguide and filter geometries, while interior PEC modeling is employed for the determination of characteristic impedance in layered coplanar waveguides and striplines. Extensive accuracy estimation studies, based on the comparison of results derived by the proposed modified MRTD schemes and the conventional FDTD technique, as well as semi-static formulas, are provided.

Green's Function Induced Wavelets and Wavelet-Like Orthogonal Systems for EM Applications

A. R. Baghai-Wadji
Vienna University of Technology
Vienna, Austria

G. G. Walter
University of Wisconsin
Milwaukee, WI, U.S.A.

Utilizing Meyer's orthogonalization technique we will discuss the construction of wavelets based on Green's functions associated with given boundary value problems. Following a brief review of standard techniques for the construction of wavelets we describe the rationale behind our ideas, and then present our first successful results concerning the scaling function $\varphi(x)$ and the wavelet $\psi(x)$ associated with Laplace operator in two spatial dimensions: $\Delta = \partial^2/\partial x^2 + \partial^2/\partial z^2$. We obtain closed-form solutions for the scaling function and the wavelet in the wavenumber domain as well as in the real-space. We have been able to identify several properties of $\varphi(x)$ and $\psi(x)$: Each of these functions corresponds to a collectively charge-neutral sequence of parallel lines. Our scaling function corresponds to the element factor of an infinite array. Our wavelet corresponds to the potential distribution of three equidistant lines with charge densities 1, -2, and 1. Furthermore, we will demonstrate the existence of an infinite family of wavelet-like orthogonal systems associated with Laplace operator. This fact guarantees great flexibilty in designing symmetric and asymmetric bases.

Then we construct the scaling function $\varphi(x, y)$, and the wavelet $\psi(x, y)$ in two independent spatial variables, associated with Laplace operator $\Delta = \partial^2/\partial x^2 + \partial^2/\partial y^2 + \partial^2/\partial z^2$.

As further examples we will consider (dyadic) Green's functions associated with bulk waves (Helmholz equation) and surface waves (Rayleigh equation), and show that these and more general Green's functions only permit wavelet-like orthogonal sequences of functions rather than wavelets which satisfy the axioms of the multiresolution analysis.

It will be shown that while the generating Green's functions are L^1 functions, the constructed scaling functions and the wavelets (wavelet-like functions) are L^2 functions: The reason for this property is that Meyer's orthogonalization scheme cancels possible singularities of the Green's functions. Furthermore, it will be pointed out that we analogously can construct wavelet-like orthogonal functions from impulse responses of linear time-invariant systems, with possible applications in instrumentation.

Our prime motivation for constructing wavelets from Green's functions has been, however, the efficient solution of singular surface integral equations which arise in the boundary element method applications. To fix the ideas we first will apply the familiar Haar wavelet to integral equations with a logarithmic kernel. We will calculate all the involved formulae in closed form and discuss the sparsity property of the system matrix which results from discretizing the underlying integral equation. Then we will proceed to the discretization of the same integral equation using our wavelet $\psi(x)$, and again calculate the system matrix in a closed-form. Finally we proceed to the solution of 3D problems by utilizing our bivariate wavelet function $\psi(x, y)$.

Finite Difference Wavelet Time Domain (FDWTD) Method for the Numerical Solution of Maxwell s Equations

M. Raugi and A. Musolino
Dipartimento Sistemi Elettrici e Automazione, Università di Pisa
Pisa, 56126, Italy

The method proposed here for the analysis of electromagnetic fields is a hybrid Finite Difference - Wavelet method.

In particular the Maxwell's equations are discretized in the space domain by the use of a standard FD technique. Then a multiresolution expansion with Daubechies Wavelets on the interval is performed in time. The representation of integral and differential operators for Daubechies wavelets on the interval, developed by the authors, is used.

The wavelets coefficients are cast in a matrix form leading to an algebraic equation in the Sylvester's form, whose matrices are sparse due to the wavelet properties. The solution of this kind of equation ($AX + XB = C$) can be performed with optimised techniques leading to reduced CPU times if compared with standard time marching schemes for the solution of MTL equations.

Interesting conclusions come from the comparison between results obtained with other methods and the proposed method: the number of wavelets functions required (directly proportional to the number of time samples of the functions) is lower given the same accuracy; furthermore considering a standard FDTD method it can be verified that situations that violate the Courant Condition, do not lead to any unstable solution in the presented method.

Wavelet Efficient Technique for the Full-Wave Modal Analysis of Arbitrary Geometry Waveguides

B. Tebar
GMV
Madrid, Spain

A. Vidal, S. Cogollos, C. Bachiller, and V. E. Boria
Universidad Politécnica de Valencia
Valencia, Spain

Wavelet techniques provide a very useful tool in electromagnetics because they offer interesting properties concerning geometry characterization and efficient numerical computation. In this work, Wavelet operators are used in an Integral Equation technique that solves the full-wave modal analysis of waveguides with arbitrary cross-section. The classical approach to the aforementioned problem involves the Method of Moments (Galerkin). Alternatively, in this work we present two innovations that, to the authors' knowledge, have never been used in waveguide modal analysis. The first one is the discretization process that is a very simple implementation of the Nyström technique. It brings major advantages in the computation of the matrix elements that are simple kernel evaluations. The second new idea is the application of a joined construction-compression process avoiding element computation of non-significant original elements in a very efficient procedure that uses Wavelet-like bases. Consequently, memory requirements and computational costs are greatly reduced. In this work, we present simulated results for a ridged waveguide that has been analyzed with the proposed method using Nyström discretization, Wavelet-like characterization, and efficient matrix construction.

The conclusion from this work is that compressed matrices are built up very efficiently and their final aspect is very disperse (see Fig. 1). This fact can be exploited in the posterior eigenvalue computation algorithm and also in matrix storage savings. Furthermore, final cut-off frequencies are compared with those obtained via a traditional solution using the Method of Moments provided by a commercial software package. The final error between both cut-off frequency sets is then analyzed, thus providing a good agreement between the classical approach and the new proposed method.

a) 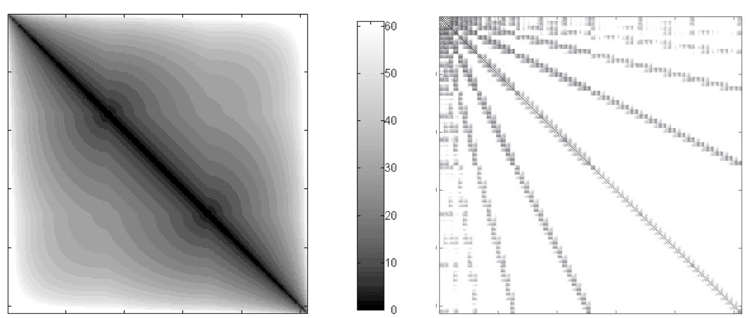 b)

Figure 1: Original kernel matrix a) and compressed kernel matrix b).

Wavelet-Based Detection and Classification of VHF Radar Meteor Trail Echoes

T. V. Chandrasekhar Sarma
National MST Radar Facility
Tirupati, India

V. M. Gadre
Indian Institute of Technology Bombay
Mumbai, India

VHF Radars have been gainfully employed over the past 25 years in atmospheric research. These radars which were designed to study atmospheric phenomena based on echoes from the radio refractive index variation in the clear air from the atmospheric regions of Mesosphere, Stratosphere and the Troposphere became known as MST radars. Only the radars with very high average power aperture products (of the order of $10^8\,\mathrm{Wm}^2$) can reach upto Mesosphere. Other moderately designed systems which are called ST or T radars depending upon the altitude coverage, proliferated for several operational and research applications. The typical operational frequency of these radars is around 50MHz. These radars are also called as atmospheric radars.

Radar study of meteors has an older history than MST studies. To study the atmospheric phenomena in the height region of 70-120km, meteor wind radars were built. These radars use the ionised meteor trail as a tracer of background wind at these heights. The occurrence of radar meteor echoes is a sporadic phenomenon.

The backscatter from the ionised meteor trail is several orders of magnitude more than the echoes from clear air. Therefore all the atmospheric radars are capable of detecting meteor trails. To exploit this capability, piggyback meteor detection systems were designed to work simultaneously with the clear-air mode of operation and separate out the meteor echoes. The radar meteor echo is broadly classified into three categories viz., underdense trail, overdense trail and the head echo. The classification of underdense and overdense is based on the ion density; $< 10^{14}\,\mathrm{m}^{-3}$ for underdense and $> 10^{14}\,\mathrm{m}^{-3}$ for overdense. The head echo is from the meteor itself.

The underdense trail is useful for deriving winds in the meteor region. The total meteor counts have use in astronomical studies.

The VHF radar records contain echoes from the ionospheric E region and the noise records, in addition to meteor echoes. Presently time-domain techniques are employed to separate out the meteor records. In these methods, many of the ionospheric records also could be classified as meteor records. The meteor trail is a transient phenomenon. The power profile of the underdense trail exhibits an exponential decay, whereas the power profile of overdense echo is more complex. The head echo is a transient with much smaller lifetime. Due to the transient nature of these echoes, time-frequency analysis methods (of which, wavelet-based methods are a popular class) is an appropriate technique for their detection and classification. This paper presents a wavelet transform-based method for the detection of meteor trail induced backscatter in the atmospheric radar records and their classification into the three categories mentioned previously.

Poetic and Scientific Representation of Infinity: A Wavelet Approach to the Impulse Function

C. F. Chen
Department of Electronic Engineering, The Chinese University of Hong Kong
Shatin, Hong Kong

Y. F. Tung
New Asia College, The Chinese University of Hong Kong
Shatin, Hong Kong

The quantity "infinity", when implemented on a computer, has been and should not be expressed by an arbitrarily chosen large number. Let us use Dirac's impulse function to illustrate the point. Dirac's unit impulse is defined by a square pulse of width "a" and a height 1/a in the limit of a→0. When we realize 1/a on the computer, one of various large numbers is chosen and therefore it never be unique. We would rather say that this kind of approach is not scientific but poetic.

In her correspondence to Einstein, Mileva Marić discussed infinity in the following way;

> "I don't think the structure of the human skill is to be blamed for man's inability to understand the concept of infinity . . . . . . If someone can conceive of infinite happiness, he should be able to comprehend the infinity of space—I should think it much easier."

Her statement shown above is qualitative or poetic; but scientist's arbitrarily chosen method for implementing infinity is no better than Marić's.

Dirac, therefore, in his later years, tried to abolish "infinity" in formulas of physics which he had established early in his life.

This paper will use the inverse Laplace formula via Haar's wavelet derived by the first author to perform the inverse Laplace transform on "1", "s" "s^2" etc or a polynomial of s in general. Fig. 1 shows the inverse Laplace of "s" while Fig. 2 is that of "-4". It is noted that if we consider the original Dirac's delta function as a particle, our new generalized Dirac's function corresponds to the wave version of the particle. This result is new.

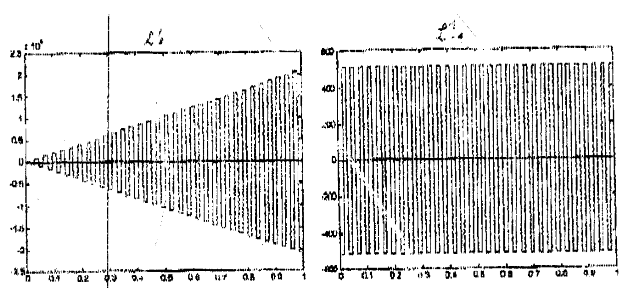

REFERENCES

1. Wu, J. L., C. H. Chen and C. F. Chen, "Numerical inversion of Laplace transform using Haar Wavelet operational matrices," *IEEE Transactions on Circuits and Systems.* Vol. 148, No. 1, Jan. 2001

Adaptive Numerical Modeling of Reconfigurable RF-MEMS Structures Using MRTD

N. Bushyager, E. M. Tentzeris, and J. Papapolymerou
School of ECE, Georgia Institute of Technology
Atlanta, GA 30332-250, U.S.A.

Interest in MEMS technology is growing in the RF field because of the lower loss characteristics of MEMS devices. These loss characteristics translate into higher Q of passive devices, a critical improvement because the Q of embedded passives is a constraining factor for their implementation in many RF technologies. Great strides are being made in the fabrication of MEMS devices, and accurate models of these devices are needed. The numerical simulation of these devices is a difficult proposition for a number of reasons. The first is the need to integrate both mechanical and electromagnetic equations. Most EM simulators are unable to compensate for the changing boundary conditions introduced by the motion of the simulated structure. A second difficulty is the complexity of modeling their intricate structure. The smallest features of the devices can be several orders of magnitude smaller than the bulk feature size, leading to numerical inaccuracies or very large computational grids. Thus, a simulator for modeling MEMS devices needs to be able to handle moving boundary conditions, the interaction between electrostatic forces and mechanical motion, and difficult to model complex geometries. In the following, the FDTD and the Haar-based MRTD algorithms are applied to the full-wave modeling of high-frequency structures that require the combination of differential equations with time-constants of different orders. The numerical coupling of Maxwell's and mechanical equations for the simulation of MEMS reconfigurable devices. Because both simulators are time domain, a change in the boundary conditions, such as would be caused by a moving metal, is not necessarily a problem. Indeed, because the boundary conditions are enforced explicitly at every time step, a moving plate simply causes the boundary conditions to be enforced at different space points for each time step. In this manner, a time varying metal plate is easy to incorporate into an FDTD or MRTD model.

Digital Filter Banks: Wavelet Transform Approach

M. V. Latte
SDM College of Engineering & Technology
Dharwad, 580002, India

S. F. Farida
Department of Applied Electronics, Gulbarga University
Gulbarga, 585106, India

S. N. Bhosale
Kittel Science College
Dharwad, 580001, India

D. K. Deshpande
Department of Physics, Karnatak University
Dharwad, 580003, India

Filter Bank is a structure that decomposes a signal into a collection of sub-signals. Depending on the applications, these sub-signals help to emphasize specific aspects of the original signal or may be easier to work with, than the original signal. Signal separation or decomposition is necessary when a signal is contaminated with interference, noise or other signals e.g., electrical activity of the heart (ECG), EEG etc. To implement the Digital Filter Banks two main techniques are used 1) Convolution 2) Wavelet Transform Analysis. Since the time and frequency localization capabilities of wavelets provide better noise detection and less signal distortion than direct filtering of the data, we have simulated a digital filter bank using wavelet transform to analyze and process the signal. A digital filter bank is implemented by convolving the original signal with the impulse coefficients of the Daubacies-4 wavelet. After convolving, the discrete wavelet transform coefficients are obtained. This decomposed signal is analyzed to determine the occurrence of various frequencies at different instances of time and can be modified so as to remove the high frequency noise. Wavelet Transform analysis provides both time and frequency information of a signal with required resolution. We have generated MATLAB code, which implements filter bank and provide denoising of the input signal and also for the reconstruction of the filter. The resolution of the signal, which is a measure of the amount of the detail information in the signal, is changed by filtering operations, and scale is changed by up-sampling and down-sampling operations. The procedure starts with passing the signal through a half-band digital low pass filter with impulse response $h(n)$. This filter removes all frequencies that are above, half of the highest frequency in the signal. Now according to Nyquist's rule, half of the samples can be eliminated by down sampling, which doubles the scale of the signal. We have implemented this algorithm for five levels. Reconstruction of the signal involves starting with up-sampling of the last level (i.e., fifth level) approximation coefficient vector, passing it through low pass reconstruction filter and then adding the result with the output of high-pass reconstruction filter, whose input would have been the up-sampled version of the fifth level detail coefficient vector.

Session 4Ac9

Poster Session - III

Nonstationary Electromagnetic Wave Scattering from a Perfectly Conducting Cone Covered with a Dielectric Layer

I. G. Efimova
Moscow State University
Moscow, 119899, Russia

Z. V. Sedel'nikova
International Research Institute of Management Sciences
Moscow, 117312, Russia

The scattering of nonstationary electromagnetic fields can be studied using either the time- or frequency-domain approaches. The frequency-domain methods are more efficient in the analysis of scattered fields when various incident pulses are scattered by one and the same body. In this case, one can calculate the frequency scattering response (FSR) of the body only once and, then, apply the Fourier transform to the product of the FSR and the spectrum of each incident signal, which appears to be a good tool to study the effect of the shape of the incident pulse on the scattered field.

We investigate the nonstationary diffraction of a plane wave from a perfectly conducting circular cone covered with a homogeneous isotropic dielectric layer and embedded in a homogeneous isotropic medium using the method of frequency-domain integral equations for axially symmetric bodies and the fast Fourier transform. Since the calculation technique is well known, here, we focus on numerical results and analyze physical effects observed. We consider the case when the incident field is a video Gaussian pulse propagating along the axis of the cone towards the vertex and towards the base. Our results show that, similarly to the scattering of a rectangular video or radio pulse by a perfectly conducting cone, in the case of the coated cone, one can also separate the fields due to the first- and second-order diffraction from the edge of the metal base. However, when the incident wave travels towards the vertex, the presence of the dielectric layer causes certain changes in the backscattered field. First of all, the amplitude of the field primarily diffracted from the edge of the metal base increases. The reason is that, in the presence of a dielectric layer, a considerable portion of the energy of this field is transformed into the energy of the quasi-surface wave, which propagates in the layer on the base and is again scattered by the edge. With the increasing permittivity, this portion of energy increases initiating the pulses of higher-order diffraction. Our results show that the edge of the cone's base is the main scattering center of the structure. The intensity of the signal reflected from the side surface and rounded vertex of the cone is much lower than the intensity of the field scattered by the edge of the cones base.

When the incident video pulse propagates towards the cone's base, the response of the coated cone resembles the response of the metal one. In the responses of both cones, the fields scattered from the base and from the edge dominate.

Dual and Dual-Cross Synchronizations in Chaotic Systems

E. M. Shahverdiev, S. Sivaprakasam, and K. A. Shore
School of Informatics, University of Wales, Bangor
Wales, UK

Chaos control is being developed for a wide base of potential applications including secure communications, optimization of nonlinear system performance, modelling brain activity and pattern recognition phenomena. A particular focus of such work is on the development of secure optical communications systems based on control and synchronization of laser hyperchaos. For practical use of this approach, particular emphasis is being given to the use of chaotic external cavity semiconductor lasers which can generate hyperchaos. In a communications system use could be made of such laser configurations to form chaotic transmitters and receivers.

In this paper we investigate dual synchronization and dual-cross synchronization between the transmitter and receiver each one consisting of two master and slave systems. In dual synchronization we investigate synchronization between the master systems from the transmitter with corresponding slave systems in the receiver. In the case of dual-cross synchronization we synchronize the master and slave systems in the cross configuration.

We demonstrate our approach using the example of synchronization of chaotic external cavity laser diodes. In the synchronization scheme under consideration the joint error signal, which is the difference between the sum of the outputs from the master systems in the transmitter and the sum of outputs from the slave systems in the receiver, is fed to each slave laser. By use of error dynamics we derive existence conditions for both dual and dual-cross synchronization between the master lasers in the transmitter and slave lasers in the receiver.

We show that synchronization is achieved when there is equality in the contributions to the joint error signal by the master and slave lasers. We show that symmetry in contributions to the coupling signal between the transmitter and the receiver plays a crucial role in the synchronization phenomenon studied here. We establish that these results may be extended to the case of a larger number of receivers and transmitters where we study multi-synchronization, multi-cross synchronization and mixed synchronization. In the latter some of master lasers are synchronized with corresponding slave lasers (multi-synchronization) and the remainder of the master lasers were synchronized with slave lasers in multi-cross configuration.

These findings are considered to be of interest in chaotic multi-channel secure communication schemes where multi-synchronization will enable multiplexed message extraction.

Total Guided Light Reflection at End Facets of High Contrast Dielectric Multimode Slabs

M. Hammer and E. van Groesen
MESA^+ Research Institute, University of Twente
Enschede, 7522 DA , The Netherlands

At the end facet of a dielectric waveguide an incoming guided light wave is partly transmitted and partly reflected, where the power fraction that is actually transferred into backwards traveling guided fields depends strongly on the waveguide geometry and the refractive index contrast. Although this problem has been studied widely [1–3], mostly with the purpose of coupling loss minimization, i.e., aiming at a low reflectivity, apparently few investigations deal with configurations where the ended waveguide supports more than one mode per polarization. In this contribution we look at these multimode waveguide facets in some detail, with interest in structures that show a high reflectivity.

We consider the problem in two spatial dimensions by means of rigorous mode expansion simulations. Given the matrix of reflection coefficients for the guided modes, one can compute the maximum power reflectance for an incident mode superposition. While even for a substantial refractive index contrast across the facet the maximum reflected power for a single incoming mode is always moderate, the reflectivity may rise to a level that justifies the attribute *total*, if one considers specific superpositions of more than one guided mode. Roughly, such a configuration can be realized with two guided fields, if the following conditions are satisfied: First, the mode angles associated with both modes in the core material have to be larger than the critical angle for total reflectance at the facet. Second, the relative amplitude of the incoming fields is such that the superposition vanishes at the edges of the core at the facet, i.e., in the comer points in the figures below.

These observations allow at least a qualitative understanding of the pronounced resonance phenomena in some recently discussed microresonator devices [4, 5], where a rectangular segment of such a high contrast multimode waveguide serves as the cavity.

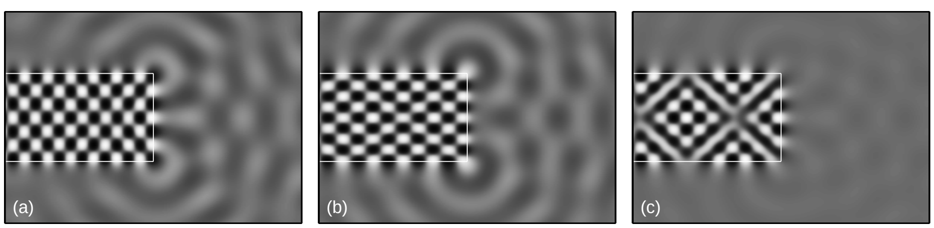

Figure 1: Snapshots of the electric field for TE light propagation across the end facet of a multimode waveguide. Incident fields are the 6th order mode (a), the 8th order mode (b), and a specific superposition of these two fields (c). Relative guided power fractions of 83%, 78%, and $> 99\%$ are reflected. Refractive indices: 3.2 (core) and 1.4 (cladding), waveguide thickness: 2.5 μm, vacuum wavelength: $1.55\,\mu$m.

REFERENCES

1. Sewell, P., M. Reed, T. M. Benson, and P. C. Kendall, "Full vector analysis of two-dimensional angled and coated optical waveguide facets," *IEEE Journal of Quantum Electronics*, Vol. 33, No. 12, 2311–2318, 1997.
2. Buus, J., M. C. Farries, D. J. Robbins, "Reflectivity of coated and tilted semiconductor facets," *IEEE Journal of Quantum Electronics*, Vol. 27, No. 6, 1837–1842, 1991.
3. Besse, P.-A., J.-S. Gu, and H. Melchior, "Reflectivity minimization of semiconductor laser amplifiers with coated and angled facets considering two-dimensional beam profiles," *IEEE Journal of Quantum Electronics*, Vol. 27, No. 6, 1830–1836, 1991.
4. Manolatou, C., M. J. Khan, S. Fan, P. R. Villeneuve, H. A. Haus, and J. D. Joannopoulos, "Coupling of modes analysis of resonant channel add-drop filters," *IEEE Journal of Quantum Electronics*, Vol. 35, No. 9, 1322–1331, 1999.
5. Lohmeyer, M., "Mode expansion modeling of rectangular integrated optical microresonators," Submitted to *Optical and Quantum Electronics*, 2001 (accepted).

Analysis of Frequency Selective Surfaces at the Millimeter Wave Band

G. R. Medeiros and A. G. d'Assunção
Department of Electrical Engineering
Federal University of Rio Grande do Norte
Natal, RN 59072-970, Brazil

A. L. P. S. Campos
Department of Electrical Engineering
Federal University of Paraíba
Campina Grande, PB 58109-970, Brazil

The analysis of frequency selective surfaces (FSS) with conducting patches on anisotropic dielectric substrates is developed for millimeter wave applications. Different types of patch geometries are considered, such as rectangular patches, thin dipoles and cross dipoles.

The analytical formulation is developed in the spectral domain, by using the immittance approach. The numerical analysis is completed by using Galerkin method with entire-domain basis functions.

In the analysis, the scattered fields of the FSS geometry are related to the surface induced currents on the conducting patches. After the formulation of the scattering problem, the numerical solution is obtained by using the moment method. The choice of the basis functions plays a very important role in the numerical efficiency of the numerical method, once they should provide a very good approximation to the real current distributions on the FSS analyzed structure.

Thereafter, the dyadic Green's function components are obtained in order to evaluate the basis functions unknown coefficients. To accomplish that, Galerkin method is used. Completing the formulation, the incident fields are determined through the incident potential, and as a consequence the FSS transmission and reflection characteristics are determined, as function of the resonant frequency and structural parameters.

The main objective of this work was to analyze FSS structures with conducting patch elements, such as thin dipoles, cross dipoles and rectangular patches, on anisotropic dielectric substrates, for high frequency applications. Therefore, numerical results for the FSS structure main characteristics were obtained in the millimeter wave band. Some of these FSS characteristics are the resonant frequency and scattering parameters, which were obtained as functions of the structural parameters. It should be pointed out that a very good agreement was observed between the results of this analysis and those available in the literature, for the particular case of FSS structures on isotropic layers. FSS structures on anisotropic substrates can be used in the development of reflecting antennas and bandpass radomes.

Image Reconstruction in Microwave Tomography

A. Danielsson and M. Persson
Department of Electromagnetics, Chalmers University of Technology
SE-412 96, Göteborg, Sweden

J. Howard
Plasma Research Laboratory
Research School of Physical Sciences & Engineering
Australian National University
Canberra A.C.T., 0200, Australia

Microwave tomography is a promising imaging method that could be used in several applications. Using this technique for mammography is an interesting application and a growing research field with great prospect. Compared to X-ray mammography there is a potential significant benefit in using microwaves in the diagnosis of breast cancer tumors due to the high contrast in the dielectric properties between tumor and surrounding tissue. In the future microwave tomography might work as a complement to X-ray mammography.

In this paper we show numerical simulations of the image reconstruction in 2D microwave tomography using an algorithm based on the FDTD-method. We use a FDTD formulation to solve the forward scattering problem and following the algorithm described by Gustafsson and He [1], the inverse problem is solved with the help of a functional. The functional is defined as the difference between the measured field and the field computed in the forward problem at the receiver locations. A dual FDTD-problem is solved backwards in time in order to compute the gradients of the functional describing how to update the dielectric properties of the reconstructed image and minimize the functional. This is an iterative process that is repeated until the functional has reached a desired minimum value in order to achieve the required accuracy in the reconstructed image.

The results obtained are compared and contrasted with the CP-MCT method described by Bertero et al. [2]. With this method the inverse imaging problem is solved using Radon transforms in a similar way as for X-ray computer tomography. The purpose of the comparison is to investigate if the FDTD-algorithm is useful and reliable in the process of reconstructing microwave tomography images.

REFERENCES

1. Gustafsson, M. and S. He, “An optimization approach to two-dimensional time domain electromagnetic inverse problems,” *Radio Science,* Vol. 35, 525–536, 2000.
2. Bertero, M., M. Miyakawa, P. Boccacci, F. Conte, K. Orikasa, and M. Furutani, “Image reconstruction in chirp-pulse microwave CT (CP MCT),” *IEEE Transactions on Biomedical Imaging,* Vol. 47, 690–699, 2000.

Electrodynamic Modeling of Wave Interaction in Strip-Slot Waveguiding Structures Containing Ferromagnetic Layers

G. S. Makeeva
Department of Radioengineering, State University of Penza, Penza, 440017
Krasnaya, 40, Russia

Mathematical simulation of distributed interaction of waves having different physical nature (electromagnetic waves (EMW), magnetostatic waves (MSW) or spin waves) in two-dimensional strip-slot structures containing magnetized ferromagnetic layers is made. Accurate modeling is based on the solution of non-uniform Maxwell's equations completed by Landau-Lifchits's equation of magnetization vector motion in a ferromagnetic.

The analytical electrodynamic approach for the investigation of resonance interaction between dynamic and magnetostatic modes in gyrotropic waveguiding structures is developed taking into account physical effects including the appearance of hybrid electromagnetic-spin waves at the condition of phase synchronism. The approach is elaborated using the solutions of equations of EMW excitation by equivalent magnetic currents (created by external fields of slow MSW propagated in magnetized ferromagnetic layers), these currents are represented as the sum of eigen magnetization waves of ferrite layers (or films) depending on the biasing magnetic field orientation.

The complex propagation constants frequency dependencies of EMW (basic and higher types) and MSW in shielded strip-slot structures containing tangent magnetized ferrite layers (or films) were calculated using numerical multimode autonomous blocks method. The spectrum of hybrid electromagnetic-spin waves as a result of the interaction between quasi-LM, quasi-LE modes (including volume or surface magnetostatic modes) in two-dimensional magnetized ferrite layers (or films) and quasi-T modes in strip lines or quasi-H modes in slot structures is analyzed . The interpretation of interaction between EMW and MSW as the intersection of partial wave dispersion surfaces in three-dimensional wave number space is proposed.

Is Lorentz Time-Space Transformation only an Approximate Calculation Method for Compressibility of Electromagnetic Field?

X. Yang
Airfoil Center, Northwest Polytechnic University
Xi'an, 710072, China

What is essential meaning of Lorenz transformation? If we compare the Maxwell equation and Euler Eq., due to the compressibility of Euler Eq., the contribution of substance derivative can not be ignored. Than we got a compressible potential Eq. (1). It can be written to small disturbance form Eq. (2).Search a transformation, which can transform Eq. (2) into incompressible form Eq. (3). This can be down by mathematical deducing software of Maple. We suppose all coefficients of transformation matrix are to be determined, these coefficients must have the character of space shorten as Lorenz Transformation, and must satisfy the transformation. With such restrictions can we derive much solution, and one is a pseudo Lorenz transformation as Eq. (4). $a^2\frac{\partial^2\phi}{\partial t^2} = (a^2-u^2)\frac{\partial^2\phi}{\partial x^2} + (a^2-v^2)\frac{\partial^2\phi}{\partial y^2} + (a^2-w^2)\frac{\partial^2\phi}{\partial z^2}$ (1)

$\frac{\partial^2\phi}{\partial t^2} - (1-\beta^2)\frac{\partial^2\phi}{\partial x^2} - \frac{\partial^2\phi}{\partial y^2} - \frac{\partial^2\phi}{\partial z^2} = 0;\ \beta = u/C$ (2) $\quad$ $\frac{\partial^2\phi}{\partial t^2} - \frac{\partial^2\phi}{\partial x^2} - \frac{\partial^2\phi}{\partial y^2} - \frac{\partial^2\phi}{\partial z^2} = 0;\ \beta = u/C$ (3)

$$\begin{bmatrix} x \\ y \\ z \\ t \end{bmatrix} = \begin{bmatrix} \frac{1}{\sqrt{1-\beta^2}} & & & \frac{-\beta}{\sqrt{1-\beta^2}} \\ & 1 & & \\ & & 1 & \\ \frac{\beta}{1-\beta^2} & & & \frac{1}{1-\beta^2} \end{bmatrix} \cdot \begin{bmatrix} x' \\ y' \\ z' \\ t' \end{bmatrix} \tag{4}$$

The relation of incompressible wave equation and compressible equation is through a space-time Variable transformation connected. Because the last incompressible wave equation is equivalent of electromagnet wave equation with time-space relation of spatial relativity, so the wave equation of compressible fluid is pretty nearly identically. The difference between Eq. (1) and the strictly Lorenz transformation is only in time dilations. Its time precision is order 1, and space precision is order 2. Compress flow is not covariant, but it is nearly covariant. In airfield, Lorentz time-space transformation, Is only a approximate calculation method for compressibility. So that we moral certainties get the conclusion: "Theory of special relativity is only a approximate calculation method of compressibility". And consider equal function fur Electromagnet Field.

How can we use aerodynamic method in construction of relation between mass and energy? Let we suppose Pressure is a measure or energy, the relation between mass and energy is same as the relation between density and Pressure: $dW/d\rho = C^2$, where W is energy, ρ is mass, let us express it by function $W = f(1/\rho)$ and use the assumption of Kammen and Qian, that is if $\beta = v/c \ll 1$, we can use a tangent to represent this curve: $dW/d(1/\rho) = f' = \text{constant}$. But $f' = dW/d(1/\rho) = -\rho^2 dW/d\ \rho = c\text{onstant}$. Combine these two Eq. $dW/d(1/\rho) = \rho^2C^2 = \rho_\infty^2 C_\infty^2 = \text{const.} = \rho_0^2 C_0^2$. Let us use low index "$_0$" to present status of stop, index "$_\infty$" to present a status without disturbance, as in infinite. The Euler equation is: $dW = -\rho V dV$. Divide two side of this Eq. by ρ, then integral from W_∞ to W can been written to

$\int_{v_\infty}^{v} v dv = -\int_{w_\infty}^{w} dw/\rho = -\int_{w_\infty}^{w} dw/d\rho * d\rho/\rho;$ and $\int_{w_\infty}^{w} dW/\rho = -c_\infty^2 * \rho_\infty^2 \int_{\rho_\infty}^{\rho} d\rho/\rho^3$ (5)

Consider the up given relation $C^2 * \rho^2$ is constant, so it can be extracted out of the integral and we write it in the form of $c_\infty^2\rho_\infty^2$ then the right of up equation change to $-\int_{w_\infty}^{w} dw/\rho = -\int_{w_\infty}^{w} c^2 * \rho^2 * d\rho/\rho^3$. Through integral: $v^2 - v_\infty^2 = -C_\infty^2 * \rho_\infty^2 * (1/\rho^2 - 1/\rho_\infty^2) = C^2 - C_\infty^2$. Further, in view of the speed in stand, $V_0 = 0$. Let me call the velocity in this stand status as C_0.

In same way get: $v^2 = C^2 - C_0^2$. Divide C^2 for both side of equation: $V^2/C^2 = 1 - (C_0/C)^2 = 1 - (\rho/\rho_0)^2$. Rewrite it, become the relations between energy and mass $\rho_0 = \rho/\sqrt{1-\beta^2}$; and $\beta = v/c$. It is same as Einstein gives. Here ρ is mass in standstill, ρ_0 is total mass, this is a measure of energy, but this is only a proximate conclusion used in situation $v/c \ll 1$.

Session 4Pc1

Randomly Rough Surface and Volume Scattering, Phenomena and Applications

High-Frequency Mode-Expansion Method for Electromagnetic Wave Scattering by Objects on Rough Surface

Y. Zhang
Volpe National Transportation Systems Center
Cambridge, MA 02142, U.S.A.

J. Pacheco, C. D. Moss, C. O. Ao, T. M. Grzegorczyk, and J. A. Kong
Research Laboratory of Electronics
Massachusetts Institute of Technology
Cambridge, MA 02139, U.S.A.

The recent attempt to understand the radar signatures of ships on rough ocean surfaces has attracted much attention in the study of electromagnetic wave scattering from the object-on-rough-surface geometry, particularly in the GHz band. In theory, the standard Method of Moments (MoM) technique can be used to solve for the unknown surface currents on the object and the rough surface; however, the dense discretization of the rough surface makes the conventional numerical approaches impractical because of the extremely large memory requirement. To overcome this limitation, several methods have been developed such as the Forward-Backward Method, the Banded Matrix Iterative Algorithm, the Fast Multipole Method, and the Fast Far Field Algorithm. Each of these methods relies on various grouping schemes and approximations for group interactions that reduce both the memory requirement and computation time. However, since these methods use point matching Sub-Domain Basis Functions (SDFs), which require the surface to be sampled with ten to twenty points per wavelength, they are still not practical for extremely large surfaces.

In this talk, a fast and memory efficient High-Frequency Mode-Expansion Method (HF-MEM) is introduced to calculate 2-D electromagnetic fields scattered by perfectly conducting objects (with sizes larger than 500λ) on a rough ocean surface. The ocean surface, with a size as large as $17,000\lambda$, is modeled as either a perfectly conducting or as a highly conducting (formulated by the impedance boundary condition) rough surface, which is described by the Pierson-Moskowitz power spectrum. By using Huygens' principle, the electric field integral equation (EFIE) is formulated to solve for the surface current distribution on both the rough ocean surface and the object. The surface current distribution is expanded as the sum of modes that represent the current components induced by both the incident wave and the waves scattered from neighboring patches. In the HF-MEM, the number of modes, which are physically the components of the induced current, is far fewer than the number of modes in the traditional Fourier expansion. In addition, in the high-frequency region (GHz), closed-form integrations can be used to reduce the impedance matrix fill time.

Using the HF-MEM, the bistatic radar cross section (RCS) of various objects, such as ship-like and low-observable objects, is calculated at 5 GHz for plane wave incidence. The simulation results of the HF-MEM are compared with those of the Physical Optics (PO) approximation and the Shooting-and-Bouncing-Ray (SBR) technique provided by the Xpatch simulation code. It is shown that HF-MEM predicts the bistatic Radar Cross-Section (RCS) of various objects above flat and rough surfaces with an accuracy comparable to SBR while incurring a computational cost that is at least 10 times lower than SBR.

Model of Radar Backscattering from Nonlinear Surface Waves

I. M. Fuks
ZelTex LLC and NOAA/ETL
Boulder, CO 80305-3328, U.S.A.

A. G. Voronovich
NOAA/ETL
Boulder, CO 80305-3328, U.S.A.

Microwave band radio wave backscattering by non-linear surface waves is considered within framework of two-scale model (F.G. Bass and I.M. Fuks, *Wave Scattering from Statistically Rough Surfaces*, Int. Ser. Nat. Phil., vol. 93, Oxford: Pergamon, 1979). Large scale (undulating) surface roughness is modeled by 2-D Stokes' or Gerstner's waves, which are the exact solutions of nonlinear hydrodynamics equations. The profile $z(x)$ of Gerstner's wave is given by trochoid's equation: $x = t/K - a \sin t$, $z = a \cos t$, where $K = 2\pi/\Lambda$ and Λ is a wavelength and a is a surface wave amplitude. The shape of these waves is characterized by the more sharpen crests and extended troughs as compared to the corresponding sinusoidal wave. For small values of steepness parameter aK the wave shape is very close to sinusoid, and for $aK = 1$ it takes the cycloid's form.

The zero-order field is calculated in the geometrical optics approximation (with shadowing effects taken into account) and by exact numerical solution of the appropriate diffraction problem. The diffuse scattering by small-scale ripples is considered in the first-order (Bragg) approximation. Spatial distribution of the specific backscattering cross section over the large scale wave profile is obtained for both polarizations of the incident wave. It is shown that the radar backscattering cross-section at horizontal polarization is modulated by the large scale wave slopes more effectively than at the vertical one. Backscattering cross-section averaged over period Λ of large-scale wave at moderate and near grazing angles is also more sensitive to the surface slope aK in the case of horizontal polarization

The Doppler frequency spectra of radar signal are not symmetrical and have the opposite skewness for *HH* and *VV* polarizations. The mean Doppler frequency shifts strongly depend on the incidence angle: for grazing angles they are approaching the limit determined by the value of orbital velocity of liquid particles plus phase velocity of small ripples and tend to zero at steep incidence. At moderate angles the mean Doppler shift for horizontal polarization exceeds essentially that one for vertical polarization, and the difference between them increases strongly with steepness parameter aK increasing. The exact account for diffraction effects reduces this difference as compared to the Kirchhoff approximation. The cause and qualitative explanation of this effect is discussed.

Random Plane Waves in 2-Dimensional Homogeneous and Isotropic Random Medium

H. Ogura
Kinki University
Uchita, Wakayama 649-6493, Japan

In 1D random medium a plane wave is shown to exist by virtue of the translational invariance due to homogeneity [1], and the solution has all exponential factor indicating the presence of localization [2]. In 2D case where the random medium is homogeneous and isotropic we can introduce both plane wave and cylindrical wave corresponding to the translational and the rotational invariances, respectively. The cylindrical mode due to the rotational invariance is discussed in [3, 4]. In this paper we show that the random plane wave of the following form

$$\psi(\boldsymbol{r}) = \exp\left[\mathrm{i}\boldsymbol{r}\cdot\boldsymbol{r} + \boldsymbol{q}\cdot\boldsymbol{r} + \int_0^r \boldsymbol{\nabla}\Phi(\boldsymbol{k})\cdot \mathrm{d}\boldsymbol{k}\right] u(\boldsymbol{r}); \quad \boldsymbol{r}^2 = k^2$$

due to the translational invariance can exist, where $\boldsymbol{q}$ denotes a complex vector, and $\Phi(\boldsymbol{r})$ and $u(\boldsymbol{r})$ are homogeneous random fields to be determined. Approximate solutions for those quantities are obtained by means of the stochastic functional approach in a manner similar to [1]. In particular, the exponential index $q = \alpha + \mathrm{i}\beta$, the amplitude of $\boldsymbol{q}$, is obtained in terms of the spectrum of the random medium, which is assumed to be a random grating with a narrowband spectrum centered at $2k$ twice as much as the unperturbed wave number k, and q is concretely calculated for a narrowband Gaussian spectrum. The same exponential factor is obtained for the random cylindrical wave [4]. The exponential factor, representing the stochastic decay or grow of the amplitude in the propagating direction, is closely related to the localized nature of random wave field although such exponentially increasing plane wave is not a physical solution by itself. Once the plane wave solutions as well as the evanecsent waves are obtained in the stochastic functional representation based on the translational and rotational invariances we will be able to construct a cylindrical wave by integration in much the same way as the Sommerfeld representation of cylindrical wave in the free space.

REFERENCES

1. Ogura, H., “Theory of waves in a homogeneous random medium,” *Physical Review A*, Vol. 11, No. 3, 942–956, 1975.
2. Ogura, H., M. Kitano, N. Takahashi, and T. Kawanishi, “Stochastic theory of localized waves in random media,” *Proceedings, URSI Int. Symp. on EMT*, 81–83, Sydney, 1992.
3. Ogura, H., “Stochastic theory of wave localization in 2-dimensional random media,” *Proceedings, URSI Int. Symp. on EMT, Victoria*, 573–576, 2001.
4. Ogura, H., Asymptotic form for random cylindrical waves and localization in 2-dimensional random medium,” *Proceedings, PIERS 2002*, Cambridge, 2002.

The Design of One-Dimensional Random Surfaces with Specified Scattering Properties

E. R. Méndez
División de Física Aplicada, Centro de Investigacion Científica
y de Educación Superior de Ensenada
Ensenada, B.C. 22800 , México

T. A. Leskova, A. A. Maradudin, and J. Muñoz-Lopez
Department of Physics and Astronomy and Institute for Surface and Interface Science, University of California, Irvine
Irvine, California 92697 , U.S.A.

We describe a method for designing a one-dimensional, random, perfectly conducting surface which, when illuminated normally by an s-polarized electromagnetic wave of frequency ω , scatters it with a prescribed distribution of intensity. It is based on the geometrical optics limit of the Kirchhoff approximation, which yields the mean differential reflection coefficient in the form

$$\left\langle \frac{\partial R}{\partial \theta_s} \right\rangle = \frac{1}{L_1} \frac{\omega}{2\pi c} \int_{-\infty}^{\infty} d\,u \int_{-\infty}^{\infty} dx_1 \exp(iqu) \langle \exp iau\zeta'(x_1) \rangle. \tag{1}$$

In this expression the angle brackets denote an average over the ensemble of realizations of the surface profile function $\zeta(x_1)$, L_1 is the length of the x_1-axis covered by the random surface, the wave number q is given in terms of the scattering angle θ_s by $q = (\omega/c) \sin \theta_s$, and $a = (\omega/c)(1 + \cos \theta_s)$. The surface profile function $\zeta(x_1)$ is given by

$$\zeta(x_1) = a_n x_1 + b_n \qquad nb < x_1 < (n + 1)b, n = 0, \pm 1, \pm 2, \dots \tag{2}$$

where the $\{a_n\}$ are independent random deviates, b is a characteristic length, and the $\{b_n\}$ are determined in such a way as to make $\zeta(x_1)$ a continuous function of x_1,

$$\begin{aligned} b_n &= b_0 + (a_1 + a_2 + \cdots + a_{n-1} - a_n)b \quad n \geq 1 && (3a) \\ b_{-n} &= b_0 - (a_{-1} + a_{-2} + \cdots + a_{-(n-1)} - (n-1)a_{-n})b \quad n \geq 1. && (3b) \end{aligned}$$

We seek the probability density function (pdf) of a_n, $f(\gamma) = \langle \delta(\gamma - a_n) \rangle$ such that the resulting surface profile function yields a mean differential reflection coefficient of a prescribed form. The result is

$$f(\gamma) = \frac{2}{1 + \gamma^2} \left\langle \frac{\partial R}{\partial \theta_s} \right\rangle (-\gamma), \tag{3}$$

where $\gamma = \tan(\theta_s/2)$. A long sequence of $\{a_n\}$ is determined from this pdf by the rejection method, and a realization of the random surface is then calculated from Eqs. (2) and (3). This method is applied to the design of a surface that scatters light uniformly within the region $-\theta_m < \theta_s < \theta_m$ and produces no scattering outside this region, a surface that acts as a Lambertian diffuser, and a surface that suppresses single-scattering processes in the interval $-\theta_m < \theta_s < \theta_m$. It is tested by computer simulations, and a procedure for fabricating such surfaces on photoresist is described.

Backscattering Enhancement: Volume Scattering in the Presence of Randomly Rough Surfaces

A. Soubret†**, G. Berginc**
Thalès Optronique
Guyancourt, France

C. Bourrely
Centre de Physique Théorique
Marseille, France

We know that backscattering enhancement occurs in the single volume scattering in a presence of a reflective boundary. The reflective surface can be smooth or rough. But few works deals with backscattering of electromagnetic waves when volume and surface disorder are considered. In this paper we present a general formalism based on the rigorous Dyson and Bethe-Salpeter equations, which take into account the scattering by the surface and the volume. We obtain an approximate expression for the coherent part of the scattered intensity under the Small-Slope approximation (SSA) of Voronovich or the Small Perturbation Method for the surfaces and the Quasi-Crystalline with Coherent Potential for the random volume. We study numerically the differential reflection coefficient for various root mean square heights, correlation lengths and densities of the volume disorder. We give an approximate expression for the diffuse intensity under the diffusion approximation. We solve numerically this equation and study how the backscattering enhancement can be produced by the interaction of the surface and the volume disorder.

† also with Centre de Physique Théorique

Non-Local Small-Slope Approximation Technique TE and TM Solutions

G. Berginc
Thalès Optronique
Guyancourt, 78283, France

Y. Béniguel
IEEA
Courbevoie, 92400, France

The vector field scattered by a rough surface is calculated by the Non Local Small Slope Approximation (NLSSA) technique [1]. The non-local small-slope approximation is a modification of the small-slope approximation for situations in which multiple scattering from points situated each other at significant distance becomes important. In this paper we will develop the technique for TE and TM wave scattering by dielectric and perfectly conducting two-dimensional surfaces. The NLSSA solution leads to expressions containing singularities for both cases of TE and TM polarization components, the TM case singularity being one order higher than the singularity corresponding to the TE case. This singularity can easily be removed for the TE case. For the TM case, far from grazing angles a similar solution is derived. For grazing angles the solution must be modified introducing statistical properties of the slope of the irregularities in order to deal with the singularity. The modified solutions for TE and TM cases will be presented at grazing angles.

With this technique, we study the back-scattering enhancement for different values of slope and we explore the validity domain of the NLSSA method for larger roughness scales. In the second part of the paper, we present results of numerical calculations of polarized waves from dielectric and metallic two-dimensional surfaces at low-grazing angles and we discuss the grazing behavior of the scattered wave for different values of slope. With the NLSSA method, we can analyze phenomena produced by roughness: for example the Brewster-angle behavior (dip in the reflection coefficient) at a specific grazing incidence angle for VV polarization over perfect conductors.

REFERENCES

1. A. G. Voronovitch, “Non-local small slope approximation for wave scattering from rough surfaces,” *Waves in Random Media*, April 1996.

Disordered Linear and Nonlinear Photonic Crystal

G. Guida and A. Priou
Groupe d'Electromagnétisme Appliqué (G.E.A.)
Université Paris X
Ville d'Avray, 92410, France

Photonic crystals [1] have recently triggered plenty of applications specially on opto-electronic devices but also on antennas control. These fascinating new materials are able to control both polarization and diffraction phenomena and are the analogue to semiconductor devices for electronics. As in Solid State Physics, strongly disordered materials (analogue to amorphous materials) can present serious advantages for the fabrication processes.

We have recently studied disordered 2D metallic photonic crystals [2, 3] for dissociated variations of three generic disturbances (position, size of the elementary pattern and inclination) and proved both theoretically and experimentally that these passive devices present a very tolerant band gap behavior.

We will present in the conference the study of a random volume (scattering volume) full with dielectric or metallic rods randomly positioned but with an averaged periodicity (random material close to a perfect photonic crystal in average). For the dielectric case, we study non linear response of the matrix appearing for a strong intensity of an incident light.

REFERENCES

1. *Journal of the Optical Society of America B*, *Special Issue on Photonic Crystals*, vol.10, 1993; *Journal of Modern Optics*, vol.41, 1994; *Photonic Band Gap Materials*, edited by C.M. Soukoulis, Kluwer Academic Publishers, 1996.
2. G. Guida, *Optics Communications*, vol.156, pp.294-296, 1998.
3. G. Guida, T. Brillat, A. Ammouche, F. Gadot, A. de Lustrac, A. Priou, *Journal of Applied Physics*, vol.88, no.8, pp.4491-7, 2000.

Shadowing Function from One-Dimensional Rough Surface with Single Reflection

C. Bourlier
Ecole polytechnique de l'Université de Nantes
Nantes, France

G. Berginc
THALES-CSF Optronique
Guyancourt, France

Conventional theories of the scattering of electromagnetic radiation from random rough surfaces [1]-[2], assume that every point of the surface contributes to the scattered wave. This assumption neglects the shadowing function, an effect that may be expected to be important at large angles of incidence. Sancer [3] showed with the geometric optics approximation that the scattering coefficient with shadow is obtained from the unshadowed scattering coefficient multiplied by the average shadowing function over the surface heights and slopes performed from either the Wagner [4] or Smith formulations [5]-[6]. To study this assumption, Bourlier et al. [7]-[9] investigated the statistical shadowing function, which depends on the surface heights and slopes in the derivation of the scattering coefficient calculated from the Kirchhoff approach.

This paper presents the Ricciardi-Sato, as well as, the Wagner and Smith formulations for calculating the monostatic and bistatic statistical shadowing functions from one-dimensional rough stationary surface, which are valid for an uncorrelated Gaussian process with an infinite surface length. The inclusion of a finite surface length is needed to extend the single-reflection shadowing function to the more general multiple-reflection case. Comparisons of these shadowing functions with exact numerical solution for the shadowing (using surfaces with Gaussian and Lorentzian auto-correlation functions for a Gaussian process) shows that the Smith formulation without correlation is a good approximation, and that including correlation only weakly improves the model.

REFERENCES

1. P. Beckmann and A. Spizzichino, 1963, "The Scattering of Electromagnetic Waves from Rough Surfaces Part I. Theory", (London, Pergamon Press).
2. F.T. Ulaby, R.K. Moore, A.K. Fung, 1982, *Microwave remote sensing*, Vol. II (Reading, MA: Addison-Wesley).
3. M. I. Sancer, 1969, Shadow-Corrected Electromagnetic Scattering from a Randomly Rough Surface, *IEEE Trans. Ant. Prop*. 17, 577–585.
4. R. J. Wagner, 1986, Shadowing of Randomly Rough Surfaces, *J. Opt. Soc. Am*. 41(1), 138–147.
5. B. G. Smith, 1967, Lunar Surface Roughness, Shadowing and Thermal Emission, *J. Geophysical Research*, 72(16), 4059–4067.
6. B. G. Smith, 1967, Geometrical Shadowing of a Random Rough Surface, *IEEE Trans. Ant. Prop.*, 15, 668–671.
7. C. Bourlier, G. Berginc, J. Saillard, 2001, Bistatic scattering coefficient from one- and two- dimensional random surfaces using the stationary phase and scalar approximation with shadowing effect -comparisons with experiments and application to the sea surface, *Waves in Random Media*, 2(1), 91–118.
8. C. Bourlier, G. Berginc, J. Saillard, 2001, Theoretical study of the Kirchhoff integral from two-dimensional randomly rough surface with shadowing effect - application on the backscattering coefficient for a perfectly conducting surface, *Waves in Random Media*, 2(1), 119–147.
9. C. Bourlier, J. Saillard, G. Berginc, 2000, The shadowing function, *PIER (Progress In Electromagnetic Research)*, Chief Editor J.A Kong, EMW, 27, 226–287.

Importance of Shadowing and Multiple Reflection in Polarization Emission

K. I. Hopcraft, J. C. Flitton, and E. Jakeman†
Theoretical Mechanics Division, School of Mathematical Sciences, University of Nottingham
Nottingham, NG7 2RD, UK

P. C. Y. Chang, and J. G. Walker
School of Electrical and Electronic Engineering, University of Nottingham
Nottingham, NG7 2RD, UK

Polarization characteristics of thermal radiation emitted from corrugated and random surfaces are investigated within the geometrical optics approximation. Analytical results are presented for photons that are emitted without subsequent reflections from surfaces having sawtooth corrugations with a variety of slope distributions for the facets comprising the surface. These analytical results are used to validate a Monte-Carlo simulation that is designed to determine and quantify the effects of multiple reflections from surface structures and, in addition, to treat two-dimensional semi-structured and randomly rough surfaces. The Monte-Carlo code evolves the Stokes vector $\boldsymbol{S}=(I,Q,U,V)$ of photons, or rays, as they are emitted, and then multiply reflect from surface features before being detected. The degree of polarization (DOP):

$$\mathrm{DOP} = \frac{Q}{I} \tag{1}$$

is calculated and it is found that the absolute magnitude of this quantity decreases with increasing RMS slope of the surface features. The degree of polarization is further reduced when multiple reflection effects are included, which incorporate shadowing of parts of the surface from others. For structured surfaces, one-dimensional corrugated, and two-dimensional regular pyramidal surfaces reveal similar features in the angular DOP spectrum that are characteristic of the value of the RMS slope. However these features become progressively less significant for sufficiently rough surfaces. This result suggests that the RMS slope is the important parameter when evaluating the degree of emission polarization irrespective of the distribution of the slopes of the facets comprising the surfaces. This observation leads to the possibility for surfaces to be designed or manipulated to have specific emission properties.

† also with the University of Nottingham.

Shadowing Function from Two-Dimensional Rough Surfaces with an Uncorrelated Arbitrary Surface Slope Distribution

C. Bourlier
Ecole polytechnique de l'Université de Nantes
Nantes, France

G. Berginc
THALES-CSF Optronique
Guyancourt, France

Shadowing function of random surfaces is originally introduced as a correction to the unshadowed scattering coefficient performed from analytical formulations as the Kirchhoff approach. The scattering analytical theories and the shadowing function (see Wagner [1] and Smith [2]-[3]) are developed with a slope and height joint Gaussian process. Gaussian process is probably adequate for the ocean, but for other surfaces such as sea ice, the density function of the surface roughness is not Gaussian [4]. Therefore it is necessary to extend the shadowing theory to two-dimensional rough surface, for any density function, in order to study its effect; such is the purpose of this paper.

In [5]-[6], the last assumption has been investigated for any one-dimensional surface height autocorrelation function, and it is proved that the discrepancy between the correlated and uncorrelated results is small. From Browns work [7] with a one-dimensional surface, Bourlier et al. [6] have expressed the Smith and Wagner monostatic shadowing functions, averaged over the surface slopes and heights, whatever the slope and height pdfs assumed to be uncorrelated.

In this paper, the monostatic and bistatic shadowing functions are performed for Gaussian, Laplacian and exponential slope probability density functions. With the method presented in [6], the one-dimensional monostatic shadowing function is also compared with the exact solution. It is obtained by generating the slope-height surfaces. The Gaussian and Laplacian slope pdfs are treated with a Gaussian surface height. The analytical results are extended to a one-dimensional bistatic configuration, and the case of a two-dimensional surface is investigated with a Gaussian and Laplacian surface slope pdfs. The last point is very relevant, since the classical shadowing functions of Smith and Wagner are assumed to be one-dimensional or isotropic.

REFERENCES

1. R. J. Wagner, 1986, Shadowing of Randomly Rough Surfaces, *J. Opt. Soc. Am*. 41(1) 138–147.
2. B. G. Smith, 1967, Lunar Surface Roughness, Shadowing and Thermal Emission, *J. Geophysical Research* 72(16) 4059–4067.
3. B. G. Smith, 1967, Geometrical Shadowing of a Random Rough Surface, *IEEE Trans. Ant. Prop*. 15 668–671.
4. G. T. Ruck, D. E. Barrick, W. D. Stuart, and C. K. Krichbaum, 1970, *Radar Cross section*, Vol. 2, Plenum Press, New York, London.
5. C. Bourlier, J. Saillard, G. Berginc, 2000, The shadowing function, *PIER (Progress In Electromagnetic Research)*, Chief Ed. J.A Kong, EMW, 27 226–287.
6. C. Bourlier, J. Saillard, G. Berginc, 2000, Effect of correlation between shadowing and shadowed points on the Wagner and Smith monostatic one-dimensional shadowing functions, *IEEE Trans. Ant. Prop*. 48(3) 437–446.
7. G. S. Brown, 1980, Shadowing by Non-Gaussian Random surfaces, *IEEE Trans. Ant. Prop*. 28(6) 788–790.

Polarization Imaging of Objects Using Ambient Illumination

K. I. Hopcraft[†], P. C. Y. Chang[*], J. C. Flitton[†], E. Jakeman[*†], and J. G. Walker[*]

[†]Theoretical Mechanics Division, School of Mathematical Sciences

[*]School of Electrical and Electronic Engineering

University of Nottingham

Nottingham, NG7 2RD, UK

We present results that exploit the polarization characteristics of multiply scattered incoherent radiation for the purpose of detecting objects that are immersed in a particulate medium. The work is motivated by the requirement to improve visibility depth in turbid environments such as the sea. Previous work [1] has shown that active illumination of objects with polarized light can discriminate against the obscuring particulates and extend the visibility depth. Here the technique is varied to consider passive or ambient illumination, such as that deriving from sunlight or a cloudy sky. The calculations use a Monte-Carlo simulation to consider the multiple scattering of unpolarized, incoherent light rays that first pass through the sea surface, then scatter from the particles comprising the medium and object before being imaged. The initially unpolarized light is partially polarized by its passage through the air-sea interface, so that each ray has a Stokes vector $\mathbf{S}=(I,Q,U,V)$ with nonzero components Q and U. Subsequent single scattering by small and large particles tends to enhance a vestige of this polarization state. By contrast, the object, which is treated as a depolarising Lambertian scatterer, erases all polarization memory of the illuminating light. Calculating the degree of polarisation

$$\frac{(Q^2+U^2+V^2)^{1/2}}{I} \tag{1}$$

of the image serves to discriminate between the ambient particles and the object. The sensitivity of the method to the turbidity, and therefore the degree of multiple scattering, of the ambient medium is investigated by changing the effective mean free scattering path length. Also the effect of changing the depth of the object is explored.

REFERENCES

1. K. Turpin, J.G. Walker, P.C.Y. Chang, K.I. Hopcraft, E. Jakeman, ‘Influence of particle size in active polarization imaging in scattering media’, *Opt. Comm.* **168**, 325-35,(1999).

Scattering by a Two-Dimensional Rough Surface with Topographic Damages

M. Bardon and G. Berginc
Thales-Optronique
Guyancourt, France

P. Bonnemason
CEA-CESTA
Le Barp, France

B. Chevalier
Thales-Optronique
Guyancourt, France

This paper deals with the modeling (3D) of the scattering of an electromagnetic wave by a damaged rough surface.

Two types of surface are studied. On the one hand, a scratched metallic rough surface with randomly distributed scratches. On the other, a metallic rough surface contaminated with randomly distributed dielectric deposits.

A statistic modeling of the damaged surface allows us to obtain some analytic results. The analytic models taken into account are the Physical Optics (PO) approximation and the Small Perturbation Method (SPM). Two numerical models are then worked out from two hybrid methods. The first model couples the small perturbation method with the method of moments (SPM/MoM). The second model couples the physical optics approximation with the method of moments (PO/MoM). Calculation of the rough surface part is worked out by the analytical methods (PO or SPM) and calculation of the distribution of scratches or dielectric contaminants is performed with the method of moments (MoM). A comparison of the scattering diagrams obtained with the hybrid methods and the scattering diagrams resulting from the analytical methods is presented for the damaged surfaces. The SPM yields very good results consistent with those obtained with the hybrid method (SPM/MoM), unlike the PO, which proves to be totally inconsistent with the hybrid method (PO/MoM) on these kinds of surface.

The Mueller matrix calculation (3D) of these surfaces is then presented. It clearly shows some polarization effects due to the scratches. This matrix clearly reveals the presence of some damages on a nanometric scale. An experimental validation is then performed using a Mueller matrix measure bench specifically designed for this research.

The modeling of the scattering by most of surfaces of the environment is thus made possible, in a relatively short computational time, thanks to the hybrid methods.

Session 4Pc2

Medical Applications and Biological Effects

An Efficient and Accurate Technique for Computations of Electromagnetic Characteristics of the Model Human Heart

L. Knisevskaja
Microwave Laboratory, Semiconductor Physics Institute
Vilnius, 2600, Lithuania

K.-F. Berggren
Department of Physics and Measurement Technology, Linköping University
Linköping, S-58183, Sweden

V. Engelson
Department Computer and Information Science, Linköping University
Linköping, S-58183, Sweden

In the present environment people are exposed to electromagnetic fields (EM) from many different kind of radiation sources over a wide range of frequencies. The biological effects of exposure to electromagnetic radiation have been a topic of scientific research over the last years. The physical basis for microwave interaction with human organs brings together the properties of both the EM field and the biologic medium within its path of propagation. The microwave parameters of biosystems contain the high-contrast information needed for dosimetric imaging.

In this paper we report on computations of the scattered EM field by a model human heart. The solution of the Maxwell equations is constructed as a superposition of hybrid quasi-E and quasi-H waves. We separate the solution of equations from satisfying the boundary conditions and at the first step we find the solution of the differential equations having a δ-function on their right side. This fundamental solution is then used in the integral representation of the components of the EM field to decide a diffraction problem for an arbitrarily shaped three dimensional body-scatterer, which can be characterized by a set of the complex dielectric permittivities. Integral representations automatically satisfy the differential equations but contain unknown density functions to be found from the boundary conditions. After the substitution of the field component expressions into the boundary conditions, a system of the Singular Integral Equations (SIE) is obtained. A solution of the system is computed numerically. The solution of the differential equations, obtained by SIE method, is rigorous. False roots do not occur when applying the SIE method. The boundary conditions are to be satisfied only on the really existing surfaces dividing different materials. For verification of the SIE algorithm we compared our computational results with experimental data for a metal disc. Our computations are in good agreement with these data.

This presentation reports on the computed dependence of the back scattering cross-section of the model human heart for a vertical-polarized plane wave, incident on the wide top part of the model heart at several complex dielectric permittivities for myocardic as well as for the blood in the auricles and ventricles. All surfaces of the model heart are defined in input file as a list of x, y, z coordinates of a triangular mesh on the heart surfaces and normal unit vectors $\vec{n}$ at the every triangle. The external myocardic surface consisted of 42 triangles and the internal surfaces were constructed from 192 triangles.

Representativeness of 24 h and 48 h Measurements of the Magnetic Field Exposure for Epidemiological Purposes and the Ratio Between the Dynamic and Static Exposure for People Living below High-Voltage Transmission Lines

G. Decat
IMS - Integral Environmental Studies
Mol, B-2400, Belgium

The results of recent epidemiological studies (Ahlbom, 2000, Greenland, 2000, Shulz 2001) suggest an association between the exposure to ELF (Extremely Low Frequency) electromagnetic fields, more specifically the 50 Hz magnetic field, from high-voltage transmission lines and childhood leukaemia. Enhanced relative risks for such an association where found at stationary home cut-off point of 0.2 μT (Shulz et al, 2001), 0.3 μT (Greenland et al., 2000) and 0,4 μT (Ahlbom et al, 2000) respectively. The determination of the 0.2 μT cut-off point observed by Shulz was based 24 h measurements while the cut-off points of both other studies were based on 'pooled data analyses' by which the magnetic field strengths were estimated by means of the wire code method, 24 h and 48 h measurements respectively. However, one of the main gaps in the ELF-epidemiology is on the one hand that there are doubts about the goodness of fit of the time integrated sample statistics (arithmetic and geometric mean, median) obtained by 24 h and even 48 h measurements for estimating the real stationary home exposure. On the other hand the estimated or measured "stationary home magnetic field exposure" doesn't fit with the real dynamic exposure of individuals living near to power lines. Since man is a dynamic human being with multiple activities, he stays alternately in ELF-rich and ELF-poor environments so that there may exist a discrepancy between the stationary home and the individual dynamic magnetic field exposure. By simultaneous one-week measurements of the static home and the dynamic personal 50 Hz magnetic fields and a data analysis by means of a 'relative exposure index' we will gain more insight in the ratio between the dynamic and stationary exposure

Comparisons of the time integrated mean exposures obtained by differentiating 24 h and 48 h from the 14 days measurements show consistency between the 24 h and 48 h measurements. A more inconsistent pattern was observed when the time integrated exposure of both measurement times are compared with the one of the measurement for 14 days.

Up to now, our results on people living under high voltage transmission lines suggest that the overall dynamic exposure may vary between 55% to about 80% from the stationary home exposure.

Model of Electromagnetic Field Distribution Calculations in the Near-Field of Microwave Antennas

R. Kubacki
Military Institute of Hygiene and Epidemiology, Department of Microwave Safety
Warsaw, 01-755, Poland

M. Wnuk
Military University of Technology, Electronics Faculty
Warsaw, 00-908, Poland

J. Kieliszek
Military Institute of Hygiene and Epidemiology, Department of Microwave Safety
Warsaw, 01-755, Poland

W. Kolosowski
Military University of Technology, Electronics Faculty
Warsaw, 00-908, Poland

Microwave antennas, like mobile phone base station antennas or radar antennas, have become popular in our environment. The increasing concerns about possible health hazards of people exposed to microwaves and the safety limits established by national standards require accurate assessment of electromagnetic field distribution around antennas.

During last years we have been flooded by different computational methods of electromagnetic (EM) field distribution around antennas. Mostly, the proposed methods of evaluations of EM field distribution have been based on methods of moments (MoM), from which the simplest one — FDTD has been especially favored. Nevertheless, there are some disadvantages of MoM, used in the near-field. They take into consideration some simplifications, which cannot be fulfilled in the case of the near-field condition. Another disadvantage is that MoM are not recommended for large antennas (e.g. radar antennas), comparing to the wavelength. In the case of large antennas there are troubles with so complex basis functions and finally, this could lead to the wrong solution.

The aim of this study was to design the numerical model of the EM field distribution in the vicinity (near-field) of microwave antennas. The calculations have been based on vector potentials, which were adapted to the near-field condition. The current distribution on the antenna surface was defined using modified synthesis method of an antenna pattern. The final formulas for E and H will be presented.

While calculating the EM field it is also very important to consider the correct value of radiation reflected from the ground. This reflected radiation can reach the value comparable with the value of direct radiation and the resultant value of EM field in the point of calculating must be considered as a vector sum of complex values. In addition, the values of electrical parameters of reflecting ground as well as the topography of the ground are also important. Nevertheless, up to now all calculations, presented in the literature, have been derived only for the case when ground surface is perfectly horizontal (perpendicular to antenna mounting). Unfortunately, such case does not occur in practice.

The calculations take into account the electrical parameters and the shape of the ground from vectorised map of the desired area. Therefore, the proposed model of calculations include the radiation reflected from the real ground.

The Safety of Using Mobile Phone under Thunder Conditions

C. N. Pai, J. H. Chou, and L. S. Chao
Department of Engineering Science
National Cheng Kung University
Tainan, Taiwan

Recently, with the increasing use of mobile phones, the relative problems caused have been discussed intensely, especially EM effect related to human safety. In this regard, Taiwan has a special concern. Taiwan is an island surrounded by seas and oceans. Thunder storms often occur during summer time and can cause damages. There are news reports suggest that persons using mobile phones might be struck by thunders. But the truth of these reports is still open. In this paper, a numerical simulation is used to address this issue.

A finite element commercial code, ANSYS, is used in this study. A human body, a mobile phone, especially its antenna, and a thunder pulse with needed parameters were modeled. After putting the mobile phone in the GSM900 and GSM1800 system respectively, the electromagnetic fields are then analyzed.

The results indicate that a mobile phone indeed can attract the thunder pulse. There are two reasons for this phenomenon. First, the thunder pulse will induce electromagnetic intensity on the body. Second, due to the antenna effect, it will make the mobile phone to produce an extra EM field to increase the EM field that is originally on the body. In other words, due to the good conductivity of the antenna of the mobile phone, coupling between the human body and the mobile phone can form an easier path for the thunder pulse. Comparing to the one without a mobile phone, the intensity of EM field can increase up to tens of times. This could cause a great threat to users safety and deserves more attention on the methods to avoid it.

High Image Quality with Low Radiation Dose in Diagnostic Radiology

A. Erdamar
Department of Biomedical Engineering, Baskent University
Ankara, 06530, Turkey

Main reason for higher society dose is Diagnosis Radiology studies. The image quality of radiographs helps the doctors for making decision. If the image quality is not sufficient for the diagnose, doctors want '*retake*', so the patient dose will increase unnecessarily. In this study, the patient dose differences caused by different system performance, various film/screen combinations and film-processing procedures are investigated. First of all, system performance were determined with quality control and acceptance testing (according to NEMA, AAPM, IPEM *etc.* standard) and skin doses were measured for every clinic study. So that irregular patient distribution created by different systems (or different dose output) is identified. According to these results, a new and a regular patient distribution among rooms is suggested. Nevertheless, the film-processing procedure has investigated during the studies and the increase of the patient dose due to changing some parameters outside the acceptance limits (developer temperature, irregular replenishment etc.) are determined. Finally, all dose output has measured with PEP (Patient Equivalent Phantom) and Knee equivalent phantom according to new suggested patient distribution.

As a result, the dose-effective organization procedure is developed for Ankara University Medicine Faculty Radiology Department.

Distribution of the Reflected Microwave Field Near the Boundary Surfaces of the Model Heart

L. Knisevskaja
Microwave Laboratory, Semiconductor Physics Institute
Vilnius, 2600, Lithuania

K.-F. Berggren
Department of Physics and Measurement Technology, Linköping University
Linköping, S-58183, Sweden

V. Engelson
Department Computer and Information Science, Linköping University
Linköping, S-58183, Sweden

Microwaves finds their way into medical noninvasive diagnosis as well as in therapeutic applications. The diffraction and absorption of microwaves are governed by the complex permittivity properties and geometry of biologic organs. There are especially important features of microwaves. The microwave frequency fields may be referred to as nonionizing electromagnetic fields. Microwave radiation penetrates some 30-100 times deeper than infrared does. These circumstances stimulate the development of Microwave Thermography, Tomography, Holography as well as Methods of Microwave Imaging for Dosimetric Applications and so on.

An electrodynamically accurate solution of the Maxwell equations for a three-dimensional dielectric model biological heart in the free space is proposed. For this purpose we use a diffraction approach. The model heart is illuminated by an incident vertically or horizontally polarized plane microwave from an external source. We determine the electric field distribution in regions near boundary surfaces of the model which depends on the polar and azimutal angles of the incidence microwave at a frequency range from 1 to 10 GHz and electrophysical parameters of some materials of the model heart. We assume in these computations that the permittivities $\dot{\varepsilon}_i = \varepsilon_i' + \varepsilon_i''$ of the relevant heart tissue and the environment are scalars. Inside the model heart there are two atria with valves bounded by surface S_1, S_2. The muscle region is defined by the permittivity $\dot{\varepsilon}_1$. In our theoretical approximation the auricles and ventricles are assumed to be always filled with blood with permittivity $\dot{\varepsilon}_2$. The magnitudes of the real and imaginary parts of the myocardial dielectric permittivity as well as for the blood in the auricles and ventricles are taken from literature. The algorithm was tested by comparision with published data for body coordinates. Good agreement is for our computations.

A Hybrid Technique for Determining the Conductivity of Tissue Layer Embedded in Multilayer Biological Structure

K. Huang
Dept. of Radio and Electronics, Sichuan University.
Chengdu, Sichuan 610064, P. R. China

X.-B. Xu
Holcombe Dept. of ECE, Clemson University
Clemson, SC 29634, U.S.A.

It has been reported in literature that there is a significant conductivity difference between normal and tumorous biological tissue, which makes it possible to diagnose the pathological tissue by measuring the change of tissue conductivity. In the previous investigations, coils, coaxial lines, and waveguides were utilized for in vivo measurements of the tissue conductivity, but the measurements were for the conductivity of homogeneous tissue or for an effective conductivity of the whole layered tissue structure.

This paper presents a new method to measure the conductivity of tissue layer embedded in stratified biological structure, which has a potential application for cancer detection. This method uses a coaxial line in contact with the top layer (skin) to measure the reflection coefficient. The Finite-Difference Time-Domain (FDTD) method is used for forward calculation to determine the electric field distribution in the stratified biological structure. The numerical results show that unlike coils used in the frequency range from 1 to 30 MHz, a coaxial line can concentrate its electric field in the vicinity of its end. This merit can protect the measurement from external interference and makes it possible to use a locally homogeneous layered model to simulate complicated biological tissue structure. Then, making use of the relationship between the conductivity of the tissue layer and the measured reflection coefficient, the conductivity of the tissue layer of interest, which is selected to be the third layer to simulate the organ tissue under skin and fat, is determined by means of an inverse calculation based on Genetic Algorithm (GA). Unlike the previous investigations, the conductivity of the third layer, rather than the effective conductivity for the stratified structure as a whole, is obtained directly through the inverse calculation. To explore the feasibility of the proposed method, the sensitivity of the reflection coefficient corresponding to the change of the conductivity of the third layer is investigated, and an optimal frequency range is selected to get the maximum sensitivity of the reflection coefficients. Also, the accuracy of the inverse calculation employing GA is verified.

Feasibility Study of Tissue Equivalent Liquids for Bodyworn and Base Station SAR Measurements at 900 and 1800 MHz

K. Ahlskog, K. Hiltunen, P. Sinisalo, and A. Toropainen
Radio Communications Laboratory, Nokia Research Center
Helsinki, Fin-00180, Finland

This paper deals with the feasibility study of tissue equivalent liquids for Specific Absorption Rate (SAR) compliance testing of bodyworn devices and miniature base stations. Measurements using base station antennas and cellular phones are done and the results are compared with FDTD simulations. In compliance testing of base stations and bodyworn devices the measured SAR values should be an overestimate of the SAR values in the human body in practical exposure situation. The aim of this study is to find out how the dielectric parameters of the body equivalent liquid should be chosen in order to meet this requirement.

A series of FDTD simulations is done in order to study the SARs in box shaped phantoms as well as in a realistic human body model. Hence the simulation results can be compared with the measurement results and also estimations of the SAR values in a realistic human body can be obtained.

The simulated results are verified by measurements. In the measurements, cellular phones and two different types of the base stations with external and internal antenna are used. The 1-g and 10-g SARs at 900 and 1800 MHz are measured using state of the art SAR measurement system and box shaped phantom.

In the measurements, two types of tissue equivalent liquids having different electrical parameters are used. The liquids used are:

1. Head tissue equivalent liquid as defined by novel mobile handset standards having electrical parameters at 900 and 1800 MHz as defined in [1]

2. Muscle tissue equivalent liquid having electrical parameters at 900 and 1800 MHz as defined in [2]

REFERENCES

1. Drossos, A., V. Santomaa, and N. Kuster, "The dependence of electromagnetic energy absorption upon human head tissue composition in the frequency range of 300-3000 MHz," *IEEE Trans. MTT,* Vol. 48, No. 11, 1988–1995, 2000.
2. Gabriel, C., "Compilation of the dielectric properties of body tissues at RF and microwave frequencies," Brooks Airforce Base Technical Report AL/OE-TR-1996-0037, 1996.

Electric and Magnetic Stimulation in Rat and Human Head using the 3D Impedance Method

M. Persson and M. Nadeem
Department of Electromagnetics, Chalmers University of Technology
SE-412-96, Göteborg, Sweden

T. Thorlin
Sahlgrens University Hospital, Institute for Clinical Neuroscience
SE 413 45, Gothenborg, Sweden

Computational results from transcrainal magnetic stimulation (TMS) and electroconvulsive therapy (ECT) in a human head model and a rat model are presented. For the TMS case, we have carried out computer simulation of a typical TMS coil of figure eight type. The magnetic field is computed in 3D using the Biot-Savrat's law after placing the coil at a standard position. Using typical currents in the coils, pulse forms and pulse widths, induced current densities and electric field distributions are computed using the 3D impedance method for a given wave form of the current in the coil. These results are compared and contrasted with the corresponding ECT calculation. Here a uniform current density is injected at one side of the head models and extracted from the opposite side again using typically used values for amplitude, wave form, and pulse widths. The numerical results obtained both in TMS and ECT cases are visualised in 3D and in 2D, by using different cuts. We find that under the conditions studied induced current and electric field in TMS is considerably weaker and less penetrating than the corresponding results for ECT.

Session 4Pa3

Advances in Integral Equations

Green's Functions of Vertical Electric Dipole in Multilayered Media Separated into Simpler Terms - Behavior, Mutual Interaction, and Formulas for the Terms

R. M. Shubair
Department of Communication Engineering, Etisalat College of Engineering
Sharjah, U.A.E.

Most of the research effort and emphasis in modeling microwave integrated circuits (MICs) using the integral equation approach and moment method has been directed towards gaining greater insight and simplifications of the Green's functions associated with a Horizontal Electric Dipole (HED) in multilayered media. The HED Green's functions are needed for the analysis of microstrip structures and multilayered transmission lines.

This paper continues that trend but for the Vertical Electric Dipole (VED) in an effort to simplify the expressions of associated Green's functions and understand their behavior. The VED Green's functions are needed when modeling multilayered structures involving vertical via interconnections. It is shown that the each of the VED Green's functions can be separated into three terms corresponding to contributions from the quasi-dynamic images, leaky waves, and surface waves. It is found that each term of the Green's function has a different attenuation rate with distance along the interfaces within the multilayered media. The different attenuation rates make the parts dominant in different distances, i.e., the quasi-dynamic term is dominant in the near-field region, the leaky wave term is dominant in the intermediate region, and the surface wave term is dominant in the far-field region. Being radiative, both the leaky wave and surface wave contributions significantly rise with frequency, dielectric constant, and thickness of the dielectric layer where the VED is located. The advantage of this three-term representation of the Green's function lies not so much on simplicity itself, but on the ability to observe the trend in behavior during practical design of MICs involving vertical vias. The accuracy, computational efficiency, and versatility of the derived VED Green's functions are verified through a number of practical examples involving one- and two-layer microstrip structures.

Quasi-static Closed-form Green's Functions for Electric Dipole Below Ground

V. Arnautovski-Toseva and L. Grcev
University "Kiril i Metodij", Faculty of Electrical Engineering
Skopje, Macedonia

The electric field due to horizontal and vertical electric dipole (HED and VED) within ground is represented by Green's functions, which take into account the influence of the air-ground interface and the electric parameters of ground as finitely conducting medium. Together with the source and image free-space terms, the corresponding Green's function consists of a term represented by Sommerfeld integral. Because of its computationally inefficiency for exact numerical integration (numerical difficulties due to oscillations, divergent behavior and singularities), Sommerfeld integrals have been studied extensively during last decades. Various numerical and analytical techniques have been developed in order to obtain accurate, fast and efficient exact numerical or approximate results.

A new approach for the derivation of closed-form Green's functions for horizontal and vertical electric dipole within ground, which are involved in the electromagnetic model of grounding system is presented. The procedure involves derivation of closed-form solution of Sommerfeld integral in the quasi-static range:

$$S_0 = \int_0^\infty f(\lambda) e^{-\gamma_1 |z+z'|} J_0(\lambda\rho)\lambda d\lambda \tag{1}$$

where $f(\lambda)$ is a complex function, k_1 is the propagation constant for the ground and $\gamma_1(\lambda) = \sqrt{\lambda^2 - k_1^2}$.

The main objective is to avoid time-consuming numerical integration of (1) when evaluating electric fields for quasi-static and near field ranges. The evaluation of such fields is the starting point in the mathematical model of grounding system, for practical lightning studies for frequency spectrum up to several MHz. Theoretically this approach is based on the quasi-static complex-image theory, which is proved to be useful in determining the quasi-static fields of antennas located near the earth's surface. The main objective of this technique is to replace the finitely conducting ground by a perfectly conducting ground located at the complex depth d using the following approximation:

$$f(\lambda) \approx e^{-\lambda d}. \tag{2}$$

The proposed approach suggests new approximation of complex function $\gamma_1(\lambda)$ that is linearly related to λ through:

$$\gamma_1 \sqrt{\lambda^2 - k_1^2} \approx A\lambda + B. \tag{3}$$

where A and B are complex constants obtained by formulas depending on electromagnetic properties of the medium and frequency. By this approximation, the closed-form solution of (1) is obtained as:

$$S_0 \approx e^{-|z+z'|B} \int_0^\infty e^{-td} e^{-|z+z'|At} J_0(\lambda\rho) d\lambda = \frac{e^{-|z+z'|B}}{\sqrt{\rho^2 + (d + A|z+z'|)^2}}. \tag{4}$$

The accuracy of the proposed approach is analyzed by comparison of closed-form results with the results of direct numerical integration. It is shown that acceptable errors of less then 3% are obtained for the range $\mathrm{Abs}(k_1\rho) \leq 2$, where ρ is radial distance from source electric dipole to the observation point. These type of closed-form Green's functions may be applied for various electromagnetic radiation problems involving highly efficient moment method technique thus drastically reducing the computational time.

Spectral Domain Green's Function for the Dielectric Coated Perfectly Conducting Elliptic Cylinder

G. Angiulli
University of Reggio Calabria, DIMET
Reggio Calabria, Italy

G. Amendola and G. Di Massa
University of Calabria DEIS
Cosenza, Italy

Radiation and scattering from cylindrical objects have been largely investigated as such structures can be used to represent many real situations. Recently, the need of reliable tools to develop printed conformal antennas has revitalized this interesting field of research. The analysis of conformal radiators is usually carried out solving the electric field integral equation with the the method of moments. This technique has been proved to be very effective but it is conditioned to the knowledge of the appropriate Green's function.

Green's functions can be obtained through the expansion, with a proper set of eigenfunctions, of the field radiated by elementary dipoles in the presence of the cylindrical object. A limitation to the method stems from the fact that complete sets of eigenfunctions are available only for a few coordinate systems and that they are very often difficult to treat. For these reasons only circular cylindrical patch antennas have been fully investigated.

The elliptic cylinder can be seen as a generalization of the circular case and it can be used to model surfaces with a variable radius of curvature.

Printed structures confromal to elliptical surfaces have been already treated with an approximate model but no attempts have been done to develop a full wave procedure. The difficulties encountered to determine the dyadic Green's function in this particular case lie in the characteristics of the set of eigenfunctions to be used, namely radial and angular Mathieu functions. Firstly, Mathieu functions depend on the wave number which assumes different values in layers which have different dielectric constants. As a result, orthogonality between angular functions cannot be invoked when boundary conditions at the separation between two layers are imposed. Furthermore, no recurrence relations are available for such class of functions and the techniques used to speed up the computation of Sommerfeld integrals adopted for the circular case cannot be applied. In this work the study of the dyadic Green's function for the dielectric coated conducting elliptic cylinder is presented. The difficulties encountered in the developments will be discussed. Results relevant to the radiation from elementary dipole placed on the interface between two layers and from more complex sources will be presented and discussed.

Well-Conditioned Integral Equations for Closed Surfaces

J. J. Ottusch
HRL Laboratories, LLC
Malibu, CA, U.S.A.

V. Rokhlin
Yale University
New Haven, CT, U.S.A.

J. L. Visher and S. M. Wandzura
HRL Laboratories, LLC
Malibu, CA, U.S.A.

The standard boundary integral equations for time-harmonic scattering problems, do not, in general, result in well-conditioned linear systems. Consequently, when iterative methods are used to solve them, the number of iterations required to obtain an accurate solution may be very large. This has a direct, negative impact on the performance of “fast” solver techniques (e.g., the fast multipole method (FMM)), which must be used in conjunction with iterative solvers. Ill conditioning also magnifies discretization and truncation errors, leading to solution inaccuracy.

The magnetic field integral equation (MFIE) and electric field integral equation (EFIE), which are commonly used in electromagnetic modeling, are suitable for illustrating the problem. The ideal formulation is a second-kind integral equation devoid of resonances. The MFIE is a second kind integral equation, but it does suffer from spurious resonances. The integral operator for the EFIE consists of a first-kind (compact) operator and a hypersingular (unbounded) operator. The EFIE suffers from its own spurious resonances. One can eliminate the spurious resonances by combining the MFIE and EFIE to form a combined field integral equation (CFIE). The cost of doing so is the introduction of the EFIE’s hypersingular piece, which spoils the conditioning for fine discretizations (or low frequencies).

We present a new integral equation for closed, impenetrable targets that is generally well conditioned. Numerical results from a dense matrix implementation of this method demonstrate improved accuracy, reduced condition number, and reduced iteration counts compared to the conventional CFIE. Implementing the new formulation in conjunction with the FMM is also simple and straightforward.

Radiation from an Arbitrarily Oriented Hertzian Dipole When It is Embedded in Two-Layered Anisotropic Medium with a Tilted Optic Axis

A. Eroglu and J. K. Lee
Department of Electrical Engineering and Computer Science
Syracuse University
Syracuse, New York 13244-1240, U.S.A.

Electromagnetic radiation from dipole antennas in stratified anisotropic medium has been studied extensively because of its numerious applications in many areas such as geophysics, microwave integrated circuit, submarine communication, etc. As a result there is a growing interest in using anisotropic substrates in electromagnetic systems containing active device substrates, microstrip antennas and circuits, and absorptive materials.

The previous work in this research area was limited to radiation of dipoles embedded in stratified medium for isotropic case or anisotropic case when its optic axis is perpendicular to the stratification. The lack of numerical data in this field is an obstacle for an accurate analysis of radiated waves especially in the far field.

Stoyer [1] has solved the multilayered problem for isotropic stratified media using the input impedance concept with the Hertz potential. Wang [2] presented general computational method for the electromagnetic problem involving stratified isotropic media. Tang [3] and Kwon and Wang [4] calculated the electromagnetic fields from dipoles embedded in anisotropic stratified medium by decomposing fields into transverse electric (TE) and transverse magnetic (TM) modes. In their analysis, the optic axis is assumed to be perpendicular to the stratification. The far field calculation of a vertical dipole over an imperfectly conducting half space when the dipole is at a specified height d is obtained by King and Sandler [5].

In this paper we calculate the far field radiation from an arbitrarily oriented dipole when it is embedded in two-layered uniaxially anisotropic medium with a tilted optic axis. Solutions to the problem of radiation are obtained analytically by using dyadic Green's function of the anisotropic medium. The stationary phase method is used to evaluate the integrals in the far field. The results are checked numerically in the limiting case with the existing results by King and Sandler [5]. It is shown that our method is practical and gives accurate results for the radiation far fields. Also our method can easily be extended to the cases involving more than two layers once the dyadic Green's functions of the multi-layer medium are calculated.

REFERENCES

1. Stoyer, C. H., "Electromagnetic fields of dipoles in stratified media," *IEEE Trans. Antennas Prop.*, Vol. 25, 547–552, 1977.
2. Wang, J. J. H., "General method for the computation of radiation in stratified media," *IEE Proc.*, part H, Vol. 132, No. 1, 58–62, 1985.
3. Tang, C. M., "Electromagnetic fields due to dipole antennas embedded in stratified anisotropic media," *IEEE Trans Antennas Prop.*, Vol. 27, No. 5, 665–670, 1979.
4. Kwon, Y. S. and J. J. H. Wang, "Computation of Hertzian dipole radiation in stratified uniaxial anisotropic media," *Radio Science*, Vol. 21, No. 6, 891–902, 1986.
5. King, R. W. P. and S. S. Sandler, "The electromagnetic field of a vertical electric dipole over the earth or sea," *IEEE Trans. Antennas Prop.*, Vol. 42, No. 3, 1994.

Efficient Computation of the Periodic Green's Function in Multilayered Media using Simulated Images

R. M. Shubair
Department of Communication Engineering, Etisalat College of Engineering
Sharjah, U.A.E.

The computation of the periodic Green's function in multilayered media is required for the analysis of the radiation or scattering characteristics of a wide class of structures including frequency-selective surfaces (FSS), optical gratings, beam couplers, and reflector antennas. The electromagnetic (EM) modeling of these periodic structures involves the formation of a boundary integral equation in which the kernel is a Green's function series that is very slowly convergent. To determine the radiation or scattering characteristics of the periodic structure, the derived integral equation is solved using the Method of Moments (MoM); in which repeated evaluations of the Green's function series are required to fill in the impedance matrix of the structures being modeled. The slow convergence of the Green's function series would, therefore, result in a considerable amount of computation time. This paper develops a technique that overcomes the slow convergence of the Green's function series allowing for a fast and efficient modeling of the periodic structure in multilayered media.

The EM modeling of a periodic structure in multilayered media using the integral equation approach requires the knowledge of the associated potential Greens function, which represents the response due to a periodic array of infinitesimal dipole point sources present in multilayered media. Using a cascaded wave-matrix approach to model the effect of the multilayered media, the periodic Greens function is expressed in terms of a spectral summation that has a very slowly convergent asymptotic behavior. To overcome this problem, we first extract from the spectral summation the slowly convergent asymptotic behavior and then add it back equivalently in the spatial domain by making use of Poissons summation formula. The equivalent asymptotic spatial function represents the inverse Fourier transform of the given spectral contribution and can be accurately calculated using a simulated image model. It is shown here that the use of the simulated image model results in a simple closed-form expression of the asymptotic spatial function consisting of a short series of decaying exponentials. The periodic Greens function then takes the form of a hybrid spectral/spatial summation. The spectral summation converges rapidly because the slowly convergent asymptotic behavior is subtracted out, whereas the spatial summation converges rapidly because the spatial function involved is expressed in terms of a short series of decaying exponentials. Numerical results are obtained to verify the accuracy, computational efficiency, and versatility of the proposed technique. The detailed analytical approach describing the proposed technique and the supporting numerical examples will be demonstrated at the conference in due date.

Session 4Pb3

Geometric and Topological Issues in Discrete Electromagnetics

Data Structures for Computational Electromagnetics Inherited from Algebraic Topology

P. R. Kotiuga
Boston University
Boston, MA 02215, U.S.A.

In both finite element analysis and the study of manifolds, the notion of a simplicial complex has long been used as a basic data structure enabling one to model spaces without making implicit geometric or topological assumptions. In electromagnetics, the basic equations are most naturally stated in terms of differential forms. That is, Maxwells equations are integral laws and information about the electromagnetic field is obtained by integrating or appealing to the generalized form of Stokes theorem to deduce differential versions of Maxwell equations and interface conditions. In the last two decades, within computational electromagnetics, Whitney forms have emerged as an ideal solution to the quest for a discrete model of differential forms phrased in terms of the data structures of simplicial complexes[1,2]. The adoption of Whitney forms has resolved many outstanding problems in vector interpolation and riddles such as the computation of spurious modes in cavities.

Given the success of simplicial data structures and Whitney forms, we examine the roots of simplicial techniques and geometric integration theory within topology, outgrowths, and inevitable technology transfer to computational electromagnetics. Specifically:

- De Rhams 1931 thesis and simplicial techniques in developing homology theory in the 1920's. (i.e. first proofs of many statements in Ch.1 of Maxwell's treatise).
- The appearance in the 1940's of Eilenberg-Steenrod axioms for a cohomology theory.
- Reaction to axiomatics; Andre Weil's paper[3] of 1952 developing the formula for Whitney forms, and Whitney's subsequent geometric integration theory.
- Milnor's theorem on CW complexes and the rejection of triangulations by the mainstream of algebraic topology in the late 1950's.
- Subsequent uses of Whitney forms in rational homotopy theory[4], combinatiorial Hodge theory and the understanding of torsion invariants[5].
- Semi-simplicial objects in algebraic topology[6] as a combinatorial abstraction of space; open problems and data structures in 3-d computational electromagnetics.

REFERENCES

1. Bossavit, A, "Computational Electromagnetism", *Academic Press Boston*, 1998.
2. Gross, P.W and P.R. Kotiuga, "Data Structures for Geometric and Topological aspects of Finite Element Algorithms", *Ch. 6 of Geometric Methods for Computational Electromagnetics, PIER Vol.32, EMW Publishing*, 2001.
3. A. Weil, "Sur les Theorems de de Rham", *Commentarii Matematicae Helvetici*, 1952.
4. Griffiths, P.A and J.W. Morgan, "Rational Homotopy Theory and Differential Forms", *Progress in Math*, Vol. 16, Birkhauser Boston, 1981.
5. Muller, W, "Analytic Torsion and R-Torsion of Riemannian Manifolds", *Advances in Math.*, Vol.28, pp 233-305, 1978.
6. Gray. B, Bull. AMS, (38)2, 217-220, "Review of: Simplicial Homotopy Theory", P. G. Goerss and J .F. Jardine, *Progress in Math*, vol.174, Birkhauser, Basel, 1999.

Convergence of Mimetic Discretization Methods

S. Steinberg
University of New Mexico
Albuquerque, NM 87131-1141, U.S.A.

The convergence of a mimetic discretization in rough grids is proven. The mimetic discretization method is based on discretizing the invariant operators divergence, gradient, and curl and then using these discretizations to discretize more general differential operators. Most importantly, mimetic method require that the discretization has exact analogs of many of the important theorems of vector calculus. For the grids, we only assume that the cells are convex. To study convergence, the family of grids under consideration are assumed to satisfy uniform convexity conditions.

Because we are focused on convergence for rough grids, we use as a model problem the simple two-dimensional Laplace equation with Dirichlet boundary conditions so that the role of grid roughness is clear. In this case, the important theorem from vector calculus we mimic is the divergence theorem. To simplify the notation, the convergence is shown on logically rectangular grids with a lower bound on the angles in the cell corners and an upper bound on the cell aspect ratios. In this situation, the best convergence rate to be expected is first order, which is what proved.

The proof involves three main steps. First, a functional analytic estimate of the error in the solution and gradient of the solution of Laplace's equation are given in terms of the truncation error of the divergence and gradient. Next, the estimates of the truncation errors for the divergence and gradient involve a detailed analysis of the geometry of a quadrilateral cell. Additionally, the gradient for the mimetic method is defined implicitly, so an analysis of the system of equations defining the gradient is given. The last step is to extend the one-cell estimates to the global grid. The techniques developed apply to far more general problems.

Multigrid FEM Using Schwarz Preconditioners and Hierarchical High Order Whitney-Like Elements

J.-F. Lee, R. Lee, and F. L. Teixeira
ElectroScience Laboratory and Department of Electrical Engineering,
The Ohio State University
Columbus, OH 43212, U.S.A.

In the finite element method (FEM), usual implementations of Whitney-like (or tangentially continuous) elements are often based on the second-order vector wave equation for the electric (or magnetic) field. This approach has been successful in modal problems, but poses obstacles in the case of driven problems. Moreover, the vector wave formulation is not suited for low frequency problems and it has been observed that the rate of convergence for iterative solvers becomes very poor. Both symptoms are caused by the lack of a frequency independent gauge.

Various vector potential approaches for the FEM have been proposed to overcome these problems. One solution has been to impose a tree gauge. This has the drawback of producing a matrix with a condition number which depend strongly on the particular choice for the tree. Another approach introduces Lagrange multipliers (with or without penalty terms).

A disadvantage of such methods is that they require extra unknowns which do not enlarge the solution space for the discrete fields. On the other hand, by using hierarchical highorder elements, the formulation can be modified in such a way that the high order unknowns are no longer affected by such problems and the above mentioned measures to improve stability need only be applied to the lowest order basis. Since the number of variables in this subspace is comparatively low, the computational burden is significantly decreased.

Another kind of problem arises when the FEM is applied to electrically large domains. In this case, the FEM matrix contains a large number of negative or close to zero eigenvalues (related to cavity modes with resonance frequency below or close to the operating frequency). Conventional preconditioners are usually unable to resolve this situation so that, in general, iterative solvers perform very poorly. However, the multilevel properties of the hierarchical elements make it easy to apply multigrid ideas. We will describe a Schwarz-type solver whose computational efficiency is barely affected when the domain gets electrically large.

Mimetic Finite Difference Methods for Maxwell's Equations on Unstructured Grids with Application to Microphotonic Devices

N. N. Carlson
Motorola Labs
Los Alamos, New Mexico 87544, U.S.A.

M. Shashkov
Los Alamos National Laboratory
Los Alamos, New Mexico 87545, U.S.A.

The previous work of Hyman and Shashkov [1] introduced high quality mimetic finite difference methods for approximating the solution to Maxwell's equations on nonorthogonal, logically rectangular computational grids. For some physical problems, however, a logically rectangular grid lacks the flexibility required to produce a high quality computational grid that conforms to the geometry of the media. Unstructured grids—consisting of triangles, tetrahedra, prisms, etc.—are well-known for their ability to discretize complex geometries. With this as motivation, we have constructed analogous mimetic finite difference methods for Maxwell's equations on unstructured grids. Like the methods in [1], these mimetic methods use discrete analogs of differential operators that satisfy the identities and theorems of vector and tensor calculus in discrete form, so that the numerical approximation is free of spurious modes and mimics many fundamental properties of the underlying physics, including conservation laws, symmetries in the solution, and divergence-free conditions.

To demonstrate the robustness of this method we numerically simulate the operation of a micron- sized channel drop filter. These semiconductor-based photonic devices consist of a pair of waveguides coupled to a microcavity resonator. Waves of the correct frequency in the input waveguide excite the resonator and are passed into the output waveguide. One example of such a device uses a ring resonator evanescently coupled to the waveguides across an air gap. Another is photonic crystal based in which the waveguides and resonator are formed by removing selected rods from a large periodic array of dielectric rods. Both cases are characterized by dielectric structures with nontrivial dielectric interface geometry, with strong discontinuities in the dielectric permittivity across the interfaces.

REFERENCES

1. Hyman, J. M and M. Shashkov, "Mimetic discretizations for Maxwell's equatio1n", *J. Comput. Phys.* 151, 881–909 (1999).

Higher Order Spatial Schemes for the Finite Integration Theory

H. Spachmann, R. Schuhmann and T. Weiland
Computational Electromagnetics Laboratory, Technische Universität Darmstadt
Darmstadt, 64289, Germany

The Finite Integration Technique (FIT) and similar techniques as Finite Differences are widely used in computational electromagnetics. The classical formulation of these techniques has a second order accuracy of the spatial operators and the dispersion error of these schemes limits the numerical analysis of electrically large structures. Higher order techniques in contrary reduce significantly the spatial dispersion but are burdened by a higher numerical effort and by accuracy and stability concerns in inhomogenious domains.

One of the key properties of FIT is the definition of matrix operators C and S representing exact transformations of the corresponding vectoranalytical operators. Beside these spatial operators, the so-called material matrices connect integral quantities on cell-facets (fluxes) with quantities on cell-edges (voltages). Whereas recent higher order approaches in Finite Differences look for higher order approximations of partial derivatives of the spatial operators (thus violating the exactness property), our innovative approach focuses on a reformulation of the FIT material matrices towards arbitrary higher order. It leaves the spatial curl and source operators untouched therefore guaranteeing vital consistency relations of the FIT. The underlying idea of the scheme is the representation of the electromagnetic quantities like field strength and flux density by piece-wise defined one- and two dimensional higher order polynomials. A three step approximation and interpolation process enables the construction of the polynomials specifying the entries of the material matrices.

Exemplarily a fourth order scheme is presented and analyzed. Hereby stability issues due to inhomogenious media, non-equidistant grid and modeling of boundary conditions are discussed. The successful application of the novel technique in frequency and time domain analysis is presented.

Weitzenbock Identities and Variational Formulations in Computational Electromagnetics

P. R. Kotiuga
Boston University
Boston, MA, U.S.A.

Given a vector field **F** with Cartesian components F_i, $i = 1, 2, 3$, we have a vector Helmholtz equation

$$\mathrm{grad}\,(\mathrm{div}\,\mathbf{F}) - \mathrm{curl}\,(\mathrm{curl}\,\mathbf{F}) + k^2\mathbf{F} = 0 \tag{1}$$

which, when referred to Cartesian coordinates becomes

$$\mathrm{div}\,(\mathrm{grad}\,F_i) + k^2 F_i = 0, \quad i = 1, 2, 3. \tag{2}$$

Equation (2) is valid only in Cartesian coordinates. If one refers the vector **F** to an orthonormal frame, the difference between the operators occurring in equations (1) and (2) involves curvature terms. The Weitzenbock identity give the precise form of these curvature terms for the Laplace-Beltrami operators acting on degree p differential forms on an n dimensional manifold. Our case corresponds to $p = 1$ and $n = 3$. These identities have many uses in electromagnetics; the $p = 2$, $n = 4$ case comes up in the context of the Sagnac effect and optical gyroscopes, while the $p = 1$, $n = 3$ case comes up once more in the context of micromagnetic exchange energy of small magnetic particles. In this way, the Weitzenbock identities give a framework for understanding the common mistakes made when Cartesian vector identities are abused in the process of trying to reduce a problem involving a vector field or differential form to a system of uncoupled scalar equations.

The current paper examines these issues in a variational setting. Specifically, the functionals

$$I(\mathbf{F}) = \frac{1}{2}\int_V (|\mathrm{curl}\,\mathbf{F}|^2 + |\mathrm{div}\,\mathbf{F}|^2 - k^2|\mathbf{F}|^2)dV \tag{3}$$

and,

$$J(\mathbf{F}) = \frac{1}{2}\sum_{i=1}^{3}\int_V (|\mathrm{grad}\,F_i|^2 - k^2|F_i|^2)dV \tag{4}$$

are the obvious variational formulations of Equations (1) and (2) respectively when **F** is suitably normalized. A key observation is that, in Cartesian coordinates, Equations (1) and (2) are equivalent but the variational formulations (3) and (4) differ by a boundary term which does not affect the Euler-Lagrange equations. The two variational formulations do however, lead to different natural boundary conditions! If the region V is a closed three-dimensional Riemannian manifold, the difference between the two functionals has an interpretation in terms of curvature and homology. In this case, the Weitzenbock identity gives us an explicit formula for the difference. This points to an explicit formula for the difference term when V is a subset of Euclidean space and gives a geometric interpretation of the difference in associated natural boundary conditions.

Within this geometric framework, we examine the finite element analysis of the vector Helmholtz operator, coercivity of bilinear forms, and the work of Martin Costabel.

A Cochain-Based Discretization Scheme for Maxwell's Equations in Complex Media and Geometries

F. L. Teixeira
ElectroScience Laboratory and Department of Electrical Engineering,
The Ohio State University
Columbus, OH 43212, U.S.A.

Discretization schemes for Maxwell's equations (ME's) which preserve discrete analogues of continuum theorems and conservation laws are important for a number of reasons. For elliptic equations, they are instrumental in supressing spurious modes. For hyperbolic or parabolic equations, they can avoid harmful unconditional instabilities in the update for irregular and unstructured grids.

We describe here a discretization approach to ME's based on the treatment of electromagnetic fields as cochains (discrete differential forms) on the first barycentric subdivision (FBS) of a simplicial lattice. We first review the convenience of treating electromagnetic field quantities as cochains and their role as a dual space of the geometric elements of the lattice (nodes, edges, faces, volumes) [1-3]. The use of a FBS to decompose the primal (simplitial) lattice and the barycentric dual (non-simplicial) lattice is then considered. We discuss some properties of barycentric subdivisions in general, including the fact that they are affinely invariant, or invariant under diffeomorphisms 'at small scales'. The distinct consequences of this fact for both static and dynamic problems are also discussed.

We illustrate the construction of discrete Hodge operators (i.e., generalized constitutive relations containing all metric information) for ME's using Whitney maps defined on the FBS. The relevance of such approach to the simulation of ME's in complex media and geometries is discussed. Finally, we cast our results against the backdrop of some recently developed discretization approaches for so-called topological field theories [4].

REFERENCES

1. Bossavit, A and L. Kettunen, "Yee-like schemes in staggered cellular grids: A synthesis between FIT and FEM approaches, *IEEE Trans. Magn.*, vol. 36, no. 4, pp. 861-867, 2000.
2. Gross, P and P. R. Kotiuga, "Data structures for geometric and topological aspects of finite element algorithms, in *Geometric Methods for Computational Electromagnetics, PIER 32*, pp. 151-169, EMW Publishing, Cambridge, MA, 2001
3. Bossavit, A, How weak is the weak solution in finite element methods, *IEEE Trans. Magn.*, vol. 34, no. 5, 2429-2432, 1998.
4. Sen, S, S. Sen, J. C. Sexton, and D. H. Adams, "A geometric discretization scheme applied to the Abelian Chern-Simmons theory, *Phys. Rev. E*, vo. 61. no. 3, 3174-3185, 2000.

Session 4Pa4

Propagation Phenomena in Indoor and Outdoor Wireless Communication Channels

Prediction of Cellular Characteristics for Various Microcell Urban Environments

N. Blaunstein
Department of Communication Systems Engineering
Ben-Gurion University of the Negev
Beer Sheva, Israel

D. Censor
Department of Electrical and Computer Engineering
Ben-Gurion University of the Negev
Beer Sheva, Israel

The strategy of cellular maps splitting on cells depends on conditions of propagation and on the topographic characteristics of built-up areas. Prediction of propagation phenomena and main propagation characteristics in urban cellular networks, as well as the frequency planning concept presented in this work is based on the multiparmetric stochastic model which can be used for optimization of the cochannel interference parameters at the preliminary stage of cellular networks planning for various built-up asreas. The propagation characteristics of cellular communication channel, as well as the cochanel interference parameter, such as carrier-to-interference ratio (C/I), are investigated for the general case of built-up areas with randomly distributed buildings placed on rough terrain. Comparison with the well-known static model of cellular map splitting and with experimental data obtained by measurements carried out in various built-up areas is presented. A good agreement between the proposed stochastic approach, the well-known static model and different experiments carried in various urban environments is obtained for cellular map performance and prediction of main characteristics of cellular networks.

Foliage Effect on Path Loss for Residential Environments

S. A. Torrico
Comsearch
Ashburn, VA, U.S.A.

R. H. Lang
Electrical and Computer Engineering Department
The George Washington University
Washington, D.C., U.S.A.

In modern wireless communication systems, there is a need to better understand the propagation channel in vegetated residential environments. In the development of Torrico, Bertoni, and Lang [IEEE Trans. Antennas Propagat., vol 46, pp. 872-880, June 1998], the effects of multiple trees and multiple buildings on the propagation loss were studied. In that approach, only the coherent field in the canopy was calculated using the discrete scattering theory of Foldy and Lax to find the characteristics of the trees.

This work describes the use of the radiative transfer equation to understand the attenuation effects of trees on the overall propagation loss, between the base station transmitter and the mobile receiver in a vegetated residential environment. As in past models, the row of houses or block of buildings are viewed as diffracting cylinders lying on the earth, and the canopy of the trees are located adjacent to and above the houses/buildings. In this approach, a row of houses or buildings is represented by an absorbing screen, and the adjacent canopy of trees by a partially absorbing phase screens. The field at the aperture of the first absorbing phase screen depends on the coherent and incoherent fields going through the first tree due to an incident plane wave. Physical optics is then used to evaluate the diffracting field at each of the successive absorbing/phase half-screens configuration, up to the mobile receiver by using the multiple Kirchhoff-Huygens integration.

In order to find the properties of a partially absorbing phase screen, such as the attenuation, the tree canopy is modeled by a random collection of branches and leaves, which are replaced by cylinders and discs respectively. At PCS frequencies, the wavelength is small compared to the size of the scatterers and, as a result, a forward scattering approximation was employed to simplify the transport analysis. In this analysis, the specific intensity in the tree canopy is split into two parts: the coherent and the incoherent intensity. The wave scattering from foliage generates the incoherent waves traversing the foliage in the forward direction in addition to the attenuated coherent wave.

Analysis of Flutuations Phenomena in Complex Structures with Applications to Wireless Propagation

R. Mazar and A. Bronshtein
Department of Electrical and Computer Engineering
Ben Gurion University of the Negev
Beer Sheva, 84105, Israel

I.-T. Lu
Department of Electrical Engineering and Computer Science
Polytechnic University
Farmingdale, NY 11735, U.S.A.

The commercial success achieved by the cellular mobile radiotelephones has stimulated development of other radio communication systems, especially those with those oriented for high data-rate transmission. Design of propagation channels for such systems operating in dense user areas requires taking into account the interaction of the propagating radiation with complex geometrical structures characteristic to modern urban and suburban environments. For example, when the transmitter and/or receiver antennas are placed below the rooftops a sharp change in the propagation character is observed because of the confinement of the propagating radiation by the building walls. In addition, there is an increase in the number of scattering events caused by traffic, trees and other obstacles characteristic of modern urban areas. All these factors result in multiple path arrival with consequent rapid phase and amplitude variations and the appearance of fast fading effects. The another factor that has a strong influence on the propagation character is related to the expanding demand for more communication channels and resulted in increasing exploitation of higher and higher frequencies, extending well into the millimeter-wave regions of the spectrum. At such high frequencies, radio waves start to interact with the propagation environment through absorption and dispersion by atmospheric gases, with scattering and absorption induced by the prevailing meteorological conditions, especially precipitation, and with the effects of fluctuations in the refractivity of the atmosphere. These factors, not generally considered in the lower-frequency regions of the spectrum, can play an important role in determining the characteristics and reliability of higher-frequency communication systems. For designers of the wireless-communication networks, this problem exposes a challenge for the analysis of complex wave - medium interactions.

In this work, we employ methods of the Stochastic Geometrical Theory of Diffraction (R. Mazar and L. B. Felsen, J. Acoust. Soc. Am., **86**(6), 2292-2308, (1989)) in order to present a model of propagation channel that accounts for all the above mentioned factors. Particularly we apply the ray-optical methods and the waveguide model for a city street with irregularly spaced buildings. This approach together with the methods developed in the coherence theory allows us to present analytical expressions for the spatial structure of the field and to account for the fluctuation phenomena induced by the turbulent motion of the air.

Generating Model of Fading in the In-Door Communication Channel

V. Lyandres
Ben-Gurion University of the Negev
Beer Sheva, Israel

There are at least two significant differences between indoor and outdoor propagation. The first is the absence of the line-of-sight component, and the second one is the strictly limited number of refracted components in the received signal. Due to these reasons the signal PDF occurs to be a non-Gaussian one and the law which is left shifted relative to the Rayleigh PDF distributes its envelope. In other words the propagation conditions in the indoor channel are more severe (with a more deep fading) than in the outdoor case.

The generating model of the corresponding narrow band random process (so called fading carrier) is presented. It is based on the interpretation of the process as a stationary output of a nonlinear dynamic system, excited by white Gaussian noise.

The model may be considered as a tool for simulating a communication channel with essentially severe fading.

Analysis of Subscriber Radio Location Techniques through a Deterministic Propagation Model

M. Porretta, P. Nepa, G. Manara, F. Giannetti
Dept. of Information Engineering, University of Pisa
Pisa, Italy

The interest in radio location algorithms originates from need to guarantee emergency services to calls made by mobile phone users; indeed, beginning October 2001, the FCC requires that, in the US, all emergency calls (911) from cellular phones must be located within 125 m in 67% of the time. Nevertheless, the number of applications for location information is growing rapidly: for example, a location-aware service is to connect the Yellow Pages with a map database giving the information about the address of a certain site (hotel, restaurant, museum) in the closeness of user. Furthermore, location information can be very useful for the network operator, especially in Radio Resource Management (RRM) functions, e.g., selection and handover.

A radio location system operates by measuring physical quantities related to radio signals traveling between a mobile station and a set of fixed base stations. The received signal is used to estimate the length and/or direction of arrival of radio paths, and the mobile position is derived from geometrical relationships. In particular, radiolocation systems can be implemented that are based on the angle-of-arrival (AOA), the signal strength, the time-of-arrival (TOA.), the time-difference-of-arrival (TDOA), or their combinations (James Caffery, Gordon Stuber, "Subscriber location in CDMA cellular networks" *IEEE Transactions on Vehicular Technology*, vol. 47, no 2, May 1998).

In this work, it is shown that a deterministic simulator of the electromagnetic propagation in urban areas can be usefully employed to optimize and validate a subscriber radio location technique for third generation cellular networks. In particular, a fully three-dimensional simulator based on high-frequency ray-techniques has been applied to validate a TOA radio location algorithm which requires the knowledge of the time of arrival delay at three different base stations. For each mobile position, the received signal is evaluated as the summation of ray contributions reaching the base station after reflections or diffractions, so that non-line-of-sight conditions can be suitably accounted for. Contributions up to the third order for reflections from the walls of the buildings have been also included. Diffractions from the edges of buildings are evaluated through approximate dyadic coefficients which are valid for impedance surface models. Moreover, computer graphics algorithms have been used to speed up the ray-tracing procedure.

The algorithm has been tested in a Manhattan-like microcellular environment and the performance have been evaluated in terms of the absolute location error. The effects of the time of arrival quantization are also taken into account. Extensive simulations demonstrated that it is possible to achieve a location error with a mean value of 33 m and a standard deviation of about 20 m. A detailed description of the radio location algorithm implemented will be given at the conference. Work is in progress to include into the algorithm other signal parameters, *e.g.*, amplitude and direction of arrival of the signal received at the base stations, with the specific aim of both increase the accuracy of the algorithm and reduce to less than three the number of base stations required.

Reflections on the PO Fresnel Model in Time and Frequency Domain

E. Van Lil and A. Van de Capelle
K.U.Leuven, div. ESAT/TELEMIC
Leuven-Heverlee, B-3001, Belgium

I. De Coster
Telindus, High Tech Institute
Heverlee-Leuven, B-3001, Belgium

In this paper the Fresnel model, used up to now for smallband indoor propagation computations, is discussed. The Fresnel model is an efficient and accurate Physical Optics (PO) model suitable for use in a propagation prediction tool, in that sense that it can handle large and rough surfaces much more efficiently than the classical theories based on Fourier transforms. It was originally derived in the frequency domain. However, its inverse Fourier transform exists as an analytical expression. The advantages of the Fresnel model over the classical Geometric Optics (GO) formulation in the frequency domain are maintained in the time domain. The time domain model has a further advantage that the classical discrete power delay profiles are replaced with continuous, finite width shapes. The conditions for the validity of the GO are not always satisfied in indoor situations. Indeed, the GO theory supposes a reflecting surface of infinite size. Moreover, the transmit and/or receive antennas are not always in the far-field of these reflectors. To satisfy the far-field condition, the separation distance between antenna and reflecting surface should be larger than the Rayleigh distance $2D^2/\lambda$. Especially in indoor situations below millimeter wave frequencies this is in general not the case.

The use of the PO theory allows to take into account the finite size of the reflectors and their position with respect to the transmitter and receiver through the calculation of the radiation integral containing the induced surface currents. But the classical theories based on Fourier transforms imply impinging plane waves and hence a large distance between the sources and the scatterers. Therefore, we focussed our research on using a parabolic incident wave, approximating the real spherical incident wave. The evaluation of this new formulation involves a Fresnel integral, hence the name Fresnel model. This model also does not suffer the classical shortcomings of Fourier models dealing with flat plates, namely that the field becomes infinite when the surface of the reflecting plate increases, so that conservation of power is guaranteed. A large number of measurements in the near-field facilities of the ESAT/TELEMIC division of the K.U.Leuven on different kinds of plates, involving planar, crenel, triangular, sinusoidal and random plates, with different materials (PE, PVC, PMMA) have been performed. For most cases, the correspondence between measurements and our PO simulations are excellent.

Since more and more broadband wireless systems are developed, it is important to have an accurate and yet simple description of the broadband behavior of the propagation channel. Classical GO prediction tools give discrete time domain profiles. However this doesn't give enough broadband information. It is obvious that the multipath waves are not impinging discretely on the receiving antenna. Measurements show that in real propagation situations a small number of significant resolvable paths can be distinguished. These have different widths in delay according to the size of the obstacles. A description in the time domain indicating the spreading in time is thus needed. Fortunately, an analytical inverse Fourier transformation of our Fresnel model exists. The time domain formulation illustrates the spreading of the waves due to the spatial distribution of the scattering object, and will be compared with more rigorous moment methods. We experienced that the shape of the time domain profiles are also similar to profiles of models obtained both from simplified geometrical considerations. This method can be generalized for higher order reflections, that can be treated as convolutions in the time domain.

Session 4Pc5

Gaussian Beams for Efficient Computation of Propagation and Scattering in Complex Environments

Universal Relationships in the Focusing of Gaussian Beams

T. L. Szabo
Boston University
Boston, MA, U.S.A.

Closed form expressions for field radiated by apertures with Gaussian and truncated Gaussian weighting have been derived from the Rayleigh-Sommerfeld diffraction integral for line sources, rectangular and circularly symmetric apertures in the frequency domain. Based on this analysis, three general observations can be made. The first is that if the closed form results above are expressed in terms of wavelength-scaled parameters, the same beam patterns apply to all frequencies (within reason). The second is that the same beam shapes occur when aperture and axial distance combine to give the same value of the universal parameter equal to the wavelength scaled distance divided by the aperture in wavelengths squared. The third is that the transition distance between near and far field can be expressed in terms of the aperture weighting function. These relationships can be shown to apply to any amplitude weighted beam.

The application of focusing to an aperture either through the application of either a thin lens or an electronic lens equivalent (array focusing), or the shaping of an aperture, can be treated by a similar analysis. In the case of focusing, the results can be written in terms of a scaled equivalent distance from the array. Through the use of this equivalent distance, the expressions for the diffraction beams from a focusing aperture can be expressed in terms of those for a nonfocusing aperture. Specifically, these results show that the entire near and far field beam evolution of a nonfocusing aperture happens within the geometric focal length with appropriate scaling. While the terms near and far field no longer apply to a focused beam, new more appropriate terms can be derived to determine depth of field. To distinguish intentional focusing from the natural focusing in a nonfocusing beam at the transition distance, new concepts based on beamwidths within a plane are proposed.

Effects of Causality on Gaussian Pulses and Beams in Lossy Media

T. L. Szabo
Boston University
Boston, MA, U.S.A.

Many solutions to wave propagation problems employ Gaussian beams or beams synthesized from Gaussian basis functions in combination with Gaussian-shaped pulses. These solutions provide analytical insight as well as answers to otherwise intractable problems. For beams formed by pulses such as arrays, accurate knowledge of the pulse shape is essential. For pulse propagation in lossy media, phase velocity dispersion is often neglected.

Many types of lossy media have an absorption characteristic that behaves as a frequency power law over the frequency range of interest. Based on a principle of causality expressed in the time-domain and the usual assumption that absorption per wavelength is small, expressions for the dispersion have been derived. These results indicate that maximum dispersion occurs when the power law exponent is one and there is no dispersion for an exponent of zero or two. Intermediate exponents with fractional powers are included in this approach.

The combined effects of absorption and dispersion can be represented by a material transfer function the Fourier transform of which is the material impulse response. For frequency-squared loss, there is no dispersion so that the material impulse response is Gaussian. This result appears paradoxical because Gaussian time responses have an infinite temporal extent, but it can be shown to be very accurate.

This study shows that for the simulation and modeling of broadband beam and pulse propagation in lossy media, even small values of dispersion can have a profound cumulative effect on pulse shape and a slight effect on pulse delay. Neglect of dispersion can, in some cases, produce acausal behavior and different pulse shapes.

Virtual Sources for Higher Order Gaussian Beams

S. R. Seshadri
Madison, WI 53705-2718, U.S.A.

A physically realizable packet of plane waves having a small range of propagation directions about a given direction, say along the z-axis, constitutes a beam. For a specified region of space, say for $z > 0$, suitable sources situated exterior to that region can generate a beam. Instead of specifying the primary source, it is usual to state the secondary source at the input plane $z = 0$ which is exterior to and at the boundary of the physical space . For generating the basic and higher order Gaussian waves, Felsen [1] and Shin and Felsen [2] have shown that it is possible to specify a simple primary source, namely a point source, located in complex space that is exterior to the specified region of physical space. There are criticisms of the Felsen method and these criticisms are discussed. The complex source point technique has been justified for the basic Gaussian wave by expanding the field in a series in terms of the small parameter $2/kb$ where k is the wave number and b is the Rayleigh distance. The leading term in the series gives the paraxial approximation. The general term in the series has been determined such that the partial sum yields the correct paraxial approximation on the axis. The infinite series has been summed up to obtain a simple expression for the Gaussian wave. This expression leads to a point source located in complex space [3].

In principle, the procedure of Couture and Belanger [3] cannot be applied to the higher order Gaussian beams. We have developed a different technique for the treatment of the higher order Gaussian beams [4]. A representation for the higher order Gaussian wave is obtained. The source is suitably chosen such that this representation gives the correct paraxial approximation. The source is a point source in complex space. The simplicity of the source enables us to determine a closed form expression for the higher order Gaussian wave. The representation for the higher order Gaussian wave includes all the nonparaxial contributions as well as the evanescent waves. Some nonparaxial contributions have been explicitly evaluated to demonstrate the advantage of this method for the evaluation of the nonparaxial contributions.

Two such higher order Gaussian waves are used to develop an electromagnetic wave which in the paraxial approximation has uniform linear polarization. The changes that occur due to the nonparaxial contributions are investigated.

REFERENCES

1. L. B. Felsen, “Evanescent waves”, *J. Opt. Soc. Am.*, 66, 751-760, 1976.
2. S. Y. Shin and L. B. Felsen, “Gaussian beam modes by multipoles with complex source points”, *J. Opt. Soc. Am.*, 67, 699-700, 1977
3. M. Couture and P. A. Belanger, “From Gaussian beam to complex-source-point spherical wave”, *Phys. Rev. A*, 24, 355-359, 1981.
4. E. Zauderer, “Complex argument Hermite-Gaussian and Laguerre-Gaussian beams”, *J. Opt. Soc. Am. A*, 3, 465-469, 1986.

Time-Harmonic Transmission of 3D Vector Fields Excited by Truncated Planar 2D Aperture Field Distributions Through Rotationally Symmetric Ogive Dielectric Layer Missile Radomes via Narrow-Waisted Gabor-Based Gaussian Beam Superposition

J. J. Maciel
Radant Technologies, Inc.
Stow, MA 01775, U.S.A.

L. B. Felsen
Boston University
Boston, MA 02215, U.S.A.

The efficient and accurate numerical calculation of wave interaction with large scale complex environments poses a major challenge in diverse forward and inverse wave propagation and scattering scenarios. It is widely acknowledged that analytic physics-based problem-matched modeling plays an important role in the construction of the relevant working algorithms. In a sequence of prototype studies, we have investigated two [1, 2] and three-dimensional (3D) [3, 4] time-harmonic electromagnetic (EM) field radiation synthesized by superposition of narrow-waisted (NW) ray-like (but without the failures of ray theory) Gaussian beams (GB) which are excited, respectively, by 1D and 2D-aperture distributions discretized via the (Gaussian-windowed) Gabor basis on an infinite lattice in the configuration(space)-spectrum(wavenumber) phase space. Using only nontilted propagating beams (tilted beams are evanescent), the NW ray-like Gabor basis, which can be conveniently modeled by the complex-source-point (CSP) method, has been shown to furnish a numerically efficient and accurate solver, via beam tracing and superposition, for interaction with complex propagation and scattering environments.

In the present paper, the NW GB algorithms are extended to tracking the 3D arbitrarily polarized fields generated by a truncated planar 2D vector aperture field distribution through polarization-sensitive reflection/transmission interactions with arbitrarily shaped 3D dielectric layers. The resulting tracking scheme is described in detail and is applied to predicting the performance of rotationally symmetric ogival ceramic missile radomes which cover 2D plane truncated apertures on gimbaled (rotatable) platforms in practical operating systems. An extensive series of numerical tests has been performed to assess the accuracy and domain of validity of the NW beam synthesis in the aperture plane $z = 0$, and away from the $z = 0$ plane in the "far zone" of the basis beams but well within the near zone of the extended aperture where the radome is located. Comparisons of power transmission and boresight error with measured data show satisfactory agreement with the analytic predictions.

REFERENCES

1. J.J. Maciel and L.B. Felsen, "Systematic study of fields due to extended apertures by Gaussian beam discretization," *IEEE Trans. Antennas Propagat.*, Vol. 37, No. 7, pp. 884-892, July 1989.
2. J.J. Maciel and L.B. Felsen, "Gaussian beam analysis of propagation from an extended plane aperture distribution through dielectric layers: Part I - Plane layer, Part II - Circular cylindrical layer," *IEEE Trans. Antennas Propagat.*, Vol. 38, No. 10, pp. 1607-1624, Oct. 1990.
3. J.J. Maciel and L.B. Felsen, "Discretized Gabor-based beam algorithm for time-harmonic radiation from two-dimensional truncated planar aperture distributions - Part I: Formulation and solution, Part II: Asymptotics and Numerical Tests," *IEEE Trans. Antennas Propagat.*, to be published, 2002.
4. J.J. Maciel and L.B. Felsen, "Gabor-based narrow-waisted Gaussian beam algorithm for transmission of aperture-excited 3D vector fields through arbitrarily shaped 3D dielectric layers," submitted to *Radio Science*, Nov. 2001.

Gabor-Based Quasi-Ray Gaussian Beam Algorithms for Scattering by Moderately Rough Surfaces

V. Galdi†, L. B. Felsen, and D. A. Castañon
Boston University
Boston, MA, U.S.A.

Gabor-based narrow-waisted (NW) Gaussian beam (GB) algorithms have emerged in the last decade as an attractive alternative to traditional high-frequency asymptotic ray methods for electromagnetic (EM) wave propagation and scattering in complex environments. In these algorithms, the excitation field is discretized self-consistently via Gabor expansions in terms of NW-GB *ray-like* basis functions, which can be tracked effectively through complex environments via *complex source point* paraxial asymptotics (*quasi-real* ray tracing), with eventual recombination at the observer. While preserving the attractive computational features of standard ray methods in the presence of *large* (on the wavelength scale) computational domains, NW-GB algorithms *do not* suffer from failures near caustics and other ray-field transition regions.

Recently, these algorithms have been applied successfully to transmission of time-harmonic three-dimensional (3D) vector EM fields (which are excited by 2D truncated planar aperture distributions) through 3D arbitrarily curved dielectric layer configurations, including those of particular interest in antenna radome design, yielding accurate, robust and computationally efficient predictions [1].

In a quite different context, we have recently succeeded in extending these methods to reflection from, and transmission through, moderately rough interfaces separating different dielectric media, both for time-harmonic and time-dependent (short pulse) excitations [2]. This problem area is of particular interest for ground penetrating radar (GPR) applications concerned with detection and classification of buried objects; in order to enhance processing of the observed data, it is important to efficiently model the distortion introduced by the twice-traversed air-ground rough interface.

This paper deals with the application of NW-GB algorithms as fast forward solvers in such inverse scattering scenarios. Two-dimensional (2D) results are reviewed for both time-harmonic and short-pulse excitations. New validations and calibrations against independently generated rigorous numerical solutions are discussed, as are the associated computational issues. Preliminary results on 3D (vector) configurations are anticipated.

REFERENCES

1. J.J. Maciel and L.B. Felsen, "Gabor-based narrow-waisted Gaussian beam algorithm for transmission of aperture-excited 3D vector fields through arbitrarily shaped 3D dielectric layers," submitted to *Radio Science*, Oct. 2001.
2. V. Galdi, L.B. Felsen, and D.A. Castañon, *IEEE Trans. Antennas Propagat.*, vol. 49, No. 9, pp. 1305-1314, Sept. 2001; ibid, "Quasi-ray Gaussian beam algorithm for short-pulse two-dimensional scattering by moderately rough dielectric interfaces," submitted to *IEEE Trans. Antennas Propagat.*, Apr. 2001.

† also with University of Sannio, Benevento, Italy

Gaussian Beams, the Time-Domain Finite-Difference Method and Geo-Acoustic Scattering from the Seafloor

R. A. Stephen
Woods Hole Oceanographic Institution
Woods Hole, MA 02543-1542, U.S.A.

Our goal is to study the physical mechanisms responsible for scattering geo-acoustic energy from the seafloor. We use Gaussian beams as the insonifying field in our two-dimensional, time-domain finite-difference (TDFD) solvers for the elastic and anelastic wave equations. Gaussian beams have these advantages: i) They give a finite size for the scattering region on the interface. ii) The incident energy is restricted to a small range of grazing angles. iii) They do not have side lobes. iv) They have a convenient mathematical expression. The major disadvantages are: i) Insonification of an interface is non-uniform. The scattered field will depend on the location of the scatterers within the beam. ii) The beams spread, so that propagation becomes an integral component of the scattering problem. A standard beam parameterization is proposed which keeps propagation effects uniform among various models so that the effects of scattering only can be compared. In continuous wave (CW) problems, for a given angle of incidence and incident amplitude threshold there will be an optimum Gaussian beam which keeps the insonified area as small as possible. For numerical solutions of pulse beams, these standard parameters provide an estimate of the smallest truncated domain necessary for a physically meaningful result. Other advantages of our TDFD approach are: i) It includes all rigidity effects in the bottom including body and interface waves. ii) It can be applied to low grazing angles. iii) Both forward and backscatter are included. iv) Multiple interactions between scatterers are included. v) Arbitrary, range-dependent topography and sub-bottom heterogeneity can be treated simultaneously. vi) Problems are scaled to wavelengths and periods so that results apply to a wide range of frequencies. vii) The method considers scattering from structures with length scales on the order of acoustic wavelengths.

Synthesis of Beam Representations of Aperture Fields in Imaging Systems Using an Orthonormal Phase-Space Basis

J. M. Arnold and J.-H. Lee
Department of Electronics and Electrical Engineering, University of Glasgow
Glasgow, G12 8LT, UK

Representation of wavefields using superpositions of beams with different centres and different directions of propagation is a very efficient method. In order to describe the effects of truncation to a finite set of beams it is necessary to have a properly formulated mathematical theory.

An arbitrary function $u(x)$ can be expanded in the Wilson basis

$$u(x) = \sum_{m \in Z} \sum_{n \in Z} U_{mn} w_{mn}(x) \tag{1}$$

with the basis functions given by

$$w_{mn}(x) = \begin{cases} \phi(x-m), & n=0 \\ \sqrt{2}\phi(x-\frac{1}{2}m)\cos(2\pi nx), \quad m+n=0\ (mod\, 2), & n \neq 0 \\ \sqrt{2}\phi(x-\frac{1}{2}m)\sin(2\pi nx), \quad m+n=1\ (mod\, 2), & n \neq 0 \end{cases} \tag{2}$$

and the mother wavelet is

$$\phi(x) = \sum_{r \in Z} \sum_{s \in Z} A_{rs} g(x - \frac{1}{2}r) \exp[2\pi isx] \tag{3}$$

with an arbitrary function $g(x)$ with sufficiently rapid decay [1]. Eq. (3) is a *frame* expansion for the function ϕ, since it oversamples the phase-space by a factor of 2. The coefficients A_{rs} are chosen so as to make the function set an orthonormal basis of the Hilbert space $L^2(\mathbf{R})$ with the usual inner product; they have been computed by Daubechies *et al.* [1] for $g = (2\nu)^{1/4} \exp[-\nu\pi x^2]$, with very good convergence properties of the terms of the series (3) as the parameter values (r, s) spread away from (0,0). It follows directly from the orthogonality that the coefficients U_{mn} are linearly related to samples of the windowed Fourier transform coefficients

$$U(m,n) = \int_{-\infty}^{\infty} u(x) g(x-m) \exp[-2\pi inx] dx. \tag{4}$$

We shall show explicitly computed examples of the application of this expansion to typical aperture distributions, in particular to some which are of geometrical optics type described by high-frequency ray-based phase and amplitude distributions [2]. In these cases, the distributions of the coefficients $U(m,n)$ and U_{mn} are strongly localised to values of (m, n) close to a Lagrange manifold, which can itself be constructed by pure geometrical optics. This property is similar to one already known for the coefficients of the discrete Gabor summation [3], but the Gabor series has some undesirable features which are not present in the Wilson basis. We consider applications of the expansion to imaging systems, and to the computation of diffraction-limited Fox-Li modes of laser resonators.

REFERENCES

1. I. Daubechies, S. Jaffard and J-L Journe, "A simple Wison orthonormal basis with exponential decay", *SIAM Jour. Math. Anal.*, Vol. 22, pp. 554-572, 1991.
2. B. Z. Steinberg, E. Heyman and L. B. Felsen, "Phase space beam summation for time harmonic radiation from large apertures", *J. Opt. Soc. Am. (A)*, Vol. 8, pp. 41-59, 1992.
3. J. M. Arnold, "Phase-space localisation in discrete representations of high-frequency wavefields", *J. Opt. Soc. Am. (A)*, Vol. 12, pp. 111-123, 1995.

A Frame Based Phase-Space Beam Summation Formulation for Wideband Radiation

A. Shlivinski, E. Heyman, A. Boag
Faculty of Engineering, Tel-Aviv University
Tel-Aviv, 69978, Israel

C. Letrou
I.N.T.
Evry, F-91011, France

Phase-space formulations are an important tool for tracking high frequency wave fields since they provide systematic framework for ray-based spectrally uniform solutions in complex configurations. Of particular interest are beam-based phase space formulations that make use of windowed configuration-spectrum transforms (e.g., the local Fourier transform in the frequency domain and the local-slant-stack-Radon transform in the time domain). An important property of these formulations is that they may be a priori discretized via the Gabor representation. Yet this representation suffers from two inherent difficulties: (a) Non-locality and instability of the expansion coefficients, and (b) the phase space beam lattice (origins and directions) varies with frequency as follows from the Gabor condition $XK = 2\pi$ where X and K are the spatial and spectral discretization step-sizes. Property (b) makes the conventional Gabor-based beam formulation inapplicable for wideband applications since it requires the tracking of different beams (with different axes) for each frequency.

In a recent paper [1], we presented a wideband frame-based beam representation that accommodates these difficulties. Using an overcomplete basis removes the Gabor constraint and adds a degree of freedom which makes it possible to use the same beam lattice for all frequencies. The overcompleteness also smoothes out the dual (analysis) function and thereby localizes and stabilizes the expansion coefficients. Using properly chosen set of iso-diffracting Gaussian-beam basis functions also provides the "snuggest" representation for all frequencies. These basis functions can also be approximately transformed in closed form into the time domain where they yield the so-called iso-diffracting pulsed beams, leading to a new frame-phase space formulation for short-pulse fields directly in the time domain [2].

This new formulation is presented here in the context of wideband radiation from a focused aperture and transmission through a radom. Emphasis is placed on analytical study of the expansion and beam parameters that render the beam representation most effective and localized. The number of phase space degrees of freedom as a function of frequency is determined, and is shown to be smaller than the Landau Pollak bound. It is shown that the frequency band for which the wideband formulation is most effective is of the order of one octave. For wider excitation bands, we introduce a specific hierarchy of frequency bands with a related set of spacial and directional discretizations that lead to a self consistent representation wherein the same beam axes are used for all the frequency bands. A time domain counterpart of the algorithm is presented in a companion paper [3].

REFERENCES

1. A. Shlivinski, E. Heyman, A. Boag, D. Lugara, and C. Letrou, "Gabor-frame phase space beam summation formulation for wideband radiation from extended apertures," *Proc. of URSI International Symposium on Electromagnetic Theory*, Victoria, Canada, May 2001, pp. 56-58.
2. A. Shlivinski, E. Heyman, A. Boag, A. Fluerasu, and C. Letrou, "A discretized-phase-space pulsed beam representation for time dependent radiation," *op cit*, 71–73.
3. A. Shlivinski, E. Heyman, A. Boag, and C. Letrou, "A discrete phase-space pulsed beam formulation for time dependent radiation from extended apertures," *This Session*.

A Discrete Phase-Space Pulsed Beam Formulation for Time Dependent Radiation from Extended Apertures

A. Shlivinski, E. Heyman, and A. Boag
Faculty of Engineering, Tel-Aviv University
Tel-Aviv, 69978, Israel

C. Letrou
I.N.T.
Evry, F-91011, France

The wideband discretized-phase-space beam summation representation introduced in the first part of this sequence [1] has several attractive features that make it amenable for an extension into the time domain (TD): (a) The same beam lattice is used for all frequencies; (b) The iso-diffracting Gaussian basis provides the "snuggest" frame representation for all frequencies; (c) The propagation parameters of the resulting beams are frequency-independent and need to be calculated only once at a reference frequency. These properties have been utilized in [3] to derive a new TD representation for radiation from extended apertures, wherein the field is expanded in a discrete lattice of shifted and tilted pulsed beam (PB) propagators. The excitation coefficients of these PBs are extracted from the aperture source distribution via the new "discretized local slant stack transform."

The theory complete the analogy between frequency domain (FD) and TD spectral representations. In the FD, the spectral framework is provided by the spatial Fourier transform and the windowed formulation may be discretized a priori via the Gabor representations or the new *frame formulation* in [1,2]. In the TD, the non-windowed formulation is based on the *slant stack transform* (SST) where the field is described as an angular spectrum of time-dependent plane waves, while the windowed approach is based on a *local-SST* comprising a phase-pace continuum of PBs that emerge from all points in the aperture and in all directions. So far there where no discretized version of the local-SST. The "missing" building block, the *discretized local-SST*, has been introduced in [3]. From a broader perspective, it is a new "discrete local Radon transform" in $\mathbf{R}^3$ that may be relevant in other disciplines, such as image processing.

This new TD formulation is further developed here. The emphasis is on an effective treatment of the time coordinate which may comprise many scales of frequencies and time. This is achieved using time-frequency discretization, such as the Gabor and the multi-resolution frames. Via this procedure the data is separated into wide bands of frequencies and for each band is then treated separately. The frequency bands then define the parameters of the spacial and spectral (directional) discretization. We determine the proper hierarchy of frequency and spacial discretizations that lead to a self consistent representation wherein the same PB axes are used for all the frequency bands. Numerical calculations of an ultra wideband focused aperture will be used to demonstrate the new concepts.

REFERENCES

1. A. Shlivinski, E. Heyman, A. Boag, and C. Letrou, "A frame-based phase-space beam summation formulation for wideband radiation," *This Session*.
2. A. Shlivinski, E. Heyman, A. Boag, D. Lugara, and C. Letrou, "Gabor-frame phase space beam summation formulation for wideband radiation from extended apertures," *Proc. of URSI International Symposium on Electromagnetic Theory*, 56–58, Victoria, Canada, May 2001.
3. A. Shlivinski, E. Heyman, A. Boag, A. Fluerasu, and C. Letrou, "A discretized-phase-space pulsed beam representation for time dependent radiation," *op cit*, 71–73.

A Beam Summation Algorithm for Fast Tracking of Wavefields in Plane Stratified Media

T. Heilpern, E. Heyman, and B. Z. Steinberg
Faculty of Engineering, Tel-Aviv University
Tel-Aviv, 69978, Israel

We present a beam summation algorithm for tracking source excited wavefields in plane stratified media, with emphasis on waves in shallow underwater environments. Ray-based algorithms may become inconvenient or even unpractical in such media due to the pile up of caustics of the multiply reflected/refracted ray fields. If the parameters of the beam basis functions (the propagators) are properly chosen, then these beams are insensitive to the caustics transition zones over large propagation ranges. Thus, since the propagators can be tracked locally using ray techniques, the beam expansion approach, when applied judiciously, combines the asymptotically uniform features of the spectral representation with the algorithmic ease of the ray representation. Furthermore, the beam representation is a priori localized in the vicinity of the Lagrange manifold (the phase space skeleton of Geometrical Optics).

Here we develop an algorithm for tracking the beam field in plane stratified medium. By approximating the medium in terms of layers with linear variation of the wave speed, we derive fast and efficient recursive algorithm for tracing the beam axes and for tracking the propagators (paraxial phase and amplitude). Using this approach we also determine the beam expansion parameters for an efficient discretization of the beam spectra.

Session 4Pa6

High-Frequency Field-to-Transmission Line Interactions

Transmission Line Models or Maxwell's Equations, Which Should You Use?

D. A. Larrabee
Physics Department, East Stroudsburg University
East Stroudsburg, PA 18301, U.S.A.

We will consider the interaction of an electromagnetic wave with a transmission line. The coupling of electromagnetic waves to transmission lines is correctly described by Maxwell's equations. The transmission line equations have been modified to include the effect of incident electromagnetic fields. It is generally assumed that the transmission line model (TLM) is accurate at low frequencies. But how low?

The transmission line model often predicts strong resonance on the line limited only by the ohmic resistance of the transmission line conductors. In such a case the line will produce a scattered electromagnetic field, taking energy out of the transmission line and limiting the peak of the current on the transmission line. This effect is not included in the traditional TLM. The strength of the effect will depend both on the wire separation distance (a) wavelength (λ), and the geometry of the line. It is generally "assumed" that the transmission line model is valid so long as $a/\lambda \ll 1$ and such scattered fields are negligible.

We will give a modified transmission line mode (MTLM) that includes the effect of the scattered electromagnetic wave and does not make the assumption that $a/\lambda \ll 1$. But rather assumes that the wire radius (r) is much smaller than a wavelength ($r/\lambda \ll 1$) [1]. This formalism allows us to compute a radiation resistance of the transmission line that is valid at low frequencies (both for the currents due to the incident electromagnetic wave as well as to signals carried by the line). The lower the transmission line's resistance the bigger this effect will become.

We will show how to solve the modified transmission line model numerically [2]. We will then compare the computational solutions of the modified and traditional models. This will allow us to examine the errors in the traditional models.

Finally, we will show how to apply this new formalism to the cross talk between two transmission lines.

REFERENCES

1. David A. Larrabee, "Interaction of an electromagnetic wave with transmission lines, including reradiation", 1998 International Symposium on Electromagnetic Compatibility, Aug. 1998, Denver CO, pp. 106-111.
2. David A. Larrabee, "Solutions of the Transmission Line Equations Modified to include Excitation by, and Reradiation of, Electromagnetic fields", 1999 International Symposium on Electromagnetic Compatibility, Aug. 1999, Seatle WA, pp. 414-416.

An Efficient Technique to Compute High Frequency Electromagnetic Field Coupling to Long Terminated Lines

S. Tkachenko
Technical University of Magdeburg
Magdeburg, Germany

F. Rachidi and M. Ianoz
Swiss Federal Institute of Technology
Lausanne, Switzerland

In this study, we present a theory for the problem of electromagnetic field coupling to a long terminated line. The theory is applicable for arbitrary line terminations and for high frequency electromagnetic field excitations, where the transmission line approximation is no longer valid. Analytical expressions are derived for the induced current along the line and at the two line terminals. The coefficients of these expressions are determined using a procedure based on the exact solutions of the integral equation for two similar line configurations, but having a significantly shorter length. In other words, the proposed method makes it possible to solve the high frequency electromagnetic field coupling to a very long line using the exact solutions for significantly shorter line configurations.

The proposed method is validated by comparing its results to exact analytical solutions obtained using NEC, and an excellent agreement is found.

The advantage of the proposed approach with respect to conventional numerical methods is that the field integral equation is to be solved only over a reduced line configuration, allowing a considerable gain in computation time and storage requirements. While the computation time and storage requirements of conventional numerical methods increase dramatically with the length of the analyzed structure (O(L^3) and O(L^2) respectively), the proposed approach makes it possible to predict the response of transmission lines to exciting electromagnetic fields in a reasonable time and using a modest memory which are practically independent of the length of the line. The method is therefore particularly efficient when considering the electromagnetic field coupling to very long lines.

On the Theory of High Frequency Electromagnetic Field Coupling to Nonuniform Terminated Lines

S. Tkachenko
Otto-von-Guericke University of Magdeburg
Institute for Fundamental Electrical Engineering and EMC
Magdeburg, 39016, Germany

F. Rachidi and M. Ianoz
Swiss Federal Institute of Technology, EPFL-DE-LRE
Lausanne, CH-1015, Switzerland

T. Steinmetz and J. Nitsch
Otto-von-Guericke University of Magdeburg
Institute for Fundamental Electrical Engineering and EMC
Magdeburg, 39016, Germany

The necessity to investigate interaction of high-frequency electromagnetic field with transmission lines is today a major issue in electromagnetic compatibility. When the wavelength of the incident electromagnetic field is comparable to or less than the cross section of the line, the classical transmission line theory (TLT) is inapplicable [1]. An effective hybrid method to obtain a closed-form approximate analytical solution for the high-frequency field (plane wave) coupling to long terminated lines was recently proposed in [2]. The method is based on a simple analytical representation for the solution of Pocklington's equation in the main part of the transmission line, enough far from the line terminals. The obtained solution contains current wave reflection coefficients from the line terminals, near which the uniformity of the line is disturbed and radiation appears.

In practice, however, line discontinuities can also appear along the line in the form of a line bend. Besides, lumped impedances and lumped voltage sources representing for example an interrupted cable shield can also be present along the line.

In the present paper, we propose a generalization of the method presented in [2] to the case of a long line containing a discontinuity (line bend or lumped impedance) in the central region. Closed-form analytical expressions are derived for line terminals reflection coefficients as well as for reflection and transmission coefficients associated with the line discontinuity.

The derived analytical expressions are compared with exact numerical results obtained using CONCEPT and a very good agreement has been found.

REFERENCES

1. Teche, F. M., M. Ianoz, and T. Karlsson, *EMC Analysis Methods and Computational Models*, John Willey and Sons, Oct. 1996.
2. Tkachenko, S., F. Rachidi, and M. Ianoz, "High-frequency electromagnetic field coupling to long terminated lines," *IEEE Transaction on Electromagnetic Compatibility*, Vol. 43, No. 2, 117–129, May 2001.

Generalized Telegrapher Equations for Radiating Nonuniform Transmission Lines

H. Haase, J. Nitsch
Institute for Fundamental Electrical Engineering and EMC, Otto-von-Guericke University
Magdebury, Germany

Nowadays, high operating frequencies of electronic equipment require the accurate knowledge of the electromagnetic behavior of the interconnection and other conducting structures. This in particular includes cables, transmission lines, three-dimensional conducting structures, traces on PCBs, and also antennas and microwave circuits. All these structures are referred to as nonuniform transmission lines. The exact analysis of such nonuniform transmission lines is a complicated procedure and usually cannot be performed analytically. Mostly, numerical methods are used to characterize these structures.

The main objective of this work is to provide a versatile "tool" for the analysis of nonuniform transmission lines and interconnection structures, which is based on generalized telegrapher equations.

In order to accomplish this a generalized transmission-line theory is proposed which is derived directly from the general solution of Maxwell's equations. It can be used to describe the wave propagation along, as well as the field coupling to those nonuniform multiconductor transmission lines. Although, the structure of the classical telegrapher equations is preserved, the generalized theory is capable to describe the intrinsic physical behavior, including radiation. This is done by redefining the per-unit-length parameters, which become not only position dependent, but also frequency dependent and complex, even for loss-less conductors. Moreover, additional per-unit-length parameters are introduced which automatically appear for nonuniform transmission lines at high frequencies. In addition the distributed sources of the telegrapher equations have to be redefined.

The per-unit-length parameters and the distributed sources are determined by the solution of two integral equations. If this solution is carried out iteratively, analytical expressions can be derived. However, these expressions involve integrals which, for the general case, cannot be solved in closed form and must be computed numerically.

Unlike the distributed sources, the per-unit-length parameters are independent from the actual excitation and thus must only be computed once for a given setup. The solution of the telegrapher equations can than be carried out very quickly.

— The Authors acknowledge the support of this work by the SUMMA-Foundation and the German Armed Forces Institute for Protection Technologies (WIS, Munster). —

Session 4Pb6

Photonic Band Gap Structures

Photonic Bandgap Planar Filters Design Based on Wave Concept

T. Garcia
Institut National Polytechnique de Toulouse (INPT), ENSEEIHT
Toulouse, 31071, France

G. Fontgalland and J. R. S. Oliveira
Centro Federal de Educação Tecnológica do Maranhão (CEFET/MA)
Department of Electronics (DEE), Microwave Laboratory and Data Communications (LMCD)
São Luís, 65.025-001, Brazil

T. P. Vuong
Institut National Polytechnique de Grenoble (INPG), ESISAR
Valence, 26902, France

H. Baudrand
Institut National Polytechnique de Toulouse (INPT), ENSEEIHT
Toulouse, 31071, France

As well known, the planar structures design has a great application in antennas, filters and scattering devices. Simply speaking, photonic bandgap filters are a class of periodic structures where a resonance peak is created by placing a defect into it. The efforts developed in recent years to efficient characterized these structures may be concentrated in the use of the traditional methods like as integral (MoM) and differential (FDTD, FEM) ones. Nevertheless, they have limitations in terms of geometry, accuracy and computing time. To overcome these restrictions an iterative method based on the wave concept is applied.

In this paper fast wave concept iterative process (FWCIP) is used to accuracy design planar filters in photonic substrates. The main features of this approach are no use of test functions and the short CPU time. The basis of the method are the definition of the incident $\mathbf{A}$ and reflected $\mathbf{B}$ waves:

$$\vec{A} = \frac{1}{2\sqrt{Z_0}}(\vec{E} + Z_0\vec{J}) \qquad \vec{B} = \frac{1}{2\sqrt{Z_0}}(\vec{E} - Z_0\vec{J}), \qquad \vec{J} = \vec{H} \times \hat{n}. \tag{1}$$

$\vec{E}$ and $\vec{H}$ are the electric and magnetic tangential fields. The waves are defined in the spatial and spectral domains. The boundary conditions of each region (metal and dielectric) and the continuity law are used to define the operators for the spatial domain. The spectral operator is written as a modes function. Once identified the operators at discontinuities plans, the iterative process begins with the definition of the waves $\mathbf{B}$ in the spatial domain. With the help of the Fast Fourier Transform (FFT) we obtain $\mathbf{B}$ in a spectral domain. The relation between $\mathbf{A}$ and $\mathbf{B}$ permit to calculate $\mathbf{A}$. By applying the inverse FFT (IFFT) $\mathbf{A}$ in a spatial domain is determined. At this point a new iteration may be implemented, if the convergence of the impedance is not attended.

The first results were obtained for a planar filter built over substrate formed by a periodic cylindrical metal posts. The simulation and experimental results are very comfortable. A new compact photonic planar filter is designed and our simulation for the filter unit cell is compared with the commercial software (Sonnet). The S parameters results are agreed.

Analysis of Fundamental Properties of Air-Hole Type Photonic Crystal Waveguide Having Sharp Bend on Uni-Axial Anisotropic Substrate

H. Satoh, N. Yoshida, and Y. Miyanaga
Division of Electronics and Information Engineering, Graduate School of Engineering, Hokkaido University
Sapporo, Japan

By use of the stop band characteristics based on the PBG in the photonic crystal which eliminates the propagation of the light wave in the specified wavelength range, it has become possible to produce the microscopic structure devices including the sharp bend with the same order of a wavelength. Due to the fine structure in those devices, the simulation is indispensable to grasp and predict the properties of those devices. So far, many analyses by FDTD and BPM have been performed.

Authors have already proposed the "Condensed Node Spatial Network for Vector Potential" that is an analysis method for the time-dependent electromagnetic fields, and has many advantages on treating various medium conditions and complicated structure models. By using this method, we have presented the dispersive propagation properties in the photonic crystal waveguide with the Lorentz-type dispersive medium, and the SHG (second-harmonic generation) characteristics in the waveguide with second-order non-linear medium, respectively [1, 2].

In various medium conditions, it is known that the anisotropy has large influences on the propagation characteristics and has been also utilized in optical and electronics devices. Recently, the air-hole type photonic crystal waveguide has been noticed for its easy fabrication than that for the pillar type one. But in this type photonic crystal waveguide, it is considered that the anisotropy of the substrate affects directly the propagation property. In the photonic crystal waveguide, the 90[deg] bend is important element to construct the fine structure devices and many studies has been performed and presented. But for the air-hole type, improvement of the performance of the bend is known not to be easy due to its complicated propagation mechanism based on both diffraction and reflection.

In this paper, after introducing the equivalent circuit treatment of uni-axial anisotropy by the mutual coupling capacitances in the condensed node spatial network for vector potential, we show the fundamental properties of air-hole type photonic crystal waveguide on the uni-axial anisotropic substrate, and present the improvement of the bend performance by changing the optical angles corresponding to control of the direction of the wave front.

REFERENCES

1. H. Satoh, N. Yoshida, and Y. Miyanaga, "Unified analyses of photonic crystal waveguide with various medium conditions by condensed node spatial network for vector potential," *Proc. PIERS 2001*, 101, July 2001.
2. H. Satoh, N. Yoshida, and Y. Miyanaga, "Analysis of fundamental properties of 2-D photonic crystal optical waveguide with various medium conditions by condensed node spatial network," *Trans. IEICE Japan*, Vol. J84-C, No. 10, 954–963, Oct. 2001 (in Japanese).

Numerical Analysis of Single-Periodic Dielectric Structures

J. Tausch
Department of Mathematics, Southern Methodist University
Dallas, TX 75275, U.S.A.

The field of a characteristic mode Ψ traveling through a periodic structure is described by Floquet's theorem. It states that

$$\Psi(\mathbf{x}) = \exp(\gamma \cdot \mathbf{x})\,\Phi(\mathbf{x}) \tag{1}$$

where Φ is periodic in z and γ is the propagation factor. To find the propagation factors for a given structure, (1) is substituted into Maxwell's equations. This results in a linear eigenvalue problem for γ on a unit cell of the period. For double-periodic domains, such as 2-D photonic crystals, the unit cell is a bounded domain and thus standard finite-element discretizations can be used to solve the eigenvalue problem to obtain the propagation factors.

This talk discusses a new numerical method for single-periodic structures, such as corrugated dielectric waveguides. In this case the periodic cell is an infinite strip, which is composed of several stratified and typically one corrugated layer, furthermore, two semi-infinite homogeneous layers, corresponding to the super- and substrate regions. In addition to radiating and propagating modes, leaky modes are possible because of the infinite geometry.

To determine the eigensolutions numerically, the strip is decomposed into an interior domain containing the non-homogeneous materials, and two exterior, semi-infinite domains. A solution of the interior domain and a solution of the exterior domain combine to a solution on the whole strip, if the field and its normal derivatives are continuous across the interfaces. Therefore a value of γ is a propagation factor if the Dirichlet-to-Neumann (DtN) operators corresponding to the interior and exterior domain match. Thus the problem on the infinite strip is reduced to an eigenvalue problem posed on the interfaces of the interior and exterior domains. Since the DtN operator depends non-linearly on γ, a Newton scheme must be employed to find the propagation modes.

Numerical results, based on discretizing the DtN operator, will be presented. They demonstrate that this approach is efficient and highly accurate. This talk presents an extension of the work which will appear in [1].

REFERENCES

1. J. Tausch and J. Butler "Efficient Analysis of Periodic Dielectric Waveguides using Dirichlet-to-Neumann Maps". SMU Mathematics Preprint 2001-01, to appear in JOSA-A.

Microwave Scattering from Macroscopic Gratings

R. D. Bardo, E. C. Fischer, A. J. Stoyanov, and H. Überall
Naval Surface Warfare Center
West Bethesda, MD, U.S.A.

Microwaves can exhibit Bragg diffraction effects when their wavelength becomes shorter than the spacing of grooves in a macroscopic grating of parallel grooves or ridges. For spacings of the order of a few centimeters, these effects will appear at about 10 GHz or above, or at lower frequencies if the incidence is closer to grazing. We study these diffraction phenomena for a general (3D) incidence of the microwave beam, both regarding their geometry, and regarding their intensity, using certain simple scattering approximations for the latter purpose.

First, we derive the Bragg scattering geometry for arbitrary (3D) incidence on a grating, which cannot be found in textbooks. The Bragg effects are studied for a specific model consisting of a large series of parallel grooves in a conducting plane, of a width of several centimeters, interspersed by parallel ridges several millimeters wide. For the grooves, standard optical Bragg theory is applicable here (Born and Wolf, Principles of Optics, 1999) and for incident microwaves of 12 or more GHz, Bragg peaks are found at $8°$ onwards (measured from the specular reflection direction at $10°$ incident grazing angles, e.g.). Note our viewpoint differs from that of recent work on groove scattering (Skigin et al., IEEE Trans. AP 47, 376, 1999) where only normal incidence was considered. The ridge scattering intensities are found from radar scattering theory (Ruck et al., Radar Cross Section Handbook, 1970), and it is seen that with increasing Bragg angles, ridge scattering increases and eventually surpasses the groove scattering intensities.

Analysis of Electromagnetic Scattering from Frequency Selective Surfaces with Anisotropic Dielectric Multilayers

A. L. P. S. Campos
Department of Electrical Engineering, Federal University of Paraíba
Campina Grande, PB 58109-970, Brazil

A. G. d'Assunção
Department of Electrical Engineering, Federal University of Rio Grande do Norte
Natal, RN 59072-970, Brazil

This work presents a theoretical analysis and experimental/numerical results for the scattering characteristics of frequency selective surfaces (FSS) using perfect conducting patches. The structures are composed by anisotropic dielectric substrates. The analysis is developed using the equivalent transmission line approach in combination with the Galerkin method to determine the transmission and reflection characteristics.

Furthermore, the analysis uses the equivalent transmission line approach which allows to model the structure as an equivalent circuit and, applying the transmission line theory, to determine the dyadic Green's function. This function relates the incident fields with the surface current densities. These fields are determined by the incident potentials by imposing the field continuity at the dielectric interfaces.

The Galerkin method is used, allowing the numerical determination of the unknown weighting coefficients and, as a consequence, the current surface densities that are expanded in terms of the known basis functions multiplied by the weighting coefficients. The determination of these functions allows the determination of the scattered fields on the top and bottom of the structure and, consequently, the determination of the transmission and reflection characteristics of these structures.

Three different types of conducting patch geometries are assumed. In addition, uniaxial anisotropic dielectric layers are considered and the optical axes are considered to be in the direction perpendicular to the dielectric interfaces.

Therefore, numerical and experimental results are presented for the reflection and transmission characteristics, such as scattering parameters, of several FSS structures with anisotropic multilayers. Thereafter, our results were compared to those available in the literature for several types of FSS structures with isotropic layers. A good agreement was observed for this particular case of our analysis.

Furthermore, it was observed that the use of anisotropic substrates increases the design flexibility of FSS structures with dielectric layers. This can be useful in developing wideband microwave filters, for instance.

Session 4Pc7

Plasmon Optics for Near Field Microscopy, Lithography and Data Storage

The One-Sided Near-Perfect Lens

S. Anantha Ramakrishna and J. B. Pendry
Imperial College
London, UK

D. Schurig, D. R. Smith, and S. Schultz
University of California
San Diego, CA, U.S.A.

It has been shown recently that a slab of negative refractive material focuses the near-field evanescent waves of a source in addition to the propagating radiative components, and hence, has been termed a *perfect lens*. Thus the diffraction limit on the resolution in conventional imaging can be overcome. The near-field evanescent components need to be effectively amplified inside the slab to restore their amplitudes, and this happens provided the perfect-lens condition, $\epsilon_s = -\epsilon_1$, and $\mu_s = -\mu_1$ (where ϵ_s and μ_s are the dielectric permittivity and the magnetic permeability of the slab medium respectively and ϵ_1 and μ_1 are the dielectric permittivity and the magnetic permeability of the outside medium (air) respectively), is met.

Subsequently, we have been able to show that a slab of negative refractive index imbedded between two media of different (positive) refractive index also behaves as a near-perfect lens whose performance is limited by only the effects of absorption and retardation. It is only necessary that the perfect-lens conditions, which are also the conditions for the existence of a surface mode, are met at *one* of the interfaces. We examine the role of the surface states in the amplification of the evanescent waves. We have shown that the asymmetry can be used to enhance the resolution of the lens against the effects of absorption in the slab. In particular, we examined for P-polarsied light the case of a negative dielectric lens consisting of a slab of silver with air on one side and any other dielectric medium on the other. We found that retardation effects due to a finite frequency of light and the mismatch in the magnetic permeability ($\mu = 1$ everywhere) limit the image resolution severely, and also results in the excitation of slab resonances that degrade the performance of the lens. Absorption alleviates the effects of the sharp resonances to some extent, and indeed, is vital to the imaging itself.

We have shown that sub-wavelength imaging at optical frequencies ($\hbar\omega \approx 2.0eV$) is possible by our asymmetric lens consisting of a slab of silver bounded by air on one side and silicon or GaAs on the other, and we obtain a spatial resolution of about 60-70 nm with this system. The possibility of having a medium to support a thin film of silver permits the construction of a nanoscopic mechanically rugged lens for optical near-field imaging. It also admits the possibility of an integrated detection system by placing, for example, an array of quantum dots at the image plane inside the GaAs.

The Role of Surface Plasmons in the Enhancement of Light Transmission Through Sub-Wavelength Apertures

R. A. Linke, A. Nahata, K. M. Pellerin and T. Thio
NEC Research Institute
Princeton, NJ 08540, U.S.A.

T. W. Ebbesen and H. J. Lezec
ISIS, Université Louis Pasteur
Strasbourg, France

It has recently been demonstrated that the optical power transmitted through a single sub-wavelength diameter aperture in a metal film with periodic surface patterning can be orders of magnitude larger than the corresponding case with no patterning. Explanations of these observations involving surface plasmon polariton (SPP) resonances have been advanced. The effect has implications for near field microscopy, optical data storage, and other applications where the attainment of high field intensities over sub-wavelength dimensions provides an advantage. In this talk, we discuss experimental results for transmission through holes in thin metal films, both with and without patterning, together with numerical finite-difference time-domain (FDTD) simulations in an effort to understand the role of the surface plasmons and to quantify the maximum gain that may be expected from this effect.

In order to understand the improvement in transmission that may be possible using SP resonant enhancement it is necessary to first understand the transmission through sub-wavelength apertures in smooth metal films. This case has been treated theoretically by Bethe, Bouwkamp, and others. In these treatments, however, three simplifying assumptions are made: (1) that the aperture is very much smaller than the wavelength, (2) that the metal film is infinitely thin, and (3) that the metal is ideal. Unfortunately, in real experimental situations, none of these assumptions is justified and experimental results typically deviate significantly from the theoretical predictions as a result.

In order to clarify this situation for the attainable case of real metals, finite thickness films, and apertures in the range of $\lambda/3$ to $\lambda/20$, we have prepared samples of silver films of various thicknesses with holes of various diameters both with and without patterning to achieve SPP resonances. We measure transmission as a function of wavelength and compare the results with FDTD solutions of Maxwells equations for the same structures.

Surface Plasmon Enhanced Illumination and its Applications

P. Stark, and D. Larson
Harvard Medical School
Boston, MA, U.S.A.

Previous attempts to create sources of light well below the Rayleigh criterion led to the development of Near-field Scanning Optical Microscopy (NSOM). A major limitation of NSOM is that the emitted light is evanescent and of very low transmission fractions, both of which severely limit its utility in applications where both resolution and power are required (e.g. photolithography). An improvement on NSOM was made by Ebbesen[1] who demonstrated unexpected levels of emission from monometallic arrays with periodic perforations. While the transmission levels are adequate for photolithography, the existence of a prolate pattern[2,3] results in resolution that is incompatible with the needs of applications where resolution is an important criterion.

A technology that eliminates the prolate pattern and delivers resolution at power levels that has great promise in applications where resolution is important has been investigated. These applications include microscopy, high-density optical data storage, and photolithography. SPEI is a technology for producing small bright nanometric light sources from apertures that are smaller than the wavelength of the emitted light. In this technique, light hitting the top surface of a composite array of apertures excites surface plasmons (electron density fluctuations) in the top metal surface layer. This energy couples through the apertures to the bottom, and is emitted as propagating light from the apertures or the rims of the apertures.

Arrays of apertures with 50nm diameter, emitting 15.3% of the incident light with a severely diminished prolate pattern have been demonstrated. Current work is focused on developing the microscopy application and advancing the core SPEI technology. In this talk the basic physics of SPEI will be presented as well as a discussion of the applications of the technology.

REFERENCES

1. Ebbesen, T. W., Lezec, H. J., Ghaemi, H. F., Thio, T. and Wolff, P. A. “Extraordinary optical transmission through sub-wavelength hole arrays.” *Nature* **391**, 667-669 (1998).
2. Sönnichsen, C., Duch, A. C., Steininger, G., Koch, M. and Plessen, G. v. “Launching surface plasmons into nanoholes in metal films.” *App. Phys. Lett.* **76**, 140-142 (2000).
3. Wannemacher, R. “Plasmon-supported transmission of light through nanometric holes in metallic thin films.” *Optics Communications* **195**, 107-118 (2001).

Breaking the Diffraction Limit for Optical Nanolithography using Plasmon Optics

O. J. F. Martin and M. Paulus
Electromagnetic Fields and Microwave Electronics Laboratory
Zurich, ETH-Zentrum 8092, Switzerland

Evanescent fields have the exciting property of not being bound to the wavelength of radiation. Their physical localization is therefore only determined by the extension of the scatterer used to generate them. In principle, an evanescent field can therefore be concentrated at the vicinity of an infinitely small volume. Unfortunately, the magnitude of such an evanescent field also depends on the scatterer volume. For near-field lithography, the utilization of evanescent fields is therefore limited by the tradeoff between the very small structures that one would like to replicate and the strong enough field required to expose the photoresist.

In this contribution, we propose to use the near-field associated with the plasmons excited in metallic particles. This near-field can be several orders of magnitudes stronger than that generated by scattering at a small dielectric defect. Our technique relies on the utilization of light-coupling masks with embedded metallic elements [1]. These masks based on structured organic polymers make conformal contact with a substrate and constitute an amplitude mask for nanolithography. By incorporating metallic elements in the polymer, we can define strongly localized electromagnetic fields, which allow the replication of structures much smaller than the wavelength of illumination.

To optimize this new approach to optical nanolithography, we present a series of simulations based on the Green's tensor technique, which incorporate the different mask elements in a fully vectorial three-dimensional model [2]. The ultimate resolution that can be achieved with this technique, as well as crosstalks effects and the possibility of simultaneously exposing small and large structures with the same mask are investigated.

REFERENCES

1. H. Schmid, H. Biebuyck, B. Michel and O.J.F. Martin, "Light-coupling masks for lensless, sub-wavelength optical lithography," Appl. Phys. Lett 72, 2379-2381 (1998).
2. M. Paulus and O.J.F. Martin, "Light propagation and scattering in stratified media: A Green's tensor approach," J. Opt. Soc. Am. A 18, 854-861 (2001).

Surface-Plasmon-Mediated Effects in Near Field Photolithography

R. J. Blaikie and S. J. McNab
Department of Electrical and Electronic Engineering
University of Canterbury
Christchurch, New Zealand

A number of group have been exploring low cost, high throughput near field photolithography techniques with nanometre-scale resolution [1–3]. Experimental demonstration of printing and pattern transfer below 100 nm has been achieved, and simulation studies predict that resolution down to 10 nm should be possible [4]. By working in the evanescent near field region the role of surface plasmons on the mask and substrate materials becomes critical in the image formation process, and there is great potential to utilize surface-plasmon-mediated effects to enhance exposure field strengths or improve resolution.

In this paper, simulation results will be presented for three surface-plasmon-mediated improvements for near field photolithography. The first is Evanescent Interferometric Lithography [5], a technique for spatial frequency doubling of periodic or quasi-periodic structures. This differs from conventional interferometric lithography in that the interfering diffracting orders are evanescent, which limits the depth of field of the resulting exposure. However, by operating at a wavelength resonant with a surface plasmon mode on the periodic mask structure, significant intensity enhancements can be achieved. The combination of mask material and structure period is critical for determining the resonant wavelength and the resultant enhanced intensity profiles — examples will be discussed.

The second is based on a recent proposal [6] that sub-diffraction-limited optical resolution can be achieved with a near field 'perfect lens' (PL) — a planar slab of metal illumined near the plasma frequency, where the real part of the permittivity is negative. The addition of a PL below a contact mask should allow near field *proximity* optical lithography with sub-diffraction-limited resolution, with relaxed mask-substrate contact conditions. Multiple multipole (MMP) simulations will be pesented for a 40 nm thick planar silver PL layer illuminated at around 340 nm. Images of gratings with periods below 100 nm can be formed beneath the PL, but the image intensity and position are affected by the loss in the silver PL layer, the grating period, Grating duty cycle and surrounding refractive index.

The third technique that will be described is Surface Plasmon Enhanced Contact Lithography (SPECL). In this case a contact mask and photoresist are in intimate contact, and it is proposed to use surface plasmons excited in a metal film immediately *beneath* the photoresist layer to enhance the near field image of the mask. MMP and Finite Difference Time Domain (FDTD) simulation results will be presented to show the improved resist profiles and increased depth of field that are expected using SPECL, and practical implementation issues will be discussed.

REFERENCES

1. Schmid, H., et al., *Appl. Phys. Lett.,* Vol. 72, 2379, 1998.
2. Alkaisi, M. M., et al., *Appl. Phys. Lett.*, Vol. 75, 3560, 1999.
3. Goodberlet, J. G., *Appl. Phys Lett.*, Vol. 76, 667, 2000.
4. McNab, S. J. and R. J. Blaikie, *Appl. Opt.,* Vol. 39, 20, 2000.
5. Blaikie, R. J. and S. J. McNab, *Appl. Opt.,* Vol. 40, 1692, 2001.
6. Pendry, J. B., *Phys. Rev. Lett.,* Vol. 85, 3966, 2000.

Plasmon Optics in High-Density Data Storage Media

T. Fukaya, J. Tominaga
Laboratory for Advanced Optical Technology
National Institute of Advanced Industrial Science and Technology (AIST)
Tsukuba, Ibaraki 305-8562, Japan

A super-resolution near-field structure (super-RENS) has an additional mask layer in the usual phase change optical disk. A thin layer of antimony (Sb) film or a silver oxide (AgOx) layer is used as a mask layer. By focusing a laser beam, a transparent aperture in Sb layer and a light scattering center in AgOx layer are formed transitionally, whose diameters are smaller than that of the laser beam spot. The changed portion can generate an intense optical near field and can be used to record and retrieve small marks beyond the diffraction limit. The nonlinear optical properties of Sb and AgOx films with protective layers were examined using a pulse laser. Optical switching, their time response and transient spectroscopic change were investigated. Light scattering property of AgOx film was also examined. A repeated optical switching action can only be realized if the illuminating spot size is confined to very small areas. Time response of Sb film shows first rise-up and then slow exponential decay. Time response of AgOx film shows more complicated decay than Sb film. Transmittance spectra just after the pump irradiation becomes flat over wide spectral range both in Sb and AgOx layers. Scattered light is extremely enhanced by increasing the input light power. From the aperture edge of the Sb film and also from the edge of the Ag particle, extremely large optical near field is expected to induce. These enhanced near field intensities are estimated to be few tens times as large as the input light intensity. We will discuss how the near field transfers to the recording material and how the recorded information can retrieve by using near field plasmon optics.

Localized Surface Plasmon Resonances in Periodic and Random Metallic Nanostructures

W.-C. Liu
Department of Physics, National Taiwan Normal University
Taipei, 11650, Taiwan

D.-P. Tsai
Department of Physics, National Taiwan Normal University
Taipei, 10617, Taiwan

Surface plasmon resonances in periodic and random metallic structures were studied with finite-difference time-domain (FDTD) simulations. Enhanced local fields and surface plasmons were found around rough metal interfaces and photo-dissociated nano-size silver particles. With periodical structures, there are two distinguishable modes - surface plasmon polaritons and localized surface plasmons associated with different periods. The surface plasmon polaritons have global, extended near-field distributions. Large phase-lag and time-delay, as well as high effective index of refraction, presented distinguished features of sharp resonances of the surface plasmon polaritons. On the other hand, the localized surface plasmons are highly concentrated around the nano-structures. For randomly distributed nanostructures, the localized surface plasmons are the predominate resonances with incident light. Randomly-distributed nano-size silver particles existed in the super-resolution near-field structure [1], which could generate optical near-field effects without a probe. Our simulations showed that clusters of the silver nanoparticles exhibited enhanced local fields and localized surface plasmons resonances with increasing particle densities. The density of the silver nanoparticles, which were generated by photo-dissociated process, corresponded to the intensity of incident light. Near-field images from a near-field scanning optical microscope confirmed that the excitations of surface plasmon could be controlled by incident intensities [2]. The controllability of the enhanced evanescent field provide a practical tool to manipulate and localize light in subwavelength scale. We also demonstrated the dynamical processes of surface plasmon coupling and importance of localized surface plasmons to transfer the evanescent waves from the subwavelength structures into propagating waves. Our research has significant implications on applications on near-field optical storages, near-field sensors, and nanophotonics.

REFERENCES

1. Tominaga, J., T. Nakano, and N. Atoda, *Appl. Phys. Lett.*, Vol. 73, 2078, 1998; H. Fukaya, D. Buechel, S. Shinbori, J. Tominaga, N. Atoda, D. P. Tsai, and W. C. Lin, *J. Appl. Phys.*, Vol. 89, 6139, 2001.
2. Tsai, D. P. and W. C. Lin, *Appl. Phys. Lett.*, Vol. 77, 1413, 2000; W.-C. Liu, C.-Y. Wen, K.-H. Chen, W. C. Lin, and D. P. Tsai, *Appl. Phys. Lett.*, Vol. 78, 685, 2001.

Study of Grating Field in the Presence of Negative Index Materials

B. K. Minhas
Department of Electrical and Computer Engineering
University of New Mexico
Albuquerque, NM 87131, U.S.A.

S. R. J. Brueck and K. J. Malloy
Center for High Technology Materials
Albuquerque, NM 87106, U.S.A.

Recently Pendry [1] has shown that a slab of negative index material can behave as a 'perfect lens' for the special case of $\varepsilon = -1$, $\mu = -1$. Extrapolating from that he has also demonstrated that in the quasistatic approximation, a slab of silver can be used to produce a perfect image. All his calculations are done for the case of homogeneous slab.

In this paper we verify Pendry's calculation by carrying out vector diffraction modeling of metallic sub-wavelength grating in the presence of a homogeneous slab having $\varepsilon < 0$ and $\mu < 0$. We modify rigorous coupled wave analysis (RCWA) [2] to study the field of metallic grating near a negative index slab and show using Maxwell's equation and appropriate boundary conditions that the grating field can indeed be perfectly imaged by this slab for the special case of $\varepsilon = -1$, $\mu = -1$. We also study the near field of the grating as the real part of ε and μ are varied in all the four quadrants. Furthermore the effects on the grating field as ε becomes complex are also presented.

REFERENCES

1. Pendry, J. B., "Negative Refraction makes a perfect lens," *Physical Review Letters*, Vol. 85, No. 18, 3966–3969.
2. Moharam, M. G. et al., "Formulation for stable and efficient implementation of the rigorous coupled — wave analysis of binary gratings," *Journal of the Optical Society of America A*, Vol. 12, No. 5, 1068–1076, May 1995.

Plasmon Printing – Pattern Replication at the Nanoscale Using Visible Light

P. G. Kik, S. A. Maier, and H. A. Atwater
California Institute of Technology
Pasadena, CA 91125, U.S.A.

We have recently proposed a new approach to optical lithography that could be used to print patterns with feature sizes below 50 nm using conventional photoresists.1 The method relies on the plasmon resonance occurring in nanoscale metallic particles. Metal nanoparticles exhibit a collective electron oscillation (surface plasmon) when placed in an optical field. This oscillation can be excited resonantly, producing a strongly enhanced dipole field around the particle. We have shown that this enhanced near field can be used to locally expose a thin resist layer.

In this talk, we show that 30 nm diameter silver nanoparticles in contact with photoresist can be resonantly excited using p-polarized 410 nm light. Using Finite Difference Time Domain (FDTD) simulations we show that broad beam illumination produces an enhanced local intensity directly below the particle, resulting in enhanced exposure in an area 20 nm in diameter (0.05 1) and extending to a depth of 15 nm in the resist. The optimum illumination wavelength coincides with the high sensitivity region of standard g-line photoresist.

Experiments were performed using silver nanoparticles deposited onto 75 nm thick g-line resist layers. The samples were exposed at various times using 410 nm light and subsequently developed. Atomic Force Microscopy on these samples reveals nanoscale depressions in exposed resist layers coated with Ag particles, providing evidence for plasmon-enhanced resist exposure. We will discuss potential applications as well as some limitations of the technique.

REFERENCES

1. Kik, P. G., S. A. Maier, and H. A. Atwater, “Plasmon Printing — a new approach to near field lithography,” *Nanopatterning — from Ultralarge-Scale Integration to Biotechnology*, Mat. Res. Soc. Proc., Boston, 2001.

Streamlines of the Poynting Vector under Subwavelength Conditions

L. Solymar and E. Shamonina
Department of Engineering Science, University of Oxford
Oxford, OX1 3PJ, UK

P. Stavrinou
Imperial College of Science, Technology and Medicine
London, SW7 2BZ, UK

There is no doubt that the Poynting vector can come to the aid of physical intuition. It is for example easy to appreciate the transmission properties of a hollow metallic waveguide by regarding the useful power as flowing inside the waveguide whereas losses are due to the component of the Poynting vector flowing into the walls. However the Poynting vector is deemed to be less useful in problems where the spatial dimensions of interest are small relative to the wavelength. We believe this not to be the case and, in fact, at frequencies where neither the wave nor the ray concepts are of any use the Poynting vector may still guide physical intuition as will be shown in the following examples.

(1) Plane wave incident upon a mismatched electrically short receiving dipole. By considering the incident and reradiated fields the streamlines of the Poynting vector ending upon or passing by the short dipole are presented. The effective aperture, defined by the streamlines reaching the dipole, is shown to decline as the mismatch increases.

(2) Subwavelength imaging by negative permittivity multi-layers. The Poynting vector is shown to converge upon the image by expanding in the positive permittivity and contracting in the negative permittivity layers.

(3) Movement of power through a 2D periodic array of slits in a metallic grating at optical wavelengths. Two resonances (the waveguide resonance and the Surface Plasmon resonance) are compared and contrasted based on the way how the streamlines of the Poynting vector behave in front of the grating, inside the slit, and behind the grating.

Subwavelength Imaging by a Negative Permittivity Material: Effect of Terminal Losses on Image Fidelity

E. Shamonina and L. Solymar
Department of Engineering Science, University of Oxford
Oxford, OX1 3PJ, UK

It was claimed [1] that perfect imaging is possible by a slab of lossless material exhibiting negative permittivity. A little later [2] it was pointed out that although perfect imaging under those conditions is not possible one can still achieve near-perfect imaging by employing multi-layers. If losses are present they can lead to further deterioration of the image. The role of the losses is particularly relevant when the image needs to deliver power, e.g., the electric field needs to excite electrons in a photoresist. The effect of a lossy material, so positioned, upon the fidelity of reproduction of the image is the main subject of the present paper. In our model the layer (or layers) of negative permittivity are lossless and loss is introduced only in the narrow region in which the image appears. Since imaging can be described in terms of the movement of power [2] we study the effect of this loss mechanism upon the streamlines of the Poynting vector, and show that they become more and more distorted as losses increase and that is closely correlated with the degradation of the image.

REFERENCES

1. Pendry, J. B., "Negative refraction makes a perfect lens," *Phys. Rev. Lett.*, Vol. 85, 3966–3969, 2000.
2. Shamonina, E., V. A. Kalinin, K. H. Ringhofer, and L. Solymar, "Imaging, compression and Poynting vector streamlines for negative permittivity materials," *Electron. Lett.*, Vol. 37, 1243–1244, 2001.

Session 4Pa8

Novel Methods in Electromagnetic Microgravity, Breaking, Ferromagnetism, and Superconductivity

Breaking of Randomly Dropped Axially Symmetrical Cylindrical Small Particles by Magnetic Ring

T. Sengor
Faculty of Electrical and Electronics Engineering, Yildiz Tech. University
Istanbul, 80750, Turkey

The dropping materials have some specific roles during some unexpected and/or unwanted conditions. We may count meteorites, missiles, rockets, discharge of firearms and more. Some examples may be count in MHD, fluid mechanics and some melting treatments. We may see such dropped things in some medical measuring processes and ballistic charge transport in FETs, too. If we consider the first group of above the breaking of such materials occurs important for defense research studies. The purpose of this paper is discuss the magnetic breaking processes and obtain the principles suitable to apply the all cases in above examples.

We consider an electric current loop I at $z = 0$ plane. A pec cylindrical cavity having length h and radius b is freely falling along the z axis with an initial velocity v_0 (see Fig. 1).

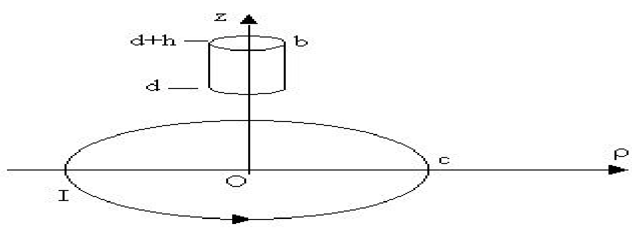

Figure 1: Falling cavity in magnetic field.

This configuration is a sample of material having time dependent and frequency varying (TDFV) and/or time varying and frequency dependent (TVFD) characteristics. The conductivity is $\sigma = \infty$ if $0 < \rho < b$ on $z = d - v_0 t - (1/2)gt^2$ and/or $z = d - v_0 t - (1/2)gt^2 + h$ and if $d - v_0 t - (1/2)gt^2 < z < d - v_0 t - (1/2)gt^2 + h$ on $\rho = b$. The conductivity is $\sigma = 0$ except these points. The environ is free space. The electromagnetic field and magnetic force on cavity supply the following equations where the tilde ($\sim$) and bar ($\_$) illustrate suitable Fourier transforms [1]:

$$\Delta \underline{H} + (-i\tilde{\omega}\tilde{\varepsilon} - \tilde{\sigma}) * \left[(i\tilde{\omega})(\tilde{\mu} * \tilde{H}) \right] = -rot\underline{J}^e - grad\left[(\tilde{\sigma} + i\tilde{\omega}\tilde{\varepsilon}) \otimes \tilde{E} \right] \quad (1)$$

$$F_z^M(\zeta;t) = \mu_0 \int_{\phi=0}^{2\pi} d\phi \int_{\rho=0}^{b} \left\{ [H_\rho(\rho,\phi,\gamma(z_{00};t);)]^2 - [H_\rho(\rho,\phi,\gamma(z_{00}+h;t);t)]^2 \right\} \rho d\rho +$$
$$\mu_0 b \int_{\phi=0}^{2\pi} d\phi \left\{ \int_{\zeta=Z_{00}}^{z_{00}+h} [H_z(b,\phi,\gamma(\zeta;t);t)]^2 d\zeta - \int_{t1}^{t_2} (v_0 + gt) [H_z(b,\phi,\gamma(\zeta;t);t)]^2 dt \right\} \quad (2)$$

Here we put $\gamma(\zeta;t) = \zeta - v_0 t - (1/2)gt^2$. The breaking condition is $R_n F_z^M - mg \le F_z^B$ where R_n, F_z^B, m and g are random density function, expected falling force, mass of the cavity and acceleration of gravity, respectively.

REFERENCES

1. Sengor, T., "Wave equation and solution in time varying and frequency dependent medium: circularly cylindrical case," *Helsinki Univ. Tech. Electromagnetics Lab. Rept.* 349, Jan 2001.

Strong-Coupling Superconductivity in Cuprates and Related Compounds

A. S. Alexandrov
Quantum Structures and Phase Transitions Group, Loughborough University
Loughborough, UK

Over the last decade several competing models of high-temperature superconductivity were proposed most of them with short-range interactions. We propose a more realistic ‘Froehlich-Coulomb’ model with strong on-site repulsive correlations, the Coulomb and strong infinite-range electron-phonon interactions [1–3]. Depending on the ratio of the inter-site Coulomb repulsion and the polaronic (Franc-Condon) level shift the ground state of the model is a polaronic Fermi (or Luttinger) liquid, bipolaronic conductor, or charge-segregate insulator for the strong, intermediate, and weak Coulomb repulsion, respectively. The phase diagram of the model is analyzed for a zig-zag ladder and the perovskite layer[3]. Charge carriers in those structures are superlight mobile inter-site bipolarons. They propagate coherently with about the same mass as single polarons. The model describes key features of the cuprates, in particular their to values, different isotope effects, normal state diamagnetism, pseudogap, spectral functions measured in tunnelling and photoemission, and different symmetries of the order parameter and gap. A parameter-free estimate of the Fermi energy of quasi-two-dimensional high -Tc superconductors [4] yields a very low value c.a. 100 meV or less, justifying our approach. We argue that the low Fermi energy and strong coupling of carriers with high-frequency phonons is the cause of high -Tc.

REFERENCES

1. Alexandrov, A. S., in “Lectures on the physics of highly correlated electron systems,” V. ed. F. Mancini, *(American institute of Physics, Melville, New York, 2001).* p 1.
2. Alexandrov, A. S., *Phys. Rev.*, Vol. 53, 2863, 1996. Alexandrov, A. S., and P. E. Kornilovitch, *Phys. Rev. Lett*, Vol. 82, 807, 1999.
3. Alexandrov49 Alexandrov, A. S., and P. E. Kornilovitch, cond-mat/0111549.
4. Alexandrov, A. S., *Physica C*, Vol. 363, 231, 2001.

Electromagnetic Analysis of a Cavity with Moving Wall under the Influence of an External Gravitational Field

M. H. Marçal
Centro de Electrodinâmica, Instituto Superior Técnico (IST)
Universidade Técnica de Lisboa (UTL)
Lisboa, 1049-001, Portugal

A simplified model is analyzed, which consists of an ideally conducting cavity whose top end is a piston moving up and down without friction. This cavity is immersed in an external gravitational field with acceleration “G”.

An electromagnetic field contained inside the cavity exerts a pressure in the cavity walls, and it is possible that these internal forces exactly compensate the action on the gravitational field on a piston of given mass “M”.

We assume therefore the existence of an initial equilibrium state where the piston is “macroscopically” at rest, which means that the average electromagnetic force acting on the piston equals the gravitational force “MG”. When this equilibrium is perturbed, namely by the addition of some extra mass “S” to the piston, it is natural to expect a transient regime converging to a second state of equilibrium.

We derive the equation of motion of the piston for a Transverse Magnetic (TM) mode, which dynamically interacts with its boundaries.

The starting point of the present analysis is an approximate solution of the Maxwell equations, which is obtained by replacing the boundary conditions at the moving wall by the static conditions, [1]. We obtain a set of differential equations coupling the motion of the piston to the amplitudes of the electric and magnetic fields. These are nonlinear differential equations, which can be solved using a fourth-order Runge-Kutta method.

For modes that are independent of the time-varying cavity length, the only restriction to the field amplitudes is that the total energy of the system is conserved. In this particular case the transient regime obtained with the electromagnetic approach used in this work exactly matches the transient regime obtained using a much simpler “physical” approach based on a “photon” energy and momentum, [2].

The interaction of electromagnetic or optical systems with external forces is a quite recent subject of research. The simple model analyzed here can be of use to the study of more complex situations, namely when the external force varies periodically in time. Such devices are presently under consideration for the detection of gravitational waves, [3].

REFERENCES

1. Blümel, R., *Phys. Rev. E,* Vol. 51, No. 6, pp. 5520–5523, 1995.
2. Abreu Faro, M., Marçal, and M. H., *Mem. Acad. Ciências de Lisboa,* Tomo XXXVII, 1998.
3. Aguirregabiria, J. M. and L. Bel, *Phys. Rev. A,* Vol. 36, No. 8, pp. 3768–3770, 1987.

Behavior of a Magnet over a Conductor Rotating Disc

A. J. S. Oliveira, A. C. Pereira, and J. M. R. dos Santos
Universidade Federal do Maranhão (UFMA)
Department of Physics
São Luís, Brazil

J. R. S. Oliveira
Centro Federal de Educação Tecnológica do Maranhão
Department of Eletronics
São Luís, Brazil

This work presents the theory of the effect of the induced current in a conductor material when it is in the presence of a magnetic material moving with velocity v. We used this theory to show that a permanent magnet can be levitated above a rotating nonmagnetic material disk. An experiment was mounted to measure the drag and lift forces involved and obtain a transmission motor (without mechanical coupling) when the magnet rotates.

A permanent magnet can be levitated over a nonmagnetic disc that rotates with angular velocity ω. This happens because the eddy current that are induced on the conductor disc, in the presence of a magnetic material, acts as an *image magnet* under the disc in opposition to the real magnet. When the angular velocity of the conducting disk increases, a better magnetic image it produces, simulating (as a limit) the behavior of a superconductor (Meissner effect).

The problem is treated as a charge over a conductor. The induced currents in the conductor are in opposition to the variation of the magnetic field due to movement of the magnet. The magnetic field produced with the eddy current is in opposition to the magnetic field of the magnet and also to the mobility of the magnet. Therefore there are two involved forces. A lift force perpendicular to the plane of the disc and a dragging forge parallel and in opposition to the movement. When we approximate the permanent magnet, the combination of these two forces makes the magnet rotates in high rotation.

The experiment used to measure the forces involved consists of an aluminum disc with a diameter of 300 mm and the width of 3 mm. The disc is then coupled to a 1/8 HP motor. The Fig. 1 shows the experiment.

Finally, voltage was obtained using this theory as can seen in Fig. 2.

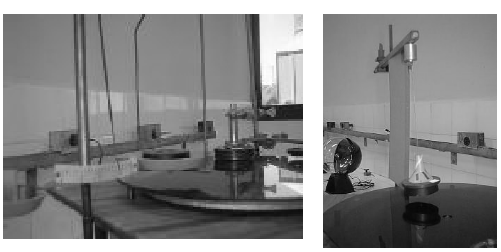

Fig. 1 Forces measure

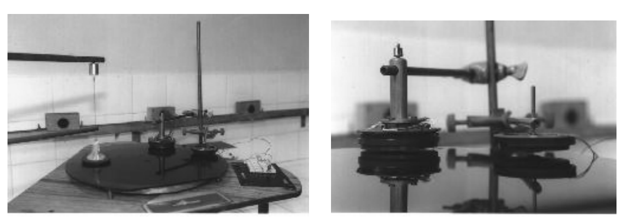

Fig. 2 Transmissions with 6 V and 250 mA

Complex Wave Equation of Electromagnetic and Gravitational Fields

V. T. Sarychev
Siberian physical-technical institute
Tomsk, Russia

The O. Heaviside's, J. Carstoiu's and L. Brillouin's ideas of the description of gravitation by classical fields are developed. The following equation for the joint description of electromagnetic and gravitational fields is offered

$$\frac{\partial^2 A^j}{\partial x_k \partial x^k} = i4\pi u_n T^{jn}; \tag{1}$$

where $A = (\varphi, \mathbf{A})$-complex 4-D potential, $x^k = (ct, \mathbf{x})$-4-D coordinates of a Minkowski space, *i* in a right part (1) -imaginary unit, u_j - components of 4-D velocity vector, T^{ij} - energy-momentum tensor. Complex field ($\mathbf{H} = rot\mathbf{A}$, $\mathbf{E} = -grad\varphi - \frac{\partial \mathbf{A}}{c\partial t}$,) corresponds to a potential *A*, where the real part represents an electromagnetic field, and imaginary - gravitational one. Accordingly, the real part of a wave equation (1) represents the Maxwell equations, and imaginary — the Heaviside-Carstoiu equations. A role of fields sources of the Maxwell and the Heaviside-Carstoiu equations are played by density of charges and currents, which behaviour should be described by substance equations. In an offered formalism a role of complex field source is played by the non-linear complex expression $i\, u_n T^{jn}$. For example, density of a complex charge is determined by the following expression: $4\pi\rho = iu_o(\mathbf{E}\cdot\mathbf{E} + \mathbf{H}\cdot\mathbf{H})/2 - i\mathbf{u}\cdot[\mathbf{EH}]$. Density of an electrical charge is determined by a real part of this expression, and density of a gravitational charge - imaginary one.

In a number of simple cases the solution (1) can be obtained strictly. At **H**=0 for a spherical symmetry case a radial component of a complex field is determined by expression

$$E_r = q/r(r + iu_o q/2), \tag{2}$$

where the integration constant $q = e + ig$ determines a full complex charge of field derivation.

At $\mathbf{H} \neq 0$ and an axial symmetry case the solution can be retrieved numerically or is submitted by series of spherical polynomials. Except for q, in this case there is a value of the complex moment $\mu = \mu_e + \mu_g$ as integral parameter (μ_e - magnetic, μ_g - mechanical moments). On large distances from an origin the field **H** is dipole, and field **E** - Coulomb. In process of decreasing *r* the behavior pattern of a field essentially changes. So for the solutions, which the values of integral parameters *q* and μ correspond to mass, electrical charge, magnetic and mechanical moment of an electron, the gravitational field changes the sign at $r < 10^{-12}$ cm. This outcome generates doubt concerning a universality of a gravitational attraction. It is easy to be convinced, that for the solution (2) the gravitational field changes the sign at r, equal to half of classical radius of an electron. Moreover, the solutions, which integral parameters correspond to antiparticles, have orientation of a gravitational field inverse to orientation of a field of normal substance. I.e. the antimatter is gravitationally repelled from matter.

The gravitational interaction is considered as most weak. However will say more correctly, that the gravitational charge of electrical charged particles is many times less electrical one on an absolute value. For an electron this relation is ~5 10^{-21}, for a proton ~2.7 10^{-18}. A little of this relation is a main interrupting of experimental confirmation of a gravitational repulsion between opposite gravitational charges (substance and antisubstance).

Session 5Ac1

Remote Sensing and Geophysical Problems

Real-Time Monitoring of Strange Sea Surface Temperature Found in Satellite Thermal Imagery After Passage of Cold Front in the Northwestern Pacific

S. Nakamura
Tanabe, Wakayama 646 0031, Japan

It was found that an ocean area of abnormal high sea surface temperature in the directly received satellite thermal data of the APT (Automatic Picture Transform) from the NOAA satellites in the northwestern Pacific. This was one case which obtained at the real-time signal receiving site in the station settled on the coast by Kyoto University. At this site, the sea surface temperature has been monitored in order to see the sea surface thermal pattern in relation to the Kuroshio flow as a western intensified ocean current. The interested area is covered by the foot prints of the satellites. The APT imageries are possible for citizen use or some other specific purposes, which can be directly obtained at a station settled on land or mounted on a boat. In this work, a specific example is introduced in order to show what was seen in the thermal pattern of the sea surface just after passage of the atmospheric cold front just off the Japanese Islands. The case was found in the thermal pattern of the sea surface in the midnight in the cold season of the northern hemisphere. The author consulted the meteorological and oceanographic data to see the abnormal high temperature in the interested area, and he could give a dynamical and thermodynamical understanding of the case by assuming the ocean as a black body (exactly, a gray body might be more appropriate to assume for the problem). Then, the long wave in the infrared band is radiated normal to the sea surface. The wind induced waves in the interested area make a patch of the sea area in which the waves make some curvatures on the sea surface. When the radius of the sea surface with a specific curvature is same to the distance between the sensor mounted on the satellite, then, the focus of the sea surface can be just at or neighbor the sensor mounted on the satellite, and, it is possible to find an abnormal high temperature on the sea surface by the satellite. A similar case is seen when swells out of a distant typhoon are observed on the coast of the northwestern Pacific as the author has ever noticed.

Radiometric Measurement of Zenith Attenuation and Estimation of Effective Rain Height to Predict Slant Path Attenuation at 19.9 GHz

I. S. Hudiara, A. Kumar, and V. Sharma
Department of Electronics Technology, Guru Nanak Dev University
Amritsar, Punjab 143005, India

The paper describes the measurement of zenith path attenuation due to rain in the year 2000 at Amritsar $(31\Upsilon\ 38'\ \mathrm{N}\ 74\Upsilon\ 52'\ \mathrm{E})$ India, using zenith looking radiometer operating at 19.9 GHz. The radiometer with antenna was housed in an air-conditioned hut with an acrylic sheet window in front of the antenna. The sky noise temperature data were collected at various rain rates using radiometer. Rain rate was measured using a tipping bucket rain gauge, which was co-located near the radiometric setup. The specific attenuation at 19.9 GHz has been calculated at different rain rates at Amritsar using lognormal drop size distribution. The effective rain height has been obtained from the analysis of radiometric data & point rainfall intensity. The point rain fall data for winter & monsoon seasons for the year 2000 & 2001 have been collected & analyzed to obtain cumulative distribution statistics for the whole year to find year to year variation of rain statistics. The values of specific attenuation, zenith attenuation and effective rain height as a function of rain rate have been shown graphically in the paper. The values of specific attenuation for the measured rain rate at Amritsar have been calculated using Marshal & Palmar (lognormal) drop size distribution. The study has shown that rain induced attenuation increases as rain rate increases. It has also been observed that the effective rain height decreases with increase in rate of rainfall. The effective rain height for rain rate exceeding 0.01% of time (89.5 mm/hr) at Amritsar was found to be 1.2 km for the year 2000. It has been found that the average value for the effective rain height estimated from the measured zenith attenuation is found to be 3 km at Amritsar which is lower than the average rain height predicted by CCIR for the latitude at which Amritsar is located. The calculated specific attenuation at various rain rates and the estimated rain height has been used to predict the slant path attenuation at Amritsar for earth space communication link. The knowledge of all these parameters is required to design an efficient communication link, which will not fail under adverse rainy conditions.

Retrieval of Forest Stem Density from Polarimetric SAR Imagery

J. Pacheco, F. Gan, B.-I. Wu, Y. Zhang, T. M. Grzegorczyk, and J. A. Kong
Research Laboratory of Electronics, Massachusetts Institute of Technology
Cambridge, MA 02139, U.S.A.

Y. Hara
Mitsubishi Electric Corporation, Kamakura Works
Kamakura, Japan

Radar technology continues to find widespread use in the long range, all weather remote sensing of earth terrain. In this talk, the use of polarimetric synthetic aperture radar (SAR) images to estimate stem density is explored. Our approach, similar to those used in the past is to use an simplified model of a forest region to study the effect of various forest parameters on the backscattering coefficient from which a method for estimating stem density from SAR imagery can be developed. In this work, the trunk layer of the forest is modeled as a collection of dielectric cylinders that are placed over a flat and possibly tilted infinite ground plane. The total scattering from the collection is approximated as the coherent sum of the independent scattering from each trunk. The double-bounce interaction between the ground plane and the trunk is also included.

First of all, a parameteric study of the backscatter coefficient's dependency on the trunk radius, height, permittivity, and stem density was done through several Monte Carlo simulations, with realizations on the order of 200, with trunks uniformly distributed over a fixed area. As expected, these simulations of the trunk layer indicate that the backscatter coefficient is a linear function of stem density. Furthermore, for a large number of trunks, the mean and standard deviation of the backscatter coefficient both approach the incoherent backscatter coefficient; the large variance being due to the coherence effects. In addition, for flat terrains, the backscatter coefficient is also a linear function of stem volume density. However, for sloped terrains the backscatter coefficient is a nonlinear function of stem volume density, a fact which leads to complications in predicting the stem density.

Next to estimate the stem density, the SAR image is segmented into several regions with sizes on the order of a resolution cell. Using the average tree height and radius, the average backscatter amplitude of one tree is calculated. Mean tree height data can be obtained through InSAR techniques, while the average radius can be determined by analyzing the polarization phase difference between the HH and VV SAR components. The number of trees within the resolution cell is then estimated by using a maximum likelihood estimator formulated on the assumption of a uniform phase distribution.

To determine the effectiveness of this estimator in the retrieval of the forest stem density, the method is applied to polarimetric SAR imagery, both simulated and experimental data obtained by Mitsubishi. The simulated SAR images are produced through the use of an efficient SAR simulation alogirthm that has been developed. The SAR simulator works by efficiently calculating the SAR back-projection integral by using a closed form analytic expression for the cross-range focusing sum. However, in this method, it is assumed that backscatter intensity of scatterers is independent of the azimuthal incidence angle. While for flat terrains with cylindrical trunks, this approximation is exact, it does not hold for sloped terrains. In this case, the wide-aperture effect is taken into account by breaking the cross range sum into several sections in which the average backscatter return is used.

Estimating Polar Ice Sheet Accumulation Rates From Interferometric Synthetic Aperture Radar Measurements

H. A. Zebker
Depts. of Electrical Engineering and Geophysics, Stanford University
Stanford, CA 94305-2215, U.S.A.

W. Hoen
Dept. of Applied Physics, Stanford University
Stanford, CA 94305-2215, U.S.A.

Mass balance estimates for the Earth's ice sheets require modeling and observation of both accumulation and wasting processes. We present here the development of models and data analysis procedures relating snow and ice accumulation rates to interferometric radar remote sensing observables. InSAR has proven a very effective method for examining the outflow of ice to the sea by resolving the surface velocity field of glaciers, however, this is only half the story as regards mass balance. It is equally important to understand the accumulation rates, the other side of the mass balance equation. Microwave methods are very helpful here as the signals penetrate meters into the firn and thereby retrieve information contained below the visible surface. Previous work relating radar remote sensing data to accumulation has used models incorporating grain size effects alone to derive accumulation rates, however we show that these models are not consistent with both radar intensity and InSAR correlation observations. Simple models indicate that adding the influence of layering within the ice medium to backscatter models resolves the inconsistency. We have developed electromagnetic scattering models for ice sheets that incorporate both the correlation and the amplitude of radar interferograms, and thereby better constrain accumulation rates. We find that correlation, in particular, is very sensitive to the near-surface wavelength-scale structure of the ice, and thus can help describe changes in grain size, layer thickness and firn density with depth over large areas. We extend existing models to include layering effects, and thereby better model the interferometric backscatter. Our theoretical development has been supported by ERS observations of Greenland, and we are now in the process of using the recently-acquired Radarsat MAMM interferometric data set to produce accumulation estimates of large regions within the Antarctic dry snow zone. MAMM observations resulted in nearly complete InSAR coverage of Antarctica north of 80° S, so that very large-scale maps may be derived. We will compare our accumulation estimates with those derived from radiometric and other instruments, as well as in situ solutions.

Spatial-Temporal Combined Doppler-Radar and Radiometer System

A. K. Hambaryan and V. K. Hambaryan
ECOSERV Remote Observation Centre
Yerevan, 375026, Armenia

A. K. Arakelyan
Institute of Radiophysics and Electronics of Armenian National Academy of Sciences
Ashtarak-2, 378410, Armenia

Combined in space and in time X-band Doppler-radar-radiometer system is described. Developed system may simultaneously operate in separate modes too, such as in Doppler, scatterometer and radiometer modes. Therefore, it allows research the regularities of relationships between the changes of radar and radiometer signals amplitudes and radar signal phase characteristics reflected from and emitted by the observed surfaces.

Time diagrams of Doppler-radar, scatterometer and radiometer channels operation, as well as the diagrams for control signals of some microwave and low frequency units of the system are presented.

On the basis of this system the Doppler-radar-radiometer detector-identifier are developed. The developed detector-identifier may be successfully used for detection and classification of 18 types of anomalous formations, originated on the background of observed surface due to natural and artificial changes of geophysical, geometrical, kinematical, bio-chemical and other characteristics of the surface. It should be used for remote control of ecological conditions of various environmental objects and areas, for instance, for sustainable monitoring of hugs of forests' tracts, internal reservoirs, lakes and seas, irrigation channels, etc. This system may be successfully used for microwave inverse problems solution too, for the determination of observed surfaces principal physical-chemical and biological parameters.

The principal parameters being used for detection and classification are the mean values and the variances of distributions of backscattered radar signal frequency, the observed surfaces radar cross sections (radar backscattering coefficients) and their brightness temperatures. Detection and classification probabilities for the developed detector are obtained, which are considerably higher than those of separate radar, radiometer or combined radar-radiometer systems.

The technical characteristics of the Doppler-radar-radiometer system are: radar pulse duration is 1 mks, pulse power is 1 W, radar receiver bandwidth is $\sim 10\%$, radar channel threshold sensitivity is -144 dB/W and the background sensitivity is -127 dB/W, radiometer receiver sensitivity at an integration time 1 s is lesser than 0.15 K. Antenna system with antenna switch provides all kinds of polarization for both radar (transmitted and received) and radiometer signals.

Spatial Size and Radar Contrast Distributions of Natural Origin, Slight Contrast Sea Surface Signatures

A. K. Arakelyan
Institute of Radiophysics and Electronics of Armenian National Academy of Sciences
Ashtarak-2, 378410, Armenia

V. K. Hambaryan
ECOSERV Remote Observation Centre
Yerevan, 375026, Armenia

The results of field experimental (airborne) investigations of distribution features of sea surface background, natural origin radar signatures (anomalous formations) are presented. Statistical characteristics of spatial sizes and radar contrasts distributions are obtained, for sea surface radar signatures of natural origin.

Airborne experimental measurements were carried out over the coastal areas of Black and Barents seas and the Pacific Ocean by X-band scatterometer. The principal conditions of observation were: front observation at the vertical polarization and at the angle of incidence of 30°–60°, the carrier height of 200–1500 m, the carrier velocity - ~ 450 m/s. The technical parameters of utilized multi-channel, panoramic scatterometer were: the radar signal central frequency - 7.5 GHz, the radar pulse duration - 4 ms, the repetition frequency - 1 KHz, the pulse power of 1 W, the number of separate radar channels - 8, each radar receiver sensitivity (background) - -127 dB/W, one channel antenna pattern beam width - 4°.

An analysis of obtained experimental data has shown that on the radar image of sea surface there are a number of anomalous formations of natural origin differing quite by their internal structure, by spatial sizes and by the values of radar contrasts. The results of performed field experiments have shown that at wind speeds of 6–22 m/s the spatial sizes of recorded signatures could reach up to 25 km. The results obtained at a calm weather condition, under the availability of short time, but powerful gusts (spurts) of wind up to 20 m/s have shown that the absolute values of radar contrasts could reach up to 15 dB.

The results of statistical processing of sea surface radar image are presented, in the forms of spatial sizes and radio contrasts distribution. The distributions were constructed for various wind speeds of 2–22 m/s.

The radar images of the Okhotsk Sea surface area just above the zone of underwater gas jet operation are presented. The spatial size of the recorded anomaly was ~ 5 km at the maximum value of radar contrast ~ -12 dB.

Electromagnetic Modelling of Vegetation with Neural Networks

F. Del Frate, L. Guerriero and D. Solimini
Tor Vergata University of Rome
Rome, 00133, Italy

Simulating scattering or emission by physically based microwave models requires the development of suitable computing codes. For instance, in case of surfaces covered with vegetation, the algorithms start from the radiative transfer theory and solve the relevant equations numerically through techniques like the matrix doubling, which include multiple scattering effects. Such an approach, while being satisfactory from the theoretical viewpoint, presents, neverthless, some shortcomings. A first one is the usually heavy computational effort, since the resulting codes can be quite demanding in terms of CPU. A second issue is that modest or no advantage is taken from previous simulations of "similar cases", e.g., if the physical parameters are changed, quite often the entire simulation has to be carried out again.

The problem of developing an electromagnetic model can be also regarded as the problem of synthesizing an associative memory that either retrieves the appropriate output when presented with the known input parameters, or is able to generalize its response when fed with new inputs.

This, at the end, is what happens during the training phase of a neural algorithm. Indeed, neural networks present attractive properties for their recognized ability to approximate multivariate, nonlinear functions. Because of their massively parallel structure, they can perform computations at a very high rate, and, because of their adaptive nature, they can learn the features of the input signals and adapt to changes in the data.

In this contribution we present a study on how neural networks can act as a multiple scattering model algorithm for computing backscattering coefficients of vegetated surfaces. The behavior of the neural network algorithm in approximating the electromagnetic features of the considered structure is analyzed from the point of view of the accuracy in producing the backscattering coefficients of the surface, i.e., after the matrix doubling procedure is applied. The results confirm that the time needed for the computations is dramatically reduced. An evaluation of the neural algorithm performance in terms of generalization and extrapolation capability with respect to a multidimensional input including geo- bio-physical and sensor parameters is reported.

Baseline Estimation for SAR Interferometry Using Ground Control Points

B.-I. Wu, J. Pacheco, T. M. Grzegorczyk, Y. Zhang, and J. A. Kong
Research Laboratory of Electronics, Massachusetts Institute of Technology
Cambridge, MA 02139-4307, U.S.A.

Y. Hara
Mitsubishi Electric Corporation, Kamakura Works
Kamakura, Japan

Generation of digital elevation map based on Interferometric Synthetic Aperture Radar requires an accurate unwrapping and inversion procedure. The uncertainties in the interferometric baseline length and orientation greatly affects the dynamic ranges and accuracies of the inverted height, which will affect the subseqeuent foreshortening and registration of the height information.

Uncertainties can be reduced by the introduction of ground control points, of which the heights and positions are known. By incorporating the information of the ground control points in the height inversion scheme, the initial estimation of the baseline parameters can be improved.

In this study, simulated interferogram of a 2-D terrain is generated and different levels of phase noise as well as uncertainties in baseline parameters are introduced. Five control points are use in a 60×60 km area. The platform height is 500 km and the frequency used is L-band. Weighted least squares method is used to reconstruct the unwrapped phase and ground control points are used to yield an improved baseline. Both the absolute and relative control points phase relations are used. The registered inverted height profiles are then compared to the original terrain and accuracy of the inversion process is studied with respect to the amount of injected noise.

Polarimetric Scattering Indexes and Information Entropy of the SAR Imagery for Surface Monitoring

Y.-Q. Jin and F. Chen
Center for Wave Scattering and Remote Sensing (CWSRS) and School of Information Science and Engineering, Fudan University
Shanghai, 200433, China

The SAR imagery technology is one of most important advances in space-borne microwave remote sensing during recent decades. Completely polarimetric scattering from complex terrain surfaces can be measured. Fully understanding and retrieving information from polarimetric scattering signatures of natural media have become a key issue for the SAR remote sensing and its broad applications.

There have been extensive researches on polarimetric scattering for SAR imagery in the CWSRS, Fudan University. It mainly includes numerical simulation of polarimetric scattering from complex natural media, the Mueller matrix solution, coherency matrix and eigen-analysis of information entropy, statistics of four Stokes parameters in multi-look SAR images, etc. To indicate the difference between vertically (*vv*) and horizontally (*hh*) co-polarized back-scatterings, the polarization index was usually defined to classify the polarized scattering signature from different natural media.

However, the study of the entropy and eigen-analysis has not been related with direct measurement of the back-scattering signatures. In this paper, the eigen-values of the coherency matrix and information entropy are derived to directly relate with co-polarized and cross-polarized back-scattering indexes. Thus, it combines the Mueller matrix simulation, the information entropy of the coherence matrix, and polarization indexes to yield an overall theory and image data analysis for quantitative understanding of the SAR imagery. As example, this theory is applied to data analysis of the fields measurements and an AirSAR image for surface monitoring.

Bistatic DBS Altimetry: Ocean Scattering Model and Simulation Results

P. T. Melacci
Physics Dept.–Univ.of Perugia
Perugia, Italy

G. Picardi and R. Seu
Infocom Dept.–University of Rome "La Sapienza"
Rome, 00184, Italy

In the classical space borne radar altimeters and in the bistatic altimeters the spatial resolution is limited by the pulse width and the orbital height to values of some kilometers, through the application of the pulse-limited (PL) concept.

We can notice that the bistatic remote sensing system consist of a constellation of satellites flying at the proper altitude with an operating geometry such that the incidence and scattering angles are equal.

Moreover, when encountering rougher surfaces, with prominent features and non zero slopes, such as land surfaces, coastal regions, ice sheets, etc. the poor spatial resolution inherent in the pulse limited approach becomes inadequate to the observed surface and the altimeter performance degrades severely. In order to overcome these problems the spatial resolution can be improved at least in the along track direction, by low-pass filtering the received echoes in the Doppler frequency domain, adapting well-known processing techniques developed for Synthetic Aperture Radar (SAR) to the illumination geometry of a Radar Altimeter. Instruments based on this concept have been called Doppler Beam Sharpened (DBS) altimeters and generally achieve this improvement in resolution at the expense of a reduction of the illuminated footprint size and thus of the non-coherent integration capability.

In this paper the application of the Synthetic Aperture concept to the bistatic altimeter is considered: the system parameters and an analytical model is derived for the average power echo received from an oceanic surface at a frequency high enough for the Kirchhoff scattering mechanism to be dominant; in particular the possibility to use the GPS signals was taken into account. The asymmetric behavior of the sea waves was also considered, modeling the surface height as a non-gaussian distributed random process. Such bistatic model will be useful to evaluate the performance of such a system in the estimate of the distance from a reference average surface, of the surface roughness and in particular the surface slope, in order to obtain the wind estimation.

A system analysis, supported by a simulator, is shown and the optimum radar parameters are evaluated.

Synergy of Altimeter and Radiometer Data for Sea Surface Microwave Signatures' Detection and Classification

A. K. Hambaryan and A. A. Arakelvan
Remote Observation Centre ECOSERV
Yerevan, 375026, Armenia

It is known that sea surface radar backscattering coefficient and sea surface brightness temperature are complicated functions of various principal parameters, namely: the wind speed and direction, the sea state (the swell or non-fully developed sea wave condition), water and air temperatures, water salinity, radio wavelength, the polarization of observation, the angle of incidence, etc. The changes some of them have comparable influence on the changes of absolute values of sea surface radar backscattering coefficient and its brightness temperature. This ambiguity is the main obstacle when one tries to solve a microwave inverse-problem by separate utilization of radar or radiometer data of observation. This problem is sufficient for tasks of microwave remote sensing applied to the detection and identification of sea surface slight-contrast signatures and targets, because the number of comparable parameters increases. Therefore, for an unambiguous and high precise solution of a sea surface microwave remote sensing inverse-problem it is necessary to have a set of independent measurements or equations.

The results of various researches have shown that microwave signals backscattered from and emitted by the sea surface are independent variables. In this aspect, the results of altimeter and down looking radiometer observations have particular interest, because under such a condition of observation it is possible to neglect the influence of wind direction on the absolute values and fluctuations of sea surface radar backscattering coefficient and its brightness temperature.

In this presentation a concept of combining of the results of altimeter and down looking radiometer observations is considered. As well as microwave, combined active-passive method is discussed, for a detection and identification of sea surface anomalous formations (signatures), originating due to separate changes of such parameters as: the wind speed (small wave spectrum characteristics), the sea state (swell or long wave spectrum characteristics), the water temperature and the condition of atmospheric stratification (the difference of near surface air and water temperatures).

Numerical estimations of sea surface altimeter backscattering coefficient and its brightness temperature were performed under various values of wind speed, sea state, water and air temperatures. The results of numerical estimations of sea surface altimeter radar and radiometer contrasts (changes) due to separate changes of the above mentioned principal parameters, are presented. The decision rules of detection and identification of various types of anomalies, as well as analytical expressions for detection probabilities' estimation, are obtained. It is shown that the probability characteristics of the developed method of detection and identification are considerably higher than those of separate radar or radiometer methods.

Session 5Ac2

Medical Applications

Dielectric Characterisation of Blood by Bio-Impedance Spectroscopy in the [1 MHz–1 GHz] Frequency Range

F. Jaspard and M. Nadi
L.I.E.N., University of Nancy 1
Vandoeuvre les Nancy, 54506, France

The electrical behaviour of biological tissue is entirely described by the permittivity and the electrical conductivity. The knowledge of these two dielectric parameters is of prime importance in the study of the interaction between electromagnetic waves and the biological tissue.

The instrumentation developed in this work is dedicated to the measurement of the dielectric parameters of blood in the frequency range [1 MHz–1 GHz]. The equipment is constituted by an impedometer (based on an extended V/I method) associated with an open ended coaxial probe. This coaxial structure is perfectly adapted for measurement on liquid and makes it easier to deal with propagating effects, which appear at high frequency. An equivalent electrical circuit allows to take into account the electrical behaviour of the probe and to connect the measured value (impedance) to the searched parameters. Measurements were performed on human and animal (beef, sheep) blood. A study of the main influence factors of the measure showed the important role of the temperature and the haematocrite.

Design and Modeling of Helical Antennas for Medical Applications Using Microwaves

A. Dietsch
Hypertechnologies
Les Clayes Sous Bois, 78340, France

J.-C. Camart, L. Dubois, and J. Pribetich
I.E.M.N. - U.M.R. C.N.R.S.
Département Hyperfréquences & Semiconducteurs
Université des Sciences & Technologies de LILLE
Villeneuve D'Ascq, 59652, France

One of the main objectives of using microwaves in medical applications is to make use of the therapeutic effects resulting from the interaction between electromagnetic waves and biological tissues in order to obtain a local heating. For this purpose, a large number of devices have been designed and tested for various medical applications. More particularly, hyperthermia using microwave applicators has proven effective in delivering therapeutic heating to tumors having different sizes in a variety of anatomic locations. We present in this paper the results concerning the design and the modeling of the helical applicator developed for various medical applications using microwaves.

The helical microwave antenna is realized from a flexible coaxial cable UT34. Several kinds of antennas with one or two helix have been realized. For the single helical antenna, the helix is obtained from the inner conductor which is rolled up around the teflon sheath. For the double helical microwave antenna , the first helix is also the inner conductor, which is rolled up around the teflon sheath. The second helix is soldered at the outer conductor and is rolled up around the cable.

For the modeling of these applicators, a complete $3D$ model based on the wellknown FDTD method has been developed. With this model, it is possible to determine the matching of the applicator inside the surrounding media. We can also obtain the specific absorption rate (SAR) at the heating frequency (915 or 434 MHz). The heating pattern is then deduced from the resolution of the bioheat transfer equation, either during the dynamic rate or in the steady state

In order to verify the theoretical results, experimental measurements have also been carried out on phantom models (polyacrylamide gel) of human tissues : measurement of the return loss (S_{11} parameter) as a function of frequency by means of a network analyzer HP 8510 in order to obtain the level of adaptation of the applicators, determination of the energy distribution and of the thermal mapping at the heating frequency using an automatic experimental system.

Several antennas with various lengths for the helix has been designed in order to obtain an increase of temperature on a short time (less than 30 seconds) with a low incident power (less than 10 W). The comparison between theoretical results and experimental measurements (concerning the power deposition diagram, the thermal mapping and the S_{11} parameter) shows a good agreement.

The theoretical results confirmed by experimental measurements show clearly the possibility to obtain a given increase of temperature on a short time with a low incident power as required in the specifications of the medical application with the designed helical antennas.

Electromagnetic and Thermal Analysis of a 915-MHz Antenna for Microwave Thermal Ablation Treatment

J. C. Lin
Department of Electrical and Computer Engineering
University of Illinois
Chicago, IL, U.S.A.

P. Bernardi, M. Cavagnaro, S. Pisa, and E. Piuzzi
Department of Electronic Engineering
University of Rome "La Sapienza"
Rome, Italy

The therapeutic use of minimally invasive transcatheter thermal ablation technology is increasingly gaining attention. Microwave energy is potentially more effective and has greater versatility for producing ablative lesions. Specifically, minimally invasive transcatheter microwave technology has been suggested as a method to improve the depth of thermally induced ablative lesions, as compared to lower frequency technologies [1]. A critical element in a minimally invasive microwave therapeutic system is the catheter antenna used to deliver the microwave energy to the target tissue, without damaging the surrounding normal tissue. This paper presents a numerical and experimental study of an antenna operating at 915 MHz, designed to operate at 915 MHz for tissue ablation. The SAR distribution and temperature elevation, induced by the antenna in a cylindrical model of phantom muscle, have been evaluated. The antenna is obtained from a coaxial cable connecting an annular cap to the enlarged inner conductor and a coaxial choke connected to the outer conductor. A dielectric junction is used to separate the cap from the outer conductor choke. In the experiment, the antenna is inserted in the center of a cylindrical phantom, filled with muscle-equivalent tissue [2]. Since both the antenna and the phantom exhibit cylindrical symmetry, in the computer simulation, this symmetry has been exploited to simplify the study. Under these conditions, the problem can be investigated using a $2D$ approach in cylindrical coordinates. To evaluate SAR distributions, the finite difference time domain (FDTD) method is applied. To evaluate the temperature rises (ΔT), an explicit finite difference solution of the bio-heat equation is used. Both SAR and ΔT values have been evaluated along lines parallel to the antenna axis at different radial distances from the antenna surface. Moreover, temperature data have been computed at different time instants (from 5 to 15 seconds from the beginning of the treatment). A good agreement between numerical and experimental results has been found.

REFERENCES

1. Nath S. and D. E. Haines, "Biophysics and pathology of catheter energy delivery systems," *Prog Cardiovasc Dis.*, Vol. 37, 185–204, 1995.
2. Pisa, S., M. Cavagnaro, P. Bernardi, and J.C. Lin, "A 915-MHz antenna for microwave thermal ablation treatment: physical design, computer modeling and experimental measurement," *IEEE Trans. on Biomedical Eng.*, Vol. 48, No. 5, 599–601, May 2001.

Hyperthermia Applicator Compatible with Non-Invasive Thermometry System

J. Vrba
Dept.of EM Field, Czech Technical University
Prague, 16627, Czech Rep.

I. Zuna and P. Peschke
German Cancer Research Institute
Heidelberg, Germany

L. Pousek
Centrum for Biomedical Engineering, Czech Technical University
Prague, Czech Rep.

M. Lapes
Hospital in Nymburk
Nymburk, Czech Rep.

G. Saliba, L. Oppl, and P. Novák
Dept.of EM Field, Czech Technical University
Prague, 16627, Czech Rep.

Our work is focused just on the design, optimisation and experimental evaluation of the microwave applicators compatible with non-invasive 3D temperature measurements systems via US and/or NMR. This means to design a microwave structure capable above all: (1) to transfer efficiently the electromagnetic energy into the biological tissue; (2) to create the required 3D temperature distribution in the area to be treated; (3) to guarantee the compatibility with US and NMR. The main goal of the planned biological experiment is a hyperthermia treatment of the experimentally induced pedicle tumors of the rat to verify the feasibility of ultrasound diagnostics and magnetic resonance imaging respectively to map the temperature distribution in the target area of the treatment. That means to heat effective volume of approximately cylindrical shape (diameter approx. 2 cm, heigth approx. 3 cm). Temperature to be reached is 41°C or more (i.e. temperature increase of at least 4°C from starting point 37°C), time period of heating is 45 minutes. Considering the necessary effective heating depth for the planned experiments, we have found 915 MHz to be suitable frequency. As an excellent compatibility of the applicator with non-invasive temperature measurement system (ultrasound or NMR) is a fundamental condition for our project, we should have to use non-magnetic metallic sheets of minimised dimensions to create the conductive elements of the applicator. Therefore the applicator itself is created by two inductive loops tuned to resonancy by capacitive elements. The position of the loops is fixed by persplex holder. There is a special cylindrical space for experimental animal in lower part of this persplex holder. As the heated tissue has a high dielectric losses, both loops are very well separated and so no significant resonance in heated area can occur. From this follows, that either the position of the loops with respect to heated area or the distance between the loops is not very critical.

First measurements to evaluate the basic properties of the discussed applicator were done on agar phantom of muscle tissue: (1) evaluation of basic microwave properties (transfer of EM energy to the tissue, reflections), (2) evaluation of compatibility with US and NMR, (3) calculation and measurement of SAR and temperature distribution and its homogeneity.

As a novel results of our work we could mention that the new type of microwave applicator for cancer treatment has been developed and evaluated. Evaluation procedures have shown, that this applicator is a very effective heating structure and excellent compatibility with US and NMR has been approved as well. Having approved this applicator in animal experiment, we are now working on development of its big version to be used in clinical praxis.

ACKNOWLEDGEMENTS

This research has been supported by program: Transdisciplinary research in BME (J04/98:210000012).

Microwave Thermotherapy in Czech Republic – Technical and Clinical Aspects

J. Vrba
Dept.of EM Field, Czech Technical University
Prague, 16627, Czech Rep.

M. Lapes
Institute of Radiation Oncology
Prague, 180 00, Czech Rep.

L. Oppl
Dept.of EM Field, Czech Technical University
Prague, 16627, Czech Rep.

J. Kvech and L. Petruzelka
Institute of Radiation Oncology
Prague, 180 00, Czech Rep.

Microwave thermotherapy (hyperthermia) is being used for cancer treatment since early 80's in many countries around the world. Since 1981 we were interested in the local external applicators working at 434 MHz and 2450 MHz. These applicators were used here in Prague for the treatment of more then 500 patients with superficial or subcutaneous tumours (up to the depth of approximately 4 cm). Now, following new trends in this field, we continue our research in two important directions: (1) deep local and regional applicators and (2) intracavitary applicators.

For the deep local thermotherapy treatment we develop above all waveguide type applicators based on the principle of evanescent mode waveguide, which is our specific solution and original contribution to the theory of microwave hyperthermia applicators. This technology enables us: (1) to design applicators with as small aperture as necessary also for the optimum frequency range for deep local and/or for regional thermotherapy treatment (the frequency band between 27 and 70 MHz); (2) using our technology we need not to fill the applicator by dielectric (necessary for deep penetration into the biological tissue – i.e. up to 10 centimetres under the body surface); (3) two to four of such applicators can be also used for regional treatment.

Waveguide type applicators are often used in the local external hyperthermia treatment of cancer and other modifications of microwave thermotherapy as they offer very advantageous properties, above all: (1) depth of penetration of the EM energy approaching the ideal case of plane wave; (2) low irradiation of the energy in the vicinity of the hyperthermia apparatus; (3) very good impedance matching, i.e. perfect energy transfer to the biological tissue.

We have studied waveguide applicators heating pattern for the aperture excitation at above and at under the cut-off frequency. It has helped us to get analytical approximations of the electromagnetic field distribution in the treated area of the biological tissue. The most important results for the effective heating depth d can be characterised as follows: (1) at high frequencies (above approx. 1000 MHz) the depth of effective heating d is above all a function of frequency f (skin effect); (2) bellow approx. 100 MHz d is the dominantly function of the diameter D of applicator aperture ($d = 0.386D$).

In the case of cancer treatment the long term statistics of clinical results can be described as follows:

Complete Response of Tumor	53%
Partial Response of the Tumor	31%
No Significant Response	16%

which corresponds to results obtained also by other groups in Europe.

ACKNOWLEDGEMENTS

This research is supported by Czech Research Programme: "Transdisciplinary Research in the Area of Biomedical Engineering" (J04/98: 210000012).

Low Frequency Magnetic Fields Interactions with Cardiac Pacemakers

A. Hedjiedj, M. Nadi, and P. Schmitt
Laboratoire dInstrumentation Electronique de Nancy, Faculté de Sciences, Université H. Poincaré de Nancy I
Vandoeuvre-les-Nancy, 54506, France

Medical implants carriers are exposed in their daily life environment to many sources of interference. The heart pacemaker through its heart-generated signal listening function is likely to be targeted by electromagnetic disruptions. Its particular functions implies to have an accurate knowledge of potentially interfering situations a carrier may be exposed to. Studies concerned with interferences between low frequency electromagnetic fields and these implants originally dealt with energy distribution network related interferences. The main objective of this work is to present a metrological protocol enabling to assess the immunity of active medical implants to low frequency electromagnetic interferences. The assessment methodology of the pacemakers immunity that we apply is in accord with the electromagnetic compatibility (E.M.C) approach. This approach starts from the victim (the implant) and known and lab-quantified disruptions (the source) then to complexity the problem by gradually integrating influence parameters. The method we suggest consists in characterizing the stimulators immunity to known and lab-quantified disruptions. The general problematic consists in checking this immunity in relation with led disruptions (the electrical voltage signals or current) and in relation with beaming disruptions (fields).

This article concerns the evaluation of pacemakers immunity to led and beaming low frequency disruptions. The studied frequencies are 50 Hz, 60 Hz, 10 kHz and 25 kHz. The presented results concern single and double chamber pacemakers. These tests are completed by in vitro measurements using an electromagnetic phantom which allow to take into account the interface which constitutes the human body, and thus to get closer to a real life situation.

A New Radiometric Imaging System for Medical Application

B. Bocquet, J. C. Van de Velde, G. Tittelein, and R. Ringot
Institut d'Electronique et de Microélectronique du Nord U.M.R. CNRS 8520, Département Hyperfréquences
et Semiconducteurs, Université des Sciences et Technologies de Lille
Villeneuve d'Ascq, 59655, France

A great activity in the characterization of breast tumors is led because X-ray mammography use alone is not sufficient to raise some diagnostic indetermination. To day, a common examination to supply X-ray is the ultrasonic exam but the specificity (or false positive) not remains so good. Other techniques, such as impedancemetry (EIT), far infrared, optical retrodiffusion, elastography, tomosynthesis or MRI, try to bring their contribution. We propose here to use a microwave technique based on the radiometric temperature measurement, but also, followed by an emissivity measurement.

We have constructed a Microwave Radiometric Mammography (near field imagery) for the early characterization of beast cancers [1, 2]. A large clinical evaluation on patients has been realized with the temperature measurement imaging system. A Receiver Operating Characteristics (ROC) statistical analyze gives a specificity upper than 80%. This results show that this technique has the same good results of the other non-invasive techniques [3]. We will present at the conference a complementarity analyze of our method with the X-ray mammography. We are going to show that radiometry has the same diagnosis power of ultrasonic investigation.

Now, we propose to develop a new radiometric imaging system based on integrated radiometers capable to measure also the emissivity factor. We will present this new system and some images we have realized on model. We will quantify the sensitivity of the radiometer in term of the emissivity factor and the potential role of this type of images.

REFERENCES

1. Leroy, Y., B. Bocquet, and A. Mamouni, "Non-invasive microwave radiometry thermometry," *Physiological Measurement*, Vol. 19, 127–148, 1998.
2. Bocquet, B., S. Mouty, R. Ringot, Y. Leroy, N. Rocourt, Y. Robert, P. Devos, and R. Beuscart, "Quantitative retrieval of temperature of breast cancers by microwave radiometric imaging," *Proc. IEEE BMES/EMBS Conf.*, Atlanta, USA, Oct. 13–16, 1999.
3. Bocquet, B., G. Tittelein, and R. Ringot, "Clinical results in microwave radiometric mammography (MRM)," *PIERS'2001*, Osaka, Japan, 18–22 July, 2001.

Microwave Spectral Radiometry for Temperature Measurement within the Neonatal Head

F. Bardati and G. Marrocco
Dipartimento di Informatica, Sistemi e Produzione
Universita Roma "Tor Vergata"
00133 Rome, Italy

P. Tognolatti
Dipartimento di Ingegneria Elettrica
Facoltà di Ingegneria, Università dell'Aquila
67100 L'Aquila, Italy

Hypothermal therapy has been recently proposed for treatment of new-born infants who have suffered hypoxia-ischaemia. This therapy is based on moderate cooling of brain and requires the deep head temperature to be monitored. Multifrequency radiometry is a candidate to this task since it enables the head temperature profile to be sensed noninvasively and atraumatically. In this paper the potentiality of microwave radiometry for this application will be examined through thermal and electromagnetic models and inversion algorithms. Examples of radiometric data inversion will be presented, using a data fitting by the matrix pencil algorithm and a Kalman filtering.

The main blocks of the procedure are i) a thermal model being used both to generate synthetic data and to obtain a-priori information for Kalman filtering; ii) an electromagnetic model being used to compute radiometric weighting functions; iii) inversion algorithms.

The head thermal model refers to a baby head, partially enveloped by a cold-liquid filled bonnet. Heat balance is modelled by classical Pennes bio-heat equation. According to previous available theoretical studies, a suitable geometry is a hemisphere of brain tissue with peripheral layers of bone and soft tissue. An adiabatic boundary condition is assumed to hold on the flat portion of the boundary.

The electromagnetic model computes the field inside the baby-head, for a realistic or a canonical model of the radiometric antenna. For the realistic model, the computation algorithm is an FDTD on cubic cells. Radiometric frequencies have been selected within 1–3 GHz band.

Numerical analysis results will be discussed, showing that the radiometric measurements can partially compensate for errors in the thermal model. As an example, if an error in the thermal model is due to a wrong knowledge of the arterial blood temperature, the temperature retrievals are still satisfactory by virtue of the additional information provided by radiometric data. If instead the error in the thermal model is caused by inaccurate estimate of the blood perfusion rate, the retrievals result unsatisfactory.

Session 5Ac3

Data Processing Techniques in Remote Sensing and Radar - I

New Possibilities to Monitor Birds Migration through Radar

L. Dinevich and I. Leshem
Tel-Aviv University
Ramat Aviv, Israel

A. B. Shupiatsky
The Central Aerological Observation
Dolgoprudny, Russia

The double-waved MRL-5 radar station was developed in the former USSR for studying the clouds physical processes and now used in Israel for ornithological research. Calculations and experimental data indicate that the technical characteristics of this radar placed 270 m a.s.l. provide the detection of Albatross size birds on 700 m flight altitude and distance of 100 km from radar disposition, and small birds like sparrow on 100 m flight altitude and distance of 40 km. The Crane flying on 3 km altitude can be detected by means of the radar second channel (l=10 cm) at a distance of almost 200 km. The narrow symmetric diagram of the antenna direction, 0.5° for l=3.2 cm and 1.5° for l=10 cm, enables to obtain more precision results in determining the height of both single birds and group flights within the covered area. The computerized system created on the basis of MRL-5 and the radar data specifying characteristics of the signals obtained enable to observe birds migration at any moment of the day. The system provides a possibility to evaluate the evolution of birds migration towards space and time, and to provide relevant operative information to the authorities engaged in airplane flights management. The peculiarity of the station and of the system as a whole is its polarimeter appliance enabling usage of more precise methods of target identification.

Researches of fluctuation of peak characteristics of birds signals have shown, that they substantially differ from similar characteristics of any other targets, including clouds, ground clutter, atmospheric phenomena etc. The filter created on this difference, enables to select the radioecho from birds with reliability exceeding 95%.

A system developed on radar technique, which is used to exert active impact on cloud formation processes, can be successfully used to solve problems related to airplane flights under complicated ornithological conditions.

Synthetic Aperture Radar Spectral Analysis Processing for Efficient ScanSAR Image Generation

A. Vidal, C. Bachiller, A. A. San Blas, and M. Ferrando
Universidad Politécnica de Valencia
Valencia, Spain

Spaceborne Synthetic Aperture Radar (SAR) instruments are becoming a very important source of data for Earth Observation, and that trend is going to be increased with the deployment of new Scanning SAR (ScanSAR) systems like RADARSAT or ENVISAT. These advanced systems generate a huge amount of data that require extensive processing before user interpretation. In this scenario, efficient algorithms for generating ScanSAR images are demanded. There are several processing techniques in the literature like Range-Doppler, Wavenumber Domain or Chirp Scaling. However, they are focused to solve high-resolution imagery with range migration features. In the case of ScanSAR data, spatial resolution is reduced by the scanning mechanism. Besides, the instrument, due to the extended swath operation, produces a high data rate that should be sent to ground. For all these reasons, new algorithms, which could provide a simple while efficient solution to generate on-board images are welcome in this scenario.

In this work, we describe and analyze a very efficient SAR processing method for reduced resolution images called Spectral Analysis (SPECAN), since data gaps reduce azimuth resolution in ScanSAR images. However, some problems due to the use of classical FFT as a spectral estimator are also identified. For that reason, Chirp-Z Transform used as a spectral estimator is then considered, and consequently interpolation can be avoided. Nevertheless, range and azimuth data require different processing features that have to be carefully studied. Therefore, this work identifies special characteristics demanded by SPECAN in range and azimuth.

Overall processing evaluation is obtained in a simulation environment using ERS raw data and simulated data (see Fig. 1). The conclusion obtained from this study is that SPECAN is a very appropriate candidate for processing ScanSAR data not only in azimuth but also in range. The results show that these new developments are very promising for obtaining fast and simple ScanSAR image generation and it could be a candidate for a potential on-board implementation.

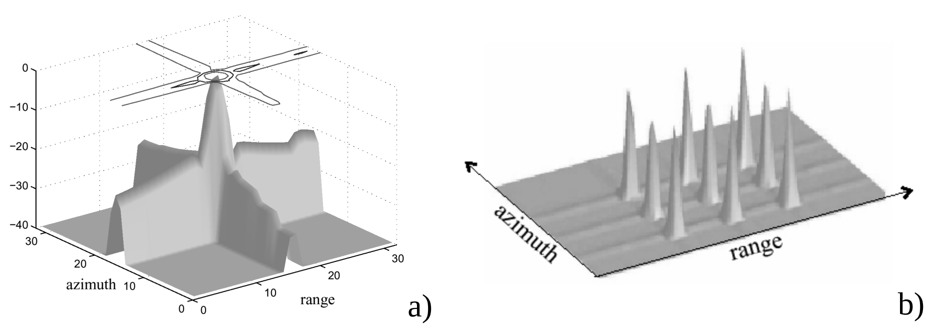

Figure 1: Impulse response (dB) with one target a) and several targets b).

Automated Extraction of Three-Dimensional Point Scatterer Target Models

S. W. Staker, J. G. Kelly, and R. G. Atkins
MIT Lincoln Laboratory
Lexington, MA 02420-9185, U.S.A.

Simulation of radar returns from dynamic objects continues to be of significant interest in hardware-in-the-loop or computer modeling of radar systems. To support such simulations, a knowledge of target signatures is required over a potentially large range of aspects and rolls. Furthermore to permit accurate Doppler modeling, these signatures must be adequately sampled to capture signature phase variations with target motion. Direct prediction or measurement of target signatures with the required Nyquist sampling in both aspect and roll is generally impractical.

To overcome these limitations point scatterer models have been suggested as providing an approach to coherently interpolate between coarsely sampled signature predictions or measurements. By identifying the three-dimensional location and complex amplitude of individual scatterers, the interference effects for small changes in target aspect can be correctly calculated. In the past, three dimensional point scatterer models of this type have been derived by hand, manually placing scatterers at appropriate locations on the target. Automatic algorithms have been developed to extract two dimensional point scatterer representations, but direct extension of these approaches to three dimensions would again require a dense sampling of signature data.

This talk presents a novel algorithm for automatically extracting three-dimensional point scatterer signature representations, from sparsely sampled predictions or measurements. The algorithm forms the equivalent of two spatially orthogonal images and identifies the projected location of the brightest spot as the correct three-dimensional position of a point scatterer. The best complex coefficient is then calculated in a least squares error sense over the data set of the orthogonal images. The complex scattered field of the point scatterer is then formed and subtracted from the original data set, forming a residual. The process is repeated using the residual until the desired number of scatterers is extracted or a minimum energy requirement is achieved. Finally, the complex coefficients of all extracted point scatterers can be refitted simultaneously via a least squares error. This point scatterer extraction algorithm is applied to a representative target and shown to place scattering centers at their correct three-dimensional locations. Evaluation of the model is further shown to provide accurate modeling of Doppler effects.

The Routing Model of Anti-Interfere Performance for the Electric Information System (EIS)

C. J. Wang
China National Software Technology & Services Company
Beijing, 100081, China

J. F. Dai
China Academy of Electronics & Information Technology
Beijing, 100041, China

The EIS consists of detection subsystem, Communication subsystem, data processing subsystem, and control subsystem, the anti-interfere ability of which is its important basic performance. In order to ensure the network system can transfer and process the information reliable and realize the electromagnetic compatibility with the environment in the condition of electromagnetic interferes. The paper is based on the information transfer, using the index of system connectivity and the average delay, to build the routing model of anti-interfere performance for information system and give out the mathematic model. The theory of non-linear integer programme (NLIP) has been used in building the model. We also have done the computer simulation test for the system.

Considering the information transmission network as show fig.1, there are m nodes, from the I-th node to the I+1-th of them having n_i communication mode.

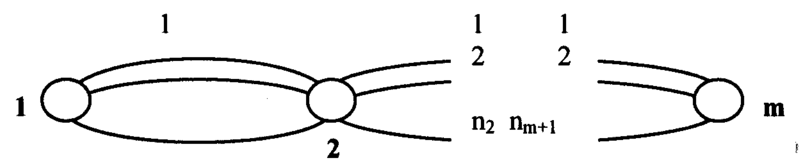

Figure 1: The schematic drawing of the information transmission network

Under the practice interference environment $k = 1, \dots, m-1$, $i = 1, \dots, n_k$, are marked as:

r_{ki}: representing the connectivity of the i-th mode from k-th node to $k+1$-th.

t_{ki}: representing the average delay of the i-th mode from k-th node to $k+1$-th.

Introducing the decision variable x_{ki} $(k = 1, 2, \dots, m-1,\ i = 1, 2, \dots, n_k)$ its supposal value is:

$$\begin{array}{ll} x_{ki} = 1 & \text{information transmission from } k\text{-th node to } k+1\text{-th via } i\text{-th comm. method} \\ x_{ki} = 0 & (others) \end{array} \tag{1}$$

In order to evaluate the average system delay the network structure, the decision variable x_{ki} must satisfy

$$\sum_{i=1}^{n_k} x_{ki} = 1 \ (k = 1, 2, \dots, m-1) \tag{2}$$

On the basis of the satisfaction of condition (2), evaluate the total system delay t and system connectivity r of network structure respectively: $t = \sum_{k=1}^{m-1} \sum_{i=1}^{n_k} t_{ki} x_{ki}$ and $r = \prod_{k=1}^{m-1} \left(\sum_{i=1}^{n_k} r_{ki} x_{ki}\right)$ The mini system delay $t^* = \sum_{k=1}^{m-1} \min\{t_{ki} | i = 1, 2, \dots, n_k\}$ max. system connectivity $r^* = \prod_{k=1}^{m-1} \max\{r_{ki} | i = 1, 2, \dots, n_k\}$ Then, two problems appear: the one is in the case of satisfaction of system delay requirement, evaluate max. system connectivity; the other is in the case of satisfaction of system connectivity requirement, to evaluate mini system delay. Because the mathematic representation of the system delay and connectivity, and the position in evaluated problem are different (either target function or restriction function). These are two perfectly different problems for evaluation method. The paper discusses the evaluation method for the min. system delay under satisfaction of the requirement of the system connectivity.

Novel Chaotic Signal Radar and Processing Scheme for Automotive Collision-Avoidance Applications

Y. Hara, T. Hara, T. Seo, and H. Yanagisawa
Mitsubishi Electric Corporation, Kamakura Works
Kamakura, 247-8520, Japan

P. Ratliff and W. Machowski
Mitsubishi Electric ITE BV, Visual Information Laboratory
Guildford, GU2 5YD, U.K.

This paper describes the development of a novel type of radar called Chaotic Signal Radar (CSR). This radar utilises chaotic or truly random continuous binary signals, in conjunction with a novel implicit sampling algorithm in the radar receiver processor, instead of a conventional correlator. This unique, but simple, processing scheme enables a very large processing gain in the receiver, which provides a very high resistance to external noise and interference, including that from the similar radar systems. Consequently, the CSR processing scheme is capable of accurately estimating obstacle distance in a complex multi-user environment. This makes it particularly well suited for applications such as automated highway monitoring (e.g. Automated Highway System - AHS), automotive collision avoidance/warning, autonomous navigation and many others.
Modelling results of the CSR using a software simulator are presented and supported by measurement results obtained from a prototype chaotic signal radar, developed for automated highway applications. The software employs the implicit sampling averaging algorithm and is capable of simulating various target scenarios and different types of interference. Additionally, several typical radar processing schemes, such as logarithmic compression, A/D conversion and signal limiting are implemented in the simulator. The software allows evaluation of the performance of the implicit sampling averaging algorithm in a basic radar system and demonstrates its attraction for interference rejection, especially in common-channel, multi-user scenarios. The characteristic waveforms (so-called *S-curves*) resulting from the simulations, indicate target ranges and may be compared with those obtained from actual measurements using the prototype CSR.

Remote Estimation of Fractal Descriptors from Transients Corrupted by Noise

Y. Laksari and H. Aubert
Institut National Polytechnique
Toulouse, France

J. Y. Tourneret
ENSEEIHT/TéSA
Toulouse, France

D. L. Jaggard
University of Pennsylvania
Philadelphia, PA, U.S.A.

This research work is placed in the framework of the time-scale analysis of waves reflected by fractal objects and the remote extraction of their fractal properties (inverse problem resolution). Based on the partition function introduced in [1] for the analysis of multifractal measures, an original partition function Z has been recently applied with success to the remote estimation of the similarity dimension of Cantor superlattices [2]. This wavelet-based partition function is computed from hierarchical structures that may appear in the time-scale domain when a wavelet analysis is performed on the impulse response of fractal objects. As an example, the figure 1 (a) displays the skeleton, i.e. the set of wavelet-transform (WT) modulus-maxima in time-scale domain, of the impulse response of a triadic Cantor superlattice. Here we explore impulse responses corrupted by white additive Gaussian noise. At first glance, for such responses, the arch-like skeleton of figure 1 (a) is broken (see figure 1 (b)) but, if we focus on fine scales hierarchical structures are apparent in time-scale domain and may be used for the computation of the partition function Z. Moreover we have established criteria for the choice of the mother wavelet used in the WT in order to enhance the extraction fractal descriptors from noisy reflected signals. In the particular case of Cantor superlattice, we have shown that the error in the remote estimation of the similarity dimension does not exceed 5% for signal to noise ratio higher than 15 dB.

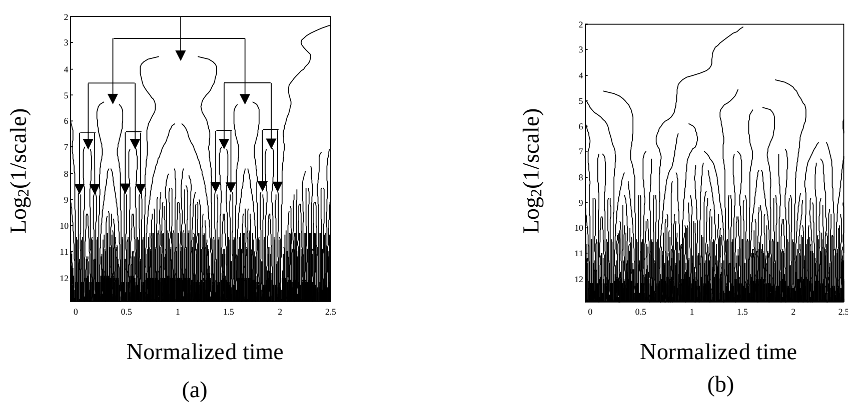

Figure 1 : Skeleton of the impulse-response (IR) of a Cantor Superlattice : (a) IR not corrupted by noise (arrows indicate the hierarchical structure from which the partition function is computed) and (b) IR corrupted by noise (S/N=20dB).

REFERENCES

1. A. Arneodo, "Wavelet analysis of fractals: from the mathematical concepts to experimental reality", in *Wavelets: Theory and Applications*, G. Erlebacher, M. Y. Hussaini, L. M. Jameson, eds., Oxford University Press (1996)
2. Y. Laksari, H. Aubert, D.L. Jaggard, "Wavelet-based Partition Function for the Analysis of Transient on Fractal Objects," *URSI International Symposium on Electromagnetic Theory*, Victoria, Canada, May 13-17, 2001.

Electromagnetic Environment and Communication System of Civil Aviation

J. F. Dai
China Academy of Electronics and Information Technology
Beijing, China

The communication of civil aviation is the important composition part of air traffic control system; it is information interactive bridge of ground and air. Because of the high-speed development of modern IT, radar equipment, navigation and communication network etc, dense distributions of various electronic information equipment, adding the electromagnetic phenomenon of nature (such as lightning etc.), make our electromagnetic environment very complex. In order to guarantee flight security, we must raise the ability of anti-interference and connectivity of ground-air communication system; realize the EMC of electromagnetic environment and the communication of civil aviation. This paper is about building the model and simulation test in the situation which ground-air communication system is interfered by electromagnetic environment.

In this paper, the airborne station is assumed to be a distance R_i from the interference source and a distance R_s from the ground station of the center of air traffic control. Assumption: Airborne radio station is the antenna of "Γ-model", ground radio station is a dimension array antenna of "double-awls", and interference source is the omnidirectional antenna or the antenna of "log-periodic". The communication equipment of civil aviation is been assumed to work in narrow-band model, spread spectrum model, hybrid model of spread spectrum and frequency stepping.

The interference-to-signal ratio of receiver for airborne communication station in input is K_{i1}:

$$K_{i1} = P_{ir}/P_{sr} = (P_iG_i/P_sG_s)(R_s/R_i)^2(G_{ir}/G_{sr})(L_i/L_s) \tag{1}$$

The interference-to-signal ratio of receiver for airborne communication station in output is K_{i2}:

$$K_{i2} = K_{i1}\{1/[3M^2(1+M)]\}(\Delta f_i/\Delta f_s) \tag{2}$$

where Δf_s and Δf_i are the bandwidths of the receiver and interference sources, and M is the signal modulability. Putting (1) into (2), we can get the following interference equation:

$$R_i = R_s(1/K_{i2})^{1/2}\{[P_iG_i/P_sG_s][L_i/L_s][\Delta f_i/\Delta f_s][1/(3M^2(1+M))]\}^{1/2}(G_{ir}/G_{sr})^{1/2} \tag{3}$$

The parameter relation among the airborne communication station, the ground station of civil aviation and the interference source are been given in the above equation.

Using the expressions of this paper to build model, we will get the simulation experiment result in different interference environment. The value of interference scope (R_i) is been given when the ground communication station of civil aviation center and the airborne communication station locate in X-Y plane, the interference source and airborne station locate in X-Z plane and the value of R_s is 150Km.

R_{i1} express the communication equipment of civil aviation working in narrow band model. R_{i2} express that working in spread spectrum mode (set up system value of spread spectrum gain for 8dB). R_{i3} express that working in the hybrid model of spread spectrum and frequency stepping (set up system value of frequency stepping gain for 17dB). This result of simulation experiment in the hybrid model of spread spectrum and frequency stepping is the best. And the ability of anti-interference for environment is the strongest. The connectivity of ground-air communication station is about one in the scope without interference. In the above situation, the EMC of electromagnetic environment and civil aviation communication system can be realized. At the same time, the air traffic control system can offer the security guarantee for the airplane of civil aviation.

Fuzzy Logic Controllers for Radar Applications

S. V. Halse, C. S. Parvati and A. B. Kulkrni
Department of Applied Electronics, Gulbarga University
Gulbarga, 585106, India

S. R. Sawant, R. R. Mudholkar
Department of electronics, Shivaji university, Kolhapur-416 004
Kolhapur, 416 004, India

Radars are versatile systems to scan the region of interest and detect and track a particular enemy aircraft. The initial position coordinates of enemy aircraft (R_i, θ_i, φ_i) can be determined by normal CW or pulsed radar systems. The Doppler shift in frequency of pulsed Doppler radar gives information about the velocity and direction of the enemy aircraft. Therefore, if the delay between the detection and the missile firing is known a priori, then the final coordinates (R_f, θ_f, φ_f) can be computed using PC. For fast, reliable, robust and automatic detection and firing system, conventional control mechanisms are inadequate, because they are not adaptive to the changing environment and not suitable for non-linear control system. However, a fuzzy logic control system can provide better solutions to such problems.

The mechanically steerable antenna system is mounted on a pedestal movable both in azimuth (AZ) and elevation (EL) with help of precision dc servomotors. During the scanning cycle, the radar detects the initial position coordinates and velocity and direction of the enemy aircraft and stores the information in the memory of the PC as a set of reference values. The scanning could also be a conical scan. Once the target is acquired, its trajectory is to be precisely determined by accurate tracking technique. The potentiometers associated with the shifts of the AZ and EL dc servomotors, give voltages proportional to the angular position. These voltages are ill-defined or fuzzy quantities. By using fuzzy set theory, appropriate membership functions are developed and the fuzzy values of the said voltages are fuzzified. The fuzzified values are compared with the rule-base in the PC and appropriate control decisions are taken by using IF-THEN rules. The received echo signals will be the strongest if the antenna is oriented directly towards the enemy aircraft. The fuzzified control signals from the inference engine (the PC with fuzzy logic algorithms) are defuzzified and fed back to the servomechanism (actuators) so as to reduce the error in angle and the rate of change of error in angle. In this case, the radar is said to be locked on the target. The direction, position, velocity and trajectory information is provided to the missile launching system by the PC, so as to shoot the enemy aircraft with high accuracy.

This paper deals with investigations on design and development of fuzzy logic controllers for accurate and precise control of the non-linear servomechanism of the radar antenna and also to provide requisite parameters to the tracking radar and the associated missile launching system. This paper demonstrates that the fuzzy logic control system is flexible, adaptive, more accurate and robust as compared to the conventional electro-mechanical control systems.

The Defect of Analytical Signal at Modelling of Oscillations with an Arbitrary Amplitude-Phase Modulation

I. D. Zolotarev
JSC "Navigational Systems" Company
Omsk, Russia

The problem of unique determination of envelope and phase of a radio signal is one of the fundamental problems of modern radio electronics ("Amplitude, Phase, Frequency" problem — APF problem). At a present time complex presentation of oscillations in the form of analytical signal (AS) — $f_a(t)$ is a popular solution of this problem. A certain difference of obtained values of envelope and phase from their physical content is the disadvantage of AS.

In [1-3] the new approach to the APF determination, which provides the adequacy of this parameters to their physical sense, is given. The solution is reached by application of complex signal (CS) — $f_k(t)$, obtained on the basis of using of a method, which simplifies Laplace Inverse Transform [4].

In known literature AS is developed for relatively simple types of amplitude modulation (saltus function, rectangular pulse) [5, 6]. However, at the practice of modern radio appliances designing complex types of radio signals modulation (when either amplitude or phase modulation present simultaneously) often take place. For the important case of arbitrary amplitude-phase modulation the new way of determination of error of oscillation process APF through AS is suggested.

For solution of this problem we write the analytical signal as,

$$\dot{f}_a(t) = \dot{f}_k(t) + \Delta\dot{f}_a(t),$$

where $\Delta\dot{f}_a(t)$ is the defect of AS.

After some transformations the expression for $\Delta\dot{f}_a(t)$ will be in the form

$$\Delta\dot{f}_a(t) = -\frac{1}{\pi}\int_{-\infty}^{0}\left[\dot{S}_1(\omega)e^{j\omega t} - \dot{S}_1^*(\omega)e^{-j\omega t}\right]d\omega = -\frac{2}{\pi}j\int_{-\infty}^{0}\dot{S}_1(\omega)\sin\left[\omega t + \psi(\omega)\right]d\omega.$$

Here $\dot{S}_1(\omega) = S_1(\omega)e^{j\psi_1(\omega)} = \frac{1}{2}F\{\dot{f}_k(t)\}$, where F is a Fourier direct transformation operator.

Thus, for the important case of arbitrary amplitude-phase modulation of a signal the expression for AS defect is obtained. As it was waited, the error takes place in the determination of imaginary component of AS, because real component of AS is established by initial real signal.

REFERENCES

1. Zolotarev I.D. Abstracts of the XXV General Assembly URSI. Lille, France. 1996. P. 148.
2. Zolotarev I.D. Proceedings of International Symposium "Acoustoelectronics, Frequency Control and Signal Generation". Moscow, 1996. P. 277281.
3. Zolotarev I.D. Proceedings of the Progress in Electromagnetics Research Symposium PIERS-97. Cambridge, Massachusetts, USA, 1997. P. 282.
4. Zolotarev I.D. Nonstationary processes in resonance amplifiers of phase-pulse measuring systems. Novosibirsk, Nauka Publishing, Siberian Division of Academy of Sciences of USSR, 1969.
5. Smolinski A.K. Bul. Acad. Pol. Sciences Techniques. 1971. V. 19, No. 6. P. 473484.
6. Zolotarev I.D. The Techniques of radio communication. 1997. Ed. 3. P. 3-10.

Session 5Ac4

EMC and Devices

A Study on Temperature Variation of the Lossy Material Inserted into the Gap of the Microwave Oven

K. Matsumoto, K. Kimura, and O. Hashimoto
Department of Electrical Engineering and Electronics, Aoyama Gakuin University
Tokyo, 157-8572, Japan

The door of microwave oven is necessary to take some food in and out. Prevention of leakage waves from the gap of the door becomes important Electromagnetic Compatibility (EMC) problem in daily life. To overcome this problem, a choke structure has been installed in the door of commercial microwave oven. The operation of the choke structure produces high shielding effectiveness (SE), however that is composed by $\lambda/4$ lines. Therefole, it is difficult to fabricate a thin door by using the choke structure.

The achievement of high SE has been confirmed theoretically by finite difference time domain (FDTD) method under the use of the lossy material inserted into the gap instead of the conventional choke structure (see in Fig. 1). It is found that an SE of 30 dB or more is obtained when the gap is filled with the lossy material. In practical use, we worry that heat from the oven cavity affects the lossy material.

In this paper, temperature variation and shielding characteristics of the lossy material by heat are examined using FDTD-HTE, (Heat Transport Equation) method. Concretely, we applied the HTE to the part of lossy material in analytical model and analyzed using time series data of real leakage waves which saved from the oven cavity model. As a result, temperature variation can be confirmed quantitatively and visually. Furthermore, we found that temperature variation is not depending on the influence on the material constant. It is also clarified that the SE of 30 dB or more is obtained under the use of the lossy material (see in Fig. 2). Consequently, it is confirmed that the thin door with the lossy material which has versatility and high SE without the influence of heat from the oven cavity is realized.

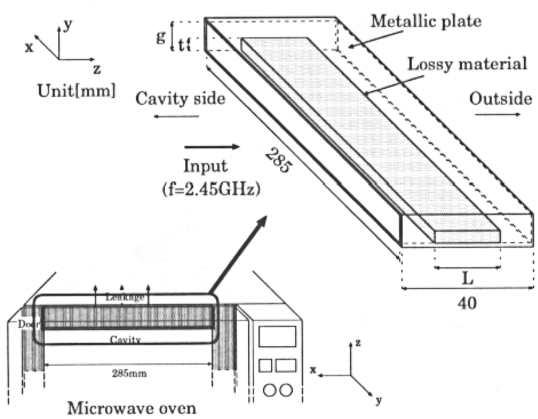

Fig. 1 The gap of the microwave oven.

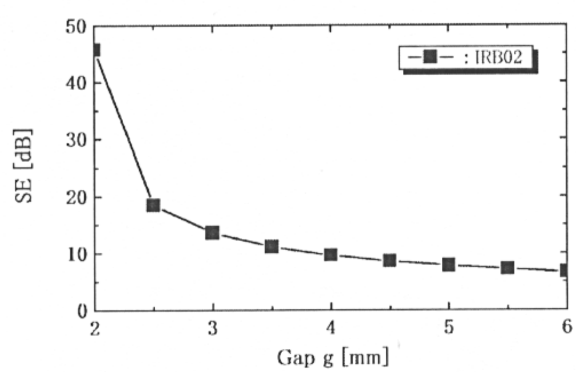

Fig. 2 SE of lossy material.

The Electromagnetic Compatibility of Heat Sinks

C. H. Ding and J. H. Chou
Department of Engineering Science, National Cheng Kung University
Tainan, Taiwan

For economic reasons, heat sinks are commonly used in consumer electronic products to enhance heat transfer to increase the reliability of these products. On the other hand, with the continuous increase in processing speed and clock frequencies of micro processors, there are concerns on the electromagnetic compatibility of heat sinks. In this paper, a FDTD numerical methods is used to solve the three dimensional Maxwell equations to investigate EMC of mounted onto a simplified electronic package. The package is of a square type with a dimension of $25\mathrm{mm} \times 25\mathrm{mm}$. The dimensions of all of the heat sinks are the same, namely, $25\mathrm{mm} \times 25\mathrm{mm} \times 12.5\mathrm{mm}$. Within the limit of 12.5mm, the heights of base and fins of the heat sink are varied. A Gaussian electric pulse is used as the EM source. The central frequency of the pulse is fixed at 5 GHz.

The numerical results indicate several features. First, the heat sink tends to play the role as an antenna. In other words, it tends to become a waveguide when the source is located outside the package and scatters the wave when the source is located inside the package. Namely, the EMS and EMI effects of a heat sink on the electronic package can be different. Second, when EMC effects of a heat sink shows up, the dominated resonance frequencies are around the frequencies at 2.5 GHz, 5 GHz and 7.5 GHz. Third, the extent of EMC depends on the number of fins on a heat sink. Thus, care should be taken when choosing heat sinks for GHz applications.

Channel Characterization of SOHO Power Distribution Wiring

R. Llorente, F. J. Martínez, J. M. Fuster, J. Marti, and R. Clavero
ITACA Research Institute, Universidad Politécnica de Valencia
Valencia, 46022, Spain

This paper presents experimental and theoretical results covering identification and statistical characterization of the different noise sources, mainly originated by the guided and radiated electromagnetic interference produced by appliances connected to the power distribution wiring deployed in office environments. S-Parameter transmission line point of view modeling has been included in this paper, enabling power wiring to be evaluated as a communication channel suitable for different technologies.

The introduction of high frequency or high bit-rate communication techniques over power distribution lines needs a complete characterization of the in-home or office power wiring. It can be pointed out that the interest on user power wirings or companies' power distribution grids as communication channel is based in several key factors: World-wide availability, near ubiquitous network connection points (several plugs in every costumer location) and no additional wiring (low deployment cost)

The results shown depict the development of coupling devices, automatic measurement set-up, statistical post-processing and theoretical modeling of the evaluated parameters: Impulsive noise, background noise, coherence time, coherence bandwidth and transmission/reflection behavior up to 100 MHz, being in the best of our knowledge the wider span modeling published in this kind of transmission channel.

The work has been carried in an office (campus) building, as potential users of emerging high bit-rate technologies are mainly small and medium companies rather than residential costumers. We have initially focused the research tasks in this SOHO (small office, home office) environment but extensions to home environments are being carrier out.

Statistical significance and de-correlation from season and repetitive patterns has been obtained through extensive in time measurement (several months time span) and carefully selection of the measuring conditions. Mathematical post-processing and best-fit strategies have been developed to obtain noise probability density functions in good agreement with the theoretical results.

A Coupled MoM-MBPE Algorithm Applied to Electromagnetic Compatibility Problems in Medical Areas

M. Schick and F. M. Landstorfer
University of Stuttgart
Stuttgart, Germany

The implementation of a model based parameter estimation (MBPE) algorithm and coupling with the field computation program FEKO is presented in the following as well as applications especially in medical areas.

Electromagnetic research in medical areas requires studies over large frequency ranges. Here the field computation program FEKO based on the Methods of Moments in the frequency domain is taken as an example. For achieving accurate results, the required computation time is usually high. In order to reduce the computational costs by minimizing the number of sampling points used the interpolation algorithm MPBE is applied to achieve a mathematically based approximation of the problems. A function sampling in the frequency domain is approximated with MBPE to represent the original function by fitting models. This is done with rational polynoms based on the Padé approximation. The complete frequency range is divided into different windows and for every window a fitting model is determined. In the end all fitting models are combined for the overall solution function.

With the adaptive sampling a more flexible algorithm is applied to further minimizing the number of required sample points by using the advantage that for sampling in the frequency domain no uniformly spaced samples are required. It is started with a small set of sampling points and with these a set of overlapping windows is determined. The whole frequency range is covered by overlapping windows so a maximum error between two fitting models can be determined for every frequency. Where the error is a maximum a new sample point will be added until the error falls under a certain threshold.

A wire loop in a cube shaped metallic housing radiates an electromagnetic field. The shielding effectiveness (the electrical field radiated through the housing's front plate with four small slots in it is compared to the electrical field without a front plate) is displayed in figure 1. In this case only 71 samples were used compared to 901 for a closely and uniformly sampled function. There is almost no difference between the two functions. The factor in time saving is $901/71 = 12.7$. In other examples containing sharp peaks in the function saving factors up to 100 can be achieved.

In a project of determining the coupling of medical devices over the human body many computations over large frequency ranges have to be performed to get universal results. In figure 2 an example is given with the voltage at the electrode at the input of a cardiac pacemaker. The pacemaker is modeled as placed within a human body model while a coagulator is working at the latter's surface. For the computation of one sample point about eight hours are needed, 18 points are used in total. The implemented algorithm converges and shows good accuracy in first examples. Consequently it was successfully applied to computations in medical areas for saving computation time.

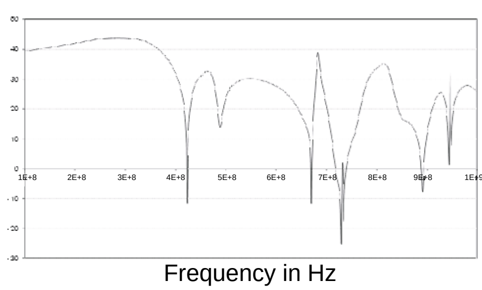

Figure 1: Shielding effectiveness of the housing in dB

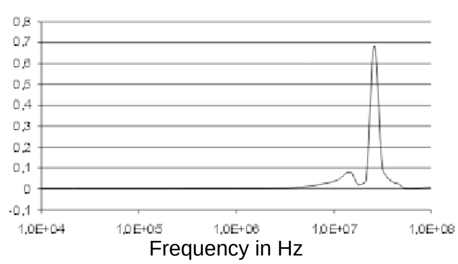

Figure 2: Voltage on the electrode at the entrance of a cardiac pacemaker in

Analysis of Hybrid Fuzzy Controller for Vector Control of an Induction Motor Drive

P. Gaur and S. Shirivastava
Netaji Subhas Institute of Agriculture & Technology, Delhi University
New Delhi, 110045, India

Many industrial applications for e.g. textile mills, cement mills, conveyer applications require very accurate fast position & speed control. D.C. motors are best suited for these kinds of applications because their control is simple as the two stator & rotor fields in D.C. machine are mutually decoupled & controlling them is easy. But D.C. motors require frequent maintenance and are costly also.

With the availability of faster & less expensive processors & solid state switches, Induction Motors drives now compare favorably to dc motor drives on considerations such as power to weight ratio, acceleration performance, maintenance etc.

Vector Control essentially decouples the two components of stator current — one providing the air gap flux & other producing torque. It provides independent control of flux & torque. The literature survey entails that till recently only conventional control has been used for vector controlled Induction motor drives. However, the conventional PI type controller cannot yield a good control performance if a controlled object is highly nonlinear & uncertain. In such cases another type of controller based on fuzzy logic is being increasingly applied to many systems with nonlinearly and uncertainty. Especially, control engineers' design the most successful fuzzy logic controllers applied into industrial plants by their expert knowledge. Unfortunately, defining membership functions of linguistic variables & formulating fuzzy rules by manual operation is time-consuming work. Also many people worry about their reliability. One of the motivations for this study is trying to answer these questions by proposing a Hybrid fuzzy P +conventional I controller. This controller is constructed by replacing the proportional term in the conventional PI controller with an incremental fuzzy logic controller. This controller incorporates the advantages of both PI and Fuzzy logic speed controller (suppression of overshoot and zero steady state error).

Synthesis of M-type Barium Hexaferrite and Effect of Substitution of Cobalt Titanium on its Microwave Dielectric Properties

S. B. Narang and I. S. Hudiara
Guru Nanak Dev University
Amritsar, India

Ferrites are very useful materials as their microwave properties make them suitable for manufacturing microwave components based on Faraday rotation principle. Cobalt titanium substituted M-type Barium hexaferrites are of great interest as they are promising materials for making permanent magnets for magnetic recording and they can also be used as microwave absorbers. It is therefore desired to study the effect of change in frequency and degree of substitution of CoTi in place of iron in the M-type Barium hexaferrite on its dielectric constant and loss factor. It is also desired to study the change in Curie temperature and Saturation magnetization as the Cobalt and Titanium percentage in the M type Barium hexaferrites is changed. A number of samples of Barium Hexaferrites $Ba(CoTi)_y\ Fe_{(12-2y)}O_{19}$ have been prepared by varying 'y' from 0.0 to 1.0 in steps of 0.1 using normal ceramic method. The density of the prepared samples was approximately 4.5 gm/cc. The complex permittivity of these samples was measured using short circuited transmission line method. A known length of the ferrite sample terminates a short-circuited air filled waveguide transmission line. The terminating impedance is determined experimentally by measurements on the standing wave pattern on the input side of the sample. Four parameters measured were, the waveguide wavelength, λg, the length of the sample (which was typically 0.62 cm), the position of the first minima from air sample interface and the voltage standing wave ratio $s \geq 1$. The measurements were made at room temperature, $23 \pm 1°C$. From the complex permittivity measurements the following conclusions have been drawn:

1. The dielectric constant of Barium HexaFerrites decreases as the frequency increases from 8.4 GHz to 12.4 GHz.
2. The loss factor also varies with frequency but does not follow a uniform pattern.
3. The dielectric constant and loss factor change at a particular frequency as the Cobalt and Titanium percentage is changed in the composition of Barium (Cobalt Titanium) Hexa Ferrite. It shows that the substitution of a part of the Fe^{3+} ions in Barium HexaFerrites with (CoTi) can be used to control the properties of ferrites at microwave frequency by varying the degree of substitution.

Currie temperature and saturation magnetization of Barium HexaFerrite has also been measured for varying amount of substitution of Cobalt and Titanium in place of Iron. It has been found that both the Curie temperature and saturation magnetisation decrease with increase in percentage of Cobalt and Titanium in place of Iron.

The chemical content of cobalt and titanium substituted Barium HexaFerrite has also been studied by means of X-ray analysis. It has been observed that the ions of Co and Ti occupy such lattice sites as to maintain the M-type hexagonal structure. The variation of lattice parameters "a" and "c" with the degree of substitution of (CoTi) has been found. All these results have been presented graphically in the paper.

Design and Simulation of Sensorless Control of Permanent Magnet Servo Drive

P. Gaur, A. Arora, and R. Kumar
Netaji Subhas Institute of Agriculture & Technology, Delhi University
New Delhi, 110045, India

Permanent magnet synchronous motors are widely used in high performance motion control systems because of their desirable features as compared to other motors. In these motors field coils are replaced by permanent magnet. Thus it eliminates losses due to field windings. The control of PMSM is entirely done through stator since there is no provision for rotor side excitation control.

The PMSM can offer significant higher advantages and efficiency over other types of motors when employed in adjustable speed drives. These motors have high torque to weight ratio, higher efficiency, good power factor, faster response etc. The typical drive of the PMSM with hysteresis or pulse width modulation technique requires the measurement of rotor position, which is usually provided by the encoder or the resolver mounted on the shaft of the motor. Among the numerous methods available for position and rotor speed detection, the technique using mechanical sensors, Hall effect transducers, tacho-generators, optical or inductive coupling sensors makes the drive system bulky, less efficient and expensive. Thus an indirect method of rotor position detection, which detects the rotor position and calculates the rotor speed from stator variable is needed.

In this paper the overall idea is to estimate the position and speed of sensor less drive of a permanent magnet synchronous motor in **SIMULINK**. As we do not know the actual position thus a model of the motor have been made in which motor is driven from known position and thus there will be some current difference between motor and model. There will bw difference in both currents in motor and model. The current difference is decomposed into two components. One is used to estimate the position and another for estimation of speed. Therefore position and speed can be estimated separately in this scheme. The results are simulated in modern software SIMULINK.

Comparative Analysis of Different Speed Controllers for Field Oriented Controlled Permanent Magnet Synchronous Motor Drive

P. Gaur, R. Kumar, and A. Arora
Netaji Subhas Institute of Agriculture & Technology, Delhi University
New Delhi, 110045, India

The PMSM is one of the types of brushless Permanent Magnet Motor, in which the windings of the motor are sinusoidally distributed & generate sinusoidal induced emfs. These motors have numerous advantages over others machines that are conventionally used for ac servo drives, such as improved efficiency, increase power density ratio, faster dynamic response, less maintenance, improved power factor, high torque to inertia ratio. To achieve desired level of performance it requires a suitable speed and current controller and that is the motive behind this work.

A conventional PI speed controller has been used in motion control applications for a long time. Numerous works reported in recent past have shown that a fuzzy logic controller has a potential to replace the conventional PI controller. Fuzzy logic control apparently offers a possibility of obtaining an improvement in the quality of the speed response, compared to PI control.

This work focuses on investigation and evaluation of the performance of a permanent magnet synchronous motor (PMSM) drive, controlled by PI, SMC (sliding mode control) and Fuzzy logic speed controllers. Performance differences due to the use of pulsewidth-modulation (PWM) and hystersis current controllers are also examined. The drive is simulated using Simulink toolbox of the MATLAB software package.

Amplification of Microwave Acoustic Modes in n-GaAs Film

S. Koshevaya, M. Tecpoyotl-Torres, J. Escobedo-Alatorre, and J. Sanchez-Mondragon
Center for Investigations on Engineering and Applied Science
Autonomous State University of Morelos
Morelos, Z.P. 62210, Mexico

V. Grimalsky
Electronics Department
National Institute for Astrophysics, Optics, and Electronics
Puebla, Z.P. 72000, Mexico

An amplification of coupled space charge — acoustic waves in thin n-GaAs film is theoretically investigated. The film is placed between two symmetrical substrates of i-GaAs without an acoustic contact. The film includes 2D electron gas with a high negative differential mobility [1] or uniform initial distribution of electrons. The length of the structure is L (along axis Oz), the thicknesses of film and substrates are $2h$ and d, respectively (along axis Ox). The other sizes are assumed as infinite. In absence of the current, the piezoactive transverse anti-symmetric acoustic wave modes of the film are:

$$u \equiv u_y = B\sin(gx)\cdot\exp(i(\omega t - kz)); \qquad \varphi \sim \cos(gx)\cdot\exp(i(\omega t - kz)), \tag{1}$$

where φ is electric potential, ω is circular frequency, $k = (\omega^2 - \omega_{crit}^2)^{1/2}/s$ is longitudinal wave number, and the parameter $g \equiv \omega_{crit}/s \approx (\pi/2h)(2n+1),\ n = 0, 1, 2\ldots$ describes the transverse distribution of displacement and potential; ω_{crit} is a cut-off frequency, $s \approx 3\cdot 10^5\,cm/s$ is a transverse sound velocity [2].

In a presence of current, an amplification of space charge wave takes place due to negative differential conductivity. This wave can excite the acoustic modes of the film, due to piezoeffect. For effective coupling, the wave numbers of interacting waves must satisfy the resonant matching condition: $k_{SCW} = k_{sound}$, or:

$$\omega/V_0 = \left(\omega^2 - \omega_{crit}^2\right)^{1/2}/s. \tag{2}$$

Here V_0 is a velocity of space charge wave. This condition is a relation between the frequency, velocities, and the thickness of the film. Because $s \ll V_0$, the higher acoustic modes $(n \sim 5)$ near cut-off can be effectively excited.

The coupled equations for slowly varying amplitudes of sound mode and space charge waves have been derived from the theory of elasticity, quasi-hydrodynamic equations of motions of electrons, and Maxwell's equations. The numerical simulations have demonstrated the effective amplification of sound in a presence of negative differential conductivity. The following parameters have been chosen: the concentration of electrons in the film is $n_0 \approx 10^{15}\,cm^{-3}$, the velocity of electrons is $V_0 \approx 2\cdot 10^7\,cm/s$, the length of the film is $L = 0.1\,cm$, the thickness of the film is $2h = 1\,\mu m$. An intensity of acoustic mode can reach $1\,W/cm^2$ at microwave frequencies $\omega = 5\cdot 10^{10} - 2\cdot 10^{11}\,s^{-1}$.

REFERENCES

1. Shur, M., *GaAs Devices and Circuits,* Plenum Press, N.Y., 1989.
2. Dieulesaint, E. and D. Royer, *Elastic Waves in Solids,* Wiley, N.Y., 1980.

Session 5Aa5

Efficient, Wideband, Electrically Small Antennas: Fantasy or Reality

Electrically Small, Efficient, Wide Band Antennas for Unattended Sensors

R. Rudish and S. Sussman-Fort
EDO/AIL Electronic Systems Group
Deer Park, NY 11729, U.S.A.

DARPA is developing concepts for achieving RF spectrum dominance in the tactical RF battlespace (20 MHz to 15+ GHz). Efficient antenna coverage over this broad spectrum for both transmit and receive functions is necessary. Coverage with the fewest number of antennas has a size advantage but requires each to achieve wide bandwidths.

As part of DARPA's programs, EDO is developing an antenna that can service over two decades of bandwidth, starting at 20 MHz. Yet this antenna is only one foot in its longest dimension and occupies less than a cubic foot in volume. Over the upper decade, because of its shape and its image in the ground, it can operate as an efficient biconical horn. Over the lower decade, it operates as a monopole. Below 200 MHz, this monopole is electrically small, which would ordinarily cause it suffer high impedance mismatch losses (low efficiency) or, if tuned, narrow bandwidth.

The impedance of an electrically small antenna is highly reactive, creating difficulty in obtaining wide band impedance match. One well known equivalent circuit for a monopole that operates well below its first resonance is a series connection of a large capacitive reactance, a small inductive reactance, and very small radiation resistance. This combination is a high-Q circuit. Furthermore, the resistance decreases as the square of frequency decrease, inversely raising circuit Q. The shape of the low frequency monopole was optimized to reduce its circuit Q.

EDO's approach is to use a non-Foster impedance network to impedance-match the antenna over its lower decade. A non-Foster impedance is one that has a negative reactance slope versus frequency, and thus doesn't obey Foster's Reactance Theorem. We cancel the conventional (Foster) reactances in the equivalent circuit over decade bandwidths by connecting them in series with equal, but opposite-signed non-Foster reactances. We also use non-Foster reactances to transform the radiation resistance to a useful fixed value, such as 50 ohms, over this same decade bandwidth.

We implement non-Foster impedances using devices called Negative Impedance Converters (NICs). A pair of negative second-generation Current Conveyors (CCII-), which are cascades of transistors arranged to provide high transconductance, implements each NIC.

The non-Foster network approach to impedance matching the low frequency monopole has the promise of yielding near isotropic gain over much of the VHF band from such a small antenna. We are currently optimizing the matching network design for both transmit and receive modes and investigating the extent of dynamic range limitations imposed by added noise and non-linear behavior. In addition to reducing mismatch loss to an acceptable level, optimization is also reducing dissipation loss (high Q non-Foster matching elements), and prime power requirements. Our progress is presented as a series of performance charts.

A Compact Dual-Band Dual-Polarization Microstrip Patch Antenna

J.-S. Row
Department of Electronic Engineering, Chien Kuo Institute of Technology
Chang-hua, Taiwan

Nowadays, some vehicles are equipped with wireless communication systems, such as DCS (Digital Communication System), and the global positioning system (GPS). In this case, the antennas for these systems are usually installed separatively, and large realty space is thus occupied. For DCS operation on a vehicle, the antenna must be capable of radiating a conical-pattern linearly polarized wave to provide low-angle coverage. As for GPS operation, it is required that the receiving antenna has a broadside circularly polarized radiation pattern. In this article, a new integrated structure of a two-element microstrip patch antenna with two feeds for DCS/GPS dual-band dual-polarization operations is proposed. The radiating element for DCS (1710-1880 MHz) operation is a broadband low-profile cylindrical monopole top-loaded with a shorted square patch, which fives linearly polarized conical-pattern radiation. The second radiating element is a square-ring microstrip patch with truncated corners for GPS operation at 1575 GHz, which provides circularly polarized broadside radiation patterns. The two radiation elements are integrated in the proposed antenna to have a compact structure. The proposed antenna meets the bandwidth requirements of DCS and GPS systems, and is suitable for mounting on a vehicle.

Slot Antenna with Chip Capacitor Loading for Size Reduction

C.-S. Hong
Department of Electrical Engineering, Chien-Kuo Institute of Technology, Changhua, Taiwan, R.O.C.
Changhua, Taiwan, 802, R.O.C.

Design of a slot antenna with a chip capacitor mounted at the slot is introduced. This design provides enhance antenna area reduction and a good crosspolarization level. The antenna design can be used as a compact antenna system where limited size is a major requirement.

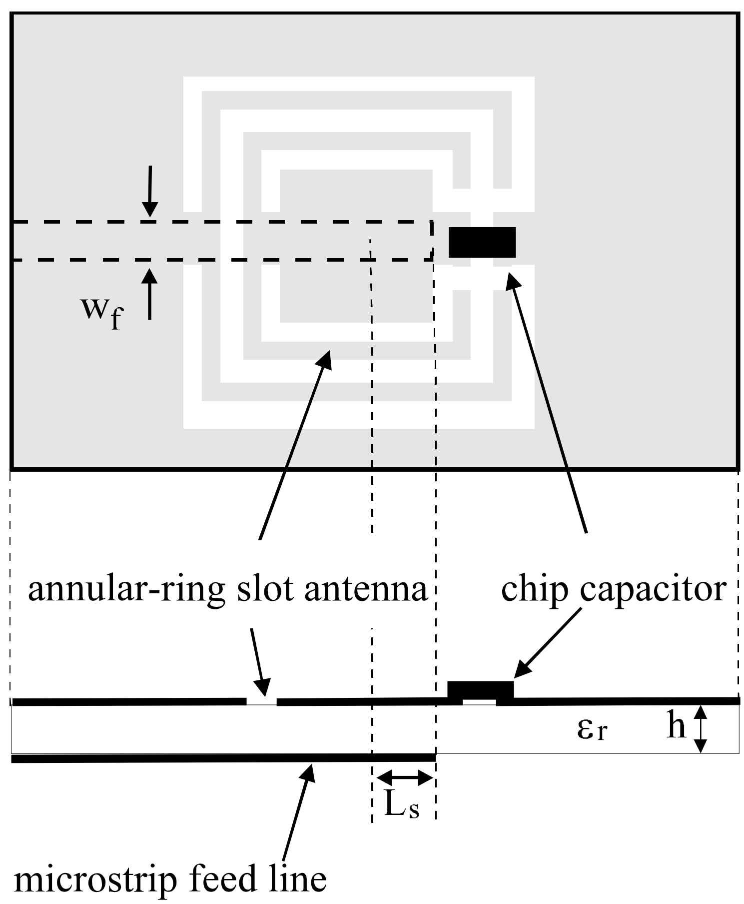

Fractal Planar Filters for Multi-band Microwave Applications

F. Surre, Y. Laksari, and H. Aubert
LEN7, ENSEEIHT
Toulouse, France

Fractal structures lead to the hope of many potential applications (see [1] and the references therein) as the design of anti-reflective coatings, dielectric mirrors, antennas arrays and selective microwave filters [2]. Recently the self-similarity property of such structures has been exploited for the design of multi-band antennas [3] and multi-band frequency selective surfaces [4]. Here, fractal geometry is explored for the synthesis of multi-band filters in the microwave or millimeter wave regimes. We focus on the realization of such filters in planar technology. Experimental data are presented and discussed. Simple rules are given for predicting the observed multi-band frequency responses.

The filter consists in two Sierpinski gaskets linked in order to realize a diamond (see figure 1). The total length of the structure is 177.8mm. The small scales are deduced from the whole triangle by a reduction factor of 1/2. In this abstract, we present a filter at stage four realized on a low-cost substrate (dielectric constant ϵ_r=4.32, height h=1.54mm and $\tan\delta = 1.8 \times 10^{-2}$). The excitation of the filtering structure is made by two 50Ω-microstrip lines. Figure 2 shows the modulus of coefficient transmission (measured on a HP8510B Network Analyzer). This response exhibits four bands: 360-680 MHz, 1.1-1.635 GHz, 3.37-3.68 GHz and 7-7.4 GHz. The ratio between two consecutive bands is close to 2 that is the inverse of the reduction factor. Therefore, the frequency response of such filter exhibits a log-periodic behavior. Another interesting result is the high rejection (lower to 50dB) in the band 4.3-6.75 GHz.

In this abstract, a new application of fractal shape is investigated by means of Sierpinski gasket. The realized filter presents four bands and a high-rejection band. Other fractal shapes produce similar filtering properties. Their explanation is underway.

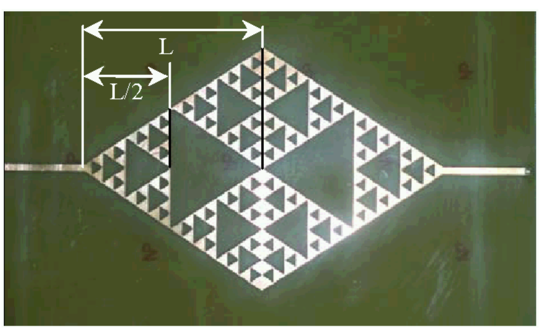

Figure 1 : Sierpinski gasket filter

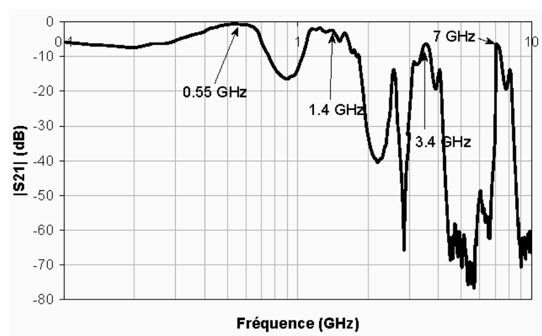

Figure 2 : |S21| versus frequency of the filter displayed on fig.1

REFERENCES

1. D. L. Jaggard, "Fractal electrodynamics: from super antennas to superlattices", in *Fractals in Engineering*, J. Lévy Véhél, E. Lutton and C. Tricot, eds., pp. 204-221, Berlin: Springer (1997).
2. A.S. Saleh and H. Aubert, "Self-similar Multi-slab Media with Variable Lacunarity for the Design of Microwave Filters", *Electronics Letters*, vol.37, No. 17, pp.1071-1073, August 2001.
3. C. Puente Baliarda, J. Romeu, R. Pous, A. Cardama, "On the Behavior of the Sierpinsni Fractal Antenna", *IEEE Transactions on Antennas and Propagation*, Vol. 46, Issue: 4 , April 1998, pp. 517-524
4. J. Romeu , Y. Rahmat-Samii, "Fractal FSS: a novel dual-band frequency selective surface", *IEEE Transactions on Antennas and Propagation*, Vol. 48, Issue: 7 , July 2000, pp. 1097 1105.

Low Q, Electrically Small Antennas: Mother Nature Can, Why Can't Electrical Engineers?

D. M. Grimes and C. A. Grimes
Department of Electrical Engineering, The Pennsylvania State University
University Park, PA 97124, U.S.A.

A radiating antenna sits in a standing energy field of its own making. Even at the shortest wavelengths for which antennas have been made if the antenna is electrically too small, that is, if the antenna length-to-radiated wavelength ratio is too small, the amount of standing field energy is so large it essentially shuts off energy exchange. Yet atoms, radiating electromagnetic energy with a wavelength-to-size ratio of several hundreds, appear to be unaffected by standing energy. Chu put the effect, as applied to constructed antennas, on a quantitative basis more than fifty years ago, for single order electric multipoles and single order, collocated dual multipoles. What happens with more complex multipolar source ensembles of sources has been the subject of much discussion since, with many concluding that the rules for single multipoles carry over to any and all ensembles. We believe the results carry over in many but not all cases, and describe important exceptions. Exceptions include the modal expansion terms of atomic radiation.

Our analysis requires careful examination of two critical concepts. The first: Near field power, as opposed to far field power, cannot be fully described using complex numbers. The logic is simple enough; it takes three numbers to describe near field power and complex numbers have but two. The second: if the source is frequency or amplitude modulated what happens to the periodically excessive portion of the standing energy? Does it return to the source or does it continue outward; in other words, does it or does it not affect antenna operation? Chu avoided both issues by working only on the source side of the antenna terminals; source power is fully expressible as a complex number and knowledge of the standing energy is unnecessary. His analysis is limited, however, since with a single source both differences in driving phases and input impedances preclude extending the technique to certain radiation sources.

We have obtained both numerical and experimental proof that the Q of certain source ensembles depends upon the relative phasing of the source elements. Although predicted by our analysis, the results would not be true if the rules for single multipoles carried over to all ensembles of sources.

The talk will review the mathematical framework, summarize numerical and experimental results, and discuss recent extensions to the theory.

Session 5Ab5

Modeling of Complex EM Structures/Media

Engineering Analysis and Design of 2-D Dielectric PBG Structure

X. Q. Shi and W. Z. Zhang
Southeast University
Nanjing, Jiangsu, P.R. China

The research work presented in this paper focus on a PBG structure that consists of an array of parallel air cylinders with circular cross section of radius r, embedded in a background dielectric material characterized by a dielectric constant ε_b. The intersection of the axes of these air cylinders with a perpendicular plane forms a rhombic lattice with side a and 60°/120° angle. The common frequency band-gap of this structure for any TM incident angle, characterized by the normalized central frequency f_0 and the relative band-gap $\Delta f/f_0$, is analyzed and programmed, based on the plane wave expansion method with computation-intensive process, in the previous work.

In the first part of this article, two estimation-oriented formulae are summarized for this kind of 2-D dielectric PBG structure. They are $\Delta f/f_0$ and λ_0/a as fitting functions of arguments ε_b and $\beta = r/a$. In order to minimize the error between the data from exact calculation and from fitting formulae, ε_b is divided into three sections: 2∼9, 10∼20 and 20∼30. The relative errors for λ_0/a are less than 7.7%, 7,2% and 8.2% at fit points in different sections respectively, and less than 7.2% at other points when ε_b=11.6 ; The errors for $\Delta f/f_0$ are less than 4% in all the sections. According to these fitting formulae, the stop-band response can be easily predicted when structure parameters (ε_b and $\beta = r/a$) are already given.

In the second part of this article, the other three design-oriented formulae are fitted too. Where the design parameters ε_b, β and a are simply calculated from the desired band-gap range (f_{min}, f_{max}), throughout $f_0 = (f_{min} + f_{max})/2$ and $\Delta f/f_0 = (f_{max} - f_{min})/f_0$. As well as the range means that at least be covered, its solution of the design is not unique. The other factors such as the structural compactness, the availability of the permittivity, should also be taken into account in practical design.

On the Refraction Index of Photonic Crystal

L. G. Zheng and W. X. Zhang
Southeast University
Nanjing, Jiangsu, China

A photonic crystal (or PBG material) is a structure whose refractive index is periodically modulated, and it possesses many attractive characteristics, such as propagation inhibition between certain frequency bands.

For 1-D periodic structure, which is well known as diffraction grating, there exists an analytical dispersion relation. From this relation, Dowling *et al.* predicted an ultra-small refraction index of photonic crystal in the higher frequency bands. Notomi argued that the same effect could be observed even for an empty lattice with the same crystal structure. In his opinion, the above effect was resulted from the reduction of wave vector **k**, which near the center of zone due to the band folding; and then he suggested that the right way to study propagation in photonic crystals should use the group velocity vector rather than **k** vector.

After a careful study of the dispersion relation, the authors of this paper obtained a good answer to this question. Although the normal dispersion curves ("reduced zone scheme") are good enough to show the band structure, it is actually not appropriate to be used to predict the refraction index curves. In order to retrieve the refraction index curves of a photonic crystal, one should use a "repeated zone scheme", which gives a complete view of the dispersion relation. Then who can find out the line segments totally belonging to a single reciprocal lattice, for example, the origin of the coordinates. If this rule is followed, one will obtain correct refraction index curves for the empty lattice structure, and who will find out that there exists no ultra-small refraction index for higher frequency band of a non-empty lattice photonic crystal.

2-D Photonic Crystals Consisting of Bianisotropic Media

L. G. Zheng and W. X. Zhang
Southeast University
Nanjing, China

L.-W. Li
National University of Singapore
Singapore

Photonic crystals got their name from the fact that their refraction indexes are modified periodically in a form of a traditional crystal lattice. So the propagation characteristics of a photonic crystal can be analyzed using classical method, such as plane wave method. Most photonic crystals researched consist of isotropic and/or anisotropic media. In this paper, a plane wave method based model for 2-D photonic crystals consisting of bianisotropic media is presented. There are many aspects necessary to be considered in the modeling phase.

1. On the wave equations —– The eigenvalue equations by using both **D** and **B** is established. The *D-B* plane, in addition to the vector **k**, comprises a *k-D-B* coordinate system. In this system, **k** is always perpendicular to both **D** and **B**, which are 2-D vectors in the *D-B* plane, thus the size of a basic matrix can be reduced from 6x6 to 4x4.

2. On the dimension —– For simplicity, a matrix-based eigen-equation solver is used. That means, only 2-D photonic crystal can be analyzed in an acceptable degree of convergence. For 3-D photonic crystal, another eigen-equation solver, such as iteration algorithm, should be incorporated to reach reasonable precision.

3. On the polarization —– For isotropic media, TE and TM waves can be analyzed independently. However, for bianisotropic media, even for Chiral material, all the eigen-modes are elliptically polarized waves and one can not decompose them into independent TE and TM waves.

The computation based on a photonic crystal consisting of square lattice of square Chiral rods surrounded by the air is performed, the results show that the band structure is similar to that of square isotropic dielectric rods. Extensive simulation is necessary in order to reveal the full characteristics of this kind of photonic crystals.

High Frequency RCS Computation of Complex Radar Targets

S. Wang, E.-P. Li
Computational Electromagnetics and Electronics
Institute of High Performance Computing
Singapore

L.-W. Li
Department of Electrical & Computer Engineering
National University of Singapore
Singapore

The application of asymptotic techniques, in conjunction with CAD tools for the Radar Cross Section (RCS) computation of the complex targets is presented in this paper.

The radar targets are modeled using I-DEAS solid modeling software in term of facets and edges. Thus there exist no limitation on the target geometry. Different modeling approximations are evaluated to provide a general guideline for complex target discritization with reasonable accuracy and computer times.

Physical theory of diffraction (PTD) is used to calculate the RCS of radar targets for its higher efficiency than classic numerical methods. Within the framework of PTD, surface reflection is analyzed by physical optics (PO), and edge diffraction is analyzed by the method of equivalent currents (MEC), in which the far field is computed as radiated by equivalent surface or edge currents, respectively.

As for complex objects, whose RCS are not only dominated by a single specula mechanism, the nonspecular components such as diffraction at edges, multiple scattering sometimes can be of similar amplitude. So the higher-order equivalent edge current expressions are introduced to take into account the edge interactions. The expressions are derived through integration of the FW surface current excited at the leading edge of the scatterer by the incident plane wave along a finite, arbitrarily oriented incremental strip extending from the leading edge to the trailing edge. They are well behaved for all directions of incidence and observation. So the higher order expressions are well suited for implementation in general computer codes calculating the radar scattering from three-dimensional structures.

The monostatic and bistatic scattering characterization of radar targets calculated by the higher order PTD are examined and compared with those obtained from PO and first order PTD, through which we can gain insight to the individual scattering contributions of different mechanisms for different types of geometry. Based on the calculation results, The following conclusions arrived:

1. Substantial improvements have been achieved by using higher order MEC;
2. The edge interaction can be significant, even though the direction of incidence is far from the plane of the scatterer;
3. Specular return is generally with large amplitude and narrow lobewidth, and diffraction arisen from field interaction with edge is generally lower in amplitude than specular returns but with a wider angular distribution.

To further improve the accuracy of the present approach, other scattering contributions such as multibounce and surface wave should be considered.

Session 5Aa6

Propagation Modeling

On Effects of Lateral Terrain Variations on Radar Propagation in 3D Environments

R. S. Awadallah, J. R. Kuttler, M. H. Newkirk, and J. Z. Gehman
Johns Hopkins University Applied Physics Laboratory
Laurel, MD, U.S.A.

Numerical simulation of long-distance tropospheric radar propagation is usually performed by marching the propagating field forward from the source to the receiver using either Fourier transform or finite difference techniques. The equation governing the field is a one-way parabolic wave equation subjected to the terrain boundary condition in addition to an absorption condition, which is enforced on the boundaries of the numerical domain to prevent reflection artifacts.

In order to facilitate efficient propagation calculations over long distances (hundreds of kilometers), several approximations of the original problem have been proposed. An important approximation among these is the assumption that the lateral terrain variations along the great circle connecting the transmitter and the receiver are negligible. This approximation effectively reduces the original vector 3D problem into a scalar, efficiently solvable 2D problem. The latter problem is then transformed from the original spherical geometry to a Cartesian geometry via the appropriate conformal map and solved via one of the aforementioned marching techniques. It is obvious that such approximation amounts to ignoring the effects of the lateral (cross-range) terrain slopes on the propagating field. These effects, which include depolarization and lateral diffraction and shadowing, may become prominent for steep cross-range terrain slopes. The inappropriate incorporation of such effects may impact terrain clutter modeling which requires accurate calculation of the propagating field.

In this paper we use our 3D vector propagation model (VEMPE) to investigate the effects associated with lateral terrain variations on radar coverage. These effects are assessed by comparing propagation results obtained by the full 3D propagation model with quasi-3D results obtained by running our 2D propagation code (TEMPER) over multiple range bearings. Numerical examples involving idealized as well as realistic terrain configurations are presented.

Advances in Radar Propagation and Clutter Modeling with Parabolic Equation Method

J. Z. Gehman, M. H. Newkirk, and J. R. Kuttler
The Johns Hopkins University Applied Physics Laboratory,
11100 Johns Hopkins Road
Laurel, MD 20723, U.S.A.

The 2-D Fourier split-step solution to the parabolic equation is a powerful tool for modeling atmospheric effects on surface-based sensors and communications systems. In the last few years, significant improvements have been achieved that make this technique more robust and better-suited for use in estimating radar clutter (backscatter), especially in littoral areas.

In this presentation, the capabilities and limitations of the Johns Hopkins University Applied Physics Laboratory (JHU/APL) Tropospheric Electromagnetic Parabolic Equation Routine (TEMPER) model are described, with a focus on the most recent improvements that facilitate radar propagation and clutter modeling in stressing scenarios.

A major TEMPER improvement is a more accurate representation of terrain diffraction and forward scattering using a piecewise-linear shift map. Using this method, along with a simple masking approach in regions where the shift map cannot be applied, provides a more capable terrain effects modeling procedure. Another improvement is better estimation of incident field grazing angles through a combination of geometric optics and spectral estimation. These grazing angles are important inputs for sea and land clutter models. The most recent improvement is an alternate formulation of TEMPER's impedance boundary condition. This slight reformulation makes TEMPER significantly more robust for very rough surfaces and higher frequencies.

We conclude with a description of a TEMPER-based method for generating clutter predictions over wide areas. This process integrates TEMPER with sea and land clutter models, making efficient use of TEMPER on the collection of radials that form a sensor's sector of coverage. Examples will demonstrate the utility of this method using actual littoral environmental data to compute the effective radar cross section for a specific platform.

Parabolic Wave Equation Based Rough Sea Surface Scattering

F. J. Ryan
Maritime Surveillance Division, CODE D7101, Space and Naval Warfare Systems Center
San Diego, CA, U.S.A.

A physics based computational electromagnetics technique is described for efficiently computing both forward scattered and backscattered (i.e., clutter) fields from realistic rough sea surfaces. The method is based on a novel split-step Fourier parabolic wave equation (PWE) method incorporating a stochastic wind and swell ocean surface wave spectral model which includes both gravity and capillary length scales.

medskip The rough surface PWE backscattering method employs a distorted wave Born approximation using a multiple forward scatter, single backscatter approach to estimate both scattered fields and the normalized surface cross section σ_0. The PWE code is computationally efficient and models both horizontally and vertically polarized signals over finite conducting surfaces. Spatial variability in both the atmospheric index of refraction n and surface dielectric properties are allowed for. The PWE method allows for surface scattering from both illuminated as well as shadow surface patches.

Stochastic rough sea surface realizations are generated from linear Gaussian process models using directional wave number spectra which include both surface gravity and capillary waves. The particular directional wave spectrum is a modified Donelan-Pearson-Banner wind wave spectrum augmented by a directional swell spectrum.

Comparisons between the PWE based scattered fields and results using the standard Miller–Brown rough surface reflection coefficient method will be shown. Examples of the rough surface scattered field vertical angle-of-arrival spectra under a variety of ducting conditions will be shown, and the impact on high precision spatial tracking (beamforming) discussed.

Influence of Random Irregularities of the Propagation Medium on the Radar Signal Structure

M. V. Tinin, M. V. Ignatenko, and S. N. Kolesnik
Irkutsk State University
Irkutsk, 664003, Russia

This paper presents the results derived from developing the methods to model the spatio-temporal structure of the sounding signal in a randomly inhomogeneous medium. They are based both on using the geometrical optics approximation and its generalization obtained using a weighted (fractional) Fourier-transform with respect to the coordinates of the source and observer. The two-dimensional version of this method within the small-angle approximation is reported in [1, 2]. This method is further developed beyond the small-angle approximation.

Using an integral representation for the wave field in a randomly inhomogeneous medium, the algorithm has been developed for improving the resolution of ray tomography of the ionosphere in the presence of multipathing and diffraction effects.

An integral representation is obtained for the field of the wave that is backscattered from a small-scale irregularity located in a large-scale randomly inhomogeneous background medium. This representation is sued to investigate the incoherently scattered signal structure.

A numerical simulation of the signal structure from beyond-the-horizon sea radar is carried out. We investigate the influence of parameters of a randomly inhomogeneous ionosphere, the methods of modulation and methods of spatio-temporal processing on the structure of this signal.

Using asymptotic methods and numerical simulation we investigate the influence of different-scale irregularities on the structure of the signal that is obliquely scattered from random irregularities of the layer (such as E_s).

REFERENCES

1. Tinin, M. V., "Quasi-geometrical optics methods in the theory of wave propagation through a randomly inhomogeneous layer," *Waves Random Media,* Vol. 8, 329–338, 1998.

2. Kravtsov, Yu. A. and M. V. Tinin, "Representation of a wave field in a randomly inhomogeneous medium in the form of the double-weighted Fourier transform," *Radio Sci.,* Vol. 35, 1315–1322, 2000.

Wave Propagation in a Multiscale Randomly Inhomogeneous Medium

M. V. Tinin
Irkutsk State University
Irkutsk, 664003, Russia

Most of currently available methods for describing the wave field in a randomly inhomogeneous medium are applicable for taking into account irregularity effects of either small or large scales. Using Fourier-transform with respect to the coordinates of the source and observer, the authors of [1, 2] obtained representations for the field of the wave and its moments, which describe effects of both large and small-scale irregularities. However, it can be shown that in this case there is no possibility of taking into account simultaneously the effects of large- and small-scale irregularities. This is due to the fact that methods [1, 2] make use of the zeroth (unperturbed) approximation of ray trajectories, whereas in the case of the scattering from small-scale irregularities it is necessary to take into account the fluctuations of rays that have propagated through large-scale irregularities.

In this paper we further develop the results reported in [1, 2] by taking into account the variations of random rays to a first approximation when calculating the phase fluctuations of partial waves, in which case the wave field in a randomly inhomogeneous medium is expanded. The expression is obtained for the scintillation index of the point source field in a turbulent medium which – at large distances – transforms to the well-known results of an asymptotic calculation of expressions obtained using Feynman path integrals.

Using the Fock method of the fifth parameter and the result reported in [1, 2] an integral representation is obtained for the wave field in a randomly inhomogeneous medium without invoking the assumption about small-angle propagation. A study is made of the influence of large-scale irregularities of the propagation medium on the structure of the signal that is backscattered from a small-scale irregularity. Furthermore, we investigate the influence of different irregularities on the oblique scattering of the spherical wave from a randomly inhomogeneous layer.

REFERENCES

1. Tinin, M. V., “Quasi-geometrical optics methods in the theory of wave propagation through a randomly inhomogeneous layer,” *Waves Random Media,* Vol. 8, 329–338, 1998.

2. Kravtsov, Yu. A. and M. V. Tinin, “Representation of a wave field in a randomly inhomogeneous medium in the form of the double-weighted Fourier transform,” *Radio Sci.,* Vol. 35, 1315–1322, 2000.

Fast Integral Methods for Calculating Microwave Propagation Over Large Rough Surfaces

C. D. Moss, Y. Zhang, H. Han, T. M. Grzegorczyk, and J. A. Kong
Massachusetts Institute of Technology
Cambridge, MA 02139, U.S.A.

The goal of this work is to develop accurate models to study the effects of terrain on the performance of ground based radar and communication systems. The types of terrain in these problems are extremely large, both in distance (typically 25 km) and height variation (up to 500 m), although we limit the scale of the local roughness to no less than a few wavelengths. Usually, a terrain profile is defined by large, flat patches that can be many hundreds of wavelengths long, and the entire geometry must take into account the spherical earth. To fully account for all surface scattering phenomena, we use an integral equation formulation which leads to an exact solution of the electromagnetic problem. Due to this terrain size, this exact formulation requires a prohibitively large number of unknowns, so we incorporate fast techniques to make the problem tractable. In particular, we use the Forward-Backward Method as an iterative solution, accelerated by a variant of the Fast Far-Field Algorithm as well as an FFT matrix-vector multiply for the self terms. These fast techniques result in huge reductions of memory requirements and computational cost, although their efficiency decreases as the surface roughness increases. The resulting algorithm that is a combination of these techniques is an approximation, and we verify the accuracy through comparison with the basic Forward-Backward Method.

Furthermore, we include a layer of random medium on the terrain to incorporate the effects of foliage (although it could be a different geophysical medium, such as snow or ocean foam). The random medium is created using Strong Fluctuation Theory to model the discrete scatterers (such as leaves in foliage), obtaining values for the effective permittivity. The tools developed in this work are general and can be applied to many problems such as radar cross section studies of ships on a rough ocean surface, or the prediction of propagation losses of microwave communication systems.

Finally, we compare the fast integral techniques to high frequency approximations, which are traditionally used for geometries of this size. In particular, we compare the integral technique to a physical optics (PO) method, which accounts for limited knife-edge diffraction over the spherical earth. We also compare to the recently developed High Frequency Mode Expansion Method, which is a combination of PO and integral techniques that can give accurate results in times unachievable by even the fastest integral techniques.

Session 5Ab6

Developments in Reflection and Propagation of Radiation Problems

Use of the Stochastic Expansion for Rough Surfaces, Compared with Lambert Law (Diffuse) Results and, for Small Surface Slopes, with Geometric Optics

W. C. Meecham
Mechanical and Aerospace Engineering Department
School of Engineering and Applied Science, University of California
Los Angeles, CA 90095-1597, U.S.A.

W.-W. Lin
Yung Vta Institute of Technology and Commerce (YTTT)
Pington, Taiwan 909, R.O.C.

Single frequency, random, surface reflection problems are characterized by ξ_0 the RMS surface displacement, Λ, the correlation length and λ, the radiation wavelength. For small λ, higher frequencies (HF), geometric optics/acoustics is useful. Indeed for HF and small-slope (ξ_0/Λ small), Gaussian surfaces, the angular distribution is itself Gaussian. For larger λ perturbation theory is usual. It will be seen that in the latter case the present expansion has substantial advantages over perturbation theory in such a (commonly occurring) regime. The stochastic expansion [also called the Wiener-Hermite (WH)] is used to represent field functions reflected from random surfaces which surfaces have Gaussian statistics. The special problem considered is for a two-dimensional conducting surface with an incident, electromagnetic wave polarized parallel to the generating element. This is the same boundary condition as that for the reflection of sound from the ocean surface, incident from the water side. The WH expansion is in terms of polynomials of a basic element. Here we use the presumed Gaussian surface as that basis. Polynomials of the basic element are constructed so as to be mutually, statistically orthogonal. The expansion of $\exp(a\xi)$ (ξ the Gaussian surface) is known to all WH orders, a decided advantage since this functional is central to reflection problems. The expansions have been used extensively for turbulence problems. In this work, we include but the first three terms. Every term has contributions to all orders in ξ_0; perturbation theory is quite different than this of course. The reflection approaches, for λ large compared with ξ_0 and Λ, a Lambert's law: the reflected field following the square of the cosine of the angle, regardless of the incident direction as is the case if the reflected field is fully diffuse. The result is shown to be greatly superior to perturbation theory, as judged by energy conservation. The method is readily extended to more general problems. Results will be presented for a variety of surface correlation lengths, for various incident angles and for several frequencies. It is emphasized that the expansion is not a perturbation one for it contains a swath composed of all perturbation orders.

Gravitomagnetic and Gravitoelectric Waves: Detectability on LIGO

I. Tolstoy
Knockvennie
Castle Douglas, Scotland

A recent article has shown how lineariztions of Einstein's field equations and isomorphisms with electromagnetic may be used to demonstrate the existence of gravitomagnetic (GM) and gravitoelectric (GE) wavefields generated by transient non-gravitational sources – as in the spin-up of a rigid sphere by an external torque [1]. Whereas such effects are too small to be measured in the laboratory, order of magnitude estimates suggest that major astrophysical events could generate signals (strains in the metric) observable by LIGO-type systems. GM/GE modes are entirely uncoupled from the quadrupole radiation of classic gravitational wave theory. However both travel at light velocity c and, since quadrupole waves might be generated by, or in the neighborhood of, the same events, it is essential to demonstrate how LIGO array geometries can discriminate between them. This is accomplished straightforwardly by determining arrival directions and polarization planes. These wavefields are exactly isomorphic with electromagnetic radiation for a model consisting particles of a single charge sign which, in the Cartesian-Minkowski limit, exert purely attractive Coulomb forces upon each other. The deformation of the spacetime metric is one of pure shear, and the fields are dipole.

REFERENCES

1. Tolstoy, I., 2001, Gravitomagnetic and Gravitoelectric Waves in General Relativity. *Int. J. of Theor. Phys.* 40, 5, 1021–1031.

Comparisons Between Analytic Approximations and Numerical Simulations for Wave Propagation in Ocean Acoustics and Atmospheric Optics

S. M. Flatté
Physics Department, University of California
Santa Cruz, CA 95064, U.S.A.

Laser-beam propagation through atmospheric turbulence has been simulated; the spectrum near the inner scale follows that of Hill and Clifford, and the turbulence strength puts the propagation into the asymptotic strong-fluctuation regime. The limits of numerical simulation from finite screen size are determined by observing the changes in variance as a function of screen size. Acoustic propagation through ocean internal waves has been simulated for multi-Megameter ranges in the presence of a deterministic waveguide (the sound channel). This propagation, unlike the optical one, is multi-frequency (broadband) in order to synthesize a pulse. The arrival time and shape of the pulse is compared, in a statistical sense, to predictions from path-integral corrections to geometrical optics. In both the optical and the acoustical cases, analytical approximations are shown to be inadequate. In the optical case, the dependence of the irradiance variance on both β_0^2 and inner scale does not follow the power-law predictions from analytics. In the acoustic case, there are two parameters that are analogous to β_0^2: the strength of the internal-wave field and the range through which the wave propagates. The dependence on range shows a marked change at several hundred kilometers; at smaller ranges, the analytics are relatively accurate, while at larger ranges the disagreement is dramatic. These two important physical cases are quite different mathematically. The optical case is three dimensional while the acoustic case is two dimensional in the wave propagation. The deterministic background for the optical case is free space, and for the acoustical case is a waveguide. The spectrum of the optical case is Kolmogorov, so $k^{-5/3}$ while the internal-wave spectrum is k^{-2}. Nevertheless these two cases can be compared approximately on a general propagation diagram of wave propagation through random media.

Bistatic Scattering by Bare and Coated Metal Targets of Simple Shape

H. C. Strifors
Detense Research Agency
Linköping, SE-58111 , Sweden

G. C. Gaunaurd
Army Research Laboratory
Adelphi, MD 20783-1197, U.S.A.

We study the scattering interaction of electromagnetic waves with a simple target. The target is a perfectly conducting sphere, either bare or coated with a thin dielectric layer. For the layer, two different hypothetical materials are specified: a non-magnetic lossy dielectric and a dielectric that has also magnetic losses. These hypothetical layers are examples of narrow-band and broadband microwave absorbing coatings. For each target, the general, far-field Mie solution for the bistatic scattered field is computed at selected frequencies. In particular, the radar cross-section (RCS) is in each case generated with a direction resolution of one degree in both azimuthal and latitudinal directions. The magnitude of the RCS is then presented as a three-dimensional surface. To best represent the magnitude of the RCS a logarithmic scale is chosen, and the distance of the surface from the origin in a given direction is proportional to the logarithm of the magnitude of the RCS in that direction. To enhance the perception of size, the 3-D surface representing the magnitude of the RCS is also colored using an arbitrary color scale (pseudocolors). The backscattering and forward scattering characteristics can be conveniently studied from the presented results, and the effect of the two different coatings on the bistatic RCS appreciated. In particular, we demonstrate that the RCS in a sector close to the forward scattering direction is very large and of similar magnitude irrespective of the choice of coating, or of no coating at all. Using a time-frequency approach, we also investigate in an ultra-wideband (UWB) frequency range the target signatures in a few scattering directions close to the forward direction. In particular, we show that the three different targets have different signatures, which can be used tor target identification purposes.

Session 5Ac7

Spectral Methods Applied to the Linear and Nonlinear Optical Response of Composite Media

Bloch Electrostatics for Arrays of Cylinders

R. C. McPhedran, N. N. Nicorovici, and M. P. Hertzberg
School of Physics, The University of Sydney
Sydney, Australia

L. C. Botten
Department of Mathematical Sciences, University of Technology
Sydney, Australia

We discuss the solution of problems in electrostatics in which a periodic set of line sources is placed in a matrix of dielectric constant ϵ_m containing an array of dielectric cylinders of constant ϵ_i. The line sources are phased according to the Bloch factor, with a Bloch vector $\mathbf{k}_0$. The quasiperiodic Green's function solving this problem, including boundary conditions on the cylinder surfaces, is evaluated using a multipole treatment, following the original method due to Lord Rayleigh.

One feature of this method is that the Green's function can be integrated over the first Brillouin zone of the array of cylinders, which results then in the Green's function for a single line source in the array. This latter is non-quasiperiodic, and its calculation has thereby been reduced to the solution and numerical integration of a set of quasiperiodic problems, and so put in a form amenable to solution on parallel computers. We explore this method of calculating non-periodic Green's functions by two-dimensional integration, We also compare it with a method of evaluating such Green's functions by one-dimensional integration, over a set of Green's functions for a grating of cylinders sandwiched between two half-planes of cylinders. This second method requires the extension to statics from dynamics of half-plane reflection matrices.

We explore the connection between this method for statics, and its equivalent for the Helmholtz equation being developed in parallel. We also explore the connection between the effective dielectric constant for the former, and the effective refractive index for the latter, relevant to problems involving homogenisation of photonic band gap systems in two-dimensions.

The Bergman Spectrum of the Effective Dielectric Constant in Composite Media

X. Li and H. R. Ma
Department of Physics, Shanghai Jiao Tong University
Shanghai, 200240, China

The first principle formulas of electric field of binary composites were obtained with use of the Bergman representation theory. The electric potential and electric field distributions for BCT, FCC and BCC structures were calculated. The Bergman spectrums of these structures were analysed, too. With use of the electric field theory, the third-order optical nonlinearity enhancement was derived directly. In the calculation, the multipole contribution as a function of the separation of particles was quantitatively discussed. Finally the valid range of the dipole approximation was given.

Spectral Methods Applied to Linear and Nonlinear Optical Response of Composite Media

T. K. Wan and K. W. Yu
Department of Physics, The Chinese University of Hong Kong
Shatin, New Territories, Hong Kong

Nonlinear optical properties of granular composite materials have attracted much attention in recent years because of their potential applications in physics and engineering. In this work, we investigate the nonlinear optical properties of randomly oriented nonlinear spheroidal metal particles in a dielectric host. Two different Maxwell-Garnett-type approximations are derived based on whether a self-consistency condition on the net polarization is invoked. These two methods lead to quite different spectral density functions. Moreover, we show that the shape of particles has a large influence on the spectral function through the depolarization effects and thereby has a pronounced effect on the optical absorption and non-linear optical susceptibility. We suggest that the self-consistent formalism can be used for large volume fractions, as mutual interaction between different polarizations is included in the theory. On the other hand, we compute analytically the spectral function for composites with a binary distribution of particle sizes. For a log-normal distribution of width s, numerical results show that the spectral density $m(s)$ changes from a delta function for zero width to a prominent peak, accompanied by a broad spectrum for a finite width s. As a result, the locations of the nonlinearity enhancement peak and the absorption spectrum shift to small frequencies with the increase of the interfacial factor I.

Nonlinear optical properties of granular composite materials have attracted much attention in recent years because of their potential applications in physics and engineering. In particular, the optical nonlinearity can be strongly enhanced by the microstructure of the composites. In this work, we investigate the effects of a distribution of size and shape on the linear and nonlinear response of metal-dielectric composites. Two different Maxwell-Garnett-type approximations are proposed based on whether a self-consistency condition on the net polarization is invoked. These two methods lead to quite different spectral density functions. We show that the shape of particles has a large influence on the spectral function through the depolarization effects and thereby has a pronounced effect on the optical absorption and nonlinear optical susceptibility. On the other hand, we compute analytically the spectral function for composites with a binary distribution of particle sizes. For a log-normal distribution of particle sizes, numerical results show that the spectral density changes from a delta function to a prominent peak, accompanied by a broad spectrum as the width of size distribution increases. As a result, the locations of the nonlinearity enhancement peak and the absorption spectrum shift to small frequencies. We suggest that the self-consistent formalism can be used for large volume fractions, as mutual interaction between different polarizations is included in the theory.

A Spectral Representation for the Dielectric Properties of Layered Materials

A. R. Day
Physics Department, Marquette University
Milwaukee, WI 53201, U.S.A.

We present a spectral representation for the effective dielectric function of a sample that consists of two homogeneous layers joined with a rough interface. This spectral representation is closely related to the Bergman-Milton spectral representation for bulk composites, and is easily extended to multilayered materials. By comparing the layered system to a reference layered system that has a flat interface we form a surface spectral function that captures all the effects of surface structure on the effective dielectric function of the layered sample, and is independent of the dielectric functions of the two layers. Because of the anisotropy of the layered system there are two surface spectral functions, one for the case where the applied field is parallel to the interface, and one for the case where the applied field is perpendicular to the interface. We discuss a reciprocity relationship between these two spectral representations and present sum rules that are directly related to the degree of surface roughness. We present numerical calculations of the surface spectral function for some model geometries, including the Gaussian random surface that has been that extensively used to study light scattering from rough surfaces, and show that the simulations verify the sum rules and reciprocity relationships. We show how the surface profile and interactions between layers of the multilayered materials are related to the features of the surface spectral function and we discuss the possibility of determining the spectral function directly from reflectivity measurements.

Microstructures and Nonlinear Optical Response of Composites

P. Sheng
Department of Physics
Hong Kong University of Science & Technology
Kowloon, Hong Kong

H. R. Ma
Department of Applied Physics
Shanghai Jiao Tong University
Shanghai, 200030, China

G. K. Wong
Department of Physics
Hong Kong University of Science & Technology
Kowloon, 200030, Hong Kong

By using the spectral approach, we calculate the third-order nonlinear optical response of metal-insulator composites with four different types of microstructures. Examples are given that demonstrate the microstructural enhancement effect through the surface plasmon resonance. Comparison with experimental data shows that large enhancement in the third-order Kerr-type nonlinear susceptibility can indeed be realized at composition below the percolation threshold.

The Effect of Geometric Anisotropy on the Optical Nonlinearity Enhancement for Periodic Composites

B. Yang
Department of Physics, Wuhan University
Wuhan, Hubei 430072, China

C. Zhang
Department of Physics, Jilin University
Changchun, Jilin 130023, P. R. China

An optical nonlinear composite material of interest is usually made of nonlinear metal or semiconductor material embedded in a linear insulation host medium. The third-order optical nonlinear susceptibility of the composite may be strongly enhanced relative to that of the nonlinear component material due to the inhomogeneity of local electric field. The inhomogeneity is sensitively dependent on both the microstructure of the composite and the polarization response of the component materials. For a particle composite, ones may make use of Stroud-Hui relation to evaluate the effective nonlinear susceptibility in two cases of isotropic and anisotropic microstructure. Robert. W. Boyd and J. E. Sipe studied the optical nonlinear susceptibility of layered composites. A layered composite can be considered as an extremely geometric anisotropic composite. In this work, we investigate the effect of geometric anisotropy on the nonlinearity enhancement for a composite with metal or semiconductor gyration ellipsoidal particles periodically in an insulating host. Two kinds of the microstructure that the inclusions are nonoverlapped and overlapped are considered. The latter forms layered networks which are the layers with periodically arranged holes. The calculations of the nonlinear susceptibility are based on Stroud-Hui relation and the series expression of space-dependent electric field in periodic composites. Our results show that the nonlinearity enhancement for the metal-and/or semiconductor-insulator composites may be increased to orders of magnitude as the cross-section of the inclusions in the direction of the applied electric field is increased. Near connection threshold, there exists a drop in the nonlinearity enhancement for metal-insulator composite due to mutual exclusion of free carriers between adjacent particles. We compare the nonlinearity enhancement in the particle composites with that calculated by using Royd-Sipe relation in layered composites and conclude that the nonlinearity enhancement increases to maximum as the granular composites are transformed into the layered composites.

Fractal-Microcavity Composites: Local-Field Optical Enhancement and Quantum-Size Effect

V. M. Shalaev and V. P. Drachev
Purdue University
West Lafayette, IN, U.S.A.

V. P. Safonov
Institute of Automation and Electrometry
Novosibirsk, Russia

W. Kim and R. L. Armstrong
New Mexico State University
Las Cruces, NM, U.S.A.

A novel class of composites for optics, microcavities doped with metal fractal aggregates, is studied. Lasing and broad-band Stokes and anti-Stokes emission from (Ag colloidal aggregates)/(adsorbed molecules)/(microcavity) composite at low-intensity cw and pulse laser excitation has been found [1-5]. At 633 nm cw excitation wavelength the emission spectrum contains many peaks, spanning a range from the wavelength of 800 nm to 200 nm. Experiments with pulse excitation of Ag/dye/microcavity composite show that duration of the observed broad-band anti-Stokes emission has exceeded considerably the pump pulse duration, dye molecule fluorescence time, and relaxation times in silver particles. It may be interpreted as a luminescence governed by long-living triplet states of dye molecules. These observations became possible due to using of a fractal-microcavity composite, where coupling the localized plasmon modes in fractal aggregates with microcavity resonances is provided. The important role of the multiphoton resonant transitions between discrete states of a finite-size metal particle in enhanced local fields is shown. Analysis, based on the model of a spherical potential well, shows that the observed spectra contain fingerprints of the quantum-size effect.

REFERENCES

1. W. Kim, V. P. Safonov, V. M. Shalaev, R. L. Armstrong, Fractals in Microcavities: Giant Coupled Multiplicative Enhancement of Optical Responses, *Phys. Rev. Lett.* 82, 4811 (1999).
2. V. P. Drachev, W. Kim, V. P. Safonov, V. A. Podolskiy, N. S. Zakovryazhin, V. M. Shalaev, and R. A. Armstrong, Low-threshold lasing and broad-band multiphoton-excited light emissionfrom Ag aggregate-adsorbate complexes in microcavity, *J. of Modern Optics*, (2001).
3. V. A. Podolskiy and V. M. Shalaev, Giant Optical Responses in Microcavity-Fractal Composites, *Laser Physics* 11, 26 (2001).
4. V. M. Shalaev, *Nonlinear Optics of Random Media: Fractal Composites and Metal-Dielectric Films*, Springer Tracts in Modern Physics, v.158, Springer, Berlin Heidelberg 2000.
5. V. M. Shalaev, "Fractal Nano-Composites: Giant Local-Field Enhancement of Optical Responses," Chapter in: *Nanoscale Linear and Nonlinear Optics*, eds: M. Bertolotti and C. Sibilia, AIP, 2001.

Anderson Localization vs. Delocalization of Surface Plasmons in Nanosystems

D. J. Bergman
School of Physics and Astronomy,
Raymond and Beverly Sackler Faculty of Exact Sciences, Tel Aviv University
Tel Aviv, 69978, Israel

M. I. Stockman
Department of Physics and Astronomy, Georgia State University.
Atlanta, GA 30340, U.S.A.

S. V. Faleev
Sandia National Laboratories. also Department of Physics and Astronomy, Georgia State University.
Livermore, CA 94551, U.S.A.

From a partial-differential eigenproblem, without use of dipole approximation, we show that the eigenmodes (surface plasmons) of disordered nanosystems (modeled as random planar composites) are not universally Anderson-localized, but can have properties of both localized and delocalized states simultaneously [1]. Their topology is determined by separate small-scale "hot spots" that are distributed and coherent over a length that may be comparable to the total size of the system. Coherence lengths and oscillator strengths vary by orders of magnitude from mode to mode at nearby frequencies. The existence of dark $vs.$ luminous eigenmodes is established (the dark eigenmodes do not contribute to optical responses, and the luminous eigenmodes do) and attributed to the effect of charge- and parity-conservation laws. Possible applications are discussed. The theory is based on the spectral representation [2].

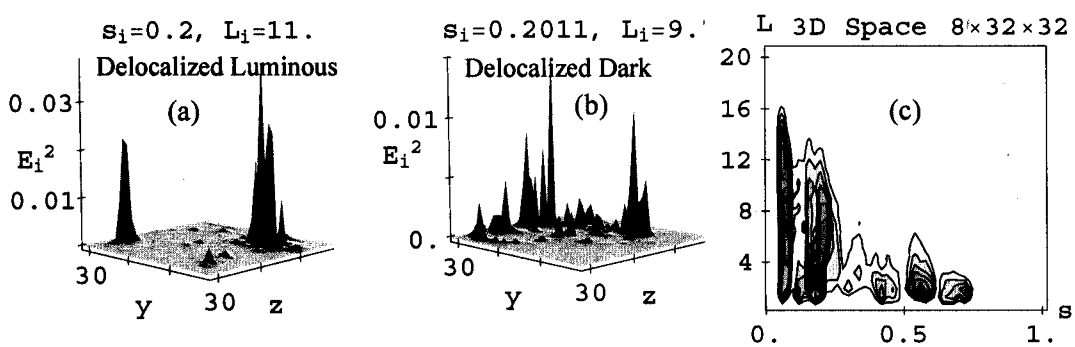

Figure 1: Examples of the delocalized luminous eigenmode (a) and delocalized dark eigenmode (b). The distribution of the eigenmodes over their localization radius L and spectral parameter S is also shown as a contour map (c). Adapted from [1].

The results for random planar nanostructured composites are illustrated in Fig.1 [1]. They show that eigenmodes with a similar geometry of local field intensities (delocalized in this case) may be either luminous or dark [cf. (a) and (b)]. The distribution over the localization lengths L is very wide, from the minimum scale to the size of the entire system [Fig.1(c)].

References

1. Stockman, M. I., S. V. Faleev and D. J. Bergman, "Localization $vs.$ Delocalization of Surface Plasmons in Nanosystems: Can One State Have Both Characteristics?" *Phys. Rev. Lett.*, Vol. 87, p. 167401, 2001.

2. Bergman, D. J., and D. Stroud, "Properties of Macroscopically Inhomogeneous Media," *Solid State Phys.*, Vol. 46, p. 147, 1992.

Femtosecond Energy Concentration in Nanosystems Controlled by Excitation Phase

M. I. Stockman
Department of Physics and Astronomy, Georgia State University
Atlanta, GA 30340, U.S.A.

S. V. Faleev
Sandia National Laboratories.
Livermore, CA 94551, U.S.A.

D. J. Bergman
School of Physics and Astronomy,
Raymond and Beverly Sackler Faculty of Exact Sciences, Tel Aviv University
Tel Aviv, 69978, Israel

We predict that excitation of a nanosystem with a correspondingly phase-modulated femtosecond pulse causes concentration of the excitation energy at a small part of that nanosystem [1]. The location of the excited site is coherently controlled by the distribution of the phase along that pulse, distinct from the "Ninth Wave" effect [2]. We discuss unique possibilities of using this in applications, in particular, for nanoscale ultrafast computing and nano-lithography.

The theory is based on the Green's function method in the spectral representation.

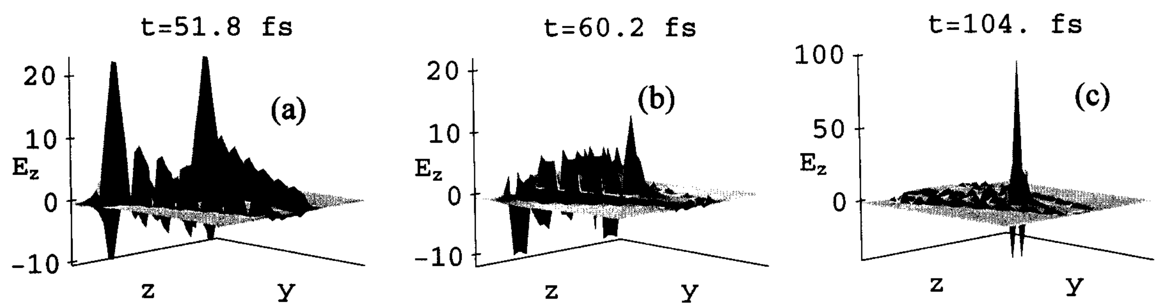

Figure 1: Spatial distributions of local electric fields (in the units of the exciting pulse amplitude) at the nanostructure for moments of time indicated. The duration of the exciting pulse is 25 fs, and the phase modulation parameter $\alpha = 0.3$ [1].

The results of the simulations [1] for a V-shaped planar nanostructure made of silver (8 nm thick) subjected of a phase-modulated 25-fs exciting light pulse ($\hbar\omega_0 = 0.95$ eV) are displayed in Fig.1. This shows that as the pulse progresses, the maximum of the local fields and, correspondingly, the energy of the excitation on the nanoscale move toward the apex of the nanostructure where they strongly concentrate at 104 fs.

References

[1] Stockman, M. I., S. V. Faleev and D. J. Bergman, "Coherent Control of Femtosecond Energy Localization on Nanoscale," *Phys. Rev. Lett.*, 2001 (Submitted).

[2] Stockman, M. I., "Femtosecond Optical Responses of Disordered Clusters, Composites, and Rough Surfaces: 'The Ninth Wave' Effect," *Phys. Rev. Lett.*, Vol. 84, 1011, 2000.

Session 5Ac8

Recent Advances in Scattering and Diffraction

Study of the Factors that Characterize the Coastline Effect for the HF and VHF Bands

M. R. Pino
Área de Teoría de la Señaly Comunicaciones
Depto. Ing. Eléctrica, Electrónica, de Computadores y Sistemas, Universidad de Oviedo
Gijón, Asturias 33204, Spain

J. A. López, F. Obelleiro, and J. L. Rodríguez
Depto. Teorí ado Sinal e Comunicacións, Universidade de Vigo
Vigo, Pontevedra 36200, Spain

The purpose of this presentation is to analyze and illustrate the propagation over a non homogeneous surface, composed by land and sea. Sometimes the communication between the transmitter and the receiver antennas passes throw some different electrical surface types. This change in the electrical properties produces important effects on the field strength expected above the terrain. The phenomenon is very salient over mixed land-sea paths, in coastline communications, and it is known as *recovery effect* or *coastal effect* [J. R. Wait and L. C. Walters, *IEEE Trans. Antennas and Propagat.*, Vol. 11, pp. 38–45, January 1963]. This event is commonly described in the literature as an increase in the field strength that appears beyond the coastline for propagation from land towards sea. Nevertheless, the field strength can also decrease beyond the coastline, depending upon the receiving height. Numerical studies performed here, show that the characterization of the *recovery effect*, should also take into account some parameters like the receiving antenna height, the frequency and the geometry of the problem.

In this work, it is proposed to use a formulation based on an Integral Equation (IE) plus Impedance Boundary Condition (IBC) approach [T. B. A. Senior, *Appl. Sci. Res.*, sec. B, Vol. 8, pp. 418–436, 1961]. Once the problem is formulated, it is solved using an iterative Method of Moments (MoM) based algorithm, named Forward-Backward (FB) joined to a spectral acceleration scheme [J. A. López, M. R. Pino, F. Obelleiro and J. L. Rodríguez, *JEMWA*, Vol. 15, No. 8, pp. 1049–1074, Aug. 2001]. The computational cost of this combined solution is $\mathcal{O}(N)$, so very large geometries can be analyzed.

In order to illustrate the phenomenon, the total electromagnetic (EM) field over a *homogeneous surface* is compared with the total EM field over a *non homogeneous terrain*. The non homogeneous surface is composed by soil. On the otherhand, the mixed-path surface (non homogeneous), is composed by two different portions. One of them is the same type of soil used in the homogeneous surface, while the second one is sea water. The field comparison shows that the field strength increases for some receiving heights while for others it decreases when the wave passes from a medium with a bigger impedance (land) to another on which the impedance is smaller (sea). In fact, the difference between the field strength over the non homogeneous surface to the homogeneous one, exhibits an undulating behavior, very similar to an interference pattern. Results showing the variations of this pattern due to different parameters will be presented.

High-Frequency Green's Function of an Infinite Slot Printed Between Two Homogeneous Dielectrics

S. Maci and A. Neto
University of Siena
Siena, Italy

This paper deals with the uniform asymptotic description of the Green's function of an infinite slot printed between two different homogeneous dielectric media. Starting from the magnetic current derived in a previous paper, the dyadic Green's function is first formulated in integral form in both spectral and spatial domain; next, the asymptotic solution for the vector potential is evaluated asymptotically. The asymptotic ray-field is structured in three contributions: a spherical wave radiated by the source (space wave), a conical leaky wave, and a lateral wave. This decomposition is first introduced by the stationary phase method applied to the space domain radiation integral. From this first investigation it is seen that the lateral wave contribution is typically negligible in actual configurations. A rigorous uniform asymptotic evaluation of the radiated field is then formulated in the spectral domain for the leaky/space wave contributions, using a steepest descent path deformation which accounts for the vicinity of the pole to the saddle point. In this description, the leaky wave contribution arises from a residue of the spectrum at a complex pole which leads to an evanescent wave. This evanescent wave is slightly different from the ray-type leaky contribution resulting from the stationary phase method, but converges to this latter for small leaky attenuation constant. Relationships between the ray regime and evanescent wave regime is fully explored. Through the rigorous steepest descent path asymptotics, the domain of existence of the leaky-wave is found to be limited by a conical shadow boundary which deviates from that defined by the stationary phase regime. Along this conical shadow boundary a phase matching between the space wave and the leaky wave is found. The compensation mechanism between space wave and leaky wave contribution is explored through the definition of a conical transition region with elliptical cross section. The radiated field in the far region as well as the interference between space and leaky waves in the Fresnel antenna region are discussed by means of illustrative examples, which also confirm the accuracy of the asymptotics.

Comparison of High-Frequency Scattering Results Using Exact and Approximate Incremental Length Diffraction Coefficients

A. D. Yaghjian
A.J. Devaney Associates
Boston, MA, U.S.A.

R. A. Shore
Air Force Research Laboratory
Hanscom AFB, MA, U.S.A.

Incremental length diffraction coefficients (ILDC's) provide a convenient, efficient method for improving upon the accuracy of the fields computed with the physical optics (PO) approximation. In particular, the accuracy of the PO scattered fields of 3-D perfect conductors can be significantly improved upon if the fields radiated by the nonuniform currents (the difference between the actual and PO currents) can be closely approximated and included in the scattering calculations. The far-field contribution from the nonuniform currents on a differential strip of surface on the 3-D scatterer transverse to a discontinuity or shadow boundary can be approximated by the ILDC's of the corresponding nonuniform currents on the conforming 2-D canonical scatterer (for example, the wedge, half-plane, cylinder, strip, and slit, channel or ridge in a ground plane). In contrast to other high-frequency techniques commonly employed to account for scattering from discontinuities, the line integration of these "physical theory of diffraction" (PTD) ILDC's along discontinuities and shadow boundaries eliminates singularities in caustic and transition regions and yields corrections to PO fields that are valid for all angles of observation. In addition, neither ray tracing nor searching for critical points (such as points of stationary phase) are involved in the application of ILDC's, and the ILDC line integrations do not add an appreciable amount to the computer time required for the PO surface integration.

By combining a direct substitution method with a planar surface-current equivalence theorem, we have been able to reduce the determination and application of PTD ILDC's to three main steps. The first step is to obtain an accurate expression for the nonuniform scattered far fields (total scattered minus PO far fields) of the 2-D cylindrical canonical scatterer that conforms to the particular discontinuity of interest. The second step is to substitute these far fields into the formulas we have derived for converting 2-D far fields to ILDC's, that is, to the 3-D far fields radiated by an increment (differential length) of the nonuniform current of the 2-D canonical scatterer. The third step is to add the ILDC correction to the PO computer code.

In this talk we concentrate on the substitution formulas used in the second step. Along the Keller-cone angles of diffraction, these substitution formulas reduce to expressions for ILDC's that would be obtained if the cylindrical spread factor of the 2-D canonical fields were simply changed to a spherical spread factor. A number of workers have used this simplified approach for obtaining approximate ILDC's at all angles of observation. Here we apply both the approximate and exact ILDC's to improve upon the accuracy of PO fields and compare the results for a number of scatterers. Although both the approximate and exact ILDC's perform comparably when the predominant scattering is along the Keller-cone angles, there are a number of geometries where the exact ILDC's produce much greater accuracy than the approximate ILDC's. Therefore, the approximate ILDC's must be applied judiciously, and are not ideal for general purpose computer codes.

Plane Wave Diffraction by a Semi-Infinite Parallel-Plate Waveguide with Five Different Material Loading

S. Okada
Department of Electrical, Electronic, and Communication Engineering, Chuo University
Tokyo, 112-8551, Japan

S. Koshikawa
Antenna Giken Co. Ltd. Laboratory
Tokyo, Saitama 330-0011, Japan

K. Kobayashi
Department of Electrical, Electronic, and Communication Engineering, Chuo University
Tokyo, 112-8551, Japan

The analysis of electromagnetic scattering by open-ended metallic waveguide cavities is an important subject in radar cross section (RCS) and target identification studies. There have been a number of investigations on the scattering by cavities of various shapes based on high-frequency asymptotic methods and numerical techniques. It appears, however, that the solutions obtained via these methods are not uniformly valid for arbitrary cavity dimensions. The authors have previously carried out a rigorous RCS analysis of various two-dimensional (2-D) cavities formed by parallel-plate waveguides using the Wiener-Hopf technique, and obtained efficient approximate solutions which are valid over a broad frequency range. In this paper, we shall consider, as a related waveguide geometry that can form a 2-D cavity, a semi-infinite parallel-plate waveguide with five different material loading, and analyze the plane wave diffraction rigorously using the Wiener-Hopf technique.

The geometry of the waveguide is shown in Fig. 1, where ψ is the incident field of E or H polarization, and the upper and lower plates at $x = \pm b$ are infinitely thin, perfectly conducting, and uniform in the y-direction. The material regions $R_m(-d_{m+1} < z < d_m)$ for $m = 1, 2, 3, 4$ and $R_5(-\infty < z < d_5)$ inside the waveguide are characterized by the relative permittivity/permeability (ϵ_m,μ_m) for $m = 1, 2, 3, 4$ and (ϵ_5, μ_5), respectively. Introducing the Fourier transform for the unknown scattered field and applying boundary conditions appropriately in the transform domain, the problem is formulated in terms of the simultaneous Wiener-Hopf equations that are solved in a formal sense via the factorization and decomposition procedure. It should be noted, however, that the formal solution involves infinite series with unknown coefficients. Using the edge condition, we shall further derive approximate expressions of the infinite series, which are then led to an efficient approximate solution of the Wiener-Hopf equations. The approximate solution requires numerical inversion of matrix equations. The scattered field is evaluated by taking the inverse Fourier transform together with the use of the saddle point method. Illustrative numerical examples on the RCS are presented and the far field scattering characteristics of the waveguide are discussed in detail.

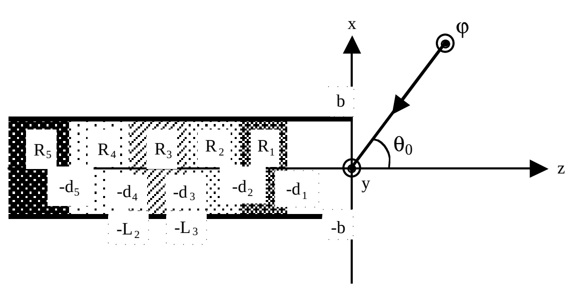

Figure 1: Geometry of the waveguide.

Iterative Solutions for the Scattering of Targets in Presence of Ocean-Like Rough Surfaces

M. R. Pino
Área de Teorí a de la Señaly Comunicaciones, Depto. Ing. Eléctrica, Electrónica, de Computadores y Sistemas, Universidad de Oviedo
Gijón, Asturias 33204, Spain

R. J. Burkholder
Department of Electrical Engineering, ElectroScience Laboratory, The Ohio State University
Columbus, OH 43212, U.S.A.

F. Obelleiro and J. L. Rodríguez
Depto. Teorí ado Sinal e Comunicacións, Universidade de Vigo
Vigo, Pontevedra 36200, Spain

The electromagnetic (EM) scattering from targets placed in complex environments has been extensively treated in the literature. This contribution deals with the EM analysis of marine targets placed on ocean surfaces and it is mainly focused on the iterative solutions used to efficiently analyze the problem.

The proposed iterative solutions are based on the Forward-Backward (FB) method [Holliday *et al.*, *IEEE Trans. Antennas and Propagat.*, Vol. 44, pp. 722–729, May 1996]. This method presents a very fast convergence when dealing with rough surfaces, but the presence of targets or obstacles on the surface makes the iterative method diverge. To overcome this limitation a generalization of the FB method, called the Generalized Forward-Backward (GFB) method has been proposed. This solution is based on a combination of the conventional FB method with the Method of Moments (MoM), where the MoM is only applied to the region close to the obstacle. The solution is found through an iterative procedure based on the same general concepts as the FB method, combining forward and backward substitution and the direct MoM solution of the obstacle region. The computational cost of the GFB method is similar to the original FB method, with the additional cost associated to the mentioned direct MoM solution. There is also an increment in the memory usage.

To reduce these costs, several improvements have been included in the method. The first proposed modification is based on a multiblock resolution of each obstacle which is divided into a set of small blocks. The solution is obtained through a standard MoM factorization for the small diagonal blocks, combined with a conventional FB iterative procedure. The computational cost of this solution is the same as the original FB method, i.e., $\mathcal{O}(N^2)$ per iteration where N is the number of unknowns modelling the problem.

Finally, these iterative procedures can be accelerated by applying a Spectral Acceleration [Pino *et al.*, *IEEE Trans. Antennas and Propagat.*, Vol. 50, No. 5, May 2002] to speed up the computation of the interactions between sea surface and targets, reducing its cost to $\mathcal{O}(N)$. Also, the Fast Multipole Method (FMM) [Rokhlin, V. *J. Comput. Phys.*, No. 86, pp. 414–439, 1990] can be used for a fast computation of the interactions between the blocks modelling the target regions, reducing this cost to $\mathcal{O}(M^{1.5})$, where M is the number of unknowns modelling those regions. The combination of both acceleration techniques yields to a very efficient algorithm where electrically large targets can be analyzed with low memory requirements and CPU time.

A Line Integral Representation of the Physical Optics Far-Field from Plane PEC Scatterers Illuminated by Hertzian Dipoles

S. Arslanagic, P. Meincke, E. Jørgensen, and O. Breinbjerg
Ørsted•DTU, Electromagnetic Systems, Technical University of Denmark
Kgs. Lyngby, Denmark

We derive a line integral representation of the physical optics field that yields the exact same result as the conventional surface radiation integral. This representation applies to the far-field radiation from a perfectly electrically conducting plane scatterer illuminated by an electric Hertzian dipole. By superposition, it also applies to three-dimensional structures formed by plane faces. The line integral representation, which is performed along the edge of the scatterer, is potentially less time-consuming than the surface radiation integral. Furthermore, it is particularly useful when the accuracy is enhanced by adding to the physical optics field a fringe wave contribution as calculated from the physical theory of diffraction equivalent edge currents. The total field is thus obtained from one single line integration along the edge of the scatterer.

In a previous work [P.M. Johansen, O. Breinbjerg, "An Exact Line Integral Representation of the Physical Optics Scattered Field: The Case of a Perfectly Conducting Polyhedral Structure Illuminated by Electric Hertzian Dipoles," *IEEE Trans. Antennas Propagat.*, vol. 43, no. 7, pp. 689–696, July 1995] we derived the line integral representation for an arbitrary observation point. This general representation obviously holds also for the case of a far-field observation point. However, it is numerically inconvenient in this case, since it contains several terms which do not contribute to the far-field but need to be calculated anyway, and since it is subject to inaccuracies resulting from the use of a large but finite observation distance. In contrast, the new line integral representation holds for the direction-dependent part of the far-field, thus leaving the far-field term, $\exp(-jkr)/r$, as an explicit factor.

The derivation of the far-field line integral representation is based on the analytical limit of the general line integral representation for $r \to \infty$. Each term of this lengthy expression has been investigated, and terms have been combined to form a more compact representation. Numerical calculations have been performed to verify the agreement between the line integral representation and the surface radiation integral, and to investigate the efficiency of the former.

Our presentation will outline the derivation of the general line integral representation and its specialisation to the case of far-field observation. Furthermore, numerical results for Hertzian dipole illumination of rectangular PEC plates will be presented.

Incremental Diffracted Floquet Waves for a Local Planar Periodic Semi-Infinite Array

A. Toccafondi, R. Tiberio, and S. Maci
Department of Information Engineering, University of Siena
Siena, 53100, Italy

Recently, a high-frequency formulation of the Green's Function for semi-infinite [1] or sectoral [2] array of dipoles, has been introduced. It has been found that an efficient representation of the Green's Function (GF) for finite arrays may be obtained when the Floquet Wave (FW) expansion of the infinite array GF is augmented by additional asymptotic ray contributions arising from edges and vertices of the array. This asymptotic formulation can be cast in the form of a generalized GTD ray theory which includes FWs truncated at appropriate shadow boundaries, with corresponding FW-induced edge and vertex diffracted waves. However, this ray-field based description of the radiation from large arrays undergoes the same impairments that are typically associated to the application of ray methods close and at caustics. In order to overcome those difficulties, it is useful to resort to local, incremental field contributions to be distributed and then integrated along the actual boundaries of the array.

In this paper, an incremental formulation of the GF for a semi-infinite array of electric dipoles is presented. The electric field radiated by the array is represented by its relevant FW expansion. Each wave species of the expansion consists of the sum of a truncated FW plus its corresponding edge diffracted field. Each FW-induced edge diffracted field contribution corresponds to the end-point contribution to the field radiated by a semi-infinite current sheet phased by the proper indexed Floquet wave-number. Its spectral integral representation exhibits the form of an edge diffracted field, excited by an incident plane wave with an indexed Floquet wave-number. According to the Incremental Theory of Diffraction (ITD) [3] a generalized localization process, based on a Fourier transform convolution pair, is applied which allows to transform the above FW-indexed spectral integral formulation into a spatial integral representation along the edge of the semi-infinite array. To this end, the spectral integral representation is recognized as a Fourier transform of the product of two spectrum functions, which directly defines its corresponding spatial convolution integral. This latter representation is naturally interpreted as a superposition of FW incremental field contributions that are localized along the edge of the semi-infinite array. As a consequence, the integrand of the spatial integral representation my be directly used to define the desired FW-indexed incremental fields. Since these latter are obtained in spectral integral form, in order to provide practical tools, asymptotic expressions of the field contributions are derived. The final expressions for the incremental diffracted FWs are well-behaved at any observation aspects and naturally lead to the generalized GTD ray-field representation, when applicable. The applicability of this formulation to large arrays with a locally large curvature of the rim is discussed.

REFERENCES

1. F. Capolino, M. Albani, S. Maci, and L. B. Felsen, *IEEE Trans. Antennas Propagat.*, part I and II, Vol. 47, No. 1, Jan. 2000.
2. S. Maci, F. Capolino, and L. B. Felsen, *Wave Motion*, 2001.
3. R. Tiberio and S. Maci, *IEEE Trans on Antennas and Propagat.* , Vol. 42, n.5, May 1994. R. Tiberio, S. Maci, and A. Toccafond, *IEICE* ,Vol.E80-C, No.11, Nov. 1997

EM Scattering from Edges in Semi-Infinite Penetrable Screens

P. Nepa, G. Manara, and A. Armogida
Dept. of Information Engineering, University of Pisa
Pisa, 56126, Italy

The scattering by non-perfectly conducting bodies has recently received an increasing attention in the context of asymptotic techniques, due to the wider and wider use of composite materials. For instance, approximate impedance boundary conditions (IBCs) have been extensively applied in the analysis of the field scattered by non-penetrable material structures. A spectral method which allows us to derive a rigorous integral representation for the total field in the presence of an isotropic impedance wedge illuminated at normal incidence was proposed by Maliuzhinets in [1]. This solution was later on extended to the oblique incidence case for specific wedge configurations, again when the wedge faces are characterized by isotropic IBCs. More recently, by resorting to the Maliuzhinets technique, three-dimensional rigorous spectral representations have been derived for wedges with anisotropic impedance faces [2]-[4]. The class of anisotropic IBCs considered in [3]-[4] is characterized by tensor impedances exhibiting a vanishing surface impedance in a principal anisotropy direction; they can be usefully applied to analyze the scattering by edges in artificially hard and soft surfaces. We note that computational costs for evaluating the fields in these more complex configurations are the same as those for the corresponding isotropic cases, since the rigorous spectral representations contain simple trigonometric terms and the well known Maliuzhinets special function. The properties of the latter function have been widely described in the literature and accurate analytical approximation proposed.

This paper is aimed to provide some details on a further extension of the Maliuzhinets method to the analysis of the scattering from edges in penetrable anisotropic screens illuminated at oblique incidence. Indeed, by applying the bisection method [5] the scattering from the edge of a penetrable screen can be rigorously reduced to a couple of full-plane impedance problems. The method can be also applied to the scattering from the planar junction between a penetrable screen and either an impedance half-plane or another penetrable screen. Samples of numerical results will be shown and compared with data obtained by some approximate solutions presented in the literature.

REFERENCES

1. G. D. Maliuzhinets, “Excitation, reflection and emission of surface waves from a wedge with given face impedances,” *Sov. Phys. Dokl.*, no. 3, pp. 752-755, 1958.
2. G. Manara, P. Nepa, “Electromagnetic diffraction of an obliquely incident plane wave by a right-angled anisotropic impedance wedge with a perfectly conducting face,” *IEEE Trans. Ant. Prop.*, AP-48, No. 4, April 2000.
3. G. Manara, P. Nepa, G. Pelosi, “High-frequency EM scattering by edges in artificially hard and soft surfaces illuminated at oblique incidence,” *IEEE Trans. Ant. Prop.*, AP-48, No. 5, May 2000.
4. P. Nepa, G. Manara, and A. Armogida, “Electromagnetic scattering by anisotropic impedance half and full planes illuminated at oblique incidence,” *IEEE Trans. Ant. Prop.*, AP-49, No. 1, Jan. 2001.
5. P. Nepa, G. Manara, and A. Armogida, “High-frequency diffraction by edges in unidirectionally conducting screens,” *Radio Science*, Vol. 35, No. 6, pp. 1265-1278, Nov.-Dec. 2000.

Session 5Pc1

Waves in Random Media

The Mueller Matrix Solution for Polarimetric Scattering from Inhomogeneous Random Media of Non-Spherical Scatterers Under a Pulse Incidence

Y.-Q. Jin and M. Chang
Center for Wave Scattering and Remote Sensing (CWSRS) and School of Information Science and Engineering, Fudan University
Shanghai, 200433, China

With the advance of radar polarimetry and imagery of SAR technology, the study of completely polarimetric scattering of the terrain surface has become of great importance. The Mueller matrix solution of vector radiative transfer has been studied for polarimetric scattering from a layer of random non-spherical particles. However, as the incidence is a plane pulse, it leads the problem of the pulse echoes for polarimetric scattering from random scatterers media and the temporal Mueller matrix solution.

There are a few works on the pulse echo from random media. For example, using two-frequency mutual coherence function, Hong and Ishimaru, Liu and Yeh, Ito studied the scalar pulse wave propagation in random media. Oguchi and Ito obtained the numerical solutions of the two frequency vector radiative transfer equation in the case where a circularly polarized plane pulse was normally incident upon a half space of spherical raindrops. Whitman *et al*. investigated the pulse propagation in a strongly forward scattering random medium. All above researches are limited to discussion of homogeneous random media. Using the ray tracing method and range calculation, Sun presented a model of forest canopy with vertical structure and calculated scattering for simulation of lidar returns. However, completely polarimetric scattering echo from inhomogeneous random media has remained to be further studied.

This paper presents a theoretical model of inhomogeneous layering random media and derives the temporal Mueller matrix solution of vector radiative transfer for polarimetric scattering of random non-spherical scatterers. Co-polarized and cross-polarized bistatic and back-scattering are numerically calculated. Variations of the shape and intensity of the polarimetric echoes well depict the inhomogeneous fraction profile, and the functional dependence upon layering thickness, incident angle and other parameters are discussed.

Evaluation of Specific Attenuation at 20 & 30 GHz from Rain Drop Size Distribution Measurements Using Distrometer

I. S. Hudiara, A. Kumar, and C. S. Sandhu
Department of Electronics Technology, Guru Nanak Dev University
Amritsar, 143005, India

The performance of terrestrial and satellite communication systems operating at microwave frequencies is severely affected by the presence of rain, fog, clouds and other hydrometers over the communication link path. Rain is the major factor that attenuates the signal propagating at these frequencies. It is desired to calculate rain-induced attenuation at different rain rates to estimate rain fade margin, which must be provided in the communication system to counter the rain effect. The specific attenuation α (dB/km) is a fundamental quantity in the calculation of rain induced attenuation statistics for terrestrial and earth space paths. Specific attenuation can be predicted from the knowledge of rain rate and drop size distribution. Various raindrop size distributions (Negative exponential distribution) reported by CCIR are based on data collected mainly in the temperate climates. When these drop size distribution models are applied for calculating specific attenuations in tropical climates, where high rainfall occurs, give unsatisfactory results. With this in view long term experimental measurements have been carried out to collect raindrop size data using distrometer to calculate raindrop size distribution at Amritsar ($31°36'N\ 74°52'E$) India, which is a tropical region. This paper describes the analysis of distrometer data for the evaluation of rainfall rate, raindrop size distribution (RDSD) and specific attenuation at 20 $\&$ 30 GHz for each rain event. The RDSD values evaluated at different rain rates have been used to develop RDSD model. We have specially calculated RDSD at a rain rate of 49.6 mm/hr for comparing it with only available Nigerian data on DSD reported by G.O. Ajayi at this rain rate. It has been found that the RDSD follows lognormal distribution and agrees with that of Nigerian data.

We have used R.G. Medhurst technique to calculate the specific attenuation at different rain rates based on our 2000 minute rain drop size data collected during monsoon periods of years 2000 $\&$ 2001, using distrometer. The specific attenuation values at 20 $\&$ 30 GHz have been evaluated at different rain rates using one-minute raindrop size data. Rain attenuation models have been developed at 20 $\&$ 30 GHz from the regression analysis of specific attenuation values estimated at various rain rates and these models have been compared with CCIR and other models based on Marshal & Palmer and Joss-Drizzle and Joss-Thunder drop size distribution.

It has been observed that the specific attenuation calculated by us based on experimentally measured DSD at this location is higher than that predicted by other models which are based on DSD data collected in temperate regions. It shows that higher rain fade margin than predicted by CCIR model (based on Laws $\&$ Parson DSD) has to be provided in the engineering of communication system at 20 $\&$ 30 GHz for our location.

Polarimetric Backscattering and Shift of Polarization Angle from Random Chiral Spheroids

Y.-Q. Jin and M. Chang
Center for Wave Scattering and Remote Sensing (CWSRS) and School of Information Science and Engineering, Fudan University
Shanghai, 200433, China

Chiralty has been studied as a novel property of some composite materials due to great potential for new applications. However, most of the researches are limited to discussion of the effective permittivity of an unbounded medium of uniformly-random small particles or continuous medium under a linearly polarized wave incidence. Actually, polarized scattering from layering chiral particulate media has not been studied.

During recent decades the polarimetry and imagery technology (such as the advance of the synthetic aperture radar, SAR) have been able to measure full 2×2 –D complex scattering amplitude matrix and 4×4 –D Mueller matrix of four scattered Stokes parameters. Jin developed a theoretical model and the Mueller matrix solution for completely polarimetric scattering from a layer of non-uniformly oriented, random non-spherical particles.

Based upon Jin's approach, this paper newly derived the scattering amplitude matrix, $f_{pq}(p, q = v, h)$, of spatially oriented, weakly chiral and electrically small spheroids. All functions of the ensemble averages $< f_{pq} f_{st}^* > (p, q, s, t = v, h)$ are explicitly formulated. They are used to construct the 4×4 –D Mueller matrix solution of the scattered Stokes parameters. Co-polarized and cross-polarized backscattering σ_c, σ_x and the polarization degree m_s, which describes partial polarization of scattered fields through random media are calculated. Numerical results can show how the chirality modulates polarimetric scattering pattern and functional dependence on the physical parameters.

It has been known that the co-polarized σ_c maximum is largely located at the polarization angles $(\chi = 0°, \psi = 0°, 180°)$ or $(\chi = 0°, \psi = 90°)$ depending on spatial orientation and particle shape. Our result first demonstrates that the chirality can asymmetrically shift this location. It is due to the chiral parameter appeared in the depolarized scattering amplitude functions. This shift can be evaluated by the measurement of the scattered Stokes parameters, and can be used to invert the chiral parameter in some simple cases.

A Hybrid Electromagnetic Technique for Modeling Radar Sea Clutter

H. W. Melief, A. P. M. Zwamborn, and H. Greidanus
TNO Physics and Electronics Laboratory
The Hague, The Netherlands

P. van Genderen, P. Hoogeboom[†]
Delft University of Technology
[†] also with TNO Physics and Electronics Laboratory
Delft, 2600, The Netherlands

When radar scattering from the ocean surface is modeled, a number of different techniques can be used. Scattering from slightly rough surfaces,i.e. a wind-roughened sea, can be modeled by Bragg scattering. The effects of larger waves are usually taken into account in two-scale models. However, very rough seas containing strongly curved components, like breaking waves, cannot be modeled in this manner. For such surfaces full-wave electromagnetic methods are needed. Unfortunately, these types of methods require high sampling of the surface, typically of the order of 10-20 points per radar wavelength in one dimension. For significant stretches of ocean surface ($\sim 100 \times 100$ m) with an X-band radar (3 cm wavelength) this quickly leads to prohibitively large sets of surface points needing to be evaluated.

In this paper we present a hybrid method for calculating the RCS from ocean type surfaces with non-linear (breaking wave) objects. The core of the method lies in a backward ray-tracing routine, which is employed to find the illumination of the surface and the local incidence angle of the radiation. This approach takes both shadowing and multiple scattering into account. The illuminated parts of the surface can then be evaluated by one of three scattering routines, Bragg scattering, physical optics or a full-wave method. The latter is a method of moments algorithm based on Rao-Wilton-Glisson basis functions and it is designed for non-perfectly conducting surfaces. The specific scattering method is chosen on the basis of the local roughness and curvature of the surface. The combination of the Bragg and the ray tracing routines leads to a two-scale model. By adding the method of moments algorithm we can model the strongly curved parts of the surface. Physical optics might be employed for very smooth surfaces, which can for instance be found in hard targets.

The advantage of this hybrid method is that only the parts of the surface that are evaluated by the method of moments code need to be sampled with 10-20 points per radar wavelength. The parts evaluated by either Bragg scattering or physical optics can be sampled with one point per few wavelengths. This results in a significant reduction of computer memory usage and calculation time.

Peculiarities of Curvature of Wave Front Surface Due to Velocity Fluctuations in Randomly Inhomogeneous Medium

G. V. Jandieri
Physics Department, Georgian Technical University
Tbilisi, 380075, Georgia

G. D. Aburjania
Vekua Institute of Applied Mathematics, Tbilisi State University
Tbilisi, 380043, Georgia

V. G. Jandieri
Physics Department, Georgian Technical University
Tbilisi, 380075, Georgia

New method of calculation of dispersion of rays shifting in random medium with velocity fluctuations randomly varying in space and time is suggested in this paper. 2D case is analysed. Stochastic kinematic nonlinear differential equation describing evolution of the curvature of wave front is derived using Serret-Frenet formulae. Unperturbed curvature has a spiral form. The expressions for fluctuations both the unit vector of wave normal and the angle of arrival are obtained by means of solution of stochastic differential equation for curvature fluctuation of the wave front. Dispersion of rays shifting which is expressed through the velocity correlation function is compared with appropriate expression in (ray–) optics approximation. Diffusion coefficient of rays is proportional to the dispersion of velocity, characteristic spatial scale of velocity pulsations and inversely to the square of the product of longitudinal component of velocity and path length of the ray in random medium. The results can be generalized for 3D case where are important both curvature and twisting of the rays. This method is universal and does not pose any restrictions on spatial scale of inhomogeneities, distance and is valid for arbitrary nonstationary media. This method is important to obtain the information about chaotic bending of phase front of wave beams due to heating spread in random media. These results may be applied for quasi-plane, quasi-cylindrical and quasi-spherical layers, such as the earth ionosphere.

Radar Cross-Section of Partially Convex Targets in Random Media

H. E. Ocla
Lakehead University
Ontario, Canada

M. Tateiba
Kyushu University
Fukuoka, Japan

We analyze the radar cross-section and backscattering enhancement for plane wave propagating in free space and continuous random media with taking into account polarization of incident wave. We consider the linear polarization including the vertical polarization (E-wave incidence) and the horizontal polarization (H-wave incidence). We assume targets with concave-convex cross-sections take sizes larger than 1.5 wavelength in free space. The backscattering enhancement is measured by the normalized RCS (NRCS). NRCS is defined as the ratio of RCS of target in random media (σ_p) to that in free space (σ_0).

From our numerical results, we have found the obvious difference in the behavior of the RCS between both of concave and convex illumination portions. RCS for concave illumination portion is larger than that for convex illumination portion due to effective illumination region widespread in case of former portion. For SCL $<< ka$, NRCS equals two due to the double passage effect irrespective of incidence wave polarization. However, NRCS deviates from two with increasing ka and/or concavity index (δ); this deviation in NRCS decreases with increasing SCL. For concave illumination portion, NRCS decreases gradually with ka. On the other hand, for convex illumination portion, NRCS fluctuates slowly around two with some anomalous increases in the NRCS with H-wave incidence and under certain circumstances of target size and δ. This analysis demonstrates clearly the effect of illumination portion curvature in conjunction with SCL of incident waves on RCS and backscattering enhancement apart from polarization of incident wave.

A Sparse Matrix Iterative Approach for Modeling Tree Scattering

K. H. Ding
Air Force Research Laboratory
Hanscom AFB, MA 01731-2909, U.S.A.

L. Tsang
Dept. of Electrical Engineering, University of Washington
Seattle, WA 98195, U.S.A.

The utilization of Foliage Penetration (FOPEN) synthetic aperture radar (SAR) to locate and detect stationary military targets hidden under the foliage faces the difficulties that the echoes from the targets are similar in strength to comparable clutter returns from trees, which cause a false alarm rate too high for robust detection of targets. A clear understanding of the fundamental scattering properties of a single tree, or a small group of trees, as resolved by an imaging radar can be important for reliable discrimination between tree and target returns.

In this paper we develop a computational electromagnetic model for modeling the foliage clutter at VHF/UHF frequencies. A structure with dielectric cylinder models is being used to simulate trees with bare branches. The method of moment is applied to calculate tree scattering signatures by discretizing the volume integral equation of the electric field and transforms it into matrix equations. An efficient numerical algorithm based on the sparse matrix iterative approach (SMIA) is used to solve the matrix equations by decomposing them into a sparse matrix for the near (strong) interactions, and a complementary matrix for the far (weak) interactions among the cylindrical sub-cells of the tree structures. Using a direct sparse solver to estimate the strong interaction part, we iteratively included the weak interaction contribution to update the solution. The key feature of this approach is that very little iteration is required to obtain convergent solutions.

We have applied the numerical tree scattering model based on SMIA to calculate scattering from various simulated trees with up to 1000 branches. We use the solutions of an exact full matrix inversion and conjugate gradient method (CGM) as baselines to illustrate the accuracy and efficiency of SMIA approach. Solutions based on the SMIA method agree very well with the exact matrix inversion. Compared to CGM, this SMIA approach reduces the number of iterations by a factor of 20 to 50 and provides a much faster numerical solution scheme for computing tree scattering.

The Ultra-Wideband Random Noise Signals and Scattering Aspects

I. Kocaman
Turkish Airforce Academy, Electronic Engineering
Yesilyurt, Turkey

O. Yildirim
Turkish Airforce Academy, Research & Development Center
Yesilyurt, Turkey

R. H. Kul
Beykent University
Istanbul, Turkey

As is well-known, electromagnetic forward scattering entails the prediction of the emission or the propagation of the radiation on the basis of known constitution of sources or scatterers. The backward scattering problems involves in deducing features of sources or scattering bodies from the emitted or scattered radiation that has propagated to a detection system. The process of deducing features of scattering bodies from the emitted or scattered radiation that has propagated to a detection system. The process of deducing features of scattering bodies from the emitted or scattered radiation that has propagated to a detection system. The process of deducing features of scattering bodies from radiation, namely inverse technique, has a vast domain of applications in geophysical and meteorological exploration and testing, etc.

This study involves the following steps; (1) computation of single scattering from a spheroidal scatterer at a single frequency, (2) computation of multiple scattering from a distribution of spheroidal scatters at a single frequency to simulate different rain rates, (3) extension of (2) to ultra-wideband (UWB) waveforms, such as stepped-frequency and random noise signals. (4) effect of dispersion on (3) above, (5) extension of (4) to target detection of, say, aircraft.

In this study, we extend the backscattering analysis from a volume filled with spheroidal raindrops and hailstones using physical optics (PO) and Rayleigh-Gans approximation (RGA) and check the validity of the theoretical derivation by using forward scattering theorem (FST). In order to reveal the multiple scattering effects, a model based on matrix doubling algorithm will be developed so that raindrops and hailstones are modelled as spheroidal particles under the Rayleigh approximation. The ultimate goal of this study is to show the scattering of the ultra-wideband random noise radar signals and to reveal the advantages of UWB radar in long-range target detection and the effects of inclement weather on system performance.

Distribution of Electromagnetic Waves in the Area of Modulation of the Superficial Relief

V. A. Komagorkin and A. I. Kukushkin
Dept. of Physics, Moscow State University
Moscow, 119899, Russia

The problem of distribution of electromagnetic waves in microwave range (200-4500 MHz) along a surface with deep modulation of a relief ($h >> \lambda$) is reviewed in case when the source of radiation is located on border or it is direct situated in Salvage's area, i.e. in the area of spatial modulation of a relief. The methods used for the decision of similar problems are analyzed, their comparative analysis is conducted, the conditions and limits of applicability are investigated, and also the most perspective approaches to development of theoretical representations and methods of the mathematical description of processes of distribution of electromagnetic waves in the area of modulation of a superficial relief are determined and proved.

Founded, that electromagnetic resonant low attenuating wave can be raised at interaction between electromagnetic waves and high-frequency component of superficial relief of the surface in one of the senior orders of diffraction, its amplitude can in some times (in some cases in tens times) surpass mirror component of diffracted fields.

Resonant surface electromagnetic wave can be distributed along a surface to significant distances, and appreciably determine structure of electromagnetic fields in shading area and in superficial areas on distances $L >> \lambda$ – wavelength of source.

Also founded, that character of intermode interaction between high frequency and the basic Fur'e-component of a superficial relief during formation of a scattering field is non-linear.

Resonant surface electromagnetic wave at distribution along a surface are similar pseudoparticles and enable to use approachings, descriptions and analogies of quantum mechanics. In particular, the underbarriering and the overbarriering transitions are resulting to originating of secondary pseudosource, which in some cases can be more brightly in the limited area of spectrum and in the allocated direction, than a real source of radiation.

Superposition of fields of resonant components in superficial areas and in shading area, and interference pictures of a field in the region of direct visibility provides practical requirements of accuracy of calculations and correctly allows taking into account wide enough class of properties of real objects.

The designed theory allows deciding quantitatively and qualitatively adequately the problem of distribution of electromagnetic waves in conditions of an actual geographic and urban landscape.

Session 5Pc2

Microwave Imaging for Biomedical Applications

Microwave Imaging Using Resonator Tomography

A. S. Omar and A. Jöstingmeier
University of Magdeburg
Magdeburg, Germany

In resonator tomography, the tomographical process takes place within a shielded cavity resonator containing the object to be imaged. Compared to free space tomography, the resonator one suffers from much less noise and interference effects. The main idea behind this type of tomography is to replace free space by a completely shielded cavity resonator of well-defined shape and geometry, illuminating antenna(s) by coupling ports and measurement of scattered field by that of the resonator generalized scattering matrix.

The inhomogeneity created by locating the object to be tomographically imaged within the cavity resonator results in coupling all resonator modes together. The modal coupling can be represented by a coupling matrix [C], which uniquely characterizes the three dimensional permittivity profile of the object. This latter can be reconstructed as a three-dimensional generalized Fourier series in terms of just one row (or column) of [C]. Coupling the resonator at properly chosen coupling ports results in a multiport, which can be externally characterized by a generalized scattering matrix [S]. Measuring the spectral dependence of the elements of [S] (the scattering parameters) provides the necessary information about the coupling matrix [C] needed for reconstructing the permittivity profile of the imaged object.

The reconstruction resolution can generally be divided into a lateral resolution describing the surface inhomogeneity of the object and a depth dependent one. The lateral resolution depends on number, distribution and geometry of the coupling ports, while the depth dependent resolution depends on the measurement bandwidth.

Experimental Imaging of Biological Objects with the Help of Microwave Tomography: I. Imaging of Excised Canine Hearts

S. Y. Semenov, A. E. Bulyshev, V. G. Posukh, Y. E. Sizov[2], A. E. Souvorov[4], R. H. Svenson, A. G. Nazarov[1], P. N. Repin[1], B. A. Voinov[3]
Biophysical Laboratory, Carolinas Medical Center
Charlotte, NC 28203, U.S.A.

[1] RRC "Kurchatov's Institute", *Moscow, Russia*
[2] Troitsk Institute of Innovative and Thermonuclear Research, *Troitsk, Moscow Region, Russia*
[3] Scientific Research Institute of Experimental Physics, *Arzamas-16, Russia*
[4] National Center of Biological Information, *Bethesda, MD, U.S.A.*

Three-dimensional (3D) microwave tomographic system (MWT) has been developed. This system is capable for measuring of a plurality of electromagnetic fields (EM) scattered by various biological objects. Using developed 3D images reconstruction algorithm, these experimental data have been inversely reconstructed into 3D tomographic images. We used a 3D-reconstruction scheme based on the gradient method.

The system itself comprises of a large working chamber (120 cm in diameter and 135 cm in height) filled with the salt solution of different concentrations. The dimensions of the working chamber allow for a whole body imaging of laboratory animals as well as excised biological organs. Precise automated system has positioned both transmitting and receiving antennas at various points inside of the working chamber, which allows for measurements of EM field with required accuracy and locations. Currently we are working in 3D scalar approximation, i.e., irradiate and measure of EM field of certain polarization and assume that it (polarization) has not changed during wave propagation.

The primary objective of our research is cardiovascular applications of microwave tomography. In particular, we study a feasibility of MWT for assessment of physiological and pathological conditions of myocardial tissue, based on an acute ischemia and chronic infarction models. Earlier, we have shown that dielectrical properties of myocardial tissue have changed in acute ischemia and chronic infarction [1] and degree of these changes is sufficient to be MW tomographically imaged. At present stage we conduct tomographic experiments on excised canine hearts with ischemia or infarction or their dielectrical models. A number of tomographic experiments have been performed. We used different experimental schemes, different number of transmitters and receivers, solutions with different dielectrical properties, varied operational frequencies and antennas configurations and optimized other parameters of the system as well as images reconstruction algorithm. This allows us to obtain microwave tomographic images of excised canine hearts.

REFERENCES

1. Semenov, S. Y., R. H. Svenson, and G. P. Tatsis, "Microwave spectroscopy of myocardial ischemia and infarction. 1. Experimental study," *Annals of Biomedical Engineering*, Vol. 28, No. 1, 48–54, 2000.

Conformal Microwave Array Applicator for Heating and Radiometric Thermometry of Large Area Superficial Disease

P. R. Stauffer and D. Neuman
University of California, Radiation Oncology Dept.
San Francisco, CA 94143, U.S.A.

S. Jacobsen
University of Tromsoe, Dept. of Physics
Tromsoe, N-9037, Norway

F. Rossetto
Vivant Medical Corp.
Mountain View, CA 94043, U.S.A.

Purpose: This presentation describes a microstrip conformal microwave array (CMA) applicator fabricated from thin and flexible multilayer printed circuit board (PCB) material for use in radiometrically controlled heating of large surface areas overlying contoured anatomy. The primary application for such a device is Hyperthermia treatment of superficial tissue disease ≤ 1 cm deep such as chestwall recurrence of breast carcinoma, and plaque psoriasis.

Methods: Microwave applicators were constructed with up to 32 individually controlled Dual Concentric Conductor (DCC) apertures, each ranging in size from 2 to 7 cm square and driven at either 915 or 433 MHz. Radiation patterns were characterized with FDTD numerical analysis in homogeneous and heterogeneous tissue loads, and compared to electric field based SAR measurements in homogeneous muscle equivalent phantom. Dual-mode applicators were also constructed from three layer flexible PCB with Archimedian spiral receive antennas integrated concentrically inside each DCC heating aperture for simultaneous non-invasive radiometric sensing of temperature under each heating aperture of the array. Using an elastic overgarment, CMA applicators with custom fabricated 5-10 mm thick temperature controlled water bolus vests were secured in place on patients with diffuse chestwall disease for one hour superficial hyperthermia treatments.

Results: SAR measurements in phantom were in close agreement with FDTD simulations, demonstrating effective heating ($\geq 50\%\ \mathrm{SAR_{max}}$) extending out to the perimeter of up to $60 \times\ 30\ \mathrm{cm}^2$ arrays. Use of a 6 mm water bolus and 3 cm DCC aperture size at 915 MHz provided good resolution control for varying the size and shape of SAR patterns under the large arrays. The broadband spirals demonstrated the potential to interrogate emitted radiation from under the center of each DCC heating antenna with an accuracy of $\pm 0.2^{\circ}\mathrm{C}$ in homogeneous test loads for 5 sec integration time and several different 500 MHz bandwidth ranges between 1-4 GHz. Temperature distributions measured with manually mapped fiberoptic sensors in the clinic confirmed the ability to heat superficial tissue uniformly above 42°C across the entire array surface, with the patient either standing, sitting or lying down comfortably during heat treatment.

Conclusions: A new flexible PCB conformal microwave array applicator has been shown to provide uniform and adjustable heating of large surface areas up to $1800\,\mathrm{cm}^2 \times 1$ cm depth over contoured anatomy, while at the same time providing temperature-related radiometric feedback control signals from integral spiral receive mode antennas. Such an applicator should significantly expand the number of patients that can be treated effectively with superficial hyperthermia.

Mathematical Model of Three-Dimensional Vector Microwave Tomography

A. E. Bulyshev, A. E. Souvorov, S. Y. Semenov, Y. E. Sizov, and V. G. Posukh
Biophysical Laboratory, Carolinas Medical Center
Charlotte, NC 28203, U.S.A.

Microwave Tomography is a novel and promising technique in biomedical imaging area. This technique has significant advantages in front of current used imaging technologies: x-ray CT, PET, SPEC, ultrasound, and NMR imaging. The major advantage of Microwave Tomography is the abilities to image dielectrical properties of living tissues, which directly reflect its physiological conditions with acceptable space and time resolution.

One of the significant problems, which have to be addressed to construct Microwave Tomograph, is a correct mathematical model of the imaging process. It has been proven that 3D vector Maxwell's equations are the adequate model for an accurate 3D-microwave imaging. In their previous investigations [1] authors have shown that a gradient method [2] was successfully applied for 3D Microwave Topography imaging in scalar approximation. The results of the computational and biophysical experiments show that the scalar approximation can provide the 3D images of internal structure of the complex biological objects as an extracted canine heart [3]. However, it is also obvious that the scalar Helmholtz is not completely adequate model for 3D case and should be improved. In the current investigation authors apply the modified gradient method to solve the inverse problem for Maxwell's equations. Some regularization procedure and two different rules to choose an iterative step are proposed. Authors suggest stopping the iterative process with accordance of the level of experimental noise. Every step of the gradient method requires two direct problems solving. In order to solve direct problems of 3D vector Maxwell's equations authors apply two iterative methods: Concus-Golub method and Conjugate Gradients Method (CGM). The first is proven to be very effective in the case of objects with small and medium contrast, and the second is more universal. A special type of preconditioner is used to apply to CGM. Another important factor, which effects the accuracy of imaging, is the model of incident field. In the current work authors investigate the incident fields produced by a rectangular waveguide.

Using theory which is introduced above authors conducted computational experiment targeting the next purposes: a) to show the abilities and effectiveness of the direct problems solvers; b) to prove the abilities of the modified gradient method to image the human heart with quality sufficient for biomedical applications; c) to make a conclusion about sensitivity and space resolution of the Microwave Tomography method.

REFERENCES

1. A. E. Bulyshev, S. Y. Semenov, A. E. Souvorov, R. H. Svenson, A. G. Nazarov, Y. E. Sizov, and G. P. Tatsis, *Inverse Problems*, Vol. 16, pp. 863–875, 2000.
2. Kleinma and P. van der Berg, *J. Comput. Appl. Math.*, Vol. 42, p. 17, 1992.
3. Semenov S. Y., Bulyshev A. E., Souvorov A. E., Nazarov A. G., Sizov Y.E., Svenson R. H., Posukh V. G., Pavlovsky A. V., Repin P. N., and Tatsis G. P., *IEEE Trans MTT*, Vol. 48, No. 6, pp. 1071–1074. 2000

FFT-Accelerated Fast Forward and Inverse Scattering Methods for Microwave Imaging of Breast Cancer

Z. Q. Zhang and Q. H. Liu
Department of Electrical and Computer Engineering
Duke University
Durham, NC 27708, U.S.A.

Recently, active microwave imaging has emerged as a promising technique for the detection of breast tumors. The impetus of these interests is the extensive study showing high electrical contrasts between malignant breast tumors and the normal breast tissue at microwave frequencies. For example, at 800 MHz, the relative permittivity, ϵ_r and electrical conductivity σ for normal mammary tissues are around $\epsilon_r = 16$ and $\sigma = 0.16$ S/m, respectively, while they are $\epsilon_r = 16$ and $\sigma = 0.16$ S/m, respectively, for a malignant breast tumor. The contrast is 3.75 for the relative permittivity, and 6.75 for the electrical conductivity (W.T. Joines et al. "The measured electrical properties of normal and malignant human tissues from 50 to 900 MHz," *Med. Phys. J.*, vol. 21, no. 4, pp. 547-550, 1994). This high contrast gives rise to a large electromagnetic scattering signal when electromagnetic waves are applied to a malignant tumor embedded in a normal tissue.

However, this high electrical contrast also increases the difficulty of forming an accurate image because of the increased multiple scattering. In order to achieve a high-resolution in the microwave breast imaging, it is essential to account for these multiple scattering effects. We have developed a series of two- and three-dimensional fast and accurate forward and inverse methods to simulate such effects and form high-resolution images from the array data. This presentation will review our recent work on (i) fast forward methods based on the combination of the extended Born approximation, conjugate-gradient, biconjugate-gradient, and stabilized biconjugate-gradient methods, and the fast Fourier transform, and (ii) two nonlinear microwave imaging algorithms for the high-contrast media encountered in microwave biomedical imaging. Numerical results for large-scale forward and inverse problems in microwave breast imaging will be presented.

Robustness of Space-Time Microwave Imaging to Breast Tissue Dielectric Properties

X. Li, E. J. Bond, S. C. Hagness and B. D. Van Veen
Deparment of Electrical Engineering and Computer Engineering, University of Wisconsin-Madison
Madison, WI 53706-1691, U.S.A.

We have recently proposed a method of microwave imaging via space-time (MIST) beamforming for detecting backscattered energy from small malignant breast tumors. In our MIST approach, each antenna in an array sequentially transmits an UWB signal into the breast and records the backscatter. Spatial focusing of the backscattered signals is required to discriminate against clutter caused by the heterogeneity of normal breast tissue. This focus can be achieved synthetically by applying signal processing techniques to the recorded signals. A beamformer time shifts the received signals, passes them through a bank of finite-impulse response (FIR) filters, and sums the filter outputs to produce the beamformer output. The beamformer output is time gated and then the energy is calculated. A display of energy as a function of location provides an image of backscattered signal strength.

The weights in the FIR filters are designed using a least squares technique so the beamformer passes the components of the backscattered signal originating from the candidate location with unit gain while compensating for frequency-dependent propagation effects. This design process uses a Debye model for the average frequency-dependent dielectric properties of normal breast tissue. The extent to which the dielectric properties vary within and between patients is not yet definitively known, due to the scarcity of published data and the preliminary status of our own measurements.

In this paper, we present a comprehensive study of the performance of our MIST beamforming approach with respect to hypothetical variations in the dielectric-properties of normal breast tissue. This study primarily relies on backscatter signals calculated using finite-difference time-domain (FDTD) simulations of anatomically realistic MRI-derived numerical breast phantoms. Backscatter signals have also been obtained from preliminary experiments using simple liquid breast phantoms. Phantoms for fatty, less fatty, more dense, and very dense normal breast tissue have been designed. First we consider the scenario where patient-specific estimates of the nominal dielectric properties of normal breast tissue are available and are incorporated into the filter design process. Small tumors are successfully detected in a wide range of phantoms, even when the contrast between malignant and normal tissue is significantly reduced due to denser normal breast tissue. We also consider the scenario where patient-specific data is not available. In this case, we apply filters that are designed using average dielectric properties that do not match that of the actual breast tissue. Small tumors are successfully detected even when a significant mismatch exists between the average normal-breast-tissue dielectric properties assumed in the beamformer design and the actual average dielectric properties of the breast being scanned. Consequently, patient-specific data on the average dielectric properties of normal breast tissue does not appear to be required for detection.

Reduced Background Contrast for Improved Microwave Imaging of the Breast: Phantom Study

P. M. Meaney, D. Li, N. Yagnamurthy, M. Fanning, S. Pendergrass, and K. D. Paulsen
Thayer School of Engineering, Dartmouth College
Hanover, NH, U.S.A.

We have recently identified a liquid that when diluted with water can provide a range of low contrast coupling media for microwave imaging of the breast. Previous studies were conducted to facilitate imaging of the breast in a saline background through the use of phase unwrapping [Meaney et al. 2001] and conformed mesh techniques [Li et al. 2001]. The general conclusion from these studies, both phantom and simulation, was that a reduction in background contrast would significantly improve image quality. The new liquid is suitable to use with human subjects and its costs are moderate. A new prototype patient interface also requires considerably less volume of liquid for each exam, which further restrains costs of the new medium.

Figure 1 shows a series of reconstructed images of a 10 cm diameter homogeneous cylindrical agar phantom in three different background media at 900 MHz. The three media had $\epsilon_r = 77.1$, 55.9 and 39.2, and $\sigma = 1.7$, 1.6 and 1.1 S/m, respectively, while the properties of the agar were $\epsilon_r = 31$ and $\sigma = 0.6$ S/m. It is interesting to note that the permittivity image in the saline background case clearly overestimated the actual property values of the cylinder, while those for the two lower contrast media recovered the properties quite well.

Patient exam data was also acquired using these different media. Figure 2 shows the scattered electric field phases for all nine receivers associated with a single transmitter for saline and the lowest contrast medium. Consistent with metrics developed in Meaney et al. [2001] (when more than 45% of the measured scattered phase values are wrapped the reconstruction process will diverge without use of a priori information or our phase unwrapping reconstruction algorithm), the images associated with the saline background diverged while those for the lower contrast medium were stable.

The consistency of these clinical results with our previous analysis is reassuring. It is very likely (based on simulation studies) that imaging with a lower contrast medium will also provide considerably more internal breast feature information which will not be obscured by the presence of such large gradients at the breast/background medium interface.

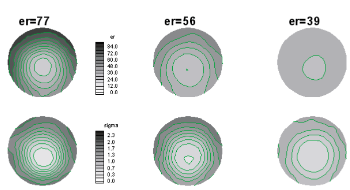

Figure 1: 900 MHz reconstructed permittivity and conductivity images for a 10 cm diameter homogeneous agar phantom for three varying contrast background media.

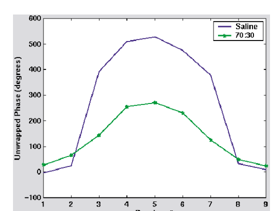

Figure 2: Unwrapped scattered phases at the 9 receiver sites for a single transmitter for two background media from a patient exam.

REFERENCES

1. Li D, Meaney PM, Paulsen KD, "Conformal microwave imaging for breast cancer detection," 2001 (submitted).
2. Meaney PM, Paulsen KD, Pogue BW, Miga MI, "Microwave image reconstruction utilizing log-magnitude and unwrapped phase to improve high-contrast object recovery," *IEEE Transactions on Medical Imaging*, vol. 20, pp. 104–116, 2001.

Development of a Printed Dipole Array Antenna for Fan Beam-Type Chirp-Pulse Microwave Computed Tomography (CP-MCT)

M. Miyakawa, E. Harada, and N. Ishii
Niigata University, Faculty of Engineering, Department of Biocybernetics
Niigata, 950-2181, Japan

M. Bertero
INFM & DIFI, University of Genova
Genova, I-16146, Italy

Originally, the chirp pulse microwave computed tomography (CP-MCT) has been developed for noninvasive temperature imaging of a human body. It has been demonstrated that the spatial resolution is approximately 10–12 mm and temperature variation from 0.3 to 0.5° C is detectable with the prototype system of CP-MCT. We have reported that high-speed imaging by the fan-beam scanner consisting of forty-seven dipole antennas is feasible [3, 4]. In this study, a printed dipole array antenna has been developed to improve the quality of images in CP-MCT and the best measuring condition with use of the antenna has also been discussed.

The pattern of the dipole antenna element printed on the laminated dielectric board (PILLAR PC-CLAD, NPC-H220A) is shown in Fig. 1(a), while the arrangement of the forty-seven elements used as a receiving antenna is given in Fig. 1(b). The dimension $L(= d1 + d2)$ has been varied from 280 mm to 315 mm in order to find the best measuring condition in respect of the spatial resolution and the maximum size of the measurable object. Relative dielectric constant and dielectric loss tangent of the dielectric board are 2.20 and 0.0001 at 3 GHz. The laminated board 0.8 mm in thickness is very soft so that the arrangement describing the circular arc is easily realized.

The distance between the adjacent two-dipole elements is 11.8 mm. It is determined numerically and experimentally. In experiment, it is determined as the minimum distance such that the input impedance varies about 6% at most when five or seven elements are arranged at the same time.

Figure 2 shows an example of the tomographic image of a cylindrical phantom 60 mm in diameter. It is filled with pure water and arranged in 0.69% bolus saline solution. Where, $L = 319$ mm and the number of effective dipole antenna elements arranged within the fan angle $(90.5°)$ are forty-three. Since the variance in the electric characteristics of the elements can be very small, the image quality is easily improved by use of the printed dipole array antenna as compared to the wired dipole elements.

Quality in images has been improved by using the printed dipole array antenna. In regard of L, we have found the best solution under the given conditions.

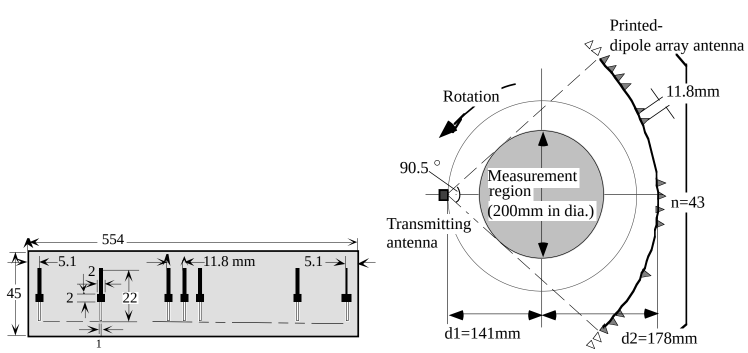

(a) Printed dipole array antenna

(b) Configuration of the element dipole antenna

Figure 1: Fan beam scanner with printed dipole antennas.

Figure 2: An example of the measured image.

Session 5Pa3

Data Processing Techniques in Remote Sensing and Radar - II

Applications of Minimum Cross-Entropy Methods to Synthetic Aperture Radar Images of Natural Landscapes

M. Grippa, I. H. Woodhouse
Department of Geography, The University of Edinburgh
Edinburgh, EH8 9XP, Scotland, U.K.

Synthetic aperture radar (SAR) has great potential for environmental mapping and monitoring, however its applications are limited by the presence of speckle, a noise-like pattern originating from the interference of the scattered waves. Significant effort has therefore been put into developing methods and algorithms that minimise their effects and/or attempt to remove them by reconstructing the underlying radar cross-section. The multi-look processing technique helps to reduce the effect of speckle by averaging separate adjacent sub-samples (or looks) of the full synthetic aperture. Although it is commonly used to reduce the influence of speckle in SAR images, its effectiveness is offset by a loss in spatial resolution.

In the first part of this paper we explore the use of a minimum cross-entropy approach to this problem of trading-off speckle reduction and resolution. Although cross-entropy techniques have been used for a wide range of scientific problems, they have rarely been applied in depth to problems in SAR imaging. A structural entropy term (that may be also interpreted in terms of information content using the Shannon information theory) is used to evaluate the goodness-of-fit between the noisy image and the underlying cross-section. This allows us to calculate an optimum effective number of looks for different targets types based on a minimum cross-entropy criterion. We then consider the dependence of this optimum with the characteristics of the natural landscape investigated (i.e. the spatial frequency of the image texture or the order parameter for clusters that are gamma distributed).

In the second part of this paper we investigate the performance of a minimum cross-entropy method for SAR image reconstruction and de-speckling. This requires solving an inverse problem and it may be done by choosing the solution that minimises the fit of the reconstructed image to the actual measurements subject to an a priori penalty function. Our approach is to employ a structural entropy term for both the goodness-of fit function and the penalty function. The potential of this new method is evaluated and discussed by presenting results obtained on both simulated and real SAR images with both single- and multi-look characteristics.

What Is the Joint Covariance Matrix of InSAR and GPS Data?

H. A. Zebker
Depts. of Electrical Engineering and Geophysics, Stanford University
Stanford, CA 94305-2215, U.S.A.

S. Jonsson
Dept. of Geophysics, Stanford University
Stanford, CA 94305-2215, U.S.A.

F. Onn
Dept. of Electrical Engineering, Stanford University
Stanford, CA 94305-2215, U.S.A.

Inverse modeling and interpretation of diverse space geodetic data sets requires a complete treatment of measurement errors. A formal method for quantifying these errors and their interdependences is found in the covariance matrix, an expression of the joint central moment of each observation datum with every other datum. While there have been many reports presenting inverse-derived solutions for subsurface slip distributions derived from InSAR, GPS, and combined InSAR-GPS data sets, most of these follow an assumption of independence for all measurements. This leads to a diagonal form for the covariance matrix, greatly simplifying the inversion calculation, but at a cost of ignoring any correlation between measurements.

The independence assumption is reasonable if the measurements are sparse enough in space or time that their cross-correlation is very small. This is often the case, say, for campaign-style GPS data. The spatial near-continuity of InSAR data, on the other hand, can lead to very significant correlations for nearby data points. The delay of radio signals propagating through the atmosphere varies as a function of many things, but is dominated by water vapor content, whose distribution can be described by a power spectrum with most of the energy at long spatial wavelengths. Since a significant part of the signal occurs at the longer wavelengths, InSAR data points located within a few km or even 10's of km of each other are highly correlated. Moreover, as GPS and InSAR observations over an area may be coincident in both space and time, these disparate measurements may follow each other as well, even in the absence of a deformation signal. Thus a surface deformation signal, which we might expect also to be spread over several km, is not readily distinguishable from natural variations in the background noise. Hence, knowledge of the spatial spectrum of atmospheric delays is critical for optimal use of the data. This is even more so if the GPS data are used to "correct" InSAR measurements. Thus an inversion algorithm may generate a solution dependent on the correlated part of the noise in the measurements instead of the underlying geophysical signal.

Here we present joint covariance matrices for interferograms and GPS data at several times and in several locations around Southern California. We used interferograms derived over short time scales so that the signals are not likely to contain deformation signals, and parameterize the matrices so that we have estimates for use in data that do include subtle deformation hiding beneath the atmospheric noise. Fully quantifying the covariance estimates also allows us to assign the proper magnitudes for weighting each element in an inverse solution for subsurface change, so that the data from each sensor may be optimally used.

Sidelobe Reduction in Range and Doppler Windows of Frequency Modulated Pulses

A. Aminaei
Iran University of Science and Technology
Tehran, Iran

A result of pulse modulation in radar systems is maximum target detection in range and Doppler domain. This is equal to a narrow and high mainlobe and low sidelobes as much as possible in ambiguity diagram of received pulses.

In this paper a comparison between phase-modulated pulses and frequency-modulated pulses is done. For the latter, Stepped Frequency and Random Frequency Pulses (RFP) are concerned.

At the end, by two examples, a method for decreasing sidelobes is presented.

Among tested methods like changing the phase and duration of subpulses, adding a zero subpulse to the duration of a RFP causes the level of sidelobes in range window decreases about 15%. Doppler window has also good characteristic. This simple method doesn't need any new hardware but saves power for long pulses as well as reducing level of sidelobes, which is important in the presence of clutter. Although adding a zero subpulse to a complex of subpulses with random frequencies increases random parameters theoretically, just its location, duration and number of zero(s) which added can optimize the ambiguity diagram. In RFP mentioned in this paper one of the random frequencies is replaced with a zero subpulse to yield sidelobe reduction. According to ambiguity diagram properties, decreasing in the level of sidelobes tend to increasing in the level or thickness of mainlobe because the volume covered by ambiguity diagram is constant.

UMTS Terrestrial Radio Access (UTRA) with Passive Intermodulation (PIM)

F. Abbas, D. Adamson, B. Clarke, and J. Miall
CETM, National Physical Laboratory, Queens Road
Teddington, TW11 0LW, UK

M. Kelly
Huber + Suhner (UK) Ltd, Telford Road
Bicester, OX26 4LA, UK

E. Weibel
Huber + Suhner AG
Herisau, CH-9100, , Switzerland

For the better quality of voice and data information must pass through a fixed bandwidth in wireless communication systems such as UTRA (W-CDMA, UMTS, 3G), PIM distortion has a significant factor which limits systems capacity. Similar as in active devices, PIM occurs when signals at two frequencies mix with each other in a nonlinear fashion to produce spurious signals. Spurious IM signals may fall within a base station's receive (Uplink) band as shown in the Figure 1 for the UTRA case, receiver desensitization can occur. This can degrade call quality or system carrier-to-interference ratio (C/I), thereby reducing the capacity of the communications system.

PIM measurements systems architectures are shown in the Figure 1. The two test frequencies are amplified in PA1 and PA2 and then combined in the filter combiner. On the input to the duplexer is a band pass filter tuned to the transmit frequencies of the system that the DUT will be used in. This has the added benefit of reducing noise from the power amplifiers (typically-65 dBm) in the system receive band where the measurements will be made. The combined carriers pass out into the DUT and then to a cable load where the power is lost. A low level IM cable with RG393 is used to make a cable load. This is just a 50-100 m reel of cable with a low power termination at the end. Most of the power is lost in the cable, and any small amount of PIM generated by the termination (they are generally good IM generators) is lost in the return up the cable. Any reflected signal then goes back into the duplexer where a band pass filter now passes only the receive frequencies (i.e. our wanted reflected IM) and reduces the level of the two test carriers. The carriers are still sufficient to cause IM in the Low Noise Amplifier (LNA) or spectrum analyzer front end, so a further band pass filter reduces them even further before passing through the LNA. The LNA has about 30 dB gain with noise figure of 2 dB, which gives a comparable reduction in the noise floor in the spectrum analyzer relative to the signal being measured. This is essential to allow measurements below -130 dBm. This work not only revealed the difficulties that industry is experiencing in making PIM measurements, but also provides UTRA equipment manufacture companies with a tool to improve their measurement capabilities as they deal with PIM-related barriers. Today, manufacturers are producing components for the third generation of mobile communications, and PIM is a major criterion for OEMs.

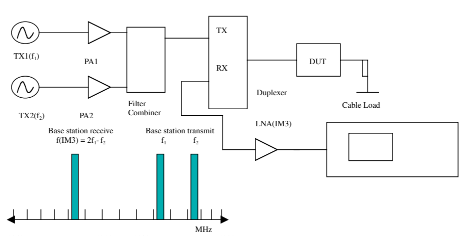

Figure 1: PIM measurements system architecture with potential third-order modulation in URTA results from collocation of two or more transceivers at a single site.

Localized Linear Operators: Application to Image Sequence Compression Using Optical Signal Progressing

D. Guha
Agilent Technologies India Limited
Kolkata, West Bengal, India

The theory of linear operators covers a large number of applications in applied mathematics and signal processing. This paper discusses three commonly used linear operators, namely, the short time Fourier transform, the wavelet decomposition and the sub-band decomposition in the light of Optical Signal Processing. Common features and differences between the above operators are examined in the framework of image sequence compression. In particular, the Gabor expansion, as a special case of short time Fourier transform in discussed in details. This has been extended to the optical domain in this paper. A new and efficient technique to perform Gabor expansion of Optical signals is introduced. The sub-band decomposition of signals and the wavelets theory are two sub-classes of linear operators which were developed in two different disciplines. However, there exist big similarities between the two approaches. After a brief introduction of sub-band decomposition and wavelet theory, the equivalence and differences between them are discussed, in both orthonormal and bi-orthonormal cases. The multi-resolution representation of data is considered in particular. A new approach to filter bank design in optical domain, using matrix formulation is introduced. Using this approach, an efficient optical filter bank with low complexity and good frequency response is designed. The characteristics of this optical filter bank are compared with that of other commonly used short kernel filter banks, for video compression applications. In this paper, a generic codec is introduced which is able to compress efficiently video image sequences using optical signal processing with any format at desired bitrate, without any change in its architecture. The approach is based on multi-resolution representation of data, which is generated by the filter bank proposed in this work. The use of multi-resolution data structure in conjunction with other components of the system such as multi-resolution motion estimation, allows a simple and efficient implementation. Simulations on typical image sequences show that it is possible to perform generic coding with reduced complexity and good efficiency.

A New Method for Designing Equiripple FIR Higher-Order Digital Differentiators by Multiple Exchange Algorithm

S. N. Bhosale
Department of Physics, Karnatak University
Dharwad, Karnataka 5800 03, India

S. Fatima
Department of Applied Electronics, Gulbarga University
Gulbarga, 585 106, India

D. K. Deshpande
Department of Physics, Karnatak University
Dharwad , Karnataka 5800 03, India

M. V. Latte
SDM College of Engineering and Technology
Dharwad, Karnataka 580 002, India

Higher-order digital differentiators (DD's) find their importance in the calculation of geometric moments and also in biological signal processing. Many methods are available in the literature for the design of higher-order DD's. One of the widely used method due to McClellan-Parks. Its modification by Rahenkamp and Vijaya Kumar is well suited for the design of first, and higher-order equiripple DD's respectively. For the design of nonequiripple DD's methods such as extension of eigenfilter method by formulating an error function in quadratic form, extension of Fourier series method in conjunction with accuracy constraints by imposing magnitude and derivative constraints at a particular frequency, are reported in the literature. Recently, Sunder et al. have suggested design methods least-squares and weighted least-squares (for the design of differentiators and Hilbert transforms using WLS method) and the latter has been extended by Bhosale et al. for the design of higherorder digital differentiators. Yet another method namely, genetic algorithm approach is suggested by Shian-Tang Tzeng.

In view of the above considerations the methods for the design of higher-order DD's are being modified from time to time. In this paper, a new method for the design of equiripple FIR higher-order DD's based on multiple exchange algorithm (MEA) introduced by C. C. Tseng and S. C. Pei is described. In the present method the extremal frequencies are searched from error response instead of magnitude response, as in the latter case it was hardly possible to search extremal frequencies. This method of searching extremal frequencies from error response has resulted in modification of MEA.

A perusal of literature suggests that even order DD's can only be designed by symmetric impulse response whereas the odd order DD's can only be designed by antisymmetric impulse response.

Bearing this in mind the present method is used for the design of
higher-order DD's (both even and odd) and the error response is studied. The peak error so estimated is smaller as compared with the values estimated using eigenfilter, least-squares and genetic algorithm approach, where as it is comparable with the values obtained from WLS and Parks-McClellan methods. Our new method for designing higher-order digital differentiators is optimal in minimax sense. This new method easily extended to design of equiripple FIR frequency selective higher-order DD's such as lowpass, highpass, bandpass, and bandstop filters. Several design examples demonstrate the efficiency and performance of this new method.

Session 5Pa4

Theory of Guided Waves

DESAFIO 1.0: A Novel CAD Tool for the Automated Design of Inductively Coupled Rectangular Waveguide Filters

J. V. Morro, H. Esteban, P. Soto, A. A. San Blas, and V. E. Boria
Dpto. de Comunicaciones, Universidad Politécnica de Valencia
Valencia, E-46022, Spain

B. Gimeno
Dpto. de Física Aplicada-ICMUV, Universidad de Valencia
Valencia, E-46100, Spain

Inductively coupled rectangular waveguide filters (see Figure 1) are used in many communication applications, specifically in satellite communications. As a consequence, many efforts have been devoted to develop very efficient and accurate tools for the analysis of such filters in the last decades. However, the design procedure of the above mentioned filters still usually requires the manual intervention of expert users. The complete automation of the inductive filters design process would extremely reduce the economic and time to market costs related to the production of such devices. Therefore, the automated design process of passive waveguide devices is receiving a considerable attention in the last times [1]. A very interesting design strategy is based on the Aggressive Space Mapping (ASM) technique well described in [2]. A major advantage of this technique is the very low CPU time required to obtain the optimal solution using a very precise simulation tool.

In this paper we present a novel Computer Aided Design (CAD) software tool for the completely automated design process of inductively coupled rectangular waveguide filters (DESAFIO 1.0). This novel CAD tool efficiently implements the ASM technique previously cited, and uses a multi-modal analysis method based on the accurate and fast solution of an Integral Equation. The paper describes in details all the optimization methods used to implement the ASM technique, as well as the analysis tool employed to determine the electrical responses of the inductive filters. Results for the full automated design procedure of a very narrow band-pass inductive filter ($f_0 = 14.25$ GHz, BW = 74 MHz, 0.5$\%$) are also offered in Figure 1.

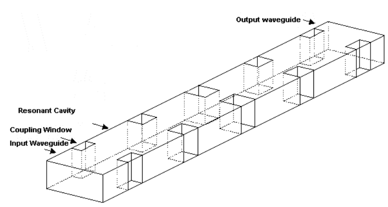

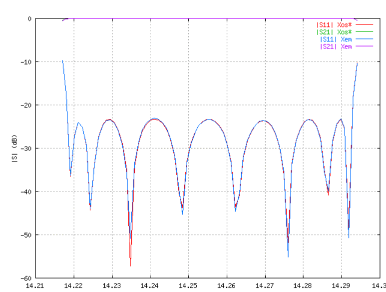

Figure 1: Inductively coupled rectangular waveguide filter in (a), and results for the automated design of a band-pass filter with an electrical response of 74 MHz bandwidth centered at 14.25 GHz in (b)

REFERENCES

1. J. W. Bandler. Special issue on "Automated circuit design using electromagnetic simulators," *IEEE Trans. Microwave Theory Tech.,* Vol. 45, No. 5 (part II), May, 1997.
2. J. W. Bandler, R. M. Biernacki, S. H. Chen, R. H. Hemmers and K. Madsen, "Electromagnetic optimization exploiting aggressive space mapping," *IEEE Trans. Microwave Theory Tech.,* Vol. 43, No. 12, 2874–2881, Dec. 1995

Millimeter-Wave Flexible Line By Using High Permittivity LSE NRD Guide at 60 GHz

F. Kuroki and A. Miyamae
Kure National College of Technology
Aga-Minami, Kure 737-8506, Japan

T. Yoneyama
Tohoku Institute of Technology
Yagiyama, Taihaku-Ku Sendai 982-8577, Japan

High permittivity LSE NRD guide, which consists of high permittivity dielectric strips inserted in a below cutoff parallel metal plate waveguide as shown in Fig. 1, has great advantage such as wide band-width, low loss, and no radiation at curved sections and discontinuities [1]. The thin sheet shaped dielectric strips can be used in this guide, because the cross-sectional dimensions are designed by

$$\frac{a_E}{\lambda_0} = 0.2 \sim 0.45 \qquad (1a)$$

$$\sqrt{\varepsilon_E - 1}\,\frac{b_E}{\lambda_0} = 0.1 \sim 0.5 \qquad (1b)$$

Choosing the ceramic compounding PTFE with the relative permittivity of 10.8, the cross-sectional dimensions are designed to be 2.25 mm in height and 0.26mm in width at 60ghz, respectively. This dielectric strip has flexibility in transverse plane because the main ingredient of the dielectric material is a soft PTFE. With this in mind, we have devised the flexible line by using this LSE NRD guide. Figure 2 (a) shows the photograph of the 180 degree bend with the curvature radius of 9mm, where it was fabricated by warping the LSE NRD guide with the length of 30mm. The transmission loss was measured by using the usually used LSM NRD guide made from the pure PTFE. The small transmission loss can be obtained as shown in Fig. (b), although the curvature was set to be drastically sharp. Figure 3(a) shows the S-shaped curve with more sharp sections. In this severe condition, though, the low transmission loss of less than 0.5 dB was also obtained. The low loss nature is due to the non-radiating performance of the NRD guide. These flexible lines will be interested in the applied fields of the several types of connections in the NRD guide integrated circuits.

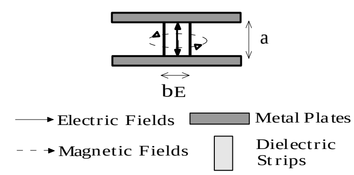

Fig. 1 Cross-sectional view of LSE NRD guide

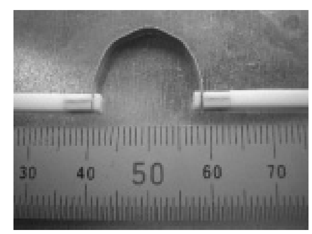

(a) Photograph

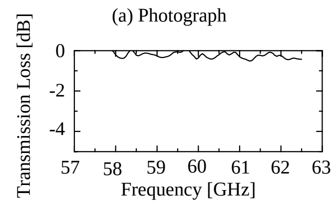

(b) Measured transmission loss

Fig. 2 180 degree bend with curvature radius of 9 mm

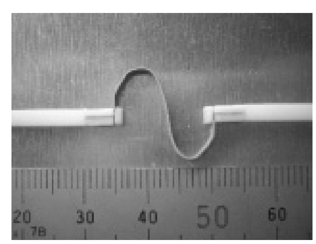

(a) Photograph

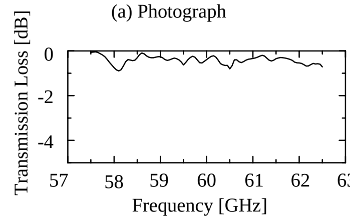

(b) Measured transmission loss

Fig. 3 S-shaped sharp curve

REFERENCES

1. Kuroki, F., K. Ikeda, and T. Matsukawa, "Transmission characteristics of LSE01 mode in high permittivity NRD guide," *APMC Proceedings*, Hong Kong, 1997.

Efficient Full-Wave Modal Analysis of Waveguides with Arbitrary Geometry Defined by Straight, Circular and Elliptical Segments

S. Marini, P. Soto, S. Cogollos, and V. E. Boria
Dpto. de Comunicaciones, Universidad Politécnica de Valencia
Valencia, Spain

B. Gimeno
Dpto. de Física Aplica - I.C.M.U.V., Universidad de Valencia
Valencia, Spain

Many modern waveguide devices, such as dual-mode filters and diplexers, can be modelled considering the whole circuit as a cascade of waveguide step discontinuities. Most of such discontinuities usually involve waveguides with arbitrary cross-section defined by linear, circular and/or elliptical segments. A fast and accurate procedure for the full-wave modal characterization of such arbitrarily shaped waveguides is based on the Boundary Integral — Resonant Mode Expansion (BI-RME) technique well described in [1].

In this paper, we present a very efficient implementation of a full-wave modal analysis tool for arbitrarily shaped waveguides based on the BI-RME theory. Novel computational and geometry capabilities have been introduced with regard to the original implementation of BI-RME method [1]. For instance, our implementation can accurately consider waveguides whose cross section is composed of circular and elliptical segments, since they are not approached by straight segments. Furthermore, very strong efforts have been devoted to improve the CPU effort required by the BI-RME method, specially for complex waveguides. Results provided by our code are successfully compared in Figure 1 for the enclosed stripline and for a coaxial rectangular waveguide.

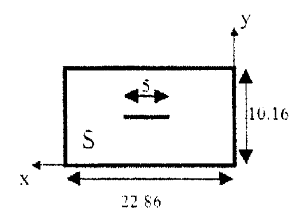

Fc (1) GHz	Fc (2) GHz	ERROR%
20.666955	20.641037	0.001
20.981585	20.961685	0.001
30.264167	30.226923	0.001
30.474869	30.429927	0.001
32.295360	32.290171	0.001
32.800748	32.760503	0.001

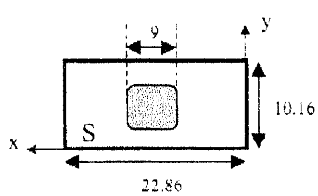

Fc (1) GHz	Fc (2) GHz	ERROR%
25.456151	25.456123	1E-04
25.458916	25.458881	1E-04
35.312001	35.311049	2E-03
35.317909	35.316954	2E-03
43.254162	43.252957	2E-03
43.262239	43.260953	2E-03

Figure 1: Cut-off frequencies of a closed stripline and of a coaxial rectangular waveguide obtained with a commercial code (1) and with our new efficient implementation (2).

REFERENCES

1. Conciauro, G., M. Bressan, and C. Zuffada, “Waveguide modes via an integral equation leading to a linear matrix eigenvalue problem,” *IEEE Trans. Microwave Theory and Tech.*, Vol. 32, 1495–1504, November 1984.

This work was supported by the European Commission under the Research and Training Networks Programme, Contract No. HPRN-CT-2000-00043.

Mode Coupling Phenomena in High Permittivity NRD Guide with Remained Small Air Gap between Dielectric and Metal Plate Interface

F. Kuroki, and M. Yamaguchi
Kure National College of Technology
Kure, Japan

T. Yoneyama
Tohoku Institute of Technology
Sendai, Japan

The NRD guide is constructed by rectangular dielectric strips inserted in a below cutoff parallel metal plate waveguide. The dominant modes can be classified into the LSM01 and LSE01 modes, the former being featured by the magnetic fields in parallel to the air-dielectric interfaces and the later being featured by the electric fields in parallel to the same interfaces. The LSM01 mode has been regarded as the operating mode, while LSE01 mode, has been dealt with as the parasitic mode. Although the NRD guide, which consists of high permittivity dielectric strips instead of usually used low permittivity ones, is expected from the view point of size miniaturization and loss reduction, such NRD guide with LSM01 mode transmission often suffers from irregular transmission. In order to clarify this phenomenon, we have analyzed the small air gap between the dielectric and metal plate interface because the high permittivity materials such as ceramics and alumina have the rough and hard surfaces. Fig.1 shows the analyzed model, where the air gap with the length of g is installed in the NRD guide with the height of a and width of b. In the first place, we will discuss the transmission characteristics of the LSM01 mode in this structure. It is considered that the TE1 slab mode is generated from the LSM01 mode by the effect of the air gap. Fig.2 (a) shows the calculated dispersion curves of two modes. From this figure, it seems that two modes having the same phase constant are liable to couple around 58GHz, and thus the irregular transmission phenomena are caused by mode coupling between the LSM01 mode and the unwanted TE1 slab mode. Next consideration is concerned with the LSE01 mode. It is predicted that the unwanted TE0 slab mode may occur in the same asymmetric structure. The calculated dispersion curves are shown in Fig.2 (b). It is considered that these modes are hard to couple due to the difference of their phased constants. As the results of the theoretical considerations, the LSE01 mode has no irregular transmission characteristics in the high permittivity NRD guide. The LSE01 mode will be therefore expected to play key role in the high permittivity NRD guide integrated circuits at the millimeter-wave frequencies.

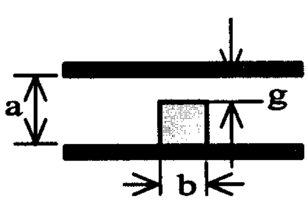

Figure 1.

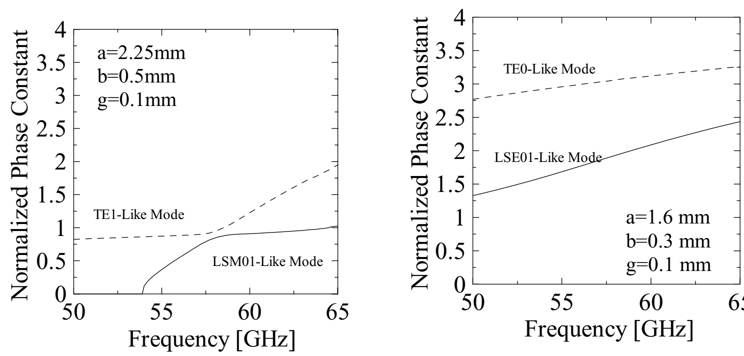

(a) LSM mode transmission (b) LSE mode transmission

Figure 2.

Description of Microstrip Propagation Modes in Terms of Modes of a Dielectric Covered Ground Plane

M. J. Lahart and C. Fazi
U.S. Army Research Laboratory
Adelphi, MD 20783, U.S.A.

I. Kohlberg
Kohlberh, Associates, Inc.
Alexandria, VA 22304, U.S.A.

Propagation modes along a microstrip are described in terms of propagation modes of a dielectric covered ground plane. The microstrip is divided into regions. One region is below the microstrip and is bounded by the microstrip, the ground plane, and two planes perpendicular to the microstrip, passing through its left and right edges. Two other regions consist of the dielectric covered ground planes and the air above them to the left and right of the microstrip.

Description of microstrip modes in terms of propagation modes of a dielectric covered ground plane permits an analysis of its modes in terms of relatively simple formulas. Modes of a dielectric covered ground plane can be described as TM and TE modes with respect to a direction of propagation along the ground plane (which may not coincide with the axis of the microstrip), and the fields of each type of mode can be described in terms of a scalar potential that obeys the wave equation. The scalar potentials in the center regions below the microstrip are computed by requiring continuity with the scalar potentials of the dielectric covered ground plane on each side of the center regions, and that conditions relevant to the conducting surfaces be obeyed. Two scalar potentials are computed. One obeys the wave equation exactly (so that the fields obey Maxwell's equations) and the other is an approximate solution to the wave equation if the function is approximately separable.

It is shown that the boundary conditions on microstrip with a homogeneous dielectric do not constrain the possible field configurations to a finite number of modes. However, if the permittivity under the microstrip is different from that under the dielectric-air boundary, the number of propagation modes can be limited on one or a finite number. In that case, it is possible to define dispersion curves that relate the propagation constant of the microstrip to the permittivity under the microstrip.

Boundary Conditions of Absorption and Excitation of the Own Decisions in a Planar Impedance Grid

C. N. Klimov
Moscow State Institute of Electronics and Mathematics
Moscow, 109028, Russia

B. V. Sestroretsky
Lavochkin Association
Moscow, 141400, Russia

The technique of construction of a boundary condition for excitation both absorption of plane and own waves rectangular waveguide, filled homogeneous dielectric is offered, which permeability can be both more, and there is less permeability of vacuum, for formation of algorithms of the electrodynamic analysis in time domain mode of structures.

The statement of a boundary condition in a method of impedance grids for absorption of own waves rectangular waveguide or plane wave in environment with homogeneous dielectric by filling means the following. If there is arbitrary waveguide structure, the statement of border of an absorber corresponds to that we limit infinite structure to absorbing border, for example, on the right, and the own decision existing to the left of border, thus does not change. Such boundary condition, corresponds to a so-called condition boundary III of a sort, which means the decision of the mixed regional task, and allows to limit infinite structure. Therefore for statement of the given boundary condition two tasks were decided: 1) The own decisions in an impedance grid previously were determined which correspond to own waves rectangular waveguide and plane wave, 2) such boundary condition was found which at restriction waveguide of structure for example on the right, at the left does not change exact own grid the decision waveguide of structure.

The received boundary condition was realized in the program. Factor of reflection from border of an absorber makes not less than 200 dB. Unfortunately it was not possible to achieve the greater absorption, as the double accuracy for representation of floating numbers was used. Such reflection is achieved and at enough large concerning length of a wave discrete of a grid (1/10), about absorption occurs in one layer of a grid.

Propagation and Interaction of Waves in Gamma- and Cross-Shaped Slotted Waveguides

Yu. V. Shestopalov and N. S. Kotik
Karlstad University
Karlstad, Sweden

We propose a semi-analytical (analytical-to-numerical) method for the analysis of interaction and calculation of waves guided by gamma- and cross-shaped slotted waveguides when several rectangular cross-sectional domains are coupled by the slots in a rather arbitrary manner.

We formulate the boundary eigenvalue problems for the Helmholtz equation that describe the wave propagation and prove the existence of eigenvalues. Then, following [1], the problems are reduced to boundary integral and infinite-matrix (summation) operator equations, where the operators are considered as multi-parameter operator-valued functions. Specifically, we obtain a system of homogeneous integral equations with a logarithmic singularity of the kernel and consider the system as a problem on characteristic numbers for the corresponding matrix Fredholm integral operator-valued function of a complex variable. Next, the slotwidths are taken as small parameters (the case of narrow slots is considered), and propagation constants are obtained in the form of segments of asymptotic series. We obtain explicit formulas expressed in powers of the characteristic small parameter (logarithm of the relative slotwidth of one of the slots). The analytical data thus obtained serve in particular as initial values for computations, which allows us to perform correct classifications of waves, and as a source for analysis of the wave interaction.

To construct summation equations, we apply the basis of Chebyshev polynomials and reduce the homogeneous systems to functional dispersion equations involving infinite determinants. To justify this procedure, we prove the existence of the determinant by verifying that the rate of decrease of the infinite-matrix elements is sufficiently high. Calculations are performed for truncated matrices of a finite order, and characteristics numbers of logarithmic integral operator-valued functions are determined numerically by calculating zeros of truncated determinants. Such a calculation technique proves to be efficient because the matrices of the summation equations turn out to be rarefied and the rate of decrease of their elements with respect to indices can be estimated, which enables one to prove the convergence of the method.

To study the interaction of waves we determine the set critical points of the determinant function (this set contains in partricular the points, at which eigenvalues of the Laplacian of the partial domains coincide) and consider the behavior of characteristics numbers in the vicinity of such points as a two-parameter family of functions. Close to these critical (degeneration) points, they exhibit a typical saddle-point structure.

This approach can be extended to slotted waveguides formed by domains of arbitrary shape if one separates a logarithmic singularity in the kernel of boundary integral equations and expands regular terms of the traces of Green's functions in a double trigonometric Fourier or Chebyshev series. The interaction can be studied under the assumption that eigenvalues of the Laplacian in partial domains are known.

REFERENCES

1. Shestopalov, Yu. V., E. V. Chernokozhin, and Yu. G. Smirnov, *Logarithmic Integral Equations in Electromagnetics*, VSP Int. Science Publishers, Utrecht, Boston, Köln, Tokyo, 2000.

Session 5Pc5

New Electrodynamics, Gravito-Electrodynamics, Gravitation, and EHD

Extended Electromagnetic Electron and Photon Models

B. Lehnert
Alfvén Laboratory, Royal Institute of Technology
Stockholm, S-100 44, Sweden

A Lorentz invariant electromagnetic theory, extended beyond Maxwell's equations, has been developed on the basis of a nonzero electric field divergence in the vacuum state. This leads to a new space charge current, in addition to the displacement current. For axisymmetric steady or time-dependent states, general solutions of the field equations are obtained from a generating function. Relevant quantum conditions are then imposed on these solutions to obtain a final and defined state.

Among the steady equilibria, an electron model results from a generating function the radial part of which diverges at the origin. Then the total electric charge, magnetic moment, mass, and angular momentum still become nonzero and finite, provided that the characteristic radius of the configuration is made to shrink to that of a point-charge-like state. This removes the problem of infinite self-energy, and presents a possible alternative to the conventional renormalization process. Further, with the subsidiary quantum conditions on magnetic moment, angular momentum, and magnetic flux, a variational analysis can be applied to find an extremum of the electronic (elementary) charge. Numerical analysis by J. Scheffel and the author then leads to a minimum charge which only deviates by 3 percent from the experimentally determined value. Possibly this small deviation can be eliminated by a quantization of the field equations already from the outset. The electronic charge would then no longer be an independent constant of nature.

Among the time-dependent states, wave-packet models have been developed for the photon, having zero net charge, no magnetic moment, a nonzero by very small rest mass, and the nonzero angular momentum of a boson. For one of these models, which is based on a divergent generating function with top-bottom anti-symmetry, the characteristic wave-packet radius can become very small. This makes possible an efficient photon-electron interaction in the photoionization effect, which cannot be understood in terms of plane waves. A proposal is finally made for the photon to appear in different quantum, states, in the form of "photon oscillations".

Mach's Principle and Weber's Electrodynamics

J. Fukai
Physics Department, Auburn University
Auburn, AL 36849, U.S.A.

A. K. T. Assis
Institut fur Geschichte der Naturwissenschaften, Universitat Hamburg
Hamburg, D 20146, Germany

Mach's principle states that there is only motion of bodies relative to other bodies, but not relative to Newton's absolute space [1]. In a mechanical world Foucault's pendulum, for example, precesses due to the earth's rotation relative to the universe (stars and galaxies). According to Mach's principle the pendulum should also precess on a stationary earth if the universe rotates the other way. In an electrodynamic world a pendulum with a charged body precesses in a uniform vertical magnetic field like Foucault's pendulum. This magnetic field can be created by a spherical shell with a uniformly distributed charge spinning around the pendulum. For a more practical analogous experiment, consider a conductor ring placed at rest inside this shell. If the rate of rotation of the shell changes in time, the magnetic flux through the ring changes accordingly. A current will be induced in the ring. Applying Mach's principle to this situation, the converse should also be true. A current should be induced in a ring spinning with varying angular velocity inside a uniformly charged sphere at rest. That is, the application of Mach's ideas to electrodynamics leads to the prediction of induction without a magnetic field! Conventional theory doesn't predict this effect, while Weber's theory can explain this phenomenon. In this work we present the account of this new phenomenon based on Weber's law. Since Weber's electrodynamics is based only on the relative motion between the interacting charges [2–4], it incorporates Mach's principle. We discuss possible experimental setups to test the existence of the new effect.

REFERENCES

1. Assis, A. K. T., *Relational Mechanics*, ISBN: 0-9683689-2-1, Apeiron, Montreal, 1999.
2. Assis, A. K. T., *Weber's Electrodynamics*, ISBN: 0-7923-3137-0, Kluwer, Dordrecht, 1994.
3. Bueno, M. d. A. and A. K. T. Assis, *Inductance and Force Calculations in Electrical Circuits*, ISBN: 1-56072-917-1, Nova Science Publishers, Huntington, New York, 2001.
4. Assis, A. K. T., J. Fukai, and H. B. Carvalho, "Weberian induction," *Physics Letters A*, Vol. 268, 274, 2000.

EHD/EMHD with Space Charge and Displacement Currents: Extension of HD and MHD

H. Kikuchi
Institute for Environmental Electromagnetics
Tokyo, 170, Japan

Electrohydrodynamics (EHD) or electromagnetohydrodynamics (EMHD) has been developed on the basis of conservations of matter and momentum together with Maxwell's equations in moving media and the equations of state, mechanical and electromagnetic, for uncharged and charged fluids, taking into account space charge and displacement currents. Accordingly EHD or EMHD is considered as an extension of HD (hydrodynamics) and MHD (magnetohydrodynamics), since HD and MHD do not have electromagnetic forces and space charge and displace- ment currents, respectively [1].

A new equation of electric field transport is introduced in addition to fluid vortex and magnetic field transport extended to include new effects of space charge and displacement currents. In addition to the fluid and magnetic Reynolds numbers familiar to HD or MHD, the electric Reynolds number with both spatial and temporal factors due to the emergence of the displacement current is newly defined, while the fluid and the magnetic Reynolds number has a spatial factor only.

One-component fluid is a continuum consisting of a single species of neutral (uncharged) or charged particles; electromagnetic forces can act on even an uncharged fluid in a non-uniform electric field. A charged fluid may be a dust fluid, positively or negatively charged, ion fluid, or electron fluid. Equations of energy transport and heat transfer are also obtained for EHD or EMHD regime.

For high electric Reynolds numbers, a new electric transport equation becomes the Kelvin-Helmholtz equation supplemented by an additional term of the space-charge current that is incorporated into the electric convection with the displacement current, implying that the frozen-in field concept still holds for the electric displacement in a dielectric fluid just like the magnetic field in a conducting fluid. For a dielectric fluid, the space-charge current term emerges in addition to the displace current but it is included in the electric convection current, leading to the identical equation for **B** and **D**. This indicates that the Kelvin-Helmholtz theorem and the frozen-in field concept still hold in a dielectric fluid.

REFERENCES

1. H. Kikuchi, *Electrohydrodynamics in Dusty and Dirty Plasmas*, Kluwer Academic Publishers, Dordrecht/The Netherlands, 2001.

Similarities and Differences between Magnetic and Electric Undulators

H. Kikuchi
Institute for Environmental Electromagnetics
Tokyo, 170, Japan

The magnetic undulator constitutes periodical magnetic cusps formed by a sequence of alternating magnetic polarities [1, 2], while a new *electric undulator* is considered an electric version of undulators, consisting of a sequence of electric quadrupoles, thereby constituting periodical electric cusps [3, 4]. Both undulators are designed to be devices for accelerating or trapping charged particles and for generating electromagnetic radiation for instance by using jointly together with a linear accelerator, ranging from radio or millimeter waves to X-rays, though the electric undulator is capable for accelerating or trapping uncharged particles as well. Their functioning or the general behavior of a particle or beam in them is very much similar to each other, although the force resulting in particles undulating motion in the electric undulator is the electric force $q\mathbf{E}$ (q: charge; $\mathbf{E}$: electric field) in contrast to the $q\mathbf{v} \times \mathbf{B}$ force in the magnetic undulator. If either electric or magnetic device is placed into an optical resonator with mirrors at both ends, coherent radiation could be produced. Then, it may be called a *free-electron laser*, although its manner of functioning is different from that of atomic or molecular lasing media. Thus, both electric and magnetic undulators are very much similar in terms of their functioning as far as a charged particle or beam is concerned. One of essential differences, however, would be their functionings for a neutral, uncharged particle or beam, although the case for the magnetic undulator has not been treated and therefore it is not clear for an uncharged particle or beam. Another remarkable difference is that the electric undulator is capable for both trapping and mirroring in contrast to trapping only in the magnetic undulator unless it is used together with a magnetic mirror.

REFERENCES

1. H. Motz, Applications of the Radiation from Fast Electron Beams, *J. App. Phys.*, 22, 527-535, 1951.
2. P. Luchini and H. Motz, *Undulators and Free-Electron Lasers*, Clarendon Press, Oxford, 1990.
3. H. Kikuchi, The Concept and Basic Properties of an Electric Undulator, in *Proc. PIERS*, 2000.
4. H. Kikuchi, *Electrohydrodynamics in Dusty and Dirty Plasmas*, Kluwer Academic Publishers, Dordrecht/The Netherlands, 2001.

Sensor of the Gravitational Turbulence and Their Application to Measures Against Large Earthquake Disasters

J. Chiba
Tohoku Institute of Technology
Sendai, 982-8577, Japan

T. Obata
Gunma National College of Technology
Maebashi, 371-0845, Japan

Y. Nemoto
Graduate School of Information Sciences, Tohoku University
Sendai, 980-8579, Japan

This paper outlines the basic analysis of seismic gravity.

We studied the turbulence of Newtonian gravitational field due to large seismic waves and the detection of the turbulent field by an interferometric gravitational field detector. The cause of the turbulent field is the variation of the mass density in the ground by the waves.

According to Einstein's general theory of relativity, gravitational field turbulence is propagated by a light velocity of 3×10^8 m/s, but on the other hand, the seismic wave itself is propagated by an elastic wave velocity of 7×10^3 m/s.

Accordingly gravitational field turbulence due to seismic waves reach instantly, whereas seismic waves arrive much later. Therefore early detection of a large seismic wave can be achieved by observing the gravitational field turbulence.

When the seismograph and the gravitational field detector are set at the same place, the seismograph does not respond until the arrival of the Primary wave, but gravitational field detector will respond to the gravitational field before the Primary wave arrival.

Assuming a great earthquake with an epicenter distance to a city is long, for instance, ~ 100km, the seismic waves then take at least 14 sec to arrive at the city. If people in the city foreknow by observing the gravitational field turbulence generated by the seismic waves, they would be warned of the arrival before the seismic waves approach.

In case of cut-off frequency of the high pass filter $f_c = 1/2$ Hz, the noise strain after the filter turns out to be $\epsilon_N \sim 9 \times 10^{-18}$ for the atmosphere noise and $\sim 1.7 \times 10^{-18}$ for the seismic noise.

On the Noise Filter for Gravitational Field Detectors

J. Chiba
Tohoku Institute of Technology
Sendai, 982-8577, Japan

T. Obata
Gunma National College of Technology
Maebashi, 371-0845, Japan

Y. Nemoto
Graduate School of Information Sciences, Tohoku University
Sendai, 980-8579, Japan

This paper outlines the optimum cutoff frequency of the noise diminishing filter for gravitational field detectors.

As stated before [1], observing the turbulence of the gravitational field due to the approach of seismic waves enables one to detect the attack of the P wave in its early stage.

Signal value due to seismic waves will exceed the theoretical photon noise limit of the sensor. Saulson, however, showed that the random gravitational forces generated by the seismic noise and by the atmosphere noise produce the dominant noise of the sensor if $f \leq 10\,\mathrm{Hz}$. The frequency spectrum of the noise generated by the random gravitational forces are well known.

A wave packet of any desired shape can be constructed upon the theory of the Fourier integral by choosing the amplitude of the component harmonic waves as an appropriate function of the frequency or wave number and integration.

The harmonic components suffer relative displacements in the phase in the direction of propagation and the wave packet arrives at a distant point in a modified form, in other words, the frequency spectrum of the seismic wave depends on the propagation distance of the seismic wave. We have discovered that the cutoff frequency for maximum signal to the noise ratio (S/N) depends on the normalized distance T.

Accordingly, an optimum filter becomes necessary. During the observations, optimum filter plays an important role. Value for optimum cutoff frequency may be read from Figures in presentation.

REFERENCES

1. J. Chiba, T. Obata, and Y. Nemoto, "*Sensor of the Gravitational Turbulence and Their Application to Measures Against Large Earthquake Disasters*," *Proceedings*, PIERS 2002 same session.

On the Gravito-Electrodynamic Plasma Modes Around a Rotating Black Hole

U. A. Mofiz
School of Science and Technology, Bangladesh Open University
Gazipur, 1705, Bangladesh

Recently, the study of plasmas around black holes and other gravito-rotating compact objects has become of much interest. It may yield the spectroscopic signatures of radiation emitted from plasma of rotating black hole. Mac Donald and Thorne have introduced Maxwell's equations in 3+1 coordinates which provides a foundation for the formulation of General Relativistic (GR) set of plasma physics equation. It provides a mean by which the electrodynamics equations and the plasma physics equations look more familiar to the usual formulations in flat space-time while taking account of general relativistic effects such as time curvature. It is possible to obtain the various wave modes at a range of fixed values of the lapse function. Secondly, gravitational and rotational effects on the equilibrium plasma are very much important to understand the various plasma modes around the rotational gravitating objects.

In this paper, firstly, we consider the electrostatic plasma modes along the open field line of a rotating neutron star. Goldreich-Julian charge density in general relativity is analysed for the neutron star with zero inclination. It is found that the charge density is maximum at the polar cap and remains almost the same in a certain extended region of the pole. For a steady state Goldreich-Julian charge density, we found the usual plasma oscillation along the field lines, plasma frequency resembles the gravitational redshift close to the Schwarzchild radius. The nonlinear plasma mode along the field lines is also studied. A nonlinear differential equation is obtained, which describes the growing plasma plasma modes near the Schwarzchild radius. For initially zero potential and field on the surface of a neutron star, Goldreich-Julian charge density is found to create the plasma mode, which is enhanced and propagates almost without damping along the open field lines.

Secondly, we studied plasma modes around a rotating black hole environment. The Kerr metric is considered in this case. For the simplicity, Langmuir oscillations in Kerr plasma is investigated. A wave equation is derived which describes the various plasma modes in Kerr plasma. GR effects on equilibrium quantities are found to be significant near the event horizon. The lapse function entering in the definition of plasma frequency describes the gravito-rotational effects on plasma oscillations. Langmuir oscillations go to zero near the event horizon, while it increases sharply near but away from the horizon, and it reaches a maximum value at a certain distance from it. Formation of nonlinear structures such as solitons and chaos in Kerr plasma in the concept of Gravito-Electrodynamics and Electro-Hydrodynamics is discussed.

Session 5Pc6

Microwave Devices

Low-Frequency Loss in Planar Ferrite Devices Having an Orthogonal Bias Field

E. Schloemann
Consultant
Weston, MA 02493, U.S.A.

Planar ferrite devices having an orthogonal bias field are widely used in microwave technology, primarily in the form of circulators and edge-mode isolators. One of their attractive features is that they have good performance over a broad bandwidth, as characterized by the lowest and highest frequency of the performance band ($f_{\min}$ and $f_{\max}$). If "good performance" is defined as "having an insertion loss less than 1 dB," the best currently available devices have a $f_{\max}/f_{\min}$ ratio of approx. 3:1. (For experimental devices the $f_{\max}/f_{\min}$ ratio has been reported [1] to be larger than 10, but in this case the insertion loss was about 3 dB.)

Hines [2] has pointed out that, according to a simple (and not necessarily accurate theory based on assuming magnetic wall boundary conditions) the $f_{\max}/f_{\min}$ ratio should be much larger than 3 for the edge-mode isolator. The theory Hines developed for this device agrees in many respects with his experiment data, but cannot explain the low-frequency loss behavior. The observed frequency dependence of the loss is similar to that characteristic of ferrite materials that are not magnetized to saturation: the loss is small at relatively high frequencies, and much larger below a certain "onset frequency", given by $f_H + f_M$ $(f_M = \gamma\mu_0 M_s,\ f_H = \gamma\mu_0 H\ \ \gamma =$ gyro-magnetic ratio, $\mu_0 = \mathrm{permeability\ of\ vacuum},\ M_s = \mathrm{saturation\ magnetization},\ H = \mathrm{internal\ magnetic\ field})$. Because of the similarity of the frequency dependence, one may be tempted to interpret the observed low-frequency loss as being the same as the low-field loss observed in incompletely magnetized ferrites, but this is not a defensible argument.

The present paper discusses two processes that are believed to contribute to the observed low-frequency loss:

1. Excitation of "slow" (quasi-static) electromagnetic waves at the ferrite/dielectric interfaces that occur at the input and output of an edge-mode isolator [3]. These waves propagate orthogonal to the primary wave. The process can account for an onset frequency given approximately by f_M, if the bias-field inhomogeneity that is likely to occur near the substrate edge is taken into account.

2. Excitation of secondary (or "parasitic") waves that propagate parallel to the strip edge. An extension of Bolle's analysis [4] of ferrite-loaded stripline is presented, which makes it very likely that such parasitic edge-guided waves occur at frequencies below f_M in typical edge-mode isolators.

REFERENCES

1. Konishi, Y. and N. Noshino, "Design of a new Broadband Isolator," *IEEE Trans. MTT*, Vol. 19, 260–269, 1971.
2. Hines, M. E., "Reciprocal and Nonreciprocal Modes of Propagation in Ferrite Stripline and Microstrip Devices," *IEEE Trans. MTT-19*, 442–451, 1971.
3. Schloemann, E., "Low-Frequency Radiation Loss. A Major Reason for bandwidth Limitations of Ferrite Microwave Devices," Paper 20BaI5 at *8th Int. Conf. on Ferrites*, Kyoto, Japan, Sept. 2000
4. Bolle, D. M., "The Modal Spectrum of Ferrite-loaded Striplines," *IEEE MTT-S, IMS Digest*, 519–522, 1977.

Nonlinear Microwave Signal Processor Based on Parametric Interactions of Dipolar Spin Waves with Localized Electromagnetic Pumping

A. N. Slavin
Department of Physics, Oakland University, Rochester
Rochester, MI 48309, U.S.A.

G. A. Melkov, Yu. Kobljanskyj, A. A. Serga and V. S. Tiberkevich
Radiophysics Faculty, Taras Shevchenko Kiev University
Kiev, Ukraine

A nonlinear microwave signal processor based on the parametric interaction of a microwave dipolar spin wave pulse, propagating in an yttrium-iron garnet (YIG) film waveguide, with a non-stationary (pulsed) electromagnetic pumping is proposed and practically realized. The proposed processor amplifies input pulsed microwave signals by up to 30 dB, performs operations of phase conjugation, time profile inversion, convolution of two pulsed signals, and controlled time delay of up to 1 μs.

Dipolar spin waves or magnetostatic waves (MSW), propagating in magnetized to saturation yttrium-iron garnet (YIG) films, can be used for processing of microwave electromagnetic signals in a way similar to that of surface acoustic waves (SAW), propagating in LiNb or other acoustic crystals. The important advantage of microwave signal processors based on MSW is a much higher working frequencies which can easily reach 10 GHz, while the working frequencies of SAW devices rarely exceed 2 GHz. The proposed nonlinear MSW signal processor is based on a conventional MSW delay-line structure, consisting of an YIG film waveguide tangentially magnetized by the external bias field H_0, input transducer situated at one end of the film waveguide, and the output transducer situated at the other end. The input transducer converts the input electromagnetic signal into a relatively slow magnetostatic wave (typical group velocity $v \sim 10^6$ cm/sec), which propagates in the film towards the output transducer, where it is again converted into the electromagnetic wave. The delay time in such a structure depends on the thickness of the YIG film, distance between the transducers, and the magnitude of the bias magnetic field H_0, and varies from several tens to several hundreds of nanoseconds.

Magnetostatic waves propagating in YIG films are dispersive and, for sufficiently large powers of the input signal ($P_{in} \sim$ several mW), are also nonlinear. Nonlinear and dispersive properties of MSW in YIG films allow us to perform several useful operations on the microwave signal during its presence in the film in the form of an MSW pulse, such as: pulse compression and formation of envelope solitons, amplification, wave front reversal and phase conjugation, convolution, etc. Detailed theoretical analysis of these effects is given in our papers.

In our current paper we describe the action of a MSW signal processor in the case when an additional pumping electromagnetic pulsed field (having frequency ω_p, which is approximately two times larger than the carrier frequency of the input microwave signal $\omega_p \approx 2\omega_s$) was supplied to the YIG film. The magnetic field $\mathbf{h}_p$ of the pumping pulse was directed mostly parallel to the bias magnetic field $\mathbf{H}_0$, so that the situation of parametric *parallell pumping* was realized in the film. Under these circumstances, the three-wave first-order parametric interaction process between the propagating MSW signal and the localized pumping magnetic field was happening in the film. As a result of this process, the signal MSW, propagating towards the output tranducer, was parametrically amplified, and a reversed and phase conjugated ("idle") MSW, having frequency $\omega_i = \omega_p - \omega_s$ and propagating from the region of pumping localization towards the input tranducer, was parametrically excited .

Microwave Spin Wave Envelope Solitons in Ferromagnetic Films

B. A. Kalinikos
Department of Electron-Ion Processing of Solids St.Petersburg Electrotechnical University
St. Petersburg, 197376, Russia

The term "envelope soliton" or simply "soliton" is used to describe nonlinear wave pulses which could preserve their shape during propagation in dispersive media and emerge unchanged after collision. In spite of great theoretical activity in the soliton area taking place in the last three decades or so, envelope solitons have been experimentally studied mainly in two systems – in optical fibers and ferromagnetic films. Ferromagnetic films present a very promising medium for spin wave soliton investigations and applications at microwaves. Recent advances in spin wave soliton area include self-generation of both bright and dark spin wave envelope soliton trains in the absence of any external radio-frequency or mirowave-frequency signal.

This paper reviews investigations of spin wave solitonic processes in ferromagnetic films with an emphasis on soliton physics, experimental work, and possible applications. Results of the experimental measurements for monocrystalline yttrium iron garnet (YIG) films and so-called "active rings" based on YIG films demonstrating both bright and dark spin wave soliton formation and self-generation effects are presented. To generate bright envelope solitons backward volume spin waves with positive dispersion coefficient and negative nonlinear response coefficient were used. To generate dark envelope solitons surface spin waves with negative dispersion coefficient and negative nonlinear coefficient were used. The soliton character of the experimentally observed waveforms was confirmed by measuring the corresponding power frequency spectra and phase-time profiles.

Theoretical explanations of the observed effects are given in the frames of the nonlinear Schödinger equation model taking into account peculiarities of wave processes in thin ferromagnetic films.

Potential applications of soliton-like processes in ferrite-film devices for signal processing at microwave frequencies are considered. For example, microwave comb-frequency oscillator and short-pulse generator are suggested.

In conclusion, we believe that the demonstrated techniques are quite general and could be extended to generate soliton pulse sequences of various widths, frequencies, and peak powers by utilising different nonlinear dispersive systems.

Inhomogeneous Internal Field in Planar Ferrites

M. Pardavi-Horvath
George Washington University
Washington, DC, U.S.A.

The lateral size of planar ferrite elements in current microwave and mm wave devices is on the order of the mm. For optimal operation the thickness of these ferrites is considerable, as compared to their lateral size, i.e. the ferrite has a finite aspect ratio, $a = h/L$ (thickness/length for a rectangular shape, or thickness/diameter for a cylinder). Approximations in the numerical analysis of these devices, used for ellipsoids of rotation or thin films, can't be used anymore. Moreover, due to the decreasing size, the surface to volume ratio increases and the effects of corners and edges become significant.

Ferrites usually operate in an external dc bias field $H_0 = 4\pi M_s$, whereas the internal field for a thin film, magnetized perpendicular to its plane $H_i = H_0 - N_{zz}M_s = 0$, ($N_{zz} = 4\pi$ is the demagnetizing tensor component for a thin film). For finite size 3D ferrites the approximation of uniform magnetization is not valid, because due to the shape N_{zz} depend on the position, and the direction of the magnetization and of the internal field H_i will deviate from the direction of the applied field, H_0.

In the present work the non-collinear magnetization ground state $M_s(\mathbf{r})$ was calculated for the case of 3D planar ferrites. The Landau-Lifshitz equation was solved iteratively by the Finite Difference Method to obtain the equilibrium magnetization distribution, assuming that the dc bias field is applied perpendicular or parallel to the plane of the ferrite. Calculations are performed for the case of YIG ($\mathrm{Y_3Fe_5O_{12}}$), as a model material. The code can be applied to arbitrary shaped ferrites, arbitrary field, and magnetization direction. The shape effect was studied for rectangular shapes, having aspect ratios $a = 4/40 = 0.1$, $8/40 = 4/20 = 0.2$, and $8/20 = 0.4$.

For a $40 \times 20 \times 8$ shape YIG in $H_0 = 4\pi M_s = 1730$ G the in-plane internal static field components around the corners are on the order of 700 G, corresponding to a canting of the internal field and the magnetic moments at the corners of about $\theta = 24°$. For a thinner plate $(40 \times 40 \times 4)$ the canting of the magnetization from the z direction is $\theta = 9.5°$. The extent of the non-uniform region of the internal field around the edges and corners persists up to $H_0 \cong 10\pi M_s$.

The inhomogeneity of the internal field and the magnetization leads to extra linewidth broadening, and the early onset of instabilities at increased power. The inhomogeneity of the internal field in the finite size magnetic element is the source of the rich MSW spectra. The excitation of a large number of magnetostatic modes over a broad frequency range makes the effective linewidth, experienced by the device, equal to the full spectral width of these modes. Unfortunately, the shape and size effects, the pronounced MSW spectra, the linewidth broadening, and the power sensitivity, all affect the operation of mm wave planar ferrite devices. The consequence of these effects is the occurrence of additional losses and incomplete non-reciprocity.

Precise FMR Spectrum Calculation of a YIG Disk Taking Inhomogeneous Demagnetization into Account

A. Sanada and I. Awai
Department of Electrical and Engineering, Yamaguchi University
Yamaguchi, 755-8611, Japan

Precise FMR spectrum calculation of perpendicularly magnetized YIG disk (the diameter is 2.0 mm, the disk thickness is $t_{YIG} = 100\mu m$) backed by a GGG substrate (the thickness is $t_{GGG} = 400\mu m$) is carried out by the full-wave FDTD method taking an inhomogeneous demagnetizing field into account.

Assuming a ferrite model in which the direction of the magnetization vector at any point coincides with the direction of the internal magnetic field, the internal demagnetizing field, as well as the distribution of the magnetization vector, was calculated by the finite-difference method based on the magnetic scalar potential before FDTD computation. Figure 1 shows the distribution of the magnetization vector in the ferrite disk with a uniform applied field perpendicular to the YIG surface H_0.

With the inhomogeneous demagnetizing field as an initial value, the motion of the magnetization based on Gilbert's equation was computed by the FDTD method. The spectrum of the resonator was obtained by Fourier-transforming the recorded data. Figure 2 shows the spectrum of the YIG resonator obtained. An experimental result of the absorption of the sample observed by a fifty-ohm microstrip transmission line is also shown in the figure. Although the magnitudes of the resonant peaks differ between the FDTD and the experimental results since the excitation and observation methods are different, it is noted that the FMR spectrum shows a rich spectrum with good agreement with the experimental result for first several modes. It is confirmed that precise calculation of the FMR spectrum of the resonator is achieved. As for the higher order resonance of less importance, on the other hand, the FDTD result has a limitation inaccuracy due to the mesh size problem. One has to choose the cell size by considering how many modes are expected to the calculated.

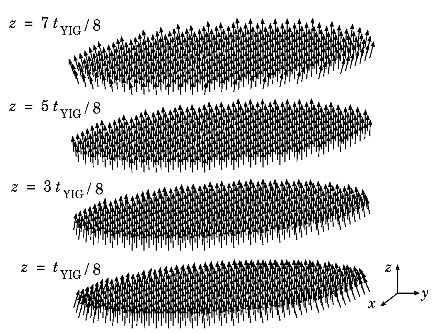

Figure 1: Distribution of the magnetization vector in the ferrite disk ($\mu_0 H_0 = 0.310T, \mu_0 M_s = 0.178T$)

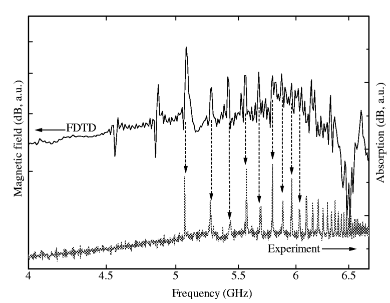

Figure 2: FMR spectrum of the YIG disk ($\mu_0 H_0 = 0.310\,T$, $\mu_0 M_s = 0.178\,T$)

Microwave and NMR Properties of Yttrium Iron Garnet Films Grown from BaO/B_2O_3 Flux

M. Maryško, K. Nitsch, and P. Novák
Institute of Physics, Academy of Sciences of the Czech Republic
Prague, 6, Czech Republic

D. Ménard, A. V. Nazarov, Y.-Y. Song, and C. E. Patton
Department of Physics, Colorado State University
Fort Collins, CO 80523, U.S.A.

M. Kuera and H. Štpánková
Faculty of Mathematics and Physics, Charles University
Prague, 18000, Czech Republic

Microwave FMR linewidth of a single crystal yttrium iron garnet (YIG) film at room temperature is given by the intrinsic Kasuya-LeCraw process (ΔH_{KL}), a part due to inhomogeneities (ΔH_{deg}), and the impurity contribution due to the valence- exchange Fe^{2+}-Fe^{3+} mechanism (ΔH_{imo}). These films are generally prepared by liquid epitaxy (LPE) from a Pb based flux on the $\{111\}$ oriented GGG substrates. They contain (Pb^{2+}, Pb^{4+}) and Pt^{4+} impurities so that it is ditficult to prevent the tormation of Fe^{2+} ions. The films with composition $Y_{3-x}Ca_xFe_5O_{12}$ used in our experiments were prepared from a lead free flux BaO/B_2O_3 on the $\{110\}$ GGG substrates. These samples contain no Pb and Pt impurities and for $x = 0$, the Fe^{2+} content c_{Fe2} is determined only by the Si^{4+} and oxygen vacancy concentrations. Doping by the divalent calcium results in the charge compensation of these impurities, which leads to a decrease of c_{Fe2}.

A new method of the study of the YIG films has been tested performing, in parallel, microwave and NMR experiments on the films with the aim to minimize the impurity linewidth contribution. The microwave parallel pumphlg measurements at room temperature yields the dependence $\Delta H_k(k)$ and the value $\Delta H_{k\to 0}$ corresponding to the magnon trequency 4.5 GHz. The extrapolated linewidth $\Delta H_{k\to 0}$ is not sensitive to inhomogeneities in the film and its value is approximately given by the sum $\Delta H_{KL} + \Delta H_{imp}$ with the second term proportional to c_{Fe2}. The NMR measurements were made at $T = 4.2\,\mathrm{K}$ on the nuclei ^{57}Fe using a spin echo technique. The main octahedral and tetrahedral lines with trequencies 76 and 65 MHz respectively as well as the corresponding spin-lattice and spin-spin relaxation times were measured. The relaxation brings an additional information on c_{Fe2}. From the intensity of the satellite lines the concentrations of Ca (denoted by x_{NMR}), Si and antisite defects were determined [1]. Comparison of the Ca concentration x determined by an electron microprobe analysis and x_{NMR} shows that $x \gg x_{NMR}$, which is indicative of an inhomogeneous distribution of Ca in the film. This represents an important tactor tor determining the Ca level, which is necessary in order to achieve the tull charge compensation.

REFERENCES

1. Englich, J., P. Novák, and H. Lütgemeier, *International Journal of Modern Physics B*, Vol. 12, 609, 1998.

X-Band High Peak Power Ferrite Devices

A. Ioachim
National Institute of Physics and Materials Technology
Bucharest - Magurele, sector 5, Romania

B. Banciu and R. Ramer
School of Electrical Engineering and Telecommunications
Sydeny, UNSW 2052, Australia

Non reciprocal high peak power microwave devices are the subject of nonlinear phenomena in ferrimagnetic materials caused by spin-wave generation. The development of materials with suitable high peak power threshold such as polycrystalline substituted yttrium iron garnets, YIG, allowed the design and the manufacturing of nonreciporcal microwave devices such as phase shifters, differential phase shift circulators and junction circulators.

Fast relaxers, fine grain structure together with controlled porosity have been considered for these materials to enhance the critical field h_c, in order to be used in high peak-power components for X-band. A series of polycrystalline samples of cobalt substituted yttrium iron garnets, with the composition Y_3 $Fe_{4.85}$ $Co_{0.075}$ $Si_{0.075}$ O_{12} were prepared using classical powder technology. An increased porosity was employed in order to enhance the critical field level; it also substantially reduced the garnet pencil crackings due to thermal shock occuring under high power conditions.

The well structured R_1-type high porous garnet (Pt=56%) was successfully used in the phase shift section of a high peak-power differential phase shift circulator handling 200 kW peak power in X-band. The material exhibited adequate values for the spin wave resonance ΔH_k, the resonance linewidth ΔH, and the resonance effective linewidth ΔH_{eff}. The nominal peak - power tests for phase shift section showed a good linearity of output power versus the input power.

The parameters of differential phase shift circulator are: insertion loss $<$ 0.5dB, isolation $>$ 22dB, and return loss $>$ 20dB, in the frequency range 9.1-9.6 GHz. The standard signal characteristics are presented in Fig. 1 and the peak-power test is presented in Fig. 2.

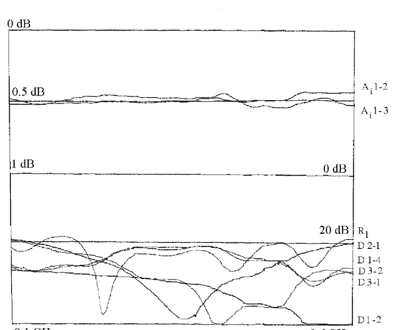

Figure 1: Standard signal characteristics of differential phase shift circulator.

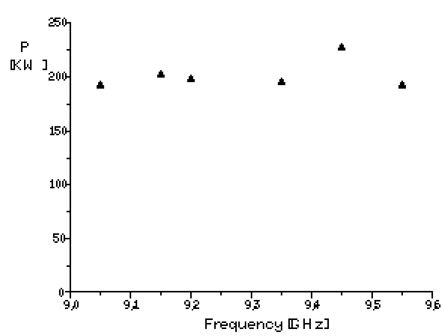

Figure 2: Nominal peak power test of differential phase shift circulator in 9.1-9.6 GHz range.

A Y type junction circulator in H plane was designed and manufactured using the porous YIG:Co garnet. The design uses full height configuration of ferromagnetic material. Insertion loss of the circulator was $<$ 0.4dB, isolation $>$ 20dB, and return loss $>$ 20 dB, in the interval 9.2 – 9.6 GHz. The circulator was tested at nominal peak power of 90 kW.

High T_c Superconductors for Microwave Devices

C. M. Srivastava
Department of Physics, Indian Institute of Technology
Powai, Mumbai-400076, India

With the discovery of superconducting cuprates development of low-loss microwave components such as resonators, delay lines and filters, and devices like microwave detectors and mixers, working at liquid nitrogen temperatures, and with far superior performance compared to those using metals, has been achieved. However the experience of more than a decade and a half shows that there are some problems that need to be solved before the rapid deployment of high T_c superconducting (HTSC) microwave devices can take place. The fabrication of these devices requires development of good quality epitaxial thin films with high critical current (J_c), low surface resistance (R_s), long term stability, as well as, methods of patterning without affecting the superconducting properties. To achieve these a proper understanding of the nature of the charge carriers and the attractive interaction that causes the formation of the cooper pairs for $T< T_c$ is required. Even in the normal state the transport and other physical properties of cuprates show an anomalous behaviour, consequently the carriers are considered to constitute, instead of Fermi liquid, a marginal Fermi liquid. We have accounted this on the basis that charge carriers in oxide superconductor are polarons and carry the local lattice deformation with them when electrical conduction occurs [1]. This explains the anomalous temperature and frequency dependence of R_s in HTSC that does not follow the conventional theory of Mattis and Bardeen for $T< T_c$ [2]. An explanation of the residual losses and the analysis of the propagation of the electromagnetic fields in a stripline using superconductors on the basis of polaronic conduction will be presented. Finally the universal correlation between the critical temperature, T_c and the ratio of the charge density to effective mass, n_s/m^*, observed in muon-spin-relaxation rate experiment on oxide superconductors is explained on the basis of the **E.p** mediated pairing in superconductivity developed be us [3]. The possibility of reduced conductor losses and enhancement of quality factor of the device in a cost effective manner will be examined on the polaron model of the charge carrier.

REFERENCES

1. C.M. Srivastava, Pramana-Journal of Physics, 50, 11, 1998.
2. C.C. Mattis and J. Bardeen, Phys. Rev., 111, 412,1958.
3. C.M. Srivastava,Ferrites, Proc. Int. Conf. on Ferrites (ICF8), Kyoto and Tokyo (Japan Society of Powder and Powder Metallurgy, 2000), p 226.

Doubling Wireless Channel Capacity using Co-polarized, Co-located Electric and Magnetic Dipoles

D. D. Stancil, A. Berson, J. P. Van't Hof, R. Negi, S. Sheth, and P. Patel
Center for Wireless and Broadband Networking
Department of ECE, Carnegie Mellon University
Pittsburgh, PA 15213, U.S.A.

It is well known that the two polarization states of electromagnetic waves can be used to transmit separate channels of information. This property has been used in microwave transmission systems and as a diversity technique for wireless fading channels. It has also been shown that multipath propagation can be exploited with spatial diversity techniques to increase capacity. Polarization diversity in a multipath environment has recently been re-examined by Andrews, Mitra, and deCarvalho [Nature, vo. 409, 18 Jan. 2001, p. 316] with the surprising conclusion that there can be as many as six separate polarization channels instead of two. This results from treating all three components of the electric field and all three components of the magnetic field as capable of transmitting independent fluctuations. To illustrate this point, a pair of tri-polarized electric dipole antennas was constructed and used to verify that three independent channels could be transmitted in a multipath environment. This demonstration left one key assertion unverified: the ability to convey independent fluctuations on the electric and magnetic fields. More specifically, to use all six degrees of freedom would require two coincident tri-polarized antennas: one composed of electric dipoles and one composed of magnetic dipoles. In such an antenna, there would be three pairs of electric and magnetic dipoles in which both antennas in each pair radiate electromagnetic waves with the same polarization. The second key concept to be verified, therefore, is whether it is possible to realize two independent channels using co-located, co-polarized electric and magnetic dipoles. If this is possible, a six-degree of freedom antenna could then be constructed of three such pairs.

In this paper, experiments are described demonstrating the ability to transmit independent information channels using co-located, co-polarized electric and magnetic dipoles in the presence of multipath propagation. The dual antennas consist of conventional electric dipoles combined with modified Kandoian loops. The complex 2×2 transfer matrix between a pair of dual antennas was measured for multiple frequencies and locations in an indoor environment with no direct line-of-sight. The measurements were made using a vector network analyzer in the 902–928 MHz unlicensed band. Statistical analysis of the measurements shows the transfer matrix to be full rank, indicating two independent transmission channels. Independence was confirmed by transmitting distinct messages simultaneously using the two antenna pairs.

RF Signal Processor for 3G+ Mobile Communication System with Large Number of Receiving and Transmitting Antennas

P. Rapajic and R. Ramer
School of Electrical Engineering & Telecommunications, UNSW
Sydney, NSW 2052, Australia

The adaptive antenna arrays concept (multisensor receivers) has been considered by many authors as a feasible way of increasing the information capacity of cellular mobile communication systems. If the N-element antenna array is used, it is shown that it is possible to accommodate $N-1$ times more users in the cellular uplink system in comparison to the omnidirectional base-station antenna system. The separation is based on different multipath-multiangle signal propagation for different users caused by different mobile terminal spatial positions. In the information capacity calculation of a space division multiple access mobile communication system is given. However, the capacity estimates are practically achievable under the condition that a sophisticated RF processor with an antenna array at the receiver side is realizable. In this paper we analyse and discuss requirements for realization of the integrated RF processor, which will provide manyfold information capacity increase of the 3G+ mobile communication network. The paper is organized as follows. In section 1, the mathematical model of multiple receiving and transmitting antenna system is considered and the information capacity of multiple receiving antenna system is presented. In section 2, realization of the integrated RF processor of the multiple receiving and transmitting antenna system is discussed. In section 3, a graphical illustration of the analytical results from previous sections is given, while conclusions are drawn in section 4.

There are two distinctive models of systems with multiple receiving antennas: 1) The single cell model with multiple antennas, and 2) The cellular system model with multiple antennas. We focus our attention to the single cell model with the space division multiple access system with a number of closely located antennas. The antennas are considered to be closely located if they are placed in a mutual distance ranging from a fraction of the carrier wavelength, or a small integer number p of the carrier wavelengths ($p = 1, 2...$). The model consists of a number of mobile stations $M_1, M_2, \ldots, M_K$ and a single base station BS with a number Ns of high directivity independent antennas $Q_1, Q_2, \ldots, Q_{Ns}$, The system, could be represented by the following matrix equation $\mathbf{y} = \mathbf{S}\mathbf{x} + \mathbf{n}$, where $\mathbf{y} = [y_1, y_2, \ldots, y_N]^T$ is the vector of the signal received by N antennas. The symbols sent by K users are denoted as $\mathbf{x} = [x_1, x_2, \ldots, x_K]^T$ and $\mathbf{n} = [n_1, n_2, \ldots, n_N]^T$ is a zero mean additive white Gaussian noise (AWGN) vector with the covariance matrix $E\{\mathbf{n}\mathbf{n}^H\} = \mathbf{I}\sigma^2$. The signature matrix is $\mathbf{S} = \{s_{k,n}\}$, where $s_{k,n}, k = 1, \ldots, K; n = 1, \ldots, N$ is the complex signal amplitude of the kth source received by the nth antenna. The normalized number of users in a multiple receiving antenna system is defined as $\rho = K/N$. Depending on how the number of users K, measures with respect to the system dimensionality N, two possible cases are of interest: 1) The **unsaturated system**, where $K < N$, $(0 < \rho < 1)$ and the **oversaturated system**, where $K > N$, $(1 \leq \rho < \infty)$.

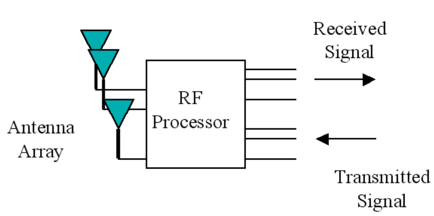

Figure 1: RF Processor for Multiple Receiving and Transmitting Antenna System Model

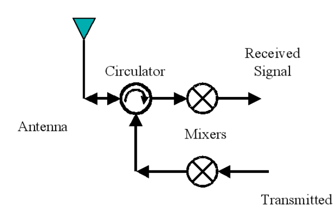

Figure 2: Single Processing Element of the RF Signal Processor

Session 5Pc7

Left-Handed Media

Waves in a Slab of Uniaxial BW Medium

S. Ilvonen and I. V. Lindell
Helsinki University of Technology
Espoo, FIN-02150, Finland

Certain isotropic and anisotropic media with negative permittivity and/or permeability parameters have recently been under active study. These materials are often labelled as left-handed media. Since these materials do not possess structural handedness (chirality), the name backward-wave media (BW media) has also been suggested [2]. This name is due to the backward waves present in these media. Various suggestions for constructing composite materials realizing such media, also called metamaterials, using e.g. photonic band gap structures have also been recently suggested.

In a recent paper [2] it was shown that a uniaxial medium with only one of its four medium parameters negative can support a backward wave along an interface with non-BW media. In the present study a slab of such an anisotropic BW medium is analyzed for guided waves. The axis of the material is assumed normal to the slab and material losses are considered negligible. In this case it is seen that, for example, when normal component of permeability is negative and all other parameters positive, the TE waves in the slab are backward waves with power propagating in the direction opposite to that of the phase. Also the power in the slab is propagating in the direction opposite to that of the power propagating outside the slab. Thus a TE wave produced in the slab results in radiation in the backward direction outside the slab. Since the ratio of the power propagating inside and outside the slab depends on the thickness of the slab, application as a backfire antenna appears possible.

REFERENCES

1. Veselago, V. S., “The electrodynamics of substances with simultaneously negative values of ϵ and μ,” *Sov. Phys. Usp.*, Vol. 10, No. 4, 509–514, 1968. (Translation from the original Russian version in *Usp. Fiz. Nauk*, Vol. 92, 517–526, July 1967.)
2. Lindell, I. V., S. A. Tretyakov, K. I. Nikoskinen, and S. Ilvonen, “BW media — media with negative parameters, capable of supporting backward waves,” *Micro. Opt. Tech. Lett.*, Vol. 31, No. 2, October 2001.

Guidance Condition for Symmetric Slab Waveguide with Negative Permittivity and Permeability

B.-I. Wu, T. M. Grzegorczyk, Y. Zhang, and J. A. Kong
Research Laboratory of Electronics, Massachusetts Institute of Technology
Cambridge, MA 02139-4307, U.S.A.

A medium with negative permittivity and permeability was introduced by Vesalago in 1968, and was called a left-handed medium because the wavevector, the electric field vector, and the magnetic field vector form a left-handed system. Theoretically, it has been shown that such medium possesses negative refraction index and has negative ϵ ad μ macroscopically. Experimentally, the left-handed medium has recently been realized by using wires and split ring resonators. A prism of such design exhibits a reversed light bending effect at microwave frequencies. Another effect of the perfect lens realization has also been suggested.

The guidance condition of the guided modes inside in a slab with negative permittivity and permeability are solved. Both real and imaginary transverse wavenumber inside the slab are considered. It is found that for real transverse wavenumber, there exist cutoff for the all mode. In addition, guidance condition of the modes with imaginary transverse wavenumber in the slab are shown to exist. Propagation of guided waves inside a less dense negative medium is shown possible. Power densities are computed in all regions and it is shown that for the guided modes with both real and imaginary transverse wavenumber, the time-averaged Poynting power densities inside the slab is opposite to the power densities outside the slab.

Plasmons in Nano-Wires and Left-Handed Plasmonic Materials

V. M. Shalaev and A. K. Sarychev
Purdue University
West Lafayette, IN, U.S.A.

V. A. Podolskiy
New Mexico State University
Las Cruces, NM, U.S.A.

The electromagnetic field distribution for thin metal nanowires is found by using the discrete dipole approximation beyond the quasi-static approximation [1] and analytical solution for a plasmon localized in nanowire [2]. Our calculations further develop simulations of [3] and treat propagating plasmon waves (surface plasmon polaritons, SPPs) in metal wires exceeding the light wavelength. The SPP modes in wires are numerically simulated and conditions for their resonant excitation are found. These modes are shown to be dependent on the incident light wavelength and direction of propagation. The theory is in agreement with the near-field optical experiments performed by Moskovits' research team in UCSB [4]. We also study ordered lattices and disordered composites fabricated from metal nano-needles. The existence of localized plasmon modes and strong local field enhancement in percolation nanowire composites is demonstrated.

We show that in plasmonic composite nanomaterials both dielectric permittivity and magnetic permeability can be negative, opening up new means for fabricating left-handed materials [5], with the negative refractive index in the visible and near-infrared parts of the spectrum. Specifically, such left-handed materials can be fabricated, using metal nano-wires or metal-dielectric percolation composites [4,6].

REFERENCES

1. V. A. Podolskiy, A. K. Sarychev, and V. M. Shalaev, "Plasmon modes in metal nanowires", *J. of Nonlinear Optical Physics and Materials* (in press).
2. D.P. Makhnovskiy, L.V. Panina, D.J. Mapps, A.K. Sarychev, *Phys. Rev.* B 64, 134205 (2001); A.N. Lagarkov and A.K. Sarychev, *Phys. Rev.* B 53, 6318 (1996).
3. J.P. Kottman, O.J.F. Martin, D.R. Smith, S. Schultz, *Chem. Phys. Lett.*, 341, 1 (2001).
4. S. Y. Yang, V. A. Podolskiy, V. Ushchinnskaya, L.-L. Tay, T. Haslett, A.K. Sarychev, M. Moskovits and V. M. Shalaev (submitted).
5. D. R. Smith, W. J. Padilla, D. C. Vier, S. C. Nemat-Nasser, and S. Shultz, *Phys. Rev. Lett.*, 84, 4184 (2000).
6. A.K. Sarychev, R.C. McPhedran, and V.M. Shalaev, *Phys. Rev.* B 62, 8531 (2000); A.K. Sarychev and V.M. Shalaev, *Phys. Reports*, 335, 275 (2000).

Observation of Coupled Plasmon-Polariton Modes of Plasmon Waveguides for Electromagnetic Energy Transport Below the Diffraction Limit

S. A. Maier, P. G. Kik, and H. A. Atwater
California Institute of Technology
Pasadena, CA 12895, U.S.A.

S. Meltzer, A. A. G. Requicha, and B. E. Koel
University of Southern California
Los Angeles, CA 90089, U.S.A.

The miniaturization of optical devices to spatial dimensions akin to their electronic device counterparts will require structures that guide electromagnetic energy below the diffraction limit of light.

We showed in previous theoretical work that plasmon waveguides consisting of arrays of closely spaced metal nanoparticles guide electromagnetic energy on the nanoscale. Energy transport in these arrays occurs via near-field coupling between metal nanoparticles that sets up plasmon modes. This coupling leads to coherent propagation of energy with group velocities of about 0.1 c and energy can be guided around 90 degree corners and split via tee structures with high efficiency [1]. We confirmed our theoretical predictions in a macroscopic analogue operating in the microwave regime both via experiment and full field electrodynamic simulations. Functional building blocks of complex networks such as 90 degree corners, tee-splitters and all-optical modulators were demonstrated [2].

We report on the optical characterization of the guiding properties of plasmon waveguides consisting of closely spaced gold and silver nanoparticles fabricated using electron beam lithography. Far-field spectroscopy confirms the existence of longitudinal and transverse collective modes of excitation and allows for the calculation of the dispersion relation of plasmon waveguides. Measurements of the polarization dependent absorption confirm that the collective mode arises from near-field optical interactions. From these far-field measurements, a maximum group velocity of 4.0×10^6 m/s for energy transport for arrays of 50 nm Au particles was calculated, in agreement with our theory. It should be possible to excite this mode of maximum group velocity for energy transport using local excitation of single nanoparticles. We report on initial measurements and will also present finite difference time domain (FDTD) simulations of the electromagnetic properties of plasmon waveguides.

REFERENCES

1. Maier, S. A., M. L. Brongersma, P. G. Kik, S. Meltzer, A. A. G. Requicha, and H. A. Atwater, "Plasmonics — a route to nanoscale optical devices," *Advanced Materials*, Vol. 13, No. 19, 1501–1505, 2001.
2. Maier, S. A., M. L. Brongersma, and H. A. Atwater, "Electromagnetic energy transport along arrays of closely spaced metal rods as an analogue to plasmonic devices," *Applied Physics Letters*, Vol. 78, 16–18, 2001.

Propagation of Electromagnetic Waves in a Left-Handed Medium

Y. Zhang, T. M. Grzegorczyk, and J. A. Kong
Research Laboratory of Electronics, Massachusetts Institute of Technology
Cambridge, MA 02139, U.S.A.

A "left-handed" (LH) medium is a medium where both the permittivity and the permeability are negative, so that the vectors $\overline{E}$, $\overline{H}$, and $\overline{k}$ form a "left-handed" dyad. After the first theoretical treatment of the LH material in 1968, studies on the subject had been elusive. It is only recently that the first experimental demonstration of the existence of LH materials in the GHz band has been offered, allowing in this way investigations on LH media to be conducted, in both academic and industrial worlds.

For example, one of the most interesting characteristic of LH slabs known to date is their ability to form a "perfect image" of a point or line source, as has been shown in a recent paper [1]. This discovery draws much attention of the researchers to explore more applications of LH materials, as well as to conduct theoretical studies to better understand their electromagnetic behavior. For example, still a challenge is how to rigorously describe the electromagnetic waves in LH media instead of using a ray-optics approximation as in many previous studies? Also, are the evanescent waves in the LH medium growing or decaying?

This talk aims at providing a rigorous derivation of the electromagnetic fields inside and outside a slab of LH material. The fields are described by using layered Green's functions in plane-wave expansion for a current source with Gaussian distribution. The coefficients in the Green's functions' kernels are solved by matching the boundary conditions for tangential electric and magnetic fields. Upon carefully carrying the algebra of the problem, it is shown that the fields possess the invariant property with respect to the choice of the wavenumber in the LH medium. Consequently, the delicate issue of having to choose between growing or decaying evanescent waves in the LH material is avoided, and the electromagnetic fields inside the LH medium are uniquely determined without any ambiguities. Finally, for the sake of validation with some recent properties discussed in the literature, we study the propagation of waves through a slab of a material with both negative permittivity and permeability, $\epsilon_1 = -\epsilon_0,\ \mu_1 = -\mu_0$ (ϵ_1 and μ_1 being the constitutive parameters of the slab).

REFERENCES

1. Pendry, J. B., "Negative refraction makes a perfect lens," *Phys. Rev. Lett.*, Vol. 85, No. 18, 3966–3969, Oct. 2000.

The Perfect Lens in a Non-Perfect World

P. G. Kik, S. A. Maier, and H. A. Atwater
California Institute of Technology
Pasadena, CA 91125, U.S.A.

We will present our approach to experimentally demonstrate sub-diffraction-limit imaging using a thin metal film. In a recent paper Pendry [1] showed that this type of system can operate as a near-field "perfect lens". The quality of the generated image is determined by a combination of the scattering losses in the film, the finite size of the source, and the roughness of the film. To assess the effect of finite source size on the image formation we performed Finite Difference Time Domain (FDTD) simulations. The model used consists of a $30 \times 30 \times 15$ nm ($L \times W \times H$) source on a 30 nm thick spacer dielectric with a 30 nm thick silver layer functioning as the lens on the opposite side of the dielectric. Despite the finite source thickness a ~ 70 nm wide image is generated, which is still well below the diffraction limit.

Our FDTD simulations suggest that experimental verification of the imaging is difficult but not impossible. Various materials systems and experimental configurations that could be used in such experiments are discussed. FDTD calculations were used to predict and optimize the image contrast and signal-to-noise ratio. We will discuss our sample fabrication method and present initial experimental results.

REFERENCES

1. Pendry, J. B., "Negative refraction makes a perfect lens," *Phys. Rev. Lett.,* Vol. 85, 3966, 2001.

Summability Method for Calculating the Field Distribution Due to a Source Below a LHM Slab

X. Chen, J. Pacheco, T. M. Grzegorczyk, Y. Zhang, B.-I. Wu and J. A. Kong
Research Laboratory of Electronics
Massachusetts Institute of Technology
Cambridge, MA 02139, U.S.A.

This paper discusses the convergence of an integral with oscillating divergent integrand in a new sense, summability.

Consider a linear antenna pointing in the $\hat{x}$ direction and lacated at the origin below a LHM slab with lower boundary $z = d_1$ and upper $z = d_2$. The H_y component in LHM is

$$H_y = -\frac{I}{4\pi} \int_{-\infty}^{\infty} dk_y e^{ik_y y} e^{ik_z (2d_1 - z)} \tag{1}$$

Since $Re\{k_z\} \geq 0$, the integrand in (1) blows up when $z > 2d_1$. In the sense of Cauchy convergence, H_y in (1) does not converge. But in fact H_y does exit physically. This paper proposes a new sense of convergence, summability, and shows that the integration (1) converges analytically in the new sense.

Here is the basic idear of summability. Consider a divergent sequence a_n ($n = 0, 1, 2 \ldots$) and its partial sum $s_n = \sum_{i=0}^{n} a_i$. In Cauchy convergence sense, s_n does not converge. But if we transform s_n into another sequence s_n' using a cettain process, such as V, s_n' may converge in Cauchy sense. Then we say that s_n is limmitable and a_n is summable by process V. Of course, the above process must satisfy some conditions. One of the most important advantages of summability is that the scope of the sequences that are limitable under the sense of summability is much enlarged, while those sequences convergent in Cauchy sense are limitable in summability sense to the same value. For example, the sum $\sum_{n=0}^{\infty} z^n$ is limitable to $\frac{1}{1-z}$ when $-\infty < z < 1$ under B or E_p process.

When $z > 2d_1$, replace $z - 2d_1$ by Z ($Z > 0$). Then (1) can be writen as

$$H_y = -\frac{I}{4\pi} \int_{-\infty}^{\infty} dk_y e^{ik_y y} e^{ik_z Z} e^{ik_z (-2Z)} = -\frac{I}{4\pi} \int_{-\infty}^{\infty} dk_y e^{ik_y y} e^{ik_z Z} \left(\sum_{m=0}^{\infty} \frac{(-2ik_z Z)^m}{m!} \right) \tag{2}$$

After exchanging the infinite sum and integration operation, we have

$$H_y = I1 + I2 + I3 \tag{3}$$

where

$$I1 = \sum_{m=0}^{\infty} \frac{(-2Z)^m}{m!} \frac{-I}{4\pi} \int_{-\infty}^{\infty} dk_y e^{ik_y y} e^{ik_z (Z)} (ik_z)^m \tag{4}$$

$$I2 = \lim_{u \to \infty} \sum_{m=0}^{\infty} \frac{(-2Z)^m}{m!} \frac{-I}{4\pi} \int_{-\infty}^{-u} dk_y e^{ik_y y} e^{ik_z (Z)} (ik_z)^m \tag{5}$$

$$I3 = \lim_{u \to \infty} \sum_{m=0}^{\infty} \frac{(-2Z)^m}{m!} \frac{-I}{4\pi} \int_{u}^{\infty} dk_y e^{ik_y y} e^{ik_z (Z)} (ik_z)^m \tag{6}$$

By Taylor expansion theorem, $I1 = \frac{iI}{4} \frac{\partial H_0^{(1)}(k\rho)}{\partial Z} = \frac{iI}{4} \frac{\partial H_0^{(1)}(k\rho)}{\partial z}$, where $\rho = \sqrt{y^2 + (z - 2d_1)^2}$. By summability under process B or E_p, $I2 = I3 = 0$. So $H_y = \frac{iI}{4} \frac{\partial H_0^{(1)}(k\rho)}{\partial z}$.

Čerenkov Radiation in Left-Handed Material

J. Lu, T. M. Grzegorczyk, Y. Zhang, J. Pacheco, B.-I. Wu, and J. A. Kong
Research Laboratory of Electronics
Massachusetts Institute of Technology
Cambridge, MA 02139, U.S.A.

A rigorous treatment of Čerenkov Radiation in Left-Handed material is presented in this work. Čerenkov radiation is generated when a relativistic charged particle passes through a medium, and whose velocity is larger than the phase velocity of light in that medium. With its special characteristics, Čerenkov radiation has many applications, such as Čerenkov detector, Čerenkov maser, etc. In normal materials the power and the particle will both go forward. In the newly emerged Left-Handed materials, which can support backward waves, the direction of the particle and the direction of the power form an obtuse angle, which can make the situation much more interesting.

Left-Handed materials were first introduced by Veselago [1]. The backward power of Čerenkov radiation was also mentioned in that paper, but no energy distribution was given. In this work, we follow the theory of Tamm and Frank [2] for normal materials, by considering the frequecy dispersion of permittivity and permeability, and we solve Maxwell's equations in Left-Handed materials. Furthermore the Poynting vector and energy distribution are calculated over the frequency and angle. For frequency dispersive materials, where the permittivity and permeability can take simultaneously negative values, the forward and backward power coexist, but in different frequency bands. Energy loss, due to Čerenkov radiation, is also derived along the unit length of the path of particle.

Finally, Čerenkov radiation in a metalic cylindrical waveguide filled with a Left-Handed material is calculated, in order to show the application of backward power. In this case, the spectrum is discrete, and only TM modes are allowed to propagate. The frequency of mth guided mode is determined by the mth root of the Neumann function. When the modes lie in the frequency band of Left-Handed regime, the real part of the Poynting vector points in the direction opposite to that of the moving particle. With this characteristic, a new kind of Čerenkov maser can be made.

REFERENCES

1. V. G. Veselago, Sov. Phys. Usp. 10, 509 (1968).
2. J. V. Jelley, 'Čerenkov Radiation and its applications', p. 15(1958).

Session 5Pc8

Quantum Computing

Small Parameters in Quantum Computation with Large Number of Qubits

G. P. Berman and D. I. Kamenev
Theoretical Division and CNLS
Los Alamos National Laboratory
Los Alamos, NM 87545, U.S.A.

V. I. Tsifrinovich
IDS Department
Polytechnic University
Brooklyn, NY 11201, U.S.A.

Quantum information processing in solid-state logic devices is always accompanied by errors. These errors can be caused by the influence of the environment on the quantum system. But even in the case when the quantum computer is completely isolated from the environment, there are always the errors associated with imperfect implementation of quantum logic gates, which is the subject of this paper. For the most effective quantum information processing, a quantum computer should have a large number of quantum bits (qubits). The number of quantum states in this many-qubit system is exponentially large. In this paper we describe a new theory which allows one to compute the errors in quantum logic operations in a quantum computer with a large number of qubits without exact solution of the quantum dynamical equations. Our theory is based on small parameters which naturally appear in solid-state quantum computer models. This theory allows one to calculate the probabilities of all essential unwanted transitions generating errors in the quantum computer. Our approach allows one to express the complicated quantum dynamics of this exponentially large time-dependent quantum system in terms of relatively simple scalable analytic formulas. To demonstrate our method, we use it to compute the error which occurs during the creation of entanglement between the end qubits in a 1000-qubit spin chain.

Quantum Effects in a Single-Spin Measurement Using Magnetic Resonance Force Microscopy

G. P. Berman, G. Chapline, P. C. Hammel, D. V. Pelekhov, and A. Suter
Los Alamos National Laboratory
Los Alamos, NM 87545, U.S.A.

F. Borgonovi
Dipartimento di Matematica e Fisica
Università Cattolica
Brescia, 25121, Italy

S. A. Gurvitz
Department of Particle Physics
Weizmann Institute of Sciences
Rehovot, 76100, Israel

V. I. Tsifrinovich
IDS Department
Polytechnic University
Brooklyn, NY 11201, U.S.A.

Modern solid-state technologies are approaching the level at which manipulating a single electron, atom, or nuclear spin becomes extremely important. The future successful development of these technologies depends significantly on single-particle measurement methods. While a single electron charge can be detected using a single-electron transistor, methods for detection of a single electron (or nuclear) spin in solids are still not available. However, many proposals for solid-state nano-devices require a single-electron (or nuclear) spin measurement. Single-spin detection is one of the important challenges facing the development of such new technologies as single-spin transistors and solid-state quantum computation. There are a few proposals for a solid-state single-spin measurement based on the swap operation of a spin state to a charge state, scanning tunneling microscopy, or magnetic resonant force microscopy (MRFM). MRFM with a cyclic adiabatic inversion, which utilizes a cantilever oscillations driven by a single spin, is a promising technique to solve the problem of a single-spin detection. We have studied the quantum dynamics of a single spin interacting with a quasiclassical cantilever. It was found that in a similar fashion to the Stern-Gerlach interferometer the quantum dynamics generates a quantum superposition of two quasiclassical trajectories of the cantilever which are related to the two spin projections on the direction of the effective magnetic field in the rotating reference frame. Our results show that quantum jumps will not prevent a single-spin measurement if the coupling between the cantilever vibrations and the spin is small in comparison with the amplitude of the radio-frequency external field.

Macroscopic Entangled Spin States in a Self-Assembled Monolayer Molecular System

D. L. Allara
Pennsylvania State University
University Park, PA 16802, U.S.A.

G. P. Berman
Los Alamos National Laboratory
Los Alamos, NM 87545, U.S.A.

V. I. Tsifrinovich
IDS Department
Polytechnic University
Brooklyn, NY 11201, U.S.A.

Entangled states of weakly interacting particles and even macroscopic objects attract much attention last years. Besides unusual physical properties such states are expected to find practical applications in quantum communication and quantum information processing.

Unlike streamline of research which concentrates on the electric properties of ordered two-dimensional arrays of organic molecules we explore magnetic properties of SAMs.

We are considering an ensemble of three-spin molecules. Every organic molecule contains three electron spins. As an example, we consider electron spins 1/2 associated with stable free radicals. We assume that the distance between three radicals in a molecule is large enough to prevent exchange interaction between the electron spins but small enough to provide strong dipole-dipole interaction between them. For our purposes the shift of the electron spin resonance (ESR) frequency of two other spins inside the molecules must be greater than the ESR linewidth. The distance between the molecules containing spin radicals must be large enough, so the ESR frequency shift caused by the dipole field from other molecules must be small. The ESR shift caused by the nuclear spins must also be small.

We discuss the opportunity for creation of a macroscopic entangled spin state in a self-assembled monolayer molecular system. A group of spin radicals in every molecule can be transferred to the entangled state using resonant electromagnetic pulses. Magnetic dipole-dipole interaction inside a molecule is taken into account while the same interaction between the molecules is shown to be negligible. A high external magnetic field at low temperature provides the identical entangled states for all molecules in a sample. We argue that the macroscopic entangled state could be detected in experiments with macroscopic magnetization of a sample.

Solid State Quantum Computing and Storage Using Optically Excited Spins

P. R. Hemmer
Department of Electrical Engineering
Texas A&M University
College Station, TX 77843-1064, U.S.A.

M. S. Shahriar
Department of Electrical and Computer Engineering
Northwestern University
Evanston, IL 77843-1064, U.S.A.

Solid state quantum computers and memories have a number of potential advantages for scalability. Unfortunately, for single atoms in solid hosts, coherence lifetimes tend to be much shorter than in other materials. One exception to this rule is dilute spin systems in non-magnetic hosts, which are known to have coherence lifetimes T_2 in excess of milliseconds and population lifetimes T_1 in excess of hours. Unfortunately, the weak interactions of spin systems with the environment, leads not only to their long coherence times but also to slow interactions between intentionally coupled spin-qubits. To overcome this limitation, we have been exploring the use of optical Raman dark resonances to address and manipulate spins in solids. The use of optical transitions to manipulate spins allows fast coupling between qubits, yet can be switched on and off at will. In addition, dark resonances offer the possibility of using adiabatic passage techniques, which greatly reduce errors and enhance fidelity.

Experimental work so far has concentrated on the use of two different materials, Pr doped Y_2SiO_5 (Pr:YSO) and nitrogen-vacancy (NV) color centers in diamond. For conditional quantum logic demonstrations, NV diamond is preferred because it is possible to detect single color centers. So far, we have demonstrated single-qubit initialization in an ensemble of NV centers, and are working toward the manipulation of individual, as well as pairs, of NV centers. The Pr:YSO has a longer spin lifetime than NV diamond, but also has a weak optical transition strength, which has so far prevented the detection of a single dopant atom. Nonetheless, this material has proved useful for the demonstration of optically driven, single spin-qubit manipulations, using an ensemble. It has also been used to demonstrate the "stopped light" storage technique in a solid. Stopped light quantum storage is of interest because it has 100% fidelity in principle, yet is relatively easy to implement in practice. In this technique the input quantum information is stored in an ensemble of active atoms, and single atom detection capabilities are unnecessary.

Determination and Teleportation of the Phase of an Electromagnetic Field via Incoherent Detection of Fluorescence

P. Pradhan and M. S. Shahriar
Department of Electrical and Computer Engineering
Northwestern University
Evanston, IL, U.S.A.

We show that the initial phase of a Rabi driving field can be determined by measuring the population of one level of a two-level system when the driving field is strong and when the rotating wave approximation is not valid. This is due to a high-frequency oscillation of the atomic population that is related to the Bloch-Siegert shift. Analytical calculation, supported by numerical simulation has been performed, and we discuss an experimental scheme by using a two-level system of a thermal beam of Rb atoms in a strong radio frequency driving field to observe this effect. It has been demonstrated that an atom is not a square law detector in this strong field regime; it has both amplitude and phase information of the coupling field, even though the measurement process detects population of only one level. Using a pair of rubidium atoms that are entangled via transferring the quantum correlation from a pair of photons, it is possible to use this process for teleportation of phase as well as frequency for possible application to clock synchronization.

Quantum-Hall Semiconductor Quantum Computer Design

V. Privman
Clarkson University
Potsdam, NY 13699-5820, U.S.A.

We survey recent advances in semiconductor spin-qubit quantum computing, both theoretical and experimental. We then outline our recent work that combined elements of the 1998 quantum computing proposals by Privman, Vagner and Kventsel, and by Kane, with the new idea of nuclear-spin qubit interactions mediated indirectly via the bound outer electrons of impurity atoms whose nuclear spins 1/2 are the qubits. These electrons, in turn, interact via the two-dimensional electron gas in the quantum Hall effect regime. The resulting quantum computing scheme retains all the gate-control and measurement aspects of the proposal by Kane, but allows qubit spacing at distances of order 100 nm, attainable with the present-day semiconductor device technologies.

In our new scheme, published by Mozyrsky, Privman and Glasser in 2001, the nuclear spins are coupled to the outer bound electrons. The latter interact via the two-dimensional electron gas. This interaction is stronger and/or of a much longer range than the couplings utilized in earlier approaches: the qubit separation can be of order 100 nm. Another advantage is that gate control of the individual qubits and of qubit-qubit interactions is possible, along the lines of Kane. We have carried out extensive perturbative many-body calculations allowing estimation of the interaction "clock" time scale and decoherence time, for both the original two-dimensional-electron-gas-involving quantum-computing proposal and its new, improved version. We also obtained estimates of relaxation and single-qubit-control time scales. The "clock speed" of the improved model is faster by two orders of magnitude, for the same quality factor.

Multi-Kilometer Atmospheric Quantum Key Distribution: Recent Results and Implications for Satellite Quantum Key Distribution

R. Hughes
Los Alamos National Laboratory
Los Alamos, NM, U.S.A.

Quantum cryptography, or more accurately, quantum key distribution (QKD), is an emerging application of quantum information science that uses single-photon transmissions to generate the shared, secret random number sequences, known as cryptographic keys, which are used to encrypt and decrypt secret communications. Because the security of QKD is based on principles of quantum physics and information theory an adversary can neither successfully tap the key transmissions, nor evade detection. QKD could therefore enable "on demand" keying of secure communications systems, with higher levels of security and convenience than present-day key distribution schemes. Particularly attractive potential uses of QKD are in free-space optical communications, both ground-based and for satellite communications. In my talk I shall describe the theory of QKD and the results of a recent experiment to demonstrate free-space QKD across a 10-km line-of-sight path in daylight and at night. This distance is six times longer than any previously reported and has optical characteristics comparable to a ground-to-space path. For the first time in QKD, secret, cryptographic quality random numbers were reliably transferred at practical rates with security against technologically feasible eavesdropping strategies. The secrecy capacity (secret bits transferred per transmitted bit) can be related to optical properties of the atmospheric channel, allowing the secrecy capacity of free-space QKD under other atmospheric conditions and over other, longer transmission distances to be inferred. I will describe the results of a satellite-to-ground QKD downlink simulation and our plans for developing a satellite QKD experiment.

The Power of Entangled Quantum Channels

S. Lloyd
Department of Mechanical Engineering
Massachusetts Institute for Technology
Cambridge, MA 02139, U.S.A.

By exploiting quantum correlations such as entanglement, coupled quantum channels can communicate at a potentially higher rate than unentangled quantum channels given the same power. In particular, given the same overall power, M coupled, entangled quantum channels can send M bits in the same time it takes a single channel to send a single bit, and in the same time it takes M unentangled channels to send $\sqrt{M}$ bits. This paper shows how the same techniques that lead to a $\sqrt{M}$ speed up for Grover's algorithm can be used to enhance communication capacity. The speed up is related to similar enhancements to the accuracy of atomic clocks, of interferometry, of lithography, and of radar and GPS. Issues of noise, errors, and the difficulty of preparing the required entangling dynamics are addressed. The method is compared with existing communication techniques.

Quantum Error Modeling and Correction in Long Distance Teleportation Using Singlet States

J. Aung and J. H. Shapiro
Research Laboratory for Electronics
Massachusetts Institute for Technology
Cambridge, MA 02139, U.S.A.

Bennett et al. [1] described the following protocol for teleporting the state of a two-level quantum system (a qubit) from one location to another. A pair of two-level systems—one at the sender and the other at the receiver—is entangled in a singlet state. The sender then performs Bell-state measurements on the joint system comprised of the qubit to be teleported and the sender's portion of the singlet. It transmits the resulting two bits of classical information to the receiver via a classical channel. The receiver completes the teleportation procedure by applying the appropriate unitary transformation, specified by this classical information, to its portion of the singlet. Bouwmeester et al. [2] reported an experimental demonstration of singlet-based teleportation. Their demonstration, however, fell several steps short of being a long-distance quantum communication system: it was a table-top demonstration that measured only one of the four Bell states and had no provision for storing the teleported state.

A team of researchers from the Massachusetts Institute of Technology (MIT) and Northwestern University (NU) has proposed a quantum communication architecture [3] that, in principle, remedies all the deficiencies of prior singlet-based teleportation experiments. This architecture uses a novel ultrabright source of entangled photon pairs [4] and trapped-atom quantum memories [5] in which all four Bell states can be measured. In this paper, we report the quantum-communication error model for the MIT/NU architecture. We show that multiple memory atoms per qubit convert multi-photon error events into erasure events, with the remaining, single-photon errors having a Werner-state density operator. Using this density operator, we quantify the fidelity versus throughput performance trade-offs afforded by the use of quantum error correcting codes [6] and/or entanglement purification protocols [7].

REFERENCES

1. Bennet, C. H., G. Brassard, C. Crépeau, R. Jozsa, A. Peres, and W. K. Wootters, *Phys. Rev. Lett.*, Vol. 70, No. 1895, 1993.
2. Bouwmeester, D., J.-W. Pan, K. Mattle, M. Eibl, H. Weinfurter, and A. Zeilinger, *Nature*, Vol. 390, No. 575, 1997.
3. Shapiro, J. H., "Long-distance high-fidelity teleportation using singlet states," *Quantum Communication, Computing and Measurement 3*, P. Tombesi and O. Hirota (eds.), 367–374, Kluwer, New York, 2001.
4. Shapiro, J. H. and N. C. Wong, *J. Opt. B: Quantum Semiclass. Opt.*, Vol. 2, No. L1, 2000.
5. Lloyd, S., M S. Shahriar, J. H. Shapiro, and P. R. Hemmer, *Phys. Rev. Lett.*, Vol. 87, No. 167903, 2001.
6. Bennett, C. H., D. P. DeVincenzo, J. A. Smolin, and W. K. Wootters, *Phys. Rev. A*, Vol. 54, No. 3824, 1996.
7. Bennett, C. H., G. Brassard, S. Popescu, B. Schumacher, J. A. Smolin, and W. K. Wootters, *Phys. Rev. Lett.*, Vol. 76, No. 722, 1996.

Simulation of Multiparticle Quantum Entanglement Using Classical Fields

K. F. Lee and J. E. Thomas
Physics Department
Duke University
Durham, NC 27708-0305, U.S.A.

Currently, there is great interest in classical-wave simulation of quantum logic and quantum measurement. Analogous to quantum systems, classical-wave fields obey a superposition principle, enabling operations with superposition states on which much of quantum information processing is based. Further, study of classical-wave systems will help to elucidate the fundamental differences between classical-wave and quantum systems.

Previously, classical-wave analogs of the Schrödinger wave function for a single particle have been explored both theoretically and experimentally. This has lead to a variety of classical-wave simulations of one-particle quantum wave-mechanics, including analogs of Fock states and Wigner phase-space distributions exhibiting negative regions [1–4].

We will describe and demonstrate a simple, general method for classical-wave simulation of entanglement of more than one-particle. The simulations employ optical heterodyne detection of fields of different frequencies. The field at each frequency is a classical analog (c-bit) of a quantum bit (qu-bit) which can be in an arbitrary polarization state, i.e., a superposition of two orthogonal polarizations. Analog multiplication of the heterodyne signals from independent spatially separated detectors is used to simulate coincidence measurement of multiple particles. The product signal so obtained contains several frequency components, one of which can be selected by band pass frequency filtering. The band passed signal generally contains several indistinguishable, interfering contributions, permitting simulation of a specific multi-particle entangle state. Results will be presented for simulation of two-particle Bell-states and three particle GHz entanglement.

REFERENCES

1. Lee, K. F., F. Reil, S. Bali, A. Wax, and J. E. Thomas, *Opt. Lett.*, Vol. 24, No. 1370, 1999, and references therein.
2. Wódkiewicz, K. and G. H. Herling, *Phys. Rev. A*, Vol. 57, No. 815, 1998.
3. Dragoman, D., *Optik*, Vol. 111, No. 393, 2000.
4. Dragoman, D., *Optik*, Vo1. 111, No. 179, 2000.

Rare Earth Doped Nano-Particles for Optically Addressable Quantum Computers

Z. Hasan, S. Dardona, and A. Konjhodzic
Physics Department
Temple University
Philadelphia, PA, U.S.A.

It is believed that arrays of isolated single atoms or small groups of a few atoms each can provide hardware for scalable quantum computers. We report the fabrication of such hardware in condensed matter. We have atomically engineered nano-particles containing as little as one atom of a rare earth impurity. Each such nano-particle could be used as an optically addressable quantum computer with a small number of qubits. All material and atomic parameters have been optimized to enhance the optical addressability and control of these rare earth qubits. The electronic transition used for optical addressing has been chosen to have very high oscillator strength, approaching the ideal value for an electric dipole allowed transition in an atom. The frequency of the transition lies in the conveniently tunable region of spectrum by dye lasers. Fine structures in the ground and excited electronic states allow for choosing the appropriate selection rules for optical loading and addressing of qubits. We have observed that most of these favorable properties are either maintained or enhanced in nano-particles as compared to the bulk.

Nano-particles of II–VI materials, doped with rare earth ions have been produced by quench condensing the laser-ablated vapors. In controlled chemical environment, our experiments have fabricated particles as small as a couple of nanometers in radius and containing one Rare Earth ion per particle. Particles with a larger number of rare earth ions are easier to fabricate. Growth parameters have been optimized to enhance yield, select size, and to narrow down the size distribution of nano-particles. These particles exhibit enhanced structural, electronic, and optical properties. Confinement induced changes in optical and thermal properties have been exploited for confirming and producing a set number of Rare Earth ions per nano-particle. This talk will review linear and non-linear optical properties of rare earth doped II–VI nano-particles especially in regard to their relevance for scalable quantum computers.

Author Index